

Special Issue  
PAPERS PRESENTED AT THE 12th INTERNATIONAL  
SYMPOSIUM ON MICROCHEMICAL TECHNIQUES (ISM '92),  
CÓRDOBA, SPAIN, SEPTEMBER 7-12, 1992

# ANALYTICA CHIMICA ACTA

An international journal devoted to all branches of analytical chemistry

**Editors:** Harry L. Pardue (West Lafayette, IN, USA)  
Alan Townshend (Hull, Great Britain)  
J.T. Clerc (Berne, Switzerland)  
Willem E. van der Linden (Enschede, Netherlands)  
Paul J. Worsfold (Plymouth, Great Britain)

**Associate Editor:** Sarah C. Rutan (Richmond, VA, USA)

**Editorial Advisers:**

F.C. Adams, Antwerp  
M. Aizawa, Yokohama  
J.F. Alder, Manchester  
C.M.G. van den Berg, Liverpool  
A.M. Bond, Bundoora, Vic.  
S.D. Brown, Newark, DE  
J. Buffle, Geneva  
P.R. Coulet, Lyon  
S.R. Crouch, East Lansing, MI  
R. Dams, Ghent  
L. de Galan, Vlaardingen  
M.L. Gross, Lincoln, NE  
W. Heineman, Cincinnati, OH  
G.M. Hieftje, Bloomington, IN  
G. Horvai, Budapest  
T. Imasaka, Fukuoka  
D. Jagner, Gothenburg  
G. Johansson, Lund  
D.C. Johnson, Ames, IA  
A.M.G. Macdonald, Birmingham  
D.L. Massart, Brussels  
P.C. Meier, Schaffhausen

M.E. Meyerhoff, Ann Arbor, MI  
J.N. Miller, Loughborough  
H.A. Mottola, Stillwater, OK  
M.E. Munk, Tempe, AZ  
M. Otto, Freiberg  
D. Pérez-Bendito, Córdoba  
C.F. Poole, Detroit, MI  
J. Ruzicka, Seattle, WA  
A. Sanz-Medel, Oviedo  
S. Sasaki, Toyohashi  
T. Sawada, Tokyo  
K. Schügerl, Hannover  
M.R. Smyth, Dublin  
M. Thompson, Toronto  
G. Tölg, Dortmund  
Y. Umezawa, Tokyo  
E. Wang, Changchun  
J. Wang, Las Cruces, NM  
H.W. Werner, Eindhoven  
O.S. Wolfbeis, Graz  
Yu.A. Zolotov, Moscow  
J. Zupan, Ljubljana

# ANALYTICA CHIMICA ACTA

**Scope.** *Analytica Chimica Acta* publishes original papers, preliminary communications and reviews dealing with every aspect of modern analytical chemistry. Reviews are normally written by invitation of the editors, who welcome suggestions for subjects. Preliminary communications of important urgent work can be printed within four months of submission, if the authors are prepared to forego proofs.

## Submission of Papers

### Americas

Prof. Harry L. Pardue  
Department of Chemistry  
1393 BRWN Bldg, Purdue University  
West Lafayette, IN 47907-1393  
USA  
  
Tel: (+1-317) 494 5320  
Fax: (+1-317) 496 1200

Prof. J.T. Clerc  
Universität Bern  
Pharmazeutisches Institut  
Baltzerstrasse 5, CH-3012 Bern  
Switzerland  
  
Tel: (+41-31) 654171  
Fax: (+41-31) 654198

Prof. Sarah C. Rutan  
Department of Chemistry  
Virginia Commonwealth University  
P.O. Box 2006  
Richmond, VA 23284-2006  
USA  
  
Tel: (+1-804) 367 1298  
Fax: (+1-804) 367 8599

### Computer Techniques

### Other Papers

Prof. Alan Townshend  
Department of Chemistry  
The University  
Hull HU6 7RX  
Great Britain  
  
Tel: (+44-482) 465027  
Fax: (+44-482) 466410

Prof. Willem E. van der Linden  
Laboratory for Chemical Analysis  
Department of Chemical Technology  
Twente University of Technology  
P.O. Box 217, 7500 AE Enschede  
The Netherlands  
  
Tel: (+31-53) 892629  
Fax: (+31-53) 356024

Prof. Paul Worsfold  
Dept. of Environmental Sciences  
University of Plymouth  
Plymouth PL4 8AA  
Great Britain  
  
Tel: (+44-752) 233006  
Fax: (+44-752) 233009

Submission of an article is understood to imply that the article is original and unpublished and is not being considered for publication elsewhere. *Anal. Chim. Acta* accepts papers in English only. There are no page charges. Manuscripts should conform in layout and style to the papers published in this issue. See inside back cover for "Information for Authors".

**Publication.** *Analytica Chimica Acta* appears in 16 volumes in 1994 (Vols. 281-296). *Vibrational Spectroscopy* appears in 2 volumes in 1994 (Vols. 6 and 7). Subscriptions are accepted on a prepaid basis only, unless different terms have been previously agreed upon. It is possible to order a combined subscription (*Anal. Chim. Acta* and *Vib. Spectrosc.*).

Our p.p.h. (postage, packing and handling) charge includes surface delivery of all issues, except to subscribers in the U.S.A., Canada, Australia, New Zealand, China, India, Israel, South Africa, Malaysia, Thailand, Singapore, South Korea, Taiwan, Pakistan, Hong Kong, Brazil, Argentina and Mexico, who receive all issues by air delivery (S.A.L.-Surface Air Lifted) at no extra cost. For Japan, air delivery requires 25% additional charge of the normal postage and handling charge; for all other countries airmail and S.A.L. charges are available upon request.

**Subscription orders.** Subscription prices are available upon request from the publisher. Subscription orders can be entered only by calendar year and should be sent to: Elsevier Science Publishers B.V., Journals Department, P.O. Box 211, 1000 AE Amsterdam, The Netherlands. Tel: (+31-20) 5803 642, Telex: 18582, Telefax: (+31-20) 5803598, to which requests for sample copies can also be sent. Claims for issues not received should be made within six months of publication of the issues. If not they cannot be honoured free of charge. Readers in the U.S.A. and Canada can contact the following address: Elsevier Science Publishing Co. Inc., Journal Information Center, 655 Avenue of the Americas, New York, NY 10010, U.S.A. Tel: (+1-212) 6333750, Telefax: (+1-212) 6333990, for further information, or a free sample copy of this or any other Elsevier Science Publishers journal.

**Advertisements.** Advertisement rates are available from the publisher on request.

**US mailing notice - *Analytica Chimica Acta*** (ISSN 0003-2670) is published biweekly by Elsevier Science Publishers (Molenwerf 1, Postbus 211, 1000 AE Amsterdam.). Annual subscription price in the USA US\$ 3035.75 (subject to change), including air speed delivery. Second class postage paid at Jamaica, NY 11431. *USA Postmasters:* Send address changes to *Anal. Chim. Acta*, Publications Expediting, Inc., 200 Meacham Av., Elmont, NY 11003. Airfreight and mailing in the USA by Publication Expediting.

# ANALYTICA CHIMICA ACTA

An international journal devoted to all branches of analytical chemistry

(Full texts are incorporated in CJELSEVIER, a file in the Chemical Journals Online database available on STN International; Abstracted, indexed in: Aluminum Abstracts; Anal. Abstr.; Biol. Abstr.; BIOSIS; Chem. Abstr.; Curr. Contents Phys. Chem. Earth Sci.; Engineered Materials Abstracts; Excerpta Medica; Index Med.; Life Sci.; Mass Spectrom. Bull.; Material Business Alerts; Metals Abstracts; Sci. Citation Index)

VOL. 283 NO. 1

CONTENTS

NOVEMBER 15, 1993

Papers presented at the 12th International Symposium on Microchemical Techniques, Córdoba, Spain, September 7-12, 1992

Foreword .....	1
<i>Extreme Trace Analysis</i>	
Problems and trends in extreme trace analysis for the elements G. Tölg (Dortmund, Germany) .....	3
<i>Surface Microanalysis and X-ray Techniques</i>	
Surface microanalysis F. Adams, A. Adriaens, P. Berghmans and K. Janssens (Wilrijk, Belgium) .....	19
Scanning tunnelling microscopy of silicon surfaces H.B. Elswijk (Eindhoven, Netherlands) .....	35
Quantitation of species on catalyst surfaces D.M. Hercules, M. Houalla, A. Proctor and J.N. Fiedor (Pittsburgh, PA, USA) .....	42
Surface analysis for the investigation of electrochemical and corrosion systems P.M.A. Sherwood (Manhattan, KS, USA) .....	52
Non-destructive 2- and 3-dimensional microanalysis with (high energy) ion microprobes G.J.F. Legge, A. Saint and N. Cholewa (Parkville, Australia) .....	62
X-Ray microanalysis of stratified specimens J.-L. Pouchou (Chatillon, France) .....	81
Synchrotron radiation-induced x-ray microanalysis K. Janssens, L. Vincze, F. Adams (Wilrijk, Belgium) and K.W. Jones (Long Island, NY, USA) .....	98
Two-photon ionization detection of adsorbed molecules on a metal surface at atmospheric pressure by 355-nm laser irradiation H. Kawazumi (Kitakyushu, Japan), T.-o. Yasuda and T. Ogawa (Fukuoka, Japan) .....	111
<i>Mass Spectrometry</i>	
Advances in inductively coupled plasma mass spectrometry: human nutrition and toxicology R.M. Barnes (Amherst, MA, USA) .....	115
Inorganic mass spectrometry for surface and thin film analysis H. Oechsner (Kaiserslautern, Germany) .....	131
Laser microprobe Fourier transform mass spectrometer with external ion source for organic and inorganic microanalysis H. Struyf, W. Van Roy, L. Van Vaeck, R. Van Grieken, R. Gijbels (Wilrijk, Belgium) and P. Caravatti (Fällanden, Switzerland) .....	139
<i>Atomic Spectrometry</i>	
Simultaneous multi-element analysis of solid samples by laser ablation-microwave-induced plasma optical emission spectrometry L. Hiddemann, J. Uebbing, A. Ciocan, O. Dessenne and K. Niemax (Dortmund, Germany) .....	152
Determination of arsenic speciation by liquid chromatography-hydride generation inductively coupled plasma atomic emission spectrometry with on-line UV photooxidation R. Rubio, A. Padró, J. Albertí and G. Rauret (Barcelona, Spain) .....	160

(Continued overleaf)

ห้องสมุดเคมีและวัสดุวิทยา

Contents (continued)

Slurry-electrothermal atomic absorption spectrometry of samples with large amounts of silica. Determination of cadmium, zinc and manganese using fast temperature programmes I. López García, J. Arroyo Cortéz and M. Hernández Córdoba (Murcia, Spain) . . . . .	167
Study of the influence of ordered media on the determination of lead by hydride generation inductively coupled plasma atomic emission spectrometry M.C. Valdés-Hevia y Temprano, B. Aizpún Fernández, M.R. Fernández de la Campa and A. Sanz-Medel (Oviedo, Spain) . . . . .	175
<b>Biological Analysis</b>	
Trace elements in medicine. Speciation: the new frontier R. Cornelis, F. Borguet and J. De Kimpe (Ghent, Belgium) . . . . .	183
Absorption and bioavailability studies of mineral nutrients by mass spectrometry F.A. Mellon, J. Eagles, T.E. Fox and S.J. Fairweather-Tait (Norwich, UK) . . . . .	190
Development of a screening method for the determination of volatile organic compounds in body fluids and environmental samples using purge and trap gas chromatography–mass spectrometry L. Dunemann and H. Hajimiragha (Düsseldorf, Germany) . . . . .	199
Systematic study of chromium determination in urine by graphite furnace atomic absorption spectrometry R. Rubio, A. Sahuquillo, G. Rauret, L. Garcia Beltran (Barcelona, Spain) and Ph. Quevauviller (Brussels, Belgium) . . .	207
Simultaneous spectrofluorimetric determination of traces of molybdenum and boron in plant leaves C. Cruces Blanco, A. García Campaña, F. Alés Barrero and M. Román Ceba (Granada, Spain) . . . . .	213
Determination of nickel in biological samples prepared by microwave dissolution using electrothermal atomic absorption spectrometry after extraction with 1,5-bis[phenyl-(2-pyridyl)methylene] thiocarbonhydrazide E. Vereda Alonso, J.M. Cano Pavon, A. Garcia de Torres and M.T. Siles Cordero (Málaga, Spain) . . . . .	224
<b>Environmental Analysis</b>	
Determination of inorganic and organic traces in the clean room compartment of Antarctica K.G. Heumann (Regensburg, Germany) . . . . .	230
Determination of bromide in snow samples by ion chromatography with electrochemical detection S. Seefeld and U. Baltensperger (Villigen, Switzerland) . . . . .	246
Characterization of organic sulphur compounds in surface water by ion-pair adsorption under different conditions S. Schullerer and F.H. Frimmel (Karlsruhe, Germany) . . . . .	251
Determination of arsenic residues in agricultural products of Milos island G.E. Miliadis and K.S. Liapis (Athens, Greece) . . . . .	258
Determination of butyltin ion species by ion-exchange chromatography with inductively coupled plasma mass spectrometric and spectrofluorimetric detection J.I. Garcia-Alonso, A. Sanz-Medel (Oviedo, Spain) and L. Ebdon (Plymouth, UK) . . . . .	261
Solid-phase extraction and spectrofluorimetric determination of triphenyltin in environmental samples R. Compañó, M. Granados, C. Leal and M.D. Prat (Barcelona, Spain) . . . . .	272
Determination of organochlorines in sea water: an assessment I. Cruz, D.E. Wells (Aberdeen, UK) and I.L. Marr (Old Aberdeen, UK) . . . . .	280
Rapid method for the determination of eight chlorophenoxy acid residues in environmental water samples using off-line solid-phase extraction and on-line selective precolumn switching J.V. Sancho-Llopis, F. Hernández-Hernández (Castelló, Spain), E.A. Hogendoorn and P. Van Zoonen (Bilthoven, Netherlands) . . . . .	287
Solid-phase extraction of pesticide residues from ground water: comparison between extraction cartridges and extraction discs J. Beltran, F.J. López and F. Hernández (Castellón, Spain) . . . . .	297
Fluorimetric study of polycyclic aromatic hydrocarbons in Brij-35 micellar solution. Evaluation of polycyclic aromatic hydrocarbons in air samples S. Rubio-Barroso, M.N. Kayali and L.M. Polo-Díez (Madrid, Spain) . . . . .	304
<b>Chromatography and Electrophoresis</b>	
Chromatography, today and tomorrow G.A. Guiochon (Knoxville, TN, USA) . . . . .	309
Standard pH values in non-aqueous mobile phases used in reversed-phase liquid chromatography J. Barbosa and V. Sanz-Nebot (Barcelona, Spain) . . . . .	320

Liquid chromatographic study of the photochemical decomposition of sodium ethylmercurithiosalicylate M. Pilar da Silva, J.R. Procopio and L. Hernández (Madrid, Spain) . . . . .	326
Determination of the stability of morphine tablets by ion-pair reversed-phase liquid chromatography I. Ismail Salem and A. Cerezo Galan (Granada, Spain) . . . . .	334
Separation and determination of betaine in an oriental medicine by liquid chromatography N. Kikuchi, K. Matsuno and T. Miki (Tokyo, Japan) . . . . .	338
On-line trace metal ion preconcentration in ion chromatography using carboxymethyl and hydroxamate dextran-coated silicas N. Ryan, J.D. Glennon (Cork, Ireland) and D. Muller (Villetaneuse, France) . . . . .	344
Simultaneous determination of lanthanum, strontium and copper in superconductor materials by ion chromatography E.A. Gautier, R.T. Gettar and R.E. Servant (Buenos Aires, Argentina) . . . . .	350
Measurement of the speciation of iron in the nanogram range: investigation of chromatographic peaks induced by iron blanks G. Weber (Dortmund, Germany) . . . . .	354
Rapid separation of fluorescein derivatives using a micromachined capillary electrophoresis system D.J. Harrison, Z. Fan, K. Seiler (Edmonton, Canada), A. Manz and H.M. Widmer (Basel, Switzerland) . . . . .	361
<i>Flow Analysis</i>	
Solid surface photoluminescence and flow analysis: a happy marriage A. Sanz-Medel (Oviedo, Spain) . . . . .	367
Flow-injection chemiluminescence determination of cobalt(II) and manganese(II) Q. Lin, A. Guiraúm, R. Escobar and F.F. De la Rosa (Seville, Spain) . . . . .	379
Flow-injection and continuous-flow systems for the determination of Se(IV) and Se(VI) by hydride generation atomic absorption spectrometry with on-line pre-reduction of Se(VI) to Se(IV) M.G. Cobo Fernandez, M.A. Palacios and C. Camara (Madrid, Spain) . . . . .	386
Flow-injection flame atomic absorption spectrometry for slurry atomization. Determination of calcium, magnesium, iron, zinc and manganese in vegetables P. Viñas, N. Campillo, I. López García and M. Hernández Córdoba (Murcia, Spain) . . . . .	393
Determination of total and free sulphur dioxide in wine with a continuous-flow microdistillation system A. Maquieira, F. Casamayor, R. Puchades and S. Sagrado (Valencia, Spain) . . . . .	401
Spectrophotometric flow-through sensor for the determination of sulphur dioxide P. Richter, M.D. Luque de Castro and M. Valcárcel (Córdoba, Spain) . . . . .	408
Continuous-flow spectrophotometric determination of amino acids with 1,2-naphthoquinone-4-sulphonate reagent J. Saurina and S. Hernández-Cassou (Barcelona, Spain) . . . . .	414
<i>Biotechnological Techniques</i>	
Flow-injection immunoassays. Review G. Gübitz (Graz, Austria) and C. Shellum (Chaska, MN, USA) . . . . .	421
Automatic determination of Michaelis–Menten constants by the variable flow-rate technique J. Marcos, A. Ríos and M. Valcárcel (Córdoba, Spain) . . . . .	429
Optosensing of D-glucose with an immobilized glucose oxidase minireactor and an oxygen room-temperature phosphorescence transducer M.J. Valencia-González, Y.M. Liu, M.E. Díaz-García and A. Sanz-Medel (Oviedo, Spain) . . . . .	439
Spectrophotometric determination of magnesium in serum by using a flow-injection system with an immobilized enzyme reactor J.M. Fernández-Romero, M.D. Luque de Castro, M. Valcárcel (Córdoba, Spain) and R. Quiles-Zafra (Toledo, Spain) . . . . .	447
<i>Kinetic Methods</i>	
Trends in kinetic methods of analysis S.R. Crouch (East Lansing, MI, USA) . . . . .	453
Simultaneous kinetic-photometric determination of imipramine and desipramine by stopped-flow mixing technique L. De la Peña, A. Gómez-Hens and D. Pérez-Bendito (Córdoba, Spain) . . . . .	471
Kinetic determination of cobalt and nickel by flow-injection spectrophotometry M.A.Z. Arruda, E.A.G. Zagatto and N. Maniasso (Piracicaba, Brazil) . . . . .	476
Simultaneous determination of arsenate and phosphate by use of the kinetic wavelength-pair method M. López Carreto, D. Sicilia, S. Rubio and D. Pérez-Bendito (Córdoba, Spain) . . . . .	481

(Continued overleaf)

*Contents (continued)*

Kinetic flow-injection spectrofluorimetric method for the determination of fluoride V. Marco, F. Carrillo, C. Pérez-Conde and C. Cámara (Madrid, Spain) . . . . .	489
<i>Chemometrics and Computers</i>	
Detecting errors in micro and trace analysis by using statistics K. Heydorn (Roskilde, Denmark) . . . . .	494
Fuzzy logic for spectra interpretation M. Otto (Freiberg, Germany) . . . . .	500
Non-linear modelling of chemical data by combinations of linear and neural net methods B. Walczak and W. Wegscheider (Graz, Austria) . . . . .	508
Expert systems in trace analysis F.X. Rius (Tarragona, Spain) . . . . .	518
Chemometric study of organic pollution in the aerosol of Madrid J. Méndez, A.J. Quejido, R. Pérez-Pastor and M. Pérez-García (Madrid, Spain) . . . . .	528
Application of an evolving factor analysis-based procedure to speciation analysis in the copper(II)-polyuridylic acid system E. Casassas, R. Gargallo, I. Giménez, A. Izquierdo-Ridora and R. Tauler (Barcelona, Spain) . . . . .	538
Factor analysis applied to the study of the effects of solvent composition and nature of the inert electrolyte on the protonation constants in dioxane-water mixtures E. Casassas, N. Domínguez, G. Fonrodona and A. De Juan (Barcelona, Spain) . . . . .	548
Computer experimentation in and teaching of modern instrumental techniques using circular dichroism measurement as an example E. Voigtman (Amherst, MA, USA) . . . . .	559
<i>Quality Control</i>	
Certified reference materials: use, manufacture and certification S. Caroli (Rome, Italy) . . . . .	573
Projects for the improvement and quality control of inorganic and organic analysis in environmental matrices Ph. Quevauviller, E.A. Maier and B. Griepink (Brussels, Belgium) . . . . .	583
Interlaboratory studies as a tool for many purposes: proficiency testing, learning exercises, quality control and certification of matrix materials E.A. Maier, Ph. Quevauviller and B. Griepink (Brussels, Belgium) . . . . .	590
Interlaboratory programme for the quality control of nitrate determination in freshwater Ph. Quevauviller, D. Van Renterghem, B. Griepink (Brussels, Belgium), M. Valcarcel, M.D. Luque de Castro and J. Cosano (Córdoba, Spain) . . . . .	600
<i>UV-Visible and Raman Spectrometry</i>	
Combining fingerprinting capability with trace analytical detection: surface-enhanced Raman spectrometry J.J. Laserna (Málaga, Spain) . . . . .	607
Analytical characteristics, applications and perspectives in thermal lens spectrometry G. Ramis-Ramos (Valencia, Spain) . . . . .	623
Extractive-spectrophotometric determination of amphetamine in urine samples with sodium 1,2-naphthoquinone 4-sulphonate C. Molins Legua, P. Campíns Falcó and A. Sevillano Cabeza (Valencia, Spain) . . . . .	635
<i>Electroanalytical Chemistry</i>	
Microdetermination of sulphate and organic sulphur: potentiometric back-titration using simple coated-wire electrodes J. Kalous, D. Brázdová and K. Vytřas (Pardubice, Czech Republic) . . . . .	645
Copper speciation analysis using a chemically modified electrode R. Agraz, M.T. Sevilla and L. Hernández (Madrid, Spain) . . . . .	650
Quinidine ion-selective electrode for potentiometric determinations in pharmaceutical preparations M.N.M.P. Alçada, J.L.F.C. Lima and M.C.B.S.M. Montenegro (Porto, Portugal) . . . . .	657

ANALYTICA CHIMICA ACTA  
VOL. 283 (1993)

# ANALYTICA CHIMICA ACTA

*An international journal devoted to all branches of analytical chemistry  
Revue internationale consacrée à tous les domaines de la chimie analytique  
Internationale Zeitschrift für alle Gebiete der analytischen Chemie*

**Editors: Harry L. Pardue (West Lafayette, IN, USA)**

**Alan Townshend (Hull, Great Britain)**

**J.T. Clerc (Berne, Switzerland)**

**Willem E. van der Linden (Enschede, Netherlands)**

**Paul J. Worsfold (Plymouth, Great Britain)**

**Associate Editor: Sarah C. Rutan (Richmond, VA, USA)**

## Editorial Advisers:

F.C. Adams, Antwerp  
M. Aizawa, Yokohama  
J.F. Alder, Manchester  
C.M.G. van den Berg, Liverpool  
A.M. Bond, Bundoora, Vic.  
S.D. Brown, Newark, DE  
J. Buffle, Geneva  
P.R. Coulet, Lyon  
S.R. Crouch, East Lansing, MI  
R. Dams, Ghent  
L. de Galan, Vlaardingen  
M.L. Gross, Lincoln, NE  
W. Heineman, Cincinnati, OH  
G.M. Hieftje, Bloomington, IN  
G. Horvai, Budapest  
T. Imasaka, Fukuoka  
D. Jagner, Gothenburg  
G. Johansson, Lund  
D.C. Johnson, Ames, IA  
A.M.G. Macdonald, Birmingham  
D.L. Massart, Brussels  
P.C. Meier, Schaffhausen

M.E. Meyerhoff, Ann Arbor, MI  
J.N. Miller, Loughborough  
H.A. Mottola, Stillwater, OK  
M.E. Munk, Tempe, AZ  
M. Otto, Freiberg  
D. Pérez-Bendito, Córdoba  
C.F. Poole, Detroit, MI  
J. Ruzicka, Seattle, WA  
A. Sanz-Medel, Oviedo  
S. Sasaki, Toyohashi  
T. Sawada, Tokyo  
K. Schügerl, Hannover  
M.R. Smyth, Dublin  
M. Thompson, Toronto  
G. Tölg, Dortmund  
Y. Umezawa, Tokyo  
E. Wang, Changchun  
J. Wang, Las Cruces, NM  
H.W. Werner, Eindhoven  
O.S. Wolfbeis, Graz  
Yu.A. Zolotov, Moscow  
J. Zupan, Ljubljana



*Anal. Chim. Acta*, Vol. 283 (1993)

ELSEVIER, Amsterdam–London–New York–Tokyo



© 1993 ELSEVIER SCIENCE PUBLISHERS B.V. ALL RIGHTS RESERVED

0003-2670/93/\$06.00

No part of this publication may be reproduced, stored in a retrieval system or transmitted in any form or by any means, electronic, mechanical, photocopying, recording or otherwise, without the prior written permission of the publisher, Elsevier Science Publishers B.V., Copyright and Permissions Dept., P.O. Box 521, 1000 AM Amsterdam, The Netherlands.

Upon acceptance of an article by the journal, the author(s) will be asked to transfer copyright of the article to the publisher. The transfer will ensure the widest possible dissemination of information.

Special regulations for readers in the U.S.A.—This journal has been registered with the Copyright Clearance Center, Inc. Consent is given for copying of articles for personal or internal use, or for the personal use of specific clients. This consent is given on the condition that the copier pays through the Center the per-copy fee for copying beyond that permitted by Sections 107 or 108 of the U.S. Copyright Law. The per-copy fee is stated in the code-line at the bottom of the first page of each article. The appropriate fee, together with a copy of the first page of the article, should be forwarded to the Copyright Clearance Center, Inc., 27 Congress Street, Salem, MA 01970, U.S.A. If no code-line appears, broad consent to copy has not been given and permission to copy must be obtained directly from the author(s). All articles published prior to 1980 may be copied for a per-copy fee of US \$2.25, also payable through the Center. This consent does not extend to other kinds of copying, such as for general distribution, resale, advertising and promotion purposes, or for creating new collective works. Special written permission must be obtained from the publisher for such copying.

No responsibility is assumed by the publisher for any injury and/or damage to persons or property as a matter of products liability, negligence or otherwise, or from any use or operation of any methods, products, instructions or ideas contained in the material herein.

Although all advertising material is expected to conform to ethical (medical) standards, inclusion in this publication does not constitute a guarantee or endorsement of the quality or value of such product or of the claims made of it by its manufacturer.

This issue is printed on acid-free paper.

PRINTED IN THE NETHERLANDS

**SPECIAL ISSUE**

**PAPERS PRESENTED AT THE 12th INTERNATIONAL  
SYMPOSIUM ON MICROCHEMICAL TECHNIQUES (ISM'92),  
CÓRDOBA, SPAIN, SEPTEMBER 7-12, 1992**

## Foreword

This special issue of *Analytica Chimica Acta* is devoted to papers presented at the *12th International Symposium on Microchemical Techniques (ISM'92)*, which took place in Córdoba (Spain) between September 7 and 12, 1992. The Symposium sessions were held at the matchless setting of the Palacio de Congresos, an old castle lying very close to the Mosque, a magnificent Arabian monument which was appointed Patrimony of Mankind by UNESCO. For the first time ever, the event was held in a peripheral European region that offers the typically warm climate of Andalusia. ISM'92 was attended by 320 scientists and included 7 plenary lectures 40 keynote lectures and 260 posters. As can be inferred from the material contained in this issue, the Symposium was concerned with general analytical chemistry rather than with microchemical techniques in particular. The Córdoba meeting consolidated the trend seen in the more recent ISM meetings. In order to avoid conflict with other European events, the Scientific Committee of ISM'92 agreed that the next meeting (ISM'96, to be held in Lyon under the direction of Professor J.M. Mermet) would go back to its roots in order that its content would be better in accord with its title.

No doubt the best memory of a Symposium is a publication like this, which contains full, refereed papers. I should therefore like to thank the publisher and editors of *Analytica Chimica Acta*,

respectively, for their cooperation with this special issue, which is a faithful reflection of the events held in Córdoba.

The active participation of the broad Scientific Committee of the Symposium and the chairpersons of past meetings was decisive in drawing up the final programme. The top-level lectures delivered by prestigious scientists and the large number of posters exhibited were supplemented by a consistent attendance at the sessions notwithstanding the touristic appeal of the Palace surroundings and the mild, inviting climate. In any case, the social programme that took place throughout the Symposium week, which included a visit to Expo'92 in Seville, was highly rewarding for the participants. I wish to thank them all for their scientific and social involvement in the symposium, which was made possible by the hard work of the staff of the Analytical Chemistry Department of the University of Córdoba and the cooperation of such institutions as the Commission of the European Communities, the University of Córdoba, the Spanish Ministry of Education and Science, the Junta de Andalucía, the National R&D Plan and the Spanish Society for Analytical Chemistry, to which we are greatly indebted.

M. Valcárcel  
Chairman, ISM'92

# Problems and trends in extreme trace analysis for the elements

Günther Tölg

*Institut für Spektrochemie und Angewandte Spektroskopie (ISAS), Dortmund, and Laboratorium für Reinststoffanalytik (LRA) des Max-Planck-Instituts für Metallforschung, Stuttgart, Bunsen-Kirchhoff-Strasse 11–13, D(W)-4600 Dortmund 1 (Germany)*

(Received 10th September 1992)

## Abstract

The continually growing challenge to find the optimum balance between technological progress and the risks that unavoidably go with it demands further innovative developments in the fields of trace, micro-distribution and speciation analysis of the elements to improve the quality criteria of the methods such as detection power, reliability and economy. It was found at a very early stage, when characterizing high-purity materials, that the fundamental problems and consequently the limits of extreme trace analysis are caused by the rapid increase in methodical systematic errors of a chemical and physical nature. These start to dominate at the ng level and increase substantially at the pg level and below. The recognition of such errors is very difficult and their minimization demands special strategies in each individual case. Most of the direct atomic spectrometric methods are in a poor position to overcome these problems when no standard reference materials are available. Long-term experience has shown that progress in the enhancement of detection power and accuracy is particularly efficient when chemical sample decomposition, separation or preconcentration steps precede the actual spectrometric determination method as closely as possible. During direct instrumental analysis of solids, sample evaporation, atomization/ionization and signal excitation steps should be independently optimized. The most promising methods of determination in extreme trace analysis such as laser spectroscopy, total-reflection x-ray fluorescence spectrometry and mass spectrometry (MS) of the elements (e.g., inductively coupled plasma-MS and glow discharge MS) together with strategies to improve further the detection capacity and accuracy are discussed.

*Keywords:* Mass spectrometry; X-ray fluorescence spectrometry; Atomic absorption spectrometry; Inductively coupled plasma-mass spectrometry; Environmental samples; Trace elements

## GENERAL STRATEGIES TOWARD EXTREME TRACE ANALYSIS

Today, modern analytical chemistry functions as a significant indicator of the optimization of the balance between technological progress and the inevitable risks that accompany it. Therefore, steadily growing challenges demand a constant effort to improve the three most important ana-

lytical figures of merit, namely power of detection, reliability and economy [1–4]. In this context, the main question is, “Is there still a demand for even more improved detection power?” In natural matrices, the lowest concentrations to be detected correspond to omnipresent concentrations which, for most elements, lie in the range  $> 1 \text{ ng g}^{-1}$ . However, as these regions are now generally analytically accessible, the question should rather be one of choosing analytical procedures of the highest possible reliability as well as of the most economic operation.

Exceptions to this rule apply to only a few rare elements such as the metals of the platinum

*Correspondence to:* G. Tölg, Institut für Spektrochemie und Angewandte Spektroskopie, Bunsen-Kirchhoff-Strasse 11–13, D(W)-4600 Dortmund 1 (Germany).

group, for which the omnipresent concentration ranges lie at  $\text{pg g}^{-1}$  levels or even lower. Any detection of elemental concentrations below omnipresent concentration levels would thus be a futile endeavour with regard to biological, medical or environmental research.

A different situation to that presented by natural matrices is the analytical characterization of technologically interesting high-purity materials (e.g., semiconductors, superconductors, high-purity metals, high-purity ceramics) [1–4,5]. Here, the improvement of detection power remains a great challenge, although only for a few highly specialized laboratories.

Most interest today is focused far more on trace analysis in micro regions than via common bulk analysis, which only yields integral information about relative concentrations of elements in large sample amounts. Micro-trace analysis opens ways to acquire more detailed information on the distribution of elements and their concentrations in micro-areas and on inner and outer border areas of the samples. The determination of the different binding forms of specific elements represents an equally great challenge.

This challenge in ultra-trace, micro-distribution and species determination, when only small amounts of sample are available, demands methods that incorporate the highest possible absolute detection power. If, for instance, a concentration of about  $1 \text{ ng g}^{-1}$  Al (representing the normal Al concentration in blood serum) is required to be detected in a biological cell of ca.  $1 \mu\text{g}$  mass, an absolute detection limit of ca.  $1 \text{ fg}$  would have to be achieved. It will be shown later that this aim has already been reached by microprobe techniques. In applied trace analysis of the bulk material, we are presently still far from reaching such levels, and as a rule, at least 10–100 mg of sample are needed in order to detect  $1 \text{ ng g}^{-1}$  Al.

The other two figures of merit are reliability and economy. The above picture of enhanced detection power soon fades when we return to the present state of trace analysis in the  $\text{ng g}^{-1}$  region in applied trace analysis. Here we are confronted with the results of inter-laboratory comparison analyses. In reality, while lower and lower concentrations are being detected, the sys-

tematic errors increase all the more rapidly, so that deviations from true concentrations are often as much as one order of magnitude [1–4,6].

In most instances, the causes of systematic errors are difficult to establish and eliminate, although such handicaps are not insurmountable. The causes of systematic errors can be traced back chiefly to insufficient qualifications and experience of the analysts and/or inadequate equipment in the laboratory, rendering any optimum analytical strategy impossible. In the former instance high-quality analytical training would be an answer and in the latter there is call for growing awareness of the fact that false analytical results may finally prove far more expensive than more elaborate equipment and operation.

It should also be reiterated in this context, that modern instrumental direct methods may be the wrong choice in ultra-trace analysis, whereas in routine analysis they have come to be indispensable because of cost-saving considerations.

One must be aware that instrumental direct determination methods are physical relative methods requiring calibration. However, it is mainly during calibration that considerable systematic errors may occur, caused by spectral and non-spectral interferences. The least problematic methods are neutron activation analysis (NAA), sputtered neutral mass spectrometry (SNMS) and x-ray fluorescence (XRF) spectrometry, if one applies very thin samples.

Matrix-dependent relative methods require standard reference materials for calibration. If these are not available, as is the case in ultra-trace or micro-trace analysis, one has to resort to multi-stage procedures with easier calibration, but these involve decomposition, separation or pre-concentration steps preceding the actual determination.

These basic problems in extreme trace analysis lead to several significant considerations. First in ultra-trace analysis, no generalizations or extrapolations are allowed. Many detection limits of analytical methods described in literature were mainly obtained by extrapolation. The fact that real detection limits in many instances are determined by blanks and their fluctuations is often overlooked. Especially for abundant elements (Si,

Al, Fe, etc.) the real detection limits can be many times larger than the “theoretical” values.

Second, optimum absolute detection power and optimum reliability can only be arrived at if the trace element to be determined is rendered for analysis in an isolated form in the smallest possible target area or excitation volume. It is for this reason that in trace analysis it will be necessary to operate for some time yet with the more elaborate combined or multi-stage procedures. It is also acknowledged that combined procedures are not free from systematic errors. However, their causes are different and for this reason better controllable. Minimization of the blank values caused by contamination of the equipment, the reagents and the laboratory air, adsorption and volatilization effects play a decisive role. Various strategies to be applied have often been reported [6–13], so it is not necessary here to go into further detail.

Another important rule for the confirmation of correct results must be that “a single method is no method at all”. Only if the results of different methods agree can one assume accuracy.

If insufficient attention is paid to these interrelated points, the uncritical application of instrumental direct methods in extreme analysis will not lead to a more economic output, but to the opposite.

#### SOME ASPECTS OF MULTI-STAGE PROCEDURES

As was pointed out many years ago [6], multi-stage procedures via solution and gaseous phases may overcome the problem of sample inhomogeneity in bulk analysis and allow a relatively simple calibration with standard solutions after the isolation of the element to be determined. However, one should be aware that the use of the standard addition technique requires careful critical assessment regarding, for example, non-linear calibration functions, background levels and various binding forms of the element to be determined in samples and standard solutions.

It should be stressed again, that the greatest attention must be paid to the minimization of contamination and the elimination of element

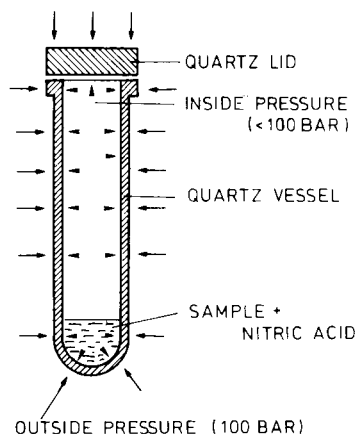


Fig. 1. Principle of the high-pressure decomposition method, after Knapp [14]. The high inside pressure of the quartz vessel will be nearly compensated by computer control for by an outside pressure of nitrogen which is several bar higher.

losses by adsorption and volatilization. The problem starts with sampling, storing the sample and further preparation techniques such as sawing, pulverizing and drying. In ultra-trace analysis, special problems arise when the sample is insoluble in the aqueous phase and during the preconcentration step.

#### Sample decomposition

For the determination of trace elements in organic samples mineralization problems existed for many years. These have now been optimally solved by the high-pressure ashing method with nitric acid in quartz vessels after Knapp (see Fig. 1) [14–17]. Complete mineralization, no losses of volatile elements and low blanks can be achieved. This means that the many other digestion methods currently used [18–21] are limited to higher concentration levels. Owing to different sources of systematic errors they must be checked from case to case.

However, for the decomposition of insoluble inorganic matrices [18,22] (such as high-temperature ceramics and many other technical matrices) there is no universal method with such low blank levels as to render it suitable for extreme trace analysis. There is a good chance of solving this problem by using elemental fluorine or gaseous fluorides as decomposition agents.

Fluorine possesses the highest known oxidation potential at relatively low temperatures. Whereas the application of appropriate gaseous fluorides, e.g.,  $\text{XeF}_4$ , has been described [23,24], elemental fluorine has not yet been used, owing to its difficult and dangerous handling and its insufficient purity. These difficulties have recently been mastered in a promising manner by Jacob [25]. He succeeded in the rapid and very reliable decomposition of such problematic matrices in a closed nickel autoclave system, which permits the on-line determination of major and minor components such as Si, B, P and S via their volatilized fluorides by Fourier transform IR spectrometry.

Investigations have now been started at the ISAS in close collaboration with Jacob to test this principle in trace analysis. Numerous matrices such as silicon nitride, silicon carbide, boron carbide and zirconium oxide can be decomposed very rapidly. The volatilized fluorides can be determined by mass spectrometry in an on-line system (see Table 1). The elements that form non-volatile fluorides can be determined in the residue after its dissolution with a special purified agent, e.g., ammonium fluoride. Possibilities of purifying

TABLE 1

Conditions for the decomposition of HT-ceramics using fluorine<sup>a</sup>

Compound	Mass (mg)	F <sub>2</sub> excess	Temperature (°C)	Yield (%)
B <sub>4</sub> C	14	4×	350	100
MgO	22	7×	500	59
			600	78
AlN	20	6×	600	96
			700	98
			750	100
Al <sub>2</sub> O <sub>3</sub>	20	9×	700	70
			700 (60 min)	84
			750	87
	3	60×	700	90
	10	18×	700 (60 min)	98
SiC	10	4×	250	100
Si <sub>3</sub> N <sub>4</sub>	20	5×	250	100
TiO <sub>2</sub>	11	15×	450	100
ZrO <sub>2</sub>	20	12×	550	77
			600	99

<sup>a</sup> Decomposition yield in 4 mmol F<sub>2</sub> in 30 min.

the nickel, which is the only suitable autoclave material, are currently being sought, because the impurities in the nickel will be the main limiting factor, which influences the detection power of the elements to be determined.

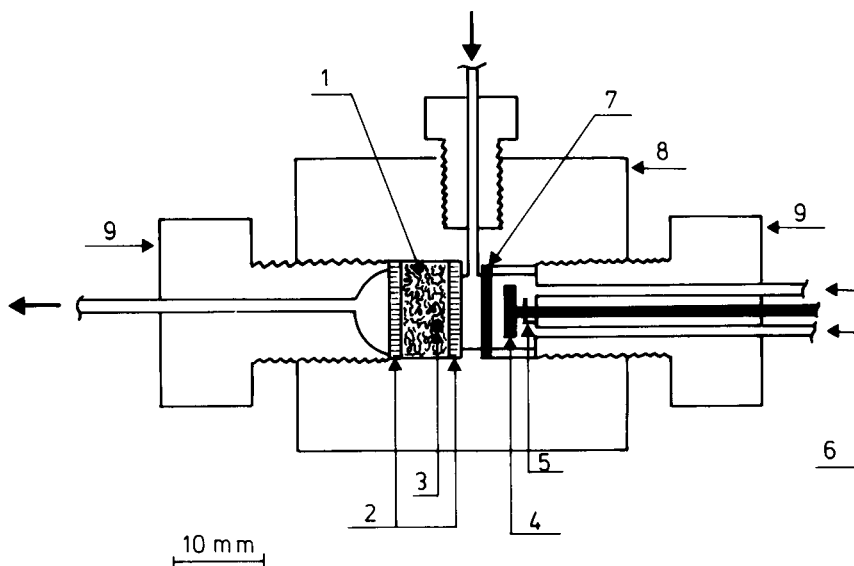


Fig. 2. Flow-through electrochemical cell [35]. 1 = Working electrode; 2 = polyethylene frits; 3 = Pt contact to the working electrode; 4 = Pt wire counter electrode; 5 = Ag reference electrode; 6 = inlet/outlet for the counter space; 7 = Ionex membrane; 8 = body of the cell; 9 = PTFE screws.

### Preconcentration

For chemical separation and preconcentration, there are many useful principles available such as coprecipitation, electrolytic deposition, volatilization, liquid–liquid extraction, ion exchange and sorption [7,26–29]. With regard to electrochemical enrichment methods [30–33], only one very innovative principle [34,35] should be specially mentioned here, because of its very low blank background, its excellent separation yield and its on-line character.

The principle is an electrochemical flow-through cell made of PTFE with a cathode made of crushed vitreous carbon (see Fig. 2). When the analyte solution passes the porous working electrode under optimized conditions (e.g., geometry of the electrode, flow-rate, acidity, potential), the electrode shows Nernstian behaviour and traces of many electroactive elements can be enriched in the porous cathode with a yield of nearly 100%. The precipitated metals can be dissolved in a second step for their determination with a

sensitive method, e.g., electrothermal atomic absorption spectrometry (ETAAS).

Further very interesting and innovative techniques for separation and preconcentration may be partition counter-current chromatography [36] and a new principle of membrane filtration using water-soluble polymers carrying chelating groups [37].

Generally, the main activities in the separation steps should be directed to closed micro-systems using the on-line flow-injection principle, as has recently been demonstrated [17,38–40]. In extreme trace analysis these techniques must permit the dropwise transfer of micro-volumes of solutions containing the preconcentrated elements on to the smallest possible target area in order to achieve highly intense analytical signals and in order to reduce drastically systematic errors in the whole multi-stage procedure. The working time can be reduced significantly by automation. An example is given later.

The concepts in extreme trace analysis can be

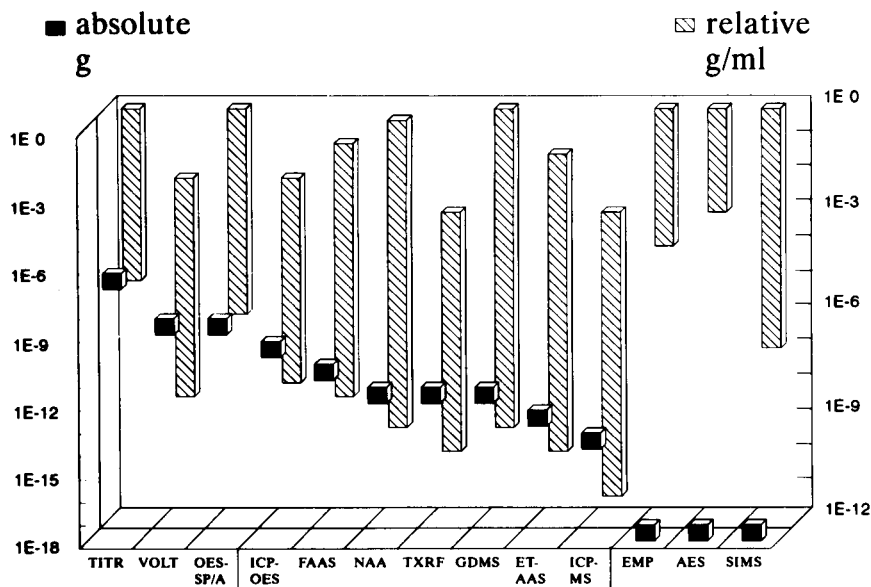


Fig. 3. Rough estimation of absolute detection limits (left) and range of relative concentrations (right) of different atomic spectrometric methods [115]. TITR = titrimetry; VOLT = voltammetry; OES-SP/A = optical emission spectrometry by spark or arc; ICP-OES = inductively coupled plasma OES; FAAS = flame atomic absorption spectrometry; ETAAS = electrothermal AAS; NAA = neutron activation analysis; GDMS = glow discharge MS; ICP-MS = inductively coupled plasma MS; EMP = electron microprobe; AES = Auger electron spectrometry; SIMS = secondary ion MS.



consequently summarized as follows. In each instance when no matrix-independent determination method or standard reference materials are available to solve a given problem in a reliable manner, at least two independent multi-stage procedures are developed, if possible, following an on-line technique in a closed system and also, if possible, using radiotracers for the optimization of the yields of the trace elements to be determined.

Before demonstrating this concept with an example later, here the most sensitive and accurate determination principles in innovative problem-oriented extreme trace analysis or micro-trace analysis are briefly compared.

#### THE MOST IMPORTANT METHODS OF DETERMINATION WITH HIGH DETECTION POWER (SEE FIG. 3 [41–43])

The classical chemical principles [44], e.g., titrimetry, spectrophotometry, fluorimetry, chelate gas chromatography, chelate liquid chromatography, ion chromatography and voltammetry, still have a useful place. They possess not only good detection abilities (some of them in the pg range), but also require relatively simple devices. In addition, the calibration of the so-called “wet chemical” methods hardly cause problems. All these methods, however, demand significant practical experience, they are often very time consuming or not simple to automate and as a rule they are suitable only for the determination on one or the simultaneous determination of a few elements. The limits of most of these methods are well known. Their detection capabilities are limited in general by blanks and some other sources of systematic errors (e.g., adsorption, desorption, volatility). Although the combination with flow-injection techniques brought many advantages with respect to reliability and economy in routine analysis, it must be mentioned that their application in extreme trace analysis is only significant when no better physical determination methods are available or independent second or third methods are necessary to prove the reliability of a newly developed procedure.

Regarding radiochemical methods, the possibilities and limitations of which are well known [45–49], it must certainly be emphasized that activation analysis and the application of radiotracers and other radiochemical methods are indispensable in innovative extreme trace analysis, first in the preparation of standard reference samples and also for the optimization of separation and preconcentration steps. In the special case of high-purity material analysis there is often no other alternative.

Concerning the atomic spectrometric methods such as atomic absorption spectrometry (AAS), optical emission (OES), spectrometry atomic fluorescence spectrometry (AFS), x-ray fluorescence (XRF) analysis and mass spectrometry (MS), only some recent developments which have helped drastically to improve the detection power will be briefly discussed here.

The current limitation of ETAAS, that it can only determine single elements, is balanced by its high detection ability which, for many elements, leads to limits of detection in the pg range with good accuracy [50–54]. Whereas the absolute detection power of AAS can be improved by about an order of magnitude only through electronic signal addition processing, there are a series of additional, very efficient possibilities based on chemical and physical preconcentration methods to improve the detection power down to the fg range with good reliability. Among these are the gas-phase separation or electrochemical enrichment of the element to be determined. Well known examples are the separation of Hg as metal vapour and of As, Se, Te, Sb and Sn as hydrides [55,56]. As has already been shown in a very early phase in the determination of Hg [57], the decisive step preceding actual determination is the condensation of the volatile component in an absorber system, followed by the pulsed release of the condensate by suddenly heating the absorber (trapping technique), which also allows, for example, accurate determinations of Se [58,59] and Ni via its tetracarbonyl [60] in the pg range. A further elegant method is the electrochemical deposition of elements in combination with ETAAS [30,34].

In the OES, there have been many compara-

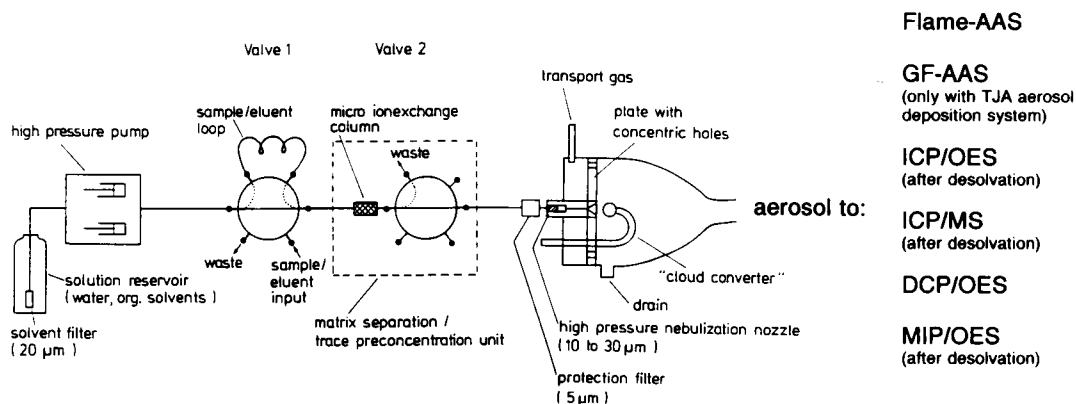


Fig. 4. On-line LC separation in combination with hydraulic high-pressure nebulization for FAAS, ETAAS, ICP-OES/MS, after Berndt [67].

tive critical investigations of different excitation principles with high-frequency or microwave plasmas [e.g., inductively coupled plasma (ICP), capacitively coupled microwave plasma (CMP) microwave-induced plasma (MIP)], cathodic sputtering and laser ablation [42]. These methods still provide new developments for problem-oriented multi-element determinations, but without substantial improvement of the detection power.

The detection powers of ICP-OES and direct current plasma (DCP)-OES are almost identical and comparable to those of spark OES and between those of flame AAS and furnace AAS

[61–65]. According to results gained empirically, interferences by alkalimetals are more severe in DCP-OES than those encountered in ICP-OES. Therefore, preference is given to ICP-OES in combination with preconcentration and high-pressure injection of the analyte solution (see Fig. 4) [66,67] or suspension techniques for the direct analysis of pulverized samples (e.g., soils, ores, oxides, and ceramics, which requires particle sizes of  $< 10 \mu\text{m}$ ) (see Fig. 5) [68–72].

Whereas CMP-OES offers no advantage over ICP-OES and DCP-OES, MIP-OES is a valuable addition. It is a simple universal micro-method suitable for the determination of a number of elements in gaseous phases and in solutions, reaching pg detection levels. Combined with suitable decomposition, separation and electrothermal vaporization methods, MIP-OES offers a very powerful, simultaneous element-specific determination of, e.g., Hg [57], Ni [60], Fe, Co, Cu, Zn, Cd, Tl and Bi [73–76]. A comparison between a conventional Beenakker resonator and a surfatron shows that with the use of the latter instrument the power of detection is improved by up to an order of magnitude [77].

MIP-OES is capable of further development in combination with gas chromatography and liquid chromatography and represents a highly sensitive element-specific detection principle in species analysis, as was successfully demonstrated some years ago in the determination of mercury and organomercury compounds [78]. Many other

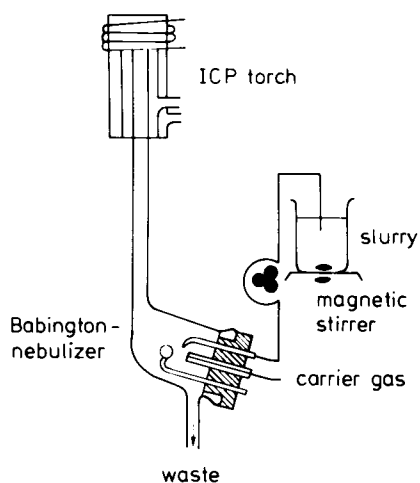


Fig. 5. ICP atomic spectrometry using slurry atomization [70].

MIP-OES detectors and their applications and limitations have been described [79–83].

The atomization and excitation of solids by glow discharge (GD) in combination with OES (GD-OES) [84,85] will remain of interest mainly for the characterization of near-surface layers of solids, but will gradually be replaced by GD-MS with its significantly higher detection power.

The greatest difficulty for the improvement of the detection power of all optical atomic spectrometric methods is the compromise (existing from the time of Bunsen and Kirchoff) that sample volatilization, atomization and excitation are made by the same source. Whereas atomization needs a high energy in order to break chemical bonds, excitation should be done with as low energy as possible in order to maintain an optimum signal-to-noise ratio.

A first attempt to deal with this problem was made by Geilmann [86] in the 1950s. Before determining a volatile trace element of interest by OES it was volatilized in a first step from non-volatile matrices in a quartz-tube furnace at temperatures of up to 1400°C (see Fig. 6), rendering these traces capable of atomization and excitation in isolated form. Both steps could be optimized independent of one another.

Today, we are coming close to meeting the requirements of operational conditions by employing twin-furnace techniques in graphite furnace (GF) AAS [87] and furnace atomic non-thermal excitation spectrometry (FANES), a combination of furnace atomization and excitation of the analyte for emission by glow discharge [88–92].

Also other tandem sources (combined sources or hybrid sources) may be considered [93].

Recently, it has been possible to optimize the different steps separately using the laser ablation principle [94]. The possibility of vaporizing very small parts of a sample by a focused laser beam (also in the case of electrically non-conductive samples) opens up new ways for the in situ micro-distribution analysis of elements possessing a lateral resolution of ca. 1  $\mu\text{m}$ .

According to the results of Niemax's group at ISAS, the earlier problem of very poor reproducibility of the laser ablation technique at the standard atmospheric pressure or in a high vacuum is no longer relevant if the vaporization is performed by laser pulses of low energy and in the presence of ca. 100 Torr of a noble gas, responsible for the energy transfer [95–98]. Recently, it was shown that laser ablation (LA) into a microwave-induced plasma in combination with time-gated OES (LA-MIP-OES) (see Fig. 7) leads to excellent results in applied micro-trace analysis of solids, e.g., quartz, superconductors or ceramics [99,100].

Other very important innovations in optical atomic spectrometry can be expected in laser spectroscopy [101,102]. This is valid for all types of excitation leading to analytical signals obtained by absorption, fluorescence or emission after the irradiation of an atomic cloud by a laser tuned to a resonant frequency. Any final judgement of the detection limits attainable would be premature, because all aspects regarding their analytical usefulness are still under development.

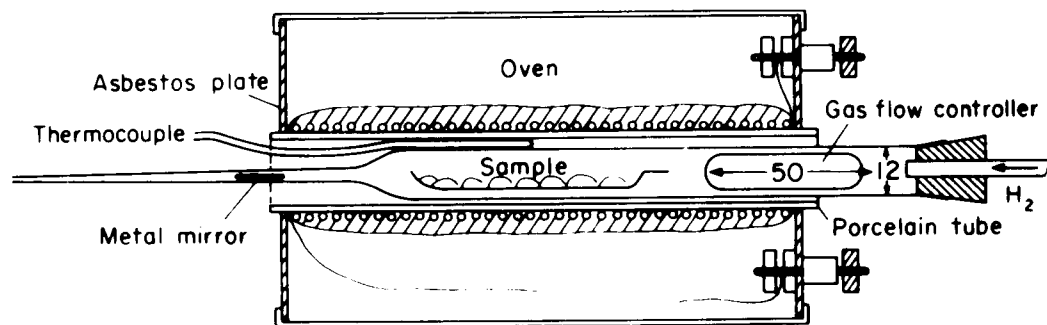


Fig. 6. Device for gas-phase separation. The volatile element or a volatile compound of the element is driven off from the sample by heating in a suitable atmosphere [86].

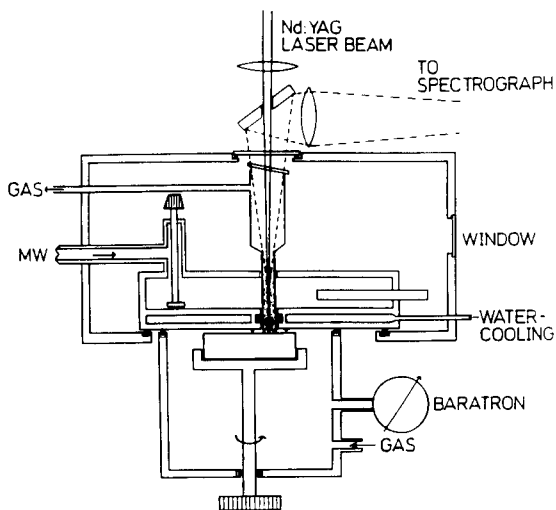


Fig. 7. Experimental apparatus for LA-MIP-OES [99].

Laser AAS (LAAS) opens up ways for multi-element determinations with great detection ability and dynamic range if simple laser systems with semiconductor diode lasers can be used [103]. Laser-induced fluorescence (LIF) already allows the determination of a few elements down to the femtogram range [104–105]. Detection limits in

the attogram range can be obtained by monitoring the products of ionization processes (ions and electrons) after resonant laser excitation.

This topic will not be considered more deeply here, but a good future for lasers can also be predicted in applied trace and micro-trace analysis. The coupling of mass spectrometry, e.g., resonant ionization MS (RIMS) [104–110], and the Doppler-free method with continuous-wave (CW) lasers that have a very narrow bandwidth allows good resolution of single isotope lines, and isotope-selective spectrometry can be carried out. In this way the problem of calibration can be solved in an elegant way using the isotope dilution technique as successfully applied in mass spectrometry. Currently, the biggest obstacle to the rapid introduction of laser spectrometry into analytical practice is the very high price of CW laser systems. However, they should soon be replaced with substantially cheaper semiconductor diode lasers when they reach shorter wavelength ranges.

The complete separation of the atomization and excitation steps in spectrometric methods is the foundation for better detection power and reliability. Therefore, the combination of sputter-

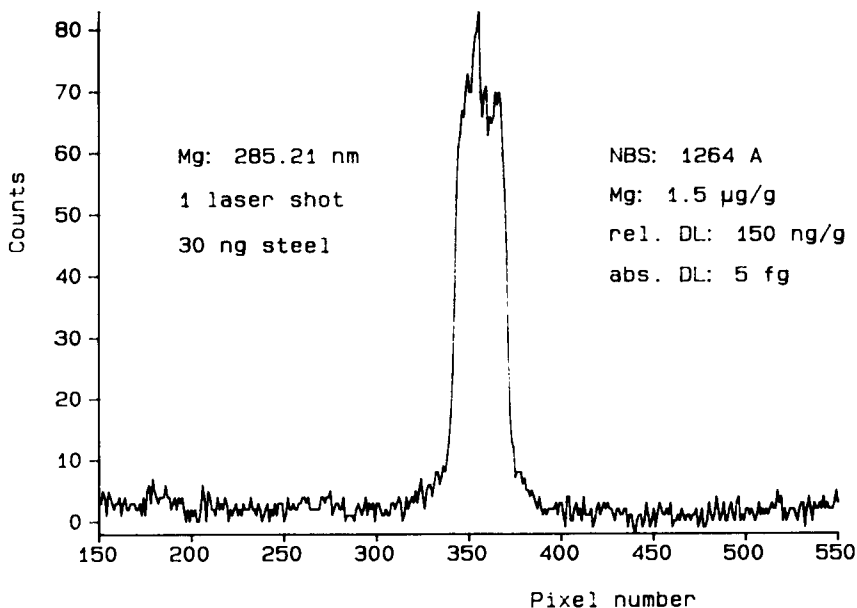


Fig. 8. Signal of the MG line at 285.21 nm produced by a single laser shot on steel [96]. A sample mass of 30 ng was evaporated from NBS SRM 1264A with an Mg content of  $1.5 \mu\text{g g}^{-1}$ . The signal corresponds to a mass of only 50 fg of Mg.

ing techniques, e.g., laser ablation, and laser spectrometry is a very promising concept in micro-trace analysis. It offers a high absolute detection ability (attogram range) for almost all elements, in situ microanalysis of atomic distribution by laser ablation, having a lateral resolution of about  $1 \mu\text{m}$ , and calibration through internal standardization.

These optimistic assessments of such developments can be supported by two examples. Figure 8 shows the signal of ca. 45 fg of magnesium in a steel sample after laser ablation and determination through LIF. The amount of the sample evaporated is ca. 30 ng and the Mg concentration is ca.  $1.5 \mu\text{g g}^{-1}$ . Consequently, this gives an absolute detection limit of 5 fg of Mg [96]. Figure 9 shows the distribution of Si ( $100 \mu\text{g g}^{-1}$ ) in the case of homogeneous and inhomogeneous distribution in steel samples.

The possibilities and limitations of conventional wavelength- and energy-dispersive XRF spectrometry are well known [111]. The method has optimum detection limits of about  $0.1 \mu\text{g}$  for elements with atomic number around 30. The most important factors that limit its detection

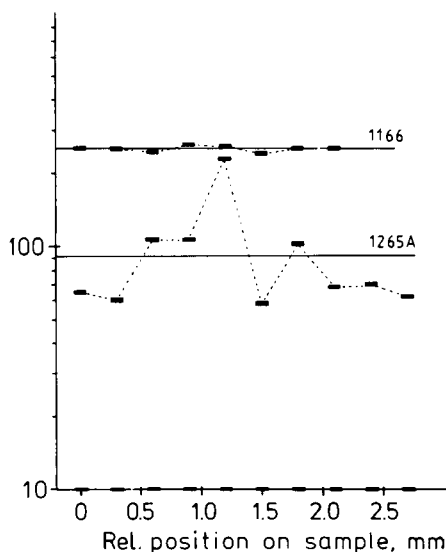


Fig. 9. Lateral distribution of Si within steel samples NBS SRM 1166 (above) and NBS SRM 1265A (below). The more or less homogeneous distribution of Si was checked by laser ablation and LIF; the step width was adjusted to  $300 \mu\text{m}$ .

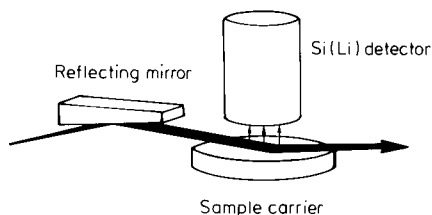


Fig. 10. Simplified principle of TXRF. The reflecting mirror can be a low-pass filter or Bragg monochromator. A sample of limited amount and thickness is placed on the carrier [114].

power are Compton and Rayleigh scattering caused by primary radiation. Moreover, the high matrix dependence also requires calibration with standard samples.

Better detection limits and higher precision will only be reached, if the signal-to-background ratio is improved and the matrix effects reduced. This can be done in three ways: by total reflection x-ray fluorescence analysis (TXRF) [112–115], particle-induced x-ray emission spectrometry (PIXE) [116–118] and synchrotron x-ray fluorescence spectrometry (SXRF) [119,120].

At ISAS most experience has been gained with TXRF. In TXRF the excitation beam impinges at a very small incidence angle on the sample holder (made of quartz, glassy carbon or acrylic glass), so that it is totally reflected (see Fig. 10). Only very thin samples on the target can be irradiated by this beam and secondary radiation excited. Owing to a smaller scattered radiation the detection limit is improved by a factor of about 1000 in comparison with standard techniques, so that the pg range is accessible. Therefore, TXRF is a very efficient method particularly in direct micro-trace analysis, but also in extreme trace analysis, when preconcentration steps are included.

Even lower absolute limits can be reached by microprobe methods [e.g., x-ray microprobe analysis (XMP), PIXE, SXRF and electron microprobe (EMP)]. The EMP even extends below the attogram detection limit, but its relative detection power is poor ( $100 \mu\text{g g}^{-1}$ ).

The advantages of the PIXE, which needs a particle (i.e. proton) accelerator, result in the possibility of bundling the particle beam down to a diameter of about  $1 \mu\text{m}$ . In this way tools are available for simultaneous micro-distribution

analysis in the  $\mu\text{g g}^{-1}$  range, e.g., over the cross-section of a human hair. Many other interesting applications for biological matrices have been described, but often they are noncritically overestimated with regard to the cost-to-benefit ratio and the reliability of the results.

Even more elaborate than PIXE is analysis by SXRF, for which a synchrotron radiation source is a prerequisite. Therefore, its advantages of high absolute detection power and good lateral resolution can only be fully exploited in special cases.

All three new excitation methods in XRF analysis represent a big step forward in the micro-distribution analysis of elements, but TXRF is the most suitable because of its lower costs.

Inorganic MS [121] is currently the most universal and the most sensitive instrumental method for the simultaneous determination of almost all elements. In comparison with OES, the mass spectra show only a few lines, which can be easily interpreted. Very good accuracy can be obtained with analytes in solution using isotope dilution techniques (except for single-isotope elements).

The conventional solid-state mass spectrometry (SSMS) remains without competition in its universal applicability mainly to the characterization of impurities in high-purity materials. However, quantitative operation is possible only with the use of standard reference samples.

Thermionic excitation is unrivalled with regard to detection power and reliability for single- or oligo-element determinations in combination with isotope dilution analysis.

However, the greatest innovative developments in the field of applied micro- and trace analysis were made with the use of two excitation techniques already well known from OES, inductively coupled plasma mass spectrometry (ICP-MS) and glow discharge mass spectrometry (GD-MS).

ICP-MS can be considered rather as a macro than a micro method for the analysis of solutions ( $> 100 \mu\text{l}$ ). The detection limits range from 0.001 to  $1 \mu\text{g l}^{-1}$  [122,123] with respect to most elements (see Fig. 11) and are two, three or even four orders of magnitude better than those for ICP-OES. Optimization of the detection power is

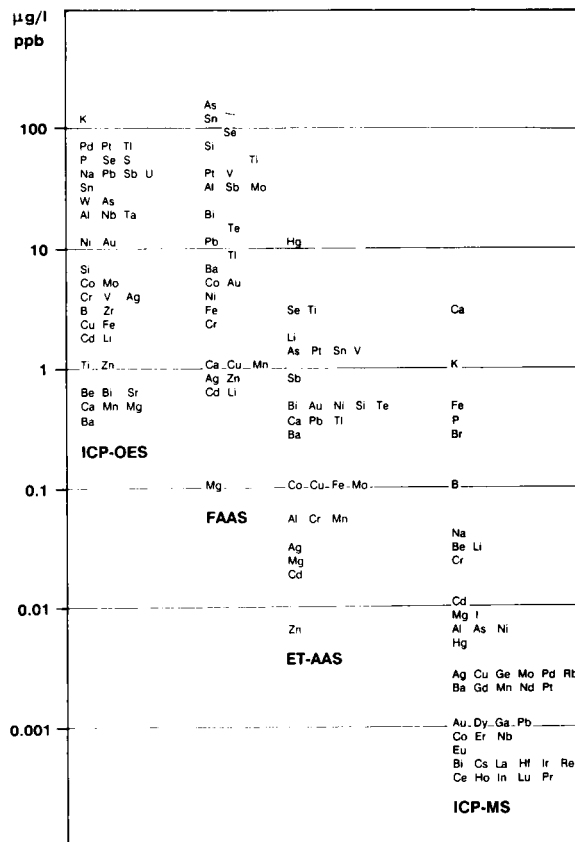


Fig. 11. Detection limits of ICP-OES, FAAS, ETAAS and ICP-MS [115].

achievable via excitation parameters, e.g., flow-rates of aerosols, electric power and observation height. High-pressure injection of the analyte into the plasma improves the detection power by about one order of magnitude [124].

Quantification in ICP-MS is often hampered by matrix effects, memory effects and spectral interferences, which can lead to systematic errors. Therefore, its combination with efficient separation methods is often required in practical extreme trace analysis.

Hitherto, GD-MS has proved to be an efficient method for the direct bulk and surface-layer analysis of solids [125,126]. It is also applicable to the micro-detection of dry residues of solutions. Thus, platinum metals have been determined with absolute detection limits extending to the lower pg region [127]. In addition, high accuracy can be

attained by isotope dilution, so that ICP-MS and GD-MS can be considered equal in merit compared with the older thermionic techniques [128,129]. In many applications, however, prior separation of interfering matrix elements also becomes necessary.

Further variants of MS are sputtered neutral MS (SNMS) and laser microprobe MS (LAMMS) employing time-of-flight spectrometers (TOF-MS) [130,131]. SNMS indicates a new approach to the matrix-independent characterization of solids and to rapid depth profiling with nm resolution [132–135], but its detection power is limited to the  $\mu\text{g g}^{-1}$  range. LAMMS is a microprobe technique with a high absolute detection power and good lateral resolution ( $\mu\text{m}$ ). However, its relative detection power also only covers the  $\mu\text{g g}^{-1}$  range.

Therefore, the most common methods for applied extreme micro-trace and trace analysis today are ETAAS, TXRF, ICP-MS and GD-MS. NAA and stripping voltammetry may be of advantage in special cases. In the future in extreme

trace analysis, laser ablation in combination with MS and laser spectrometry will open up many very innovative possibilities. For their optimization, multi-stage procedures will be essential over a longer period.

#### DETERMINATION OF PLATINUM AS AN EXAMPLE OF APPLIED EXTREME TRACE ANALYSIS

This last section is intended to demonstrate briefly the strategy for solving a practical problem of applied extreme trace analysis. This example is related to the general problem that progress in technology inevitably introduces risks to safety and health. Although great efforts may be made to minimize such risks, such efforts may in fact introduce new problems that are not recognized immediately as the systems are very complex.

Such a situation arose when platinum catalysts were introduced in “catalytic converters” in automobiles [136]. These catalysts substantially de-

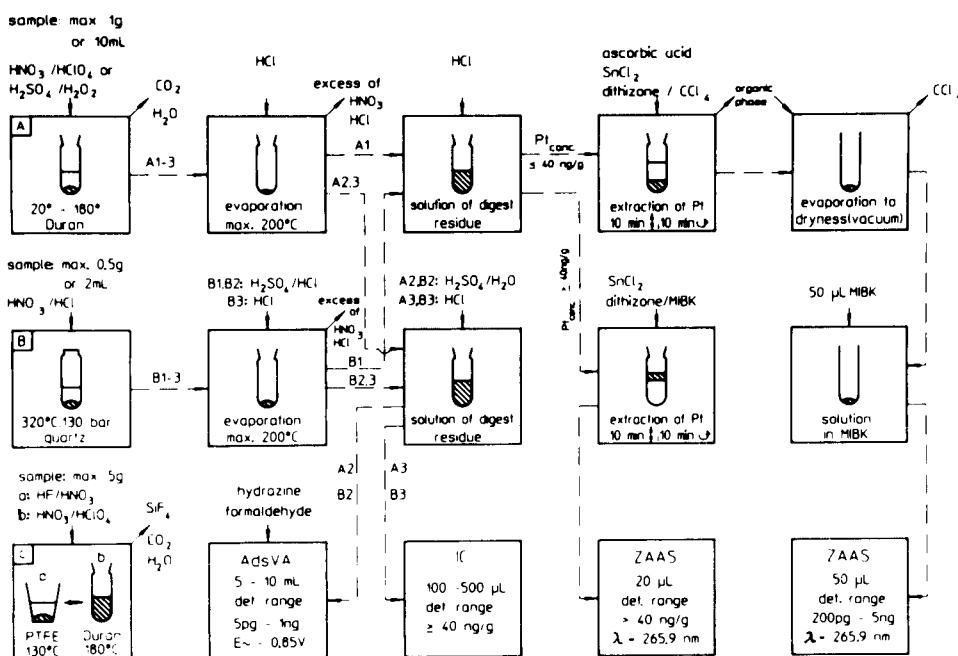


Fig. 12. Scheme of multi-stage procedures for the determination of very low platinum concentrations in environmental matrices [137–139]. (A) Open wet digestion; (B) high-pressure digestion; (C) open wet digestion ( $\text{SiO}_2$ -containing material, further treatment as in A 1–3. AdsVA = adsorption voltammetry with catalytic hydrogen wave; IC = ion chromatography; ZAAS = Zeeman-effect graphite furnace atomic absorption spectrometry.  $\text{Pt conc.} \leq 40 \text{ ng/g}$  = Platinum-containing phase, shake, centrifuge.

crease the emission pollutants such as  $\text{NO}_x$  and polycyclic aromatic hydrocarbons, but small amounts of platinum are released and accumulate in the environment. At present it is too early to make any general statements about the physiological effects of the platinum such as platinum asthma, platinosis and cancer, as the distribution patterns and the binding forms of platinum are significant parameters that are not yet well known.

As the natural omnipresent concentrations of platinum in the human body are of the order of  $10^{-8}$ – $10^{-9}\%$ , several years ago the development of several independent procedures for the extreme trace determination of platinum was begun [137–141]. Here just a multi-step procedure will be considered (Fig. 12), which at present is the most suitable mode for routine analysis but is also the basis for the optimization of other instrumental methods such as TXRF, ICP-MS and GD-MS. The development of this combined procedure includes sample decomposition, preconcentration and determination by ETAAS and an efficient voltammetric method [139].

The decomposition method presented the most difficult step. Especially for the voltammetric determination, complete mineralization was necessary, which could only be achieved by decomposition of the sample using high-pressure decomposition with high-purity nitric acid [17]. The separation of Pt from the other components was effected by liquid–liquid extraction of the dithizonate complex and optimization of the recovery was only possible by using a radiochemical means with the aid of the  $^{190}\text{Pt}$  isotope as a tracer. With this combined procedure, which can be easily calibrated, pg amounts of Pt can be determined with great reliability in virtually all environmental matrices.

More progress with respect to a more sensitive simultaneous determination procedure can be expected from on-line preconcentration steps based on an electrochemical [34,35,141] or a sorbent extraction flow-through system [142]. The first case has already been mentioned. The metals will be collected in a porous working electrode and can be determined, e.g., by ETAAS after their redissolution or directly by ETAAS using the graphite electrode as furnace (see Fig. 13).

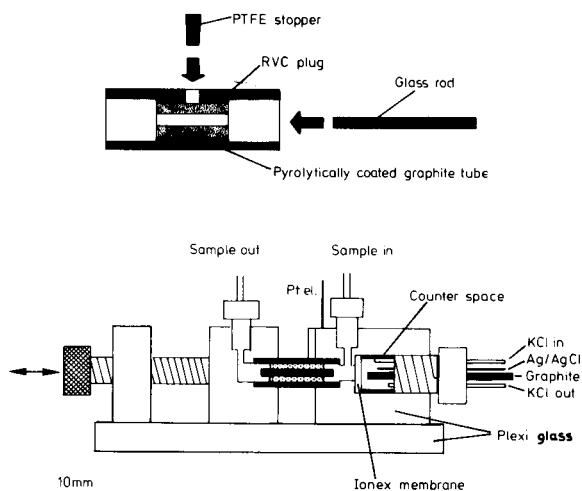


Fig. 13. Schematic diagrams of the flow-through cell for electrochemical preconcentration of Pt in a porous graphite electrode for platinum determination by ETAAS [141].

In the second case, the platinum metals Pd, Pt and Rh are initially complexed as bis(carboxymethyl)dithiocarbamates. These chelates are ac-

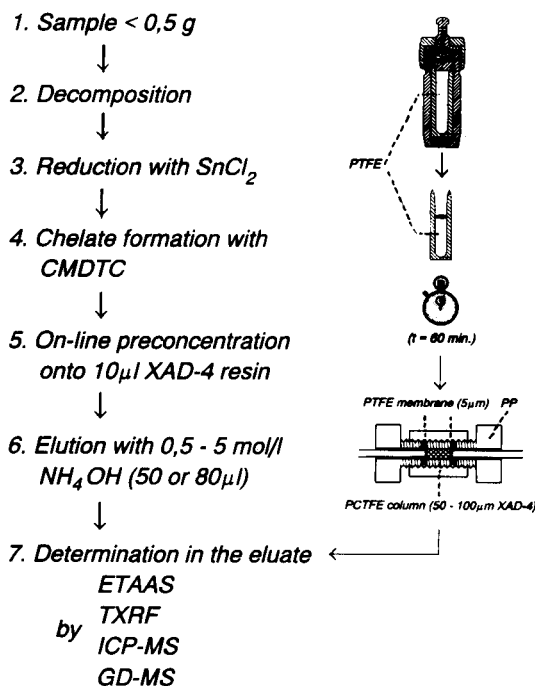


Fig. 14. Scheme of preconcentration steps by sorbent extraction in a flow-through cell for Pt determination by, e.g., ETAAS, TXRF, ICP-MS, GD-MS [142].



cumulated on a very small column (total volume 10  $\mu$ l) packed with XAD-4 resin. The adsorbed metal complexes can be desorbed by using a basic eluent, e.g., ammonia solution, and transferred to the determination method (see Fig. 14). The determination of the enriched metals in the solution can be performed by ETAAS, ICP-OES, TXRF or GD-MS.

GD-MS seems to be the most sensitive principle. The mineralized solution with the isolated Pt-group metals is transferred on to a copper carrier which operates as a hollow cathode in the glow discharge source. After evaporation of the small solution volume, the Pt-group metal ions are reduced to their metallic forms by the copper. The metals thus formed can be sputtered and ionized for MS determination [127]. This last step has already been worked out and Pt can be determined down to the fg range with good reliability.

### Conclusion

A general statement about which trace element analytical method should be recommended for the characterization of real complex materials is not possible. Often one tends to over-estimate the attributes of a specific method, which may hinder innovative analysis. The best method or the most suitable combination of methods can be discussed only with regard to the particular analytical problem. The optimum solution of an analytical problem is less a question of tools or methods than a question of the right analytical strategy. Consequently, advanced analysis is greatly accelerated through a narrow symbiosis of chemical and physical methods. Finally, only with efficient analysis will it be possible to balance correctly the positive and the negative effects of today's technological advances.

### REFERENCES

- G. Tölg and R.P.H. Garten, *Angew. Chem.* 97 (1985) 439.
- G. Tölg, *Fresenius' Z. Anal. Chem.*, 331 (1988) 226.
- J.A.C. Broekaert and G. Tölg, *Nachr. Chem. Tech. Lab.*, 38 (1990) 145.
- G. Tölg, *GIT Fachz. Lab.*, 33 (1989) 971.
- H.M. Ortner, *Fresenius' J. Anal. Chem.*, 343 (1992) 695.
- G. Tölg, *Naturwissenschaften*, 63 (1976) 99.
- J.A.C. Broekaert and G. Tölg, *Nachr. Chem. Tech. Lab.*, 40 (1992) 146.
- G. Tölg, *Talanta*, 19 (1972) 1489.
- G. Tölg, *Fresenius' Z. Anal. Chem.*, 294 (1979) 1.
- P. Tschöpel, L. Kotz, W. Schulz, M. Veber and G. Tölg, *Fresenius' Z. Anal. Chem.*, 302 (1980) 1.
- P. Tschöpel and G. Tölg, *J. Trace Microprobe Tech.*, 1 (1982) 1.
- G. Tölg and P. Tschöpel, *Anal. Sci.*, 3 (1987) 199.
- K. Hoppstock, R.P.H. Garten, P. Tschöpel and G. Tölg, *Fresenius' J. Anal. Chem.*, 343 (1992) 778.
- G. Knapp, *Int. J. Environ. Anal. Chem.*, 22 (1985) 71.
- G. Knapp, in P. Brätter and P. Schramel (Eds.), *Trace Element Analytical Chemistry in Medicine and Biology*, Vol. 5, de Gruyter, Berlin, 1988, p. 63.
- B. Griepink and G. Tölg, *Pure Appl. Chem.*, 61 (1989) 139.
- G. Knapp, *Mikrochim. Acta (Wien)*, (1991) 445.
- R. Bock, *A Handbook of Decomposition Methods in Analytical Chemistry*, International Textbook, London, 1979.
- R. Bock, in H. Kienitz, R. Bock, W. Fresenius, W. Huber and G. Tölg (Eds.), *Analytiker Taschenbuch*, Vol. 1, Springer, Berlin, 1980, pp. 19–42.
- G.M. Kimber and S. Kokot, *Trends Anal. Chem.*, 9 (1990) 203.
- L. Dunemann, *Nachr. Chem. Tech. Lab.*, 39 (1991) M2.
- Z. Sulcek and P. Povondra, *Methods of Decomposition in Inorganic Analysis*, CRC, Boca Raton, FL, 1989.
- V.I. Rigin and A.O. Eremina, *Zh. Anal. Khim.*, 39 (1984) 510.
- V.N. Mit'kin, A.A. Vasil'eva, T.M. Korda, S.V. Zemskov, V.G. Torgov and A.N. Tatarchuk, *Zh. Anal. Khim.*, 44 (1989) 1589.
- E. Jacob, *Fresenius' Z. Anal. Chem.*, 333 (1989) 761.
- A. Mizuike, *Enrichment Techniques for Inorganic Trace Analysis*, Springer, Berlin, 1983.
- Yu.A. Zolotov and N.M. Kuz'min, *Preconcentration in Analytical Chemistry (Wilson and Wilson's Comprehensive Analytical Chemistry, Vol. XXV)*, Elsevier, Amsterdam, 1990.
- J.P. Brunette and M.J.F. Leroy, *Anal. Chem.*, 20 (1992) M30.
- K. Terada, *Anal. Sci.*, 7 (1991) 187.
- G. Volland, P. Tschöpel and G. Tölg, *Anal. Chim. Acta*, 90 (1977) 15.
- M. Hiraide, P. Tschöpel and G. Tölg, *Anal. Chim. Acta*, 186 (1986) 261.
- T. Tanaka, Y. Maki, Y. Kobayashi and A. Mizuike, *Anal. Chim. Acta*, 252 (1991) 211.
- J. Shiowatana and J.P. Matousek, *Talanta*, 38 (1991) 375.
- E. Beinrohr, *Fresenius' J. Anal. Chem.*, 338 (1990) 735.
- E. Beinrohr, M. Németh, P. Tschöpel and G. Tölg, *Fresenius' J. Anal. Chem.*, 343 (1992) 566.
- Yu.A. Zolotov, B.Ya. Spivakov, T.A. Maryutina, V.L. Bashlov and I.V. Pavlenko, *Fresenius' Z. Anal. Chem.*, 335 (1989) 938.

- 37 K.E. Geckeler, E. Bayer, B.Ya. Spivakov, V.M. Shkinev, G.A. Vorob'eva and B.Y. Spivakov, *Anal. Chim. Acta*, 189 (1986) 285.
- 38 J.F. Tyson, *Spectrochim. Acta Rev.*, 14 (1991) 169.
- 39 Z. Fang, *Spectrochim. Acta Rev.*, 14 (1991) 235.
- 40 V. Carbonell, A. Salvador and M. de la Guardia, *Fresenius' J. Anal. Chem.*, 342 (1992) 529.
- 41 J.A.C. Broekaert and G. Tölg, *Fresenius' Z. Anal. Chem.*, 326 (1987) 495.
- 42 G. Tölg, *GIT Fachz. Lab.*, 10 (1989) 971.
- 43 G.M. Hieftje, *Fresenius' Z. Anal. Chem.*, 337 (1990) 528.
- 44 G. Tölg, *Elemental Analysis with Minute Samples (Wilson and Wilson's Comprehensive Analytical Chemistry, Vol. III)*, Elsevier, Amsterdam, 1975, pp. 1–184.
- 45 V. Krivan, in G. Günzler, R. Borsdorf, W. Fresenius, W. Huber, H. Kelker, I. Lüderwald, G. Tölg and H. Wisser, (Eds.), *Analytiker Taschenbuch, Vol. 5*, Springer, Berlin, 1985, pp. 35–68.
- 46 V. Krivan, in G. Günzler, R. Borsdorf, W. Fresenius, W. Huber, H. Kelker, I. Lüderwald, G. Tölg and H. Wisser, (Eds.), *Analytiker Taschenbuch, Vol. 10*, Springer, Berlin, 1991, pp. 153–187.
- 47 S.J. Parry, *Activation Spectrometry in Chemical Analysis*, Wiley, New York, 1991.
- 48 P. Hoffmann and K.H. Lieser, *Methoden der Kern- und Radiochemie*, VCH, Weinheim, 1991.
- 49 E. Bujdoso, *J. Radioanal. Nucl. Chem.*, 141 (1990) 443.
- 50 R.E. Sturgeon, *Fresenius' J. Anal. Chem.*, 337 (1990) 538.
- 51 R.E. Sturgeon, *Analyst*, 117 (1992) 233.
- 52 G.M. Hieftje, *J. Anal. At. Spectrom.*, 4 (1989) 117.
- 53 G.M. Hieftje, *J. Anal. At. Spectrom.*, 6 (1991) 192.
- 54 W. Slavín, *Anal. Chem.*, 63 (1991) 1033A.
- 55 J. Dedina, *Chem. Anal. (Warsaw)*, 35 (1990) 108.
- 56 M. Valcarcel and M.D. Luque de Castro, *Non-Chromatographic Continuous Separation Techniques*, Royal Society of Chemistry, Cambridge, 1991.
- 57 G. Kaiser, D. Götz, G. Tölg, G. Knapp, B. Maichin and H. Spitz, *Fresenius' Z. Anal. Chem.*, 291 (1978) 278.
- 58 J. Piwonka, G. Kaiser and G. Tölg, *Fresenius' Z. Anal. Chem.*, 321 (1985) 225.
- 59 F. Alt, J. Messerschmidt and G. Tölg, *Fresenius' Z. Anal. Chem.*, 327 (1987) 233.
- 60 W. Drews, G. Weber and G. Tölg, *Anal. Chim. Acta*, 231 (1990) 265.
- 61 P.W.J.M. Boumans (Ed.), *Inductively Coupled Plasma Emission Spectroscopy, Parts I and II*, Wiley, New York, 1987.
- 62 M. Thompson and J.N. Walsh, *Handbook of Inductively Coupled Plasma Spectrometry*, Chapman and Hall, New York, 1989.
- 63 A. Varma, *CRC Handbook of Inductively Coupled Atomic Emission Spectroscopy*, CRC, Boca Raton, FL, 1990.
- 64 J.W. Olesik, *Anal. Chem.*, 63 (1991) 12A.
- 65 A. Sanz-Medel, *Mikrochim. Acta* (1991) 265.
- 66 H. Berndt, G. Schaldach and E. Ivanova, in B. Welz (Ed.), *6. Colloquium Atom-spektrometrische Spurenanalytik*, Konstanz, Bodenseewerk Perkin-Elmer, Überlingen, 1991, pp. 481–488.
- 67 H. Berndt, *Nachr. Chem. Tech. Lab.*, 40 (1992) 820.
- 68 L. Ebdon and M.E. Foulkes, *Chem. Anal. (Warsaw)*, 35 (1990) 109.
- 69 J.A.C. Broekaert, *Chem. Anal. (Warsaw)*, 35 (1990) 5.
- 70 B. Docekal, J.A.C. Broekaert, T. Graule, P. Tschöpel and G. Tölg, *Fresenius' J. Anal. Chem.*, 342 (1992) 113.
- 71 R. Lobinski, W. Van Borm, J.A.C. Broekaert, P. Tschöpel and G. Tölg, *Fresenius' J. Anal. Chem.*, 342 (1992) 563.
- 72 C. Xhoffer, C. Lathen, W. Van Borm, J.A.C. Broekaert, W. Jacob and R. Van Grieken, *Spectrochim. Acta, Part B*, 47 (1992) 155.
- 73 J.A.C. Broekaert and F. Leis, *Mikrochim. Acta*, (1985) 261.
- 74 K.A. Forbes, E.E. Reszke, P.C. Uden and R.M. Barnes, *J. Anal. At. Spectrom.*, 6 (1991) 57.
- 75 Gy. Heltai, J.A.C. Broekaert, F. Leis and G. Tölg, *Spectrochim. Acta, Part B*, 45 (1990) 301.
- 76 Gy. Heltai, J.A.C. Broekaert, P. Burba, F. Leis, P. Tschöpel and G. Tölg, *Spectrochim. Acta, Part B*, 45 (1990) 857.
- 77 U. Richts, J.A.C. Broekaert, P. Tschöpel and G. Tölg, *Talanta*, 38 (1991) 863.
- 78 D. Kollotzek, D. Oechsle, G. Kaiser, P. Tschöpel and G. Tölg, *Fresenius' Z. Anal. Chem.*, 318 (1984) 485.
- 79 K. Bächmann, U. Hamm, A. Werner, P. Tschöpel and G. Tölg, in R.M. Barnes (Ed.), *Developments in Atomic Plasma Spectrochemical Analysis*, Heyden, London, 1982, p. 361.
- 80 K. Cammann and H. Müller, *Fresenius' Z. Anal. Chem.*, 331 (1988) 336.
- 81 P.L. Wylled and B.J. Quimby, *J. High Resolut. Chromatogr.*, 12 (1989) 813.
- 82 Q. Jin, F. Wang, C. Zhu, D.M. Chambers and G.M. Hieftje, *J. Anal. At. Spectrom.*, 5 (1990) 487.
- 83 R.M. Alvarez Bolainez, M.P. Dziejatkoski and Ch.B. Boss, *Anal. Chem.*, 64 (1992) 541.
- 84 W.W. Harrison, C.M. Barshik, J.A. Klinler, P.H. Ratliff and Y. Mei, *Anal. Chem.*, 62 (1990) 943A.
- 85 H. Hocquaux, *Spectra 2000*, 18 (1990) 11.
- 86 W. Geilmann, *Fresenius' Z. Anal. Chem.*, 160 (1958) 410.
- 87 W. Frech, D.C. Baxter and B. Hütsch, *Anal. Chem.*, 56 (1986) 1973.
- 88 H. Falk, C. Luedke and E. Hoffman, *Chem. Anal. (Warsaw)*, 35 (1990) 126.
- 89 S. Geiss, J. Einax, J. Mohr and K. Danzer, *Fresenius' J. Anal. Chem.*, 338 (1990) 602.
- 90 J.M. Harnley, D.L. Styris and N.E. Ballou, *J. Anal. At. Spectrom.*, 5 (1990) 139.
- 91 K. Dittrich, H. Fuchs, H. Berndt, J.A.C. Broekaert and G. Schaldach, *Fresenius' Z. Anal. Chem.*, 336 (1990) 303.
- 92 K. Dittrich, B. Radzink and B. Welz, *J. Anal. At. Spectrom.*, 6 (1991) 465.
- 93 M.W. Borer and G.M. Hieftje, *Spectrochim. Acta Rev.*, 14 (1992) 463.

- 94 L. Moenke-Blankenburg, *Laser Micro Analysis*, Wiley, New York, 1989.
- 95 F. Leis, W. Sdorra, J.B. Ko and K. Niemax, *Mikrochim. Acta*, (1989) 185.
- 96 K. Niemax and W. Sdorra, *Appl. Opt.*, 29 (1990) 5000.
- 97 A. Quentmeier, W. Sdorra and K. Niemax, *Spectrochim. Acta, Part B*, 45 (1990) 537.
- 98 J. Uebbing, J. Brust, W. Sdorra, F. Leis and K. Niemax, *Appl. Spectrosc.*, 45 (1991) 1419.
- 99 U. Uebbing, A. Ciocan and K. Niemax, *Spectrochim. Acta, Part B*, 47 (1992) 601.
- 100 A. Ciocan, J. Uebbing and K. Niemax, *Spectrochim. Acta, Part B*, 47 (1992) 611.
- 101 K. Niemax, *Fresenius' J. Anal. Chem.*, 337 (1990) 551.
- 102 K. Niemax, in G. Günzler, R. Borsdorf, W. Fresenius, W. Huber, H. Kelker, I. Lüderwald, G. Tölg and H. Wisser (Eds.), *Analytiker Taschenbuch*, Vol. 10, Springer, Berlin, 1991, pp. 1–28.
- 103 R. Hergenroeder and K. Niemax, *Trends Anal. Chem.*, 8 (1989) 333.
- 104 J. Phab, *Anal. Proc.*, 28 (1991) 415.
- 105 M.A. Bolshov, C.F. Boutron, F.M. Ducroz, U. Görlach, O.N. Kompanetz, S.N. Rudniev and B. Hütsch, *Anal. Chim. Acta*, 251 (1991) 169.
- 106 A. Zysin, C. Schnürer-Patschan and K. Niemax, *Spectrochim. Acta, Part B*, in press.
- 107 H. Rinke, G. Herrmann, M. Mang, C. Mühleck, J. Riegel, P. Sattelberger, N. Trautmann, F. Anes, H.-J. Kluge, E.-W. Otten, D. Rehklau, W. Ruster and F. Scheerer, *Mikrochim. Acta*, (1989) 223.
- 108 E.B. Saloman, *Spectrochim. Acta, Part B*, 46 (1991) 319.
- 109 M.E. Barthe, J.L. Debrun, T. Gilbert and B. Dubreuil, *J. Trace Microprobe Techn.*, 9 (1991) 1.
- 110 N.S. Nogar and R.C. Estler, *Anal. Chem.*, 64 (1992) 465.
- 111 K.H. Janssens and F.C. Adams, *J. Anal. At. Spectrom.*, 4 (1989) 123.
- 112 A. Prange, *Spectrochim. Acta, Part B*, 44 (1989) 437.
- 113 R. Klockenkämper, in G. Günzler, R. Borsdorf, W. Fresenius, W. Huber, H. Kelker, I. Lüderwald, G. Tölg and H. Wisser (Eds.), *Analytiker Taschenbuch*, Vol. 10, Springer, Berlin, 1991, pp. 111–152.
- 114 R. Klockenkämper and A. von Bohlen, *J. Anal. At. Spectrom.*, 7 (1992) 273.
- 115 R. Klockenkämper and G. Tölg, *Spectrochim. Acta, Part B*, in press.
- 116 R.P.H. Garten, in W. Fresenius, H. Günzler, W. Hüber, I. Lüderwald and G. Tölg (Eds.), *Analytiker Taschenbuch*, Vol. 4, Springer, Berlin, 1984, pp. 259–286.
- 117 S.A.E. Johansson and J.L. Campbell, *PIXE: A Novel Technique for Elemental Analysis*, Wiley, Chichester, 1988.
- 118 R.D. Vis, *Fresenius' Z. Anal. Chem.*, 337 (1990) 622.
- 119 A. Knöchel, *Fresenius' J. Anal. Chem.*, 337 (1990) 614.
- 120 K.W. Jones and B.M. Gordon, *Anal. Chem.*, 61 (1989) 341A.
- 121 F. Adams, R. Gijbels and R. van Grieken, *Inorganic Mass Spectrometry*, Wiley, New York, 1988.
- 122 J.A.C. Broekaert, in H. Günzler, R. Borsdorf, W. Fresenius, W. Hüber, H. Kelker, I. Lüderwald, G. Tölg and H. Wisser (Eds.), *Analytiker Taschenbuch*, Vol. 9, Springer, Berlin, 1990, pp. 127–163.
- 123 K.E. Jarvis, A.L. Gray, I. Jarvis and J. Williams (Eds.), *3rd Surrey Conference on Plasma Source Mass Spectrometry*, 16–19 July 1989, Royal Society of Chemistry, London, 1989.
- 124 N. Jakubowski, I. Feldmann, D. Stüwer and H. Berndt, *Spectrochim. Acta, Part B*, 47 (1992) 119.
- 125 D. Stüwer, *Fresenius' J. Anal. Chem.*, 337 (1990) 737.
- 126 D. Stüwer, in H. Günzler, R. Borsdorf, W. Fresenius, W. Hüber, H. Kelker, I. Lüderwald, G. Tölg and H. Wisser (Eds.), *Analytiker Taschenbuch*, Vol. 9, Springer, Berlin, 1990, pp. 165–189.
- 127 N. Jakubowski, D. Stüwer and G. Tölg, *Spectrochim. Acta, Part B*, 46 (1991) 155.
- 128 D. Tancer and K.G. Heumann, *Anal. Chem.*, 63 (1991) 1984.
- 129 P. Herzner and K.G. Heumann, *Mikrochim. Acta*, 106 (1992) 127.
- 130 *Proceedings of the 6th Working Conference on Applied Surface Analysis*, Kaiserslautern, L.H. Oechsner (Ed.), *Fresenius' J. Anal. Chem.*, 341 (1991) 1–448.
- 131 W. Reuter, *Trends Anal. Chem. (Pers. Ed.)*, 8 (1989) 203.
- 132 W. Husinsky, P. Wurz, A. Traumfellner and G. Betz, *Fresenius' J. Anal. Chem.*, 341 (1991) 12.
- 133 P. Wilhartitz and H.M. Ortner, *Fresenius' J. Anal. Chem.*, 341 (1991) 125.
- 134 U.C. Schmidt, M. Fichtner, J. Goschnick, M. Lipp and H.J. Ache, *Fresenius' J. Anal. Chem.*, 341 (1991) 260.
- 135 H. Jenett and Y. Kikuta, *Spectrochim. Acta, Part B*, 47 (1992) 143.
- 136 F. Alt, in P. Brätter and P. Schramel (Eds.), *Trace Element Analytical Chemistry in Medicine and Biology*, Vol. 5, De Gruyter, Berlin, 1988, pp. 279–296.
- 137 F. Alt, J. Messerschmidt and G. Tölg, *Fresenius' Z. Anal. Chem.*, 327 (1987) 233.
- 138 F. Alt, U. Jerono, J. Messerschmidt and G. Tölg, *Mikrochim. Acta (Wien)*, III (1988) 299.
- 139 K. Hoppstock, F. Alt, K. Cammann and G. Weber, *Fresenius' Z. Anal. Chem.*, 335 (1989) 813.
- 140 J. Messerschmidt, F. Alt, G. Tölg, J. Angerer and K.H. Schaller, *Fresenius' J. Anal. Chem.*, 343 (1992) 391.
- 141 E. Beinrohr, M.L. Lee, P. Tschöpel and G. Tölg, *J. Anal. At. Spectrom.*, in press.
- 142 M.-L. Lee, E. Beinrohr, P. Tschöpel and G. Tölg, *Anal. Chim. Acta*, in press.

# Surface microanalysis

F. Adams, A. Adriaens, P. Berghmans and K. Janssens

*Department of Chemistry, University of Antwerp (UIA), B-2610 Wilrijk (Belgium)*

(Received 10th September 1992)

## Abstract

Methods are discussed which combine surface, interface and thin-film measurements with the analysis of limited spatial domains. The progress which is now occurring rapidly is illustrated. The methods treated are selected from the beam-imaging methods, based on electron, ion, x-ray beam and laser interaction with the solid sample. Two examples are given concerned on one side with the ion microprobe analysis of micro structures in electronic devices and on the other side with the characterization of surface-modified asbestos by electron energy loss spectrometry and electron spectroscopic imaging.

**Keywords:** Electron probe methods; Mass spectrometry; Surface techniques; X-ray diffraction; X-ray fluorescence spectrometry; Microsurfaces; Surface microanalysis

Surface characterization of materials is presently amongst the most active, dynamic and rapidly expanding areas in analytical chemistry. It is of increasing importance in materials science and microelectronics and vital for the study of the environment and biological systems. The recognition in many practical problems that surfaces are often spatially inhomogeneous, leads to the increased need for exploitation of spatially resolved surface analytical techniques.

In materials science, increasingly small structures must be fabricated with high material uniformity and interface smoothness. This requirement demands appropriate device fabrication techniques, such as cold vapour deposition and molecular beam epitaxy, impractical until a short time ago, since it is essential in some cases to have control of composition and structure down to the atomic level [1]. Also, many of the most critical properties of materials involve their sur-

faces. Surface-modification chemistry provides an answer to many dilemmas in materials science by decoupling the surface properties of materials from those of the bulk solid. Monolayers or thin surface layers of organic and inorganic surfaces increasingly determine electroactive, optical and catalytic properties of many materials. Electronic materials require an ever more detailed understanding of the deposition of extremely small amounts of matter in precise physical arrangements and locations. Many catalysts consist of highly dispersed support particles whose size, morphology, structure and nature of metal-support and metal-promoter interfaces need to be studied more and more in detail.

In environmental chemistry, examples of microscopical surface characterization are abundant. The composition or structure of microscopically sized environmental particles are important parameters for their persistence and fate in the environment, their toxicology and for inferring the assignment of particles to specific sources of pollution. Sometimes microsurface analysis (or

*Correspondence to:* F. Adams, Department of Chemistry, University of Antwerp (UIA), B-2610 Wilrijk (Belgium).

surface enrichment) provides insight information mechanisms and heterogeneous surface reactions [2].

Microsurface analysis plays an important role in some of the newest and most exciting discoveries: high-temperature superconductors, fullerenes, biomaterials and high-performance composites, to give only a few examples. In general, there is a tremendous drive for the analytical developments of the enormous range of applications in fields such as the environment, biomedical research and health care, and electronic and structural materials, which serve as the fabric of modern technology. Hence, during the past decade there has been a substantial and continuing

growth of interest among researchers for the development of truly microscopical surface-characterization techniques. Actually, today the number of surface analytical techniques with some kind of microscopical potential has grown so large that it has become a difficult task for the user to select an appropriate technique to solve a given problem. Over a hundred different techniques exist which aim at identifying one or more specific properties at the microscopical or surface level in condensed matter. Together they often provide a reasonably good understanding of a material's properties, structure and composition. The main application areas and a number of these methods are shown in Table 1. This, by all

TABLE 1

Characterization of solid materials

Main application area	Analysis method	Abbreviation
Layer thickness/composition	Transmission electron microscopy	TEM
	Auger emission spectrometry	AES
	X-ray photon spectrometry	XPS
	Secondary-ion mass spectrometry	SIMS
	Spectroscopic ellipsometry	
Low level impurities	Rutherford backscattering spectrometry	RBS
	Laser mass spectrometry	LAMMS
	Glow discharge mass spectrometry	GDMS
	Instrumental neutron activation	INAA
	SIMS	
Chemical information/bond form	X-ray photon spectrometry	XPS
	Fourier-transform infrared spectrometry	FT-IR
	Fourier-transform mass spectrometry	FT-MS
	Infrared spectrometry	IR
	Raman spectrometry	RAMAN
	Electron spin resonance spectrometry	ESR
	Nuclear magnetic resonance	NMR
Two-dimensional/three-dimensional impurity distribution	Laser spectrometry	
	Ion microscopy/microprobe imaging	SIMS
	Scanning electron microscopy	EPMA/SEM
	Electron energy loss spectrometry	EELS
	LAMMS, FTIR, laser RAMAN	
Electrical information	Imaging NMR	
	Spreading resistance, C-V, Hall measurements	
	Deep level transition spectrometry	DLTS
	Time resolved luminescence / transient optical measurements	
Structural/crystallographic	X-ray diffraction	XRD
	High-resolution EM	HREM
	Scanning transmission EM	STEM
	RBS, Raman, ESR, ab initio calculations	

means incomplete, list of techniques nevertheless represents a large and expensive collection of instrumentation. Moreover, it requires experienced scientists with diverse interests and backgrounds in analytical chemistry, physics, computer science and instrument engineering, which can be made available only in very large institutes or through the establishment of a collaborating network. The University of Antwerp, for example, has assembled the infrastructure and know-how of 15 laboratories belonging to the departments of physics and chemistry in an Institute of Materials Science (IMS) with the purpose of joining resources for materials research, especially with the aim of materials characterization. Even then, in order to cover the range of instrumentation required for materials characterization in Belgium, it is necessary to pool resources with other Belgian Institutes, the Interuniversity Microelectronic Centre (IMEC, Leuven) and another Institute of Materials Research (IMO) in Diepenbeek. Only then access is gained over a more or less full range of analytical and physical instrumentation for the purpose. As far as their application relates to the characterization of microelectronic materials and devices most of these methods (and indeed many more) are covered in the recent book edited by Grasserbauer and Werner [1].

In this paper we will focus the attention on a few methods concerning the combination of sur-

face, interface and thin-film analysis on limited spatial areas and the progress which is now rapidly occurring in these methods. They were selected from the group of techniques termed “beam-imaging methods”, based on electron, ion or x-ray beam interactions with the solid sample.

#### METHODS OF SURFACE MICROANALYSIS

Table 2 summarizes different types of interactions of particle beams or radiation with a solid material, and the main phenomena which give rise to analytical information confined to small spatial domains coupled to a more or less well defined surface discrimination capability. Spatial resolution and imaging are either obtained via the source (such as in the scanning electron microscope or the ion microprobe) or via the detector (as in the transmission electron microscope or the ion microscope). The surface was defined here in a rather general, generic manner as this part of the sample, which by composition or properties, is analytically different from the bulk material. This definition differs from that specified by surface chemists who define the surface as nothing more than the outermost atomic layer [3]. Elemental composition, molecular information or structural inhomogeneity may be of interest in the surface layer.

Figure 1 shows a graph comparing the spatial

TABLE 2

Beam methods for microsurface analysis and state-of-the-art resolution

Excitation	Analytical signal	Resolution	
		Lateral	Surface
Electrons	Auger electrons (SAM)	50 nm	1–2 nm
	Transmitted electrons (EELS)	10 nm	thin sample
	Reflected electrons (HREELS)	50–500 $\mu\text{m}$	0.25–3 nm
X-ray photons	Photoelectrons (XPS)	10 $\mu\text{m}$ (tube)	nm
	Auger electrons (XAES)	$\mu\text{m}$ (synchrotron)	nm
KeV ions	Secondary ions (SIMS)	0.1 $\mu\text{m}$	3 nm
	Secondary ions (SSIMS)	1 $\mu\text{m}$	nm
Low energy ions	Backscattered ions (ISS)	none	nm
UV photons (laser)	Molecular fragments (LMMS) (LAMMA/LIMA, FT-LMMS)	5 $\mu\text{m}$	50 nm
X-rays (synchrotron)	Fluorescence x-rays (SRXRF)	1 $\mu\text{m}$	none

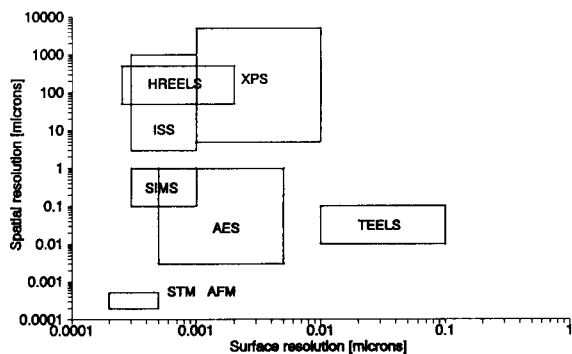


Fig. 1. Spatial and surface resolution of a number of surface microanalytical techniques [1,39].

and surface resolution of a number of techniques. Generally speaking the spread in lateral resolution of the methods illustrates the progress realized over time since the original introduction of the methodology. The lateral resolution of the beam methods is primarily related to the confinement of the impinging radiation on the sample surface, although various diffusion effects in the interaction may contribute in limiting the lateral resolution practically achievable. Hence, progress in ion beam focalization is responsible for the steady gain in lateral resolving power of e.g. ion microprobe analysis. Laser beam interaction methods are not included in Fig. 1. Their optimum lateral resolution is 5–10  $\mu\text{m}$ , their depth resolution  $\leq 0.1 \mu\text{m}$ . In Fig. 1, only scanning tunnelling microscopy (STM) and atomic force microscopy (AFM) approach a resolution at the atomic dimensions, necessary in many examples of nano-fabrication technology. Tremendous progress has occurred in the lateral resolution of methods based on x-ray interaction due to the developments in x-ray photon-focusing technology which was realized recently.

#### *Techniques based on the measurement of electrons*

Three techniques will be briefly reviewed as far as their surface microscopical potential is concerned: Auger electron spectroscopy (AES), x-ray photoelectron spectroscopy (XPS, or ESCA), and electron energy loss spectroscopy (EELS). Both AES and XPS involve the ejection

of secondary electrons, possessing an energy characteristic of the target's elemental composition, while EELS studies the primary electrons which have impinged and interacted with the sample.

AES is based on the detection of Auger electrons induced in the bombardment with an electron or (see later) an x-ray photon beam. The emitted Auger electrons have energies unique to each atom and are accordingly analyzed as a function of their energy, yielding both qualitative and quantitative information on the sample. AES has proven to be a powerful technique in scanning Auger microprobing (SAM), allowing localized analyses, element mapping, and, when used with a sputtering ion gun for etching away layers of material, depth profiling. The characterization of semiconductor devices [4], superlattice structures [5] and metallurgical specimens [6] are important fields of application of SAM.

Electron ejection may also be induced by photons of a characteristic energy, as in XPS. The core electrons, emitted at bombardment by x-rays, obtain discrete kinetic energies. Apart from the capability to identify elements, the advantage of XPS is situated in the possibility to determine the chemical state of the element studied. The main applications of XPS are located in corrosion studies [7], catalysis [8], and polymer science [9]. Theory and applications of both XPS and AES are discussed extensively in the recent edition of the handbook of Briggs and Seah [3].

Both methods involve the study of the energy distribution of the emitted electrons, which implies that the information depth or surface resolution is determined by the electron mean free path. This is a function of the electron energy and the composition of the matrix. The low escape depth (0.5–5 nm) of Auger- and photoelectrons, up to a few hundred eV, provides surface analysis within the first few monolayers, which classifies the method as a very surface-sensitive technique. The lateral resolution of SAM is dominated by the diameter of the primary-electron beam and is well into the sub-micron domain.

There are advantages in using continuous x-rays for excitation of the Auger electrons (x-ray-induced AES or XAES) as near-threshold pho-

toionization cross sections can be several orders of magnitude higher than the maximum electron cross sections. Moreover, there is a gain in signal-to-noise ratio as the high secondary-electron backgrounds are significantly reduced. High-resolution spectrometry of high-energy (several keV) Auger electrons could furthermore provide information on chemical species [10]. All this should indicate that conventional electron-induced AES and SAM is a choice resulting from the ease with which electron beams can be produced and focused. Siegbahn coined the acronym ESCA (electron spectroscopy for chemical analysis, as opposed to XPS), to underline the fact that both photoelectron and Auger electron peaks appear in the electron spectrum obtained under x-ray irradiation [11]. The progress in x-ray optics gave rise to increasingly small x-ray photon beams, while synchrotron radiation sources deliver extremely intense beams in the UV to the hard x-ray energy region. Both technologies now tend to change the electron spectroscopy situation completely from what it has been only recently. Spatial resolution of XPS has improved from areas of millimetre dimensions in “large-area” XPS systems to nowadays lateral resolutions of 5–20  $\mu\text{m}$  in imaging systems based on rotating-anode x-ray tubes [12]. Spatial resolutions of 1  $\mu\text{m}$  may eventually be possible in routine XPS systems while a considerably better resolution, approaching 0.1  $\mu\text{m}$ , has recently been reached in synchrotron-based instruments [3,13,14].

In addition to evolving into a microscopical technique, XPS has developed into a widely applicable method for the analysis of the outermost atomic layers of solid samples. Recently, attention has been focused on the use of angle-dependent methods to extract information as a function of depth in the top few nanometres below the surface of the sample. Indeed, measurements with a tilted sample, from almost grazing ejection angle to the normal of the surface, give rise to the observation of different surface layers. These surface layers change with the normal effective depth times the sine of the angle, hence from the top atomic surface layer at angles near grazing incidence to the full depth corresponding to the complete electron mean free

path. Many depth-profile deconvolution algorithms have been reported for acquiring data at a number of angles and for computing a depth profile throughout the film analyzed [15]. This concept of angle-dependent measurements is not new; it has been applied in many other methods. Nevertheless, despite its obvious shortcomings, the angle-resolved application of XPS avoids a major drawback of the conventional sputter-assisted depth-profile measurements, where ion-bombardment-induced modifications (ion mixing, ion-induced surface roughening, projectile implantation) can otherwise falsify results.

Concomitantly with the progress described till now, there is the continuing development of detection systems which increase both the AES and XPS imaging capability. Progress in the quantization of surface analysis with the electron spectroscopies have been rapid over the last ten years. In well characterized and simple systems errors are now of the order of 5%. Accuracy becomes more limited for materials lacking homogeneity in the surface region or showing surface roughness [16] and for UV-induced photoelectrons (UPS). The topic is of industrial importance and international organizations have been formed to follow and direct the quantification effort [17].

The energy distribution of bombarding electrons, which have interacted with the atoms of a specimen, is studied in electron energy loss spectroscopy (EELS). This method provides elemental information on minute locations of the sample [18]. In transmission EELS, the spectrometer, which separates the energy of the electrons, is integrated in a transmission electron microscope. Lateral resolution is limited by aberrations of the optical system and operation parameters of the microscope. The information depth of the method is determined by the sample thickness and ranges typically between 10 and 100 nm. We will illustrate the surface microanalytical potential of this method with an example in a later section of this paper. Reflected EELS, which is also understood as high-resolution EELS (HREELS), studies the energy loss of reflected low-energy bombarding electrons. Promising applications of HREELS are situated in semiconductor research and polymer technology [19]. The information depth depends



on the energy of the bombarding electron beam and the angle of incidence. The surface sensitivity of this method can go down to probing a single monolayer adsorbed on well defined surfaces. Lateral resolution is limited by the incident beam spot size and ranges between 50 and 500  $\mu\text{m}$  [20]. The understanding of the interaction mechanism between monochromatic electrons and the vibrations of the solid are not yet fully understood and hamper at present quantization [21].

#### *Techniques based on the measurement of ions*

Secondary-ion mass spectrometry (SIMS) and ion scattering spectroscopy (ISS) are two techniques which are based on ion detection. SIMS is an analytical method in which bombardment of energetic primary ions on a solid specimen removes particles by sputtering [11]. These emitted particles are partially ionized and are accelerated into a mass spectrometer. The so-called secondary ions are characteristic for the elemental and isotopic composition of the sample. SIMS analyses allow localized depth profiling, line scans, elemental micromapping and isotopic analyses. SIMS has achieved great success as a materials characterization tool because of its  $\mu\text{g ml}^{-1}$  to  $\text{ng ml}^{-1}$  sensitivity, excellent depth and lateral resolution, and even for its capability for three-dimensional analyses. It is best known for its applications in the microelectronics industry, but is now increasingly used in many other fields.

Quantification with an accuracy of 10–20% is now commonplace for simple, conductive materials [22,23].

The recent evolution in one microanalytical SIMS system, the CAMECA ion microscope–microanalyzer, is shown in Table 3. The gradual improvements in the lateral resolution show the remarkable progress achieved in SIMS microsurface analysis. The lateral resolution obtained in SIMS is determined by its mode of operation. The ion microprobe mode rasters a focused ion beam over the surface of the sample, and the resultant lateral resolution is determined by the beam diameter (0.1  $\mu\text{m}$ , even better in some ion microprobe systems). In the ion microscope mode, on the other hand, a magnified image of the surface is produced using a relatively large beam (up to several hundreds of  $\mu\text{m}$ ) in combination with an ion optical system. The lateral resolution in this case is determined by the ion optical system and its aberrations. In dynamic SIMS instruments, such as those of Table 3, material is quickly sputtered from the exposed surface and in a dynamic way sub-surface layers are analyzed leading eventually to three-dimensional data stacks of elemental analytical data [24].

In static SIMS systems (SSIMS) the primary-ion beam current density is lowered to values corresponding with sputtering rates as long as several hours [25,11]. Under such conditions SIMS becomes a true surface analytical technique of

TABLE 3

Main characteristics of the Cameca range of ion microscopes/ion microprobes

Characteristics	IMS 3f	IMS 4f	IMS 5f	IMS 1270
Year of introduction	1979	1985	1991	1991
Mode of operation	Microscope	Microscope Microprobe	Microscope Microprobe	Microscope Microprobe
Lateral resolution	1000 nm	1000 nm 200 nm	500 nm 150 nm	350 nm 50 nm
Information depth	0.3–1 nm	0.3–1 nm	0.3–1 nm	0.3–1 nm
Mass range	1–280	1–500	1–2000	1–2000
Maximum mass resolution	$10^4$	$10^4$	$4 \times 10^4$	$10^5$
Transmission	30% (MRP = 800)	30% (MRP = 800)	40% (MRP = 800)	50% (MRP = 6000)
Sensitivity	$\text{ng ml}^{-1}$ – $\mu\text{g ml}^{-1}$	$\text{ng ml}^{-1}$ – $\mu\text{g ml}^{-1}$	$\text{ng ml}^{-1}$ – $\mu\text{g ml}^{-1}$	$\text{ng ml}^{-1}$ – $\mu\text{g ml}^{-1}$
Charge compensation	No	Yes	Yes	Yes
Vacuum sample chamber	$8 \times 10^{-9}$ torr	$5 \times 10^{-10}$ torr	$5 \times 10^{-10}$ torr	$5 \times 10^{-10}$ torr
Detection	Sequential	Sequential	Sequential	Simultaneous (up to 5 detectors)

the top surface layer of the sample with high detection sensitivity. The method has evolved over the last two decades from a large-area technique into a microanalytical technique. It is a scanning microprobe configuration where a focused and pulsed liquid metal ion source is used as primary radiation and a high-transmission reflection type time-of-flight (TOF) tube as the mass analyzer in a UHV environment ( $10^{-11}$  torr) [26,27]. This configuration combines parallel mass registration with high sensitivity, high mass resolution and a high mass range. It allows elemental and molecular surface analysis in small surface areas of a few  $\mu\text{m}$  in imaging mode and extremely high (sub-monolayer) sensitivity for inorganic as well as organic materials at high mass resolution. In particular the potential of this kind of mass spectrometric surface analysis is documented for the analysis of microelectronic materials, processes and devices. Applications in this area range from the detection of metal contaminants and organic molecules [28] to the control of surface reactions on silicon wafers [29].

Ion scattering spectrometry (ISS) is based on the energy analysis of backscattered ions from the target surface atoms [30]. An important aspect of ISS is its high sensitivity for the outermost surface layer. This is due to the low-energy primary

ions (0.1 keV to a few keV). Lateral resolution is limited to  $10 \mu\text{m}$ . The technique is frequently used in adsorption and reaction studies of surfaces. High-energy equivalents of ISS range up to the Rutherford backscattering spectrometer (RBS) using MeV ions. Micro-RBS is available on a number of nuclear microprobes in combination with proton-induced x-ray emission (PIXE) and scanning transmission ion microscopy (STIM). Resolutions down to 50 nm have been achieved with high-energy and low-current ion beams [31,32]. RBS mapping and cross-sectional (in-depth) RBS measurements can be combined when a proton microprobe is scanned over a sample. The depth information is derived from the RBS spectra at each pixel point and is also called RBS tomography [33]. The method provides information on the atomic composition and distribution of matrix elements and impurities beneath insulating layers in semiconductors.

Both SIMS and ISS show a strong dependence of their information depth upon the kinetic energy and the mass of the primary ions. It ranges between 0.3 and 1 nm. In SIMS the attainable depth resolution is determined by the initial surface roughness and by ion beam mixing. The minimum achievable depth resolution for the easiest matrices (semiconductors) at 2–3 atomic lay-

TABLE 4  
Comparison of characteristics of TOF-LMMS and FT-LMMS

Characteristics	TOF-LMMS	FT-LMMS
Mass resolution	850	$10^5$
Mass range	1–unlimited	$1-15 \times 10^3$
Sensitivity	$10^{-13}$ g	$10^{-11}-10^{-12}$ g
Geometry	Transmission	Reflection
Lateral resolution	$1 \mu\text{m}$	$> 1 \mu\text{m}$
Information depth	100 nm	100 nm
Measured species	Promptly generated ions (+ / -)	Prompt ions and post-laser ionization ions (+ / -)
Special remarks	Post-ionization is not possible in commercially available instrumentation	Post ionization
Applications	Organic: detailed structure characterization Inorganic: speciation	Organic: detailed structure characterization Inorganic: speciation

ers ties in nicely with the stochastic nature of the sputtering process and the depth of origin of the ejected particles [34].

#### *Laser microprobe analysis as a microscopical surface tool*

There are numerous examples [2,35] proving the utility of laser microprobe mass spectrometry (LMMS) for microsurface analysis with one of two instruments which became available around 1980, the laser microprobe mass analyzer (LAMMA) [36] and the laser ionization mass analyzer (LIMA) [37]. Both instruments are based on low-resolution ( $m/z = 800$ ) TOF mass spectrometers to analyze the ionized species released upon impact by a focused and pulsed UV radiation of a Nd-YAG laser. The analytical characteristics are compared in Table 4 with those of a recent contender, in which Fourier-transform laser mass spectrometry (FT-LMMS) is used for high-resolution mass spectrometric detection [38]. The tremendously high mass resolution and the other features offered by FT-MS indicate that this quite new method for microsurface analysis may provide an unrepresented specificity for inorganic and organic structural surface analysis.

In Table 5 its characteristics for organic surface analysis are compared with those of TOF-SSIMS. The possibilities for structural identification are superior to those of TOF-SSIMS due to the inherent possibilities of the FT-MS technique, directly through the high mass resolution and indirectly, e.g. by collision-activated dissocia-

tion (CID) or electron impact post-ionization. Structural specific fragmentation also facilitates identification.

#### *Atomic resolution imaging techniques*

Scanning tunnelling microscopy (STM) and atomic force microscopy (AFM) are two techniques which do not fit into the classical particle-in-particle-out scheme of other analytical surface methods. The principle of STM is based on the quantum mechanical tunnelling of electrons through the region between the sample and a sharp metallic tip, which is brought very close (1 nm) to the specimen surface. A voltage applied across the sample and the tip, causes the electrons to cross the region in a narrow channel. The measured intensity is very sensitive to the distance between sample and tip. Once the interaction is established, the surface is scanned by the probe, and the measured intensity will be used to create an image. The lateral resolution of the surface is limited by the sharpness of the tip (0.2–1.2 nm) [39]. Aside from measuring the surface topography, STM provides information on the atomic composition, since the measured current depends on the electronic structure of the surface. Applications are reviewed by Ray et al. [40]. Considerable effort has recently been directed towards using STM to characterize, under close to physiological conditions, the structure of biological macromolecules deposited on a clean surface. Despite the atomic resolution, the method is not yet capable of providing a reproducible and unambiguous visualization of the structure or to identify bases [41].

Atomic force microscopy is a surface technique which is closely related to STM [42]. It consists of measuring the atomic forces between a tip and the surface of a sample, the tip now being attached to a cantilever. When the tip approaches the surface, the cantilever will tilt due to the impact of interatomic forces. Optical methods are then used to measure these deflections. The advantage of this method over STM is the possibility to analyze non-conducting samples. Applications of both STM and AFM are situated in several fields: surface physics and chemistry, electrochemistry, biology and the study of electronic

TABLE 5

Comparison of TOF-SSIMS and FT-LMMS for organic surface analysis

Characteristics	TOF-SSIMS	FT-LMMS
Mode of operation	Imaging	Spot analysis
Lateral resolution ( $\mu\text{m}$ )	5	5
Information depth (nm)	1	50
Detection limit	$10^{-12}$	$10^{-10}$
Mass resolution	10000	100000 (up to $m/z = 1000$ )
Mass range	Limited by mass resolution	15000
Structural discrimination	Good	Excellent

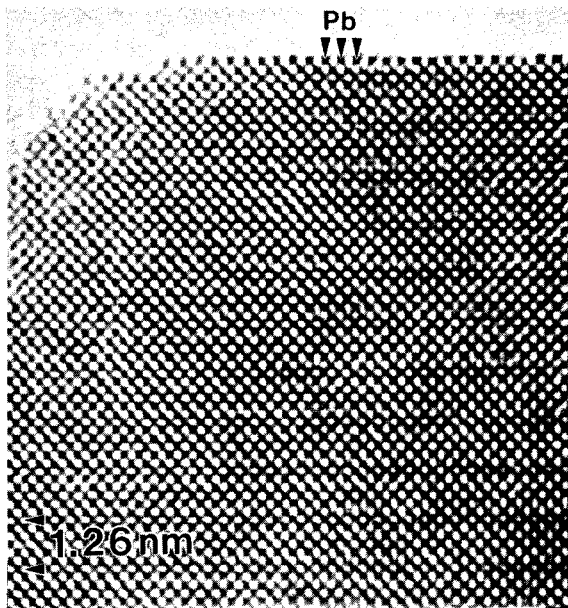


Fig. 2. HREM image showing a surface located at the level of the plane between SrO and PbO layers in  $(\text{Pb}, \text{Bi})_2\text{Sr}_{2-x}\text{La}_x\text{Cu}_2\text{O}_{6+y}$  superconductor. Black dots at the surface can be identified as Pb atom configurations [43].

devices. High-resolution electron microscopy (HREM) has also reached the level of atomic imaging on a more or less routine basis. HREM images are obtained by allowing the transmitted and one or more diffracted beams through the objective aperture of a point-resolution TEM. Image formation occurs by the interference of these selected electron beams. However, the interpretation of the images which contain the characteristic periodicities of the crystalline specimen in terms of atomic identity and structure remains tedious. Image simulation must be used to compare simulated (calculated) and experimental images so as to obtain unambiguous atomic images. An example of the application of this methodology is shown in Fig. 2 [43]. The presence of particular atoms at the top surface of a superconducting sample is directly evidenced.

#### *Synchrotron radiation in surface microanalysis*

The high brightness of synchrotron radiation sources has significantly enhanced the research capability for methods relying on UV or x-rays.

Synchrotron radiation x-ray fluorescence spectrometry (SRXRF) is coming to the fore as a very promising analytical method, complementing other techniques based on x-rays, such as electron probe microanalysis and the nuclear microprobe. SRXRF will mostly be used to attain lower detection limits, to perform dynamic observations for the study of transient phenomena and to obtain high spatial resolution for element mapping. Applications of the micro SRXRF technique are numerous. They range from the analysis of micro-heterogeneities in materials of different composition over sensitive bulk analysis of technologically important materials to the study of distributions of elements across different kinds of interfaces. In x-ray fluorescence analysis under total reflection conditions, monochromatic x-rays are directed onto a sample surface under glancing incident angle. The primary-ion beam then excites a surface layer of about 3 nm in depth. The fluorescent x-radiation, as detected by a Si(Li) detector, provides detection limits of about  $10^8$ – $10^{10}$  atoms  $\text{cm}^{-2}$  for impurities like Fe, Cu, Zn and Ni [44]. With high-intensity synchrotron radiation, the technique can be used for microscopical samples or spot analyses [45].

Synchrotron radiation (SR) plays an increasingly important role in microscopical surface analysis in (i) the study of chemical composition, (ii) structural studies and (iii) electronic structure studies. About 50% of the actual SR beam time is used for the study of condensed matter and surface research (about 500 000 hours per year now) using diverse techniques. We cannot give a complete overview of the role of SR sources but want to stress a few emerging trends. The role of synchrotron radiation in imaging XPS was already emphasized in the section “Techniques based on the measurement of electrons”.

The important advantage of SR in surface studies is that it gives continuously variable photon energies which in photoemission allows one to optimize (i) the sensitivity to particular species, (ii) the surface sensitivity by setting the photoelectron kinetic energy in the energy range of minimum escape depth around 50–100 eV and (iii) energy resolution, state-of-the-art at 100 eV is now 25 meV. In the past few years extended

x-ray absorption fine-structure analysis (EXAFS) was widely used for the investigation of the local structural environment of specific atoms. The method is based on the small oscillations in the absorption cross section as a function of energy for several hundred eV above the absorption edge. Surface-specific versions of the technique (surface EXAFS or SEXAFS) have been developed and are widely exploited, e.g. for the study of catalysts.

Unique new possibilities will be offered by the new generation of high-energy SR sources (ESRF at Grenoble, France; APS in Argonne, IL; and SPring-8 in Harima, Japan).

## APPLICATIONS

### *Ion microprobe study of microstructures in electronic devices*

Secondary-ion mass spectrometry (SIMS), using the ion microprobe or ion microscope configuration in combination with image processing, is a technique which couples lateral imaging and dynamic ion beam sputtering. It allows the extension of the common capabilities of SIMS with a number of interesting features such as local area depth profiling, line analysis and the acquisition of three-dimensional image depth profiles. This technique is applied here to locate and analyze micro structures in electronic devices.

Similar types of applications have been performed, having analyzed elements of either high concentration or high sensitivity [46,47]. The fact that micron-scale structures of very low concentration are analyzed, makes this study an exception. In these types of analyses, it is necessary to make a compromise between the spatial resolution obtained and the precision acquired. These two aspects are of course linked. Since in the microprobe mode, the probe size is critical for a good spatial resolution, a reduction in the primary beam intensity will improve it. On the other hand the volume analyzed will be reduced, implying an inevitable reduction of the signal and hence the precision of the analysis. The purpose of this study therefore is to develop a procedure

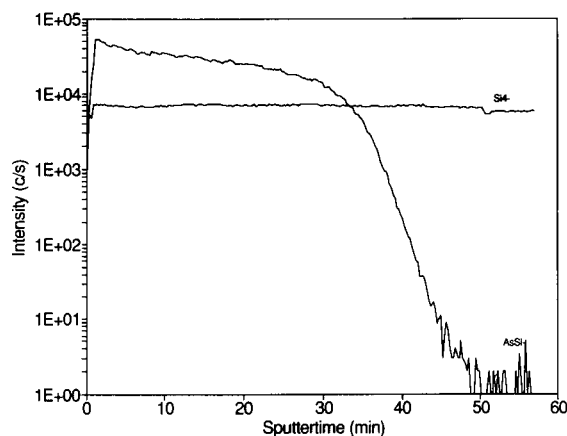


Fig. 3. Depth profile of the  $\text{AsSi}^-$  signal, measured in the centre of the  $\text{n}^+$  diode.

to measure microstructures of very low concentration with an acceptable precision.

The sample analyzed consists of an  $\text{n}^+$  (arsenic) diode, which has an area of a few square microns and a depth of a few hundreds nanometres, located in a silicon wafer. The arsenic has a maximum concentration of the order of  $10^{19}$ – $10^{20}$  at  $\text{cm}^{-3}$  ( $\leq 1$  at%). The purpose of these analyses was to check the lateral and in-depth distribution of As in the Si matrix. The instrument used to analyze the sample was a Cameca IMS 4f ion microprobe. The surface was scanned with a focused  $\text{Cs}^+$  beam of 1 nA over an area of  $10 \mu\text{m}^2$ . Negative secondary ions were accelerated into the mass spectrometer and were detected with an electron multiplier in pulse-counting mode. The  $\text{AsSi}^-$  signal was measured to prove the presence of arsenic in the sample. This signal was preferred over the  $\text{As}^-$  signal because of its higher sensitivity. The sample was analyzed with a high mass resolution of 3000 to eliminate the isobaric interference of  $^{29}\text{Si}_3\text{O}^-$ . In Fig. 3, a profile of the  $\text{AsSi}^-$  signal, which is measured in the centre of the  $\text{n}^+$  diode, is shown as a function of time (which can be correlated with depth). The  $\text{Si}_4^-$  signal is measured to have a reference signal. The plot shows a fairly flat signal close to the surface, but then it decreases gradually as the border is reached, showing a smooth bottom interface of the diode, where the pn junction is located, with its environment.

In order to have a two- and three-dimensional view of the arsenic distribution in the silicon wafer, a set of images was taken while the surface was gradually being disintegrated during the ion beam bombardment. A Kontron imaging system was applied for the acquisition of the images. This computer is linked with a SEM box, through which signals are sent to a set of deflectors having the primary beam scan the selected area. The imaging system is synchronized with the scanning of the primary beam: it accumulates and stores the measured intensity for each position scanned, after which the images can be reconstructed. About 50 images were taken over a period of an hour. Figure 4 illustrates the selected area over which the ion probe is scanned. The lateral distribution of the  $\text{AsSi}^-$  signal taken close to the surface is shown in Fig. 5a, demonstrating a lower  $\text{As}^-$  intensity near the edges of the diode. The image-processing software allows advanced operations such as real-time display of vertical slices in any direction of the image stack. The line drawn in Fig. 5a represents the region where a cross section is made through the 50 images stored underneath each other as a function of depth. The result is demonstrated in Fig. 5b, showing a smooth crossing of the diode with the silicon wafer. The cross section makes it possible to evaluate parameters such as lateral and in-depth diffusion of the arsenic as a function of, e.g. thermal treatment of the sample.

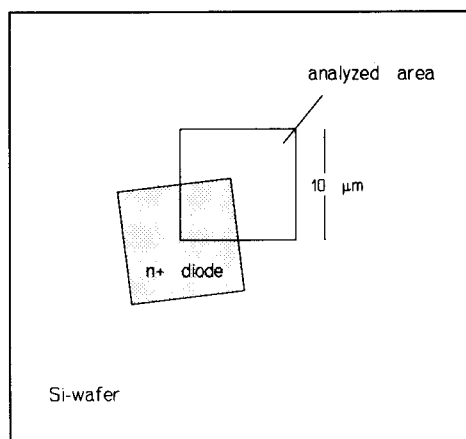


Fig. 4. The selected area over which the ion probe is scanned.

As a final step, the distribution of arsenic can also be represented in a three-dimensional solid object. In this case a two-dimensional area needs to be selected. This is displayed in Fig. 5c, in which the selected area shows part of an image taken on the surface of the diode. The bottom image represents an image taken near the base of the diode. A three-dimensional cross section is made through the entire stack of images, after which the solid block is rotated in order to have a view indicated by the arrow, as is demonstrated in Fig. 5d.

The sample analyzed here was a test sample, which demonstrates the possibility to obtain both a good spatial resolution and still have a good precision while analyzing very low concentrations. The analysis of these types of materials will be a challenge for a further analytical methodology development. The importance of these analyses can be situated in a number of areas. It serves on one hand as a control procedure, in which the shape of the analyzed structure and the element distribution within the structure can be examined. Furthermore, it provides the possibility to prove the presence of contaminants within and around the structure. On the other hand these analyses create a possibility for process engineers to have a means for evaluation or feedback, in order to control the fabricated structure.

#### *Characterization of surface-modified asbestos by EELS*

The cytotoxic and hemolytic properties of asbestos fibres may be strongly influenced through chemical modification of the mineral surfaces with  $\text{TiCl}_3$  [48]. Biological investigations already have demonstrated a significant reduction in the binding ability of a carcinogen such as benzopyrene to the titanium-treated fibres [49]. Systematic studies of the characterization of the surface and the inside of the fibre tubes are therefore essential in the development of less pathogenic chrysotile fibres. The characterization of the fibers' condition is not easy. The short-range inhomogeneity of the composition of the asbestos fibres and the small fibre size (typically 20–100 nm diameter) requires the use of analytical techniques providing extremely high lateral resolution. Furthermore, if

these additional titanium species are present at the surface, they are present generally as very thin surface layers. In this case a highly sensitive microanalytical technique for investigating the local elemental composition is required. Given these constraints, EELS is an analytical technique very well suited to address this problem.

With EELS inner-shell loss edges are studied; these are characteristic of the chemical composition of the sample. Furthermore, there is a minimal lateral electron scatter and so electron spectroscopic imaging (ESI) has the added advantage to monitor elemental images of the sample with spatial resolutions approaching the diameter of

the electron beam. The electron-loss near-edge structure (ELNES) can also be used to acquire information on both the spatial distribution and the atomic environment. Even though the origin of the details of the different edge features is not well understood, the technique can be used to probe local bonding and oxidation states.

Energy-loss spectra and images were obtained with the Zeiss EM 902 (Oberkochen, Germany) instrument operating at 80 kV. Due to the high electron beam intensity required for high-magnification electron microscopy a cryo-stage cooled with liquid nitrogen at  $-150^{\circ}\text{C}$  was used to reduce the irradiation damage of the hyrous min-

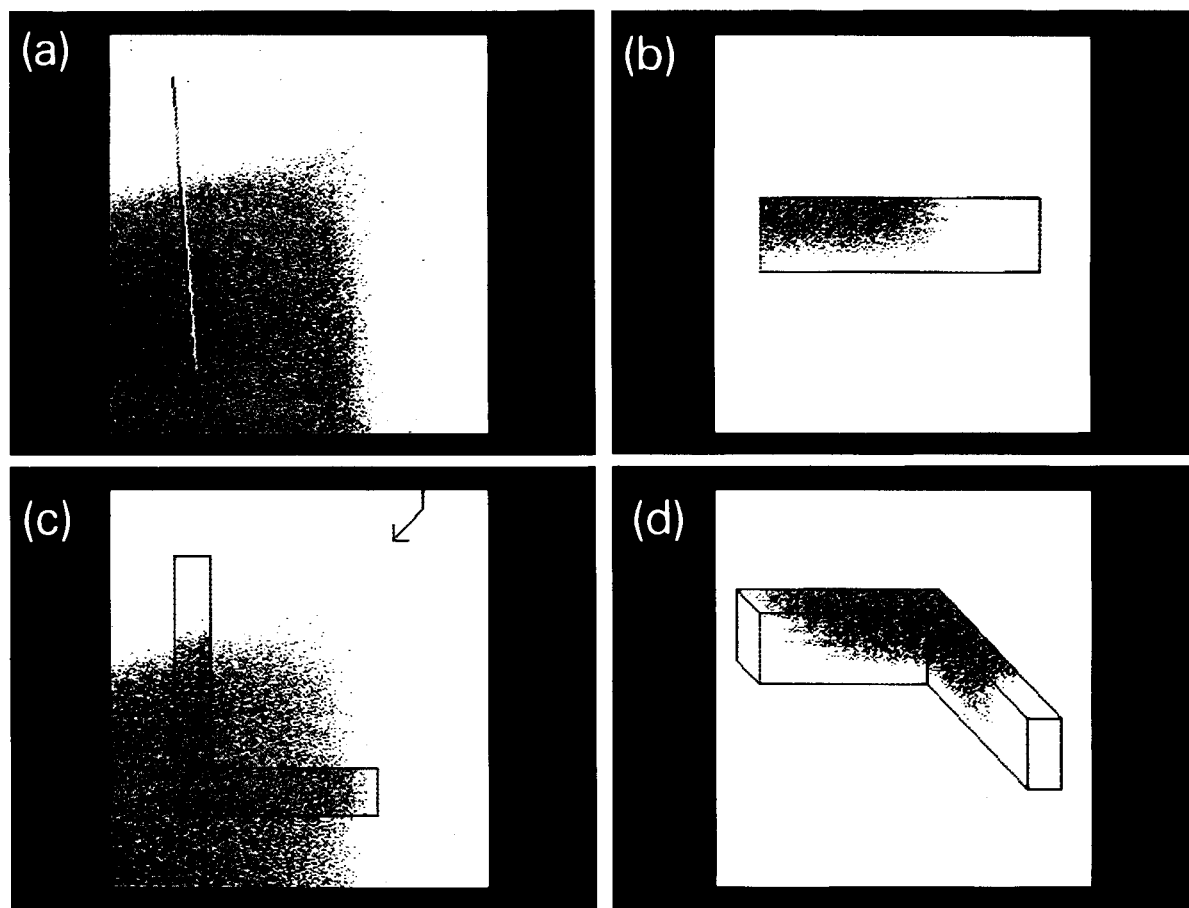


Fig. 5. (a) Lateral distribution of the AsSi<sup>-</sup> signal taken close to the surface. The line represents the region where a cross section is made through the fifty images stored underneath each other as a function of depth. (b) Vertical slice through the image stack. (c) Selected two-dimensional area showing part of an image taken on the surface of the diode. The bottom image represents an image taken near the base of the diode. (d) A three-dimensional cross section through the entire stack of images.

eral fibres. The resolution in the electron spectroscopic images clearly depends on the susceptibility of the asbestos fibres to radiation damage. Although the typical dose was  $3 \times 10^5 \text{ e nm}^{-2}$ , it remains important to establish how the electron spectroscopic images are affected by mass loss. With the use of a cooled sample holder it is possible to obtain chemical information from cross-sectioned asbestos fibres at a high spatial resolution, provided that the counting time used to collect the spectra is long enough to ensure adequate statistics. The present work was done with serial EELS acquisition, which means that the different energy-filtered images are acquired successively. For detection limits we estimate the minimum detectable signal-to-background ratio to be about 0.01, corresponding to a titanium concentration of ca. 1 atom percent.

Two approaches were considered for the sample observation: as cross sections and with the fibres deposited on holey carbon film. The use of cross-sectioned samples is very useful because it provides structural and morphological information, while the deposition method reveals more local information about the surface of the modified fibres.

Figure 6 shows a high-magnification ESI transmission electron microscope image ( $\times 140\,000$ ) of

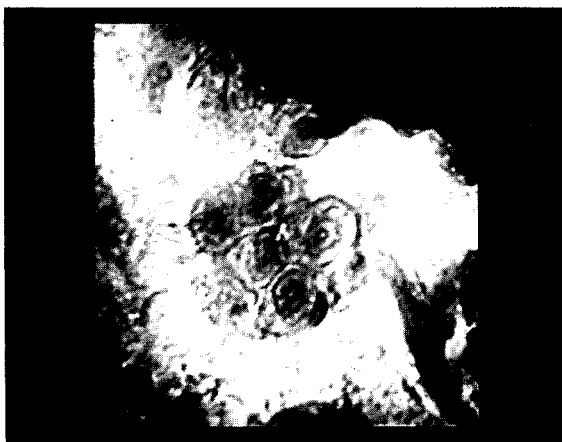


Fig. 6. Transmission electron microscope image of a cross-sectioned chrysotile fibre. The entire picture corresponds to 185 nm.

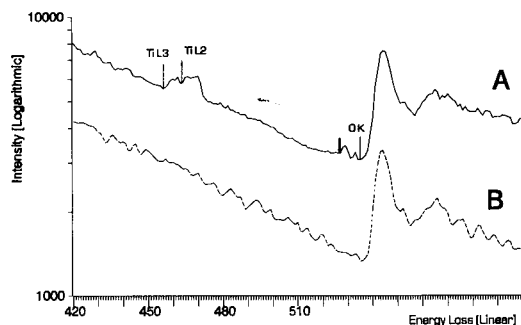


Fig. 7. Energy-loss spectrum of chrysotile asbestos modified with  $\text{TiCl}_3$  showing the titanium  $L_{2,3}$  and oxygen K edges after background subtraction and Fourier deconvolution (A). The dashed lines display the spectrum of the non-modified standard chrysotile fibres (B).

a cross-sectioned fibre. It shows the smaller fibrils within the fibre.

In the experimental curve in Fig. 7A the ELNES above the titanium  $L_{3,2}$  edge is indicated as well as the oxygen K edge. The spectrum was processed in the following way. The background absorption curve preceding the edge was fitted to an inverse power law  $AE^{-r}$  where  $E$  is the energy loss of the transmitted electron. The curve was extrapolated beyond the edge and subtracted. The remaining contribution of the inner-shell excitation was deconvoluted with respect to the low-loss spectrum (mainly interband transitions and plasmon loss) using a Fourier log deconvolution method. The spectrum reveals the  $L_{3,2}$  edges of titanium which are marked by prominent features with a sharp increase in intensity at the threshold of the edge. These features are caused by the excitation of the electrons from the  $2p_{3/2}$  ( $L_3$ ) and  $2p_{1/2}$  ( $L_2$ ) spin-orbit split levels to the unfilled  $3d$  levels [50]. The titanium  $L_{3,2}$  threshold peak shows two dissimilar peaks with multiplet structures at both  $L_3$  and  $L_2$ . In addition to the above, in comparison with the spectrum of the non-modified standard chrysotile fibre in Fig. 7B, a substantial variation in the near-edge fine structure of the oxygen K edge is observed. The appearance of a shoulder at the onset of the oxygen K edge in the spectrum of the  $\text{TiCl}_3$ -modified asbestos could be assigned to a state arising by hybridization of the oxygen



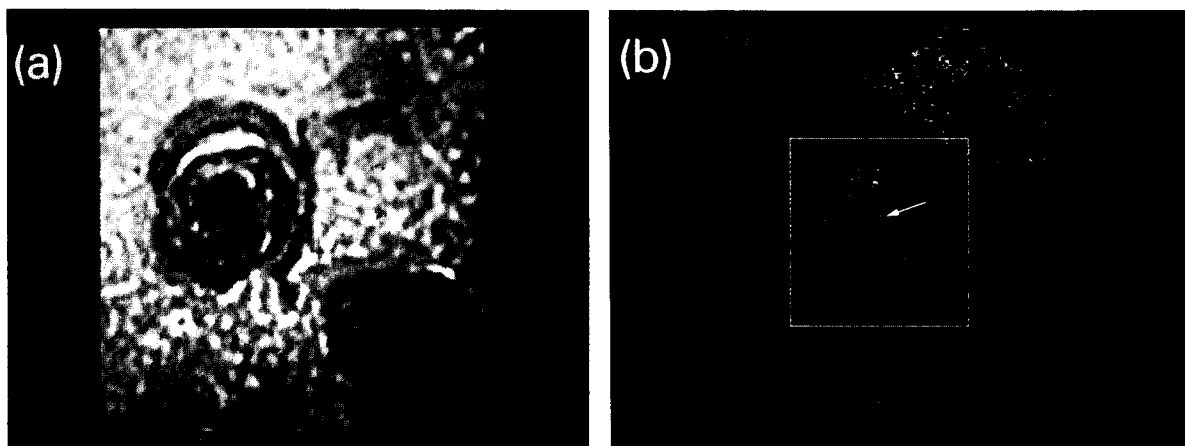


Fig. 8. (a) Brightfield image of a selected part of the analyzed area of a cross section of  $\text{TiCl}_3$ -treated chrysotile fibres embedded in a Spurr resin (full picture is 95 nm). (b) Net-titanium image obtained by calculating a background image at 460 eV with a least-squares fitting procedure.

$2p$  and the titanium metal  $3d$  level. This might be an indication that  $\text{TiCl}_3$  has chemically reacted with the chrysotile fibres.

Around the titanium  $L_{3,2}$  absorption edge, a series of ten energy loss images from 380 to 470 eV loss at a 10-eV interval were recorded. By using a data-analysis program, PV ~ WAVE (Precision Visuals, Boulder, CO), a least-squares fitting procedure was performed in parallel for all pixels in the series of images. The background counts underlying the characteristic core edge were subtracted from the measured intensity at each pixel by fitting and extrapolating the pre-edge spectrum. This calculation ensures that the images represent a true titanium distribution and not mass thickness variations.

Figure 8a displays the brightfield image of a selected part of the analyzed area at a higher magnification than in Fig. 8b, showing the fine structure of a cross section of a chrysotile fibril. The net titanium distribution image of the analyzed area is shown in Fig. 8b. In Fig. 9  $I(\Delta E)$  versus  $E$  is plotted, together with the fitted curve for the background  $I_b$ , for one pixel located on the asbestos section. The signal from the titanium  $L_{3,2}$  edge is seen as the clean rise above the extrapolated background. The procedure can be very easily modified to take the uncertainty on the intensities in the original images into account.

In this way, next to the net image, also a corresponding uncertainty image can be calculated which allows the identification of the area in the image with a net intensity significantly different from zero. By selecting different locations in the net image, the selected part of the EEL spectrum, its background and the cross sections through the net image at that location can be interactively inspected. An example of two orthogonal cross sections starting from one pixel located on the asbestos section is shown in Fig. 10a and b.

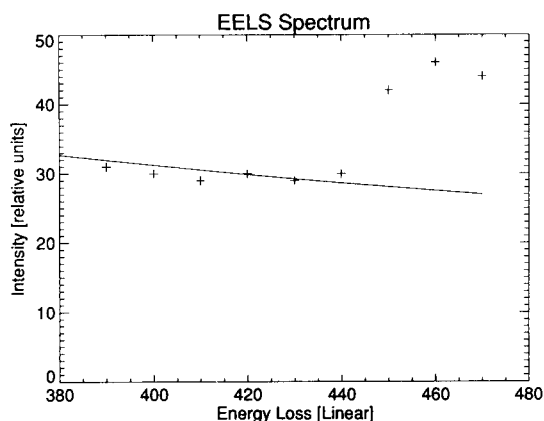


Fig. 9. Datapoints (+) of a selected part of the EEL spectrum at one pixel location near the surface of a fibril, together with the fitted curve of the background.

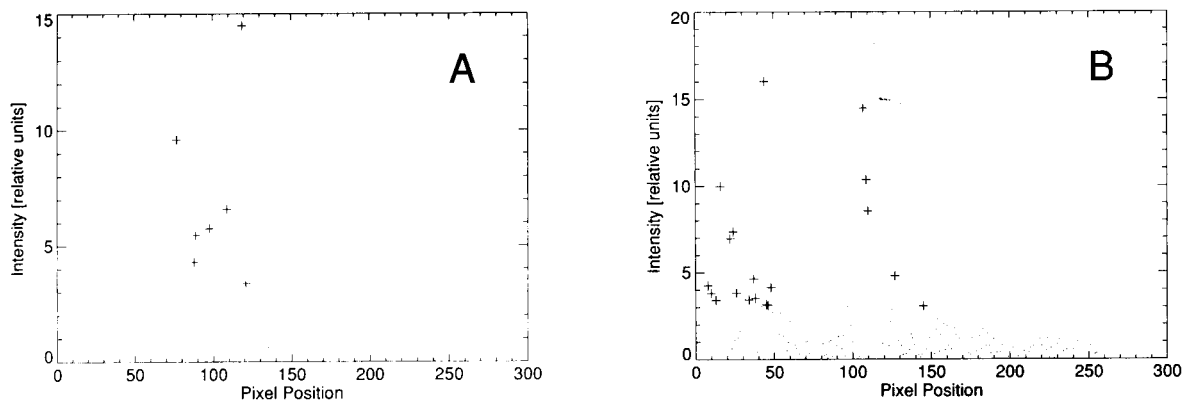


Fig. 10. (A) *x*-section and (B) *y*-section at this location through the net image, showing the pixels in the image with a net intensity significantly different from zero (+) while the other pixels (·) indicate noise.

From these images and other images we could conclude that the titanium atoms are concentrated at the surface of the fibre and form an encapsulation around the material. Some elemental maps display also a contribution of titanium inside the fibre tubes which follow a spiral curvature, typical for chrysotile asbestos. These results indicate that low *Z* core shell energy loss images from adequately prepared specimens can provide useful chemical information about asbestos fibres.

A.A. is a research fellow at NFWO/FNRS (Belgium). This work was funded by FKFO, Brussels and DPWB, Brussels (IUAP-III program).

#### REFERENCES

- 1 M. Grasserbauer and H.W. Werner, *Analysis of Micro-electronic Materials and Devices*, Wiley, Chichester, 1991.
- 2 R. Van Grieken and C. Xhoffer, *J. Anal. At. Spectrom.*, 7 (1992) 81.
- 3 D. Briggs and M.P. Seah, *Practical Surface Analysis*, Vol. 1, Auger and X-ray Photoelectron Spectroscopy, Wiley, Chichester, 1990.
- 4 J.L. Zilko and R.S. Williams, *J. Electrochem. Soc.*, 129 (1982) 406.
- 5 R.E. Ericson, *Surf. Interface Anal.*, 18 (1992) 381.
- 6 G.W. Stupian and P.D. Fleischauer, *Appl. Surf. Sci.*, 9 (1981) 250.
- 7 J.E. Castle, in T.L. Barr and L.E. Davies (Eds.), *Application of XPS Analyses to Research into the Causes of Corrosion*, Applied Surface Analysis, ASTM STP 699, American Society for Testing and Materials, Philadelphia, PA, 1980, p. 182.
- 8 T.E. Fischer, *J. Vac. Sci. Technol.*, 11 (1974) 252.
- 9 D.T. Clark, in D.W. Dwight, T.J. Fabisch and H.R. Thomas (Eds.), *The Modification, Degradation and Synthesis of Polymer Surfaces Studied by ESCA*, in Photon, Electron and Ion Probes of Polymer Structure and Properties, ACS Symp. Ser. Vol. 162, American Chemical Society, Washington DC, 1981, p. 247.
- 10 L. Köver, D. Varga, I. Cserny, J. Toth and K. Tötkei, *Surf. Interface Anal.*, 19 (1992) 9.
- 11 H.W. Werner, in L. Fiermans, J. Vennik and W. Dekeyser (Eds.), *Introduction to Secondary Ion Mass Spectrometry. Electron and Ion Spectroscopy of Solids*, Plenum Press, New York, 1978, p. 324.
- 12 M.P. Seah and G.C. Smith, *Surf. Interface Anal.*, 11 (1988) 69.
- 13 H. Ade, C.H. Ko, E.D. Johnson and E. Anderson, *Surf. Interface Anal.*, 19 (1992) 17.
- 14 *Ultramicroscopy*, 36 (1991) entire issue.
- 15 G.C. Smith and A.K. Livesey, *Surf. Interface Anal.*, 19 (1992) 175.
- 16 P.H. Holloway and T.D. Bussing, *Surf. Interface Anal.*, 18 (1992) 251.
- 17 A. Jablonski and K. Wandelt, *Surf. Interface Anal.*, 17 (1991) 611–627.
- 18 R.F. Egerton, *EELS in the Electron Microscope*, Plenum Press, New York, 1986.
- 19 J.J. Pireaux, C. Gregoire, M. Vermeersch, P.A. Thiry and R. Caudano, *Surf. Sci.*, 189/190 (1987) 903.
- 20 A.J. Bevolo, *Scanning Electron Microsc.*, IV (1985) 1449.
- 21 J.J. Pireaux, P.A. Thiry, R. Sporken and R. Caudano, *Surf. Interface Anal.*, 15 (1990) 189.
- 22 A. Benninghoven, F.G. Rüderer and H.G. Werner (Eds.), *Secondary Ion Mass Spectrometry; Basic Concepts, Instrumental Aspects, Applications and Trends*, Wiley, New York, 1987.
- 23 F.A. Stevie, *Surf. Interface Anal.*, 18 (1992) 81.

- 24 F. Michiels, W. Vanhoolst, P. Van Espen and F. Adams, *J. Am. Soc. Mass Spectrom.*, 1 (1990) 37.
- 25 A. Benninghoven, *Surface Sci.*, 35 (1973) 427.
- 26 J. Schwieters, H.G. Cramer, T. Heller, U. Jürgens, E. Niehuis, J. Zehnfening and A. Benninghoven, *J. Vac. Sci. Technol.*, A9 (1991) 2864.
- 27 B.T. Chait and K.G. Standing, *Int. J. Mass Spectrom. Ion Phys.*, 40 (1981) 185.
- 28 H. Van der Wel, J. Lub, P.T.N. Van Velzen and A. Benninghoven, *Microchim. Acta (Wien)*, 11 (1990) 3.
- 29 H. Van der Wel, P.N.T. Van Velzen, U. Jürgens and A. Benninghoven, in M. Grasserbauer and H.W. Werner (Eds.), *Analysis of Microelectronic Materials and Devices*, Wiley, Chichester, 1991, p. 461.
- 30 H.W. Werner and R.P.H. Garten, *Rep. Prog. Phys.*, 46 (1984) 221.
- 31 G.J.F. Legge, A. Saint, G. Bench, J. Laird and M. Cholewa, *Nucl. Instrum. Methods*, B64 (1992) 342.
- 32 M.B.H. Breese, J.P. Landsberg, P.J.C. King, G.W. Grime and F. Watt, *Nucl. Instrum. Methods*, B64 (1992) 505.
- 33 M. Takai, *Scanning Microsc.*, 6(1) (1992) 147.
- 34 P.C. Zalm, in A. Benninghoven, K. Janssen, J. Tümpner and H.W. Werner (Eds.), *Secondary Ion Mass Spectrometry SIMS VIII*, Wiley, Chichester, 1992, p. 307.
- 35 H.J. Heinen and R. Holm, *Scanning Electron Microsc.*, 111 (1984) 1129.
- 36 A.H. Verbueken, F.J. Bruynseels and R.E. Van Grieken, *Biomed. Mass Spectrom.*, 12(9) (1985) 438.
- 37 F. Adams, R. Gijbels and R. Van Grieken (Eds.), *Inorganic Mass Spectrometry*, Wiley, New York, 1988.
- 38 M. Pelletier, G. Krier, J.F. Muller, J. Campana and D. Well, in P.E. Russell (Ed.), *Microbeam Analysis — 1989*, San Francisco Press, San Francisco, CA, 1989, p. 1089.
- 39 G. Binnig and H. Rohrer, *Sci. Am.*, 235 (1985) 40.
- 40 M.A. Ray, G.E. McGuire, I.H. Musselman, R.J. Nemanich and D.R. Chopra, *Anal. Chem.*, 63 (1991) 99R.
- 41 Y. Kim and C.M. Lieber, *Scanning Microsc.*, 5(2) (1991) 311.
- 42 G. Binnig, C.F. Quate and C. Gerber, *Phys. Rev. Lett.*, 56 (1986) 930.
- 43 H.W. Zandbergen, W.T. Fu, G. Van Tendeloo, S. Amelinckx, *J. Cryst. Growth*, 96 (1989) 716.
- 44 M. Hein, P. Hoffmann, K.L. Lieser and H.M. Ortner, *Fresenius' Z. Anal. Chem.*, 343 (1992) 760.
- 45 B. Lengerer, *Microchim. Acta*, 1 (1987) 455.
- 46 A. Brown, P. Humphrey and J.C. Vickerman, in A. Benninghoven (Ed.), *Secondary Ion Mass Spectrometry SIMS VI*, Wiley, New York, 1987, p. 393.
- 47 S.R. Bryan, W.S. Larkin, J.H. Gibson and G.G. Leiniger, in A. Benninghoven (Ed.), *Secondary Ion Mass Spectrometry SIMS VI*, Wiley, New York, 1987, p. 369.
- 48 F.M. Kimmerle and P. Roberge, *US Pat.* 4,388,149 (1983).
- 49 D. Cozak, C. Barbeau, F. Gauvin, J.-P. Barry, C. DeBlois, R. De Wolf and F. Kimmerle, *Can. J. Chem.*, 61 (1983) 2753.
- 50 L.A. Grunes, R.D. Leapman, C.N. Wilker, R. Hoffmann and A.B. Kunz, *Phys. Rev. B*, 25 (1982) 7157.

# Scanning tunnelling microscopy of silicon surfaces

Herman B. Elswijk

*Philips Research, P.O. Box 80000, 5600 JA Eindhoven (Netherlands)*

(Received 21th September 1992)

## Abstract

The fundamentals and some applications of scanning tunnelling microscopy and scanning tunnelling spectroscopy are introduced. Atomic-scale studies of thermal cleaning, sputtering and Sb adsorption on Si(111) surfaces are discussed to illustrate the potential of the techniques.

*Keywords:* Surface techniques; Scanning tunnelling microscopy; Scanning tunnelling spectroscopy; Silicon

In the scanning tunnelling microscope (STM), a sharp metallic probe tip is brought close to a conducting sample surface to the point where the wavefunctions of electrons of the surface and of the outermost atom of the tip start to overlap. Electrons can then pass from the surface to the tip and vice versa by tunnelling through the vacuum barrier and a net tunnelling current will flow if a small bias is applied over the gap between sample and tip. The current will depend strongly on the amount of overlap of the electron wavefunctions and hence on the gap width. As the wavefunctions decay exponentially into the vacuum gap, the current depends exponentially on the gap width. As a rule of thumb, each 0.1 nm changes the current by an order of magnitude. The great sensitivity of the current to the gap width confers on the STM its capability to measure atomic corrugations on surfaces. In order to image a surface in atomic detail, the STM tip is laterally scanned over the surface while the current is kept constant by continuously adjusting the height of the tip. The required signal applied to the height actuator of the STM needle is a

direct measure of the topography of the sample surface.

In an alternative mode of operation of the STM, the position of the tip is kept constant and the current is measured while the voltage is varied. At a constant gap width the current changes with voltage because the number of electrons available for tunnelling depends on the voltage difference between the tip and the sample. This allows the instrument to be used as an electron spectroscopy tool with extremely high spatial resolution.

Both modes of operation are combined in scanning tunnelling spectroscopy (STS) where current–voltage ( $I$ – $V$ ) curves are measured as a function of position in a lateral scan. A fundamental problem in the use of the STM and in STS is that geometrical and electronic information are always intermixed. A protrusion in a topograph can be a result of the presence of an atom but can also result from a localized surface electronic state.

A number of excellent review articles on the STM and STS are already available [1–6]. Likewise, the theoretical foundations of tunnelling spectroscopy are well known from the investigation of bulk tunnel junctions [4,7,8]. The theory

*Correspondence to:* H.B. Elswijk, Philips Research, P.O. Box 80000, 5600 JA Eindhoven (Netherlands).

was applied to tunnelling spectroscopy with the STM in some recent publications [9–15]. This contribution attempts to cover the essentials of the theory of the STM and gives some selected examples of applications.

### ONE-DIMENSIONAL TUNNELLING

The potential energy diagrams in Fig. 1 illustrate a system consisting of a metal tip with a featureless density of electronic states, a sample with a distribution of surface states and the intermediate vacuum gap. If the tip and the sample are sufficiently far apart, the vacuum levels of the electron potential energy are equal (Fig. 1(top)).

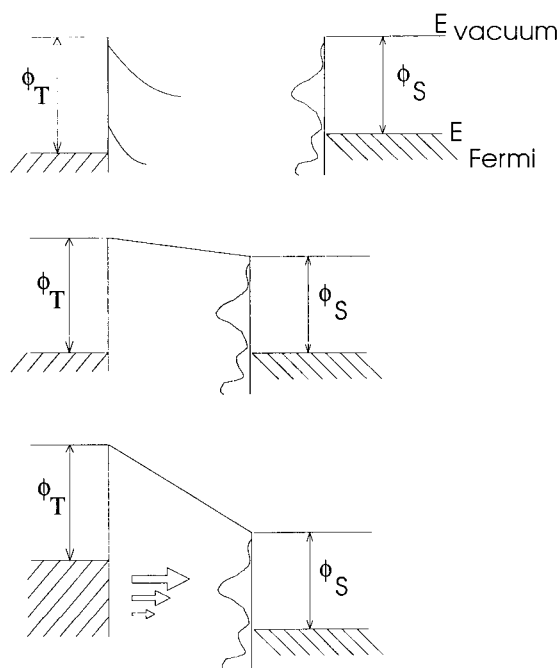


Fig. 1. Electron potential energy diagrams illustrating one-dimensional tunnelling between a conducting tip and a sample with a distribution of surface states.  $\phi_t$  and  $\phi_s$  are the work functions of tip and sample, respectively. In the upper part tip and sample are far apart, in the middle part they are in close contact and thermodynamic equilibrium and in the lower part a voltage difference is applied. The size of the arrows indicates the contribution to the total tunnelling current of the corresponding states.

The difference in the work functions of both materials then determines the difference in Fermi levels. Also indicated in Fig. 1(top) is the exponential decay of the quantum mechanical wavefunctions of the electrons into the vacuum. In the bulk the wavefunctions are periodic but in the vacuum they decay as  $A \exp\{-[2m(\phi - E)]^{1/2}(z/\hbar)\}$ , where  $z$  is the distance into the vacuum and  $E$  is the energy measured with respect to the Fermi level. The decay length is larger for wavefunctions with higher energy and consequently these wavefunctions penetrate further into the vacuum. If the tip and the sample are brought in close proximity, electrons will tunnel from the lower to the higher work function material and an electrostatic field will be set up in the tunnel barrier until thermodynamic equilibrium is achieved (Fig. 1(middle)). Both Fermi levels are then equalized and an approximately trapezoidal tunnel barrier is established. If a voltage difference is applied to the junction, a rigid shift is introduced in the energy diagram, as depicted in Fig. 1(bottom). In the case of a negative potential applied to the tip, electrons will tunnel from occupied states at the tip to empty states at the sample. The tunnel current depends on the density of states involved in the tunnelling process and on the transmission probability, which in turn depends on the height and shape of the barrier. The current can be expressed as [5]

$$I = \int_0^{eV} d_s(r, E) d_t(r, -eV + E) T(E, eV, r) dE \quad (1)$$

where  $V$  is the applied bias,  $e$  the elementary charge and  $d_s(r, E)$  and  $d_t(r, E)$  the density of states at location  $r$  at the sample and tip, respectively, and at energy  $E$  measured with respect to their individual Fermi levels.

Assuming a constant density of states at the tip, in the WKB approximation the transmission probability for planar electrodes is given by [8]

$$T(E, eV) = \exp\left[-\frac{z\sqrt{2m}}{\hbar} \left(\frac{\phi_s + \phi_t}{2} + \frac{eV}{2} - E\right)^{1/2}\right] \quad (2)$$

Then,

$$\begin{aligned} \frac{dI}{dV} = & d_s(r, eV)d_t(r, 0)T(eV, eV, r) \\ & + \int_0^{eV} d_s(r, E)d_t(r, -eV + E) \\ & \cdot \frac{dT(E, eV, r)}{dV} \cdot dE \end{aligned} \quad (3)$$

The first term in Eqn. 3 is the product of the density of states of the sample at the energy  $eV$

corresponding to the applied bias  $V$ , the density of states at the Fermi level at the tip and the tunnelling transmission probability  $T$ . The second integral contains the derivative of  $T$  vs.  $V$  and gives a slowly varying background on which the spectroscopic information is superimposed. From Eqn. 3 it is clear that electron spectroscopic information can be obtained with the STM, but only states which give an appreciable overlap with the tip states ( $T$  is sufficiently large) are visible to the STM. For example,  $d$  states of transition

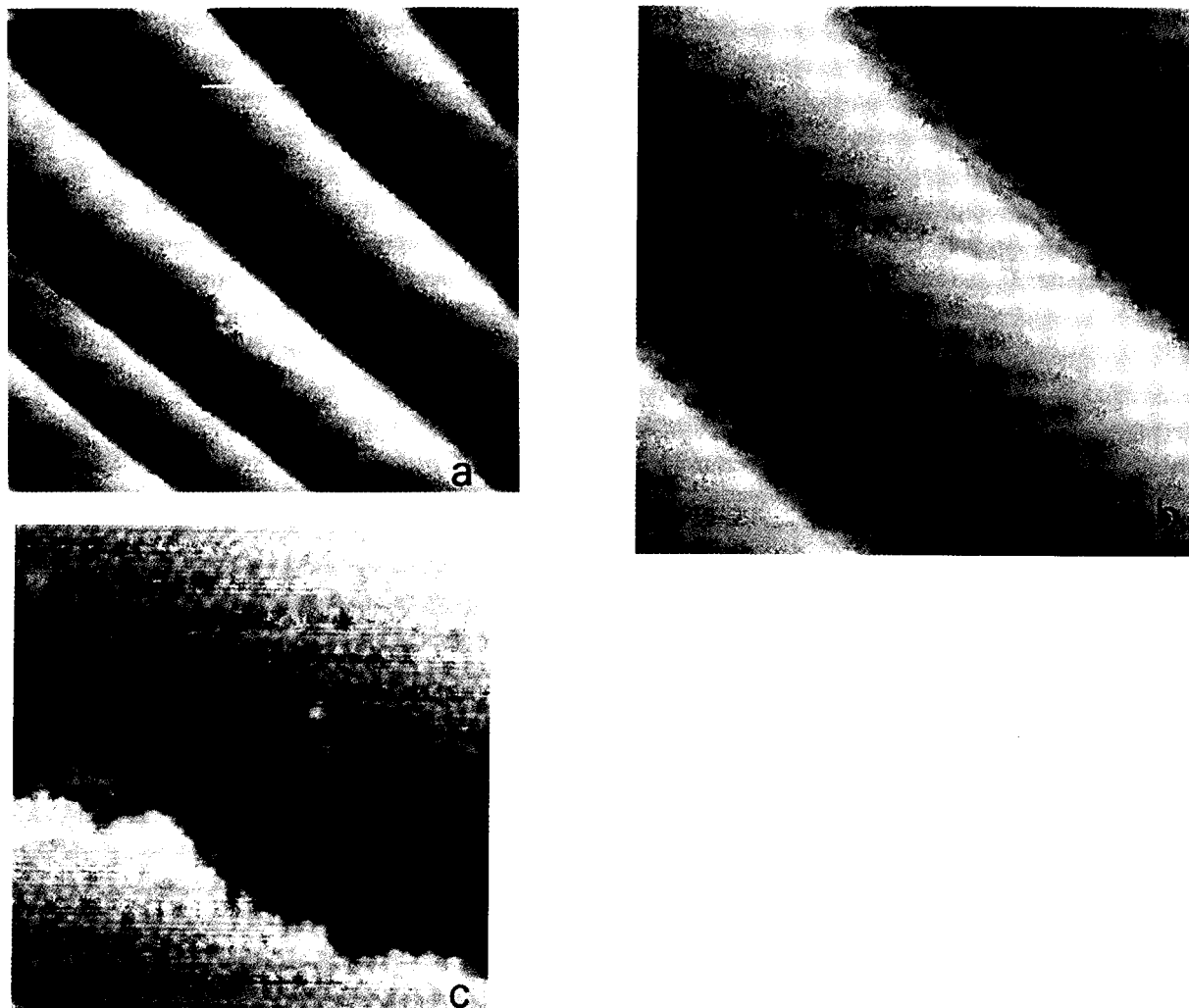


Fig. 2. STM images of a vicinal Si(111) surface cleaned by thermal flashing to 1500 K. (a)  $350 \times 350$  nm image. An array of steps running diagonally separates (111) oriented terraces. (b)  $80 \times 80$  nm image of the same surface; the steps are shown to be composed of multiple atomic steps. (c)  $20 \times 20$  nm image revealing the adatoms in the  $7 \times 7$  reconstruction and a step of two atomic layers high.

metals have a smaller principal quantum number than the outermost  $p$  and  $s$  orbitals (for Mo  $4d$ ,  $5s$  and  $5p$ ) and are located closer to the atomic core and turn out to be invisible in STM experiments [16]. Also, states which are further than a few electronvolts from the Fermi level are inaccessible, since at bias voltages exceeding the work function field emission occurs and the current is governed by standing wave states between tip and sample [17,18]. This makes true chemical identification of single atoms impossible in most instances.

#### SELECTED APPLICATIONS OF THE STM

Figure 2a–c show a clean vicinal Si(111) surface at three different magnifications. The surface was prepared in ultra-high vacuum (UHV) by outgassing at 900 K for 10 h followed by several flashes of a few seconds to 1500 K. The pressure never exceeded  $1 \times 10^{-9}$  Torr. The flashes are required to remove the oxide layer and to obtain a surface with well developed long-range order.

Figure 2a shows a regular array of steps separated by terraces with a normal in the [111]

direction. The macroscopic orientation of the vicinal Si(111) sample is  $3.8^\circ$  away from [111], giving rise to the steps in order to accommodate the misorientation. In Fig. 2b the steps are shown in more detail to reveal that they are composed of many monatomic steps. Recently, it has been shown that on vicinal Si(111) surfaces two phases exist: one with bunched steps and the other with monatomic steps depending on the misorientation angle and the temperature [19]. In Fig. 2c the well known atomic structure of the  $7 \times 7$  reconstruction of Si(111) can be observed in combination with a double atomic step.

In Fig. 3a and b the result of a different sample preparation procedure is shown. Here the sample was not flashed to 1500 K but kept at 1200 K for a few minutes instead. Also here the oxide is removed by evaporation but at this temperature the surface is very susceptible to carbon contamination from residual gases in the vacuum. The hydrocarbons crack at the hot surface and form carbides which are stable at this temperature. At 1500 K the carbides evaporate. The carbide clusters at the surface pin the step edges which move over the surface through the evaporation of Si. If evaporation is continued for some time the surface will roughen, which is detrimen-

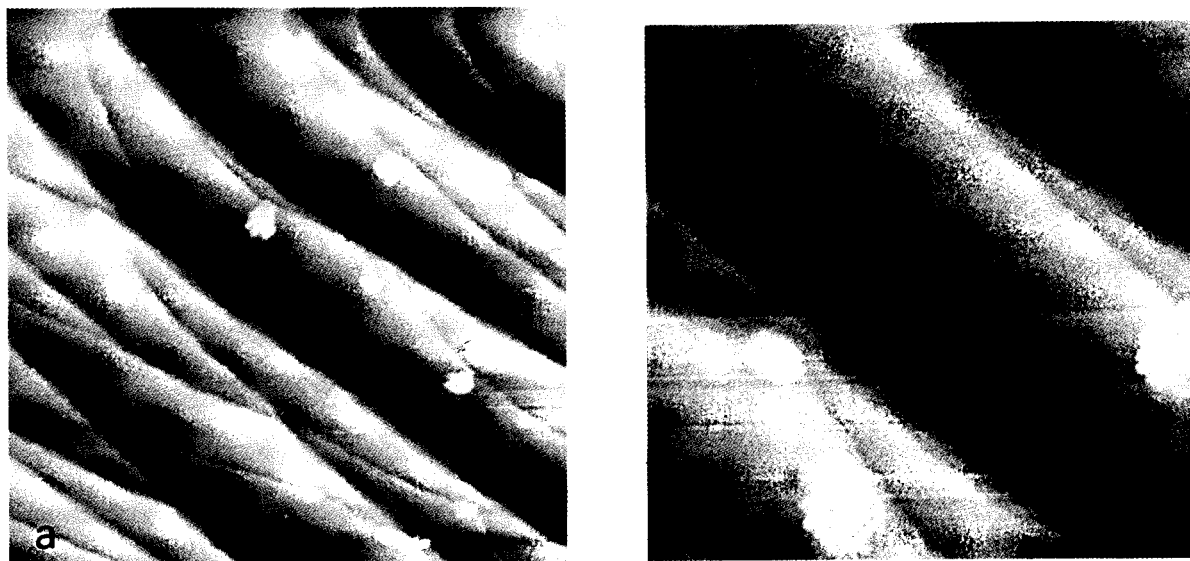


Fig. 3. STM images of a vicinal Si(111) surface cleaned by thermal flashing to 1200 K. Carbide particles remain on the surface and pin the steps. (a)  $400 \times 400$  nm; (b)  $80 \times 80$  nm.

tal for subsequent structuring processes such as molecular beam epitaxy. This study shows a strong point of the STM, i.e., the possibility of detecting isolated defects which are present at a low density. The concentration of carbon at the surface in Fig. 3 is much less than 1% and therefore very hard to detect with averaging techniques such as Auger spectroscopy, but it can still have a pronounced effect on the surface topography.

Another example of a recent study which makes use of this asset is an atomic-scale investigation of sputtering of Si surfaces [20]. Again some results on Si(111) are presented. Figure 4 shows a  $20 \times 20$  nm area on a  $7 \times 7$  reconstructed Si(111) surface after bombardment with  $\text{Ar}^+$  ions with an energy of 3 keV. The ion dose as determined from measuring the ion current in a Faraday cup was  $3 \times 10^{12}$  ions  $\text{cm}^{-2}$ , which translates into ca. 12 ion impacts on the imaged area. In a series of similar measurements there appeared to be an approximate 1:1 correlation between the density of “craters” induced by the ion impact and the ion dose. It was found that only the topmost layer of so-called adatoms in the  $7 \times 7$  structure was removed by the  $\text{Ar}^+$  ion impacts, a result which is in accordance with the conven-

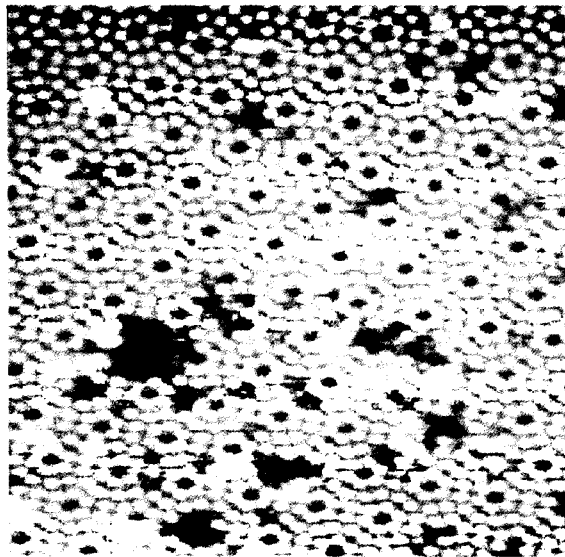


Fig. 4. Si(111) surface with defects which are induced by individual  $\text{Ar}^+$  ion impacts.

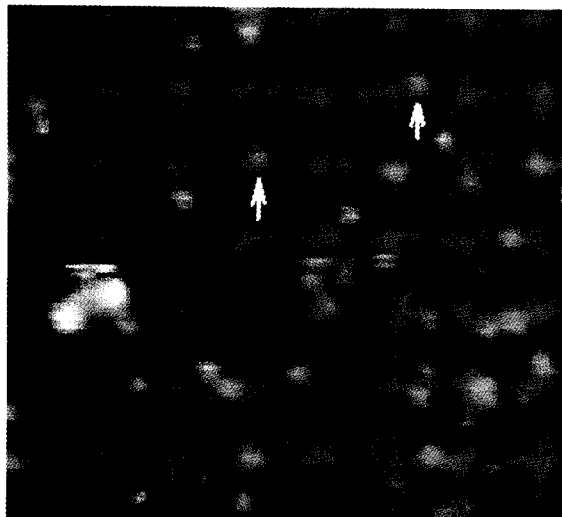


Fig. 5. Si(111) surface with 0.03 atomic layer Sb adsorbed imaged at  $-2.5$  V sample voltage. Arrows point to Sb atoms substituted for Si adatoms in the  $7 \times 7$  reconstruction.

tional models of sputtering where sputtering takes place only from the top layer of the surface.

In the next application of the STM, a study of adsorption of Sb on Si(111) surfaces the potential of STS is highlighted [21]. In Fig. 5, an Si(111)  $7 \times 7$  surface is depicted after adsorption of about 1% of an atomic layer of Sb at a temperature of 1000 K during adsorption. The applied bias voltage to the sample was  $-2.5$  V so tunnelling occurs from occupied states at the sample (tip at zero potential). Brightly imaging atoms can be distinguished (see arrows in Fig. 5) corresponding to the expected density of Sb atoms. The density of these bright spots increases with Sb coverage so that we concluded that they are Sb atoms. Careful examination of the registration of their position with the Si lattice showed that the Sb atoms substitute for Si adatoms in the  $7 \times 7$  reconstruction. These Si adatoms form three bonds with atoms of the underlying Si layer and have an unsaturated dangling bond sticking out into the vacuum and giving rise to a filled and empty electron state close to the Fermi level. An Sb atom with five valence electrons at the same position will also form three bonds with underlying Si atoms but will have a lone pair orbital sticking out into the vacuum. Owing to this pair



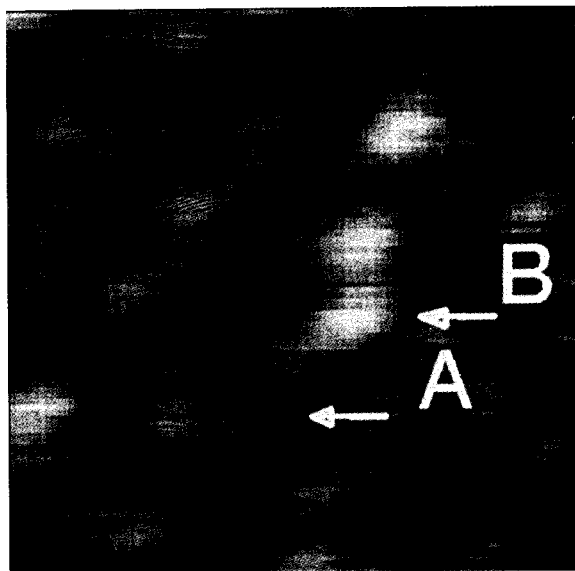


Fig. 6.  $3 \times 3$  nm image at  $-2.5$  V sample voltage of Si(111)  $7 \times 7$  cell with at some sites adsorbed Sb atoms (B site) and Si atom at others (A site).

formation, the density of filled states is higher. The higher density of filled states at Sb atoms as compared with Si atoms gives Sb the bright appearance in a constant-current topograph taken at negative bias applied to the sample. In Eqn. 1, if  $d_s$  is higher at the relevant energies,  $T$  should be lower at constant  $I$ , so  $z$  in Eqn. 2 is increased by the feedback mechanism of the STM and the atom appears higher, which is equivalent to brighter.

In Fig. 6 an area equal to about two  $7 \times 7$  cells is shown on which  $I-V$  spectra were acquired by temporarily holding the tip at a constant position, ramping the sample voltage between  $-2.5$  and  $+2.5$  V and measuring the current. Figure 7 shows the  $I-V$  spectra taken at (A) a Si adatom and (B) an Sb adatom. In the case of a Si adatom the current at small applied sample voltage is much larger than at an Sb adatom because of the presence of the dangling bond states close to the Fermi level. In Fig. 8 the value of the current at a voltage difference of  $0.5$  V applied to the sample is imaged as a function of position. This current image can be loosely interpreted as an image of

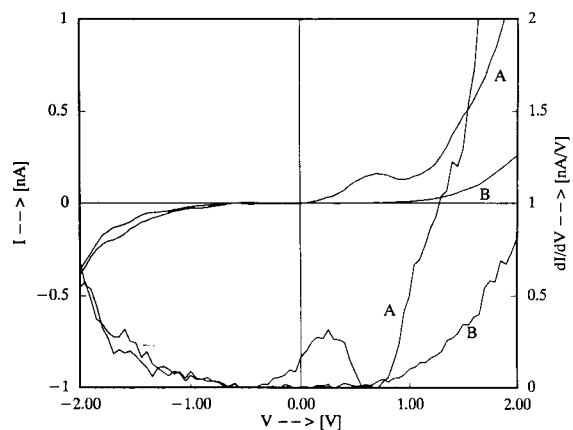


Fig. 7.  $I-V$  measurements taken at the Si adatom site indicated by A in Fig. 6 and at the Sb adatom site (B in Fig. 6). Top curves are the current vs. sample voltage and the bottom curves  $dI/dV$ . The empty dangling bond state is only apparent at the Si adatom.

the electron states between  $E_F$  and  $E_F + 0.5$  eV. It is immediately obvious that this empty state close to  $E_F$  is absent at the Sb adatom (B).

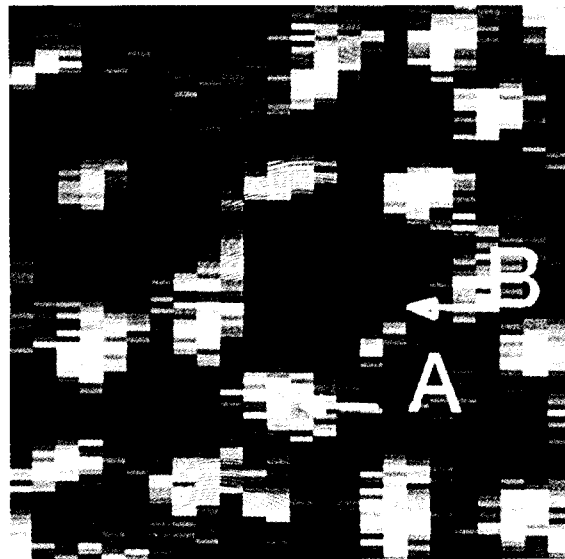


Fig. 8. A current imaging tunneling spectroscopy image of the same area as in Fig. 6. The current at  $0.5$  V sample voltage as a function of position is keyed to the brightness in the image. Sites A and B are indicated. At site B (Sb atom) the current at  $0.5$  V is smaller than at site A (Si adatom), indicating the absence of an unpaired dangling bond for the Sb atom.

Although the present example may suggest that chemical analysis is possible with the STM, this is not truly the case. Only because we already know which species is adsorbed on which substrate and we also know their chemical properties can we safely guess what the bright and dim features in the image are. If, however, we were to be confronted with an unknown sample with unknown adsorbates, it would be impossible to determine either, as the electrons that carry the chemically specific information, the core level electrons, are not accessible by the STM.

The author thanks H.J.W. Zandvliet and I.S.T. Tsong for their work on sputtering damage on Si(111) and E.J. van Loenen and D. Dijkkamp for many collaborative efforts.

#### REFERENCES

- 1 G. Binnig and H. Rohrer, *IBM J. Res. Dev.*, 30 (1986) 355.
- 2 G. Binnig and H. Rohrer, *Helv. Phys. Acta*, 55 (1982) 726.
- 3 G. Binnig and H. Rohrer, *Surf. Sci.*, 126 (1983) 236.
- 4 P.K. Hansma, *Tunnelling Spectroscopy: Capabilities, Applications, and New Techniques*, Plenum, New York, 1982.
- 5 R.J. Hamers, *Annu. Rev. Phys. Chem.*, 40 (1989) 531.
- 6 R.M. Tromp, *J. Phys. Condens. Matter*, 1 (1989) 10211.
- 7 E.L. Wolf, *Principles of Electron Tunnelling Spectroscopy*, Int. Series of Monographs on Physics, Vol. 71, Oxford University Press, Oxford, 1989.
- 8 J.G. Simmons, *J. Appl. Phys.*, 34 (1963) 1793.
- 9 N. Garcia, F. Flores and F. Guinea, *J. Vac. Sci. Technol.*, A6 (1988) 323.
- 10 J. Tersoff and D.R. Hamann, *Phys. Rev. B*, 31 (1985) 805.
- 11 J. Tersoff and D.R. Hamann, *Phys. Rev. Lett.*, 50 (1983) 1998.
- 12 A. Baratoff and B.N.J. Persson, *J. Vac. Sci. Technol.*, A (1988) 331.
- 13 B.N.J. Persson and A. Baratoff, *Phys. Rev. Lett.*, 59 (1987) 339.
- 14 N.D. Lang, *Phys. Rev. B*, 34 (1986) 5947.
- 15 C.J. Chen, *J. Vac. Sci. Technol.*, A6 (1988) 319.
- 16 N.D. Lang, *Phys. Rev. Lett.*, 58 (1987) 45.
- 17 R.S. Becker, J.A. Golovchenko and B.S. Swartzentruber, *Phys. Rev. Lett.*, 55 (1985) 987.
- 18 J.H. Coombs and J.K. Gimzewski, *J. Microsc.*, 152 (1988) 841.
- 19 R.J. Phaneuf and E.D. Williams, *Phys. Rev. Lett.*, 58 (1987) 2563.
- 20 H.J.W. Zandvliet, H.B. Elswijk, E.J. van Loenen and I.S.T. Tsong, *Phys. Rev. B*, 46 (1992) 758.
- 21 H.B. Elswijk, D. Dijkkamp and E.J. van Loenen, *Phys. Rev. B*, 44 (1991) 3802.

# Quantitation of species on catalyst surfaces

David M. Hercules, Marwan Houalla, Andrew Proctor and Joseph N. Fiedor

*Department of Chemistry, University of Pittsburgh, Pittsburgh, PA 15260, (USA)*

(Received 28th September 1992; revised manuscript received 20th November 1992)

## Abstract

Methodology for the quantitation of the distribution of oxidation states in reduced catalysts is reviewed. The adopted approach is based on curve fitting the x-ray photoelectron spectroscopy (ESCA, XPS) envelope using a non-linear least squares curve fitting (NLLSCF) routine. The procedure was applied to the study of the reduction of Mo/TiO<sub>2</sub> and Mo/Al<sub>2</sub>O<sub>3</sub> catalysts. The distribution of Mo oxidation states obtained by ESCA was corroborated by chemical measurements and correlated with catalytic activity. The limitations of the NLLSCF approach are discussed. It is shown that the uncertainties inherent in curve fitting methods can be minimized by the use of factor analysis. This data analysis technique provides an independent estimate of the number, positions, and shapes of components required to describe the Mo 3d envelopes in the reduced catalysts.

*Keywords:* Catalytic methods; Principal component analysis; Catalyst surfaces; Non-linear least squares curve fitting

The final stage in the preparation of supported catalysts often involves an “activation” step. This usually consists of reduction of the oxidic precursor, or reduction–sulfidation in the case of hydro-treating catalysts. The catalytic activity of the final catalyst is a function of the nature of the supported species present in the activated catalyst and their abundance. One can thus readily see the interest in quantitatively analyzing the distribution of supported species on catalysts surfaces. By varying the distribution of supported species and correlating the results with catalytic activity one can gain insight into the identity of the active species. This will allow “tailoring” of the catalyst preparation method to maximize the abundance of the active phase.

For catalysts which consist of “weakly interacting” carriers (SiO<sub>2</sub>, C) and oxides readily reducible to the metal (e.g., Rh<sub>2</sub>O<sub>3</sub>, PtO<sub>2</sub>, NiO, Co<sub>3</sub>O<sub>4</sub>), the structure of the supported phase in

its active form (i.e., reduced) can be adequately defined by conventional characterization techniques (gravimetric analysis, chemisorption measurements, electron microscopy, etc.). The situation is, however, more challenging for supported oxides which form intermediate oxidation states on reduction [e.g., (Mo, W, V, Cr, Re) oxides/Al<sub>2</sub>O<sub>3</sub>]. A careful study of the catalyst structure will require a detailed knowledge of the distribution of oxidation states for given treatment conditions.

Supported Mo catalysts are a dramatic illustration of the complexity of the active surfaces described above. These catalysts have been the subject of many investigations primarily because of their role in hydrotreating. It is well known, however, that depending on the activation conditions, they can catalyze a wide range of industrially important reactions. In their oxidic form, they catalyze selective oxidation reactions. Reduced Mo catalysts are active for metathesis, isomerization, hydrogenation and hydrogenolysis [1–15]. It was also quickly recognized that the versatility of

*Correspondence to:* D.M. Hercules, Department of Chemistry, University of Pittsburgh, Pittsburgh, PA 15260 (USA).

supported Mo catalysis is related to the formation of intermediate Mo oxidation states. However, direct correlation between the catalytic activity and the abundance of a specific oxidation state has been difficult to establish. This can be mainly ascribed to the lack of adequate means for measuring the distribution of Mo oxidation states in reduced Mo catalysts. In most instances, Mo oxidation states are inferred from gravimetric analysis (weight change on reduction or reoxidation) or volumetric measurements (amounts of  $H_2$  or  $O_2$  consumed during a redox cycle). While this approach provides a useful parameter for correlation with catalytic activity it can only measure an average Mo oxidation state. A direct measure of the distribution of Mo oxidation states can, however, be achieved by x-ray photoelectron spectroscopy (XPS, ESCA). This has been recently illustrated in the case of  $Mo/TiO_2$  and  $Mo/Al_2O_3$  catalysts [16,17]. The present paper is an overview of the methodology we have used for the determination of the distribution of Mo oxidation states in reduced  $Mo/TiO_2$  and  $Mo/Al_2O_3$  catalysts by XPS. The results are corroborated by other techniques (gravimetric measurements, data analysis procedures) and correlated with catalytic activity.

#### DISTRIBUTION OF Mo OXIDATION STATES IN REDUCED $Mo/TiO_2$ AND $Mo/Al_2O_3$ CATALYSTS

##### *Methodology*

The distribution of Mo oxidation states in reduced  $Mo/TiO_2$  and  $Mo/Al_2O_3$  catalysts was determined by XPS. The procedure involves curve fitting the ESCA Mo 3d envelope using a standard non-linear least squares curve fitting routine (NLLSCF) [18]. A detailed description of the methodology used for curve fitting and the assumptions made for quantitative analysis has been given [16,17]. The most salient features of the adopted approach are as follows. For a given system ( $Mo/TiO_2$  or  $Mo/Al_2O_3$ ) and a given oxidation state, the ESCA parameters were kept constant. For both systems and all Mo oxidation states, the  $Mo\ 3d_{5/2}/Mo\ 3d_{3/2}$  area ratio was set

equal to its theoretical value (3:2); the spin-orbit doublet separation ( $Mo\ 3d_{5/2}-Mo\ 3d_{3/2}$ ) was kept essentially constant (3.1–3.2 eV). An integral type background was assumed for each peak. Except for Mo metal [16,17], the  $Mo\ 3d_{5/2}/Mo\ 3d_{3/2}$  FWHM ratio was considered to be unity. One serious source of uncertainty in the methodology described above, is the assignment of Mo 3d binding energy values to a specific Mo oxidation state. This is due to the lack of availability of model compounds containing Mo with oxygen ligands in “intermediate” oxidation states [Mo(V), Mo(III), Mo(II)]. The limitations inherent in the use of NLLSCF routine will be addressed later.

##### *Distribution of Mo oxidation states in reduced $Mo/TiO_2$ catalysts*

The reduction studies were performed on a 5 wt.%  $Mo/TiO_2$  catalyst prepared by incipient wetness impregnation [16]. It has been previously shown [19] that the Mo phase is present as a surface compound.

Mo 3d XP spectra indicate a broadening of the Mo 3d envelope and a shift to lower binding energies with increasing the reduction temperature. The Mo 3d envelopes were curve-fitted according to the procedure described earlier. Representative curve-fitted spectra are shown in Fig. 1. The Mo 3d doublet binding energy values for the oxidic catalyst are characteristic of Mo(VI). Curve-fitting of the Mo 3d envelopes for catalysts reduced between 200 and 600°C indicates the presence of multiple oxidation states. Three doublets were required to curve-fit the Mo 3d envelope for the catalyst reduced at 304°C. These doublets, designated as A, B and C (Fig. 1), are attributed to Mo(VI), (V) and (IV) (as in  $MoO_2$ ), respectively. Curve fitting results for the catalyst reduced between 304 and 662°C indicate the presence of Mo oxidation states between (IV) and 0. The Mo 3d envelope of the catalyst reduced at 662°C was identical to that obtained for Mo metal. Figure 2 shows the distribution of Mo oxidation states in  $Mo/TiO_2$  catalysts reduced between 200 and 700°C. Note that for any given reduction temperature between 200 and 700°C, the catalyst surface contains at least three different Mo oxidation states. This is a clear

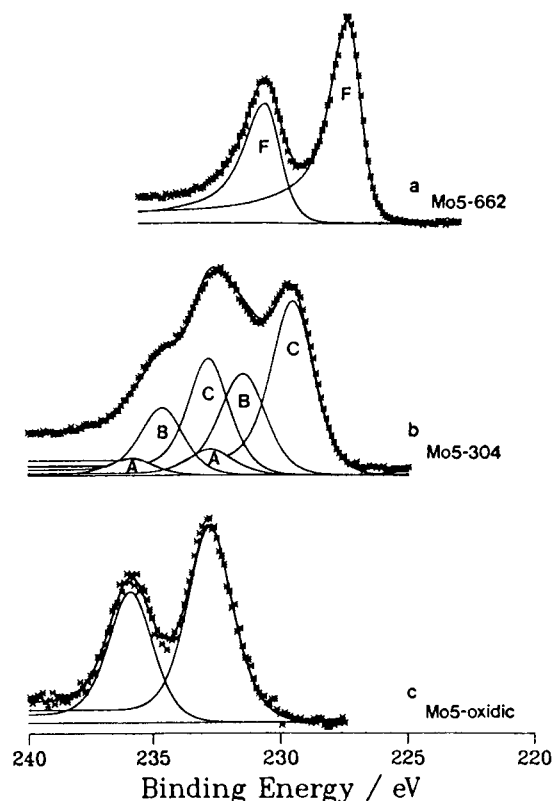


Fig. 1. Curve-fitted Mo 3d spectra of Mo/TiO<sub>2</sub> in the oxidic form Mo5 and after two reduction treatments at 304 and 662°C: (a) Mo5-662, (b) Mo5-304, (c) Mo5-oxidic. Doublets A, B, C and F refer to Mo oxidation states (VI), (V) (IV) and (0), respectively.

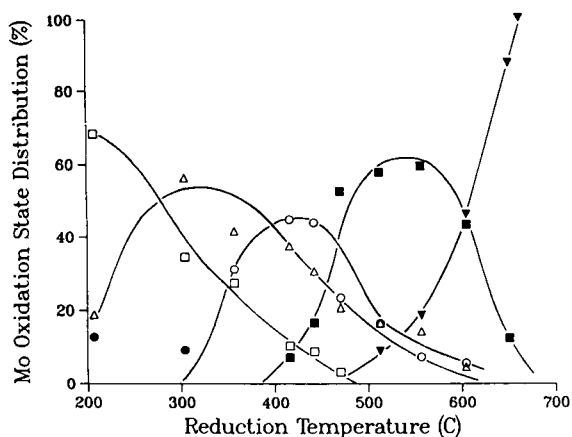


Fig. 2. Mo oxidation state distribution versus reduction temperature: (●) Mo(VI), (□) Mo(V), (△) Mo(IV), (○) Mo(III), (■) Mo(II), (▼) Mo(0).

illustration of the complexity of the reduced Mo catalysts surfaces described earlier in the Introduction.

#### Distribution of Mo oxidation states in reduced Mo/Al<sub>2</sub>O<sub>3</sub> catalysts

The methodology described above was applied to the study of the reduction of Mo/Al<sub>2</sub>O<sub>3</sub> catalysts. The catalyst used in the study (8% Mo/Al<sub>2</sub>O<sub>3</sub>) was prepared by incipient wetness impregnation [12] and reduced at various temperatures between 500 and 900°C. Figure 3 shows typical Mo 3d curve-fitted spectra for oxidic and reduced Mo/Al<sub>2</sub>O<sub>3</sub> catalysts. The Mo 3d<sub>5/2</sub>/3d<sub>3/2</sub> doublets are designated by their assigned oxidation states. The results show that in addition to Mo(VI) and Mo metal, intermediate Mo oxidation states Mo(V), (IV), (III) and (II) are formed on reduction. However, in variance with the results reported for the Mo/TiO<sub>2</sub> system which show that complete reduction to Mo metal can be achieved at 662°C, reduction of Mo/Al<sub>2</sub>O<sub>3</sub> catalysts at temperatures up to 900°C always leads to mixed oxidation states. The distribution of Mo oxidation states as a function of the reduction temperature is shown in Fig. 4 for Mo/Al<sub>2</sub>O<sub>3</sub> catalysts reduced between 500 and 900°C. Note the heterogeneity of the surface structure for catalysts reduced between 500 and 800°C (at least 4 different Mo oxidation states are detected at any given temperature). The Mo 3d binding energies for different oxidation states were the same as those obtained for the Mo/TiO<sub>2</sub> system. The full width of half maximum values (FWHM) obtained for the Mo 3d level were, however, consistently larger in the case of Mo/Al<sub>2</sub>O<sub>3</sub> catalysts.

#### Correlation with chemical measurements

The distribution of Mo oxidation states determined by ESCA was used to estimate the average Mo oxidation state for each reduction temperature. Details concerning the assumptions required for such determination are given in Ref. 17. The average Mo oxidation states estimated by XPS were compared to those determined by gravimetric analysis for Mo/TiO<sub>2</sub> (Fig. 5) or from oxygen consumption measurements for Mo/

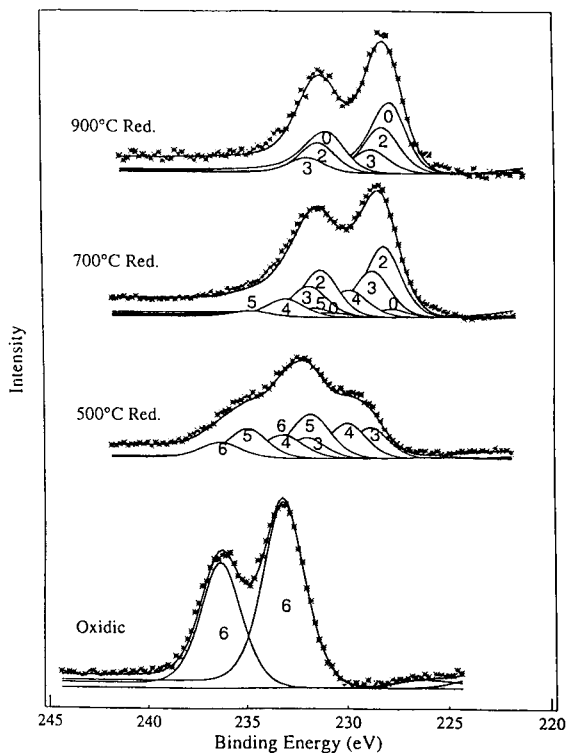


Fig. 3. Typical Mo 3d curve-fitted spectra for oxidic and reduced Mo/Al<sub>2</sub>O<sub>3</sub> catalysts. The Mo 3d<sub>5/2</sub>-3d<sub>3/2</sub> doublets are designated by their assigned oxidation states.

Al<sub>2</sub>O<sub>3</sub> (Fig. 6). Clearly, for both systems there is good agreement between the average oxidation state calculated from ESCA and that obtained by chemical measurements.

#### CORRELATION BETWEEN DISTRIBUTION OF Mo OXIDATION STATES AND CATALYTIC ACTIVITY

The purpose of the detailed analysis of the surface structure of reduced Mo/TiO<sub>2</sub> and Mo/Al<sub>2</sub>O<sub>3</sub> catalysts is to investigate how it correlates with the catalytic activity for various probe reactions. This should provide insight into Mo oxidation state requirements for various catalytic functions. Such Mo oxidation state/catalytic activity relationships have been investigated for benzene hydrogenation on reduced Mo/TiO<sub>2</sub> and Mo/Al<sub>2</sub>O catalysts. The results were described in detail elsewhere [16,17]. Recently, we have also

studied [20,21] the hydrogenolysis of propane on reduced Mo/Al<sub>2</sub>O catalysts. Figure 7 shows the comparison between propane hydrogenolysis activity measured at 250°C and the distribution of Mo oxidation states obtained by ESCA. The abundance of Mo(VI) (V) and (IV) are not shown for the sake of clarity. It can be seen from Fig. 7 that catalysts reduced at temperatures lower than 550°C which contain Mo oxidation states higher than Mo(II), are not active for this reaction. The sharp increase in activity observed for the catalyst reduced at 700°C coincides with the formation of

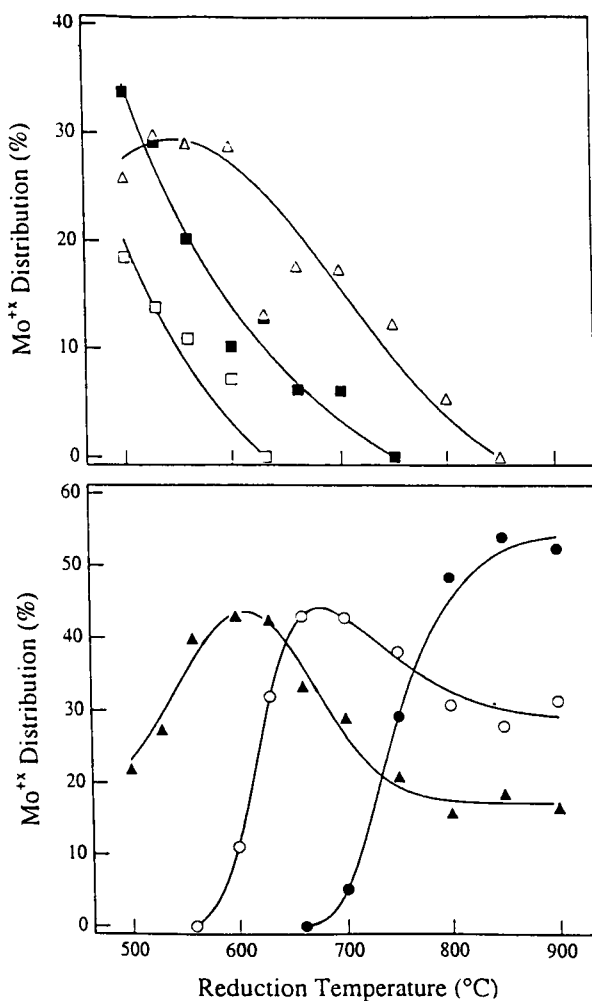


Fig. 4. Distribution of Mo oxidation states in Mo/Al<sub>2</sub>O<sub>3</sub> catalysts as a function of reduction temperature: (□) Mo(VI); (■) Mo(V), (△) Mo(IV); (▲) Mo(III); (○) Mo(II); (●) Mo(0).

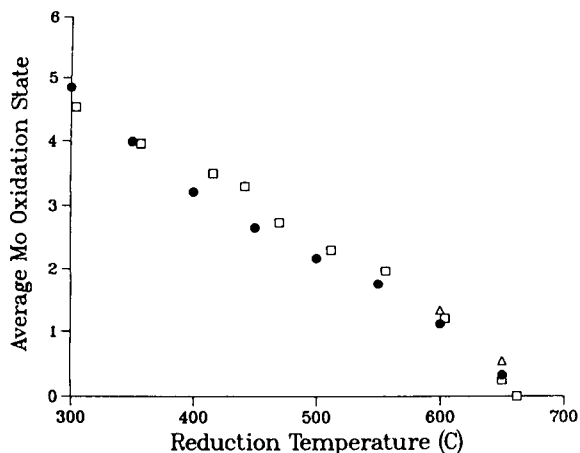


Fig. 5. Average Mo oxidation state versus reduction temperature from gravimetric analysis (●, △) and from curve-fitted ESCA Mo 3d spectra (□).

significant amounts of Mo metal. Figure 7 also shows a close correlation between the catalytic activity and the abundance of Mo metal. This suggests that Mo metal is the most active species for propane hydrogenolysis. Similar results were reported by Burwell and co-workers [5-8] for conventionally prepared and carbonyl based Mo/Al<sub>2</sub>O<sub>3</sub> catalysts.

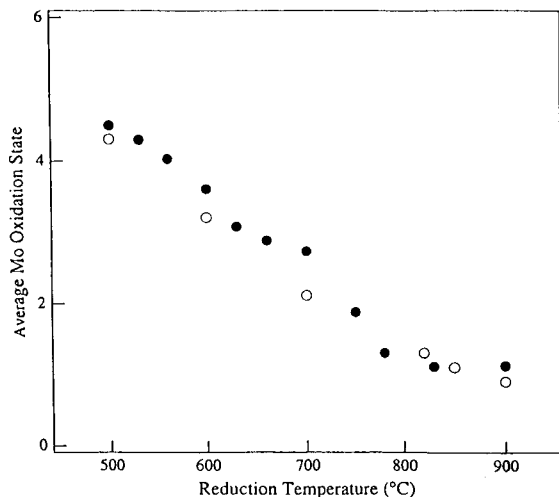


Fig. 6. Variation of the average Mo oxidation state in Mo/Al<sub>2</sub>O<sub>3</sub> catalysts estimated from XPS (■) and O<sub>2</sub> consumption measurements (○) as a function of reduction temperature.

#### FACTOR ANALYSIS FOR THE DETERMINATION OF THE DISTRIBUTION OF Mo OXIDATION STATES IN REDUCED CATALYSTS

As noted above, the distribution of Mo oxidation states was achieved by curve fitting the Mo 3d envelope using a non-linear least squares curve fitting (NLLSCF) routine [16,17]. While this approach is justified, there is frequently a significant uncertainty in the analysis because of the assumptions made in NLLSCF. The major problem with NLLSCF of XPS data lies in estimating the number and positions of components (Mo(VI), Mo(V) etc.) under the Mo 3d envelope. Unconstrained, a curve fitting routine will relax into a local minimum regardless of whether or not the result is spectroscopically meaningful. Thus some spectroscopic intuition must be exercised in the choice of curve fitting parameters such as peak positions and widths. However, this choice, especially for the intermediate Mo oxidation states, becomes extremely difficult because of the lack of appropriate model compounds. This highlights

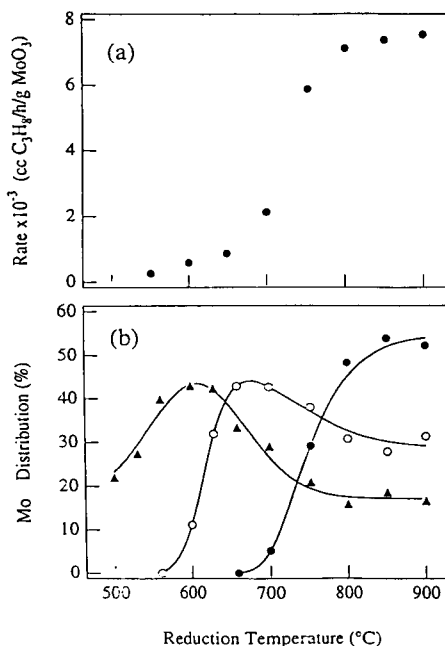


Fig. 7. (a) Propane hydrogenolysis rate versus reduction temperature. (b) Distribution of Mo oxidation states in Mo/Al<sub>2</sub>O<sub>3</sub> catalysts as a function of the reduction temperature: (▲) Mo(III); (○) Mo(II); (●) Mo(0).

the limitations associated with employing only one data analysis technique for evaluating the XPS envelope in reduced Mo catalysts. Therefore, it is desirable to have a complementary technique which would lend more credence to NLLSCF results. We have recently shown [22] that factor analysis (FA), which is comprised of principal component analysis (PCA) and target testing (TT), can provide an *independent* estimate of the number, positions, and shapes of components required to describe the XPS envelopes of Mo 3d in reduced Mo/TiO<sub>2</sub> catalysts.

#### Principle, methodology

The requirements for, as well as a detailed description of the overall FA technique are given

in Ref. 22. Figure 8 gives a short synopsis of the FA procedure performed in this work. As understood here FA is comprised of PCA and TT. PCA involves the decomposition of a data matrix (Fig. 8A: a series of Mo 3d spectra) into  $c$  abstract components (Fig. 8B: components which have no physical meaning in the spectroscopic sense). Through PCA it is possible to determine which abstract components account for signal ( $1 - n$ ) and which account for noise ( $n + 1 \dots c$ ). This study will focus on the weight of evidence obtained from several statistical methods, such as the  $F$  test, indicator function (IND), and the reduced eigenvalue (REV) ratio, as well as other non-statistical methods to determine  $n$ . A more detailed explanation for the determination of  $n$

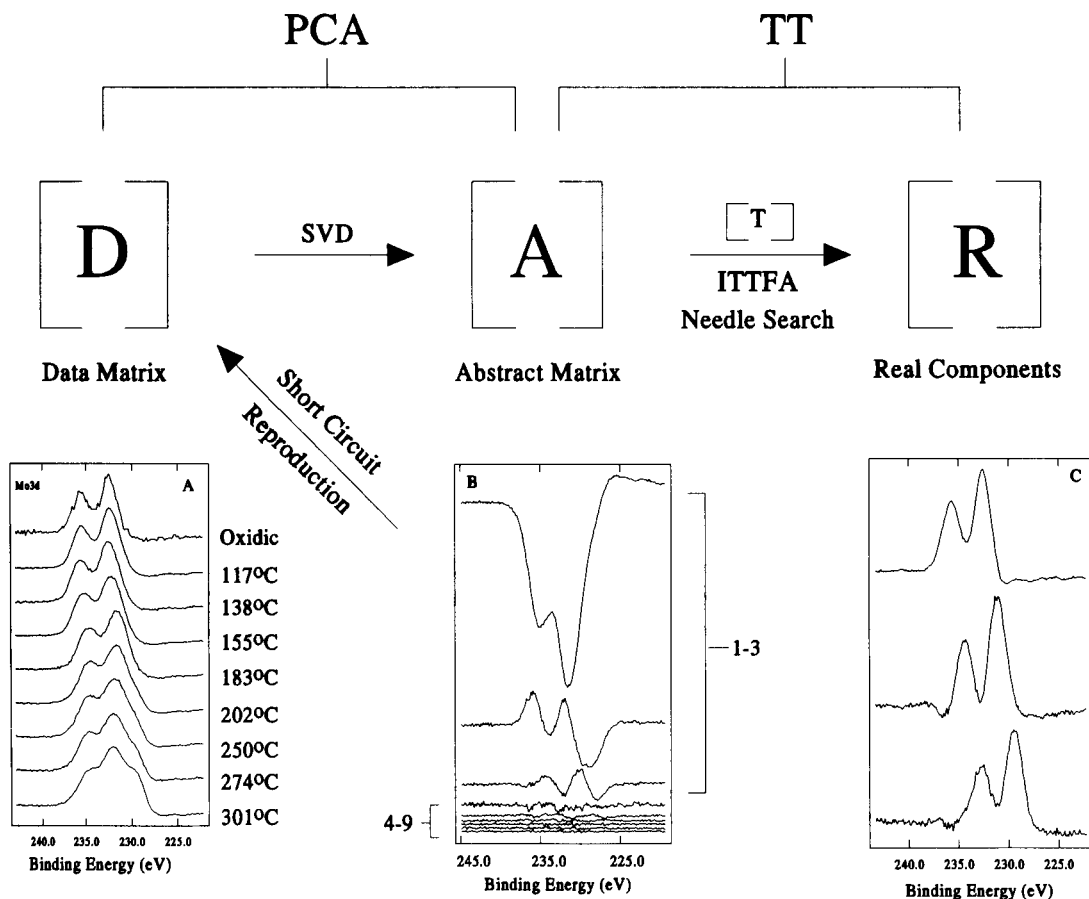


Fig. 8. Short synopsis of FA. (A) Original data matrix consisting of a series of Mo 3d spectra for oxidic and reduced 5 wt.% catalysts. (B) Abstract component matrix for the Mo 3d spectra of Fig. 8A. (C) Predicted Mo 3d spectra after several iterations.



by these various techniques can be found in Ref. 23. These criteria were chosen for this work because they do not require prior knowledge of the noise content in the original data matrix [23–26].

Once  $n$  has been determined, the next step is to transform these  $n$  abstract components into real spectroscopic components through TT (see Fig. 8C: real spectroscopic components). The main thrust of TT involves a target or test spectrum which is transformed into a predicted spectrum. The predicted spectrum is simply a weighted sum of the abstract components. The weighting coefficients or transformation vector [T] is derived from a least squares procedure which minimizes the differences between the test and predicted spectra. By using the  $n$ th predicted spectrum as the  $(n + 1)$ th test spectrum the process can be iterative [iterative target transformation factor analysis (ITTFA)] to produce a better match between test and predicted spectra. The key aspect of the iterative procedure is the applied constraints [22].

If there is a good understanding of the data then a reasonable guess may be made for the first test spectrum. Unfortunately, this may not always be possible. However, in these cases, it is possible to use a “needle” search to help find positional information about the individual peaks [23,26]. A “needle” search uses a series of  $N$  ( $N =$  number of points in a spectrum) test spectra where each spectrum is represented by a delta function. Thus the delta function has a value of unity at the  $p$ th data point and zero at all other data points. The delta function (i.e., test spectrum) is transformed into a predicted spectrum. The most likely position of the spectral peak corresponds to the data point where the test and predicted spectra are most similar. This is seen graphically by plotting the TT response (TTR = residual variance between the test and predicted spectra) as a function of the position of the delta function.

*Application: example for the use of FA to analyze the reduction of Mo / TiO<sub>2</sub> catalysts.*

*Principal component analysis.* Figure 8A illustrates the original data matrix used in PCA and TT. It consists of nine Mo 3d spectra from a series of reduced 5 wt.% MoO<sub>3</sub>/TiO<sub>2</sub> catalysts.

TABLE 1

Principal components analysis results for the data matrix consisting of the smoothed oxidic and reduced 5 wt.% MoO<sub>3</sub>/TiO<sub>2</sub> catalysts<sup>a</sup>

Factor	E.V.(%)	IND	Q(%)	REV ratio
1	96.436	$2.13 \cdot 10^{-4}$	$6.63 \cdot 10^{-4}$	26.81
2	3.185	$9.72 \cdot 10^{-5}$	0.10	8.31
3	0.334	$4.92 \cdot 10^{-5}$	0.33	16.02
4	0.018	$6.03 \cdot 10^{-5}$	25.82	1.44
5	0.010	$8.30 \cdot 10^{-5}$	33.24	1.31
6	0.006	$1.35 \cdot 10^{-4}$	41.57	1.28
7	0.004	$3.00 \cdot 10^{-4}$	54.29	0.56
8	0.004	$1.03 \cdot 10^{-3}$	52.68	0.84
9	0.003	0.00	0.00	1.00

<sup>a</sup> Results obtained using a smoothed oxidic spectrum. For identity of terms, see text.

It is evident from Fig. 8A that the original data matrix consists of more than one component. The PCA results for this data matrix are given in Table 1. The PCA criteria conclusively indicate the presence of *three* primary components. The IND function minimizes at the third factor, the  $Q$  value drops dramatically from factor 4 (25.82%) to factor 3 (0.3%), and the REV ratio rises strongly from factor 4 (1.437) to factor 3 (16.02).

Examining the abstract component matrix (Fig. 8B) offers a visual gauge in determining the number of importance of the primary components. The abstract components which exhibit shape (low frequency components) are considered to be responsible for signal and those which are random are responsible for the noise in the data matrix. The relative intensity, as well as the importance of the abstract components to the signal content in the original data matrix, decreases from component 1 to component 9. From this figure it is seen that the first three abstract components (1–3) represent the major portion of the signal while components 4–9 contain little or no low frequency information.

Through a process known as short circuit reproduction (see Fig. 8), a data matrix can be reconstructed using any number of abstract components. If *all* the abstract components are chosen for use, the original data matrix will be reconstructed *completely*. However, the original data matrix can be reconstructed with a high degree of

statistical significance (i.e., minus noise) by using only the  $n$  abstract components. Figure 9 shows the original data matrix (—) overlaid with a data matrix (\*) that has been reconstructed using the *three* primary components. The reconstructed data matrix overlays very well with the original data matrix, thus verifying that the original nine Mo 3d spectra consist of various combinations of only *three* components.

**Target testing.** The first step of TT was to carry out a “needle” search to obtain the binding energy values of the real spectral components. Since PCA indicated the presence of *three* primary components, the positions of the real spectral components will be located at the three largest maxima. Figure 10 shows the results of the “needle” search. The TTR shows the presence of three major peaks indicated by A, B, and C. The

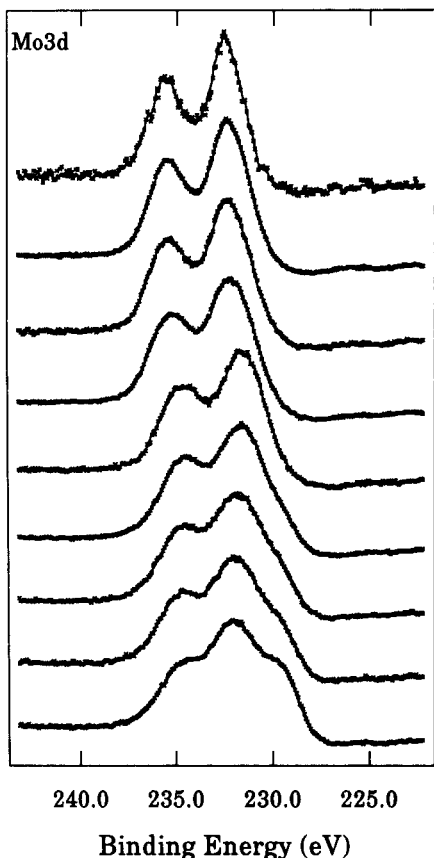


Fig. 9. Overlay of the original data matrix with a data matrix reconstructed using 3 components.

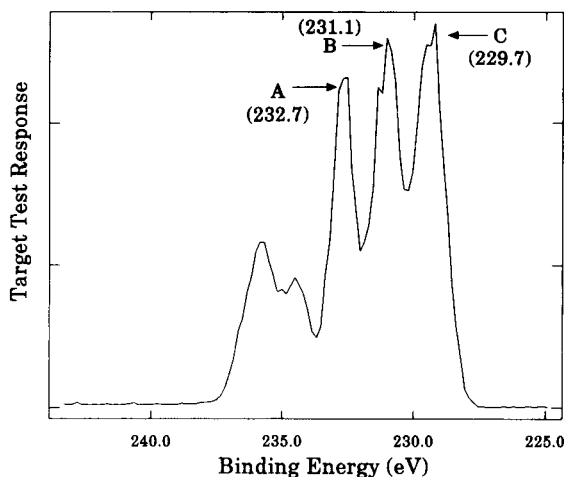


Fig. 10. The results of the “needle” search carried out on the experimental data matrix with the positions of the spectral components indicated by A, B and C.

positions of these peaks agree with those obtained earlier by NLLSCF [16] and are attributed to the Mo  $3d_{5/2}$  positions of Mo(VI), Mo(V), and Mo(IV). The presence of the response peaks around 236 eV simply correspond to the Mo  $3d_{3/2}$  peaks of Mo(VI) and Mo(V).

Transformation of the original delta function into true spectroscopic components was carried out by using the positions of the spectral components obtained from the “needle” search. The predicted spectra (Fig. 11) obtained from using the delta function as the test spectrum were rather crude but they did somewhat resemble normal Mo 3d doublets. However, it is clear that they exhibit features (i.e., negative portions) which are not characteristic of typical XPS spectra. Thus, it is necessary to apply certain constraints to obtain better representative Mo 3d spectra. The constraints applied modify the predicted spectra. These spectra are then used as the test spectra. This type of iterative procedure continues until there is little difference between the test and predicted spectra. Figure 8C shows the predicted spectra after several iterations. These spectra are overlaid with theoretical Mo 3d doublets (Fig. 12) used in the previous published NLLSCF analysis [16]. The similarity is remarkable considering that curve fitting uses sound theoretical knowledge about peak shapes while

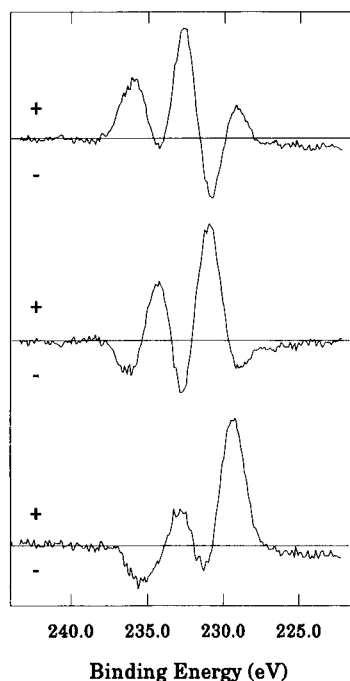


Fig. 11. Predicted components obtained using a delta function at points A, B and C: top plot, Mo(VI); middle plot, Mo(V); bottom plot, Mo(III).

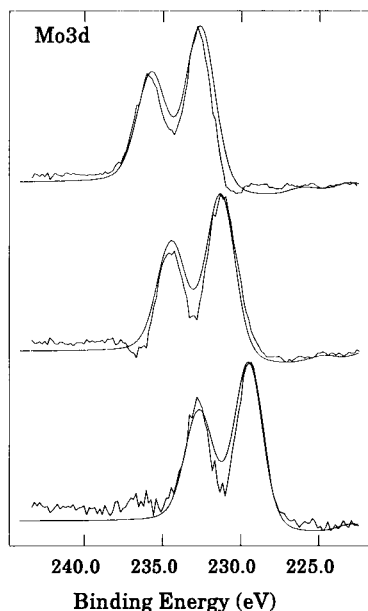


Fig. 12. Overlay of the predicted components with the theoretical Mo 3d doublets used in curve fitting: plots as in Fig. 11.

FA requires no such input. Thus in summary, F, performed on a series of reduced 5 wt.% MoO<sub>3</sub>/TiO<sub>2</sub> catalysts is able to determine the number, positions, and shapes of principal components (i.e., Mo oxidation states) in Mo 3d spectra *without any prior assumptions*. This should prove to be a valuable tool in assisting NLLSC analysis.

The authors acknowledge financial support for this work from the Department of Energy, Grant DE-FG02-87ER13781. J.N.F. acknowledges B.I. America for a graduate fellowship.

#### REFERENCES

- 1 W.K. Hall, in R. Vanselow and R. Howe (Eds.), *Chemistry and Physics of Solid Surfaces VI*, Springer Verlag Weinheim, 1986.
- 2 E.A. Lombardo, M. Lo Jicano and W.K. Hall, *J. Catal.*, **6** (1980) 150.
- 3 E.A. Lombardo, M. Houalla and W.K. Hall, *J. Catal.*, **5** (1978) 256.
- 4 W.S. Millman, D.C. Smrz, K. Segawa and W.K. Hall, *Polyhedron*, **5** (1986) 169.
- 5 R.L. Burwell, Jr., in S. Kaliaguine and A. Mahay (Eds.), *Catalysis on the Energy Scene*, Elsevier, Amsterdam, 1986, p. 45.
- 6 R.L. Burwell, Jr. and J. Chung, *React. Kinet. Catal. Lett.* **35** (1987) 381.
- 7 J. Chung, J.P. Zhang and R.L. Burwell, Jr., *J. Catal.*, **11** (1989) 505.
- 8 J. Chung and R.L. Burwell, Jr., *J. Catal.*, **116** (1989) 51.
- 9 A. Wambeke, L. Jalowiecki, S. Kasztelan, J. Grimblot and J.B. Bonnelle, *J. Catal.*, **109** (1988) 320.
- 10 Y. Holl, R. Touroude, G. Maire, A. Muller, P.A. Engelhard and J. Grosmanin, *J. Catal.*, **104** (1987) 202.
- 11 Y. Holl, F. Garin, G. Maire, A. Muller, P.A. Engelhard and J. Grosmanin, *J. Catal.*, **104** (1987) 211.
- 12 A. Redey, J. Goldwasser and W.K. Hall, *J. Catal.*, **11** (1988) 82.
- 13 K. Segawa, D.S. Kim, Y. Kurusu and I.E. Wachs, in M. Phillips and M. Ternan (Eds.), *Proceedings of the 9th International Congress on Catalysis*, The Chemical Institute of Canada, Ottawa, 1988, p. 1960.
- 14 W. Grünhert, A.Y. Stakheev, R. Feldhaus, K. Anders, E.S. Shpiro and K.M. Minachev, *J. Phys. Chem.*, **95** (1991) 1323.
- 15 W. Grünhert, A.Y. Stakheev, W. Mörke, R. Feldhaus, K. Anders, E.S. Shpiro and K.M. Minachev, *J. Catal.*, **13** (1992) 269.
- 16 R.B. Quincy, M. Houalla, A. Proctor and D.M. Hercules, *J. Phys. Chem.*, **94** (1990) 1520.

- 17 M. Yamada, J. Yasumaru, M. Houalla and D.M. Hercules, *J. Phys. Chem.*, 95 (1991) 7037.
- 18 A. Proctor and D.M. Hercules, *Appl. Spectrosc.*, 38 (1984) 505.
- 19 R.B. Quincy, M. Houalla, A. Proctor and D.M. Hercules, *J. Phys. Chem.*, 93 (1989) 5882.
- 20 J. Yasumaru, M. Yamada, M. Houalla, W.K. Hall and D.M. Hercules, *J. Phys. Chem.*, submitted for publication.
- 21 J. Yasumaru, M. Yamada, M. Houalla and D.M. Hercules, in *Proceedings of the 10th International Congress on Catalysis, Budapest, 1992*.
- 22 J.N. Fiedor, A. Proctor, M. Houalla and D.M. Hercules, *Surf. Int. Anal.*, in press.
- 23 E.R. Malinowski, *Factor Analysis in Chemistry*, Wiley, New York, 2nd ed., 1991.
- 24 E.R. Malinowski, *J. Chemom.*, 3 (1988) 49.
- 25 E.R. Malinowski, *J. Chemom.*, 4 (1990) 102.
- 26 P.J. Gemperline and J.C. Hamilton, in H.L.C. Meuzelaar (Ed.), *Computer-Enhanced Analytical Spectroscopy*, Vol. 2, Plenum, New York, 1990, p. 40.

# Surface analysis for the investigation of electrochemical and corrosion systems

Peter M.A. Sherwood

*Department of Chemistry, Willard Hall, Kansas State University, Manhattan, KS 66506 (USA)*

(Received 8th September 1992; revised manuscript received 4th January 1993)

## Abstract

The use of surface analysis in investigating electrochemical and corrosion systems is discussed. In particular x-ray photoelectron spectroscopy (XPS) in both the core and valence band region are described. Examples are given for metallic and carbon fiber electrode systems, and the role of core XPS chemical shifts analyzed by curve fitting is demonstrated. Valence band XPS is shown to have the ability to probe subtle differences in chemical structure, and is more effective in this respect than core XPS. Unfortunately, since all compounds possess valence electrons, the spectra contain features that cannot readily be interpreted without the help of reliable calculations. Examples illustrate how X-alpha cluster and other calculations can be used to interpret such spectra, allowing subtle chemical differences to be detected and thus enabling the approach to be used as a sensitive analytical surface chemistry probe. New  $X\alpha$  and ab initio calculations for the valence band of tetragonal  $ZrO_2$  are presented.

*Keywords:* Surface techniques; Corrosion; X-ray photoelectron spectroscopy

Electrochemical processes that involve reactions of the electrode are a surface chemical process, since the bulk of the electrode merely serves as an electrical connection to the electrode surface. Many corrosion processes are electrochemical in nature. This paper will focus upon the use of surface analysis, particularly x-ray photoelectron spectroscopy (XPS or ESCA) in both the core and valence band region, in investigating such systems.

The key to understanding electrochemical processes that involve the electrode is thus to determine the surface chemistry of the electrode. This may be quite complex, involving subtle chemical changes. In metal systems oxidation will often occur at appropriately oxidizing potentials leading to a range of oxides, hydroxides and oxohy-

droxides. In fact oxohydroxides are quite commonly involved in electrochemical process, and these compounds may often contain variable oxidation states. In carbon electrode systems electrochemical oxidation may lead to hydroxy, epoxy, keto, or carboxylic acid groupings. The analytical challenge is to be able to determine which of these species is present under particular conditions.

An important added complication is the fact that electrochemical processes occur in solution, but the analysis of the surface chemistry often requires the electrode to be removed from solution and placed in a vacuum system. This approach means that ex situ analytical techniques must be used. Valuable information has been obtained from in situ analytical techniques such as Raman and infrared (IR) spectroscopy, but this method cannot provide all the information required about all systems. They are not inherently surface sensitive, but may provide valuable

*Correspondence to:* P.M.A. Sherwood, Department of Chemistry, Willard Hall, Kansas State University, Manhattan, KS 66506-3701 (USA).

surface information because the spectroscopic information is clearly coming only from the surface region (such as for carbon monoxide adsorbed on a nickel metal surface). The traditional range of *ex situ* surface analytical techniques will of course provide information only about the surface region, but the sample must be taken from the electrode into a vacuum system. This presents the problem that the sample surface may react with the atmosphere during the transfer process, and the sample may decompose by being placed in an ultra-high vacuum (UHV) system, and as a result of the surface analytical probe being used. Thus electron and ion beams may decompose the surface, and the electrical double layer may decompose and hydroxides and oxohydroxides decompose and dehydrate in the vacuum system. Therefore careful monitoring of decomposition and surface chemical changes is needed when *ex situ* surface analytical techniques are used, however these techniques provide very valuable information about many of these systems.

In the case of corrosion systems a highly complex surface chemistry often results. If corrosion is to be understood and prevented this chemistry needs to be understood. Real corrosion systems are not normally single crystals, are frequently amorphous, and often contain impurities. They therefore provide a particularly serious challenge to the surface scientist.

Ultra-high vacuum surface analytical techniques have been successfully applied to electrochemical and corrosion systems for a number of years [1,2]. In particular the problem of transfer from the electrochemical cell (or environment for interaction of the solid with the solution) has involved the construction of a variety of electrochemical cells inserted into the vacuum system of a subsidiary chamber attached to the main surface analytical area. In the author's laboratory this is done by having a UHV chamber designed with gate valves which allow an electrochemical cell to be introduced from the bottom, and a Luggin capillary tube from the top so that the electrochemical or solution exposure experiment can be performed in an inert atmosphere, and then all the glass cell components removed from the UHV chamber and the electrode surface

pumped down to UHV. An important feature of this approach is that it allows the electrode surface to be examined and prepared under UHV conditions before exposure to the solution in the cell. While this type of approach is still *ex situ*, it does allow the method of sample transfer from solution to the surface analytical region with the minimum of surface chemical change.

A range of surface analytical techniques could be applied to this situation, but in this paper a focus will be placed on methods which will allow surface chemical information to be applied to a range of samples, amorphous or crystalline, and samples which may have significant impurities present. In particular XPS in the core and valence band region has considerable potential for extracting important surface chemical information.

Core XPS gives chemical shifts which can be used to identify surface chemistry, but often these shifts are quite small, and indeed compounds that are chemically different may not give different chemical shifts. Thus epoxide groupings will give the same core O1s binding energy as hydroxide groupings. Different oxides frequently give the same O1s chemical shift. So, while valuable, core XPS still leaves considerable uncertainty about surface chemical differences.

Valence band XPS gives a spectrum which depends upon the changes in energy levels that arise due to the way in which the molecular orbitals are composed of various atomic orbitals, and thus is very sensitive to subtle chemical differences. The valence band region (0–30 eV binding energy) will be present for all materials, so the challenge is to be able to understand the main valence band features, and to be able to relate these to surface chemical changes. Model compounds (i.e., compounds whose composition is known) may be helpful in generating sample spectra, but since one can never be sure that the surface of a compound is representative of its bulk composition, then there is always uncertainty associated with the use of model compounds. In the author's laboratory the valence band spectra of model compounds is recorded for model compounds whose bulk composition has been determined by x-ray powder diffraction

methods. However the most important analytical component is to generate an expected valence band spectrum by calculating the spectrum from a molecular orbital calculation based upon a model cluster representative of the bulk surface composition.

#### CALCULATION APPROACHES

Calculations using the  $X\alpha$  multiple scattered wave method (a useful review of this method has been provided by Case [3]) have been found to be especially valuable (examples from the author's laboratory are given in [4–16]) in interpreting the valence band region. Useful results can also be obtained by using extended basis set ab initio methods. The approach is based upon taking a cluster of sufficiently large size to represent the solid surface under study. In the case of ionic materials this involves taking a charged cluster, but the  $X\alpha$  method provides a convenient method for such systems by placing an oppositely charged sphere (the Watson sphere) around the ion so that a neutral species is calculated. An important aspect of this approach is that the calculation provides information about *differences* between peaks in the spectrum. Since the difference between peaks in the valence band can accurately be calculated, and is unaffected by any sample charging effects, the approach has considerable analytical potential.

Figure 1 illustrates spectra calculated using this approach. The calculated spectra [in (b) and (c)] are compared with the experimental spectrum in (a) which has had a Tougaard type background removed [17,18]. The calculated spectra are shown as being composed of a number of component calculated peaks (these are not attempts to fit experimental data) which correspond to the calculated energy level positions. The area under the peaks are obtained by multiplying the number of electrons by the atomic population for the level adjusted by the appropriate atomic photoelectron cross-section (in this case using the values of Scofield [19]). The process has been described in more detail elsewhere [11]. The experimental data correspond to the

tetragonal form of  $ZrO_2$  (yttria-stabilized zirconia) and is taken from the work of Majumdar and Chatterjee [20]. In both of the calculated spectra a  $ZrO_8^{12-}$  cluster is used. In the X-alpha case (Fig. 1b) an oppositely charged Watson sphere is placed around the cluster. In the extended bases set ab initio case, the cluster is surrounded by an octahedral symmetry set of eight positive charges. In both cases the calculated spectra were aligned with the experimental spectra since we are interested in the width and relative peak separations in the valence band. Calculation details are given in Table 1. For X-alpha calculations the atomic character is readily obtained. For the ab initio case the net atomic populations were used (using the Gelius model approach [21]). These calculations were carried out using the HONDO program and both calculations were performed on an IBM RISC/6000 Model 320 computer with 1.25 GB of hard disk space. The ab initio calculation needing substantial quantities of disk space is needed for

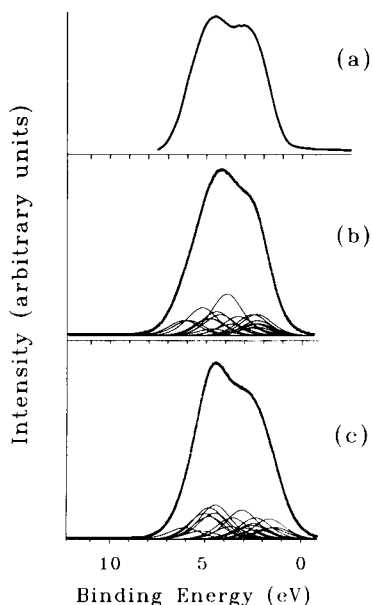


Fig. 1. XPS outer valence band region of tetragonal  $ZrO_2$  (yttria-stabilized zirconia) from the data of Majumdar and Chatterjee [20] using monochromatic aluminum x-radiation shown in (a) with a Tougaard background removed. This spectrum is compared with a spectrum generated from an  $X\alpha$  calculation in (b) and from an ab initio calculation in (c) in both cases using a  $ZrO_8^{12-}$  cluster.

TABLE 1

Parameters used and features of the calculations of a tetragonal  $ZrO_8^{12-}$  cluster( $\alpha$  Values in the  $X\alpha$  calculation: outer = intersphere, 0.74000; zirconium, 0.70424; Oxygen, 0.74447. Maximum  $l$  value in the  $X\alpha$  calculation: outer, 4; zirconium, 4; oxygen, 1. Basis sets in the ab initio calculation: zirconium, STO-6G; oxygen, 6-31G)<sup>a</sup>

Symmetry	$D_{2d}$	
Symmetry of point charges (ab initio)	$O_h$	
Distance of point charges from Zr (ab initio)	2.2675 Å for a charge of 2.5 units	
Zr–O bond lengths (Å)	2.0647 (4)	2.4634 (4)
$X\alpha$ -zirconium sphere radius (Å)	1.5175	
$X\alpha$ -oxygen sphere radius (Å)	1.1600 (4)	1.4652 (4)
$X\alpha$ -outer sphere radius (Å)	3.9286	
$X\alpha$ -Watson sphere radius (Å)	2.2640	
$X\alpha$ -virial ratio ( $-2T/V$ ) <sup>a</sup>	1.00364	

*X $\alpha$ -convergence:* When the difference in potentials at the beginning and end of the iteration were less than  $10^{-5}$  of the potential at the start of the iteration. This gives energy levels that differed by less than  $10^{-6}$  Rydbergs between the last two iterations

*X $\alpha$ -treatment of core electrons:* “Thawed” so that they retained atomic character while being fully included in the iterative process. Alls, Al2s, and O1s electrons were treated as core electrons

<sup>a</sup>  $T$  = Potential energy;  $V$  = kinetic energy;  $l$  = secondary quantum number.

integral storage (there were nearly 12 million two electron integrals that needed to be stored). When symmetry is not used the number of integrals to be calculated increases substantially (to some nearly 59 million needing more than 0.5 GB of hard disk space for storage). Each component in the calculated spectrum corresponds to a 50% Gaussian–Lorentzian product function [21,22] with each peak having the same full width at half-maximum (FWHM) (1.0 eV for all the spectra discussed here) and an area generated as described above. The data in Fig. 1 were generated using monochromatic x-radiation, but in most cases achromatic x-radiation is used and thus the calculations include x-ray satellite features for the x-radiation used. The inclusion of these x-ray satellite features is an important aid to analysis since in many oxide situations there is an intense O2s feature that contributes significant x-ray satellite intensity to the low binding energy part of the spectrum.

#### EXAMPLES OF THE APPLICATION OF CORE AND VALENCE BAND PHOTOEMISSION TO ELECTRO-CHEMICAL AND CORROSION SYSTEMS

Electrochemical and corrosion systems may be either metallic or involve a conducting non-

metallic material such as carbon. These two situations will be dealt with separately.

#### *Metallic systems*

Metallic systems generally involve the formation of oxides, oxyhydroxides of hydroxides on the surface as a result of a corrosion process. Core XPS is a valuable method for distinguishing between the substrate metal and an oxidized surface. As expected, hydroxides will be formed at the least oxidizing potentials, with oxides being formed at the most oxidizing potentials. Identification and distinction between these materials is not always easy. The O1s core region is valuable in distinguishing between oxide and hydroxide features in most cases, the latter feature occurring at the lower binding energy and the former at a higher binding energy. In most cases the metal core region clearly distinguishes between the metal and the oxidized species, but it is not always possible to distinguish between different types of oxidized materials. This is unfortunate since this information is essential in order to understand the electrochemical or corrosion process. In this section examples will be given which describe how valence band X-ray photoemission generally provides this missing information.

In some cases clear shifts can be seen between oxides of different formal oxidation state, for



example in the case of molybdenum. However, sometimes, such as in the case of molybdenum, the valence band region shows a marked change leading to the appearance of a new peak in the spectrum. One can understand how this occurs if one notes that reduction in oxidation state leads to more electrons in the valence band, and thus it is reasonable to find that this may lead to the appearance of a new band. An example is provided by molybdenum [23] where reduction from the VI oxidation states leads to the population of new levels ( $t_{2g}$  levels involving molybdenum d electrons in the case of an octahedral molybdenum complex).

In many cases it is not easy to distinguish between different formal oxidation state oxides from core XPS. An example is the case of SnO and SnO<sub>2</sub> which have only a small difference in Sn3d core binding energy. The valence band region however shows significant differences, which can be understood by X $\alpha$  calculations [10]. Unfortunately this problem is found for many important corrosion systems. Thus the Fe2p core region can clearly distinguish between metallic iron and its oxides, but it is almost impossible to unambiguously distinguish between different oxidized forms of iron. Again valence band XPS provides some clear differences. For example, FeOOH and Fe<sub>2</sub>O<sub>3</sub> can be distinguished, and the differences understood by comparison with spectra generated from X $\alpha$  calculations [7].

Some of the most important practical systems present serious problems for surface chemical identification. Aluminum provides a good example, for while it is relatively unreactive due to its protective oxide layer, the nature of this oxide layer plays a significant role in the corrosion of aluminum. Aluminum has a range of oxides, oxohydroxides and hydroxides, the principal ones being  $\alpha$ - and  $\gamma$ -Al<sub>2</sub>O<sub>3</sub>, the oxohydroxides  $\alpha$ - (diaspore) and  $\gamma$ -AlOOH (boehmite) and the hydroxides [Al(OH)<sub>3</sub>] gibbsite, bayerite and nordstrandite. Recently we have found [15] that these oxidized compounds can be distinguished by subtle differences in the valence band, even though it is very hard to distinguish between them from core XPS studies (there are some differences in the Auger parameter). Figure 2 shows the near

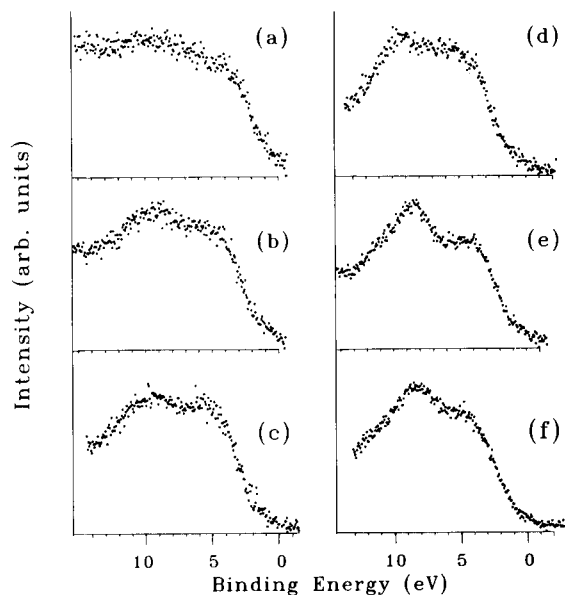


Fig. 2. XPS outer valence band region of various aluminum compounds: (a) gibbsite, (b) bayerite, (c) nordstrandite, (d) boehmite, (e)  $\alpha$ -Al<sub>2</sub>O<sub>3</sub>, (f)  $\gamma$ -Al<sub>2</sub>O<sub>3</sub>.

valence band region (it excludes the intense O2s peak at higher binding energy), and close examination shows that there are significant differences between these spectra. In particular there are two peaks in this region whose separation and relative intensity can be used to distinguish between aluminum compounds. This separation can be understood by X $\alpha$  and ab initio calculations on AlO<sub>6</sub><sup>9-</sup> clusters, and is related to the Al–O separation in these compounds. Note how gibbsite is significantly different from the other oxidized compounds, and how the separation between the two peaks is less (by 0.6 eV) for  $\gamma$ - compared with  $\alpha$ -Al<sub>2</sub>O<sub>3</sub>. This difference can be exploited in trying to understanding the changes that occur on electrochemical oxidation of aluminum in nitric acid [24]. Thus one notices substantial changes in the valence band region as the potential is made more oxidizing (Fig. 3). Figure 3 shows the wide valence band region including the O2s feature around 24 eV. At normal take-off angles one notices the metal as a shoulder around 0 eV binding energy whose intensity falls off and disappears with increasingly oxidizing potentials. At surface sensitive take-off angles however one no-

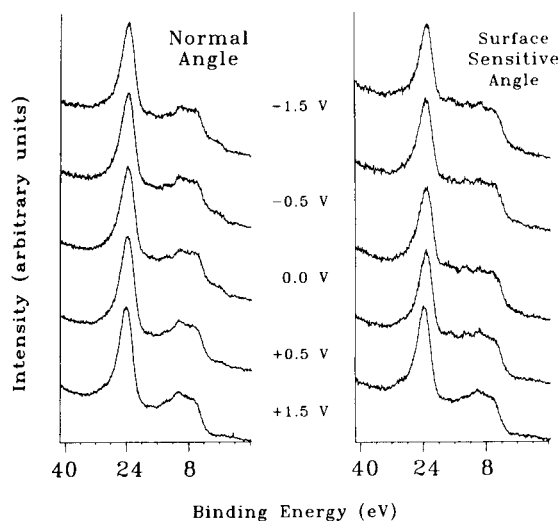


Fig. 3. XPS valence band region of aluminum polarized in 0.5 M nitric acid (10 min polarization time).

tices substantial change in the near valence band region with the spectrum changing from that of gibbsite to that of  $\gamma\text{-Al}_2\text{O}_3$ . This ties in with one's chemical expectation since hydroxide would be expected at less oxidizing potentials and oxide at more oxidizing potentials.

Interestingly one sees here how valence band photoemission can allow differences in chemical composition to be identified within a thin oxide film. This type of experiment, which gives information about changing composition with depth into the film, should be distinguished from changes seen in the valence band of orientated homogeneous single crystals as the take off angle is varied [4–6]. These experiments show how valence band photoemission can provide substantial information about the surface film. They also illustrate how the combination of surface science and electrochemistry can provide mutually supportive explanations. Thus if one interprets a spectrum in a particular way, and then has to use this interpretation in a consistent manner to explain a series of chemically changing spectra, one has a strong test of interpretative model. Thus in this case the differences in the valence band predicted by the model compounds interpreted by calculations [15] is supported by an experiment where the chemical composition is changed in a

controlled manner [24]. In the core region we have been applying this approach for many years in the curve fitting of spectra to a series of component peaks [1,21,22] in a situation where electrochemistry changes the relative amounts of these components in a chemically controlled manner. The curve fitting parameters in these cases must be used consistently over the whole set of spectra.

Other features of concern in electrochemical and corrosion systems are the presence of carbonates and hydrogencarbonates. We have shown that these can be clearly distinguished in the valence band region [25].

A region that has considerable analytical potential is the O2s region. In metallic systems its energy is usually widely separated from the rest of the valence band region, and it behaves more like the core O1s region. Thus oxide features are usually found at lower binding energy and hydroxide features at higher binding energy (aluminum is an exception perhaps because the hydroxide and oxide Al–O bond lengths lie within the same range). However the shift between oxide and hydroxide is often somewhat greater than in the O1s region due to a small amount of interaction with the other valence electrons. A good example is provided by  $\text{Fe}_2\text{O}_3$  and  $\text{FeOOH}$  [7].

Corrosion inhibitors provide an important challenge for surface analysis. We still have little understanding of how such inhibitors act. One might suppose that an ideal inhibitor would remove any unprotective oxide film and then form a chemically and mechanically stable protective film on the material. In trying to achieve this goal it is important to be able to analyze the surface chemistry of generally complex and often amorphous compounds. Such potentially “messy” systems can be analyzed by valence band photoemission, an example being provided by the reaction of iron and steel with calcium etidronate [9,13]. The oxidized iron film on iron and steel react with the etidronate ion to give the phosphate ion, and valence band photoemission can clearly distinguish between these two ions.

An important aspect of the examination of “messy” systems is that even though they may

have significant C1s intensity due to hydrocarbon contamination, the low cross section for carbon means that hardly any carbon features are seen in the valence band region of metallic systems.

### Carbon systems

Carbon systems show important electrochemical behavior. Carbon fibers are of interest to us because of the importance of the surface chemistry in understanding and enhancing their application in composite materials. Carbon fiber surface chemistry provides a good example of a case where changes in surface chemistry can lead to major changes in material properties. Thus composites formed from carbon fibers that have been surface treated can typically take more than three times the load of composites formed from the same fibers without surface chemical treatment.

XPS has proved a powerful method for examination of carbon and carbon fiber surfaces [13,26] since it can examine the chemistry of the outer region alone and causes little surface decomposition. Carbon is not the best system for surface science studies, especially because surface functionality is subject to rapid loss when the carbon surface is exposed to electron and ion beams.

Figure 4 illustrates the type of information provided by core and valence band XPS and x-ray powder diffraction for a high modulus pitch based carbon fiber electrochemically oxidized in 0.1 M nitric acid solution for 20 min at various voltages [vs. the saturated calomel electrode (SCE)]. The overall XPS spectrum immediately shows the relative amounts of carbon and oxygen [to be quantitative these need to be adjusted for the instrument transmission function, the relative photo-

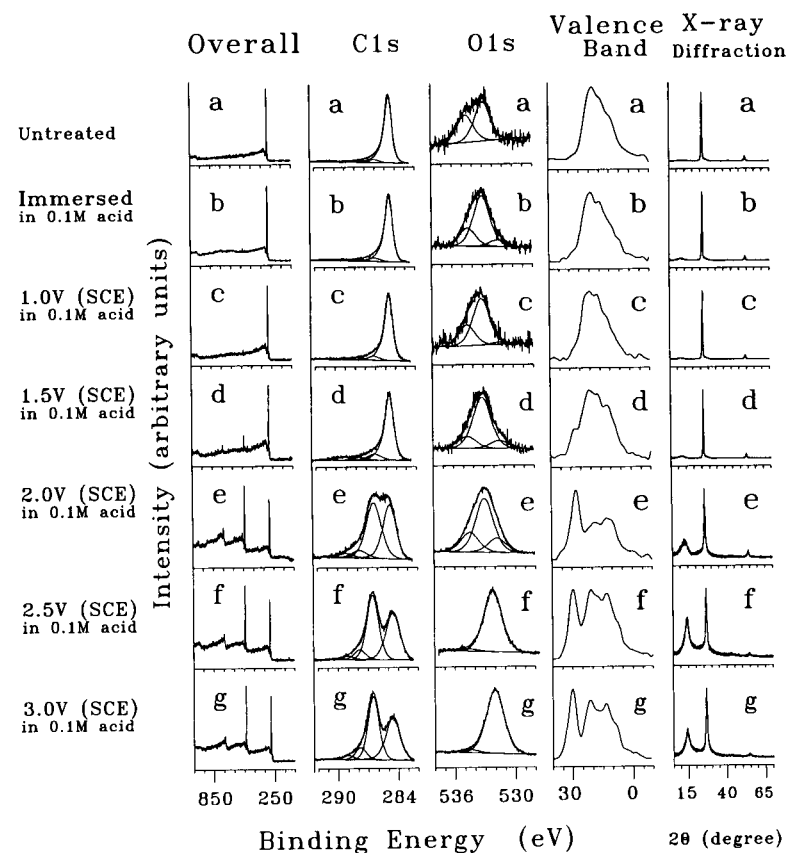


Fig. 4. XPS and XRD data for a high modulus pitch based fiber before and after electrochemical treatment for 20 min in 0.1 M nitric acid electrolyte.

electron cross sections, and homogeneity (or lack of it) in the surface region)). The intense peak at higher binding energy corresponds to C1s, and the peak at lower binding energy which becomes intense at positive potentials corresponds to O1s. A high resolution scan of both these regions reveals a number of chemically shifted features which are curve fitted by non-linear least squares fitting methods [21,22]. This curve fitting is an example of the case discussed above of a need to consistently fit a series of spectra whose chemical composition is changing in a controlled manner. The lowest binding energy C1s feature is due to graphitic carbon and this is fitted to an exponential tail due to conduction band interaction from the graphite  $\pi$ -system, which becomes lost at this system is broken down by oxidation. Other features in the C1s spectrum correspond to C–OH, C–O–C, and C=O functionality. The O1s region also shows features corresponding to such groups and consists of one to three overlapping peaks. The valence band region is complex, and can be understood by calculations and model compounds [12], but provides more information than the core region, and in particular can distinguish between C–O–C and C–OH functionalities. The x-ray diffraction spectrum is little changed below 2.0 V (vs. SCE) oxidation, and then shows new features which may be associated with the considerable bulk changes caused by this extensive oxidation.

The O2s region warrants further discussion. It can be identified as the intense feature in the 24–30 eV energy range which appears after extensive oxidation. Similar intense features are often found in oxidized metals (for example, see Fig. 3), however unlike the metal case where this region is rather core-like with little interaction with the other valence levels from which it is widely separated in energy, this region strongly interacts with the carbon 2s region which lies close in energy. The O2s region in carbon compounds thus behaves differently and shows important features that can be used for analytical purposes. When x-radiation is used the C2s intensity is much greater than the C2p intensity thus enhancing the importance of C2s interaction. The effect of this interaction is that O2s features due

to C–OH and C=O functionality are found in *opposite* positions compared with the O1s region. This can be understood by a simple molecular orbital picture where one considers the C–OH group to have the least C–O interaction and thus the smallest separation between the principally C2s and O2s regions. The shorter C=O bond would cause a greater interaction and thus a greater separation, and finally the C–O–C group having two carbons about each oxygen might lie to higher or lower binding energy than the C=O group. In our calculations [12] of model compounds we find the epoxide group to lie at the highest binding energy.

We have used the valence band region for the examination of a number of hydrocarbon systems including polymers [14]. This has particular relevance to carbon fibers since the interface between the carbon fiber surface and a polymer matrix will be significantly affected by the carbon fiber surface functionality [26,27]. Optimization of any chemical interaction in this situation will have an important effect in developing improved composites. Figure 5 illustrates how the XPS valence band spectrum of the fiber Nomex aramid in Fig. 5a can be predicted by extended basis set *ab initio* calculations on the two principal compo-

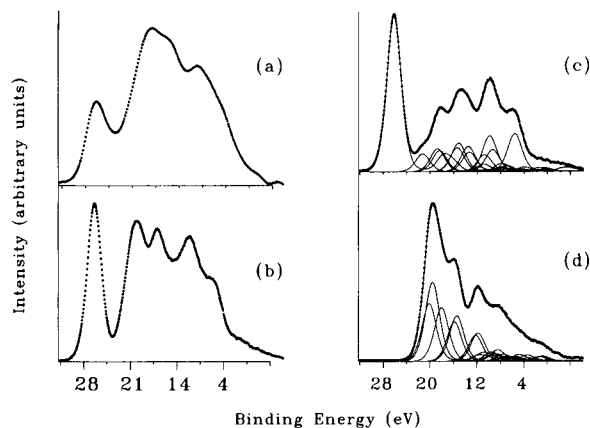


Fig. 5. XPS valence band region of Nomex aramid showing the experimental spectrum obtained in the author's laboratory with Mg  $K\alpha$  x-radiation: (a) after removal of a non-linear background compared with a calculated spectrum (b) obtained by combining the calculated spectrum for (c) isophthalaldehyde and (d) *m*-phenylenediamine (1,3-diaminobenzene) from *ab initio* calculations.

nents of the repeat unit of the polymer [16]. Thus the spectrum in Fig. 5d represents that of *m*-phenylenediamine (1,3-diaminobenzene) and that in Fig. 5c of isophthalaldehyde with the first peak in the latter spectrum (due largely to N2s contributions) being shifted 6 eV from the first peak in the former spectrum (due largely to O2s contributions) to obtain correct alignment. When aligning different polymeric units one usually uses spectral features from a common chemical unit (such as a benzene ring) as an alignment aid. The resulting valence band was linearly contracted on the energy scale by a factor of 1.3 in all cases. The contraction results since the spectra predicted by *ab initio* Hartree–Fock calculations always overestimates, by a factor of about 1.3, the spread of valence band energy levels. The approach has been found to be very valuable in a number of polymeric and other organic systems [16], and the use of a linear contraction was a feature of nearly all these studies.

Another aspect of the XPS valence band region is that it probes more deeply into the surface than the core regions since the photoelectrons from this region have a higher kinetic energy. We have used this feature to probe the changes in chemical composition with depth, and in particular any changes in carbon fiber surface functionality from the heating produced by the X-ray gun.

### Conclusions

The surface analysis of electrochemical and corrosion systems has been actively pursued for more than twenty years by a variety of techniques. It can be seen that the use of valence band photoemission, in conjunction with calculations that predict the spectra, and compound characterization by x-ray diffraction, provides important surface chemical information for both metallic and carbon systems. An attractive feature of this analytical approach is that it is relatively non-destructive compared with other surface analytical methods, it can be applied to amorphous as well as crystalline samples, and it can be used for less than ideal systems (practical systems with some surface contamination). In particular, angle resolved photoemission in the valence band has the ability to probe variations in

surface composition with depth into the sample which can be especially valuable for systems where the core region shows no spectral differences between surface components.

This material is based upon work supported by the National Science Foundation under Grant No. CHE-8922538. The U.S. Government has certain rights in this material. The carbon fiber work was funded by the Air Force Office of Scientific Research, NASA Langley Research Center, and Dupont. We are grateful to the U.S. Department of Defense for funding the x-ray diffraction equipment. HONDO calculations used the MOTECC™ Package. Dr. Debasis Majumdar is thanked for presenting his data on zirconium dioxide prior to publication, and for helpful discussions. Various members of my research group were involved in this work, especially, Dr. Yaoming Xie, Dr. Sajan Thomas, Dr. Cara Weitzsacker, Professor Dilip Paul, Ian Welsh, Tiejun Wang, Xiaoying Wang, Mike Bellamy, Mike Rooke, and Yuanling Liang.

### REFERENCES

- 1 P.M.A. Sherwood, in D.M. Hercules, G.M. Hieftje, L.R. Snyder and M.A. Evenson (Eds.), *Contemporary Topics in Analytical and Clinical Chemistry*, Vol. 4, Plenum, New York, 1982, pp. 205–293.
- 2 P.M.A. Sherwood, *Chem. Soc. Rev.*, 14 (1985) 1.
- 3 D.A. Case, *Ann. Rev. Phys. Chem.*, 33 (1982) 151.
- 4 K. Broomfield and P.M.A. Sherwood, *J. Chem. Soc., Faraday Trans. II*, 79 (1983) 785.
- 5 K. Broomfield and P.M.A. Sherwood, *J. Chem. Soc., Faraday Trans. II*, 79 (1983) 799.
- 6 K. Broomfield and P.M.A. Sherwood, *J. Chem. Soc., Faraday Trans. II*, 79 (1983) 1321.
- 7 I.D. Welsh and P.M.A. Sherwood, *Phys. Rev. B*, 40 (1989) 6386.
- 8 I.D. Welsh and P.M.A. Sherwood, *Proc. Electrochem. Soc.*, 89 (1989) 417.
- 9 Y. Xie and P.M.A. Sherwood, *Chem. Mater.*, 1 (1989) 427.
- 10 P.M.A. Sherwood, *Phys. Rev. B*, 41 (1990) 10151.
- 11 P.M.A. Sherwood, *J. Vac. Sci. Technol.*, A9 (1991) 1493.
- 12 Y. Xie and P.M.A. Sherwood, *Chem. Mater.*, 3 (1991) 164.
- 13 I.D. Welsh and P.M.A. Sherwood, *Chem. Mater.*, 4 (1992) 133; and references cited therein.
- 14 P.M.A. Sherwood, *J. Vac. Sci. Technol.*, A10 (1992) 2783.
- 15 S. Thomas and P.M.A. Sherwood, *Anal. Chem.*, 64 (1992) 2488.

- 16 L.E. Hamilton, P.M.A. Sherwood and B.M. Reagan, *Appl. Spectrosc.*, 47 (1993) 139.
- 17 S. Tougaard and P. Sigmund, *Phys. Rev. B*, 25 (1982) 4452.
- 18 S. Tougaard, *Surf. Interface Anal.*, 8 (1988) 11.
- 19 J.H. Scofield, *J. Electron Spectrosc.*, 8 (1976) 129.
- 20 D. Majumdar and D. Chatterjee, *J. Appl. Phys.*, 70 (1991) 988.
- 21 P.M.A. Sherwood, in D. Briggs and M.P. Seah (Eds.), *Data Analysis in XPS and AES in Practical Surface Analysis*, Second Edition, Vol. 1, Auger and X-ray Photoelectron Spectroscopy, Wiley, New York, 1990, Appendix 3, pp. 555-586.
- 22 P.M.A. Sherwood, in D. Briggs and M.P. Seah (Eds.), *Practical Surface Analysis by Auger and X-Ray Photoelectron Spectroscopy*, Wiley, New York, 1983, Appendix 3, pp. 445-475.
- 23 I.D. Welsh and P.M.A. Sherwood, in preparation.
- 24 S. Thomas and P.M.A. Sherwood, *J. Chem. Soc., Faraday Trans.*, 89 (1993) 263.
- 25 S. Thomas and P.M.A. Sherwood, *Surf. Interface Anal.*, in press.
- 26 P.M.A. Sherwood, *Materials Research Society Proceedings*, 270 (1992) 79; and references cited therein.
- 27 C. Kozlowski and P.M.A. Sherwood, *Carbon*, 25 (1987), 751.

# Non-destructive 2- and 3-dimensional microanalysis with (high energy) ion microprobes

G.J.F. Legge, A. Saint and N. Cholewa

*Micro Analytical Research Centre (MARC), School of Physics, University of Melbourne, Parkville, Vic. 3052 (Australia)*

(Received 11th September 1992; revised manuscript received 29th November 1992)

## Abstract

Ion microprobes operating at energies of a few to many MeV are now readily available for quantitative elemental and structural analysis. These ion microprobes are more analogous to the electron microprobe than to the low energy (or sputter) ion microprobe and initially were developed for their low minimum detection limits, their quantitative accuracy and their depth sensitivity. More recently they have been exploited for their abilities to analyse crystal properties, to perform 3-dimensional tomography, to analyse microcircuitry beneath overlayers and study single event upsets, to investigate single ion radiation effects and to perform micromachining and microlithography. New applications are continuing to appear. This paper sets out the basic properties and strengths of these ion microprobes and discusses how they can be used alone or to complement the work of other microprobes, particularly in elemental or structural microanalysis.

*Keywords:* Ion microprobes; Microanalysis

This paper presents the wide range of analytical techniques available to an ion microprobe operating at energies of several MeV and discusses them in the general context of microprobe analysis, making a comparison with other complementary microprobe instruments. Strict comparisons can be made only in specific instances and here only order of magnitude figures can be given. The emphasis will be on the basic interactions between beam and specimen and the information that can be extracted from the specimen. It should be emphasised also that all these microprobe instruments have their specific advantages and, in elaborating and concentrating on the modes of operation of one instrument, we can not give adequate coverage to the other instruments. Ion induced x-ray emission is the first ion

microprobe technique to be discussed, because it is the most generally familiar technique and can be most readily compared with the complementary techniques of other instruments. Then the other ion microprobe techniques are introduced, with examples of their use.

The efficient collection, storage and quantitative analysis of data is discussed as a feature of major concern to users of all scanning instruments and of particular importance to the ion microprobe.

A large range of interactions is employed in elemental microanalysis which, for this paper, means the elemental analysis of microscopic samples or of larger samples with microscopic resolution. There are many properties of a sample which may be analyzed at microscopic level, by means of a microprobe: (1) elemental composition (major, minor and trace elements); (2) isotopic composition; (3) chemical composition; (4) crystalline structure; (5) porosity; (6) surface

*Correspondence to:* G.J.F. Legge, Micro Analytical Research Centre (MARC), School of Physics, University of Melbourne, Parkville, Vic. 3052 (Australia).

properties; (7) electrical properties; (8) magnetic properties.

Of these, the chemical composition, involving as it does the valence electrons, is generally investigated directly by means of low energy interactions or indirectly by means of low energy effects in high-energy spectra. In this paper, the emphasis is on high-energy ( $> 1$  keV) effects and interactions; but a distinction is drawn between the energy of the interaction and the energy of the radiation, in contrasting the interactions available to several types of microprobe. We shall be concerned with the cross sections of the principal analytical reactions and of the various mechanisms for energy or intensity loss. Thus x-ray beams are principally affected by the total absorption of individual photons by electrons in the sample, leading to the attenuation of the x-ray beam intensity, but no change in energy. In contrast, each particle in a beam of high velocity charged particles loses energy continuously at approximately the same rate, principally through ionization of atoms along its path through the specimen. This will result also in a small statistical spread in the energy distribution of the beam (known as energy straggling) but little attenuation.

It is important to note that the cross section for removal of any orbital electron by a passing electron or ion is a maximum when this charged particle traverses the atom with approximately the same velocity as that of the electron in its orbital, provided of course that the energy of the charged particle is greater than the ionization energy that it is to supply. Thus it is velocity that determines the probability of ionization and not energy. It should also be noted that the principal mode of energy loss by ions changes from ionization (“electronic stopping”) to interactions with nuclei, individually or together with their surrounding cloud of orbital electrons, (“nuclear stopping”) as the velocity of the charged particle drops well below that of the orbital electrons. In contrast to “electronic stopping”, the low energy ion transfers a large fraction of its energy in such an atomic collision, because the interacting particles have comparable mass, and this energy remains localized with the atom. This has a major

effect on the specimen-beam interaction, as is discussed below.

#### X-RAY MICROPROBE

The most direct means of probing elemental composition is provided by a beam of x-rays. There are many spectroscopic techniques that may be used in single point measurements with a focused beam [1]. Elements may be identified by their x-ray absorption edges, as the energy of the x-ray beam is swept over the range of interest. It may be possible also to identify the chemical attachment of an element by means of a small shift of the elemental edge. It is feasible thus to analyze a single point on a specimen for all elements or, by scanning over a large area with beam energy on either side of an edge, to map the distribution of an element over that area. However, to map the distribution of many elements over an area, it is generally necessary to measure all simultaneously with the technique of x-ray fluorescence. A wavelength dispersive detector (crystal spectrometer) does provide a means to identify small chemical dependent shifts in the fluorescent x-ray spectrum. However, this too is limited to one x-ray energy at a time and is therefore too inefficient for the multiple mapping of elements. An energy dispersive detector [generally a Si(Li) crystal] provides the means to distinguish and record the fluorescence of all elements simultaneously and hence to allow their simultaneous, individual mapping over an area, though the energy resolution is then insufficient to detect chemical shifts. Obviously, for such energy dispersive x-ray analysis (EDXRA), the energy of the x-ray beam must be greater than the ionization energy of the heaviest element to be detected. Most work to date has been carried out with unfiltered (so-called white) radiation, in which only a small fraction of the x-ray beam satisfies the above energy requirement. Even so, the peak to background ratio for the characteristic radiation is very good and detection limits of 0.1 ppm have been reached in x-ray microprobe analysis [2]. Radiation damage is also low, though not negligible [2]. Such damage will be greatly



reduced when the radiation is filtered with a monochromator and it will be possible to consider some *in vivo* biological measurements.

The major limitation of the x-ray microprobe (XMP) at present is the spatial resolution, which until recently has been about 5  $\mu\text{m}$  for practical analysis with a synchrotron source [2]. Recently it has been shown that 1  $\mu\text{m}$  or better may be achieved with focusing by a tapered, glass capillary tube [3,4] and this holds great promise for future development and activity.

Unlike the microprobes to be considered below, the XMP generally has its beam fixed and any scanning is performed through movement of the specimen. Also the beam from a capillary tube has a divergence angle set by the acceptance angle for x-ray reflection and so the working distance must be short (1 mm or less). Another distinguishing feature of the x-ray beam is its attenuation in passage through the specimen, without change of energy, apart from the so-called "hardening" effect. The high penetration of the x-ray beam means that relatively thick specimens may be examined, provided some correction is made for absorption of both primary and secondary radiation. This, of course, is a disadvantage if surface analysis is required. The analysis of thick specimens suggests a need for 3-dimensional tomography and this is discussed later, after introducing the other microprobes. Likewise, the analysis of crystalline properties is discussed later.

#### ELECTRON MICROPROBE

The electron microprobe (EMP) was the first to be developed and is the general workhorse, now being found most often in the form of a Si(Li) detector attachment to a scanning electron microscope (SEM). The characteristic x-rays are excited by the electron beam and therefore this must have an energy well above the highest ionization energy of interest. This means that the electrons in the beam must have velocities greater than those of the electrons to be ejected. It is desirable that this "overvoltage" not be too great, an "overvoltage" factor of 4 or greater being

recommended [5]. Unfortunately, the background of bremsstrahlung from the deceleration of electrons in the specimen is severe and elemental detection limits for EDXRA with an EMP are frequently of the order of 100 ppm or worse, unless very good statistics are accumulated at high beam currents.

At low beam currents, the spatial resolution of an SEM utilizing the secondary electron signal may be less than a nanometre; but, whereas such electrons come only from the surface, the characteristic x-rays originate at considerable depth beneath the sample surface, where the incident electron beam has been considerably broadened by scattering. Consequently, the effective resolution may be more than 1  $\mu\text{m}$  in a sample of several  $\mu\text{m}$  thickness to the beam. If the sample is not thin, the effective thickness may be reduced by taking advantage of the rapid loss of energy by electrons in the beam as they pass through the specimen. Thus, by limiting the beam energy, the analysis may be restricted to a region within a few  $\mu\text{m}$  of the surface. For a given yield of characteristic x-rays, and hence for given information, the energy dissipated in the specimen by a beam of electrons is very much greater than that from a beam of primary x-rays. Hence the damage is more severe and *in vivo* biological analyses are generally out of the question, though the EMP is still classified as a nondestructive analytical instrument, because the specimen usually remains intact.

#### SPUTTER ION MICROPROBE

This instrument is often known as a SIMS (secondary ionization mass spectrometry) microprobe (SIMSMP). It could also be described as a low velocity ion microprobe, since it is the low velocity of the ions in its primary beam which characterises it. The ion source supplies large beam currents of positive or negative ions and a wide range of ion masses may be available. It commonly operates at an accelerating potential of about 20 kV. This is comparable with the accelerating potential of an EMP, but of course

results in heavy ions of very low velocity. Consequently, the ion beam suffers mainly “nuclear stopping” in the specimen, losing a large fraction of its energy with every collision and causing the target atoms to act in turn as energy carriers, thus producing a chain reaction over a short distance in the specimen. So much energy is dissipated to the target atoms in a short distance by this explosive interaction that secondary ions are boiled off to be collected and analyzed. As the surface of the specimen is steadily sputtered away by the action of the focused, incident ion beam, the elemental composition may be recorded as a function of depth. Thus this form of analysis, like that of the laser microprobe, is essentially destructive and, although the primary ion beam may be focused to about 1 nm in some instances, the spatial resolution and depth resolution are limited to the diameter of the interaction volume, which may be up to 100 nm.

The elemental detection limits are very low (of the order of 0.01 ppm) but the quantitative accuracy is limited by the strong dependence of elemental sputtering yields on local chemical composition of the specimen. However this limitation does not apply to the determination of isotopic ratios, for which the instrument can obtain unrivalled accuracy. We shall not discuss the SIMSMP further in this paper, because it is not closely analogous to the other instruments.

## ION MICROPROBE AND A COMPARISON OF MICROPROBES

If a beam of ions is accelerated to velocities comparable to those of the electrons in an EMP, they will have comparable cross sections for ionization and hence excitation of characteristic x-radiation as they traverse the sample. The cross sections will be most similar if the ions are protons, as these also have the same charge as the electron. Such an ion microprobe (IMP) is closely analogous to an EMP. It also goes by the name of proton microprobe and nuclear microprobe, though neither of these names is fully descriptive. Because the IMP and EMP have comparable cross sections for ionization, they also show comparable rates of energy loss by their particles. There are, however, several major points of distinction between these two instruments. An ion having the same velocity as an electron will have a much greater energy. Consequently, the IMP can operate at lower velocities than the EMP and still be well above all ionization thresholds. Having similar ionization cross sections and losing the same energy per ionizing event, but with much greater total energy to dissipate, the ions will have much greater ranges in the specimen and will show less energy straggling and related range straggling, expressed as fractions of the total energy and range. Also, being heavier, the ions will

TABLE 1

Microprobes and their major distinguishing properties

[The fundamental natures of the x-ray, electron and ion microprobes (XMP, EMP and IMP), as used for x-ray analysis, are compared with each other and with the SIMS microprobe (SIMSMP). Only with the SIMSMP is the depth of sample analyzed determined solely by the interaction range of the primary beam. With the other microprobes it is determined to a great extent by the attenuation of the secondary x-rays in the specimen. Approximate energies of the primary radiation are used to show the crucial role of its velocity (compared to the velocity,  $v$ , of orbital electrons)]

MP	Primary radiation	Typical energy	Velocity	Energy loss	Signal	Depth	Scatt
XMP	Photon	10 keV	$c$	Electronic	X-Ray	100 $\mu\text{m}$	Medium
EMP	Electron	10 keV	$v - 3v$	Electronic	X-Ray	10 $\mu\text{m}$	Medium
IMP	Proton or light ion	3 MeV	$v/3 - v$	Electronic	X-Ray	100 $\mu\text{m}$	Small
SIMSMP	Heavy ion	10 keV	$v/200$	Nuclear	Secondary ion	10 nm	-

show less angular straggling (from scattering by nuclei in the specimen). Thus the IMP has spatial resolution of about 1  $\mu\text{m}$  or better, but it can maintain this resolution over a depth of about 10  $\mu\text{m}$ . The damage per  $\mu\text{m}$  is similar for high velocity light ions and electrons; so the IMP is also classified as a nondestructive analytical instrument.

Comparison of the IMP with the XMP is more complex. A comparison of peak to background ratios with both operating at sufficiently high energies to detect all elements of interest would slightly favour the XMP [6], as commonly used for microprobe work with a primary beam of white radiation. The background would be significantly decreased with use of a monochromatic primary beam; but the minimum detection limits in a given time depend also on the brightness of the beam, which is currently low for the IMP. Some of these points are summarised in Table 1, which emphasises the inherent properties of the above four types of microprobe, and not their current state of development.

All of these microprobes (except the XMP) give rise to copious emission of secondary electrons, which may be used to image the specimen and, since these low energy electrons can come only from the surface of the specimen, the spatial resolution obtained is that of the focused beam spot. This has the advantage of identifying the exact position of the scan on the specimen. However, further discussion of this aspect would be outside the scope of this paper.

#### DATA HANDLING

Trace elemental microanalysis requires high efficiency in the handling of data. This is particularly so if multiple elemental mapping is to be performed and quantitative results are required. The low beam currents available from a high energy ion accelerator for high resolution work with the IMP made it essential to utilise 100% of the detectable signals quantitatively and this appears to have been the first instrument for which total quantitative scanning analysis (TQSA) was

achieved, though it was introduced as a technique applicable to all scanning instruments [7].

The principle of the technique is that all signals from all detectors viewing the specimen should be permanently recorded, without any restrictions, that is without any "windowing" of the energy spectra. When in scanning mode, the  $x$ - and  $y$ -deflections of the beam are treated as parameters analogous to the energy parameter. Each radiation event is recorded by a computer as a set of 3 words, identifying the detector and specifying the energy of the radiation, the  $x$ -deflection of the beam and the  $y$ -deflection of the beam. With such a system of recording, local heating of the specimen by the beam may be avoided, by continuous rapid scanning of the beam spot over the surface to be analyzed. The beam will then make multiple passes over every point. Alternatively, the beam may be allowed to dwell, for some predetermined beam charge, at each point in a slow raster scan and the complete spectrum recorded at each point. The word complete here means only that again no energy restrictions are set (no windowing). However the data are collected, the computer is able to sort the events for each detector notionally into a 3-dimensional block, which can be carved up by computer analysis. Thus, on demand, the computer can produce the map of any element (by windowing the corresponding elemental peak in the total energy spectrum stored in the computer memory), the line scan of any element (by windowing the elemental peak and the position of the line) or the complete spectrum of any region of interest (by specifying the boundary). The data having been recorded in time sequence, it is also possible to inspect the progress of the analysis, thus detecting any elemental losses that may have resulted from the irradiation of a sensitive specimen. In general, any information that was recordable during the progress of the analysis is retrievable, immediately or at any time in the future. Thus elements which were not originally looked for can have their maps extracted, new regions of interest can be defined and analyzed and ratios of elemental abundances or other relationships can be sought, without reirradiation of the specimen. This form of total data handling has greatly

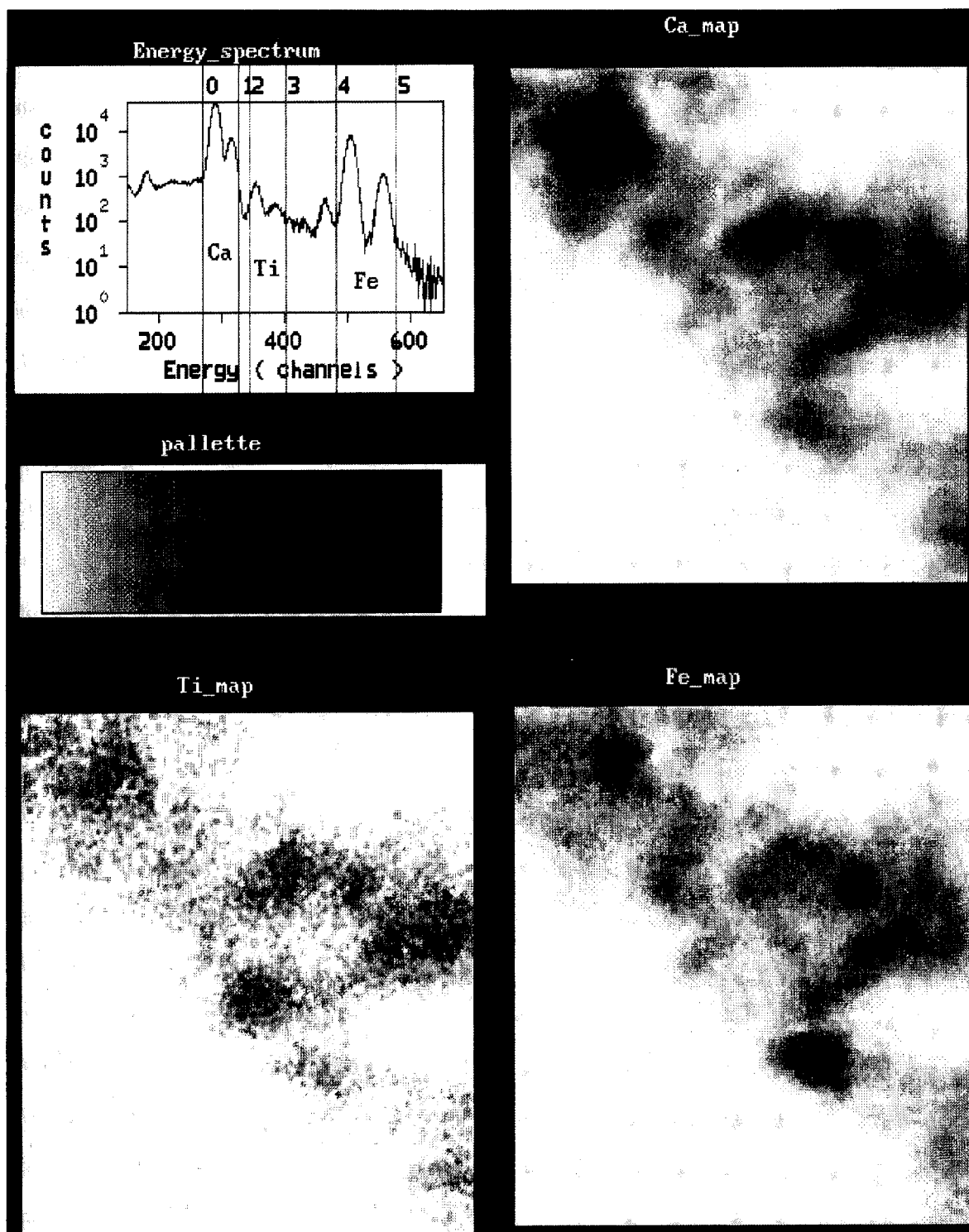


Fig. 1. The total x-ray spectrum from the IMP analysis of a flyash sample and the maps of Ca, Ti and Fe distributions. A map is presented by the computer in response to the windowing of any region of the spectrum.

expanded the available techniques of the IMP. The employment of a modern fast graphics workstation enables the computer system to keep up with very high data collection rates and to present multiple maps and spectra live during the

collection of data, as seen in Fig. 1. In this case, TQSA is applied to the IMP analysis of flyash. A 3-MeV beam of protons was focused to a spot of diameter  $2\ \mu\text{m}$  and scanned over an area of  $50 \times 50\ \mu\text{m}$ . The beam current was 100 pA for

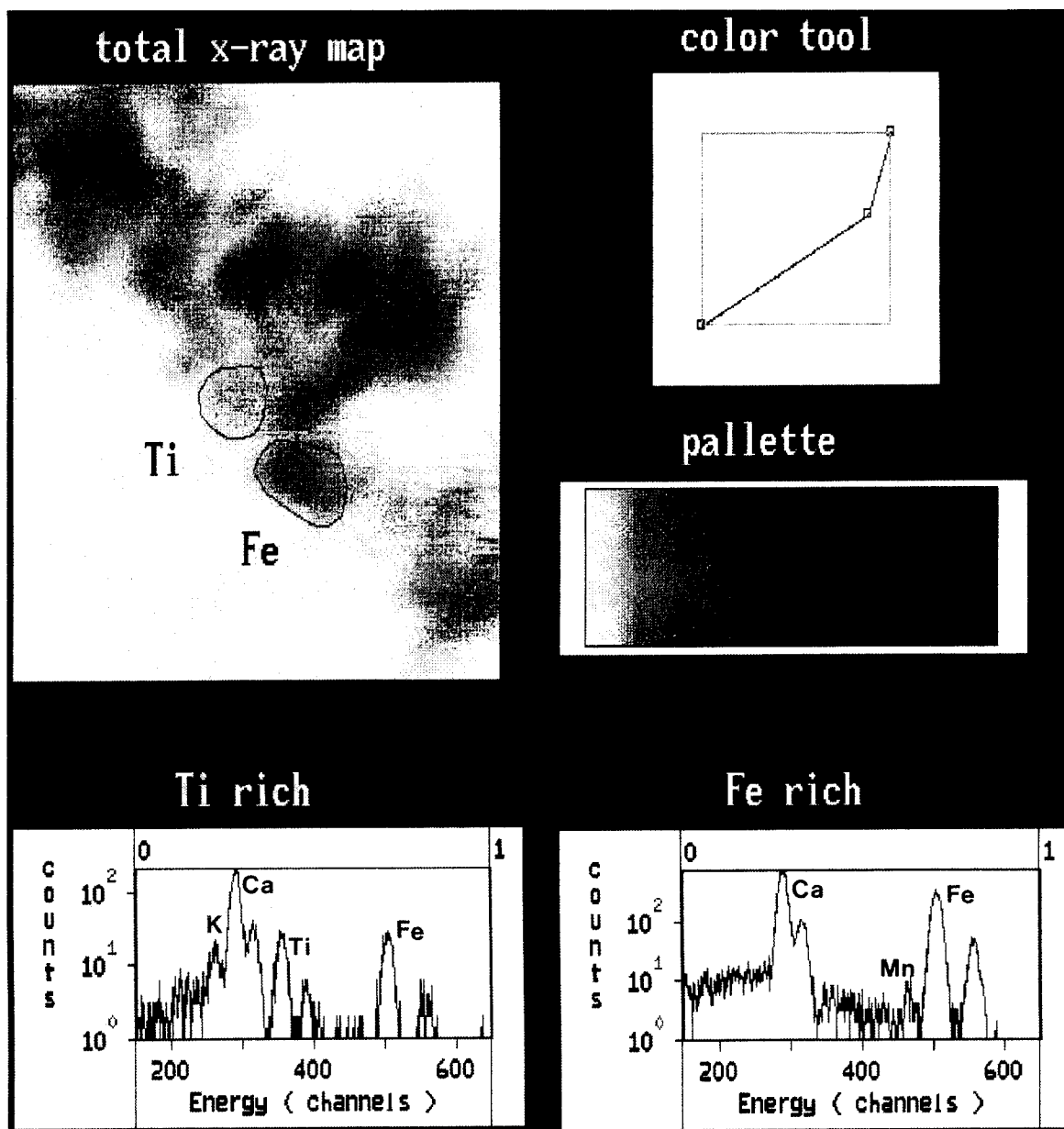


Fig. 2. The map of all events in the x-ray spectrum of Fig. 1 is presented and, in response to the tracing of any boundary to define a "region of interest", the computer extracts the spectrum of events for that region. Two such regions are shown here analyzed.

900 s and the x-rays produced were detected with an Si(Li) detector at a backward angle of 450 (so-called particle induced x-ray emission or PIXE). Figure 1 shows the complete x-ray spectrum on a logarithmic scale. The  $K_{\alpha+\beta}$  peaks of Ca, Ti and Fe have been framed with markers and the distributions of these three elements thereby extracted from the complete data set and displayed as grey scale maps. The grey scale palette may be manipulated with a “colour tool” to enhance contrast or this may be used with a false colour scale for even greater contrast.

For each element several regions of high concentration are seen and Fig. 2 shows the map of all elements, with two regions of interest defined by the operator. The spectra thereby extracted from these two regions are also displayed and allow the concentrations of Ti and Fe to be extracted quantitatively for these two regions. The region strong in Ti is of interest because it shows, not only the major element Ca, to the low energy side of Ti, but at slightly lower energy, channel 250, a well defined peak of K an element not previously looked for, because it was not visible in the total spectrum. Thus, without further irradiation, K may be mapped, its regions of concentrations examined and so on. Additional information on peak identification and energy has been deliberately suppressed for the purposes of this discussion.

There are three important and related points in TQSA which often have been misunderstood, leading to data handling systems of limited power. The first is that windowing is to be carried out only on the recorded complete set of data, not on the data as they are collected. Otherwise, it will not be possible to extract all required quantitative information from the data block. The second is that space must not be reserved in computer memory (hard or disc) for the complete spectrum at every point in the scan. Minor and trace elements will not register a count at many points in the scan and reserving memory for all possible energy events is impractical.

Windowing the energies of all elements of interest also defeats the purpose of TQSA, because it is then impossible to fit and subtract backgrounds to the spectra, in order to achieve

quantitative results. For example, if the scan contained  $1000 \times 1000$  points, then the number of events for each point would be very small. The only efficient way of recording events is in “event-by-event” or “list” mode. Thus the 3-dimensional data block is only a notional block of addresses, each of which could have any number of the spectral events assigned to it.

This raises the third point. It is sometimes stated that the number of pixels, and hence the spatial resolution, must be limited in order to achieve meaningful statistics in each pixel. However, it is not necessary to achieve meaningful statistics in each pixel, and certainly not for every element. The pixel resolution should be as good as the resolution of the focused beam spot. The major tenet of TQSA is that it is unnecessary and undesirable to throw away any information, and this includes the spatial information available with good resolution, it being possible always to improve statistics by smoothing or binning data, but impossible to recover information that was not recorded. If data are recorded in event-by-event mode, the number of channels available for each dimension (energy or displacement) does not affect the memory or disc space required to store the data. It will affect the requirements for sorting the data, but this is not a serious problem.

As an illustration of the above point, it is often crucial to know on which side of some boundary a trace element is to be found. As long as the boundary can be identified precisely by some means (optical, secondary electron or major element image, for example), we do not need good statistics of the trace element of interest for every point (only for the total region of interest) but it is vital that we know precisely from which side of the boundary the trace elemental counts come. With this in mind, the first version of TQSA used a data block of  $8000$  (energy)  $\times$   $1000$  ( $X$ )  $\times$   $1000$  ( $Y$ ), although the core memory then available was only 48 kB. Modern developments have led to much cheaper memory and discs; but rather than affect the size of the data block, these developments, like that of much faster central processor units (CPUs), have greatly increased the speed of data analysis and enabled more to be done on-line, during collection of the data.

## NUCLEAR REACTION ANALYSIS

The above section on the IMP covered only the identification of elements by means of the characteristic x-rays emitted following ionization, so-called particle induced x-ray emission (PIXE). An event of much lower probability, but great interest is the initiation of a nuclear reaction leading to the emission of some readily identifiable nuclear radiation. Such radiation usually has an energy which is specific to the isotope, not just the atomic number. Coulomb repulsion from the nucleus forms an effective barrier around heavy nuclei; but nuclear reaction analysis (NRA) is often employed to detect light elements, such as C, N, O and F, which are difficult to detect with x-rays. However the small cross sections for nuclear reactions make it difficult to obtain good statistics with high resolution. The high energy requirement and the small cross section follow from the strength and short range of the nuclear force. Nuclear reactions are not to be confused with so-called “nuclear stopping” (discussed above); the latter is an atomic effect involving only Coulomb forces and having a large cross section at low energies.

## RUTHERFORD BACKSCATTERING ANALYSIS

At high energies, where “electronic stopping” is of greatest importance, some “nuclear stopping” also occurs. The energies of the ions are such that they and the nuclei of the specimen atoms interact independently of any orbital electrons and this type of Coulomb scattering is historically known as Rutherford back scattering (RBS). The interaction is an elastic one but the ion loses a fraction of its energy to the target nucleus, determined by the angle of scatter and the relative masses of the two particles, the heavy specimen nuclei taking least energy. Thus the energy spectrum from a charged particle detector placed at some known backward angle provides a mass spectrum of the specimen atoms. However the ion also loses energy as it penetrates the specimen on the way in and out; so the energy of the scattered ion also depends linearly on the

depth of the RBS interaction below the surface of the specimen and the energy spectrum provides a depth profile of each element.

This nondestructive depth profiling technique finds major use in materials research, where the surface properties are crucial and, with a detector placed at a glancing angle of emergence, a depth sensitivity of 2 nm is obtainable, but this falls to 12 nm at depths of 200 nm [8]. With a thick specimen, the depth profiles for the various elements will overlap at low energies in the spectrum. So RBS is most useful for profiling heavy elements near the surface of a light matrix, such as heavy dopants in Si, SiC or diamond. With TQSA, the distribution of elements at any given depth may be mapped. If the detector is placed at a forward angle, even H may be mapped, by detection of either the scattered ions or the knocked on target atoms.

## CHANNELING CONTRAST MICROSCOPY

If the specimen is crystalline, the rate of energy loss by ions in the beam is reduced by 10–20% when the beam enters along a crystal axis and the ions can “channel” through the specimen. Of greater significance to RBS is the accompanying very large reduction in scattering cross section as the alignment of atomic nuclei makes the crystal somewhat transparent to the beam of ions. These effects can be calculated for a perfect crystal and hence the measured energy spectrum may be used to provide a measure of crystal perfection. In channeling contrast microscopy (CCM), the beam is channeled, the RBS spectrum recorded whilst the specimen is scanned by the beam and maps of the RBS yield are extracted to show regions of crystal imperfection or misalignment. CCM will also reveal the nature of subsurface layers as, compared to the yield when the beam is not channeled, the lower scattering cross section for a channeled beam will lead to an increased signal to background ratio for scattering from an interstitially located element in contrast to that from an element located on lattice sites. The PIXE yield may also be used with CCM, to locate the lattice sites of elements

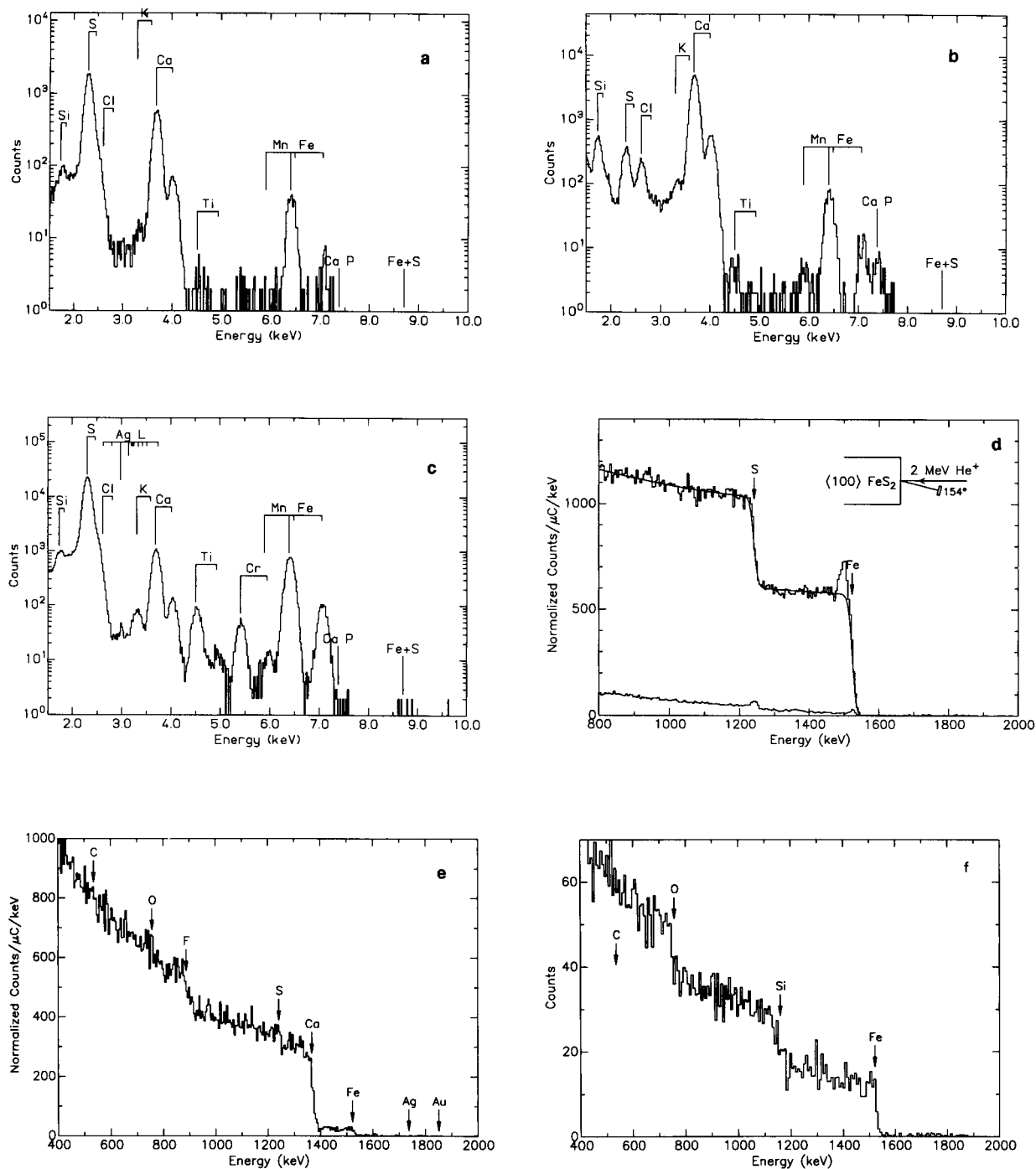


Fig. 3. The analysis of a crystalline sample (pyrite) by the IMP. (a) PIXE spectrum from the matrix, showing FeS and several trace elements, (b) and (c) PIXE spectra from two inclusions, (d) RBS spectrum from (above) a randomly aligned beam of 2 MeV He<sup>+</sup> ions and (below) a beam aligned with the <111> crystal axis, (e) and (f) RBS spectra from inclusions, with the beam channeling in the matrix, and (g) a comparison of elemental maps obtained by windowing the PIXE total spectrum both with the beam aligned to channel along the <111> axis and with a random direction of incidence.



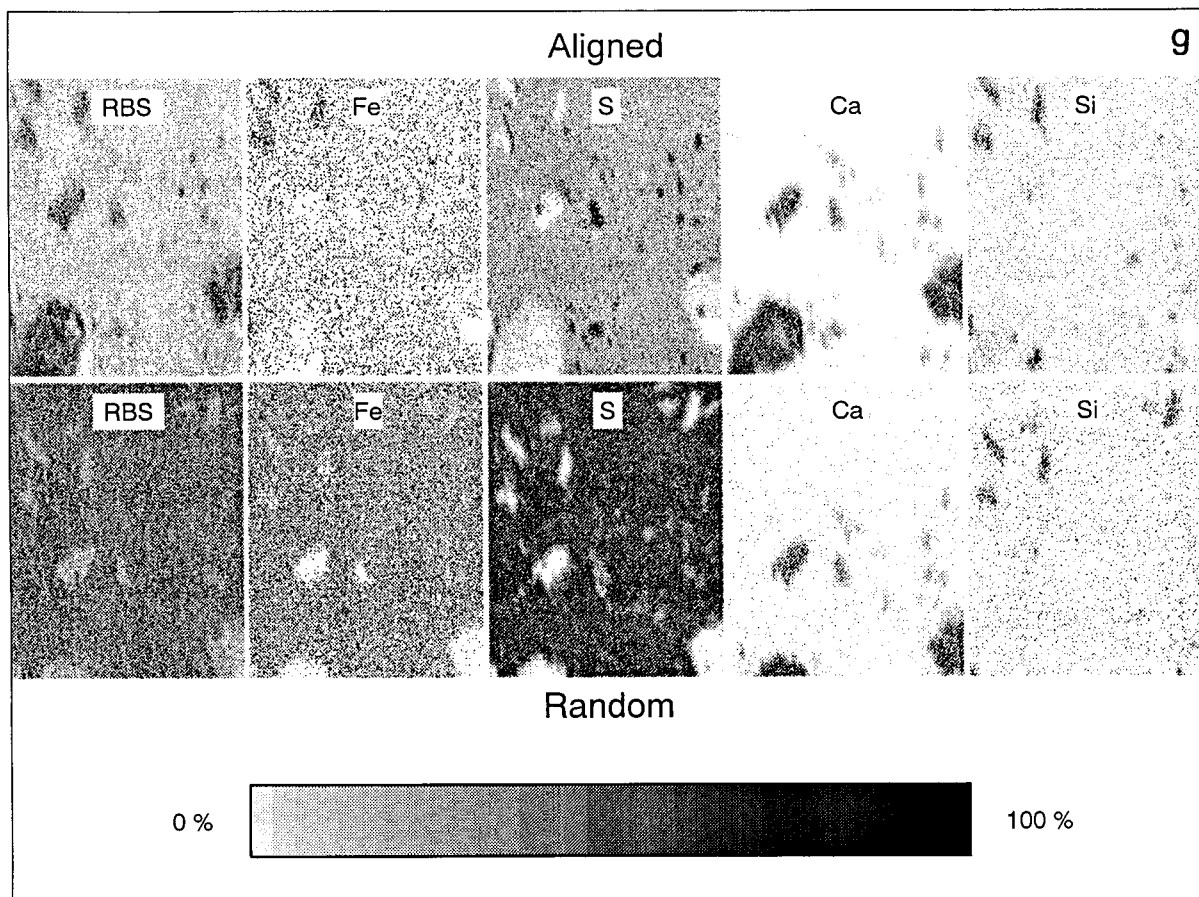


Fig. 3 (continued).

that may be undetectable in the RBS spectrum. Again, with a channeled beam, the yield will depend on the lattice site of the atom in question. These techniques are finding wide application in the analysis of semiconductor materials and other new crystalline materials [9].

A very recent development, the application to mineral specimens, has been very successful and will serve well as an illustration [10]. PIXE has been an accepted sensitive and quantitative microanalytical technique in geology and mineralogy for many years and Fig. 3a shows a PIXE spectrum of natural pyrite crystal measured on the Melbourne IMP. With this beam and energy (He ions of 2 MeV), the sensitivity of PIXE drops rapidly for elements heavier than Ca and it is obvious that the major composition is FeS, as

expected, but with considerable inclusion of other elements. Figure 3b is from an area rich in Ca and Fig. 3c from an area rich in heavier elements. These can be shown as inclusions by calling for the maps of these elements. In this analysis, the backscattered ions were also detected and the RBS spectrum from the matrix is shown in Fig. 3d, with the expected energies of the Fe and S edges marked. The upper spectrum was collected with random orientation of the crystal to the incident beam direction. When the crystal was aligned to bring the beam in along the  $\langle 100 \rangle$  crystal axis, the spectrum changed to the lower one. The dramatic decrease in yield (a factor  $\chi = 3.3\%$ ) corresponds to that expected for an almost perfect crystal. This provides a valuable aid to analysis because, under such conditions,

the yield from any amorphous or off-axis inclusions will be greatly enhanced compared with the yield from the matrix. This is seen in Fig. 3g, where the maps of four elements have been extracted from the PIXE data sets for both the aligned and random directions. The maps labelled RBS are of the total RBS signal. The scanned region of  $1\text{ mm} \times 1\text{ mm}$  shows many inclusions, some of which are only visible in the aligned maps. Figure 3e and f shows RBS spectra extracted from 2 of these inclusions. These RBS spectra show the light elements, as well as the heavier ones seen in PIXE spectra, and also enable a quantitative estimate of the stoichiometry and hence an identification of the inclusion.

#### SCANNING TRANSMISSION ION MICROSCOPY

Since the rate of energy loss for an ion depends on the nature and density of the material, in a thin sample the energy loss of transmitted ions may be used to map the spatial distribution of these characteristics. This was first done with the SIMSMP [11], where it was, of necessity, used with very thin specimens. The technique, scanning transmission ion microscopy (STIM), was ideally suited to the IMP, for which the energy loss is fairly linear as a function of areal density. Because of the high detection efficiency when a detector is placed in the transmitted beam immediately after the specimen, the ion beam current

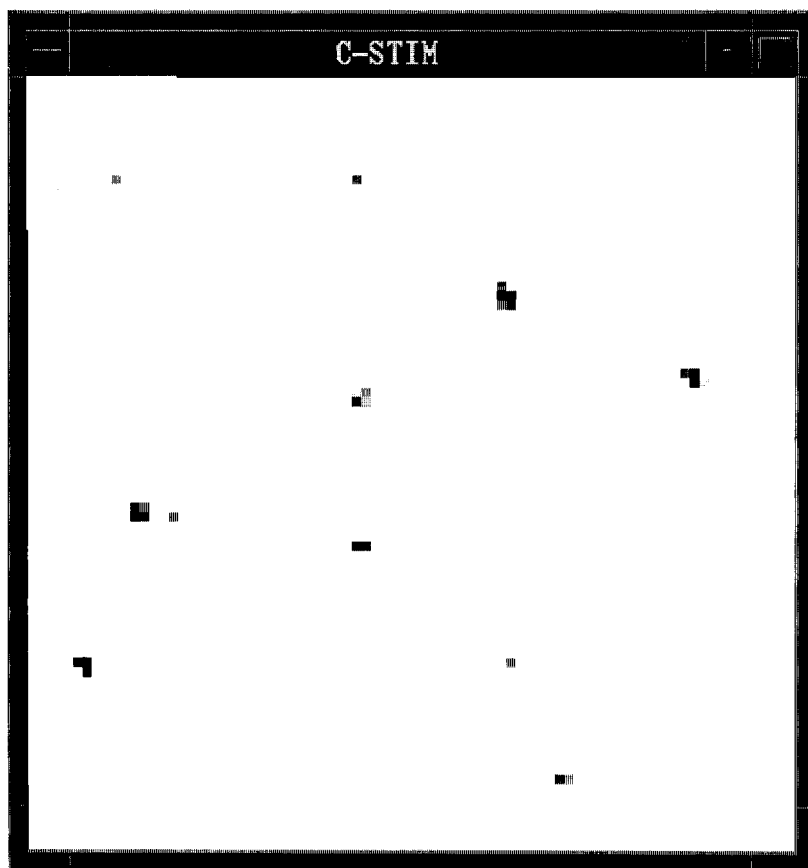


Fig. 4. Channeling STIM map of a thin SiC crystal analyzed in an IMP. The energy loss contrast shows regions of poor channeling and hence large energy loss. The scan size is  $300 \times 300\ \mu\text{m}$ . Less than an fA of beam current is required for such work (performed at ETL, Tsukuba).

must be very small and this allows the spatial resolution to be reduced to about 50 nm [12]. The sensitivity to thickness variations is about the same. The energy loss is actually a measure of apparent electron areal density. Generally the most quantitative information is obtained by taking several measurements of transmitted ion energy at the one point and calculating the median value [13]. However the second moment of the energy distribution for the one point provides information on the porosity or granularity existing within the area of the focused beam spot [14]. Instead of the above “bright field” image, a dark field” image may be collected by stopping the direct beam from entering the detector; and, for

both “bright” and “dark field” modes, the contrast mechanism may be energy loss, as above, or scattering, in which case the number of events is the parameter plotted [15]. For most situations, energy loss provides the greater contrast, because the statistical nature of the ion beam fluctuations are then of no consequence and the large number of ionization events involved in the energy loss process make its statistics (which lead to the so-called energy straggling) much better.

#### CHANNELING STIM

The two techniques of CCM and STIM may be combined, if the degree of channeling is made

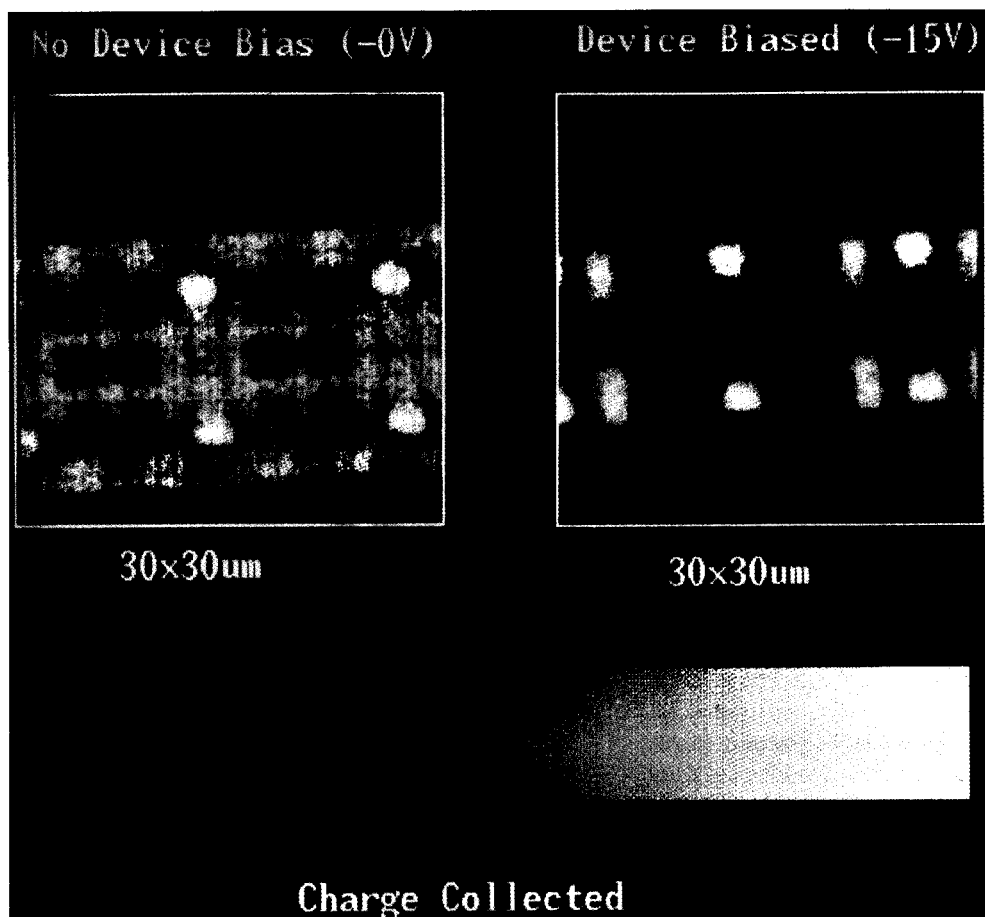


Fig. 5. IBIC images of memory cells in an integrated circuit, under two different states of bias. The state of the circuit is revealed by the level of charge collection. The 3- $\mu\text{m}$  thickness of overlayers does not prevent clear resolution of the 2- $\mu\text{m}$  spacing between components.

the source of variation in the transmitted ion energy. Channeling STIM can only be used on thin specimens, but it has great sensitivity and, like all STIM measurements, creates negligible damage in the specimen.

Figure 4 shows a channeling STIM map of a thin specimen (12  $\mu\text{m}$  thick) of SiC with its Si substrate etched away, prepared at ETL Laboratories in Tsukuba and scanned over  $300 \times 300 \mu\text{m}$  with a beam of 2 MeV protons from the ETL IMP aligned along the  $\langle 111 \rangle$  axis of the sample. The map of median transmitted energy shown reveals several small areas of relatively high energy loss (dark areas) and hence poor channeling. In view of the method of preparation, they are unlikely to be merely denser regions of the specimen. This was tested by looking at the same map with the beam tilted to avoid channeling. These patches were then seen to have the same areal density as the surrounding material. They represent either amorphous material or, more likely, small crystals with tilted planes [16].

#### ION BEAM INDUCED CHARGE AND SINGLE EVENT UPSETS

Bright field STIM with an IMP is analogous to bright field STEM with an electron microscope in the handling of the beam; but there is a major difference in the quantitative aspects of data handling and image formation, because STIM provides a quantitative measurement with each individual beam particle. Therefore we speak of probing the specimen with single ions, each of which is under our control. This opens up other possibilities. The ion may not be transmitted, as in STIM, but may stop in the specimen. For example, the measurement of charge collection in a microcircuit, which is itself both specimen and detector, enables us to measure response to ionizing particle radiation under different operating conditions of a commercial chip, without the need to strip off the protective overlays. This ion beam induced charge (IBIC) is analogous to EBIC in a SEM, but IBIC will probe to greater depths, maintaining spatial resolution of about 1  $\mu\text{m}$  at depths of several  $\mu\text{m}$ . An example is shown in

fig. 5, IBIC images from a TA670 IC (a CMOS 16K Static RAM), taken under two different bias conditions [17]. The images clearly reveal the state of operation of the microcircuit. The left image shows the junction between two memory cells. The four dark squares (representing no charge collection, because biased off) are the driving transistors for the bit lines of the upper memory cell. (Below these drivers is the lower memory cell.) The blank area at the top of the image is the p-region of the device, where no charge is collected by the supply rail connected to the charge-sensitive amplifier. The bright spots are the constituent n-sources of the MOSFETS comprising the memory elements, while the darker regions to either side represent the n-drains, seen to be noncollecting due to the large path impedance from them to the supply rail. The right image shows the same memory cells under reverse bias. The larger electric field in this case substantially increases the collection efficiency for charge pairs created along the track of an incident ion. Most marked is the dramatic increase in the charge collected by the 2 n-sources (bright squares) and 2 of the 4 n-drains (bright rectangles) in each memory cell. Whether or not an n-drain is seen depends on the state of the memory, no collection by a n-drain denoting an “off” state and collection denoting an “on” state. The 2- $\mu\text{m}$  gaps between memory components are clearly visible beneath the 3- $\mu\text{m}$  thickness of overlayers, which had not been removed from the commercial device. The IMP beam was of 2.4 MeV  $\text{He}^+$ .

A related technique is the probing of a microchip for its susceptibility to “single event upset” under ion irradiation [18], a topic of growing concern with satellite operation and communication because the smaller and faster devices are more readily upset.

#### CONTROLLED DAMAGE

The IMP is now being used for microlithography, because the long range with only small deflection of the high energy ions enables the fabrication of relatively thick masks of high aspect

ratio [19,20]. It is even possible to etch the tracks of accurately placed single ions to form microstructures [21]. Single ions may also be fired in a controlled manner through components of a live biological cell, in order to measure accurately radiation effects which have previously been deduced only through approximate statistical studies, in many cases extrapolated from conditions of much higher dose [22].

### 3-DIMENSIONAL STIM AND PIXE TOMOGRAPHY

It has been mentioned that a highly penetrating radiation is at a disadvantage in analyzing

surface properties because underlying specimen material will interfere in the analysis. That, of course, does not apply when the detected radiation carries depth information, as is the case with RBS. However, even with depth insensitive radiation, the apparent weakness may be turned into a strength if the specimen can be examined from more than one angle, so that depth information can be extracted from the data. Qualitative information may be obtained from a stereo image pair, which the human eye and brain is programmed to interpret [23]. However, for quantitative information we need full three-dimensional tomography [24]. Such tomography has been per-

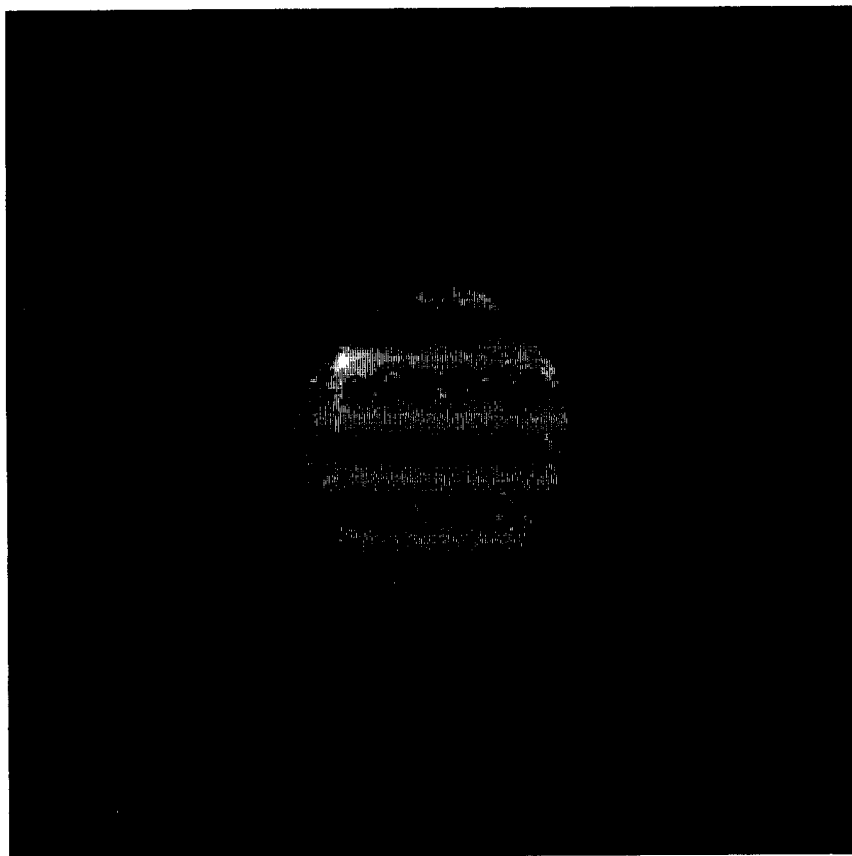


Fig. 6. Two-dimensional STIM tomographic slice: one of 256 comprising a complete 3-D PIXE tomographic image of a polymer particle. Many of the slices, like this one, reveal a small catalyst particle (white = high density) near the surface of the polymer particle. The polymer particle has a diameter of about 100  $\mu\text{m}$ .

formed with EMP, XMP and IMP. STIM tomography is generally carried out on specimens of dimensions between 10 and 1000  $\mu\text{m}$ , in which region it provides greater accuracy and sensitivity than the EMP or XMP. The advantages of STIM tomography with the IMP are the ability to map the density quantitatively in three dimensions in samples of thickness limited only by the stopping power of the available ions. These are selected to ensure that a large fraction of the incident energy is lost in the sample but the energy loss remains in the well understood region of “electron stopping”. With appropriate choice of beam projectile and energy, a spatial and depth resolution of less than 1  $\mu\text{m}$  is achievable and an absolute density accuracy of about 10–20%. The relative accuracy will probably be better than this.

To perform STIM tomography, the specimen is mounted centrally on a single axis goniometer and scanned with a two-dimensional raster of  $n \times n$  resolution elements (resels) to give a quantitative two-dimensional STIM image, formed from the median of several energy loss measurements at each resel. This constitutes one projection. The specimen is then rotated about an axis

perpendicular to the beam in order to record 3n such projections evenly spaced through 180° or 360°. A three-dimensional tomograph of  $n \times n \times n$  pixels is then computed from these data and stored in the form of  $n$  slices. Although STIM is almost 100% efficient and only about 8 measurements may be needed at each resel, depending on the accuracy required in the median, pixel dimensions of  $n = 500$  will still require the accurate measurement of  $3 \times 10^9$  events. So the data handling requirements call for speed and efficiency. A versatile program allows the tomograph to be rotated, viewed as a whole from any direction (with adjustable transparency), sectioned or sliced in any direction.

Figure 6 shows one two-dimensional “slice” taken from a complete three-dimensional tomograph of a polymer particle. The particle had been examined with a 3-MeV beam of protons, and a spatial resolution of 500 nm. The particle dimensions here are about 100  $\mu\text{m}$  and the significant observation is that dense catalyst particles (needed to grow such polymer particles) remain near the surface, where they can remain active. One such catalyst particle is seen top left in this

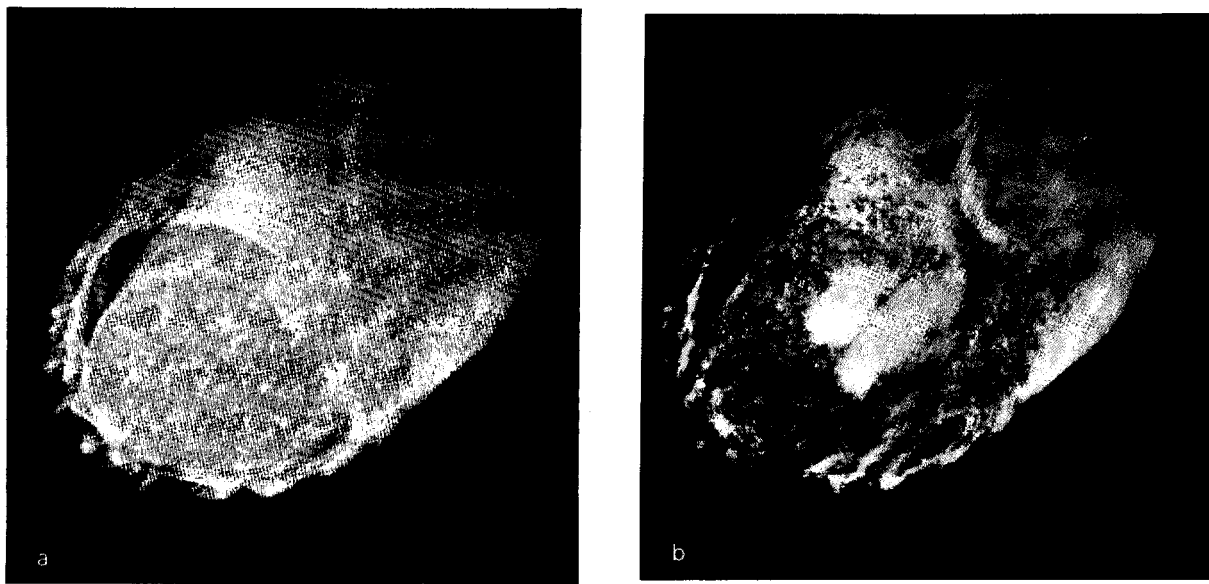


Fig. 7. Complete 3-D STIM tomograph of a *Lilium longiflorum* L. Thunb. cell. In these two presentations of the one data set, the threshold density is first set to show surface structure (left) and then internal structure (right).

slice, near the surface of the polymer particle. We also see signs of density variations in the polymer [25]. The complete data may be examined slice by slice or as a whole with the transparency adjusted to enable a view through the sample. In an earlier experiment with a XMP [26], larger catalyst particles were identified in several tomographic slices through larger polymer particles, the two instruments filling complementary roles.

Figure 7 shows a biological example. The complete tomograph of a pollen grain of *Lilium longiflorum* L. Thunb. is displayed, at left, with a threshold density set to enhance the grain surface and, at right, set to enhance the two nuclei of high density seen near the centre of the grain. We can see surface structure and also the un-

usual internal structure of such a cell, there being two nuclei clearly visible: the vegetative cell nucleus and the generative cell nucleus. Thus, it is possible to manipulate this data set so as to examine the surface structure of the grain or to peer deep into the structure of the nuclei themselves [27].

The beam currents needed for STIM are very low and this enables the achievement of high spatial resolution, limited ultimately by scattering of the beam. High energy heavy ions here have an advantage over electrons and over x-rays. X-rays are generally used on specimens of greater thickness, a mm or more, though high energy accelerators could also be used.

Three-dimensional tomography can also be applied to x-ray elemental analysis, thus making an

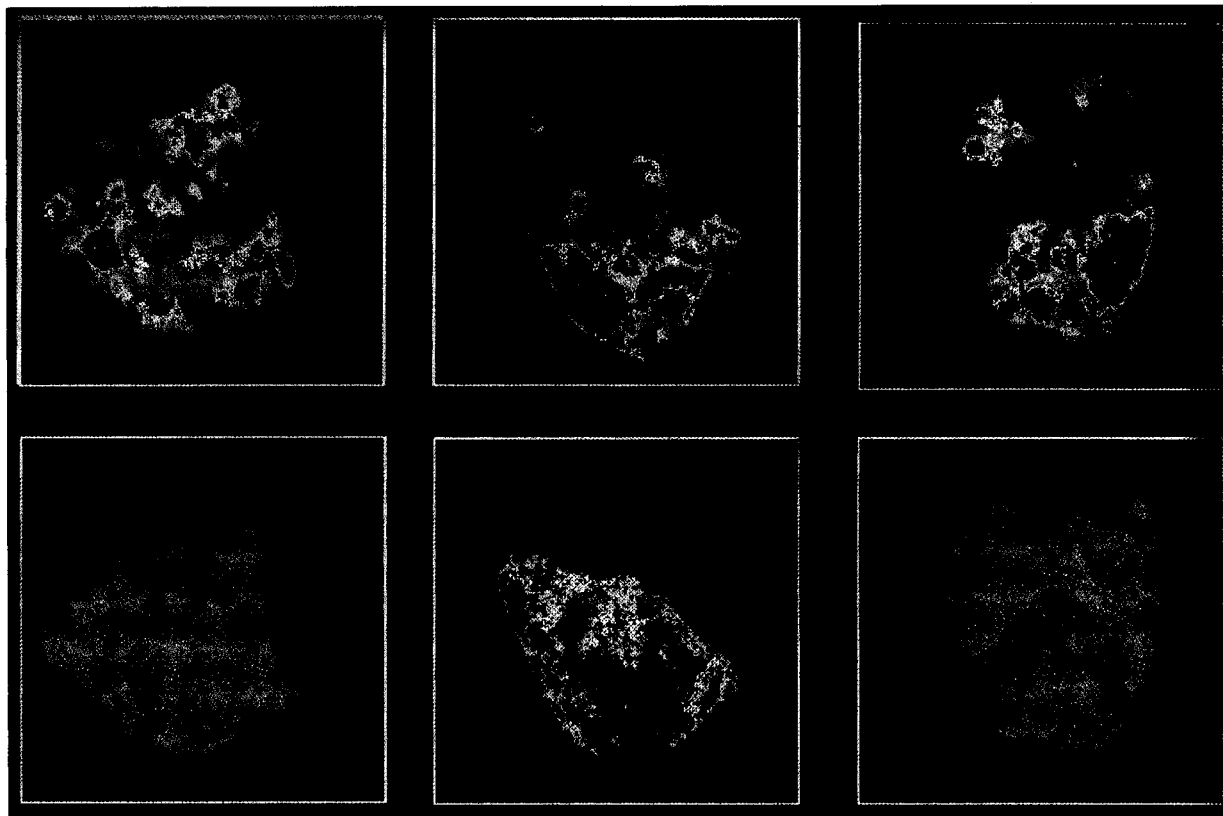


Fig. 8. Three projections (1200 apart) of Fe (top row) and Si (bottom row) forming part of the data set for a 3-D PIXE tomograph. The sample of mine tailings was examined with a 3.5-MeV beam of protons and tomographs of different elements were formed, by extracting the relevant data from the complete data set. As well as showing local concentrations of the major elements, the projections reveal shadowing of the detector and other effects from the thick specimen, of about 90  $\mu\text{m}$  diameter.

advantage of its lack of depth sensitivity. The cross section for ionization and subsequent detection of an x-ray is very low compared with that for STIM; so larger beam currents are required, with a consequent worsening of spatial resolution. Also we are now involved in poor counting statistics, compared with the excellent statistics of energy loss measurements. Nevertheless, work has recently commenced to develop this powerful analytical technique [28–30]. The experimental configuration is similar to that of STIM tomography, but instead of a particle detector at 0° and the need to record the median energy loss for each pixel, we now have an x-ray detector at 135° (a backward angle) and the need to record x-rays from anywhere in a complete energy spectrum for each pixel. If we were to reserve memory addresses for all possible x-ray events for a three-dimensional tomographic resolution of only 64 re-sels, we would require about a GB of computer memory, thus emphasising the need for TQSA. In Fig. 8 the data for 2 elements (Si and Fe) are extracted from the total data set and, for each element, 3 equally spaced projections are shown (from a total of 120 taken through 360°). This is only a small fraction of the total set but there is sufficient to show the very different distributions of these two elements in the three dimensional sample: a 90  $\mu\text{m}$  fragment of tailings from a copper mine in Northern Queensland [28,29]. The ion beam was 200 pA of 3.7 MeV protons focused to a spot size of 2  $\mu\text{m}$ . Shadowing effects, from attenuation of x-rays and energy loss of the ions in the relatively thick specimen are also observable and the first correction programs have been developed to handle such problems for quantitation [30].

### Conclusion

The basic requirements for microanalysis and hence for a microanalytical instrument are:

(1) high spatial resolution: high lateral resolution and high depth resolution; (2) high signal resolution; (3) low minimum detection level: low background; (4) quantitative accuracy; (5) efficiency: efficient detection, efficient data collection, efficient data analysis and efficient data presenta-

tion; (6) maximum information and versatility; (7) minimum damage.

The IMP, operating at MeV energies, shows good performance in all these areas, with particularly good characteristics in quantitative accuracy, efficiency, range of information and versatility. The range of applications is steadily expanding; for many areas it offers the only means of obtaining some information; in other areas it competes with or complements the information from other microanalytical instruments.

We wish to thank Drs. Nishijima and Sekiguchi of Electro Technical Laboratories, Tsukuba for their kind permission to show the data on channeling STIM before full publication of this work. We thank Dr. Jamieson of our laboratory and Dr. Ryan of CSIRO Division of Exploration Geoscience for permission to show some of their results which are in publication and others which are unpublished. The tailing sample was kindly supplied by Dr. Espiosa-Gomez of the Mount Isa Mining Co. and the pollen grain sample by Phil Taylor of the Department of Botany in the University of Melbourne. We are indebted for the IBIC work to Jamie Laird and to Dr. Doyle of Sandia Laboratories, Albuquerque, who supplied the sample. This work was supported by the Australian Research Council.

### REFERENCES

- 1 H. Winick and S. Doniach (Eds.), *Synchrotron Radiation Research*, Plenum Press, New York, 1980.
- 2 K.W. Jones, *Synchrotron-Radiation-Induced X-ray Emission (SRIXE)*, in R. Van Grieken and A. Markowicz (Eds.), *Handbook on X-Ray Spectrometry: Methods and Techniques*, Marcel Dekker, New York, 1992.
- 3 P. Engström, S. Larsson, A. Rindby, A. Buttkewitz, S. Garbe, G. Gaul, A. Knöchel and F. Lechtenberg, *Nucl. Instrum. Methods*, A302 (1991) 547.
- 4 D.J. Thiel, D.H. Bilderback and A. Lewis, *Nucl. Instrum. Methods*, A317 (1992) 597–600.
- 5 J.I. Goldstein, D.E. Newbury, P. Echlin, D.C. Joy, C. Fiori and E. Lifshin, in *Scanning Electron Microscopy and X-Ray Microanalysis*, Plenum Press, New York, 1981, p. 105.
- 6 K.H. Janssens, F. van Langevelde, F.C. Adams, R.D. Vis, S.R. Sutton, M.L. Rivers, K.W. Jones and D.K. Bowen, *Adv. X-ray Anal.*, 35 (1992) in press.



- 7 G.J.F. Legge and I. Hammond, *J. Microsc.*, 117 (1979) 201.
- 8 J.S. Williams, J.C. McCallum and R.A. Brown, *Nucl. Instrum. Methods*, B30 (1988) 480.
- 9 D.N. Jamieson, R.A. Brown, C.G. Ryan and J.S. Williams, *Nucl. Instrum. Methods*, B54 (1991) 213.
- 10 D.N. Jamieson and C.G. Ryan, *Nucl. Instrum. Methods*, B77 (1993) 415.
- 11 R. Levi-Setti and T.R. Fox, *Nucl. Instrum. Methods*, 168 (1980) 139.
- 12 G.S. Bench and G.J.F. Legge, *Nucl. Instrum. Methods*, B40/41 (1989) 655.
- 13 J.C. Overley and H.W. Lefevre, *Nucl. Instrum. Methods*, B10/11 (1985) 237.
- 14 J.C. Overley, R.M.S. Schofield, F.D. Macdonald and H.W. Lefevre, *Nucl. Instrum. Methods*, B30 (1988) 337.
- 15 R.M. Sealock, D.N. Jamieson and G.J.F. Legge, *Nucl. Instrum. Methods*, B29 (1987) 557.
- 16 H. Sekiguchi, T. Nishijima and A. Saint, in preparation.
- 17 K.M. Horn, B.L. Doyle, F.W. Sexton, D.S. Walsh, J. Laird, A. Saint, M. Cholewa and G.J.F. Legge, B77 (1993) 355.
- 18 B.L. Doyle, K.M. Horn, D.S. Walsh and F.W. Sexton, *Nucl. Instrum. Methods*, B64 (1992) 313.
- 19 B.E. Fischer, *Nucl. Instrum. Methods*, B30 (1988) 284; and B54 (1991) 401.
- 20 M.B.H. Breese, G.W. Grime, F. Watt and D. Williams, *Nucl. Instrum. Methods*, B77 (1993) 169.
- 21 R. Spohr, in K. Bethge (Ed.), *Ion Tracks and Microtechnology – Principles and Applications*, Vieweg, Braunschweig, 1990.
- 22 C.R. Geard, D.J. Brenner, G. Randers-Pehrson and S.A. Marino, *Nucl. Instrum. Methods*, B54 (1991) 411.
- 23 H.W. Lefevre, R.M.S. Schofield, G.S. Bench and G.J.F. Legge, *Nucl. Instrum. Methods*, B54 (1991) 363.
- 24 A.E. Pontau, A.J. Antolak, D.H. Morse, A.A. Ver Berkmoes, J.M. Brase, D.W. Heikinnen, H.E. Martz and I.D. Proctor, *Nucl. Instrum. Methods*, B40/41 (1989) 646.
- 25 M. Cholewa, A. Saint, G.J.F. Legge, W. Curtis Conner, S.W. Webb, P. Spanne and K. Jones, in preparation.
- 26 W. Curtis Conner, S.W. Webb, P. Spanne and K. Jones, *Macromolecules*, 23 (1990) 4742.
- 27 G. Bench, A. Saint, M. Cholewa, G.J.F. Legge, D.L. Weirup and A.E. Pontau, *Nucl. Instrum. Methods*, B68 (1992) 481.
- 28 A. Saint, G. Bench, G. Moloney and G.J.F. Legge, *Proc. 7th Australian Conf. on Nuclear Techniques of Analysis*, Melbourne Univ., 1991, Australian Nuclear Science and Technology Organization, Sydney, 1991, pp. 209–211.
- 29 A. Saint, M. Cholewa and G.J.F. Legge, *Nucl. Instrum. Methods*, B75 (1993) 504.
- 30 R.M.S. Schofield and H.W. Lefevre, *Nucl. Instrum. Methods*, B72 (1992) 104.

# X-Ray microanalysis of stratified specimens

Jean-Louis Pouchou

*Office National d'Etudes et Recherches Aéronautiques (O.N.E.R.A.), Department of Materials, 29 avenue de la Division Leclerc,  
92320 Chatillon (France)*

(Received 10th September 1992; revised manuscript received 15th March 1993)

## Abstract

This paper presents a description of the state of the art methodology and software for the application of x-ray microanalysis to thin surface layers and more generally to the characterization of stratified specimens. The sensitivity of the technique to near-surface segregation is demonstrated. Some emphasis is given on the  $\phi(\rho z)$  function (the distribution in depth of the primary generated x-ray intensity), which is the key to all advanced quantitative procedures presently available. The main characteristics of the recently developed software packages *Strata* and *Multifilm* are briefly described (physical basis, incorporation of fluorescence by lines and continuum, graphically assisted modes of operation, iterative mode of operation for the automatic determination of compositions and thicknesses). The capability of the technique is illustrated by three different applications: a bilayer on a substrate (case with no common element), a coated fibre (case with common elements and very light element analysis), a coated substrate analyzed in various geometrical conditions and by an "as soon as possible" procedure.

*Keywords:* Stratified specimens; Thin surface layers; X-Ray microanalysis

For 25 years, electron probe x-ray microanalysis (XRMA) has been conventionally applied to bulk specimens to obtain elementary chemical analyses of microvolumes of the order of  $1 \mu\text{m}^3$ . Contrary to other analytical techniques, XRMA has the advantage of providing quantitative results in an absolute way, i.e. it is actually not necessary to refer to standards similar to the specimen. For a given characteristic line, any standard (pure or compound) containing the element of interest permits to define an experimental relative intensity  $k$  (usually called  $k$ -ratio in the case of a pure standard), which can be converted into a mass concentration by use of a "correction" procedure. However, the conventional quantitative procedures used for 20 years (the most popular was the ZAF method) had a

limited field of applicability: low absorption situations (less than 30% of the x-rays emitted in the spectrometer direction should be absorbed by the specimen itself), and homogeneous microvolumes.

During the nineteneighties, several groups have made a real effort to promote new procedures in order to overcome the above limitations, extend quantitative analysis to very light elements (low energy, i.e., strongly absorbed lines), and characterize specimens with a depth-dependent composition. The key to those problems is the  $\phi(\rho z)$  function, defined by Castaing [1] in his pioneering work, and representing the distribution in depth of the primary ionizations generated per incident electron in the target. New models based on accurate  $\phi(\rho z)$  descriptions are now superseding the conventional procedures, namely the gaussian MSG model of Packwood and Brown [2] and Packwood et al. [3] and the PAP and XPP models of Pouchou and Pichoir [4–6]. Although they use different starting points

*Correspondence to:* J.-L. Pouchou, Office National d'Etudes et Recherches Aéronautiques (O.N.E.R.A.), Dept. of Materials, 29 av. de la Division Leclerc, 92320 Chatillon (France).

and mathematical expressions, these models aim to produce realistic distributions in depth of the primary generated x-ray intensity, in a wide range of electron and x-ray energies. The reliability of their  $\phi(\rho z)$  parameterization permits to evaluate accurately the strong absorption effects for soft x-rays, and to compute directly, in the case of stratified specimens, meaningful values of the x-ray intensity emitted by a surface layer, a buried layer, or a substrate.

This paper gives experimental evidences of the sensitivity of XRMA to the surface. Some basic principles are then recalled. Typical problems of near-surface analysis that can be solved in an effective manner by advanced x-ray microanalysis procedures are presented. The new computer programs *Strata* and *Multifilm*, developed recently in cooperation with SAMx on the basis of our PAP and XPP models, are used for this purpose.

#### ANALYZED DEPTH AND SENSITIVITY

As far as the resolution in depth is concerned, x-ray microanalysis under electron beam bombardment cannot compete with surface techniques like Auger emission spectrometry, x-ray photoelectron spectrometry or secondary ion mass spectrometry: in practice, as shown in Fig. 1, the depth of x-ray production cannot be significantly less than about  $10 \mu\text{g}/\text{cm}^2$  (i.e. 10 nm for a material with a density of  $10 \text{ g}/\text{cm}^3$ ), even in the

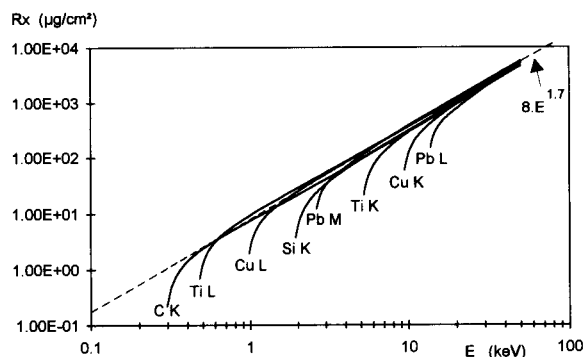


Fig. 1. Ultimate ionization depth vs. accelerating voltage in pure targets, according to the PAP model.

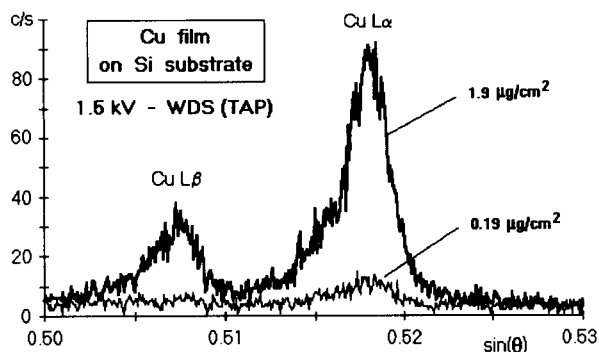


Fig. 2. WDS spectrum in the Cu L lines region corresponding to Cu layers on Si substrate. Layer thicknesses 1.9 and  $0.19 \mu\text{g}/\text{cm}^2$  ( $\sim 2$  and  $0.2 \text{ nm Cu}$ ). Accelerating voltage 1.5 kV. Beam current 150 nA. TAP monochromator. Camebax microprobe.

most favourable situation (electrons with an energy of about 1 keV generating soft x-rays). In spite of this poor resolution in depth, the technique offers however an interesting sensitivity to the surface: Fig. 2 demonstrates that a segregation of Cu less than  $0.1 \mu\text{g}/\text{cm}^2$  (equivalent to about 0.1 nm pure Cu) on top of a Si substrate can actually be detected by wavelength dispersive spectrometry (WDS). Figure 3 shows that with an energy dispersive (ED) spectrometer, although the limit of detection is slightly poorer because of a less favourable peak-to-background ratio, it still remains of the order of  $0.1 \mu\text{g}/\text{cm}^2$ . It can be noted that for the thinnest layer ( $0.19 \mu\text{g}/\text{cm}^2$ ) shown on Figs. 2 and 3, the Cu L $\alpha$  k-ratio would be 3.2% at 1.5 kV and 0.67% at 2.5 kV. Even for very light elements, the sensitivity to surface seg-

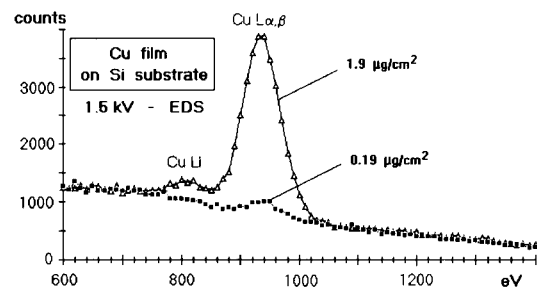


Fig. 3. ED spectrum in the Cu L lines region corresponding to the same specimen as in Fig. 2. Accelerating voltage 1.5 kV. Super Quantum Kevex Si(Li) detector. Zeiss DSM 960 scanning electron microscope.

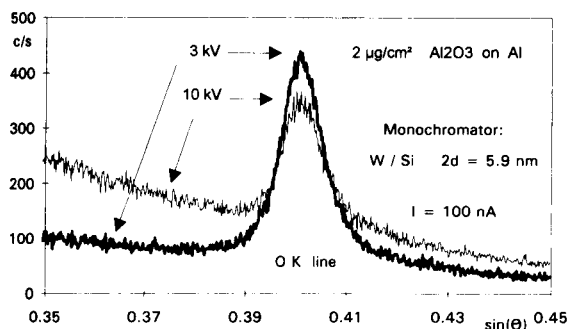


Fig. 4. WDS spectrum of the oxygen K line corresponding to a surface oxide layer on mechanically polished aluminium (mass thickness of  $\text{Al}_2\text{O}_3 \sim 2 \mu\text{g}/\text{cm}^2$ ). Accelerating voltages 3 and 10 kV. Beam current 100 nA. Multilayer W/Si monochromator. Camebax microprobe.

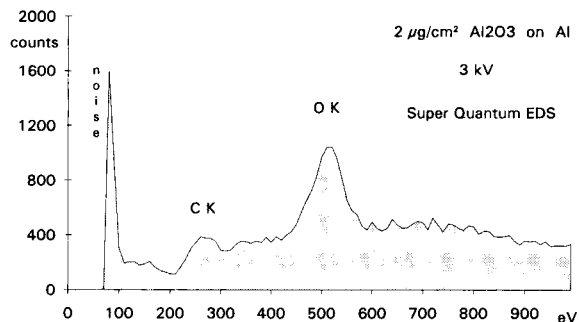


Fig. 5. ED spectrum of the same specimen as in Fig. 4. Accelerating voltage 3 kV. KeveX Super Quantum Si(Li) detector. Zeiss DSM 960 scanning electron microscope.

TABLE 1

Peak count rates and peak-to-background ratios measured for  $M\alpha$  and  $L\alpha$  lines of pure Pb at low overvoltage. (Camebax microprobe. Vertical spectrometers with PET monochromator for M line and LiF monochromator for L line. Beam current 100 nA)

Line (critical energy)	Accelerating voltage (kV)	Excited depth (nm)	Overvoltage ratio	Net count rate (counts $\text{s}^{-1}$ )	Peak to background ratio
Pb $M\alpha$ (2.5 keV)	2.7	15	1.08	10	5
	2.8	20	1.12	25	12
	3.7	50	1.48	40	50
Pb $L\alpha$ (13.05 keV)	13.8	150	1.06	140	0.5
	14.2	200	1.09	320	1.1
	15.0	300	1.15	1050	2.9

TABLE 2

Peak count rates and peak-to-background ratios measured for  $L\alpha$  and  $K\alpha$  lines of pure Cu at low overvoltage (Camebax microprobe. Inclined spectrometer with TAP monochromator for L line. Vertical spectrometer with LiF monochromator for K line. Beam current 100 nA)

Line (critical energy)	Accelerating voltage (kV)	Excited depth (nm)	Overvoltage ratio	Net count rate (counts $\text{s}^{-1}$ )	Peak to background ratio
Cu $L\alpha$ (0.933 keV)	1.26	10	1.34	150	60
	1.67	20	1.80	700	80
	2.84	50	30.4	2700	100
	3.46	70	3.71	4200	105
	4.10	100	4.40	5800	110
Cu $K\alpha$ (8.98 keV)	9.46	70	1.05	110	4
	9.70	100	1.08	350	11
	10.14	1500	1.13	1000	24
	10.60	2000	1.18	2000	40
	11.76	3000	1.31	5500	75

regation is high: Figures 4 and 5 show that an oxygen amount of  $\sim 1 \mu\text{g}/\text{cm}^2$  at the surface of a freshly polished aluminium standard (such an oxygen amount corresponds to  $\sim 5 \text{ nm}$  oxide) is strongly above the limit of detectability, since it gives at 3 kV, which is not a very low accelerating voltage, a peak-to-background ratio close to 5 with a WDS spectrometer and close to 1.7 with an ED spectrometer. Note that the  $k$ -ratios of the O K line would be for this thin oxide film about 3.5% at 3 kV, 1.3% at 5 kV, and 0.4% at 10 kV.

As a general rule, if very thin films have to be characterized, one should preferably use soft characteristic lines and operate at low accelerating voltage, to combine a low depth of excitation with a degree of excitation of the atomic shells sufficient to obtain a favourable peak-to-background ratio. Thus, for the high  $Z$  elements, the M lines should be preferred to the L lines (Table 1); similarly, the L lines of the medium  $Z$  elements would give more sensitivity to near-surface applications than the K lines (Table 2). However, some of these lines have to be used with great care; for example, the  $L\alpha$  lines of the transition elements of the 4th period (Sc to Ni) can be a source of problems in the quantitation, since they exhibit significant changes in their intensity and in their coefficients of self-absorption, depending on chemical bonding [7].

The capability of detecting elements located at some distance below the surface depends firstly on the electron accelerating voltage. The highest voltage available in the commercial instruments (scanning electron microscope or electron probe microanalyzer) is generally between 30 and 50 kV. Figure 1 shows that in such conditions, the ultimate ionization depth is of the order of a few  $\text{mg}/\text{cm}^2$  (i.e. a few micrometers for a target with a density of  $10 \text{ g}/\text{cm}^3$ ). When a buried layer is excited by the electrons, the capability of detecting an element present in this layer depends on the mass thickness of this element, but also on the absorption of its characteristic radiation, which depends on the mass thickness and on the nature of the material(s) covering the buried layer. This will be illustrated in the next paragraph.

#### DISTRIBUTION IN DEPTH OF THE PRIMARY IONIZATION

Several rough approximations of the depth distribution of ionizations, called  $\phi(\rho z)$  by Castaing [1], have been used for a long time to perform the absorption correction in the conventional ZAF procedure for quantitative analysis. The most popular have been the exponential model of Philibert [8] and the square model of Bishop [9]. The latter had the interest of demonstrating that even with an oversimplified model, satisfactory absorption corrections could be obtained in many cases, provided that the mean depth for x-ray generation was well parameterized. Unfortunately, these approximate models were not able to produce good quantitative results in the case of light element analyses (B, C, N, O...) and could not be applied successfully to stratified specimens, in spite of several attempts.

During the 1980s, new models based on more realistic descriptions of the  $\phi(\rho z)$  distribution have been developed. As far as we know, the three models below are employed in most laboratory or commercial software packages presently available.

(i) The MSG (modified surface-centered Gaussian) model of Packwood and Brown [2,3] is based on a random walk approach, which leads to describe the  $\phi(\rho z)$  function by a surface-centred gaussian, which, however, has to be modified by an exponential transient near the surface to account for the progressive scattering of the beam penetrating the specimen:  $\phi(\rho z) = \gamma \{1 - [\gamma - \phi(0)]/\gamma \exp(-\beta\rho z)\} \cdot \exp[-(\alpha\rho z)^2]$ . Four shape parameters define the distribution: the width  $1/\alpha$  of the gaussian (the calculation of which involves mainly the Bethe electron slowing down expression); the amplitude  $\gamma$  of the gaussian (which involves the ionization cross-section); the actual value  $\phi(0)$  of the distribution at the surface (which involves mainly the electron backscattering coefficient); the argument  $\beta$  of the exponential term, which alters the pure gaussian near the surface. The original parameters of Packwood and Brown have been revised by Bastin to improve the results for light element analyses. However, when it

is based on the above shape parameters, the resulting  $\phi(\rho z)$  function leads to difficulties for the evaluation of the so-called atomic number effects. It is why, instead of relating empirically the argument  $\beta$  to  $\alpha$  as in the initial approach, Bastin et al. [10] later proposed to set it so that the  $\phi(\rho z)$  distribution would have the same area as in the models of Pouchou and Pichoir.

(ii) The PAP model by Pouchou and Pichoir [4–6] uses two connected parabolas to describe the distribution:  $\phi(\rho z) = a_1(\rho z - R_m)^2 + \phi(0)$  from  $\rho z = 0$  to  $R_c$  (connection point) and  $\phi(\rho z) = a_2(\rho z - R_x)^2$  from  $\rho z = R_c$  to  $R_x$  (ultimate ionization depth). The model has been designed to be in agreement with the definition of  $\phi(\rho z)$  by Castaing, i.e. the area  $F$  of  $\phi(\rho z)$  is proportional to the number  $N_j$  of primary ionizations produced per incident electron on the level  $j$  of atoms A:  $N_j = C_A N^\circ Q_j(E_0) F/A$ .

$Q_j(E_0)$  is the ionization cross section of level  $j$  at initial electron energy  $E_0$ ;  $\rho$  is the specific weight of the target;  $A$  is the atomic mass of the element;  $C_A$  is its mass concentration;  $N^\circ$  is the Avogadro's number). The computation of  $N_j$  involves expressions for the electron energy loss  $dE/d\rho s$ , the ionization cross-section, and the losses  $1 - R$  due to backscattered electrons:

$$N_j = C_A (N^\circ/A) R \int_{E_0}^{E_j} Q_j(E) / (dE/d\rho s) dE$$

In addition to the fundamental area parameter, three shape parameters are used to define completely the distribution: the ultimate ionization range  $R_x$  for the level of interest, the location of the maximum of the distribution  $R_m$  and the surface ionization  $\phi(0)$ . The PAP model has been principally parameterized on the basis of stratified specimen experiments. It has been shown to give reliable results in this field as well as for light element analysis [11–14].

(iii) The XPP model is the latest model produced by Pouchou and Pichoir [6,15]. The aim was to build a reliable but simple mathematical model, able to describe properly with a single set of expressions the  $\phi(\rho z)$  distribution even at oblique electron beam incidence (this allows to use it efficiently in all practical EDS/SEM situa-

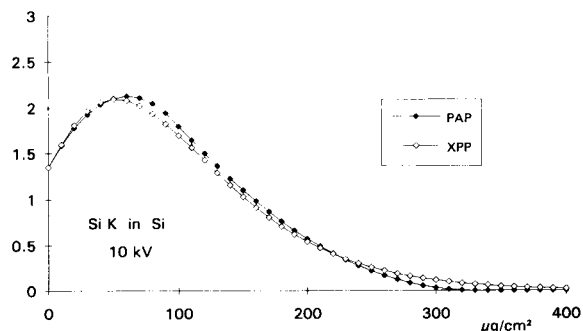


Fig. 6. Comparison of the  $\phi(\rho z)$  functions predicted by PAP and XPP models for the Si  $K\alpha$  radiation in pure Si.

tions). A satisfactory description of the distribution is obtained by combining exponential and linear functions, as follows:  $\phi(\rho z) = a \exp(-\alpha\rho z) + [\phi(0) - a] \cdot \exp(-\beta\rho z)$ . The basic parameter is still the area below the  $\phi(\rho z)$  curve, as in the PAP model. The surface ionization  $\phi(0)$  is also unchanged; the two other shape parameters are the mean depth for x-ray generation  $R_b$  and the slope of the distribution at the surface  $\phi'(0)$ . A unique feature of XPP is that its parameters are expressed as a function of the specimen tilt angle [16].

Figures 6 and 7 compare the  $\phi(\rho z)$  distributions predicted by PAP and XPP models for Si K ionizations by 10 keV electrons in light and heavy targets (pure Si and the  $\text{ReSi}_2$  compound) at normal beam incidence. Although the models use different mathematical descriptions, it can be verified that they produce very similar distributions.

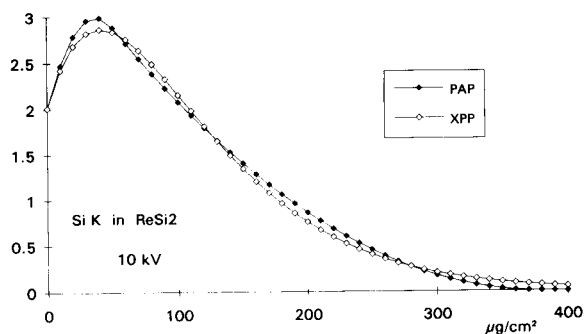


Fig. 7. Comparison of the  $\phi(\rho z)$  functions predicted by PAP and XPP models for the Si  $K\alpha$  radiation in the compound  $\text{ReSi}_2$ .

It is also interesting to note that for a given line at a given voltage, the ultimate ionization depth (expressed in mass units) does not depend strongly on the atomic number of the target. This is a great advantage in the study of layered specimens, since it permits to estimate the excited depth without knowing the nature of the specimen. In practice, if an estimation of the ionization depth is needed, for example to initialize a procedure, the following modification of the Castaing formula can be used ( $R_x$  in  $\mu\text{g}/\text{cm}^2$ ,  $E_0$  and  $E_j$  in keV):

$$R_x = 8(E_0^{1.7} - E_j^{1.7})g(U_0)$$

with

$$g(U_0) = 1 + 3/[E_j^{0.5}(U_0 + 0.3)^2] \text{ and } U_0 = E_0/E_j$$

When soft x-rays are used for the analysis, one has to be aware that the actual depth of analysis for these lines may differ strongly from the excited depth, because of the influence of absorption. Figures 8 and 9, relative to the oxygen K line respectively in chromium and titanium at 5 and 15 kV, illustrate this point. Although Cr and Ti are very close in the periodic table, they behave differently for the oxygen analysis, because they have very different mass absorption coefficients for the O K line:  $\mu/\rho = 2900 \text{ cm}^2/\text{g}$  in Cr and  $22100 \text{ cm}^2/\text{g}$  in Ti. While in Cr (Fig. 8) the distribution of the emerging intensity changes significantly with the accelerating voltage (the maximum effective depth of x-ray emission drops from 100 to about  $500 \mu\text{g}/\text{cm}^2$  from 5 to 15 kV),

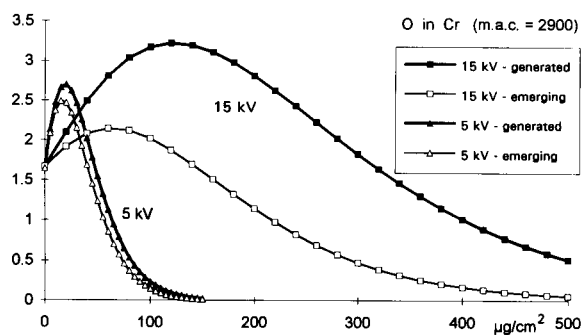


Fig. 8. Distributions of the generated and of the emerging O K $\alpha$  intensity at 5 and 15 kV in a Cr matrix ( $40^\circ$  take-off angle assumed).

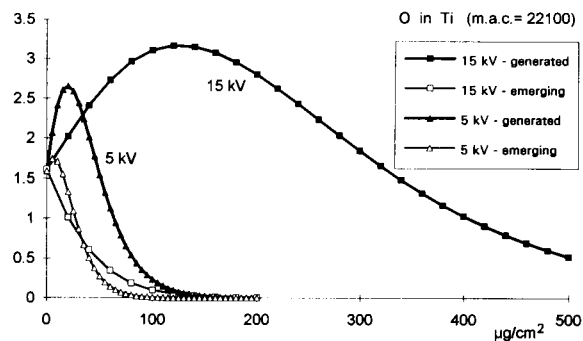


Fig. 9. Distributions of the generated and of the emerging O K $\alpha$  intensity at 5 and 15 kV in a Ti matrix ( $40^\circ$  take-off angle assumed).

the effective depth of O K emission in a Ti matrix (Fig. 9) is almost independent of the voltage, and is limited to about  $100 \mu\text{g}/\text{cm}^2$  by the strong absorption in Ti.

#### USE OF THE $\phi(\rho z)$ FUNCTION FOR LAYERED SPECIMENS

In the general case of a stratified specimen, a layer of index  $s$  located from mass depth  $\rho z_s$  to  $\rho z_{s+1}$  and containing element A with mass concentration  $C_A^s$  emits in a characteristic line of A a x-ray intensity proportional to:

$$I_A^s = C_A^s T_A^s \int_{\rho z_s}^{\rho z_{s+1}} \phi_A(\rho z) \exp(-\chi_A^s \rho z) d\rho z$$

with

$$T_A^s = \prod_{k=1}^{s-1} \exp[\Delta\rho z_k (\chi_A^s - \chi_A^k)]$$

$T_A^s$  takes into account the absorption of A radiation emitted in layer  $s$  by the upper layers of mass thicknesses  $\Delta\rho z_k = \rho z_k - \rho z_{k-1}$ .  $\chi_A^s$  and  $\chi_A^k$  are the absorption factors of A radiation in the layers  $s$  and  $k$  ( $\chi = \mu/\rho \text{csc}\theta$ ).

The intensity of a bulk standard would be obtained by setting  $T_A^s = 1$  and by integrating from  $\rho z = 0$  to infinity (or  $R_x$  for the PAP model). The above expression is general, and is valid for every  $\phi(\rho z)$  model.

In the analytical  $\phi(\rho z)$  models presently available, it is assumed that the distribution is not basically different in a layered target and in a

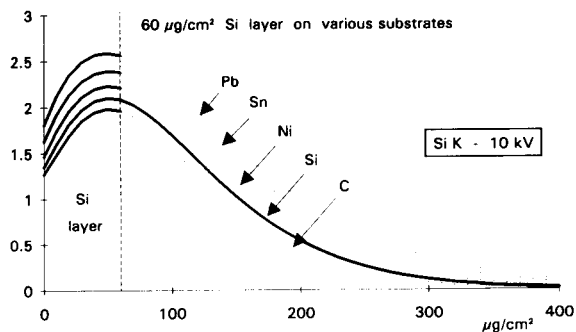


Fig. 10.  $\phi(\rho z)$  functions of a  $60 \mu\text{g}/\text{cm}^2$  Si layer ( $\sim 250 \text{ nm}$ ) for light to heavy substrates. Si  $K\alpha$  line at 10 kV. XPP model.

homogeneous target which would have the same mean atomic number. Obviously, this assumption is strictly valid only when the layers have similar diffusion and stopping powers of the impinging electrons (i.e. when the layers have similar mean atomic numbers). In most cases where these conditions are not satisfied, the basic parameters of every  $\phi(\rho z)$  model can be computed with a satisfactory accuracy by use of an appropriate weighting law for each of them [3,6,17]. Figures 10 and 11 illustrate for the XPP model the distortion of the  $\phi(\rho z)$  curve predicted by such a weighting method in the case of a Si layer on different substrates and for Si layers of variable thickness on a heavy substrate. However, it should be pointed out that when the layers have very different atomic numbers, the approximation of a progressive distortion of the  $\phi(\rho z)$  curves becomes more questionable: Monte-Carlo simulations actually indicate that non negligible distortion of

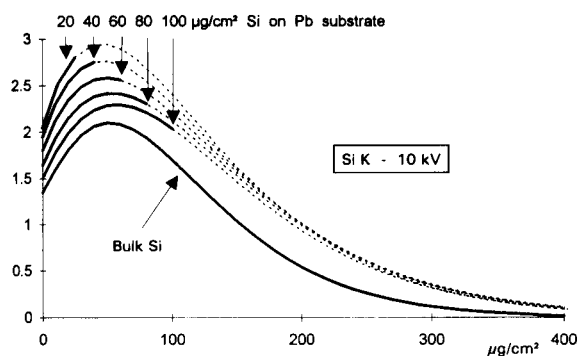


Fig. 11.  $\phi(\rho z)$  functions of Si layers of variable thickness on a heavy Pb substrate. Si  $K\alpha$  line at 10 kV. XPP model.

the  $\phi(\rho z)$  curves may appear near the interfaces [18]. In the case of a single layer on a substrate, the most critical situation occurs for extreme differences in the atomic numbers (e.g. very light element on heavy substrate), and when the depth of the interface is of the order of half the ultimate ionization depth. In these particularly unfavourable situations, we believe that the error on the computed intensities may reach up to 20% relative. Fortunately, for all the elements of a given layer, the error is almost the same. Hence, since the process of simultaneous determination of thickness and composition of a layer requires to normalize the concentrations, the error on the chemical analysis is limited, and most of the uncertainty lies in the thickness determination. In those extreme situations where the quantitation may become uncertain, the operator should always try to select the most appropriate analytical conditions. For example, in the case of a thin film of low atomic number at the surface of a heavy substrate, it may be better, even if the experimental peak-to-background ratio becomes poorer, to operate at a rather high voltage, so that the film will appear very thin compared to the ultimate ionization depth. Hence, it will become possible to approximate almost perfectly the  $\phi(\rho z)$  curve of the specimen by that of the substrate.

Before introducing the computer programs available for the characterization of layered specimens, it is useful to explain with simple arguments how a set of  $k$ -ratios makes it possible to get simultaneously the mass thickness and the composition of a layer on a substrate, and to correlate this with the conventional analysis of homogeneous volumes. Basically, in the case of homogeneous volumes, it is not necessary to analyze all  $N$  elements present in the sample: the analysis of  $N - 1$  elements and the computation of the last one by difference is actually sufficient. In practice however, all the elements are generally measured when possible, because the extra information allows to check that the sum of the concentrations is close to 100%. In the case of stratified specimens, one can use the extra information given by the sum of the  $k$ -ratios to deduce the mass thickness of the layer, provided that all the elements of the layer are measured and that



their concentrations are normalized at each step of the computation.

#### THE STRATA AND MULTIFILM PACKAGES

*Strata* and *Multifilm* are two software packages developed in cooperation with SAMx for advanced applications in x-ray microanalysis, mainly for the characterization of surface segregation and stratified specimens.

*Strata* is available either in a *PC / Windows* or in a *SUN / Sunview* version; it is a general purpose and user-friendly off-line program that uses *k*-ratios as input data. *Multifilm*, which has been specially designed for the Kevex ED spectroscopy system, can additionally handle Kevex ED spectra directly to produce a *k*-ratio file. Both programs enable to process data measured at one or several accelerating voltages. The voltage(s) can be completely different from one element to another. Either the PAP model or the XPP model can be applied. The latter allows to use oblique electron beam incidence.

The latest version of *Multifilm* offers also a ASAP option (“as soon as possible”). Whatever the number of elements to be analyzed, and whatever the number of accelerating voltages used, the ASAP mode allows to measure only a limited set of standards (at least one, which does not necessarily needs to contain an element present in the specimen). The x-ray intensities of all missing pure standards are then computed on the basis of the measured one(s). Contrary to the case of conventional analysis of homogeneous microvolumes, it is not easy in the case of stratified specimens to work with no standard at all, because this would require to know very accurately the beam current and the solid angle of detection. This is why *Multifilm*/ASAP requires at least one standard. Presently, the ASAP quantitation may be applied successfully for K lines. For L and M lines, further basic work is needed, because some physical parameters involved in the computation of the characteristic L and M intensities (namely the Coster-Kronig radiationless transition rates and the relative weights of the

lines in a series) are not known presently with enough accuracy [15,20,21].

The *Strata* and *Multifilm* programs both include the secondary emission due to the fluorescence excited by characteristic lines and by the x-ray continuum. The formulae developed by the authors are used [6]. The implementation of the fluorescence by the continuum has led to a revision in the original PAP and XPP models of the expressions for the primary intensity [19]. Taking into account both types of fluorescence is very important; actually, in some cases where high energy radiation is used, omitting the secondary emission can lead to strong errors, even when only a qualitative understanding of the experimental data is required. Since a full computation of the fluorescence at several voltages and for a layered specimen requires time (the computing time almost doubles when the fluorescence is included), a switch in the program allows skipping this secondary effect, if so desired. Actually, the fluorescence may be neglected every time only soft x-rays (with energy in the keV region or less) are considered, but it must definitely be taken into account for more energetic lines. Several experimental examples have already shown [6,16] that, although the excitation by fluorescence is for every atom of the target a low probability event compared to the primary ionization by electrons, the secondary emission represents, as a whole, a non negligible intensity since it is produced in a volume larger by several orders of magnitude than the primary emission (the range of excitation by 10 keV photons is typically 10 times the range of excitation by 20 keV electrons). Figure 12 gives a set of theoretical curves computed with the *Strata* program, showing the contribution of the fluorescence in the simple case of Zn coatings (0.2 to 5  $\mu\text{m}$  thickness) on a Cu substrate. At the lowest voltages, just above the Zn K critical energy, one can observe that, because of the fluorescence by the continuum, the *k*-ratio for the Zn  $K\alpha$  line is not equal to 1, but lies between 0.93 and 1 (the amount of Zn that can be excited by fluorescence is less in the film than in a bulk standard). On the other hand, at voltages just above the Cu K critical energy where the electrons are not able to produce Cu K exci-

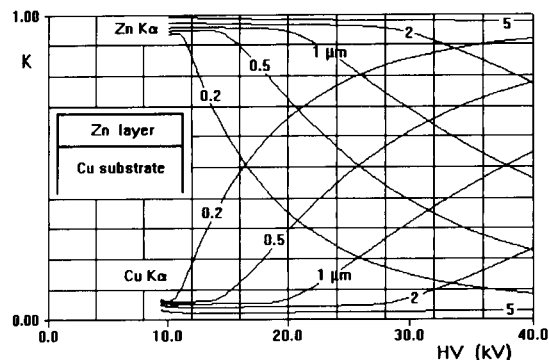


Fig. 12. Curves of Zn  $K\alpha$  and Cu  $K\alpha$   $k$ -ratios vs. accelerating voltage for Zn layers of different thicknesses (0.2 to 5  $\mu\text{m}$ ) on a Cu substrate, showing the fluorescence mainly due to the excitation by the continuum (40° take-off assumed).

tations in the substrate, the Cu  $K\alpha$   $k$ -ratio is not zero, but lies between 0 and 7%, depending on the layer thickness. In the present case, this represents mainly the excitation of the substrate by the continuum, since the excitation of Cu by the Zn  $K\beta$  line is only a small fraction of the total fluorescence effect. It should be pointed out that for the thickest Zn film (5  $\mu\text{m}$ ), no primary ionization of the Cu substrate occurs up to 40 kV, but the Cu fluorescence emission still represents about 3% of the intensity of a pure bulk Cu standard. This shows the danger of assuming that a thick film is equivalent to a bulk specimen and of analyzing it by means of conventional software programs, which neglect most often the fluorescence by the continuum. We believe that this is a frequent source of misinterpretation of x-ray microanalysis data.

#### OPERATING STRATA AND MULTIFILM PROGRAMS

*Strata* and *Multifilm* offer two principal modes of operation, and additional accessory features.

(1) The more general mode is a graphical mode called “K vs. HV”, in which  $k$ -ratios curves are calculated and displayed as a function of the accelerating voltage, for a given description of the specimen (mass thicknesses and compositions of the layers). In this mode, the specimen description may be either a hypothesis of the operator

(as in Fig. 12), or the result of another working mode, the iterative mode. It is very useful to operate “K vs. HV” prior to an experiment, to verify if one can reasonably expect to solve a given problem, and to define the best operating conditions for this problem (analytical line, voltage range ...). “K vs. HV” can also be used after the experiment, to process the data by a trial and error approach, in which the operator formulates reasonable hypotheses, to obtain the best agreement between the calculated and the experimental  $k$ -ratios. This operating mode is of general use and can be applied in any case. However, this does not imply that all problems can be solved completely with this method: it should not be forgotten that, in complex cases, a satisfactory agreement between computed and experimental  $k$ -ratios can be obtained for several hypotheses on the specimen structure! Starting from the 3.0 version, *Strata* provides a forward and backward switch, from the “K vs. HV” display to a “K vs.  $R_x$ ” display, which may help in understanding the structure of the specimen (for a given line,  $R_x$  is the ionization depth corresponding to HV). On a “K vs.  $R_x$ ” graph, the elements located in the same layer appear at the same abscissa, whatever their critical energy, unlike on a “K vs. HV” plot.

(2) The other important operating mode is the automatic mode, whereby the thicknesses and the compositions of the strates can be obtained simultaneously by an iterative procedure. This powerful mode of operation can be applied under certain conditions:

(i) all elements in a layer of unknown composition should be measured, except those determined by stoichiometry;

(ii) all the layers to be chemically characterized (including the substrate) should be excited, and their radiation should not be completely absorbed by the upper layers;

(iii) an element may be present in several layers, but it is allowed to have an unknown concentration in one layer only. (It is recalled that an element determined by stoichiometry is not considered as having an unknown concentration);

(iv) every layer is supposed to have a uniform composition.

In order to determine concentrations and thicknesses, different iterative schemes are used, depending on whether some elements (index  $i$ ) are present in several layers (index  $s$ ) or not. In both cases, at each iteration step  $j$ , the concentrations  $C_j(i, s)$  and the thicknesses  $T_j(s)$  are determined inside separate loops. The concentrations are always obtained by a simple iteration:  $C_{j+1}(i, s) = C_j(i, s) \cdot K_{\text{exp}}(i)/K_{\text{calc}}(i)$ . Here,  $K_{\text{exp}}(i)$  represents the experimental  $k$ -ratio of element  $i$  at a given voltage, and  $K_{\text{calc}}(i)$  the computed value corresponding to the current specimen description.

When there is no common element, the thicknesses are also determined by simple iteration:

$$T_{j+1}(s) = T_j(s) \sum_i K_{\text{exp}}(i) / \sum_i K_{\text{calc}}(i).$$

When there are common elements, we adopted a different iteration scheme. The concentrations are still computed by a simple iteration, as in the previous case. But for the thicknesses, the iterative technique is to look for the least deviation  $\Delta$  between the calculated  $k$ -ratios  $K_{\text{calc}}(i)$  and the experimental data  $K_{\text{exp}}(i)$ . The thickness leading to the least deviation is estimated from the deviations  $\Delta^0$ ,  $\Delta^+$  and  $\Delta^-$  corresponding respectively to the current thickness  $T_j$ , to  $T_j + \delta T_j$  and to  $T_j - \delta T_j$  (a convenient value for  $\delta T_j$  is  $T_j/20$ ). The iteration is stopped when all the concentrations and thicknesses are stationary within  $10^{-4}$ .

(3) Two accessory working modes of the *Strata* and *Multifilm* programs are the plot of  $\phi(\rho z)$

curves (see Figs. 6-11). Starting from the 3.0 version, *Strata* also enables to compute and plot calibration curves of  $k$ -ratios versus the mass thickness, for layers of known composition on a known substrate.

#### EXAMPLES OF STRATA OR MULTIFILM APPLICATION

The examples in this paragraph illustrate different types of applications of *Strata* or *Multifilm*, from very simple situations to more complex ones. In the following examples, the thicknesses will frequently be expressed in Angströms, nanometers or micrometers for an easier understanding. However, it should be emphasized that only mass thicknesses make sense and can actually be determined by the technique. The use of linear thicknesses implies that a value of the density is assumed in the computation. If not specified, the nominal density of the bulk material is assumed.

##### Example 1: bilayer on substrate (no common element)

The first example is a typical problem of simultaneous determination of thickness and composition for which no other method can give a reliable result as easily and as quickly as XRMA can do. An experiment of Willich [14] has been selected. The specimen consists of two layers (Ni-Cr

Layer #	Element	# atoms	Mass thick. ( $\mu\text{g}/\text{cm}^2$ )	Thick. ( $\text{\AA}$ )	Density
1	Ni	0.0000	7.4	100.0	7.41
	Cr	0.0000			
2	Fe	0.0000	10.6	100.0	10.60
	Gd	0.0000			
	Pt	0.0000			
Substrate	Si	1.0000			

Fig. 13. Specimen description window of the *Strata* software before applying the iteration to the experimental  $k$ -ratios of Table 3.

TABLE 3

$k$ -ratios for Ni, Cr and Fe  $K\alpha$ , Gd  $L\alpha$  and Pt  $M\alpha$  (from [14]) used by *Strata* for the characterization of the layered specimen described in Figure 13 (take-off  $40^\circ$ )

$E_0$ (keV)	Ni $K\alpha$	Cr $K\alpha$	Fe $K\alpha$	Gd $L\alpha$	Pt $M\alpha$
20	0.0151	0.0744	0.0258	0.0123	0.0083
25	0.0084	0.0443	0.0147	0.0076	0.0058
30	0.0054	0.0299	0.0098	0.0052	0.0048

and Fe–Gd–Pt) on top of a Si substrate. The  $k$ -ratios of the Ni, Cr and Fe  $K\alpha$  lines, of the Gd  $L\alpha$  line and of the Pt  $M\alpha$  line, measured with respect to pure standards at 20, 25 and 30 kV are given in Table 3. Figure 13 is the initial description of the problem in *Strata* (the unknown concentrations are set to zero, the unknown thicknesses of both layers are initialized to 100 Angströms, the assumed densities are respec-

tively 7.41 and 10.60). Figure 14 shows a black and white copy of the screen at the end of the iteration, using the PAP model with full fluorescence effects (lines and continuum). After 5 iterations, the compositions and mass thicknesses of both layers are obtained, with a mean relative deviation between the experimental data and the computed  $k$ -ratios slightly less than 1%. For this specimen, the technique of Rutherford Backscattering Spectrometry is applicable, and can give the same type of information. Table 4 shows the excellent agreement between the results of *Strata* and the RBS results reported by Willich. After the iterative process, the “K vs. HV” mode of *Strata* can be executed to check the agreement between the computed curves and the experimental data (Fig. 15). This comparison may also be done by switching to the “K vs.  $R_x$ ” mode (Fig. 16). The interest of the latter mode is obvious: as

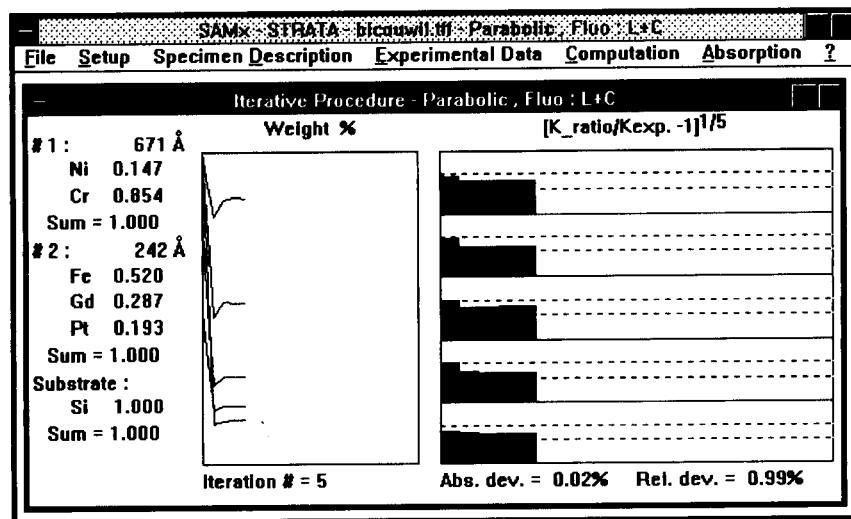


Fig. 14. Iteration window of the *Strata* software at the end of the iterative procedure.

TABLE 4

Comparison of the XRMA results using *Strata* with the RBS results for a Ni–Cr/Fe–Gd–Pt/Si stratified specimen (experimental data from [14])

	Surface layer			Buried layer			
	wt.% Ni	wt.% Cr	Thickness (nm)	wt.% Fe	wt.% Gd	wt.% Pt	Thickness (nm)
XRMA	14.7	85.4	67.1	52.0	28.7	19.3	24.2
RBS	14.4	85.6	68.3	51.4	28.6	20.0	24.6

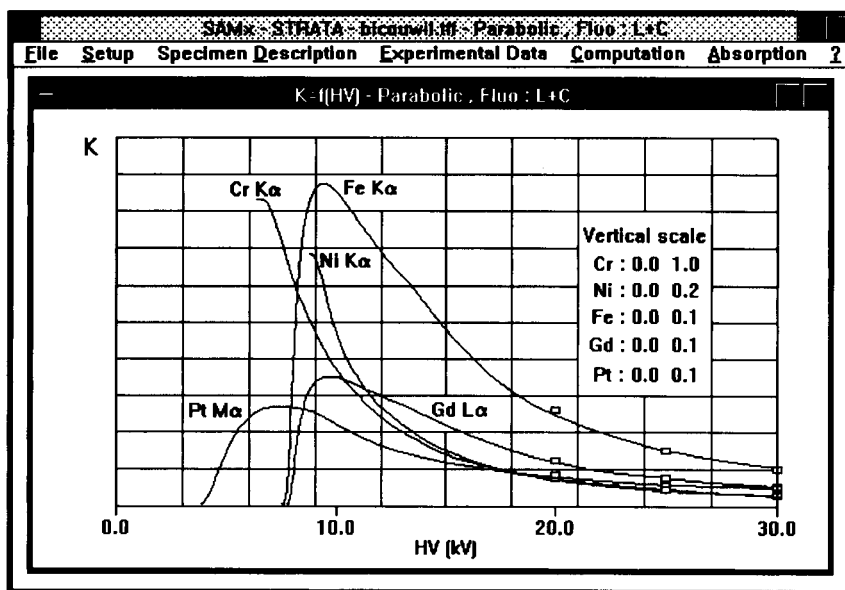


Fig. 15. Comparison of the experimental  $k$ -ratios of Table 3 with the “K vs. HV” curves computed as a function of accelerating voltage for the specimen description of Fig. 14.

mentioned earlier, the curve corresponding to the Pt  $M\alpha$  line lies in the same  $R_x$  range as the curves for Fe and Gd (elements present in the same layer), whereas in the “K vs. HV” display mode, the curve for Pt  $M\alpha$  was appearing at a

lower energy, because of its critical excitation energy significantly lower than the Fe K and Gd  $L_3$  levels. This example gives the opportunity of four additional comments:

(i) since there is no common element in the

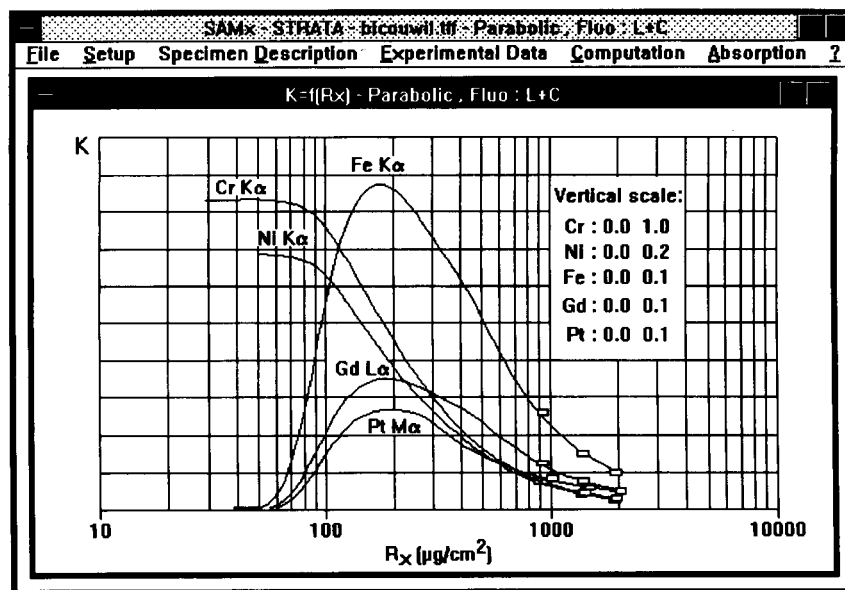


Fig. 16. Comparison of the experimental  $k$ -ratios of Table 3 with the “K vs.  $R_x$ ” curves plotted vs. the ultimate excitation depth for the specimen description of Fig. 14.

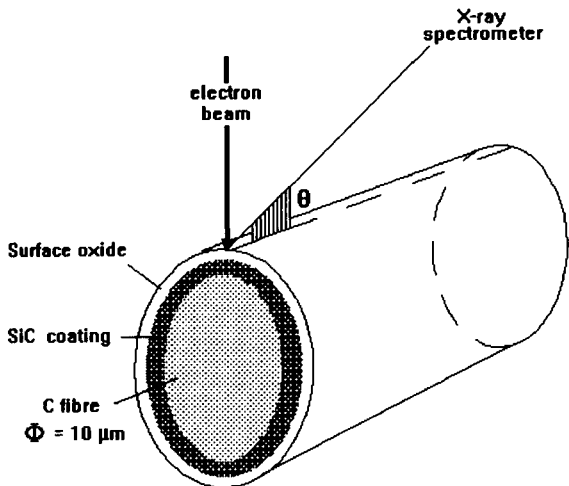


Fig. 17. Analytical geometry used for in-depth analysis of a coated fibre.

different strates, the sum of the concentrations obtained for both strates is necessarily 100%;

(ii) since there is no common element in the different strates, it would have been sufficient to measure the *k*-ratios at a single voltage to get the full information. The measurements at three different voltages were made just to verify the consistency of the results;

(iii) it can be observed that the measurements have been made at rather high voltages. In such conditions, the films represent a small fraction of the excitation range, so that the *k*-ratios are small and the peak-to-background ratios are poor. Consequently, a great care is needed in the measurements to avoid systematic errors and ensure a sufficient statistical precision. Willich was em-

ploying such extreme conditions to be able to process the data with his own simplified software, in which it is assumed that the  $\phi(\rho z)$  function in the whole specimen can be approximated by that of the substrate. With the more sophisticated model used in *Strata*, this approximation is not needed; thus, it would be easier (mainly if an ED spectrometer was used) to perform the analysis at a lower voltage, for instance 15 kV;

(iv) in such a specimen, it would be interesting, mainly in the case of a single voltage, to measure also the *k*-ratio of the Si substrate. This additional information would allow to check the global consistency of the experiment.

*Example 2: characterization of a coating on a fibre (common elements, very light elements)*

This second example has several particularities: the geometry of the specimen, the analysis of very light elements, and the presence of common elements in several layers. The specimen is a carbon fibre (typical diameter 10 μm) coated with silicon carbide (thickness in the range 100-200 nm). The objective of the experiment was to control the composition of the coating and its thickness, as well as the oxidation of the coating at the surface. Because of the special shape of the specimen, and because light elements have to be analyzed, this type of experiment requires a great deal of care, mainly to avoid experimental errors that could come from a bad geometrical configuration of the specimen with respect to the spectrometer. In particular, it is essential for the electron beam to be accurately focused on top of

SALC - STRATA - elcsurc.tif - Parabolic - Fluo - None					
File Setup Specimen Description Experimental Data Computation Absorption					
Specimen Description					
Valid		Cancel		Help	
Layer		+		-	
Element		+		-	
Layer #	Element	# atoms	Mass thick. (μg/cm <sup>2</sup> )	Thick. (Å)	Density
1	Si	1.000	2.3	100.0	2.33
	O	2.000			
2	Si	0	3.2	100.0	3.15
	C	0			
Substrate	C	1.000			

Fig. 18. Specimen description window of the *Strata* software before applying the iteration to the experimental data of Table 5.

TABLE 5

Relative intensities of C, O and Si  $K\alpha$  lines measured at several electron energies on the specimen of Fig. 17 (take-off angle  $40^\circ$ )

$E_0$ (keV)	Si $K\alpha$ (pure standard)	$E_0$ (keV)	O $K\alpha$ ( $Y_3Fe_5O_{12}$ standard)	C K (SiC standard)
2.3	0.623	1.1	0.3000	0.800
3.0	0.646	2.3	0.0780	0.900
3.5	0.646	3.0	0.0682	1.036
5	0.591	5.0	0.0240	1.149
7.5	0.346	7.5	0.0200	2.038

the fibre, and for the fibre to be oriented towards the spectrometer port (Fig. 17), so that the angle of incidence of the electrons and the take-off angle of the x-rays are well defined.

Table 5 gives the relative intensities measured for the  $K\alpha$  lines of Si, O and C in the low accelerating voltage range (1.1–7.5 kV). For oxygen analysis, a conductive  $Y_3Fe_5O_{12}$  standard was used; a SiC compound standard was used for carbon. For this element, area measurements of the emission band were necessary, as shown later.

Figure 18 is the specimen description window of *Strata* prior to the actual calculation. The

Si–C layer of unknown composition (concentrations set to zero) and of unknown thickness (initial thickness set to 10 nm) is supposed to be covered at the surface by an oxide film of composition  $SiO_2$  and unknown thickness.

This example, where two elements (Si and C) are simultaneously present in two components of the layered structure, can be solved by the iterative method, since the concentrations of Si and C are unknown in one layer only. Figure 19 shows the copy of the screen at the end of the calculation, applying the XPP model with full fluorescence effects. The procedure converges after 18 iterations, with a mean relative deviation of 2.7% between the computed and the experimental data. The Si–C layer is found to have a thickness of approximately  $53 \mu\text{g}/\text{cm}^2$  (168 nm assuming a density of  $3.15 \text{ g}/\text{cm}^3$ ) and a composition very close to the SiC stoichiometry (the bottom window displays weight fractions without normalization, while the top window gives the corresponding normalized atom fractions). The thickness of the oxide film at the outer surface of the coating is found to be  $0.9 \mu\text{g}/\text{cm}^2$  (3.7 nm assuming a density of  $2.33 \text{ g}/\text{cm}^3$ ).

Switching to the “K vs. HV” mode allows to compare the curves of relative intensities corre-

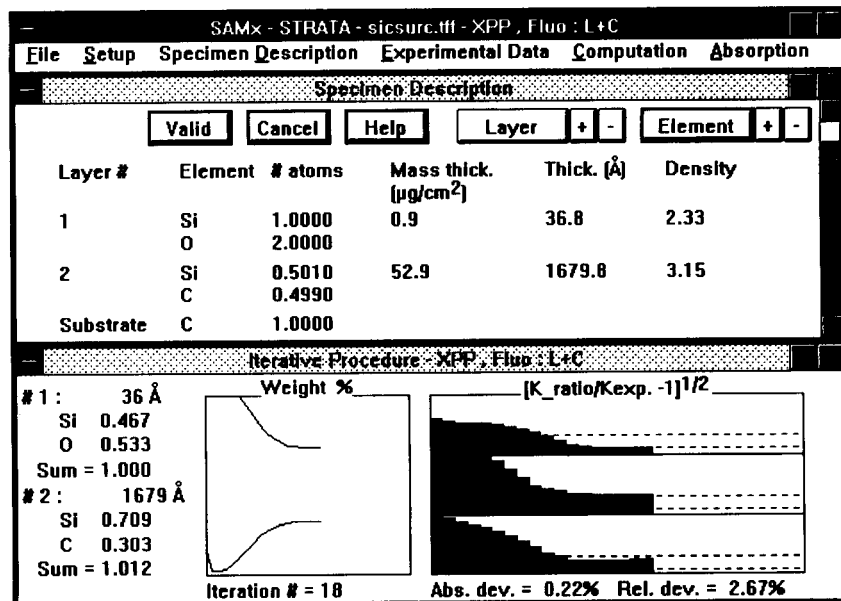


Fig. 19. Result of the *Strata* iterative procedure applied to the problem defined by Fig. 18 and Table 5.

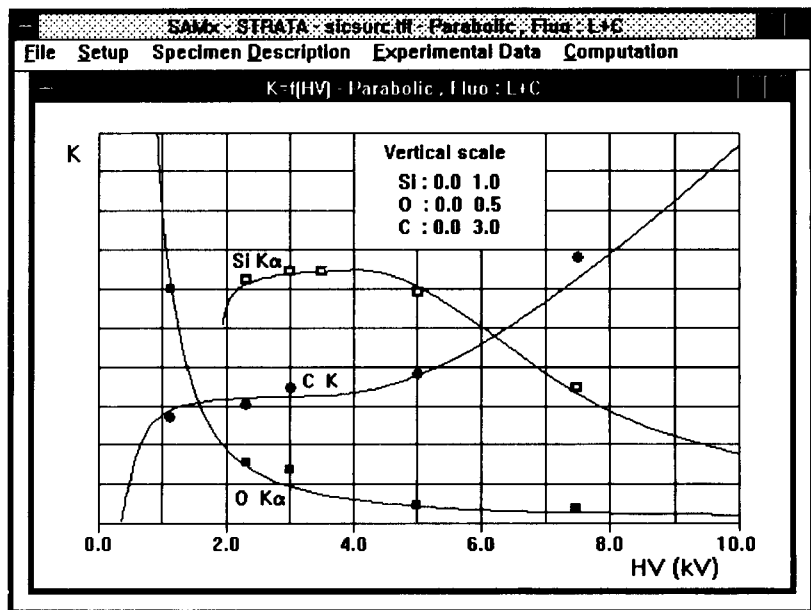


Fig. 20. Comparison of the experimental data of Table 5 with the "K vs. HV" curves computed as a function of accelerating voltage for the specimen description of Fig. 19.

sponding to this result with the experimental data (Fig. 20). It can be seen that with two accelerating voltages only (typically 3 kV and 7.5 kV), a full characterization of this particular specimen would have been possible.

Figure 21 compares the WDS spectra obtained for the C K line in different operating conditions. At 3.5 kV, the primary electrons are able to excite the SiC coating only, as can be verified on

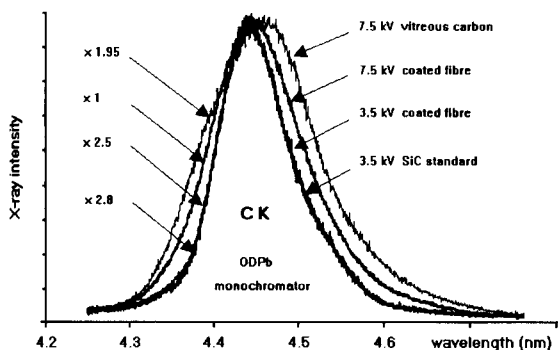


Fig. 21. WDS spectra of the C K line recorded on the SiC-coated carbon fibre at two different voltages (3.5 and 7.5 kV). Comparison with the characteristic lines of vitreous carbon and of SiC. Synthetic multilayer monochromator (W/Si 2d = 5.9 nm).

Fig. 20. Consequently, the C K band is narrow, and has the same shape as a SiC standard. On the contrary, at 7.5 kV, the electrons excite also the carbon substrate, which produces approximately one half of the emerging intensity. Hence, the C K emission band becomes wider, and tends to that of vitreous carbon (which is similar to that of an uncoated fibre). This illustrates that whenever very light elements are present in stratified specimens under different chemical forms, it is necessary to perform area measurements at every voltage, to take into account the continuous change of the line shape with the analyzed depth.

*Example 3: "As soon as possible (ASAP)" analysis of a coated substrate and determination of the coating thickness*

This last example illustrates the capability of the *Multifilm* software to characterize stratified specimens by ED spectrometry with a reduced set of standards (ASAP option). This example has two other particularities: firstly, the specimen component which is supposed to have an unknown composition is the substrate; secondly, to illustrate the wide capability of the procedure,



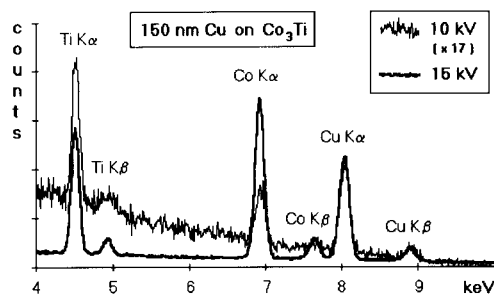


Fig. 22. ED spectra in the region of the Ti K to Cu K lines for a Cu/Co<sub>3</sub>Ti layered specimen at 10 and 15 kV. Spectra recorded at the same beam current. Normal incidence. 35° take-off angle. Super Quantum detector.

some of the measurements have been done at oblique electron beam incidence and variable take-off angle.

The specimen is a compound close to the Co<sub>3</sub>Ti composition (20.7 wt.% Ti nominal), covered by a copper layer having a thickness in the range 100–200 nm. The problem is to analyze the coated compound and to evaluate simultaneously the layer thickness. Figure 22 shows typical EDS spectra recorded at 10 and 15 kV using the same beam current and normalized at the Cu K $\alpha$  peak.

In this example, there is no common elements in the layers. Hence, one voltage is sufficient to characterize the specimen. Several spectra have

been acquired at the same voltage setting (15 kV), but in different geometrical configurations (normal or oblique incidence, variable take-off angle). In every configuration, the spectra of pure Cu, Co, Ti and additionally Cr standards have been recorded with the same beam current as the specimen spectra. Table 6 shows that the normal *Multifilm* quantitation procedure referring to the Cu, Co and Ti standards gives a composition very close to the nominal one and a Cu thickness of 144 nm in average (the assumed density is 8.96 g/cm<sup>3</sup>). In the ASAP mode, any standard can be used, even if it does not correspond to an element present in the specimen. Using only a pure Cr standard, the composition of the coated specimen and the thickness of the copper layer are found to agree very well with the results obtained using the full set of standards.

This example shows that for routine control applications, the ASAP procedure allows the user to avoid spending too much time in acquiring and processing the spectra of the standards. In the present state, we consider that its full reliability is limited to the K lines of light to medium Z elements. For the very light elements and the L and M lines, some improvements are expected as the result of the effort recently undertaken in a few laboratories to improve the standardless quantitative techniques in general [15,20–22].

TABLE 6

Characterization of a Co–Ti compound (20.7 wt.% Ti nominal) coated with pure Cu, applying the *Multifilm* program to EDS spectra acquired at 15 kV for different tilt and take-off angle [Comparison of the results obtained either using the full set of standards (Cu, Co, Ti) or using a single reference standard (“ASAP” procedure). KeveX Super Quantum Si(Li) detector. Zeiss DSM 960 scanning electron microscope]

Azimuth (deg.)	Tilt (deg)	Take-off (deg)	Full set of standards (Cu, Co, Ti)			ASAP with single Cr standard		
			Cu thickness (nm)	wt.% Co (nm)	wt.% Ti	Cu thickness	wt.% Co	wt.% Ti
0	0	35.0	141	79.1	20.9	–	–	–
0	20	55.0	150	79.5	20.5	163	79.5	20.5
40	20	48.9	142	79.7	20.3	149	79.8	20.2
60	20	42.7	140	80.0	20.0	150	80.0	20.0
80	20	36.0	144	79.6	20.4	149	79.9	20.1
100	20	29.3	147	79.3	20.7	150	79.5	20.4
Average			144	79.5	20.5	152	79.8	20.2
Relative r.m.s.			2.6%	0.4%	1.5%	4.1%	0.3%	0.3%
Deviation from nominal				+0.3%	–1.0%		+0.6%	–2.4%

### Conclusions

The potential of x-ray microanalysis under electron beam excitation is much higher than commonly considered. In particular, the technique can be applied very successfully to the detection of near-surface segregation and the characterization of stratified specimens, from 0.1 to about 1000  $\mu\text{g}/\text{cm}^2$ . The advantages of the technique are that it is local and in principle non-destructive, that it can be performed using any commercial instrument (electron microprobe or analytical scanning electron microscope), and that it provides truly quantitative compositions and/or mass thicknesses of stratified specimens. As far as the thickness range, the sensitivity and the accuracy are concerned, the capability of the method is similar to that of RBS. Hence, advanced x-ray microanalysis techniques actually fill the domain between the “surface” techniques (x-ray photoelectron and Auger electron spectrometry) and the “bulk” techniques such as x-ray fluorescence spectrometry.

The easiest problems of in-depth analysis correspond to specimens with a known layer sequence and where every element is present in a single layer. In such situations, one obtains very rapidly, by applying an iterative procedure to the  $k$ -ratios measured at a single voltage (as in conventional microanalysis), a non ambiguous chemical and in-depth characterization of the specimen. If some elements are common to several strates, but have an unknown concentration in only one of them, an other iteration scheme, which frequently requires  $k$ -ratios measured at several voltages, can be applied successfully. Any more complex specimen structure may be solved (sometimes only partially) by a graphically assisted trial and error method.

The commercial software packages *Strata* and *Multifilm* developed with SAMx are powerful tools for these applications. Since they allow to simulate many situations, they also represent a didactic means of education in the field of advanced quantitative x-ray microanalysis.

*Strata* and *Multifilm* have been developed in cooperation with SAMx under contract ON-

ERA/SAMx No. 6361. The author acknowledges J.F. Thiot and his collaborators at SAMx for their efficient contribution to the software development. The experimental contribution of D. Boivin and Y. Pioche (ONERA) is also acknowledged. *Strata* is distributed by SAMx (Support for Applications in x-ray Microanalysis), Guyancourt, France. *Multifilm* is distributed by Kevex.

### REFERENCES

- 1 R. Castaing, Thesis, University of Paris, 1951.
- 2 R.H. Packwood and J.D. Brown, X-Ray Spectrom., 10 (1981) 138.
- 3 R.H. Packwood, G. Rémond and J.D. Brown, Proc. ICXOM 11, Univ. W. Ontario, 1987, p. 274.
- 4 J.L. Pouchou and F. Pichoir, Proc. ICXOM 10, J. Physique, 45 (1984) C2–47.
- 5 J.L. Pouchou and F. Pichoir, Proc. ICXOM 11, Univ. W. Ontario, 1987, p. 249.
- 6 J.L. Pouchou and F. Pichoir, Electron Probe Quantitation, Plenum Press, New York, 1991, p. 31.
- 7 J.L. Pouchou and F. Pichoir, Microbeam Analysis, San Francisco Press, 1988, p. 319.
- 8 J. Philibert, Métaux, 465 (1964) 157.
- 9 H.E. Bishop, J. Phys. D: Appl. Phys., 7 (1974) 2009.
- 10 G. Bastin and H. Heijligers, Electron Probe Quantitation, Plenum Press, New York, 1991, p. 145.
- 11 P. Willich, Proc. ICXOM 11, Univ. W. Ontario, 1987, p. 238.
- 12 P. Willich, D. Obertop and J. Krumme, Microbeam Analysis, San Francisco Press, 1988, p. 307.
- 13 P. Willich and D. Obertop, Surf. Interface Anal., 13 (1988) 20.
- 14 P. Willich, Mikrochim. Acta, Suppl., 12 (1992) 1.
- 15 J.L. Pouchou, F. Pichoir and D. Boivin, Microbeam Analysis, San Francisco Press, 1990, p. 120.
- 16 J.L. Pouchou, F. Pichoir and D. Boivin, Proc. ICXOM 12 (Krakow 1989), Academy of Mining and Metallurgy Univ. Krakow, 1, 1989, p. 52; also in ONERA Report TP 157, Publ. ONERA (1989).
- 17 J.L. Pouchou and F. Pichoir, Scanning, 12 (1990) 212.
- 18 P. Karduck, N. Ammann and W. Rehbach, Microbeam Analysis, San Francisco Press, 1990, p. 21.
- 19 J.L. Pouchou and F. Pichoir, Scanning Microscopy, in press.
- 20 J.L. Labar, Microbeam Analysis, San Francisco Press, 1988, p. 253.
- 21 J.L. Labar, C.E. Fiori and R.L. Myklebust, Proc. EMSA/MAS meeting, San Francisco Press, 1992, p. 1636.
- 22 J.L. Pouchou and F. Pichoir, in Rios et al. (Ed.), Electron Microscopy 92, Univ. Granada Spain, Vol. 1, 1992, p. 293.

# Synchrotron radiation-induced x-ray microanalysis

K. Janssens, L. Vincze and F. Adams

*Department of Chemistry, University of Antwerp (UIA), Universiteitsplein 1, B-2610 Wilrijk / Antwerp (Belgium)*

K.W. Jones

*Department of Applied Science, Brookhaven National Laboratory, Upton, Long Island, NY 11973 (USA)*

(Received 12th October 1992)

## Abstract

The qualities and limitations of synchrotron radiation-induced x-ray microfluorescence (SRXRF) spectrometry are discussed in comparison with those of more conventional microchemical techniques such as secondary ion microscopy and electron probe microanalysis. Examples of the analysis of particulates and the two-dimensional mapping of elemental species are given. Two new developments in connection with SRXRF are discussed: the use of microscopic x-ray absorption spectrometry and the predicted performance of SRXRF spectrometers installed with third-generation synchrotron sources.

*Keywords:* X-ray fluorescence spectrometry; Synchrotron radiation

Synchrotron radiation-induced x-ray microfluorescence (SRXRF) spectrometry is the microscopic analogue of the well established multi-elemental bulk analysis method of (energy-dispersive) x-ray fluorescence (EDXRF) spectrometry. In the latter method, radiation from bremsstrahlung tubes or radioactive sources is employed to induce emission of element-specific radiation by sample atoms; usually sample areas of 1–2 cm<sup>2</sup> are irradiated to yield (in the case of EDXRF) detectable count rates in the range 10<sup>3</sup>–10<sup>4</sup> counts s<sup>-1</sup>. To achieve the same count rate when an area of only, e.g., 100 μm<sup>2</sup> (10<sup>-6</sup> cm<sup>2</sup>) is employed, x-ray sources that are typically 10<sup>6</sup> times more intense are required. Such extremely intense x-ray fluxes are provided by electron storage rings where radiation is produced by forcing a beam of light elementary particles (elec-

trons, positrons) in a quasi-circular orbit. At the location where the relativistic particle beam is forced to alter its direction by means of suitable magnetic fields, an intense beam of polarized, polychromatic radiation is produced in a cone oriented tangentially to the particle beam path. The vertical opening angle of the cone (typically a few mrad) is related to the energy of the circulating particles which is in the range 0.1–10 GeV. The maximum intensity is emitted in the plane of the storage ring itself. This radiation is linearly polarized in the plane; slightly above and below the storage ring plane, the radiation is elliptically polarised.

Typical energy distributions of the x-rays produced at bending magnets are shown in Fig. 1. In addition to bending magnets, other magnetic structures called wigglers and undulators are employed to produce even higher x-ray fluxes. These devices operate by forcing the particle beam into multiple oscillatory trajectories and are installed in the straight sections of the storage rings.

*Correspondence to:* K. Janssens, Department of Chemistry, University of Antwerp (UIA), Universiteitsplein 1, B-2610 Wilrijk/Antwerp (Belgium).

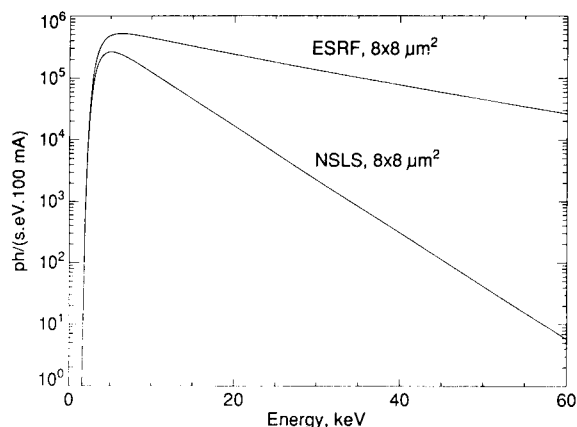


Fig. 1. Photon flux available at (0.8-T) ESRF and NSLS bending magnet beam lines using a  $8 \times 8 \mu\text{m}^2$  pin hole collimator at 30 and 10 m, respectively, from the tangent point.

In the last 5 years, as a result of the increasing availability of electron storage rings as sources of highly intense, collimated and polarized x-rays in the energy range between 1 and 30–40 keV, a number of x-ray fluorescence microprobes have been constructed. An overview of some of the characteristics of these instruments is presented in Table 1.

The analytical properties of the various instruments are mainly determined by two factors: the characteristics of the storage ring/x-ray source at which they are installed and the way in which radiation originating from the ring is transformed into a microbeam. At Hasylab (Hamburg, Germany) [1] and the NSLS (Brookhaven National

Laboratories, Upton, NY) [2], white light microprobes are in operation; at these stations, collimated pencil beams are used to perform sensitive trace element mapping with minimum detection limits (MDLs) in the 1–10 ppm range and with a lateral resolution of the order of  $10 \mu\text{m}$ . At SRS (Daresbury, UK) [3], SSRL (Stanford, Ca) [4] and the Photon Factory (Tsukuba) [5], focused monochromatic microbeams are employed. Some of the optical configurations listed in Table 1 have only very recently been tested in practice and the analytical qualities of the corresponding SRXRF spectrometers still need to be evaluated [6,7].

In their most recent biannual review of x-ray spectrometry, Török and Van Grieken [8] considered the availability of intense small-sized beams for use in XRF experiments as one of the major developments in x-ray spectrometry, in addition to the use of laser-plasma sources, ultra-trace analysis by total reflection XRF (TXRF) and structural analysis by means of extended x-ray absorption fine structure (EXAFS) [9].

Most microanalytical methods such as secondary ion mass spectrometry (SIMS), proton-induced x-ray emission ( $\mu$ -PIXE) and electron probe x-ray microanalysis (EPXMA) combine a number of useful qualities with one or more undesirable properties. This also applies to SRXRF. However, SRXRF also represents a unique combination of advantageous properties that are not found elsewhere. Similarly to SIMS, SRXRF is capable of trace level microanalysis but does not have any of the disadvantages asso-

TABLE 1

Characteristics of currently operating X-ray microprobes

Storage ring	$E_c$ (keV) <sup>a</sup>	Optical system	Energy (keV)	Spot size ( $\mu\text{m}^2$ )
DCI	1.9	Curved graphite crystal	8–20	–
Hasylab	31.7	Bragg–Fresnel lens	10	$2 \times 2$
		Pin hole	White	$3 \times 3$
NSLS	5	Conical capillary	White	?
		Pin hole	White	$5 \times 5$ , or larger
Photon Factory	1.9	Wolter	10	$3 \times 10$
SSRL	2.0	KirkPatrick–Baez	10–20	$3 \times 3$
VEPP-3	5.4	Channel-cut monochromator	10–60	–

<sup>a</sup>  $E_c$  = critical energy of electron storage ring.

ciated with a destructive mass spectrometric technique. In addition to the damage that is inflicted by an ion beam on a sample surface, another significant disadvantage of SIMS is that the collected secondary ion intensities are very difficult to quantify; the use of elaborate empirical calibration procedures is required in order to do so. This calibration problem arises mainly as a result of the very complicated processes that give rise to the formation of the secondary ions. In contrast, the interaction of x-ray photons with matter is relatively simple, very well known and analytically describable. The combination of the capability to perform sensitive elemental mapping with the proven accuracy and reliability of quantitative XRF makes SRXRF a very interesting analytical technique.

Some of the weak and strong points of SRXRF can be understood when SRXRF is considered in comparison with its closest analogues,  $\mu$ -PIXE and EPXMA. Essentially, these three methods differ only in the type of energy carriers that are being used in the micro beam. In all instances, the energetic particle is used to eject a core-level electron from a target atom, while the intensity and energy of the resulting characteristic radiation are measured with an Si(Li) detector. The overall efficiency of photon-induced x-ray emission (i.e., the number of characteristic photons produced per primary photon) is  $10^2$ – $10^3$  times higher than in the case of electron- or proton-induced emission, and this quantity increases with increasing atomic number [10]. Accordingly, SRXRF is more suitable than EPXMA or  $\mu$ -PIXE for trace determinations of the heavier elements (atomic number  $Z > 20$ –25). Also, per characteristic photon produced, the energy deposited in the sample using SRXRF is a factor of  $10^2$ – $10^3$  lower than in EPXMA; the difference is even larger with  $\mu$ -PIXE [11,12].

In addition to the production efficiency for characteristic radiation, the MDLs achievable with an x-ray-based technique are also determined by the importance of the continuous background in the collected EDXRF spectra. In this respect, another important difference between the interaction of photons and charged particles with matter is the probability of scattering inter-

actions. As a result of many (in)elastic collisions, the retardation of energetic charged particles in solids gives rise to a bremsstrahlung continuum. In the case of x-ray fluorescence, each primary photon either does not undergo any scattering interaction at all or (in the worst case) encounters one or two (in)elastic collisions with sample atoms before it is either absorbed (photoionization) or escapes from the solid. Accordingly, nearly background-free XRF spectra can be obtained when monochromatic photon excitation is employed, yielding (sub-)ppm level detection limits for selected elements (see Fig. 4). Only in the region at or just below the primary energy do (in)coherent scatter peaks contribute significantly to the background.

Owing to the linear polarization of the synchrotron radiation in the storage ring plane, a further decrease in the scatter background level can be realised if the detector is also positioned in this plane and at  $90^\circ$  to the incident beam. As shown in Fig. 4, this effect makes it possible to achieve ppm MDL values with SRXRF employing polychromatic excitation [2].

An additional advantage of an x-ray microprobe (XRM) is that it can be operated in air or in an inert gas atmosphere such as helium; also, samples need not be conducting. A weak point of an XRM is its limited lateral resolution (see Table 1). This property is directly related to the currently attainable beam sizes but is also influenced by other factors (see next section).

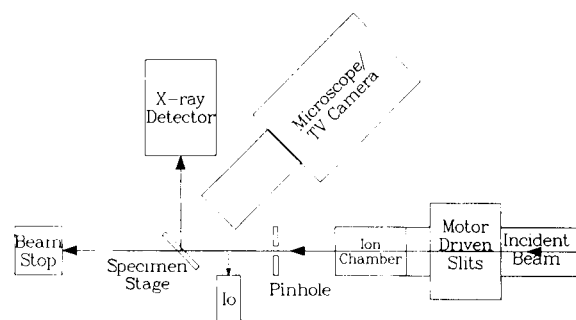


Fig. 2. Schematic diagram of the NSLS XRM. The pin hole-sample and sample-detector distances are of the order of a few cm.

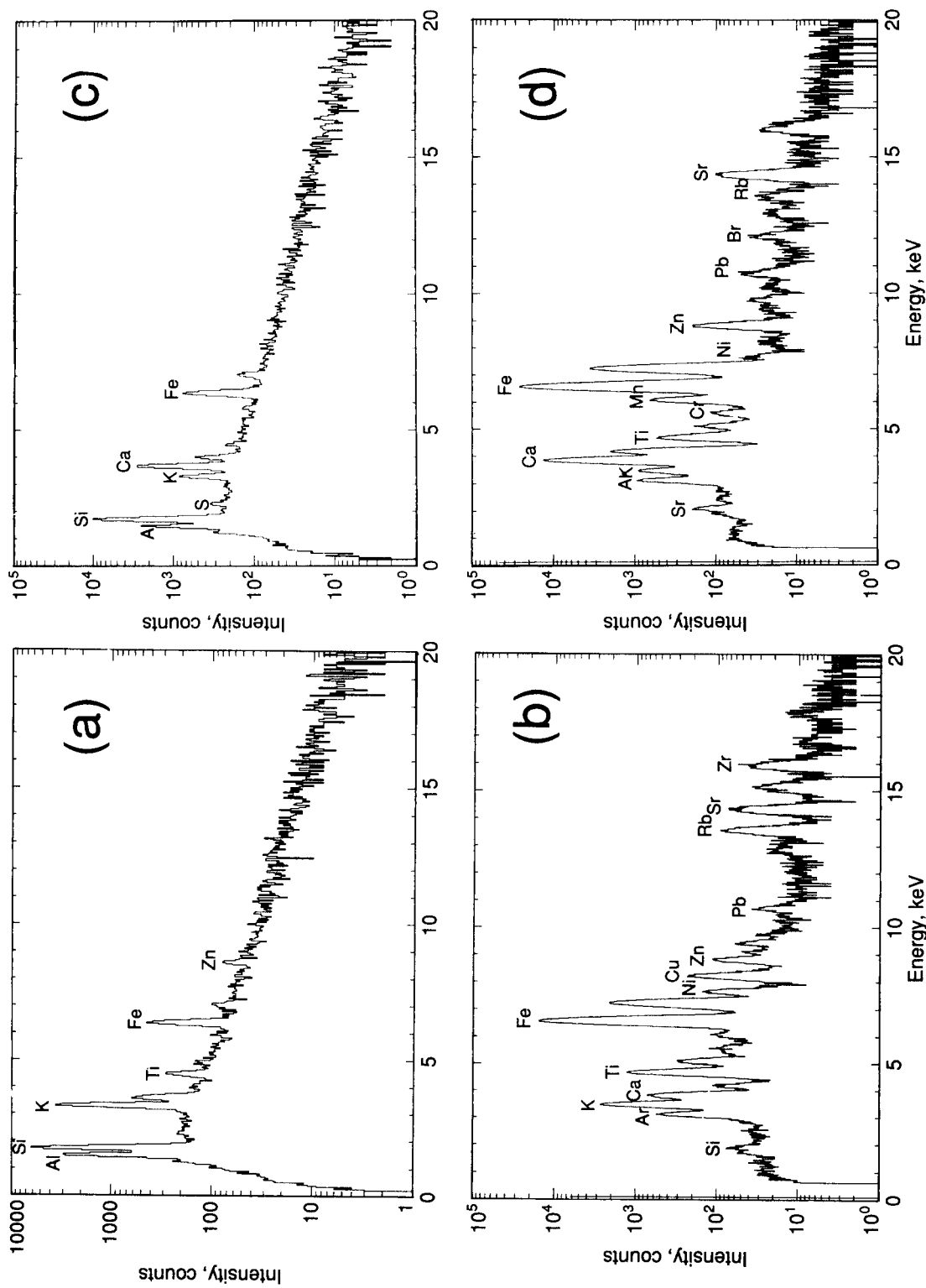


Fig. 3. X-ray spectra of two environmental particles of diameter 10–15  $\mu\text{m}$ . (a, c) Electron-induced x-ray spectra; (b, d) synchrotron radiation-induced x-ray spectra.

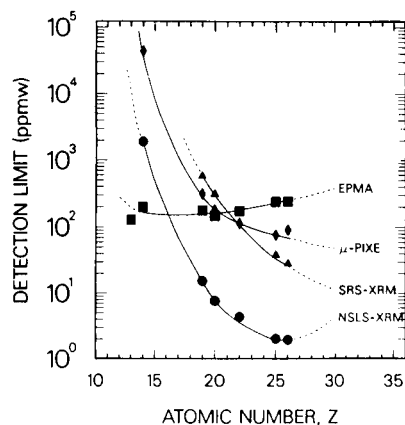


Fig. 4. MDL values derived from x-ray spectra of K309 glass microspheres of 20–30  $\mu\text{m}$  diameter generated using different instruments and techniques. Adapted from [13].

In what follows, first the capabilities and limitations of currently operating SRXRF instruments are outlined by means of a few examples. The applicability of SRXRF to individual particle analysis is briefly discussed and a comparison of SRXRF with SIMS and EPXMA illustrates some of the (dis)advantages of SRXRF as a multi-elemental mapping technique. Next, the use of x-ray absorption near edge structure ( $\mu$ -XANES) as a technique combinable with  $\mu$ -SRXRF in the same experimental set-up and which yields chemical information on selected elemental species is mentioned. Finally, the predicted performance and applications of future SRXRF spectrometers, to be installed with third-generation synchrotron rings such as the European Synchrotron Radiation Facility (ESRF, Grenoble) or the APS (Advanced Photon Source, Argonne, IL), are discussed.

## EXPERIMENTAL

For the x-ray microprobe experiments, the instrument at the X26A beamline of the NSLS (National Synchrotron Light Source) was employed. After emerging from the storage ring ultra-high vacuum (UHV), the beam is defined by four tantalum slits and further collimated by a  $5 \times 5$  or  $8 \times 8 \mu\text{m}^2$  crossed slit system. The sam-

ple is positioned at  $45^\circ$  to the incoming beam. A schematic diagram of the instrument is shown in Fig. 2.

As shown in Fig. 1, the low-energy part of the polychromatic energy spectrum impinging on the sample is heavily absorbed by the beryllium end windows of the beam pipe and the air path between the collimator slits and the sample. The specimen is viewed by a horizontally mounted stereozoom binocular microscope, equipped with a TV camera. For the analysis of particulates, an  $8 \times 8 \mu\text{m}^2$  collimator was employed to define the beam size. X-ray spectra were collected by locating a particle on the filter using the microscope, moving it into the beam and maximizing the detectable count rate. For the elemental mapping experiments, a specific  $100 \times 100 \mu\text{m}^2$  area of a grain of Carnmenellis Granite was studied. In this area, elemental maps were collected, first by EPXMA (using a 25-kV electron beam), then by SRXRF and finally by SIMS (employing a 30-kV  $\text{O}^-$  beam). During the SRXRF experiment, a collimator yielding a  $5 \times 5 \mu\text{m}^2$  photon beam was employed. The collection of the  $512 \times 512$  pixel SIMS maps took about 2 h of instrument time, including the alignment of the ion-optical system. The collection of the potassium and sodium x-ray maps ( $140 \times 200$  pixels) using EPXMA took about 1 h. The synchrotron radiation-induced x-ray images were collected using a dwell time of 50 s per pixel; x-ray images  $25 \times 35$  pixels in size were collected taking a total instrument time of about 12 h to acquire. The XANES spectra were also collected at the NSLS XRM and took ca. 1 h each to acquire, using a 1-s collection time at each energy. The spectra in Fig. 7a and b were collected using an energy increment of 0.6 eV and those in Fig. 7c with a 0.3-eV step size.

## SRXRF AT CURRENT SYNCHROTRON FACILITIES

In general, microchemical techniques may be employed for two generic types of studies: the analysis of minute samples such as microscopic particles and fibres, and the visualization of the distribution of elemental species in or on the surface of samples of larger dimensions with

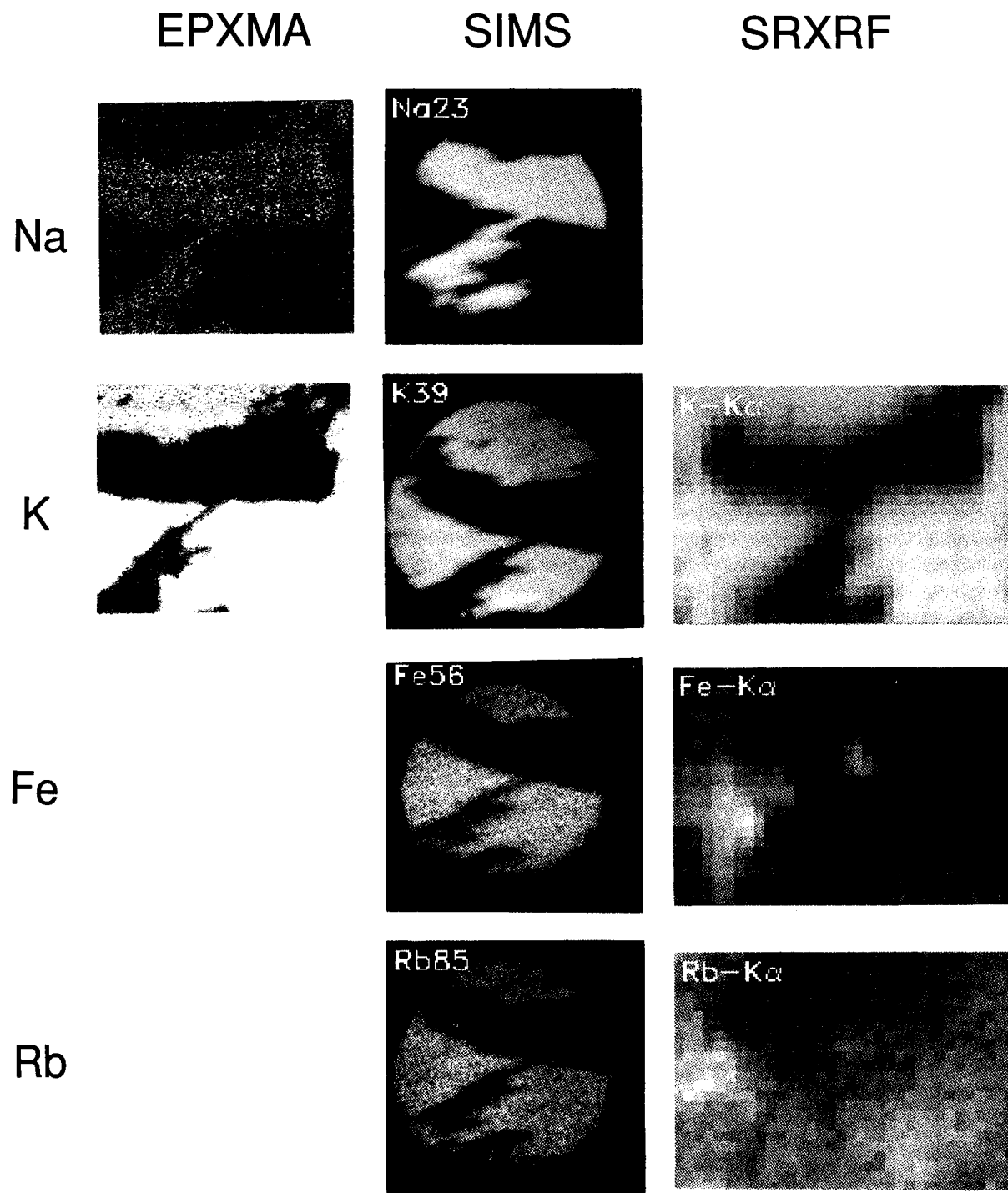


Fig. 5. Elemental maps of various major and trace constituents in selected area of a grain of micropertthitic granite. Left column, EPXMA images; middle column, SIMS images; right column, SRXRF images. The dimensions of the lamellae shown in most of the maps are ca.  $30 \times 100 \mu\text{m}^2$ . Adapted from [17].



$\mu\text{m}$ -size lateral resolution. In this section, examples of both types of analysis are discussed.

#### *Particulate analysis*

In Fig. 3, the applicability of SRXRF for the characterization of individual microscopic particles is illustrated. Individual particle analysis of aerosols by means of an automated electron microprobe analyser has proved to be a convenient technique for revealing the composition and relative importance of air pollution sources. In Fig. 3a–d, synchrotron radiation (SR) and electron-induced x-ray spectra of individual environmental particles having a mean diameter of ca. 10–15  $\mu\text{m}$  are presented. Whereas in the EPXMA spectra (Fig. 3a and c), only the major constituents of the aluminosilicate particles are visible, in the x-ray-induced spectra (Fig. 3b and d) peaks corresponding to trace and minor constituents such as Ni, Cu, Pb, Br, Rb, Sr and Zr can be observed (e.g., the Rb signal in Fig. 3d corresponds to a concentration of ca. 50 ppm). As the NSLS XRM is operated in an air atmosphere, the low energetic Si and Al  $K\alpha$  lines are heavily absorbed in the air path between the sample and detector.

In Fig. 4, the MDLs achievable at this instrument for the analysis of National Institute of Science and Technology (NIST) K309 Glass Microspheres of diameter 20–30  $\mu\text{m}$  are compared with those obtained at the SRS XRM (see Table 1) and with those derived from electron- and proton-induced x-ray spectra of the same material (see [13] for details). In contrast to the NSLS XRM, at SRS a 15-keV monochromatic beam of primary radiation is employed. In the case of EPXMA, a more or less uniform sensitivity in the 100 ppm range is obtained; for the other techniques, the MDL values vary considerably with atomic number. Corresponding to the maximum near 8 keV in the excitation spectrum available at the NSLS XRM (Fig. 1), the lowest MDL values are obtained for elements such as Mn and Fe. The optimum MDL of 2 ppm for Fe corresponds for a 26- $\mu\text{m}$  diameter particle to an absolute detectable amount of ca. 3 fg of Fe. With the SRS microprobe, an MDL of Fe of ca. 30 ppm is obtained.

The MDL values plotted in Fig. 4 are valid for

a 300-s counting time and for fairly large particles (diameter 20–30  $\mu\text{m}$ ), compared with the average size distribution of environmental aerosol particles (0.1–10  $\mu\text{m}$ ). For particle diameters smaller than 10  $\mu\text{m}$ , a much diminished x-ray yield is observed while the background intensity increases as a significant portion of the primary photons interact with the substrate rather than with the particles themselves. Accordingly, higher MDL values than those plotted in Fig. 4 are obtained and a smaller difference in sensitivity between SRXRF and EPXMA is observed. Nevertheless, for the smallest particles analysable using current SRXRM instrumentation (ca. 7  $\mu\text{m}$  in diameter), the NSLS XRM is still 5–10 times more sensitive than EPXMA for Ca and Pb [13].

#### *Elemental mapping*

In Fig. 5, elemental maps of various elements obtained using SIMS, EPXMA and SRXRF (at the NSLS XRM) from the same area of a geological material are shown. The material studied was a grain of Carnmenellis granite [14], consisting of a potassium-rich feldspar groundmass in which ex-solution lamellae of albite (a sodium-rich feldspar mineral) are found. The dark rectangular area in most of the images in Fig. 5 corresponds to such a lamella (approximate dimensions 30  $\times$  100  $\mu\text{m}^2$ ).

In addition to a difference in major composition (Na/K) between the two phases, the average abundance of trace elements such as Fe, Rb and Sr in the two phases is also different. Most minor and trace elements are predominantly present in the K-rich phase; Goossens et al. [14] reported, e.g.,  $\text{Rb}_2\text{O}$  concentrations of 840 and 3 ppm in the K- and Na-rich feldspar phases, respectively.

The elemental maps shown in Fig. 5 illustrate several of the strong and weak points of SRXRF. First, in contrast to EPXMA, by means of which only the distribution of the major elements could be mapped (Fig. 5, left column), the NSLS XRM allows the study of the distribution of trace elements such as Fe and Rb, similarly as in SIMS (Fig. 5, right and middle columns). The most striking difference between SRXRF and the other two methods obviously is the lateral resolution of the various images. Whereas in EPXMA and

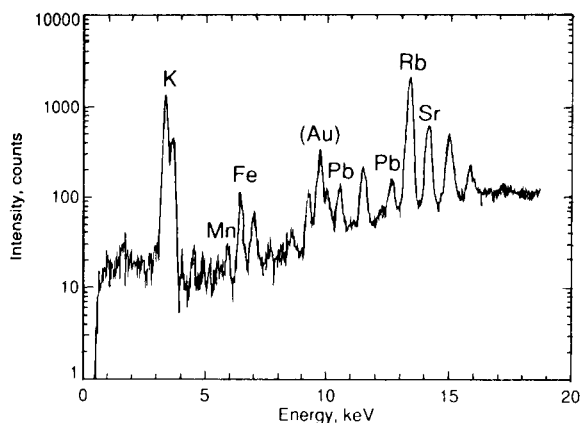


Fig. 6. SRXRF spectrum collected from a location in the K-rich phase of the granite samples shown in Fig. 5.

SIMS particle beams with submicrometre cross-sections are employed, for the SRXRF experiments a  $5 \times 5 \mu\text{m}^2$  beam was used. In this way, the area of interest could be scanned in a reasonable amount of time (ca. 12 h) while a 50-s dwell time allowed for the collection of an EDXRF spectrum of sufficient statistics at each pixel.

Figure 6 shows one of these spectra, corresponding to a location in the K-rich phase. Owing to the limited spatial resolution, many of the finer details of the elemental distributions (such as the interconnection between the two lamellae) that are visible in both the SIMS and EPXMA images are lost in the SRXRF images.

Another factor affecting the lateral resolution is the difference in penetration depth between the three microbeam methods. Whereas using SIMS only the top 10–100 nm of the materials is being sampled (depending on the sputter time and beam intensity), 25-kV electrons will penetrate ca. 3–5  $\mu\text{m}$  into the material, causing characteristic x-rays to emerge from a pear-shaped interaction volume of comparable size. For high-energy photons of, e.g., 10 and 20 keV, the  $1/e$  penetration depth is ca. 130 and 950  $\mu\text{m}$ , respectively, in the K-feldspar phase. Although the K  $K\alpha$  radiation only escapes from the uppermost 10  $\mu\text{m}$ , the more energetic Rb  $K\alpha$  photons still have a comparable escape probability when originating from 300  $\mu\text{m}$  deep. Accordingly, instead of only visualizing the two-phase structure on the upper

surface of the grain (as in the SIMS maps in Fig. 5), the high-energy SRXRF images yield information on the distribution of elements deeper in the material. The highly penetrative character of photons can be used advantageously, e.g., for non-destructive structural investigations using computed microtomographic (CMT) techniques [15] or in the analysis of submerged structures such as fluid inclusions in minerals (see, e.g., [16]). On the other hand, as discussed in [17], it can also cause significant problems regarding the quantification of elemental maps as shown in the right-hand column of Fig. 5.

#### NEW DEVELOPMENTS IN SRXRF

Currently, two new developments related to SRXRF merit attention. By employing more brilliant and more energetic x-ray sources, some of the limitations of current SRXRF instruments outlined in the previous section can be eliminated. Another development is the combination of the elemental speciation capabilities of SRXRF with the possibilities of x-ray absorption spectrometry ( $\mu$ -XAS) to yield chemical information on selected elemental species.

##### *Microscopic x-ray absorption spectrometry*

In contrast to the relatively limited number of XRFs available worldwide (see Table 1), one of the major application areas of SR is absorption spectrometry. This technique is based on the irradiation of a sample with a highly monochromatic ( $\Delta E/E \approx 10^{-4}$ ) x-ray beam of tunable energy. By scanning the energy over an absorption edge of an element of interest, called the central atom (e.g., Fe, when the Fe K-edge is scanned) in fractional eV steps and recording either the absorption of the beam in the sample (absorption XAS) or the intensity of the fluorescent radiation that is produced (fluorescence XAS), the fine structure on the absorption edge can be recorded. Two regions of x-ray absorption, the near edge (XANES) and the extended region (EXAFS), provide different structural information. The processing and interpretation of these features is not a trivial task, although efforts at standardization

are being made [18,19]. From EXAFS, information on the number, the atomic number and the distance of the neighbours of the central atoms may be derived. In the XANES region, data on the oxidation and coordination state of the central atom can be extracted from the position of the major edge and from the pre-edge features.

Both variants of absorption spectrometry have predominantly been used for bulk investigations of high-technology and catalyst materials (see, e.g., [20]). Iida and co-workers [21,22] reported  $\mu$ -XAS measurements using fluorescent detection with a lateral resolution of 20  $\mu\text{m}$  in an instrument very similar to a monochromatic XRM. Iida [23] also demonstrated differences in the XANES spectra of Cr in the chromite, olivine and pyroxene phases of a peridotite rock sample. Using the microscopic arrangement of Fig. 2, but with the use of a Pt-coated 8:1 ellipsoidal mirror and a double-channel monochromator to focus and monochromate, respectively, the primary beam, Sutton et al. [24] also studied Cr in rocks using  $\mu$ -XANES and inferred the oxidation state of this element in 200- $\mu\text{m}$  sized individual grains of lunar olivine and pyroxene from lunar basalt 15555. A beam of  $180 \times 205 \mu\text{m}$  was employed to obtain sufficient sensitivity for the detection of Cr at the 100 ppm level.

As an illustration of the applicability of  $\mu$ -XANES to the investigation of industrially important materials, in Fig. 7, Ti K-edge XANES spectra are shown which were collected using the same instrumentation as in [24]. In Fig. 7a, the XANES spectra of Ti metal and  $\text{Ti}^{4+}$  in NIST 1832 standard glass demonstrate the shift to higher energies that the Ti K absorption edge undergoes with increasing oxidation state. The origin of the energy scale in Fig. 7 was arbitrarily fixed at the top of the sharp pre-edge peak visible in the  $\text{Ti}^{4+}$  spectrum of Fig. 7a. This peak can be attributed to the  $1s \rightarrow 3d$  transition; transitions of this type are forbidden by selection rules but can occur as a result of orbital mixing. Between the two profiles shown in Fig. 7a, a shift in half-height of about 13 eV can be observed, corresponding to ca. 3.25 eV per charge unit. Similar results were obtained by Waychunas [25]. Sutton et al. [24] observed a shift of 17 eV between Cr

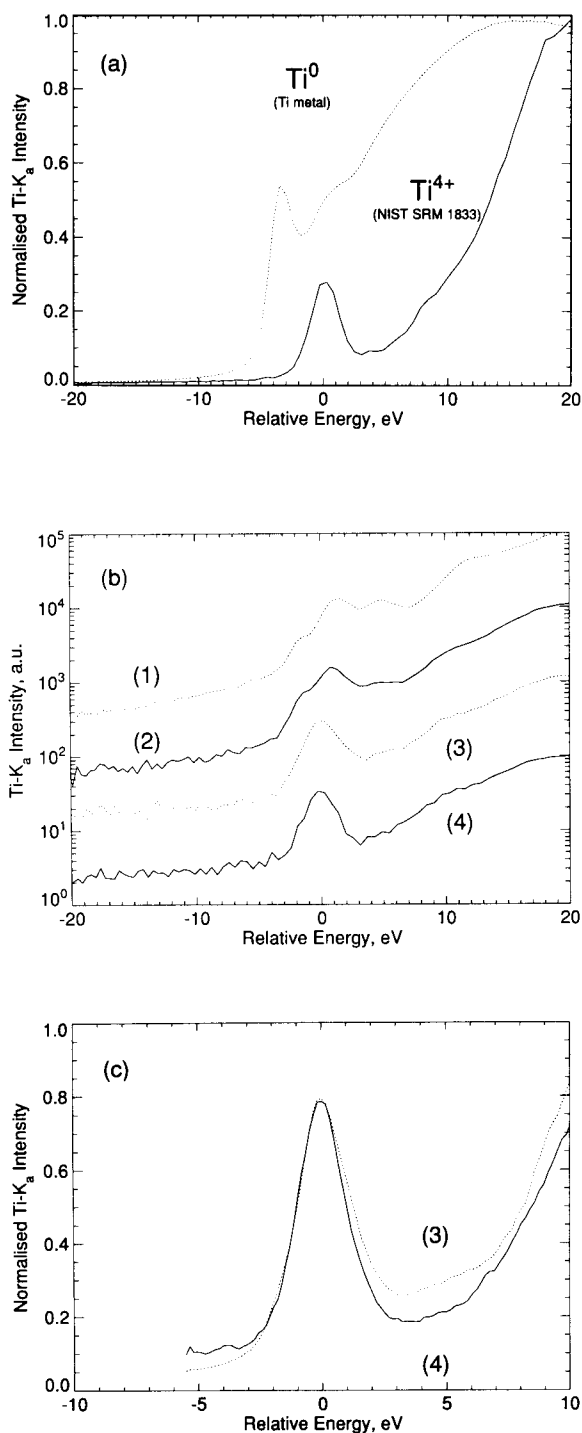


Fig. 7. (a) XANES spectra of the Ti K-edge for  $\text{Ti}^0$  (Ti metal) and  $\text{Ti}^{4+}$  ( $\text{TiO}_2$  in NIST 1832 glass); (b) the same for  $\text{Ti}^{4+}$  in various materials (see text); (c) high-resolution scan of the pre-edge peaks on curves 3 and 4 in (b).

metal ( $\text{Cr}^0$ ) and  $\text{K}_2\text{CrO}_4$  ( $\text{Cr}^{6+}$ ) and arrived at approximately the same number.

As pointed out by various workers [21,24,25], a linear relationship between the edge position and the oxidation state of the central atoms can be readily established. In this way, by performing rapid energy scans over an absorption edge at various locations of the microbeam on the sample, chemical state mapping can be performed.

In addition to information on the chemical state of an element, data on the coordination of the central atom can also be extracted from the XANES region. In Fig. 7b, Ti K XANES spectra of  $\text{Ti}^{4+}$  in various materials are shown. Curves 1 and 2 are very similar and correspond to anatase ( $\text{TiO}_2$ ) and the so-called "Grace" silica, a co-gel of  $\text{SiO}_2$  and  $\text{TiO}_2$ , respectively. Curves 3 and 4 were obtained from materials prepared from the co-gel through crystallization and which feature a zeolite structure (medium-pore zeolite ZSM-5) [26]. Curve 4 corresponds to titanium silicalite-1 (TS-1), a material which is an efficient catalyst for oxidation of organic compounds with hydrogen peroxide. The material from which curve 3 was obtained has the same structure as TS-1 but does not show the above-mentioned catalytic activity. Comparison of curves 1 and 2 indicates that the coordination of Ti in the co-gel is not very different from that in anatase. The typical three-peak pre-edge feature which can be observed in curves 1 and 2 has also been found by other workers [25,26] and is indicative of a regular octahedral site of Ti.

On the basis of Ti K XANES spectra of various Ti minerals, Behrens et al. [26] observed that with increasing distortion of the octahedral site, the central peak gains intensity and moves to slightly lower energies, as is the case in profiles 3 and 4. The width of the pre-edge peak in curve 3, which is broader than those obtained from compounds with uniform coordination (see the lower curve in Fig. 7a) indicates a co-existence of several environments for Ti in the inactive zeolite structure. Behrens et al. [26] suggested a 10:15:75 mixture of tetrahedral, square-pyramidal and octahedral coordinations. The shapes of the pre-edge peaks in curves 3 and 4 were recorded a second time with 0.3-eV resolution

and are compared in Fig. 7c. Together with the deconvolution results presented in [26], the smaller width of the peak in curve 4 may indicate that in the catalytically active product, more Ti atoms are coordinated in a non-octahedral way. Further work, employing for instance data extracted from the EXAFS region of the Ti edge, needs to be done to confirm this hypothesis.

#### *Third-generation synchrotron sources*

A number of the limitations of SRXRF discussed in the previous section can be eliminated by using more intense photon sources. At currently operating storage rings, this can be done by using undulator or wiggler radiation instead of x-rays originating from a bending magnet. Rivers et al. [27] discussed SRXRF experiments at the 5-T superconducting wiggler of NSLS beamline X17B1. In addition to the advantage conferred by the higher intensity of the source, they pointed out that as a result of the higher divergence of the wiggler beam in the vertical plane, a poorer degree of polarization of the x-ray micro-beam is obtained than at the X26A bending magnet beamline [28].

An alternative is to employ bending magnet radiation from one of the third-generation synchrotron rings now currently under construction in Japan (SPRING-8 in Harima), the USA (APS at Argonne National Laboratories, IL) and in Europe (ESRF at Grenoble). For the last facility, the construction phase of which is virtually completed [29], the expected improvement in flux density and achievable MDLs when a collimated x-ray microprobe is installed at a 0.8-T bending magnet beamline was estimated. The predictions are based on a detailed Monte Carlo simulation of the interaction of a polarized, polychromatic photon beam with sample atoms [30,31]. The details of these calculations, which also include a comparison of the performance of optical devices for generating high-energy x-ray microbeams other than pin holes, are presented elsewhere [32]. Only the alternatives employing polychromatic forms of excitation will be discussed here.

Owing to the higher operating energy of the ESRF ring (6 GeV compared with 2.5 GeV for the NSLS), as shown in Fig. 1, the white syn-

chrotron spectrum obtained from an ESRF bending magnet is far more energetic than that obtained from an NSLS port. Whereas SRXRF trace elemental analysis at an NSLS bending magnet beamline is in practice restricted to the energy interval 3–30 keV (K lines of S to Cs) [33], using an ESRF x-ray source of similar type will allow for the excitation of the K lines of much heavier species such as the rare earth series or the platinum group elements. Although these elements can currently be determined using L-line radiation, detection limits for L lines are higher than those for K lines because the L fluorescence yields are smaller [33]. As a result of peak overlap, employing L lines for quantitative determinations is also more error prone and difficult than when K lines are used.

In Fig. 8, the predicted XRF spectrum which would be obtained if the white ESRF spectrum shown in Fig. 1 were used to excite an 80 mg cm<sup>-2</sup> sample of NIST SRM 1571 Orchard Leaves is compared with the corresponding experimental spectrum collected using the NSLS XRM. The simulated spectra in Fig. 8 were calculated assuming a degree of polarization of the primary radiation of 96%. (The discrepancies in the intensities of the K, Ti and Mn peaks between the simulated and experimental spectra for the NSLS case are attributed to microheterogeneity of the

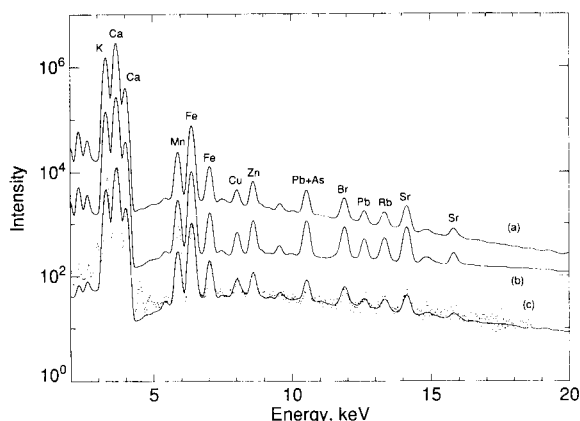


Fig. 8. Simulated (lines) and experimental (dots) SRXRF spectra derived from an 80 mg cm<sup>-2</sup> sample of NIST 1572 Orchard Leaves under different excitation conditions: (a) ESRF, capillary (see text); (b) ESRF, pin hole; (c) NSLS, pin hole.

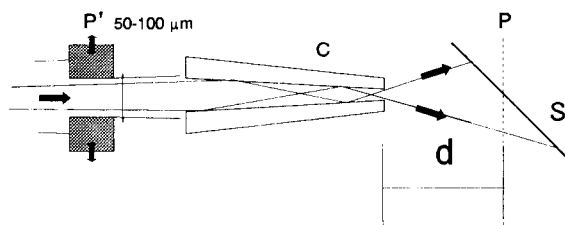


Fig. 9. Principle of capillary optics.  $d$  = Distance between the far end of the capillary and the sample being irradiated; C = capillary; P = projection plane for the distributions of Fig. 11; S = sample at an angle of 45°; P' = pin hole.

sample material [31].) Overall, in the low-energy region of the spectra (7–10 keV), for the ESRF case, an increase in the x-ray yield by a factor of 10 is observed compared with the NSLS case. As can be expected from the plots in Fig. 1, at higher energies a higher sensitivity increase is obtained while improved peak-to-background (P/B) ratios are also observed for, e.g., the Br, Sr and Rb peaks. These two phenomena cause the MDL values for this type of sample, which for the NSLS XRM are at the 2–3 ppm level for elements heavier than Fe, to decrease to the 0.3–1 ppm range [32].

In Fig. 8, the EDXRF spectrum that would be obtained if, instead of a simple pin hole arrangement, a conical glass capillary were to be used to define the ESRF x-ray beam is also shown. The operating principle of this type of device is shown in Fig. 9. X-ray photons of energy  $E$  originating from the storage ring enter the capillary and are reflected on the inner walls of the glass tube, provided that they impinge on the walls at an angle smaller than the critical angle of total reflection  $\theta_c(E)$ . Whereas parallel capillaries are used as x-ray wave guides (e.g., in microfluorescence and microdiffraction instruments employing conventional x-ray tubes [34]), tapered capillaries of the type shown in Fig. 9 can act as polychromatic focusing devices with high-energy filtering properties.

Engström et al. [6] demonstrated the use of these devices for focusing of SR beams. In view of their simplicity compared with e.g., ellipsoidal or toroidal mirrors, and the fact that they may be used to focus radiation for  $\mu$ -XAS experiments,

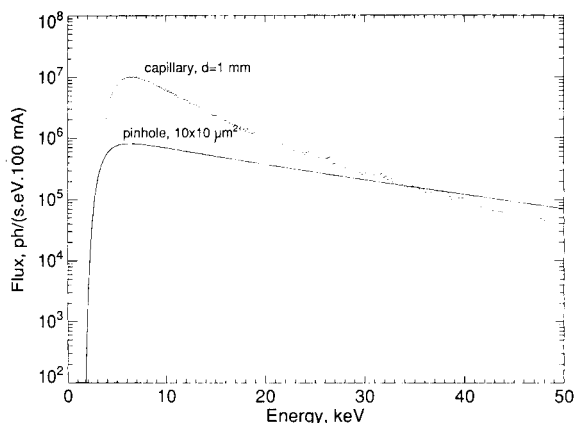


Fig. 10. X-ray flux available at an ESRF 0.8-T bending magnet transmitted by a  $10 \times 10 \mu\text{m}^2$  pin hole (line) and by a glass capillary yielding the same spot at 1 mm from the capillary end (dots). See text.

these capillaries are currently considered to be very promising optical elements for hard x-ray focusing. For one of the devices tested in [6] (a capillary of 25 cm length, with i.d.. 58 and  $1 \mu\text{m}$  at the beginning and end, respectively), Fig. 10 illustrates the energy-dependent focusing properties and the effect on the white ESRF spectrum. These results were obtained by means of a ray tracing code developed in this laboratory.

In Fig. 11, the predicted dimensions of the microbeam emerging from the capillary tip at different distances  $d$  (see Fig. 9) are shown. Be-

cause the x-rays emerge from the tapered glass tube at an angle  $\theta \leq \theta_c(E)$  (which in general is larger than the divergence of the incoming SR beam), in order to maintain the small beam cross-sections defined by the end diameter of the capillary, the sample material to be investigated must be placed extremely close to the capillary end. As can be seen from Fig. 11, the beam cross-section rapidly increases with larger values of  $d$ . For the above-mentioned capillary and for a distance  $d$  equal to 1 mm, a microspot of  $100 \mu\text{m}^2$  is obtained. In Fig. 10 the unfocused flux passing through a pin hole of the same area is also plotted. The gain in flux by a factor of 10–20 at the lower excitation energies results in a comparable sensitivity gain for elements in the  $Z$  range from 19 (K) to 26 (Fe), as shown in Fig. 8. As a result of the diminishing focusing capabilities of the capillary with increasing energy, for heavier elements such as Rb and Sr, less favourable P/B ratios are obtained than in the pin hole case (Fig. 8, curve b).

#### Conclusions

Some of the strong and weak points of SRXRF as implemented at currently operating XRM facilities have been highlighted. It can be concluded that SRXRF is a valuable method for the determination of trace, minor and major elements and this it can profitably be used in parallel with electron and ion beam methods. Exciting

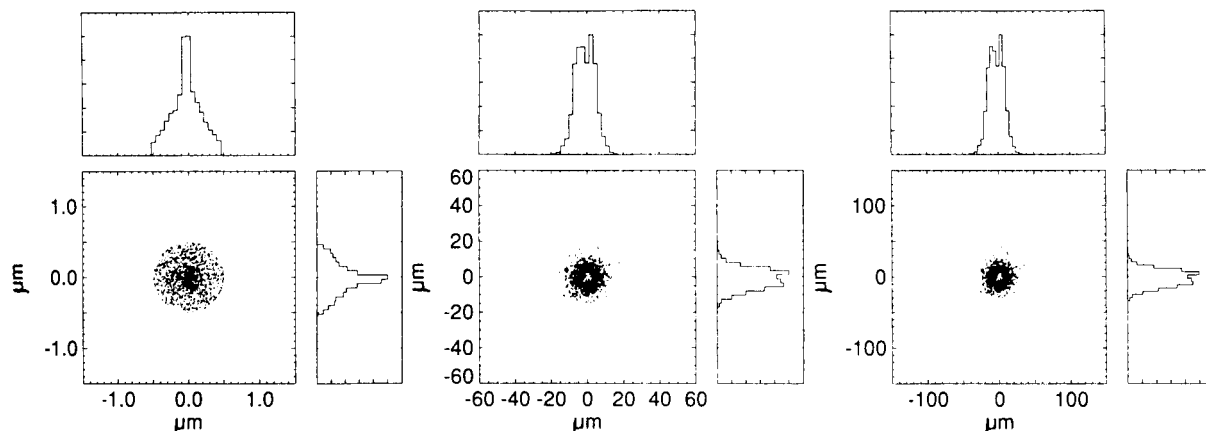


Fig. 11. Variation of the cross-section of the beam emerging from the capillary as a function of the distance  $d$ . Left 0 mm; middle 5 mm; right, 10 mm. Spot sizes of 1, 25 and  $50 \mu\text{m}$ , respectively are achieved.

new horizons are opening up for SRXRF as third-generation X-ray sources become available, providing highly energetic and polarized photon beams of unprecedented intensity. In addition to the improvement in lateral resolution and in sensitivity that these new x-ray sources will induce, the enhancement of the elemental mapping capacity of SRXRF with the chemical speciation possibilities of  $\mu$ -XAS will significantly improve the scope and breath of x-ray microprobe analysis.

This work was supported by the Belgian National Science Fund NFWO and in part by the US Dept. of Energy under Contract DE-ACO2-76CH00016.

#### REFERENCES

- 1 M. Bavdas, A. Knöchel, P. Ketelsen, W. Petersen, N. Gurker, M.H. Salehi and T. Dietrich, *Nucl. Instrum. Methods*, A266 (1988) 308.
- 2 K.W. Jones, and B.M. Gordon, *Anal. Chem.*, 61 (1989) 341A.
- 3 F. Van Langevelde, D.K. Bowen, G.H.J. Tros, R.D. Vis, A. Huizing and D.K.G. de Boer, *Nucl. Instrum. Methods*, A292 (1990) 719.
- 4 A.C. Thompson, J.H. Underwood, Y. Wu, R.D. Giaque, K.W. Jones and M.L. Rivers, *Nucl. Instrum. Methods*, A266 (1988) 318.
- 5 Y. Goshi, S. Aoki, A. Iida, S. Hayakawa, H. Yamaji and K. Sakurai, *Jpn. J. Appl. Phys.*, 26 (1987) L1260.
- 6 P. Engström, S. Larsson, A. Rindby, A. Buttkewitz, S. Garbe, G. Gaul, A. Knöchel and F. Lechtenberg, *Nucl. Instrum. Methods*, A302 (1991) 547.
- 7 D. Erko and P. Chevallier, in A. Michette, G. Morrison and C. Buckley (Eds.), *X-Ray Microscopy III*, Springer, Berlin, New York, 1992, pp. 105–107.
- 8 S.T. Török and R.E. Van Grieken, *Anal. Chem.*, 64 (1992) 180R.
- 9 J.W. Gilfrich, *X-Ray Spectrom.*, 19 (1990) 45.
- 10 L.S. Birks et al., *Appl. Phys.*, 35 (1964) 2578.
- 11 A.P. Mazzolini, G.J.F. Legge and C.K. Palaghy, *Nucl. Instrum. Methods*, 191 (1981) 217.
- 12 R.D. Vis, *Scanning Microsc.*, 2 (1988) 977.
- 13 K. Janssens, F. Van Langevelde, F.C. Adams, R.D. Vis, S.R. Sutton, M.L. Rivers, K.W. Jones and D.K. Bowen, *Anal. Chim. Acta*, 25 (1992) 1265.
- 14 D. Goossens, L. Van't Dack and R. Gijbels, in D.L. Miles (Ed.), *Water-Rock Interaction*, Balkema, Rotterdam/Brookfield, 1989, pp. 267–270.
- 15 K.W. Jones, P. Spanne, G. Schidlovsky, D. Xue, R. Bockman, M. Rabinowits, P. Hammond, R. Bornschein and D. Hoeltzel, in A. Michette, G. Morrison and C. Buckley (Eds.), *X-Ray Microscopy III*, Springer, Berlin, New York, 1992, p. 431.
- 16 J.D. Frantz, H.K. Mao, Y. Zhang, Y. Wu, A. Thompson, J. Underwood, R. Giaque, K. Jones and M. Rivers *Chem. Geol.*, 69 (1988) 235.
- 17 K. Janssens, F. Adams, M.L. Rivers and K.W. Jones, presented at 11th Pfefferkorn Conference, Amherst, MA, August 7–14, 1992.
- 18 W.T. Elam., *Synchrotron Radiat. News*, 3 (1990) 14.
- 19 A. Edwards, D. Sayers., *Synchrotron Radiat. News*, 3 (1990) 16.
- 20 A.J. Davenport and H.S. Isaacs, *Corros. Sci.*, 21 (1990) 105.
- 21 S. Hayakawa, A. Iida, S. Aoki and Y. Goshi, in A. Michette, G. Morrison and C. Buckley (Eds.), *X-ray Microscopy III*, Springer, Berlin, New York, 1992, p. 376.
- 22 S. Hayakawa, Y. Goshi, A. Iida, S. Aoki and K. Sato, *Rev. Sci. Instrum.*, 62 (1992) 2545.
- 23 A. Iida, *Trends Anal. Chem.*, 10 (1991) 215.
- 24 S.R. Sutton, K.W. Jones, B.M. Gordon, M.L. Rivers, S. Bajt and J.V. Smith, *Geochim. Cosmochim. Acta*, submitted for publication.
- 25 G.A. Waychunas, *Am. Mineral.*, 12 (1987) 89.
- 26 P. Behrens, J. Felsche, S. Vetter and G. Schulz-Ekloff, *J. Chem. Soc., Chem. Commun.*, (1991) 678.
- 27 M.L. Rivers, S.R. Sutton and K.W. Jones, in A. Michette, G. Morrison and C. Buckley (Eds.), *X-Ray Microscopy III*, Springer, Berlin, New York, 1992, pp. 212–216.
- 28 M.L. Rivers and S.R. Sutton, *National Synchrotron Light Source Annual Report*, Brookhaven Natl. Laboratories, Dept. of Energy, Upton, NY, 1990.
- 29 *European Synchrotron Radiation Facility Newsl.*, No. 14, July (1992), p. 1.
- 30 L. Vincze, K. Janssens and F. Adams, *Spectrochim. Acta*, Part B, in press.
- 31 K. Janssens, L. Vincze, P. Van Espen and F. Adams, *X-Ray Spectrom.*, in press.
- 32 L. Vincze, K. Janssens and F. Adams, in P.J. Duke, G.W. Lorimer, T. Mulvey (Eds.), *Proceedings of the 13th International Conference on X-Ray Optics and Micro Analysis*, Manchester, September 1992, in press.
- 33 S.R. Sutton, M.L. Rivers, S. Bajt and K.W. Jones, presented at the Sixth International PIXE Conference, July 1992.
- 34 B.A. Carpenter, *Adv. X-Ray Anal.*, 32 (1989) 115.

# Two-photon ionization detection of adsorbed molecules on a metal surface at atmospheric pressure by 355-nm laser irradiation

Hirofumi Kawazumi

*Division of Science, Kitakyushu University, Kokura-minami, Kitakyushu 802 (Japan)*

To-oru Yasuda and Teiichiro Ogawa

*Department of Molecular Science, Kyushu University, Kasuga, Fukuoka 816 (Japan)*

(Received 8th September 1992)

## Abstract

Two-photon ionization was applied to the sensitive detection of aromatic molecules and dyes on a metal surface in ambient air by using the third harmonic of an Nd:YAG laser. The better quality of the Nd:YAG laser beam compared with a nitrogen laser improved the sensitivity. The detection limits were of the order of  $10^{-3}$  monolayer coverage. The dependence of the ionization signal on the molar absorptivity and the metal substrate was measured.

*Keywords:* Surface techniques; Aromatic compounds; Dyes; Laser photoionization; Photoionization spectroscopy

Cleanness is an important characteristic of a surface. For the detection of trace organic molecules on a surface, mass spectrometry using a laser for desorption and ionization is a versatile technique [1–6], although it requires a high-vacuum system. Many practical surface characterization, however, need on-line and in situ measurements under atmospheric pressure.

A laser can be used to ionize a photo-absorbing molecule efficiently through a stepwise multi-photon process. This technique has been successfully applied to the determination of trace amounts of molecules in solution [7–14]. In previous papers [15,16], the highly sensitive two-photon ionization detection of aromatic molecules adsorbed on a metal surface by using a nitrogen laser was reported; photo-current measurement

in ambient air is simple and sensitive. Laser radiation of 337 nm provides soft excitation without extensive ionization of the bulk surface, because the photoelectric effect of the metal surface is smaller at 337 nm in comparison with that below 200 nm [17].

In this work, the two-photon ionization detection of aromatic molecules and dyes on metal surfaces under atmospheric pressure by using the third harmonic of an Nd:YAG laser was investigated. The dependence of the ionization signal on the molar absorptivity and the metal substrate was also investigated.

## EXPERIMENTAL

The experimental apparatus and the sample preparation were essentially the same as those reported previously [15,16]. The third harmonic

*Correspondence to:* T. Ogawa, Department of Molecular Science, Kyushu University, Kasuga, Fukuoka 816 (Japan).



of an Nd:YAG laser (Quanta-Ray GCR-11, 355 nm, 6 ns) was focused softly on one of the electrodes, on which a sample layer had been prepared. The laser was operated with a pulse energy of 3–4 mJ and a frequency of 3–5 Hz in order to reduce any effects of charging and desorption of the sample. The electrodes were placed in an electrically shielded box. The typical applied voltage was  $2.5 \text{ kV cm}^{-1}$ . The effect of ambient gases was measured in an evacuable chamber with a nitrogen laser (Molelectron UV-12, 337 nm, 10 ns).

The photocurrent was measured through a current amplifier (Keithley 427). A time profile was obtained by using a digital storage scope (Iwatsu DS6411) with a time resolution of  $10 \mu\text{s}$ . A precise signal intensity was obtained by using an A/D converter (Canopus Analog Pro II) with a time resolution of  $20 \mu\text{s}$  and integrating the signal over 0–200  $\mu\text{s}$ . The signal intensity was divided by the square of the pulse energy in order to correct for laser fluctuations [14].

A hexane solution (10  $\mu\text{l}$ ) of the sample molecule was dropped into a circular dimple ( $1.0 \text{ cm}^2$ ) on a metal plate which served as the electrode, then the solution was dried in air. The metal plate was either platinum, copper or nickel. The abbreviations of some of the samples used are 7-amino-4-methylcoumarin = coumarin 440, 1,6-diphenylhexa-1,3,5-triene = DPH, 2,5-bis(5-*tert*-butyl-2-benzoxazolyl)thiophene = BBOT, 2-(4-biphenyl)-5-phenyl-1,3,4-oxadiazole = PBD and 4,4'-bis[(2-butyloctyl)oxy]-*p*-quaterphenyl = BBQ.

The absorption spectra of adsorbates were recorded on a Shimadzu UV2200 spectrophotometer with a spherical integration attachment.

## RESULTS AND DISCUSSION

The two-photon ionization signal was observed with the laser pulse energy in the range  $30 \mu\text{J}$ – $5 \text{ mJ}$  with the metal substrate as the cathode [15,16,18]. The time-resolved photocurrent consisted of a sharp and a broad component; the former was due to fast negative species and the latter from slow negative species. The former was

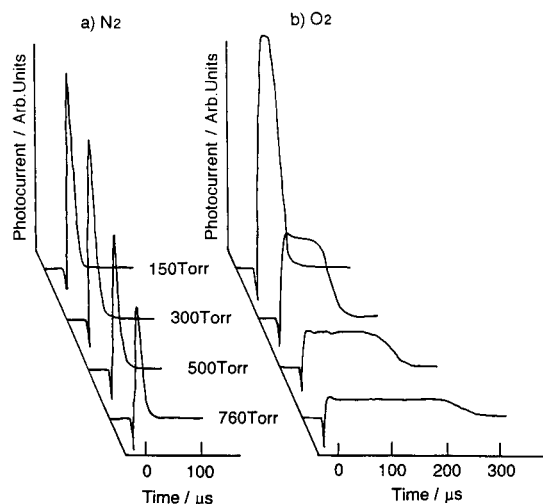


Fig. 1. Time profile of two-photon ionization current from pyrene on platinum in nitrogen and oxygen. Surface density of molecules,  $1.0 \times 10^{-9} \text{ mol cm}^{-2}$ ; laser,  $250 \mu\text{J}$  per pulse at 337 nm; applied voltage,  $2.5 \text{ kV cm}^{-1}$ .

assigned to emitted electrons and the latter to oxygen anions produced by capture of emitted electrons by measuring the dependence of the ambient pressure, applied voltage and ambient gas on the time profile [16].

The effects of nitrogen and oxygen as the ambient gas on the time profile are shown in Fig. 1. The sample was pyrene on a platinum plate and the surface density was  $1.0 \times 10^{-9} \text{ mol cm}^{-2}$ . The energy of the nitrogen laser was  $250 \mu\text{J}$  per pulse to avoid space-charge effects. When the chamber is filled with nitrogen, only the sharp component appears. As the time resolution used is slower than the electron drift, a change in the nitrogen pressure induces a corresponding change in the signal intensity but does not affect the time profiles. However, only the slow component appears for oxygen. The time-of-flight behaviour varies with the oxygen pressure because the mobility of the oxygen anion changes steadily. These results confirm the previous assignment of the charge carriers [16].

The signal intensity was proportional to the irradiation area of the laser up to at least  $1.5 \text{ cm}^2$ . The sample was BBQ on a nickel plate and the surface density was  $1.0 \times 10^{-10} \text{ mol cm}^{-2}$ . An iris trimmed the laser spot size. The energy of the

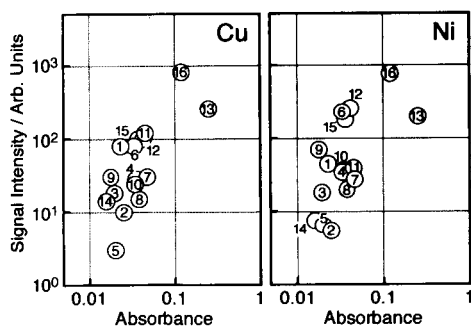


Fig. 2. Dependence of two-photon ionization signal of aromatic hydrocarbons on copper and nickel on absorptivity in ambient air. Surface density of molecules,  $1.0 \times 10^{-10}$  mol  $\text{cm}^{-2}$ ; laser, 3.0 mJ per pulse at 355 nm. 1 = 9-Methylanthracene; 2 = 1-chloroanthracene; 3 = 9-bromoanthracene; 4 = anthracene; 5 = naphthacene; 6 = 2-methylanthracene; 7 = coumarin 440; 8 = 2-aminoanthracene; 9 = 9,10-dimethylanthracene; 10 = perylene; 11 = DPH; 12 = tetraphene; 13 = BBOT; 14 = PBD; 15 = pyrene; 16 = BBQ.

Nd:YAG laser was 3.5 mJ per pulse at 355 nm when the laser spot size was  $1.0 \text{ cm}^2$ . This finding indicates that the sample molecule adsorbs uniformly on the surface. Two-photon ionization detection with a small laser spot allows a mapping analysis for surface samples by using a beam scanning technique. In subsequent measurements, the whole sample surface was irradiated to increase the sensitivity.

The two-photon ionization signals of sixteen molecules were observed on copper and on nickel and their dependence on the molar absorptivity is summarized in Fig. 2; the absorbance of the adsorbate was measured by using a quartz substrate. The absorption bands of these molecules on the surface shifted to longer wavelengths by more than 10 nm compared with those in hexane solution. The photocurrent of the molecules on copper and nickel is roughly proportional to the absorbance at 355 nm. The effect of the copper and nickel substrate is not as large as that of the molar absorptivity. The efficiency of excitation to the initial singlet excited state seems to be a dominant factor for the ionization. Similar results have been obtained for molecules in solution [9,11,14] and adsorbed molecules excited by a 337-nm nitrogen laser on nickel [17].

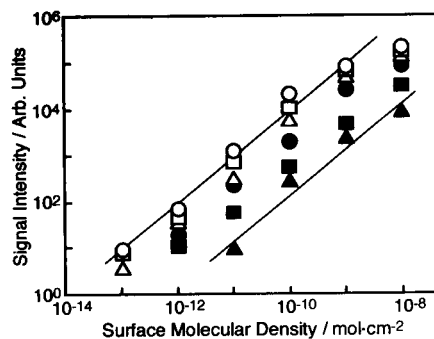


Fig. 3. Analytical response curves of aromatic hydrocarbons on platinum.  $\circ$  = BBQ;  $\square$  = 2-methylanthracene;  $\triangle$  = pyrene;  $\bullet$  = anthracene;  $\blacksquare$  = coumarin 440;  $\blacktriangle$  = 1-chloroanthracene. The solid line shows slope = 1.

Analytical response curves were measured for BBQ 2-methylanthracene, pyrene, anthracene, coumarin 440 and 1-chloroanthracene on platinum, as shown in Fig. 3. The surface molecular density was varied by adjusting the concentration of the hexane solution dropped. All the graphs are linear over more than three orders of magnitude. The detection limits of BBQ, 2-methylanthracene, pyrene, anthracene, coumarin 440 and 1-chloroanthracene are  $1.0 \times 10^{-13}$ ,  $1.7 \times 10^{-13}$ ,  $2.9 \times 10^{-13}$ ,  $5.5 \times 10^{-13}$ ,  $1.5 \times 10^{-12}$  and  $7.1 \times 10^{-12}$  mol  $\text{cm}^{-2}$ , respectively, at signal-to-noise ratio of 3.

The relationship between the detection limits and the molar absorptivities is summarized in Fig. 4. BBQ presents the lowest detection limit ( $1.0 \times 10^{-13}$  mol  $\text{cm}^{-2}$ ) because of the largest ab-

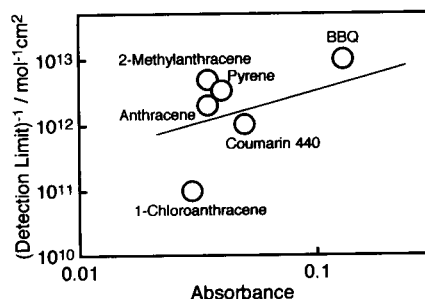


Fig. 4. Detection limits and absorptivities of aromatic hydrocarbons. Absorptivity is evaluated by the absorbance of a  $1.0 \times 10^{-10}$  mol  $\text{cm}^{-2}$  sample on the quartz plate. Solid line shows slope = 1.

sorbance. The detection limit of BBQ corresponds to about 1/500 monolayer coverage, which was estimated by assuming flat adsorption with a surface area of 3 nm<sup>2</sup> per molecule. The sensitivity for 1-chloroanthracene is low, probably because initially excited states were quenched by the halogen atom [14]. The detection limits with the Nd:YAG laser are about three times lower than those with a nitrogen laser [15,16], mainly because the former can irradiate a wide area uniformly.

In conclusion, laser two-photon ionization excited by 355-nm laser radiation is a very sensitive technique for trace molecules on a surface in ambient air. As laser radiation with a comparatively long wavelength prevents the photoelectric effect from a bulk metal surface, selective detection of adsorbates has been achieved.

#### REFERENCES

- 1 R. Tembreull and D.M. Lubman, *Anal. Chem.*, 59 (1987) 1003.
- 2 R.N. Zare, J.H. Hahn and R. Zenobi, *Bull. Chem. Soc. Jpn.*, 61 (1988) 87.
- 3 B. Stahl, M. Steup, M. Karas and F. Hillenkamp, *Anal. Chem.*, 63 (1991) 1463.
- 4 S.E. Egorov, V.S. Letokhov and A.N. Shibanov, *Chem. Phys.*, 85 (1984) 349.
- 5 M. Yang, J.R. Millard and J.P. Reilly, *Opt. Commun.*, 55 (1985) 41.
- 6 K.R. Gopidas and P.V. Kamat, *J. Phys. Chem.*, 93 (1989) 6428.
- 7 E. Voigtman, A. Jurgensen and J.D. Winefordner, *Anal. Chem.*, 53 (1981) 1921.
- 8 S. Yamada, K. Kano and T. Ogawa, *Bunseki Kagaku*, 31 (1982) E247.
- 9 S. Yamada, A. Hino, K. Kano and T. Ogawa, *Anal. Chem.*, 55 (1983) 1914.
- 10 S. Yamada and T. Ogawa, *Prog. Anal. Spectrosc.*, 9 (1986) 429.
- 11 S. Yamada, T. Ogawa and P.H. Zhang, *Anal. Chim. Acta*, 183 (1986) 251.
- 12 N. Sato, S. Yamada and T. Ogawa, *Anal. Sci.*, 3 (1987) 109.
- 13 S. Yamada, N. Sato, H. Kawazumi and T. Ogawa, *Anal. Chem.*, 59 (1987) 2719.
- 14 T. Ogawa, M. Kise, T. Yasuda, H. Kawazumi and S. Yamada, *Anal. Chem.*, 64 (1992) 1217.
- 15 T. Ogawa, T. Yasuda and H. Kawazumi, *Anal. Sci.*, 8 (1992) 81.
- 16 T. Ogawa, T. Yasuda and H. Kawazumi, *Anal. Chem.*, 64 (1992) 2615.
- 17 H. Kiriata and M. Uda, *Rev. Sci. Instrum.*, 52 (1981) 68.
- 18 R. Naaman, A. Petrank and D.M. Lubman, *J. Chem. Phys.*, 79 (1983) 4608.

# Advances in inductively coupled plasma mass spectrometry: human nutrition and toxicology

Ramon M. Barnes

*Department of Chemistry, Lederle Graduate Research Center, University of Massachusetts, Amherst, MA 01003-0035 (USA)*

(Received 7th November 1992; revised manuscript received 28th January 1993)

## Abstract

Inductively coupled plasma mass spectrometry (ICP-MS) has been applied with increasing frequency in the study of human nutrition and heavy metal toxicity. ICP-MS provides reliable isotope ratio determinations and superior metal concentration sensitivity. When combined with compound separation technology as part of the sample introduction phase, ICP-MS extends the tools available for studies of human metabolism and heavy metal poisoning. The basis for ICP-MS in these fields is reviewed, and examples are presented for zinc nutrition and lead toxicity to demonstrate the advances achieved in ICP-MS. The prospect for kinetic models with ICP-MS data is explored.

**Keywords:** Inductively coupled plasma mass spectrometry; Isotope dilution analysis; Isotope ratios; Kinetic models; Metals; Nutrition; Toxicity

In the elemental analysis of biological materials, three primary goals are considered: the identification and quantification of elemental concentrations, the identification and quantification of compounds containing metals, and the evaluation of bioavailability and/or toxicity. Typically, when a biological sample is analyzed the elemental composition of the material is sought first, and then the concentration of an individual element or group of elements is judged to be normal or abnormal. Information about the spatial and temporal distributions of an element within a fluid, organ, tissue, or cell magnifies the analysis requirements. The response of the element concentration and distribution to system perturbations

(e.g., disease, diet, environment, poison) extends simple analysis to involve critical and sometimes unknown *in vivo* processes. Furthermore, the identification of specific metal-containing compounds in addition to, or in lieu of, total metal concentration is desirable but often is restricted by the relative and absolute sensitivity of element-specific detection. To measure these metal-containing compounds, they are usually separated from the matrix and other similar complex materials, typically with chromatographic or electrophoretic techniques, and the metal-containing molecules are then identified, generally with the aid of on-line spectroscopic detectors. Identifying the chemical form of the metal in the compound is also critical. Changes in chemical form often alter the role played by the species in biological systems. Although molecular (UV, NMR) and mass spectroscopic (MS) techniques provide invaluable information about metal

*Correspondence to:* R.M. Barnes, Department of Chemistry, Lederle Graduate Research Center, University of Massachusetts, Amherst, MA 01003-0035 (USA).

species, applications are limited by the sensitivity of the technique. The bioavailability and nutrition of minerals and trace metals is established with animal and human subjects through element balance, isotope tracer, or radioisotope studies. The chemical form of the metal in these investigations is of growing concern, especially when the mechanisms of metabolism and toxicity are to be characterized. In each of these aspects of biological material analysis, inductively coupled plasma (ICP)-MS can provide a valuable and sometimes unique contribution.

Stable isotope analysis methods for biological materials are well established with conventional mass spectrometric and nuclear approaches [1–3]. Typically, stable isotopes are employed to characterize absorption, excretion, and kinetics of trace minerals [1]. Among the elements applied for these studies are Li, Mg, K, Ca, V, Cr, Fe, Ni, Cu, Zn, Se, Cd, Rb, Sr, Ba, Tl, and Pb. An extensive literature of isotope methodology already exists for conventional ion source mass spectrometry. Accepted techniques such as stable isotope dilution analysis (IDA) or administration of multiple isotopes of the same element, and valuable applications with these conventional isotope techniques can be extended by ICP-MS (e.g. for Br) [2].

The motivation to apply stable isotope techniques in biomedical research is growing as their advantages are recognized and the requirements are satisfied with novel instrumentation capabilities. ICP-MS and new isotope measurement technologies enhance the other approaches commonly used because the sample preparation is easy, the analysis rapid, and the precision sufficient for most biomedical applications. Furthermore, nutritional, pharmacological and toxicological models of animals and humans can be expanded with sufficient data, and the sample throughput of ICP-MS significantly increases the range and usefulness of stable isotope measurements for these kinetic models [4].

In most studies, the interactions and cooperation among professionals, including nutritionists, toxicologists, clinicians, and analytical chemists, is critical to maximize the utility of stable isotope methods with biomedical materials [5].

## INDUCTIVELY COUPLED PLASMA MASS SPECTROMETRY

The general applications, instrumentation, principles, and features of ICP-MS are examined in a number of recent books and conference proceedings [6–10]. Included are chapters describing stable isotope tracer applications to biological samples [11–13]. Relative to ICP atomic emission spectrometry (ICP-AES), ICP-MS provides much lower limits of detection, simpler spectral interpretation with fewer spectral interferences, and reliable isotope ratio and isotope dilution analysis results. On the other hand, ICP-AES uses simpler and lower cost instrumentation than ICP-MS, operates with lower daily running costs, displays better tolerance to total sample salt content, exhibits lower matrix effects, and draws on a large, mature applications database. For example, limits of detection reported by ICP-mass spectrometer manufactures with state-of-the-art instrumentation are orders of magnitude better than either ICP-AES or earlier ICP-MS systems [7,14]. More than 50 elements can be detected below the  $10 \text{ pg ml}^{-1}$  level, which translates into the reliable isotope ratio determination of many mineral and trace elements of concern in human nutrition studies. For example, higher sensitivity for zinc with current ICP-MS systems should improve the measurement precision of  $^{70}\text{Zn}$  to  $^{68}\text{Zn}$  ratios in human serum [15]. With ICP quadrupole MS, the precision range of stable isotope measurements is typically better (0.1–2% relative standard deviation) than either neutron activation analysis (NAA) or gas chromatography–mass spectrometry (GC–MS). However, the precision is poorer than thermal ionization mass spectrometry (TIMS) with a magnetic sector mass spectrometer. Quadrupole TIMS and fast-atom bombardment MS (FAB-MS) appear to be comparable with ICP-MS [3]. Moreover, ICP-MS with a high-resolution, double focusing magnetic sector mass analyzer equipped with multiple detectors matches the accuracy and precision of TIMS stable isotope measurement [16].

In considering the applications of ICP-MS to biological and botanical (plants, feeds, foods, and animal tissues), and clinical-medical (blood and

blood components; urine and feces; bone, kidney, liver, lung tissues; hair; milk; drugs and drug metabolites) materials [17], both elemental and isotope ratio analyses furnish survey and quantitative results. Semiquantitative analysis provides survey data of total element content of biological and clinical materials [18]. Quantitative analysis of major, minor, and trace impurities depends upon external calibration, standard additions, or isotope dilution techniques. Obtaining an elemental mass spectrum of a biological sample is essentially simple; however, the spectrum requires interpretation especially with low-resolution quadrupole MS instruments. Isobaric species are not resolved, and poly-atomic ion species from the matrix, sample preparation steps, and argon plasma cause interferences when coincident with analyte ions. Polyatomic ions arising from biological materials include combinations of C, Cl, S, O, P, and Na (e.g.,  $^{35}\text{ClO}^+$ ,  $\text{ArC}^+$ ,  $^{37}\text{ClO}^+$ ,  $\text{ArO}^+$ ,  $\text{PO}_2^+$ ,  $\text{ArNA}^+$ ,  $^{35}\text{Cl}_2^+$ ,  $\text{Ar}_2^+$ ). Spectral overlap by polyatomic species from sample matrix and argon plasma background limits the method for some critical major isotopes (e.g., Cr, Mn, V, Ca, Se).

The rapid, multi-element capability of ICP-MS is an ideal match for the requirements of many biological and clinical analyses. Examples of semi-quantitative ICP-MS determinations include reports by Yoshinaga et al. [19], who evaluated 61 elements in six human internal organ tissues (cerebrum, cerebellum, heart, spleen, liver, kidney) from 45 cadavers, and by Vaughan et al. [20], who surveyed 13 elements in serum, 15 elements in whole blood, and 25 elements in saliva using available software. Polyatomic ion interferences limited the number of elements identified, however. Subtraction of interfering signals in the blank might be sufficient to correct some spectral interferences, but the approach yields low results for other elements (i.e., B, Mg, and Al) resulting from signal suppression with digested plasma or whole-blood samples. Reliable concentration estimates were achieved for numerous elements with matrix matched standards, internal reference elements, or by adding a multi-element standard to a sample aliquot.

As an example of quantitative multi-element

analysis, Lyon and coworkers [21,22] evaluated the accuracy of ICP-MS analysis of human autopsy tissues. ICP-MS results for Al, Mg, Mn, Fe, Cu, Zn, and Cd were obtained faster than with atomic absorption spectrometry (AAS) and with comparable accuracy. Shiraishi and McInroy [23] also determined five elements (Ba, Tl, Bi, Th, and U) in human autopsy tissues (liver, lung, spleen, and kidneys). The sample solutions prepared from approximately 3 g of soft tissues were estimated to contain about  $1000 \mu\text{g ml}^{-1}$  of salts. Maximum dilution to reduce matrix effects was balanced by the requirement for high sensitivity at ultratrace concentrations. Advanced techniques are needed to address this dilemma. Vanhoe et al. [24] determined Fe, Cu, Co, Zn, Rb, Mo, and Cs in human serum after subtraction of polyatomic ion signals obtained with a blank solution containing matched concentrations of Na, S, Cl, and Ca.

In order to achieve accurate ICP-MS element concentrations and isotope ratio analyses in complex clinical and biological samples, preconcentration and separation techniques are applied either to remove the matrix or to concentrate the analyte [25]. The analyte is typically separated chemically from the sample prior to determination. For example, Janghorbani and Ting [2] developed sample preparation and separation schemes for each of their stable isotope analyses. After sample digestion, they applied ion exchange for Li, precipitation with ammonium phosphate for Mg, precipitation with ammonium pyrrolidinedithiocarbamate (APDC) for Fe, Cu, and Zn followed by dissolution for Zn, complexation with ammonia for Fe, ion exchange for Cu, hydride generation for Se, and distillation for Br. In another example Heithmar et al. [26] adopted a semiautomatic system with a macroporous iminodiacetate resin to preconcentrate Ti, V, Mn, Fe, Co, Ni, Cu, Cd, and Pb and separate them from a high-salt content, waste water matrix. Organic samples generally require complete digestion prior to separation and preconcentration steps to free organically bound elements.

In an elegant example, Lyon and Fell [27] separated copper in serum from sodium and phosphate ions ( $\text{ArNa}^+$ ,  $\text{PO}_2^+$ ), which interfere

with  $^{63}\text{Cu}^+$ , by size-exclusion chromatography of copper-bound ceruloplasmin, albumin, and transthyretin proteins. Accurate direct measurement of the  $^{63}\text{Cu}:^{65}\text{Cu}$  ratio was achieved with a precision of 0.2% in the desalted protein solution.

Slight improvement in the mass spectrometric resolution is sufficient to minimize spectral interferences. For example, in the determination of bromine in human serum, the two stable isotope  $^{79}\text{Br}$  (50.7%) and  $^{81}\text{Br}$  (49.3%) signals can be affected by broadening of the  $^{80}\text{Ar}_2^+$  [28]. Most commercial quadrupole ICP-MS systems allow some adjustment to the resolution ( $\Delta\text{amu} = 1-0.6$ ) with a commensurate sacrifice in sensitivity (half). Thus, to resolve the bromine and argon dimer signal overlaps, higher resolution and reduced sensitivity were utilized. Minimum sample dilution was a prerequisite. Thus with no digestion, only a 5- to 10-fold dilution of the serum sample was needed to reduce salt blockage of the plasma torch, solid deposition on the sampler and skimmer cones, and signal suppression from the matrix. A blank solution signal was subtracted to correct for  $^{40}\text{Ar}^{38}\text{ArH}^+$  on  $^{79}\text{Br}$  and  $^{40}\text{Ar}^{40}\text{ArH}^+$  on  $^{81}\text{Br}$  interferences.

Contamination also limits the accuracy of ICP-MS determinations [29]. Appropriate sample preparation and field sampling blanks are essential, and cleanroom facilities and pure reagents are needed for accurate results. Another practical problem arises from sample carry-over in the ICP-MS sample introduction system. For a few elements (i.e., B, I, Hg, Os), extended cleanout periods are required to wash the nebulizer and spray chamber. By substituting a nebulizer arrangement without aerosol spray chamber (e.g., a direct injection nebulizer), this memory effect is significantly reduced [30]. With this arrangement Smith et al. [30] determined boron and  $^{10}\text{B}:^{11}\text{B}$  ratio in biological materials with a detection limit of  $1\text{ ng g}^{-1}$  and isotope ratio precision of 0.4–1.5% (R.S.D.).

The quantitative analysis of trace impurities by ICP-MS employs either external calibration, standard additions, or isotope dilution analysis [31]. External calibration results in the highest sample throughput, but the accuracy and precision obtained are best at low concomitant concentra-

tions. The performance is improved with matrix matched standards or internal reference element additions. The method of additions reduces the sample throughput, but good accuracy results in the absence of spectral interferences.

Isotope dilution analysis (IDA) also decreases sample throughput, but very good accuracy and precision are obtainable [31]. Two isotopes free of spectral interferences are required. The technique provides compensation for a variety of physical and chemical interferences, as well as for analyte loss during sample preparation. The isotope ratio acts as an ideal internal standard, and the method is absolute. However, some elements have only one stable isotope, and the stable isotopes can be expensive, if available. In practical ID-ICP-MS, spectroscopic overlap interferences may be a severe problem. The steps in an ID-ICP-MS experiment include preparation of a solution of the unspiked sample, verification of the isotope ratios of the unspiked sample to evaluate polyatomic ion interference, isobaric interference, and natural variations, preparation of a solution of the sample with a stable isotope spike allowing ample time for equilibration of the isotopes, measurement of the altered isotope ratio, correction for mass discrimination when needed, and calculation of the element concentration in the unspiked sample, with correction for mass discrimination [6]. The analytical error of isotope dilution MS was evaluated theoretically and verified experimentally by Van Heuzen et al. [32], and the best IDA achieved with an optimum mixture of the spike and sample [33]. ICP-MS operating conditions should be selected to optimize isotope ratio precision rather than analyte count rate.

McLaren et al. [34] pioneered the application of stable isotope dilution ICP-MS in the analysis of marine standard reference materials including sediments, sea water, and marine lobster tissue. Okamoto [35] determined total tin in fish tissue reference material by isotope dilution ICP-MS. Campbell et al. [36] determined mercury in cod muscle after evaluating the influence of chemical form on the accuracy. Biological applications of stable isotope dilution ICP-MS include the determination of lead in environmental (soil, sediment,

dust, paint) and clinical (blood, feces) samples [37,38]. Igarashi et al. [39,40] used ID-ICP-MS for the determination of Th and U in human tissues and other biological samples.

In vivo uptake and retention studies in living organisms by ICP-MS was considered by Russ [41] as one of the most exciting and potentially useful areas of IDA. The in vitro stable isotope dilution method involves the addition of a known amount of highly enriched isotope to the biological sample, which differs from the in vivo tracer [2]. When these two techniques are combined, at least three stable isotopes are required and at least two isotope ratios are measured.

In summary, the advantageous characteristics of ICP-MS for stable isotope ratio analysis include the rapid sample analysis (5 min per sample) and high throughput, minimum sample preparation, broad multi-element capability, and determination of elements with high ionization potential. The most serious problem is the relatively limited precision (1–0.1% R.S.D. in the best measurement case) and spectral overlap interference in the worst case with quadrupole MS.

#### STABLE ISOTOPES FOR TRACER STUDIES

A variety of methods exist for the measurement of stable isotopes: NAA, TIMS, GC-MS, fast-atom bombardment mass spectrometry (FAB-MS), ICP-MS, electron impact and chemical ionization mass spectrometry (EI- and CI-MS), and field desorption mass spectrometry (FD-MS) [1–4]. Selection of the instrumental approach applied depends upon the instrument availability, the isotopes analytes, and the precision and sensitivity required. TIMS is the definitive and most precise method for most analyses, but ICP-MS provides shorter sample preparation and analysis time with a precision that is generally adequate for most tracer studies [1].

Stable isotope tracers in nutritional studies permit following the dynamic/equilibrium transport of chemical elements or their compounds. This can aid the understanding of the metabolism of minerals in foods or those administered as

therapeutic agents under a broad range of conditions of health or disease [4]. Stable isotopes as in vivo metabolic tracers are introduced through the alimentary canal or respiratory system, the integument, or by injection, and lead to exchange with endogenous elements. Thus, stable isotope tracers are useful for metabolic modelling, especially in infants and pregnant women to whom administration of a radioisotope is undesirable. Numerous multiple isotope labelling options exist, and no limit is fixed for the period of the experiment, as might occur with a short-lived radioisotope [2].

The application of ICP-MS for stable isotope tracer has been relatively limited, although the area is developing [2]. The target human population groups include both normal and preterm infants, healthy adults, patients, and women of child-bearing age. Studies of mineral metabolism (Ca, Mg, Fe, Cu, Zn, Pb, and Se), such as the dietary availability of iron to infants, and exchangeability of dietary pools of Zn, Se and Mg turnover studies and Cu transport in animals, are typical examples [2]. Other elements for which ICP-MS stable isotope ratio analyses have been performed with non-clinical samples include Li, B, Mg, Cl, K, Cr, Fe, Cu, Zn, Se, Br, Rb, Sr, Re, Os, Pb, U, and Th [6,41].

A general limitation of stable isotope applications includes the unavailability of more than one stable isotope for some elements [2]. Stable isotopes are accessible from a limited number of suppliers, sometimes in restricted quantities. Secondly, adequate enrichment of the tracer in the endogenous pools is needed for detection. Furthermore, the costs of the stable isotope, sample preparation, and type of mass spectrometer can also constrain isotope selection. Isotope ratio analysis is more difficult than a simple quantitative measurement, and the measurement precision ultimately limits the analysis utility. Unlike radioisotopes, in vivo localization of the stable isotope is not readily detected without taking a sample for external analysis [2,3].

Two important requirements need be considered before applying stable isotopes to tracer studies. First, the measurement precision and accuracy should be evaluated relative to the isotope



enrichment achievable after in vivo administration of the stable isotope dose. Enrichment should be sufficient to provide signal count differences adequate to be measured statistically. Secondly, the feasibility of achieving acceptable isotopic enrichment in the target fluid, tissue, or subcompartment should be evaluated in order to quantify the tracer with the requisite accuracy and precision [2].

The degree of isotopic enrichment in biological systems depends upon the amount of isotope administered, the efficacy of absorption and retention, the specific compartment distribution, the amount of element in the target compartment, distribution of the chemical forms in the compartment, the natural stable isotopic abundances and composition, and the cost of the stable isotope to achieve 10% enrichment [4]. For example, the feasibility of measuring iron absorption by incorporating stable iron isotopes into red blood cells was evaluated by Whittaker and coworkers [42,43]. In their clinical protocol 10 mg of  $^{57}\text{Fe}$  were administered orally and 0.5 mg  $^{58}\text{Fe}$  were given intravenously. A 1-ml blood sample was taken before administration and a second was drawn 14 days later. The  $^{57}\text{Fe}:^{56}\text{Fe}$  and  $^{58}\text{Fe}:^{56}\text{Fe}$  ratios were determined to obtain the iron absorption. ICP-MS instrument measurement precision was  $<0.4\%$  for the former and  $<0.6\%$  for the latter when the Fe concentration was  $10 \mu\text{g ml}^{-1}$ . Their optimized procedure allowed a 3% minimum detectable absorption for  $^{57}\text{Fe}$ .

Single isotope erythrocyte analysis required an assumption of the level of oral Fe incorporation into the erythrocytes. In contrast, the double isotope method dispensed with this assumption, because the intravenously administered isotope was equivalent to 100% absorption. This compensated for redistribution of the tracer in the body. The approach provides greater accuracy than the single isotope technique. The two least abundant stable iron isotopes were administered to achieve maximum enrichment, and the reliability of the  $^{56}\text{Fe}$  measurement was critical. Enrichment of the administered isotopes was limited by their cost (i.e.,  $^{58}\text{Fe}$  is approximately 20-fold more expensive than  $^{54}\text{Fe}$  and 5 times more costly than

$^{57}\text{Fe}$ ) and the desire to give physiological doses of iron comparable to the daily dietary intake. Since the natural abundance of  $^{54}\text{Fe}$  is 2.6 times that of  $^{57}\text{Fe}$ , 2.6 times as much  $^{54}\text{Fe}$  would be required to give the same enrichment as  $^{57}\text{Fe}$ . However, administration of this quantity of  $^{54}\text{Fe}$  would exceed the target daily iron requirement. The use of  $^{58}\text{Fe}$  is most expensive and is limited to intravenous administration. In order to minimize the counting error to  $<0.5\%$  for the two isotope ratios,  $^{56}\text{Fe}$  counts must be  $>10^7$  above the signal from polyatomic background ( $^{40}\text{Ar}^{16}\text{O}^+$ ). Thus, the  $^{40}\text{Ar}^{16}\text{O}^+$  must be minimized. Minor adjustments in mass bias were made for unknowns by comparing standards with accepted natural abundances. The high concentration of Fe in whole blood permitted 10 replicate analyses (after 1 + 24 dilution) each taking 2 min. The analysis time for 5 blanks and 10 sample replicates was 40 min [42,43].

A number of recent studies on animals and humans demonstrate the power of ICP-MS. Studies of very low birth weight premature infants is one example. In general, Fe, Se, Cu, Mg, and Zn have been examined for human metabolism studies by ICP-MS. Investigation of Zn metabolism in preterm infants by ICP-MS is especially applicable, since some of the sample amounts are limited, stable isotope additions are desirable, and potential interferences exist in the measurements [15].

Definition of the optimal diet for premature infants is focussed on achieving normal post-natal development and nutrient accretion, but the composition of this diet requires measurement of dietary mineral bioavailability and retention. Naturally occurring, non-invasive, non-radioactive isotope traces are added in infant diets as extrinsic tags to quantify absorption and incorporation [44]. Sample analyses in these studies performed earlier by NAA are being replaced by ICP-MS [45]. Zn [15,46], Cu [44], Se [47], and Fe [48] have been investigated, and extrinsic stable isotope tag and standard nutrient balance methods were found to correlate well. To obtain quantitative descriptions of Zn metabolism, a stable Zn isotope tracer ( $^{70}\text{Zn}$ ) was administered orally or intravenously to infants, and plasma, red blood

cells, urine, feces, and nutrients were sampled. For example, we measured total Zn by ICP-AES and Zn isotope ratios by ICP-MS [49]. The data obtained was evaluated with a model of Zn metabolism [50].

In another example, the organ turnover rate, exchangeable pool size, and the dynamics of administered minerals were studied in mice and rats for Mg [51,52], Cu [53], and Se [54] by ICP-MS. In the long-term organ Mg turnover kinetics experiment, the normal isotope abundance of Mg ( $^{24}\text{Mg}$  77.95%,  $^{25}\text{Mg}$  10.28%,  $^{26}\text{Mg}$  11.77%) in tissue was altered by substituting highly enriched (> 98%)  $^{24}\text{Mg}$  in the diet. The change in organ content of  $^{25}\text{Mg}$  with time was quantified accurately by *in vivo* isotope dilution with an  $^{26}\text{Mg}$  (99.72%) spike. This measurement cannot be accomplished by radioactive  $^{28}\text{Mg}$ , because of its short half life (21.3 h) relative to the equilibrium time required (120 h). With conventional stable isotope analysis, NAA imprecision limited the isotope ratio determinations of the minor isotopes  $^{25}\text{Mg}$  and  $^{26}\text{Mg}$  at low isotopic enrichment. On the other hand, ICP-MS provided precisions for  $^{25}\text{Mg}$ : $^{24}\text{Mg}$  and  $^{26}\text{Mg}$ : $^{24}\text{Mg}$  in the range of 0.1–1%. In summary, ICP-MS has made the *in vivo* study of Mg biokinetics possible and practical.

Stable isotope bioavailability studies thus can be approached in four ways: classical mass balance, single oral tracer, dual tracer, and continuous tracer administration. The mass balance approach gives a direct measure of the net absorption/retention, is relatively inexpensive, and widely applicable. However, no information about the source or kinetics is obtained, complete sample collection is challenging, absorption values depend on the completeness of stool collection, and the procedure is difficult to apply to neonates and older children. With a single oral tracer true absorption is obtained, but fractional absorption is dependent on the mass balance. Furthermore, differentiation between unabsorbed metal from the diet and the metal endogenously excreted in feces is difficult. In the dual tracer approach, kinetic analysis is possible, the results are verifiable, and true fractional absorption is available (e.g., from a 24-h urine sample). However, both

oral and intravenous tracer administration is required. In the continuous tracer technique cumulative enrichment and true fractional absorption are obtained, but the method is expensive and difficult [51,52].

A recent example of the dual tracer technique with FAB-MS was described by Fennessey et al. [55] for Zn and 120 human subjects. Oral  $^{68}\text{Zn}$  and intravenous  $^{70}\text{Zn}$  were administered. For feces the fractional absorption was determined by extrapolating the curve of cumulative fecal  $^{68}\text{Zn}$  isotope excretion, the slope of which is constant after > 95% of the unabsorbed isotope was eliminated, to zero administering time of the oral dose. Correction for excretion of systemic Zn was made by the use of the cumulative fecal  $^{70}\text{Zn}$  excretion data. Similar results could be achieved with ICP-MS. Another example of a dual isotope tracer experiment was described by Schuette et al. with Mg [51,52].

#### TOXICOLOGY AND TOXICOKINETICS

Whereas nutrition is the science or study of proper, balanced diet to promote health, especially in humans, and pharmacology is the science dealing with the preparation, qualities, and uses of drugs and their effect on living organisms, toxicology is the science of poisons, their effects, antidotes, etc. [56]. In a parallel fashion, whereas pharmacodynamics is the branch of pharmacology that deals with the effects and reactions of drugs within the body and pharmacokinetics considers all processes involved in the uptake, deposition, transportation, degradation, and elimination of a drug, the definition of toxicodynamics and toxicokinetics is the branch of toxicology that deals with the effects and reactions of poison within the body, and all the processes involved in the uptake, deposition, transportation, degradation, and elimination of a toxicant, respectively.

Toxicology and toxicokinetics represent fields of significant potential development for stable isotope analysis by ICP-MS. Yet, relatively little experience has resulted, probably because of the ethical question of conducting human experiments with heavy metal poisons. A valuable toxi-

ecological application of ICP-MS isotope analysis has been source identification involved in childhood lead poisoning cases. Whenever unique environmental lead sources such as paint, dust, or soil are ingested by children, the lead isotope composition in the child's blood and feces changes to reflect the isotope abundance of the source [37,38]. Unique sources can be pinpointed by their congruency with the blood lead isotopic composition. With source identification, lead abatement can be directed to the appropriate specific lead supply.

The status of toxicokinetics was reviewed by Frazier [57], who considered the organ toxicity of cadmium. The major challenge facing toxicology was identified as the ability to predict the concentration–time profile of a toxicant in the essential organ as a function of exposure conditions. A number of critical questions were posed concerning the toxicokinetics of the cumulative toxin cadmium in humans: “Why is the biological half-life of cadmium so long? Why is the kidney a target organ for chronic chromium toxicity following systemic absorption? Why is there an apparent threshold for cadmium renal toxicity? What is the biological basis of the critical organ concentration?” Frazier observed that “very little is known about the fundamental processes which control the toxicokinetic of metals in biological systems”. Membrane transport and intra- and extra-cellular protein–metal interactions are important for cadmium. Furthermore, he indicated that “there is no complete physiologically based toxicokinetic model for cadmium kinetics in humans”. Existing models of human cadmium kinetics do not account for many of the non-linear phenomena of the kinetic processes and toxicological responses of specific compartments under wide cadmium exposure levels. A useful model must incorporate cadmium-binding proteins, including plasma proteins and metallothionein.

Surprisingly, no reports have appeared on the application of stable isotope ICP-MS analysis to the toxicokinetics of cadmium (or other heavy metal toxins), although cadmium binding to metallothionein and similar proteins has been detected by ICP-MS after chromatographic separations [58,59]. Lead is an exception, owing to the

interest in lead poisoning. However, speciation studies of As, Hg, Sn, and Pb with ICP-MS detection have been reported [60].

#### KINETIC MODELLING WITH STABLE ISOTOPE ANALYSIS

In metabolism, nutritional, pharmaco-, and toxicodynamic studies the primary objects are to identify the system sinks and sources, establish the dynamics and kinetics between them, define their physiological relationships, and characterize the biochemical mechanisms. Biokinetic parameters can be determined with stable and radioactive isotopes by measuring the change of tracer concentration in body fluids or tissues after *in vivo* tracer administration (e.g., Te in rabbits [61]). Mathematical functions are fitted to concentration–time data to characterize kinetic uptake and loss parameters. Kinetic modelling has become an important component in nutrition, and the modelling resources available were described recently by Collins [62].

Kinetic models have been studied widely using isotope tracers. For example, a kinetic model of Cu metabolism in lactating dairy cows employed  $^{65}\text{Cu}$  as an *in vivo* tracer [63]. After administration, the distribution of tracer and natural concentration of Cu in liver, plasma, and milk were monitored, and a popular kinetic modelling program (SAAM/CONSAM) was applied with seven compartments (i.e., liver, two plasma forms (ionic and ceruloplasmin-bound), remaining body, gut, milk, and feces) and five loss routes. The solution to the model provided kinetic data on the absorption and transfer among compartments. The model was not in a steady state, which resulted in about half of the kinetic parameters varying with time.

State-of-the-art of mineral metabolism modelling was the theme of in a recent conference [64]. One kinetic modelling program (Simulation, Analysis and Modelling: SAAM/CONSAM) demonstrated there expresses models in terms of physiological pools and flows, constructs and solves mathematical equations, displays model curve fits against observed data, and includes built-in convergence routines that provide the

best estimate of model parameters. Models for Ca, Cu, I, Fe, Mn, Se, and Zn metabolism, and Cd, Hg, and Pb kinetics were described. The meeting papers will be published [65].

One excellent example of the application of this kinetic modeling program is a model developed to describe the biokinetics of sodium selenite metabolism in humans, based on plasma, urine, and fecal samples obtained over a four-week period after a single oral dose of enriched stable isotope tracer  $^{74}\text{Se}$  [66,67]. The model described absorption, distribution along the gastrointestinal tract, and enterohepatic recirculation with four kinetically distinct plasma pools, a liver–pancreas subsystem, and a slow turn over pool. Separating selenium metabolism into several distinct kinetic components was the first step in identifying the efficacious, nutritious, and toxic forms of Se. The kinetically distinct pools suggested the possibility of different chemical species of Se, each of which may have had a specific, perhaps different mechanism of absorption. The pharmacokinetics of an organically bound form of Se  $^{74}\text{Se}$  L-selenomethionine (SeMet), also was studied with the aid of a kinetic model [68]. The amounts of  $^{74}\text{Se}$  tracer, unenriched Se, and total Se were determined by IDA-GC-MS. A model similar to the selenite model was proposed for SeMet data. The oral SeMet dose was better absorbed and conserved than was the selenite. However, the observed plasma data suggested two kinetically distinct peripheral tissue pools, and a significantly higher reutilization and turnover of SeMet than selenite.

Moser-Veillon et al. [69] administered sodium [ $^{76}\text{Se}$ ] selenite and [ $^{74}\text{Se}$ ] SeMet simultaneously to lactating and non-lactating women. The two chemical forms were metabolized differently by the physiologically distinct groups of women. Multiple isotopes permitted simultaneous intrinsic and extrinsic labelling of food, simultaneous intravenous and oral tracer administration, and the use of IDA techniques.

Although the  $^{74}\text{Se}$  and  $^{76}\text{Se}$  were determined by IDA-GC-MS after a suitable complexation and extraction, the extensive development of  $^{74}\text{Se}$  isotope tracer analysis with ICP-MS by Janghorbani et al. [46] suggests that ICP-MS will become a valuable tool in future kinetic modeling. How-

ever, isotope selection with ICP-MS detection may be different owing to potential spectral overlap interferences.  $^{74}\text{Se}$  has been used as an in vivo tracer and  $^{82}\text{Se}$  as an in vitro IDA spike by Janghorbani et al. [46].

The kinetic analysis of zinc metal metabolism has been studied extensively with radioisotope tracers (i.e.,  $^{65}\text{Zn}$  oral or intravenous injection) for example to determine sites of regulation of zinc metabolism [70]. In these models the native and radioactive zinc activity were measured in plasma, erythrocytes (RBC), urine, and feces by flame AAS and  $\gamma$ -ray spectrometry, and by external counting over the whole body, liver, and thigh. Zinc metabolism studies in children were limited by the lack of an accurate technique [71]. Human zinc metabolism can be studied with an in vivo  $^{70}\text{Zn}$  stable tracer to determine parameters of whole body zinc metabolism, including absorption, excretion and secretion [72].  $^{70}\text{Zn}$ ,  $^{68}\text{Zn}$ , and  $^{64}\text{Zn}$  were determined by NAA. Values obtained with two zinc tracers ( $^{65}\text{Zn}$  and  $^{70}\text{Zn}$ ) from multiple tissues and analyzed by a compartmental model were the same. Furthermore, the stable  $^{70}\text{Zn}$  can be used safely with children.

Zinc kinetic studies have benefited significantly from the ICP-MS determination of stable Zn isotope tracers ( $^{67}\text{Zn}$ ,  $^{68}\text{Zn}$ , and  $^{70}\text{Zn}$ ) [2,15,73–75]. Our own ICP-MS zinc analyses [49] have been undertaken in support of kinetic modelling of zinc metabolism in neonates [50]. The determination of zinc by ICP-AES and  $^{70}\text{Zn}$ : $^{68}\text{Zn}$  by ICP-MS is required in infant serum, urine, feces, and food. As indicated earlier, appropriate sample preparation steps and contamination control in a cleanroom environment are essential. The determination of  $^{70}\text{Zn}$  in serum requires sample preconcentration and separation [15,73]; however, measurement precision can be limiting without the application of an ultrasonic nebulizer or the sensitivity of second-generation ICP-MS instrumentation.

Measurement of fractional absorption of zinc based upon a dual tracer ( $^{68}\text{Zn}$  and  $^{70}\text{Zn}$ ) experiment with urine rather than feces also should be feasible by ICP-MS instead of FAB-MS [76]. A critical assumption is that the infused  $^{70}\text{Zn}$  exchanges completely with the plasma zinc pool.

## CHEMICAL SPECIATION AND STABLE ISOTOPE ANALYSIS

The metabolic behavior or toxicity of an element, especially at trace concentration levels, depends on its chemical forms in biological systems [77]. Speciation of a trace element in a biological matrix represents the identification of the biologically active compounds to which the element is bound and the quantification of the element in relation to the particular compound [78]. Toxic effects generally involve speciation of small molecules (e.g., methyl mercury, triethyltin, tetraethyllead) or of free ionic forms, while biological functions concern evaluation of large molecules (e.g., metallo-enzymes, metallo-proteins). Either direct species determination or analysis after separation are employed [77]. The recovery of the biomolecule and the trace element should be reported. Identifying different oxidation states of elements in tissues and fluids is another area of biological speciation research.

Cornelis [78] described the application of radiotracer labelling for speciation. Lund [79] reviewed techniques for the determination of various elemental species and discussed the relationship between speciation and bioavailability. Behne [77] discussed current trends and problems. He concluded that no available method [i.e., liquid chromatography (LC) or electrochemical separation] met the requirements for the determination of protein-bound trace element compounds by combined analysis. The resolving ability of most fractionating techniques is insufficient to distinguish among the large number of molecular components in biological fluids. However, when combined with an element-specific detector like ICP-MS, the added detection selectivity sometimes relaxes the requirement for high resolution.

Numerous combinations of separation and detection approaches are available for chemical speciation analysis [80,81]. ICP-MS among other plasma sources (e.g., ICP-AES, microwave-induced plasma) has become a valuable partner in chemical speciation of metals especially, because of its very low detection limits and high selectivity [13,27,58–60]. On the other hand, separation of bound metal species prior to ICP-MS detection is

advantageous because the matrix electrolytes (e.g., Na) are separated and do not generate an MS signal suppression during the analysis [27]. Active development is underway of LC-ICP-MS for the separation and identification of metal-containing molecules [6, e.g., Table 4.9, p. 114; 82]. For example, organic forms of arsenic [83–86], cadmium [58,59,87], chromium, iron [88,89], lead [90,91], mercury [90,92,93], rare earth elements [94], tellurium [95], tin [96–99], and zinc [100] have been separated and/or quantified in environmental and biological materials. As an example, the detection limit was 0.2 pg absolute and  $0.1 \mu\text{g l}^{-1}$  relative for Pb and 7 pg absolute and  $4 \mu\text{g l}^{-1}$  relative for Hg [90]. Peak area precision, however, was only 2–5%.

Stable isotope analysis of chromatographically separated, metal-bound molecules is not well developed, and only a limited number of studies have been conducted. For example, Owen et al. [100] recently described a multi-isotopic study (i.e.,  $^{54}\text{Fe}$ ,  $^{57}\text{Fe}$ ,  $^{59}\text{Co}$ ,  $^{63}\text{Cu}$ ,  $^{65}\text{Cu}$ ,  $^{64}\text{Zn}$ ,  $^{66}\text{Zn}$ ,  $^{67}\text{Zn}$ ,  $^{68}\text{Zn}$ ,  $^{88}\text{Sr}$ ,  $^{95}\text{Mo}$ ,  $^{98}\text{Mo}$ ,  $^{111}\text{Cd}$ ,  $^{112}\text{Cd}$ ,  $^{114}\text{Cd}$ ,  $^{127}\text{I}$ ,  $^{138}\text{Ba}$ ,  $^{204}\text{Pb}$ ,  $^{206}\text{Pb}$ ,  $^{207}\text{Pb}$ ,  $^{208}\text{Pb}$ ) of proteins by ICP-MS after a size-exclusion or reversed-phase chromatographic separation. For the Zn isotope ratios ( $^{64}\text{Zn} : ^{67}\text{Zn}$ ,  $^{66}\text{Zn} : ^{68}\text{Zn}$ ,  $^{67}\text{Zn} : ^{68}\text{Zn}$ ) in intrinsically labelled chicken meat following reversed-phase chromatographic separation, they demonstrated that data were in good agreement with direct nebulization and TIMS analysis. Some variation in the individual Zn peak height ratios was attributed to polyatomic overlap interference from  $\text{S}_2^+$  and  $\text{SO}_2^+$  at  $m/z$  64, 66, 68 and  $\text{ArN}_2^+$  at  $m/z$  68, and the isotope ratios were corrected after the response was normalized to  $^{67}\text{Zn}$ . For the most part, zinc recoveries from the separation were quantitative.

One potential limitation of this approach is the analytical precision obtained for isotope ratio analysis resulting from the transient chromatographic signal, especially for low metal concentrations or low ion abundances. In general, isotope ratio analysis for samples introduced by transient techniques exhibit a precision of 1–3%, which is somewhat poorer than achieved by continuous nebulization, because the sample measurement time is short or signal averaging is not effective

[101]. A primary factor in determining the precision and accuracy of isotope ratio measurements with transient sampling techniques is the amount of material injected. These measurements could certainly benefit from the high sensitivity of second generation ICP-MS instrumentation. Furthermore, software for obtaining data and calculating isotope ratios from online chromatographic signals requires more development.

Biological applications of combined separation and ICP-AES techniques, like element-specific detection of metallodrugs and their metabolites, can be generally extended by ICP-MS. For example, pharmacokinetic studies of platinum-based drugs by LC-ICP-AES [102] and their independent determination by ICP-MS [103] establish the basis for LC-ICP-MS of platinum-based drugs and their metabolites. Similar analyses have been demonstrated for gold-drug therapy [104,105].

Another separation technique which might provide detailed characterization of macromolecules and particles with ICP-MS is field-flow fractionation (FFF) [106,107]. FFF has significant potential for biomedical research and applications, because the technique is gentle on delicate and shear liable species, with minimal loss of biological activity; the analysis time is relatively short and procedures are simpler and more convenient than traditional methods, with comparable or better resolution, purity, and yield; and the theoretical background is well established and provides straightforward optimization procedures [108]. The two systems of choice for biomedical applications are sedimentation and flow field-flow fractionation. FFF-ICP-MS has not yet been applied to biological materials, however.

Furthermore, the potential combination of capillary electrophoresis [109] and ICP-MS has only recently been considered [110]. Capillary zone electrophoresis (CZE) is a technique for high-resolution, low flow-rate separations of macromolecules. However, these flow-rates are too low for stable operation of most MS ion sources (i.e., continuous fast-atom bombardment, electrospray, ICP), and appropriate interface design using a make-up solvent is required [111,112]. An electrospray arrangement for inorganic ions was implemented by converting a conventional

ICP-MS [113], and the prospect is good for achieving some type of effective CZE-ICP-MS system in the near future.

#### LEAD TOXICOKINETICS STUDIES

The toxicokinetics of lead is of considerable importance, because preventing lead poisoning in young children has become a national objective [114]. Mahaffey et al. [115] have critically reviewed the environmental and human exposure status of lead. They conclude that the subclinical lead toxicity syndrome involves multiple organ systems and requires sophisticated measuring devices beyond routine clinical observation. The mechanisms of the toxic action of lead at the molecular level are not known, and the biochemical mechanisms of low-level lead neurotoxicity is not clearly established. The effects of lead must be analyzed at the subcellular level. However, sample contamination and analytical measurement sensitivity limit systematic studies. For example plasma lead content may be a better measure of available lead than blood lead, but plasma lead ( $10 \text{ ng dl}^{-1}$ ) is difficult to measure. The general objective of this analysis is to devise chemical and molecular concepts, involving the interactions of metal ions and their associated ligands with cellular constituents, that could be used for developing a predictive, toxicokinetic model for lead compound toxicity.

Establishing lead bioavailability, distinguishing skeletal and soft tissue lead pools, characterizing skeletal lead mobilization and removal, and identifying effects of redistribution of endogenous lead on organs during chelation therapy or pregnancy are among the objectives of kinetic modeling and experiments with radioactive ( $^{203}\text{Pb}$ ,  $^{210}\text{Pb}$ ) and stable ( $^{204}\text{Pb}$ ,  $^{206}\text{Pb}$ ,  $^{207}\text{Pb}$ ,  $^{208}\text{Pb}$ ) lead isotopes. The lead isotope ratios found in animal and human fluids and tissues vary depending on the tissue type and the external sources of exposure.

The tools are available for reliable lead isotope dilution and stable isotope analyses. Since three of the four lead isotopes ( $^{206}\text{Pb}$ ,  $^{207}\text{Pb}$ ,  $^{208}\text{Pb}$ ) are radiogenic, the isotopic abundances in

nature are variable and depend upon the age of the source and the original uranium and thorium content. The least abundant isotope  $^{204}\text{Pb}$  (1.45%) is not radiogenic and is suitable for isotopic enrichment. Furthermore, enriched standard reference material (NIST SRM 981, 982, and 983) and reagent lead isotopes are accessible.

ICP-MS is a powerful innovation for the quantification of lead concentrations in human body fluids and tissues by isotope dilution [37], and it provides isotopic information that can be used for lead poisoning source identification [38,116–118]. Excellent agreement was demonstrated for lead isotope analysis with ICP-quadrupole MS and TIMS for environmental and clinical samples [110,119,120], and 1–5% changes of lead isotope ratios in blood upon lead exposure can be determined accurately. Practically, <1% change can be determined with samples containing >300 ng ml<sup>-1</sup> Pb in less than 5 min. The 200-fold enhanced lead sensitivity obtained with state-of-the-art compared to first-generation ICP-MS systems [7,14] is likely to extend this lead isotope analysis by improving the precision or permitting analysis of lower lead blood concentrations and smaller samples.

With a double focusing magnetic sector mass analyzer, ICP ion source, and seven Faraday detectors, the precision of lead isotopic ratio measurements equalled that obtained by TIMS [16,121]. Furthermore, the sector MS system minimizes spectral interferences, because of its superior resolution compared to a quadrupole instrument. By extending the accuracy and precision of lead isotope ratios to <0.5%, the reliability of lead source identification and discrimination can be improved significantly. However, the cost of high-resolution ICP-MS instruments is at least double the quadrupole-based systems.

The application of ICP-MS for lead poisoning source identification has become routine in our laboratory. The combination of size-exclusion LC with ICP-MS [91] for the identification of lead-binding proteins (PbBP) in blood serum and red blood cells extends the capability of ICP-MS for lead toxicokinetic studies with specific lead-binding species. ICP-MS is the only practical on-line LC detector for lead species, because its sensitiv-

ity is orders of magnitude superior to alternatives [122]. Characterization of PbBP is not well developed, although Fowler and coworkers [123,124] have identified and delineated several distinct low-molecular-weight, high-affinity PbBP in rat kidney and brain which appear to be critical in intracellular lead bioavailability processes. The PbBP from rat kidney was a specific cleavage product of  $\alpha_2$ -microglobulin. This renal PbBP was localized selectively in certain nephrons and specific segments of the renal proximal tubule.

Enriched  $^{206}\text{Pb}$  tracer was employed to label lead compartments in rats with ultralow lead concentrations [125] and to investigate lead mobilization (redistribution and excretion) by the lead chelator DMSA (2,3-dimercaptosuccinic acid) [126]. Stable lead isotope ratios were measured by TIMS in hard and soft tissue and fluids. Lead isotopic compositions were indistinguishable in skeletal and soft tissues prior to the enrichment study. A DMSA-induced lead redistribution to the skeleton was observed, but no redistribution to the brain was detected. Extending these experiments with ICP-MS isotope analysis would be beneficial.

Multi-compartmental kinetic models have been developed to systematize lead exposure, retention, and excretion [127]. Recently, O'Flaherty [128] identified the need for physiologically based toxicokinetic models capable of integrating exposure over time by incorporating growth, development, and aging. Physiologically based kinetic models for bone-seeking elements (i.e., Pb, Ra, Sr, U, Ba, Al) in which the whole-body behavior is determined principally by the balance among excretion, uptake, and release from bone was formulated to include growth and maturation dependence of physiological and biochemical functions [129]. A model was developed for lead kinetics in the growing rat from birth to childhood which incorporated the processes controlling lead distribution to bone and soft tissues [128]. The model assumed that lead behaved like calcium in its interaction with bone, but it did not incorporate lead accumulation by the kidney nor lead binding to specific proteins. A model of human body and bone growth from birth to maturity also was described [130].

Rabinowitz [131] reviewed the toxicokinetics of bone lead and lead models and outlined some research with stable isotope analysis to obtain data on skeletal lead uptake and release. Rabinowitz et al. [132,133] were pioneers in the application of stable isotope tracers in the study of human lead metabolism. Based upon this isotopic data and other results, Marcus [134–136] developed a number of multicompartiment kinetic models for lead with CONSAM/SAAM. Based on these models, an uptake-biokinetic model for lead in children was developed by the US Environmental Protection Agency to estimate lead concentrations that might result from exposure to lead in a multifold environment (paint, soil, and dust) [137]. However, none of these models has utilized yet data provided by ICP-MS.

Stimulated by the hazard of lead poisoning of children through environmental exposure, the application of stable isotope analysis by ICP-MS together with high-resolution protein separation could be combined effectively with physiologically based toxicokinetic models and applied to human children. Once accomplished, then risk assessment evaluation based upon environmental or in vivo exposure to lead could be established reliably. The ICP-MS measurement of lead isotope ratios can provide the essential data efficiently, but design of experiments and adaptation of models is needed.

### *Conclusions*

Nutritional kinetic modeling with stable isotope tracers is an established and productive approach for a limited number of elements (e.g., Ca, Cu, Fe, I, Se, Zn). With ICP-MS, data can be collected for new experiments with additional elements (e.g., Te, Br), including non-traditional ones that might be encountered in pharmacokinetics (e.g., Au, Gd, Pt, Tc). In parallel, quantification of metal-binding molecules in nutrition and pharmacology is under-utilized, because most emphasis has been focused on the toxic heavy metals (As, Cd, Sn, Pb, Hg). Why has Tl be excluded from this list, whereas Mn is included? The major undeveloped aspect is chemical speciation of mineral-binding forms in nutritional modeling.

In toxicokinetics heavy-metal modeling has been limited [115,128], and the potential to apply stable isotope tracer techniques is significant. Single and dual tracer studies are practical, but the large number of stable isotopes available for most toxic heavy metals (e.g., Cd has 8, Sn has 10, Te has 8, Hg has 7, Pb has 4) offers the practical opportunity for multiple stable isotope tracers and in vivo isotope dilution. For example, repeating the continuous replacement experiment of Schuette et al. [51] for  $^{25}\text{Mg}$  with Cd or Pb isotopes might provide insight into their toxicodynamics.

Furthermore, combination of stable isotope tracers with chemical speciation is a unexplored field for nutritional and toxicological modeling. Preliminary experiments with Zn- and Pb-binding proteins detected by ICP-MS [91,100] indicate a reasonable likelihood that isotope ratio analysis could be accomplished with separated species but with a sacrifice of precision. Sensitive, new ICP-quadrupole MS instruments give higher counts and better precision than the first generation systems. Including isotope tracers of specific chemical species in modeling can be expected to expand the potential of biokinetic models. Iyengar [138] predicted that “biochemical investigations involving chemical speciation to understand the mode of action of trace elements will undoubtedly dominate future biological trace element research”. He concluded that “biological trace element research is presented with a unique opportunity for interdisciplinary investigations on a massive scale...”. This forecast remains a contemporary goal, and ICP-MS is likely to contribute to its realization.

Preparation and presentation of this paper was sponsored by the ICP Information Newsletter and a University of Massachusetts Faculty Research Grant for Conference Travel, respectively.

Keynote lectures presented in part at the *12th International Symposium on Microchemical Techniques, Cordoba, Spain, September 6–11, 1992*, and the *1993 Winter Conference on Plasma Spectrochemistry, Granada, Spain, January 10–15, 1993*.



- 1 P.E. Johnson, *J. Micronutr. Anal.*, 6 (1989) 59.
- 2 M. Janghorbani and B.T.G. Ting, *J. Nutr. Biochem.*, 1 (1990) 4.
- 3 J.R. Turnlund, *Crit. Rev. Food Sci. Nutr.*, 30 (1991) 387.
- 4 M. Janghorbani, B.T.G. Ting and N.E. Lynch, *Mikrochim. Acta (Wien)*, III (1989) 315.
- 5 G.V. Iyengar, in K.S. Subramanian, G.V. Iyengar and K. Okamoto (Eds.), *Biological Trace Element Research*, American Chemical Society, Washington, DC, 1991, Chap. 1, p. 1.
- 6 K.E. Jarvis, A.L. Gray and R.S. Houk, *Handbook of Inductively Coupled Plasma Mass Spectrometry*, Blackie, Glasgow, 1992.
- 7 A. Montaser and D.W. Golightly (Eds.), *Inductively Coupled Plasmas in Analytical Atomic Spectrometry*, VCH Publishers, New York, 2nd edn., 1992.
- 8 G. Holland and A.N. Eaton (Eds.), *Application of Plasma Source Mass Spectrometry*, Royal Society of Chemistry, Cambridge, 1991.
- 9 A.R. Date and A.L. Gray (Eds.), *Applications of Inductively Coupled Plasma Mass Spectrometry*, Blackie, Glasgow, 1989.
- 10 K.E. Jarvis, A.L. Gray, I. Jarvis and J. Williams (Eds.), *Plasma Source Mass Spectrometry*, Royal Society of Chemistry, Cambridge, 1990.
- 11 M. Janghorbani and B.T.G. Ting, in A.R. Date and A.L. Gray (Eds.), *Applications of Inductively Coupled Plasma Mass Spectrometry*, Blackie, Glasgow, 1989, Chap. 5, p. 115.
- 12 J.R. Dean, H.M. Crews and L. Ebdon, in A.R. Date and A.L. Gray (Eds.), *Applications of Inductively Coupled Plasma Mass Spectrometry*, Blackie, Glasgow, 1989, Chap. 6, p. 141.
- 13 R.M. Barnes, in K.S. Subramanian, G.V. Iyengar and K. Okamoto (Eds.), *Biological Trace Element Research*, American Chemical Society, Washington, DC, 1991, Chap. 12, p. 158.
- 14 G. Horlick, *Spectroscopy (Eugene)*, 7 (1992) 22.
- 15 R.E. Serfass, J.J. Thompson and R.S. Houk, *Anal. Chim. Acta*, 188 (1986) 73.
- 16 A.J. Walder, P.A. Freedman, I.D. Abell, P. Walkden and I. Platzner, 40th American Society for Mass Spectrometry Conference on Mass Spectrometry and Allied Topics, Washington, DC, 1992, Conference Abstracts.
- 17 A. Taylor, S. Branch, H.M. Crews and D.J. Halls, *J. Anal. At. Spectrom.*, 7 (1992) 67R.
- 18 C.J. Amarasiwardena, B. Gercken, M.D. Argentine and R.M. Barnes, *J. Anal. At. Spectrom.*, 5 (1990) 457.
- 19 J. Yoshinaga, N. Matsuo, H. Imai, M. Nakazawa, T. Suzuki and N. Morita, *Intern. J. Environ. Anal. Chem.*, 41 (1990) 27.
- 20 M.-A. Vaughan, A.D. Baines and D.M. Templeton, *Clin. Chem.*, 37 (1991) 210.
- 21 T.B. Lyon, G.S. Fell, K. McKay and R.D. Scott, *J. Anal. At. Spectrom.*, 6 (1991) 559.
- 22 T.D.B. Lyon and G.S. Fell, *Food Chem.*, 43 (1992) 299.
- 23 K. Shiraishi and J.F. McInroy, *J. Trace Elem. Exp. Med.*, 4 (1991) 191.
- 24 H. Vanhoe, C. Vandecasteele, J. Versieck and R. Dams, *Anal. Chem.*, 61 (1989) 1851.
- 25 Z. Horvath, A. Laszity and R.M. Barnes, *Spectrochim. Acta Rev.*, 14 (1991) 45.
- 26 E.M. Heithmar, T.A. Hinnners, J.T. Rowan and J.M. Riviello, *Anal. Chem.*, 62 (1990) 857.
- 27 T.D.B. Lyon and G.S. Fell, *J. Anal. At. Spectrom.*, 5 (1990) 135.
- 28 C. Vandecasteele, H. Vanhoe and R. Dams, *Anal. Lett.*, 23 (1990) 1827.
- 29 H.T. Delves, *Food Chem.*, 43 (1992) 277.
- 30 F.G. Smith, D.R. Wiederin, R.S. Houk, C.B. Egan and R.E. Serfass, *Anal. Chim. Acta*, 248 (1991) 229.
- 31 J.D. Fassett and P.J. Paulsen, *Anal. Chem.*, 63 (1989) 643A.
- 32 A.A. van Heuzen, T. Hoekstra and B. van Wingerden, *J. Anal. At. Spectrom.*, 4 (1989) 483.
- 33 K. Chiba, I. Inamoto and M. Saeki, *J. Anal. At. Spectrom.*, 7 (1992) 115.
- 34 J.W. McLaren, K.W.M. Siu, J.W. Lam, S.N. Willie, P.S. Maxwell, A. Palepu, M. Koether and S.S. Berman, *Fresenius J. Anal. Chem.*, 337 (1990) 721.
- 35 K. Okamoto, *Spectrochim. Acta Part B*, 46 (1991) 1615.
- 36 M.J. Campbell, G. Vermeir, R. Dams and P. Quevauviller, *J. Anal. At. Spectrom.*, 7 (1992) 617.
- 37 A. Laszity, M. Viczian, X. Wang and R.M. Barnes, *J. Anal. At. Spectrom.*, 4 (1989) 761.
- 38 M. Viczian, A. Laszity and R.M. Barnes, *J. Anal. At. Spectrom.*, 5 (1990) 293.
- 39 Y. Igarashi, Y. Ishikawa, Y. Takaku, K. Masuda, K. Shiraishi and R. Seki, *Radioisotopes*, 40 (1991) 226.
- 40 Y. Igarashi, K. Shiraishi, Y. Takaku, K. Masuda, R. Seki and M. Yamamoto, *Anal. Sci.*, 8 (1992) 475.
- 41 G.P. Russ III, in A.R. Date and A.L. Gray (Eds.), *Applications of Inductively Coupled Plasma Mass Spectrometry*, Blackie, Glasgow, 1989, Chap. 4, p. 90.
- 42 P.G. Whittaker, J.F.R. Barrett and J.G. Williams, *J. Anal. At. Spectrom.*, 7 (1992) 109.
- 43 J.F.R. Barrett, P.G. Whittaker, J.G. Williams and T. Lind, *Clin. Sci.*, 83 (1992) 213.
- 44 R.A. Ehrenkranz, B.A. Ackerman, C.M. Nelli and M. Janghorbani, *Am. J. Clin. Nutr.*, 40 (1984) 72.
- 45 J.J. Fardy and I.M. Warner, *J. Radioanal. Nucl. Chem.*, 157 (1992) 239.
- 46 R.A. Ehrenkranz, P.A. Gettner, C.M. Nelli, E.A. Sherwonit, J.E. Williams, B.T.G. Ting and M. Janghorbani, *Pediatr. Res.*, 26 (1989) 298.
- 47 R.A. Ehrenkranz, P.A. Gettner, C.M. Nelli, E.A. Sherwonit, J.E. Williams, B.T.G. Ting and M. Janghorbani, *J. Pediatr. Gastroenterol. Nutr.*, 13 (1991) 125.
- 48 R.A. Ehrenkranz, P.A. Gettner, C.M. Nelli, E.A. Sherwonit, J.E. Williams, H.A. Pearson, B.T.G. Ting and M. Janghorbani, *J. Pediatr. Gastroenterol. Nutr.*, 15 (1992) 270.

- 49 C.J. Amarasiriwardena, A. Krushevskaja, H. Foner, M.D. Argentine and R.M. Barnes, *J. Anal. At. Spectrom.*, 7 (1992) 915.
- 50 M.E. Wastney, G.E. Gordon, C. Amarasiriwardena, A. Krushevskaja, R.M. Barnes and K.N.S. Subramanian, *FASEB J.*, 6 (1992) A1788.
- 51 S. Schuette, J. Hong, D. Vereault, B. Ting and M. Janghorbani, *J. Nutr. Biochem.*, 1 (1990) 355.
- 52 S.A. Schuette, S.C. Hartmann, B.T.G. Ting and M. Janghorbani, *J. Nutr. Biochem.*, 3 (1992) 38.
- 53 B.T.G. Ting, C.C. Lee, M. Janghorbani and J.R. Rohaska, *J. Nutr. Biochem.*, 1 (1990) 249.
- 54 M. Janghorbani, C.S. Moores, M.A. Smith, T. Hazell, K. Blanock and B.T.G. Ting, *J. Nutr.*, 121 (1991) 345.
- 55 P.V. Fennessey, L. Lloyd-Kindstrand and K.M. Hambridge, *Int. J. Mass Spectrom. Ion Proc.*, 111 (1991) 355.
- 56 D.B. Guralnik (Ed.), *Webster's New World Dictionary*, World Publishing, New York, 1974.
- 57 J.M. Frazier, in D.H. Hemphill and C.R. Cothorn (Eds.), *Trace Substances in Environmental Health—XXIV, Supplement to Environmental Geochemistry and Health*, 13 (1991) 55.
- 58 J.R. Dean, S. Munro, L. Ebdon, H.M. Crews and R.C. Massey, *J. Anal. At. Spectrom.*, 2 (1987) 607.
- 59 H.M. Crews, J.R. Dean, L. Ebdon and R.C. Massey, *Analyst*, 114 (1989) 895.
- 60 G. Lespes, M. Potin-Gautier and S. Struc, *Environ. Technol.*, 13 (1992) 207.
- 61 T. Kron, K. Wittmaack, C. Hansen and E. Werner, *Anal. Chem.*, 63 (1991) 2603.
- 62 J.R. Collins, *J. Nutr.*, 122 (1992) 695.
- 63 W.T. Buckley, *Can. J. Anim. Sci.*, 71 (1991) 155.
- 64 *Trace Element/Mineral Metabolism During Development, Mathematical Modeling in Experimental Nutrition IV*, Georgetown University Medical Center, Washington, DC, June 8–10, 1992.
- 65 M.E. Wastney and K.N.S. Subramanian (Eds.), *Kinetic Models of Trace Element and Mineral Metabolism During Development*, CRC Press, Boca Raton, FL, 1993.
- 66 B.H. Patterson, O.A. Levander, K. Helzlsouer, P.A. McAdam, S.A. Lewis, P.R. Taylor, C. Veillon and L.A. Zech, *Am. J. Physiol.*, 257 (1989) R556.
- 67 B.H. Patterson and L.A. Zech, *J. Nutr.*, 122 (1992) 709.
- 68 C.A. Swanson, B.H. Patterson, O.A. Levander, C. Veillon, P.R. Taylor, K. Helzlsouer, P.A. McAdam and L.A. Zech, *Am. J. Clin. Nutr.*, 54 (1991) 917.
- 69 P.B. Moser-Veillon, A.R. Mangels, K.Y. Patterson and C. Veillon, *Analyst*, 117 (1992) 559.
- 70 M.E. Wastney, R.L. Aamodt, W.F. Rumble and R.I. Henkin, *Am. J. Physiol.*, 251 (1986) R398.
- 71 M.E. Wastney, O.M. Rennert and K.N.S. Subramanian, in R. Dulbecco (Ed.), *Encyclopedia of Human Biology*, Vol. 7, Academic Press, New York, 1991, p. 879.
- 72 M.E. Wastney, I.G. Gökmen, R.L. Aamodt, W.F. Rumble, G.E. Gordon and R.I. Henkin, *Am. J. Physiol.*, 260 (1991) R134.
- 73 R.S. Houk, S.C.K. Shum and D.R. Wiedering, *Anal. Chim. Acta*, 250 (1991) 61.
- 74 R.E. Serfass, E.E. Ziegler, B.B. Edwards and R.S. Houk, *J. Nutr.*, 119 (1989) 1661.
- 75 C.B. Egan, F.G. Smith, R.S. Houk and R.E. Serfass, *Am. J. Clin. Nutr.*, 53 (1991) 547.
- 76 J.K. Friel, V.L. Naake, Jr., L.V. Miller, P.V. Fennessey and K.M. Hambridge, *Am. J. Clin. Nutr.*, 55 (1992) 473.
- 77 D. Behne, *Analyst*, 117 (1992) 555.
- 78 R. Cornelis, *Analyst*, 117 (1992) 583.
- 79 W. Lund, *Fresenius J. Anal. Chem.*, 337 (1990) 557.
- 80 J.C. Van Loon and R. Barefoot, *Analyst*, 117 (1992) 563.
- 81 P.C. Uden, in P.C. Uden (Ed.), *Element-Specific Chromatographic Detection by Atomic Emission Spectroscopy*, American Chemical Society, Washington, DC, 1992, Chap. 1, p. 1.
- 82 L.K. Olson, D.T. Heitkemper and J.A. Caruso, in P.C. Uden (Ed.), *Element-Specific Chromatographic Detection by Atomic Emission Spectroscopy*, American Chemical Society, Washington, DC, 1992, Chap. 17, p. 288.
- 83 D. Beauchemin, K.W.M. Siu, J.W. McLaren and S.S. Berman, *J. Anal. At. Spectrom.*, 4 (1989) 285.
- 84 D. Heitkemper, J. Creed, J. Caruso and F.L. Fricke, *J. Anal. At. Spectrom.*, 4 (1989) 279.
- 85 Y. Shibata and M. Morita, *Anal. Sci.*, 5 (1989) 107.
- 86 M. Morita and J.S. Edmonds, *Pure Appl. Chem.*, 64 (1992) 575.
- 87 K. Takatera and T. Watanabe, *Anal. Sci.*, 8 (1992) 469.
- 88 K. Takatera and T. Watanabe, *Anal. Sci.*, 7 (1991) 695.
- 89 L. Stuhne-Sekalec, S.X. Xu, J.G. Parkes, N.F. Olivier and D.M. Templeton, *Anal. Biochem.*, 205 (1992) 278.
- 90 S.C.K. Shum, H. Pang and R.S. Houk, *Anal. Chem.*, 64 (1992) 2444.
- 91 B. Gercken and R.M. Barnes, *Anal. Chem.*, 63 (1991) 238.
- 92 D.S. Bushee, *Analyst*, 113 (1988) 1167.
- 93 D.S. Bushee, J.R. Moody, and J.C. May, *J. Anal. At. Spectrom.*, 4 (1989) 773.
- 94 D.S. Braverman, *J. Anal. At. Spectrom.*, 7 (1992) 43.
- 95 H. Klinkenberg, S. van der Wal, J. Frusch, L. Terwint and T. Beeren, *At. Spectrosc.*, 11 (1990) 5.
- 96 H. Suyani, J. Creed, T. Davidson and J. Caruso, *J. Chromatogr. Sci.*, 27 (1989) 139.
- 97 H. Suyani, D. Heitkemper, J. Creed and J. Caruso, *Appl. Spectrosc.*, 43 (1989) 962.
- 98 J.W. McLaren, K.W.M. Siu, J.W. Lam, S.N. Willie, P.S. Maxwell, A. Palepu, M. Koether and S.S. Berman, *Fresenius J. Anal. Chem.*, 337 (1990) 721.
- 99 S. Branch, L. Ebdon, S. Hill and P. O'Neill, *Anal. Proc.*, 26 (1989) 401.
- 100 L.M.W. Owen, H.M. Crews, R.C. Hutton and A. Walsh, *Analyst*, 117 (1992) 649.
- 101 R.S. Houk and J.J. Thompson, *Mass Spectrom. Rev.*, 7 (1988) 425.
- 102 A. Alimonti, C. Dominici, F. Petrucci, F. La Torre and S. Caroli, *Acta Chim. Hung.*, 128 (1991) 527.

- 103 P. Tothill, K. McKay, L.M. Matheson, M. Robbins and J.F. Smith, in H. Grenville and A.N. Eaton (Eds.), *Applications of Plasma Source Mass Spectrometry*, Royal Society of Chemistry, Cambridge, 1991, pp. 89–95.
- 104 R.C. Elder, W.B. Jones and K. Tepperman, in P.C. Uden (Ed.), *Element-Specific Chromatographic Detection by Atomic Emission Spectroscopy*, American Chemical Society, Washington, DC, 1992, Chap. 18, p. 309.
- 105 S.G. Matz, R.C. Elder and K. Tepperman, *J. Anal. At. Spectrom.*, 4 (1989) 767.
- 106 R. Beckett, *At. Spectrosc.*, 12 (1991) 228.
- 107 H.E. Taylor, J.R. Garbarino, D.M. Murphy and R. Beckett, *Anal. Chem.*, 64 (1992) 2036.
- 108 S. Levin, *Biomed. Chromatogr.*, 5 (1991) 133.
- 109 F.-T.A. Chen, C.-M. Liu, Y.-Z. Hsieh and J.C. Sternberg, *Clin. Chem.*, 37 (1991) 14.
- 110 J. Wang, H.E. Evans, J.G. Dorsey and J.A. Caruso, *ICP Inf. Newsl.*, 18 (1992) 75; 1992 Pittsburgh Conference, Paper 216, New Orleans, LA, 1992.
- 111 M.J.-F. Suter, B.B. DaGue, W.T. Moore, S.-N. Lin and R.M. Caprioli, *J. Chromatogr.*, 553 (1991) 101.
- 112 R.D. Smith, J.A. Loo, R.R. Ogorzalek Loo, M. Busman and H.R. Udseth, *Mass Spectrom. Rev.*, 10 (1991) 359.
- 113 G.R. Agnes and G. Horlick, *Appl. Spectrosc.*, 46 (1992) 401.
- 114 Preventing Lead Poisoning in Young Children, U.S. Department of Health and Human Services/Public Health Service/Centers for Disease Control, October 1991.
- 115 K.R. Mahaffey, J. McKinney and J.R. Reigart, in M. Lippmann (Ed.), *Environmental Toxicants. Human Exposure and Their Health Effects*, Van Nostrand Reinhold, New York, 1992, Chap. 12, pp. 360–391.
- 116 R.M. Barnes, *Anal. Chem.*, 62 (1990) 1023A.
- 117 H.T. Delves and M.J. Campbell, *J. Anal. At. Spectrom.*, 3 (1988) 343.
- 118 E.S. Hall and J. Higgins, *ICP Inf. Newsl.*, 18 (1992) 442.
- 119 M.J. Campbell and H.T. Delves, *J. Anal. At. Spectrom.*, 4 (1988) 235.
- 120 M.E. Ketterer, M.J. Peters and P.J. Tisdale, *J. Anal. At. Spectrom.*, 6 (1991) 439.
- 121 A.J. Walder and P.A. Freedman, *J. Anal. At. Spectrom.*, 7 (1992) 571.
- 122 A. Al-Rashdan, D. Heitkemper and J.A. Caruso, *J. Chromatogr. Sci.*, 29 (1991) 98.
- 123 B.A. Fowler and G. DuVal, *Environ. Health Persp.*, 91 (1991) 77.
- 124 P.L. Goering, P. Mistry and B.A. Fowler, *J. Pharmacol. Exp. Ther.*, 237 (1986) 220.
- 125 D.R. Smith, J.D. Osterloh, S. Niemeier and A.R. Flegal, *Environ. Res.*, 57 (1992) 190.
- 126 D.R. Smith and A.R. Flegal, *Toxicol. Appl. Pharmacol.*, 116 (1992) 85.
- 127 M.R. Moore, in *Lead Toxicity*, R. Lansdown and W. Yule, editors, Chapter 5, pp. 54, John Hopkins University Press, Baltimore, 1986.
- 128 E.J. O'Flaherty, *Toxicol. Appl. Pharmacol.*, 111 (1991) 313.
- 129 E.J. O'Flaherty, *Toxicol. Appl. Pharmacol.*, 111 (1991) 299.
- 130 E.J. O'Flaherty, *Toxicol. Appl. Pharmacol.*, 111 (1991) 332.
- 131 M.B. Rabinowitz, *Environ. Health Perspect.*, 91 (1991) 33.
- 132 M. Rabinowitz, G.W. Wetherill and J.D. Kopple, *Environ. Health Perspect.*, 7 (1974) 145.
- 133 M. Rabinowitz, G.W. Wetherill and J.D. Kopple, *J. Clin. Invest.*, 58 (1976) 260.
- 134 A.H. Marcus, *Environ. Res.*, 36 (1985) 441.
- 135 A.H. Marcus, *Environ. Res.*, 36 (1985) 459.
- 136 A.H. Marcus, *Environ. Res.*, 36 (1985) 473.
- 137 R.W. Elias, 24th Annual Conference on Trace Substances in Environmental Health, Cincinnati, OH, 8–12 July, 1990, Conference Abstracts.
- 138 G.V. Iyengar, *Sci. Total Environ.*, 100 (1991) 1.

# Inorganic mass spectrometry for surface and thin film analysis

Hans Oechsner

*Fachbereich Physik und Institut für Oberflächen- und Schichtanalytik, Universität Kaiserslautern, W-6750 Kaiserslautern (Germany)*

(Received 10th September 1992)

## Abstract

After a discussion of several fundamental aspects connected with the mass spectrometry of sputter-removed particles for surface and thin-film analysis and a comparison between secondary neutral mass spectrometry (SNMS) and glow discharge mass spectrometry, novel instrumental developments in SNMS for the analysis of electrically insulating materials are described. Subsequently, the utilization of  $\text{MCs}^+$  molecular ions in secondary ion mass spectrometry (SIMS) is discussed. In both instances the instrumental and methodical progress is elucidated by appropriate examples of SNMS and SIMS depth profiling analysis of various dielectric and metal multi-layer structures, and of the application of  $\text{HCs}^+$  ions to hydrogen detection.

**Keywords:** Mass spectrometry; Surface techniques; Depth profiling; Dielectrics; Hydrogen; Thin films

The mass spectrometric analysis of solids requires an efficient transformation from the solid phase into the atomic or molecular state in connection with an effective ionization process. For bulk analysis this is well accomplished by spark source mass spectrometry (SSMS) using radiofrequency or d.c. micro-arcs for the simultaneous evaporation and ionization of the sample material [1]. This technique has, in particular, been shown to be very useful for the purity control of solids with detection limits down to the  $\text{ng g}^{-1}$  range [2]. Similar detection limits for bulk analysis can be achieved by glow discharge mass spectroscopy (GDMS) where a rod-shaped sample is used as an active element for the generation of d.c. discharges at pressures up to the mbar region [3]. The atomized sample material is predominantly ionized in such instances by Penning processes

involving metastable  $\text{Ne}^*$  or  $\text{Ar}^*$  particles in the  $^3\text{P}_{2,0}$  states with potential energies around 16.6 or 11.6 eV, respectively. Laser ion microprobes [laser microprobe mass analysis (LAMMA) or laser ionization mass analysis (LIMA)] represent another more recent method for solids mass spectrometry, where pulsed laser beams are focused on to a solid surface and create transient microplasmas of evaporated surface material. Ions escaping or being extracted from the plasma are subsequently analysed using a time-of-flight mass spectrometer [4].

Although all these techniques are very useful for the analysis of solids with high detection sensitivity, they suffer in general from a lack of surface sensitivity which is essential, e.g., for the compositional characterization of thin-film structures. Apart from appropriate versions of laser microprobes, the lateral resolution of these techniques is also very poor. This paper therefore concentrates on secondary ion (SIMS) and secondary neutral mass spectrometry (SNMS) as sur-

*Correspondence to:* H. Oechsner, Fachbereich Physik und Institut für Oberflächen- und Schicht-analytik, Universität Kaiserslautern, W-6750 Kaiserslautern (Germany).

face-sensitive mass spectrometric methods that permit the analysis of solid structures with sometimes excellent depth resolution, and that can also be operated with high lateral resolution. After a brief discussion of some fundamental aspects of both methods and a comparison between SNMS and low-pressure GDMS, the application of the electron gas version of SNMS to the analysis of dielectric samples, and possible progress in the quantification of SIMS by utilizing  $MCs^+$  ions (where M denotes the sample constituent to be measured) will be elucidated in some detail.

#### MASS SPECTROMETRY OF SPUTTERED SURFACE PARTICLES

##### *SIMS and SNMS: some fundamental aspects*

In comparison with electron spectroscopy of solid surfaces, mass spectrometric identification of atomic and molecular species removed from a solid surface by “atomic spoons” in the form of primary bombarding ions delivers the most direct information about the sample composition. Whereas Auger and photoelectron spectrometry, the most frequently used electron spectroscopic methods, monitor what is left at the surface after the mostly selective attack of ions or other probe species, the original surface composition is obtained with mass spectrometric methods when all or a constant fraction of the particles removed from the sample are collected with well defined detection sensitivities.

Because of the direct availability of positively or negatively charged ions ejected from an ion-bombarded solid, SIMS has developed to a widely employed technique with highly sophisticated instrumentation. One of the most attractive features of SIMS is its excellent detection sensitivity based on the high collection efficiency with which secondary ions can be extracted into the entrance optics of a mass spectrometer. While “useful yields” up to  $10^{-3}$  secondary ions per ejected ion are achievable for instruments employing double-focusing mass spectrometers, even higher collection efficiencies are obtained by recent versions of time-of-flight (TOF) mass spectrometers,

particularly with reflector-type instruments. Such attractive features of TOF-SIMS are mainly due to the “parallel” detection of the analysed particles in contrast to the sequential particle registration in conventional magnetic or quadrupole mass spectrometers. As TOF instruments are especially appropriate for heavy species with their long flight times resulting in a high mass dispersion, mass spectrometry of organic samples has become an important domain of TOF-SIMS (for recent information see, e.g., [5]).

Despite its excellent figures of merit and its high level of instrumentation, SIMS suffers from severe quantification problems because of the well known matrix influences on the formation probability of secondary ions. The electron transition probabilities during particle ejection that decide whether a surface particle leaves the sample as an ion or as a neutral particle depend strongly on the local electronic conditions, i.e., the chemical binding structure at the individual ejection site. Recent microscopic theories on secondary ion formation have succeeded in describing the respective electron transition probabilities quantitatively only for a few well defined situations [6]. In general, however, the secondary ion yields  $Y_X^\pm$  for positive or negative secondary ions of a species X vary strongly with the actual surface composition in an unknown manner.  $Y_X^\pm$  is given by the product  $\alpha_X^\pm Y_X$ , where  $\alpha_X^\pm$  is the ionization and  $Y_X$  the ejection probability for the detected species X.  $Y_X$  is identical with the partial sputtering yield of X. Whereas under stationary conditions  $Y_X$  is linearly correlated with the concentration  $c_X$  of X in the sample,  $\alpha_X^\pm$  is determined not only by  $c_X$ , but also by the concentrations of other surface constituents. Therefore, the partial sputter yield  $Y_X$  and subsequently  $c_X$  cannot be extracted from the secondary ion signals being determined by the in general not separable product  $\alpha_X^\pm Y_X$ .

The problems with the quantification of SIMS result merely from the fact that ejection and ionization of the analysed particles takes place in the same event. Such difficulties are resolved by SNMS, in which both processes are strictly separated by post-ionizing the removed neutral surface particles after their ejection with a well

known constant probability  $\alpha_X^0$ . Quantification of the SNMS signals, which are proportional to  $\alpha_X^0 Y_X$  and, hence, directly to  $c_X$ , is then straightforward, and additionally favoured by the circumstance that apart from a few exceptions the overwhelming fraction of all sputter-removed particles consists of neutral species [7].

Since its introduction in 1972, secondary (or sputtered) neutral mass spectrometry based on electron impact post-ionization by a hot Maxwellian electron gas, formed by the electron component of a resonantly excited low-pressure noble gas plasma has developed into a routinely used technique for surface and thin-film analysis [8,9]. It has recently been expanded to a secondary neutral microprobe for surface imaging via post-ionized sputtered neutral species by scanning a highly focused ion beam across the sample surface [10].

Within the last few years, non-resonant laser post-ionization has also been employed as an effective means for surface analysis by sputtered neutral species [11]. In such arrangements an ionizing laser pulse is used as the triggering signal for parallel detection of a bunch of post-ionized neutral species in a TOF mass spectrometer. Imaging of the elemental surface composition via the generated photo-ions has been shown to be a very attractive application of laser SNMS [12]. In contrast to the electron gas method, quantification of laser SNMS is still problematic for different reasons, in particular when multi-photon ionization along different schemes of atomic or molecular energy levels or photofragmentation of sputtered molecules must be considered. Ionization up to a saturation level for all species in the

sputtered particle flux would be a possible remedy, but requires laser intensities up to  $10^{11}$  W  $\text{cm}^{-2}$ , which are hardly possible with currently available laser systems [13].

Some characteristic properties of the mass spectrometric methods discussed in this section are collected in Table 1.

#### *Comparison of electron gas SNMS with low-pressure GDMS*

GDMS operated at noble gas pressures of the order of  $10^{-2}$ – $10^{-1}$  mbar [14] is often argued to display similar properties to electron gas SNMS as another plasma-based analytical technique. There are, however, very distinct differences which arise from mainly two characteristic aspects.

First, Penning ionization as utilized for GDMS necessarily involves a strong collisional interaction between sputter-removed surface particles and metastable species in the respective neon or argon plasma. Such interactions destroy the kinetic properties of the sputtered neutral species, lead to the formation of new molecular species (“argides”) by associative ionization [15] and cause backscattering of sputtered neutral species again on to the surface of the analysed sample. Obviously, the formation of novel species in the plasma volume may seriously hamper the quantification of the GDMS spectra from an unknown sample. Backscattering of previously sputter-removed particles to the sample deteriorates depth resolution during the analysis of thin film systems.

Second, the (necessarily conductive) sample forms in most GDMS arrangements one of the electrodes between which the glow discharge

TABLE 1

Characteristic properties of mass spectrometric techniques for surface and depth profile analysis

Parameter	SIMS	SNMS (electron gas)	Laser SNMS
Primary ions	$\text{O}_2^+$ , $\text{Cs}^+$ ( $\text{Ga}^+$ ), 5–20 keV	Noble gases ( $\text{Ar}^+$ ), 50–2000 eV	$\text{Ar}^+$ , $\text{Ga}^+$ , several keV
Detection sensitivity	$\sim 10$ ng $\text{g}^{-1}$	$\sim 100$ ng $\text{g}^{-1}$	$\sim$ ng $\text{g}^{-1}$
Depth resolution	$\sim 10$ nm	$\sim 1$ nm	$\sim 5$ nm
Useful yield	$\leq 10^{-3}$ , magnetic sector MS	$\leq 10^{-8}$ , quadrupole; $10^{-6}$ , magnetic sector MS	$10^{-3}$ , time-of-flight MS
Quantification	Difficult	High	Problems

plasma is excited. Hence, the plasma properties change with the nature of the sample. Varying plasma properties, however, also cause varying detection probabilities during the analysis of inhomogeneous samples as thin-film structures of different composition.

On the other hand, electron gas SNMS employs under ultra-high vacuum conditions a resonantly excited r.f. plasma at much lower working pressures (some  $10^{-4}$  mbar for argon), which is completely independent of the nature of the actual sample. Post-ionization of sputtered neutral species is performed via electron impact ionization through the hot Maxwellian electron gas with electron temperatures corresponding to 15 eV, which is established by the electron component of the r.f. plasma [7]. The post-ionization probability  $\alpha_X^0$  for a sputter-removed species X is determined by the convolution integral between the ionization function of X and the energy distribution of the plasma electrons [9]. For fixed operating conditions, the  $\alpha_X^0$  values are particle-specific apparatus constants independent of the sample composition.

Because of the low working pressure, collisional interaction between the sputtered neutral particles and heavy species in the SNMS plasma is negligible along the travelling length of a few cm of the analysed particles through the plasma volume. Hence, the original energy distribution of the sputter-removed surface particles with average energies of the order of 10–20 eV remains undisturbed even after the electron impact post-ionization has been performed. Thus, the fast

post-ionized neutral species can be separated from the low-energy plasma ions by an appropriate potential step in the ion extraction optics in front of the mass spectrometer. This allows a considerable background reduction in the SNMS spectra down to count rates of a few cps, whereas, depending on the operating conditions, the SNMS signals for sample components with concentrations in the atomic percentage range amount to  $10^4$ – $10^5$  cps.

#### ANALYSIS OF DIELECTRIC SAMPLES WITH ELECTRON GAS SNMS

As a particular advantage, electron gas SNMS offers the possibility of analysing electrically non-conducting, i.e., dielectric, samples. Figure 1 displays the different operating modes of this method which are successfully employed for quantitative analysis of such systems. The respective operating modes are always based on the availability of the post-ionizing electron gas as an electron reservoir from which a constant or time-dependent electron flux can be directed on to the sample in a controlled manner, to compensate for the positive charge applied by the bombarding primary ions.

In the so-called separate bombardment mode (SBM) of SNMS, the ion bombardment of the sample is performed by an ion beam traversing the post-ionizing SNMS plasma. The dielectric sample is separated from the plasma by a space-charge sheath that is automatically built up to

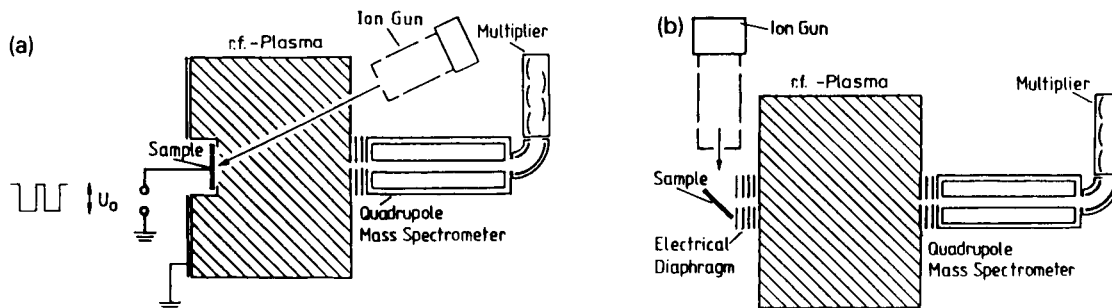


Fig. 1. Schematic diagrams of electron gas SNMS instruments. (a) Separate bombardment and high-frequency mode SBM and HFM. The square-wave, high-frequency voltage used for HFM is switched off for SBM. (b) External bombardment mode (EBM).

achieve a saturation current of low-energy plasma ions and a retardation current of plasma electrons of equal height on to the sample surface. Any additional charge deposited on the sample surface by the bombarding ion beam is then automatically compensated for by corresponding local changes in the electron retardation current from the SNMS plasma [16].

In the so-called external bombardment mode (EBM) of SNMS, the sample is positioned outside of the post-ionizing chamber and bombarded with an ion gun under conditions similar to those in SIMS instruments. The sputtered secondary neutral species enter the SNMS plasma through an electrical diaphragm that prevents the passage of any charged particles in both directions. This diaphragm, consisting of electrostatic lenses, can be opened for low-energy plasma electrons in such a way that the ion charge transported to a dielectric sample by the primary ion beam becomes precisely compensated [17].

This operating mode of SNMS is of particular importance for the analysis of oxidic glasses in which any minor surface charging causes stoichiometry changes by field-induced migration of highly mobile cations such as alkali metal ions through the silicate network. As an example, an SNMS depth profile through a dielectric layer structure on float glass measured using the charge-compensated EBM is presented in Fig. 2. As an important result, outdiffusion of Na from the glass substrate into the oxidic multi-layer structure at the surface consisting of two  $\text{TiO}_2$  layers of 65 nm with an intermediate  $\text{SiO}_2$  layer of 90 nm is clearly detected. Obviously, the  $\text{SiO}_2$ - $\text{TiO}_2$  interfaces form a diffusion barrier for the  $\text{Na}^+$  ions, both on their diffusion-induced transport out to the surface and the back-diffusion from the Na-rich surface segregation layer. As no net charge was built up at the actual sample surface during sputter depth profiling through this completely insulating layer structure, and as the SNMS signals are directly proportional to the individual concentrations in the sample, the depth-dependent variations of the Na, Ti and Si signals can be directly attributed to the true concentration profiles in the sample.

In the direct bombardment mode (DBM) of

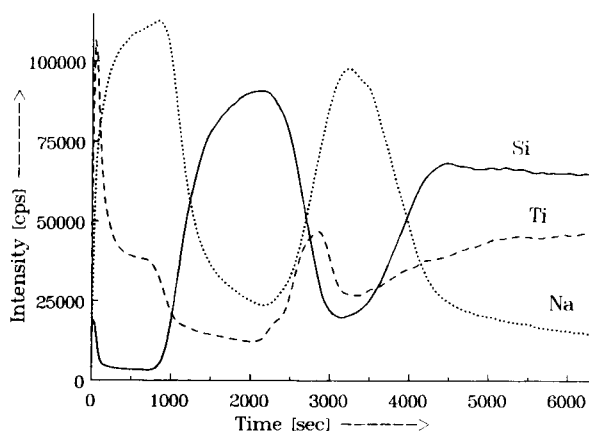


Fig. 2. SNMS depth profile of an oxidic layer structure on a float glass substrate. Analysis with charge compensated external bombardment mode (EBM) of SNMS with a 5-keV  $\text{Kr}^+$  beam scanned across the dielectric sample. Float glass coated with 65 nm  $\text{TiO}_2$ -90 nm  $\text{SiO}_2$ -65 nm  $\text{TiO}_2$ .

SNMS [7,9], the sample is bombarded by low-energy ions which are extracted from the SNMS plasma with high lateral homogeneity by simple ion optics in front of the sample. This operating mode is ideally suited for high-resolution depth profiling, as any distortion of the concentration profiles at interfaces by collisional mixing effects is avoided at bombarding ion energies down to the  $10^2$  eV range. The characteristic feature of the DBM can be also maintained for dielectric samples when the recently developed high-frequency mode (HFM) of SNMS is employed. In order to establish charge compensation, a square-wave, high-frequency potential is applied to the sample, i.e., basically a d.c. voltage that is switched off periodically to admit short electron pulses on to the surface for compensating for the positive charge from the preceding ion bombardment time interval (see Fig. 1a). The bombarding ion energy is controlled by the amplitude  $U_0$  of the square-wave potential. As constant ion optical conditions are established during the ion bombardment interval, the same lateral homogeneity and, consequently, the same high depth resolution are achieved for dielectric samples as for conducting specimens with the usual DBM using a constant d.c. potential at the sample.



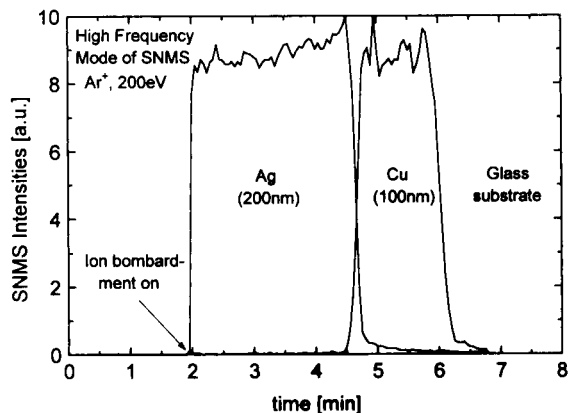


Fig. 3. SNMS depth profile analysis of an Ag–Cu double layer of 200 and 100 nm thickness on a glass substrate measured with the high-frequency mode (HFM) of SNMS under normal bombardment with 200 eV  $\text{Ar}^+$  ions.

Figure 3 shows an intensity versus sputter time profile that was acquired by this novel method for a metallic double layer of 200 nm Ag and 100 nm Cu on a glass substrate. No electric current was transported through the dielectric substrate to the sample holder. The very narrow Ag–Cu interface width of about 10 nm demonstrates that even in this instance, where the dielectric properties of the sample structure vary by several orders of magnitude between the metallic layers and the glass substrate, the sample is eroded with high lateral homogeneity, permitting depth profiling of such previously inaccessible structures with unrivalled depth resolution.

#### SIMS ANALYSIS USING $\text{MCs}^+$ MOLECULAR IONS

$\text{Cs}^+$  ions have long been employed as primary species in SIMS to enhance ion formation for electronegative species, and it was also noticed very early that the yields of positive  $\text{MCs}^+$  molecular ions vary significantly less than the respective atomic ion yields [18]. Nevertheless, the possibility of minimizing the often deleterious matrix influences in SIMS by the detection of  $\text{MCs}^+$  ions has been recognized only recently [19,20]. Such species have in particular been shown to provide the most sensitive detection scheme for

Group II elements such as Zn, Cd or Hg [5] or for noble gases [19]. The advantages of  $\text{MCs}^+$  detection for depth profile analyses have been demonstrated recently for various multi-layer structures of semiconductors and metals [21].

Results for the analysis of a Cr–Ni multi-layer sample with a double layer thickness of 70 nm are shown in Fig. 4 [21]. The measurements were made using a Cameca IMS 4f ion microscope with 5.5 keV  $\text{Cs}^+$  primary ions at an incidence angle of  $42^\circ$  with respect to the surface normal.  $\text{MCs}^+$  intensities of the order of  $10^4$ – $10^5$  cps were obtained for primary  $\text{Cs}^+$  currents around 20 nA.

The  $\text{CrCs}^+$  and  $\text{NiCs}^+$  signals reflect the compositional variations in the sample with reasonably good depth resolution. The sensitivity of the  $\text{MCs}^+$  method is demonstrated by the detection of low Si concentrations that agglomerate within the Ni sublayers presumably by diffusion from the Si substrate. Under the assumption of almost equal sputtering yields for Cr and Ni under the present bombarding conditions, the ratio between the  $\text{MCs}^+$  intensities for pure Cr and Ni was only of the order of 6, whereas the simultaneously

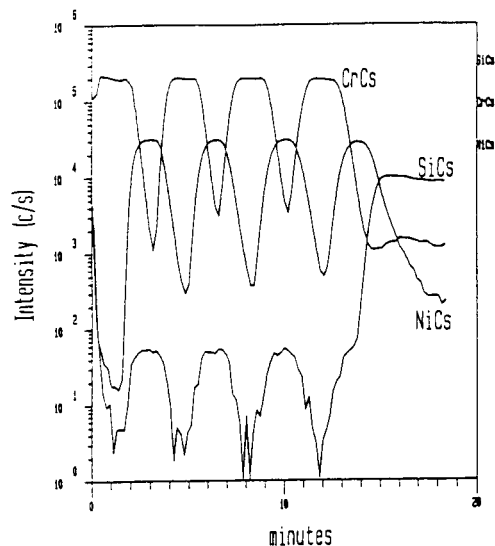


Fig. 4. SIMS depth profile analysis of a Cr–Ni multi-layer structure on Si using  $\text{MCs}^+$  ions. Ion bombardment with 5.5 keV  $\text{Cs}^+$  ions at  $42^\circ$  to the surface normal. Thickness of a Cr–Ni double layer = 70 nm. (From [21].)

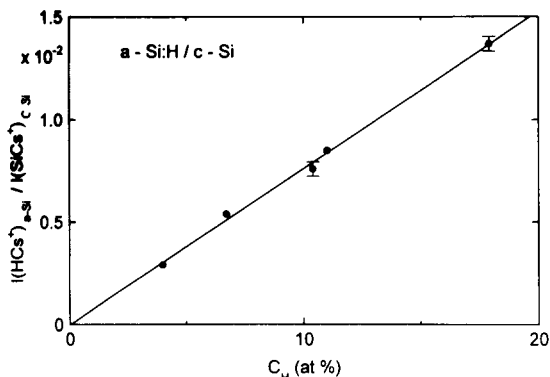


Fig. 5. Hydrogen detection for different hydrogenated amorphous Si films (a-Si:H) on crystalline Si substrates. The SIMS signals of  $\text{HCs}^+$  normalized to the respective  $\text{SiCs}^+$  signals from the substrates are plotted versus the hydrogen concentrations,  $c_{\text{H}}$ , in the layers determined by Fourier transform IR spectrometry. Analysis conditions as in Fig. 4. (From [22].)

detected signals for the respective atomic species exhibited much stronger differences and severe distortions at the interfaces. In particular, the  $\text{Cr}^+$  signals have been found to be strongly influenced by small impurities of oxygen at the interfaces between the sublayers [21].

The determination of hydrogen by using  $\text{HCs}^+$  ions is another promising aspect of the  $\text{MCs}^+$  method [22]. When applied to hydrogen detection in amorphous hydrogenated Si layers on single-crystal Si substrates, detection limits around  $10^{19}$  H atoms  $\text{cm}^{-3}$  are obtained for sputter removal rates of the order of 3 monolayers  $\text{s}^{-1}$ . According to Fig. 5 the  $\text{HCs}^+$  signals detected for such systems are strictly proportional to the hydrogen concentration,  $c_{\text{H}}$ , for values up to 20 at.%. Hence, the detection of  $\text{HCs}^+$  molecular ions offers an interesting alternative to other methods for the determination of hydrogen concentration profiles for which, e.g., the detection of sputter-generated neutral monohydride molecules by SNMS has been shown to be another useful approach [23].

The results in Fig. 5 favour a model according to which  $\text{MCs}^+$  ions are formed via a combination of  $\text{Cs}^+$  ions being re-ejected from the "caesiated" sample surface with sputtered neutral atoms M during the ejection process [20]. This model has recently been confirmed in more detail by

correlating the flux of  $\text{MCs}^+$  ions normalized to that of  $\text{Cs}^+$  with the number density of sputtered M atoms in the agglomeration region [24]. Such a mechanism for the formation of  $\text{MCs}^+$  molecular ions matches well the atomic combination model for the formation of sputtered molecules, which has been shown to be valid for a number of binary sample materials [25].

### Conclusion

Although SIMS and SNMS have developed into routinely used methods for the compositional analysis of surfaces and thin-film structures, their full potential has still not been realized with respect to instrumentation or to novel detection schemes. As an example, new methodical developments in SNMS permit the analysis of the dielectric sample structures with the same quantifiability and depth resolution as were previously available for conducting specimens. Although being fraught with some quantification problems, laser SNMS has developed into a very useful tool for matrix effect-free imaging of elemental surface distributions with extremely high detection sensitivity. Finally, even in SIMS as an already classical surface analytical technique, novel detection schemes such as the use of  $\text{MCs}^+$  signals offer new possibilities for the reduction of the well known problems with the quantification of secondary ion signals.

The author thanks V. Rupertus, M. Kopnarski and M. Strack for skilful performance of the measurements presented in Figs. 2 and 3.

### REFERENCES

- 1 A.J. Ahearn (Ed.), Trace Analysis by Mass Spectrometry, Academic, New York, London, 1972.
- 2 J.A. Jansen and A.W. Witmer, Fresenius' Z. Anal. Chem., 309 (1981) 262.
- 3 J.E. Cantle, E.F. Hall, C.J. Shaw and P.J. Turner, Int. J. Mass Spectrom. Ion Phys., 46 (1983) 11.
- 4 H.J. Heinen, S. Meier, H. Vogt and R. Wechsung, Int. J. Mass Spectrom. Ion Phys., 47 (1983) 19.
- 5 A. Benninghoven, F.G. Rüdener and H.W. Werner, Secondary Ion Mass Spectrometry, Wiley, New York, 1987.
- 6 Z. Sroubek, Spectrochim. Acta, Part B, 44 (1989) 317.
- 7 H. Oechsner, Scanning Microsc., 2 (1988) 9.

- 8 H. Oechsner and W. Gerhard, *Phys. Lett. A*, 40 (1972) 211.
- 9 H. Oechsner, *Nucl. Instrum. Methods Phys. Res.*, B33 (1988) 918.
- 10 W. Bieck, M. Karr, J. Steltmann, H. Gnaser and H. Oechsner, *Dünnschichttechnologien* 92, VDI, Düsseldorf, 1992, p. 759.
- 11 C.H. Becker and K.T. Gillen, *Anal. Chem.*, 56 (1984) 1671.
- 12 S.P. Mouncey, L. Moro and C.H. Becker, *Appl. Surf. Sci.*, 52 (1991) 39.
- 13 S. Kaesdorf, H. Schröder and K.L. Kompa, *Vacuum*, 41 (1990) 1699.
- 14 J.W. Coburn and E. Kay, *Appl. Phys. Lett.*, 19 (1971) 350.
- 15 J.W. Coburn, H.W. Eckstein and E. Kay, *J. Appl. Phys.*, 46 (1975) 2828.
- 16 K.H. Müller, K. Seifert and M. Wilmers, *J. Vac. Sci. Technol.*, A3 (1985) 1367.
- 17 J.F. Geiger, M. Kopnarski, H. Oechsner and H. Paulus, *Mikrochim. Acta*, I (1987) 497.
- 18 H.A. Storms, K.F. Brown and J.D. Stein, *Anal. Chem.*, 49 (1977) 2023.
- 19 M.A. Ray, J.E. Baker, C.M. Loxton and J.E. Greene, *J. Vac. Sci. Technol.*, A6 (1988) 44.
- 20 Y. Gao, *J. Appl. Phys.*, 64 (1988) 3760.
- 21 H. Gnaser and H. Oechsner, *Fresenius' J. Anal. Chem.*, 341 (1991) 341.
- 22 H. Gnaser and H. Oechsner, *Surf. Interface Anal.*, 17 (1991) 646.
- 23 J. Sopka and H. Oechsner, *J. Non-Cryst. Solids*, 114 (1989) 208.
- 24 H. Gnaser and H. Oechsner, in A. Benninghoven, K.T.F. Jansen, J. Tümpner and H.W. Werner (Eds.), *SIMS VIII*, Wiley, Chichester, 1992, p. 95.
- 25 H. Oechsner, *Int. J. Mass Spectrom. Ion Phys.*, 103 (1990) 31.

# Laser microprobe Fourier transform mass spectrometer with external ion source for organic and inorganic microanalysis

H. Struyf, W. Van Roy, L. Van Vaeck, R. Van Grieken and R. Gijbels

*Department of Chemistry, University of Antwerp (UIA), Universiteitsplein 1, B-2610 Wilrijk (Belgium)*

P. Caravatti

*Spectrospin AG, Industriestrasse 26, CH-8117 Fällanden (Switzerland)*

(Received 8th September 1992; revised manuscript received 27th January 1993)

## Abstract

The earlier laser microprobe (LM) mass spectrometer with a time-of-flight (TOF) analyser showed that the irradiation of solids by a focused UV laser represents an interesting means of performing local analysis. However, the subsequent measurement of the generated ions is done under low-resolution conditions. The characterization of heterogeneous samples and the occurrence of poorly understood ion formation mechanisms motivated the development of an instrument with superior mass spectrometric performance. Specifically, Fourier transform (FT) mass spectrometry potentially provides the required high mass resolution and accurate mass determination in combination with adequate sensitivity. In this work an FT-LM mass spectrometer with an external source was developed. Analysis is performed in the reflection mode with a 5- $\mu\text{m}$  spot from a Q-switched Nd:YAG laser. Transfer of ions from the external source into the cell is performed by static electrical fields. The resulting mass separation imposes limitations on the panoramic spectrum registration in the case of pulsed laser microbeam ionization of solids, producing ion bunches over not more than a few hundred microseconds. This paper addresses instrument design and performance with respect to sensitivity, spatial resolution and accuracy of  $m/z$  determination and the problem of panoramic registration. Attention is focused on the comparison of results from FT- and TOF-LM mass spectrometry in relation to the determination of the speciation of inorganic compounds and diagnostic analysis of organic molecules.

*Keywords:* Mass spectrometry; Laser microprobe

Laser microprobe (LM) mass spectrometry (MS) is a relatively recent technique for the measurement of organic and inorganic constituents at the surface of solids with a spatial resolution of the order of a few  $\mu\text{m}$ . A microvolume is irradiated by a focused laser and the ions produced are mass analysed. The local excitation of the sample by means of a photon beam eliminates the charg-

ing problems. The first commercial instruments were time-of-flight (TOF) LM mass spectrometers [1–3]. The high transmission ensured good sensitivity and no scanning was needed, so that complete mass spectra could be obtained from each single laser interaction. The applicability of TOF-LMMS to a wide range of research problems from science and industry has been demonstrated [4–6].

The results indicated the analytical potential of laser microbeam irradiation for inorganic and organic local analysis, but also revealed the limi-

*Correspondence to:* L. Van Vaeck, Department of Chemistry, University of Antwerp (UIA), Universiteitsplein 1, B-2610 Wilrijk (Belgium).

tations of the TOF instrument for mass analysis. On the one hand, fine speciation capabilities are offered while the mass spectra for organic compounds usually yield molecular weight information and numerous fragments to characterize the functionalities in the molecule. However, mass resolution of TOF-LMMS is limited to less than 1000 [7,8]. Hence the exact chemical composition of the detected ions cannot be derived, which is a prerequisite because of the lack of knowledge about the ion formation under laser microbeam irradiation of heterogeneous solids. Additionally, TOF-MS relies on prompt ion formation, which essentially occurs during the laser pulse. Organic compounds tend to form ions for a long time after the laser pulse [9].

The well known capabilities of Fourier transform (FT) MS with respect to high mass resolution, accurate  $m/z$  determination and spectrum registration without scanning and the additional use of ion–molecule reactions and multiple MS experiments to elucidate the ion structure makes the idea of FT-LMMS particularly appealing on the condition that the sensitivity is sufficient to detect the extremely small number of ions generated from the irradiated microvolume.

The feasibility of the FT-LMMS approach has been evidenced by the experimental set-ups developed at the University of Metz (France) and the IBM Laboratories (San Jose, CA, and Endicott, NY, USA) [10–12]. These instruments used laser microbeam ionization of the samples *inside* the FT-MS cell. Hence, the optical systems for laser focusing, sample observation and illumination and the micropositioner of the specimen have to be mounted at least partially within the narrow bore of the superconducting magnet. This often makes the design complicated. Moreover, preliminary results suggested that ion formation inside the magnetic field is responsible for second-order interactions between the orbiting ions and the slowly pumped-off neutral species [13]. This could explain at least in part the observed differences between FT- and TOF-LMMS of, e.g., polymers.

In this work, the development of FT-LMMS with an external ion source was investigated. The first reason was the accessibility and roominess

around the sample so that the implementation of the laser focusing and viewing optics and the sample positioning system could be fully optimized. Additionally, the ion lenses required to guide the ions into the ion transfer system can offer the possibility of studying the kinetics and characteristics of the generated species with respect to, e.g., energy distribution and gas-phase vs. surface ionization. The short residence time of the ions in the laser-generated micro-cloud just above the sample surface should minimize the ion–molecule interactions. Second, a high vacuum is maintained in the cell, even when, e.g., post-chemical ionization would be used in the source, and hence good mass resolution can be expected.

However, the use of an external source in FT-MS also implies the problem of ion transfer. Specifically, the injection of ions through the inhomogeneous fringing field of the magnet is not trivial [14,15]. Tandem quadrupoles have been used [16,17], the first acting as a mass filter while the second is used as a lens in the r.f.-only mode. Also, mass selection by tandem quadrupoles has been combined with an electrostatic lens to guide the ions through the fringing field into the cell [18]. However, a single quadrupole-based FT mass spectrometer has been proved to show excellent sensitivity and resolution [19]. Alternatively, the use of static electrical fields allows high transmission efficiency in combination with simple construction [20]. Purely electrostatic lenses have been applied to inject the ions from a metal cluster beam [21]. The retention of the ions in the low trapping field of the cell is not obvious because this conflicts with the relatively high kinetic energy of the ions required for efficient ion transfer [22]. Some accumulation effects occur during ion trapping, e.g., collisional deceleration of injected ions by the neutral species in the cell [22], ion–molecule reactions [23] or possibly deflection of injected ions by radial magnetic field inhomogeneities induced by the trap plates [24].

The purpose of this paper is to describe the FT-LM mass spectrometer and to illustrate the basic specifications with respect to sensitivity and spatial and mass resolution. Analysis is performed in the reflection mode by a frequency-

quadrupled Nd:YAG laser beam, which is focused to  $5\ \mu\text{m}$ . Post-ionization of the laser-generated neutral species can be performed using a 70-eV electron beam. With laser microbeam irradiation of solids, ion formation occurs over less than a few hundred microseconds. The time dispersion of the laser-generated ion bunches in the electrostatic transfer line conflicts with the simultaneous registration of ions within a wide  $m/z$  range. It will be shown, however, that this problem may provide interesting clues to the basic ion formation mechanisms induced by laser microbeam irradiation of organic vs. inorganic solids. Subsequently, attention will be devoted to representative results in relation to the speciation analysis of inorganic compounds and structural analysis of organic molecules. Comparative data from FT-LMMS and TOF-LMMS show characteristic differences, which will be tentatively interpreted in terms of the ion formation mechanism.

## EXPERIMENTAL

Figure 1 shows a schematic diagram of the MicroFocus<sup>TM</sup> instrument, based on a Spectrospin CMS 47X with a 4.7-T superconducting magnet and a single cylindrical cell of 60 mm length and 60 mm diameter (Spectrospin, Fällanden, Switzerland). Instrument control and data acquisition are performed using an Aspect 3000 computer upgraded with a 20-MHz, 9-bit fast ADC and 256K memory. A full description of the basic instrumentation is available elsewhere [25]. The ion source–ion transfer–cell assembly is mounted on a movable vacuum cart to facilitate maintenance.

Ionization is performed by a frequency Q-switched Nd:YAG laser (Quanta-Ray DCR-2A, Spectra-Physics, San Jose, CA), delivering 20 mJ per pulse of 4–5 ns at 266 nm and equipped with fill-in optics for a Gaussian beam profile. The laser head is flashlamp-pumped at 10 Hz. The

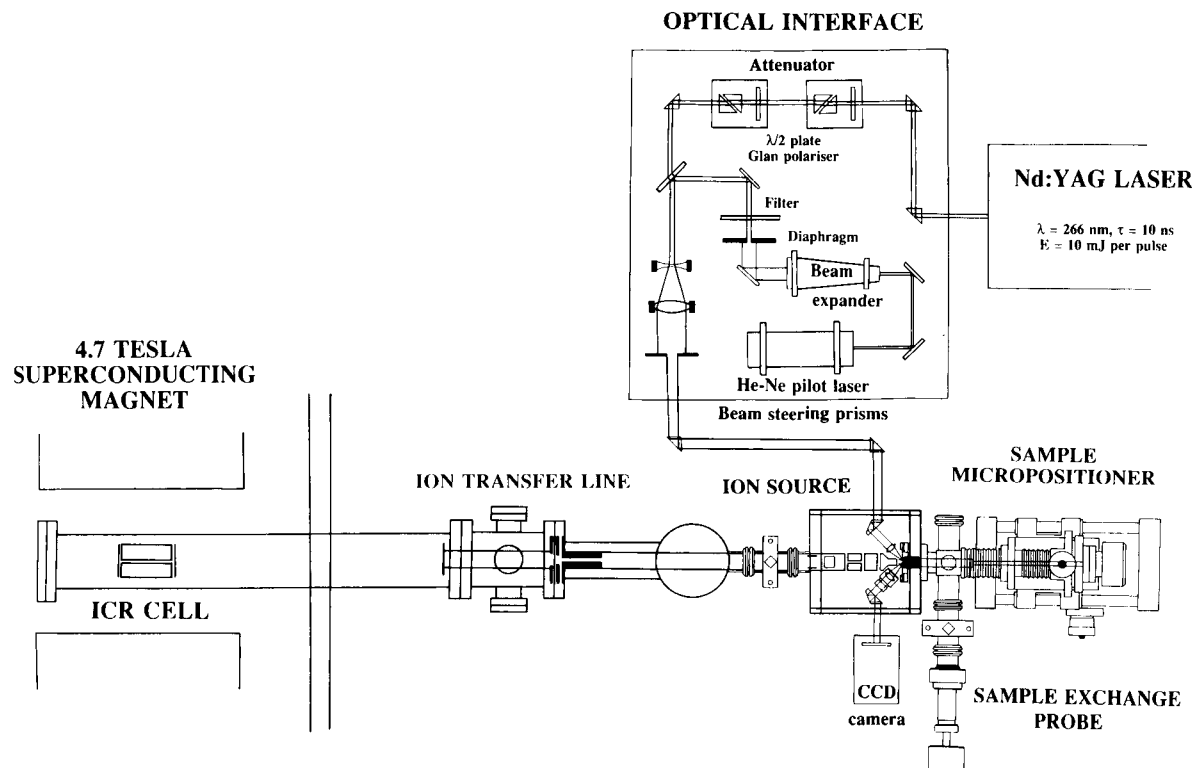


Fig. 1. Schematic diagram of the developed FT-LM mass spectrometer with the external source.

Pockell cell is controlled by a special interface board, triggered by the ionization pulse. The internal clock of the Aspect computer is disabled until the next flashlamp event. The analyses were performed under the so-called threshold conditions, involving the use of less than 100 nJ per shot.

Apart from the obvious diaphragms, filters and steering prisms, the optical interface essentially contains an expanded He–Ne laser, coupled collinearly with the UV beam at a 45° quartz plate, a 2.5 × Galilean-type beam expander and two sets of  $\lambda/2$  waveplates in front of Glan air-spaced polarizers for rough and fine attenuation of the UV beam. A 15 × microscope lens (OFR, NJ) inside the vacuum performs the final focusing. The laser irradiates the sample in reflection under 45° over an ellipsoid spot, of which the long side is 5  $\mu\text{m}$ . All UV optics are anti-reflection coated and adjustable for tilt around two orthogonal axes, except for the beam expander lenses. The front optic is fixed and the exit optic is adjustable for tilt and in the  $x$ ,  $y$ ,  $z$ -directions. The number of steering prisms is optimized to permit partial readjustment when the laser or the ion source is being maintained.

The sample viewing system consists of a microscope objective with ultra-long working distance (M Plan SLWD 20X, Nikon, Tokyo) inside the vacuum, a CCD camera (CCD 500; Bishcke, Switzerland), and a high-resolution monitor (TVM 12HI; Bishcke) for display. The final magnification is 700 ×, so 1 mm on the screen represents 1.4  $\mu\text{m}$  on the specimen. The depth-of-focus (DOF) permits the position of the sample surface to be assessed critically within the waist of the ionizing laser. The observation under 45° with a high-magnification microscope lens means that the sample is only imaged over 12  $\mu\text{m}$ . A complementing low-magnification (10–63 ×) binocular (Nikon SMZ-2T), mounted outside the vacuum chamber, permits an overview of the sample. An area of 4 mm diameter is illuminated by a common halogen light source (Intralux; Volpi, Switzerland) outside the manifold and by prisms inside the vacuum.

The sample holder is designed for specimen with a size up to 20 × 20 × 10 mm. Microposition-

ing of the sample is performed by means of a commercial  $x$ ,  $y$ ,  $z$ -manipulator (Huntington, CA) with a 1- $\mu\text{m}$  precision and 25-mm travel. The additional chamber with appropriate interlock and probe allows the exchange of the sample within 5 min without interruption of the vacuum in the ion source.

The standard configuration of the electrodes in the ion source and at the beginning of the transfer line has been redesigned. The sample is electrically isolated from the manifold and can be used as a repeller electrode. The first extracting electrode consists of a perforated cone of 6 mm diameter and 9 mm length, placed 2 mm above the sample surface. Post-ionization in the external source by 70 eV of laser-generated neutral species is feasible. Additional details of the system are described elsewhere [26].

Comparative results were recorded on a LAMMA 500 transmission-type instrument (Leybold Heraeus, Germany). Powdered particles of about 1–3  $\mu\text{m}$  were attached to a Formvar film over a usual electron microscopy grid. The mass spectra were registered using the described procedure for threshold mode analysis [27].

### *Samples*

Most samples were applied to a polished stainless-steel sample holder by evaporating a 10- $\mu\text{l}$  aliquot of a solution, typically containing 2 mg of material per 100 ml methanol or water. Gold coatings were made by sputtering with  $\text{Ar}^+$  under vacuum.

## RESULTS AND DISCUSSION

### *Basic performance*

Routinely, the mass resolution is over 100 000 for  $m/z$  values up to 500. Naturally, in the lower range higher values are attained. Figure 2 shows a few examples of the signals. Determination of  $m/z$  values yields results which lie within 1 ppm around the values calculated by calibration on perfluorotributylamine, which was introduced through the gas inlet and ionized with 70-eV electrons.

The sensitivity of the instrument in the laser ionization mode depends on the compound under consideration. Consumption of less than 1 pg of coronene gives a fairly intense signal in the narrow-band mode with a signal-to-noise ratio ( $S/N$ ) of 7.5 at a resolution of 240 000. In general, the detectability of FT-LMMS allows the recording of at least the base peak from a single shot with a 5- $\mu\text{m}$  spot size. Irradiation of a gold layer of less than 100 nm thickness with a 5- $\mu\text{m}$  spot yields a very prominent signal for the positive elemental ions with  $S/N > 100$  and a resolution of  $1.2 \times 10^6$ . Under these conditions, the crater depths exceeds the thickness of the upper layer. However, the total amount of evaporated material only contains about  $1.2 \times 10^{10}$  gold atoms.

An interesting feature of the LM irradiation under threshold conditions is the very limited information depth, i.e., the recorded mass spectral data only issue from the upper 100 nm whereas the crater goes several  $\mu\text{m}$  deeper. This makes the method appealing as a surface technique. No iron ions could be detected during the irradiation of stainless steel covered with a gold layer of about 100 nm. In principle, this phenomenon depends on the relative ionization yield of the upper and underlying component on the condition that the ion characteristics are compa-

rable with respect to, e.g., energy distribution and formation time. Of course, the broadband mode is less sensitive than the high-resolution mode, by a factor of at least 50, depending on the ion trapping procedure (see the next section).

The availability of post-electron impact (EI) in the external ion source has been demonstrated to be a substantial asset for particular organic compounds. For structures giving the same ions with laser ionization and post-EI, e.g., coronene, the detection limit improves by a factor of five or more. Alternatively, post-EI can be applied to overcome the poor ionization efficiency of the laser for certain molecules. Finally, post-EI allows the generation of additional fragment peaks, which increase the diagnostic information of the registered mass spectra. Figure 3 illustrates several aspects in the spectra of methylene blue obtained by FT-LMMS. The TOF-LMMS results are included for comparison. The latter method detects the intact cations with virtually no fragmentation. The situation is more or less comparable for the laser-only mode in FT-LMMS, but still some small additional peaks are present. Ionization of the laser-generated neutral species yields a substantial increase in the signal at  $m/z$  268 in the presence of the corresponding fragments. The latter peaks certainly increase the information

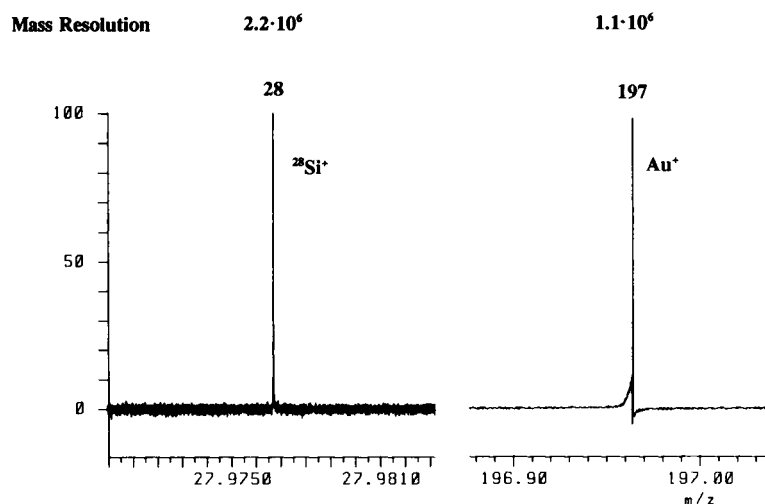


Fig. 2. Typical high-resolution measurements by FT-LMMS of the elemental ions from a silicon wafer (left) and a 100-nm gold layer (right).



content of the spectra and allow the description of the functionalities in the molecule, which is hardly feasible from the laser-only mode data. Moreover, the signal at  $m/z$  149 is related to the phthalate contamination of the sample, which is almost inevitable although not detected in the laser-only mode. For some reason, this compound

is not very sensitive under laser microbeam irradiation conditions, in spite of its aromatic functionality.

#### *Panoramic registration*

Depending on the application, local analysis research may involve the localization of a given

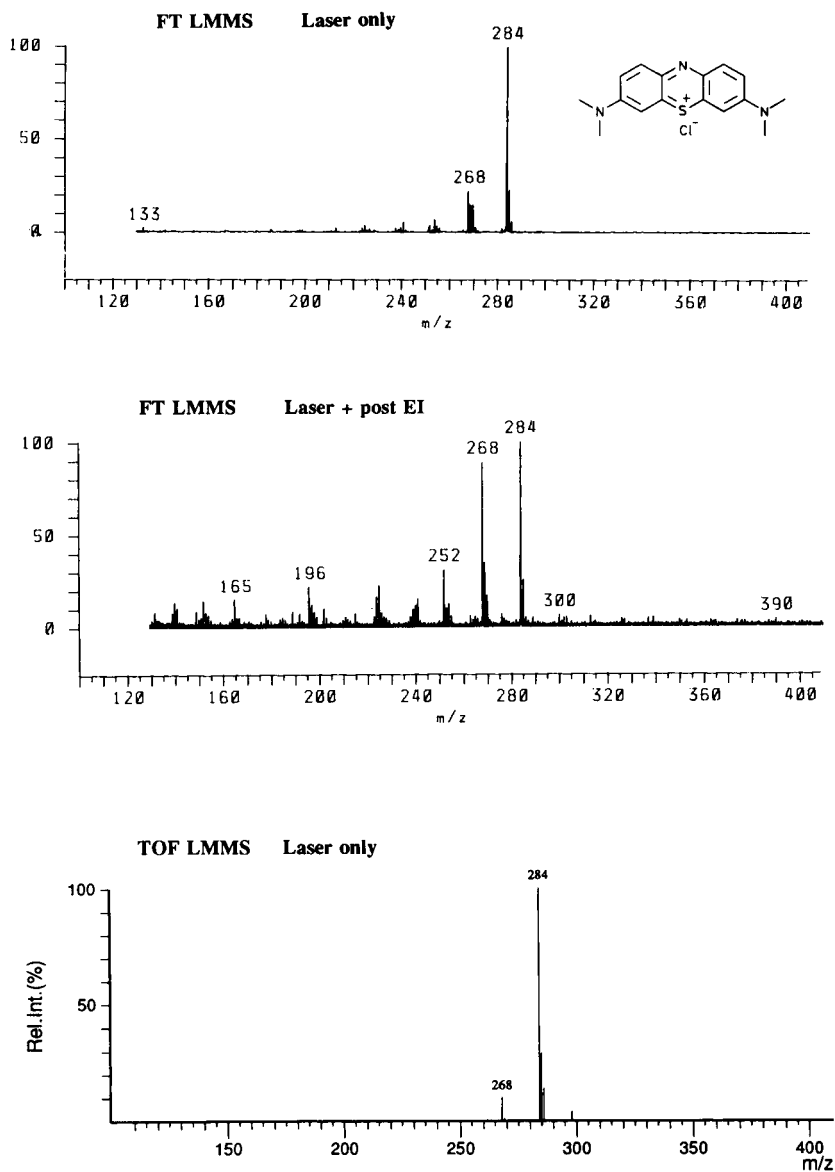


Fig. 3. Positive-ion detection mode mass spectra of methylene blue recorded by TOF-LMMS and FT-LMMS with or without post-electron ionization.

target or the identification of an unknown substance in, e.g., a microscopic heterogeneity. In the former case, single ion monitoring in the high-resolution mode can be considered as an adequate means, because the  $m/z$  accuracy and the available mass resolution in FT-LMMS make the determination of the compound under consideration almost unambiguous in practice. How-

ever, multiple ion monitoring would be desirable to allow the localization of several components in the same shot. In the latter case, a mass spectrum over a wide  $m/z$  range is required.

Whenever an external source is coupled to the FT-MS analyser cell over static electrical fields, a mass-dependent time separation occurs during the ion transfer. Hence, the low- $m/z$  ions arrive

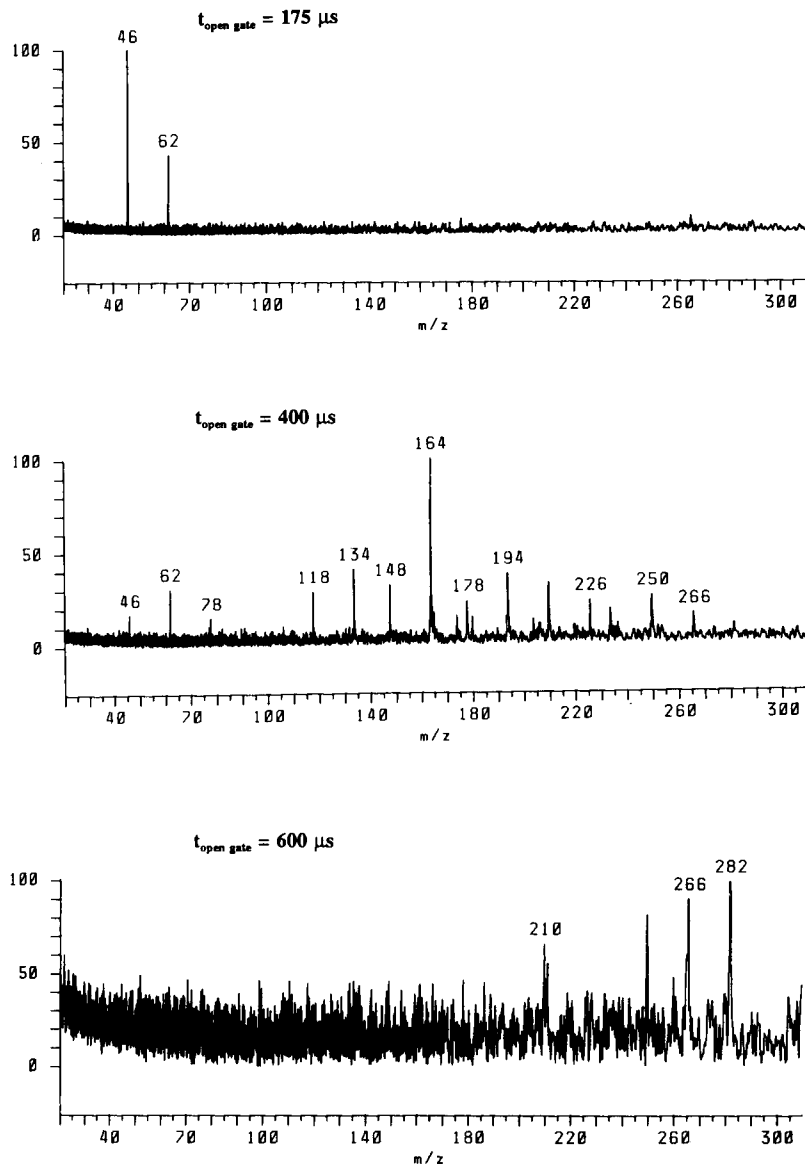


Fig. 4. Negative-ion mass spectra of calcium nitrate recorded by FT-LMMS a function of the duration of the ionization pulse ( $t_{\text{open gate}}$ ).

first at the “cell gate”. These ions are allowed to enter the cell when the repulsing field situated in the central perforation of the first trapping electrode is reduced to zero. Subsequently, the ions are reflected by the second trapping plate. Obviously, the repelling field in the front electrode has to be restored before the ions have returned. At the same time, the higher  $m/z$  ions which arrive later can no longer enter the cell. Stated differently, to determine the mass range for panoramic registration one has to consider the lowest  $m/z$  to be recorded. The trap residence time (i.e., the period in which the ions travel from one trap plate to the other) of these ions, which arrive first, determines the time during which the cell can be opened for the slower, higher  $m/z$  ions. These effects have been extensively described [15,28]. Note that these problems arise whenever the ionization method used produces ion bunches within extremely short time periods. When, for instance, EI is applied to a continuous sample supply, ions can be produced at a fairly constant rate over thousands of  $\mu\text{s}$ , i.e., several times the flight time of even the heaviest ions. Hence the TOF effect rules out completely because, at each moment, the cell contains ions that were generated at different times. Further, the use of two half-electrodes in front of the first trapping plate, permitting the repulsing trapping field to be compensated upon entering, partially prevents the escape of the ions from the cell. As a result, ions are accumulated in the cell [29]. Of course, in the present instance this is not feasible.

Figure 4 shows a few broadband spectra of calcium nitrate as a function of the duration of the ionization pulse. The indicated times refer to the ionization pulse time, which roughly corresponds to the time between the laser firing and the disabling of the half-electrodes in front of the cell. The assignment of the signals shown in Fig. 4 is summarized in Table 1 and will be discussed later.

It is clear, however, that the TOF effect causes severe problems but the situation can be dealt with on the condition that the considered  $m/z$  range can be limited, especially with respect to the low mass limits. A coverage of the  $m/z$  range from 100 to 500 is acceptable for practical applications. Note that the elemental ions in the low-mass range require different laser ionization conditions than the organic compounds and the higher mass ion clusters used for speciation analysis of inorganic compounds.

Hence it is worth comparing the mentioned times for the ionization pulse with the values in Table 2, which were calculated using the SIMION program (Idaho National Engineering Laboratory), for the flight times and the trapping residence times. The former were calculated for the voltages on the transfer optics as used in the present experiments. This essentially involves a stepwise acceleration up to 3 kV followed by a gradual decrease to 550 V in the last flight tube, ending about 50 cm before the cell. The ions then drift through a zero-voltage tube towards the cell. The trapping residence times are calculated for a

TABLE 1

Assignment of the major signals in the negative-ion mass spectrum of calcium nitrate

$m/z$	Species	$m/z$	Species
46	$\text{NO}_2^-$	178	$\text{CaO} \cdot \text{NO}_2 \cdot \text{NO}_2 \cdot \text{NO}^-$
62	$\text{NO}_3^-$	192	$\text{CaO} \cdot \text{CaO} \cdot \text{H}_2\text{O} \cdot \text{NO}_3^-$
118	$\text{CaO} \cdot \text{NO}_3^-$	194	$\text{Ca}(\text{NO}_3)_2 \cdot \text{NO}^-$
134	$\text{CaO} \cdot \text{O}_2 \cdot \text{NO}_2^-$	205	$\text{CaO} \cdot \text{HNO}_2 \cdot \text{CaO} \cdot \text{NO}_2^-$
148	$\text{CaO} \cdot \text{NO}_2 \cdot \text{NO}_2^-$	210	$\text{Ca}(\text{NO}_3)_2 \cdot \text{NO}_2^-$
149	$\text{CaO} \cdot \text{HNO}_2 \cdot \text{NO}_2^-$	221	$\text{CaO} \cdot \text{HNO}_2 \cdot \text{CaO} \cdot \text{NO}_3^-$
164	$\text{CaO} \cdot \text{NO}_2 \cdot \text{NO}_3^-$	226	$\text{Ca}(\text{NO}_3)_2 \cdot \text{NO}_3^-$
165	$\text{CaO} \cdot \text{HNO}_2 \cdot \text{NO}_3^-$	234	$\text{CaO} \cdot \text{NO}_2 \cdot \text{CaO} \cdot \text{NO}_2 \cdot \text{NO}^-$
174	$\text{CaO} \cdot \text{CaO} \cdot \text{NO}_3^-$	237	$\text{Ca}(\text{NO}_3)_2 \cdot \text{CaO} \cdot \text{OH}^-$
176	$\text{CaO} \cdot \text{CaO} \cdot \text{H}_2\text{O} \cdot \text{NO}_2^-$	250	$\text{Ca}(\text{NO}_3)_2 \cdot \text{CaO} \cdot \text{NO}^-$

TABLE 2

Calculation of flight times and trapping residence times for ions at different  $m/z$  in FT-LMMS with external source

$m/z$	Flight time ( $T_f$ ) ( $\mu\text{s}$ )	Trapping residence time ( $T_{tr}$ ) ( $\mu\text{s}$ )	Optimum time calculated ( $T_f + T_{tr}$ ) ( $\mu\text{s}$ )
20	46	52	98
50	72	82	154
100	102	116	218
250	161	183	344
500	227	259	486
1000	321	366	687

trap potential of 1.5 V and ions arriving with 0.3–1.4 eV in the cell. The spread of the trapping residence time for ions with different energies in that range is about 2.4%.

Assume that abstraction can be made from the time dispersion resulting from the initial velocity and angular emission spread of the ions and that all ions are generated within 5 ns. If one uses an

ionization pulse time of 344  $\mu\text{s}$ , i.e., the sum of the flight time and the trap residence time for the ions at  $m/z$  250, it should be possible to trap all ions (i.e., up to  $m/z$  1000) that arrive at the “cell gate” within that time. At the same time, however, all ions below  $m/z$  100 arrive sooner and have a shorter trap residence time and hence will have escaped from the cell by then. As a result, the TOF effects are particularly annoying when the low-mass range is aimed at. For organic compounds, it is often sufficient to record the spectral information from ions between  $m/z$  150 and 500. In order to overcome these TOF effects the instrumentation will be modified with respect to the ion transfer and/or trapping system, according to the results of Beu and Laude [28].

#### Comparison of FT-LMMS with TOF-LMMS

For convenience, let us discuss the possible reasons for the differences between mass spectra obtained in TOF- and FT-LMMS.

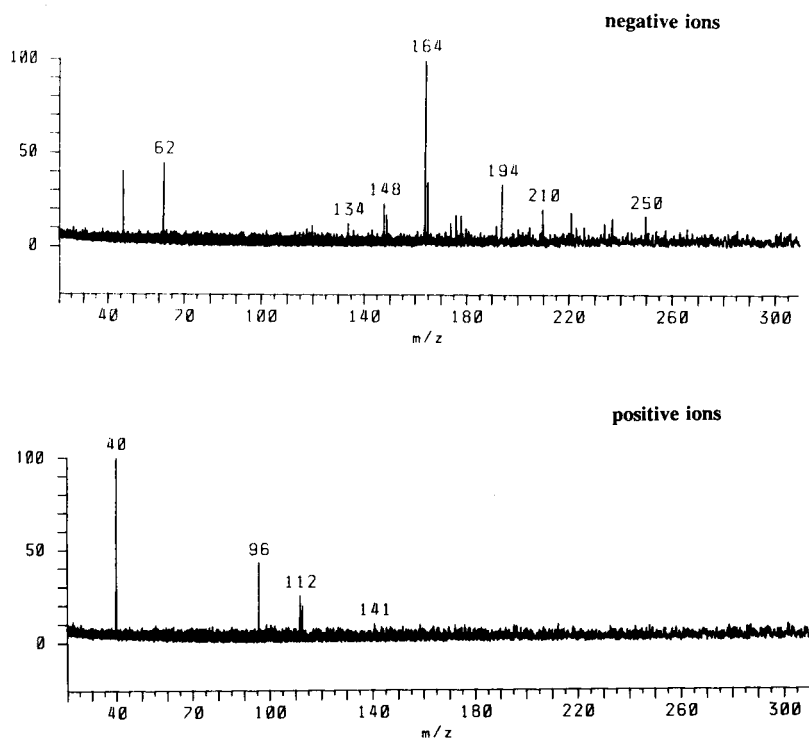


Fig. 5. Positive- and negative-ion mass spectra of calcium nitrate recorded by FT-LMMS.

**Laser microbeam irradiation.** The power density distribution within the irradiated area can be different simply because of the spot size. Further, it is difficult to reproduce the irradiate conditions exactly on two different instruments because the energy in the final spot cannot be measured. Finally, the proposed FT-LM mass spectrometer uses reflection geometry, i.e., the laser impinges on the sample and the ions are extracted from the same side, whereas the TOF-LM mass spectrometer works in transmission geometry, i.e., the laser beam and spectrometer are on the same axis but at opposite sides of the thin sample.

**Time domain for ion collection.** The TOF instrument deals essentially with the prompt ions whereas the FT-LM spectrometer allows the measurement of the total ion current, generated within a fraction of a millisecond, unless special precautions are taken.

**Duration of the experiment.** In TOF-LMMS there is a period of only 500  $\mu\text{s}$  between ion generation and registration. In FT-LMMS the basic duty cycle of even a simple experiment lies in the range of milliseconds.

**Kinetic energy acceptance.** This is high in TOF-LMMS where only the distribution width matters as long as the average ion velocity allows preservation of the calibration. The kinetic energy acceptance is low in FT-LMMS, depending on the trapping potential and the characteristics of the ion transfer system.

**Extraction field.** This is high in TOF-LMMS, hence the residence time within the laser microplasma is minimal. There is a low to very low or even repelling field in the external source of the FT-LM mass spectrometer, which causes a longer residence time. It is better, however, than in the alternative set-ups, using laser microbeam irradiation of the sample inside the cell [13].

**Inorganic speciation analysis.** The positive- and negative-ion mode mass spectra of calcium nitrate in Fig. 5 illustrate the features one expects from LMMS for measurement of speciation. Note that the intensity of the elemental ions in the positive-ion mass spectrum is possibly underestimated because of the TOF effect. The same is true for the negative ions below  $m/z$  100 in the negative-ion mass spectrum. The main informa-

TABLE 3

Assignment of the major signals in the positive-ion mass spectrum of calcium nitrate

$m/z$	Species
40	$\text{Ca}^+$
96	$\text{CaO} \cdot \text{Ca}^+$
112	$\text{CaO} \cdot \text{CaO}^+$
113	$\text{CaO} \cdot \text{CaO} \cdot \text{H}^+$
152	$\text{CaO} \cdot \text{CaO} \cdot \text{Ca}^+$

tion that can be derived from the positive ions comes from cations in the form of elemental ions and oxides in the case of oxo salts (see Table 3). Depending on the structure, higher clusters consist of these units attached to one or more neutral entities. The low- $m/z$  ions in the negative ion mode usually characterize the anionic moiety by means of the base peak (cf., Table 1). Highly relevant in this respect is the presence of intense signals referring to the combination of the salt ionic pair with a stable anionic moiety. Sometimes, however, higher clusters are not detected, depending on the compound studied. The combination of all of these signals clearly allows the identification of a salt in a very obvious way. In this respect, laser microbeam irradiation has been proved superior to, e.g., secondary ion MS or other microprobe methods.

The LM irradiation conditions are kept identical in both the TOF and FT-LM instruments as far as possible, but there is no absolute guarantee that this is really the case. Owing to the extreme dependence of the spectral intensities on the exact irradiation conditions, i.e. focusing, particle size, etc., it is justified to classify the signals in three or four intensity ranges. From comparison of the two methods, it is clearly observed that the FT-LMMS data contain in general fewer peaks than the corresponding TOF spectra; the main diagnostic information is preserved but the spectra look cleaner.

The interpretation of this observation is not yet clear. One of the reasons is the lack of knowledge on the ion formation mechanisms. In principle, desorption as an ion pair and subsequent association with a charged species or dissociation into the detected low- $m/z$  ions can occur in

competition with direct emission of the registered ions from the solid. A relevant observation in this respect concerns the fact that the detection of higher clusters in FT-LMMS is favoured if one increases the residence time of the ions in the first part of the ion transfer system. This can be achieved by increasing the voltage on the first extraction lens, which is very near to the sample surface, above that on the sample holder, which consequently ceases to act as a real repeller. In contrast, elemental ions still pass through when there is a small accelerating field between the extractor and repeller. Also, the experimentally optimized pulse ionization times agree better with the calculated values for elemental ions, com-

pared with the higher clusters. This may point to prompt ionization processes for the former ions and delayed mechanisms for the latter.

So far, little is known about the possible fragmentation rates of inorganic ions. Exploration of this field using the capabilities of FT-LMMS for ion decomposition studies of laser-generated ions provides an exciting research topic for the near future.

*Organic compounds.* Figure 6 compared the TOF- and FT-LMMS results for haloperidol in the positive-ion detection mode [30]. The general trend with respect to the relative ion intensities concerns the fact that the base peak is more dominant over the other signals in FT- than in

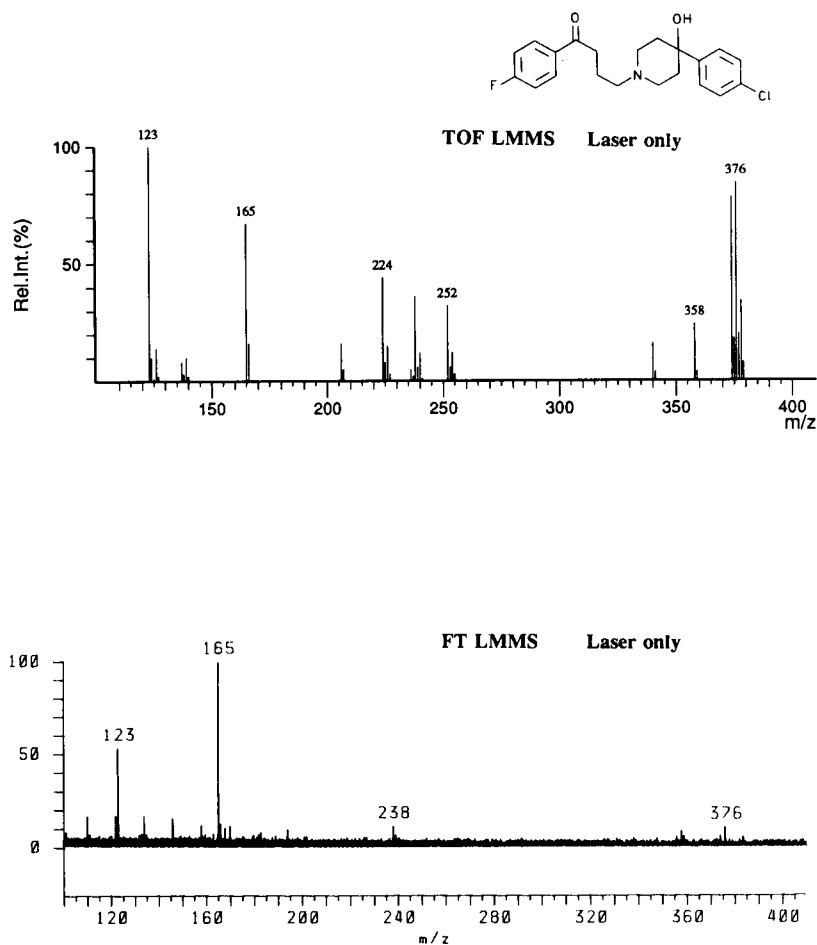


Fig. 6. Positive-ion detection mode mass spectra of haloperidol recorded by TOF-LMMS and FT-LMMS.

TOF-LMMS. The abundance of the stable fluoro-benzoyl fragment ion “suppresses” the other signals in the former instance. Qualitatively, TOF-LMMS produces more signals, e.g., the ions at  $m/z$  252 and 224, which are not detected in FT-LMMS. The tentative rationalization of the observed differences is straightforward. The effect of sampling the total ion bunch and not only the promptly generated species in FT-LMMS results in a lower energy distribution for the ion population. This hypothesis can be deduced, for instance, from the draw-out pulse measurements on a TOF instrument [9]. The later generated ions have smaller energy distributions and undergo less fragmentation down to none at all.

The FT-LMMS data remain adequate for localization of this target in a mixture or a complex sample. One should bear in mind that the signals still remain structure specific and that the peaks can be measured in high resolution. It was also noted that the  $[M - H]^+$  signal is consistently lower in FT-LMMS than in TOF-LMMS, which may be due to a relative increase in the  $[M + H]^+$  ions in FT-LMMS.

A substantially longer pulse ionization time is required in comparison with the SIMION calculations for the ions in the molecular region, which points to a prevalent formation process after the laser pulse.

### Conclusions

Preliminary results have shown the feasibility of the developed FT-LM mass spectrometer with an external ion source to perform high mass resolution measurements of the ions, generated from a 5- $\mu$ m spot on organic and inorganic samples. At least the base peak can be detected in the single shot mode. The high mass resolution and accurate  $m/z$  determination provide valuable identification possibilities for the localization of the target, depending, of course, on its structure. The benefits from the application of post-EI on the laser-generated neutral species also depend on the structure studied. If the laser ionization yields ions at the same  $m/z$  as post-EI, the sensitivity is improved by a factor of five. On the other hand, the fragmentation caused by post-EI disperses the additional ion yield over several

$m/z$  signals. To overcome this problem, the ion source is currently modified to perform post-CI on laser-desorbed neutral species. There are some differences between FT- and TOF-LMMS data, which are tentatively interpreted in terms of ion formation mechanisms, but further research is required. There is evidence for the occurrence of thermal degradation during the analysis. It can be concluded that the sensitivity of FT-LMMS is sufficient to register the base peak but it still remains a factor of 100 lower than in TOF-LMMS. In the authors' opinion, the price to be paid for the higher mass resolution with FT-LMMS system is very reasonable. At present, panoramic spectrum registration by FT-LMMS is hindered by the time-of-flight problem. Under these conditions, only limited  $m/z$  ranges can be recorded in the broadband mode. The comparison of experimental and SIMION-calculated data suggest that the situation is aggravated by the delayed ion formation. This problem will be dealt with in the immediate future. FT-LMMS results for inorganic compounds are characterized by fewer lines in comparison with TOF-LMMS data, but the main diagnostic information is preserved. It is not yet clear which factor is responsible for this, e.g., kinetic energy distribution or time scale. FT-LMMS fulfills the expectations for inorganic and organic analysis, with fine speciation analysis capabilities in the former field and good structural characterization information for the latter application.

Luc Van Vaeck and Wim Van Roy are indebted to the National Science Foundation, Belgium (NFWO) as research associate and research assistant, respectively. Eng. R. Saelens is acknowledged for technical support. This work was partially sponsored by the Belgian Ministry of Public Health and the Environment and by the Belgian Prime Minister's Services, Science Policy Office, in the framework for the Impulse Programme on Marine Sciences.

### REFERENCES

- 1 H. Vogt, H.J. Heinen, S. Meier and R. Wechsung, *Fresenius' Z. Anal. Chem.*, 308 (1981) 195.

- 2 H.J. Heinen, S. Meier, H. Vogt and R. Wechsung, *Int. J. Mass Spectrom. Ion Phys.*, 47 (1983) 19.
- 3 J.C. Ruckman, R. Davey and N.S. Clarke, *Vacuum*, 34 (1984) 911.
- 4 A.H. Verbueken, F.J. Bruynseels, R. Van Grieken and F. Adams, in F. Adams, R. Gijbels and R. Van Grieken (Eds.), *Inorganic Mass Spectrometry*, Wiley, New York, 1988, p. 173.
- 5 L. Van Vaeck and R. Gijbels, *Fresenius' J. Anal. Chem.*, 337 (1990) 743.
- 6 L. Van Vaeck and R. Gijbels, *Fresenius' J. Anal. Chem.*, 337 (1990) 755.
- 7 R. Kaufmann, F. Hillenkamp, R. Wechsung, H.J. Heinen and M. Schurmann, *Scanning Electron Microsc.*, 2 (1979) 279.
- 8 L. Van Vaeck, J. Claereboudt, P. Van Espen, F. Adams, R. Gijbels and W. Cautreels, *Adv. Mass Spectrom.*, 9B (1986) 957.
- 9 R.J. Cotter and J.C. Tabet, *Int. J. Mass Spectrom. Ion Phys.*, 53 (1983) 151.
- 10 M. Pelletier, G. Krier, J.F. Muller, D. Weil and M. Johnston, *Rapid Commun. Mass Spectrom.*, 2 (1988) 146.
- 11 J.T. Brenna, W.R. Creasy, W. McBain and C. Soria, *Rev. Sci. Instrum.*, 59 (1988) 873.
- 12 R.B. Cody, A. Bjarnason and D.A. Weil, in D. Lubman (Ed.), *Lasers in Mass Spectrometry*, Oxford University Press, New York, 1990, p. 316.
- 13 J.T. Brenna, in P.E. Russell (Ed.), *Microbeam Analysis—1989*, San Francisco Press, San Francisco, 1989, p. 306.
- 14 P. Köfel and T.B. McMahon, *Int. J. Mass Spectrom. Ion Processes*, 98 (1990) 1.
- 15 P. Köfel, M. Alleman, H. Kellerhals and K.P. Wanczek, *Int. J. Mass Spectrom. Ion Processes*, 72 (1986) 53.
- 16 R.T. McIver, Jr., R.L. Hunter and W.D. Bowers, *Int. J. Mass Spectrom. Ion Processes*, 64 (1985) 67.
- 17 D.F. Hunt, J. Shabanowitz, J.R. Yates, III, P.R. Griffin and N.-Z. Zhu, *Anal. Chim. Acta*, 225 (1989) 1.
- 18 W.G. Millen, J.T. Meek, G.W. Stockton, M.L. Thomson and R.S. Wayne, in *Proceedings of 36th ASMS Conference on Mass Spectrometry and Allied Topics*, San Francisco, CA, June 5–10, 1988, p. 1247.
- 19 C.B. Lebrilla, I.J. Amster and R.T. McIver, Jr., *Int. J. Mass Spectrom. Ion Processes*, 87 (1989) R7.
- 20 P. Köfel, M. Alleman, H. Kellerhals and K.P. Wanczek, *Int. J. Mass Spectrom. Ion Processes*, 65 (1985) 97.
- 21 J.M. Alford, P.E. Williams, D.J. Trevor and R.E. Smalley, *Int. J. Mass Spectrom. Ion Processes*, 72 (1986) 33.
- 22 S.C. Beu and D.A. Laude, *Int. J. Mass Spectrom. Ion Processes*, 97 (1990) 295.
- 23 D.F. Hunt, J. Shabanowitz, R.T. McIver, R.L. Hunter and J.E.P. Syka, *Anal. Chem.*, 57 (1985) 765.
- 24 M. Bamberg and K.P. Wanczek, in *Proceedings of the 37th ASMS Conference on Mass Spectrometry and Allied Topics*, Miami Beach, FL, May 21–26, 1989, p. 456.
- 25 P. Grossmann, P. Caravatti, M. Alleman and H. Kellerhals, in *Proceedings of the 36th ASMS Conference on Mass Spectrometry and Allied Topics*, San Francisco, CA, 1988, p. 616.
- 26 L. Van Vaeck, W. Van Roy, H. Struyf, F. Adams and P. Caravatti, *Rapid Commun. Mass Spectrom.*, in press.
- 27 L. Van Vaeck, J. Bennett, W. Lauwers, A. Vertes and R. Gijbels, *Mikrochim. Acta*, III (1990) 283.
- 28 S.C. Beu and D.A. Laude, Jr., *Int. J. Mass Spectrom. Ion Processes*, 104 (1991) 109.
- 29 P. Caravatti, *US Pat.*, 4 924 089 (1990).



# Simultaneous multi-element analysis of solid samples by laser ablation–microwave-induced plasma optical emission spectrometry

L. Hiddemann, J. Uebbing, A. Ciocan, O. Dessenne and K. Niemax

*Institut für Spektrochemie und Angewandte Spektroskopie (ISAS), Bunsen-Kirchhoff-Str. 11, P.O. Box 101352, W-4600 Dortmund 1 (Germany)*

(Received 23rd November 1992; revised manuscript received 18th January 1993)

## Abstract

An experimental arrangement for multi-element microanalysis of solid samples by laser ablation–microwave-induced plasma optical emission spectrometry is introduced. The application of optical fibres as the interface between an échelle spectrograph and a gateable optical multi-channel detector head allows simultaneous measurements of up to ten elements with single laser shots and investigations of element correlations in samples from shot to shot. Correlation measurements of trace elements in steel and aluminium and sodium and lithium in high-purity quartz are given as examples.

*Keywords:* Laser ablation; Microwave-induced plasma; Optical-emission spectrometry; Solid samples; Trace elements

Focused laser radiation allows the ablation of small amounts of solid samples with spatial resolution limited by the diffraction of the laser radiation. Therefore, it is a microanalytical technique of moderate resolution. Under optimum conditions (short laser wavelength and focusing lens of short focal length), spatial areas of the sample with a diameter of a few micrometres can be analysed [1–3].

This paper discusses the experimental conditions and instrumentation for matrix-independent, precise and accurate simultaneous multi-element microanalysis with single laser shots. Application of the technique is demonstrated by multi-element analysis of trace elements in glass and metallic matrices, and by microanalytical correlation measurements of trace elements in

metallic matrices and in synthetic, high-purity quartz.

## EXPERIMENTAL

### *Conditions for quantitative elemental analysis*

The basic conditions for accurate element analysis by laser ablation (LA) are that the ablated material must have the stoichiometric composition of the solid sample irradiated by the focussed laser beam and the material has to be atomized completely. The first condition can be fulfilled by the application of lasers with short pulses, e.g., lasers with pulse lengths of a few nanoseconds. The material (particles, droplets and vapour) is ejected from the surface of the sample in a plasma burst. As long irradiation times and heating of the sample, e.g., with continuous-wave lasers, would favour fractional evaporation, short pulses are essential. The second

*Correspondence to:* K. Niemax, Institut für Spektrochemie und Angewandte Spektroskopie, Bunsen-Kirchhoff-str. 11, P.O. Box 101352, W-4600 Dortmund 1 (Germany).

condition requires a hot plasma in which the droplets and particles ejected from the sample are introduced and completely vaporized. If samples are ablated into a buffer gas atmosphere, e.g., a noble gas, there is also plasma breakdown in the buffer gas and heating of this plasma by laser radiation just above the irradiated region of the sample surface. This buffer gas plasma serves as the atomizer. Complete atomization can be proved by investigations of the spatial and temporal distribution of atomized sample material [4] and of the radial distribution of the plasma temperature [5] and electron density [6]. It has been shown that there is an optimum pressure of the buffer gas for analytical applications [7–9]. If the pressure is too low, laser heating is not efficient and the atomization may be not complete. If the pressure is too high, the viscosity of the buffer gas plasma is too large and fewer particles and droplets ejected from the surface of the sample penetrate into the buffer gas plasma. For example, with argon as a buffer gas the optimum pressure for analytical applications was found to be in the range 100–250 hPa [7–9].

The analytical radiation source used in this work was a Bennakker-type microwave-induced plasma (MIP) continuously operating in a low-pressure argon gas flow (200 hPa) through a quartz capillary [10,11]. An Nd: YAG laser pulse (pulse length ca. 5 ns) ablates microsamples from solids and atomizes the material inside the MIP. Depending on the matrix and the ablated mass, the MIP conditions are affected only for typical 100–200  $\mu\text{s}$ , but emission from the analytes can be observed for several milliseconds (time of transport through the MIP) [10].

With laser ablation–microwave-induced plasma optical emission spectrometry (LA–MIP–OES), low detection limits can be obtained. Depending on the element and the matrix, detection limits for single laser shots as low as  $0.3 \mu\text{g g}^{-1}$  have been obtained [12].

#### *Arrangement for simultaneous microanalysis of solid samples*

The experimental arrangement included an Nd: YAG laser ( $\lambda = 1.06 \mu\text{m}$ ), sample cell, gas-handling system, the MIP and gateable optical

multi-channel detector as described in recent papers [10–12]. However, there is an important improvement in the present apparatus that allows simultaneous multi-element detection by single laser shots. Instead of a Czerny–Turner-type monochromator, a 0.5-m échelle spectrograph (Carl Zeiss, Jena) is now used. The experimental half-widths of the apparatus function of the échelle instrument are, for example, about 15 and 10 pm at 300 nm (80th order) and 200 nm (120th order), respectively. In this system, 149 optical fibres are set to selected spectral lines in the focal plane. Up to ten of these fibres can be plugged simultaneously into an array holder. The radiation guided through the fibres is imaged by a large-aperture quartz lens system on to the sensitized detector head (IRY 1024SB) of the multi-channel analyser (OSMA; Stanford Instruments), which allows time-resolved measurements. The measurement of the intensities started typically 200  $\mu\text{s}$  after the ablation process and the gate width of the detector was in the range 2–8 ms.

The net intensities of the analyte lines were measured by subtraction of the intensities without a laser shot from the intensity measurement with laser ablation. In order to look for spectral interferences, the spectral range near the analyte lines could be measured by scanning the camera mirror of the spectrometer with a step motor (about 0.5 pm per step).

The focus diameter of the Nd: YAG laser beam on the sample surfaces was about 100–150

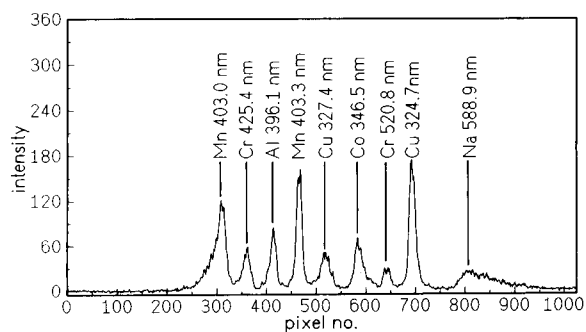


Fig. 1. Simultaneous, time-gated intensity measurement of nine different lines by an optical multi-channel analyser. Only one laser shot was applied to a nickel sample.

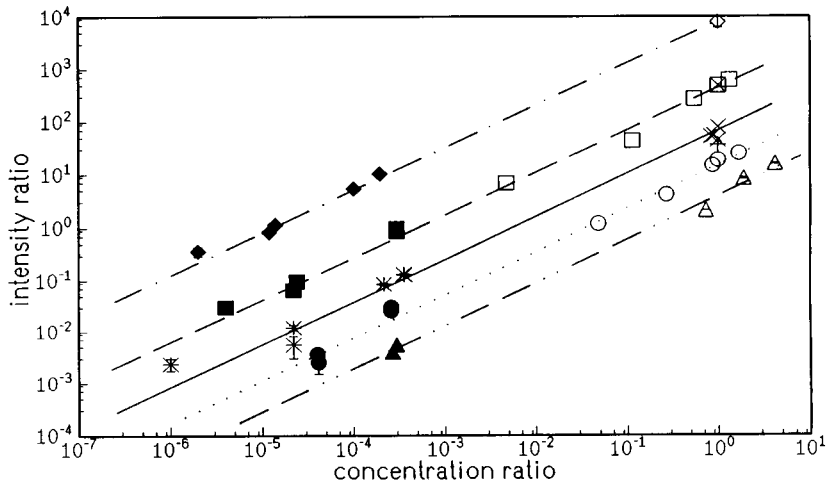


Fig. 2. Simultaneously measured calibration graphs for Be/Cu (diamonds, dashed-dotted line), Mg/Cu (squares, dashed line), Cr/Cu (crosses, full line), Al/Cu (circles, dotted line) and Mn/Cu (triangles, double dashed-dotted line). The Cu line at 327.3 nm was used as a reference. The Be, Mg, Cr, Al and Mn wavelengths are given in the text. For better graphical representation, the Be/Cu, Cr/Cu and Mn/Cu data are multiplied by factors of 10, 2 and 0.1, respectively. Matrices: ( $\diamond$ ,  $\blacksquare$ ,  $*$ ,  $\bullet$ ,  $\blacktriangle$ ) copper; ( $\square$ ,  $\times$ ,  $\circ$ ,  $\triangle$ ) nickel; ( $\langle$ ,  $\boxtimes$ ,  $+$ ) borax glass.

$\mu\text{m}$ , which allowed microanalysis with moderate spatial resolution.

## RESULTS AND DISCUSSION

### Calibration graphs for multi-element analysis

Figure 1 shows, as an example, simultaneous intensity measurements of six elements with the

échelle spectrometer and the OSMA detector using nine out of the ten channels. The intensities for manganese ( $2700 \mu\text{g g}^{-1}$ ), copper ( $650 \mu\text{g g}^{-1}$ ), aluminium ( $1100 \mu\text{g g}^{-1}$ ), cobalt ( $8200 \mu\text{g g}^{-1}$ ), sodium (concentration not specified) and chromium ( $550 \mu\text{g g}^{-1}$ ) were obtained with one laser shot on a nickel sample (17519 G; Willan Metals, Rotterdam, UK). The intensity distributions of the Mn 403.0-nm and Na 588.9-nm lines

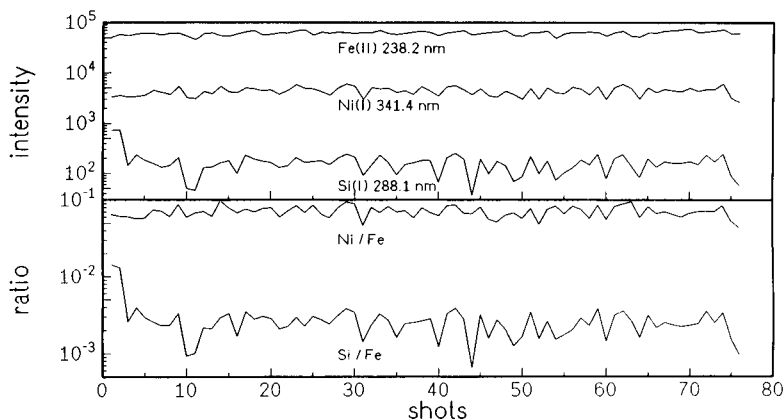


Fig. 3. Top: simultaneous intensity measurements of an iron, a nickel and a silicon line as a function of single laser shots applied to a low-alloy steel sample. Bottom: corresponding Ni/Fe and Si/Fe intensity ratios.

in the outer channels are asymmetric due to image defects.

Similar measurements were made with samples of various matrices (steel, copper, aluminium, nickel and borax glass) in order to obtain calibration graphs for multi-element analysis. For example, multi-element calibration graphs for Be (313.0 nm)/Cu, Mn (257.6 nm)/Cu, Al (396.1 nm)/Cu, Cr (425.4 nm)/Cu and Mg (279.5 nm)/Cu measured simultaneously in copper, nickel and borax glass matrices are shown in Fig. 2. Samples from Kabel und Metallwerk (Osnabrück) (copper), Willan Metals (nickel) and Hoesch (Dortmund) (borax) were used. The copper reference line selected for calibration was 327.3 nm. The slopes of the calibration graphs are ca. 0.9. The deviation from unit slope is due to a slight optical thickness of the copper line in the data from the copper samples (full symbols and \* in Fig. 2). Note that optically thick copper lines lead to analyte/copper intensity ratios that are systematically too large.

#### Correlation measurements in steel and aluminium

Figure 3 (top) shows intensity measurements for nickel ( $510 \mu\text{g g}^{-1}$ ) and silicon ( $250 \mu\text{g g}^{-1}$ ) together with iron ( $0.992 \text{ g g}^{-1}$ ) obtained with the first 76 shots on a low-alloy steel sample (NBS 1166). It can be seen that, from the first shot on, the signals of nickel and iron were constant within the experimental uncertainties. Taking into ac-

count the data for these 76 shots, the relative standard deviations (R.S.D.s) of single-shot detection for iron and nickel were 9% and 19%, respectively. For silicon, the intensities of the first two shots were significantly larger than the average intensity of the following shots (R.S.D. 34%). Measurements at different positions on sample 1166 gave qualitatively the same results. The data indicate that from the first shot the amount of steel ablated by the laser was constant. The higher silicon signal of the first shots was due to contamination of the sample surface. The mass ablated by a single shot estimated from measurements with an optical microscope was about 75 ng.

Figure 3 (bottom) shows plots of the Ni/Fe and Si/Fe ratios. The R.S.D.s calculated for the ratios for single shots were 17% and 31% for Ni/Fe and Si/Fe, respectively. This means that the R.S.D.s of the ratios are smaller than the corresponding single-shot standard deviations of the nickel and silicon intensities, owing to compensation for the fluctuations in the ablation process.

Figure 4 shows the data for the same elements as in Fig. 3 for a high-alloy steel sample (RU 11 by Dillinger Hüttenwerke). The composition is nickel  $2.95 \text{ mg g}^{-1}$ , silicon  $5.2 \text{ mg g}^{-1}$  and iron  $0.85 \text{ g g}^{-1}$ . Here the laser needed about ten shots to produce, within the limits of uncertainty, constant intensities for the matrix element iron and the minor constituent nickel and silicon (see top diagram in Fig. 4). Obviously the amount of ab-

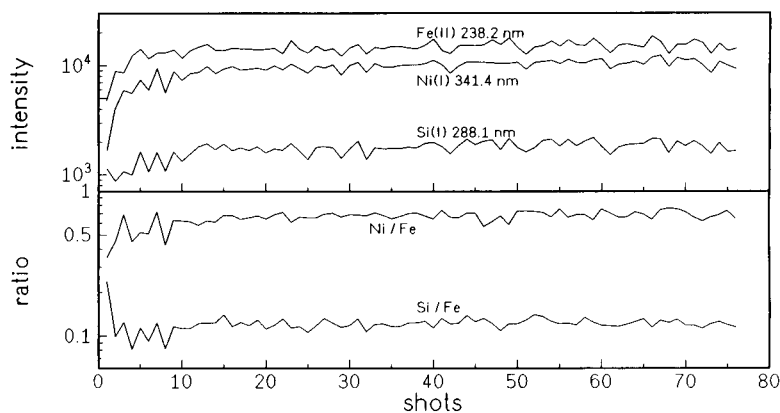


Fig. 4. Top: simultaneous intensity measurements of an iron, a nickel and a silicon line as a function of single laser shots on a high-alloy steel sample. Bottom: corresponding Ni/Fe and Si/Fe intensity ratios.

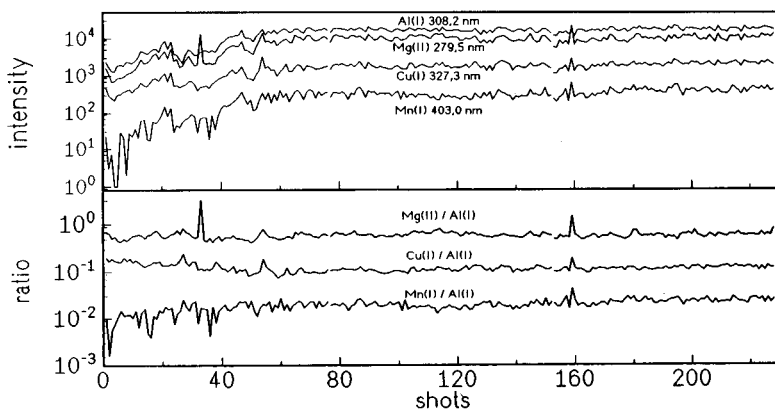


Fig. 5. Top: simultaneous intensity measurements of aluminium, magnesium, copper and manganese as a function of single laser shots on an aluminium sample. Bottom: corresponding Mg/Al, Cu/Al and Mn/Al intensity ratios.

lated matrix material increased for the first shots. The Ni/Fe ratios are given in the bottom diagram in Fig. 4. It is interesting to see that the scatter of the intensity ratios is significantly larger for the first ten shots than for the later shots. It is concluded that it took more shots for high- than for low-alloy steel to produce the final shape of the shallow crater which guarantees reproducible laser ablation.

Taking into account the signal from the 11th to the 76th shots, the R.S.D.s of the iron, nickel and silicon signals for single laser shots were 10%, 12% and 14%, respectively. The R.S.D.s for the Ni/Fe and Si/Fe ratios were found to be about 8% each.

Successive single-shot measurements on an aluminium sample (Pechiney 1211) are shown in Fig. 5. The line intensities of magnesium (8 mg

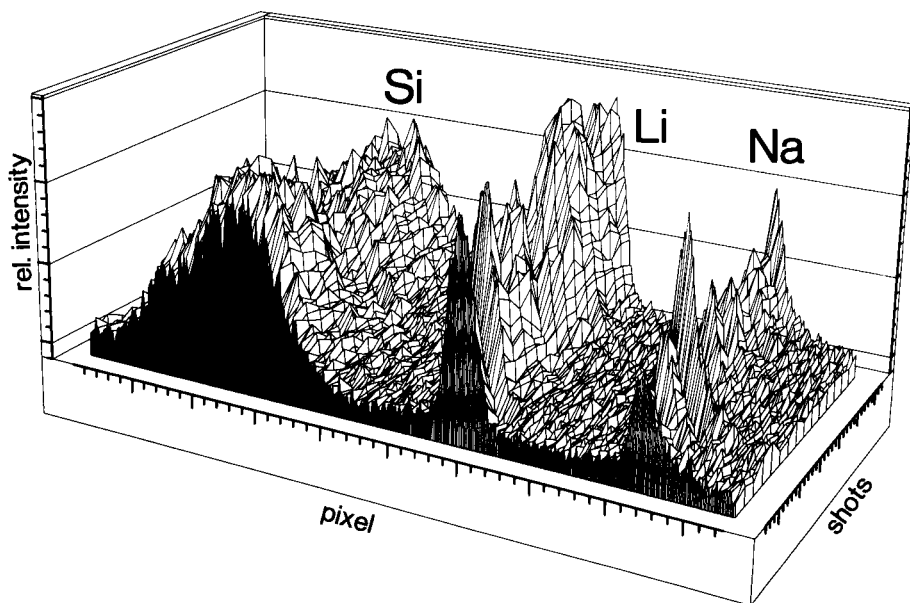


Fig. 6. Simultaneous intensity measurements of silicon (212.41 nm), lithium (670.78 nm) and sodium (588.99 nm) lines as a function of sixteen successive laser shots on a high-purity quartz sample.

$\text{g}^{-1}$ ), copper ( $35 \text{ mg g}^{-1}$ ), manganese ( $10 \text{ mg g}^{-1}$ ) and the matrix element aluminium were recorded simultaneously. About 150 ng per shot was ablated from the sample. It took about 50 shots to obtain constant ablation (top diagram in Fig. 5), whereas the Mg/Al, Cu/Al and Mn/Al ratios were almost constant from the beginning (bottom diagram in Fig. 5). However, as with high-alloy steel (Fig. 4), the scatter of the intensity data was larger at the beginning of the ablation. It is believed that the relatively slow equilibration of the ablation process is due to oxidation of the sample surface. Other aluminium samples showed qualitatively the same behaviour.

Taking into account 76 shots in the range of constant intensities, the R.S.D.s of the single-shot intensities were about 10% (Al), 15% (Mg), 14% (Cu) and 19% (Mn), and the R.S.D.s for the ratios were found to be 10% (for Mg/Al and Cu/Al) and 15% (Mn/Al).

#### *Measurements of sodium and lithium in high-purity quartz*

Recently preliminary measurements were made on sodium in high-purity quartz used for the production of optical fibres [11]. In particular sodium but also lithium are the most critical contaminants, which act as catalysts for the diffu-

sion of hydrogen in quartz. In turn, hydrogen forms Si–OH and Ge–OH bonds, both of which cause absorption losses at the diode laser wavelengths of 1.3 and 1.55  $\mu\text{m}$  used for telecommunication [13]. In recent measurements relatively large fluctuations of the sodium concentration were observed depending on the number of shots applied to the quartz samples. Therefore, it was of interest to study this behaviour from shot to shot in more detail. Further, using the échelle spectrometer it was now possible to study sodium simultaneously with the concentration of lithium and the matrix element silicon.

The relative intensities of sodium, lithium and silicon for sixteen successive shots are shown in Fig. 6. As the alkali metal concentrations were very low, it was necessary to increase the pulse power of the Nd:YAG laser to about 30 mJ per pulse. At this power, depending on the depth of the crater, about 4–35 ng were ablated with one shot (see below) and the depth of the crater increased about 0.5  $\mu\text{m}$  per shot on average. The integrated intensities of the following lines were measured: 588.99 nm (sodium), 670.78 nm (lithium) and 212.41 nm (silicon). Whereas the intensity of the silicon line varied only slightly from shot to shot (R.S.D. 14%), the differences for the lithium and sodium signals were much

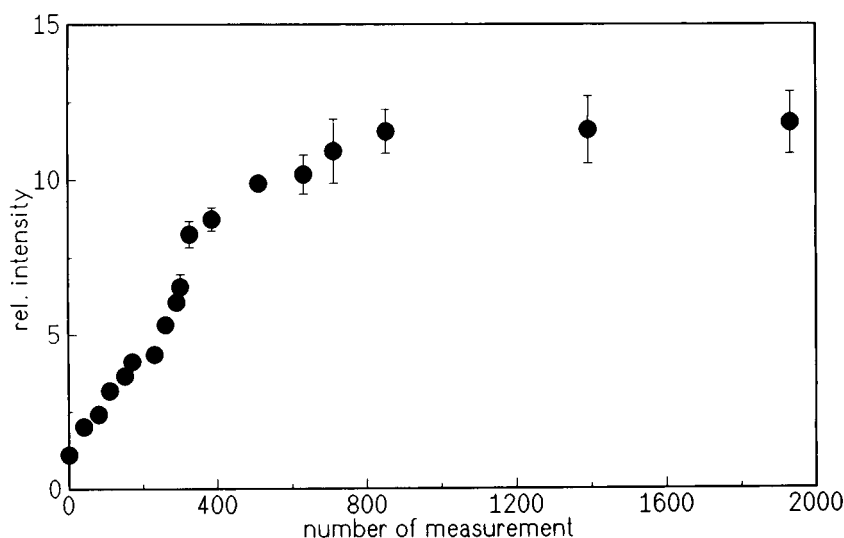


Fig. 7. Intensity of an optically thin silicon line as a function of single laser shots on a synthetic quartz sample.

larger (R.S.D.s: lithium 75% and sodium 60%). Obviously there are inhomogeneous distributions of sodium and lithium in the synthetic quartz. However, it is of interest that there are no visible correlations of the lithium and sodium signals, i.e., the distributions of sodium and lithium are independent of each other.

Figure 7 shows the intensity of the silicon line measured over 1930 single shots. As the intensity is proportional to the mass ablated by the laser, the measurement indicated that the amount of material increases as a function of the shot number and reaches, within the limits of uncertainty, a constant value at about 800 shots. This behaviour is different from that observed with metallic matrices, e.g., steel or aluminium (see Figs. 4 and 5). It is due to the formation of a narrow and deep crater in quartz. After 2000 shots the crater diameter was about 240  $\mu\text{m}$  and its depth about 1 mm. With quartz the laser pulses shiver the sample into small pieces around the irradiated area, but with metals the crater area melts, and therefore laser craters are much wider than in quartz at comparable depths.

Despite the strong dependence of the ablated mass on the depth of the crater, and except for the first shots where surface contamination by alkali metals could be observed [11], the average of the Na/Si and Li/Si intensity ratios were constant within the limits of experimental uncertainty. In order to determine the sodium and lithium concentration in four quartz samples, company standards by Alusuisse with known Na/Si and Li/Si concentrations and five quartz standards from fibre-producing company were used. The sodium and lithium concentrations in the quartz standards were 0.5–1.1 and 0.6–3.4  $\mu\text{g g}^{-1}$ , respectively. These data were measured in the chemical laboratories of the company by inductively coupled plasma optical emission spectrometry (ICP-OES), taking great care to avoid alkali metal contamination in the dissolution process of the quartz. Figure 8 shows the calibration data for the Na/Si ratio from the aluminium samples and the standard quartz samples. A calibration line with a slope of unity was constructed, giving a higher statistical weight to the quartz measurements. Nevertheless, taking into account

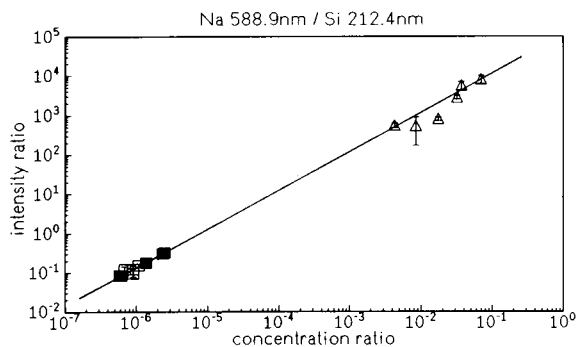


Fig. 8. Na/Si intensity ratio as a function of the Na/Si concentration ratio. Calibration data:  $\Delta$  = aluminium standard and  $\square$  = quartz standard;  $\blacksquare$  = data for unknown quartz samples.

the statistical error bars, only one value of the aluminium measurements is clearly off the calibration line. Note that the calibration line covers five orders of magnitude. The data for the four unknown quartz samples are plotted on the calibration line. The sodium concentrations determined in the unknown samples were in the range 0.6–2.5  $\mu\text{g g}^{-1}$ .

The results of the lithium measurements are given in Fig. 9. As in the sodium measurement, the data for the quartz standards were given a high statistical weight and a calibration line with a slope of unity was determined. As the scatter of the aluminium data was larger than that in the sodium calibration (Fig. 8) and the values for two quartz standards did not fit with the other data in

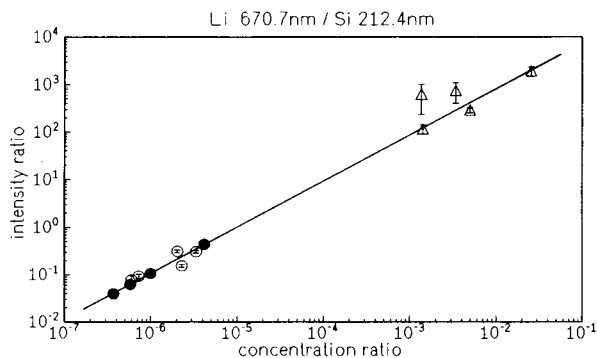


Fig. 9. Li/Si intensity ratio as a function of the Li/Si concentration ratio. Calibration data:  $\Delta$  = aluminium standard and  $\circ$  = quartz standard;  $\bullet$  = data for unknown quartz samples.

the calibration, the uncertainty of the calibration for lithium can be regarded as larger than that for sodium. The lithium concentrations in the four unknown quartz samples were found to be in the range 0.4–4.2  $\mu\text{g g}^{-1}$ .

The single-shot detection limits ( $3\sigma$  criterion) for sodium and lithium in quartz were ca. 35 and 70  $\text{ng g}^{-1}$ , respectively. As expected from statistics, the detection limits decreased with increasing number of shots  $N$  as  $N^{-1/2}$ .

### Conclusions

Correlation measurements of different species in steel, aluminium and quartz were performed by LA-MIP-OES. It has been shown that time-gated simultaneous measurements of line intensities not only allow rapid, matrix-independent multi-element bulk analysis of solid samples but also reduce statistical and systematic uncertainties. On the other hand, as LA-MIP-OES offers very low detection limits, simultaneous recording of intensities with single laser shots permits powerful microanalyses of moderate spatial resolution.

The authors gratefully acknowledge financial support by the Deutsche Forschungsgemeinschaft, the Bundesministerium für Forschung und

Technologie and the Ministerium für Wissenschaft und Forschung (Nordrhein-Westfalen).

### REFERENCES

- 1 E.H. Piepmeier, in E.H. Piepmeier (Ed.), *Analytical Applications of Lasers*, Wiley, New York, 1986, p. 627.
- 2 D.A. Cremers and L.J. Radziemski, in L.J. Radziemski, R.W. Solarz and J.A. Paisner (Eds.), *Laser Spectroscopy and Its Applications*, Dekker, New York, 1987, p. 351.
- 3 L. Moenke-Blankenburg, *Laser Micro Analysis*, Wiley, New York, 1989.
- 4 W. Sdorra and K. Niemax, *Spectrochim. Acta*, Part B, 45 (1990) 917.
- 5 W. Sdorra, J. Brust and K. Niemax, *Mikrochim. Acta*, 108 (1992) 1.
- 6 X.Z. Zhao, L.J. Shen, T.X. Lu and K. Niemax, *Appl. Phys. B*, 55 (1992) 327.
- 7 F. Leis, W. Sdorra, J.B. Ko and K. Niemax, *Mikrochim. Acta*, II (1989) 195.
- 8 W. Sdorra, A. Quentmeier and K. Niemax, *Mikrochim. Acta*, II (1989) 201.
- 9 W. Sdorra and K. Niemax, *Mikrochim. Acta*, 107 (1992) 319.
- 10 J. Uebbing, A. Ciocan and K. Niemax, *Spectrochim. Acta*, Part B, 46 (1992) 601.
- 11 A. Ciocan, L. Hiddemann, J. Uebbing and K. Niemax, *J. Anal. At. Spectrom.*, in press.
- 12 A. Ciocan, J. Uebbing and K. Niemax, *Spectrochim. Acta*, Part B, 46 (1992) 611.
- 13 M. Ogai, A. Iino and K. Matsubara, *J. Lightwave Technol.*, 5 (1987) 611.



# Determination of arsenic speciation by liquid chromatography–hydride generation inductively coupled plasma atomic emission spectrometry with on-line UV photooxidation

R. Rubio, A. Padró, J. Albertí and G. Rauret

*Departament de Química Analítica, Universitat de Barcelona, Avda. Diagonal 647, 08028 Barcelona (Spain)*

(Received 13th October 1992; revised manuscript received 4th January 1993)

## Abstract

The determination is described of the six arsenic species arsenite, arsenate, monomethylarsonate (MMA), dimethylarsinate (DMA), arsenobetaine and arsenocholine by hydride generation inductively coupled plasma atomic emission spectrometry after liquid chromatographic separation and on-line photooxidation. An anion-exchange polymer-based column is used for separation. The details of the photoreactor designed to transform arsenobetaine and arsenocholine into simpler species that can be reduced are presented. The reducing conditions to obtain the arsine from arsenate (as the final product of the photooxidation process) are optimized. The overall assembly is presented and using the optimized operating conditions the quality parameters (detection limits, precision and accuracy) for all the arsenic species are reported. These parameters for arsenite, arsenate, MMA and DMA are compared with those obtained without photooxidation. The introduction of a new step on-line in the coupling does not produce any loss of quality of information or a significant increase in analysis time.

**Keywords:** Atomic emission spectrometry; Liquid chromatography; Inductively coupled plasma spectrometry; Arsenic; Speciation; Waters

To determine the speciation of arsenic, several coupled techniques have been proposed. Some of them use the direct coupling between liquid chromatography (LC) and inductively coupled plasma atomic emission spectrometry (ICP-AES) [1–5], but the detection limits achieved are not low enough to apply this combination to environmental analysis. Recently, ICP mass spectrometry (MS) [6–11] has been applied successfully but the technique is not available in many laboratories and even if it is the cost is too high to use it in routine analysis. Other workers have proposed

postcolumn generation of the volatile hydrides of the arsenic species before detection by atomic absorption spectrometry (AAS) [12–14] or ICP-AES [15–17] in order to reach lower detection limits.

The coupled technique LC–hydride generation (HG)–ICP-AES allows the determination of arsenite, arsenate, MMA and DMA, as all these species are able to generate the corresponding arsine by reduction. However, neither arsenobetaine nor arsenocholine can be reduced to arsines. Some workers have reported the decomposition of arsenocholine and arsenobetaine by means of thermo-hydride generation [18] or of arsenobetaine by means of a photolytic process [19]. Recently, the decomposition of these two

*Correspondence to:* G. Rauret, Departament de Química Analítica, Universitat de Barcelona, Avda. Diagonal 647, 08028 Barcelona (Spain).

arsenic compounds was achieved by means of a UV photooxidation process, yielding simpler species and if the oxidation is completed, As(V) is obtained, which can be reduced to arsine [20]. The next challenge was the coupling of the photoreactor on-line for the determination of the six arsenic species in order to obtain a reliable and inexpensive system that can be used in routine analysis.

This paper presents the optimum coupling conditions to introduce the photooxidation process on-line between LC elution and hydride generation. The optimum conditions for the separation step were established using different columns and elution systems.

The conditions for subsequent photooxidation and hydride generation were also optimized and the performance parameters (detection limits, short- and long-term precision and recoveries) were studied for the six arsenic compounds using the coupled LC–UV–HG–ICP/AES technique.

## EXPERIMENTAL

### Apparatus

**LC system.** A Perkin-Elmer 250 LC binary gradient pump was used. The anion-exchange column was Hamilton PRP X-100, 10- $\mu\text{m}$  particle size (250 mm  $\times$  4.1 mm i.d.). A Rheodyne Model 7125 injector with a 100- $\mu\text{l}$  loop was employed.

**Photoreactor.** A Heraeus TNN 15/32 low-pressure mercury vapour lamp (254 nm, o.d. 2.5 cm, length 17 cm, 15 W) placed inside a PVC tube (i.d. 7.5 cm) with the inner wall and the ends covered with aluminium foil was used. PTFE tubing (9.5 m  $\times$  0.35 mm i.d.) and a Gilson Minipuls 3 peristaltic pump were used. The photoreactor is shown in Fig. 1.

**Hydride generation (HG) system.** The system used was a Varian VGA-76 with the sample channel connected to the outlet of the LC system or of the photoreactor.

**ICP-AES.** The instrumentation consisted of a Plasmatherm source (27.12 MHz) operating at 1 kW, a Jobin Yvon thermoregulated monochromator with a holographic grating (2400 grooves  $\text{mm}^{-1}$ ), focal length 1 m, resolution 0.1  $\text{\AA}$ , 80/45-

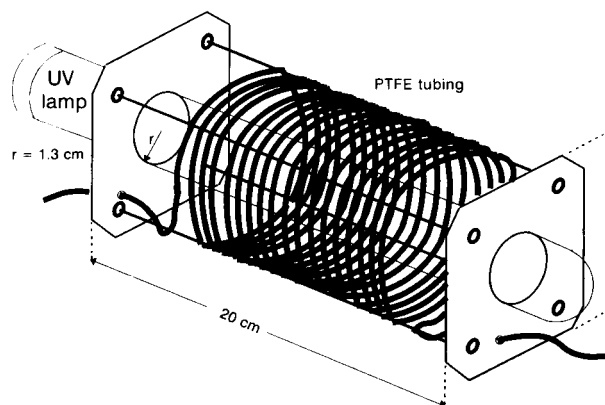


Fig. 1. Scheme of the photoreactor.

$\mu\text{m}$  slits. Argon was used as the coolant and carrier gas. The wavelength was 193.696 nm. Data acquisition and processing were carried out as described [16].

### Reagents and solutions

Stock standard solutions of arsenic compounds (1000 mg  $\text{As l}^{-1}$ ) were prepared as follows: arsenite,  $\text{As}_2\text{O}_3$  (Merck) primary standard, was dissolved in NaOH (4 g  $\text{l}^{-1}$ ); arsenate,  $\text{Na}_2\text{HAsO}_4 \cdot 7\text{H}_2\text{O}$  (Carlo Erba), was dissolved in water; monomethylarsonate,  $\text{CH}_3\text{AsO}(\text{ONa})_2 \cdot 6\text{H}_2\text{O}$  (Carlo Erba), was dissolved in water; dimethylarsinate,  $(\text{CH}_3)_2\text{AsNaO}_2 \cdot 3\text{H}_2\text{O}$  (Fluka), was dissolved in water; arsenocholine (AsChol),  $(\text{CH}_3)_3\text{As}^+\text{CH}_2\text{CH}_2\text{OHBr}^-$  and arsenobetaine (AsBet),  $(\text{CH}_3)_3\text{As}^+\text{CH}_2\text{COO}^-$ , were supplied by the Service Central d'Analyse, CNRS (Vernaison, France).

For the mobile phases, phosphate buffers prepared from  $\text{NaH}_2\text{PO}_4 \cdot \text{H}_2\text{O}$  (Carlo Erba) and  $\text{Na}_2\text{HPO}_4 \cdot 2\text{H}_2\text{O}$  (Carlo Erba) were dissolved in water and these solutions were filtered through a 0.22- $\mu\text{m}$  membrane filter.

Solutions of peroxodisulphate,  $\text{K}_2\text{S}_2\text{O}_8$  (Fluka), dissolved in the NaOH solution, and  $\text{NaBH}_4$  (Alfa Venton), 1% in 0.5% NaOH, were prepared immediately before use.

All solutions were prepared using doubly deionized water (Culligan Ultrapure GS) of 18.3  $\text{M}\Omega$  cm resistivity.

### Procedure

A 100- $\mu$ l volume of sample solution was injected on to the Hamilton PRP X-100 column and a gradient was applied using a flow-rate of 1 ml min<sup>-1</sup>. As mobile phases solution A (NaH<sub>2</sub>PO<sub>4</sub>-Na<sub>2</sub>HPO<sub>4</sub>, 20 mmol l<sup>-1</sup>, pH 5.75) and solution B (NaH<sub>2</sub>PO<sub>4</sub>-Na<sub>2</sub>HPO<sub>4</sub>, 100 mmol l<sup>-1</sup>, pH 5.75) were used with the following gradient programme: 100% A for 2 min, decreasing to 50% A in 0.1 min, this ratio maintained for 3 min, then to 100% A in 0.1 min and maintained for 7 min. The eluate was introduced into a photoreactor connected to the outlet of the column with addition of 3% K<sub>2</sub>S<sub>2</sub>O<sub>8</sub> in 3% NaOH (0.2 ml min<sup>-1</sup>) as photooxidation reagent. The stream emerging from the photoreactor was introduced into the hydride generation system, which was connected to the outlet of the photoreactor. As hydride generation reagents, 8 mol l<sup>-1</sup> HCl (1 ml min<sup>-1</sup>) and 1% NaBH<sub>4</sub> in 0.5% NaOH (1 ml min<sup>-1</sup>) were used. The resulting solution reached the gas-liquid separator and then the plasma torch.

## RESULTS AND DISCUSSION

### Separation conditions

Once the optimization of the photooxidation process had been established [20], efforts were made to improve the separation conditions for the six arsenic species to be determined.

The separation conditions for arsenite, arsenate, MMA, DMA, AsBet and AsChol were studied with a polymer-based anion-exchange column [Hamilton PRP X-100, poly(styrene-divinyl benzene)trimethylammonium exchanger]. The separation of the six arsenic species was studied using phosphate buffer as eluent at different pH values and different concentrations. In Figure 2 the variation of the retention times with pH for the arsenic species is shown. From this study a pH of 5.75 was chosen for further separation. The concentration of the phosphate buffer had no significant effect on the resolution of the less retained components.

With this column only five compounds can be separated as AsBet co-elutes with arsenite. Nev-

ertheless, if arsenite occurs in a sample two independent determinations are recommended, one using the photooxidation step and the other with the UV lamp switched off. Figure 3 shows the chromatograms corresponding to these two determinations. The major advantage of this column is its long life time and it was observed that using the conditions described here about 600 injections can be performed without a significant decrease in resolution.

### Photoreactor

The design was developed to be easily coupled on-line between the exit of the LC column and the entrance to the reduction chamber. The length and inner diameter of the PTFE coil and the flow-rate were considered in order to minimize the broadening of the chromatographic peaks, as

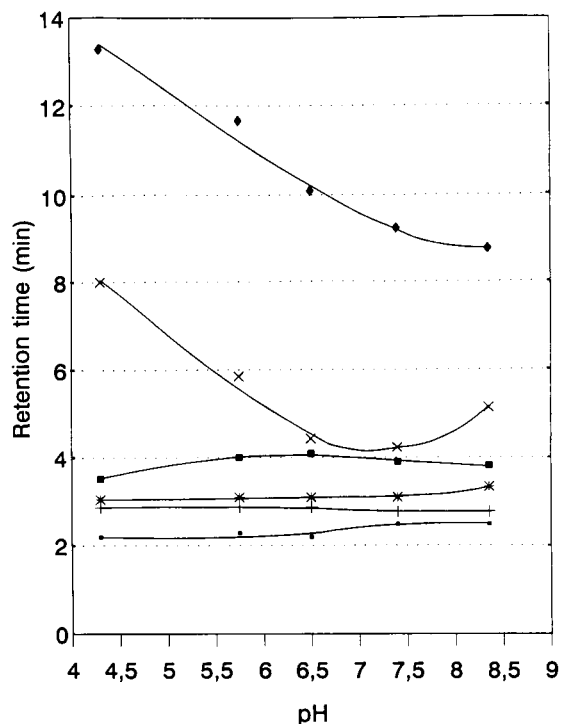


Fig. 2. Retention time of six arsenic species versus pH using the Hamilton PRP X-100 column and 20 mmol l<sup>-1</sup> phosphate buffer with the LC-ICP-AES system. ● = AsChol; + = AsBet; ■ = DMA; × = MMA; \* = arsenite; ◆ = arsenate.

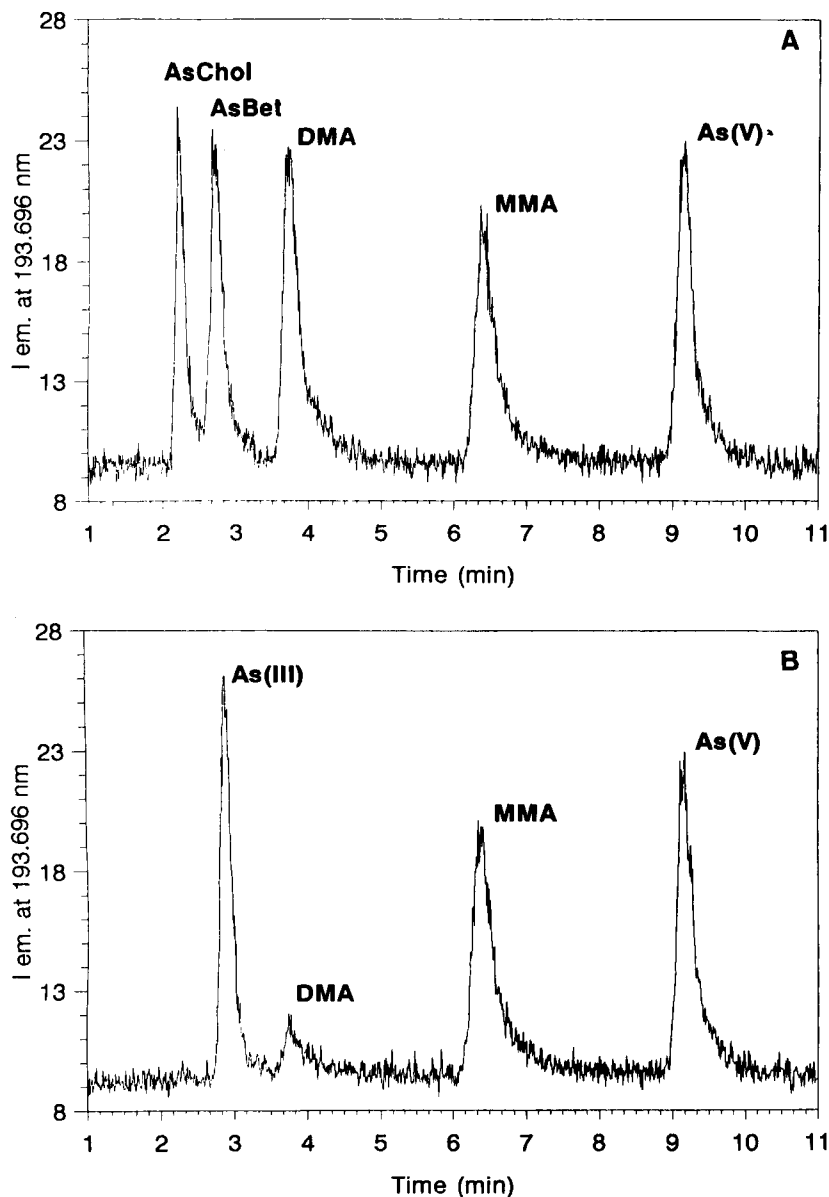


Fig. 3. (A) Chromatogram obtained with the proposed procedure. The concentrations of AsChol, AsBet, DMA, MMA and arsenate are 100, 135, 160, 160 and 160  $\mu\text{g As l}^{-1}$ , respectively. (B) Chromatogram obtained with the proposed procedure but with the UV lamp switched off. The concentrations of arsenite, DMA, MMA and arsenate are 80, 160, 160 and 160  $\mu\text{g As l}^{-1}$ , respectively. AsBet and AsChol are also present in the sample at 135 and 100  $\mu\text{g As l}^{-1}$ .

this depends on  $L$ ,  $r$  and  $\phi$  [21], according to the equation

$$\sigma_v^2 = k \frac{\pi r^4 L}{24 D_m} \phi$$

where  $r$  = internal radius of the capillary tube,

$L$  = capillary tube length,  $\phi$  = liquid flow-rate,  $D_m$  = molecular diffusion coefficient for analyte in the solvent and  $k$  = proportionality factor, which depends on the flow profile in the capillary tube.

The flow-rate from the separation system was

1 ml min<sup>-1</sup>. To avoid a significant increase in the band broadening, the flow-rate of peroxodisulphate solution was established as 0.2 ml min<sup>-1</sup>. For a fixed reactor volume the variance can be minimized when the length of the tube is increased and its inner diameter is reduced. Thus, 0.35 mm, the narrowest readily available PTFE tube, was chosen. The optimum length of the tube was determined by the time necessary to complete the photooxidation reaction. In a previous study [20], the conditions established for the total conversion of both AsBet and AsChol into arsenate were an irradiation time of 30 s and 1% of peroxodisulphate in the reaction medium. Under these conditions the generation of bubbles in the solution is a serious inconvenience as it increases the background noise. Therefore 0.5% peroxodisulphate was used in the reaction medium, which corresponds to the addition of 3% peroxodisulphate solution. Under these conditions the irradiation time established was 40 s, which corresponds to a capillary tube length of ca. 9 m.

#### Optimization of conditions for hydride generation

Although the conditions for arsine generation had been optimized in a previous study, it was necessary to establish these conditions again taking into account that after the photooxidation step all the arsenic species are converted into arsenate. Thus, HCl and H<sub>2</sub>SO<sub>4</sub> at different concentrations were applied in order to obtain the maximum signal-background ratio (SBR) for arsenate using a system without the photolytic device. The results are shown in Fig. 4, and the best values were obtained when HCl was used. The assay was repeated including the photooxidation process before hydride generation and using HCl at different concentrations. The SBR values obtained for different HCl concentrations were 2.61 (4 mol l<sup>-1</sup>), 3.05 (6 mol l<sup>-1</sup>), 3.16 (8 mol l<sup>-1</sup>) and 3.07 (10 mol l<sup>-1</sup>). It can be concluded that 8 mol l<sup>-1</sup> HCl gives the most efficient conversion of arsenate into arsine.

NaBH<sub>4</sub> at concentrations higher than 1% gives a considerable evolution of hydrogen, which increases the signal fluctuations and even causes

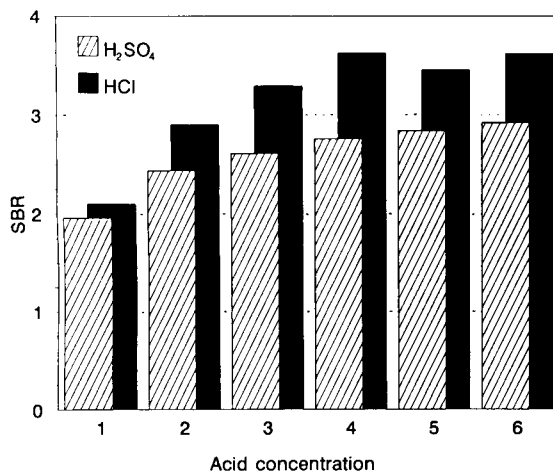


Fig. 4. Comparison of SBR obtained for 100 μg As l<sup>-1</sup> as arsenate using HCl and H<sub>2</sub>SO<sub>4</sub> at different concentrations in the hydride generation step of the LC-HG-ICP-AES system. The acid concentration is expressed as [H<sup>+</sup>] (mol l<sup>-1</sup>).

the extinction of the plasma [16], hence a concentration of 1% was chosen.

Different tubing lengths (80 and 150 cm × 0.35 mm i.d.) between the hydride generator and gas-liquid separator were tried, and no significant difference was observed; hence an 80-cm tubing length was used.

#### Determination of arsenic species under optimized conditions

Figure 5 shows the overall scheme of the LC-UV-HG-ICP-OES coupled system.

Figure 3A shows the chromatogram corresponding to the separation of arsenate, MMA, DMA, AsBet and AsChol using this system according to the proposed procedure. Figure 3B shows the separation of arsenate, arsenite, MMA and DMA in a sample that also contained AsBet and AsChol, using the same procedure but with the UV lamp switched off. Under these conditions the performance parameters were studied. In Tables 1–3 the results for the detection limits (LOD), short- and long-term precision and accuracy, obtained using the proposed procedure and those obtained with an LC-HG-ICP-AES system [16], are reported. The detection limits (Table 1) were calculated as twice the standard deviation

TABLE 1

Detection limits ( $\mu\text{g As l}^{-1}$ ) obtained for arsenic compounds using the two different methods.

As compound	LC-UV-HG-ICP-AES	LC-HG-ICP-AES
AsChol	6.1	–
AsBet	7.9	–
Arsenite	2.6 <sup>a</sup>	3.5
DMA	9.8	21.3
MMA	13.0	3.8
Arsenate	9.6	9.2

<sup>a</sup> LOD value obtained with UV lamp switched off.

(S.D.) of the background signal. The values are the means for three different days. Short-term precision (Table 2) was calculated with a solution approximately five times the LOD concentration, which was injected ten times on the same day, and the relative standard deviation (R.S.D.) was calculated. The R.S.D. values reported are the

TABLE 2

Short- and long-term precision

As compound	LC-UV-HG-ICP-AES		LC-HG-ICP-AES	
	Short-term R.S.D. (%)	Long-term R.S.D. (%)	Short-term R.S.D. (%)	Long-term R.S.D. (%)
AsChol	4.6	7.9	–	–
AsBet	4.9	5.4	–	–
Arsenite	–	–	4.3	5.4
DMA	6.8	6.6	5.4	5.9
MMA	6.3	6.1	3.8	4.3
Arsenate	5.2	6.1	5.3	5.8

means of three replicates. For long-term precision (Table 2) the same procedure was applied, but using three non-consecutive days, and the overall R.S.D. was calculated from the 30 values obtained. Accuracy values (Table 3) were calculated for a mineral water sample from the

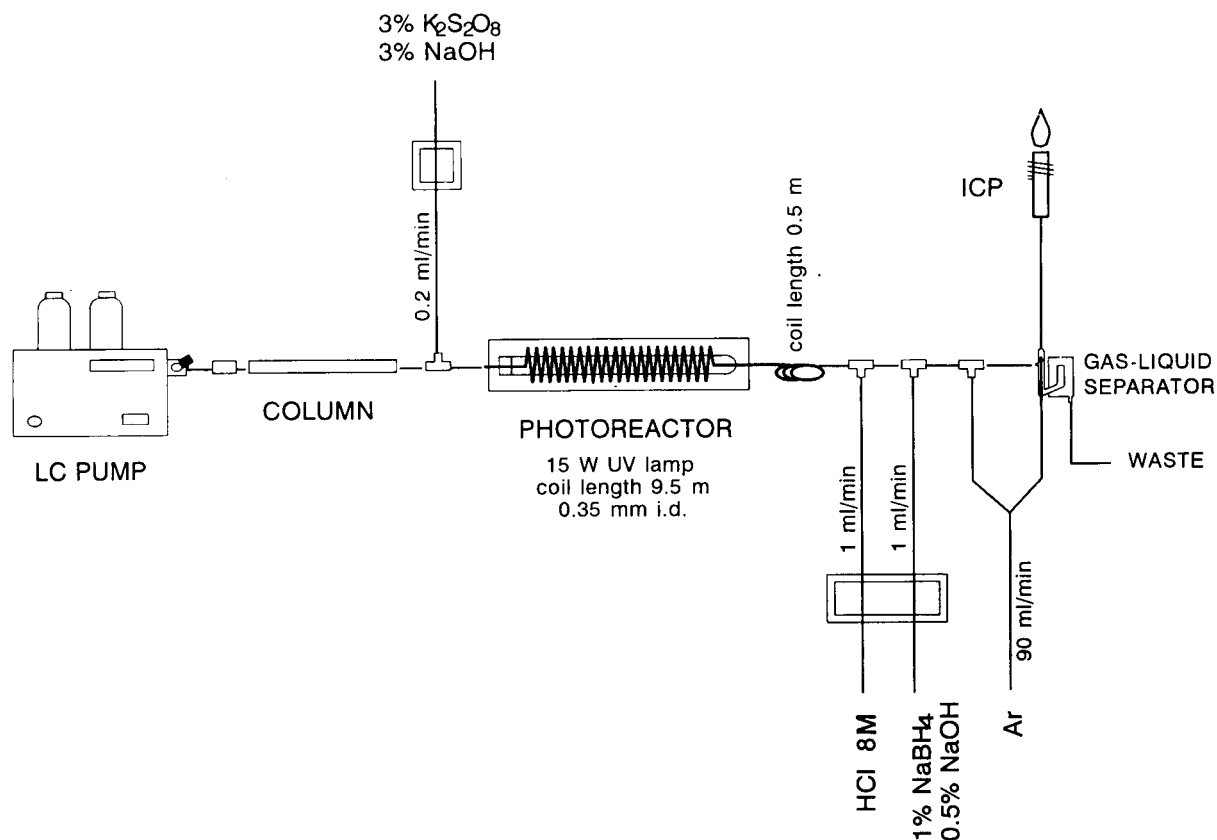


Fig. 5. Overall scheme of the LC-UV-HG-ICP-AES coupled system.

TABLE 3

Accuracy of arsenic species determination, expressed as percentage recovery, of analytes added to a mineral water sample

As compound	LC-UV-HG-ICP-AES		LC-HG-ICP-AES	
	LOD $\times 5^a$	LOD $\times 10^a$	LOD $\times 5^a$	LOD $\times 10^a$
AsChol	90.0	80.4	–	–
AsBet	80.4	86.5	–	–
Arsenite	–	–	77.0	90.0
DMA	97.0	97.8	101.3	99.1
MMA	97.7	97.5	101.7	95.3
Arsenate	95.3	101.2	99.5	102.1

<sup>a</sup> Concentration level

Montseny area zone (Catalonia, Spain) spiked with the different arsenic species at two concentration levels corresponding to five and ten times the LOD. Each value is the mean of two injections.

Similar detection limits were obtained for inorganic arsenic compounds using both procedures. For MMA lower detection limits are obtained using LC-HG-ICP-AES, probably owing to the elution conditions, which are advantageous for this compound, whereas DMA shows a higher detection limit using the same procedure. This behaviour could be attributed to its higher retention time under the separation conditions applied, and to the poorer yield in the arsine generation. The precision and recovery were similar using the two procedures.

### Conclusions

The LC-UV-HG-ICP-AES method represents a reliable and inexpensive system for separating and determining the arsenic species of main interest, including AsBet and AsChol, added to mineral water samples.

The introduction of the on-line photooxidation does not produce any loss of precision or a significant increase in analysis time. The detection limits are similar to those obtained without photooxidation.

The proposed technique represents an important contribution to coupled systems and to speciation studies, as it can be expected that many

organometallic compounds of toxicological and biological interest can be decomposed by photolysis and generate volatile hydrides.

The authors thank CIRIT (Comissió Interdepartamental de Recerca i Innovació Tecnològica de la Generalitat de Catalunya) for financial help, and the Service Central d'Analyse, CNRS, for supplying the AsBet and AsChol standards.

### REFERENCES

- 1 M. Morita, T. Uehiro and K. Fuwa, *Anal. Chem.*, 53 (1981) 1806.
- 2 K.J. Irgolic, R.A. Stockton, D. Chakraborti and W. Beyer, *Spectrochim. Acta, Part B*, 38 (1983) 437.
- 3 K.A. Francesconi, P. Micks, R.A. Stockton and K.J. Irgolic, *Chemosphere*, 14 (1985) 1443.
- 4 W.D. Spall, J.G. Lynn and L.R. Gurlay, *Anal. Chem.*, 58 (1986) 1340.
- 5 K.E. Lafreniere, V.A. Fassel and D.E. Eckels, *Anal. Chem.*, 59 (1987) 879.
- 6 O.F.X. Donard and F.M. Martin, *Trends Anal. Chem.*, 11 (1992) 17.
- 7 D. Beauchemin, M.E. Bednas, S.S. Berman, K.W.N. Sim and R.E. Sturgeon, *Anal. Chem.*, 60 (1988) 2209.
- 8 D. Beauchemin, K.W.M. Sim, J.W. McLaren and D.D. Berman, *J. Anal. At. Spectrom.*, 4 (1989) 285.
- 9 Y. Shibata and M. Morita, *Anal. Chem.*, 61 (1989) 2116.
- 10 S.C.K. Shum, R. Neddersen and R.S. Houk, *Analyst*, 117 (1992) 577.
- 11 C. Demesmay, PhD Thesis, Université Claude Bernard Lyon 1, Lyon, 1992.
- 12 B.S. Chana and N.J. Smith, *Anal. Chim. Acta*, 197 (1987) 177.
- 13 L. Ebdon, S. Hill, A.P. Walton and R.W. Ward, *Analyst*, 113 (1988) 1159.
- 14 A.J. Mürer, A. Abildtrup, O.M. Poulsen and J.M. Christensen, *Analyst*, 117 (1992) 677.
- 15 D.S. Bushee, I.S. Krull, P.R. Demko and S.B. Smith, *J. Liq. Chromatogr.*, 7 (1984) 861.
- 16 G. Rauret, R. Rubio and A. Padró, *Fresenius', J. Anal. Chem.*, 340 (1991) 157.
- 17 R. Rubio, A. Padró, J. Albertí and G. Rauret, *Mikrochim. Acta*, 109 (1992) 39.
- 18 J.S. Blais, G.M. Monplaisir and W.D. Marshall, *Anal. Chem.*, 62 (1990) 1161.
- 19 R.H. Atallah and D.A. Kalman, *Talanta*, 38 (1991) 167.
- 20 R. Rubio, J. Albertí and G. Rauret, *Int. J. Environ. Anal. Chem.*, in press.
- 21 J.W. Birks and R.W. Frei, *Trends Anal. Chem.* 15 (1982) 361.

# Slurry-electrothermal atomic absorption spectrometry of samples with large amounts of silica. Determination of cadmium, zinc and manganese using fast temperature programmes

Ignacio López García, Jesus Arroyo Cortéz and Manuel Hernández Córdoba

*Department of Analytical Chemistry, Faculty of Chemistry, University of Murcia, 30071-Murcia (Spain)*

(Received 28th September 1992; revised manuscript received 22nd February 1993)

## Abstract

The determination of cadmium, zinc and manganese in diatomaceous earth, as well as in other materials with high silica content, is carried out by first suspending the ground samples in dilute hydrofluoric acid. Following this, aliquots of the slurries are directly injected into the electrothermal atomizer. Using the fast-temperature methodology, the drying and ashing steps are replaced by a modified drying stage in which temperature and hold time are experimentally optimized by studying the temperature changes inside the atomizer with a thermocouple. Zinc and cadmium are atomized from a platform using ammonium phosphate as a matrix modifier. Wall atomization and no modifier other than hydrofluoric acid is used for manganese determination. Calibration is performed using aqueous standards. The optimized conditions for diatomaceous earth samples are applicable to other materials with high silica content, as is shown by the analysis of five standard reference materials.

**Keywords:** Atomic absorption spectrometry; Cadmium; Diatomaceous earth; Manganese; Zinc; Slurry-electrothermal AAS

The conventional practice of electrothermal atomic absorption spectrometry (ETAAS) involves dissolving the solid samples to obtain a solution suitable for measurement. The dissolution step is time-consuming and prone to contamination due to prolonged sample manipulation. If this step can be avoided, a considerable saving of time as well as a decrease in the risk of external contamination can be achieved. For this reason, a number of researchers have addressed their attention to the direct use of solid samples in ETAAS [1], and particularly to the slurry-based

methodology in which, instead of a solution, a suspension prepared from the finely ground sample is introduced into the atomizer. This approach, first proposed by Brady et al. [2,3] for the determination of zinc and lead in plant leaves and marine sediments, offers a rapid alternative to the dissolution-based procedures for the analysis of materials that might normally require lengthy digestion or fusion steps. For the slurry methodology to be successful, the particle size must be sufficiently small, a requisite that can be fulfilled in many instances using a simple pre-treatment. This is the case with many samples of a high silica content, whose physical characteristics mean that their particle size can be decreased by grinding.

*Correspondence to:* Manuel Hernández Córdoba, Department of Analytical Chemistry, Faculty of Chemistry, University of Murcia, 30071-Murcia (Spain).



On the other hand, it is also a common practice to include in the ETAAS furnace programmes successive steps to perform the drying, ashing, atomization and clean-out of the aliquot of sample introduced into the furnace. However, the extensive work of Halls and co-workers [4–10] has proved that, in many instances, steps can be omitted or conveniently modified in such a way that a considerable decrease in the time necessary to run the programme is achieved. This fast methodology has also been successfully applied to slurry-based procedures for a number of samples, including coal and fly ash [11], glass [12,13], soils [14] and diatomaceous earth [15].

In this paper, cadmium, zinc and manganese are determined in materials with a high silica content using both slurry-based and fast-programme methodologies. The study was performed on diatomaceous earth (DE), a commercial product with very high silica content and a wide variety of industrial applications, and is an extension of a previous study of the determination of lead, copper and chromium in the same matrix [15]. The conclusions here reached concerning the analysis of this easily available, very pure commercial product can be extended to others silicate-based materials, as is shown by the results obtained using five different certified reference materials. For this reason, the approach here discussed can be of interest to those interested in trace elements in geochemical analysis.

## EXPERIMENTAL

### *Apparatus*

All measurements were obtained with a Perkin-Elmer Model 1100B atomic absorption spectrometer equipped with deuterium-arc background correction and an HGA-400 electrothermal atomizer. The measurements were made at 228.8, 213.9 and 279.5 nm using hollow cathode lamps operated at 10, 20 and 20 mA and bandwidths of 0.7, 0.7 and 0.2 nm for cadmium, zinc and manganese, respectively. Argon was used as the inert gas. Pyrolytic graphite coated tubes and pyrolytic graphite platforms inserted in pyrolytically coated tubes with grooves were obtained

from Perkin-Elmer (Parts B013–5653 and B012–1092, respectively). Background corrected peak areas were used as the analytical signal.

The study of the temperature changes in the drying step was performed using an iron–constantan (Type J) thermocouple (Herten, Castellón, Spain). The output of the thermocouple was connected to a personal computer by means of a PCLab 818 PG data acquisition card (Advantech). A home-made software written in C language together with a commercial package for plotting scientific data permitted the direct plotting of the time–temperature relationship. The response time of the device to a change from 20 to 500°C was estimated to be about 5 s.

### *Reagents*

Doubly distilled water proved inadequate for the work due to high blank values. High quality water obtained using a Milli-Q system (Millipore, USA) proved to be satisfactory and was used exclusively. Severe problems of contamination from cadmium and zinc arising from the micropipette tips and plasticware used were found. To avoid this, micropipette tips were immersed overnight in 2 M nitric acid and thoroughly washed with water before use. The same precaution against contamination was followed for all the volumetric equipment used. Hydrofluoric and nitric acids were obtained from Fluka.

### *Procedure*

The DE samples were first ground for 10 min using an agate ball mill. It was checked that the ground samples passed entirely through the 30  $\mu\text{m}$  sieve. The slurries were prepared by adding 25 ml of a suspending solution to weighed amounts (10–1000 mg) of the ground samples in 50 ml plastic beakers. When slurries more dilute than 0.04% (w/v) were required, the volume of suspending solution was increased to 50–100 ml in order to decrease the weighing error. For the determination of zinc and cadmium a solution containing 0.1% (w/v) of ammonium dihydrogenphosphate and variable percentages (0.1–3% for slurries in the 0.02–2% range) of hydrofluoric acid was used as the suspending medium. For the determination of manganese, no ammonium

TABLE 1  
Optimized furnace programmes

Step	Furnace parameter	Cadmium <sup>a</sup>	Zinc <sup>a</sup>	Manganese <sup>b</sup>
Dry	Temperature (°C)	400	400	200
	Ramp (s)	1	1	1
	Hold (s)	20	20	15
Atomize <sup>c</sup>	Temperature (°C)	1600	1600	2500
	Ramp (s)	0	0	0
	Hold (s)	3	3	3
Clean-out	Temperature (°C)	2650	2650	–
	Ramp (s)	1	1	–
	Hold (s)	2	2	–

<sup>a</sup> Platform atomization. <sup>b</sup> Wall atomization. <sup>c</sup> The flow of argon was stopped except in the case of zinc, for which a miniflow condition was used.

phosphate was added. The suspensions were submitted to ultrasound for 5 min. Aliquots were taken while the suspensions were magnetically stirred. The optimized heating programmes are given in Table 1. Calibration was performed using aqueous standards.

## RESULTS AND DISCUSSION

The distinctive feature of the fast-programme methodology [4] in ETAAS is the replacement of the conventional drying and ashing steps by a modified fast drying stage. This is performed by rapidly heating at a temperature ( $T_d$ ) higher than that of the boiling point of the solvent. The power supply of the furnace is programmed to hold this temperature over a sufficiently long time ( $t_h$ ) to dry the sample completely and permit smoke to be removed before the atomization stage. The optimal values of  $T_d$  and  $t_h$  are closely related. Thus, for high values of  $T_d$ , the holding times can be decreased, although there is the risk of sputtering due to an excessively fast rate of heating. If  $T_d$  is fixed too low, at only a few degrees above the boiling point of the solvent,  $t_h$  must be increased to achieve complete drying of the sample, thus unnecessarily prolonging the total programme time. Furthermore, these parameters are related with a number of factors, including the atomization mode used (wall or platform),

the volume and physical-chemical properties of the sample and the temperature of the cooling water. A recent paper by Hinds et al. [14] describes a systematic study of the relation between  $T_d$  and  $t_h$  both for aqueous solutions and for slurries prepared from soils. Their results indicate that temperatures as high as 500°C can be used for  $T_d$ , which agrees with the reports of Bradshaw and Slavin [11] and Slavin et al. [16] for platform atomization.

In addition to the above factors, the performance of the furnace used should be taken into account when the values of  $T_d$  and  $t_h$  are to be optimized. This is due to the inertia of the temperature response of commercial atomizers, a point already indicated several years ago [4,9]. In an attempt to ascertain the optimal values of  $T_d$  and  $t_h$  for use in the equipment available in our laboratory, a number of experiments were performed in which the temperature response of the furnace was measured using a thermocouple [4]. Figure 1 shows the results obtained when wall atomization was used and different  $T_d$  temperatures, as indicated in the graph, were programmed on the HGA-400 power supply. In all cases, a holding time of 30 s was selected and the suggestion of Halls [4] of using a 1-s ramp was followed. Curves labelled as A were obtained, with no solvent in the atomizer, by directly placing the tip of the thermocouple on the wall of the graphite tube, through the injection hole. Curves labelled as B were obtained by first pipetting into the graphite tube 25  $\mu$ l water and then inserting the tip of the thermocouple into the drop. It is important to point out that the graphs were not corrected for the response time of the thermocouple and the results must be seen as approximate, rather than absolute, as there is no means of ensuring the totally accurate response of the thermocouple due to the small area of contact between the tip of the thermocouple and the graphite, and to kinetic factors. In spite of this, as has already been pointed out by Halls [4,9], it is apparent that the actual temperature of the atomizer lags behind the programmed temperature for a noticeable interval of time.

Figure 2 shows the results obtained for a similar set of experiments carried out using platform

atomization. The evaporation of the solvent is clearly seen in both Figures as the temperature response for curves B is constant at around 100°C. This is more apparent in the platform atomization experiments because of the slower heating rate involved in this atomization mode. As could be predicted, the time necessary for the total drying of the sample markedly increased with the volume injected. Figure 3 demonstrates that for platform atomization and using a  $T_d$  value of 400°C, about 5 s were needed to completely evaporate a 25- $\mu$ l volume of water, once the constant response was obtained.

Figures 1 and 2, as is to be expected, also show that the time necessary for total drying decreased when  $T_d$  was increased. This experimental condi-

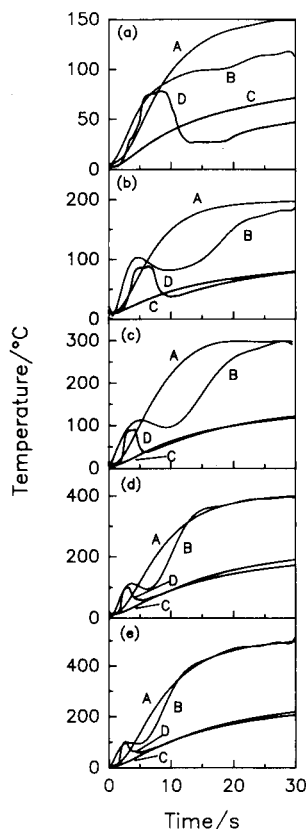


Fig. 1. Temperature response of the thermocouple in the drying stage using wall atomization. Graphs (a–e): temperatures of 150, 200, 300, 400 and 500°C, respectively, were programmed on the power supply of the atomizer (see text for details).

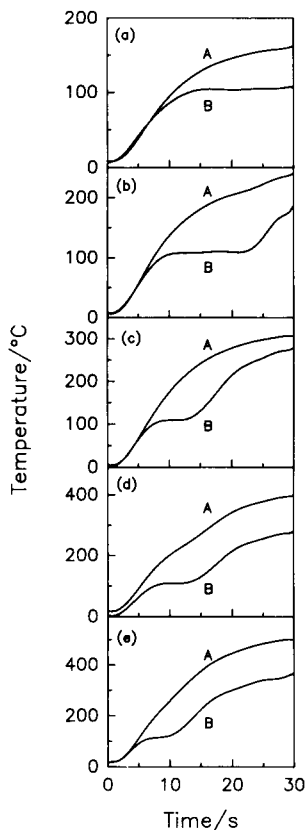


Fig. 2. Temperature response of the thermocouple in the drying stage using platform atomization. Graphs (a–e): temperatures of 200, 300, 400, 500 and 600°C, respectively, were programmed on the power supply of the atomizer. Curves: (A) no water injected, (B) 25  $\mu$ l of water.

tion of using high  $T_d$  values involves a serious risk of analyte loss through sputtering, because the heating rate is very high. The highest  $T_d$  value which can be used has usually been estimated by visual observation of sputtering signs and then studying the reproducibility of the integrated peak area in a further atomization step. We tried to estimate the highest useful  $T_d$  value using a different approach. For this, the tip of the thermocouple was placed inside the injection hole without touching the graphite material and a response to the temperature of the inert gas which was continuously flowing through the atomizer was obtained. The experiments were designed to register different responses of the thermocouple in the case of the water being expelled as a

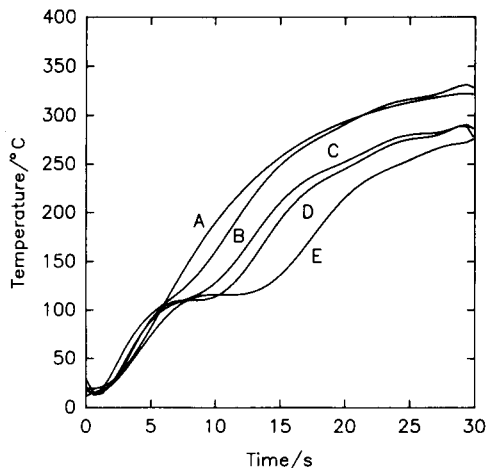


Fig. 3. Temperature response of the thermocouple in the drying stage using platform atomization. A 1-s ramp and a final temperature of 400°C were programmed. (A) no water injected. (B–E) 5, 10, 15 and 25  $\mu\text{l}$  of water, respectively.

vapour or as a liquid. The results obtained for wall atomization using 150 and 200°C for  $T_d$  showed that, once the evaporation process took place, the response was lower than that obtained for the same experiment in the absence of water inside the graphite tube (curves C and D of Fig. 1, respectively). This might be taken as a sign that water is expelled from the tube as a vapour. No conclusions could be obtained for a similar set of experiments performed using platform atomization, as no differences were observed in the temperature of the gas when 25  $\mu\text{l}$  of water was evaporated and for the same experiments performed in the absence of the solvent. All the experiments quoted were repeated using dilute suspensions prepared from DE instead of water and the results were practically identical to that obtained for the pure solvent.

To summarize, the results obtained using the described approach indicate that a 25  $\mu\text{l}$  volume of sample is completely dried on the platform using 400°C for  $T_d$  and a hold time of 15 s. For wall atomization  $T_d$  must be lowered to 200°C and the hold time to 10 s. As the atomizer switches to the reduced or null gas flow condition 5 s before of the atomization step, this time must be added to the mentioned hold times. These results basically agree with those reported by Hinds et

al. [14] and by ourselves [15] based on visual observation of sputtering and on the study of the reproducibility of the analytical signal obtained in a further atomization stage.

#### Determination of cadmium, zinc and manganese in DE

The atomization of suspensions prepared from DE produced a serious deterioration of the graphite as a consequence of chemical attack due to the high silica content [17,18]. To overcome this and considerably prolong the useful lifetime of the pyrolytic material, the approach first studied by Bendicho and de Loos-Vollebregt [13] and later used by us [15] of using hydrofluoric acid as the suspending medium was used. Under this experimental condition, a fraction of the analytes is extracted from the solid matrix into the suspending solution. As has been reported for the analysis of glass [12,13] and for the determination of lead, copper and chromium in DE [15], complete extraction is not required, as the peak areas obtained in the atomization stage were the same regardless of the fraction of the analyte introduced into the furnace as a solution or as a slurry. This can be seen in Fig. 4 where absorbance signals of zinc and cadmium obtained

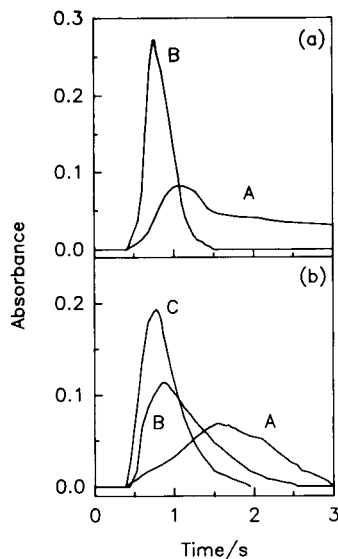


Fig. 4. Atomization profiles of (a) Zn in a 0.02% DE slurry and (b) Cd in a 0.3% slurry. Curves: (A) no hydrofluoric acid, (B) and (C) 0.1 and 1% hydrofluoric acid, respectively.

for platform atomization from slurries prepared from DE, both in the presence and in the absence of hydrofluoric acid, are shown. So, as a matter of routine to increase the lifetime of the atomizers, slurries were prepared in the presence of hydrofluoric acid.

#### Atomization stage

Platform atomization was used for the determination of cadmium and zinc. As no ashing step was used, a matrix modifier did not appear to be necessary because, although  $T_d$  was programmed as 400°C, the actual temperature was only slightly above 100°C at the end of the drying stage (Fig. 2), which suggested no risk of analyte loss before the atomization step. However, the peak areas due to cadmium were dependent on the atomization temperature. Figure 5 shows atomization profiles obtained from 0.6% DE suspensions and from aqueous standards of cadmium, which are

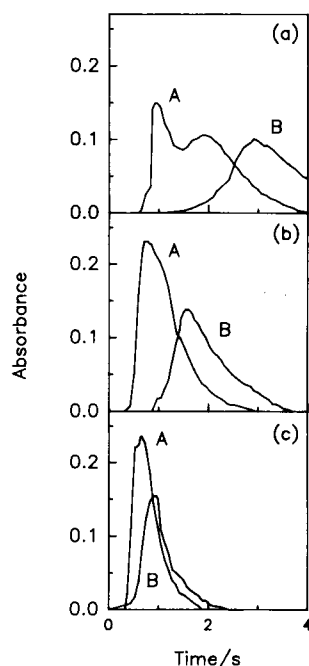


Fig. 5. Atomization profiles of cadmium at different atomization temperatures. Curves: (A) 21 pg of aqueous cadmium, (B) 17 pg in a 0.6% DE slurry. (a) 1000°C; peak area values: 0.243 and 0.183 A s for aqueous cadmium and for the slurry, respectively. (b) 1300°C; 0.199 and 0.147. (c) 1600°C; 0.152 and 0.122.

included for comparison. In both cases, the peak areas were considerably decreased when the atomization temperature was increased. The loss of signal can be attributed to the high volatility of the analyte together with the thermal expansion of the gas inside the atomizer due to the rapid heating. Moreover, as can be seen in the Figure, the signals from the slurries were delayed with respect to those of the aqueous standards, This is not the most desirable situation, because, as has been reported [14], it is more advantageous when the profiles from aqueous standards and slurries are coincident. The effect of atomization temperature on the peak area is a drawback that affects reproducibility and for this reason ammonium dihydrogen phosphate was assayed as a matrix modifier. When the suspensions were prepared in the presence of 0.1% of this compound, the profiles from aqueous standards and from slurries were nearly identical and the peak areas were independent of the atomization temperature in the 1300–1700°C range.

Due to the high sensitivity and relatively high content of zinc in the DE samples, the atomization stage for this analyte was performed using miniflow for the inert gas flow. This probably explains why no effects attributable to thermal expansion were observed and why the peak areas were nearly independent of the atomization temperature in the 1300–1600°C range. When atomization was performed at temperatures higher than 1500°C the appearance time  $t_{ap}$  of the signal was less than 1 s. To delay the  $t_{ap}$  and ensure the atomization takes place under isothermal conditions, 0.1% ammonium dihydrogenphosphate was added to the slurries as a matrix modifier and 1600°C was selected as the atomization temperature.

Wall atomization was used for the determination of manganese. The peak areas were constant for atomization temperatures ranging from 1600 to 2500°C and as the peak profiles were nearly identical to those obtained from aqueous standards, no modifier was considered necessary. A temperature of 2500°C was selected as adequate as the clean up stage could thus be omitted [15] without signs of cross-contamination. This also decreased the total time of the programme.

TABLE 2

Comparison of the results for a DE sample analyzed by the suspension and acid-dissolution procedures

Element	Slurry procedure		Acid-dissolution procedure	
	Found <sup>a</sup> ( $\mu\text{g g}^{-1}$ )	R.S.D. <sup>b</sup> (%)	Found <sup>a</sup> ( $\mu\text{g g}^{-1}$ )	R.S.D. <sup>b</sup> (%)
Cadmium	0.102 ± 0.008	7.8	0.118 ± 0.030	25.4
Zinc	9.0 ± 0.3	3.3	8.5 ± 0.6	7.1
Manganese	36 ± 1	2.8	35 ± 3	8.6

<sup>a</sup> Mean ± standard deviation ( $n = 7$ ). <sup>b</sup> Relative standard deviation.

### Reproducibility

The great sensitivity of ETAAS for the three analytes studied necessitates the preparation of very dilute suspensions, especially for the determination of zinc and manganese, and this could lead to a poor reproducibility. To study this, a number of slurries covering a wide range of percentages were prepared from DE samples and the suspensions analyzed for the three determinands. The percentages were chosen in such a way that the peak areas were in the linear response range of the instrument, which was previously established using aqueous standards under identical experimental conditions. The results are summarized in Fig. 6, where vertical bars indicate the confidence intervals at the 95% confidence level (ten measurements in each case) for each percentage studied. The errors inherent in sampling slurries greatly decrease with particle size and when using samples with a narrow particle size distribution [19]. The grinding of DE samples

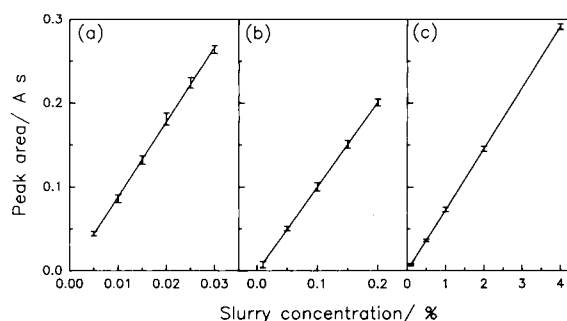


Fig. 6. Effect of the slurry percentage. (a) Manganese, (b) zinc, (c) cadmium.

considerably reduces the particle size [15], which probably explains why even the most diluted suspensions assayed showed relative standard deviations (R.S.D.) < 7%.

Calibration was carried out using aqueous standards. The validity of this simplest approach was checked by comparing the slopes of calibra-

TABLE 3

Results for the determination of Cd, Zn and Mn in Standard Reference Materials

Sample	Cadmium ( $\mu\text{g g}^{-1}$ )		Zinc ( $\mu\text{g g}^{-1}$ )		Manganese ( $\mu\text{g g}^{-1}$ )	
	Certified	Found <sup>a</sup>	Certified	Found <sup>a</sup>	Certified	Found <sup>a</sup>
SRM 1633a coal fly ash	1.00 ± 0.15	0.94 ± 0.05	220 ± 10	226 ± 3	179 ± 8	175 ± 5
BCS 375 soda feldspar	–	–	12 ± 2	11.4 ± 0.5	20 ± 4	20 ± 2
BCS 376 potash feldspar	–	–	5 ± 2	5.6 ± 0.5	18 ± 4	17 ± 0.6
SARM 1 granite	–	–	50	52 ± 1	160	166 ± 4
SRM 688	–	–	58 <sup>b</sup>	55 ± 2	1293	–

<sup>a</sup> Mean ± standard deviation ( $n = 6$ ). <sup>b</sup> This is an approximate, not certified, value given for information. The content of Mn in the SRM 688 sample is too high to be determined by the studied procedure.

tion lines obtained using aqueous standards with those found for standard additions calibration graphs obtained from slurries. Under the experimental conditions used the slopes for aqueous standards were  $7.109 \pm 0.123$ ,  $0.6770 \pm 0.0321$  and  $1.777 \pm 0.042$  A s ng<sup>-1</sup> and values for the characteristic mass of 0.6, 6.3 and 2.4 pg/0.0044 A s were obtained for cadmium, zinc and manganese, respectively. The mean slope for the standard additions graphs obtained for fourteen commercial DE samples were  $7.144 \pm 0.157$ ,  $0.6728 \pm 0.0315$  and  $1.766 \pm 0.051$  A s ng<sup>-1</sup>, for cadmium, zinc and manganese, respectively.

To assess reproducibility and accuracy, a commercial DE sample was completely dissolved using digestion with nitric and hydrofluoric acids and the content of the three analytes determined. Table 2 compares the results obtained by the procedure here discussed with those found by means of the acid-dissolution methodology. The application of an ordinary t-test [20] revealed no significant differences between the two procedures. Another thirteen samples were also analyzed using both procedures. There was complete correlation between the two sets of results, for 0.02–0.2 μg g<sup>-1</sup> Cd, 7–14 μg g<sup>-1</sup> Zn and 20–70 μg g<sup>-1</sup> Mn. To further check the reliability of the procedure, five certified reference materials with high silica content were also analyzed. In this case the samples were first ground for 30 min to decrease the particle size and then the slurries prepared as indicated in Experimental. The results, which are shown in Table 3, agreed with those certified.

Financial support from the Spanish DGICYT (Project PB90–0302) is gratefully acknowledged.

J.A.C. thanks the Venezuelan Foundation Gran Mariscal de Ayacucho for a scholarship.

## REFERENCES

- 1 C. Bendicho and M.T.C. de Loos-Vollebregt, *J. Anal. At. Spectrom.*, 6 (1991) 353.
- 2 D.V. Brady, J.G. Montalvo, J. Jung and R.A. Curran, *At. Absorpt. Newsl.*, 13 (1974) 118.
- 3 D.V. Brady, J.G. Montalvo, G. Glowacki and A. Pisciotta, *Anal. Chim. Acta*, 70 (1974) 448.
- 4 D.J. Halls, *Analyst*, 109 (1984) 1081.
- 5 D.J. Halls and G.S. Fell, *Analyst*, 110 (1985) 243.
- 6 D.J. Halls, C. Mohl and M. Stoeppler, *Analyst*, 112 (1987) 185.
- 7 D.J. Halls, M.M. Black, G.S. Fell and J.M. Ottaway, *J. Anal. At. Spectrom.*, 2 (1987) 305.
- 8 A.D. Keating, J.L. Keating, D.J. Halls and G.S. Fell, *Analyst*, 112 (1987) 1381.
- 9 D.J. Halls, *J. Anal. At. Spectrom.*, 4 (1989) 149.
- 10 U.K. Kunwar, D. Littlejohn and D.J. Halls, *Talanta*, 37 (1990) 555.
- 11 D. Bradshaw and W. Slavin, *Spectrochim. Acta, Part B*, 44 (1989) 1245.
- 12 C. Bendicho and M.T.C. de Loos-Vollebregt, *Spectrochim. Acta, Part B*, 45 (1990) 679.
- 13 C. Bendicho and M.T.C. de Loos-Vollebregt, *Spectrochim. Acta, Part B*, 45 (1990) 695.
- 14 M.W. Hinds, K.E. Latimer and K.W. Jackson, *J. Anal. At. Spectrom.*, 6 (1991) 473.
- 15 I. López García, J. Arroyo Cortéz and M. Hernández Córdoba, *J. Anal. At. Spectrom.*, 8 (1993) 103.
- 16 W. Slavin, D.C. Manning and G.R. Carnrick, *Spectrochim. Acta, Part B*, 44 (1989) 1237.
- 17 J.C. Eames and J.P. Matousek, *Anal. Chem.*, 52 (1980) 1248.
- 18 G. Müller-Vogt and W. Wendl, *Anal. Chem.*, 53 (1981) 651.
- 19 J.A. Holcombe and V. Majidi, *J. Anal. At. Spectrom.*, 4 (1989) 423.
- 20 J.C. Miller and J.N. Miller, *Statistics for Analytical Chemists*, Wiley, New York, 2nd edn., 1988, Chap. 6.

# Study of the influence of ordered media on the determination of lead by hydride generation inductively coupled plasma atomic emission spectrometry

M.C. Valdés-Hevia y Temprano, B. Aizpún Fernández, M.R. Fernández de la Campa and A. Sanz-Medel

*Department of Physical and Analytical Chemistry, Faculty of Chemistry, University of Oviedo, c/ Julián Clavería 8, 33006 Oviedo (Spain)*

(Received 3rd October 1992; revised manuscript received 12th January 1993)

## Abstract

Continuous-flow generation of plumbane from different media for sample introduction into an inductively coupled plasma (ICP) for the determination of lead by atomic emission spectrometry (AES) was investigated in detail. Different "organized molecular assemblies" (micelles and vesicles) were tried for plumbane generation using the ammonium peroxodisulphate–nitric acid system as oxidant and sodium tetrahydroborate as the reducing agent. Cetyltrimethylammonium bromide (CTAB) or, alternatively, didodecyltrimethylammonium bromide was found to accelerate plumbane generation in the oxidant mixture. The advantages of hydride generation using aqueous, micellar or vesicular media are discussed and critically compared in terms of sensitivity, selectivity and accuracy of the corresponding ICP-AES determination of low levels of lead. The method using ammonium peroxodisulphate–nitric acid–CTAB proved to be superior (detection limit  $9 \text{ ng ml}^{-1}$  and precision 1.4% at the  $50 \text{ ng ml}^{-1}$  level) to conventional hydride generation, and was applied to the determination of low levels of lead in soft drinks by ICP-AES. Validation of the results was carried out successfully by graphite furnace atomic absorption spectrometry.

*Keywords:* Atomic emission spectrometry; Inductively coupled plasma spectrometry; Fruit juices; Hydride generation; Lead; Organised molecular assemblies

The extensive industrial application of lead in recent years and especially its use in petrol has resulted in relatively high concentrations of this toxic element in the atmosphere. Although the exact threshold above which lead in the organism has adverse effects is still not known [1], the need for control and assessment of its risk, and thus for the determination of lead concentrations that are toxic for the organism, is obvious (e.g., the

European Community admits a maximum level of only  $10 \text{ ng ml}^{-1}$  [2] in drinking water for human consumption). Hence there is great interest in developing more sensitive, selective and reliable methods to determine traces and ultratraces of this element in biological and environmental samples.

Analytical atomic spectrometric techniques, particularly inductively coupled plasma atomic emission spectrometry (ICP-AES), have been widely used for such a purpose. However, the low levels to be determined in foods, beverages and environmental samples are demanding the use of

*Correspondence to:* A. Sanz-Medel, Department of Physical and Analytical Chemistry, Faculty of Chemistry, University of Oviedo, c/ Julián Clavería 8, 33006 Oviedo (Spain).



hydride generation (HG) techniques or other means in order to increase the sensitivity for lead of conventional nebulization ICP-AES.

Plumbane ( $\text{PbH}_4$ ) is the least known of the hydrides of the Group IVB elements owing to its instability at room temperature [3]. The slow kinetics and the relatively poor generation efficiency of  $\text{PbH}_4$  are well known. It is recognized that the generation of lead hydride requires the presence of an oxidant and a complexing agent of metastable Pb(IV) before final reduction to  $\text{PbH}_4$  with sodium tetrahydroborate ( $\text{NaBH}_4$ ). Among all the systems published, the most commonly used was the ammonium peroxodisulphate–nitric acid system for lead preoxidation [4–9]. The generation of plumbane has also been achieved from organic solvents [10–12]. Detection by atomic absorption spectrometry (AAS) has been used as a rule. However, plasma detectors including direct current plasma (DCP)-AES [4] and ICP-AES [13,14] have also been tried with plumbane generation as the means of sample introduction.

Surfactant organised media, or organized molecular assemblies [15], have been shown to alter chemical equilibria, reaction rates and other important chemical features owing to their capacity to create a special microenvironment for reactions at a molecular level. These aggregates have proved to be very useful in many fields of analytical chemistry [15–18]. The use of surfactants in atomic spectrometry, however, has been limited

mainly to enhancing the efficiency of nebulization in flame atomic absorption spectrometry, and their benefits in plasma atomization/excitation are controversial [19,20]. It has been shown previously that organized media can improve hydride formation [21] as related to generation from an aqueous phase. This effect has been applied to improve the determination of arsenic by ICP-AES with arsine generation [22].

In the context of studying the effects of such organized assemblies on plumbane generation and its possible application to increasing the sensitivity of ICP-AES, in this work the addition of different types of organized media, including normal micelles and vesicles, on the HG-ICP-AES of lead was investigated. Some preliminary experiments were carried out by AAS in order to select the more convenient organized assembly to be used in connection with ICP-AES measurements and so those AAS results are also included. The more commonly used lead preoxidation system, ammonium peroxodisulphate–nitric acid, was selected in order to study the effect of the addition of different organized molecular assemblies to such reaction medium, with sodium tetrahydroborate as the reducing agent. The application of micellar enhanced HG-ICP-AES to the determination of lead in real samples using a cetyltrimethylammonium bromide (CTAB) micellar medium for accelerated plumbane generation is also reported.

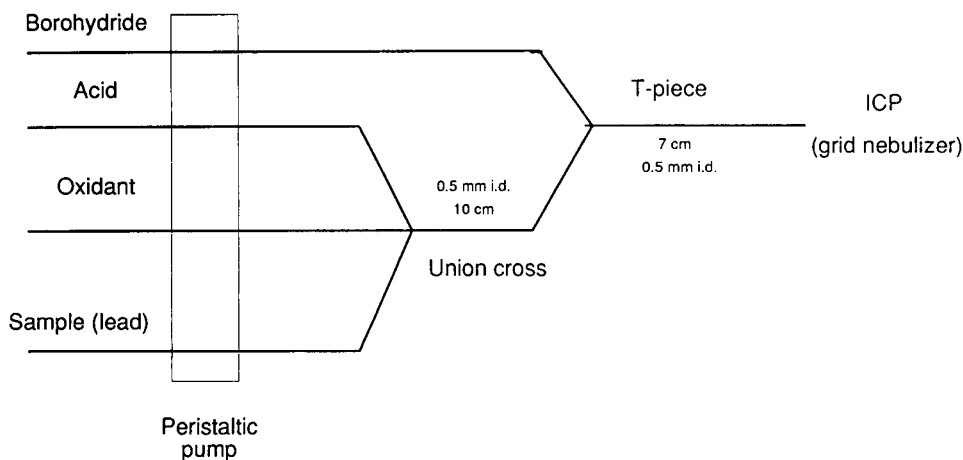


Fig. 1. Continuous HG flow system.

## EXPERIMENTAL

*Instrumentation*

A Philips Model PU7000 ICP was used for ICP-AES detection. Other details of the experimental flow system and the ICP-AES set-up used are given in Table 1 and Fig. 1.

*Reagents*

A 1000  $\mu\text{g ml}^{-1}$  lead(II) stock standard solution (Merck) was diluted daily as appropriate to give working standard solutions.

Sodium tetrahydroborate solutions were prepared by dissolving  $\text{NaBH}_4$  (Carlo Erba) in ultrapure water, stabilized in a 0.1% (w/v) sodium hydroxide solution. Solutions were prepared weekly and filtered before use.

Ammonium peroxodisulphate (Carlo Erba) and nitric acid (Merck, 65%) solutions were prepared by appropriate dissolution of the required amounts of the reagents in ultrapure water.

Cetyltrimethylammonium bromide (CTAB) solution (0.01 M) was prepared by dissolving the surfactant powder (Fluka) in water by gentle warming. Other surfactant solutions such as sodium lauryl sulphate (SLS) (Sigma) (0.01 M), Triton X-100 (TX-100) (Merck) (2%, v/v) and Zwittergent-3.16 (ZW-3.16) (Carbiochem-Behring) (0.01 M) were prepared in a similar way. Didodecyldimethylammonium bromide (DDAB) vesicles solution (0.01 M) was prepared by dissolving the surfactant powder (Kodak) in water

and after sonication at room temperature at 60 W for ca. 12 min.

All mineral acids and metal salts used were of analytical-reagent grade and ultrapure water obtained using a Milli-Q system (Millipore) was used throughout.

*General HG-ICP-AES procedure*

*Continuous generation of plumbane.* In the flow system described here (Fig. 1), the sample, 6% (w/v) ammonium peroxodisulphate and 2% (v/v) nitric acid solutions were passed through a four-channel union cross by a peristaltic pump at a rate of 0.75  $\text{ml min}^{-1}$  each. The sample solution carries the required amount of CTAB in the sample channel. The resulting mixture (see Fig. 1) is merged with a 10% (w/v) sodium tetrahydroborate solution (flow-rate 0.75  $\text{ml min}^{-1}$ ) via an ordinary T-piece, producing a final flow-rate of 3  $\text{ml min}^{-1}$ . This solution feeds the grid nebulizer of the PU7000 ICP, which is detuned in order to separate the volatile species, going up to the plasma, from the liquid phase. Lead is measured at the 220.353-nm emission line and under the conditions detailed in Table 3.

*Juice samples.* These were analysed as received, without any sample pretreatment, following the continuous-flow plumbane generation described above.

## RESULTS AND DISCUSSION

*Preliminary studies: organized media enhancement studied by HG-AAS*

In the search for more sensitive and selective methods for the determination of ultratrace amounts of lead in environmental samples, the potential of organized media to improve the kinetics of plumbane generation was first investigated by using a commercial batch hydride generator (Perkin-Elmer MSH 10) in conjunction with a heated quartz tube atomiser-AAS system and the most commonly used ammonium peroxodisulphate-nitric acid system [4–9] for lead preoxidation. It was observed that addition of CTAB and DDAB above a given concentration brought about a significant increase in the slope of the calibra-

TABLE 1

## Instrumentation

ICP spectrometer	Philips Model PU7000 equipped with a 40-MHz source unit
Gas-liquid separation interface	"Grid" type nebulizer provided with the instrument
Peristaltic pump (four channels)	Gilson Minipuls 2
Atomic absorption spectrometer	Perkin-Elmer Model 2280; chart recorder, Perkin-Elmer Model 56
Hydride generator for AAS measurements	Perkin-Elmer Model MSH-10
High-intensity ultrasonic processor	Sonics and Materials Model 500W

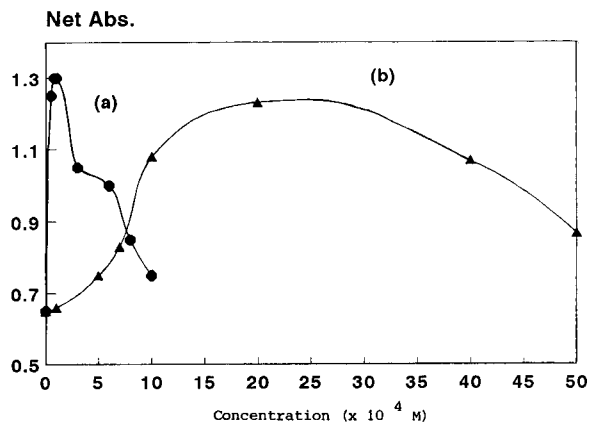


Fig. 2. Effect of surfactant concentration on AAS lead signal.  $[Pb] = 100 \text{ ng ml}^{-1}$ . (a) CTAB; (b) DDAB.

tion graphs while negatively charged or zwitterionic surfactants did not produce such a positive effect on the AAS transient lead signal.

Table 2 shows a summary of the observed effects of different organized media on the slope and detection limits for lead determination by batch HG-AAS. The best results were observed for CTAB and DDAB and the influence of surfactant concentrations is shown in Fig. 2a for CTAB. The effect of DDAB concentration on vesicle formation is shown in Fig. 2b. It can be seen that the analytical signal increased with increasing vesicle concentration until a plateau was reached (between  $1 \times 10^{-3}$  and  $4 \times 10^{-3}$  M of the surfactant monomers).

In order to investigate further the nature of the observed AAS signal enhancement, the peak shapes obtained by generating  $PbH_4$  from water,

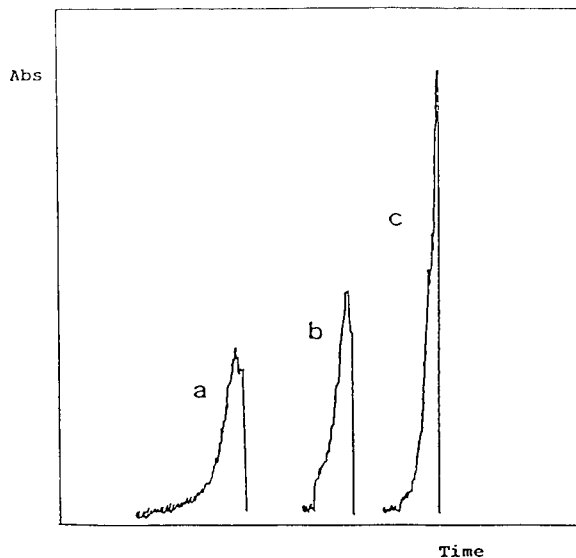


Fig. 3. Effect of the different organized media on the lead AAS peak profile. (a) Water; (b)  $2 \times 10^{-3}$  M DDAB; (c)  $1 \times 10^{-4}$  M CTAB. Time in seconds.

from CTAB or DDAB media using 3% ammonium peroxodisulphate–2% nitric acid and 3%  $NaBH_4$  for reduction were studied. The results are shown in Fig. 3 and indicate that the presence of organized assemblies seems to accelerate the hydride generation kinetics and thus to provide higher and sharper lead peaks.

Having established the possibility of improving the analytical characteristics of plumbane generation by cationic aggregates (micelles and vesicles), the application of such organized media to the

TABLE 2

Comparison of lead hydride generation with peroxodisulphate–nitric acid from water and organized molecular assemblies using AAS detection <sup>a</sup>

Medium	Surfactant concentration	Slope <sup>b</sup> ( $\text{ml ng}^{-1}$ )	$A_B \pm \sigma_B$ <sup>c</sup>	DL <sup>d</sup> ( $\text{ng ml}^{-1}$ )	Micellar factor <sup>e</sup>
Water	–	$2.2 \times 10^{-3}$	$0.039 \pm 0.005$	7	1.0
DDAB	$2 \times 10^{-3}$ M	$3.6 \times 10^{-3}$	$0.054 \pm 0.007$	6	1.7
TX-100	0.02%	$3.4 \times 10^{-3}$	$0.029 \pm 0.006$	5	1.6
ZW-3.16	$1 \times 10^{-3}$ M	$2.0 \times 10^{-4}$	$0.012 \pm 0.009$	135	0.1
SLS	$1 \times 10^{-3}$ M	$9.0 \times 10^{-4}$	$0.050 \pm 0.03$	99	0.4
CTAB	$1 \times 10^{-4}$ M	$5.8 \times 10^{-3}$	$0.026 \pm 0.002$	1	2.6

<sup>a</sup> Total sample volume used in the batch procedure = 5 ml. <sup>b</sup> Slope of the calibration line:  $A = A_B + \text{slope}[\text{ng ml}^{-1} \text{ Pb}]$ . <sup>c</sup>  $A_B$  blank (mean value of absorbance for ten blanks). <sup>d</sup> DL (detection limit) =  $3 \sigma_B / \text{slope}$  ( $\sigma_B$  = standard deviation of the blank). <sup>e</sup> Micellar enhancement factor = organized media slope/water slope.

TABLE 3

Optimum conditions for lead hydride generation by ICP-AES

Plasma experimental conditions:	
Wavelength	220.353 nm
R.f. forward power	0.7 kW
Nebulizer pressure	30 p.s.i.
Coolant gas flow-rate	13 l min <sup>-1</sup>
Auxiliary gas flow-rate	0.1 min <sup>-1</sup>
Final sample flow-rate	3 ml min <sup>-1</sup>
Drain flow-rate	3 ml min <sup>-1</sup>
Integration time	3 s
Chemical parameters:	
(NH <sub>4</sub> ) <sub>2</sub> S <sub>2</sub> O <sub>8</sub>	6% (m/v) (flow-rate 0.75 ml min <sup>-1</sup> )
HNO <sub>3</sub>	0.2 M (flow-rate 0.75 ml min <sup>-1</sup> )
NaBH <sub>4</sub> <sup>a</sup>	10% (w/v) in 0.1% (w/v) NaOH (flow-rate 0.75 ml min <sup>-1</sup> )
CTAB	1 × 10 <sup>-4</sup> M (flow-rate 0.75 ml min <sup>-1</sup> )
DDAB	1 × 10 <sup>-3</sup> M (flow-rate 0.75 ml min <sup>-1</sup> )

<sup>a</sup> Maximum concentration assayed.

determination of lead by HG-ICP-AES was studied using the ammonium peroxodisulphate–nitric acid system for preoxidation and NaBH<sub>4</sub> for final reduction to plumbane.

#### Conventional HG-ICP-AES of lead

**Optimization of instrumental and chemical parameters.** Using continuous gas–liquid separation in the ICP instrument, the effect of varying instrumental parameters was studied by following the general HG-ICP-AES procedures for the ammonium peroxodisulphate–nitric acid system for plumbane generation [13]. The optimum ICP instrumental values obtained are summarized in Table 3. Optimum chemical parameters (concentration of reactants, flow-rates, etc.) for continuous PbH<sub>4</sub> generation and introduction into the plasma were then investigated, looking for the maximum signal-to-background ratio. The effect of sample flow-rate was studied from 1 to 10 ml min<sup>-1</sup> and, as expected, the signal increased almost linearly with increasing sample flow-rate. A flow-rate of 3 ml min<sup>-1</sup> was selected as a compromise in order to avoid flooding of the spray chamber in the commercial set-up.

The optimum values selected for both the ICP plasma conditions and continuous chemical generation of PbH<sub>4</sub> are summarized in Table 3.

**Analytical performance characteristics.** Using the experimental conditions given in Table 3 the analytical parameters of the method were evaluated. The calibration graphs were linear up to 1 µg ml<sup>-1</sup> and the detection limit (3 σ<sub>B</sub>, IUPAC recommendation [23]) was 13 ng ml<sup>-1</sup> of lead. The precision, evaluated by analysing ten replicates containing 50 ng ml<sup>-1</sup> of lead, was 2.2%.

With the above reference data, the addition of surfactants to the PbH<sub>4</sub> generation medium was investigated.

#### Lead HG-ICP-AES using organized molecular assemblies

Triton X-100 produced a great deal of foam, which eventually extinguished the ICP. Therefore, this non-ionic surfactant was ruled out and only CTAB micelles and DDAB vesicles (see Table 2) were tried in further ICP-AES work. Addition of both types of surfactants to sample solutions produced an important increase in the lead signal, as can be seen from Fig. 4. The maximum enhancement was produced when the concentrations of CTAB and DDAB monomers were 1 × 10<sup>-4</sup> and 1 × 10<sup>-3</sup> M, respectively. This is in accordance with the results obtained by AAS (see Fig. 2).

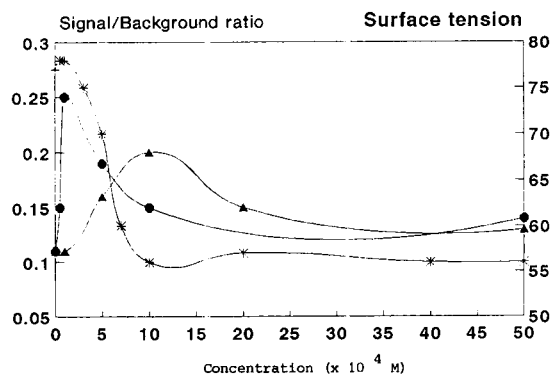


Fig. 4. Effect of the organized media concentration on HG-ICP-AES Pb signal using ammonium peroxodisulphate–nitric acid and CTAB c.m.c. measurements. [Pb] = 50 ng ml<sup>-1</sup>. ● = CTAB; ▲ = DDAB; \* = CTAB at the c.m.c.

**Analytical figures of merit: a comparison.** The ICP and chemical generation parameters were optimized for all three reaction media tested: peroxydisulphate–nitric acid, peroxydisulphate–nitric acid–CTAB and peroxydisulphate–nitric acid–DDAB. The results obtained are summarized in Table 4. The comparison of the different media shows that the best analytical performance is provided by the peroxydisulphate–nitric acid–CTAB reaction medium. The detection limits and precisions obtained in both organized systems are better than in aqueous media.

Therefore, the determination of low levels of lead by HG-ICP-AES enhanced by CTAB was investigated in detail. First, the critical micellar concentration (c.m.c.) of CTAB in the reaction medium for HG was determined using surface tension ( $\sigma$ ) measurements. The results obtained (plotted in Fig. 4) showed that maximum efficiency in HG is obtained before the “normal” c.m.c. of the surfactant (ca.  $8 \times 10^{-4}$  M) is reached. This indicates that pre-micellar aggregates seem to be responsible for the observed enhancement.

**Nature of the acid used for plumbane generation from CTAB.** The acids HCl, HClO<sub>4</sub>, HNO<sub>3</sub>, H<sub>2</sub>SO<sub>4</sub> and HF (with boric acid) were investigated because they are currently used in many sample digestions. Citric acid was also tested as it

TABLE 4

Comparison of analytical performances of different lead hydride generation systems by ICP-AES

Parameter	P–N– CTAB <sup>a</sup>	P–N– DDBA <sup>a</sup>	P–N– water <sup>a</sup>
Slope <sup>b</sup>	$8.2 \times 10^2$	$6.4 \times 10^2$	$4.9 \times 10^2$
$I_B$ <sup>c</sup>	193 700	217 600	187 900
DL (ng ml <sup>-1</sup> ) <sup>d</sup>	9	11	13
R.S.D. (%) <sup>e</sup>	1.4	1.2	2.2
Enhancement of slope	1.7	1.3	1.0

<sup>a</sup> P = peroxydisulphate; N = nitric acid. <sup>b</sup> Slope (ml ng<sup>-1</sup>) of the calibration lines obtained:  $I_L = \text{slope} [\text{ng ml}^{-1} \text{Pb}] + I_B$ , where  $I_L$  = line intensity.  $I_B$  = background intensity.  $I_L + B$  = total intensity. <sup>c</sup>  $I_B$  = mean value of the emission intensity for ten independent blanks. <sup>d</sup> DL (detection limit) =  $3 \sigma_B / \text{slope}$ . <sup>e</sup> R.S.D. = relative standard deviation for ten replicates of 50 ng ml<sup>-1</sup>.

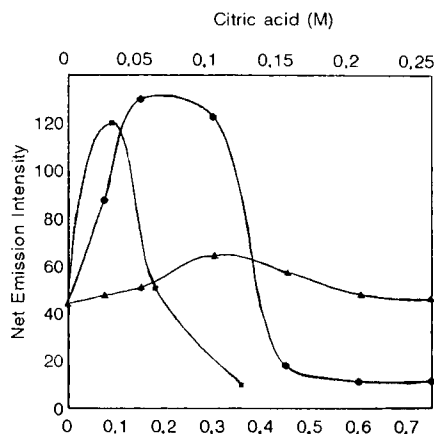


Fig. 5. Effect of (●) nitric acid, (■) sulphuric acid and (▲) citric acid concentrations on the HG-ICP-AES Pb signal. Conditions as in Table 3.

is normally present in the soft drinks to be analysed for their lead content. All the mineral acids tested, with the exception of H<sub>2</sub>SO<sub>4</sub> (which produced maximum intensity at 0.1 M and at a level of 0.4 M the emission signal of lead was zero) showed similar behaviour to that illustrated for nitric acid in Fig. 5. As can be seen, the optimum acid concentration occurs at 0.15 M.

The effect of citric acid, as shown in Fig. 5, is different because the lead signal increases very slowly to reach a maximum at around 0.1 M. This maximum signal is much lower, probably owing to its complex formation ability with lead and to its character being a not very strong acid.

**Interference studies.** Using the optimum conditions for lead (Table 3), the effect of the presence of foreign elements in the ICP-AES signal of lead was investigated.

Table 5 summarizes all the potentially interfering elements tested and the levels of tolerance observed in the lead determinations. As shown, hydride-forming elements interfere in aqueous and organized media. These interferences by hydride-forming elements may be explained by competitive reactions in which such elements successfully compete with lead for the NaBH<sub>4</sub>. Some elements, as As, Se, Hg and Sn, seemed to be less troublesome for lead determinations when HG is performed from CTAB medium. High levels of alkali and alkaline earth metals or com-

mon anions were found not to affect lead hydride generation in the CTAB medium.

#### Analysis of real samples

Once the optimum plumbane generation conditions (ammonium peroxodisulphate–nitric acid–CTAB) for lead determination by HG-ICP-AES had been determined, the recommended method was applied to the determination of low levels of lead in soft drinks. Samples of apple, pineapple and orange juices were analysed directly by HG-ICP-AES without any pretreatment. Background correction (at 220.371 and 220.339 nm) was employed and the other conditions were as detailed in Table 3. Calibration was accomplished using lead standards in citric acid (0.1 M) because the latter is a major component in these samples. HG from 0.2 M HNO<sub>3</sub> in the presence of 0.1 M citric acid increased the lead signal by 0.5%.

The results obtained by the proposed method were compared with those obtained by graphite furnace atomic absorption spectrometry (GFAAS) for the same samples and the comparative values are summarized in Table 6. Very good agreement was observed. Therefore, the validity of the proposed organized medium-enhanced HG-ICP-AES

TABLE 5

Interference studies on 100 ng ml<sup>-1</sup> of Pb with peroxodisulphate–nitric acid–CTAB plumbane generation medium

Interferent ion	Weight excess	Pb recovery (water) (%)	Pb recovery (CTAB) (%)
Se <sup>a</sup>	1:500	88.7	95.4
As <sup>a</sup>	1:500	71.8	108
Ni	1:100	45.6	50.3
Cr	1:500	105	103
Fe	1:500	100	100
Hg <sup>a</sup>	1:500	108	100
Sn <sup>a</sup>	1:500	67.7	87.5
Zn	1:500	41	50
Na	1:10000	102	100
K	1:1000	100	103
Ca	1:1000	101	100
Mg	1:10000	99	98
Chloride	1:50000	100	101
Nitrate	1:50000	101	101

<sup>a</sup> Elements that seemed to be less troublesome for lead determinations when HG is performed from CTAB medium.

TABLE 6

Analysis of commercial fruit juices with the peroxodisulphate–nitric acid–CTAB system

Sample	Pb concentration (ng ml <sup>-1</sup> ) <sup>a</sup>	
	HG-ICP <sup>b</sup> (ng ml <sup>-1</sup> )	GFAAS (ng ml <sup>-1</sup> )
A	77.3 ± 3.1	75.1 ± 2.1
B	91.7 ± 4.2	89.8 ± 1.0
C	85.1 ± 5.7	86.3 ± 2.3

<sup>a</sup> Mean ± S.D. (*n* = 3). <sup>b</sup> Analysis using calibration line (0.1 M citric acid).

method for the determination of low levels of lead in soft drinks has been demonstrated.

#### Conclusions

The sensitivity (slope of the calibration graph) of the ICP-AES determination of lead in water using hydride generation from a peroxodisulphate–nitric acid oxidant medium is increased twofold by adding CTAB while the detection limit is also slightly lowered. Batch HG-AAS experiments (Fig. 3) showed that the generation reaction in organized molecular assemblies increased the kinetics of such hydride generation. Therefore, the potential ability of micelles, vesicles, etc., to organize reactants at a molecular level, improving the kinetics of reactions, has been realized in the problematic generation of plumbane with commonly used preoxidation reagents. The presence of complexing agents of Pb(IV) [24] can change the effects of surfactants. In any case, the effect of surfactants and other molecular assemblies in hydride generation reactions seems to be very complex and depends on the nature of the surfactant, the relative charge of the analyte/surfactant and the particular mechanisms of the reduction reaction considered for each particular volatile species-forming element considered.

The authors acknowledge financial support from FICYT (Fundación para el Fomento en Asturias de la Investigación Científica Aplicada y la Tecnología) and CICYT (Comisión Interministerial de Ciencia y Tecnología), and also FICYT grants to M.C. Valdés-Hevia y Temprano and B. Aizpún Fernández. The loan of the ICP PU7000

instrument by Unicam Analytical Systems (Cambridge) is also gratefully acknowledged.

#### REFERENCES

- 1 A. Taylor, *J. Clin. Endocrinol. Metab.*, 14 (1985) 658.
- 2 *Off. J. Eur. Commun.*, 23 (1980) 11.
- 3 F. Paneth and E. Rabinowitsch., *Chem. Ber.*, 58 (1925) 1138.
- 4 I.D. Brindle and X. Le, *Anal. Chem.*, 61 (1989) 1175.
- 5 K. Jin and M. Taga, *Anal. Chim. Acta*, 143 (1982) 229.
- 6 K. Jin, H. Taga, H. Yoshida and S. Himike, *Bunseki Kagaku*, 27 (1978) 759.
- 7 Y. Madrid, M. Bonilla and C. Cámara, *J. Anal. At. Spectrom.*, 3 (1988) 1097.
- 8 Y. Madrid, M. Bonilla and C. Cámara, *J. Anal. At. Spectrom.*, 2 (1989) 167.
- 9 J. Sanz, P. Basterra, J. Galbán and J.R. Castillo, *Mikrochim. Acta*, I (1989) 271.
- 10 J. Aznarez, F. Palacios, J.C. Vidal and J. Galbán, *Analyst*, 109 (1984) 713.
- 11 J. Aznarez, J.C. Vidal and R. Carnicer, *J. Anal. At. Spectrom.*, 2 (1987) 55.
- 12 C. Nerín S. Olavide and J. Cacho, *Anal. Chem.*, 59 (1987) 1918.
- 13 M. Ikeda, J. Nishibe, S. Mamada and R. Tujino, *Anal. Chim. Acta*, 125 (1981) 109.
- 14 V. Porta, C. Sarzanini and E. Mentasti, *Mikrochim. Acta*, III (1989) 247.
- 15 E. Pelizzetti and E. Pramauro, *Anal. Chim. Acta*, 169 (1985) 1.
- 16 G. Ramis Ramos, M. Khashwneh, M.C. García de Coque and J.D. Winefordner, *Talanta*, 35 (1988) 41.
- 17 L.J. Cline Love, J.G. Habarta and J.G. Dorsey, *Anal. Chem.*, 56 (1984) 1133A.
- 18 A. Sanz-Medel, P.L. Martínez García and M.E. Díaz García, *Anal. Chem.*, 59 (1987) 774.
- 19 Z. Yin Yan and W. Zhang, *J. Anal. At. Spectrom.*, 4 (1989) 797.
- 20 J. Mora, A. Canals and V. Hernandis, *J. Anal. At. Spectrom.*, 6 (1991) 139.
- 21 M.R. Fernández de la Campa, C. García Ortíz M.E. Díaz García and A. Sanz-Medel, Abstracts of XII Reunión Nacional de Espectroscopía, Barcelona, 1990, Communication AA-10.
- 22 B. Aizpún Fernández, M.C. Valdés-Hevia y Temprano, M.R. Fernández de la Campa, A. Sanz-Medel and P. Neal, *Talanta* 39 (1992) 1517.
- 23 J.C. Miller and J.N. Miller, *Statistics for Analytical Chemistry*, Wiley, New York, 2nd edn.
- 24 M.C. Valdés-Hevia y Temprano, M.R. Fernández de la Campa and A. Sanz-Medel, *J. Anal. At. Spectrom.*, in press.

# Trace elements in medicine

## Speciation: the new frontier

R. Cornelis, F. Borguet and J. De Kimpe

*Laboratory for Analytical Chemistry, University of Ghent, Proeftuinstraat 86, B-9000 Ghent (Belgium)*

(Received 11th September 1992)

### Abstract

Speciation of trace elements in body fluids and tissues consists of defining the many biocomponents to which the trace elements are bound and to explain their mobility, storage, retention and toxicity. Such new frontiers are now open for interdisciplinary research. It is necessary to maintain the integrity of the metal–ligand binding and to check the mass balance of the protein and the trace element throughout the isolation steps. A distinction is made between chemical speciation of the trace element and speciation as a part of cytology. Some methods are discussed for the speciation of As and Cr in serum, together with the limitations of the speciation procedure. It is assumed that the biomolecule and the trace element which are subsequently detected in the same fraction, are indeed associated with one another. This is not necessarily the case, so that confirmation with different means of identification of the biocomponent is imperative. A major problem in speciation work is due to the fact that immense hazards exist for contamination and losses of the trace element. In cytology, meaningful speciation cannot be achieved by ultracentrifugation of the different cell organelles. The best approach nowadays is to use microbeam techniques which are able to locate the trace element in situ, and even to attribute a semiquantitative value to its presence.

*Keywords:* Gel permeation chromatography; Speciation of trace elements; Trace element speciation

Today, very few physicians, if any, would request a total iodine content of a plasma sample. This type of analysis, which was based on the Sandell–Kolthoff reaction [Ce(IV)–As(III) catalysis, with first order reaction rate based on the iodide concentration] [1], has been deleted from the list of standard procedures for the routine clinical laboratory. It has been replaced by measurement of the concentrations of the thyroid hormones T<sub>3</sub>, T<sub>4</sub> and related hormonal compounds. These became the parameters to control the thyroid function and so the I-stores of the body. Iodine provides a good example of a trace

element whose role and pathways are now so well understood that the century-long interest in its total concentration has been completely superseded by that of the components which need the iodine for their biosynthesis.

For most of the other trace elements, and surely for the ultratrace elements, very little is known about their exact biochemical behaviour. On the basis of epidemiological surveys and of animal experiments, they were classified into 3 broad categories: essential, non-essential and toxic. Epic difficulties were encountered in the attempt to determine their total content in a body fluid or a tissue. These problems seem now to be under control, and yet it is not surprising that few attempts have been made to define the many biocomponents to which the trace elements are

*Correspondence to:* R. Cornelis, Laboratory for Analytical Chemistry, University of Ghent, Proeftuinstraat 86, B-9000 Ghent (Belgium).



linked and to explain their mobility, storage, retention and toxicity. Such new frontiers are now open for interdisciplinary research.

It is the aim of this paper to show the need for speciation and to discuss the methods to be developed and the problems that may occur.

#### DEFINING "SPECIATION OF TRACE ELEMENTS IN MEDICINE"

Webster's dictionary still limits the meaning of speciation to "the formation of biological species or the processes leading to this end, whether constituting gradual divergence from related groups or occurring abruptly by combination or transformation of genomes". The chemists borrowed this term and define it in many different ways depending on their discipline and the type of "species" or group of chemicals they are able to isolate with their techniques. In medical sciences two different lines are explored: chemical speciation and cytology of an element.

##### *Chemical speciation in medical sciences*

The more common approach for speciation of trace elements in body fluids consists of the identification and quantification of the biologically active compounds to which the trace element is bound and the quantification of the element in relation to those particular molecules. First, these investigations entail the separation of the bio-components, followed by the determination of the trace element in the different fractions. It is assumed that the biomolecule and the trace element which are subsequently detected in the same fraction, are indeed associated with one another. This is an indirect way to determine species, different from the direct measurement of a specific property, such as, for instance, Cr(V) detection by electron paramagnetic resonances (EPR) spectrometry.

Determination of the different oxidation states of the trace element is another area of speciation research. When different oxidation states can prevail, the problem of their possible oxidation state specific association with biomolecules has still to be investigated. Well known examples are

As(III) and As(V), Cr(III) and Cr(VI), Fe(II) and Fe (III).

Another approach measures the concentration of the compounds which contain the trace element, such as the above mentioned example of iodine in the thyroid hormones. Determination of the enzyme activity of a metal containing enzyme, or the opposite, the inhibition of the enzyme activity, is also used to measure the content of toxic trace element species in body fluids [2,3].

##### *Speciation in cytology*

Speciation of the trace element in cytology deals with the search for its distribution in the cell. It is possible to reveal the location of a trace element in a cell with high resolution microbeam techniques. It can also be investigated by sub-cellular fractionation of the cell organelles by differential centrifugation to be followed by total element detection in the separated fractions.

#### CHEMICAL SPECIATION

In the study of trace element toxicity it has been long known that great differences in toxic properties occur among the species of an element. Many metals are capable of forming small organometallic compounds, and their toxic effects exceed those of the inorganic forms of the elements or of the compounds formed with large molecules. Methylmercury, triethyltin and tetraethyllead are examples of this.

Total element determinations of the trace element are obsolete because the different species follow completely different metabolic pathways. This may also be exemplified with the increasing toxicity of As compounds in the following order: As(III) inorg. > As (V) inorg. > monomethylarsenic acid (MMAA) > dimethylarsenic acid (DMAA) > As(0) > arsenobetaine. In the human body  $\text{AsO}_4^{3-}$  seems to be first reduced from As(V) to As(III), to diffuse through the cell wall and be methylated, as a kind of a detoxifying mechanism, first to MMAA and then to DMAA, the major metabolite in urine. The As(III) species are toxic because they react with free SH groups and inhibit enzymes by blocking the active sites.

In seafood arsenic is present as arsenobetaine, which presumably is not transformed by man and is very rapidly excreted without any toxic effect.

The essential role of a trace element is very often due to its key function as an active component of a large molecule. There are a series of compounds present in human serum which contain a particular element as an essential building stone. A well known example is vitamin B<sub>12</sub>, which is present in different forms, listed as cobalamin, each containing a single Co atom which has a +I, +II or +III oxidation state [4]. Comparing the total vitamin B<sub>12</sub> concentration of about 400 pmol l<sup>-1</sup> with the total concentration of Co in serum at 0.2 μg l<sup>-1</sup> or 3 nmol l<sup>-1</sup>, it appears that the presence of vitamin B<sub>12</sub> only accounts for 13% of total Co, leaving a substantial part unidentified, supposedly bound to other compounds. The procedures which led to understanding cobalamin are alien to analytical chemistry. First the compound was purified, then crystallized and the complex three-dimensional structure elucidated by x-ray diffraction crystallography by Dorothy Hodgkin in 1956 (Nobel Prize in 1964). A few more elements are known to be the essential building stones of particular compounds, for example Cu in ceruloplasmin, and Zn in a series of enzymes. The elemental content of such a protein is expected to be constant. This essential knowledge was mainly investigated by biochemists who used techniques where the risk for inaccurate results by elemental loss or contamination is very limited.

Today some analytical chemists, who originally specialized in total trace element determinations in various body fluids and tissues, now venture into speciation work. An interdisciplinary approach is needed, combining knowledge about the composition of the matrix and of separation methodologies for the biocompounds, with expertise to investigate the trace elements [5]. A qualitative picture is unsatisfactory. The aim goes for the quantitative determination of the biocompound and of the trace element associated with it. One of the main difficulties is that the element is complexed on certain binding sites of a protein, from which it can be easily released depending on the equilibrium constants concerned. Serum albu-

min functions as a complexing agent for many trace elements, but bonds are very weak so that the trace element is available if needed, to be taken up as an essential building stone by other components.

The methods used for separation of the biocomponents are fractionation techniques such as: affinity chromatography, gel permeation chromatography (GPC), ion-exchange chromatography, precipitation and ultrafiltration. The detection of the biomolecules during chromatographic separation occurs through measuring the absorption of radiation in the UV or visible region of the spectrum. It is based on the fact that large molecules, such as proteins, contain chromophores which absorb part of the light. This type of detection offers very little specificity and is hardly semiquantitative. The quantification of the proteins is performed with techniques such as nephelometry, radial immunodiffusion, kinetic immunoturbidity. None of the separation methods meets the requirements for trace element determination and they all pose huge hazards of contamination and loss of the trace element. Another divergence of interest is connected to the fact that developments in biotechnology are focusing on systems that process very small quantities of the biocompounds, offering increasing resolution and specificity. As the proteins carry just one or a few atoms per molecule, the diluted fractions of the isolated proteins, more often than not, contain trace element quantities far below the detection limit of the analytical methods. Therefore separations of proteins for speciation studies have to be performed on a preparative scale with far less resolution and questionable specificity. To improve the sensitivity of the detection of the trace elements, 100 times enrichment procedures of the trace element in the fractions have to be developed.

As mentioned above, contamination hazards and insufficient sensitivity to detect the element are 2 major obstacles in speciation work. They can be partially remedied by performing feasibility studies with *in vivo* and *in vitro* labelled radioactive compounds. To a great extent it facilitates the workload of determining the very low concentrations in the various fractions and virtu-

ally eliminates the immense hazard of distorting the results with exogenous amounts of the trace element: because they are not radioactive, they escape detection. Some second thoughts about radiolabelling have to be kept in mind. In the case of *in vitro* labelling, the radio tracer is only representative for that fraction of the trace element which has been metabolised since its administration. A thorough exchange with body stores would often take a major part of the normal lifespan of the organism, which is usually not feasible. Add to this that Woittiez et al. [6] express a very diminutive view about the use of radiolabels for *in vitro* and *in vivo* experiments, by describing such incubation studies as deliberate contaminations.

#### Methods of speciation

So far there is no ideal method for speciation of protein-bound trace element compounds. To give an idea of procedures which are currently investigated, a separation scheme for a procedure applied to trace element speciation in serum or plasma on fractionating columns is given in Fig. 1. The serum sample will be stored for as short as a period of time as possible at 5°C. For the separation of the proteins several systems are in use: gel permeation chromatography, anion and cation chromatography, affinity chromatography, etc. The eluted-fractions are screened on-line with

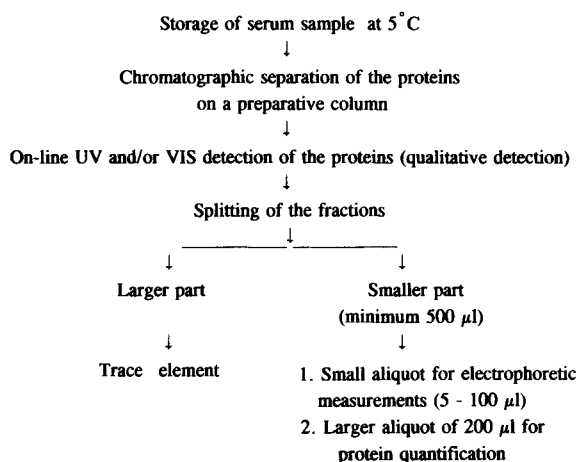


Fig. 1. Separation scheme for trace element speciation in serum or plasma.

a UV-visible monitor and give a qualitative, un-specific indication of the presence of proteins. There exist systems where the apparatus for trace element detection [inductively coupled plasma (ICP)-atomic absorption spectrometry, ICP-mass spectrometry, etc.] is hyphenated to the chromatographical unit. This is a major asset to ensure a quick throughput of the samples. However, the unequivocal identification and the quantification of the eluted protein in the same fraction, as the one processed for trace element determination, is fundamental to establish the link between both components. Proteins can be qualitatively identified by analyzing 5- $\mu$ l aliquots of the eluted fraction by various electrophoretic techniques [iso-electric focusing (IEF) for *pI* determinations, sodium dodecylsulphate polyacrylamide gel electrophoresis (SDS-PAGE) for molecular weight determination], through which the presence of the major proteins can be ascertained.

The quantification of the proteins can be done for instance by nephelometric measurement of the protein-antibody complex. In case the trace element detection occurs on-line, the sample is completely used up, and the determinations of the proteins will have to be done on a separate run.

Experience has learnt that it is necessary to reduce the duration of the chromatographic elution to as short a time as possible, in order to reduce the risk of disturbing the original metallo-protein complexes [7]. The use of fast protein liquid chromatography (FPLC) is a big asset for this type of work. Previous experiments with high capacity (5 ml plasma) standard GPC columns had to be abandoned because of problems associated with both the column retention of Cr and the formation of an unidentified Cr component with a molar mass of  $\pm 5000$ . Irregularities were also observed using the anion exchange chromatography (AEC) column. The original Cr-protein bond cleaved, probably as a result of the long retention time on the columns.

An example of a more detailed chromatographic separation for plasma proteins, as used for the speciation of Cr species, is shown in Fig. 2. The method focused on the separation of transferrin (MW = 80 000) and albumin (MW =

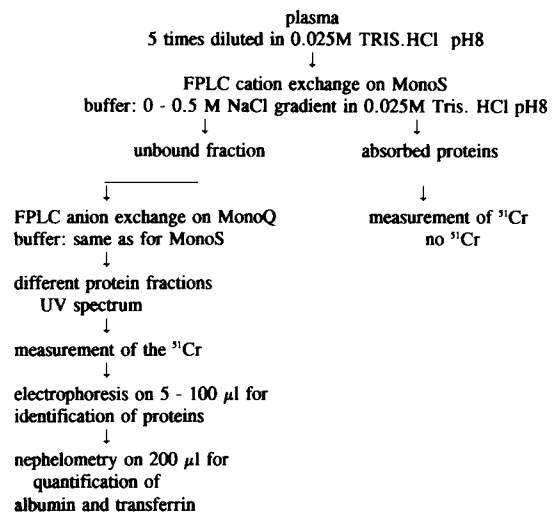


Fig. 2. Separation procedure applied to human plasma for Cr speciation purposes using the radiolabel  $^{51}\text{Cr}$ .

64500), the two main Cr-binding proteins. Because all biocompounds were in vitro labelled with  $^{51}\text{Cr}$ , it was very easy to trace the element by measuring its radioactivity. Furthermore the main proteins were identified in all fractions. From these data it was concluded that Cr is bound to transferrin for 80% and to albumin for 10%. It may be said that it took considerable developing work before the separation scheme was optimized to such a degree that the mass balance for Cr, transferrin and albumin matched the expectations.

The assumption that the biomolecule and the trace element, detected in the same fraction, are indeed associated with one another does not necessarily hold true in all cases. Because of the lack of specificity of these chromatographic separations, it is essential to confirm the identity of the species in different ways. The attempt to speciate As in human serum provided food for thought. The cation-anion separation scheme given in Fig. 2 was applied to serum incubated in vitro with carrier-free  $^{74}\text{AsO}_4^{3-}$  for 24 h. All  $^{74}\text{As}$  was completely eluted from the cation exchanger together with the negatively charged, unbound proteins. Figs. 3 and 4 show the UV-chromatogram of the cation- and anion-exchange elution, as well as the  $^{74}\text{As}$  distribution over the different fractions. The

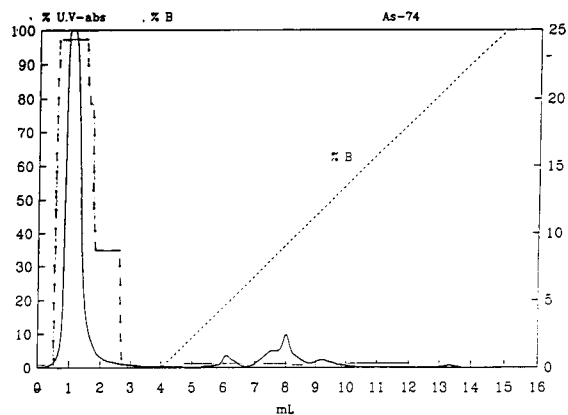


Fig. 3. Elution chromatogram of human plasma incubated with carrier-free  $^{74}\text{AsO}_4^{3-}$  for 24 h on FPLC cation exchange chromatography MonoS and  $^{74}\text{As}$  profile.

proteins present during the main UV absorption peaks were submitted to isoelectric focusing. The fraction identified as asialotransferrin carried 17.7% of the total  $^{74}\text{As}$  radioactivity, the sialotransferrin carried 25.3% and the albumin 56.3%. Unsuspectingly, one might have concluded that the As is bound respectively to transferrin and to albumin in these proportions. However, when the albumin fractions were subjected to GPC on a Superose column (Fig. 5), differentiating the molecules according to molar mass instead of charge, the elution patterns of the albumin and the  $^{74}\text{As}$  did not coincide any more. The  $^{74}\text{As}$  activity became completely dissociated from the

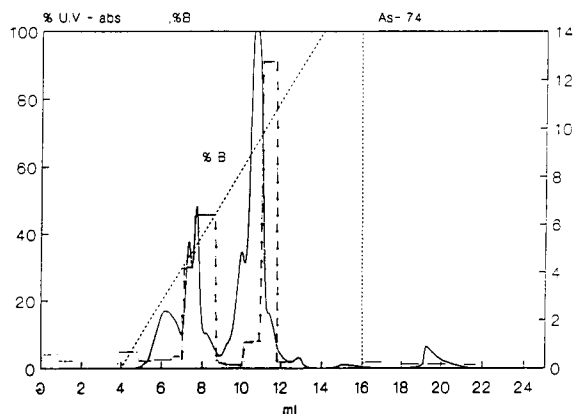


Fig. 4. Elution chromatogram of unbound proteins using cation-exchange chromatography on FPLC anion-exchange chromatography MonoQ together with the  $^{74}\text{As}$  profile.

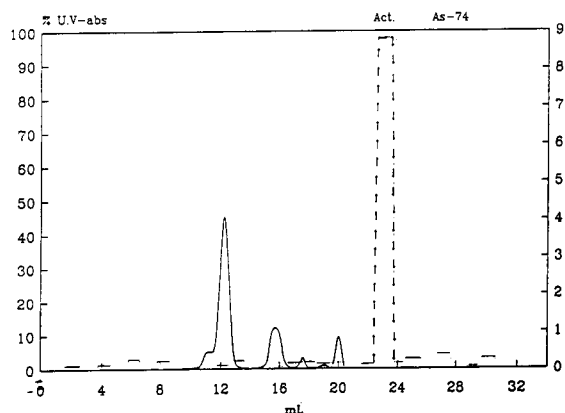


Fig. 5. Gel permeation chromatography (Superose) of fraction containing albumin of the anion-exchange chromatography elution, together with the  $^{74}\text{As}$  profile.

albumin and eluted as a low-molecular-weight compound with an elution volume  $V_e$  far beyond the interstitial volume  $V_i$  of the column (see Fig. 5).

In order to improve the reliability of the results it is necessary to subject the fractions containing the trace element to other separation techniques based on different properties of the molecules. If there is no contradiction between the findings of the cation–anion chromatography, and the isoelectric focusing tests on the one hand, with those of GPC, SDS-PAGE and ultrafiltration on the other hand, then the probability of having made an erroneous association between a protein and the trace element decreases to a great extent. The uncertainty of the conclusion is, however, something one has to live with if one approaches speciation of the trace element with such indirect methodologies. It is evident that the availability of a reference material for quality control in speciation work is very much needed.

Whereas trace element speciation in serum or plasma is still in its infancy, the study of the group of the metal complexing protein metallothioneins has received a lot of attention during the past three decades [8]. Thioneins are well known for their functions in protecting the cells and tissues from the toxic action of cadmium and other soft metal ions. Kägi [9], who performed pioneering work in this field, actually attributed to metallothioneins the very characterizing epi-

theton: “Thionein, a Protein for all Seasons”. Metallothioneins have been mainly studied in liver tissue, which entails all kind of difficulties in handling solid samples. The methods currently used to analyze metallothioneins are radioimmunoassay (RIA)–ELISA, but also chromatographic analyses coupled to trace element detection equipment are explored. As the approach of the RIA–ELISA methods is such that nearly all attention goes to the molecule, this domain is somewhat alien to the analytical chemist specialized in trace element analyses. More information on metallothioneins can be found in Refs. 6, 8 and 9.

#### *Speciation in cytology*

An endless way to determine the location of a trace element in the different organelles consists in the homogenization of the tissue followed by differential centrifugation.

The homogenization is done with a Potter–Elvehjem homogenizer, so that the cells erupt without harming the subcellular structure. This will be followed by differential centrifugation: at 700 g the nuclei, at 9000 g the mitochondriae, at 30 000 g the lysosomes; at 10 500 g the microsomes; the remaining fraction consists of cytosol. In principle the trace element content of all these fractions could be investigated, but it would be very naive to attribute too much value to that data.

There are many pitfalls in this procedure when applied to trace element analyses of the different organelles. First of all, not all the cells will have been homogenized. The intact cells and their fragments can be discarded by sieving through nylon. Furthermore it is very doubtful that the metal–organelle binding remains intact throughout the long subcellular fractionation process in the homogenization buffer solution. Add to this that the hazard of contamination (from all the reagents and the walls of the vessels), is so great that the mass of the trace element will probably exceed the original total trace element mass by many orders of magnitude. Sucrose can serve as a suitable homogenizing buffer, but this reagent cannot be obtained with a sufficiently low blank value for reliable trace element speciation work.

Another major criticism consists in the observation that not a single fraction consists of one type of organelle only. Each fraction will contain a mixture of all organelles, largely enriched in one type.

The more relevant way to discover the location of a trace element on a cellular level is to use microbeam techniques, such as laser microprobe mass analysis (LAMMA), electron energy loss spectroscopy (EELS), electron beam analytical techniques and microbeam particle induced x-ray emission (PIXE). In a first approach this is a qualitative technique, although some researchers succeeded in giving these determinations a semi-quantitative character [10].

### *Conclusions*

Speciation of trace elements in body fluids and tissues has been approached in many different ways, during the last decades. Although the discipline of the researcher seems to play an important role in defining “speciation”, every approach adds some knowledge about the composition of the compounds to which the trace element is bound and how it acts in the human body. Such speciation analyses are, however, extremely difficult because of the complexity of the body. All analytical measurements should be accurate and precise, and systematically checked for the yields of both the trace element and the biocompound.

The availability of a reference material certified for particular species would be a formidable asset in this endeavour.

### REFERENCES

- 1 W.T. Binnerts in D. Glick (Ed.), *Determination of Iodine in Biological Material (Methods of Biochemical Analysis, Vol. 22)*, Wiley, New York, 1974, pp. 253–306.
- 2 D. Behne, *Analyst*, 117 (1992) 7.
- 3 R. Cornelis, *Analyst*, 117 (1992) 583.
- 4 L. Stryer, *Biochemistry*, Freeman, New York, 3rd edn., 1988.
- 5 R. Cornelis in: J.A.C. Broekaert, Ş. Güçer and F. Adams (Eds.), *Speciation of Trace Elements in Serum or Plasma (NATO ASI Series Vol. G. 23), Metal Speciation in the Environment*, Springer Verlag, Berlin, Heidelberg, 1990.
- 6 J.R.W. Woittiez, H.T. Wolterbeek, G.J. Van den Berg and O.M. Steinebach, presented at the 6th International Workshop on Trace Element Analytical Chemistry in Medicine and Biology, Neuherberg, April 24–26, 1991, to be published in *J. Trace Elements Electr. Health Dis.*, (1993).
- 7 F. Borguet and R. Cornelis, *Biol. Trace Element Res.*, 26–27 (1990) 439.
- 8 G.E. Batley, *Trace Element Speciation: Analytical Methods and Problems*, CRC Press, Boca Raton, FL, 1989.
- 9 J.H.R. Kägi, presented at the ISTERH third Int. Conf. & NTS fourth Nordic Conf. on Trace Elements in Health and Disease, Stockholm, May 25–29, 1992, *Scand. J. Work Environ. Health*, (1993) in press.
- 10 D.F. Vandeputte, J. Savory, R.E. Van Grieken, W.A. Jacob, R.L. Bertholf and M.R. Wills, *Biomed. Environ. Mass Spectrom.*, 18 (1989) 589.

# Absorption and bioavailability studies of mineral nutrients by mass spectrometry

F.A. Mellon, J. Eagles, T.E. Fox and S.J. Fairweather-Tait

*AFRC Institute of Food Research, Norwich Laboratory, Norwich Research Park, Colney, Norwich, Norfolk NR4 7UA (UK)*

(Received 8th September 1992)

## Abstract

Minerals are essential for the maintenance of a wide range of metabolic functions in human beings, yet there is a lack of adequate information regarding their absorption, bioavailability and metabolism. Enriched stable isotopes provide safe, ethically acceptable and scientifically rigorous tools for investigating the metabolism of mineral nutrients in human subjects. Microchemical and mass spectrometric techniques used for conducting human studies of the metabolism of essential minerals are described and discussed with reference to the precision of stable isotope ratio measurement normally required in these experiments. Specific examples are given, involving both single and double isotope labelling procedures. These include investigations of calcium and zinc absorption from different foodstuffs and a study of zinc metabolism aimed at the determination of body pool sizes. The convenience and precision of different mass spectrometric methods are discussed and stable isotope methodology is compared to radio-labelling techniques.

**Keywords:** Mass spectrometry; Calcium; Isotope ratio measurements; Mineral nutrients; Zinc

Nutrient minerals and other elements are essential for the maintenance of a wide range of metabolic functions in the human body. The importance of iron as the binding site of oxygen in haemoglobin has long been recognised, however the prominence of other nutritional minerals has been appreciated more recently. Zinc, for example, was only proposed as an essential mineral for humans in 1960; it is now recognised to be a co-factor in the functioning of over 100 enzymes (a list which is still growing). Iron, zinc, calcium, copper, magnesium, chromium, and selenium are nutritionally important minerals which are amenable to mass spectrometric (MS) techniques

for studying their metabolism because they possess more than one isotope.

The early focus of mineral nutrition research was on the prevention of gross conditions such as anaemia (resulting from iron deficiency), zinc-responsive growth retardation, and acute zinc deficiency syndromes which manifest themselves in a clear and striking manner. However the possibility of more subtle effects of marginal, rather than extreme, deficiencies of nutrient minerals are now been recognised as important. For example, manifestations of iron deficiency in blood tests are usually only found after the body has diverted iron from other essential areas, such as promoting brain growth in infants, in order to attempt to maintain erythrocyte iron at levels sufficient to support oxygen carrying function. Thus overt deficiency symptoms are only be the tip of the

*Correspondence to:* F.A. Mellon, AFRC Institute of Food Research, Norwich Laboratory, Norwich Research Park, Colney, Norwich, Norfolk NR4 7UA (UK).

iceberg. There are strong arguments supporting the maintenance of *optimal* function as a basis for defining micronutrient requirements, rather than the levels necessary to prevent or cure deficiencies. This has always been the case, but is only just becoming widely appreciated. An understanding of optimal nutrition requires a firm base of scientific evidence regarding the bioavailability, absorption and metabolism of micronutrients; unfortunately, these data are lacking for many nutrient minerals.

The use of stable isotopes as tools for the investigation of nutrient metabolism has a long history. However, the increased adoption of these techniques in the study of mineral nutrition is relatively recent, having previously been overshadowed by the extensive use of radioisotopes as tracers of mineral metabolism. Concerns over the hazards of ionizing radiation have caused the shift towards stable isotope techniques, particularly where studies of such vulnerable groups as pregnant women, infants and young children are concerned. Even for population groups where low level radiation exposure is considered to be relatively safe, it is increasingly difficult to find volunteers willing to participate in radiolabelling studies.

Enriched stable isotopes provide harmless, ethically acceptable and scientifically rigorous tools for investigating the absorption and metabolism of mineral nutrients in human subjects [1]. Their main drawback is that a stable isotope label is not a true tracer. Isotopes must be measurable above the natural abundance of those already present in the sample. The administration of excessive amounts of label will perturb the biological system under investigation, yielding atypical data and possibly even resulting in toxic overload. On the other hand, dispensation of small amounts of label relative to the size of body pools or to quantities of excreted mineral may result in changes in isotope ratio too small to measure accurately. Body pool sizes, the precision of isotope ratio measurement achievable and mineral excretion rates are among the factors which must be considered in designing mineral nutrition studies. It is also possible that isotopes may be metabolised at different rates (“isotope

effects”), but this is unlikely to be a significant problem with essential minerals because of their high atomic mass.

An additional important consideration is the form in which the isotope is administered when oral dosing is used. The two basic techniques used with foods are intrinsic and extrinsic labelling. Extrinsic techniques are the simplest and the cheapest methods of labelling foods and are achieved by mixing the isotope with the food prior to consumption. Implicit in this approach is the assumption that the label exchanges completely with the endogenous food mineral, an assumption which is, in many cases, invalid. Intrinsic labelling incorporates the isotope into the food in exactly the same manner as the endogenous mineral. This is accomplished by growing food plants in nutrients incorporating the label, or (in the case of meat, eggs or milk) by injection of solutions of the label into the producer animal. Intrinsic labelling is expensive and time-consuming, consequently extrinsic labelling is far more common, however an awareness of the limitations of this technique is absolutely essential in planning nutritional experiments.

The initial exploitation of techniques of fast atom bombardment mass spectrometry (FAB-MS) for measuring isotope ratios has been superseded, in our laboratory, by thermal ionization mass spectrometry (TIMS) using a relatively inexpensive, simple, quadrupole mass spectrometer. The TIMS methods developed are sufficiently precise, accurate and rapid for conducting the vast majority of mineral nutrition experiments and have been applied to studies of calcium and zinc absorption in a number of nutritional studies, described below, and have also been compared with alternative approaches involving inductively coupled plasma mass spectrometry (ICP-MS) and FAB-MS.

## EXPERIMENTAL

### *Human volunteers*

Details of the numbers and sex of volunteers used in these studies are given in the appropriate references. All studies were approved by the Institute of Food Research Ethical Committee.



### *Stable isotope solutions*

Enriched stable isotopes ( $^{67}\text{Zn}$ ,  $^{70}\text{Zn}$ ,  $^{42}\text{Ca}$ ,  $^{44}\text{Ca}$ ) were purchased from Technical and Optical Equipment (London), Medgenix (Ratingen) or Oak Ridge National Laboratory (Oak Ridge, TN). Isotopic composition was always checked mass spectrometrically before use in any experiments. Solutions of stable isotopes were made up according to published methods. The concentration of the solutions was determined by atomic absorption spectrometry, or by isotope dilution.

### *Administration of stable isotopes*

Isotopes were administered orally and/or by intravenous (i.v.) injection. Carmine and/or radio-opaque markers were also given with labelled meals. Fuller details are given in the appropriate references, cited in the text.

### *Sample collection and processing*

**Faecal samples.** Faecal samples were collected until all markers (carmine or radio-opaque) had been excreted, plus one further collection. Samples were stored at  $-18^{\circ}\text{C}$  until studies had been completed. Collections from each subject for each period were combined, thawed, autoclaved at  $121^{\circ}\text{C}$  for 20 min, freeze-dried, and ground to a fine powder and sieved (if necessary) to remove radio-opaque markers.

**Blood samples.** Blood samples for zinc isotope analysis (5–10 ml) were either taken by venepuncture, using veins in the arm or ankle, or through a venous catheter (collection methods varied according to the type of experiment performed, full details are given in the references cited below). The blood was centrifuged at 1500 g for 5 min and the plasma removed and stored at  $-18^{\circ}\text{C}$  until analysis.

Samples for calcium analysis were collected in heparinized tubes, centrifuged and the plasma removed. Trichloroacetic acid ( $35\text{ g l}^{-1}$ ) was added in the ratio 3:1. The mixture was allowed to stand for 15 min at  $4^{\circ}\text{C}$ , and was then centrifuged and the deproteinized supernatant fraction removed.

**Urine samples.** Complete urine collections were made for each 24-h period. All containers used for the collection were acid washed and deionised.

**Saliva samples.** Saliva samples were provided by subjects in acid washed plastic tubes at regular intervals. These samples were stored at  $-18^{\circ}\text{C}$  prior to analysis.

### *Sample purification*

The methods for purifying zinc and calcium in biological matrices outlined below describe the most recent techniques in use in our laboratory. Earlier techniques, described in some of our publications cited below, have now been superseded by these methods. Urine, saliva and plasma samples used for measuring Ca isotopes by fast atom bombardment were either used directly (after addition of HCl or  $\text{HNO}_3$ ) or after oxalate precipitation to concentrate samples low in Ca.

**Zinc in faeces.** Sub-samples of the powdered faeces were burned to ash in silica crucibles at  $480^{\circ}\text{C}$  for 48 h. Portions (0.1 g) of the ash were dissolved in 2 ml of warm, 9 M HCl (Aristar, BDH) overnight in silica crucibles. A further 2 ml of 9 M HCl was added and the resulting solution transferred to a plastic vial by washing with 8 ml of distilled water.

A 200–400 mesh AG 1-X8 anion exchange resin (Bio-Rad Labs., Richmond, VA) was prepared by swelling in water for two days prior to stirring with a PTFE magnetic bar and packing into a short form glass Pasteur pipette. The 7-cm pipette packing was plugged with glass wool, washed with 60 ml of 2 M  $\text{HNO}_3$  using a peristaltic pump operating at a flow of  $1\text{ ml min}^{-1}$  and regenerated to the chloride form with 60 ml of 0.5 M HCl. After addition of the sample solution, the pipette was washed with a further 30 ml of 0.5 M HCl and the zinc was eluted with 20 ml of 0.04 M HCl and collected in 1 ml fractions. Individual fractions were dried by evaporation under an infrared lamp in a laminar flow cabinet. Fractions contained approximately  $10\text{ }\mu\text{g}$  of zinc.

**Zinc in blood and urine.** Plasma (1 ml plus 5 ml acid) and urine (5 ml of 5-fold concentrated plus 10 ml acid) were digested in 15 M  $\text{HNO}_3$  in a microwave oven (MDS-81D, CEM Co., Matthews, NC) in pressurized PTFE vessels. The heating time was 20.5 min per 12 samples (50% power for 30 s, 100% power for 4 min and 50% power for 16 min). The solutions were then evap-

orated to dryness in PTFE vessels on ceramic hotplates in a filtered air fume hood. The residue was dissolved in 2 ml concentrated HCl (Aristar grade) and 8 ml of quartz distilled water was added. Zinc was extracted by anion exchange, as described above, with the exception that polypropylene (rather than glass) columns were used.

*Calcium in urine and saliva.* Urine and saliva samples were ashed according to procedures very similar to those described for zinc in blood. The ashed sample solutions were adjusted to give a nitric acid concentration of 0.2 M. Anion-exchange columns of 200–400 mesh Dowex 50W-X8 (Aldrich, Gillingham) were prepared and pre-washed with 2 M HNO<sub>3</sub> as for zinc. Columns were then treated with 0.2 M HNO<sub>3</sub> for 30 min and calcium samples when loaded in 0.2 M HNO<sub>3</sub>. The columns were washed with 0.2 M HNO<sub>3</sub> for 30 min and the calcium was eluted with 2 M HNO<sub>3</sub>. The eluent was evaporated and the residue dissolved in 0.04 M HCl.

A further step of ion-exchange purification was found to be necessary, especially for low sample levels and low enrichments. A 200–400 mesh Dowex AG 50 W × 12 (H<sup>+</sup> form) column was used, following pre-washing with 30 ml of 6 M HCl and 30 ml of distilled water. Sample solutions were then added to the columns in 0.04 M HCl. The columns were washed with 20 ml of distilled water and the calcium was eluted with 1.8 M HCl. The first 9 ml of eluent were discarded and the next 10 1.5-ml fractions collected and evaporated to dryness.

#### *Mass spectrometry*

*Fast atom bombardment.* FAB-MS was conducted using an MS80 RFA mass spectrometer (Kratos Analytical, Manchester) [2–4]. Samples were analyzed in triplicate, interposed between two bracketing standards of known isotopic composition in order to correct for instrumental variables and fractionation.

*Thermal ionization mass spectrometry.* TIMS was carried out on a Thermoquad (THQ) mass spectrometer (Finnigan MAT), as described previously [4,5]. The instrument was checked regularly against isotopic standards, yielding 0.1–0.5%

relative standard deviation (R.S.D.) for isotope ratios with sample loadings down to 1 µg and < 1% R.S.D. with loadings between 100 ng and 1 µg.

*Inductively coupled plasma mass spectrometry.* ICP-MS of zinc samples was performed using a Plasma Quad (VG Elemental, Winsford) instrument. Operating conditions have been described in previous publications [6,7]. Samples were introduced into the plasma by either flow injection (FI) or continuous nebulization (CN).

## RESULTS AND DISCUSSION

### *Calcium absorption from milk and watercress: an FAB-MS study*

Bioavailability is a key concept in nutritional research and is defined as the proportion of a nutrient in particular foods and diets that can be absorbed and utilised by the body. Calcium in milk has been judged to be more bioavailable than that in cereals or vegetables although firm experimental evidence for this opinion has been lacking. A study was therefore designed to compare Ca absorption from skimmed milk and Ca-enriched skimmed milk (Vital<sup>TM</sup>, Express Foods Group, South Ruislip) with that from watercress soup, a non-dairy food high in Ca [3]. A double-label technique, <sup>44</sup>Ca to label the food and intravenously injected <sup>42</sup>Ca to label plasma and urine, was used to allow for excretion of endogenous Ca [8,9]. The validity of extrinsically labelling watercress with Ca has been established previously by using a radiolabel (<sup>47</sup>Ca) in a rat study. Other groups have shown that Ca in milk can be labelled extrinsically [10].

Ten adult male volunteers were divided into two equal groups with similar Ca intakes and were each given (after an overnight fast) 250 g of watercress soup, containing 131 mg Ca, to which 30 mg <sup>44</sup>Ca (98.78 atom%) had been added as calcium chloride. Subjects were given an intravenous injection of <sup>42</sup>Ca 2–3 h later, i.e., when the plasma concentration of <sup>44</sup>Ca was at its highest. Blood and saliva samples were taken 12 h later and 24-h urine collections were made for 6 days, commencing immediately after the labelled

meal. This procedure was repeated on a separate occasion, the only difference being the substitution of 136 ml of skimmed milk (containing 154 mg Ca) or 83 ml Vital (calcium gluconate enriched skimmed milk containing 154 mg Ca) for the labelled meal. An additional 30 mg of  $^{44}\text{Ca}$  was added to the milk portions. If one makes the reasonable assumption that orally and i.v. administered isotopes are metabolized at the same rate when equilibrium has been reached, absorption from the oral dose can be calculated in plasma, urine and saliva by the simple equation [9]:

$$\text{ABS} = \frac{(\text{na}^{44}\text{Ca})(^{42}\text{Ca i.v.}) \times \Delta\% \text{XS}^{44}\text{Ca} \times 100}{(\text{na}^{42}\text{Ca})(^{44}\text{Ca oral}) \times \Delta\% \text{XS}^{42}\text{Ca}} \quad (1)$$

where ABS is the %absorption, na the natural abundance of the particular Ca isotopes (relative to  $^{40}\text{Ca}$ ), i.v. and oral refer to the exact doses of  $^{42}\text{Ca}$  and  $^{44}\text{Ca}$  given, and  $\Delta\% \text{XS}$  represents the %difference by which the measured enriched ratio exceeds natural abundance.

The mean results of measurements of Ca absorption from the two milks and from watercress soup are shown in Table 1.

Statistical analysis of these data confirms that there is no significant difference between the absorption of Ca from skimmed milk and Vital. A wide range of absorption values was found in the Vital group, consequently no statistically significant difference between absorption from Vital and watercress soup could be detected. However, absorption of Ca from skimmed milk was significantly higher ( $P < 0.001$ ) than from watercress soup.

The work described above clearly demonstrates that stable isotope double-labelling tech-

niques can be used to measure Ca absorption from milk and vegetable products. Further measurements, not recounted in detail here but described fully elsewhere [3], indicated a good correlation between  $^{44}\text{Ca}$  absorption measurements in urine, saliva and plasma.

The isotope ratios measured by FAB-MS yielded precisions averaging 0.5% R.S.D., in general agreement with data obtained in pioneering work, carried out in other laboratories, evaluating the FAB technique for measuring Ca absorption [11–13]. This degree of precision is perfectly adequate for measuring the changes of isotope ratio of 5–15% above normal found in the course of this experiment. It is desirable to maintain changes in isotopic abundance at these or similar levels (less than 50% has been suggested [13]), given the main constraints of the need to maintain normal metabolism by administering typical doses, and the desirability of keeping the cost of experiments down to a reasonable level.

This study provided useful data on absorption of Ca with the aid of relatively accessible FAB-MS which is widely available on conventional, medium resolution organic mass spectrometers. Sample preparation was straightforward and tests showed that measurements could be conducted on as little as 100 ng quantities of Ca. The main drawbacks of the method were the lengthy period of development required to optimise the FAB technique, and the operator-intensive nature and lack of automation of the measurements. Interferences due to monohydride formation present difficulties in FAB isotope ratio determinations of some minerals, however this was not a problem in the case of Ca because of the 2 mass unit gap between the measured isotopes. Because of the drawbacks of the FAB method we have used a thermal ionization mass spectrometer (see experimental), a dedicated instrument for inorganic analysis similar to that used in other laboratories [14–16]. However the FAB technique still has much to offer and has been successfully exploited and evaluated in metabolic studies of a variety of trace elements [17–21]. Ultimate choice of instrumentation will depend on a number of factors, including cost, accessibility, sensitivity, precision, ease of use and degree of automation.

TABLE 1

Mean Ca absorption from skimmed milk, Ca-fortified skimmed milk and watercress soup in ten adult males, measured in plasma 24 h post-dosing

	Mean	S.E.M. <sup>a</sup>	Range (%)
Skimmed milk	45.5%	1.9	41.0–52.3
Vital <sup>TM</sup>	35.7%	4.7	20.5–48.9
Watercress soup	27.4%	1.9	17.6–36.7

<sup>a</sup> S.E.M. = Standard error of mean,  $n = 10$ .

*Zinc absorption: a stable isotope study of the effects of food processing and an evaluation of TIMS, ICP-MS and FAB-MS for determining  $^{64}\text{Zn}/^{67}\text{Zn}$  isotope ratios*

It has been suggested that thermal processing of foods may have deleterious effects on the bioavailability of nutrients. Experimental evidence has been presented which indicates that extrusion cooking of a high fibre cereal product reduces the bioavailability of zinc, magnesium and phosphorus when compared to conventionally cooked products [22]. Extrusion cooking is now in widespread use in the food industry, consequently it was decided to conduct further investigations into the potentially adverse effects of food processing techniques on the availability of Zn and Fe in the presence of high fibre processed wheat bran products [17]. The Zn study was performed with the aid of isotope ratio MS but iron isotopes were measured by neutron activation analysis since the methodology for measuring  $^{57}\text{Fe}$  by MS had not been developed sufficiently at the time the experiment was carried out, a situation that has since been remedied.

Eleven volunteers were given a meal comprising either 40 g of extrusion-cooked wheat bran/white wheat flour (50:50 mix), consumed with 100 ml milk, or the same quantity of flour/bran heated with the milk to form a conventionally-cooked porridge. At the same time, the subjects were given 170 ml of a cola drink containing a solution of  $^{67}\text{Zn}$  (5.51 mg of 93.11 atom%  $^{67}\text{Zn}$  in 1.0 ml of 0.5 M HCl). Markers (radio-opaque and carmine) were administered with the test meal and a normal evening meal respectively, consumed on the same day. Faecal collections were made for each subject and the  $^{64}\text{Zn}/^{67}\text{Zn}$  ratios were determined by FAB-MS, TIMS and ICP-MS, following extraction and purification of the zinc as described above. Total zinc content was measured by atomic absorption spectrometry.

The apparent absorption of zinc is calculated very simply from the values for total Zn content and the  $^{64}\text{Zn}/^{67}\text{Zn}$  ratio of faecal Zn. For males, extrusion-cooked cereal gave an apparent absorption of  $22.2 \pm 3.3\%$  (mean  $\pm$  S.D.), and a conventionally cooked sample,  $19.0 \pm 1.8\%$ . For females,

the values were  $17.2 \pm 2.0$  and  $21.0 \pm 3.2\%$ , respectively.

Statistical analysis demonstrates that these data indicate no significant differences between Zn absorption for the two different meals, and no differences between male and female subjects. The lack of any effect on Zn absorption compared to the Swedish study [22] may be due to differences in foodstuff composition, however a more likely explanation is provided by the major differences in intestinal physiology between the normal, healthy subjects used in the current study compared to the ileostomy patients used in the Swedish experiment.

The above study on Zn absorption had an additional dimension in that it provided an opportunity to evaluate different mass spectrometric methods for determining  $^{64}\text{Zn}/^{67}\text{Zn}$  ratios on zinc derived from labelled faecal samples [4,7]. Isotopically-enriched zinc isolated from the samples collected during the course of the extrusion experiment was subjected to measurement by quadrupole TIMS, FAB-MS and ICP-MS. In the case of ICP-MS, two different sample introduction techniques were used: continuous nebulization (CN) and flow injection (FI). A typical sample (a more comprehensive list of ratios is reported elsewhere [7]) of some of the results is shown in Table 2. Statistical analysis of the full set of data demonstrated that there were no significant differences between the ratios determined by the different mass spectrometric methods. FAB-MS, TIMS and ICP-MS (CN) all yielded isotope ratios with a precision of 1% R.S.D. or better, generally considered to be adequate for

TABLE 2

Example data from comparison of FAB-MS, TIMS and ICP-MS measurements of  $^{64}\text{Zn}/^{67}\text{Zn}$  isotope ratios in  $^{67}\text{Zn}$  enriched faecal extracts

Sample	Isotope ratio			
	FAB	TI	ICP (CN)	ICP (FI)
45/1	5.55	5.42	5.52	5.63
38/2	4.29	4.24	4.20	4.12
19/2	2.90	2.96	2.97	3.14
Mean R.S.D. (%)	0.5	0.5	0.3	4.9

studies of human mineral metabolism [23–24]. Only flow-injection ICP-MS gave results too imprecise to be acceptable for general nutritional work (although the data would be acceptable for quantitative isotope dilution, rather than tracer, measurements).

Both ICP-MS and quadrupole TIMS have advantages over FAB-MS in terms of their sensitivity, degree of automation and freedom from metal hydride interferences. ICP-MS and quadrupole TIMS methods have also been developed for measuring a wider range of nutrient minerals than FAB and inter-laboratory comparisons have shown that they are capable of achieving the requisite levels of accuracy and precision for successful metabolic studies [25]. ICP-MS has advantages over TIMS for Zn measurements in that a lesser degree of sample processing is required and isotope ratio measurement is more rapid.

The final choice of mass spectrometric method will be dependent on a number of factors, as discussed in more detail elsewhere [7]. However, it is fair to conclude that studies of Zn metabolism are feasible with the aid of any of the methods described above.

#### *Exchangeable pools of zinc measured by TIMS determination of $^{70}\text{Zn}$*

Nutritional status is a measure of how well dietary intake meets physiological needs. An essential prerequisite for establishing dietary zinc requirements is the clarification of the relationship between intake and body Zn status. As yet, no method of measuring Zn status has been developed, thus alternative approaches must be considered. The measurement of plasma Zn kinetics has the potential to yield important information regarding this relationship. A preliminary study of the kinetics of Zn metabolism has been conducted using  $^{70}\text{Zn}$  and TIMS to measure the movement of this label [26].

Two volunteers were injected with a zinc solution containing 1.355 mg (male) and 0.290 mg (female) of  $^{70}\text{Zn}$  (65.51 atom%). Blood samples were then collected over 9 days, initially more frequently (9 collections in 2 h, 10 further collections in 24 h) then daily. Complete urine and faecal collections were also made every 24 h. The

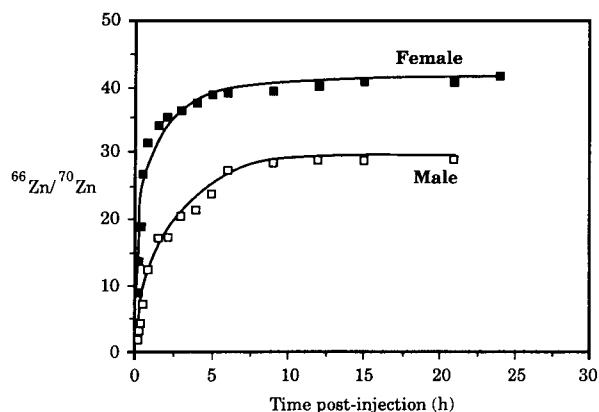


Fig. 1. Change in plasma  $^{66}\text{Zn}/^{70}\text{Zn}$  ratio during first 24-h post-injection in female and male subjects injected with  $^{70}\text{Zn}$ .

$^{70}\text{Zn}/^{66}\text{Zn}$  isotope ratios of the plasma, urine and faecal samples were then determined. Curves plotting the changes in the  $^{66}\text{Zn}/^{70}\text{Zn}$  ratio in plasma over the 24-h period after injection are shown in Fig. 1.

These data, in addition to  $^{66}\text{Zn}/^{70}\text{Zn}$  isotope ratios in urine and faecal samples, can be subjected to kinetic modelling to calculate the total  $^{70}\text{Zn}$  present in different pools over a period of time and the rate of turnover of the pool [26]. The study demonstrated that the method could be used to predict body pool sizes and, in addition to the plasma zinc pool, indicated the presence of a rapidly exchangeable (0–1 h) pool of 10 mg and one or more slowly exchanging pools of approximately 200 mg. Although further research is needed to refine and test the validity of the assumptions implicit in the models used, the methodology shows great promise as a technique for analyzing body zinc pools and may lead to useful means of assessing zinc status.

#### *Conclusions*

Three different mass spectrometric techniques FAB-MS, quadrupole TIMS and ICP-MS, have sufficient accuracy and precision to conduct a wide range of human studies on the metabolism of enriched stable isotopes of Zn and Ca. FAB is extensively available in mass spectrometry laboratories because of its widespread use as a routine technique for the analysis of complex organic

molecules, however achievement of the levels of precision and accuracy needed in metabolic studies requires a high level of technical skill and commitment. TIMS and ICP-MS have the considerable advantages of higher sensitivity and increased automation and sample throughput over the FAB technique, as well as being well-established techniques of inorganic mass spectrometry. TIMS with a magnetic sector mass analyzer is capable of a high degree of precision and has been used to conduct metabolic studies on a wide range of nutrient elements, including Fe, Zn, Ca, Cu and Mg<sup>27</sup>. The less expensive technique of quadrupole TIMS yields lower precision isotope ratios than magnetic sector TIMS, however the data are still more than adequate for conducting nearly all metabolic studies. A possible exception might be the measurement of excreted stable isotopes in population groups which are very efficient at absorbing particular mineral nutrients, where high precision data would be needed because of the consequently low enrichments found in urine and faeces.

ICP-MS is more rapid than TIMS and can often be used with minimal amounts of sample processing and purification, although subject to interference problems at some masses (a not insuperable problem for most minerals, with the possible exception of Ca) and is rapidly becoming the most popular technique for conducting mineral metabolism studies. Both TIMS and ICP-MS are capable of determining isotopes of all the multi-isotopic trace minerals (Fe, Zn, Ca, Cu, Cr, Se and Mg) which are important human micronutrients.

Stable isotope techniques have advantages and disadvantages compared to radioisotopes in metabolic studies. On the one hand, radioisotopes are relatively easy to measure non-invasively and are capable of pinpointing sites of absorption and metabolism in the body quite precisely. Stable isotopes, on the other hand, must be determined using expensive and complex equipment, often after extensive sample purification, and can only be measured either invasively (blood sampling or biopsy) or indirectly (faecal and urine collection). Radioisotopes are also genuine tracers, in that it is possible to administer

them in very small (carrier-free) quantities, however stable isotopes must be administered at levels where changes in isotope ratio can be detected. This may represent a substantial fraction of, or even more than, the body's normal daily intake and may result in metabolic disturbance unless given in multiple doses over several days. This type of problem is likely to arise if attempts are made to label a mineral which has a large body pool (e.g., iron in blood). Stable isotopes have the practical advantage over radioisotopes that their activity does not decay, consequently samples can be analyzed long after collection, allowing considerably more flexibility in experimental protocols. Additionally, it is much simpler to conduct multiple-labelling experiments using stable isotopes and it is even possible to carry out multielement studies. However, the strongest argument in favour of stable isotopes is found in the overriding need to conduct experiments safely and ethically.

The authors wish to thank the Agricultural and Food Research Council, Ministry of Agriculture Fisheries and Food, Milk Marketing Board and the European Community for funding.

#### REFERENCES

- 1 J.R. Turnlund, in R.G. Whitehead and A. Prentice (Eds.), *New Techniques in Nutritional Research*, Academic Press, New York, 1991, pp. 113–130.
- 2 D.E. Pratt, J. Eagles and S.J. Fairweather-Tait, *J. Micro-nutr. Anal.*, 3 (1987) 107.
- 3 S.J. Fairweather-Tait, A. Johnson, J. Eagles, S. Ganatra, H. Kennedy and M.I. Gurr, *Br. J. Nutr.*, 62 (1989) 379.
- 4 J. Eagles, S.J. Fairweather-Tait, D.E. Portwood, R. Self, A. Götz and K.G. Heumann, *Anal. Chem.*, 61 (1989) 1023.
- 5 A. Götz and K.G. Heumann, *Fresenius, Z. Anal. Chem.*, 325 (1986) 24.
- 6 J.R. Dean, L. Ebdon, H.M. Crews and R.C. Massey, *J. Anal. At. Spectrom.*, 3 (1988) 349.
- 7 J. Eagles, S.J. Fairweather-Tait, F.A. Mellon, D.E. Portwood, R. Self, A. Götz, K.G. Heumann and H.M. Crews, *Rapid Commun. Mass spectrom.*, 3 (1989) 203.
- 8 J.A. DeGrazia, P. Ivanovich, H. Fellows and C. Rich, *J. Lab. Clin. Med.*, 66 (1965) 822.
- 9 A.L. Yergey, N.E. Vieira and D.G. Covell, *Biomed. Environ. Mass Spectrom.*, 14 (1987) 603.
- 10 B.R. Martin, C.M. Weaver and D.L. Smith, *FASEB J.*, 3 (1989) A771.

- 11 D.L. Smith, *Anal. Chem.*, 55 (1983) 2391.
- 12 D.L. Smith, C. Atkin and C. Westfelder, *Clin. Chim. Acta*, 146 (1985) 97.
- 13 J. Xiangyu and D.L. Smith, *Anal. Chem.* 59 (1987) 2570.
- 14 L.S. Hillman, E. Tack, D.G. Covell, N.E. Vieira and A.L. Yergey, *Pediatric Res.*, 23 (1988) 589.
- 15 A.L. Yergey, S.A. Abrams, N.E. Vieira, R. Easthill, L.S. Hillman and D.G. Covell, *Can. J. Physiol. Pharmacol.*, 68 (1990) 973.
- 16 R.I. Price, G.N. Kent, J.B. Rosman, D.H. Gutteridge, J. Reeve, J.P. Allen, B.G.A. Stuckey, M. Smith, G. Guelfi, C.J. Hickling and S.L. Blakeman, *Biomed. Environ. Mass Spectrom.*, 19 (1990) 353.
- 17 S.J. Fairweather-Tait, D.E. Portwood, L.L. Symss, J. Eagles and M.J. Minski, *Am. J. Clin. Nutr.*, 49 (1989) 151.
- 18 W.D. Lehmann, R. Fischer and H.C. Heinrich, *Anal. Biochem.*, 172 (1988) 151.
- 19 P.L. Peirce, K.M. Hambridge, C.H. Goss, L.V. Miller and P.V. Fennessey, *Anal. Chem.*, 59 (1987) 2034.
- 20 L.V. Miller, M. Hambridge and P.V. Fennessey, *Anal. Chim. Acta*, 241 (1990) 249.
- 21 P.V. Fennessey, L. Lloyd-Kindstrand and K.M. Hambridge, *Int. J. Mass Spectrom. Ion Proc.*, 111 (1991) 355.
- 22 B. Kivisto, H. Anderson, G. Cederblad, A.-S. Sanberg and B. Sandström, *Br. J. Nutr.*, 55 (1986) 255.
- 23 M. Janghorbani, *Progr. Food Nutr. Sci.*, 8 (1984) 303.
- 24 B.T.G. Ting and M. Janghorbani, *Anal. Chem.*, 58 (1986) 1334.
- 25 H.M. Crews, V. Ducros, J. Eagles, P. Kastenmayer, J.B. Luten, B.A. McGaw, F.A. Mellon and P. Solgaard, unpublished results.
- 26 S.J. Fairweather-Tait, M.J. Jackson, T.E. Fox, S.G. Wharf, J. Eagles and P.C. Croghan, *Br. J. Nutr.*, (1993) in press.
- 27 J.R. Turnlund and W.R. Keyes, *J. Micronutr. Anal.*, 7 (1990) 117.

# Development of a screening method for the determination of volatile organic compounds in body fluids and environmental samples using purge and trap gas chromatography–mass spectrometry

Lothar Dunemann and Hossein Hajimiragha

*Department of Analytical Chemistry, Medical Institute for Environmental Hygiene at the Heinrich-Heine-Universität Düsseldorf, Auf'm Hennekamp 50, D-W-4000 Düsseldorf 1 (Germany)*

(Received 30th October 1992)

## Abstract

A sensitive screening method with low sample consumption is presented for the simultaneous determination of 48 volatile organic compounds (VOCs) by capillary gas chromatography with flame ionization detection (FID) or mass spectrometric ion trap detection (ITD). The method is applicable to body fluids (blood, urine and human milk) and environmental samples (well water and waste water). Sample preparation and introduction are performed with a purge and trap system. For low-concentration analytes this has the advantage of including an enrichment step prior to gas chromatographic separation. Four different media in combination are used for the adsorption of the VOCs. The carrier gas purges the compounds through these media during the adsorption step and the subsequent thermodesorption step is performed in the reversed direction. From whole blood the VOCs are adsorbed within 15 min at 40°C with helium as a purge gas. For desorption the tube is heated to 250°C. Forty-eight compounds, both non-halogenated aromatic and chlorinated and brominated aliphatic and aromatic VOCs, were separated by two capillary columns with both FID and an ITD instruments in parallel with a chromatographic run time of 28 min per sample. Detailed reproducibility, precision and accuracy data are given. Applications to both body fluids and water samples are presented. The limit of detection is better than  $0.1 \mu\text{g l}^{-1}$  for most of the compounds. Compared with the static headspace technique for some VOCs this method is 100 times more sensitive.

*Keywords:* Gas chromatography; Blood; Milk; Purge and trap; Urine; Volatile organic compounds

The physico-chemical behaviour of volatile organic compounds (VOCs) make them ubiquitous not only in the atmosphere but also in aqueous and biological systems and in humans [1]. This inexactly defined group of compounds includes aromatic and halogenated organic substances of low molecular weight with low boiling points and

potential hazards to environmental and/or biological systems. A wide range of sources have led to the widespread occurrence of VOCs, e.g., emissions from combustion processes including those from automobiles, chlorination reactions with organic matter in drinking water due to disinfection with chlorine, dry-cleaning shops and the production of chlorinated hydrocarbons. VOCs are present in thinners, degreasers, paints, adhesives and other industrial products [2,3] which are commonly used in many areas, including the home and workplaces. In addition to

*Correspondence to:* L. Dunemann, Department of Analytical Chemistry, Medical Institute for Environmental Hygiene at the Heinrich-Heine-Universität Düsseldorf, Auf'm Hennekamp 50, D-W-4000 Düsseldorf 1 (Germany).



direct impact on humans via the air, there is also a potential path via the food chain, especially for those foodstuffs with high fat contents [4].

The VOCs included in this investigation were chosen from the EPA method 524.2 [5]. All these VOCs have specific environmental and/or health risks. VOCs are incorporated via the lungs or by food and drinking water via the gastrointestinal tract and to some extent via the skin [6]. Some aromatic hydrocarbons have serious detrimental effects, such as benzene, which is a carcinogen. Chlorinated hydrocarbons have effects on the liver and there is a strong accumulation in fatty tissues [7]. Brominated hydrocarbons also have a high potential to cause adverse health effects [6].

The main problem in the determination of such substances at low levels is the low sensitivity of most established methods (e.g., headspace sampling). Analytes in environmental matrices can be enriched from a large sample volume (e.g., [8]), but this is normally not possible for biological and human sample materials. Nevertheless, with purge and trap as a sample preparation step, enrichment by a factor of 100 or more can be obtained even in these matrices.

The aims of this study were to increase the number of VOCs that can be determined in a single gas chromatographic (GC) run and to reduce the amount of sample necessary for each determination; this is of special importance for blood samples from children. Although one cannot expect to find all of the 48 components in low-exposure samples by a single method, it is useful, especially for the screening of unknown environmental exposures, for providing a rapid and reliable method for a wide range of analytes and matrices.

#### EXPERIMENTAL

Forty-eight VOCs (Table 1) were purged from different human and environmental samples (blood, urine, human milk, well water and waste water). The VOCs were separated from the matrix, followed by an enrichment step. Subsequently they were thermodesorbed in to the GC column and detected using flame ionization detection (FID) and ion trap detection (ITD). The VOCs were chosen from the EPA method 524.2

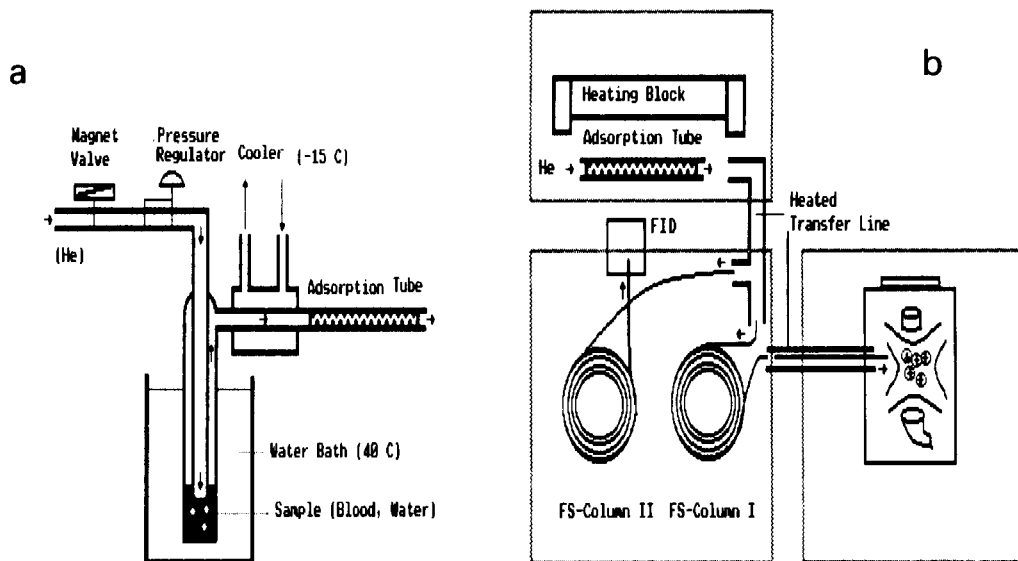


Fig. 1. Schematic diagram of the purge and trap GC-ITD technique. (a) Adsorption of VOCs from the sample solution to the adsorption tube; (b) desorption of VOCs from the adsorption tube and GC-ITD analysis.

[5]; their boiling points ranged between 40 and 220°C.

#### *Sampling and sample preparation*

**Blood.** A 10-ml volume of whole blood was collected from volunteers with 20-ml sterile syringes (Discardit; Becton Dickson) previously filled with 200  $\mu$ l of 8.75% (w/v) EDTA solution. The venipuncture was prepared by disinfection of the puncture site with 3% (v/v) hydrogen peroxide solution. The blood collection itself was performed with the sampling site in a laminar flow cabin to avoid contamination of the samples by the laboratory atmosphere. All syringes were from a single charge. Blood samples were stored in Wheaton 200 borosilicate glass bottles at 4°C after sampling and analysed immediately or, if not possible, within 24 h.

**Human milk.** At least 5 ml of milk were collected by volunteers without the use of any mechanical aids (pumps, etc) to minimize the risk of contamination. The milk was stored in Wheaton 200 borosilicate glass bottles at 4°C after sampling and analysed within 24 h.

**Well water and waste water.** The sampling was performed according to the DEV [9].

#### *Apparatus*

For off-line purge and trap sample preparation, a modified CLSA (closed-loop stripping apparatus) and subsequently a TDAS 5000 (thermal desorption autosampler) (both from Carlo Erba) were used (Fig. 1).

Analytical separation and detection were carried out on a Mega HRGC gas chromatograph (Carlo Erba). The carrier gas was helium (Messer Griesheim 5.0). The carrier gas stream was split (1:1) to allow the use of two fused-silica capillary columns in parallel (J&W Scientific 30 m  $\times$  0.25  $\mu$ m i.d. DB-5 column, 0.25  $\mu$ m film thickness). The temperature programme started at 37°C with a 10-min hold, followed by a ramp at 6°C/min to the final temperature of 130°C, which was held for 5 min. One of the columns was equipped with an FID and the other was coupled to an ITD (Finnigan ITD 700). Detection was performed in the full-scan mode from 35 to 310 u with a scan rate of 1 s<sup>-1</sup> (tune segments 75, 75, 100 and 125).

The temperature of the manifold was 260°C and that of the trap was 230°C. The voltage of the multiplier was 1800 V. For quantification normally the most intense mass ( $m/z$ ) was used (Table 1).

#### *Purge and trap procedure*

The VOCs were purged from the sample matrix and enriched on the adsorption media. Subsequently the thermodesorption and cryofocusing were performed.

**Adsorption.** Adsorption was performed using a combination of four components: (a) 3% SP-2100 (Supelco) on Chromosorb W AW; (b) Tenax-TA (Macherey-Nagel), 60–80 mesh; (c) silica gel (Alltech), 60–80 mesh; and (d) Carbotrap (Supelco), 20–40 mesh. The end-caps of the adsorption tubes were closed with silanized glass-wool [coated with dimethylchlorosilane (DMCS)]. During enrichment the carrier gas flowed from adsorption medium (d) to medium (a) and vice versa for the following desorption step.

**Enrichment.** For enrichment of the analytes from blood samples on to the adsorption media, 2 ml of whole blood, 25  $\mu$ l of 10% Antifoam B emulsion (Sigma) and 50  $\mu$ l of the internal standard solution (fluorobenzene) were pipetted into a test-tube. Enrichment was performed for 15 min at 40°C in a water-bath with helium as a purge gas. The purge gas flowed through a Pasteur pipette and was dispersed to very small bubbles; in this way the contact between purge gas and sample solution was optimum. The purge volume was 600 ml (for a 40 ml min<sup>-1</sup> purge flow). The other samples were treated in a corresponding procedure with suitable adequate amounts of Antifoam B emulsion. A freezing trap (-15°C) was fitted between the sample inlet and the adsorption tube to condense water vapour and other polar components from the sample.

**Thermodesorption and cryofocusing.** Four steps were necessary for thermodesorption of the VOCs. Purging: the adsorption tube was purged with helium at room temperature for 30 s; residues of oxygen and condensed water were removed. Preheating: the tube was heated at 250°C for 3 min (with vents closed); the components (VOCs) were desorbed from the adsorption

TABLE 1

Basic data on the example of a spiked blank water sample (six replicates each)

No. <sup>a</sup>	<i>m/z</i>	Compound	R.S.D. (%)		Recovery (0.2 $\mu\text{g l}^{-1}$ ) <sup>b</sup> (%)	Detection limit (0.2 $\mu\text{g l}^{-1}$ ) <sup>b</sup> ( $\mu\text{g l}^{-1}$ )	CAS-No
			10 $\mu\text{g l}^{-1}$ <sup>b</sup>	0.2 $\mu\text{g l}^{-1}$ <sup>b</sup>			
1	96	Fluorobenzene (int.std.)	–	–	–	–	462-06-6
4	96	1,1-Dichloroethene	4	19	99	0.12	75-34-3
5	49	Dichloromethane	5	12	112	0.10	75-09-2
6	43	Methyl ethyl ketone (MEK)	7	45	193	0.41	78-93-3
7	77	2,2-Dichloropropane	5	21	112	0.14	590-20-7
8	49	Bromochloromethane	6	7	112	0.09	74-97-5
9	83	Trichloromethane	6	22	94	0.17	67-66-3
10	97	1,1,1-Trichloroethane	3	7	95	0.05	71-55-6
12	75	<i>cis</i> -1,3-Dichloropropene (qual.)	7	3	103	0.02	10061-01-5
13	78	Benzene (BTX)	3	9	99	0.04	71-43-2
14	117	Tetrachloromethane	8	3	113	0.04	56-23-5
15	63	1,2-Dichloropropane	3	4	104	0.03	78-87-5
16	132	Trichloroethene (TRI)	3	3	101	0.03	79-01-6
17	83	Bromodichloromethane	3	2	109	0.03	75-27-4
18	75	<i>trans</i> -1,3-Dichloropropene (qual.)	4	6	106	0.04	10061-02-6
19	43	Methyl isobutyl ketone (MIBK)	3	17	93	0.08	108-10-1
20	75	1,1-Dichloroprop-1-ene	3	10	104	0.07	563-58-6
21	91	Toluene (BTX)	7	42	110	0.23	108-88-3
22	83	1,1,2-Trichloroethane	2	2	110	0.02	79-00-5
23	76	1,3-Dichloropropane	2	5	103	0.04	142-28-9
24	129	Dibromochloromethane	3	3	106	0.05	124-48-1
25	107	Dibromomethane	2	3	85	0.04	74-95-3
26	166	Tetrachloroethene (PER)	4	14	106	0.14	127-18-4
27	112	Chlorobenzene	5	5	105	0.04	108-90-7
28	131	1,1,1,2-Tetrachloroethane	2	14	106	0.13	630-20-6
29	91	Ethylbenzene	6	16	117	0.09	100-41-4
30	91	<i>m</i> -Xylene (BTX) <sup>c</sup> }	5	23	266	0.60	108-38-3
30	91	<i>p</i> -Xylene (BTX) <sup>c</sup> }					106-42-3
31	91	Styrene	6	5	107	0.04	100-42-5
32	91	<i>o</i> -Xylene (BTX)	5	12	108	0.07	95-47-6
33	83	1,1,2,2-Tetrachloroethane	4	2	101	0.02	79-34-5
34	74	1,2,3-Trichloropropane	2	45	100	0.36	96-18-4
35	105	Isopropylbenzene (cumene)	7	6	114	0.04	98-82-8
36	77	Bromobenzene	5	6	109	0.06	108-86-1
37	120	<i>n</i> -Propylbenzene	6	1	111	0.06	103-65-1
38	126	4-Chlorotoluene	5	5	111	0.04	106-43-4
39	105	1,3,5-Trimethylbenzene	7	7	110	0.04	108-67-8
40	119	<i>tert</i> -Butylbenzene	8	8	113	0.04	98-06-6
41	105	1,2,4-Trimethylbenzene	6	16	108	0.09	95-63-6
42	146	1,3-Dichlorobenzene	6	4	110	0.04	541-73-1
43	146	1,4-Dichlorobenzene	5	16	93	0.11	106-46-7
44	105	<i>sec</i> -Butylbenzene	8	9	122	0.05	135-98-8
45	119	<i>p</i> -Isopropyltoluene ( <i>p</i> -cymene)	9	13	119	0.07	527-84-4
46	146	1,2-Dichlorobenzene	6	7	108	0.05	95-50-1
47	91	<i>n</i> -Butylbenzene	9	11	125	0.07	104-51-8
48	180	1,2,4-Trichlorobenzene	9	5	115	0.05	120-82-1
49	128	Naphthalene	10	8	108	0.05	91-20-3
50	180	1,2,3-Trichlorobenzene	10	6	108	0.04	87-61-6
51	225	Hexachlorobutadiene	11	11	131	0.14	87-68-3

<sup>a</sup> No. 11 not evaluated<sup>b</sup> Calculated on the basis of 0.2 or 10  $\mu\text{g l}^{-1}$  standard solutions.<sup>c</sup> Not separated.

media but remained in the tube (first desorption step). Desorption: the vents were opened at 250°C for 1 min. The VOCs entered the cryotrap (–120°C) via a heated deactivated fused-silica column. After heating to 250°C the substances were desorbed to the two separation columns of the gas chromatograph (second desorption step). Cleaning: after desorption the tube was heated at 250°C for 15 min for reconditioning.

### Calibration

**Standard solutions.** Standard solutions and the internal standard solution (fluorobenzene) were prepared by dissolving the pure substances in acetone and diluting to the appropriate concentrations with VOC-free water (treated with a UV reactor: Gränzel). Volumes of 50  $\mu\text{l}$  each of the diluted standard solutions and the internal standard solution were added to the samples for the calibration procedure.

**Calibration procedure.** A blank sample was prepared to ensure a very low loaded sample with the same matrix as the real samples. This sample was prepared by purging with the carrier gas (helium) for 30 min. A GC-ITD control run demonstrated that after this step the concentra-

tions of all components were below the detection limit. The standard solutions of all VOCs and the internal standard solution were added to this blank sample and the calibration function was recorded.

**Determinations.** All determinations were performed twice. If there were deviations of more than 20%, two more determinations were made.

### RESULTS AND DISCUSSION

Table 1 shows the reproducibility of the method for all the compounds in a single analysis cycle on the example of two standard solutions (10 and 0.2  $\mu\text{g l}^{-1}$ , respectively). The use of the more concentrated standard (10  $\mu\text{g l}^{-1}$ , representing the upper limit of the expected concentration range for low-exposure samples) gives good relative standard deviations (R.S.D.s) between 2 and 11%. For the less concentrated standard (0.2  $\mu\text{g l}^{-1}$ ) the result is different. For most analytes the reproducibility is excellent (R.S.D. < 10%) whereas for the three [methyl ethyl ketone (MEK), toluene and 1,2,3-trichloropropane] the R.S.D. is not acceptable (> 40%).

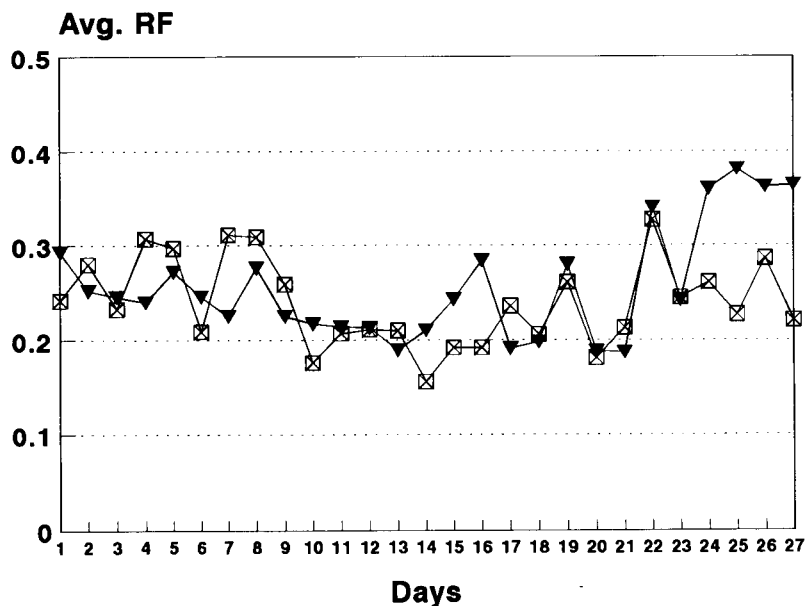


Fig. 2. Reproducibility (peak areas) from day to day.  $\blacktriangledown$  = 1,2-Dichlorobenzene- $d_4$ ;  $\square$  = 4-bromofluorobenzene.

TABLE 2

Concentrations of VOCs in different matrices ( $\mu\text{g l}^{-1}$ )<sup>a</sup>

No.	Compound	Blood	Urine	Milk	Water	Waste
1	Fluorobenzene (int.std.)					
4	1,1-Dichloroethene	0.03	– <sup>b</sup>	0.06	0.14	0.68
5	Dichloromethane	0.22	0.19	–	0.87	0.39
6	Methyl ethyl ketone (MEK)	–	–	–	–	200
7	2,2-Dichloropropane	0.08	0.38	–	–	4.52
8	Bromochloromethane	–	0.17	–	0.30	0.23
9	Trichloromethane	–	0.22	–	–	1.26
10	1,1,1-Trichloroethane	0.08	0.26	0.17	0.37	1.96
12	<i>cis</i> -1,3-Dichloropropene	0.06	0.07	0.04	0.03	0.29
13	Benzene (BTX)	0.15	0.20	0.12	–	3.60
14	Tetrachloromethane	–	–	–	–	–
15	1,2-Dichloropropane	0.07	0.05	0.07	–	0.12
16	Trichloroethene (TRI)	0.03	–	0.06	3.13	–
17	Bromodichloromethane	0.2	0.08	0.21	–	0.81
18	<i>trans</i> -1,3-Dichloropropene	0.03	0.12	–	–	–
19	Methyl isobutyl ketone (MIBK)	0.06	0.97	0.52	–	16
20	1,1-Dichloroprop-1-ene	0.25	–	0.10	–	–
21	Toluene (BTX)	0.63	0.64	0.58	–	95
22	1,1,2-Trichloroethane	0.03	–	–	–	0.52
23	1,3-Dichloropropane	–	0.09	0.05	0.08	0.05
24	Dibromochloromethane	–	–	0.29	–	–
25	Dibromomethane	–	–	0.11	–	–
26	Tetrachloroethene (PER)	0.50	1.15	0.13	35	1.27
27	Chlorobenzene	0.05	0.01	0.04	0.41	0.13
28	1,1,1,2-Tetrachloroethane	–	0.71	–	–	0.09
29	Ethylbenzene	0.30	0.23	0.02	–	50
30	<i>m,p</i> -Xylene (BTX)	1.28	0.88	0.79	–	45
31	Styrene	0.79	0.04	0.20	0.56	110
32	<i>o</i> -Xylene (BTX)	0.20	0.13	0.05	–	180
33	1,1,2,2-Tetrachloroethane	–	–	–	0.06	0.70
34	1,2,3-Trichloropropane	0.23	0.28	0.01	0.39	0.40
35	Isopropylbenzene (cumene)	0.04	0.03	0.05	0.55	15
36	Bromobenzene	0.06	0.02	0.05	0.68	6.82
37	<i>n</i> -Propylbenzene	0.10	0.02	0.06	0.51	15
38	4-Chlorotoluene	–	0.01	–	–	0.31
39	1,3,5-Trimethylbenzene	0.36	0.02	0.09	0.28	22
40	<i>tert</i> -Butylbenzene	0.07	0.12	0.04	–	15
41	1,2,4-Trimethylbenzene	0.60	0.12	0.24	–	90
42	1,3-Dichlorobenzene	0.04	0.42	–	–	–
43	1,4-Dichlorobenzene	0.39	0.21	0.05	–	–
44	<i>sec</i> -Butylbenzene	0.97	0.60	0.44	0.36	7.21
45	<i>p</i> -Isopropyltoluene ( <i>p</i> -cymene)	0.07	0.09	0.06	0.32	35
46	1,2-Dichlorobenzene	–	–	–	0.75	–
47	<i>n</i> -Butylbenzene	–	–	–	0.34	22
48	1,2,4-Trichlorobenzene	0.02	–	–	–	–
49	Naphthalene	0.10	0.14	0.02	0.65	4.45
50	1,2,3-Trichlorobenzene	–	–	–	–	–
51	Hexachlorobutadiene	–	–	–	–	–

<sup>a</sup> Values > 10  $\mu\text{g l}^{-1}$  are given in qualitative terms.<sup>b</sup> Dashes indicate concentrations below detection limit (see Table 1).

Therefore, in the low concentration range ( $< 1 \mu\text{g l}^{-1}$ ) these VOCs were just evaluated in qualitative terms. For a screening procedure, the R.S.D.s of all other VOCs are acceptable even at the  $0.2 \mu\text{g l}^{-1}$  level. The recoveries (Table 1) are between 90 and 115% for most of the substances. Because of the low peak purity for MEK and *m*- and *p*-xylene, these compounds were also evaluated in qualitative terms only. The detection limits, given as three times the standard deviation ( $3\sigma$ ) of six replicates of the  $0.2 \mu\text{g l}^{-1}$  standard solution, are below  $0.1 \mu\text{g l}^{-1}$  for 35 VOCs, between  $0.1$  and  $0.2 \mu\text{g l}^{-1}$  for 8 VOC and above  $0.2 \mu\text{g l}^{-1}$  for 4 VOCs. The reproducibility from day to day is shown in Fig. 2

The results (Table 2 and Fig. 3) show that most of the analytes are determinable in samples such as blood, urine, human milk and well water of low-exposure origins. The well water that had been chosen for this study showed a high concentration of tetrachloroethane ( $35 \mu\text{g l}^{-1}$ ). The waste water sample showed high values for some aromatic hydrocarbons with concentrations two to three decades higher than those of the four low-exposure samples; no special stress was found for halogenated compounds.

The most important advantages of purge and trap sample preparation are the matrix separation and the enrichment of the now almost matrix-free analytes by a factor of 100 or more. This method is more sensitive than the static headspace technique. Therefore, concentrations of many VOCs in blood can be determined even in samples from low-exposure persons.

Other advantages are the elimination of water in the cooling trap and the elimination of oxygen in the adsorption tube prior to the thermodesorption step. Therefore, especially in conjunction with the ion trap detector, there are fewer problems with poor detection limits. Another advantage is the extension to such different organic compounds as aromatic and halogenated compounds because of the parallel use of two detection systems. This can be further optimized by using an electron-capture detector, which is even more sensitive, especially for the highly chlorinated compounds. Moreover, the use of two different GC columns (e.g., a polar and a non-polar

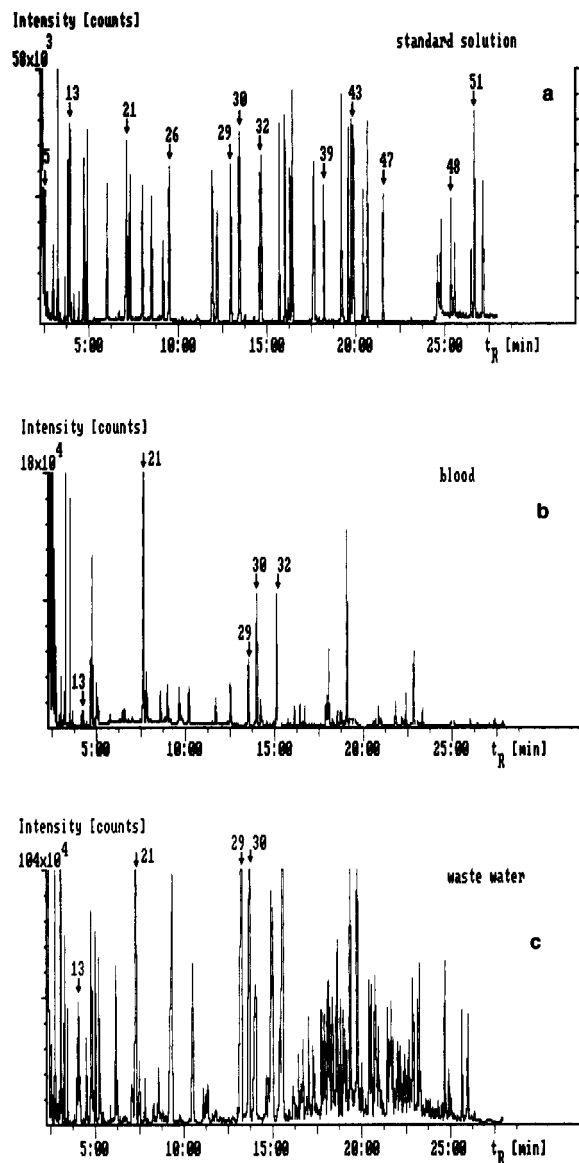


Fig. 3. Peaks obtained for the determination of VOCs in absolute intensities (counts) for (a) a standard solution (spike blank water), (b) a blood sample and (c) a waste water sample. For peak numbers, see Table 1.

column) can extend the range of VOCs still further. Moreover, this feature can be used as a further quality control item for the quantitative identification of VOCs in biological and environmental samples.

Although many purge and trap procedures have been used in the determination of VOCs in environmental samples, there are only a few for foods [4], breath [8] and blood [10]. A very sensitive technique has been described for purge and trap GC with electron-capture detection [11]. A spray extraction procedure has been described as a similar technique to the purge and trap method for the analysis of some VOCs by GC-MS [12]; the special item here is the use of a mobile mass spectrometer for on-site environmental monitoring. In a recent study [10], 10 ml of blood were needed as a minimum for the determination of 32 VOCs in a single sample.

Compared with the above papers dealing with the detection of VOCs, the present method has the advantages of low sample consumption, rapidity and applicability to a wide range of matrices. It is applicable especially for the rapid screening of body fluids, water and air, and can be used as an "early-warning system". Moreover, for most analytes it can be extended to air samples (including breath) [13] and even to solid matrices. The method can therefore contribute to the better control of environmental hazards and human health risks due to volatile organic compounds.

Current investigations include improving the method by adapting the off-line system described here to an automatic on-line system with two different separation columns and electron-capture detector and mass spectrometric detector.

The advantages are better reproducibility, higher sample throughput and less labour intensity.

#### REFERENCES

- 1 S.R. Antoine, I.R. DeLeon and R.M. O'Dell-Smith, *Bull. Environ. Contam. Toxicol.*, 36 (1986) 364.
- 2 T. Inoue, Y. Takeuchi, N. Hisanaga, Y. Ono, M. Iwata, M. Ogata, K. Saito, H. Sakurai, I. Hara, T. Matsushita and M. Ikeda, *Ind. Health*, 21 (1983) 175.
- 3 M. Kumai, A. Koizumi, K. Saito, H. Sakurai, T. Inoue, Y., Takeuchi, I. Hara, M. Ogata, T. Matsushita and M. Ikeda, *Ind. Health*, 21 (1983) 185.
- 4 R. Barcarolo, P. Casson and C. Tutta, *J. High Resolut. Chromatogr.*, 15 (1992) 307.
- 5 J.W. Eichelberger and W.L. Budde, *Measurements of Purgeable Organic Compounds in Water by Capillary Column Gas Chromatography/Mass Spectrometry*, Method 524.2, Revision 3.0, US Environmental Protection Agency, Cincinnati, OH, 1989.
- 6 R.D. Thomas, *J. Am. Coll. Toxicol.*, 8 (1989) 779.
- 7 A. Sato and T. Nakajima, *Scand. J. Work Environ. Health*, 13 (1987) 81.
- 8 L.A. Wallace, E.O. Pellizzari, T.D. Hartwell, R. Withmore, H. Zelon, R. Perrit and L. Sheldon, *Atmos. Environ.*, 22 (1988) 2141.
- 9 *Deutsche Einheitsverfahren zur Wasser-, Abwasser- und Schlamm-Untersuchung*, VCH, Weinheim, 1992.
- 10 D.L. Ashley, M.A. Bonin, F.L. Cardinali, J.M. McCraw, J.S. Holler, L.L. Needham and D.G. Patterson, Jr., *Anal. Chem.*, 64 (1992) 1021.
- 11 L. Lepine and J.-F. Archambault, *Anal. Chem.*, 64 (1992) 810.
- 12 G. Baykut and A. Voigt, *Anal. Chem.*, 64 (1992) 677.
- 13 H. Hajimiragha and U. Ewers, to be published.

# Systematic study of chromium determination in urine by graphite furnace atomic absorption spectrometry

R. Rubio, A. Sahuquillo and G. Rauret

*Departament de Química Analítica, Universitat de Barcelona, Avda. Diagonal 647, 08028 Barcelona (Spain)*

L. Garcia Beltran

*Servei de Bioquímica, Hospital General Universitari Vall d'Hebron, Pg. Vall d'Hebron s/n, 08035 Barcelona (Spain)*

Ph. Quevauviller

*Community Bureau of Reference (BCR), Directorate-General for Science, Research and Development, Rue de la Loi 200, B-1049 Brussels (Belgium)*

(Received 13th October 1992; revised manuscript received 4th January 1993)

## Abstract

The optimized measurement of Cr in urine samples using graphite furnace atomic absorption spectrometry, with a tungsten lamp and Zeeman-effect background correction is described. Sample dilution and slow hot injection were studied in an effort to improve the precision. Parameters such as detection limit ( $0.08 \mu\text{g l}^{-1}$ ) and precision are reported. Based on this study, the Zeeman effect with slow hot injection of diluted sample is recommended. The method was evaluated by applying the conditions established to a certified reference urine. The method was applied to the determination of chromium in urine from healthy subjects and total parenteral nutrition patients.

*Keywords:* Atomic absorption spectrometry; Chromium; Urine

Chromium is an essential element that controls normal physiological functions in humans, and it is believed to be involved in glucose metabolism [1,2]. Chromium deficiency is associated with cardiovascular diseases and diabetes [1,3,4]. It is reported that patients subjected to long-term total parenteral nutrition (TPN) develop symptoms similar to those attributed to chromium deficiency [4,5] and a chromium supplement to these patients of  $10\text{--}20 \mu\text{g day}^{-1}$  [1,6] as chromium chloride is recommended.

The human biological fluid with the highest Cr concentration is urine [4,7], and there is increas-

ing interest in the determination of Cr contents in this fluid as it can give information with which to assess the chromium nutritional status of humans [2], for Cr balance studies and for monitoring patients receiving Cr supplements [1].

The levels of chromium reported in human urine are very low in healthy subjects, ranging from 0.2 to more than  $12 \mu\text{g l}^{-1}$  [8,9]. This wide range could be attributed to difficulties in the determination of the element at low concentrations and in a complex matrix [10]. More recently, graphite furnace atomic absorption spectrometry (GFAAS) has been used to measure Cr in urine. Nevertheless, sample treatment, instrumental performance and measurement conditions are now of critical importance, owing to the demand for high sensitivity and reproducibility in

*Correspondence to:* R. Rubio, Departament de Química Analítica, Universitat de Barcelona, Avda. Diagonal 647, 08028 Barcelona (Spain).



metabolic, biological and toxicological assays. In recent years some rigorous studies on the reduction of the background signal in the determination of Cr in urine have been reported [7,11–13], and the use of the Zeeman-effect correction and pyrolytic graphite-coated tubes is highly recommended to decrease matrix interferences, although deuterium background correction is also reported to be useful [13].

This paper describes an attempt to optimize the measurement of chromium in urine by GFAAS. The temperatures and times for the graphite furnace programme were optimized by the simplex approach [14]. Slight modifications to this programme were introduced for its application to urine samples.

Two procedures for sample pretreatment, sample dilution and microwave digestion were examined in order to minimize the spattering observed with direct sample introduction.

The decrease in the background signal using continuous correction with a tungsten lamp and with the Zeeman effect was studied.

With the conditions established, the linearity ranges, detection limit and short- and long-term precision were determined. Taking into account the lack of data on the determination of these quality parameters in the literature, the results reported here may provide valuable information.

The method was evaluated by applying the proposed procedures to two standard reference material (SRM) freeze-dried urine samples. As an application, Cr was determined in two sets of samples, urine from a random population of healthy subjects (laboratory staff) and urine from TPN patients at different hospital units.

## EXPERIMENTAL

### *Apparatus*

A Perkin-Elmer Model 4000 atomic absorption spectrometer equipped with an HGA-500 graphite furnace assembly, an AS 40 autosampler (standard version) and a Perkin-Elmer Model 561 recorder was used. A tungsten lamp was used for background correction. This instrument is referred to as PE. A Varian SpectrAA-30 atomic

absorption spectrometer equipped with a GTA autosampler and DS-15 data station was used when Zeeman-effect background correction was applied. This instrument is referred to as VS. In both instances a hollow-cathode chromium lamp was used as a radiation source and pyrolytic graphite-coated graphite tubes were used.

Rainin edp2 digital electronic automated micropipettes were used to prepare spiked samples. A domestic microwave oven was used for sample pretreatment assays.

### *Reagents*

A stock standard chromium solution of 1000 mg l<sup>-1</sup> was prepared from potassium dichromate (Merck, analytical-reagent grade). Stock solutions of 10 mg l<sup>-1</sup> were prepared weekly and more dilute working standard solutions were prepared daily. The final medium of all solutions was 2% HNO<sub>3</sub> prepared from Merck Suprapur acid.

Working solutions were prepared with doubly deionized water (Culligan Ultrapure GS) of 18.3 MΩ cm resistivity.

Standard reference urines obtained from NIST were two freeze-dried urines, CRM 2670, containing different Cr levels after reconstitution with 20 ml of doubly deionized water: “normal level” 0.013 mg l<sup>-1</sup> Cr (value given only for information) and “high level” (spiked sample) 0.085 ± 0.006 mg l<sup>-1</sup> Cr (certified value). Reconstituted urine was used after 30 min of preparation, occasionally shaking very slowly.

### *Collection and handling of urine samples*

Urine samples from healthy subjects and patients on TPN were collected using 50-ml plastic containers and, when analysis was not carried out immediately, the samples were stored at 4°C.

### *Working conditions*

A class 100 clean room (NBS) [15] was used to prepare the solutions.

### *Procedure*

To 5.00 ml of urine (normal or TPN), 0.5 ml of concentrated HNO<sub>3</sub> was added and the solution was diluted with doubly deionized water to 25.00 ml. The solution was homogenized and Cr was

TABLE 1

Graphite furnace programme

Step	T (°C)	t <sub>r</sub> (s)	t <sub>h</sub> (s)
Drying	110 <sup>a</sup>	18	19
	140 <sup>b</sup>		
Ashing 1	700	18	2
Ashing 2	1300	5	15
Atomizing <sup>c</sup>	2400	3	10
Cleaning	2600	2	4

<sup>a</sup> PE instrument. <sup>b</sup> VS instrument. <sup>c</sup> Stopped flow of inert gas.

measured by GFAAS at 357.9 nm using the PE instrument.

For TPN patients, 2.00 ml of urine were diluted with 2% HNO<sub>3</sub> to 10.00 ml and final measurement was performed at 357.9 nm using the VS instrument.

For samples from healthy subjects, 1.00 ml of 2% HNO<sub>3</sub> was added to 1.00 ml of urine for the final measurement using the VS instrument.

The modified furnace programme for the determination of Cr in urine samples and the instrumental conditions used are given in Tables 1 and 2.

## RESULTS AND DISCUSSION

### Samples pretreatment

The introduction of the TPN urine without pretreatment was tried initially. The results obtained with both instruments were not reproducible, probably owing to the high viscosity of the matrix. The relative standard deviations

(R.S.D.) obtained for five injections were 50% and 16% for the PE and VS, respectively. Sample pretreatment was therefore necessary.

Two different dilutions of TPN and spiked normal urines (1 + 4 and 1 + 1) with media of different acidity containing up to 1%, 2% and 8% HNO<sub>3</sub> and microwave digestion under the conditions given below, were tried as pretreatments. Figure 1 shows the results obtained, expressed as R.S.D., with the different pretreatments. The best precision corresponds to a sample diluted 1 + 5 with a final acid concentration of 2% HNO<sub>3</sub>; the viscosity of the sample was reduced and the reproducibility was increased.

In microwave digestion assays, the time of digestion and the sample-to-acid volume ratio were optimized. From all the conditions tested, the best reproducibility was obtained when 2 ml of sample and 5 ml of concentrated HNO<sub>3</sub> were placed in a Teflon vessel and digested at the maximum oven power (650 W) for 5 min, but this treatment did not improve the reproducibility of the sample injection compared with simple sample dilution with nitric acid (Fig. 1).

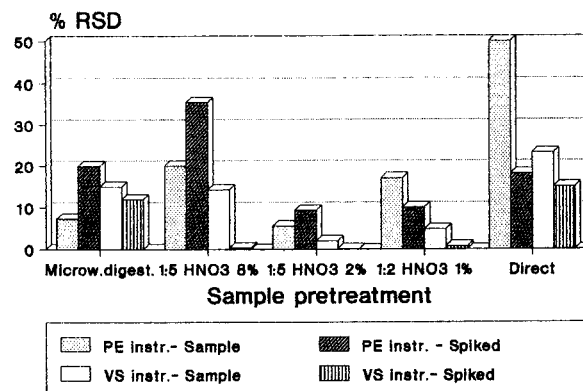
Hence the recommended urine pretreatment procedure is a 1 + 4 sample dilution with a final medium containing 2% HNO<sub>3</sub>. Nevertheless, for the determination of Cr in urine from healthy subjects, owing to the low concentrations, a dilution of only 1 + 1 in 2% HNO<sub>3</sub> is recommended when the VS instrument is used.

The use of a surfactant (Triton X-100) as diluting agent was also tried, but the reproducibility

TABLE 2

Instrumental parameters for urine analysis

Parameter	PE instrument	VS instrument
Lamp intensity (mA)	10	7
Type of signal	Peak area	Peak area
Background corrector	Tungsten lamp	Zeeman-effect
Inert gas	Ar	Ar
Slit width (nm)	0.7	0.2 (height decreased)
Sample volume (μl)	20	40
Injection mode	Usual	Hot injection (95°C, rate factor 6)



obtained was not better than that obtained with a simple dilution with  $\text{HNO}_3$ . Therefore, to simplify the method and owing to the facility of obtaining nitric acid of high purity, the addition of Triton X-100 was discarded.

#### *Instrumental parameters*

Optimization of the instrumental parameters for chromium determination by GFAAS was carried out in different ways for the continuous and non-continuous variables.

The continuous variables considered were the different temperatures and the ramp and hold times for each step of the furnace programme. These variables were optimized by means of the simplex approach [14]. The response considered for simplex application was the slope value obtained with four standard solutions of Cr(VI), i.e., optimizing the instrumental conditions to obtain the maximum sensitivity.

The non-continuous variables considered were the type of signal treatment (peak area or peak height), the use of a background corrector, the intensity of the hollow-cathode lamp, the interrupted flow mode of inert gas during the atomization step, the inert gas used and the slit width. These variables were established in sequential assays.

The wavelength used was 357.9 nm, the most sensitive line for Cr, and both uncoated and pyrolytic graphite-coated tubes were tested. All the assays and the simplex study were performed with standard solutions of Cr(VI) in 2%  $\text{HNO}_3$  in the concentration range 10–500  $\mu\text{g l}^{-1}$ .

The optimized values of the non-continuous variables obtained for the PE instrument are given in Table 2. Under these conditions, better sensi-

tivity was achieved when using pyrolytic graphite-coated tubes.

For urine samples, the programme of temperatures and times giving the highest sensitivity for Cr(VI) solutions in  $\text{HNO}_3$  had to be modified by adding a second ashing step at 700°C in order to avoid spattering of the sample. Table 1 gives the optimized programme.

The hot injection mode using the VS instrument was also tried, as recommended for urine analysis in the literature [11]. With the programme used, the tube was heated to 95°C before sample introduction. Injection was made slowly at a deposition rate six times slower than in the normal mode. This hot injection mode allowed the introduction of 40  $\mu\text{l}$  of sample, improving the sensitivity.

#### *Performance parameters*

Under the optimum conditions established, performance parameters were determined for both instruments and for both standard solutions and urine samples. The linear range, detection and quantification limits and short- and long-term precision were calculated.

For standard Cr(VI) solutions the linear range found was up to 30  $\mu\text{g l}^{-1}$  Cr. The detection limit was calculated considering the concentration corresponding to three times the standard deviation of the absorbance of three blank solutions (2%  $\text{HNO}_3$  solution) and performing ten measurements on each. The quantification limit was calculated as ten times the standard deviation of the absorbance of a blank solution. The corresponding concentrations were calculated using the calibration graph. Precision was established at two different Cr concentrations within the linear

TABLE 3

Performance parameters for Cr(VI) standard solutions

Parameter	PE instrument	VS instrument
Detection limit ( $\mu\text{g l}^{-1}$ )	0.34	0.05
Quantification limit ( $\mu\text{g l}^{-1}$ )	1.12	0.23
Short-term precision R.S.D. (%) ( $n = 30$ )	6.0 (at 6 $\mu\text{g l}^{-1}$ ) 1.5 (at 24 $\mu\text{g l}^{-1}$ )	1 (at 2.5 $\mu\text{g l}^{-1}$ ) 0.5 (at 10 $\mu\text{g l}^{-1}$ )
Long-term precision R.S.D. (%) ( $n = 30$ )	7.5 (at 6 $\mu\text{g l}^{-1}$ ) 3.3 (at 24 $\mu\text{g l}^{-1}$ )	1.3 (at 2.5 $\mu\text{g l}^{-1}$ ) 1 (at 10 $\mu\text{g l}^{-1}$ )

TABLE 4

Performance parameters for 1+4 diluted TPN urine sample

Parameter	PE instrument	VS instrument
Detection limit ( $\mu\text{g l}^{-1}$ )	1.12	0.08
Quantification limit ( $\mu\text{g l}^{-1}$ )	3.4	0.27
Within-day R.S.D. (%) ( $n = 20$ )	– <sup>a</sup>	1.6 <sup>b</sup>

<sup>a</sup> Value lower than the quantification limit after dilution. <sup>b</sup> At  $2.4 \mu\text{g l}^{-1}$  (concentration after dilution).

range. The standard deviation was calculated from the mean values of ten readings for each standard solution, in three periods of ca. 2 h within the same working day for the short-term precision, and within three non-consecutive days for the long-term precision. The results are given in Table 3.

For TPN urine samples, the linearity range in spiked urines was up to  $30 \mu\text{g l}^{-1}$  Cr. The detection and quantification limits were established as above and, for the VS instrument, the within-day R.S.D. was also calculated. The results are given in Table 4.

#### Validation of the method

For the validation of the method, the Cr contents in two NIST certified reference materials (CRM 2670; freeze-dried normal and “elevated level” spiked urine) were determined following the proposed procedure using direct calibration and the standard addition methods. The dried material was reconstituted with 20 ml of doubly deionized water and analysed on the same day. The results obtained are given in Table 5.

#### Application

Chromium was determined in two sets of samples, urine from a random population of healthy

TABLE 6

Analysis of TPN urine samples with the VS instrument

Sample No.	Direct calibration ( $\mu\text{g l}^{-1}$ )	Standard addition ( $\mu\text{g l}^{-1}$ )
1	8.0	8.4
2	4.7	5.2
3	0.35	0.24

subjects and urine from TPN patients in different hospital units and for different nutrition periods from 3 days to 2 months. Twenty samples of each type were analysed using direct calibration as the standard addition and direct calibration methods did not give significantly different results compared with the certified reference material value or values for some TPN samples previously analysed (see Table 6).

Using the PE instrument the levels of Cr found for healthy subjects were below the detection limit and the Cr levels found on dilution for TPN patients were between the detection and quantification limits.

Using the VS instrument and the slow hot injection mode, the mean Cr content in the twenty urine samples were as follows: healthy subjects ( $n = 20$ ),  $0.33 \pm 0.18 \mu\text{g l}^{-1}$ ; and TPN patients ( $n = 20$ ),  $5.19 \pm 3.03 \mu\text{g l}^{-1}$ . The values found for healthy subjects were close to, and sometimes below, the quantification limit of the technique.

#### Conclusions

In the determination of Cr in urine, sample dilution is necessary in order to achieve satisfactory reproducibility in the injection step. The use of microwave digestion does not decrease the R.S.D. for the injection.

TABLE 5

Analysis of NIST CRM 2670

Background corrector	NIST value ( $\text{mg l}^{-1}$ )	Experimental values ( $\text{mg l}^{-1}$ ) <sup>a</sup>	
		Direct calibration	Standard addition
PE instrument	(0.013) informative	$0.010 \pm 0.001$ <sup>b</sup>	$0.012 \pm 0.001$ <sup>b</sup>
VS instrument		$0.010 \pm 0.002$	$0.012 \pm 0.002$
PE instrument	$0.085 \pm 0.006$	$0.080 \pm 0.003$	$0.083 \pm 0.005$
VS instrument		$0.089 \pm 0.001$	$0.082 \pm 0.002$

<sup>a</sup> Mean  $\pm$  2 S.D. ( $n = 3$ ). <sup>b</sup> Value lower than the quantification limit.

The direct calibration and the standard addition methods do not give significantly different results, so direct calibration with Cr(VI) in 2% HNO<sub>3</sub> is recommended.

The use of the VS instrument with Zeeman-effect background correction and the hot injection mode gives a good detection limit, slightly lower than those reported [10], and also good within-day and long-term precision. The PE instrument with tungsten lamp correction is only applicable when the concentration is high enough, that is, for toxic levels of Cr in urine.

A urine SRM at normaler levels would be necessary for the best validation of the method, as the SRM analysed has a much higher Cr content than the physiological levels.

#### REFERENCES

- 1 E.G. Offenbacher and F.X. Pi-Sunyer, *Annu. Rev. Nutr.*, 8 (1988) 543.
- 2 C. Veillon, *Methods Enzymol.*, 158 (1988) 334.
- 3 R.A. Anderson, N.A. Bryden and M.M. Polansky, *Am. J. Clin. Nutr.*, 41 (1985) 571.
- 4 J. Gaughofer and V. Bianchi, in E. Merian (Ed.), *Metals and Their Compounds in the Environment*, VCH, Weinheim, 1991, pp. 853–878.
- 5 R.O. Brown, S. Forloines-Lynn, R.E. Cross and W.D. Heizer, *Digest. Dis. Sci.*, 31 (1986) 661.
- 6 C.I. Kien, C. Veillon, K.Y. Patterson and P.M. Farrell, *J. Parent. Nutr.*, 10 (1986) 662.
- 7 P. Dube, *Analyst*, 113 (1988) 917.
- 8 Z. Mianzhi and R.M. Barnes, *Spectrochim. Acta, Part B*, 38 (1983) 259.
- 9 D.J. Halls and G.S. Fell, in P. Bratter and P. Schramel (Eds.), *Trace Element Analytical Chemistry in Medicine and Biology*, Vol. 2, Walter de Gruyter, Berlin, 1983, pp. 667–673.
- 10 R. Rubio, A. Sahuquillo, G. Rauret and Ph. Quevauviller, *Int. J. Environ. Anal. Chem.*, 47 (1992) 99.
- 11 M.B. Knowles, *J. Anal. At. Spectrom.*, 4 (1989) 257.
- 12 D.J. Halls and G.S. Fell, *J. Anal. At. Spectrom.*, 3 (1988) 105.
- 13 D.J. Halls and G.S. Fell, *J. Anal. At. Spectrom.*, 1 (1986) 135.
- 14 L.A. Yarbro and N. Deming, *Anal. Chim. Acta*, 73 (1974) 391.
- 15 J.R. Moody, *Anal. Chem.*, 54 (1982) 1358.

# Simultaneous spectrofluorimetric determination of traces of molybdenum and boron in plant leaves

C. Cruces Blanco, A. García Campaña, F. Alés Barrero and M. Román Ceba

*Department of Analytical Chemistry, Faculty of Sciences, University of Granada, 18071 Granada (Spain)*

(Received 8th September 1992; revised manuscript received 29th January 1993)

## Abstract

A method is described for the simultaneous determination of molybdenum and boron in plant leaves, based on the highly sensitive fluorescence reaction with Alizarin Red S. Simplicity is achieved by using first and second derivatives of the synchronous spectra. Appropriate calibration equations were established between 0.1–0.9 and 0.3–0.7  $\mu\text{g ml}^{-1}$  for molybdenum and boron, respectively, with a mean relative standard deviation of 2.2%.

**Keywords:** Fluorimetry; Boron; Derivative spectroscopy; Molybdenum; Plant materials; Synchronous derivative spectrofluorimetry

Molybdenum and boron are important trace elements in nature, especially in soils and plants [1,2]. Their contents in plants depend on numerous factors (vegetable species, plant parts, climatic conditions, etc.) but, usually no more than a few  $\text{ng g}^{-1}$  are found.

The increasing interest in plant growth studies has created the need not only for increasingly sensitive methods of analysis for numerous micronutrients but also highly sophisticated techniques for providing complete characterization of complex environmental samples. In order to simplify routine analyses of large numbers of samples, simple analytical concepts and inexpensive instrumentation are needed.

Fluorescence spectrometry is an important method in environmental analysis. Its sensitivity is well established but its selectivity has to be increased by applying separation techniques or by using modified forms of spectroscopic analysis.

*Correspondence to:* C. Cruces Blanco, Department of Analytical Chemistry, Faculty of Sciences, University of Granada 18071 Granada (Spain).

Among the latter, synchronous scanning fluorimetry [3,4] combined with derivative spectroscopy [5] has demonstrated its usefulness in the analysis of single- [6–10] and multi-component samples [11–20].

Numerous methods for the determination of boron [21–24] and molybdenum [25–29] at the microgram level have been proposed, but most of them involve their prior isolation from interfering species. Among the methods used for the determination of boron and molybdenum, fluorescence methods based on complex formation are the most frequently used [30–33].

Alizarin Red S (the sodium salt of 1,2-dihydroxyanthraquinone-3-sulphonic acid) is one of the most sensitive reagents for the fluorimetric determination of boron [34], but it is not very selective as it forms fluorescent chelates with a large number of ions, including molybdenum. This paper shows the utility of the synchronous derivative method, using isodifferential point measurements [16,35], for the simultaneous determination of boron and molybdenum as a simple and rapid screening method for these ions in plant leaf

samples. The results obtained for synthetic mixtures and interferences usually found in plant materials show that the association of the two techniques leads to a straightforward method for analysing mixtures.

## EXPERIMENTAL

### *Apparatus*

Fluorescence was monitored with a Perkin-Elmer Model MPF-66 spectrofluorimeter, equipped with a 150-W xenon arc lamp and an R-928 photomultiplier. All measurements were made in standard 10-mm pathlength quartz cells, thermostatically controlled at  $25.0 \pm 0.5^\circ\text{C}$  with a water-bath circulator (Frigiterm S-382). Excitation and emission monochromators were locked together and scanned simultaneously with a constant difference  $\Delta\lambda = \lambda(\text{em}) - \lambda(\text{ex})$ . The scanning speed and response time of the spectrometer were set at  $480 \text{ nm min}^{-1}$  and 0.5 s, respectively.

The spectrometer was connected to a Perkin-Elmer Model 7300 Professional Computer provided with PETLS application software (C 646-0280). A 101 Rhodamine quantum counter sample (Perkin-Elmer) was used for source intensity adjustment. Fluorescence data are given without spectral correction.

A Crison Digit-501 pH meter was used for all pH measurements.

### *Reagents*

All chemicals were of analytical-reagent grade, unless stated otherwise. Doubly distilled, demineralized water was used throughout.

Stock standard solutions of boron and molybdenum ( $1 \text{ g l}^{-1}$ ) were prepared from  $\text{H}_3\text{BO}_3$  and  $(\text{NH}_4)_6\text{Mo}_7\text{O}_{24} \cdot 4\text{H}_2\text{O}$  (Merck), respectively. The solutions were stored in polyethylene bottles. Working standard solutions ( $100 \mu\text{g ml}^{-1}$ ) were obtained by dilution with water.

Alizarin Red S was purchased from Carlo Erba. A  $1.0 \times 10^{-3} \text{ M}$  solution was prepared in water.

A pH 6.3 buffer solution was prepared by mixing appropriate volumes of 0.1 M disodium hydrogenphosphate and potassium dihydrogenphosphate.

A 3 M potassium chloride solution was prepared in water.

A strongly acidic cation-exchange resin, Amberlite IR-120 ( $\text{H}^+$ -form), 100–200 mesh, was used. An appropriate amount of resin was purified by placing it in a large column and backwashing with water to remove fine particles. It was then washed with 4 M hydrochloric acid and subsequently with demineralized water until the effluent gave a negative test with silver nitrate.

### *General procedure*

Synthetic mixtures were prepared in 10-ml volumetric flasks containing  $0.3\text{--}7 \mu\text{g ml}^{-1}$  or  $0.1\text{--}0.9 \mu\text{g ml}^{-1}$  of Mo; 3 ml of buffer solution (pH 6.3), 4 ml of 2.5 M KCl solution and an appropriate reagent excess were added. The mixture was diluted to volume with demineralized water. The synchronous fluorescence spectra, with a constant wavelength difference ( $\Delta\lambda$ ) of 150 nm, were recorded against a reagent blank and stored in the Perkin-Elmer data station.

For the determination of boron, the stored synchronous spectra of the mixtures were smoothed by using 25 experimental points and the first and second derivatives were calculated with  $\Delta\lambda' = 25$ . The amplitudes at 477 nm (first derivative) and 447 nm (second derivative) were proportional to the boron concentration.

For the determination of molybdenum, the same procedure was carried out with measurements of amplitudes at 447 nm (first derivative) and 475 nm (second derivative), which were proportional to the molybdenum concentration.

The fluorescence intensities of these derivative signals are directly related to the concentration of each ion in their individual calibration graphs, previously plotted.

### *Plant analysis*

Finely pulverized plant samples (melon and tomatoes leaves) were dried at  $60^\circ\text{C}$ . An accurately weighed portion (3 g) of the powder was calcined in a muffle furnace at  $500^\circ\text{C}$  for several hours and then left to cool inside the furnace. The resulting ash was wetted with demineralized water and 1 ml of concentrated hydrochloric acid was added. The mixture was heated at  $70^\circ\text{C}$  on a

hot-plate and subsequently filtered and washed with hot water. A 1.25-ml volume of 0.1 M EDTA solution was added and the resulting solution neutralized with sodium hydroxide solution. The mixture was finally transferred into a 25-ml volumetric flask and diluted to volume with demineralized water. To eliminate the main interferences, an aliquot of 10 ml was passed through the resin column at a flow-rate of  $0.5 \text{ ml min}^{-1}$ . After washing the column with 10 ml of demineralized water, the total volume for the determination of both ions was neutralized with sodium hydroxide solution, collected and transferred into a 25-ml volumetric flask and diluted to volume with demineralized water. Aliquots of 2.25 ml were used for the determination of boron and molybdenum by the procedure described above.

## RESULTS AND DISCUSSION

### *Selection of experimental conditions*

The individual determination of boron and molybdenum by fluorescence spectrometry has been reported previously [33,36]. The methods are based on the fluorescent complexes formed with Alizarin Red S in aqueous media.

In this work, these methods were modified for analysing binary mixtures of molybdenum and boron. In order to investigate whether the simultaneous determination was possible, a detailed study of the influence of pH on the fluorescence intensity of the two complexes in aqueous solution was carried out. The results are presented in Fig. 1. It is clear that pH is a very important variable to be controlled for the appropriate formation of both complexes. To obtain the maximum fluorescence signal for both complexes simultaneously, a pH of 6.3 was selected. This optimum pH was obtained by addition of a pH 6.3 disodium hydrogenphosphate–potassium dihydrogenphosphate buffer.

Little change in fluorescence intensity with the buffer concentration was observed, but a final concentration of 0.15 M was chosen to ensure the final pH desired for both complexes.

As previously established for Mo [36], an increase in fluorescence intensity was obtained on

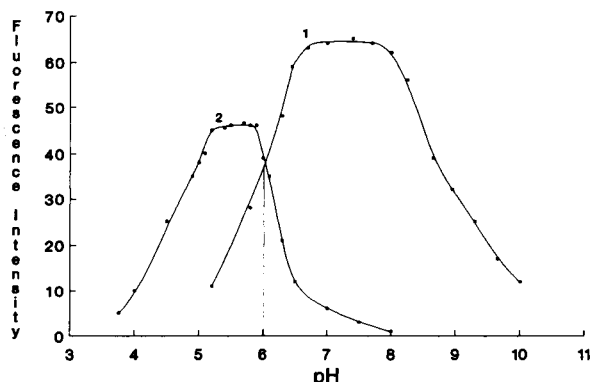


Fig. 1. Effect of pH on the fluorescence intensity of aqueous solutions of (1) boron complex ( $[B]=[R]=8 \times 10^{-5} \text{ M}$ ) and (2) molybdenum complex ( $[Mo]=[R]=1 \times 10^{-5} \text{ M}$ ).  $\lambda(\text{ex})=465 \text{ nm}$ ,  $\lambda(\text{em})=615 \text{ nm}$ ;  $[R]=$  reagent conc.

addition of KCl to the final solution. The effect of the concentration of this salt (0.4–2.0 M) on the fluorescence intensity of boron was studied and no changes were observed in this concentration range. A 1 M concentration was found to give the highest fluorescence intensity for molybdenum and boron complexes.

In order to obtain an appropriate reagent excess in solution to ensure the simultaneous complexation of both ions in a binary mixture, a detailed study of the effect of the Alizarin Red S concentration on the fluorescence intensity of both chelates was carried out. No changes in the fluorescence intensities of the two complexes were observed when the reagent molar concentration to cation ratio was maintained between 5:1 and 15:1 for molybdenum and 0.22:1 to 4:1 for boron. Throughout the experimental work, a reagent excess to ensure the simultaneous complexation of both ions in a binary mixture was used.

Although no temperature effect was observed for the molybdenum complex, the strong temperature dependence with the boron complex required thermostating at  $25^\circ\text{C}$ .

The order of addition of the reagents is not important and the complexes remain stable for at least 5 h.



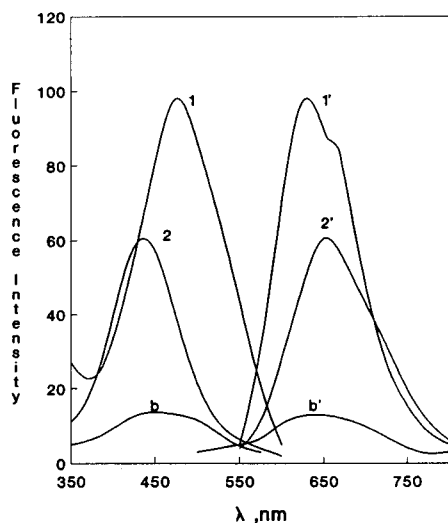


Fig. 2. Fluorescence spectra of (1, 1') molybdenum and (2, 2') boron complexes with Alizarin Red S and the reagent blank.  $[Mo] = 0.5 \mu\text{g ml}^{-1}$ ;  $[B] = 0.7 \mu\text{g ml}^{-1}$ ;  $[R] = 7 \times 10^{-5} \text{ M}$ ;  $[KCl] = 1 \text{ M}$  at pH 6.0.

#### Selection of instrumental parameters

The excitation and emission spectra of molybdenum and boron complexes under the optimum experimental conditions previously selected for their simultaneous determination are shown in Fig. 2.

The molybdenum complex shows an excitation maximum at 478 nm and the boron complex at 435 nm. The emission spectra show maxima at 623 and 610 nm, respectively.

As Fig. 2 shows, the emission spectra of both complexes consist of broad overlapping spectral bands and the analysis of mixtures of molybdenum and boron conventional spectrofluorimetry will not be feasible.

Here, a simple and rapid method is proposed for the individual and simultaneous determination of boron and molybdenum, using the well demonstrated advantages of synchronous derivative spectrofluorimetry (SDS).

The most important variable to be optimized in SDS is the wavelength difference between excitation and emission monochromators ( $\Delta\lambda$ ) at which a good separation between fluorescence maxima could be achieved with a minimum loss of sensitivity.

As the Stokes shift for molybdenum and boron complexes alone were 145 and 175 nm, respectively, the most intense and well shaped synchronous spectra for each compound alone will presumably appear between these two values.

In order to select the optimum  $\Delta\lambda$  value, a wide range (80–220 nm) was examined. The position of the maximum of the synchronous spectra and the fluorescence intensity for molybdenum and boron as a function of  $\Delta\lambda$  is shown in Fig. 3a and b, respectively. As can be seen, both the spectral distribution and the fluorescence intensity depend strongly on  $\Delta\lambda$ . Figure 3a shows a hypsochromic shift for both complexes as  $\Delta\lambda$  increases. As can be expected, when the value chosen for  $\Delta\lambda$  equals the difference between the excitation and emission wavelength maxima of

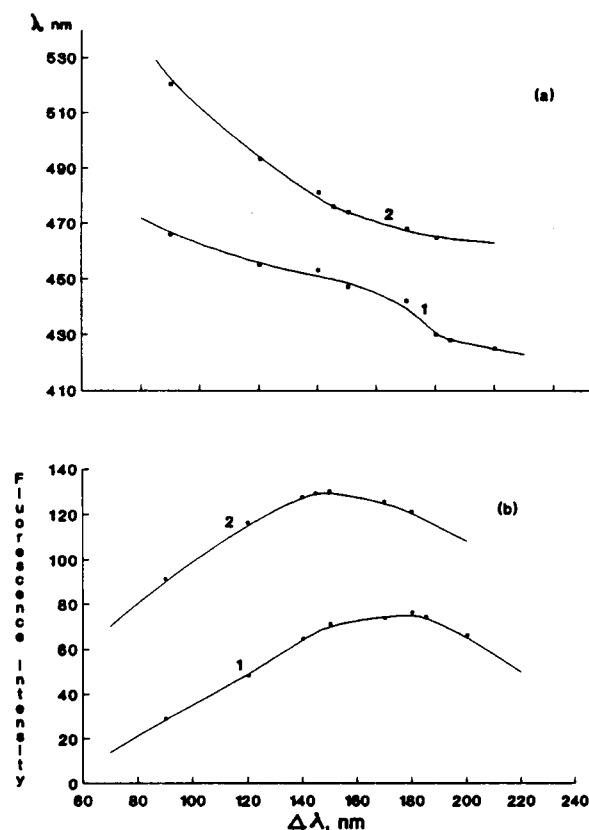


Fig. 3. Effect of  $\Delta\lambda$  on the synchronous spectra of (1) boron and (2) molybdenum. (a) Effect on the wavelength of the synchronous maxima; (b) effect on the fluorescence intensity.

TABLE 1

Analytical figures of merit

Element	Method <sup>a</sup>	Calibration graph <sup>b</sup>	$S_A$ <sup>c</sup> ( $\mu\text{g ml}^{-1}$ )	LOD <sup>d</sup> ( $\mu\text{g ml}^{-1}$ )	LOQ <sup>e</sup> ( $\mu\text{g ml}^{-1}$ )	Error (%)	R.S.D. <sup>f</sup> (%)
Mo	A	$I = 149.1[\text{Mo}] + 5.2$	0.010	0.009	0.031	1.36	1.90
	B	$I = 150.2[\text{Mo}] + 4.4$	0.006	0.014	0.045	0.75	1.05
	C	$I = 38.8[\text{Mo}] + 1.1$	0.009	0.008	0.026	1.56	2.18
	D	$I = 4.7[\text{Mo}] + 0.2$	0.017	0.064	0.174	2.46	3.44
B	A	$I = 53.9[\text{B}] + 9.0$	0.037	0.075	0.250	4.47	6.24
	B	$I = 53.1[\text{B}] + 6.3$	0.044	0.066	0.220	5.11	7.14
	C	$I = 10.8[\text{B}] + 1.5$	0.046	0.092	0.305	3.37	4.71
	D	$I = 2.1[\text{B}] + 0.8$	0.052	0.124	0.414	6.12	8.56

<sup>a</sup> A = direct; B = synchronous; C = synchronous first derivative; D = synchronous second derivative. <sup>b</sup>  $I$  = signal intensity; concentrations in  $\mu\text{g ml}^{-1}$ . <sup>c</sup> Analytical sensitivity. <sup>d</sup> Limit of detection. <sup>e</sup> Limit of quantification. <sup>f</sup> Relative standard deviation at  $0.5 \mu\text{g ml}^{-1}$  for  $n = 10$ .

conventional spectra (Stokes shifts), the fluorescence signals for both complexes exhibit a maximum. This occurs at  $\Delta\lambda = 150$  and  $180$  nm for molybdenum and boron, respectively (see Fig. 3b).

The selection of these  $\Delta\lambda$  values causes a reduction in the peak half-band width from  $126$  to  $83$  nm (molybdenum) and from  $81$  to  $64$  nm (boron). This band-narrowing effect is very valuable in the application of the derivative technique, especially for binary mixtures.

To obtain conditions for the individual and simultaneous determination of both complexes in a single scan, an unique  $\Delta\lambda$  should be selected.

The first and second derivatives were applied to the synchronous spectra of molybdenum and boron alone, recorded at three wavelength intervals ( $150$ ,  $170$  and  $180$  nm), in order to select the most appropriate interval for the greatest separation between derivative peaks. At a wavelength interval of  $150$  nm, the mutual spectral interference in a mixture was a minimum and, as is derived from Fig. 3b, for boron at  $\Delta\lambda = 150$  nm the fluorescence intensity is nearly the same as at its Stokes shift ( $180$  nm), whereas  $\Delta\lambda = 150$  nm corresponds to the maximum fluorescence intensity for Mo.

For recording the synchronous spectra, a scan

TABLE 2

Effect of foreign ions on the simultaneous determination of Mo and B ( $0.2 \mu\text{g ml}^{-1}$ )

Tolerance ratio (w/w)	Molybdenum <sup>a</sup>			Boron <sup>a</sup>		
	B	C	D	B	C	D
1000	$\text{K}^+$ , $\text{Ca}^{2+}$ , $\text{NO}_3^-$ , $\text{NO}_2^-$ , tartrate	$\text{K}^+$ , $\text{Ca}^{2+}$ , $\text{NO}_3^-$ , $\text{NO}_2^-$ , $\text{SO}_4^{2-}$	$\text{K}^+$ , $\text{Ca}^{2+}$		$\text{K}^+$ , $\text{NO}_2^-$ , $\text{NO}_3^-$ , $\text{SO}_4^{2-}$ , tartrate, $\text{F}^-$	$\text{K}^+$ , $\text{Ca}^{2+}$ , $\text{NO}_2^-$ , $\text{NO}_3^-$ , $\text{SO}_4^{2-}$ , tartrate, $\text{F}^-$
500	$\text{F}^-$ , $\text{Mn}^{2+}$	$\text{F}^-$ , tartrate	$\text{Mn}^{2+}$	$\text{F}^-$ , $\text{SO}_4^{2-}$ , $\text{K}^+$ , $\text{Ca}^{2+}$ , $\text{NO}_2^-$ , $\text{NO}_3^-$	$\text{Mn}^{2+}$ , $\text{Mg}^{2+}$ , $\text{Ca}^{2+}$	$\text{Mn}^{2+}$
100		$\text{Mn}^{2+}$ , $\text{Mg}^{2+}$	$\text{Zn}^{2+}$ , $\text{Mg}^{2+}$			$\text{Mg}^{2+}$
50	$\text{Zn}^{2+}$ , $\text{Mg}^{2+}$	EN	EDTA, EN	$\text{Mg}^{2+}$ , $\text{Mn}^{2+}$	EN	$\text{Zn}^{2+}$ , EDTA, EN
25	EDTA, EN <sup>b</sup>	$\text{Zn}^{2+}$ , EDTA		$\text{Zn}^{2+}$ , EDTA, EN	$\text{Zn}^{2+}$ , EDTA	
5			$\text{Cu}^{2+}$			
3	$\text{Cu}^{2+}$	$\text{Cu}^{2+}$			$\text{Cu}^{2+}$	$\text{Cu}^{2+}$
2	$\text{Fe}^{3+}$		$\text{Fe}^{2+}$ , $\text{Fe}^{3+}$	$\text{Cu}^{2+}$		
1	$\text{Fe}^{2+}$	$\text{Fe}^{3+}$			$\text{Fe}^{3+}$	$\text{Fe}^{2+}$ , $\text{Fe}^{3+}$
0.5		$\text{Fe}^{2+}$		$\text{Fe}^{2+}$ , $\text{Fe}^{3+}$	$\text{Fe}^{3+}$	

<sup>a</sup> Methods B, C and D as indicated in Table 1. <sup>b</sup> EN = ethylenediamine.

TABLE 3  
Linearity data for different synthetic binary mixtures

Composition ( $\mu\text{g ml}^{-1}$ )	Slope <sup>a</sup>				Intercept <sup>a</sup>				Correlation coefficient <sup>a</sup>				
	Molybdenum	Boron	A	B	C	D	A	B	C	D	A	B	C
0.1–1.0	0.0	149.1 ± 10.3	150 ± 6.6	38.8 ± 1.7	4.7 ± 0.2	2.05 ± 5.9	20.1 ± 3.8	3.6 ± 1.5	0.3 ± 0.1	0.9934	0.9982	0.9979	0.9830
	0.1	149.0	145.9	38.0	4.5	22.7	23.6	3.1	0.2	0.9998	0.9998	0.9999	0.9937
	0.2	146.0	145.3	37.8	4.7	26.7 <sup>b</sup>	27.0 <sup>b</sup>	3.1	0.3	0.9995	0.9992	0.9994	0.9952
	0.5	142.5	141.4 <sup>b</sup>	37.3	4.7	34.8 <sup>b</sup>	35.3 <sup>b</sup>	2.1	0.0 <sup>b</sup>	0.9999	0.9996	0.9995	0.9996
	1.0	141.3	142.8 <sup>b</sup>	37.1	4.9	48.7 <sup>b</sup>	49.6 <sup>b</sup>	1.4 <sup>b</sup>	0.2 <sup>b</sup>	0.9998	0.9997	0.9998	0.9980
	3.0	111.8 <sup>b</sup>	110.3 <sup>b</sup>	34.0 <sup>b</sup>	3.2 <sup>b</sup>	98.1 <sup>b</sup>	12.3 <sup>b</sup>	3.1 <sup>b</sup>	0.4 <sup>b</sup>	0.9994	0.9999	0.9979	0.9784
	0.0	0.1–0.3	53.9 ± 5.0	53.1 ± 3.6	10.8 ± 1.6	2.1 ± 0.2	23.1 ± 3.7	1.5 ± 0.8	0.8 ± 0.5	0.9921	0.9954	0.9937	0.9941
	0.1	58.4	56.7	11.4	2.3	28.4 <sup>b</sup>	26.1 <sup>b</sup>	0.9	0.3	0.9967	0.9999	0.9999	0.9999
	0.2	53.9	52.9	10.9	2.1	41.6 <sup>b</sup>	39.7 <sup>b</sup>	1.7	0.4	0.9985	0.9996	0.9995	0.9995
	0.5	39.7 <sup>b</sup>	50.5	10.0	2.0	71.7 <sup>b</sup>	65.1 <sup>b</sup>	1.6	0.4	0.9910	0.9997	0.9997	0.9980
	1.0	27.1 <sup>b</sup>	44.5 <sup>b</sup>	9.2	1.9	119.5 <sup>b</sup>	111.5 <sup>b</sup>	2.3	0.5	0.9658	0.9992	0.9998	0.9996

<sup>a</sup> Methods A–D as indicated in Table 1. <sup>b</sup> Values out of calibration graph standard deviation ( $n = 3$ ).

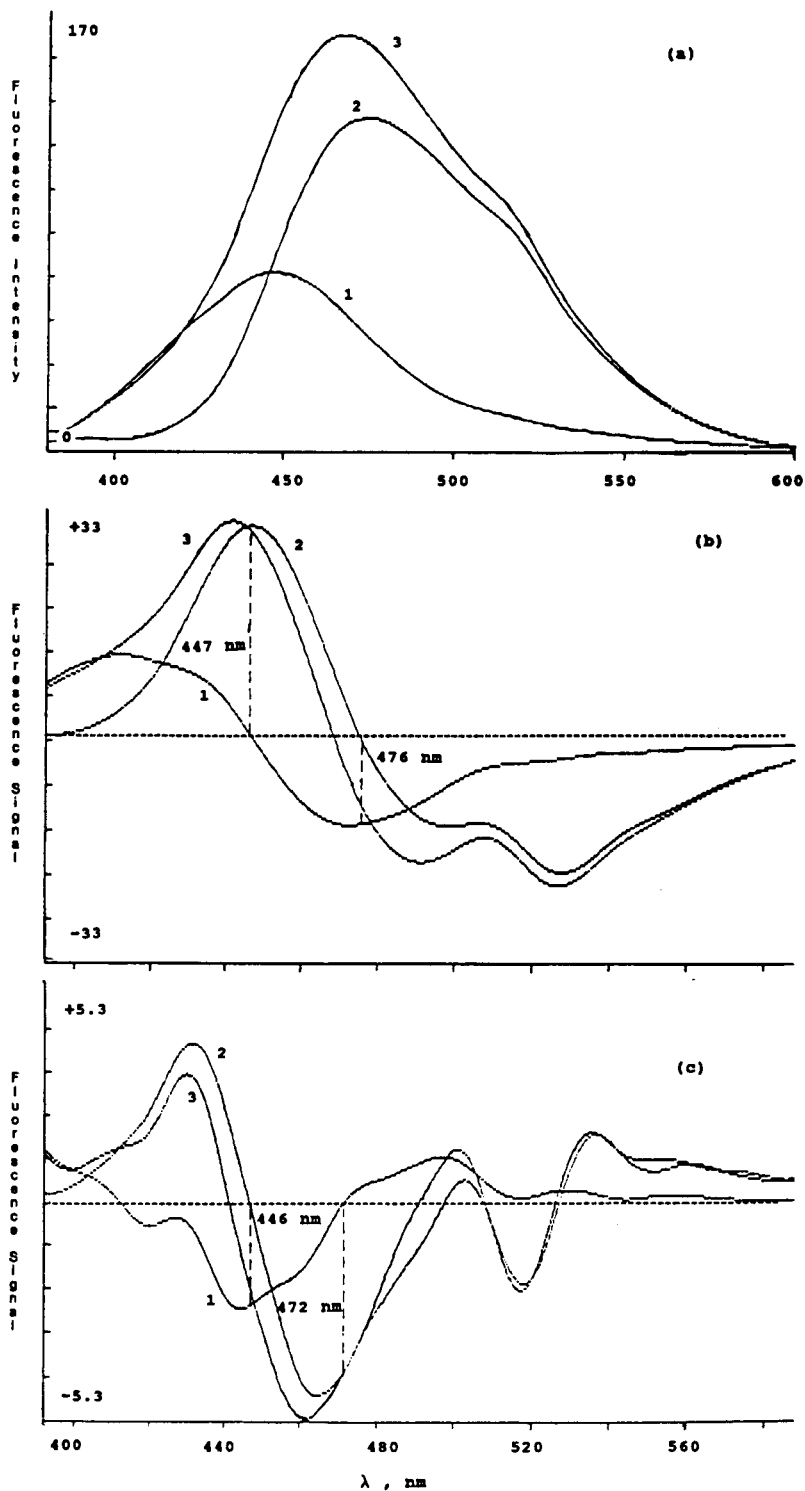
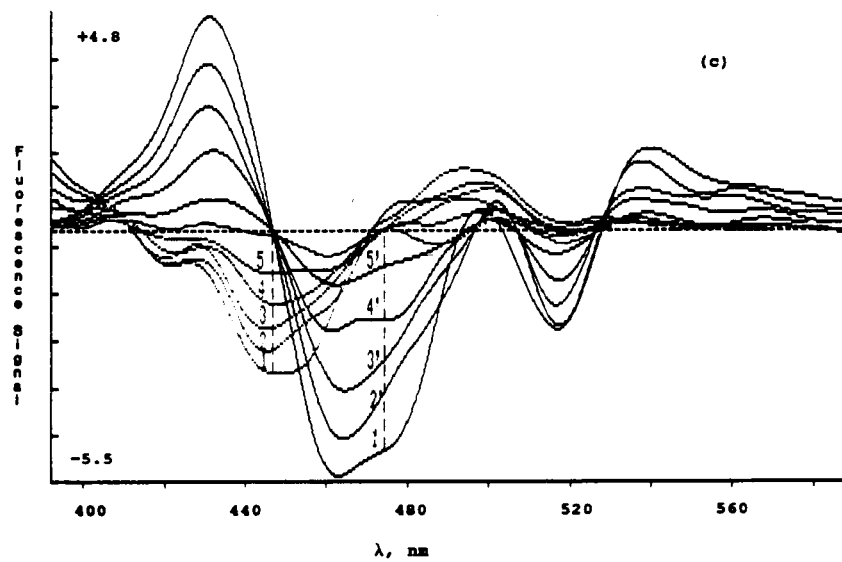
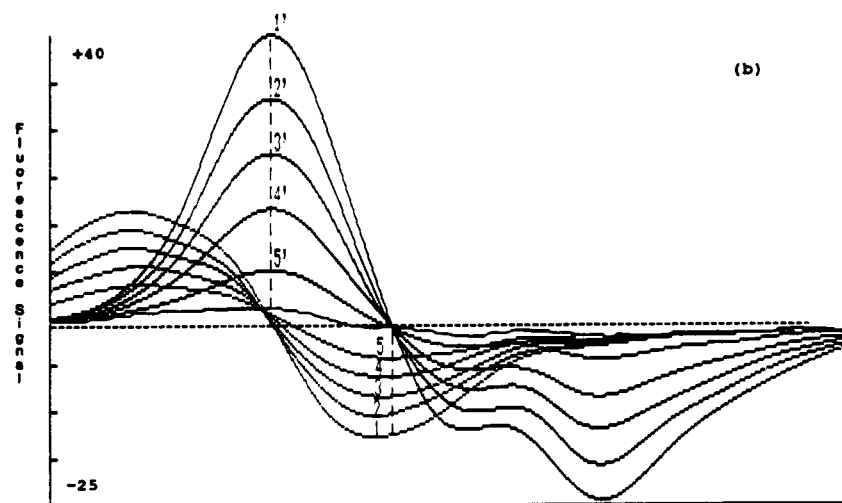
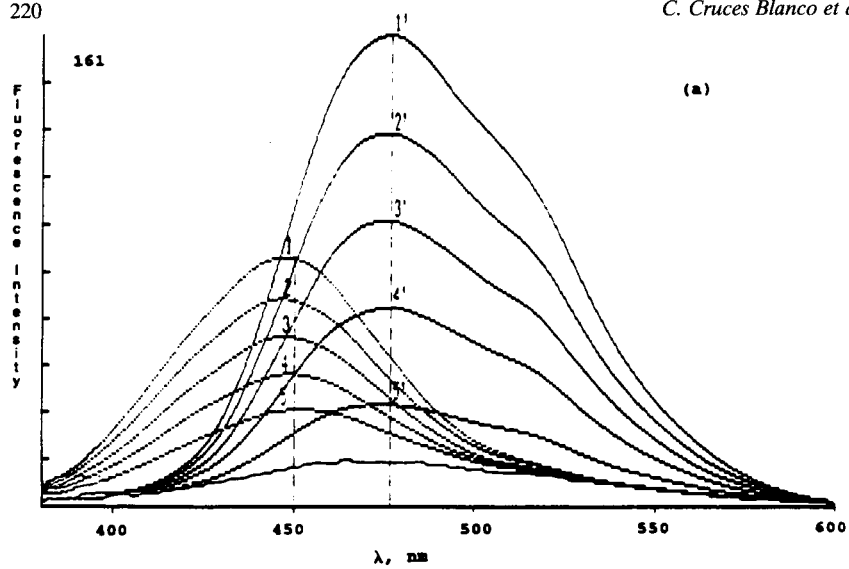


Fig. 4. (a) Synchronous fluorescence spectra and (b) their first derivative and (c) second derivative for (1) boron, (2) molybdenum and (3) a mixture of both at  $\Delta\lambda = 150$  nm.  $[\text{Mo}] = [\text{B}] = 1 \mu\text{g ml}^{-1}$ . The analytical wavelengths for the determination are indicated.



speed of  $480 \text{ nm min}^{-1}$  and a response time of 0.5 s were selected. For calculation of the derivatives of the synchronous spectra of molybdenum and boron complexes, filter sizes of 25 points were used. As can be seen in Fig. 4a, the synchronous spectra of the molybdenum and boron complexes overlap, hence the quantitative analysis of mixtures is not possible even if these spectra are recorded. However, as shown in Fig. 4b and c, the first and second derivatives of the corresponding synchronous spectra have zero values of differential fluorescence. These so-called isodifferential points [16,35] show no signal contribution of one compound to the other at the measurement wavelength indicated.

#### Analytical characteristics

Under the recommended conditions, the analysis of mixtures of boron and molybdenum is carried out in only one scan. The method involves the establishment of individual calibration graphs for each compound. The direct, synchronous, synchronous first- and second-derivative signals vary linearly with molybdenum ( $0.1\text{--}0.9 \mu\text{g ml}^{-1}$ ) and boron ( $0.3\text{--}7.0 \mu\text{g ml}^{-1}$ ) concentration. The analytical figures of merit are summarized in Table 1, and representative plots are shown in Fig. 5.

The limits of detection (LOD) and quantification (LOQ) were calculated as described previously [37,38]. The analytical sensitivity [8] varied depending on the method applied. The higher LOD of boron with respect to molybdenum in the synchronous and synchronous-derivative method is due to the fact that the wavelength interval used in the single scan favours the molybdenum response (see Fig. 3b).

In order to test the precision of the method, four series of samples covering the range of interest for Mo (0.1, 0.2, 0.5 and  $1.0 \mu\text{g ml}^{-1}$ ) were analysed and the corresponding mean relative standard deviations (R.S.D.s) ( $n = 10$ ) using the synchronous first derivative were 4.7% and 5.1% for molybdenum and boron, respectively.

#### Interference study

To assess the applicability of the proposed method to the determination of both molybdenum and boron in plant leaves, the effect of the ions commonly found in these material was studied.

The spectral interferences were measured with the direct, synchronous and the two derivative methods. The maximum concentration tested of each potentially interfering ion was  $200 \mu\text{g ml}^{-1}$ . If interference occurred, the concentration was decreased until no interference was observed. The tolerance criterion used was a deviation of twice the standard deviation,  $S_S$ , of the mean value of ten measurements of  $0.5 \mu\text{g ml}^{-1}$  of molybdenum and boron by the different methods.

It is observed in Table 2 that except for iron and copper, the ions tested do not interfere at the levels usually encountered in plant leaves. A concentration of  $5 \times 10^{-4}$  M EDTA as masking agent is recommended, taking into account that an excess of EDTA will cause interference itself (see Table 2).

The results indicate that the SDS technique is very useful for obtaining more selective determinations in real samples, as pointed out previously [39].

#### Simultaneous determination of molybdenum and boron in synthetic mixtures

To study the efficiency of the proposed methods for the simultaneous determination of both ions in a real sample, the effect of one ion on the linearity of the response of the other was tested. The fluorescence signals of a series of solutions containing molybdenum ( $0.1\text{--}1.0 \mu\text{g ml}^{-1}$ ) or boron ( $0.1\text{--}3.0 \mu\text{g ml}^{-1}$ ), measured by the different methods, were compared with and without the presence of increasing concentrations of boron and molybdenum, respectively. The different concentrations tested gave Mo:B and/or B:Mo ratios from 1:1 to 1:30 which, as demon-

Fig. 5. (a) Synchronous fluorescence spectra and (b) their first derivative and (c) second derivative of two superimposed series of Mo (1'–5') and B (1–5). [Mo] =  $0.1\text{--}0.9 \mu\text{g ml}^{-1}$ ; [B] =  $0.3\text{--}1.2 \mu\text{g ml}^{-1}$ .

strated subsequently, are those usually found in plant material.

Table 3 summarizes the results obtained, from which the following conclusions can be drawn. For the conventional and synchronous methods, the slopes and intercepts are greatly affected by the presence of small concentration ratios of the two ions, only a ratio 1:1 for each ion being possible. For the synchronous first- and second-derivative methods, both the slopes and the intercepts are found to be within the standard deviation of the calibration graph of the compound alone, allowing ratios of 1:30 (Mo:B) and 1:10 (B:Mo), which were the maximum ratios tested.

The facts that the slopes are nearly identical for these last methods and that the intercepts are in good agreement with those corresponding to the compounds alone, demonstrate the absence of interference of one ion with the fluorescence signal of the other at the measurement wavelengths previously chosen (see Fig. 4).

#### *Analysis of plant leaf samples*

Plant leaf samples (melon and tomato), containing unknown amounts of molybdenum and boron, were analysed directly by measuring the

fluorescence signals by the synchronous first-derivative method.

Although good results were obtained in the analysis of synthetic mixtures by both synchronous first- and second-derivative spectrometry, the detection limit and precision are slightly poorer for the latter (see Table 1). Therefore, synchronous first-derivative spectrometry is recommended for further routine work.

Three individual extractions and three determinations for each extraction were carried out for the two samples tested. The average molybdenum contents were 1.29 and 2.36  $\mu\text{g ml}^{-1}$  for melon and tomato leaves, respectively, and those for boron were 29.20 and 23.62  $\mu\text{g ml}^{-1}$ , respectively.

The results summarized in Table 4 indicate that good recoveries are obtained with different amounts of molybdenum and boron added to three samples analysed.

In conclusion, the combination of derivative spectroscopy and the synchronous fluorescence technique have permitted the simultaneous determination of two complexes with very similar fluorescence spectra, with the advantage that only one scan is required, which results in very short

TABLE 4

Simultaneous determination of molybdenum and boron in plant leaves by the synchronous first-derivative method

Sample	Mo			B		
	Added ( $\mu\text{g g}^{-1}$ )	Found <sup>a</sup> ( $\mu\text{g g}^{-1}$ )	Recovery (%)	Added ( $\mu\text{g g}^{-1}$ )	Found <sup>a</sup> ( $\mu\text{g g}^{-1}$ )	Recovery (%)
Melon leaves	–	1.29 ± 0.05	–	–	29.20 ± 0.55	–
	9.26	9.70	90.8			
	27.78	28.03	96.3	27.78	55.83	95.9
	46.30	45.00	94.4	46.30	73.74	96.2
	64.63	62.50	94.7	64.63	92.77	98.4
	82.96	82.80	98.4	82.96	110.81	98.5
Tomato leaves	–	2.36 ± 0.07	–	–	23.62 ± 0.03	–
	9.26	11.32	96.8			
	27.78	27.41	96.0	27.78	48.96	91.2
	46.30	47.43	97.6	46.30	70.01	100.1
	64.63	66.27	99.0	64.63	87.62	99.0

<sup>a</sup> Mean of three determinations.

measurement times. The present method developed for molybdenum and boron determination in plant leaves provides a sensitive and rapid procedure for field work and could be extended to other ions in different real samples.

## REFERENCES

- 1 M. Ya. Shkolnik, *Trace Elements in Plants*, Elsevier, Amsterdam, 1984, p. 195.
- 2 J. Bonner and J.E. Vaner, *Plant Biochemistry*, Academic, New York, 1975.
- 3 J.B.F. Lloyd, *Nature (London)*, 231 (1971) 64.
- 4 T. Vo-Dinh, in E.E. Wehry (Ed.), *Modern Fluorescence Spectroscopy*, Vol. 4, Plenum, New York, 1981, Chap. 5.
- 5 P. John and I. Soutar, *Anal. Chem.*, 48 (1976) 520.
- 6 C. Cruces Blanco and F. García Sánchez, *Anal. Chem.*, 56 (1984) 2035.
- 7 C. Cruces Blanco and F. García Sánchez, *Anal. Chim. Acta*, 166 (1984) 277.
- 8 F. García Sánchez and C. Cruces Blanco, *Anal. Chem.*, 58 (1986) 73.
- 9 F. Capitán, A. Navalón, E. Manzano, L.F. Capitán-Vallvey and J.L. Vilchez, *Fresenius' Z. Anal. Chem.*, 340 (1991) 10.
- 10 F. García Sánchez, A. Aguilar Gallardo and C. Cruces Blanco, *Talanta*, 40 (1992) 135.
- 11 J.N. Miller, A.F. Fell and T.A. Ahmad, *Anal. Proc.*, 19 (1982) 37.
- 12 E.L. Inman, Jr., and J.D. Winefordner, *Anal. Chem.*, 54 (1982) 2018.
- 13 S. Rubio, A. Gómez-Hens and M. Valcárcel, *Anal. Chem.*, 57 (1985) 1101.
- 14 F. García Sánchez, J.C. Márquez Gómez and M. Hernández López, *Analyst*, 112 (1987) 649.
- 15 A. Muñoz de la Peña, F. Salinas and I. Durán Marás, *Anal. Chem.*, 60 (1988) 2493.
- 16 F. García Sánchez and C. Cruces Blanco, *Anal. Chem.*, 60 (1988) 323.
- 17 F. García Sánchez and C. Cruces Blanco, *Talanta*, 37 (1990) 537.
- 18 Y.Q. Li, X.Z. Huang, J.C. Xu and G.Z. Chen, *Anal. Chim. Acta*, 256 (1992) 285.
- 19 D.G. Konstantianos and P.C. Loannov, *Analyst*, 117 (1992) 877.
- 20 F. Capitán, G. Sánchez-Palencia, A. Navalón, L.F. Capitán-Vallvey and J.L. Vilchez, *Anal. Chim. Acta*, 259 (1992) 345.
- 21 C.A. Parker and W.J. Barnes, *Analyst*, 85 (1960) 828.
- 22 W. Tkacz and L. Psonicki, *Anal. Chim. Acta*, 90 (1977) 339.
- 23 B. Liebich, D. Monnier and A. Marcantonatos, *Anal. Chim. Acta*, 52 (1970) 305.
- 24 F. Salinas, A. Muñoz de la Peña, J.A. Murillo and J.C. Jiménez Sánchez, *Analyst*, 112 (1987) 913.
- 25 P.Y. Peng and E.B. Sandell, *Anal. Chim. Acta*, 29 (1963) 67.
- 26 K. Kawabuchi and R. Kuroda, *Talanta*, 17 (1970) 67.
- 27 J. Korkisch and H. Gross, *Talanta*, 20 (1973) 1153.
- 28 J.L. Martínez Vidal, A.R. Fernández Alba and F. Salinas, *Analyst*, 115 (1990) 329.
- 29 K. Jiao, W. Jin and H. Metzner, *Anal. Chim. Acta*, 260 (1992) 35.
- 30 G.F. Kirkbright, T.S. West and C. Woodward, *Talanta*, 13 (1966) 1645.
- 31 F. Salinas, A. Muñoz de la Peña, L.F. Capitán-Vallvey and A. Navalón, *Analyst*, 114 (1989) 1297.
- 32 S. Motomizu, M. Oshima and Z. Jun, *Anal. Chim. Acta*, 251 (1991) 269.
- 33 A. García Campaña, F. Alés Barrero and M. Román Ceba, *Analyst*, 117 (1992) 1189.
- 34 L. Szebellady and S. Tomay, *Fresenius' Z. Anal. Chem.*, 107 (1936) 26.
- 35 F. García Sánchez, M. Hernández López and J.C. Márquez Gómez, *Spectrochim. Acta, Part A*, 43 (1987) 101.
- 36 A. García Campaña, F. Alés Barrero and M. Román Ceba, unpublished results.
- 37 *Spectrochim. Acta, Part B*, 37 (1978) 242.
- 38 *Anal. Chem.*, 52 (1980) 2242.
- 39 M. Valcárcel and A. Rios, *Analisis*, 18 (1990) 469.



# Determination of nickel in biological samples prepared by microwave dissolution using electrothermal atomic absorption spectrometry after extraction with 1,5-bis[phenyl-(2-pyridyl)methylene] thiocarbonhydrazide

E. Vereda Alonso, J.M. Cano Pavon, A. Garcia de Torres and M.T. Siles Cordero

*Department of Analytical Chemistry, Faculty of Sciences, University of Málaga, 29071 Málaga (Spain)*

(Received 16th September 1992; revised manuscript received 2nd December 1992)

## Abstract

An electrothermal atomization atomic absorption spectrometric method for the determination of traces of nickel after extraction of the metal into methyl isobutyl ketone containing 1,5-bis[phenyl(2-pyridyl)methylene] thiocarbonhydrazide is suggested. The chief advantage of the method lies in its maximum allowable aqueous-to-organic phase volume ratio of 37. The method was applied to the determination of nickel in various biological tissues, serum and human urine.

*Keywords:* Atomic absorption spectrometry; Biological samples; Extraction; Microwave dissolution; Nickel; Serum; Urine

The relevance of nickel from the health point of view has grown markedly over the last few years as a result of toxicological and physiological research on this element [1–5]. The fact that nickel can cause allergy and in some of its compounds is carcinogenic has made the monitoring of nickel levels in biological materials of great importance. Hence there is an increasing demand for suitable, sensitive and selective analytical methods for this purpose.

Under normal conditions, nickel occurs in body fluids and tissues at very low concentrations. As the nickel concentrations in biological materials usually lie at the  $\text{ng ml}^{-1}$  level, atomic absorption spectrometry with electrothermal atomization (ETAAS) has become the most appropriate tech-

nique for its determination. However, in certain kinds of samples, the sensitivity of this method is not sufficient for direct determination, so that prior preconcentration by liquid–liquid extraction is necessary. The extraction step has a twofold purpose, namely concentrating the metals of interest and isolating them from a potentially interfering matrix. The concentration range achieved depends on the ratio of the aqueous to organic phase volume. On the other hand, isolation from the matrix significantly decreases any background signal arising from the occurrence of concomitants.

1,5-Bis[phenyl-(2-pyridyl)methylene] thiocarbonhydrazide (BPTH) is a suitable complexing reagent for a number of metal ions. Most of the complexes formed can be extracted into a variety of organic solvents. As it is amphoteric, its partitioning between water and an organic solvent is markedly dependent on the pH.

*Correspondence to:* J.M. Cano Pavon, Department of Analytical Chemistry, Faculty of Sciences, University of Málaga, 29071 Málaga (Spain).

In this work, a systematic study was made to determine the optimum conditions for the determination of nickel in biological samples by graphite furnace AAS after extraction of the metal into methyl isobutyl ketone (MIBK) containing BPTH. The chief advantage of the proposed method lies in its maximum allowable aqueous-to-organic phase volume ratio of 37.

## EXPERIMENTAL

### *Apparatus*

AAS measurements were made with a Varian Model 475 atomic absorption spectrometer with a standard air–acetylene burner, a Perkin-Elmer Model 372 atomic absorption spectrometer equipped with an HGA 2200 graphite furnace and a deuterium arc background corrector and a Perkin-Elmer Model 4100 ZI Zeeman electrothermal atomic absorption spectrometer equipped with a Model As-70 automatic sampling system, a Zeeman-effect background correction system and a PC-ICL computer. Pyrolytic graphite-coated graphite tubes and L'vov-type graphite platforms were used.

pH measurements were made with the aid of a Crison Digit-501 pH meter furnished with a combined glass–calomel electrode.

Separating funnels were shaken on a Galenkamp flask agitator.

For sample digestion, a Panasonic Model NN-8507/8557 domestic microwave oven with a 700-W magnetron and rotating antenna was used. The oven was placed in a laboratory fume-hood. The samples were placed in Parr Model 478 microwave acid digestion bombs. The bombs were cleaned before use with 10% nitric acid for 1 day following by repeated rinsing with water.

All glassware used was washed with 10% nitric acid for 1 day and rinsed with water just before use.

### *Reagents*

All chemicals were of at least analytical-reagent grade and doubly distilled, deionized water was used throughout.

A stock standard solution of Ni(II) was pre-

pared from the nitrate and standardized gravimetrically with dimethylglyoxime. Working standard solutions were prepared by appropriate dilution as required. Standard solutions were prepared daily.

Boric acid–sodium borate buffer (pH 8.8) was prepared by mixing 25 ml of 0.2 M boric acid and 15 ml of 0.2 M sodium borate in a 100-ml volumetric flask and diluting to volume with water.

A 0.2% (w/v) BPTH solution in MIBK was prepared dissolving the appropriate amount of the reagent, prepared and purified as described under *Synthesis of the reagent*, in hot MIBK and diluting to 100 ml. The solution was stable for at least 1 week in a refrigerator.

### *Synthesis of the reagent*

A 1.0-g amount of thiocarbonhydrazide was dissolved in 80–100 ml of distilled water and 4.3 g of phenylpyridine in 10 ml of ethanol were added. The mixture was then refluxed for 4 h and the yellow product was filtered, washed with hot ethanol and dried in a vacuum desiccator (yield 70%, m.p. 165–175°C). Elemental analysis gave C 68.62, H 4.59, N 19.14, S 7.40; C<sub>25</sub>H<sub>20</sub>N<sub>6</sub>S requires C 68.80, H 4.59, N 19.27, S 7.34%. The structure of the compounds was confirmed by IR, NMR and mass spectrometry.

### *Procedures*

*Choice of optimum extraction conditions.* The metal ion was extracted as follows: in 250-ml separating funnels were placed 40 µg of nickel with various volumes of HCl, NaOH and NaClO<sub>4</sub> solutions and the mixture was diluted to an overall volume of 40 ml in the aqueous phase. Variable volumes of BPTH solution at different concentrations in MIBK were then added and the mixture was shaken vigorously on a mechanical agitator for different periods of time. Once the two phases had separated, the aqueous phase was collected and the equilibrium pH measured. The remaining metal ion concentration in the aqueous phase was determined by flame AAS, using appropriate calibration graphs. From the concentration found the fraction of metal extracted was calculated. Appropriate blanks were prepared and run in the same manner.

TABLE 1  
Temperature programme of HGA 2200 graphite furnace

Temperature (°C)	Time (s)		Flow-rate of argon (ml min <sup>-1</sup> )
	Ramp	Hold	
110	1	30	250
130	5	30	250
1100	10	10	250
2300	0 <sup>a</sup>	5	0 (read 5 s)
2400	1	2	250

<sup>a</sup> Maximum power heating.

**Recommended procedure.** In 250-ml separating funnels aliquots of samples or standards solutions containing nickel were placed and the pH of the aqueous phase was adjusted by means of borate buffer solution (pH 8.8). A 0.2% solution of BPTH in MIBK was used as organic phase. The maximum volume ratio of the aqueous to organic phase for a single-stage extraction of 99–100% was 37:1. The mixture was shaken vigorously at 3000 rpm for 7 min and the phases were allowed to separate. The organic solvent layer was transferred into a polypropylene centrifuge tube (some samples, e.g., human urine and blood serum, may need centrifugation for up to 10–15 min to improve the separation between the layers). Aliquots of 20  $\mu$ l of organic phase were injected, in triplicate, into the graphite furnace and the analytical signal (peak area) was measured at 232.0 nm using a band pass of 0.2 nm and a lamp current of 25 mA. Other instrumental parameters used are given in Table 1. The nickel concentration was evaluated from a calibration graph constructed

with standard solutions treated in the same way; alternatively, one can also apply the standard additions method. Blanks were always run in the same way and for each sample examined the value of the blank was subtracted.

#### Sample preparation

**Biological tissues.** Samples of the various types of material considered were first dried in accordance with the directives of the respective analysis certificates. Each dried sample was mineralized according to the following procedure. Samples (ca. 200 mg) were weighed directly into the digestion vessels on a digital electronic balance and 4 ml of concentrated HNO<sub>3</sub> were added. The mixture was allowed to stand for 30 min and then 2 ml of concentrated HCl were added. Next, the bomb was closed and placed in a microwave oven together with a beaker filled with 10 ml of water. This procedure minimizes the risk of damage to the magnetron as the small sample loads may cause magnetron failure because most of the microwave power is reflected back to the waveguide and magnetron. The power and treatment time of the microwave oven for the different types of samples are given in Table 2.

After digestion, the solutions were evaporated to a small volume and neutralized with NaOH, then 10 ml of boric acid–sodium borate buffer (pH 8.8) and 2 ml of 0.2 M glycine were added and the solutions were diluted to 100 ml with deionized water in a volumetric flask. Aliquots of these samples solutions were placed in 250-ml separating funnels and the analysis of each sam-

TABLE 2  
Operating conditions of microwave oven

Sample	Power (%) + time (min)	No. of treatments	No. of bombs
Olive leaves	2 min at 80% + 4 min at 20%	1	2
Aquatic plant	2.5 min at 80% + 4.5 min at 50%	1	2
Aquatic moss	2 min at 100% + 4 min at 50%	2	2
Dogfish muscle	4 min at 50% + 10 min at 20%	1	3
Dogfish liver	4 min at 50% + 10 min at 20%	1	3
Lobster hepatopancreas	4 min at 50% + 10 min at 20%	1	3
Citrus leaves	4 min at 50% + 10 min at 20%	1	3
Pig kidney	4 min at 50% + 10 min at 20%	1	3
Bovine muscle	4 min at 50% + 10 min at 20%	1	3

ple, in triplicate, was completed as described above.

**Human urine.** The urine was acidified to 1% (v/v) with concentrated  $\text{HNO}_3$  and stored frozen until analysis for nickel. In 100-ml separating funnels were placed 50 ml of acidified urine plus 2 ml of 0.2 M glycine and 8 ml of borate buffer (pH 8.8, adjusted by addition of 3 M NaOH). Then, 3 ml of 0.2% BPTH solution in MIBK were added and the nickel content was determined by the recommended procedure using the method of standard additions.

**Human blood serum.** Samples of serum (4 ml) were placed in centrifuge tubes and concentrated  $\text{HNO}_3$  (200  $\mu\text{l}$ ) was added to each sample and mixed for 1 min. Each tube was placed in a water-bath at 70°C for 5 min, then, the tubes were mixed for 10 s and centrifuged for 10 min. The protein-free supernatants were decanted and centrifuged for 10 min; if necessary, concentrated  $\text{HNO}_3$  was added drop to drop in order to see if further precipitation of proteins was produced. If this occurred, mixing for 1 min was applied, followed by recentrifugation. The protein-free serums were transferred into separating funnels together with 0.6 ml of borate buffer (pH 8.8) plus 0.1 ml of 0.2 M glycine. The pH was adjusted to 8.8 by adding various volumes of 3 M NaOH. Then, 1 ml of the 0.2% BPTH solution in MIBK was added and the nickel content was determined by the recommended procedure using the method of standard additions.

The precipitated proteins were tested for the presence of nickel but none was found.

## RESULTS AND DISCUSSION

### Analytical conditions

Extraction of metal ions by organic reagents is known to depend on several factors such as type and amount of reagent, organic solvent, pH of solution and shaking time. The extraction process was investigated in order to establish the optimum conditions. MIBK has a significant solubility in water but was chosen as the organic solvent because of its high extraction efficiency for the Ni(II)–BPTH complex.

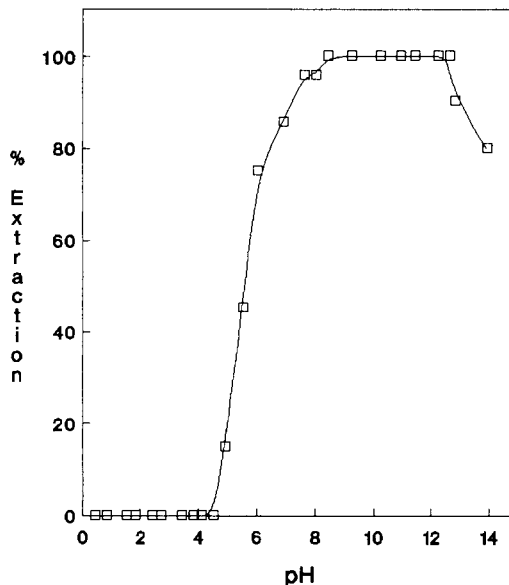


Fig. 1. Extraction of nickel into MIBK versus pH using BPTH as extractant.

The effects of pH on the extraction of nickel with BPTH into MIBK are shown in Fig. 1. The optimum pH range for quantitative extraction of the complex is ca. 8.5–12.0. All subsequent studies were carried out at pH 8.8, adjusted using borate buffer solution. The volume of buffer added had no effect. Increasing the ionic strength produced no significant changes in the extraction.

The minimum shaking time was determined by varying the shaking time from 1 to 10 min; 5 min was sufficient, but as prolonged shaking had no adverse effect on the extraction of metal ion, 7 min was selected.

The reagent concentration in the organic phase was varied while keeping its final volume at 5 ml. The results obtained showed that the extracted fraction remains constant for reagent concentrations  $\geq 1.15 \times 10^{-3}$  M (0.065%). A concentration of 0.2% of BPTH was used in practice in order to prevent reagent depletion by other extractable ions potentially occurring in the aqueous medium.

Variation of the concentration of the analyte at the optimum pH and a constant reagent concentration of 0.05% had no effect on the distribu-

tion ratio, which suggests that only the mononuclear species was extracted.

The composition of the extracted complex was studied by the equilibrium shift method based on the following equation [6], assuming that only the species  $ML_n$  is extracted and the metal is present in the aqueous phase predominantly as the cation  $M^{n+}$ :

$$\log D = \log K_{ex} + n\text{pH} + n \log[\text{HL}]_0$$

where  $D$  is the metal distribution ratio,  $K_{ex}$  is the extraction constant of the complex and  $[\text{HL}]_0$  is the concentration of the extracting agent in the organic phase. The results obtained by plotting the logarithm of the distribution coefficient versus the logarithm of the ligand concentration, at the optimum pH, indicate a ratio of the metal to ligand of 1:2, with the liberation of two protons during complexation.

The volume of the aqueous phase was varied between 10 to 200 ml while keeping that of the organic phase constant at 5 ml (0.2% BPTH); hence the phase volume ratios were varied between 0.5 and 40. For a ratio  $> 37$ , the phase separations were unsatisfactory and the procedure was thus inapplicable. This phase ratio allows the sensitivity of the direct non-extractive method to be increased by a factor of 37.

Under these optimum conditions, the recovery factors for the extraction of nickel were calculated by means of a series of experiments in which the atomic absorption of this element in the aqueous or organic phase was compared with that of an appropriate standard. In all instances, nickel in the range 0.5–100  $\mu\text{g}$  was extracted completely from the aqueous solution by a single extraction under the recommended conditions.

On the other hand, prior to the analysis of real samples, it was necessary to optimize the instrumental conditions for the determination of Ni by ETAAS. The complete programme developed as a result of normal optimization procedures was as described under *Recommended procedure*.

#### *Sensitivity and precision*

The limits of detection and determination of the method were established according to the definitions of the American Chemical Society

Committee on Environmental Improvement [7] and the values found were 0.2 and 0.9  $\text{ng ml}^{-1}$ , respectively, of nickel in the aqueous phase for an aqueous-to-organic phase volume ratio of 37. The blank value, in units of absorbance, was  $0.021 \pm 0.002$ .

The precision of the method was studied by the analysis solutions containing known amounts of nickel. The results of the determination of 1.1  $\text{ng ml}^{-1}$  of nickel showed a maximum relative error of 3.5%.

#### *Effect of foreign ions*

The effect of various ions on the determination of nickel by the proposed method was examined under the optimum working conditions. For this study, different amounts of the ionic species tested were added to a 2.5  $\text{ng ml}^{-1}$  solution of nickel in the aqueous phase, the volume of which was 185 ml, whereas that of the organic phase was 5 ml. The starting point was an interferent-to-Ni weight ratio of 4000; if any interference occurred, the ratio was gradually lowered until the interference disappeared. The tolerance limits found (Table 3) show that nickel can be determined in the presence of a variety of ions including most of those which commonly occur with nickel in natural samples. The tolerance level for some metal ions can be increased by addition of

TABLE 3

Tolerated levels of foreign species in the determination of Ni(II)

Ion or species	Tolerated ratio
Li(I), Na(I), K(I), Mg(II), Ca(II), Sr(II), Ba(II), Cd(II), Hg(I), Hg(II), Pb(II), V(V), Mo(VI), Mn(II), Bi(III), Sb(III), As(III), As(V), Cr(III) <sup>a</sup> , Ag(I), Al(III), bromide, chloride, fluoride, iodide, nitrate, phosphate, sulphate, oxalate, thiosulphate, thiourea	> 4000
Fe(III) <sup>a</sup> , Fe(II) <sup>b</sup>	2000
Co(II)	1500
Zn(II)	1300
Glycine	1000
Cu(II)	900

<sup>a</sup> With 2.5 ml of 0.2 M glycine. <sup>b</sup> With 2.5 ml of 0.2 M glycine + 1 drop of  $\text{H}_2\text{O}_2$ .

glycine. Thus, the tolerated ratio of Cr(III) can be increased to > 4000. Likewise, Fe(III) and Fe(II) can be determined at concentrations up to 2000 by using 2.5 ml of 0.2 M glycine. To the Fe(II) one drop of H<sub>2</sub>O<sub>2</sub> also has to be added.

#### Sample analysis

In order to test the accuracy and applicability of the proposed method to the analysis of real samples, some reference biological materials were analysed. Matrix interference was checked by comparison of the slopes of calibration graphs with those using the standard addition method. Only for human urine and blood serum were matrix effects apparent for the ETAAS measurements and determination was performed with the standard additions method. The results are given in Tables 4 and 5 as the averages of three replicates. As can be seen, the nickel concentrations determined by the proposed methods are in close agreement with the certified values. For the analysis of human serum, the results obtained show a satisfactory recovery of nickel. The certified reference materials analysed were Community Bureau of Reference (BCR) Certified Reference Materials (CRMs) 062 Olive Europaea (Olive

TABLE 4

Determination of nickel in biological tissues and human urine

Sample	[Ni] ( $\mu\text{g g}^{-1}$ )	
	Certified	Found <sup>a</sup>
Olive leaves	8.0	7.8 ± 0.1
Aquatic plant	40.0	40.8 ± 7.4
Aquatic moss	420.0	424.5 ± 66.0
Dogfish muscle	1.20 ± 0.30	1.06 ± 0.02
Dogfish liver	0.26 ± 0.06	0.28 ± 0.06
Lobster hepatopancreas	2.3 ± 0.3	2.7 ± 0.1
Citrus leaves	0.6 ± 0.3	0.6 ± 0.1
Pig kidney	0.42	0.40 ± 0.03
Bovine muscle	0.27	0.29 ± 0.02
Human urine (normal level)	70.0	70.0 ± 10.0
Human urine (elevated level)	300.0	280.0 ± 10

<sup>a</sup> Mean ± standard deviation ( $n = 3$ ).

TABLE 5

Determination of nickel in human serum

Sample No.	Ni added ( $\text{ng ml}^{-1}$ )	Ni found ( $\text{ng ml}^{-1}$ )
1	–	0.6 ± 0.3 <sup>a</sup>
	5.0	5.7
	7.5	7.8
	10.0	10.8
2	–	0.6 ± 0.2 <sup>a</sup>
	5.0	5.4
	7.5	8.7
	10.0	10.2

<sup>a</sup> Mean ± standard deviation ( $n = 3$ )

Leaves), 060 Lagarosiphon Major (Aquatic Plant), 061 Platihypnidium Riparioides (Aquatic Plant), 184 Bovine Muscle, 186 Pig Kidney, National Research Council Canada (NRCC) CRMs DORM-1 Dogfish Muscle, DOLT-1 Dogfish Liver, TORT-1 Lobster Hepatopancreas and National Institute of Standards and Technology (NIST) Standard Reference Materials (SRMs) 1572 Citrus Leaves, 2670 Freeze-Dried Urine (Toxic Metals at Normal and Elevated Levels) and 909a Human Serum.

The authors are grateful to the Comisión Interministerial de Ciencia y Tecnología (CICYT) for supporting this study (Project PB90-0809) and also the Regional Government of Andalucía.

#### REFERENCES

- Agency for Toxic Substances and Disease Registry (Atlanta, GA, USA), 89 (11) (1989) Abstr. No. 930 616.
- F.W. Sunderman, Jr., Arch. Toxicol., Suppl. 13 (Biol. Monit. Exposure Response Subrell. Level Toxic Subst.) (1989) 40.
- A.B. Fischer, Life Chem. Rep., 7 (1989) 149.
- R. Maximilien, Comm. Eur. Commun., [Rep]. EUR, EUR 12456, Pt. 1 (1989).
- International Committee on Nickel Carcinogenesis in Man, Scand. J. Work Environ. Health, 16 (1990) 1.
- F.R. Hartley, G. Burgess and R.M. Alcock, Solution Equilibria, Horwood, Chichester, 1980.
- ACS Committee on Environmental Improvement, Anal. Chem., 52 (1989) 2242.

# Determination of inorganic and organic traces in the clean room compartment of Antarctica

Klaus G. Heumann

*Institut für Anorganische Chemie der Universität Regensburg, Universitätsstrasse 31, W-8400 Regensburg (Germany)*

(Received 15th October 1992)

## Abstract

The concentration of most elements and of their species as well as of organic compounds in Antarctica is in an extremely low range, normally at the  $\text{pg g}^{-1}$  and pptv level or even below. Sensitive and reliable analytical methods must therefore be applied to determine these substances in this remote area. Differential pulse anodic stripping voltammetry, ion chromatography, and gas chromatography with electron capture detection can be used directly in Antarctica under strict contamination control for the determination of some heavy metals, anions, and volatile halogenated hydrocarbons, respectively. Isotope dilution mass spectrometry can be applied in the home laboratory for the calibration and completion of this data.

The concentration of most of the heavy metals in Antarctic snow and ice lies in the low  $\text{pg g}^{-1}$  range and below. Evidently higher concentrations were only found in hoar-frost samples. It could be shown that even at such a low concentration level lead is partially of anthropogenic, chromium only of terrestrial origin. First indications have been obtained that cadmium is possibly influenced by biological processes in the polar sea. The nitrate content of precipitation in Antarctica agrees with the natural background level of 200–230  $\text{ng g}^{-1}$  found in remote areas of the North and South Atlantic.  $\text{HNO}_3$  is the most dominant nitrate form in the Antarctic atmosphere and can be re-emitted from snow on the surface after its deposition. A natural cycle of nitrate in Antarctica is presented.

High enrichment factors for iodine in relation to the chloride concentration have been observed in Antarctic snow compared with the seawater composition. In the Antarctic atmosphere, iodine is preferably associated with the smallest aerosol particles in contrast to chloride which shows the highest concentration in the larger sea salt particles. From this it follows that different types of substances must be responsible for this enrichment effect. HI,  $\text{I}_2$ , HOI, and organoiodine have been identified as volatile iodine species in the atmosphere. Biogenically produced methyl iodide is the most abundant organoiodine compound and, after photodissociation, can act as a natural iodine contaminant in the interior of Antarctica. From these results a natural cycle could also be established for iodine. However, the most dominant biogenic halogenated methane in Antarctica is bromoform with average concentrations of about 6  $\text{ng l}^{-1}$  in the polar surface seawater and 6 pptv in the atmosphere measured during the Antarctic spring.  $\text{CHBr}_3$  correlates well in its seawater concentration with those of other brominated methanes, e.g.  $\text{CH}_2\text{Br}_2$  and  $\text{CHBrCl}_2$ . Under high biological production rates these halogenated methanes can possibly contribute to the greenhouse effect and they will also influence, at least, the tropospheric ozone.

**Keywords:** Gas chromatography; Ion chromatography; Isotope dilution analysis; Mass spectrometry; Biogenic halogenated methanes; Halogens; Heavy metals; Iodine cycle; Nitrate cycle; Trace detection

*Correspondence to:* K.G. Heumann, Institut für Anorganische Chemie der Universität Regensburg, Universitätsstraße 31, D(W)-8400 Regensburg (Germany).

Many people only connect Antarctica with synonyms like desolate area, ice desert, and adventure. Only a few people know that the sixth

continent has become one of the most intensive research areas on Earth. One reason for these research activities lies in the fact that we know less about the real geological surface of this continent with an average ice shield of about 2000-m thickness than about the surface of the moon. On the other hand, Antarctica is the most extensive clean room compartment on Earth, slightly larger in size than Europe. In this connection the ice shield of up to 4000 m in its maximum acts as a natural archive of events in the past. The different layers of the ice shield preserve, for example, the atomic test bomb experiments of the last few decades but also volcanic activities from the last several hundred years by the specific trace substances deposited on the surface of Antarctica at the time of the special event.

The most important aspect for analytical investigations in Antarctica are the clean room conditions in this part of the world. Here, the determination of the ubiquitous concentration of elements is a strong challenge for extreme trace analysis. By comparing the actual concentration of substances in today's surface snow of Antarctica with those contents obtained from ice core samples, anthropogenic influences can be determined. The age of the corresponding ice layer can be obtained by means of isotopic methods [1]. The seasonal variation of the  $^2\text{H}$  and  $^{18}\text{O}$  concentration in the  $\text{H}_2\text{O}$  precipitation, which is based on a temperature dependent isotope fractionation effect, allows the dating of the different ice layers. It is therefore no fundamental problem to correlate trace compound depositions in a definite ice layer with the age of the corresponding event, e.g. a volcanic eruption.

Natural cycles of trace substances can normally not be followed in the Northern Hemisphere because in most cases the natural concentrations of these compounds are overlapped by more or less strong anthropogenic influences. The clean room compartment of Antarctica, on the other hand, opens the possibility to determine interactions of natural trace compounds with the atmosphere, the ocean, the ice and snow, and the geological formation. Thus, in this part of the world there is a chance to elucidate natural cycles of trace elements and of their species.

About 90% of all anthropogenic emissions into the atmosphere take place in the Northern Hemisphere, especially from heavy metal sources [2]. The determination of north–south concentration profiles in the atmosphere from Europe to Antarctica yields a better knowledge of the global distribution rates and mechanisms of anthropogenic substances and their sinks.

Cosmological information can be obtained by the analysis of Antarctic meteorites. The blue ice fields in the interior of Antarctica are the most important reservoirs on Earth for cosmological material. More than 10 000 meteorites have been found in Antarctica since 1969 [3]. The conserving conditions in Antarctica, which prevent fast weathering of the meteorite pieces, is the reason why the average terrestrial age of the Antarctic meteorites is about 200 000 years [4]. Inorganic and organic cosmological substances in the meteorites as well as (natural) contaminations during the long storage of the meteorites in Antarctica are interesting analytical questions to be answered [5,6].

After an introduction into general problems of trace analyses in Antarctica and on the instrumentation, which can be used, selected examples of trace substance determinations carried out by my group at the University of Regensburg will show some interesting aspects of trace analysis in Antarctica.

#### GENERAL ASPECTS OF TRACE ANALYSES IN ANTARCTICA

After sampling, the treatment of sample and their instrumental measurements are strongly dependent on the equipment one has available in Antarctica. Many nations run research stations in Antarctica where, under certain preconditions, simple sample treatments and/or measurements are possible. A more convenient alternative we used during our stays at the German stations "Georg-von-Neumayer" on the Ekström ice shelf and at "Filchner" station on the Ronne–Filchner ice shelf is a survival container 1–2 km upwind from the station. During the Antarctic summer we equipped this container with a clean flow box



and the necessary analytical instrumentation. During sampling at the container (especially for aerosol samples) an automatic wind controller was used, which immediately switched off the sampling unit if the wind came from the direction of the station. As an alternative, chemical laboratories are also available on board some research ships, e.g. the German research vessel *Polarstern*.

Contamination is the major problem for sampling and analyses at the extreme low concentration levels of Antarctica. Therefore, contamination control is the most important precondition for accurate analyses. Man's activities and installations are the main contamination sources even if the clean room atmosphere of Antarctica yields advantages with respect to contamination by the environment. Sample treatments have to be carried out under the normal preconditions, which means that suprapure chemicals and ultrapure vessels must be used. If the sample treatment and the instrumental measurements are not carried out in Antarctica, the samples must be conserved until their analysis in the home laboratory, for example, snow and ice samples should be deep-frozen.

The risks of contamination during sampling are very different. With certain precautions the risk of contamination during sampling of surface snow is relatively low. The sampling procedure we normally used for surface snow samples is schematically shown in Fig. 1. To prevent contamination by man, the sampling procedure is always carried out against the wind direction. As shown in the figure a triangular piece of snow is first removed from the surface with a precleaned

plastic scraper. Especially the leeward frontside of the snow hole is not touched with anything else but the scraper. A precleaned sample container (1000 ml polyethylene (PE) wide necked bottle) is pressed by hand, covered with cleaned plastic gloves, to a depth of 15–30 cm into the snow wall. Immediately after filling the bottle it is closed by a screw plug, put in PE wrapping twice, and stored frozen until the treatment of this sample. Samples from field landings are taken by covering a distance of 0.5–1 km from the airplane by foot against the wind direction.

In contrast to surface snow samplings ice core samples obtained with metallic drilling systems are highly contaminated. Boutron and Batifol [8] developed a time-consuming analytical procedure to determine the real heavy metal concentration in ice core samples by analysing the horizontal concentration profile from the surface to the inner sections of the ice core samples. Only in cases where a low and constant concentration plateau in the inside of the ice core sample is found, can no contamination be assumed for this plateau data.

Aerosol samplings in Antarctica are mainly limited by the contamination of the sampling system itself if the wind direction from man's activities is under control. On board of a ship aerosol samplings are only acceptable in front of the foredeck under strict control of the ship's exhaust gases.

#### ANALYTICAL METHODS

Analytical instruments, which are used in Antarctica, must be, in general, easy to handle, relatively independent of temperature and other climatic influences and it should be possible to operate them electrically from a generator or a battery with their known instabilities. On the other hand, the methods must be sensitive enough for the low concentration levels to be analysed in Antarctica.

From our experience, electroanalytical methods for the analysis of metals [9], ion chromatography for the detection of anions [10], and gas chromatography with element specific detection

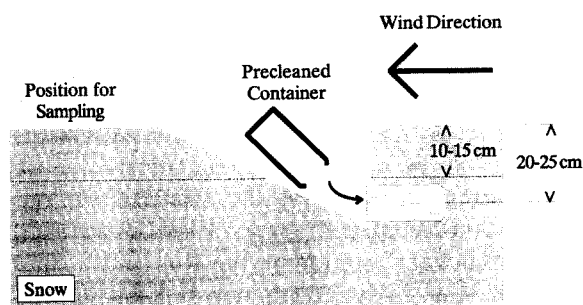


Fig. 1. Sampling procedure for surface snow samples in Antarctica [7].

for the determination of element species and organic compounds [11,12] are the most suitable instruments to be used under Antarctic conditions. We were able to analyse the low lead, cadmium, nitrate, chloride, and sulfate concentrations in Antarctic snow with differential pulse anodic stripping voltammetry (DPASV) and ion chromatography (IC), respectively, in the above mentioned containers near the German stations [9,10]. Volatile organohalogen compounds and organic sulfur or selenium species could be analysed in a laboratory of the German station and aboard the research ship *Polarstern* using capillary gas chromatography with an electron capture detector (GC-ECD) or a flame photometric detector system (GC-FPD) [11,12].

The application of these methods does not automatically guarantee accurate analytical results as well. However, accurate results are at least an essential precondition for the comparison of analytical data, which has been produced and which will be produced in the future in different parts of Antarctica. It is therefore necessary to check the results obtained directly in Antarctica with independent and reliable analytical methods. This can be done, for example, in the home laboratory, well equipped for analyses

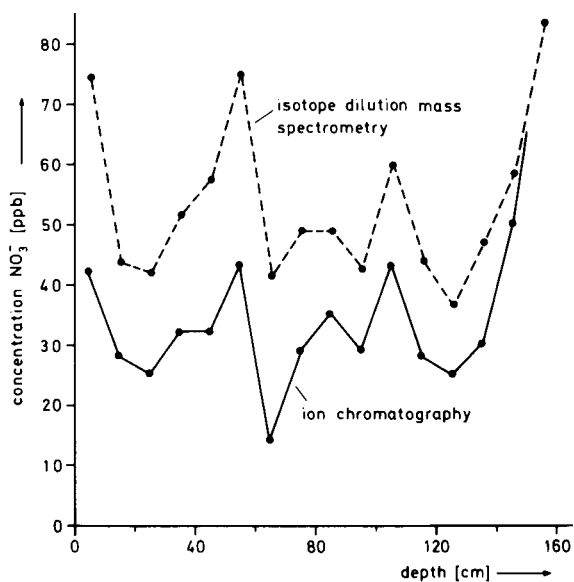


Fig. 2. Depth profile of nitrate in Antarctic firn core samples analysed by IDMS and IC with a conductivity detector.

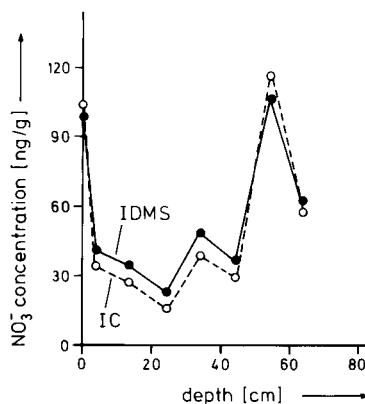


Fig. 3. Depth profile of nitrate in Antarctic firn core samples analysed by IDMS and IC with a UV detector.

at very low levels, by the determination of parallel samplings or with aliquots of a sample previously analysed in Antarctica. In most cases we used isotope dilution mass spectrometry (IDMS), which is known as a method of high precision and accuracy [13], to calibrate, check or complete our analytical results from Antarctica.

Figure 2 represents a depth profile of the nitrate concentration in Antarctic firn core samples analysed by IDMS and IC. The depth profile curves show the same shape for both methods but the absolute values disagree by a factor of up to about two. After we changed the IC measurements from the conductivity detector to the UV detector we obtained much better agreements of nitrate concentrations in another depth profile (Fig. 3), which shows the urgent necessity of calibrating analytical methods used in Antarctica.

#### HEAVY METAL TRACE ANALYSIS

In Table 1 a selection of heavy metals analysed in the Antarctic summer 1989/90 in surface snow samples of the Ronne-Filchner ice shelf with IDMS is listed [7]. The given results are the concentration ranges analysed in different samples taken from a nearly  $100 \times 200 \text{ km}^2$  large section of the ice shelf about 70–270 km away from the ice edge. The mean concentration for thallium and cadmium is distinctly below  $1 \text{ pg g}^{-1}$  whereas the lead and copper concentrations are

in the low  $\text{pg g}^{-1}$  level. Previous determinations of samples from the Ekström ice shelf have shown that iron, as a more abundant element in the environment, is the only heavy metal which can be found in a higher concentration range of (0.5–1.5)  $\text{ng g}^{-1}$  in Antarctic surface snow samples [9]. The mean thallium concentration of 0.5  $\text{pg g}^{-1}$  is equivalent to about 1 atom of thallium per  $2 \times 10^{13}$  molecules of  $\text{H}_2\text{O}$  which could be analysed with the sensitive IDMS method.

First measurements of hoar-frost samples in Antarctica have shown distinctly higher concentrations for cadmium and lead [9] as well as for nitrate [10] compared with snow precipitations in the same area. We therefore investigated this enrichment of trace substances in hoar-frost samples in more detail for the element lead. The lead enrichment factors determined for three different hoar-frost events in Antarctica are listed together with the corresponding concentrations in Table 2. The enrichment factors are calculated as the ratio of the lead concentration in the hoar-frost sample (collected on acid precleaned Nylon nets of  $40 \times 60 \text{ cm}^2$ ) to the concentration found at the same location and at the same time in surface snow samples. The measured lead enrichment factors of 9–31 demonstrate the effective collection of aerosol traces by hoar-frost. Although the collection mechanism is not quite clear, up to now, similar effects were also observed in anthropogenic areas [14]. Because hoar-frost is also deposited in thin layers on the surface of Antarc-

TABLE 1

Concentration ranges of heavy metals analysed in Antarctic surface snow samples of the Ronne-Filchner ice shelf with IDMS [7]

Element	Concentration range ( $\text{pg g}^{-1}$ )	Number of samples	Mean <sup>a</sup> ( $\text{pg g}^{-1}$ )
Tl	0.2– 1.3	19	0.5
Cd	< 0.5– 2.3	20	< 0.5
Pb	< 0.9– 7.6	18	4.0
Cu	5.5–32.3	18	12.2

<sup>a</sup> For calculation of the mean the detection limits (“<” values) are used. For Cd only 4 of 20 samples showed concentrations above the detection limit. Therefore < 0.5  $\text{pg g}^{-1}$  is regarded as the mean for this element.

TABLE 2

Lead enrichment factors in hoar-frost (HF) samples compared with surface snow (SS) from identical locations [7]

Sample		Concentration ( $\text{pg g}^{-1}$ )	Enrichment factor
Filchner ice shelf			
location 1	HF	123	31
	SS	4	
location 2	HF	91	13
	SS	7	
Ekström ice shelf			
location 1	HF	178	9
	SS	19	

tica, possible high concentration spots must be taken into consideration when analysing ice core samples.

#### SOURCE IDENTIFICATION OF HEAVY METALS

##### *Terrestrial and anthropogenic origin*

Even if it is possible to determine accurately the extremely low concentrations in Antarctic snow, the question, “Where do the heavy metals come from?” still remains. The primary source of the trace elements cannot be identified from the determined concentrations alone. Therefore, indirect methods must be applied for source identification.

In principle, anthropogenic and natural sources must be taken into consideration. The most probable pathway for a transportation of heavy metals to the ice shield of Antarctica is the atmosphere. Different combustion processes, which especially emit substantial amounts of heavy metals into the atmosphere of the Northern Hemisphere, are anthropogenic sources to be discussed. Natural influences can be the result of material from terrestrial, volcanic or marine origin. Also biological activities or natural burning must be taken into consideration [2].

For source identification with respect to the terrestrial origin, enrichment factors *EF*, defined by Eqn. 1, can be determined

$$EF(\text{Fe}) = \frac{(c_{\text{element}}/c_{\text{Fe}})_{\text{sample}}}{(c_{\text{element}}/c_{\text{Fe}})_{\text{crust}}} \quad (1)$$

TABLE 3

Heavy metal enrichment factors  $EF(Fe)$  with respect to crustal material in different surface snow samples from the Ekström ice shelf

Element	Range of $EF(Fe)$	Interpretation
Cr	0.5– 2	Terrestrial origin
Cu	8 – 20	Probably also other influences
Pb	32 – 97	Significantly other influences
Cd	100 –820	Predominantly other influences

with  $c_{\text{element}}$  as the concentration of the element of interest,  $c_{\text{Fe}}$  as the concentration of the reference element iron and  $(c_{\text{element}}/c_{\text{Fe}})_{\text{crust}}$  as the mean abundance ratio of the element to iron in the Earth's crust (values from [15]). Fe is one of the most commonly used reference elements for crustal materials [16]. Due to natural variations of the corresponding ratio in the Earth's crust, only  $EF(Fe)$  values significantly different from unity can be used for interpretations of non-terrestrial origin.

In Table 3  $EF(Fe)$  values are listed, which had been calculated from results obtained in different surface snow samples on the Ekström ice shelf near the German station "Georg-von-Neumayer" in 1987 [9]. From these results it is very probable that the low chromium concentrations in Antarctic snow (measured range:  $< 0.8\text{--}15 \text{ pg g}^{-1}$ ) are mainly the result of terrestrial sources. In contrast to chromium, the other listed heavy metals show more or less high enrichment factors. From the data for lead it can be concluded that influences other than terrestrial have significantly affected the lead content in Antarctic snow. However, the highest  $EF(Fe)$  values have been found for cadmium.

The discussed  $EF(Fe)$  data in Antarctic snow is very well reflected in the analysis of particulate heavy metals in the marine atmosphere over the Atlantic Ocean from Europe to Antarctica [16,17]. Figure 4 represents such a north–south profile of  $EF(Fe)$  values for chromium and lead [17]. Whereas lead enrichment factors of up to  $10^3$  are not very rare, the corresponding chromium enrichment factors are mostly below 10.

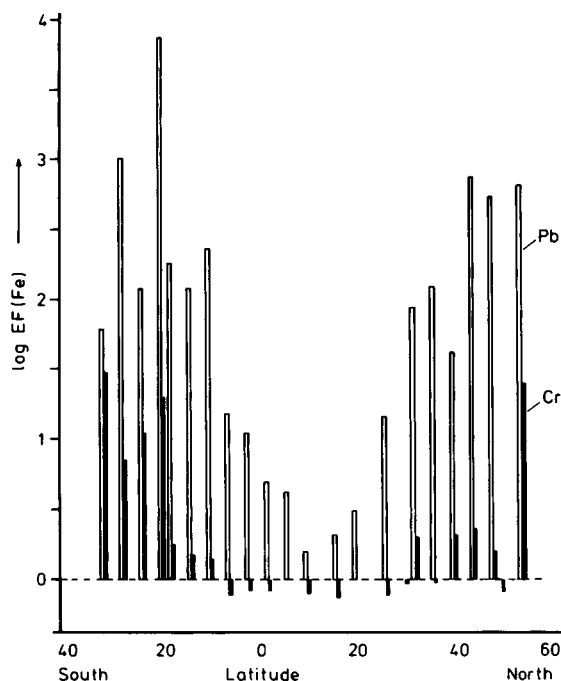


Fig. 4. Enrichment factors  $EF(Fe)$  of lead and chromium with respect to crustal material in marine aerosols over the Atlantic Ocean [17].

The results given in Table 3, e.g. for lead, only allow the conclusion that non-terrestrial material strongly influences the lead content of today's Antarctic snow. The question remains, whether the lead is of other natural or of anthropogenic origin. An answer can be obtained by the analysis of ice core samples. Figure 5 represents the results of lead concentration in ice core samples

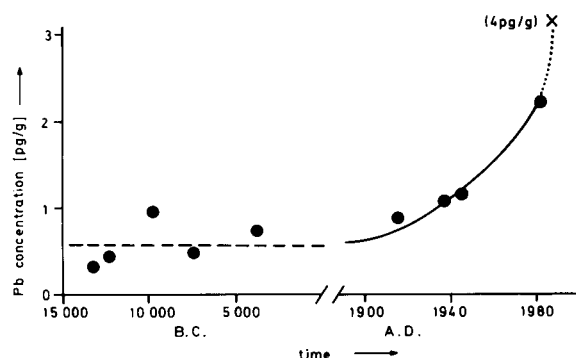


Fig. 5. Lead concentrations in Antarctic ice core samples. (●) Data from [18,19]; (×) 1990 mean value from Table 1.

[18,19]. The figure includes data from samples of snow and ice from this century but also from ice samples several thousand years old. Additionally, our newest result from surface snow in 1989/90 (see Table 1) is also shown in the figure. From Fig. 5 it can be seen that the lead concentration of ancient snow, which could only have been influenced by natural sources, is in the range of  $0.2\text{--}1\text{ pg g}^{-1}$ . The excess lead compared with this natural background level must therefore be attributed to anthropogenic lead. Only a slight increase can be observed in the 1940s but for 1980 and 1990 significantly higher concentrations have been found. Therefore, a high proportion of the total lead found in today's Antarctic snow must be of anthropogenic origin. Man's activities in Antarctica as well as a long range transportation of lead-containing aerosols by the atmosphere from anthropogenic emission sources may contribute to the lead in Antarctica. In contrast to other trace substances, which are deposited relatively fast from the atmosphere on the Earth's surface, a more continuous decrease of lead is found in the marine atmosphere over the Atlantic Ocean from Europe to Antarctica. This is obvious from the lead data presented in Table 4 [16,17,20,21]. The relatively long atmospheric residence time, especially of very small lead containing particles in the atmosphere, also makes the contribution of anthropogenic lead in Antarctica from the Northern Hemisphere possible. In contrast to the more remote region of Antarctica, it was recently shown by Boutron et al. [22] that the anthropogenic lead content of Greenland snow has been decreasing since the late 1960s, probably as a particular consequence of the reduced lead emission into the air by the use of unleaded gasoline, after a

TABLE 4

Normal concentration ranges of lead analysed in the near surface aerosol from Europe to Antarctica [16,17,20,21]

Region	Concentration range ( $\text{ng m}^{-3}$ )
Cities of Central Europe	100 – 1000
North Atlantic	10 – 100
South Atlantic	1 – 10
Antarctica (south of $60^\circ\text{S}$ )	0.01– 1

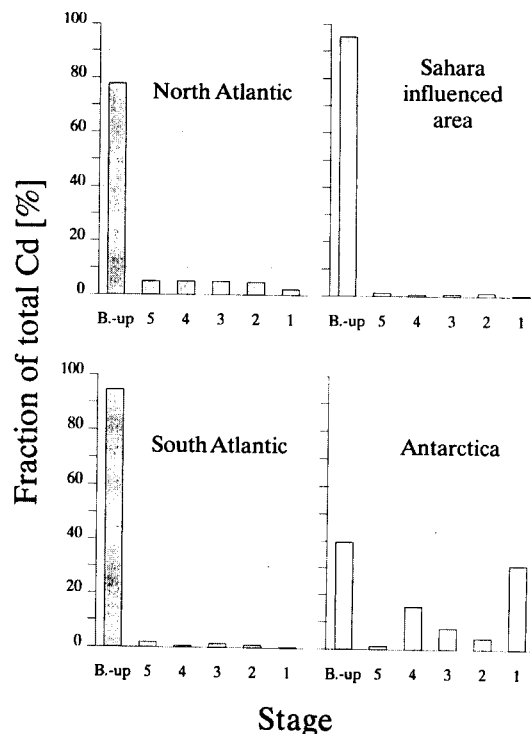


Fig. 6. Cadmium size distribution pattern in aerosols from different regions over the Atlantic Ocean and from Antarctica [23]. Sampling by an impactor system, the 50% cut-off diameters for the different impactor stages are as follows: (1) =  $7.2\ \mu\text{m}$ , (2) =  $3.0\ \mu\text{m}$ , (3) =  $1.5\ \mu\text{m}$ , (4) =  $0.95\ \mu\text{m}$ , (5) =  $0.49\ \mu\text{m}$ . (B.up) = back-up  $< 0.49\ \mu\text{m}$ .

tremendous increase of concentrations up to about  $400\text{ pg g}^{-1}$  in the 1950s.

#### Biogenic origin

It is difficult to explain the extremely high enrichment factors  $EF(\text{Fe})$  for cadmium in Antarctic snow (Table 3) by anthropogenic sources. Recently, we obtained the first indications that the emission of cadmium from the polar sea may possibly cause the high enrichment factors.

Using an impactor system for sampling of aerosol particles, we found a distinctly different cadmium size distribution pattern in aerosols of Antarctica compared with other regions of the Atlantic Ocean (Fig. 6) [23]. The large particles, which are mainly sea-salt particles in the marine atmosphere, are collected on the first impactor

TABLE 5

Range of cadmium concentrations in different Antarctic surface snow samples dependent on the distance from the ice edge [7]

Distance (km)	Concentration range ( $\mu\text{g g}^{-1}$ )
70	0.7–2.3
120	< 0.5–0.6
170–270	< 0.5

stage(s) whereas the small particles are collected on the last stages, especially on the back-up filter. As can be seen from Fig. 6, about 80% or more of the total particulate cadmium was always found at the smallest particles in aerosols of the North Atlantic, over the Atlantic Ocean in an area where Sahara sand strongly influences the atmospheric particles, and of the South Atlantic. In contrast to these findings, an essential amount of the total cadmium was found on the largest aerosol particles in Antarctica. This association with the large particles originating from sea-salt indicates a marine origin of cadmium. This assumption is supported by the dependence of the concentration on the distance from the ice edge, which we found for cadmium in surface snow samples (Table 5) [7].

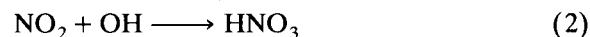
Without any further investigations, only speculations can be made about the type of primary cadmium compounds formed in the polar sea. One of our postulations is a biogenic production of volatile organocadmium compounds (probably  $\text{Cd}(\text{CH}_3)_2$ ) as it is known for other elements, such as for iodine and sulfur [11,12]. Due to their low chemical stability organocadmium compounds should decompose very quickly in the atmosphere. However, the existence of such biogenically produced organic cadmium compounds must first be proved, e.g. by GC methods with element specific cadmium detection using an atomic emission system.

#### NITRATE ANALYSES

Whereas in the atmosphere of the European Continent nitrate is mainly of anthropogenic ori-

gin, in the remote area of Antarctica one should definitely find only a natural background level. In contrast to other trace substances, e.g. the heavy metals (see Table 4 for lead) or the Freons (see Table 10), nitrate is effectively washed out of the atmosphere by precipitation. As a consequence, nitrate in the atmosphere does not show a continuous decrease from the north to the south but rather a strong difference in the concentration level between areas directly affected by anthropogenic nitrate and those where nitrate is not emitted into the atmosphere by man. This is reflected in the average nitrate concentration determined in marine precipitation from Europe to Antarctica (Table 6). Precipitation collected over the North Sea show more than ten times higher nitrate levels [24] when compared with precipitation collected over the open North Atlantic, South Atlantic and in Antarctica [25]. The strong wash-out effect of anthropogenic nitrate is demonstrated by a nearly constant background level in the range of 200–230  $\text{ng g}^{-1}$  for the last three mentioned areas with neglectable nitrate sources of anthropogenic origin [10,25]. It must therefore be assumed that this background level is of natural origin.

Naturally formed nitrate mainly consists of gaseous nitric acid. The most probable formation process in the atmosphere under daylight is the reaction of  $\text{NO}_2$  with OH radicals



The following sequence of reactions can also produce nitric acid without daylight

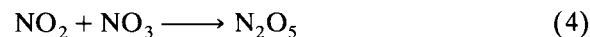
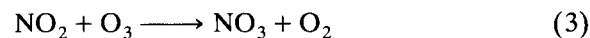


TABLE 6

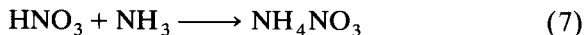
Average nitrate concentrations in marine precipitation from Europe to Antarctica [10,24,25]

Region	$\text{NO}_3^-$ concentration ( $\text{ng g}^{-1}$ )
North Sea	2750
North Atlantic	231
South Atlantic	226
Antarctica	206

The gaseous nitric acid can be converted into nitrate salt, for example by a reaction with sea-spray particles



or by a gas phase reaction with ammonia



In the case of Eqn. 6 the corresponding process takes place in atmospheric particles. In the case of the process given in Eqn. 7 the so formed ammonium nitrate associates with particles and is then deposited on the Antarctic surface by dry or wet deposition. The process, which corresponds to Eqn. 7, is only of minor importance because the nitrate concentration in Antarctic snow and ice essentially exceeds the concentration of  $\text{NH}_4^+$  which is in the range of 1–25  $\text{ng g}^{-1}$  [26].

To determine the fraction of particulate nitrate and gaseous  $\text{HNO}_3$  in the Antarctic atmosphere a filter sampling system was applied, which is schematically shown in Fig. 7 [27]. Two consecutive PTFE filters were used for sampling of the particulate nitrate and two Nylon filters were used for the absorption of the gaseous nitric acid. The results of four samplings in January and February 1992 on the Ronne–Filchner ice shelf near the ice edge are listed in Table 7. In all cases the gaseous  $\text{HNO}_3$  concentration exceeds the particulate nitrate, resulting in ratios for gaseous  $\text{HNO}_3$ /particulate nitrate between 1.1 and 8.5. The different gaseous/particulate ratios may be the consequence of various atmospheric conditions with respect to the possible reactions given in Eqns. 2–7.

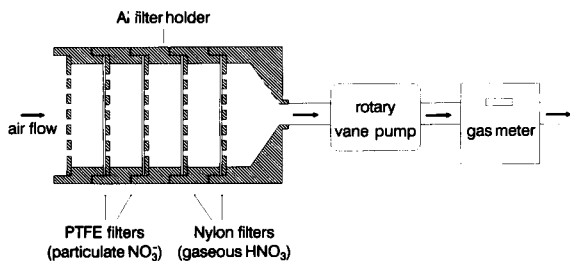


Fig. 7. Schematic figure for the sampling of particulate nitrate and gaseous  $\text{HNO}_3$  [27].

TABLE 7

Determination of gaseous  $\text{HNO}_3$  and particulate nitrate in the Antarctic atmosphere of the Ronne–Filchner ice shelf [27]

Date	Concentration ( $\text{ng m}^{-3}$ )		Ratio gaseous/ particulate
	Gaseous $\text{HNO}_3$	Particulate $\text{NO}_3^-$	
Jan. 31, 1992	46.7	13.4	3.5
Febr. 8, 1992	17.5	15.3	1.1
Febr. 14, 1992	27.9	3.3	8.5
Febr. 16, 1992	27.0	6.7	4.0

Independent of short-term variation by different meteorological conditions, the drastic seasonal changes in the duration of sunshine in Antarctica, with no sunrise during the Antarctic winter months, should be reflected in the nitrate deposition. This can be seen from Fig. 3 where a nitrate depth profile in firn core samples from the Ekström ice shelf down to 70 cm is shown. With respect to the yearly snow accumulation rate of about 60 cm in this area [1], maximum nitrate concentrations were obtained for summer on the surface and to a depth of 60 cm of the firn core. A minimum was observed for winter between these maxima because of a lower probability for the  $\text{HNO}_3$  production by the daylight reaction of Eqn. 2.

However, such well defined seasonal variation cannot be observed in all depth profiles so that other effects than the increased photochemically induced formation of  $\text{HNO}_3$  must also be taken into consideration to interpret the nitrate concentration in Antarctic snow. Investigations of new snow (up to a few hours after snowfall), old surface snow (at least some days old), and firn core samples have distinctly shown a decreasing nitrate concentration with the increasing age of the snow [10,28]. The nitrate abundance distribution curves for these three types of Antarctic snow are shown in Fig. 8 where the results of a total of 136 samples are represented. A strong dependence of concentration on deposition age is found. The average nitrate concentration in new snow is 206  $\text{ng g}^{-1}$  (see Table 6), in old surface snow 146  $\text{ng g}^{-1}$ , and in firn core samples 61  $\text{ng g}^{-1}$ . The average value of the firn core samples is

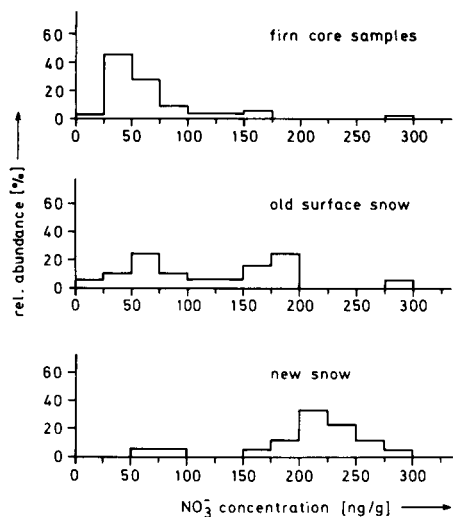


Fig. 8. Dependence of nitrate abundance distribution curves in Antarctic snow on the age of the deposition [10].

influenced by the discussed seasonal variation. However, the mean of the new and old surface snow should be in the same range because they are always collected during Antarctic summer within a small time period. A re-emission of  $\text{HNO}_3$  into the atmosphere and a photochemical decomposition of  $\text{HNO}_3$  must therefore be assumed after its primary deposition by snow. The assumption that sunlight reduces the nitrate concentration in Antarctic surface snow could be confirmed by following the concentration for 160 h after a snowfall in Antarctica. During this time of sunshine the nitrate concentration in the snow sample dropped from  $255 \text{ ng g}^{-1}$  to  $180 \text{ ng g}^{-1}$  [10].

Taking into account the results of all these analyses, a geochemical nitrate cycle in Antarctica can be established (Fig. 9).  $\text{NO}_x$  is oxidized in the atmosphere and converted into gaseous  $\text{HNO}_3$  and particulate nitrate, which are deposited on the surface of Antarctica by dry and, more effectively, by wet deposition. The re-emission of  $\text{HNO}_3$  from the snow into the atmosphere, especially during sunshine, and the photolytic decomposition of  $\text{HNO}_3$  strongly reduces the amount of nitrate primarily deposited in Antarctic snow. This also influences the total nitrate budget in the Antarctic atmosphere. Ni-

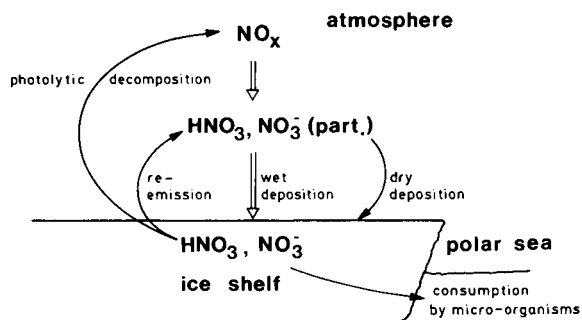


Fig. 9. Geochemical nitrate cycle in Antarctica.

trate conserved in the ice shield of Antarctica will reach the polar sea after hundreds or thousands of years. Ice from the ice shelf edge breaks off and falls into the polar sea. The nitrate is then consumed by microorganisms in the ocean. Additional investigations have shown that the contribution of marine nitrate on the total nitrate in Antarctic snow, for example by sea-spray, can be neglected [28].

#### IODINE SPECIATION

Iodine and chloride concentrations have been analysed by IDMS in snow samples from the Ekström and Riiser Larsen ice shelves at locations a few kilometers away from the ice edge in the range of  $0.03\text{--}0.8 \text{ ng g}^{-1}$  and  $1\text{--}10 \mu\text{g g}^{-1}$ , respectively [6]. High enrichment factors  $EF(\text{Cl}^-)$

$$EF(\text{Cl}^-) = \frac{(\text{Iodine}/\text{Cl}^-)_{\text{sample}}}{(\text{Iodine}/\text{Cl}^-)_{\text{seawater}}} \quad (8)$$

TABLE 8

Iodine/chloride ratio and enrichment factor  $EF(\text{Cl}^-)$  in Antarctic snow [6]

Sampling site	(Iodine/chloride) $\times 10^4$	$EF(\text{Cl}^-)$
Ekström ice shelf		
20 km from ice edge	0.3	10
Riiser Larsen ice shelf		
5 km from ice edge	1.4	47
15 km from ice edge	5.6	187
Ocean water [29]	0.3	1



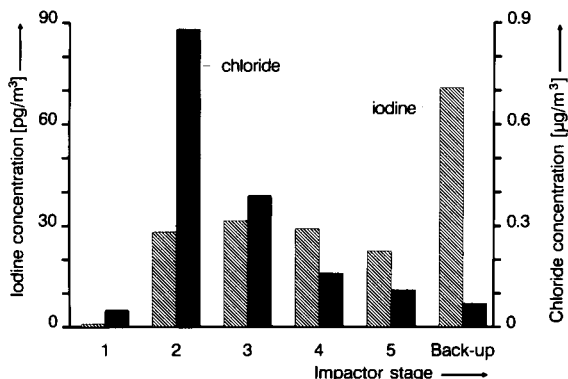


Fig. 10. Determination of the size distribution pattern of Antarctic aerosol particles associated with iodine and chloride using an impactor system [30].

of up to more than 100 were calculated for iodine from these data. The results of some selected snow samples are listed in Table 8. Because the primary source of iodine and chloride is certainly the polar sea, different emission mechanisms for iodine and chloride, and therefore different types of substances, must be responsible for this relative iodine enrichment.

The size distribution pattern of Antarctic aerosol particles associated with iodine and chloride was determined by an impactor system (Fig. 10; for particle sizes collected on the different impactor stages see Fig. 6) [30]. The corresponding  $EF(\text{Cl}^-)$  values are represented in Fig. 11. Iodide and iodate, on the one hand, and chloride, on the other hand, are the most probable species

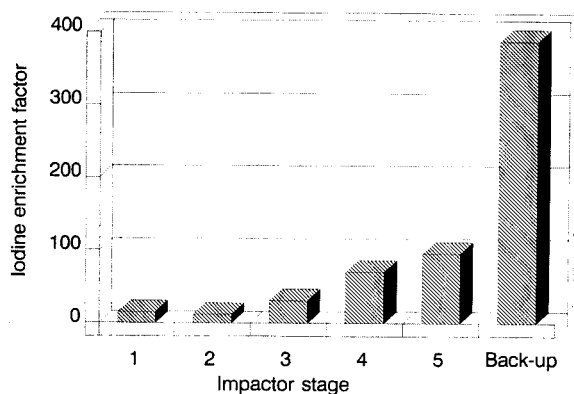


Fig. 11. Iodine enrichment factor  $EF(\text{Cl}^-)$  in Antarctic aerosol particles of different sizes [30].

collected on the impactor filters. The given iodine concentrations in Fig. 10 are the sum of iodide and iodate (and possibly also of other iodine compounds with an oxidation state higher than  $-1$ ) because the filters were always leached with a sulfite solution to reduce iodate to iodide, which could be then analysed by IDMS using an  $^{129}\text{I}^-$  spike solution for the isotope dilution process.

Whereas iodine is preferably associated with the smallest particles (collection at the back-up filter), the opposite behaviour is found for chloride where the highest concentration is analysed at the second impactor stage. This result for chloride is caused by the relatively large sea-spray particles. The same behaviour as for chloride salt must also be expected for iodide and iodate salt dissolved in seawater. Other natural but volatile iodine species must therefore cause the high enrichment factor of iodine found in the smallest particles. These species are probably converted in the atmosphere or in the aerosol particles into an inorganic iodine salt.

An additional impactor experiment was carried out where the one half of all filters was leached only with water for iodide speciation and the other half with a sulfite solution to determine the sum of iodide and iodate. The results are represented in Fig. 12 [30], which shows that a substantial amount of the total particulate iodine exists in the form of iodate, or, more correctly, in the form of an iodine species which can be converted into iodide by a sulfite solution.

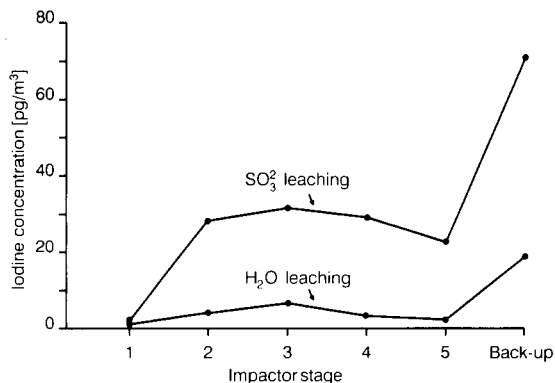


Fig. 12. Iodide and iodate speciation by leaching with  $\text{H}_2\text{O}$  and  $\text{SO}_3^{2-}$  solution, respectively, in an impactor sampling experiment [30].

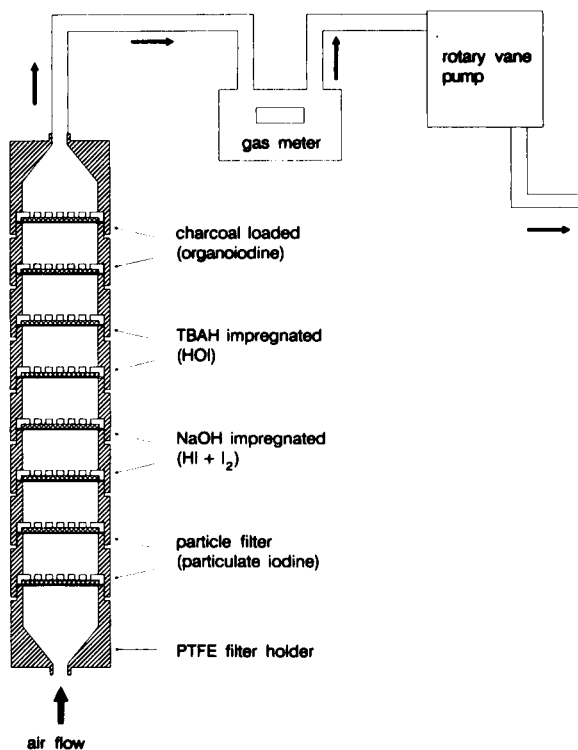


Fig. 13. Schematic diagram of the sampling system with specifically prepared filters for iodine speciation in the atmosphere [31].

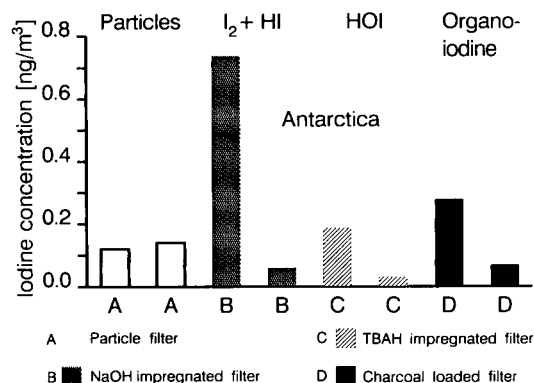


Fig. 14. Determination of atmospheric iodine species with a sampling system of specifically prepared filters and IDMS [31]. A = particle filter; B = NaOH impregnated filter; C = TBAH impregnated filter; D = charcoal loaded filter.

To determine other iodine species than particulate iodide and iodate in the atmosphere a sampling system with specifically prepared filters has been developed (Fig. 13) [31]. First, this sampling system collects particulate iodine with a particle filter. Then, HI and I<sub>2</sub> are absorbed on a NaOH impregnated filter, HOI on a tetrabutylammonium hydroxide (TBAH) impregnated filter, and

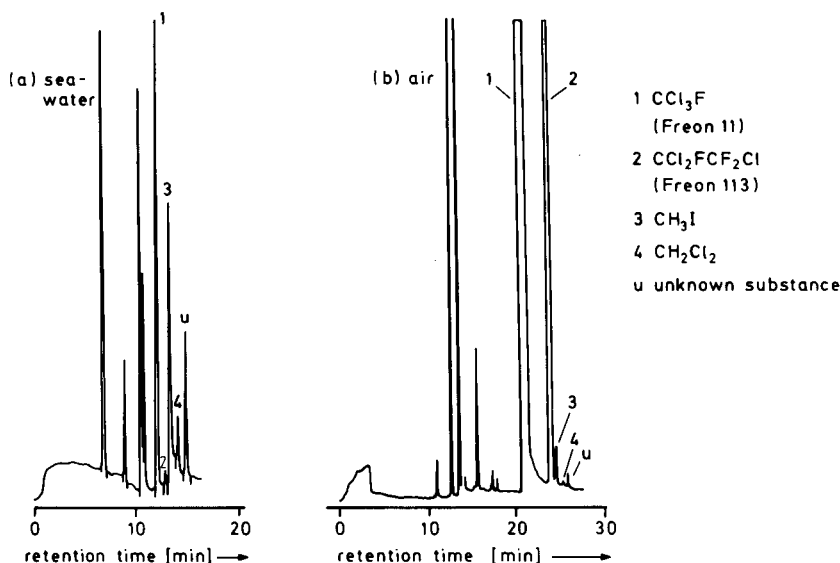


Fig. 15. ECD gas chromatogram of an Antarctic seawater and an air sample [34].

organoiodine on a filter loaded with activated charcoal. At least two filters of the same type were used in series to guarantee a complete collection of one special iodine species. Evident concentration differences between the second filter for the absorption of one species and the first filter for the next species shows that really different iodine compounds are absorbed on the various filters. This behaviour was tested in model experiments.

The results of one sampling on the Ronne-Filchner ice shelf near the ice edge are represented in Fig. 14 using IDMS as the analytical method [31]. All different species could be analysed in the range of  $0.1\text{--}0.8\text{ ng I m}^{-3}$  with the  $\text{I}_2/\text{HI}$  fraction as the most abundant. Compared with similar measurements in Europe, the absolute concentrations of the two inorganic fractions  $\text{I}_2/\text{HI}$  and HOI are in the same range, whereas the particulate iodine and the organoiodine is lower in Antarctica by a factor of about ten [31]. However, with respect to the usually higher atmospheric stability of organoiodine compounds compared with the inorganic species  $\text{I}_2$ , HI, and HOI, the organoiodine species will play an important role in the atmosphere of Antarctica.

From investigations in non-polar regions it is known that methyl iodide is the dominant organic iodine species in the marine atmosphere [32]. Rasmussen et al. [33] have detected methyl iodide

at the South Pole. We therefore assumed that methyl iodide is also the most abundant species of the organic iodine fraction presented by our results in Fig. 14. The evidence of this assumption was obtained by GC-ECD measurements in the atmosphere and corresponding surface seawater samples from around the Antarctic Peninsula [34]. Figure 15 represents sections of two gas chromatograms, one from an Antarctic air sample and the other one from the corresponding seawater sample after isolating the volatile organic compounds from seawater by a purge and trap system [34]. Methyl iodide could be detected in both types of samples in addition to other iodinated hydrocarbons such as diiodomethane, chloriodomethane, propyl iodide, and butyl iodide [35], other biogenic halocarbons and the anthropogenic Freons. The average methyl iodide concentration in a total number of 21 air samples and of 34 seawater samples collected from October to December 1987 near the Antarctic Peninsula on board the R.V. *Polarstern* was found to be 2.4 pptv and  $2.6\text{ ng l}^{-1}$ , respectively. The surface seawater, where this iodine compound is biogenically produced, contained concentrations in the range of  $0.2\text{--}7.5\text{ ng l}^{-1}$  depending on the biological activity.

Summarizing all the results on iodine species a geochemical cycle in Antarctica can be presented by the schematic Fig. 16. Sea-salt particles from

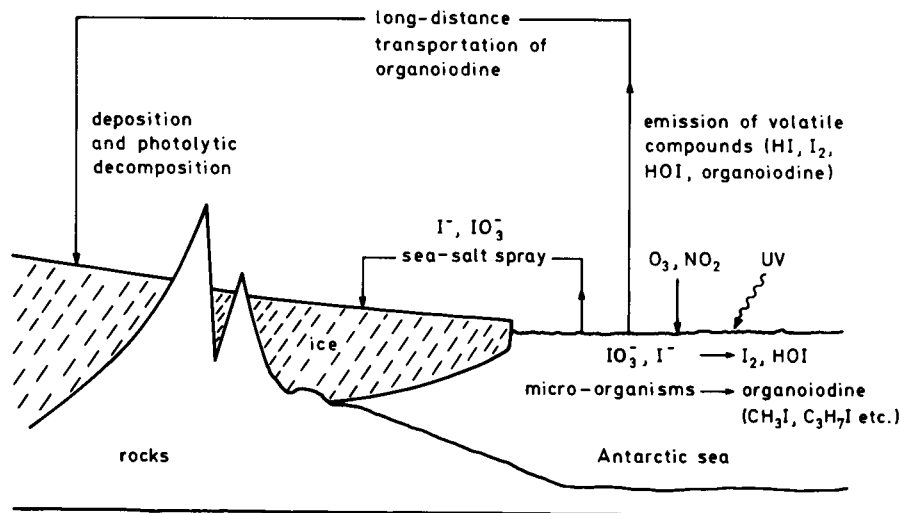


Fig. 16. Geochemical iodine cycle in Antarctica.

TABLE 9

Iodine enrichment in the surface layers of an Antarctic rock and an Antarctic meteorite analysed by IDMS [6,37]

Sample	Part of sample analysed	Iodine concentration ( $\mu\text{g g}^{-1}$ )	Enrichment factor
Granite rock	Surface	0.73	5
	Interior	0.14	
Iron meteorite	Surface	6.4	91
	Interior	0.05	

sea-spray, which preferably affect the region near the ice edge, contain mainly iodide and iodate. In addition, volatile inorganic and organic compounds (elemental iodine,  $\text{I}_2$ , for example, can be formed by oxidation of iodide with  $\text{O}_3$  or  $\text{NO}_2$ ) are emitted from the seawater surface into the atmosphere. The volatile inorganic species have relatively low atmospheric half-lives and should therefore not be transported over long distances. On the other hand, the longer atmospheric residence time of about 8 days for methyl iodide [36] permits its transportation from the polar sea to inner Antarctica. By the possible photodissociation of methyl iodide



the organic iodine can be converted into inorganic iodine. The inorganic iodine is deposited on the ice shield and is then again transported by the ice movement within hundreds of years to the polar sea. The iodine radicals formed by reaction (9) can also react with other substances, for example with the surface layers of Antarctic rocks and meteorites. This was demonstrated by the iodine enrichment analysed in the surface layers of Antarctic rocks and meteorites compared with the inner sections of the same samples [6,37]. As an example, the results of a granite rock and an iron meteorite are listed in Table 9. This is the first time that a long-term contamination effect of a natural trace compound could be observed in a remote area of the world.

## BIOGENIC BROMOMETHANES

From Fig. 15 one can see that also other halogenated hydrocarbons than methyl iodide are detected with the GC-ECD system. Besides the anthropogenic Freons the different bromomethanes, which are all of biogenic origin, are of special interest. In this connection Reifenhäuser and Heumann determined for the first time  $\text{CHBr}_3$ ,  $\text{CH}_2\text{Br}_2$ ,  $\text{CHBr}_2\text{Cl}$ , and  $\text{CHBrCl}_2$  in air and seawater samples near the Antarctic Peninsula [12]. These compounds have retention times between 40 and 60 min under the same gas chromatographic conditions (two coupled capillary columns of different polarity, OV 1701 and SE 54) as they were used for the record of Fig. 15. The average concentrations of the bromomethanes detected in 67 air and 34 seawater samples are listed in Table 10. The corresponding values for freon 11 are also given for comparison.

Bromoform is the most dominant bromomethane in the Antarctic atmosphere as well as in the south polar sea with a maximum of up to about  $50 \text{ ng l}^{-1}$  in the ocean. It is interesting to point out that the concentration of freon 11 in seawater is in the same range as determined for all other bromomethanes except  $\text{CHBr}_3$ , although the atmospheric content of this anthropogenic compound is much higher. This reflects the low solubility of freon 11 in seawater. The distribution of  $\text{CH}_2\text{Br}_2$  in an area westward of the Antarctic Peninsula is shown in Fig. 17 [38]. The height of the black bars in Fig. 17 represents the concentration in seawater. Dibromomethane, and also the other bromomethanes, normally show

TABLE 10

Average concentrations of bromomethanes in the atmosphere and in surface seawater samples near the Antarctic Peninsula (October–December 1987) [12]

Compound	Atmosphere (pptv)	Seawater ( $\text{ng l}^{-1}$ )
$\text{CHBr}_3$	6.3	6.2
$\text{CH}_2\text{Br}_2$	3.7	0.9
$\text{CHBrCl}_2$	3.8	0.3
$\text{CHBr}_2\text{Cl}$	Not determined	0.6
$\text{CCl}_3\text{F}$ (Freon 11)	215	0.6

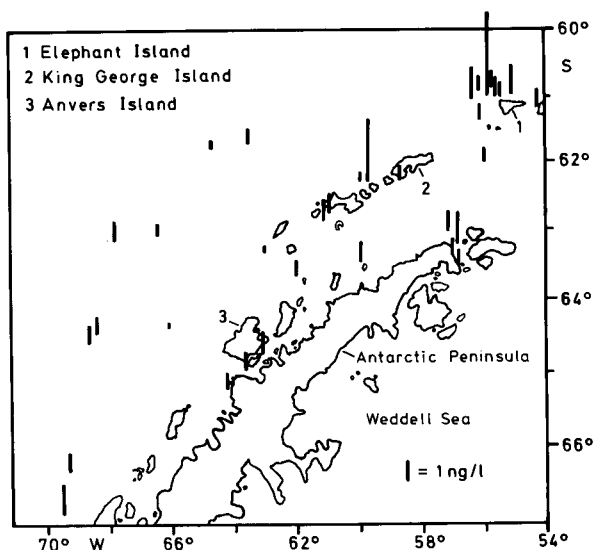


Fig. 17. Distribution of  $\text{CH}_2\text{Br}_2$  in seawater samples obtained westward of the Antarctic Peninsula [38].

higher concentrations along the coast-line of the Antarctic Peninsula and around the islands than in the open sea. This correlates well with bioactivity at the different locations. Further investigations have shown that probably the chlorophyll content can be used for correlation with the biogenically produced bromomethanes [35].

The seawater concentrations of the different bromomethanes correlate well as can be seen from Fig. 18 for  $\text{CHBr}_2\text{Cl}$  and  $\text{CH}_2\text{Br}_2$  [38]. This indicates an identical, or at least a similar, path-

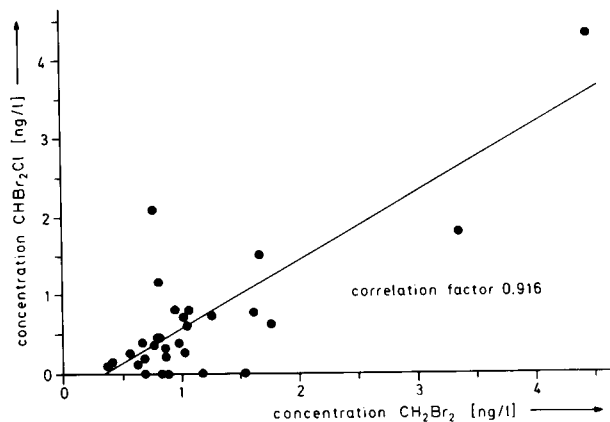


Fig. 18. Correlation between  $\text{CHBr}_2\text{Cl}$  and  $\text{CH}_2\text{Br}_2$  in Antarctic surface seawater samples [38].

way for the biological production for these compounds. Although the exact mechanism of formation is still not known today, it is assumed that  $\text{CH}_2\text{Br}_2$  and  $\text{CHBr}_3$  are produced in marine organisms via a successive enzymatic bromination of ketone metabolites [39,40]. The mixed bromochloro compounds can be directly released from algae into the seawater, as experiments by Class and Ballschmiter have shown [41], or they can be formed by nucleophilic substitution of bromide by chloride in seawater itself



On the other hand, we did not find a correlation between methyl iodide and the brominated methanes [34], which indicates different biological pathways of formation.

Further investigations must be carried out to obtain better knowledge on the important correlations between biological species and the production of the biogenic halogenated compounds. Another important topic is that halogenated hydrocarbons are able to absorb IR radiation more strongly than many of the other commonly discussed greenhouse gases. Whether these biogenic compounds can also contribute to the global warming or not is a question of the abundances of these gases in the atmosphere. It is unlikely that the today's level of biogenic halogenated hydrocarbons in the atmosphere can essentially contribute to the global warming, although the real influence by these substances has not been examined. However, in connection with recent ideas to control the  $\text{CO}_2$  level in the atmosphere by fertilizing the Antarctic Ocean with iron for an enhanced uptake of  $\text{CO}_2$  by phytoplankton and macroalgae [42], the potential influence of all biogenically produced halocarbons in the polar regions on the global warming gains new dimension.

In the troposphere, photodissociation is one of the major sinks for organobromides and organoiodides. Because the decomposition of ozone by halogen radicals is well known, it may therefore be possible that the bromo- and iodomethanes influence the tropospheric ozone concentration.

Additionally, it cannot be totally ruled out that these compounds also partially influence the stratospheric ozone.

Trace analysis is a wide field in Antarctica and should be more intensively applied in the future for a better knowledge of the behaviour and interaction of organic molecules as well as of trace elements and their species in the environment of the clean room compartment of this remote continent.

I thank all my co-workers, who contributed to the reported results, and all colleagues, who have cooperated in these scientific investigations in an excellent and effective way. I am grateful to the Alfred-Wegener-Institut für Polar- und Meeresforschung, Bremerhaven, to the crew of the polar research vessel *Polarstern* and to the different crews of the German Antarctic station "Georg-von-Neumayer" for all logistic support and continuous assistance. The financial support of the Deutsche Forschungsgemeinschaft is gratefully acknowledged.

#### REFERENCES

- O. Reinwarth, W. Rauert, W. Stichler and H. Moser, *Ann. Glaciol.*, 3 (1982) 274.
- J.M. Pacyna, in J.O. Nriagu and C.I. Davidson (Eds.), *Toxic Metals in the Atmosphere*, Wiley, New York, 1986, p. 1.
- A.L. Graham and J.O. Annexstad, *Antarctic Sci.*, 1 (1989) 3.
- L. Schultz, *Naturwissenschaften*, 69 (1982) 220.
- R. Froböse, *Geowiss. unserer Zeit*, 2 (1984) 45.
- K.G. Heumann, M. Gall and H. Weiss, *Geochim. Cosmochim. Acta*, 51 (1987) 2541.
- N. Rädlein, Thesis, University of Regensburg, 1991.
- C.F. Boutron and F.M. Batifol, *Ann. Glaciol.*, 7 (1985) 7.
- J. Völkening and K.G. Heumann, *Fresenius' Z. Anal. Chem.*, 331 (1988) 174.
- J. Neubauer and K.G. Heumann, *Fresenius' Z. Anal. Chem.*, 331 (1988) 170.
- D. Tanzer and K.G. Heumann, *Intern. J. Environ. Anal. Chem.*, 48 (1992) 17.
- W. Reifenhäuser and K.G. Heumann, *Chemosphere*, 24 (1992) 1293.
- K.G. Heumann, in F. Adams, R. Gijbels and R. van Grieken (Eds.), *Inorganic Mass Spectrometry*, Wiley, New York, 1988, p. 301.
- L. Hütter, *Chem. Labor Betr.*, 36 (1985) 104.
- S.R. Taylor, *Geochim. Cosmochim. Acta*, 28 (1964) 1273.
- J. Völkening and K.G. Heumann, *J. Geophys. Res.*, 95D (1990) 20623.
- N. Rädlein and K.G. Heumann, *Intern. J. Environ. Anal. Chem.*, 48 (1992) 127.
- C.F. Boutron and C.C. Patterson, *Geochim. Cosmochim. Acta*, 47 (1983) 1355.
- C.F. Boutron and C.C. Patterson, *Nature*, 323 (1986) 222.
- J. Völkening, H. Baumann and K.G. Heumann, *Atmos. Environ.*, 22 (1988) 1169.
- H. Baumann and K.G. Heumann, *Fresenius' Z. Anal. Chem.*, 320 (1985) 512.
- C.F. Boutron, U. Görlach, J.-P. Candelone, M.A. Bolshov and R.J. Delmas, *Nature*, 353 (1991) 153.
- N. Rädlein and K.G. Heumann, *Fresenius' J. Anal. Chem.* (1992) in press.
- K.G. Heumann and M. Unger, *Fresenius' Z. Anal. Chem.*, 315 (1983) 454.
- J. Neubauer, Thesis, University of Regensburg, 1988.
- M.R. Legrand, M. De Angelis and R.J. Delmas, *Anal. Chim. Acta*, 156 (1984) 181.
- J. Wittenzellner, Thesis, University of Regensburg, 1993.
- J. Neubauer and K.G. Heumann, *Atmos. Environ.*, 22 (1988) 537.
- K.H. Wedepohl (Ed.), *Handbook of Geochemistry*, Vol. II-4, Springer, Heidelberg, 1974.
- H.-E. Gäbler and K.G. Heumann, *Intern. J. Environ. Anal. Chem.* (1992) in press.
- H.-E. Gäbler and K.G. Heumann, *Fresenius' J. Anal. Chem.* (1992) in press.
- H.B. Singh, L.J. Salas, H. Shigeishi and E. Scribner, *Global Distribution of Selected Halocarbons, Hydrocarbons, SF<sub>6</sub> and N<sub>2</sub>O*, Report Atmos. Sci. Lab., Stanford Res. Inst., 1978.
- R.A. Rasmussen, M.A.K. Khalil, R. Gunawardena and S.D. Hoyt, *J. Geophys. Res.*, 87 (1982) 3086.
- W. Reifenhäuser and K.G. Heumann, *Atmos. Environ.*, 26A (1992) 2905.
- C. Schall, Thesis, University of Regensburg, 1993.
- W.L. Chameides and D.D. Davis, *J. Geophys. Res.*, 85 (1980) 7383.
- K.G. Heumann, J. Neubauer and W. Reifenhäuser, *Geochim. Cosmochim. Acta*, 54 (1990) 2503.
- W. Reifenhäuser, Thesis, University of Regensburg, 1989.
- R.S. Beissner, W.J. Guilford, R.M. Coates and L.P. Hagner, *Biochemistry*, 20 (1981) 3724.
- R. Theiler, J.C. Cook and L.P. Hagner, *Science*, 202 (1978) 1094.
- T. Class and K. Ballschmiter, *J. Atmos. Chem.*, 8 (1988) 35.
- R. Baum, *Chem. Eng.*, (1990) 21.

# Determination of bromide in snow samples by ion chromatography with electrochemical detection

S. Seefeld and U. Baltensperger

*Paul Scherrer Institute, CH-5232 Villigen PSI (Switzerland)*

(Received 29th September 1992)

## Abstract

Ion chromatography with electrochemical detection was applied to the determination of bromide in snow samples. Greater reproducibility and increased sensitivity was obtained by coating the silver electrode with a highly insoluble AgI surface. Without preconcentration, a detection limit of less than  $1 \mu\text{g l}^{-1}$  was achieved. With preconcentration, snow samples from a high-alpine site with bromide concentrations as low as  $90 \text{ ng l}^{-1}$  could be analysed.

*Keywords:* Ion chromatography; Bromide; Environmental samples; Snow

Bromide is a sea salt constituent with a concentration of  $60\text{--}70 \text{ mg l}^{-1}$  [1], i.e., about 300 times lower than the chloride concentration. The annual sea salt production amounts to about  $10^9 \text{ t}$  [2], resulting in an annual  $\text{Br}^-$  aerosol production of about  $2 \times 10^6 \text{ t}$  [3]. In addition, the worldwide anthropogenic annual bromine production amounted to about  $350\,000\text{--}400\,000 \text{ t}$  in the early 1980s [1]. In the 1970s, up to 70% of this production was due to ethylene dibromide, which was added together with ethylene dichloride to leaded petrol; however, later this proportion decreased owing to the increasing use of unleaded fuel [1]. These compounds form volatile compounds such as  $\text{PbBrCl}$  in the exhaust gas, thus increasing lead volatility [4]. In the atmosphere,  $\text{PbBrCl}$  is decomposed, leading to more stable lead salts such as  $\text{PbSO}_4$  and to  $\text{HBr}$ ,  $\text{HCl}$  and other halide compounds [5]. As a result,  $\text{Br}^-$  in rain and snow can be an interesting tracer for leaded automobile fuel consumption. The combined measurement of  $\text{Br}^-$  and  $\text{Pb}$  in ice samples should reveal

the importance of the automobile source for these two elements. A history of the  $\text{Pb}$  and  $\text{Br}^-$  concentrations is conserved in ice of high-alpine glaciers and should therefore give access to the history of leaded fuel consumption in Central Europe. In addition, bromine is of interest in the Arctic atmosphere because of a spring pulse of particulate bromine that has been observed at several sites throughout the Arctic [6], and methods to reveal its speciation are of great importance.

There are a variety of techniques available for the determination of bromide.  $\text{Br}^-$  can be determined by several spectrophotometric techniques [7], by an indirect spectrophotometric technique [8] or by chemiluminescence [9]. In addition, several techniques such as neutron activation analysis [10], total reflection x-fluorescence analysis (TRXF) [11] or particle-induced x-ray emission (PIXE) [12] offer the possibility of measuring total bromine. Many of these techniques, however, need very sophisticated equipment or do not provide a detection limit below  $1 \mu\text{g l}^{-1}$ .

In principle,  $\text{Br}^-$  could easily be determined by ion chromatography with standard conductiv-

*Correspondence to:* U. Baltensperger, Paul Scherrer Institute, CH-5232 Villigen PSI (Switzerland).

ity detection, but  $\text{NO}_3^-$ , often present in a 100-fold excess in environmental samples, interferes with the determination of  $\text{Br}^-$ . Therefore, several workers have described methods with ion chromatography and electrochemical detection [13–15]. However, no bromide data for real samples were presented, presumably because of a lack of reproducibility. In this paper it is shown that this technique provides a very suitable means for the determination of  $\text{Br}^-$  in real samples, with excellent sensitivity.

## EXPERIMENTAL

A Sykam ion chromatographic system [16] was used. The columns as well as the conductivity detector were placed in a thermostated cabinet. The electrochemical detector (Metrohm, 656, together with a Metrohm 641 VA detector) was based on the wall-jet principle and consisted of a silver working electrode, a gold counter electrode and a  $3 \text{ mol l}^{-1} \text{ Ag/AgCl}$  reference electrode, with a cell volume of  $< 1 \mu\text{l}$ . The sensitivity of the detector was normally set to 100 nA (full-scale), which allowed the determination of  $\text{Br}^-$  concentrations from the detection limit up to  $1 \text{ mg l}^{-1}$ . Data were recorded with a Hewlett-Packard multi-channel interface (HP 35900C) connected to a personal computer. Data evaluation was performed by ChemStation software (HP3365).

A Dionex column (IonPac AS4A) was used for the separations, with  $1.7 \text{ mM NaHCO}_3$ – $1.8 \text{ mM Na}_2\text{CO}_3$  as eluent. Chemical conductivity suppression (Dionex membrane suppressor, AMMS) was only used for combined experiments with electrochemical and conductivity detectors (Sykam S3110). All reagents were of analytical-reagent grade. In order to check for interferences,  $\text{Br}^-$  standard solutions were usually prepared with  $1 \text{ mg l}^{-1}$  of  $\text{Cl}^-$ ,  $\text{NO}_3^-$  and  $\text{SO}_4^{2-}$ . For  $\text{Cl}^-$ , NaCl rather than KCl was used, as the KCl contains 0.05%  $\text{Br}^-$ .

The electrochemical detector was extremely sensitive to pressure pulsations, with pulse amplitudes up to 4 nA. Therefore, an additional pulse damper (Portmann PM-PD 800) was installed,

which reduced baseline pulsations by a factor of about 100. In addition, the detector was subject to electrostatic interferences. This effect could be eliminated by connecting the injection loop to earth.

## RESULTS AND DISCUSSION

### *Response of the detection system*

Han et al. [17] showed that the condition of the surface of the working electrode has a profound influence on its response characteristics. They noted that a platinum electrode showed an increased response to iodide oxidation after the electrode had been immersed in an iodizing solution. We tested this effect with the present silver electrode and obtained similar findings. An untreated silver electrode gave a very low response, which decreased even more during use (Fig. 1). Immersing the electrode in a saturated solution of KBr or KI resulted in a much higher sensitivity, which even increased during the first few hours of use (Fig. 1). Immersion in KI gave a slightly lower sensitivity than in KBr, but the time needed for a constant signal was shorter with KI, and also the reproducibility was better. Immersion in  $\text{Na}_2\text{S}$  was also tested, as  $\text{Ag}_2\text{S}$  has the lowest solubility product of all silver salts, which should result in the most stable deposit on the silver electrode. Indeed, the sensitivity was initially about a factor of 5 higher than with KI, but decreased to the values for the iodized electrode

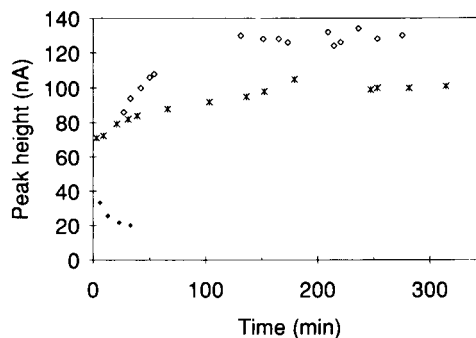


Fig. 1. Bromide peak height as a function of time for several electrode pretreatments: ◆ = without pretreatment; ◇ with KBr conditioning; \* = with KI conditioning.



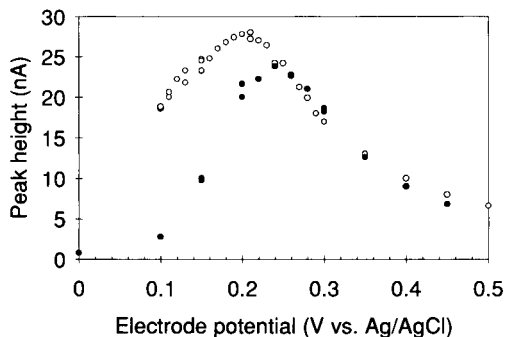


Fig. 2. Bromide peak height as a function of electrode potential (vs. Ag/AgCl).  $\circ$  = With KBr conditioning;  $\bullet$  = with KI conditioning.

within about 5 h. In addition, the reproducibility with sulphide was poorer than with iodide. Therefore, only the KBr and KI procedures were continued.

Figure 2 shows the response of the silver electrode as a function of the applied potential. Data obtained with KBr and KI electrode pretreatment are given, and appear similar to those described by Rocklin and Johnson [13] for  $I^-$ . As the potential is increased from negative to positive, the peak height increases as the diffusion-controlled plateau is reached. Beyond this potential, the peak height decreases as other reactions compete with the reaction of interest [13]. Because of the better reproducibility, in subsequent experiments all  $Br^-$  determinations were performed with an iodized silver electrode, with an applied potential of 0.2 V (vs. Ag/AgCl). Typically, the electrode was polished with  $Al_2O_3$  (Metrohm) for about 30 s, immersed in saturated KI solution overnight and then rinsed with water prior to the first use. A newly iodized electrode was used for 4 days before a new iodizing procedure was necessary. Overnight either the eluent flow-rate was reduced to  $0.2 \text{ ml min}^{-1}$  with the electrode potential left at 0.2 V, or the electrode was stored dry in air. Storing in air for 14 days did not affect the response of the electrode.

Figure 3 shows a standard chromatogram for  $10 \mu\text{g Br}^- \text{ l}^{-1}$  obtained with the electrochemical detector. The bromide peak exhibits a characteristic peak shape, with an undershooting of the baseline. This effect has also been reported by

other workers [12,18] and is probably due to the formation and subsequent dissolution of AgBr on the electrode surface [19]. For peak height evaluation a horizontal baseline extrapolation was made, thus minimizing interferences by this undershooting.

The calibration graph obtained for  $Br^-$  concentrations  $\leq 20 \mu\text{g l}^{-1}$  was linear: peak height (nA) =  $0.21[Br^- (\mu\text{g l}^{-1})] + 0.00$ ;  $r = 0.999$ ,  $n = 21$ . All samples also contained  $1 \text{ mg l}^{-1}$  of  $Cl^-$ ,  $NO_3^-$  and  $SO_4^{2-}$ . No interferences were found with these ions at the given concentrations. A detection limit of  $< 1 \mu\text{g l}^{-1}$  was achieved. Repeated measurements of  $1 \mu\text{g l}^{-1}$  standard samples gave relative standard deviations between 8 and 19%, depending on the baseline stability. The calibration graph was linear up to  $100 \mu\text{g l}^{-1}$ .

#### Combination of detection techniques

Electrochemical detection can be used in conjunction with conductivity detection to determine in one run ions detectable by either method [13]. Several arrangements were tested. First, the membrane suppressor and conductivity detector were placed behind the electrochemical detector. Owing to the low volume of the electrochemical detector, this set-up did not adversely affect the peak resolution in the conductivity detector. Good chromatograms were obtained for higher  $Br^-$  concentrations, but the back-pressure of the membrane suppressor increased the pressure pul-

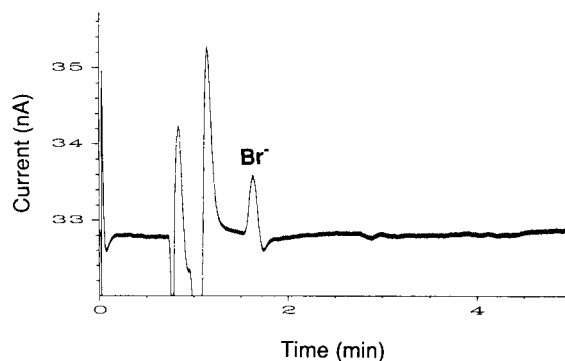


Fig. 3. Chromatogram obtained with a standard sample containing  $10 \mu\text{g Br}^- \text{ l}^{-1}$  and  $1 \text{ mg l}^{-1}$  of  $Cl^-$ ,  $NO_3^-$  and  $SO_4^{2-}$ .

sations of the electrochemical detector output by about a factor of 100, resulting in a detection limit of about  $10 \mu\text{g Br}^- \text{l}^{-1}$ . Second, the electrochemical detector was placed behind the suppressor and the conductivity detector in order to eliminate the pressure pulses. This arrangement did not adversely affect the  $\text{Br}^-$  peak shape significantly, as the total dead volume of the conductivity detector was only about  $20 \mu\text{l}$ . However, under these conditions the conductivity in the electrochemical detector is much lower than recommended. Any ion passing the detector increases the conductivity considerably, which increases the baseline oxidation current. Hence all ions, including non-oxidizable ions, produce a peak in the electrochemical detector output, and the electrochemical detector reacts somehow as a combination of an electrochemical and a conductivity detector. However, as this approach did not eliminate possible interferences between  $\text{Br}^-$  and  $\text{NO}_3^-$ , it was not pursued further. Third, the suppressor, conductivity detector and electrochemical detector were again placed in series, but the conductivity in the electrochemical detector was increased by adding a salt solution behind the conductivity detector;  $20 \text{ g l}^{-1}$  of  $\text{NaNO}_3$  and  $20 \text{ g l}^{-1}$  of  $\text{NaNO}_3 + 0.29 \text{ g l}^{-1}$  of  $\text{NaOH}$  were added by means of an infusion pump (Precidor 5003-1) and a T-connector. With this approach the peaks caused by  $\text{Cl}^-$ ,  $\text{NO}_3^-$  and  $\text{SO}_4^{2-}$  disappeared almost completely. Sufficiently high  $\text{Br}^-$  concentrations could easily be determined, but the increased baseline noise increased the detection limit again to  $10 \mu\text{g Br}^- \text{l}^{-1}$ . Thus, although several approaches for simultaneous multi-anion analysis could be shown to work, in all instances the  $\text{Br}^-$  detection limit was increased by more than a factor of 10.

#### Determination of ions other than bromide

A variety of other anions can be determined simultaneously by electrochemical detection [13,17]. Figure 4 shows a chromatogram of  $\text{Cl}^-$ ,  $\text{Br}^-$ ,  $\text{SO}_3^{2-}$ ,  $\text{I}^-$ ,  $\text{HS}^-$  and  $\text{SCN}^-$  obtained at an applied electrode potential of  $0.2 \text{ V vs. Ag/AgCl}$ . Most detection limits were about one order of magnitude lower than with the untreated silver electrode [13] or with the iodized platinum elec-

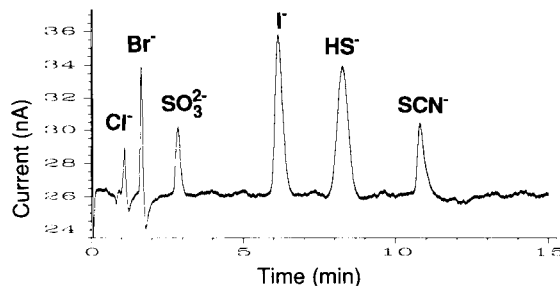


Fig. 4. Chromatogram of  $\text{Cl}^-$  ( $1 \text{ mg l}^{-1}$ ),  $\text{Br}^-$  ( $0.1 \text{ mg l}^{-1}$ ),  $\text{SO}_3^{2-}$  ( $1 \text{ mg l}^{-1}$ ),  $\text{I}^-$  ( $0.05 \text{ mg l}^{-1}$ ),  $\text{HS}^-$  ( $0.1 \text{ mg l}^{-1}$ ) and  $\text{SCN}^-$  ( $1 \text{ mg l}^{-1}$ ) obtained with electrochemical detection at an applied potential of  $0.2 \text{ V vs. Ag/AgCl}$ .

trode [17].  $\text{CN}^-$  had about the same retention time as  $\text{Br}^-$ , and the  $\text{CN}^-$  peak showed considerable tailing under these conditions. Hence  $\text{CN}^-$  has the potential to interfere with the determination of  $\text{Br}^-$ .

#### Preconcentration procedure

Even though the detection limit achieved without preconcentration was low, the expected bromide concentrations in high-alpine snow samples are even lower. Therefore, a preconcentration technique was tested. A six-way injection valve was used where the injection loop was replaced with a preconcentration column (Dionex IonPac TAC-1). Samples of  $10 \text{ ml}$  were pumped through the preconcentration column by means of an infusion pump (Precidor 5003-1). The amount of sample introduced was controlled by a time measurement. The calibration graph was linear, and the desired detection limit of less than  $0.1 \mu\text{g l}^{-1}$  was finally reached.

#### Analysis of fog and snow samples

The  $\text{Br}^-$  concentrations in fog and snow samples are presented in Table 1. For the fog and snow samples from the Swiss plains values greater than  $1 \mu\text{g l}^{-1}$  result, which means that these bromide concentrations can be determined without preconcentration. This is not so for high-alpine sites during winter. Owing to reduced vertical transport processes atmospheric aerosol concentrations at high-alpine sites are normally at least a factor of ten lower during winter than during summer [20]. Hence it is reasonable to

TABLE 1  
Bromide concentrations of fog and snow samples <sup>a</sup>

Sample	Br <sup>-</sup> concentration (μg l <sup>-1</sup> )	Preconcentration
Fog	73	No
Snow 1	2.0	No
Snow 2	7.0	No
Snow 3	2.8	No
Snow 4	0.09	Yes

<sup>a</sup> The fog sample and snow samples 1–3 were taken in rural areas of the plain in northern Switzerland; snow sample 4 was taken on the Jungfrauoch (3450 m).

expect the lowest Br<sup>-</sup> concentrations in high-alpine winter snow. As an example, Fig. 5 shows a chromatogram of a snow sample taken at the Jungfrauoch (3450 m) in January. The Br<sup>-</sup> peak was obtained by preconcentration of a 10-ml sample and represents a concentration of 90 ng l<sup>-1</sup>. Thus, even high-alpine samples can be analysed for Br<sup>-</sup> with the proposed technique, but only after preconcentration.

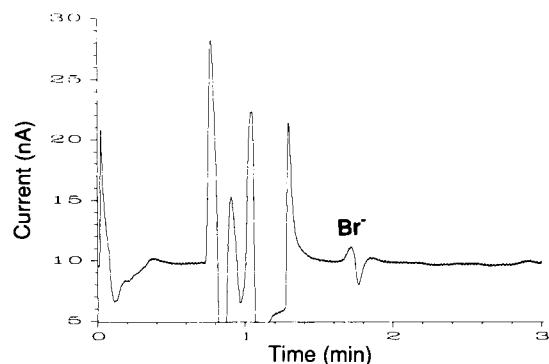


Fig. 5. Chromatogram of a snow sample from the Jungfrauoch (3450 m) containing 90 ng Br<sup>-</sup> l<sup>-1</sup>.

## REFERENCES

- 1 W.R. Merriman and H.E. Arkens, in D. Price, B. Iddon and B.J. Wakefield (Eds.), *Bromine Compounds, Chemistry and Applications*, Elsevier, Amsterdam, 1988, p. 385.
- 2 R. Jaenicke, in G. Fischer (Ed.), *Landolt Börnstein, New Series, Physical and Chemical Properties of Air, Group V, Vol. 4b*, Springer, Berlin, 1988.
- 3 B.J. Finlayson-Pitts and J.N. Pitts, Jr., *Atmospheric Chemistry: Fundamentals and Experimental Techniques*, Wiley, New York, 1986, p. 784.
- 4 H. Baumann and K.G. Heumann, *Fresenius' Z. Anal. Chem.*, 320 (1985) 512.
- 5 P.D.E. Biggins and R.M. Harrison, *Environ. Sci. Technol.*, 13 (1979) 558.
- 6 W.T. Sturges and L.A. Barrie, *Atmos. Environ.*, 22 (1988) 1179.
- 7 C. Zhu and G.M. Hieftje, *Anal. Chim. Acta*, 256 (1992) 97, and references cited therein.
- 8 G.S. Pyen, M.J. Fishman and A.G. Hedley, *Analyst*, 105 (1980) 657.
- 9 A.T. Pilipenko, A.V. Terletskaia and O.V. Zui, *Fresenius' Z. Anal. Chem.* 335 (1989) 45.
- 10 S. Landsberger, J.J. Drake and S.J. Vermette, *Chemosphere*, 17 (1988) 299.
- 11 A. Prange, *Spectrochim. Acta, Part B*, 44 (1989) 437.
- 12 G. Henrici, D. Hofmann, H.W. Georgii and K.O. Groeneveld, *J. Atmos. Chem.*, 12 (1991) 391.
- 13 R.D. Rocklin and E.L. Johnson, *Anal. Chem.*, 55 (1983) 4.
- 14 G.S. Pyen and D.E. Erdmann, *Anal. Chim. Acta*, 149 (1983) 355.
- 15 H.C. Mehra and W.T. Frankenberger, Jr., *Microchem. J.*, 41 (1990) 93.
- 16 U. Baltensperger and S. Kern, *J. Chromatogr.*, 439 (1988) 121.
- 17 K. Han, W.F. Koch and K.W. Pratt, *Anal. Chem.*, 59 (1987) 731.
- 18 G. Schwedt and B. Rössner, *Fresenius' Z. Anal. Chem.*, 327 (1987) 499.
- 19 W. Terzer, Metrohm, Herisau, Switzerland, personal communication, 1991.
- 20 U. Baltensperger, H.W. Gäggeler, D.T. Jost, M. Emmenegger and W. Nägeli, *Atmos. Environ.*, 25A (1991) 629.

# Characterization of organic sulphur compounds in surface water by ion-pair adsorption under different conditions

Susanne Schullerer and Fritz H. Frimmel

*Lehrstuhl für Wasserchemie der Universität Karlsruhe (TH), Postfach 6980, D-7500 Karlsruhe 1 (Germany)*

(Received 26th September 1992; revised manuscript received 29th January 1993)

## Abstract

Organic sulphur compounds belong to the main pollutants of surface water. Due to their hydrophilic character, analytical determination has been severely hampered. In a new concept, which uses ion-pair formation, the advantages of integrated quantification and chromatographic determination are unified. Three solid phase methods for enrichment of organic sulphur compounds were applied to gain information on their character. The integrated determination with ICP-AES led to the conclusion that ion-pair adsorbable organic sulphur mainly reflects the different organic sulphonic acids. The example of naphthalene-1,5-disulphonic acid shows that the individual acids can be assigned using LC with UV and fluorescence detection. The methods were applied to determine organic sulphur compounds along the River Rhine, and a sulphonic acid was followed through a water treatment plant down to a level of  $0.1 \mu\text{g l}^{-1}$ .

**Keywords:** Atomic emission spectrometry; Ion chromatography; Inductively coupled plasma; Liquid chromatography; Extraction; Sulphur compounds; Waters

Chromatographic methods are important tool methods in the classification of water quality and a huge number of organic substances have been identified and determined. Liquid chromatography is especially useful in detecting relatively polar substances without further derivatization.

Chromatographic methods work well with most organic substances having a defined molecular structure. However, there is a lack of analytical methods applicable to substances of high molecular weight such as humic acids and ligninsulphonic acids, which may significantly influence water quality. High resolution chromatography with identification of individual compounds is often not the method of choice in this instance. The development of sum parameters brought an

advantageous application in water analysis. Sum parameters try to cover all substances of a group. So far two important sum parameters have proved successful: DOC and AOX. The parameter DOC (dissolved organic carbon) quantifies all organic substances dissolved in a water sample. The method works mostly without a preconcentration step [2,3]. The parameter AOX (adsorbable organic halogens) covers a wide range of organic halogenated substances [4]. A preconcentration step using activated carbon guarantees the enrichment of even fairly polar organic compounds. On the other hand, the desorption of the preconcentrated substances and their chromatographic separation are often not possible.

Owing to their broad application, organic sulphur compounds have a well known influence on surface water quality [5,6]. Aromatic sulphonic acids, for example, have been applied in the paper and textile industries as dyes and as optical

*Correspondence to:* F.H. Frimmel, Lehrstuhl für Wasserchemie der Universität Karlsruhe (TH), Postfach 6980, D-7500 Karlsruhe 1 (Germany).

brighteners [7]. Frequently used detergents such as the linear alkylbenzenesulphonic acids are also important [8]. Ligninsulphonic acids arise from the production of cellulose and may reach surface waters in considerable amounts [9].

In a new concept for the determination of organically bound sulphur in aquatic samples, the advantages of integrated quantification and chromatographic determination are unified. A suitable pre-enrichment step for the substances to be determined leads to their transfer into a suitable solvent. Using this concentrate, all further analytical investigations are possible [10]. This concept for the analysis of aquatic samples uses solid-phase adsorption on a non-polar octadecyl-modified reversed phase (RP-C<sub>18</sub> material).

The aim of the work was to use the principle of solid-phase adsorption under different conditions for the pre-enrichment of organically bound sulphur in aqueous samples; to determine the

sulphur compounds in the obtained extracts by spectroscopic [inductively coupled plasma atomic emission spectrometry (ICP-AES)] and chromatographic methods [ion chromatography (IC) and liquid chromatography (LC) with UV and fluorescence detection]; to draw some conclusions on the character and behaviour of the organically bound sulphur in the River Rhine as raw water for drinking water production.

#### THE ANALYTICAL CONCEPT

The concept for the characterization of organically bound sulphur is based on solid-phase adsorption. For more detailed information on the character of the organic sulphur compounds, aquatic samples were split and either applied unchanged at neutral pH, acidified to pH 2.0 before contact with the solid phase or equili-

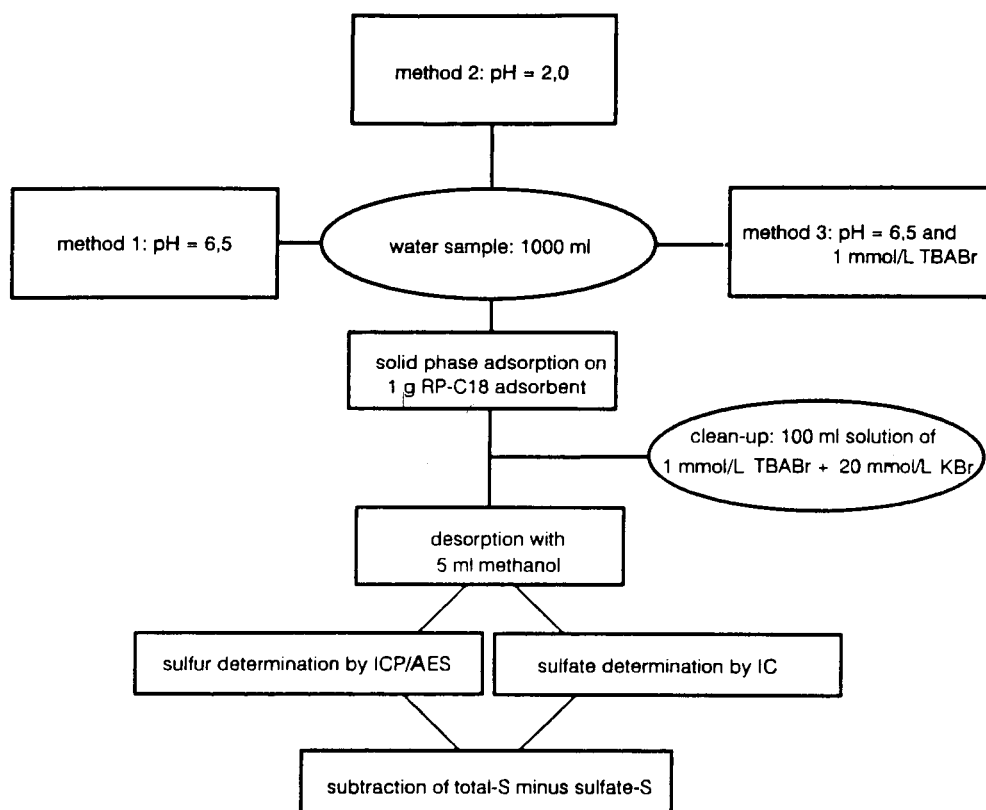


Fig. 1. Three possibilities for solid-phase enrichment of organic sulphur compounds in water with RP-C<sub>18</sub> adsorbent.

brated with the solid phase after addition of tetraalkylammonium bromide for ion-pair formation. The three parallel extracts were further characterized. The whole procedure is shown schematically in Fig. 1.

Sulphur can be determined by ICP-AES [11]. Depending on the chosen enrichment procedure, the extract may contain co-adsorbed inorganic sulphate, which is detected by IC [12,13]. The amount of total sulphur minus the amount of inorganically bound sulphur equals the amount of the preconcentrated sulphur present in organic compounds.

The extract can also be used for LC and identification of the fractions [14]. A great advantage lies in the possibility of determining the total sulphur species first and deciding from the results whether or not there is a need for an advanced analytical approach to identify the individual compounds.

## EXPERIMENTAL

### *Origin of samples*

Samples were taken from the River Rhine and from a water treatment plant in Düsseldorf during a sampling campaign in August 1992. The river samples were taken daily over a period of 2 weeks. Samples were also taken after different treatment steps in a water treatment plant near the city of Düsseldorf, which uses bank filtrate of the River Rhine as raw water. The samples of the bank filtrate were taken at a distance of 350 m from the river bank. For ozonation, 1.5 mg l<sup>-1</sup> of ozone were applied.

### *Sample treatment*

The composite samples were brought to the laboratory at a temperature of 4°C. They were filtered through a glass-fibre filter (Sartorius, Göttingen, Germany). Parallel samples of 1 l were neutralized to pH 6.5 (method 1), acidified with 2 M HCl to 2.0 (method 2) and mixed with tetrabutylammonium bromide (TBABr) (0.32 g) to give a 1 mM solution (method 3). In method 3 the TBABr serves as an ion-pair reagent. The organic cation is adsorbed on the solid phase during the

pre-enrichment step. This allows the preconcentration via ion-pair formation of the anionic sulphur compounds on the positively charged surface of the solid phase.

### *Solid-phase adsorption*

The samples were passed through a glass column (100 mm × 10 mm i.d.: bottom Glas fritte No. 1) filled with 1 g of RP-C<sub>18</sub> solid-phase material (J.T. Baker, Phillipsburg, NJ) at a rate of ca. 500 ml h<sup>-1</sup>. The RP-C<sub>18</sub> phase had been brought into the column as a methanolic slurry and had been washed thoroughly with distilled water. The samples were sucked through by vacuum. In the application of methods 1 and 2, the amount of co-adsorbed inorganic sulphate was negligible. Using method 3, the amount of the co-adsorbed sulphate reached values up to 80 µg S l<sup>-1</sup>. To remove the inorganic sulphur compounds, the loaded column was washed with 100 ml of a solution containing 1 mM TBABr and 20 mM KBr. After this clean-up step, the concentrations of adsorbed sulphate were lower than 10 µg S l<sup>-1</sup>. This is a tolerable value which allows the determination of organic sulphur compounds even in the range of 20 µg S l<sup>-1</sup> with a relative standard deviation below 15%. After this the RP-C<sub>18</sub> phase was dried thoroughly using nitrogen. For desorption of the adsorbed substances, 5 ml of methanol were passed through the dried column. The methanol was evaporated and the residue was dissolved in 5 ml of doubly distilled water. In this aqueous extract, total sulphur and sulphate were determined and used for the calculation of the amount of adsorbed organic sulphur compounds.

### *Sulphur determination by ICP-AES*

Scandium was used as the internal standard. A 0.5-ml volume of a 0.25 g Sc l<sup>-1</sup> standard solution was added to 2.0 ml of aqueous extract prior to determination by ICP-AES. The samples were introduced at a rate of 1 ml min<sup>-1</sup> into the inductively coupled argon plasma of a sequential atomic emission spectrometer (Perkin-Elmer Plasma 2000). Sulphur was determined at 180 and 731 nm and scandium at 420–424 nm. Details of the spectroscopic set-up have been described

elsewhere [11]. Calibration was done with external standard solutions made from a sulphate standard solution ( $30 \text{ mg l}^{-1}$ ). Five individual determinations for each sample were made leading to a relative standard deviation of  $\leq 2\%$  at sulphur concentrations  $> 10 \text{ mg l}^{-1}$ .

#### Sulphate determination by IC

The sulphate concentrations in the aqueous extracts were determined using a Dionex 2000 IC system (Dionex, Idstein, Germany) with a precolumn (Dionex AG 4A), an analytical column (Dionex AS 4A) and electrical conductivity detection according to standard methods [13].

#### Liquid chromatography

The extracts were chromatographed using a Hewlett-Packard 1090 M LC system with diode array UV detection (DAD) and fluorescence detection. A Hypersil ODS/ $C_{18}$  column with a particle size of  $5 \mu\text{m}$  was used ( $250 \text{ mm} \times 4.6 \text{ mm}$  i.d.). The eluents [A = water; B = methanol-water (75 + 25)] contained 1 mM tetrabutylammonium hydrogensulphate and 5 mM sodium dihydrogenphosphate. A gradient was used for elution 0 min, A:B = 70 + 30; 50 min, A:B = 0 + 100; 70 min, A:B = 70 + 30). The samples were injected as aqueous solutions (A:B = 70 + 30). The injection volume was 50–100  $\mu\text{l}$ .

## RESULTS AND DISCUSSION

The different pretreatment procedures had a strong influence on the amount of preconcentrated sulphur compounds. Figure 2 shows the results for water samples taken along the River Rhine. The ordinate shows the concentration of the adsorbed organic sulphur compounds.

It is obvious that the neutralized samples (method 1, pH 6.5) show the lowest yields ( $< 1\text{--}21 \mu\text{g S l}^{-1}$ ). Acidifying the water to pH 2.0 (method 2) leads to increased adsorption ( $14\text{--}43 \mu\text{g S l}^{-1}$ ) and ion-pair formation (method 3) shows by far the largest amount of adsorbable organic sulphur compounds (IOS:  $20\text{--}85 \mu\text{g S l}^{-1}$ ) [applying method 3, the sum of adsorbed organic sulphur compounds is called IOS (ion-pair-adsorbable or-

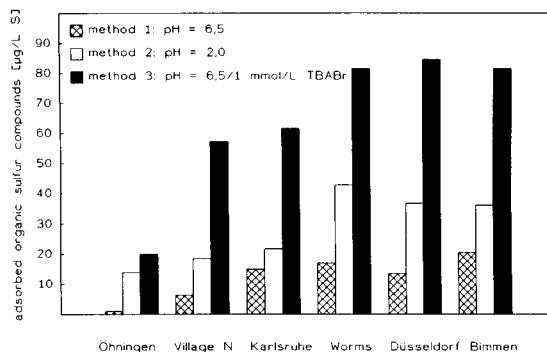


Fig. 2. Amount of organic sulphur compounds in River Rhine water obtained with different enrichment methods.

ganic sulphur)]. Even though the values are operationally defined, the trends are clear. In model experiments it could be shown that the recoveries of many aromatic sulphonic acids added to distilled water and Rhine water were 80% in the ion-pair adsorption method described [15]. The standard deviation for the reproducibility in Rhine water was  $3.5 \mu\text{g S l}^{-1}$ , which corresponds to a relative standard deviation of 15% for the determination limit of the IOS, which has been statistically calculated to be  $20 \mu\text{g S l}^{-1}$ . For methods 1 and 2 the determination limits and the analytical errors at the given concentrations were even lower (determination limit =  $5 \mu\text{g S l}^{-1}$ , standard deviation =  $1.5 \mu\text{g S l}^{-1}$ ). Comparison between the yields of organic sulphur compounds adsorbable on activated carbon (AOS) [16] and the yields of IOS lead to the conclusion that both methods come close to the total amount of organic sulphur in aqueous solutions. For comparison and validation, Rhine water samples were analysed using both methods (determination of IOS and AOS). The statistical interpretation of the data showed a bias of  $-2.1 \mu\text{g S l}^{-1}$  and a relative standard deviation of 10% [15].

It was concluded that IOS is a suitable parameter for the integrated assessment of organic sulphonic acids in surface water as an important example of anthropogenic pollution. Compared with AOS, IOS includes the possibility of a straightforward identification of individual compounds, if necessary. However, the amount of co-adsorbed sulphate has to be eliminated in an

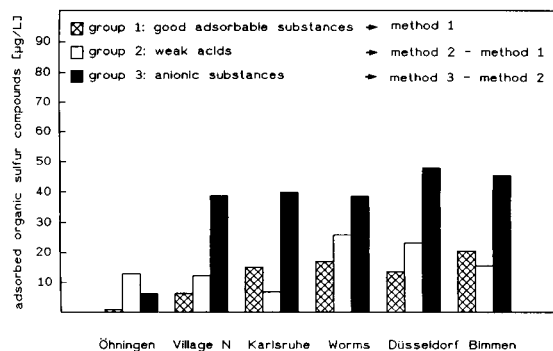


Fig. 3. Separation of organic sulfur compounds into three groups: group 1 as readily adsorbable substances, group 2 as weak acids and group 3 as anionic substances.

additional clean-up step. Mostly a washing procedure with an aqueous TBABr–KBr solution (Fig. 1) is sufficient.

The different results obtained on applying the three pretreatment methods allow some general conclusions to be drawn on the structure of the sulphur compounds isolated. Method 1 preconcentrates only highly adsorbable substances with a relatively small number of anionic functional groups and therefore hydrophobic in character. On acidifying according to method 2 weak acids and phenols are converted into their protonated uncharged form and thus gain hydrophobicity. Adsorption of the protonated substances in addition to the originally non-polar compounds occurs. Finally ion-pair formation (method 3) converts most of the sulphonic acids originally present in anionic form into uncharged complexes so that they readily adsorb on the RP-C<sub>18</sub> phase.

The operationally defined character of the substances according to the methods applied leads to the fractions given in Fig. 3.

From the additional information, conclusions on the sources of pollution and on the behaviour of the substances in water treatment can be drawn. The River Rhine in Öhningen (23 km from Lake Constance) seems to be influenced less by industrial waste water. Natural organic sulphur compounds and some biotransformed lignin sulphonates can explain the dominance of the substances isolated according to method 2. The Rhine at Düsseldorf (732 km) not only reflects a much higher degree of pollution (85 µg S l<sup>-1</sup>) but also a higher relative amount of IOS. Poorly biodegradable aromatic sulphonic acids from the production or use of detergents, dyes, drugs, etc., may contribute to the mixture of compounds present.

The identification of single compounds is demonstrated by an example. The application of IC, which has become a well established method [17,18], leads to an analytical fractionation of the compounds in the extract from ion-pair adsorption (method 3).

Liquid chromatograms obtained with DAD and fluorescence detection are shown in Fig. 4a. It is clearly seen that the UV absorption is highly disturbed by the background absorption of compounds that possibly also form ion pairs and need not necessarily contain sulphur, such as acids of the humic type. The combination of  $\lambda(\text{ex}) = 230$  nm and  $\lambda(\text{em}) = 340$  nm for fluorescence detection leads to a much clearer chromatogram. How-

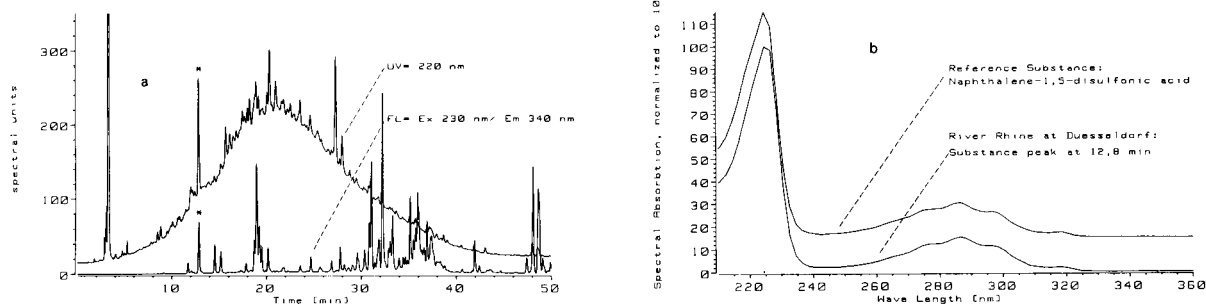


Fig. 4. (a) LC of naphthalene-1,5-disulphonic acid with UV (DAD) and fluorescence detection and (b) its identification in River Rhine water from Düsseldorf from its UV spectrum.



TABLE 1

Amounts of the naphthalene-1,5-disulphonic acid in bank filtrate of River Rhine water and its behaviour during water-treatment steps

Sample	Naphthalene-1,5-disulphonic acid ( $\mu\text{g l}^{-1}$ )
Bank filtrate	3.5 (100%)
After ozonation	1.8 (51%)
After activated carbon filtration	< 0.1 (< 3%)

ever, one must bear in mind that the lack of sulphur specific detection methods does not allow a clear assignment of sulphur containing fractions. The availability of UV-visible spectra for some of the industrially synthesized sulphonic acids, however, allows an identification of the compounds. Figure 4b shows the good match of the UV spectrum of naphthalene-1,5-disulphonic acid and the DAD spectrum of the peak marked with an asterisk in Fig. 4a. Calibration gave a concentration of  $3 \mu\text{g l}^{-1}$  of naphthalene-1,5-disulphonic acid in a river water sample from Düsseldorf. The limited availability of reference materials and the complexity of partly biotransformed samples make further identification and quantification difficult.

According to general practice in producing drinking water from river water by bank filtration and water treatment, naphthalene-1,5-disulphonic acid was followed on its way through a treatment plant. Table 1 shows that little is removed by bank filtration. The poorly biodegradable and adsorbable character of the compound can explain that observation. Ozonation of the bank filtrate, followed by activated carbon filtration, is able to decrease the concentration to levels ( $< 0.1 \mu\text{g l}^{-1}$ ) that are acceptable for drinking water supply.

### Conclusions

Hydrophilic organic substances in aqueous systems have been widely neglected in water analysis. They range from naturally occurring compounds to anthropogenic products that lead to marked pollution, especially of surface waters. The need for analytical methods for the investigation of this situation is clear. Organically bound

sulphur is a major contributor to the man-made pollution of aquatic systems and has to be monitored. The variety of individual compounds and their biotransformation require integrated information on their occurrence. Sum parameters with low detection limits are necessary to reach that goal. The use of solid-phase adsorption after ion-pair formation has proved to be a promising method that not only supplies integrated information on the group of compounds but also includes the possibility of their analytical fractionation. Identification of the individual compounds is still difficult, limited by the availability of reference compounds. However, the example of naphthalenedisulphonic acid showed that it is achievable. The methods described are suitable for following the real concentrations of organic sulphur compounds in surface waters and in their passage through water-treatment procedures. The application of mass spectrometry for the identification of hydrophilic compounds seems promising. Answers can be expected on the type of organically bound sulphur (e.g.,  $-\text{SH}$ ,  $-\text{SO}_3^-$ , heterocyclic). Additional information on the fate of organic sulphur compounds in aquatic systems and on the ecological implications is urgently needed.

### REFERENCES

- 1 F.H. Frimmel, in E.M. Perdue and E.T. Gjessing (Eds.), *Organic Acids in Aquatic Ecosystems*, Wiley, Chichester, 1990, p. 5.
- 2 P. Wölfel, Dissertation, Universität Karlsruhe, Karlsruhe, 1974.
- 3 S.A. Huber and F.H. Frimmel, *Anal. Chem.*, 63 (1991) 2122.
- 4 Deutsche Einheitsverfahren zur Wasser-, Abwasser- und Schlammuntersuchung: DIN 38 409, H14: Bestimmung der adsorbierbaren organischen Halogene (AOX), Beuth Verlag, Berlin, 1985.
- 5 F.H. Frimmel, K. Haberer and K.-E. Quentin, Ermittlung der Belastung von Fließgewässern mit organischen Heteroverbindungen, DVGW-Schriftenreihe Wasser Nr. 107 (1988) 65.
- 6 H.-J. Brauch, M. Fleig and W. Kühn, Vorkommen wichtiger organischer Mikroverunreinigungen im Rhein unter Berücksichtigung des Zusammenhangs von Einzelstoffanalytik und Summenparametern sowie der Trinkwasserrelevanz, 46. Jahresbericht der Arbeitsgemeinschaft Rhein-Wasserwerke, Karlsruhe, 1989, pp. 60–131.

- 7 E.A. Clarke and R. Anliker, in O. Hutzinger (Ed.), *Handbook of Environmental Compounds, Part A, Vol. 3*, Springer, Berlin, 1980, p. 181.
- 8 W. Giges, A.C. Alder, P.H. Brunner, A. Marcomini and H. Siegrist, *Tenside Surfact. Deterg.*, 26 (1989) 95.
- 9 K.H. Schweer, F. Fuchs and H. Sontheimer, *Wasser*, 45 (1975) 29.
- 10 S. Schullerer, G. Koschenz, H.-J. Brauch and F.H. Frimmel, *Wasser*, 78 (1992) 229.
- 11 B. Raue, H.-J. Brauch and F.H. Frimmel, *Fresenius' Z. Anal. Chem.*, 340 (1991) 395.
- 12 J. Weiss, *Handbuch der Ionenchromatographie*, VCH, Weinheim, 1985.
- 13 Deutsche Einheitsverfahren zur Wasser-, Abwasser- und Schlammuntersuchung, DIN 39 405, D 19: Bestimmung von Sulfat mit der Ionenchromatographie, Beuth Verlag, Berlin, 1984.
- 14 S. Schullerer, H.-J. Brauch and F.H. Frimmel, *Wasser*, 75 (1990) 83.
- 15 S. Schullerer, Thesis, Universität Karlsruhe, Karlsruhe, 1992.
- 16 M. Schnitzler, G. Levay, W. Kühn and H. Sontheimer, *Wasser*, 61 (1983) 263.
- 17 E. Tomlinson, T.H. Jefferies and C.M. Riley, *J. Chromatogr.*, 159 (1978) 315.
- 18 C.T. Hung and R.B. Taufer, *J. Chromatogr.*, 202 (1980) 333.

# Determination of arsenic residues in agricultural products of Milos island

G.E. Miliadis and K.S. Liapis

*Pesticide Residues Laboratory, Benaki Phytopathological Institute, 7 Ekalis Str., 145 61 Kifissia, Athens (Greece)*

(Received 8th September 1992; revised manuscript received 23rd February 1993)

## Abstract

A geothermal plant was shut down and part of the agricultural production was destroyed in 1989 on the island of Milos following the claims of a private laboratory about arsenic residues in olive oil samples. Analysis by two methods of the same olive oil and fruit and vegetables of the island showed no residues of arsenic. The silver diethyldithiocarbamate method was applied for olive oil, with a limit of determination of  $0.02 \mu\text{g g}^{-1}$ . The recovery of arsenic was 86–98% at  $0.025$ – $0.1 \mu\text{g g}^{-1}$  fortification levels.

*Keywords:* UV-Visible spectrophotometry; Arsenic; Foods; Olive oil

The historic island of Milos is located in the Aegean sea. Electric energy produced from a geothermal pilot plant was introduced on the island in 1985. In 1989 a private laboratory, belonging to an ecological organization, claimed to have found, among others, high concentrations of arsenic residues in olive oil samples taken from the island. The residues found were attributed by that organization to pollution by the geothermal plant. As a result, unrest arose among the inhabitants of the island, they destroyed part of their agricultural production and they demanded and finally succeeded in having the plant shut down. The value of this plant is estimated to be 7 million dollars.

In this work a study was undertaken to reinvestigate the occurrence of arsenic in samples from Milos island.

*Correspondence to:* G.E. Miliadis, Pesticide Residues Laboratory, Benaki Phytopathological Institute, 7 Ekalis Str., 145 61 Kifissia, Athens (Greece).

## EXPERIMENTAL

Samples were collected, in January 1989, by Agronomists of the Ministry of Agriculture. Olive oil samples were taken from the same six containers that the private laboratory had sampled. Two separate 1-l glass bottles were filled with olive oil from each container. The containers contained 200–800 kg of olive oil and emanated from six different olive oil producers of the island. Agricultural products other than olive oil were also sampled: 2-kg samples of lemons, oranges, tangerines, spinach and chicory and samples of cabbage and lettuce were taken from various farms at locations adjacent to the geothermal plant. The samples were forwarded to the laboratory and analysed within 1 week.

The dry ashing procedure [1] was applied to the olive oil samples. According to this method, 20 g of olive oil were mixed with MgO and cellulose powder and water was added. The slurry formed was dried at  $100^\circ\text{C}$  and pre-charred under

an infrared lamp.  $\text{Mg}(\text{NO}_3)_2 \cdot 6\text{H}_2\text{O}$  was added, the sample was ashed at  $550^\circ\text{C}$  and the resulting residue was dissolved in HCl and transferred into an evolution flask.

Fruits and vegetables were analysed by the wet digestion procedure [2]. According to this procedure, 25 g of homogenized sample were gently heated with  $\text{HNO}_3$  and  $\text{H}_2\text{SO}_4$  until evolution of brown nitrogen oxide fumes. The temperature was then raised and  $\text{HNO}_3$  was added in small increments periodically to prevent sample charring. Heating was continued until  $\text{SO}_3$  fumes appeared. A 25-ml volume of ammonium oxalate was then added slowly and heating was continued until all the water had evaporated and the  $\text{H}_2\text{SO}_4$  began to fume. The sample was then cooled to room temperature, diluted with water and transferred into an evolution flask.

Arsenic was determined in all samples by the silver diethyldithiocarbamate (Ag-DDC) method [1]. KI and  $\text{SnCl}_2 \cdot 2\text{H}_2\text{O}$  were added to the evolution flask, then zinc (arsenic free) was added and the arsine evolved during 2 h, after passing through lead acetate-coated glass-wool, was absorbed in a pyridine solution of Ag-DDC to give a red colour. The colour intensity, which is related to the arsenic content in the sample, was measured with a spectrophotometer at 536 nm against Ag-DDC solution.

## RESULTS AND DISCUSSION

The dry ashing procedure that has been used with various categories of food [1,3] was applied in this work to olive oil. The treatment was found to be suitable and simple. The well established wet digestion procedure [4] was applied to fruits and vegetables. The reagent blanks that were carried out with each set of samples produced zero absorbance in the spectrophotometer.

Calibration graphs were prepared, for each batch of Ag-DDC solution, by adding appropriate volumes of  $\text{As}_2\text{O}_3$  solution, containing 0.2, 0.5, 1, 2 and 3  $\mu\text{g}$  of  $\text{As}_2\text{O}_3$ , to the evolution flask and evolving the arsine according to the above method. Olive oil from other regions of Greece, that produced zero absorbance in the spectropho-

TABLE 1

Recovery of arsenic added to olive oil at different levels

Addition ( $\mu\text{g g}^{-1}$ )	Mean recovery (%) <sup>a</sup>	R.S.D. (%) <sup>a</sup>
0.025	86	8.2
0.05	98	11.7
0.1	95	7.6

<sup>a</sup> Three analyses of each sample.

tometer after been treated according to the method, was used as a control sample.

The recovery of arsenic from olive oil was determined by spiking olive oil control samples with known amounts of  $\text{As}_2\text{O}_3$  and analysing each spiked sample to determine the concentration of arsenic. Table 1 gives the recoveries and relative standard deviations (R.S.D.s) obtained at various fortification levels.

As can be seen, the recoveries values ranged from 86 to 98% and the R.S.D.s from 7.6 to 11.2%. These values are within the accepted range for residue determinations [5]. The limit of determination was  $0.02 \mu\text{g g}^{-1}$  for arsenic in olive oil and  $0.01 \mu\text{g g}^{-1}$  for arsenic in fruits and vegetables.

No arsenic residues were detected in any of the olive oil, fruit and vegetable samples that were analysed. The results obtained in this laboratory were collaboratively verified by analysis of the same olive oil samples in an official laboratory in another European country by atomic absorption spectrometry, with a detection limit of  $0.05 \mu\text{g g}^{-1}$ .

It is of particular interest that the private organization that originally reported arsenic contamination revised their first results, giving a new series of results ca. 400% lower than the initial values. This difference was attributed by them to malfunctioning of the ashing apparatus during the original analyses, and they finally claimed to have found arsenic residues in olive oil at levels up to  $50 \mu\text{g g}^{-1}$ , a value which is 2500 times above the determination limit of our method. It should also be emphasized that the olive oil samples that were analysed in this work and found to be free from arsenic originated from the same containers that the private organization had sam-

pled. There is no evidence of significant arsenic losses due to adsorption on container walls [6,7].

It must be mentioned that the samples of olive oil that were analysed in this work were taken at the same time period as those taken by the private organization. Although from another study in New Zealand arsenic residues in lakeweed were possibly associated with geothermy [8], the results of this study gave no evidence for arsenic residues in agricultural products from Milos island.

Considering the adverse economic effects that was caused by the partial destruction of the 1989 agricultural production in Milos due to fears about arsenic residues and by the shutting down of the geothermal plant, it is concluded that any data concerning toxic residues in agricultural products and foods should be considered with extreme care and should be verified collaboratively before being released.

#### REFERENCES

- 1 H.K. Hundley and J.C. Underwood, *J. Assoc. Off. Anal. Chem.*, 53 (1970) 1176.
- 2 G. Zweig and J. Sherma, *Analytical Methods for Pesticides and Plant Growth Regulators*, Vol. X, Academic, New York, 1978, p. 385.
- 3 G.M. George, L.J. Frahm and J.P. McDonnell, *J. Assoc. Off. Anal. Chem.*, 56 (1973) 793.
- 4 R.G. Lewis, *Residue Rev.*, 68 (1977) 123.
- 5 P.A. Greeve, in A. Ambrus and R. Greenhalgh (Eds.), *Pesticide Residue Analysis*, WHO/FAO, Rome, 1984, p. 281.
- 6 National Bureau of Standards, Special Publication No. 260, US Department of Commerce, Washington, DC, 1973, p. 50.
- 7 J.E. Portmann and J.P. Riley, *Anal. Chim. Acta*, 31 (1964) 509.
- 8 R.J. Lancaster, M.R. Coup and J.W. Hughes, *N. Z. Vet. J.*, 19 (1971) 141.

# Determination of butyltin ion species by ion-exchange chromatography with inductively coupled plasma mass spectrometric and spectrofluorimetric detection

J.I. Garcia-Alonso and A. Sanz-Medel

*Department of Physical and Analytical Chemistry, Faculty of Chemistry, University of Oviedo, Julian Claveria s/n, 33007 Oviedo (Spain)*

L. Ebdon

*Plymouth Analytical Chemistry Research Unit, Department of Environmental Sciences, University of Plymouth, Drake Circus, Plymouth PL4 8AA (UK)*

(Received 29th September 1992; revised manuscript received 29th March 1993)

## Abstract

Separation of mono-, di- and tributyltin (TBT) ions was accomplished by ion-exchange chromatography (Zorbax SCX 250 × 4.6 mm, 10 μm particle size) using a relatively little (30%) methanol containing eluent with 5% acetic acid and 0.05 M ammonium citrate. This low methanol content allowed sensitive detection by inductively coupled plasma mass spectrometry (ICP-MS) and micellar spectrofluorimetry after post-column reaction with morin in a Brij-35 micellar solution. Detection limits ( $3\sigma$ ) for TBT were 0.2 and 1.5 ng (as Sn), respectively, for 100 μl injection. Inductively coupled plasma atomic emission spectrometry (ICP-AES) was also tested as detection system with much lower sensitivity. The spectrofluorimetric method was applied to the determination of TBT in blind aqueous solutions supplied by the Community Bureau of Reference (BCR) of the EC after preconcentration on ODS cartridges and elution with a methanol–water–acetic acid mixture (80:17:3, v/v/v). The relative standard deviation ranged from 3 to 7% for 5 independent analyses of each of 4 samples and the accuracy obtained by the proposed method was satisfactory.

**Keywords:** Fluorimetry; Inductively coupled plasma mass spectrometry; Ion exchange; Liquid chromatography; Butyltin ions; Micellar systems; Tin; Waters

The determination of tributyltin ions (TBT) and their degradation products dibutyltin (DBT) and monobutyltin (MBT) in waters and sediments is a matter of growing environmental concern due to the extensive use of TBT-based antifouling paints to protect sea vessels and its adverse effects against non-target organisms like shellfish. The Community Bureau of Reference (BCR) of

the EC has undertaken the task of preparing a sediment Certified Reference Material [1] for its use in the development and application of reliable analytical procedures for TBT determination in environmental samples.

Different techniques have been proposed for the determination of TBT and its degradation products in environmental samples [2–16] and virtually all of them include a chromatographic technique (gas, supercritical fluid or liquid chromatography) coupled to a selective or specific detector. Gas chromatography (GC) after chemi-

*Correspondence to:* L. Ebdon, Plymouth Analytical Chemistry Research Unit, Department of Environmental Sciences, University of Plymouth, Drake Circus, Plymouth PL4 8AA (UK).

cal derivatization (alkylation [2–5] or hydride formation [6–8]) is one of the most popular techniques for butyltin analysis. Chau and Wong [9] recommend the use of non-conventional selective or specific detectors for speciation work. The flame photometric detector is very selective for tin and has been one of the most commonly applied, in spite of its instability [2–5]. Other specific detectors proposed include mass spectrometry (MS) [2], atomic absorption spectrometry (AAS) [6–8] and microwave plasma-MS [10]. Supercritical fluid chromatography (SFC) with inductively coupled plasma (ICP)-MS detection has also been proposed for tin speciation [11] but the separation obtained was not suitable for trialkyltin compounds.

Liquid chromatography (LC) offers several advantages over GC. First, the separation can be performed at room temperature without the need for derivatization. Thus, sample preparation and manipulation are minimized. Moreover, a larger variety of separation mechanisms can be explored and also a larger number of detector systems can be tested which could give the required sensitivity and selectivity. Ion-exchange chromatography (IEC) for organotin compounds was proposed by Jewett and Brickman [12] using graphite furnace atomic absorption spectrometry (GFAAS) detection. The separation of TBT and DBT ions was accomplished using a 70:30 (v/v) methanol-water eluent containing 0.06 M ammonium citrate. Similar conditions were used by Ebdon and coworkers [13,14] for the determination of TBT using AAS [13] or spectrofluorimetric detection [14]. ICP-MS can also be applied with the advantages of lower detection limits and specific Sn detection [15,16]. However, the high methanol content in the eluent reduces significantly the achievable sensitivity compared to pure aqueous solution [15]. In order to improve the sensitivity of ICP-MS detection Suyani et al. [17] applied micellar LC for the separation of alkyltin compounds and ICP-MS detection. Unfortunately TBT could not be eluted adequately with the conditions used in such micellar separation [17].

In this paper we present an improved separation scheme which allows the determination of TBT, DBT and MBT in 12 min using ICP-MS or

spectrofluorimetric detection. A relatively reduced methanol content in the ion-exchange eluent used increased the sensitivity for ICP-MS and spectrofluorimetric detection.

## EXPERIMENTAL

### *Instrumentation*

The chromatographic system used consisted of an LKB Model 2150 high-pressure pump (Bromma, Sweden), a Rheodyne 7125 sample injector fitted with a 100- $\mu$ l sample loop and a Zorbax SCX 250  $\times$  4.6 mm i.d., 10  $\mu$ m particle size ion-exchange column. The spectrofluorimetric detector used was a Perkin-Elmer Model LS-3 spectrofluorimeter equipped with a 12- $\mu$ l flow cell. Excitation and emission wavelengths were set at 408 and 534 nm respectively using 10-nm slits. The output from the detector was fed to a BBC Master 128 microcomputer during the optimization stage and to a Shimadzu CR3A integrator for quantitative analysis. The post-column reagent was pumped, using a Gilson HP4 peristaltic pump, to a PTFE mixing T-joint. A 2 m  $\times$  0.5 mm i.d. PTFE reaction coil was placed between the T-joint and the detector. Excitation and emission spectra were measured with a Shimadzu RF-5000 spectrofluorimeter.

ICP-atomic emission spectrometry (AES) detection was carried out with a Perkin-Elmer Model 5000 emission spectrometer using a cross-flow nebulizer connected to the output of the chromatographic column. Best signal-to-noise ratio was obtained at the wavelength of 303.41 nm.

ICP-MS detection was made with a VG PlasmaQuad II instrument at the most abundant Sn mass (120 a.m.u.). The output from the column was fed to a concentric nebulizer fitted in a Scott-type refrigerated spray chamber.

### *Reagents*

All chemicals used were of analytical-reagent grade unless stated otherwise. Milli-Q water (Millipore) was used throughout this work. MBT, DBT and TBT were obtained as their chlorides from Sigma and used as received. TBT acetate

was supplied by the BCR. Stock solutions (1000  $\mu\text{g ml}^{-1}$  as Sn) were prepared in LC-grade methanol. Working solutions were prepared daily in water by dilution of the stock. Morin (2',3,4',5,7-pentahydroxyflavone) was obtained from Sigma and a 0.1% stock solution was prepared in methanol. Brij-35 [polyoxyethylene(23) dodecanol], a non-ionic surfactant, was obtained from Aldrich and prepared as a 10% solution in water.

The chromatographic eluent, prepared freshly every day, consisted of 0.05 M ammonium citrate (Merck), 5% (v/v) acetic acid (Merck) and 30% (v/v) methanol in Milli-Q water, with final degassing using He for 10 min. ODS Sep-pak cartridges (Millipore) were used for the preconcentration of TBT in aqueous solutions.

#### Procedures

**Preconcentration.** TBT contained in 100 ml of the aqueous sample was preconcentrated by passing the volume through ODS Sep-Pak cartridges at 4  $\text{ml min}^{-1}$  with the help of a peristaltic pump. The ODS cartridges were previously conditioned with 5 ml of methanol and 5 ml of water. Elution was carried out with 5 ml of a 80% methanol and 3% aqueous acetic acid solution. This solution was injected directly for quantification.

**Chromatographic separation.** Optimum operating conditions for the separation of MBT, DBT and TBT were obtained using 0.05 M ammonium citrate, 5% acetic acid and 30% methanol in Milli-Q water as eluent at 1  $\text{ml min}^{-1}$  flow-rate. Those conditions could be slightly changed for better sensitivity using ICP-MS detection.

**ICP-MS.** ICP-MS operating conditions are summarized in Table 1. The output from the column was fed directly to the input port of the concentric nebulizer. The forward power had to be increased to 1800 W when nebulizing a 30% methanol solution with a moderate increase in the reflected power (up to 22 W). Chromatograms were obtained with the single-mass monitoring program which allowed the determination of the peak heights and areas of the chromatographic peaks. 1535 channels of the multi-channel analyser were used to collect each chromatogram (1006 s).

TABLE 1

ICP-MS operating conditions

Forward power	1800 W
Reflected power	22 W
Nebulizer flow-rate	0.65 $\text{l min}^{-1}$
Cooling flow-rate	14 $\text{l min}^{-1}$
Auxiliary flow-rate	0.5 $\text{l min}^{-1}$
Spray chamber	110 ml; double-pass, water cooled
Mass monitored	120 a.m.u.
Dwell time	0.655 s

**Post-column reaction and spectrofluorimetric detection.** Optimum sensitivity for TBT detection was obtained with 0.6% Brij-35 and 0.005% morin at pH 3.5. The flow-rate of this post-column derivatization reagent was 1.5  $\text{ml min}^{-1}$ . Excitation and emission wavelengths selected were 408 and 534 nm respectively providing the highest analytical signals for TBT determinations.

## RESULTS AND DISCUSSION

#### Chromatographic separation

The initial aim of this work was to obtain chromatographic conditions that allowed the detection of the three ionic butyltin compounds in the same chromatogram. Previous conditions applied by us [13–15], as derived from those proposed by Jewett and Brickman [12], did not allow the elution of MBT or DBT from the column. DBT could be eluted using ammonium citrate instead of ammonium acetate [12] but MBT, probably in hydrolysed form, was strongly retained by the ion-exchange support. The use of acetic acid in the eluent proved to be the solution to this problem. This allowed also the reduction of the methanol content in the eluent from 80% [14,15] to just 30% as stated before. Figure 1 shows the variation of the retention time of MBT, DBT and TBT with acetic acid concentration in the eluent. As can be observed MBT is eluted practically in the dead volume of the column and is not affected by the acetic acid concentration above 3%. TBT is eluted next and finally DBT. The elution order observed did not follow the expected order for an ion-exchange separation:



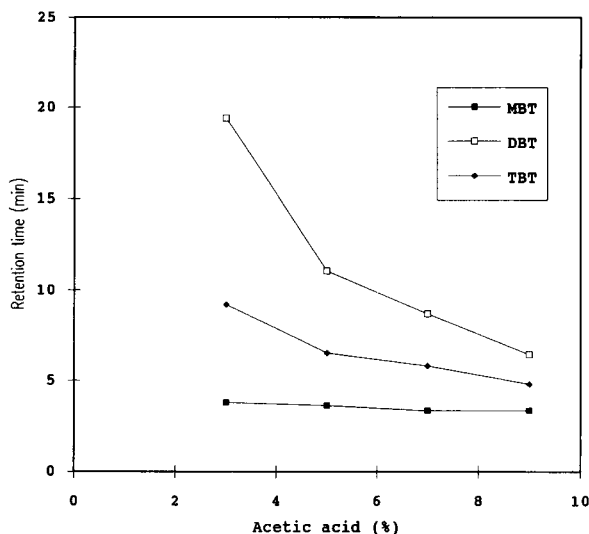


Fig. 1. Influence of acetic acid concentration on the retention time for MBT, DBT and TBT. [Methanol] = 30% (v/v). [Ammonium citrate] = 0.05 M.

the fact that MBT (which should have a 3+ charge) elutes close to the dead volume could indicate the formation of hydrolysed species, perhaps  $\text{MBTO}^+$ .

The observed influence of ammonium citrate concentration, using 5% acetic acid and 30% methanol, is given in Fig. 2. As can be observed the retention time for TBT is reduced initially with citrate concentration but it stabilizes above 0.03 M ammonium citrate. We think that above this concentration the retention mechanism for TBT is no longer governed by ion-exchange, but hydrophobic interactions with the chromatographic support are responsible for this effect. The retention of DBT follows a more usual ion-exchange pattern, although hydrophobic interactions could take place as well. MBT retention time increases slightly as the ammonium citrate concentration is increased. Figure 3 shows the influence of the concentration of methanol for 5% acetic acid and 0.05 M ammonium citrate. The abrupt changes in retention times between 20 and 40% methanol for DBT and TBT indicate that hydrophobic interactions play a major role in the separation mechanisms involved. At the chromatographic conditions selected finally (30% methanol, 5% acetic acid and 0.05 M ammonium

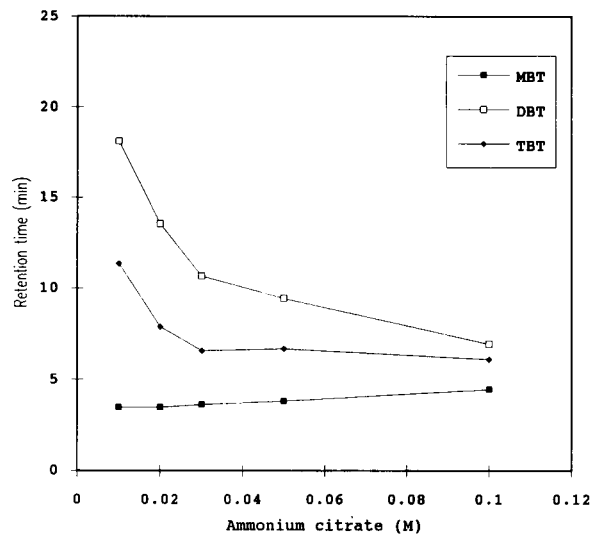


Fig. 2. Influence of ammonium citrate concentration on the retention time for MBT, DBT and TBT. [Methanol] = 30% (v/v). [Acetic acid] = 5% (v/v).

citrate) the capacity factor for TBT is close to 1 which is considered optimum for LC determination.

#### ICP-MS detection of butyltin compounds

Tin has 10 naturally occurring isotopes among which  $^{120}\text{Sn}$  is the most abundant. Single-mass

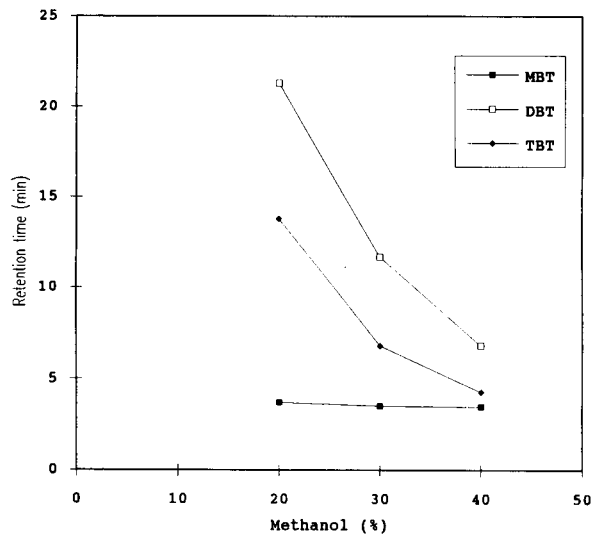


Fig. 3. Influence of methanol concentration on the retention time for MBT, DBT and TBT. [Ammonium citrate] = 0.05 M. [Acetic acid] = 5% (v/v).

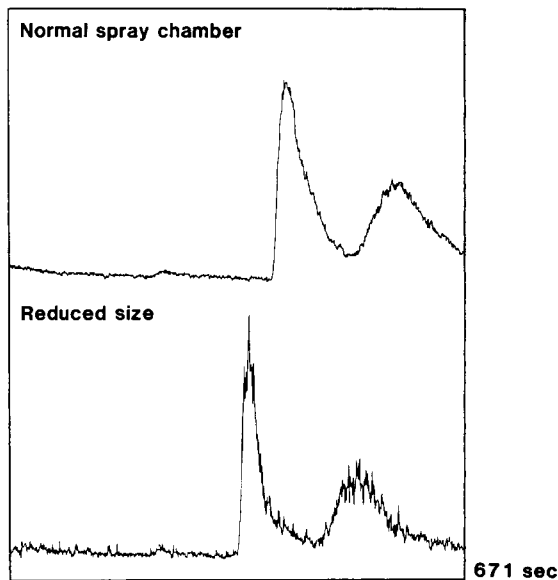


Fig. 4. Comparison of standard and smaller spray chambers for ICP-MS detection of DBT and TBT.

monitoring at this mass was selected. Optimum sensitivity for a TBT standard solution containing 30% methanol was accomplished with 1800 W forward power and  $0.65 \text{ l min}^{-1}$  nebulizer flow-rate. Both parameters were critical for optimum sensitivity. Two different spray chambers were tested in order to reduce detector band broadening to a minimum. Figure 4 compares the results obtained with a conventional Scott-type double-pass spray chamber (internal volume 110 ml) and a laboratory-constructed reduced-size spray chamber of only 11 ml volume. The separation of TBT and DBT peaks is improved by the use of the small spray chamber. However, the reflected power increased to 70 W and the signal-to-noise ratio worsened drastically (see Fig. 4). The conventional water-cooled spray chamber was then selected in spite of its greater band broadening problems.

Tin sensitivity was strongly affected by the methanol concentration in the eluent. Figure 5 shows the chromatograms obtained for the separation of 100 ng of each of DBT and TBT at various methanol concentrations (ammonium citrate concentration 0.03 M and acetic acid content 5%). As can be observed, the peak area corre-

sponding to TBT decreased as the methanol content increased. The TBT peak areas for the three chromatograms shown are close to the ratio 1:2:4, which is indicative of exponential decay, as observed previously [15]. Sensitivity was not greatly affected, however, by the ammonium citrate or by the acetic acid concentration in the eluent. The peak shape for both TBT and DBT improved as the acetic acid content was increased from 3 to 9%, and this effect was more noticeable for DBT, which showed a pronounced skewing.

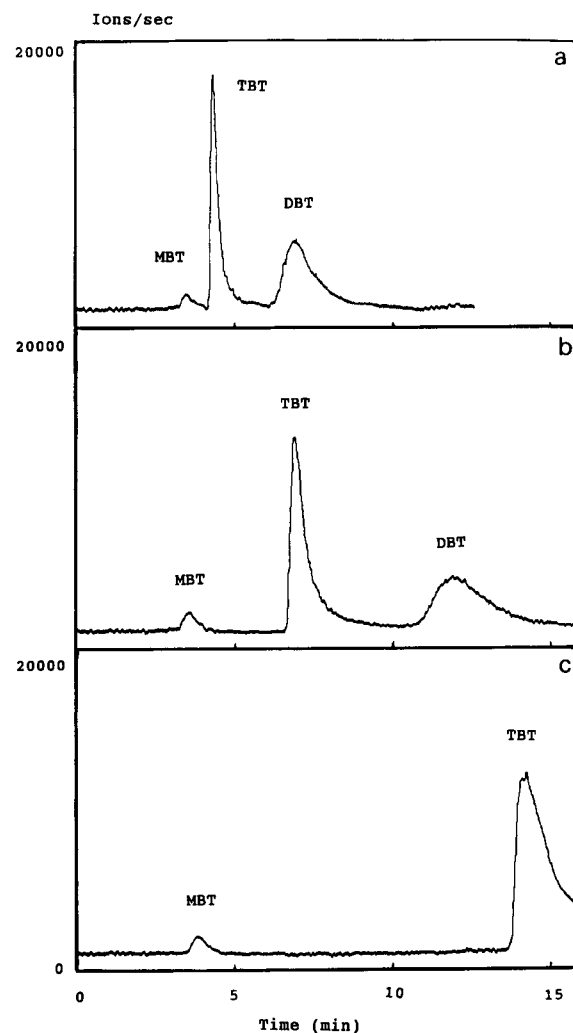


Fig. 5. Influence of methanol concentration on the separation of DBT and TBT with ICP-MS detection. (a) 40; (b) 30; (c) 20% (v/v).

Peak skewing was not affected by the ammonium citrate concentration. In Fig. 5 the small peak close to the dead volume corresponds to MBT impurities in the DBT standard. The MBT peak was identified by spectrofluorimetry (see below). Both the acetic acid and methanol used showed detectable quantities of Sn impurities. A typical background count rate for the eluent was ca. 1000 ions  $s^{-1}$ . Taking into account background noise the detection limit was calculated as 0.7 ng of TBT acetate (0.2 ng of Sn), which is similar to other detection limits found with ICP-MS [15,16]. Calibration for TBT was linear up to 1000 ng of TBT injected both in peak height or peak area mode.

#### ICP-AES detection of butyltin compounds

ICP-AES was also tested as a possible alternative for Sn detection after LC separation. A 10  $\mu g ml^{-1}$  TBT acetate solution was prepared in 30% methanol, 5% acetic acid and 0.05 M ammonium citrate in order to optimize the ICP-AES detection conditions. Using the 189.99-nm Sn(II) line no difference was detected between the sample and the blank for a range of ICP operating conditions. Atomic lines gave better sensitivity but presented highly structured background. The best signal-to-background ratio was obtained for the 303.41-nm Sn(I) line, which is rated as the seventh best for Sn in aqueous solutions [18]. Simplex optimization was carried out at this line and an optimum background equivalent concentration of 0.01  $\mu g ml^{-1}$  of TBT acetate was found. Due to this low sensitivity observed in our eluent no actual chromatogram was run with ICP-AES detection.

#### Spectrofluorimetric detection of butyltin compounds

Organotin compounds have no native fluorescence but can be made fluorescent by forming a chelate with an organic reagent like morin (2',3,4',5,7-pentahydroxyflavone). Morin is known to form fluorescent chelates with inorganic tin in acid media and with dialkyltin compounds in organic solvents [19,20], but the reaction was reported to be poorly sensitive for TBT [20]. In a previous paper [14] we have demonstrated that

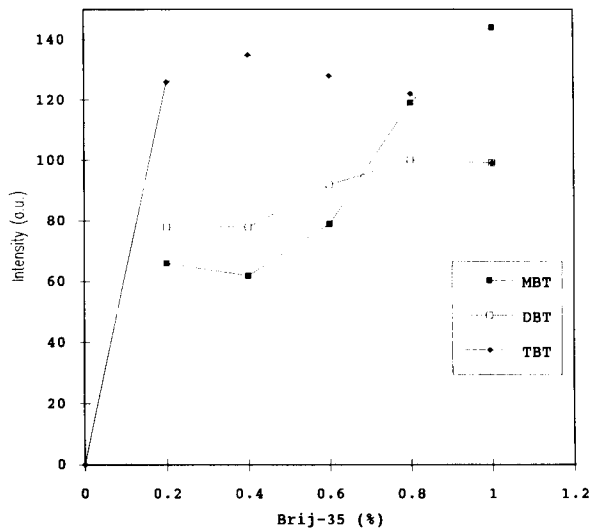


Fig. 6. Effect of Brij-35 concentration in the post-column reagent on the peak height for MBT, DBT and TBT with spectrofluorimetric detection.

TBT could be detected spectrofluorimetrically with morin in the presence of non-ionic surfactants. However, the high methanol content in the eluent used there (80%) reduced the attainable sensitivity due to disruption of the micellar medium. Using 30% methanol in the eluent, Brij-35 proved to be the surfactant of choice. Figure 6 shows the influence of the concentration of Brij-35 on the fluorescence signal (peak height) obtained for MBT, DBT and TBT after post-column reaction at pH 3.5. Optimum sensitivity for TBT was obtained with 0.2–0.6% Brij-35. It is clear that both MBT and DBT would require higher Brij-35 concentrations for optimum signal. No signal for TBT was observed in the absence of surfactant as described previously [14].

When the post-column reagent contained only morin and Brij-35, the pH at the exit of the detector was 3.5 due to the 5% acetic acid in the eluent. TBT reacts better with morin at higher pH values [14]. Thus a detailed study of the optimum pH was carried out by adding different amounts of sodium acetate to the post-column reagent and measuring the signal and the resulting pH at the exit of the detector. Figure 7 shows the results obtained in peak height mode. Both MBT and DBT show optimum values at pH 3.5–4,

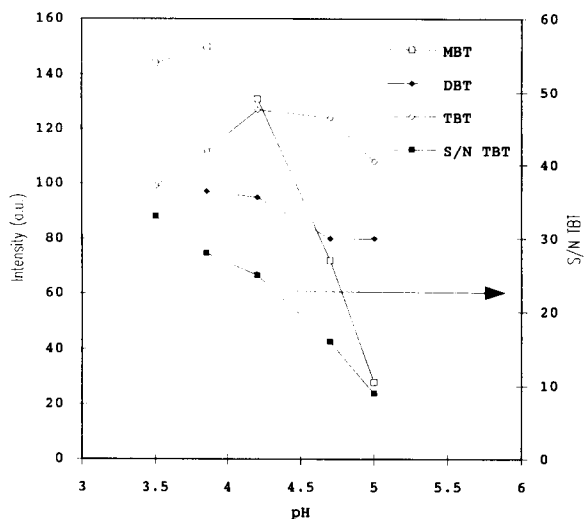


Fig. 7. Influence of pH on the peak height for MBT, DBT and TBT with spectrofluorimetric detection and on the signal-to-noise (*S/N*) ratio for TBT.

whereas TBT signal was maximum at pH 4.5. The baseline intensity and noise, however, increases with the pH. Figure 7 shows also the signal-to-noise ratio observed for TBT at different pH values. Based on these data a pH of 3.5 (i.e., no addition of sodium acetate) was selected. The height of the TBT peak was independent of the morin concentration above 0.003% morin up to 0.010% (m/v). The baseline signal increased slowly with morin concentration and a compromise value of 0.005% was selected for the morin concentration.

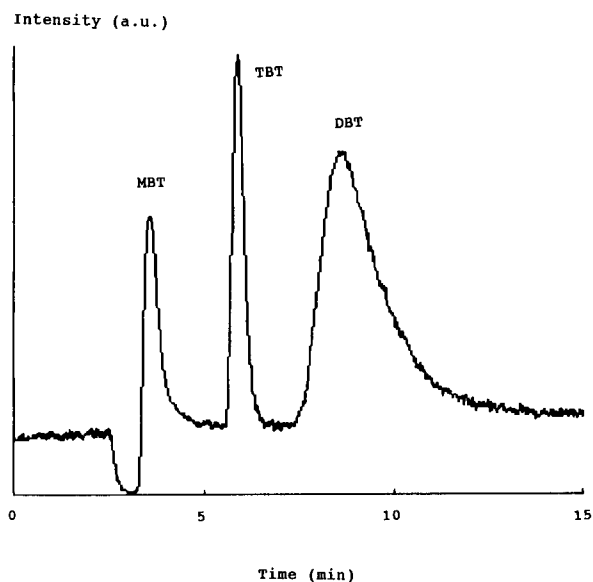


Fig. 8. Typical chromatogram for the separation of MBT, DBT and TBT with spectrofluorimetric detection under the recommended conditions.

Under these conditions, a typical chromatogram for 200 ng of MBT, DBT and TBT injected with spectrofluorimetric detection is shown in Fig. 8. The fluorescence signal was fed to a BBC microcomputer as described previously [21]. As can be observed MBT elutes close to the dead volume, then TBT and finally DBT (which shows a poor peak profile).

Analytical performance characteristics for TBT determination were obtained using a chromato-

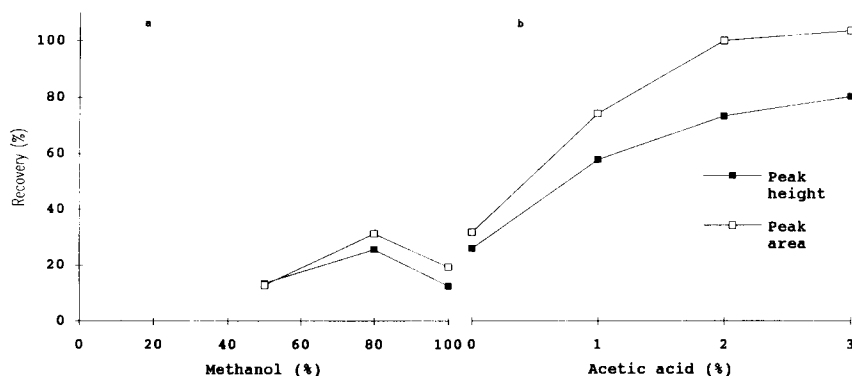


Fig. 9. Recovery for the elution of TBT from ODS Sep-pak cartridges using various methanol and acetic acid concentrations. (a) [Acetic acid] = 0% (v/v), (b) [Methanol] = 80% (v/v).

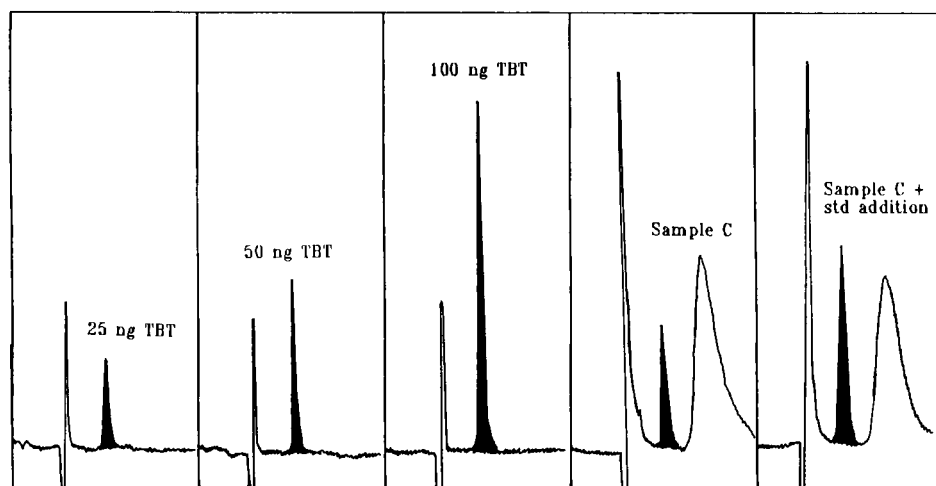


Fig. 10. Determination of TBT in blind aqueous solutions. Chromatograms obtained for the analysis of sample C containing MBT, DBT and TBT.

graphic integrator. The calibration graph for TBT was linear up to 1500 ng of TBT acetate injected both in peak area and peak height mode. The slopes of the log–log calibrations were, however, 0.9028 and 0.9831 for peak area and peak height respectively. Precision was also better in peak height mode. Typical values ranged from 2.2 to 5.1% for 25, 50 and 100 ng TBT acetate injected. Detection limit, calculated from three times the standard deviation of the baseline, was 5 ng of TBT acetate (1.5 ng Sn).

#### *Preconcentration of TBT in waters*

Organotin compounds present in waters are usually preconcentrated using long and tedious solvent extraction procedures [1]. Different extractants have been proposed in the presence [2,4] or absence [22–24] of tropolone. However, solid-phase extraction, which simplifies the sample preparation stage, can be applied. Kadokami et al. [25] used bonded-phase extraction with ODS cartridges and tetrahydrofuran–acetic acid (95 + 5) containing 0.5% (m/v) tropolone for the elution of the organotin compounds. In our previous paper [14] we observed that TBT was quantitatively retained on a 4 cm × 4.6 mm i.d., 10 μm particle size ODS chromatographic column. In order to develop a preconcentration method which could be used when and where the samples

are collected, we investigated commercially available ODS preconcentration cartridges for TBT preconcentration from waters in situ.

The Sep-pak ODS cartridges were conditioned with 10 ml of methanol and washed with 10 ml of water. The retention of TBT from spiked standard aqueous solutions was found to be quantitative as 5 ml of 1–2.5 μg ml<sup>-1</sup> of TBT in water passed through the cartridge were injected in the LC system, using the spectrofluorimetric procedure previously described, and no TBT could be detected in the eluate for those samples. In order to study the elution of TBT from the ODS cartridge, the following procedure was applied: 5 ml of the aqueous TBT standard solutions were loaded on a new, conditioned Sep-Pak cartridge, 10 ml of water were injected and then succes-

TABLE 2

Analysis of blind aqueous samples (BCR) by the present method and by interlaboratory studies

Sample	TBT found <sup>a</sup> (μg ml <sup>-1</sup> )	S.D. <sup>b</sup> (n = 7)	TBT found <sup>c</sup> (μg ml <sup>-1</sup> )	S.D. <sup>b</sup> (n = 12) <sup>d</sup>
A	3.22	0.14	2.61	0.32
B	3.02	0.22	2.71	0.15
C	3.05	0.10	2.74	0.32
D	2.87	0.13	2.59	0.30

<sup>a</sup> This work. <sup>b</sup> S.D. = Standard deviation. <sup>c</sup> Mean of interlaboratory studies. <sup>d</sup> 12 laboratories.

TABLE 3  
Some LC methods for the determination of TBT

Species detected	Column used	Mobile phase	Detector used	TBT detection limit (ng ml <sup>-1</sup> as Sn)	Reference
MBT, DBT, TBT	Zorbax SCX-10 250 × 4.6 mm	30% Methanol 5% Acetic acid 0.05 M Ammonium citrate	ICP-MS Spectrofluorimetry	2 1.5	This work
DBT, TBT, TPT	Partisil SCX-10 250 × 4.6 mm	70% Methanol 0.06 M Ammonium citrate	GFAAS	80	12
TBT	Partisil SCX-10 250 × 4.6 mm	80% Methanol	FAAS	100	13
TBT	Partisil SCX-10 250 × 4.6 mm	0.1 M Ammonium acetate 80% Methanol	Spectrofluorimetry	90	14
TBT, TPT	Partisil SCX-10 250 × 4.6 mm	0.15 M Ammonium acetate 80% Methanol	ICP-MS	9	15
MBT, DBT, TBT	Partisil SCX-10 250 × 4.6 mm	60% Methanol 0.18 M Ammonium citrate pH = 6	ICP-MS	0.2	16
MMT, MBT, DMT, DBT, DPT, TMT, TBT, TPT	TSK gel ODS-80TM 250 × 4.6 mm	54% THF 8% Acetic acid 0.2% Tropolone	FAAS	25	25
TBT, TBT, TMT	SCX	80% Methanol 0.2 M Ammonium acetate pH = 4	Flame LEAFS <sup>a</sup>	35	26
TBT, TPT, TMT	Spherisorb ODS-2 250 × 4.6 mm	80% Methanol 1% Acetic Acid 0.004 M Sodium pentane sulphonate	ICP-MS	2	28
TBT, TPT, TMT	Absorbophere SCX-5 250 × 4.6 mm	85% Acetonitrile 0.1 M Ammonium acetate	ICP-MS	4	28
TBT, DBT	Cyanopropil Silica-5 250 × 4.6 mm	Toluene 7.5 mg l <sup>-1</sup> Tropolone	GFAAS	20	27

<sup>a</sup> LEAFS = laser-excited atomic fluorescence spectrometry.

sively 5 ml of the selected eluent passed through. 100  $\mu\text{l}$  of this eluate were injected in the LC system and peak height and peak area for the TBT peak were compared with those obtained for the standard aqueous solution. Figure 9 shows the results obtained for the different eluents tested containing various amounts of methanol, water and acetic acid. In the absence of acetic acid recovery values were generally low (Fig. 9a). Using 80% methanol in the eluent the recovery in peak area mode was quantitative when 2–3% acetic acid was added (Fig. 9b). Recovery values in the peak height mode approached only 80% due to the wider peaks obtained when TBT was injected in the preconcentration eluent instead of in an aqueous standard.

#### *Analysis of blind aqueous TBT samples*

Four aqueous samples containing traces of TBT and various interfering tin compounds were supplied by the BCR. TBT acetate standard was also supplied for calibration purposes. For quantitative analysis the samples had to be diluted (100 and 10000 times) prior to the actual measurement. Sample A contained only TBT; sample B contained TBT and inorganic tin; sample C contained MBT, DBT and TBT and sample D contained TBT and TPT (triphenyltin). 1 ml of each sample was diluted to 100 ml with water and subjected to the preconcentration procedure described with the help of a peristaltic pump at 4 ml  $\text{min}^{-1}$ . TBT standards were prepared in the preconcentration eluent. Seven independent dilutions were made for each sample and two of them were spiked with 1.25 and 2.5  $\mu\text{g}$  of TBT acetate, respectively, to check for recovery. All samples were then directly analysed against a calibration graph. As an example, Fig. 10 shows the chromatograms obtained for the analysis of sample C with and without the addition of 2.5  $\mu\text{g}$  of TBT acetate and the type of calibration obtained. Mean overall recovery for the four samples was found to be 70.6% (range 68.6–72.3%) based on the slopes of the plot TBT spiked vs. TBT found. Table 2 shows the final results in the original samples taking into account such recovery factors along with the mean results provided by the inter-comparison exercise. In all cases our results are

higher than the mean of the laboratories but no significant differences were found. It has to be taken into account that all those samples were prepared at 3.00  $\mu\text{g ml}^{-1}$  originally by BCR before being sent for interlaboratory comparison.

#### *Conclusions*

A separation method for MBT, DBT and TBT was developed allowing for the elution of all three butyltin compounds in less than 12 min. Detection limits were in the  $\leq \text{ng ml}^{-1}$  range, by ICP-MS, which also offered higher selectivity.

Table 3 compares the present results with those obtained by other LC methods published for TBT determination, in which most of the separations are carried out on strong cation-exchange columns with eluents containing a high methanol concentration. In general, the lowest detection limits are obtained by ICP-MS [15,16,27], which could be further improved by decreasing the methanol concentration by using larger injection volumes and by decreasing tin contamination in the eluant by, perhaps, using an on-line chelating column just before the injector.

Spectrofluorimetry, after post-column reaction with morin in a micellar solution, provided less sensitivity but the instrumentation was cheaper, which is an added advantage for low-budget laboratories. The spectrofluorimetric method was applied to the determination of TBT in blind aqueous solutions provided by the BCR of the EC with satisfactory results. The preconcentration of TBT from waters on ODS cartridges provided a viable alternative to the other methods.

The provision of a research grant to J.I.G.A. by the University of Oviedo in order to perform the ICP-MS measurements in Plymouth (UK) is gratefully acknowledged.

#### REFERENCES

1. L. Ebdon, S.J. Hill and B. Griepink, *Env. Technol. Lett.*, 9 (1988) 965.
2. I. Tolosa, J.M. Bayona, J. Albaigés, L.F. Alencastro and J. Tarradellas, *Fresenius' J. Anal. Chem.*, 339 (1991) 646.
3. T. Ishizaka, S. Nemoto, K. Sasaki, T. Suzuki and Y. Saito, *J. Agric. Food Chem.*, 37 (1989) 1523.

- 4 R.J. Maguire, Y.K. Chau, G.A. Bengert, E.J. Hale, P.T.S. Wong and O. Kramar, *Environ. Sci. Technol.*, 16 (1982) 698.
- 5 G.B. Jiang, P.S. Maxwell, K.W.M. Siu, V.T. Luong and S.S. Berman, *Anal. Chem.*, 63 (1991) 1506.
- 6 M. Chamsaz, I.M. Khasawneh and J.D. Winefordner, *Talanta*, 35 (1988) 519.
- 7 R.C. Forster and A.G. Howard, *Anal. Proc.*, 26 (1989) 34.
- 8 Ph. Quevauviller and O.F.X. Donard, *Fresenius' J. Anal. Chem.*, 339 (1991) 6.
- 9 Y.K. Chau and P.T.S. Wong, *Fresenius' J. Anal. Chem.*, 339 (1991) 640.
- 10 H. Suyani, J. Creed, J. Caruso and R.D. Satzger, *J. Anal. At. Spectrom.*, 4 (1989) 777.
- 11 W.-L. Shen, N.P. Vela, B.S. Sheppard and J.A. Caruso, *Anal. Chem.*, 63 (1991) 1491.
- 12 K.L. Jewett and F.E. Brickman, *J. Chromatogr. Sci.*, 19 (1981) 583.
- 13 L. Ebdon, S.J. Hill and P. Jones, *Analyst*, 110 (1985) 515.
- 14 L. Ebdon and J.I. Garcia Alonso, *Analyst*, 112 (1987) 1551.
- 15 S. Branch, L. Ebdon, S. Hill and P. O'Neill, *Anal. Proc.*, 26 (1989) 401.
- 16 J.W. McLaren, K.W.M. Siu, J.W. Lam, S.N. Willie, P.S. Maxwell, A. Palepu, M. Koether, and S.S. Berman, *Fresenius' J. Anal. Chem.*, 337 (1990) 721.
- 17 H. Suyani, D. Heitkemper, J. Creed and J. Caruso, *Appl. Spectrosc.*, 43 (1989) 962.
- 18 P.W.J.M. Boumans, *Line Coincidence Tables for ICP-AES*, Pergamon Press, Oxford, 1984.
- 19 W. Langseth, *Talanta*, 31 (1984) 975.
- 20 Y. Arakawa, O. Wada and M. Marabe, *Anal. Chem.*, 55 (1983) 1901.
- 21 L. Ebdon, J.I. Garcia Alonso, S.J. Hill and A. Hopkins, *J. Automat. Chem.*, 9 (1987) 132.
- 22 C. Donaghy, M. Harriott and D.T. Burns, *Anal. Proc.*, 26 (1989) 260.
- 23 M. Chamsaz and J.D. Winefordner, *J. Anal. At. Spectrom.*, 3 (1988) 119.
- 24 D. Adelman, K.R. Hinga and M.E.Q. Pilson, *Environ. Sci. Technol.*, 24 (1990) 1027.
- 25 K. Kadokami, T. Uehiro, M. Morita and K. Fuwa, *J. Anal. At. Spectrom.*, 3 (1988) 187.
- 26 A.P. Walton, G.-T. Wei, Z. Liang, R. Michel and J.B. Morris, *Anal. Chem.*, 63 (1991) 232.
- 27 A. Astruc, R. Lavigne, V. Desauziers, R. Pinel and M. Astruc, *Appl. Organomet. Chem.*, 3 (1989) 267.
- 28 H. Suyani, J. Creed, T. Davidson and J. Caruso, *J. Chromatogr. Sci.*, 27 (1989) 139.



# Solid-phase extraction and spectrofluorimetric determination of triphenyltin in environmental samples

R. Compañó, M. Granados, C. Leal and M.D. Prat

*Departament de Química Analítica, Universitat de Barcelona, Avda. Diagonal 647, 08028 Barcelona (Spain)*

(Received 8th September 1992; revised manuscript received 30th November 1992)

## Abstract

The effects of several micellar and aqueous–organic media on the fluorescence of the 3-hydroxyflavone–triphenyltin complex are reported. The relationship between emission intensity and experimental variables was studied in order to establish a spectrofluorimetric method for the determination of triphenyltin in a micellar medium of Triton X-100. Linear calibration graphs were obtained in the ranges 0.1–10, 5–120 and 50–400  $\mu\text{g l}^{-1}$  Sn as triphenyltin. The detection limit was 0.07  $\mu\text{g l}^{-1}$ . The stoichiometric composition of the complex was determined to be 1 : 1, with  $\log K_f = 7.0$ . The solid-phase extraction of triphenyltin from sea water with  $\text{C}_{18}$  cartridges was studied. The breakthrough volume was greater than 1 l. Elution profiles with methanol and a solution of 3-hydroxyflavone in methanol were obtained. A concentration factor of up to 100 was achieved.

**Keywords:** Fluorimetry; Sample preparation; Extraction; Preconcentration; Sea water; Solid-phase extraction; Triphenyltin; Waters

Organotin compounds have found widespread industrial applications as biocides, antifouling paints, catalysts and PVC stabilizers. As a result, there are a variety of pathways for their entry into the environment. Although inorganic tin in natural media is basically harmless, some organotin compounds, especially tri-substituted organotin species (tributyl and triphenyl), are highly toxic [1]. Therefore, there is a need for methods for the determination of these compounds, which should be sensitive and able to distinguish between species.

Determination is usually carried out by atomic spectrometric techniques, coupled with a chromatographic or a vaporization separation method [2–5]. Liquid chromatography has also been coupled with spectrofluorimetric detection and morin

has been described as a sensitive pre- or postcolumn fluorogenic reagent for the simultaneous determination of dialkyltin and diphenyltin compounds [6–8]. However, there are large differences in fluorescence intensities among different organotin–morin systems, and early studies showed that this reaction was not sufficiently sensitive for the detection of triorganotin compounds. Further studies have shown that the use of aqueous micellar media enhances the fluorescence of tributyl and triphenyl species and improves their determination [9,10]. 3-Hydroxyflavone, which is similar to morin in structure, has also been used for the determination of triphenyltin in different substrates [11–14] after extraction with hydrocarbon solvents, but no reference to micellar enhancement of fluorescence has been found.

In this work, the fluorescence of the complex of triphenyltin (TPHT) with 3-hydroxyflavone in micellar media and the use of this ligand in the

*Correspondence to:* R. Compañó, Departament de Química Analítica, Universitat de Barcelona, Avda. Diagonal 647, 08028 Barcelona (Spain).

presence of Triton X-100 for the determination of TPhT in sea-water samples were studied. The fluorescence of this complex proved to be much greater than that given by the morin chelate.

As some organotin compounds, including TPhT, are toxic at very low trace levels, preconcentration processes are common in their analysis, even when sensitive detection techniques are used. Among the preconcentration techniques, liquid–liquid extraction is a classical approach, and its advantages and disadvantages are well known. More recently, solid-phase extraction (SPE) has been recognized as an attractive technique for the enrichment of trace constituents and it has been applied to a broad range of samples, including environmental samples. In this field SPE has been reported as a suitable technique for the preconcentration of organotin compounds [9,15–17]. In this work the SPE of TPhT from sea water on an octadecyl phase was optimized, in combination with the spectrofluorimetric method developed.

## EXPERIMENTAL

### *Apparatus*

Fluorescence measurements were made on a Perkin-Elmer LS-50 spectrofluorimeter equipped with a xenon discharge lamp and 10-mm silica cells. The slit widths were set to 5 nm in both the excitation and emission monochromators, unless stated otherwise. The spectrofluorimeter was calibrated daily using a Perkin-Elmer fluorescence intensity standard of ovalene. All fluorescence data are given without spectral correction. Measurements were performed at 20°C in a thermostated room.

A Radiometer pHM64 pH meter equipped with an Orion combined electrode was used for pH measurements.

The preconcentration step was achieved using a Gilson Minipuls peristaltic pump. As adsorption of TPhT on the pump tubes was observed, with either standard, silicone or Solvaflex tubes, a reverse pumping manifold was used in the preconcentration step, the sample being aspirated through the column.

All glassware used for experiments was previously soaked in 10% nitric acid for 24 h and rinsed with doubly deionized water.

Disposable 1-ml SPE columns (average particle diam., 40  $\mu\text{m}$ ), containing 100 mg of octadecyl ( $\text{C}_{18}$ ) (Bond Elut; Analytichem International) and octyl ( $\text{C}_8$ ), phenyl (Ph) and cyano (CN) (Supelclean; Supelco) bonded silica were used in the TPhT extractions.

### *Reagents*

Doubly-deionized water (Culligan Ultrapure GS) of 18.3 M $\Omega$  cm resistivity was used to prepare solutions.

*Tin(IV) solutions.* A standard solution of 1 g l<sup>-1</sup> Sn(IV) (Merck) in 5 M hydrochloric acid was used. Working solutions were prepared daily by diluting this standard solution with 0.01 M HCl. Stock solutions (0.5 g l<sup>-1</sup> tin) of triphenyltin (TPhT), tributyltin (TBT), dibutyltin (DBT), trimethyltin (TMT), diphenyltin (DPhT) and monophenyltin (MPHT) were prepared by dissolving the corresponding chlorides (Fluka or Aldrich, purity > 95%) in methanol, while tricyclohexyltin (TCHT) chloride was dissolved in cyclohexane. These stock solutions were stored at 4°C in dark glass bottles and appropriate dilutions were prepared freshly prior to use by dilution with water, except for TCHT, which was diluted with methanol.

*3-Hydroxyflavone (FIOH) solution.* The reagent was purchased from Aldrich and 1  $\times 10^{-3}$  and 4  $\times 10^{-3}$  M methanolic solutions were prepared daily.

*Morin solution.* A 1  $\times 10^{-3}$  M solution in methanol was prepared from the reagent supplied by Merck

*Surfactant solutions.* Stock aqueous solutions of 0.05 M Triton X-100 (Merck), 5  $\times 10^{-3}$  M Brij-35 (Scharlau), 0.05 M cetyltrimethylammonium bromide (CTAB) (Merck) and 0.4 M sodium lauryl sulphate (SLS) (Merck) were prepared.

*Buffer solutions.* The buffer solutions used were 0.05 M formic acid–sodium hydroxide, 0.05 M acetic acid–sodium hydroxide, 0.05 M succinic acid–sodium hydroxide, 0.05 M Tris–hydrochloric acid and 0.05 M ammonium chloride–ammonia.

### Fluorimetric determination of triphenyltin

Transfer up to 5 ml of sample solution, containing 0.004–3  $\mu\text{g}$  (as TPhT tin) into a 25-ml volumetric flask. Add 5 ml of Triton X-100 solution, 0.5 ml of  $1 \times 10^{-3}$  M FIOH solution and 2.5 ml of 0.05 M succinate buffer solution (pH 5.5) and dilute to volume with water. Measure the fluorescence intensity at 490 nm against a reagent blank, using an excitation wavelength of 392 nm. Use a calibration graph obtained from standard TPhT solutions treated in the same way.

### Solid-phase extraction

Condition the disposable  $C_{18}$  cartridge by rinsing with 5 ml of methanol at a flow-rate of  $1 \text{ ml min}^{-1}$ , followed by 10 ml of a  $35 \text{ g l}^{-1}$  sodium chloride solution at pH 2 at a flow-rate of  $5 \text{ ml min}^{-1}$ . During this activation process, care must be taken to keep the column wet. Pump a known sample volume, between 100 ml and 1 l, through the column at a flow-rate of  $5 \text{ ml min}^{-1}$ . After extraction has been achieved, wash the column with 10 ml of water, in order to remove any residual inorganic ions, and dry it by drawing room air through the cartridge for about 5 min. Elute with 2 ml of  $1 \times 10^{-4}$  M FIOH solution in methanol at a flow-rate of  $0.5 \text{ ml min}^{-1}$  in the back-flush mode. Collect the eluate in a 10-ml volumetric flask, add 2 ml of Triton X-100 solution and 1 ml of buffer solution, dilute to volume with water and measure the fluorescence intensity at 490 nm using an excitation wavelength of 392 nm.

**Caution:** TPhT is toxic by inhalation and if swallowed and is an irritant to the eyes and skin. The use of suitable protection for eyes, skin and respiratory tract is strongly recommended when handling the pure substance and its stock solutions.

## RESULTS AND DISCUSSION

### Fluorimetric studies

The effect of micellar solutions of SLS, CTAB, Triton X-100 and Brij-35 on the fluorescence intensity of the TPhT–FIOH complex was studied. Although the complex exhibited fluorescence

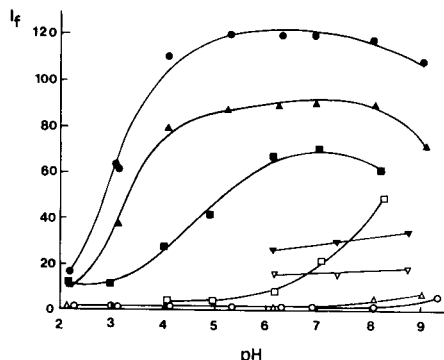


Fig. 1. Effect of pH on the fluorescence intensity of TPhT–FIOH complex in micellar media. ● = Triton X-100,  $6 \times 10^{-3}$  M; ▲ = Brij-35,  $1.8 \times 10^{-3}$  M; ▼ = SLS,  $1.6 \times 10^{-1}$  M; ■ = CTAB,  $1.8 \times 10^{-2}$  M. Open symbols are the corresponding blank fluorescence intensities. [TPhT] =  $50 \mu\text{g as Sn l}^{-1}$ ; [FIOH] =  $4 \times 10^{-5}$  M.

in all the media tested, large differences were observed between the surfactants. Figure 1 shows the relative fluorescence intensity as a function of pH in different media. The highest intensity was obtained in Triton X-100 micellar solutions and the lowest in SLS. In the latter medium the fluorescence was similar to those observed in aqueous–organic media, such as methanol–water or acetonitrile–water. The higher fluorescence obtained in the presence of non-ionic surfactants compared with other micellar media agrees with the fluorescence enhancement observed for the TBT complex of morin in those micellar media [10].

Instability of the triphenyltin chloride–FIOH complex in benzene or toluene solutions, which has been attributed to the quenching effect of chloride ions [12,13], was not observed in Triton X-100 micellar medium.

The fluorescence characteristics of FIOH with other organotin compounds, including phenyl derivatives (DPhT and MPhT) and trialkyl derivatives (TMT, TBT, TCHT), were also studied. Measurements were made in Triton X-100 at different pH values (in the range 2–8) and no appreciable fluorescence was obtained, except for DPhT, which showed an emission about 20 times lower than TPhT. Although it has been reported

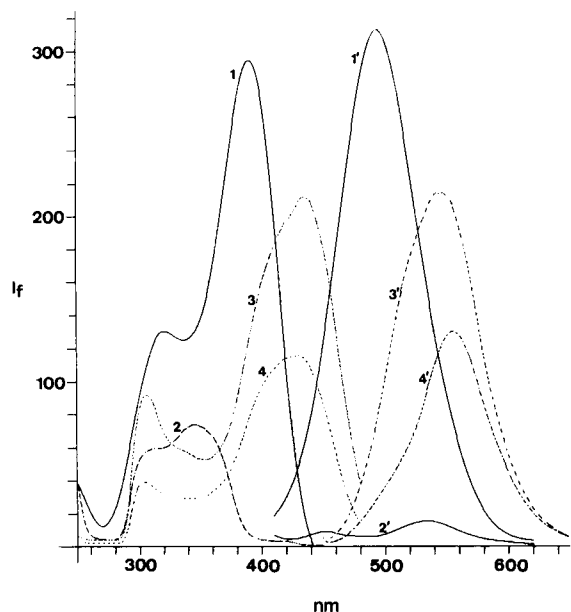


Fig. 2. Fluorescence spectra of TPhT complexes of FIOH and morin. 1, 1' = excitation and emission spectra of TPhT complex of FIOH; 2, 2' = corresponding blank spectra; [TPhT] =  $50 \mu\text{g as l}^{-1} \text{ Sn}$ ; [FIOH] =  $2 \times 10^{-5} \text{ M}$ ; [Triton X-100] =  $9 \times 10^{-3} \text{ M}$ ; pH = 5.5. 3, 3' = excitation and emission spectra of TPhT complexes of morin; 4, 4' = corresponding blank spectra; [TPhT] =  $200 \mu\text{g l}^{-1} \text{ Sn}$ ; [morin] =  $8 \times 10^{-5} \text{ M}$ ; [Triton X-100] =  $2.5 \times 10^{-2} \text{ M}$ ; pH = 5.5.

that TMT forms fluorescent complexes with FIOH when extracted in toluene, no signal was detected from Triton X-100 micellar solutions, even for relatively high concentrations. Inorganic tin(IV) also gave a fluorescent complex, with an intensity of about 40% of that of the TPhT.

Comparison between the TPhT–FIOH and TPhT–morin systems showed that the former fluoresces much higher (about 15 times) than the latter, making FIOH more sensitive than morin for the determination of triphenyltin. Figure 2 shows the excitation and emission spectra of both complexes in Triton X-100 at pH values corresponding to maximum emission.

*Effects of experimental variables.* The influence of the experimental variables on the fluorescence intensity of the TPhT–FIOH complex in Triton X-100 micellar media was tested at a tin level of  $50 \mu\text{g l}^{-1}$ . As can be seen in Fig. 1, the fluores-

cence intensity was maximum and constant in the pH range 5–8. Further work was carried out at pH 5.5, obtained with a succinic acid–sodium succinate buffer.

The fluorescence intensity increased when the concentration of FIOH was increased up to  $1 \times 10^{-5} \text{ M}$  (corresponding to an FIOH to TPhT molar ratio of ca. 25). Higher concentrations of FIOH had no effect on the fluorescence intensity. A  $2 \times 10^{-5} \text{ M}$  concentration was chosen for subsequent work to ensure an excess of ligand.

Studies on the effect of surfactant concentration showed that the fluorescence reaches a maximum at a Triton X-100 concentration of  $3 \times 10^{-3} \text{ M}$  (ten times the critical micellar concentration). At higher concentrations the intensity remained constant. Concentrations lower than  $1.5 \times 10^{-3} \text{ M}$  could not be studied because precipitation of the ligand and the complex occurred.

Concentrations of methanol below 25% (v/v) had little effect on the fluorescence of the complex. Above this level there was a marked decrease in intensity with increasing concentration of alcohol until, on reaching 50% (v/v), the intensity was identical with that obtained without surfactant.

In all experiments the blank values were low and almost independent of the experimental variables. The order in which the reagents were mixed had no influence on the fluorescence intensity.

The fluorescence intensity decreased on increasing the temperature of the solution. A coefficient of  $0.8\% \text{ } ^\circ\text{C}^{-1}$  was obtained between 15 and  $35^\circ\text{C}$ . For practical reasons, a temperature of  $20^\circ\text{C}$  was used in subsequent measurements.

The fluorescence intensity reached a maximum in a few seconds and remained constant for at least 6 h.

*Characteristics of the fluorimetric method.* Under the experimental conditions outlined for the fluorimetric determination of TPhT, there is a linear relationship between fluorescence intensity and TPhT concentration in the ranges  $5\text{--}120 \mu\text{g l}^{-1} \text{ Sn}$  as TPhT (5-nm slits for both emission and excitation monochromators) and  $0.1\text{--}10 \mu\text{g l}^{-1}$  (10-nm slits for both monochromators). Linear calibration was also obtained in the range  $50\text{--}400 \mu\text{g l}^{-1}$  tin (2.5-nm slits) when the final reagent

TABLE 1

Regression data for calibration graphs

Concentration range ( $\mu\text{g l}^{-1}$ )	No. of data points	Relative slope <sup>a</sup>	Relative intercept <sup>a</sup>	$r^2$
0.1– 10	17	8.07 (0.03)	– 0.4 (0.4)	0.9998
5 –120	8	2.07 (0.02)	1.3 (1.9)	0.9996
50 –400	8	0.343 (0.004)	2.7 (1.4)	0.9991

<sup>a</sup> Values in parentheses are standard deviations.

concentration was  $1.5 \times 10^{-4}$  M. Regression data are summarized in Table 1.

The limits of detection ( $3\sigma$ ) and quantification ( $10\sigma$ ) are 0.07 and  $0.15 \mu\text{g l}^{-1}$ , respectively.

Three series of fifteen determinations on standard solutions containing 1, 20 and  $100 \mu\text{g l}^{-1}$  tin gave relative standard deviations of 3.1, 1.9 and 0.4%, respectively.

The effect of different inorganic ions on the fluorescence of the TPhT–FIOH–Triton X-100 system is shown in Table 2. The tolerance limit was taken as that concentration which did not cause more than a 5% change in the fluorescence intensity. Ions that form fluorescent complexes with FIOH, such as Al(III) or Pb(II), increased the signal obtained, whereas Fe(III), Hg(II), Cu(II), Cd(II), Ni(II), Co(II) and Zn(II) de-

TABLE 2

Maximum tolerance limits of foreign ions in the determination of  $50 \mu\text{g l}^{-1}$  Sn as TPhT

Ion added	Tolerance limit ( $\text{mg l}^{-1}$ )	
	Without masking	With masking agent
$\text{NO}_3^-$ , $\text{Cl}^-$ , $\text{Br}^-$ , $\text{I}^-$ , Li(I), Na(I), K(I), $\text{NH}_4^+$ (I)	No interference, even at high concentrations	
Ba(II), Ca(II), Mg(II), $\text{F}^-$	100 <sup>a</sup>	
Zn(II)	8	
Mn(II), Cd(II), Ni(II), Co(II)	4	
Cu(II)	1	5 <sup>a</sup> ( $\text{S}_2\text{O}_3^{2-}$ $1 \times 10^{-3}$ M)
Pb(II)	1	
Al(III)	0.8	50 <sup>a</sup> ( $\text{P}_2\text{O}_7^{4-}$ $5 \times 10^{-2}$ M)
Hg(II)	0.05	
Fe(III)	< 0.05	50 <sup>a</sup> ( $\text{P}_2\text{O}_7^{4-}$ $5 \times 10^{-2}$ M)

<sup>a</sup> The highest ratio tested.

TABLE 3

Effect of other organotin species on the determination of  $10 \mu\text{g l}^{-1}$  Sn as TPhT

Ion added <sup>a</sup>	TPhT found ( $\mu\text{g l}^{-1}$ ) <sup>a</sup>	Ion added <sup>a</sup>	TPhT found ( $\mu\text{g l}^{-1}$ ) <sup>a</sup>
MPhT ( $100 \mu\text{g l}^{-1}$ )	9.8	DBT ( $100 \mu\text{g l}^{-1}$ )	9.5
DPhT ( $100 \mu\text{g l}^{-1}$ )	11.7	TBT ( $100 \mu\text{g l}^{-1}$ )	9.8
DPhT ( $50 \mu\text{g l}^{-1}$ )	10.5	TBT ( $250 \mu\text{g l}^{-1}$ )	9.5
TMT ( $100 \mu\text{g l}^{-1}$ )	9.7	TBT ( $500 \mu\text{g l}^{-1}$ )	9.0

<sup>a</sup> Concentration as Sn.

creased the fluorescence. Addition of pyrophosphate as a masking agent overcame the interference of Fe(III) and Al(III) and thiosulphate considerably increased the tolerance limit for Cu(II). However, the interference of Hg(II), when occurring at concentrations equal to the TPhT concentration, could not be avoided. Nevertheless, inorganic ions were easily removed when SPE on a non-polar phase was performed. In spite of the great quenching observed for Hg(II), no effect was detected when methylmercury was present, even at high concentrations.

The influence of other organotin species on the determination of TPhT was also studied. The compounds selected included degradation products of TPhT and also as other organotin species that have been detected in environmental samples, such as TBT. The results obtained (Table 3) show that an excess of the compounds tested of up to a tenfold molar excess had no effect on the determination of TPhT, except for DPhT, whose tolerance limit was found to be a fivefold molar excess.

**Composition of TPhT–FIOH complex.** The stoichiometric composition of the complex was determined to be 1:1 by continuous variation and mole ratio methods. From the measurements obtained when the continuous variation method was applied, following Likussar and Boltz [18], the complex formation constant was estimated to be  $\log K_f = 7.0$ .

#### Solid-phase extraction

In a preliminary study, some silica-based bonded phases were tested (octyl, octadecyl,

phenyl and cyanopropyl). In all instances good retention of TPhT was observed, and no significant difference was detected in its elution behaviour when methanol was used as the eluting solvent. As an octadecyl ( $C_{18}$ ) bonded phase has been reported [9,15–17] to be suitable for the SPE of organotin compounds from water, all subsequent experiments were performed using  $C_{18}$  cartridges.

In order to examine the influence of the eluent on the recovery of TPhT from the  $C_{18}$  phase, methanol, acetonitrile (ACN), tetrahydrofuran (THF) and aqueous solutions of Triton X-100, which could be advantageous from the point of view of the spectrofluorimetric determination of TPhT, were assessed. In these experiments an elution flow-rate of  $1 \text{ ml min}^{-1}$  was used. ACN gave very low recovery values (about 22% with 5 ml), whereas with THF no reproducible results were obtained. This may be attributed to the low stability of TPhT in THF solutions, which is converted into diphenyltin [16]. On the other hand no elution was achieved with Triton X-100 solutions.

The best recovery results were obtained with methanol as eluent, i.e., about 85% with 5 ml of methanol. Taking into account that, in the spectrofluorimetric determination of TPhT, a low methanol content in the solution is desirable, elution from the  $C_{18}$  cartridge with methanol–water mixture (80:20) was assessed. The results were discouraging, as only a 5% of recovery was achieved using 5 ml of this mixture. This suggests that the elution behaviour of TPhT from  $C_{18}$  is rather different from that described for tributyltin, which undergoes complete elution with methanol–water containing more than 70% of methanol [9]. Based on these results, methanol was selected as the eluent.

**Breakthrough volume.** In this study some parameters concerning the nature of the matrix sample were taken into account. Because the final aim was the determination of TPhT in sea water, solutions of TPhT were prepared in an aqueous matrix containing  $35 \text{ g l}^{-1}$  of sodium chloride. Two pH conditions were studied: neutral, which approximately emulates the natural sample pH, and pH 2, which is a representative

value for stored samples. Finally, the effect of the addition of methanol to the sample was also considered.

The breakthrough characteristics were measured for solutions containing  $1 \text{ mg l}^{-1}$  of TPhT in  $35 \text{ g l}^{-1}$  sodium chloride at neutral pH, at pH 2, with 15% methanol at neutral pH and with 15% methanol at pH 2. These solutions were continuously pumped through the  $C_{18}$  columns at  $5 \text{ ml min}^{-1}$ ; 5-ml fractions were collected and retention was determined by the spectrofluorimetric procedure described above.

For a sample modified with 15% methanol at pH 2, the breakthrough volume was observed at 530 ml. In the other instances the breakthrough volume was higher than 1 l, the maximum volume examined.

**Influence of elution flow-rate.** Experiments using 5 ml of methanol as eluent were carried out in order to determine the influence of flow-rate on the TPhT recovery. Three flow-rates were tested, 3, 1 and  $0.5 \text{ ml min}^{-1}$ . When the highest flow-rate was used a 66% recovery was achieved, whereas for 1 and  $0.5 \text{ ml min}^{-1}$  no significant difference was detected and a recovery of 87% was obtained. Further experiments were performed with a flow-rate of  $0.5 \text{ ml min}^{-1}$  to ensure no influence of this parameter.

**Elution profile.** Elution profile studies were carried out with spiked sea-water samples, as previous experiments had shown some differences between the TPhT elution behaviour of synthetic and natural sea water, i.e., lower recoveries were obtained with real samples. Sea-water samples were collected from several points along the Catalanian coast (Spain), filtered through  $0.45\text{-}\mu\text{m}$  cellulose filters, acidified with HCl to pH 2 and stored in dark glass bottles at  $4^\circ\text{C}$ .

A 100-ml volume of sea water sample at pH 2, containing 15% methanol, spiked with  $5 \mu\text{g l}^{-1}$  of TPhT was pumped through the column. After rinsing, elution was performed and separate eluate fractions of 1 ml were collected. The same procedure was performed with non-spiked samples to obtain a blank elution profile. The recoveries for each fraction were determined by the spectrofluorimetric procedure after subtracting the signal of the corresponding blank fraction.

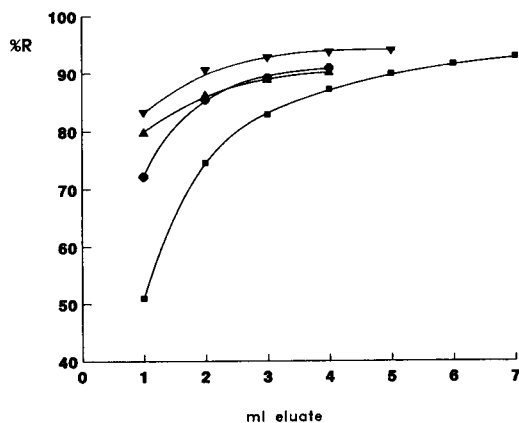


Fig. 3. Elution profiles of TPhT. (a) Sample = 100 ml of spiked sea water, pH 2, 15% methanol; eluent, ■ = methanol, ● =  $1 \times 10^{-4}$  M FIOH in methanol and ▲ =  $1 \times 10^{-4}$  M FIOH in methanol in the back-flush mode. (b) Sample = 100 ml of spiked sea water, pH 2; eluent; ▼ =  $1 \times 10^{-4}$  M FIOH in methanol in the back-flush mode.

Two eluents were tested, methanol and  $1 \times 10^{-4}$  M FIOH in methanol. The results are shown in Fig. 3. The addition of FIOH to the eluent improved the elution of TPhT; and 86% recovery was obtained with 2 ml of FIOH solution, whereas a 75% recovery was achieved with the same volume of methanol. No significant difference was observed when elution with FIOH solution was performed in the back-flush mode, i.e., with the eluent pumped through the cartridge in the opposite direction to that of the sample during the

preconcentration step. Nevertheless, better results would be expected in the back-flush mode if the sample is not modified with methanol. Hence, an elution profile of a sea-water sample containing no methanol was obtained in this mode with FIOH solution as eluent. This system led to the best elution results, i.e., a 90% recovery with 2 ml of FIOH solution. No significant retention of FIOH on  $C_{18}$  cartridges was observed.

From these results, and taking into account the spectrofluorimetric detection method described previously, the following conditions were adopted: sea-water sample not modified with methanol, 2 ml of  $1 \times 10^{-4}$  M FIOH in methanol as eluent in the back-flush mode, the eluate being collected in a 10-ml volumetric flask. In this way the solution to be measured contained 20% methanol, which has little effect on the fluorescence intensity.

**Recovery experiments.** The whole process of SPE and spectrofluorimetric determination was tested with several spiked sea-water samples. In the first step, samples from seven points along the Catalanian coast were spiked with  $2 \mu\text{g l}^{-1}$  Sn as TPhT and 100 ml of each sample were analysed in triplicate with the proposed method. In spite of the very different origins of the samples (S1 = clean area; S2 and S3 = urban areas; S4 and S5 = industrial and urban areas; S6 = trading port, S7 = sports harbour), no significant difference was found among the recoveries obtained (Table 4).

TABLE 4

Recovery of TPhT from spiked sea-water samples with 2 ml of  $1 \times 10^{-4}$  M FIOH in methanol as the eluent in the back-flush mode

Sample	Sampling area	Volume (ml)	Concentration <sup>a</sup> ( $\mu\text{g l}^{-1}$ )	Recovery <sup>b</sup> (%)
S1	Clean	100	2	87 (1)
S2	Urban	100	2	85 (6)
S3	Urban	100	2	89 (1)
S4	Urban and industrial	100	2	84 (1)
S5	Urban and industrial	100	2	88.5 (0.5)
S6	Trading port	100	2	84.5 (0.1)
S7	Sports harbour	100	2	84 (2)
S2	Urban	100	0.1	82 (1)
S7	Sports harbour	100	0.1	88 (15)
S5	Urban and industrial	1000	0.1	81 (2)

<sup>a</sup> Concentration as Sn. <sup>b</sup> Values in parentheses are relative standard deviations (%) from triplicate analyses.

In order to study the influence of TPhT concentration, in the second step two sea-water samples were spiked with  $0.1 \mu\text{g l}^{-1}$  Sn as the organotin compound and 100 ml of each were treated by the general procedure. The recoveries shown in Table 4 suggest that there is no influence of this variable.

Finally, in order to ascertain the effect of the sample volume, a 1-l sample, with a concentration of  $0.1 \mu\text{g l}^{-1}$  Sn as TPhT was analysed. No significant difference was found between this result (Table 4) and those corresponding to 100-ml samples.

### Conclusions

A method for the determination of TPhT in sea water has been developed. It combines a preconcentration procedure in a  $\text{C}_{18}$  cartridge and spectrofluorimetric detection. SPE offers a maximum concentration factor of 100, when 1-l sample is processed. Further, SPE acts as a clean-up treatment to remove the inorganic ions from the sample. On the other hand, the spectrofluorimetric method is highly sensitive, with a detection limit of  $0.07 \mu\text{g l}^{-1}$  Sn as TPhT; therefore, its combination with SPE ensures a powerful procedure for TPhT determination, which allows the detection of TPhT at  $\text{ng l}^{-1}$  levels.

The financial support of the Spanish Ministry of Education and Science (CICYT, Project

NAT91-1339) is gratefully acknowledged. C. Leal also thanks the Spanish Ministry of Education and Science for an FPI grant.

### REFERENCES

- 1 S.J. Blunden and A. Chapman, in P.J. Craig (Ed.), *Organometallic Compounds in the Environment. Principles and Reactions*, Longman, Harlow, 1986, Chap. 3.
- 2 A.O. Valkirs, P.F. Seligman, G.J. Olson, F.E. Brinkman, C.L. Matthias and J.M. Bellama, *Analyst*, 112 (1987) 17.
- 3 H. Harino, M. Fukushima and M. Tanaka, *Anal. Chim. Acta*, 264 (1992) 91.
- 4 X. Dauchy, A. Astruc, M. Borsier and A. Astruc, *Analisis*, 20 (1992) 41.
- 5 J. Ashby, S. Clark and P.G. Craig, *Spec. Publ. R. Soc. Chem.*, No. 66 (1988) 263.
- 6 T.H. Yu and Y. Arakawa, *J. Chromatogr.*, 258 (1983) 189.
- 7 W. Langseth, *Talanta*, 31 (1984) 975.
- 8 W. Langseth, *J. Chromatogr.*, 315 (1984) 351.
- 9 L. Ebdon and J.I. García-Alonso, *Analyst* 112 (1987) 1551.
- 10 W. Kleiböhmer and K. Cammann, *Fresenius' Z. Anal. Chem.*, 335 (1989) 775.
- 11 F. Vernon, *Anal. Chim. Acta*, 71 (1974) 192.
- 12 S.J. Blunden and A.H. Chapman, *Analyst* 103 (1978) 1266.
- 13 W.N. Aldrige and B.W. Street, *Analyst*, 106 (1981) 60.
- 14 P.G. Baker, D.S. Farrington and R.A. Hoodless, *Analyst*, 105 (1980) 282.
- 15 G.A. Junk and J.J. Richard, *Chemosphere*, 16 (1987) 61.
- 16 K. Kadomaki, T. Uehiro, M. Morita and K. Fuwa, *J. Anal. At. Spectrom.*, 3 (1988) 187.
- 17 O. Evans, B.J. Jacobs and A.L. Cohen, *Analyst*, 116 (1991) 15.
- 18 W. Likussar and D.F. Boltz, *Anal. Chem.*, 43 (1971) 1265.



# Determination of organochlorines in sea water: an assessment

Isabel Cruz and David E. Wells

*SOAFD Marine Laboratory, P.O. Box 101, Victoria Road, Aberdeen AB9 8DB, Scotland (UK)*

Iain L. Marr

*Chemistry Department, University of Aberdeen, Old Aberdeen, Scotland (UK)*

(Received 16th September 1992; revised manuscript received 11th January 1993)

## Abstract

Multi-matrix multi-determinand methods of analysis are needed when studying the fate and transport of trace organic compounds in the aquatic environment. These methods are cost effective and provide information about the distribution of the determinands within the sample. The current method of this laboratory for the determination of persistent organochlorine contaminants was extended to the analysis of large volumes of sea water (28 l) and suspended particles. The method was validated in each stage of the analysis by a series of experiments using spiked samples, reference materials and replicates. The results showed that the precision for the determination of the organochlorines in the aqueous and particulate fractions were similar, at the sub-nanogram per litre level, whilst the initial extraction from the sample matrix contributed over 80% of the total variance in the analysis.

*Keywords:* Gas chromatography; Organochlorines; Sea water; Ultra-trace analysis; Waters

Natural waters are ultimately contaminated from inputs from all other compartments of the environment. Effluents are discharged into rivers, lakes and seas, whilst ground waters receive leachates and run off from the land which are contaminated with persistent organic contaminants. The oceans of the world constitute the main environmental repository of persistent anthropogenic chemicals [1].

An understanding of the behaviour of pollutants in aquatic systems is necessary to assess their distribution, their fate and their ultimate environmental impact. Organochlorine pesticides (OCPs) and chlorobiphenyls (CBs) are generally hydrophobic in nature, having low solubilities in

water. They tend to associate with organic-rich sedimentary particles and are concentrated in fatty biological tissues.

In the sea water column the organochlorine (OC) contaminants are distributed between the water and the particulate material. In estuaries the bulk of the CBs are associated with the suspended solids, this fraction accounting for as much as 80% of the total CBs, on a mass to volume basis [2,3]. However, in open waters the distribution can vary with the change in particulate loading.

Any assessment of the occurrence and fate of OCs in the marine environment requires a detailed understanding of the partitioning and the dynamics of the sorption/desorption processes [4], particularly as sewage sludge or dredge spoil dumped at sea constitute a major source of anthropogenic contamination.

*Correspondence to:* I. Cruz, SOAFD Marine Lab., P.O. Box 101, Victoria Road, Aberdeen AB9 8DB Scotland (UK).

Reliable analytical methods are required to separate the sea water and particulate fractions and to determine organochlorines at the sub-nanogram per litre level in both fractions.

In this study, the accuracy and precision of an analytical method was investigated, and the source of errors identified.

## METHODS

### Sample preparation

The particulate and aqueous fractions of the sea water samples were separated with a stainless steel pressurised extraction and filtration system (PEFS) designed and built in this laboratory, and described in detail elsewhere [5,6]. In brief, the PEFS system comprises of two containers, (28 l) and a filtration holder (stainless steel) which is suitable for operation under pressure, and provides a closed system in which all separations are carried out.

Water samples were collected in the first container. The water was filtered by pressurising the system (30–40 psi N<sub>2</sub>) to force the sample through the glass fibre filter (0.7 μm pore size and 142

mm diameter) [6]. This process took 10–15 min, depending on the particle loading. The filtrate was collected in the second container, and the OCs were extracted in pentane (500 ml) with the addition of sulphuric acid (5 M; 20 ml) to assist the extraction of acidic compounds, such as pentachlorophenol [7] (PCP). The water and extraction mixture were stirred rapidly with an air-driven stirrer (3000 rpm, 5 min). After the two phases had separated (15 min), the container was pressurised and the aqueous and organic phases were collected separately. The water was discarded, while the extract in pentane was refrigerated (5°C) prior to analysis.

The pentane extract was dried with anhydrous sodium sulphate and the solvent volume reduced in a clean air stream, prior to the clean-up and group separation. The filters containing the particulate material were acidified with sulphuric acid (0.2 M; 1.5 ml) and extracted in a soxhlet with hexane–acetone (40:60) (100 ml) for 4 h, at a syphon rate of 20 cycles per hour. When the extraction cycle was completed, the water–acetone phase was washed with dilute sulphuric acid (pH 2, 250 ml), and the hexane separated and dried with anhydrous sodium sulphate. The

TABLE 1

Chromatographic conditions for the determination of organochlorine compounds

	Chlorobiphenyls and hexachlorobenzene	Organochlorine pesticides	Pentachlorophenol
Instrument	Varian 3500 with automated on-column injection	Varian 3500 with automated on-column injection	Varian 3500 with automated on-column injection
Column	CP-SIL8 50 m × 0.22 i.d., 0.2 μm phase thickness	CPSIL19 50 m × 0.22 i.d., 0.2 μm phase thickness	CP-SIL19 50 m × 0.22 i.d., 0.2 μm phase thickness
Carrier gas	Hydrogen, 35 cm s <sup>-1</sup>	Hydrogen, 40 cm s <sup>-1</sup>	Hydrogen, 40 cm s <sup>-1</sup>
Oven programme	80°C, 1 min, 3°C min <sup>-1</sup> to 270°C, hold 10 min	80°C, 1 min, 3°C min <sup>-1</sup> to 270°C, hold 10 min	80°C, 1 min, 3°C min <sup>-1</sup> to 210°C, 1 min, 10°C min <sup>-1</sup> to 270°C, hold 5 min
Injection	0.5 μl on-column	0.5 μl on-column	0.5 μl on-column
Injector	120°C, 1 min, 300°C min <sup>-1</sup> to 280°C, hold 60 min	120°C, 1 min, 300°C min <sup>-1</sup> to 280°C, hold 60 min	120°C, 1 min, 300°C min <sup>-1</sup> to 280°C, hold 60 min
Detector	ECD, 320°C	ECD, 320°C	ECD, 320°C

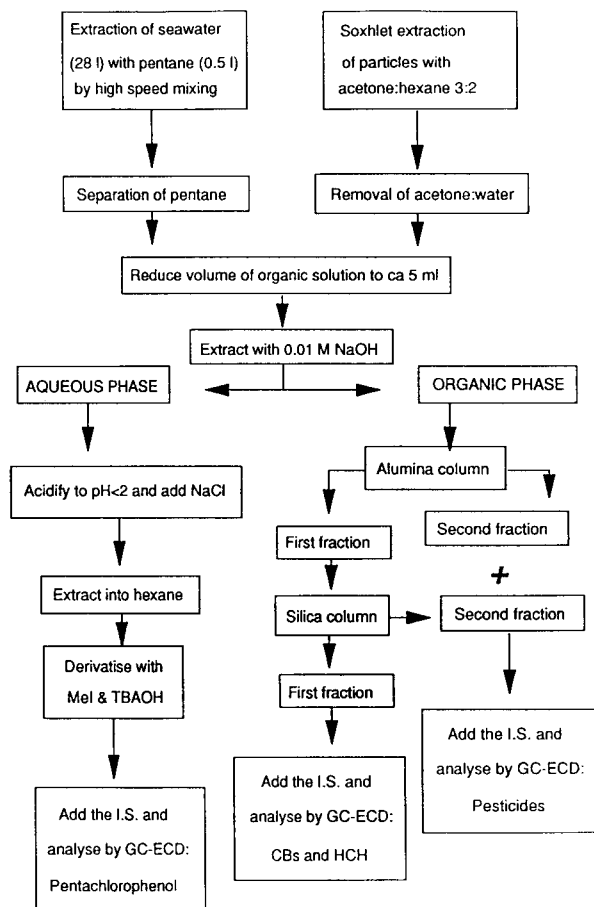


Fig. 1. Schematic diagram for the extraction, clean-up, group separation and GC-ECD determination of OCs in sea water and suspended solids.

extracts from the particles were then treated in the same manner as the water extracts.

The clean-up and group separation for CBs, hexachlorobenzene (HCB), hexachlorocyclohexane ( $\alpha$ -HCH and  $\gamma$ -HCH), DDT, dieldrin, endrin and PCP are based on the method used in this laboratory [8], and have been extended to include this particular study [5,8]. The outlines of the methodology are presented in Figure 1. Details of instrumental and chromatographic conditions for the final determination are listed in Table 1.

#### *Recovery of OCs from the aqueous fraction*

Filtered sea water (28 l), was spiked with a multi-component solution containing a mixture of

CBs and pesticides in methanol (20 ml) in the PEFS vessel. The OCs had a range of water solubilities covering four orders of magnitude. The spiked sea water was extracted, and the OCs analysed to determine the recovery of the method.

The experiment was carried out at three concentration levels: 4–3 ng l<sup>-1</sup>, 0.6–0.4 ng l<sup>-1</sup> and 0.3–0.2 ng l<sup>-1</sup> for CBs, HCB, PCP, 2,4-DDE and 4,4-DDE and 1.6–1.4 ng l<sup>-1</sup>, 0.3–0.2 ng l<sup>-1</sup> and 0.2–0.1 ng l<sup>-1</sup> for  $\alpha$ -HCH,  $\gamma$ -HCH, dieldrin, endrin, 2,4-DDT and 4,4-DDT.

There were 10 recovery trials in total, three were replicates at the highest and the lowest levels and four at the intermediate level.

The same batch of filtered sea water was also extracted to determine the background concentrations of the contaminants.

#### *Extraction of OCs from the particulate fraction*

The comparability of the analysis of the suspended particles for OC determination was studied using a contaminated sediment (Laboratory Reference Material, LRM 125 [9]). It was assumed that the mechanisms of the extraction matrix effects were comparable. The dried sediment was wetted with dilute sulphuric acid and allowed to equilibrate with the electrolyte for a minimum of 2–4 h to reconstitute the wet sediment and improve the extraction of pentachlorophenol [7].

LRM 125 (1 g portions) were analysed using the described method. The mean concentrations and coefficient of variation for the individual organochlorines were calculated, and compared with the results of the on-going quality control in this laboratory which employs soxhlet extraction (dichloromethane) of dry material.

#### *Precision of the determination of OCs by gas chromatography with electron capture detection (GC-ECD)*

The variability of the GC-ECD determination was assessed by the repeated analysis of the GC-ECD calibration solutions corresponding to the three fractions [9]. This test determined the short-term coefficient of variations associated with the instrumental errors.

### Reproducibility of the clean-up, separation and GC-ECD determination

Aliquots (1 ml) of a multi-component standard solution was subjected to clean-up, class separation and GC-ECD determination. The short-term coefficient of variation for the analytical separation, clean-up and determination was obtained.

## RESULTS AND DISCUSSION

Results for the recovery test in the aqueous fraction are given in Table 2, which lists the mean recoveries and the standard deviations for the individual congeners at each concentration level, together with the *F* factors calculated from the analysis of the variance (one-way ANOVA) [10].

The analysis of the unspiked sea water showed background levels of CB 28, 0.17 ng l<sup>-1</sup>;  $\gamma$ -HCH, 0.22 ng l<sup>-1</sup>;  $\alpha$ -HCH, 0.1 ng l<sup>-1</sup>, and presence of dieldrin, CB 44 and CB 170. These concentrations were subtracted from the levels found in the spiked samples.

Recovery for PCP was consistently lower at each of the concentration levels. This probably arises as PCP is the most water soluble of the

compounds studied. Furthermore, the analytical method for PCP determination, includes a derivatisation step which gives systematic losses [8].

The recovery of HCB might appear to be concentration-dependent, however assessment of coefficients of variation led to the conclusion that there were no significant difference between levels.

Recoveries for  $\alpha$ -HCH and  $\gamma$ -HCH varied greatly between and within levels. This was due to background concentrations, found in the analysis of the unspiked trial.

The efficiency of the analytical method for the aqueous fraction should be independent of the concentration in the water and the solubility of the OCs, within defined limits. Horwitz [11] has shown that the variance of experimental results increases at lower concentrations. Although the "Horwitz correlation" is only indicative relationship based on earlier intercomparison studies, it is necessary to assess whether the method is free of bias of this type. The ANOVA of the determination of OCPs and CBs at the three concentrations showed that there was no dependence of recovery upon the level of determinand ( $P <$

TABLE 2

Means and standard deviations (*s*) of the recoveries at the three concentration levels and at all levels. [Values of the *F* factor for the individual determinands ( $F = 4.26$ ,  $p < 0.05$ )]

Determinand	High level ( <i>n</i> = 3)		Median level ( <i>n</i> = 4)		Low level ( <i>n</i> = 3)		<i>F</i>	All levels ( <i>n</i> = 10)	
	Mean	<i>s</i>	Mean	<i>s</i>	Mean	<i>s</i>		Mean	<i>s</i>
HCB	77	6.7	95	12.9	99	17.8	2.5	91	13.2
CB52	87	5.0	106	22.8	93	13.9	1.1	96	15.7
CB101	88	5.3	92	10.0	85	9.3	0.6	89	8.7
CB118	92	3.1	94	10.1	81	9.5	2.2	89	8.5
CB153	87	2.7	93	12.1	80	9.3	1.8	87	9.5
CB138	85	2.1	93	12.7	79	7.0	2.0	86	9.2
CB180	84	3.2	89	11.7	67	3.2	6.3	81	8.1
2,4-DDE	85	7.0	78	10.7	74	4.5	1.3	79	8.3
4,4-DDE	85	5.5	85	12.2	74	3.5	1.7	82	8.7
$\alpha$ -HCH	76	5.1	90	11.9	85	17.7	1.1	84	12.6
$\gamma$ -HCH	70	3.6	81	27.7	44	14.1	3.0	67	19.9
Dieldrin	72	4.6	82	8.1	88	4.6	4.9	81	6.3
Endrin	91	7.9	96	9.2	107	6.7	3.0	97	8.2
2,4-DDT	69	10.3	96	4.9	94	22.6	3.7	87	13.7
4,4-DDT	85	7.8	97	22.3	94	11.7	0.5	93	16.4
PCP	72	19.0	75	19.8	81	19.9	0.2	76	19.9

0.05). The two apparent exceptions were for CB180 ( $F = 6.3$ ) and dieldrin ( $F = 4.9$ ). There is no apparent explanation for this except for the small sample size and the relatively low concentrations. There is no reason to suspect these compounds should selectively have a concentration-recovery dependence over this concentration range (Table 2).

Table 3 compares the results for the wet soxhlet extraction of sediment, in presence of sulphuric acid, with the results obtained using the standard laboratory method for the determination of OCs in the sediment, LRM 125. The material used for this test was the LRM125 normally analysed as part of the quality control for sediment analysis in this laboratory. The main differences in the magnitude of the coefficients of variation between the two data sets arise because the values for the standard method are derived from a large data set obtained over a period of months by different workers. Taking this into account, the data sets did not appear to be significantly different from each other.

The variance for the GC-ECD determinations should always be kept as low as possible, and

TABLE 3

Means ( $\mu\text{g kg}^{-1}$ ) and coefficients of variation for the sediment LRM 125

Determinand	Standard method <sup>a</sup> (dry)		Wet extraction with $\text{H}_2\text{SO}_4$	
	Mean ( $n = 10$ )	CV (%)	Mean ( $n = 4$ )	CV (%)
HCB	2.5	40.8	2	10.5
CB28	30	22.1	34	16.6
CB52	51	28.9	37	10.8
CB101	32	19.0	39	9.0
CB118	25	15.0	29	5.8
CB153	38	18.0	47	7.5
CB138	33	11.7	40	3.0
CB180	33	14.1	38	6.7
$\gamma$ -HCH	5	38.6	6	13.1
Dieldrin	88	25.6	55	11.2
2,4-DDE	15	35.4	13	9.6
4,4-DDE	12	21.9	13	11.1
4,4-DDD	36	43.0	41	8.7
4,4-DDT	24	53.1	27	9.0

<sup>a</sup> Method used in this laboratory using soxhlet extraction with dichloromethane under dry conditions.

TABLE 4

Coefficients of variation associated with the GC-ECD determination ( $\text{CV}_{\text{det}}$ ) and with the analytical separation, clean-up and GC-ECD determination ( $\text{CV}_{\text{sep}}$ )

Determinand	$\text{CV}_{\text{det}}$ ( $n = 5$ )	$\text{CV}_{\text{sep}}$ ( $n = 3$ )
HCB	3.5	7.1
CB52	3.5	8.3
CB101	4.5	4.8
CB118	3.4	4.2
CB153	0.4	4.0
CB138	1.9	2.6
CB180	3.2	3.9
$\alpha$ -HCH	4.5	8.9
$\gamma$ -HCH	4.5	6.7
Dieldrin	2.7	3.8
Endrin	–	4.9
2,4-DDT	4.3	11.0
4,4-DDD	4.4	6.8
PCP	2.2	3.5

always less than other steps in the method in order to make a valid assessment of the contribution of recovery and sample preparation to the overall method precision (Table 4). A high variance for the final determination would clearly indicate that the instrument was not optimised.

#### Statistical analysis of the coefficients of variation

There are three main stages in the analytical method:

- (i) the extraction of the sample from the matrix;
- (ii) the clean-up, compound class separation and, where necessary, derivatisation;
- (iii) the determination by GC-ECD.

The coefficients of variation ( $\text{CV}\%$ ) associated with each of the three stages were estimated from the experimental results. For these calculations it has been assumed that the  $\text{CV}\%$  were independent of the concentration for the concentration range tested, and that there was no covariance between the different stages.

Hence the coefficient of variation of the whole method,  $\text{CV}_t$ , was expressed as a function of the coefficients of variation associated with each of the three stages:

$$\text{CV}_t^2 = \text{CV}_i^2 + \text{CV}_{ii}^2 + \text{CV}_{iii}^2$$

$CV_i$  for the aqueous and for the particulate fractions were derived from the mean values in Table 2 ( $CV_i$ ) water, in Table 3 ( $CV_i$ ) particles and  $CV_{iii}$  from Table 4.

The coefficients of variation associated with the second stage was calculated from Table 4.

$$CV_{ii}^2 = CV_{an}^2 - CV_{iii}^2$$

Finally,  $CV_i$  which is a measure of the coefficient of variation of the initial extraction plus the matrix effect, was obtained from:

$$CV_i^2 = CV_t^2 = CV_{an}^2$$

The results from these calculations are listed in Tables 5 and 6 for the analyses of the aqueous (AF) and particulate fraction (PF) respectively.

The estimated coefficients of variation showed that the weakest link of the whole method was the initial extraction of the determinands from the sample matrix and accounted for over 80% of the total variance for both the AF and the PF. The coefficients of variation for the whole analyses averaged 11% for PF and 14% for AF. The exceptions were PCP in the PF (29%) and  $\gamma$ -HCH in the AF (30%).

The high coefficient of variation for the determination of PCP in solid matrices was due, in

TABLE 5

Statistical analysis of the coefficients of variation associated with each step of the water analysis, extraction ( $CV_i$ ), clean-up and separation ( $CV_{ii}$ ) and GC-ECD determination ( $CV_{iii}$ )

Determinand	$CV_t$ (n = 10)	$CV_i$	$CV_{ii}$	$CV_{iii}$
HCB	14.6	12.8	6.2	3.4
CB52	16.3	14.0	7.5	3.5
CB101	9.8	8.5	1.7	4.5
CB118	9.5	8.5	2.5	3.4
CB153	10.8	10.0	4.0	0.4
CB138	10.7	10.4	1.8	1.9
CB180	10.0	9.2	2.2	3.2
$\alpha$ -HCH	15.0	12.1	7.7	4.5
$\gamma$ -HCH	29.9	29.1	5.0	4.5
Dieldrin	8.9	8.1	2.7	2.7
Endrin	8.4	6.8	4.9	–
2,4-DDT	15.6	11.1	10.1	4.3
4,4-DDD	17.7	16.3	5.2	4.4
PCP	26.1	25.9	2.7	2.2

TABLE 6

Statistical analysis of the coefficients of variation associated with each step of the solids analysis, extraction ( $CV_i$ ), clean-up and separation ( $CV_{ii}$ ) and GC-ECD determination ( $CV_{iii}$ )

Determinand	$CV_t$ (n = 10)	$CV_i$	$CV_{ii}$	$CV_{iii}$
HCB	10.5	7.7	6.2	3.4
CB52	10.8	7.0	7.5	3.5
CB101	9.0	7.7	1.7	4.5
CB118	5.8	4.0	2.5	3.4
CB153	7.5	6.3	4.0	0.4
CB138	3.1	1.6	1.8	1.9
CB180	6.7	5.4	2.2	3.2
$\gamma$ -HCH	18.0	16.7	5.0	4.5
Dieldrin	11.0	10.3	2.7	2.7
4,4-DDD	10.0	7.3	5.2	4.4
PCP	29.0	28.8	2.7	2.2

part, to the nature of the solid-PCP chemical adsorptive and ionic interactions within the sample matrix [5]. The chemical interactive forces binding the PCP are partially overcome by the addition of sulphuric acid, but the variability of the recovery suggests that further soaking or sonication with acid prior to extraction might be advantageous.

The relatively high values of the coefficients of variation for the determination of  $\gamma$ -HCH and PCP of AF are largely due to the relatively high water solubilities of these compounds. A general observation is that the variance of the method increases with increasing water solubilities (Table 2).

### Conclusions

The method described here is suitable for the determination of individual OCs in sea water at the sub-nanogram per litre concentration level. The mean recovery of the OCs was 88% (range 67 to 97%) for different compounds with a range of water solubilities covering four orders of magnitude, and a range of water concentrations from 0.1 to 4 ng l<sup>-1</sup>. Other methods describing sampling apparatus for large volumes of water (over 20 l), followed by liquid-liquid extraction of the organochlorines into an organic solvent, quote recoveries below 80% for individual organochlo-

rines at similar concentrations in sea water [12–14]. Some workers have investigated the efficiency of the extraction by comparison with adsorption onto resins. It was concluded that liquid-liquid extraction yielded higher concentrations for hydrocarbons in sea water than adsorption onto resins [15].

The analytical method for the determination of OCs on particulate material was comparable to that used for the analysis of similar compounds in contaminated sediments. The wet soxhlet method was suitable for further studies on these contaminants in the sea water column.

Random errors (measured as  $CV_i$ ) for the analysis of the aqueous and particulate fractions were of the same order, giving a consistency for the analytical methods for the determination of these compounds in sea water.

The weakest link in the methodology, for both the aqueous and the particulate fraction, was the initial extraction from the sample matrix, especially for those compounds with higher water solubilities. This must be borne in mind if other determinands are included in the analysis, with different physico-chemical properties from those of the compounds studied here.

We wish to thank the Ministerio de Educacion y Ciencia of Spain for the financial support, and the colleagues at the Marine Laboratory in par-

ticular Lesley Campbell, Douglas Campbell and Alan Kelly for their support in this work.

#### REFERENCES

- 1 S. Tanabe and R. Tatsukawa, in J.S. Waid (Ed.), *PCBs and the Environment*, CRC Press, Boca Raton, FL, 1986.
- 2 J.S. Latimer, L.A. Leblanc, J.T. Ellis, J. Zheng and J.G. Quinn, *Sci. Total Environ.*, 97/98 (1990) 155.
- 3 R. Van Zoest, and G.T.M. van Eck, *Neth. J. Sea. Res.*, 26 (1990) 89.
- 4 S.W. Karickhoff, *J. Hydraul. Eng.*, 110 (1984) 707.
- 5 I. Cruz, PhD Thesis, University of Aberdeen 1992.
- 6 A.G. Kelly, I. Cruz and D.E. Wells, *Anal. Chim. Acta*, in press.
- 7 I. Cruz and D.E. Wells, *Int. J. Environ. Anal. Chem.*, 48 (1992) 1001.
- 8 D.E. Wells, A.E. Cowan and E.G. Christie, *J. Chromatogr.*, 328 (1985) 372.
- 9 D.E. Wells and A.G. Kelly, *Mikrochim. Acta.*, III (1991) 23.
- 10 J.C. Miller and J.N. Miller, *Statistical Analysis for Analytical Chemistry*, Ellis Horwood, Chichester, 1989.
- 11 W. Horwitz, *Anal. Chem.*, 54 (1982) 67A.
- 12 B. Stachel, K. Baetjer, M. Cetinkaga, J. Dueszeln, U. Lahl, K. Lierse, W. Thieman, B. Gabel, R. Kozicki and A. Podbielski, *Anal. Chem.*, 53 (1981) 1469.
- 13 J.C. Duinker and M.T.J. Hillebrand, in K. Grasshoff, M. Ehrhardt and K. Kremling (Eds.), *Methods of Seawater Analysis*, VCH, Weinheim, 1983, pp. 290–309.
- 14 B.G. Oliver and K.D. Nicol, *Int. J. Environ. Anal. Chem.*, 25 (1986) 275.
- 15 J.I. Gomez-Belinchon, J.O. Grimalt and J. Albaiges, *Environ. Sci. Technol.*, 22 (1988) 677.

# Rapid method for the determination of eight chlorophenoxy acid residues in environmental water samples using off-line solid-phase extraction and on-line selective precolumn switching

J.V. Sancho-Llopis and F. Hernández-Hernández

*Laboratorio de Medio Ambiente, Universitat Jaume I, P.O. Box 224, 12080 Castelló (Spain)*

E.A. Hogendoorn and P. van Zoonen

*Laboratory of Organic–Analytical Chemistry, National Institute of Public Health and Environmental Protection (RIVM), P.O. Box 1, 3720 BA Bilthoven (Netherlands)*

(Received 8th September 1992; revised manuscript received 21st January 1993)

## Abstract

A rapid procedure for the determination of eight chlorophenoxy acid herbicides in environmental water samples is described. The method involves two off-line solid-phase extraction (SPE) procedures prior to analysis by liquid chromatography with (pre)column switching and UV detection at 228 nm. SPE sample pretreatment consists in loading a 50-ml sample on a 100-mg C<sub>18</sub> cartridge followed by clean-up of the extract on a 100-mg silica cartridge. The extracts obtained by this procedure are analysed with coupled column liquid chromatography (LC) using a precolumn packed with internal surface reversed-phase material (5- $\mu$ m GFF II) and an analytical column packed with C<sub>18</sub> material (3- $\mu$ m Microspher). The separation of the extracts from the SPE procedure takes less than 15 min, rendering an overall procedure with a throughput of 40 samples per day. The chlorophenoxy acids 2,4-D, MCPA, 2,4-DP, MCPP, 2,4,5-T, 2,4-DB, MCPB and 2,4,5-TP can be assayed in the various water samples down to a level of 0.1  $\mu$ g l<sup>-1</sup>. Drinking, ground and surface water samples spiked at levels of 0.5 and 2.0  $\mu$ g l<sup>-1</sup> yielded average recoveries between 80 and 110% ( $n = 5$  for each sample type and spiked level) with relative standard deviations between 1 and 10%. The calibration graphs are linear over at least three orders of magnitude.

**Keywords:** Liquid chromatography; Sample preparation; Chlorophenoxy acids; Herbicides; Solid-phase extraction; Waters

Chlorophenoxy acids are widely used as herbicides in agriculture. Their persistence combined with their polar nature renders them mobile in more vulnerable types of soil, thus possibly threatening drinking water supplies. The Euro-

pean Community Drinking Water Directive prescribes a maximum allowable concentration of 0.1  $\mu$ g l<sup>-1</sup> for an individual pesticide in drinking water. Consequently, the availability of sensitive, selective and high-throughput methods of analysis for controlling drinking water and drinking water-related samples is essential. Productivity can be ensured by the application of multi-residue methods, able to detect several pesticides in one run combined with automated procedures for

*Correspondence to:* P. van Zoonen, Laboratory of Organic–Analytical Chemistry, National Institute of Public Health and Environmental Protection (RIVM), P.O. Box 1, 3720 BA Bilthoven (Netherlands).



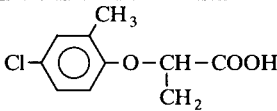
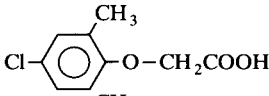
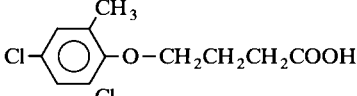
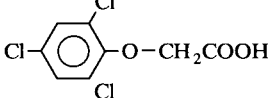
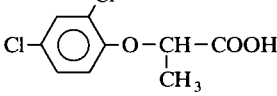
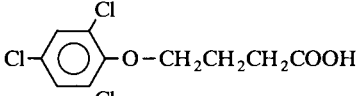
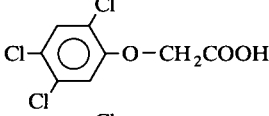
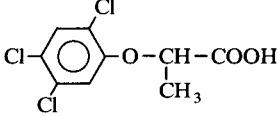
sample clean-up. Selectivity and sensitivity can be enhanced by the use of coupled column chromatographic techniques.

Chlorophenoxy acid herbicides (CPAs) are relatively polar compounds with low vapour pressures. Hence, their analysis is simpler by liquid chromatography (LC) [1–14], since for gas chromatography (GC) volatile derivatives have to be prepared [15–19]. Unfortunately, UV detection as generally applied in LC is not particularly selective or sensitive for the compounds involved, thus making the application of a laborious pre-concentration step followed by a selective clean-up necessary in order to reach the low limits required.

Nowadays, sample pretreatment has become less laborious by replacing the conventional liquid–liquid extraction step with solid-phase extraction (SPE) [2,3,5]. An important problem encountered in the pre-concentration of acidic compounds from natural water samples is that many matrix interferences are co-extracted and often co-eluted, resulting in a broad hump in the baseline whenever UV detection at short wavelengths is applied. This general problem [7,20], arising from humic substances, is clearly illustrated in Fig. 1, showing the reversed phase (RP)LC (UV detection) analysis of a ground water extract obtained (A) with and (B) without the addition of acid before the SPE  $C_{18}$  enrichment. In order to

TABLE 1

Systematic names and structural formulae of the chlorophenoxy acid herbicides

Herbicide	Systematic name	Structural formula
MCPP (mecoprop)	2-(4-Chloro-2-methylphenoxy)propanoic acid	
MCPA	(4-Chloro-2-methylphenoxy)acetic acid	
MCPB	4-(4-Chloro-2-methylphenoxy)butanoic acid	
2,4-D	(2,4-Dichlorophenoxy)acetic acid	
2,4-DP (dichloroprop)	2-(2,4-Dichlorophenoxy)propanoic acid	
2,4-DB	4-(2,4-Dichlorophenoxy)butanoic acid	
2,4,5-T	(2,4,5-Trichlorophenoxy)acetic acid	
2,4,5-TP (fenoprop)	2-(2,4,5-Trichlorophenoxy)propionic acid	

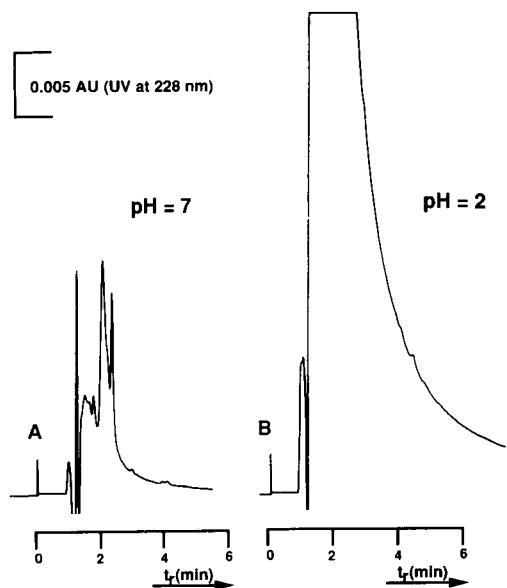


Fig. 1. RP-LC-UV analyses of groundwater sample extracts obtained after loading (25 ml) on a 100-mg SPE  $C_{18}$  cartridge at a pH value of the sample of (A) 7.0 and (B) 2.0. Injection of 100  $\mu$ l of extract (= 2.5 ml of sample) in 0.05% aqueous TFA on a 100 $\times$ 4.6 mm i.d. column packed with 3- $\mu$ m Microspher  $C_{18}$ . Mobile phase, methanol–0.05% aqueous TFA (60+40, v/v) at 1 ml  $\text{min}^{-1}$ . For SPE  $C_{18}$  procedure, see Experimental.

overcome this problem, several techniques such as membrane trapping [7], selective detection [8–10] and application of selective sorbents for off-line [6] and on-line [7–14] trapping of the CPAs have been applied to improve selectivity. Fully

automated precolumn-switching systems have been described [13,14] for the determination of some CPAs in drinking and surface water. However, unattended analysis of larger series of water samples is not possible owing to the lack of commercially available autosamplers capable to accommodate a sufficient number of samples for the injection of large volumes of water (> 25 ml).

Coupled column LC [21–24] is a powerful technique for improving the selectivity and sensitivity of the procedure and to automate the cleanup of samples or extracts. The object of this study was to develop a productive, sensitive and selective LC assay for monitoring chlorophenoxy acid herbicides in environmental aqueous samples using favourable features of both off-line SPE and on-line column switching. The eight chlorophenoxy herbicides studied are listed in Table 1.

## EXPERIMENTAL

### Chemicals

All the chlorophenoxy acid herbicides (content > 99%) were obtained from Dr. S. Ehrenstorfer (Promochem, Wesel, Germany). Acetone, acetonitrile, dichloromethane, methanol and 2,2,4-trimethylpentane (isooctane), all of LC grade, were obtained from Promochem. Analytical-reagent grade anhydrous sodium sulphate and trifluoroacetic acid (TFA), orthophosphoric acid

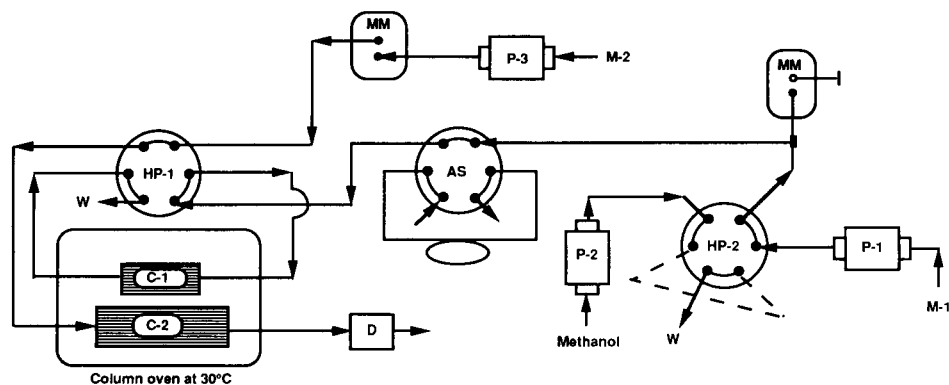


Fig. 2. LC scheme for column switching. AS = autosampler with 400- $\mu$ l sample loop; HP-1 and HP-2 = high-pressure valves; P-1, P-2 and P-3 = LC pumps; MM = manometric modules; C-1 = precolumn; C-2 = separation column; M-1 and M-2 = mobile phases; W = waste; UV detector set at 228 nm.

(89% pure), hydrochloric acid (37%) and acetic acid (100%) were bought from Merck. LC-grade water was obtained by purifying demineralized water in a Milli-Q system (Millipore, Bedford, MA, USA).

Stock standard solutions (ca. 500  $\mu\text{g ml}^{-1}$ ) of the herbicides were prepared in acetonitrile. For LC analysis, the stock solutions were diluted and mixed with LC-grade water containing 0.05% (v/v) TFA. Methanol–0.05% aqueous TFA (5 + 95, v/v) and methanol–0.05% aqueous TFA (60 + 40, v/v) were used as the first (M-1) and second (M-2) mobile phases respectively.

Disposable 1-ml SPE cartridges containing 100 mg of  $\text{C}_{18}$ -bonded or bare silica material (40  $\mu\text{m}$ ) were obtained from J.T. Baker (Deventer, Netherlands).  $\text{C}_{18}$  cartridges were preconditioned with 1 ml of methanol, 1 ml of acetone, 1 ml of methanol and 2 ml of 0.1% aqueous TFA and silica cartridges with 1 ml of methanol–dichloromethane (75 + 25, v/v), 1 ml of dichloromethane and 1 ml of isooctane.

#### Equipment

A Baker-10 system (J.T. Baker) was used to perform SPE. The LC set-up is illustrated in Fig. 2. The system consists of a Model 232 autosampler (AS) equipped with an auxiliary switching valve (HP-1), three Model 305 LC pumps (P-1, P-2, P-3), two Model 805 manometric modules (MM) and a Model 316 UV detector (D) from Gilson (Villiers-le-Bel, France), two Type 7010 high-pressure valves (HP-1 and HP-2) from Rheodyne (Cotati, CA, USA), a  $10 \times 3$  mm i.d. precolumn (C-1) packed with 5- $\mu\text{m}$  GFF II from Pinkerton (obtained from Regis, Morton Grove, IL, USA) and a  $100 \times 4.6$  mm i.d. separation column (C-2) packed with 3- $\mu\text{m}$  Microspher  $\text{C}_{18}$  from Chrompack (Bergen op Zoom, Netherlands). The LC pumps and valves for column switching and eluent supply were controlled by the autosampler (AS).

The columns were kept at 30°C with a laboratory-made column oven connected to a Model 1441 circulating water system from Braun (Melsungen, Germany).

Quantitative measurements of peak heights were made with a Model 3388A integrator from

Hewlett-Packard (Waldbronn, Germany) and UV spectra were recorded with a Model 1000S diode-array detector from ABI (Foster City, CA, USA).

A Model 691 pH meter and (200- and 1000- $\mu\text{l}$ ) Pipetmans were purchased from Metrohm (Herisau, Switzerland) and Gilson, respectively.

#### Sample pretreatment

Aqueous samples (50 ml) were acidified with 100  $\mu\text{l}$  of TFA and percolated through a preconditioned 100-mg  $\text{C}_{18}$  cartridge at a flow-rate of 5  $\text{ml min}^{-1}$ . After the sample had passed through the cartridge, it was rinsed with 1 ml of methanol–0.05% aqueous TFA (10 + 90, v/v) and dried by passing air for 10 min. The valve was closed and 500  $\mu\text{l}$  of acetone were brought on to the cartridge. Next, the cartridge was removed from the Baker-10 system and by means of overpressure, i.e., with a syringe placed on top of the cartridge, the acetone was passed through the cartridge and collected in a calibrated tube. The extract was evaporated to dryness under a gentle stream of nitrogen and the residue was dissolved by adding 200  $\mu\text{l}$  of dichloromethane and 800  $\mu\text{l}$  of isooctane. The 1-ml extract was loaded on to a preconditioned 100-mg silica cartridge placed in the SPE system and removed to waste with a mild vacuum (ca. 400 mbar). Next, the valve was closed and 1 ml of methanol–dichloromethane (50 + 50, v/v) was passed through the cartridge (overpressure) into a calibrated tube. The solution was evaporated to dryness using a hot water-bath and a gentle stream of nitrogen. The residue was dissolved in 1 ml of 0.05% aqueous TFA prior to LC analysis.

#### LC analysis

The mobile phases (see Fig. 2) were adjusted to a flow-rate of 1  $\text{ml min}^{-1}$ . A volume of 400  $\mu\text{l}$  obtained after the SPE clean-up procedure was injected on to C-1. After clean-up with 1.0 ml of M-1 (injection volume included), C-1 was switched on-line with C-2 for 30 s to transfer the CFA-containing fraction (0.50 ml of M-2) to C-2. Simultaneously, the high-pressure valve (HP-2) was switched for 3 min to rinse C-1 with 3 ml of methanol. Quantification of the CPAs was done

by external calibration with standard solutions of CPAs in 0.05% aqueous TFA.

## RESULTS AND DISCUSSION

### Selection of RP-LC–UV detection conditions

The use of an acidic buffer in the mobile phase for ion suppression of the CPAs results in suitable chromatographic behaviour on  $C_{18}$  materials [3,6,8]. Experiments indicated that the efficiency of the RP-LC separation of CPAs increases with a decrease in the pH of the mobile phase and the use of methanol instead of acetonitrile or tetrahydrofuran as modifier. Working in the allowable pH range of the  $C_{18}$ -bonded material, a  $100 \times 4.6$  mm i.d. column packed with  $3\text{-}\mu\text{m}$   $C_{18}$  (ca. 10000 plates) and a mobile phase of methanol–aqueous solution (pH 2.4) (60 + 40, v/v) were selected for the isocratic separation of the CPAs given in Table 1. As illustrated in Fig. 3, aqueous solutions of 0.05% TFA or 0.03 M phosphate can be used as the aqueous mobile phase constituent. The considerable change in elution time and/or order of some analytes can be very useful for confirmatory purposes. Because of the slightly better elution (smaller peak volumes) of the last three compounds, 0.05% aqueous TFA was selected as the aqueous mobile

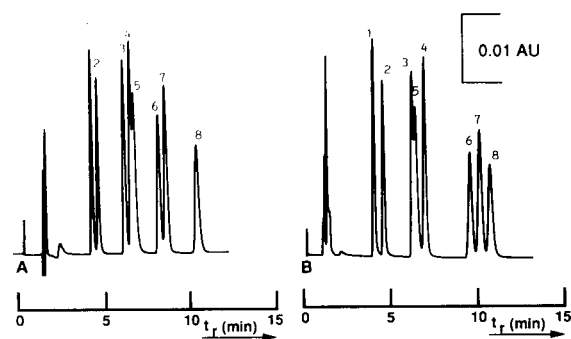


Fig. 3. Isocratic separation of CPAs on a  $100 \times 4.6$  mm i.d. column packed with  $3\text{-}\mu\text{m}$  Microspher  $C_{18}$  and a mobile phase ( $1\text{ ml min}^{-1}$ ) consisting of 60% (v/v) of methanol in an aqueous solution of pH 2.4 of (A) 0.05% TFA and (B) 0.03 M phosphate buffer. Injection of  $400\ \mu\text{l}$  of standard solution of CPAs in 0.05% aqueous TFA (ca.  $0.5\ \mu\text{g}$  per analyte). UV detection at 228 nm. 1 = 2,4-D; 2 = MCPA; 3 = 2,4-DP; 4 = MCPB; 5 = 2,4,5-T; 6 = 2,4-DB; 7 = MCPB; 8 = 2,4,5-TP.

TABLE 2

UV absorption data for the chlorophenoxy acid herbicides

Herbicide	Molar absorptivity ( $\text{l mol}^{-1}\text{ cm}^{-1}$ )		
	205 nm	228 nm	280 nm
2,4-DP	24900	8000	1330
2,4-D	23800	8050	1490
MCPA	16000	8300	1350
2,4,5-T	33750	8790	1390
MCPB	18400	8230	1290
MCPB	17850	5760	730
2,4-DB	11450	3090	620
2,4,5-TP	16100	7980	1380

phase constituent. An increasing separation efficiency, viz., decrease in chromatographic analysis with similar resolution, was observed on increasing the temperature of the column up to  $60^\circ\text{C}$ . Unfortunately, the column lifetime decreases considerably at higher temperatures. Therefore, a column temperature of  $30^\circ\text{C}$  was selected for further analysis. With reference to the UV detection of these compounds, the UV spectra were recorded with photodiode-array detection. The results of the calculated molar absorptivities at three different wavelengths are given in Table 2. As a compromise between sensitivity and selectivity, a wavelength of 228 nm was used for the detection of all the compounds.

### Selection of extraction and clean-up procedure

From the molar absorptivity data in Table 2, it can be inferred that a ca. 50-fold concentration factor of the sample is necessary to obtain a limit of detection (LOD) of  $0.1\ \mu\text{g l}^{-1}$  in a water sample, injecting  $400\ \mu\text{l}$  from a final extract of 1 ml.

SPE using small 100-mg  $C_{18}$  disposable cartridges was chosen for the rapid isolation of the chlorophenoxy acids from 50 ml of sample acidified to pH 2 with TFA. In a first approach, the possibility of on-line clean-up of the crude SPE  $C_{18}$  extract with coupled-column RP-LC was investigated using the method development strategy described previously [21,24]. To perform on-line clean-up with column switching, two  $50 \times 4.6$  mm i.d. columns (C-1 and C-2) packed with  $3\text{-}\mu\text{m}$  Microspher  $C_{18}$  were selected instead of a  $100 \times$

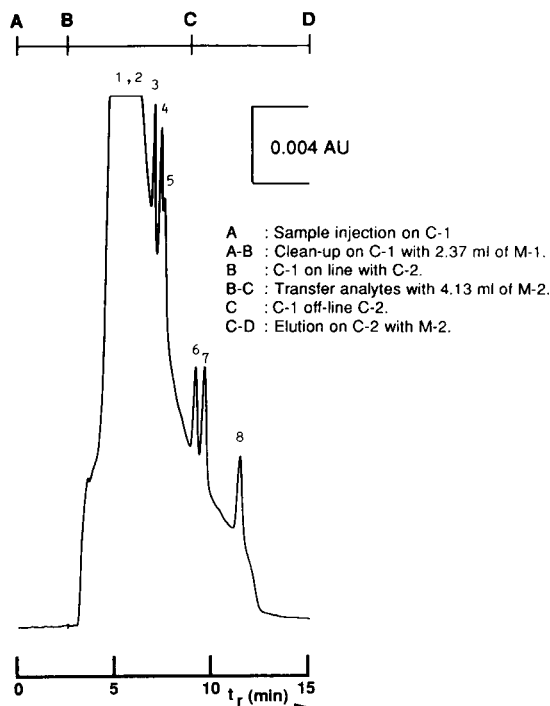


Fig. 4. Coupled-column RP-LC analysis of an SPE  $C_{18}$  extract of a surface water sample spiked with CPAs at a level of  $2.0 \mu\text{g l}^{-1}$ . C-1 and C-2,  $50 \times 4.6$  mm i.d. column packed with  $3\text{-}\mu\text{m}$  Microspher  $C_{18}$ ; M-1 and M-2, methanol–0.05% aqueous TFA (60+40, v/v) at flow-rate of  $1 \text{ ml min}^{-1}$ . Injection of  $400 \mu\text{l}$  of extract (= 20 ml of sample) on C-1; UV detection at 228 nm. 1–8 as in Fig. 3.

4.6 mm i.d. column. With the selected composition (see above) for both the mobile phases M-1 and M-2 on C-1 and C-2, a clean-up volume of 2.37 ml could be applied on C-1 after injection of an SPE  $C_{18}$  sample extract (see Experimental). As shown in Fig. 4, the clean-up performance of the coupled-column system, for the analysis of a surface water spiked at the  $2 \mu\text{g l}^{-1}$  level is certainly not sufficient. The broad and strongly tailing interfering peak makes the analysis of the first analytes (2,4-D and MCPA) impossible and disturb the determination of the other analytes at (required) lower levels. The application of a larger clean-up volume (5.5 ml) by lowering the elutropic strength of M-1 to 40% (v/v) methanol did not improve the selectivity sufficiently. Obviously, additional clean-up prior to the RPLC procedure is necessary.

First, improving the SPE sampling conditions was studied, e.g., increasing the pH of the sample (range 2.0–4.5), addition of different contents of methanol (range 0–20%) to the water and the use of the ion-pairing reagent tetrahexylammonium hydrogensulphate (THA), in addition to the application of liquid–liquid extraction (LLE) with dichloromethane at low pH, or LLE with the ion-pairing reagent. None of these approaches suppressed the early eluting interfering peak sufficiently.

Second, an additional clean-up procedure on a 100-mg silica cartridge was developed (see Experimental) using small volumes of mixtures of dichloromethane in isooctane and methanol with carefully adjusted compositions to perform adsorption and desorption of the analytes. The results of such a procedure, resulting in a substantial improvement in the clean-up, is shown in Fig. 5A. In spite of the improvement, the first two peaks (2,4-D and MCPA) still elute on the top of the remaining part of the interference(s), making quantification difficult at the low LODs required.

So far, the interferences seem to elute from a  $C_{18}$  column with a mobile phase at a low pH always in a broad hump near the first-eluting analytes. Considering the nature of water samples, such a retention behaviour can be expected from humic acids showing both acidic and basic properties causing retention and band broadening due to interaction with the residual silanol groups of  $C_{18}$  material. Based on the results described so far, it can be concluded that coupled-column LC with two  $C_{18}$  columns is not particularly suitable for solving this separation problem. Therefore, as an alternative step towards selectivity improvement, two other hydrophobic materials in the first column were tested, rendering a more or less multi-dimensional separation system. For reasons of convenience and costs, small (pre)columns were tested as C-1. In order to maintain the resolution of the chromatographic system, the two  $50 \times 4.6$  mm i.d.  $C_{18}$  columns used in previous experiments were joined, acting as one 100-mm  $C_{18}$  column (C-2). As illustrated in Fig. 5B, the first tested column ( $15 \times 3.2$  mm i.d.) packed with  $7\text{-}\mu\text{m}$  RP-8 from Brownlee (Santa Clara, CA, USA) resulted in

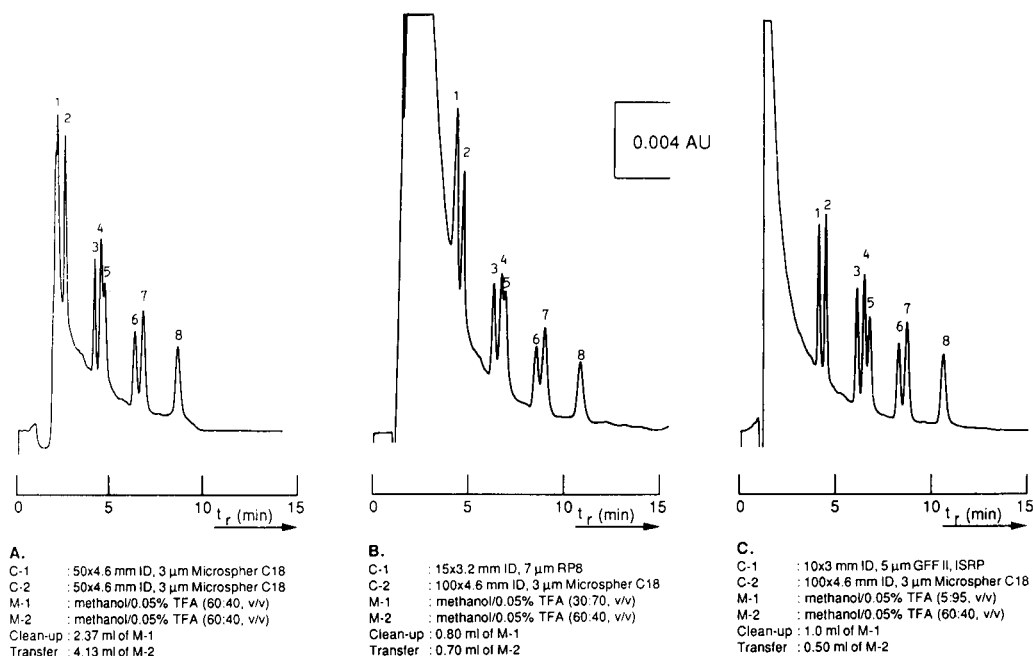


Fig. 5. Various column-switching RP-LC procedures for the analysis of a spiked surface water sample ( $2 \mu\text{g l}^{-1}$  level) obtained after enrichment on  $\text{C}_{18}$  and clean-up on silica SPE cartridges (for SPE procedures, see Experimental). UV detection at 228 nm. All flow-rates set at  $1 \text{ ml min}^{-1}$ . Displayed chromatograms start after clean-up on C-1. 1–8 as in Fig. 3.

more favourable elution of the first analytes. However, experiments with surface and ground waters indicated that the separation between the first-eluting CPAs and the interference is still insufficient to obtain on a LOD of  $0.1 \mu\text{g l}^{-1}$ . As shown in Fig. 5C, the selectivity was further improved with the use of a precolumn ( $10 \times 3 \text{ mm i.d.}$ ) packed with  $5\text{-}\mu\text{m}$  GFF II internal surface reversed-phase material. The column-switching system obtained made it possible to trace the analytes in water samples down to levels of  $0.1 \mu\text{g l}^{-1}$  in less than 15 min. In combination with off-line SPE sample pretreatment an efficient procedure has been developed capable to assay 40 samples per day. As an example, a chromatogram of a surface water sample spiked with the CPAs at a level of  $0.5 \mu\text{g l}^{-1}$  and analysed with the proposed procedure is given in Fig. 6.

#### Performance of the procedure

Using standard mixtures within a wide range of concentrations ( $25\text{--}5000 \mu\text{g l}^{-1}$ ), the response was linear ( $n = 5$ ,  $r \geq 0.99999$ ) for analytes. The

recovery and repeatability of the method at two concentration levels of the eight CPAs were assessed in different environmental aqueous matrices. Samples of drinking, surface and groundwater were divided into two portions that were spiked with the analytes at levels of  $0.5$  and  $2 \mu\text{g l}^{-1}$  for surface and groundwater and  $0.1$  and  $0.5 \mu\text{g l}^{-1}$  for drinking water. Aliquots of  $50 \text{ ml}$  of these samples were analysed by this procedure in quintuplicate. The quantitative results, reported in Table 3, are acceptable with regard to both recovery and repeatability. The relatively high recovery of MCPB in drinking water at the level of  $0.1 \mu\text{g l}^{-1}$  was caused by the elution of a broad interfering peak close to the analyte, making quantification difficult at this low level.

Moreover, surface water samples spiked at the  $2.5 \mu\text{g l}^{-1}$  level were loaded on to  $\text{C}_{18}$  SPE cartridges, according to the present procedure, and stored for 2 weeks at room temperature in the laboratory, trying to check the possibility of field sampling. The results, given in Table 4, confirm the stability of the eight chlorophenoxy

TABLE 3

Data on recovery and repeatability for various water samples spiked with CPAs at two levels <sup>a</sup>

Herbicide	Mean recovery (%) $\pm$ R.S.D. of CPAs spiked in					
	Drinking water		Surface water		Ground water	
	0.1	0.5	0.5	2.0	0.5	2.0
2,4-D	90 $\pm$ 3.5	93 $\pm$ 9.0	101 $\pm$ 3.0	97 $\pm$ 2.0	87 $\pm$ 1.5	79 $\pm$ 7.0
MCPA	95 $\pm$ 4.0	95 $\pm$ 8.0	101 $\pm$ 1.0	104 $\pm$ 2.0	98 $\pm$ 8.2	88 $\pm$ 10
2,4-DP	99 $\pm$ 2.0	100 $\pm$ 8.0	102 $\pm$ 1.0	103 $\pm$ 2.0	112 $\pm$ 9.0	95 $\pm$ 9.5
MCPP	95 $\pm$ 3.0	100 $\pm$ 5.0	102 $\pm$ 2.0	109 $\pm$ 2.0	116 $\pm$ 11	97 $\pm$ 8.0
2,4,5-T	88 $\pm$ 3.0	97 $\pm$ 3.0	93 $\pm$ 2.5	97 $\pm$ 3.0	92 $\pm$ 4.0	78 $\pm$ 8.0
2,4-DB	101 $\pm$ 4.0	99 $\pm$ 3.0	102 $\pm$ 3.0	97 $\pm$ 2.0	89 $\pm$ 4.0	93 $\pm$ 7.0
MCPB	127 $\pm$ 3.0	104 $\pm$ 4.5	105 $\pm$ 2.0	99 $\pm$ 2.0	85 $\pm$ 6.5	101 $\pm$ 7.0
2,4,5-TP	99 $\pm$ 3.0	98 $\pm$ 7.5	96 $\pm$ 2.0	98 $\pm$ 2.5	94 $\pm$ 8.0	93 $\pm$ 12

<sup>a</sup>  $n = 5$  for each level.

acid herbicides sorbed on  $C_{18}$  cartridges during this period.

Finally, the potential of this method was checked with dicamba, a chlorobenzoic acid herbicide usually analysed together with the eight herbicides studied in this work. Usually, gradient

elution will be necessary to elute CPAs together with a significantly more polar analyte in one chromatographic run. To speed up analysis, linear gradient elution can be applied to overcome the large difference in the retentions of the analytes. However, using a buffered system and sensitive non-selective UV detection, the baseline will be severely disturbed during the period of gradient elution [8,14]. Previous studies [25,26] indicated that step-gradient elution can serve as a good alternative for the adequate separation of compounds with a large difference in retention. By selecting a favourable time for eluent switching, an overall improvement of the baseline can be obtained, enhancing the sensitivity and reducing the time for chromatographic analysis [25,26]. The performance of step-gradient elution for the separation of dicamba and the eight CPAs was roughly investigated. A chromatogram obtained

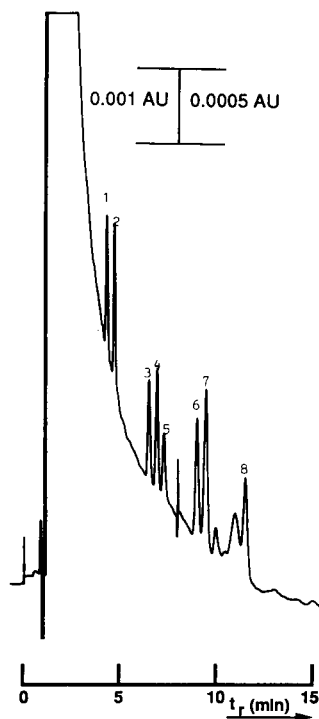


Fig. 6. Column-switching RP-LC of a surface water sample spiked with CPAs at the  $0.5 \mu\text{g l}^{-1}$  level. Sample pretreatment and LC conditions as in Fig. 5C. 1–8 as in Fig. 3.

TABLE 4

Data on recovery ( $n = 2$ ) for surface water samples spiked with CPAs at  $2.5 \mu\text{g l}^{-1}$  and stored for 2 weeks

Herbicide	Recovery (%)	
2,4-D	92	85
MCPA	94	99
2,4-DP	95	98
MCPP	100	104
2,4,5-T	91	98
2,4-DB	101	103
MCPB	97	99
2,4,5-TP	91	92

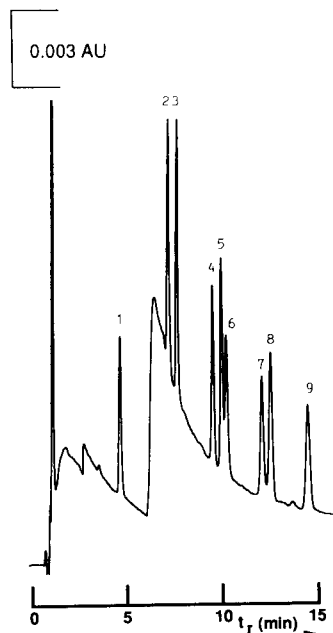


Fig. 7. Column-switching RP-LC and step-gradient elution on C-2 of a surface water sample spiked at a level of  $2 \mu\text{g l}^{-1}$  with dicamba and CPAs. Injection of  $400 \mu\text{l}$  of extract obtained after SPE sample pretreatment on  $\text{C}_{18}$  and silica cartridges. LC conditions: C-1,  $10 \times 3 \text{ mm}$  i.d. column packed with  $5\text{-}\mu\text{m}$  GFF II; M-1, methanol–0.05% aqueous TFA (5 + 95, v/v); C-2,  $100 \times 4.6 \text{ mm}$  i.d. column packed with  $3\text{-}\mu\text{m}$  Microspher  $\text{C}_{18}$ ; M-2A, methanol–0.05% aqueous TFA (50:50, v/v); M-2B, methanol–0.05% aqueous TFA (60 + 40, v/v); clean-up volume, 1.0 ml of M-1 (injection volume included); transfer volume, 0.50 ml of M-2A. After transfer, a step gradient on C-2 was applied of 5.2 ml of M-2A and 10 ml of M-2B. Displayed chromatogram starts after clean-up on C-1. 1 = Dicamba; 2 = 2,4-D; 3 = MCPA; 4 = 2,4-DP; 5 = MCPP; 6 = 2,4,5-T; 7 = 2,4-DB; 8 = MCPB; 9 = 2,4,5-TP.

for the analysis of a surface water sample spiked at the  $2 \mu\text{g l}^{-1}$  level is shown in Fig. 7, which illustrates the effect of step-gradient elution on the interfering peak, with compression of the interfering peak and distortion of the baseline, but the method is still capable of detecting residues of all the compounds studied at very low levels.

#### Confirmation of CPAs

The proposed method above provides a rapid screening method for the presence of CPAs in water samples. However, UV detection at 228 nm is not very selective. Therefore, positive samples

are usually confirmed by means of mass spectrometry. For this purpose the CPAs are derivatized with pentafluorobenzyl bromide. Direct phase transfer-catalysed derivatization of CPAs in water samples to pentafluorobenzyl derivatives prior to gas chromatography with electron-capture detection and negative-ion chemical ionization mass spectrometry has been applied [27].

#### Conclusions

A major problem encountered in the determination of acidic pollutant residues in natural water samples is obtaining sufficient separation between analytes and the large excess of co-extracted more polar interferences, e.g., fulvic and humic acids. It appeared that prior to the tested RP-LC column-switching procedures, rapid clean-up on SPE silica cartridges was highly efficient. Further, multi-dimensional precolumn switching using internal surface reversed-phase material and conventional  $\text{C}_{18}$  material provided better separations between co-extracted interferences and analytes in comparison with coupled-column RP-LC.

Combination of two off-line SPE procedures with an on-line multi-dimensional precolumn switching system yielded an overall procedure capable of determining eight chlorophenoxy acid herbicides down to a level of  $0.1 \mu\text{g l}^{-1}$  in various aqueous environmental samples with a high sample throughput.

Preliminary experiments indicated that the developed procedure is amenable to more polar acidic pesticides, e.g., dicamba, and that step-gradient elution can serve as an adequate separation technique.

#### REFERENCES

- 1 C.W. Vaughan, *Anal. Chim. Acta*, 131 (1981) 307.
- 2 S.H. Hoke, E.E. Brueggeman, L.J. Baxter and T. Trybus, *J. Chromatogr.*, 357 (1986) 429.
- 3 M.J.M. Wells and J.L. Michael, *Anal. Chem.*, 59 (1987) 1739.
- 4 A. Betti, G. Lodi and S. Coppi, *J. Chromatogr.*, 513 (1990) 219.
- 5 E.R. Bogus, T.L. Watschke and R.O. Mumma, *J. Agric. Food Chem.*, 38 (1990), 142–144.



- 6 A. Di Corcia, M. Marchetti and R. Samperi, *Anal. Chem.*, 61 (1989) 1353.
- 7 G. Nilvé, G. Audnsson and J.A. Jönsson, *J. Chromatogr.*, 471 (1989) 151.
- 8 W. Schlüsser, *Chromatographia*, 29 (1990) 24.
- 9 C. De Ruiter, W.A. Minnaard, H. Lingeman, E.M. Kirk, U.A.Th. Brinkman and R.R. Otten, *Int. J. Environ. Anal. Chem.*, 43 (1991) 79.
- 10 T. Suzuki and S. Watanabe, *J. Chromatogr.*, 541 (1991) 359.
- 11 R. Hamann and A. Ketrup, *Chemosphere*, 16 (1987) 527.
- 12 R.L. Smidt and D.J. Pietrzyk, *J. Chromatogr. Sci.*, 21 (1983) 282.
- 13 R.B. Geerdink, C.A.A. van Balkom and H. Brouwer, *J. Chromatogr.*, 481 (1986) 275.
- 14 V. Coquart and M.C. Hennion, *Sci. Total Environ.*, in press.
- 15 W. Wang and S. Huang, *J. Chromatogr.*, 483 (1989) 121.
- 16 T. Tsukioka and T. Murakami, *J. Chromatogr.*, 469 (1989) 351.
- 17 N.P. Hill, A.E. McIntyre, R. Perry and J.N. Lester, *Int. J. Environ. Anal. Chem.*, 15 (1983) 107.
- 18 F. Ngan and T. Ikeskaki, *J. Chromatogr.*, 537 (1991) 385.
- 19 R.E. Cline, G.D. Todd, D.L. Ashley, J. Grainger, J.M. McCraw, C.C. Alley and R.H. Hill, *J. Chromatogr. Sci.*, 28 (1990) 167.
- 20 V. Coquart and M.-C. Hennion, *J. Chromatogr.*, 553 (1991) 329.
- 21 E.A. Hogendoorn, C.E. Goewie and P. van Zoonen, *Fresenius' J. Anal. Chem.*, 339 (1991) 348.
- 22 P. van Zoonen, E.A. Hogendoorn, G.R. van der Hoff and R.A. Baumann, *Trends Anal. Chem.*, 11 (1992) 11.
- 23 E.A. Hogendoorn, R. Hoogerbrugge, C.E. Goewie, P. van Zoonen and P.J. Schoenmakers, *J. Chromatogr.*, 552 (1991), 113.
- 24 E.A. Hogendoorn, C. Verschraagen, U.A.Th. Brinkman and P. van Zoonen, *Anal. Chim. Chim. Acta*, 268 (1992) 205.
- 25 E.A. Hogendoorn and P. van Zoonen, *Meded. Fac. Landbouwwet. Rijksuniv. Gent*, 55 (1991) 1275.
- 26 E.A. Hogendoorn, E. Dijkman, S.M. Gort, R. Hoogerbrugge, U.A.Th. Brinkman and P. van Zoonen, *J. Chromatogr. Sci.*, in press.
- 27 H.D. Meiring, G.D. den Engelsman and A.P.J.M. de Jong, *J. Chromatogr.*, submitted for publication.

# Solid-phase extraction of pesticide residues from ground water: comparison between extraction cartridges and extraction discs

J. Beltran, F.J. López and F. Hernández

*Environmental and Natural Resources Laboratory, Department of Experimental Sciences, Jaume I University, P.O. Box 224, 12080 Castellón (Spain)*

(Received 8th September 1992; revised manuscript received 9th February 1993)

## Abstract

Octadecyl (C<sub>18</sub>) bonded porous silica sorbent cartridges and Empore membrane extraction discs were evaluated for the solid-phase extraction (SPE) of organochlorine (lindane, dicofol, chlorfenson and tetradifon) and organophosphorus pesticides (dimethoate, fenitrothion and methidathion) from ground water. The 500-mg C<sub>18</sub> cartridges quantitatively adsorbed these pesticides, including the most polar (dimethoate), with recoveries ranging from 68 to 113% for a ground water sample spiked at the 0.1  $\mu\text{g l}^{-1}$  level. SPE with 500-mg C<sub>18</sub> Empore discs also quantitatively adsorbed the pesticides with recoveries between 73 and 115% for the 0.1  $\mu\text{g l}^{-1}$  level, but only after eluting with 15 ml of ethyl acetate compared with 4 ml using cartridges and a longer analysis time per sample. After elution with ethyl acetate, the extract was concentrated to an appropriate volume, between 100 and 500  $\mu\text{l}$ , under a gentle stream of nitrogen. Detection limits were lower than 0.1  $\mu\text{g l}^{-1}$ , which is currently the maximum level allowed by the EEC for pesticide residues in drinking water. Determination was effected by capillary gas chromatography using electron-capture and nitrogen-phosphorus detectors.

*Keywords:* Gas chromatography; Extraction; Pesticides; Waters

One of the most important environmental concerns is pesticide residue levels in water, mainly in ground water in predominantly agricultural areas, and their movement in the ecosystem. This has led to the development of multi-residue methods for the determination of pesticides in environmental samples. Unfortunately, classical analytical procedures based on solvent partitioning in separation funnels are time consuming and require large volumes of costly and toxic solvents. The solid-phase extraction (SPE) system using bonded silica sorbents applied to the extraction of pesticides from water offers the advantages of

a shorter analysis time, lower cost and the consumption of very low volumes of organic solvents.

Organochlorine and organophosphorus pesticides have been determined in water samples using SPE using a variety of sorbents such as C<sub>18</sub> [1–6], C<sub>8</sub> [7–9] and Amberlite XAD [10–13]. Empore membrane extraction discs can be used as an alternative to cartridge SPE. These can be used in the off-line mode with a filtration apparatus [14] and in the on-line mode using a membrane holder [15,16].

The pesticides studied in this work included some of the most commonly applied compounds in this area of Spain. They include the organophosphorus (OP) pesticides dimethoate, fenitrothion and methidathion and the organochlorine (OC) pesticides lindane, dicofol, chlor-

*Correspondence to:* F. Hernández, Environmental and Natural Resources Laboratory, Department of Experimental Sciences, Jaume I University, P.O. Box 224, 12080 Castellón (Spain).

fenson and tetradifon. In a previous paper [17] the extraction of these compounds using cartridge SPE (100 mg C<sub>18</sub>) was reported, with successful results except for the most polar dimethoate. In this paper, a modified procedure of cartridge SPE to improve the recovery of dimethoate is described, and compared with SPE using Empore membrane extraction discs.

## EXPERIMENTAL

### *Apparatus and conditions*

The following were used: solid-phase extraction cartridges, 100, 200 and 500 mg C<sub>18</sub> (Analytichem); Vac Elut solid-phase extraction system (Analytichem); vacuum pump with pressure controller; Empore C<sub>18</sub> solid-phase extraction discs, 47 mm diameter, and filtration system; graduated and assay tubes; Multiblock Selecta heating block, supplied with a nitrogen stream; a Hewlett-Packard 5890 Series II gas chromatograph, equipped with two detectors (electron-capture and nitrogen-phosphorus) and an HP Ultra 2 capillary column (25 m × 0.20 mm i.d., 0.33 μm film thickness); and a Hewlett-Packard 7630A autosampler.

Determinations were carried out under the following conditions: injector temperature, 275°C; electron-capture detector temperature, 300°C; nitrogen-phosphorus detector temperature, 270°C; column temperature programme, 90°C, held for 1 min, increased at 30°C min<sup>-1</sup> to 180°C, increased at 4°C min<sup>-1</sup> to 270°C, held for 15 min; carrier gas, helium at 1 ml min<sup>-1</sup>; and injection, 2 μl using the autosampler and the splitless mode.

### *Chemicals*

Sodium sulphate, anhydrous, of pesticide residue analysis grade (J.T. Baker), was purified by heating at 350°C overnight. NaCl of analytical-reagent grade (Panreac), was purified by heating. Organic solvents of pesticide residue analysis grade (methanol, dichloromethane, ethyl acetate and hexane) were purchased from Scharlau. Pesticide standards (Riedel-de Haën) were purchased from Scharlau. Stock standard solutions (ca. 500 μg ml<sup>-1</sup>) were prepared in acetone and

stored at -18°C. Working standard solutions were prepared by dilution with acetone (for fortification) and with hexane (for injection).

### *Recommended procedure*

A 500-mg C<sub>18</sub> cartridge was conditioned with two cartridge volumes (12 ml) of methanol, ethyl acetate, methanol again and finally distilled water. Then, 200 ml of ground water sample containing 20% NaCl were passed through the cartridge using a vacuum (8–10 ml min<sup>-1</sup>). The cartridge was rinsed with 12 ml of distilled water and then dried by passing air for 20 min. The pesticides were eluted with 4 ml of ethyl acetate. This extract was evaporated at 40°C under a gentle stream of nitrogen to a volume of ca. 100 μl. The final extract volume was measured with a syringe and injected into the gas chromatograph.

## RESULTS AND DISCUSSION

The pesticides studied were selected from the most commonly used insecticides and acaricides used in the Plana de Castellón for control of citrus pests. Of the seven pesticides used, three were OPs (dimethoate, fenitrothion and methidathion) and four were OCs (lindane, dicofol, chlordifon and tetradifon).

The SPE study was divided into two parts, a study with disposable cartridges and Vac Elut system and a study with Empore membrane extraction discs, in order to compare the characteristics and suitability of the two systems.

The general scheme proposed by Wells and Michael [2] was followed to establish the optimum conditions for the extraction of pesticides from ground water. The retention step was kept constant with regard to the sample volume, fortification level and cartridge used, in order to optimize the elution step. The retention step was subsequently optimized, by adjusting the pH, salinity, sorbent mass, sample volume and sample concentration.

### *SPE cartridges*

A fixed sample volume (100 ml), sample concentration (10 μg l<sup>-1</sup> each pesticide) and car-

tridge type (100 mg C<sub>18</sub>) were used to retain the pesticides.

As shown previously [17], elution with dichloromethane, methanol, acetone or ethyl acetate gave good recoveries for all these pesticides, except for the most polar pesticide dimethoate. Under these conditions, all of the pesticides eluted in the first 1-ml fraction and none in the subsequent fractions. Dichloromethane (1 ml) was chosen for this study because it was the most volatile and easy to evaporate, although any of the other solvents previously tested were equally suitable.

All attempts to improve the dimethoate recovery (above 40%) were unsuccessful, even with adjustment of the sample pH and salinity. Cartridges containing more polar sorbents such as C<sub>8</sub>-, C<sub>2</sub>-, phenyl- and cyclohexyl-bonded types were equally unsuccessful.

These findings agree with other published data [8] indicating that dimethoate gave consistently low recoveries on C<sub>18</sub> and C<sub>8</sub> sorbents, whereas

TABLE 1

Recoveries of selected pesticides in groundwater after SPE with 500-mg C<sub>18</sub> cartridges using different eluents<sup>a</sup>

No.	Pesticide	Ethyl acetate (4 ml)		Dichloromethane (4 ml)	
		ECD <sup>b</sup>	NPD <sup>b</sup>	ECD <sup>b</sup>	NPD <sup>b</sup>
1	Dimethoate	87	86	87	89
2	Lindane	90		59	
3	Fenitrothion	101	83	94	86
4	Dicofol	73		76	
5	Methidathion	97	90	101	96
6	Chlorfenson	82		83	
7	Tetradifon	91		87	

<sup>a</sup> Conditions: 100-ml water sample containing 20% NaCl, sample pesticide concentration 10 µg l<sup>-1</sup> each. <sup>b</sup> ECD = electron-capture detection; NPD = nitrogen-phosphorus detection.

other organophosphorus pesticides studied gave good recoveries. The cause of such low recoveries was attributed to the polar *N*-methylamido group,

### Recoveries %

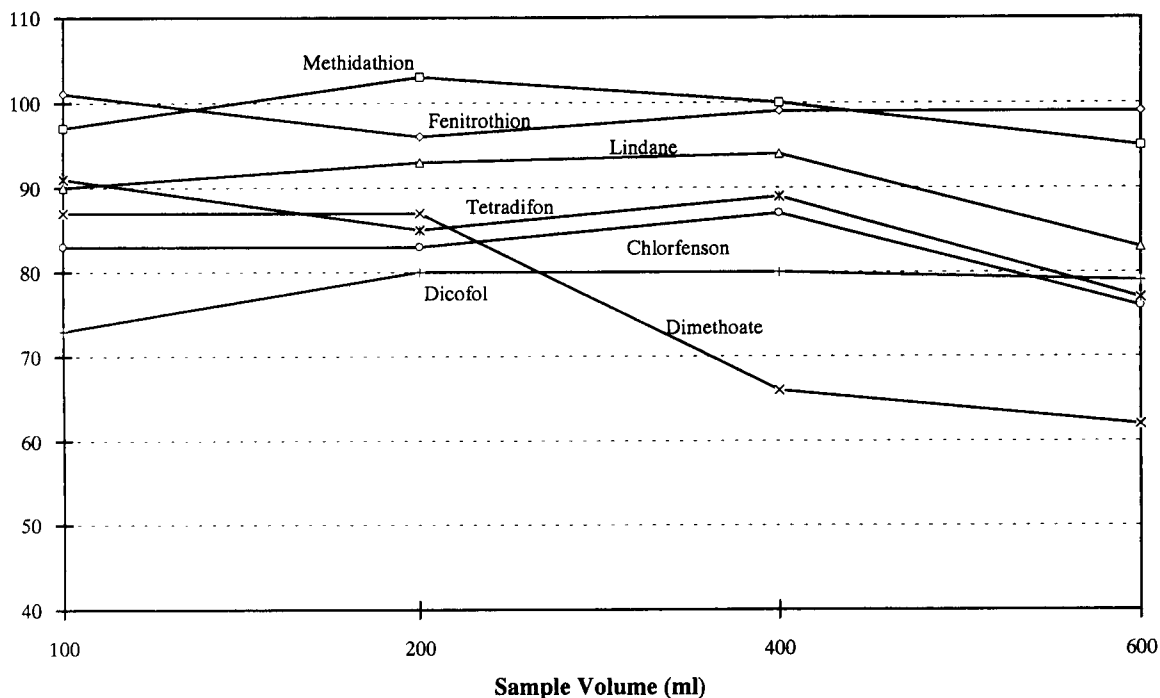


Fig. 1. Recovery of selected pesticides as a function of sample volume with a 500-mg C<sub>18</sub> cartridge.

TABLE 2

Mean recoveries and standard deviations <sup>a</sup> of selected pesticides in groundwater fortified at two different levels after SPE with 500-mg C<sub>18</sub> cartridges, and limits of detection <sup>b</sup>

Pesticide	1 $\mu\text{g l}^{-1}$		0.1 $\mu\text{g l}^{-1}$		Limit of detection ( $\mu\text{g l}^{-1}$ )	
	ECD	NPD	ECD	NPD	ECD	NPD
Dimethoate	75 ± 8	82 ± 7		83 ± 7	–	0.02
Lindane	83 ± 11		68 ± 8		0.004	
Fenitrothion	96 ± 1	90 ± 6		85 ± 8	0.007	0.012
Dicofol	79 ± 13		78 ± 12		0.05	
Methidathion	–	107 ± 8		113 ± 9	–	0.03
Chlorfenson	90 ± 7		88 ± 14		0.009	
Tetradifon	85 ± 7		83 ± 8		0.01	

<sup>a</sup> Calculated for five replicates. <sup>b</sup> Conditions: 200-ml water sample, containing 20% NaCl, elution with 4 ml of ethyl acetate.

<sup>c</sup> Detection limits calculated using results for the 0.1  $\mu\text{g l}^{-1}$  sample.

with stronger aqueous hydrogen bonding and therefore reduced C<sub>8</sub> or C<sub>18</sub> interaction.

The study was therefore focused on the opti-

mization of the retention step to increase the adsorption of dimethoate.

The sorbent mass was increased by using 200-

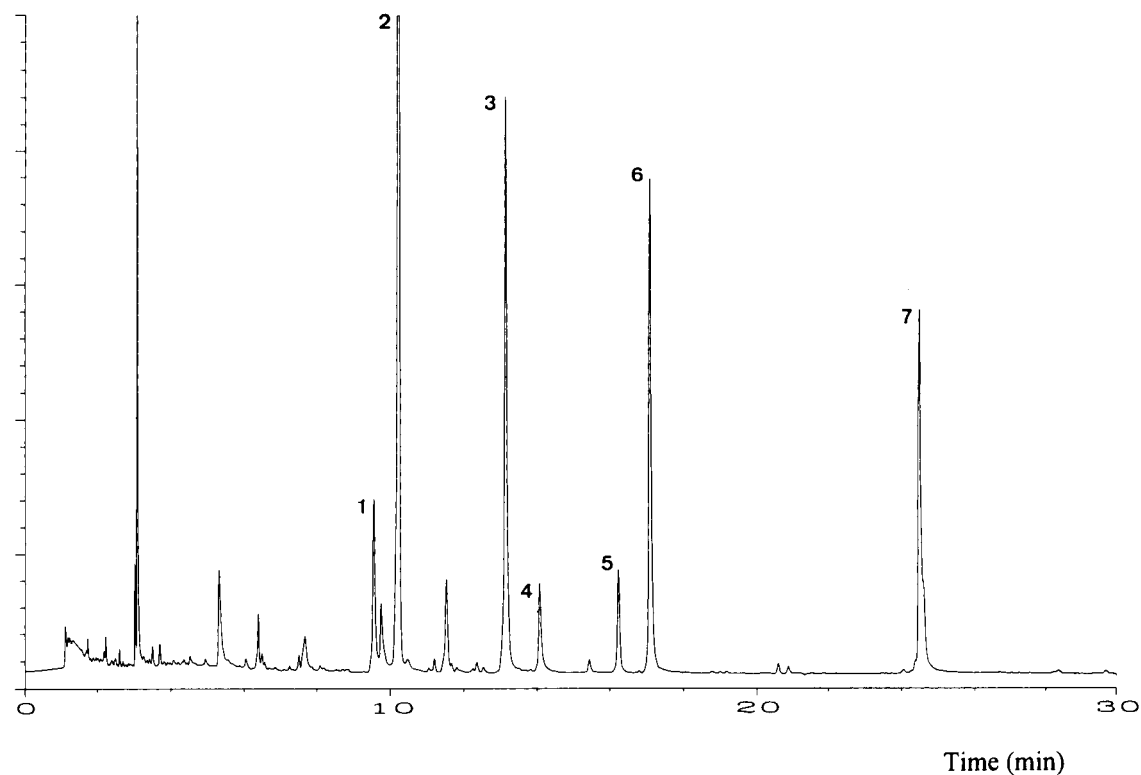


Fig. 2. Gas chromatogram with electron-capture detection of a fortified ground water sample extract after SPE with a 500-mg C<sub>18</sub> cartridge (ca. 1 ng each injected). For column and temperature programme see Experimental. Peaks: pesticides as numbered in Table 1.

and 500-mg C<sub>18</sub> cartridges, with a 100-ml water sample spiked at the 10 µg l<sup>-1</sup> level. The results, compared with those obtained using a 100-mg cartridge showed that the recovery of dimethoate increased with increase in the mass of sorbent. However, the use of larger amounts of sorbent also required an increase in the elution volume to elute the pesticides quantitatively, particularly the non-polar chlorfenson or tetradifon, which were strongly retained on the cartridge. The previous elution volumes with three 2-ml fractions of ethyl acetate or dichloromethane needed to be increased to at least 4 ml each. Moreover, the recovery of dimethoate was also considerably improved when NaCl was added to the water sample, reaching values near 100%. Table 1 shows the recoveries of pesticides obtained using a 500-mg C<sub>18</sub> cartridge.

The effect of sample volume was studied using

volumes of 100, 200, 400 and 600 ml of water, fortified at levels of 10, 5, 2.5 and 1.7 µg l<sup>-1</sup>, respectively, to maintain constant the total pesticide mass (1 µg each). The pesticide recoveries after passing different volumes of sample and eluting with 4 ml of ethyl acetate are shown in Fig. 1.

The maximum volume of sample suitable with the 500-mg cartridge was 200 ml. Larger volumes cause losses of dimethoate by exceeding the breakthrough volume. However, larger volumes of water, up to 600 ml, could be used if the determination of dimethoate is not required without any losses of the remaining pesticides studied.

The effect of sample concentration was studied at fortification levels of 10, 5, 1 and 0.1 µg l<sup>-1</sup>, using a 200-ml water sample.

The results obtained (Table 2) indicate that

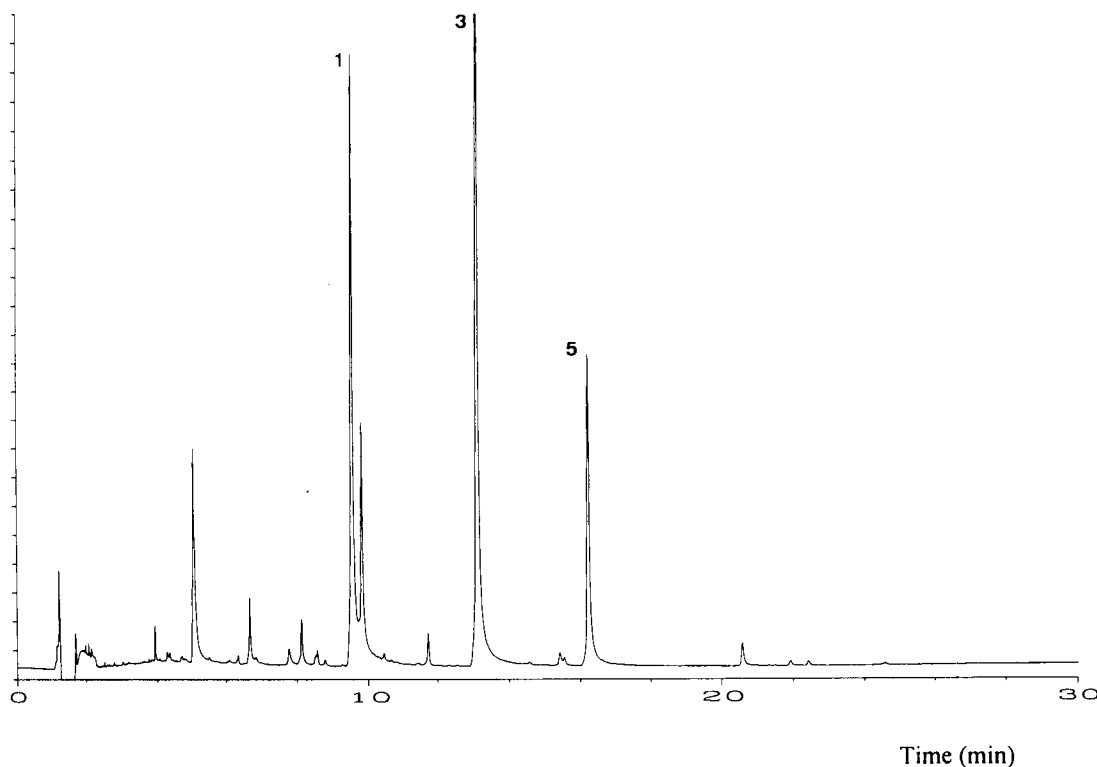


Fig. 3. Gas chromatogram with nitrogen–phosphorus detection of a fortified ground water sample extract after SPE with a 500-mg C<sub>18</sub> cartridge (ca. 1 ng each injected). For column and temperature programme see Experimental. Peaks: pesticides as numbered in Table 1.

TABLE 3

Recoveries of selected pesticides after SPE with Empore C<sub>18</sub> discs using different eluents<sup>a</sup>

Pesticide	Ethyl acetate (10 + 5 ml)		Dichloromethane (10 + 5 ml)	
	ECD	NPD	ECD	NPD
Dimethoate	51	51	31	29
Lindane	63		20	
Fenitrothion	96	97	67	63
Dicofol	78		56	
Methidathion	112	116	72	72
Chlorfenson	95		66	
Tetradifon	108		77	

<sup>a</sup> Conditions: 200-ml water sample; sample pesticide concentration 10  $\mu\text{g l}^{-1}$  each.

recoveries are suitable for application of this method to the determination of these pesticides in ground water. The limits of determination were calculated for a sample spiked at the 0.1  $\mu\text{g l}^{-1}$  level and are also given in Table 2. All the pesticides can be determined at levels below 0.1  $\mu\text{g l}^{-1}$ . Dimethoate and methidathion should be determined using the nitrogen–phosphorus detector signal because of its higher sensitivity, as the electron-capture detector signal does not allow be such low concentration levels to be reached.

Figures 2 and 3 show gas chromatograms of a ground water sample fortified at the 1  $\mu\text{g l}^{-1}$  level, after SPE (200-ml water sample containing 20% NaCl, 500-mg C<sub>18</sub> cartridge, elution with 4

ml of ethyl acetate; extract evaporated to a volume of ca. 200  $\mu\text{l}$  under a gentle stream of nitrogen).

#### Empore SPE discs

The general procedure with the discs was similar to that used with the cartridges. The variables, sample volume (200 ml), concentration (10  $\mu\text{g l}^{-1}$ ) and disc type (C<sub>18</sub>), were fixed initially.

The elution efficiencies of different solvents were measured with the cartridges. Therefore, only dichloromethane and ethyl acetate were checked with the discs using elution volumes of 4 × 2 ml followed by 5 ml. Each fraction was evaporated to dryness, the residue was dissolved in hexane and the solution was chromatographed. The chromatograms obtained showed that a small amount of pesticide was still eluted from the last fraction. The recoveries were similar using ethyl acetate and dichloromethane. The elution volume was increased to 10 ml plus 5 ml of ethyl acetate. Before injection into the gas chromatograph, the extract was evaporated under a gentle stream of nitrogen to a suitable volume, which was measured with a syringe prior to injection into the gas chromatograph (Table 3).

The recoveries of dimethoate and lindane were low, which indicated poor retention in the disc. In order to improve the retention, 20% NaCl was added to the water sample prior to extraction. The recovery of dimethoate was still low (Table 4) and the salting-out effect of NaCl was minimal.

TABLE 4

Mean recoveries and standard deviations<sup>a</sup> of selected pesticides in groundwater fortified at three different levels after SPE with Empore C<sub>18</sub> disc, and limits of detection<sup>b</sup>

Pesticide	10 $\mu\text{g l}^{-1}$		1 $\mu\text{g l}^{-1}$		0.1 $\mu\text{g l}^{-1}$		Limit of detection ( $\mu\text{g l}^{-1}$ ) <sup>c</sup>	
	ECD	NPD	ECD	NPD	ECD	NPD	ECD	NPD
Dimethoate	45	44	107 ± 16	88 ± 11	–	84 ± 3	–	0.03
Lindane	71		70 ± 4		73 ± 6		0.003	
Fenitrothion	95	89	118 ± 4	92 ± 1	115 ± 19	94 ± 1	0.008	0.02
Dicofol	75		76 ± 12		93 ± 10		0.04	
Methidathion	85	93	98 ± 14	99 ± 7	–	114 ± 14	–	0.04
Chlorfenson	99		97 ± 13		97 ± 9		0.01	
Tetradifon	101		117 ± 16		113 ± 13		0.009	

<sup>a</sup> Calculated for five replicates. <sup>b</sup> Conditions: 200-ml water sample containing 20% NaCl. <sup>c</sup> Detection limits calculated from results for the 0.1  $\mu\text{g l}^{-1}$  sample.

However, the recoveries of all compounds studied were quantitative at fortification levels down to  $1 \mu\text{g l}^{-1}$  (Table 4). This establishes an upper limit of determination of  $1 \mu\text{g l}^{-1}$  for dimethoate and of more than  $10 \mu\text{g l}^{-1}$  for the other pesticides studied. According to these results, extraction of 200 ml of water fortified at  $0.1 \mu\text{g l}^{-1}$  was carried out, and the recoveries calculated were satisfactory (Table 4).

The effect of sample volume was checked by extracting 400 ml of water fortified at 0.5 and  $0.1 \mu\text{g l}^{-1}$ . The results indicated that lower recoveries of some pesticides (dimethoate, lindane and dicofol) occurred when this sample volume was used at the  $0.1 \mu\text{g l}^{-1}$  level (exceeding the breakthrough volume).

Hence the final recommended procedure is to use 200 ml of water with the addition of 20% NaCl and extract with a 500-mg  $\text{C}_{18}$  disc. The disc should be eluted with  $10 + 5$  ml of ethyl acetate and concentrated under a gentle stream of nitrogen to a final volume of ca.  $100 \mu\text{l}$  prior to gas chromatographic analysis. When this procedure was applied to a ground water sample fortified at  $0.1 \mu\text{g l}^{-1}$ , the detection limits were satisfactory (Table 4).

In conclusion, the use of 500-mg  $\text{C}_{18}$  cartridges allows the quantitative extraction of all the pesticides studied, including the most polar dimethoate. The use of this amount of sorbent requires higher elution volumes (at least 4 ml of ethyl acetate). After concentration to ca.  $100 \mu\text{l}$ , the extract is injected into the chromatograph, reaching detection limits below  $0.1 \mu\text{g l}^{-1}$  for all the compounds studied.

Similar results are obtained when using Em-pore membrane extraction discs, although the use of cartridges has some advantages: smaller elution volumes (4 ml compared with 15 ml; hence less time required for evaporation); the possibility of extracting up to ten samples simultaneously using the Vac Elut system; and cartridges are about four times cheaper than discs with the same mass of sorbent.

Current studies are being focused on clean-up

procedures, based on packed-column chromatography with silica, Florisil or alumina, to be coupled with SPE cartridges in order to analyse samples with more complex matrix (such as surface water or water from the unsaturated zone).

J. Beltran is the recipient of a grant of Formación de Profesorado Universitario y Personal Investigador from the Ministerio de Educación y Ciencia. The purchase of the capillary gas chromatograph was possible with the help of Generalitat Valenciana. This work forms part of a research project (reference AGR91-1165) of the CICYT del Ministerio de Educación y Ciencia.

#### REFERENCES

- 1 J.J. Richard and G.A. Junk, *Mikrochim. Acta*, 1 (1986) 387.
- 2 M.J.M. Wells and J.M. Michael, *J. Chromatogr. Sci.*, 25 (1987) 345.
- 3 G.A. Junk and J.J. Richard, *Anal. Chem.*, 60 (1988) 451.
- 4 J. Mañes, J.C. Moltó, C. Igualada and G. Font, *J. Chromatogr.*, 472 (1989) 365.
- 5 D.M. Swineford and A.A. Belisle, *Environ. Toxicol. Chem.*, 8 (1989) 465.
- 6 P. Branca and P. Quaglino, *Boll. Chim. Igiene.*, 40 (1989) 71.
- 7 D.A. Hinckley and T.F. Bidleman, *Environ. Sci. Technol.*, 23 (1989) 995.
- 8 P.R. Loconto and A.K. Gaid, *J. Chromatogr. Sci.*, 27 (1989) 569.
- 9 E.R. Bogus, T.L. Watschke and R.O. Mumma, *J. Agric. Food Chem.*, 38 (1990) 42.
- 10 J.J. Richard, G.A. Junk, M.J. Avery, N.L. Nehring, J.S. Fritz and H.J. Svec, *Pestic. Monit. J.*, 9 (1975) 117.
- 11 E.E. McNeil, R. Otson, W.F. Miles and F.J.M. Rajabalee, *J. Chromatogr.*, 132 (1977) 277.
- 12 A. Przyjazny, *J. Chromatogr.*, 346 (1985) 61.
- 13 A. Verweij, M.A. van Liempt-van Houten and H.L. Boter, *Int. J. Environ. Anal. Chem.*, 21 (1985) 63.
- 14 G. Durand, R. Alonso and D. Barceló, *Quím. Anal.*, 10 (1991) 157.
- 15 D.F. Hagen, C.G. Markell, G.A. Schmitt and D.D. Blevins, *Anal. Chim. Acta*, 236 (1990) 257.
- 16 E.R. Brouwer, H. Ligeman and U.A.Th. Brinkman, *Chromatographia*, 29 (1990) 415.
- 17 F. Hernández, J. Beltran and J.V. Sancho, *Sci. Total Environ.*, 132 (1993) 297.



# Fluorimetric study of polycyclic aromatic hydrocarbons in Brij-35 micellar solution. Evaluation of polycyclic aromatic hydrocarbons in air samples

S. Rubio-Barroso, M. Nour Kayali and L.M. Polo-Díez

*Department of Analytical Chemistry, Faculty of Chemistry, Complutense University of Madrid, 28040 Madrid (Spain)*

(Received 23rd October 1992; revised manuscript received 26th April 1993)

## Abstract

The fluorescence intensity of polycyclic aromatic hydrocarbons (PAHs) is higher in Brij-35 micellar solution than in methanol. Pyrene, benzo[*ghi*]perylene and benzo[*a*]pyrene could be determined in the presence of up to a 100-fold excess of other PAHs, the errors being lower than 5%. The relative standard deviation was 5% at the  $\text{pg ml}^{-1}$  level. The detection limit for benzo[*a*]pyrene was particularly low at  $4 \text{ pg ml}^{-1}$ . The method was applied to the determination of pyrene, benzo[*ghi*]perylene and benzo[*a*]pyrene in particulate air samples; a comparison of the results with those given by gas chromatography shows the usefulness of the proposed method for evaluating these PAHs in air samples.

**Keywords:** Fluorimetry; Air; Micellar solution; Polycyclic aromatic hydrocarbons

Polycyclic aromatic hydrocarbons (PAHs) are environmental contaminants present at low ( $\text{ng ml}^{-1}$ ) concentrations in air, water, smoked foods and soil samples. Incomplete combustion of organic material leads to pyrosynthetic reactions which are responsible for the formation of PAHs. Many PAHs cause cancer in various animal species and perhaps in humans [1–3]. There are sixteen PAHs on the Environmental Protection Agency (EPA) priority pollutant list [4].

The techniques most often used for determining PAHs are gas chromatography (GC) [5–8] and liquid chromatography (LC) with spectrophotometric or fluorimetric detection [8–11]. Other techniques such as fluorimetry and phosphorimetry at room temperature on filter-paper or in organized media [12–15] have also been used.

*Correspondence to:* S. Rubio-Barroso, Department of Analytical Chemistry, Faculty of Chemistry, Complutense University of Madrid, 28040 Madrid (Spain).

Recently the possibility of the selective spectrofluorimetric determination of PAHs in organized media such as pluronic-F68 micellar solutions was evaluated [16].

This paper reports a systematic fluorimetric study of the behaviour of thirteen PAHs in micellar solution prepared with non-ionic Brij-35 surfactant. The sensitivity and hence the selectivity of PAH determinations in this medium are higher than in methanol and in Pluronic-F68 media [16]; this allows the development of a method for evaluating pyrene, benzo[*a*]pyrene and benzo[*ghi*]perylene in particulate air samples. Pyrene and benzo[*ghi*]perylene are considered to be among the most abundant PAHs and benzo[*a*]pyrene is one of the most studied for its carcinogenicity and its usefulness as an indicator of domestic and industrial contamination [17,18]; consequently, the development of simple methods for the determination of these compounds continues to be a matter of concern.

## EXPERIMENTAL

*Apparatus*

A Perkin-Elmer MPF-44A spectrofluorimeter and Perkin-Elmer No. 1 standard fluorescent samples were used to standardize the source intensity daily. A Selecta Frigitherm S-382 ultrathermostat, able to control the temperature to  $\pm 0.05^\circ\text{C}$ , and an Ultrasons P-Selecta bath were used. A MCV high-volume sampler equipped with 15-cm diameter Whatman GF/A glass-fibre filters was used for collecting particulate air samples.

*Reagents*

All chemicals were of analytical-reagent grade. Water was obtained from a Milli-Q system (Millipore). Stock standard methanolic solutions of different PAHs from Sigma at concentration in the range  $1.7 \times 10^{-3}$ – $1.1 \times 10^{-4}$  M, were prepared by weighing and dissolving the solid products in methanol (Carlo Erba). More dilute solutions were prepared by dilution with methanol.

An aqueous micellar solution of Brij-35 [polyoxyethylene 23 lauryl ether,  $\text{C}_{12}\text{H}_{25}(\text{OCH}_2\text{-CH}_2)_{23}\text{OH}$ ; formula weight = 1199.6; 30% (w/v)] from Sigma was prepared by dissolving 3.6 ml in 1.0 l of water to give a final concentration of  $9.0 \times 10^{-4}$  M; critical micellar concentration (c.m.c.) =  $10^{-4}$  M [2].

*Calibration procedure*

Calibration graphs were prepared using the methanolic PAH stock standard solutions. Volumes of these solutions suitable for PAH concentrations in the range  $1.2 \times 10^{-2}$ – $44.1 \text{ ng ml}^{-1}$  were transferred into 10.0-ml volumetric flasks (the concentration ranges for each particular PAH are specified in Table 3), diluted to volume with  $9.0 \times 10^{-4}$  M Brij-35 solution and stirred for 5 min by sonication in an ultrasonic bath. The fluorescence intensity was measured at  $10 \pm 0.05^\circ\text{C}$  at the selected excitation and emission wavelengths (Table 1) and corrected for the blank.

*Air sample collection*

The sampler was placed on the roof of a building and samples were taken at a flow-rate of

$30 \text{ m}^3 \text{ h}^{-1}$  for 24 h in winter of 1991.

*Sample extraction*

The PAHs were extracted ultrasonically with 50 ml of cyclohexane for 20 min and centrifugation at 4000 rpm (3100 g) for 20 min. The extract was concentrated first in a rotary vacuum evaporator and then to 0.5 ml with a stream of nitrogen.

*Clean-up*

Clean-up was carried out with silica gel, activated at  $130^\circ\text{C}$  for 24 h and deactivated with 5% of water, in a glass column (40 cm  $\times$  1 cm i.d.). Elution was effected first with 25 ml of hexane and then with 40 ml of hexane–methylene chloride (4 + 1). The second fraction was concentrated in a rotary vacuum evaporator and the solvent was eliminated under a stream of nitrogen. The residue was dissolved in 25.0 ml of methanol and then the above fluorimetric procedure was applied to 100–200- $\mu\text{l}$  aliquots.

## RESULTS AND DISCUSSION

*Fluorimetric study of PAHs in Brij-35 micellar solution*

The emission intensity of PAHs generally increases with increasing Brij-35 concentration up

TABLE 1

Spectral characteristics of PAHs in Brij-35 micellar solution

PAH	$\lambda(\text{ex})/\lambda(\text{em})$ (nm)		$I_{\text{Brij-35}}/I_{\text{MeOH}}^a$
	Brij-35	MeOH	
Pyrene	338/391	334/376	13.8
Benzo[ghi]perylene	300/420	376/425	6.7
Benzo[a]pyrene	297/410	294/408	3.5
Benzo[e]pyrene	289/394	286/393	3.5
Benzo[a]anthracene	288/393	283/390	3.1
Chrysene	267/384	263/383	2.6
Dibenzo[a,h]anthracene	298/400	294/398	2.4
Phenanthrene	248/365	245/365	2.4
Acenaphthene	291/329	294/327	2.0
Naphthalene	275/328	272/328	2.0
Fluoranthene	285/460	283/460	1.8
Fluorene	267/311	260/310	1.0
Anthracene	249/406	246/402	0.6

<sup>a</sup> Sensitization factors of PAHs in micellar solution.

TABLE 2  
Effects of time and temperature on micellar solution stability

PAH	$\Delta I_{F,24h}$ (%) <sup>a</sup>	$-\Delta I_{F,10-30^\circ C}$ (%) <sup>b</sup>
Pyrene	-1.9	28.6
Benzo[ghi]perylene	0.9	8.1
Benzo[a]pyrene	-6.3	10.7
Benzo[e]pyrene	0.1	7.3
Benzo[a]anthracene	-2.6	12.2
Chrysene	3.6	5.5
Dibenzo[a,h]anthracene	-2.8	4.3
Phenanthrene	0.2	8.2
Acenaphthene	-12.4	8.3
Naphthalene	-15.4	11.7
Fluoranthene	-6.4	4.7
Fluorene	-5.7	5.4
Anthracene	-17.5	5.5

<sup>a</sup> Difference between fluorescence intensities at 0 and 24 h.

<sup>b</sup> Difference between fluorescence intensities at 10 and 30°C.

to the c.m.c. ( $10^{-4}$  M), above which it remains virtually constant. A higher concentration ( $9 \times 10^{-4}$  M) was therefore chosen for further work.

The excitation and emission wavelength maxima (Table 1) show that in most instances the

TABLE 3  
Analytical characteristics of PAHs in Brij-35 micellar solution

PAH	Range studied (ng ml <sup>-1</sup> ) <sup>a</sup>	R.S.D. <sup>b</sup>	DL (ng ml <sup>-1</sup> ) <sup>c</sup>
Pyrene	0.07– 2.63	2.3	0.02
Benzo[ghi]perylene	0.06– 5.53	3.5	0.02
Benzo[a]pyrene	0.01– 1.77	5.6	0.004
Benzo[e]pyrene	0.05– 8.83	1.8	0.01
Benzo[a]anthracene	0.03–20.5	2.1	0.01
Chrysene	0.02– 4.79	1.6	0.005
Dibenzo[a,h]anthracene	0.04– 2.50	1.8	0.01
Phenanthrene	0.21– 6.24	1.8	0.06
Acenaphthene	0.32–15.4	2.9	0.09
Naphthalene	0.85–44.1	1.6	0.2
Fluoranthene	0.17– 9.71	6.2	0.05
Fluorene	0.07– 6.32	1.9	0.02
Anthracene	0.03– 2.14	3.8	0.01

<sup>a</sup> The first value is the limit of determination ( $k = 10$ ). <sup>b</sup> Relative standard deviation ( $n = 10$ ). <sup>c</sup> Limit of detection ( $k = 3$ ).

spectra are not shifted significantly with respect to those in methanol. Only the shifts for pyrene [ $\Delta\lambda(\text{em}) = 15$  nm] and benzo[ghi]perylene [ $\Delta\lambda(\text{ex}) = 76$  nm] are notable; these shifts should increase the selectivity of benzo[ghi]perylene de-

TABLE 4  
Interference study of pyrene, benzo[ghi]perylene and benzo[a]pyrene in Brij-35 micellar solution

PAH	PAH/Pyr <sup>b</sup>	$E_r$ (%) <sup>a</sup>	PAH/B[ghi]Pery <sup>b</sup>	$E_r$ (%) <sup>a</sup>	PAH/B[a]Pyr <sup>b</sup>	$E_r$ (%) <sup>a</sup>
Pyrene	–	–	1	11	10	32
					1	3.3
Benzo[ghi]perylene	1	12	–	–	1	10
Benzo[a]pyrene	1	7.6	1	10	–	–
Benzo[e]pyrene	1	3.6	1	11	10	56
					1	–0.8
Benzo[a]anthracene	1	16	1	14	1	9.7
Chrysene	10	6.0	10	22	10	27
	1	2.4	1	–2.6	1	4.6
Dibenzo[a,h]anthracene	1	8.0	1	63	1	16
Phenanthrene	1	–7.2	10	14	10	21
			1	–4.8	1	2.4
Acenaphthene	100	15	100	18	100	18
	10	2.0	10	2.2	10	–7.6
Naphthalene	1000	12	1000	49	1000	26
	100	0.8	100	–4.0	100	5.2
Fluoranthene	1	15	10	45	10	9.2
			1	–4.0	1	0.4
Fluorene	100	7.4	1	62	10	8.7
	10	0.8			1	0.1
Anthracene	1	5.8	1	27	1	38

<sup>a</sup> Average of two determinations. <sup>b</sup> Pyr = pyrene; B[ghi]Pery = benzo[ghi]perylene; B[a]Pyr = benzo[a]pyrene.

terminations. The fluorescence sensitization factors, defined as the ratio of fluorescence intensity in Brij-35 to that in methanol, are also given in Table 1; these factors are  $> 2$  in most instances; the highest values are 13.8 for pyrene and 6.5 for benzo[ghi]perylene. These results suggest that the selectivity for pyrene and benzo[ghi]perylene should increase in micellar solution.

The stability results in Table 2 show that all the solutions studied were stable for at least 24 h, except naphthalene, anthracene and acenaphthene, whose fluorescence intensity decreased by 15.4, 17.5 and 12.4%, respectively, in 24 h. No significant changes in emission fluorescence were observed when it was measured in the first hour.

The effect of temperature on quantum emission efficiency (Table 2) is fairly critical for pyrene, which has the highest sensitization factor.

#### Analytical characteristics

Individual standard solutions were used to obtain the analytical characteristics summarized in Table 3. The range of linearity (which was the studied range) was adjusted so that there were no more than about 100 arbitrary fluorescence units at the upper concentration, and depended on the individual PAH sensitivities. The relative stan-

dard deviation was 5% at the  $\text{ng ml}^{-1}$  level ( $n = 10$ ). The detection limits for benzo[a]pyrene and chrysene were particularly low (about  $5 \text{ pg ml}^{-1}$ ), between 0.5 and 1.5 orders of magnitude lower than in Pluronic-F68.

The selectivity studies are summarized in Table 4 in terms of relative errors ( $E_r$ ). The effect of the presence of the other PAHs on the fluorescence intensities of pyrene, benzo[ghi]perylene and benzo[a]pyrene was studied. Pyrene and benzo[ghi]perylene were chosen because they showed the highest wavelength shift and sensitization factor; on the other hand, benzo[a]pyrene has the highest toxicity [1–3]. Certain PAH/analyte ratios are particularly notable. Pyrene, benzo[ghi]perylene and benzo[a]pyrene could be determined in the presence of a 100-fold excess of naphthalene, pyrene and benzo[ghi]perylene could be determined in the presence of a tenfold excess of acenaphthene and pyrene could be determined in the presence of a tenfold excess of fluorene, the errors being lower than 5%.

#### Evaluation of PAHs in air samples

The proposed fluorimetric method was applied to the determination of pyrene, benzo[ghi]perylene and benzo[a]pyrene in particulate air sam-

TABLE 5  
Evaluation of PAHs in air samples

Sample <sup>a</sup>	Medium	Method	Concentration ( $\text{ng m}^{-3}$ air) <sup>b</sup>			
			Benzo[a]pyrene	Pyrene	Benzo[ghi]perylene	Total
1	Brij-35	SS <sup>c</sup>	3.5	2.7	9.1	
		SA <sup>d</sup>	3.8	2.9	10.7	
	P-F68	SS	3.0	2.0	11.1	
		SA	2.9	2.0	10.3	
2	Brij-35	GC <sup>e</sup>	2.6	1.6	7.4	32
		SS	4.8	5.0	10	
		SA	4.1	4.2	9.1	
	P-F68	SS	5.9	5.6	13.5	
		SA	5.7	5.6	12.5	
		GC	3.6	4.0	8.5	80
3	Brij-35	SS	9.7	11	14	
		SA	9.5	10	13	
	P-F68	SS	12	13	16	
		SA	11	13	15	
		GC	6.6	7.9	9.9	

<sup>a</sup> Samples were collected in the city of Madrid in winter, 1991. <sup>b</sup>  $n = 3$  (average of three determinations on the same sample).

<sup>c</sup> SS = series of standards method. <sup>d</sup> SA = standard additions method. <sup>e</sup> GC = EPA gas chromatographic TO-13 method [19].

ples for screening purposes. The results are shown in Table 5. There were only small differences between the results of the standard additions method (SA) and the series of standards method (SS). The slopes of the two calibration graphs were similar, indicating that matrix effects are not significant, and this may explain the small differences in the results of the two calibration methods. These results were generally higher than those obtained by gas chromatography (GC).

Pluronic-F68 (P-F68) was also used instead of Brij-35 to prepare the micellar solutions [16]. The results were similar to those found with Brij-35 with respect to the calibration graphs. The contents of each particular PAH are included in Table 5.

The results for samples 2 and 3 are higher when using P-F68 than when using Brij-35. It seems that Brij-35 is more suitable than P-F68 when the complexity of the sample, indicated by its total PAH content, is higher. This can be explained by taking into account that the sensitization factors for Brij-35 are higher than for P-F68 and, consequently, the selectivity is higher using Brij-35.

The fact that the results for sample 1 obtained using P-F68 are lower than those obtained with Brij-35 can only be attributed to the different nature of this sample.

### Conclusions

The fluorescence emission of most PAHs, in particular pyrene and benzo[ghi]perylene, in Brij-35 micellar solution is significantly higher than in methanol; the most significant excitation and emission wavelength shifts are those of benzo[ghi]perylene and pyrene, respectively. This allows the development of a simple and rapid method for evaluating these two compounds and benzo[a]pyrene in particulate air samples. The results are higher than those obtained by gas chromatography owing to lack of selectivity. However, the method may be useful for screening purposes because these three compounds are of significance in environmental studies.

The financial support of the Spanish CICYT (project PB89-0109) is gratefully acknowledged.

### REFERENCES

- 1 W. Stahl and G. Eisenbrand, in R. Macrae (Ed), HPLC in Food Analysis, Academic Press, New York, 1988, p. 377.
- 2 M. Zander, in T. Vo-Dinh (Ed.), Chemical Analysis of Polycyclic Aromatic Compounds, Wiley, New York, 1989, p. 171.
- 3 J. Jaklin and P. Krenmayr, in J. Albaigés and R.W. Frei (Eds.), Fate of Hydrocarbons in the Environment, Gordon and Breach, New York, 1986, p. 73.
- 4 L.H. Keith and W.A. Telliard, Environ. Sci. Technol., 13 (1979) 416.
- 5 K. Speer, E. Stees, Th. Kuehn and A. Montag, J. High Resolut. Chromatogr., 13 (1990) 104.
- 6 W. Auer and H. Malissa, Anal. Chim. Acta, 237 (1990) 451.
- 7 A. Bemgard and A. Colmsjö, J. Chromatogr. Sci., 30 (1992) 23.
- 8 H.A.M.G. Vaessen, P.J. Wagstaffe and A.S. Lindsey, Fresenius' Z. Anal. Chem., 336 (1990) 503.
- 9 S.N. Sivaswamy, B. Balachandran and V.M. Sivaramakrishnan, Curr. Sci., 59 (1990) 480.
- 10 M.D. Nuñez and F. Centrich, Anal. Chim. Acta, 234 (1990) 269.
- 11 N. Hethrington and M. Dong, Am. Environ. Lab., 2 (1990) 31.
- 12 S.M. Inmann, P. Thibado, G.A. Theriault and S.H. Lieberman, Anal. Chim. Acta, 239 (1990) 45.
- 13 S.G. Schulman, Molecular Luminescence Spectroscopy. Methods and Applications, Parts 1 and 2, Wiley, New York, 1985 and 1988.
- 14 R.J. Hurtubise, Phosphorimetry. Theory, Instrumentation and Applications, VCH, New York, 1990.
- 15 T. Vo-Dinh, Room Temperature Phosphorescence for Chemical Analysis, Wiley, New York, 1984.
- 16 S. Rubio-Barroso, D. López-López, C. Val-Ontillera and L.M. Polo-Díez, Quím. Anal., 10 (1991) 127.
- 17 B. Muel and S. Saguem, Int. J. Environ. Anal. Chem., 19 (1985) 111.
- 18 H.C. Steinmetzer, W. Baumeister and O. Vierle, Sci. Total Environ., 36 (1984) 91.
- 19 Compendium of Methods for the Determination of Toxic Organic Compounds in Ambient Air, Environmental Protection Agency, Washington, DC, 1988, EPA 600/4-89/017.

# Chromatography, today and tomorrow

Georges A. Guiochon

*Department of Chemistry, University of Tennessee, Knoxville, TN 37996–1600; and Division of Analytical Chemistry,  
Oak Ridge National Laboratory, Oak Ridge, TN (USA)*

(Received 7th October 1992)

## Abstract

The history of chromatography is briefly reviewed. Current trends are documented, pointing to the advanced degree of maturation of the method. Its future as a research area results from its unique position as an extremely powerful technique of investigation of the thermodynamics and kinetics of phase equilibria, in the same time as it is the most powerful method of separation available in the life sciences.

*Keywords:* Chromatography; History of chromatography

A number of reviews have been published recently under a similar title [1–4]. The basic rules of the exercise seem to call for a thorough review of the present status of the method, followed by a list of the unresolved problems as seen by the author, and a more or less careful extrapolation to the future of the trends observed over the recent past. Given the poor state of the art of crystal ball detectors, and the current lack of attention devoted to the development of divination methods, it is not surprising that the quality of the latter part rarely measures up to that of the first one. The human mind experiences tremendous difficulties at imagining what could happen besides the normal continuation of the present course of events.

Most people extrapolate along the slope of the current trend. Only the most gifted and best trained in the art of forecasting can take the current curvature into account. Almost by definition, new discoveries cannot be forecasted, although their annunciation would be the best pos-

sible contribution of an exercise such as the one I am attempting. As a particularly striking example, we can refer to the remarkable development of the personal computers in the early 1980s, to the change they made in the very concepts of modern instrumentation, and to the costly decisions made by companies whose managers did not anticipate this development when the first inexpensive microprocessors appeared in the late 1970s.

After this careful disclaimer, and noting that the unique crystal-ball detector known<sup>a</sup> is currently borrowed by the Department of Economics, I will follow the traditional approach. We have to remember first that chromatography [5,6] is celebrating its 90th birthday this year, while gas chromatography reaches the mature age of forty [7]. During this long time span chromatography has evolved, spread and is maturing. It is useful to briefly recall the salient steps of this impressive

<sup>a</sup> This detector belonged to Napoleon I, who inadvertently dropped it on the ground under his tent the night before Waterloo. It is now conserved in the Museum of the Ecole Polytechnique (Palaiseau, France).

*Correspondence to:* G.A. Guiochon, Department of Chemistry, University of Tennessee, Knoxville, TN 37996–1600 (USA).

TABLE 1

Stages of development of a technique

- 
- Discovery of a new technique
  - Spread of the discovery
  - Commercialization of the proper instruments
  - Maturity of the technique
  - Inclusion in the cultural background
- 

career. Table 1 summarizes the various steps in the evolution of a technique [1].

#### DISCOVERY OF CHROMATOGRAPHY

Almost everybody knows now the sad life story of Tswett [5,6]. What is not fully realized, however, is the extreme care which was paid by Tswett to experimental details, and the considerable grasp he had of the fundamental problems encountered in the use of this new analytical method [8]. Unfortunately, published in Russian in a Polish Journal of Botany [9,10], the first papers languished a long time on dusty shelves. The PhD dissertation escaped oblivion and the destructions of a civil war because a copy was passed on to Willstätter [11], who had a German translation made and eventually gave it to Kuhn.

Eventually, Kuhn used Tswett's results to begin the series of investigations which lead to the rebirth of chromatography [12]. Plant pigments are extremely sensitive to isomerization, and to various degradation reactions. They do not survive well to extended contacts with silica. The first chromatograms were obtained by Tswett with finely divided calcium carbonate, a very gentle adsorbent. This detail escaped the German chemists in their earlier attempts at reproducing Tswett's results using silica gel. This explains the early hostility of Willstätter [8] towards the method, and why, rather typically, the new technique faded away after a brilliant discovery was made. The method began to take off only thirty years later, after Kuhn and Lederer had overcome the artifact problems.

Note that already at this early stage, chromatography was the realm of biochemists. A botanist interested in the composition of plant

pigments, or a chemist involved in the unraveling of the structure of carotenoids would now be called biochemists. Truly, chromatography belongs to biochemists. Some of the current trends we are witnessing now and that we will discuss later are merely the continuation of an original inclination attested by the long list of affairs chromatography had with biochemistry. The period that follows the rediscovery by Kuhn and Lederer shows a rapid succession of progress and innovation, sanctioned by a long series of Nobel prizes. The work of Martin and Synge on paper chromatography [13], followed ten years later by the development of gas chromatography [7], already seeded in the original paper of Martin and Synge, are examples of the many fields which were explored and the techniques which were developed before, during, and immediately after World War II.

#### THE SPREADING OF CHROMATOGRAPHIC TECHNIQUES

The spreading of chromatography as an analytical technique has proceeded by leaps and bounds. By birth, chromatography is a 19th century technique, which could have been understood, or at least assimilated and used, by the Founding Fathers of chemistry. In contact with the electronic revolution of the 1960s, it undertook a remarkable evolution which transformed it completely. This is illustrated, for example, by the progressive replacement of "conventional" by "high performance" column liquid chromatography<sup>a</sup>. In the first period, the instrumentation was minimum. A glass column was packed, and the mobile phase was left percolating under the driving force of its mere weight. Fraction collection, off-line analysis, lack of control, slow analysis, and intensive human labor were the rule. The kinetics of chromatographic phenomena was not studied. During the second period, all the modern conquest of electronic based instrumentation were progres-

<sup>a</sup> HPLC has been used to mean many different things during the last 20 years, high-pressure LC, high-performance LC, or high-price LC.

TABLE 2

Implementations of the chromatographic principle

- 
- Gas–solid chromatography
  - Gas–liquid chromatography
  - Supercritical fluid chromatography
  - Normal phase liquid chromatography
  - Reversed-phase liquid chromatography
  - Hydrophobic interaction chromatography
  - Ion-exchange chromatography
  - Size-exclusion chromatography
  - Ligand-exchange chromatography
  - Affinity chromatography
  - Thin-layer chromatography
- 

sively included in the chromatograph. In present-day chromatographs, detection is on-line, the eluent is pumped through the column, most parameters are controlled, computer data acquisition and handling have become universal. While the equipment has become automatic, the analysts are leaving the laboratory for offices.

Indicative of the power of the chromatographic principle, is the rapid multiplication in the number of the different techniques implementing it, a number which increased from a few to a dozen in the 1950s and 1960s (Table 2). Each of these techniques, in turn, underwent the same cycle of discovery, spreading, explosive growth, commercialization and maturity. Some chromatographic techniques have even undergone the cycle twice. As explained above, liquid–solid chromatography, the very technique discovered by Tswett was entirely changed and rejuvenated by the incorporation of the developments which had made gas chromatography such a successful technique in the 1960s. Size exclusion chromatography appeared a mature technique in the early 1970s. It has continued developing at a steady pace by putting to use the progress made in liquid–solid chromatography (instrumentation, data handling techniques), and especially in the design of new stationary phases.

Three types of fluids with widely different sets of physico-chemical properties, liquids, low and high density gases (those including supercritical fluids) can be used as the mobile phase. A wide

variety of retention mechanisms, including all types of molecular interaction known, have been studied, and appropriate stationary phases made available for their application. Adsorption remains the premier retention mechanism, having spawned at least five different methods, normal and reversed-phase liquid–solid chromatography, hydrophobic interaction chromatography, besides the classical gas–solid and supercritical fluid–solid chromatography. Even the total absence of molecular interactions in the stationary phase has found its place in the array of possibilities; it is the basis of size exclusion chromatography. Again, we must observe that biochemists have been at the origin of most of these methods. All this activity has created an explosion in the number of papers published, hence the number of citations, reviews, abstracts, books and computer programs. This fact has not been lost on the publishing companies.

#### POPULARIZATION OF CHROMATOGRAPHY

Whichever standard we use to measure it, the number of papers published in analytical chemistry journals, whether broad-based or dedicated to chromatography, has increased most rapidly between 1950 and 1980. The current trend shows certainly the approach of a maximum (Fig. 1).

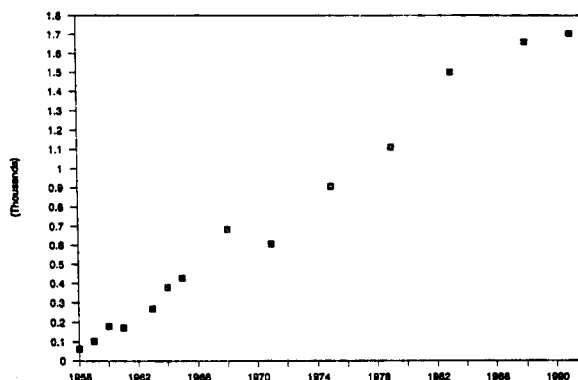


Fig. 1. Number of papers published yearly by the *Journal of Chromatography* since its foundation in 1958.



Quite significantly, fewer and fewer papers deal with instrumentation or with fundamental issues, although every now and then a spur of activity is still observed on some special problem. On the other hand, more and more papers discuss new applications of one of the chromatographic methods to the solution of these analytical problems which were ignored yesterday, have become critical today, and will be mere routine tomorrow.

Obviously, this type of activity is necessary in many industries, or for countless applications in academic or industrial research, and the publication of its results, being of potential use to many, is legitimate. However, method development or the investigation of technological improvements is not the main stay of academic research. So, the rising tide of application papers is probably the result of the conjunction (i) of a publication system geared to handle a massive number of papers, and needing material to process; (ii) of the large number of new method developments which must be studied each year because of the expanding needs of analysis in the life sciences and related industries; and of (iii) the considerable effort which is still required to develop these methods, and which justifies the writing of a paper, at least in the author's mind. The statistical studies of Giddings [14,15] and Oros and Davis [16] on the resolution power of a column and the number of components which are likely to be resolved on this column explain the fundamental source of the difficulties of method development.

Be as it may, we can safely state that the main thrust of research in chromatography is now returning to biochemistry, after having for many years laid in the area of physical chemistry where it was the central purpose of the activities of many scientists from a wide variety of walks. Most fundamental chromatography problems are solved now. What are not solved, are problems in other fields of chemistry that the chromatographer has to elucidate in order to perform separations. Most of them are problems of the thermodynamics of phase equilibria, and problems of material sciences. They revolve around the key question of chromatography, how to make and use better stationary phases.

## THE COMMERCIALIZATION OF CHROMATOGRAPHY

More striking still than the explosion in the number of papers, is the blossoming of a large market, supporting a multi-billion dollar industry, and served by several dozen companies of widely different sizes, selling instruments, accessories, dedicated products, and services. A number of instrumentation giants have come into chromatography through their own research and development effort, but more often by buying successful small companies created by imaginative, persistent inventors. Many medium size companies have been started by far-sighted analytical chemists, and produce highly reputable instruments. They often survived with difficulties the loss of their founder, especially when it resulted from a sale and lead to the misguided efforts of the purchasing company at boosting revenues. A vast number of small companies make or sell the variety of instruments, stationary phases, accessories, chemicals, gadgets, tubings, valves fittings, etc. that a chromatographer needs.

A single visit to the annual *Pittsburgh Conference on Analytical Chemistry and Applied Spectroscopy* (which had to add Analytical Chemistry to its name because chromatographers were outnumbering spectroscopists) suffices to convince anyone of the huge size and the vitality of this industry. The visit of any trade show on instrumentation the world over confirms the reality of this conclusion. Now, all this industry is here to stay, whatever happens to the research field of chromatography. Not long ago, there were still more money spent on buying gas than liquid chromatographs, although the papers published on liquid chromatography outnumbered those on gas chromatography years earlier. But the market of chromatographic instrumentation has become a replacement market. To understand what this means, we have to remember that we still buy balances, but we rarely meet to discuss the science of weighing.

What may be in doubt, however, is the future of another aspect of the popularization and commercialization of chromatography, the symposium industry. The number of these meetings has in-

creased rapidly over the years. If they have contributed usefully to spread the technique, they have also largely contributed to fragment it, or rather to consolidate its fragmentation. For example, we see rarely specialists of affinity chromatography in HPLC symposia. Ten years ago, I collated the lists of the attendants to HPLC'81 (ca. 600 people) and to the symposium on affinity chromatography organized the same year in Strasbourg (ca. 300 people). There were only 2 people whose names were on both lists! Symposia on planar chromatography, open tubular column chromatography, microcolumn chromatography, supercritical fluid chromatography, chiral chromatography, preparative chromatography, have multiplied, while each and every meeting on analytical chemistry needs one or several sessions on chromatography, and meetings on technique X like a session on X-chromatography coupling. You may not think seminars are a business. My travel agent does. I wonder how long this will last, and whether the reduction in attendance observed at minor meetings this year is the fruit of the recession or the harbinger of a new trend.

#### MATURITY AND ITS PROBLEMS

History tells us that people who live through a transition period have had always great difficulties to observe it. We, chromatographers, are in such a period for two reasons. Our very field is in transition, and the world around us is also in transition, causing analytical chemistry to spread, develop and evolve. The present crisis of our technical society, induced in part by the fatigue of its actors, in part by the immensity of the new problems it is causing to itself, creates new needs. Some of them can be solved only through more frequent or more intense uses of chromatography. So, while chromatography is maturing and slowly fading as an area of fundamental scientific research, society is requiring from us new progress, and wants many more of us. This will provide for what I believe will be an intense flurry of activity in the short or medium term, may be a dozen years, followed by a rapid melting in the background of chemical culture.

#### *Driving force for the expansion of research in chromatography*

Today, research in chromatography remains very active in several areas involving the thermodynamics and kinetics of the retention mechanisms, the fundamentals of method development (including optimization and the statistics of band overlap), the extension of chromatographic separations to new classes of compounds of biochemical importance, large scale preparative chromatography and microcolumn technologies. An increasing fraction of this effort, however, is devoted more to technological development than to fundamental problems.

The reason for the extraordinary level of interest and funding we have received in the past twenty years and are still receiving now is the constant stream of new legislations boiling out from our political centers. In the United States, the innumerable Acts watching over the safety of our foods, drugs and cosmetics, the safety of our air, water and environment, the safety of our industrial practices, have made necessary the multiplication of countless analysis types (Table 3<sup>a</sup>). Most of them require the use of chromatography, alone or in combination with other techniques. Since we have decided that we should be in perfect health and live forever, the maintenance of our body requires also analyses in increasingly large numbers, and analyses of an ever deeper complexity. As we, academic chromatographers and biochemists, make more chromatographic analysis possible, we feed a system which, through the combination of their potential usefulness and the threat of malpractice liability, forces physicians to require more analysis, thus making necessary the employment of more chromatographers. Although we have lost many jobs to computers in those last ten years, we have created many more through the operations of the legal system. Because of the increasingly complex requirements of a more and more sophisticated

<sup>a</sup> Understanding what it is exactly that the laws require to do, when and how can keep busy teams of lawyers and chemists which many medium size companies can ill or even no longer afford [see A.M. Thayer, *Chem. Eng. News*, 38 (1992) 9].

TABLE 3

List of US acts <sup>a</sup> relevant to the production and handling of chemicals

---

Federal food, drug and cosmetic act
Toxic substances control act (TOSCA)
Clean air act
Clean water act
Resource conservation and recovery act (RCRA)
Safe drinking water act
Occupational safety and health act
Hazardous materials transportation act
Comprehensive environmental response, compensation and liability act (CERCLA or Superfund)
Federal hazardous substance act
Federal insecticide, fungicide and rodenticide act (FIFRA)
Consumer product safety act
Pollution prevention act of 1990
Emergency planning and community right-to-know act (Part of Superfund amendment and reauthorization act, or SARA)
Poison prevention packaging act
Ports and waterways safety act
Marine protection, research and sanctuaries act

---

<sup>a</sup> Many of these acts have been modified by amendments passed later (e.g., SARA). This greatly enhances the complexity of the legal field.

society, new demands will continue to fuel chromatographic research for a long time. Analytical chemistry and especially chromatography is a field full of promises, because it holds one of the most important keys to safety, the goal of our modern society.

Is there any reason for this process to stop before everybody has become a chromatographer, or before we know how to detect a molecule of any thing in any sample? Obviously there is, the question is when. Before discussing it, let us review the problems we have to face and solve to accomplish our mission. I will divide these problems into those which are purely chromatographic, and those which are found in other areas of science and technology, where we have to take the answers from. These are mainly phase equilibrium thermodynamics and detection methods.

#### *Thermodynamic problems*

Chromatographers would like, and will need, to be able to call a computer data bank and

determine rapidly the retention data of some new components on a series of phases. This could be done by selecting data previously measured by another scientist on the same phase or on a similar one from some computer file, by correlating data previously measured for some similar components on the same, or a similar phase, or by using some computer program based on correlations between retention data and chemical structure. This would save considerable time and avoid wasting precious chemicals in the acquisition of new data. It should be emphasized that now is the time to invest in any project whose results will contribute to reduce wastes later.

Many current difficulties arise from our lack of understanding of retention mechanisms <sup>a</sup>. This has nothing to do directly with chromatography, and is truly a thermodynamic problem. The trouble is that so many chromatographers have unknowingly turned themselves into thermodynamicists without really knowing the basics nor the tools of this field. Whether gas or liquid chromatography is used, we still cannot predict retention times, retention factors, nor separation factors. Many of these problems arise because we do not have standard compounds or mixtures, which is reasonable as the variety of our problems is just too immense, and because we do not have enough retention data, which may seem surprising but is too real. There are few collections of good retention data, and most of them are insufficient to properly characterize the stationary phases. The work of McReynolds [17] and Park et al. [18] should be continued and expanded. Chemometrics offers us very powerful tools which we cannot really use for the lack of the relevant data. Unfortunately, many chemometricians seem to be content to acquire data for fiftish monofunctional components, and use that data set to train their procedure to identify a few more. We need no more chemometric studies now; we need chro-

<sup>a</sup> In a recent symposium on *Fundamental Advances in Liquid Chromatography* (Washington, DC, August 1992), a group of a dozen well-known leaders in the field were unable to agree on a definition of what exactly is the stationary phase when chemically bonded silica is used as the column packing.

matographic studies using chemometrics.

The lack of sufficiently large retention data bases prevents us from normalizing stationary phases, from drawing meaningful comparisons, or from extending the work of Rohrschneider [19]. In the same time, the number of stationary phases available increases rapidly, and it becomes impossible to perform any systematic investigation to select the best phase system for the solution of but the most complicated problems. It is not even possible to require a normalized set of retention data to characterize new phases. These conclusions apply to all types of chromatography, gas (GC), liquid (LC) or dense gas (SFC) chromatography, whatever their exact retention mechanism (Table 2).

In GC, the role of adsorption at the gas–liquid interface is still misunderstood and difficult to account for. The choice of standard solutes is made difficult by the rapid variation of their vapor pressure, hence retention volume, with temperature. Several series of standard solutes would be necessary, but the choice of those used at high temperatures is especially difficult. To increase their vapor pressure, we need to increase their molecular weight, but cannot simply take higher homologs: the polarity would decrease with increasing chain length. On the other hand, polyfunctional solutes are difficult to handle in all but the most sophisticated correlations. The use of polyfunctional solutes in which the same group is repeated twice or three times and these groups are separated with a short alkyl leash appears as an attractive solution (e.g., at high temperatures, methanol is replaced by 1,3-propanediol, acetonitrile by succinonitrile, benzene by dibenzyl).

Two other problems deserve serious attention in GC. First, as shown by Kersten and Poole [20], there are no stationary phases available which are strong proton donors. This is most surprising in view of the several hundred stationary phases described in the literature, many of which being very similar. It might be due to the poor thermal stability of such compounds, but a systematic investigation would certainly be worthwhile. Finally, it is surprising to see how little interest has been devoted to the use of computers in method

development, optimization, data handling and correlation with computers in GC, especially compared to what has been done in LC in the recent past. But may be no new methods are developed in GC any longer [1].

In normal phase liquid chromatography, we have no adsorbent of standard, reference activity. We cannot predict correctly the change in retention factors occurring when we replace the strong solvent in a binary mobile phase by another one at constant eluotropic strength, nor even the changes in separation factors. In reversed-phase LC, the dependence of the retention factor on the composition of a binary mobile phase is no better understood. We know that the linear dependence of  $\log k'$  on the composition is simplistic, but we have no better model yet. More sophisticated approaches, such as the unified theory of retention of Martire and Boehm [21] and the solvatochromic theory as used by Cheong and Carr [22] and Johnson et al. [23] have not yet been applied to the full of their potentiality. The inability of chromatographers to predict the variation of the separation factors with the composition of a multi-solvent mobile phase prevents them from anticipating peak cross-over during the optimization of the mobile phase composition.

Needless to say, considerable work will have to be performed before we understand retention mechanisms better. The most sensible approach would probably start by studying selective mechanisms and try to predict the relative retention of closely related compounds. This way, most non-selective molecular interactions can be ignored, as they cancel out. A case in point is the separation of enantiomers, for which all behaviors are identical, except for what concerns the enantioselectivity. But if progress has been made recently along these lines for phases using selective complexation or similar interaction types, we do not have much of an inkling on what controls the selective separation mechanism with cellulose and cyclodextrin phases.

Finally, as far as supercritical fluid chromatography (SFC) is concerned, the use of dense gases as the mobile phase provides first and foremost a unique opportunity to learn more about the

physico-chemical properties of those fluids, which are still poorly understood. We know that the fact that the mobile phase is supercritical or not has nothing to do with the separation mechanism. All phase equilibrium properties vary smoothly with the gas density around the critical point. What counts is the gas density, which controls molecular interactions. While we begin to understand retention in high density carbon dioxide through the work of Yonker and Smith [24], Schoenmakers [25] and Martire and Boehm [21], the physical basis of the influence of polar modifiers is still controversial.

Even simple parameters, such as the diffusion coefficients of solutes in mixtures of associated solvents like water–methanol or water–acetonitrile which is a function of their composition, are impossible to predict simply. The classical correlation equations provide often no more than the proper order of magnitude.

To conclude this section, I think that there is a great future for research in phase equilibrium thermodynamics, in connection with the retention mechanisms used in chromatographic separations. Already an important part of the true research done in chromatography belongs to this area. The investigation of mass transfer properties is less advanced, but holds at least as many promises.

#### *Chromatographic problems*

There are not many unsolved problems left which can be properly qualified as chromatographic. There remain a few nagging problems, and much mopping up to do, however. This involves particularly problems related with the operation of columns under non-linear conditions, whether for preparative applications or to perform particular analysis. This includes also some analytical problems, and a few other problems which are instrumental in nature.

So far, multidimensional chromatography has attracted much more interest among academics than practitioners. It is not clear whether analysts are too preoccupied by their current problems, or happy enough with the separation tools presently available. In most cases, what is called multidimensional analysis is truly mere multi-column

analysis. Compared to a real bidimensional analysis, where component zones are spread over the entire plane, they involve only separations along too perpendicular narrow bands in the plane, thus affording much less separation power. Bi- and tri-dimensional analyzers could provide either much faster analysis or much higher resolution power. The question is whether there are any analytical problems requiring such progress. It does not seem that the pressure to develop that kind of technique has been great over the last ten years, in spite of the potentiality of the method, which has been clearly illustrated by Giddings [14] and Oros and Davis [16].

Preparative chromatography is still in the early stages of development. At present, the technique seems to be in a stage intermediate between spreading and popularization. The advantages, drawbacks, and limitations of several possible implementations of the method, overloaded elution, displacement, annular rotating column, simulated moving bed, are not yet clear, nor which segment of the market they can claim for [26]. Packing and operating large diameter columns is a complex process. We can no longer assume the radial homogeneity of the column, and we have no simple way to take radial heterogeneity into account. There is little information available regarding either the degree of packing homogeneity which is really achieved, or the influence of packing homogeneity on column performance. A number of facets of the problem have been investigated. The synthesis of these results and wider scope investigations are required. This is an area where the combination of modelling, computer simulations and experiments will be particularly fruitful.

Among the analytical problems which are still under active investigation, the most challenging by far is the analysis of peptides and proteins. Because these compounds are so numerous and their physico-chemical properties vary so very widely, we cannot expect any general method. The problem is complicated by the fragility of their tertiary structure, key to their biological activity. Depending whether pure analytical information is sought, or whether the recovery of purified material for further biochemical investi-

gation is needed, the separation method can be aggressive or must be gentle towards this structure. Combinations of size exclusion, ion-exchange and hydrophobic interaction chromatographies could achieve very powerful separations in short periods of time, if they could be combined into a tridimensional process. We are currently observing an intense proliferation of analytical schemes taking place in this area. The acute need for streamlining separation methodologies for protein analysis will surface soon, and true multi-dimensional analysis is probably the most effective way to approach it.

There is a growing recognition of the existence of the many artifacts that take place during a chromatographic analysis, a fact that had been forgotten all these years when LC was essentially applied to small molecules, mostly of industrial origin, or to environmental samples. Tswett had recognized them [9,10], and they slowed the adoption of chromatography by German chemists [12]. The causes of these artifacts and the conditions under which they are most prone to take place need to be better identified. They can be extremely damaging, for example in most applications of LC in the life sciences. Ignorance and an excessive confidence in your own skills and in the performance of the procedures used magnify the consequences of these damages.

Surprisingly, there are still a few nagging problems in GC which have been left behind when research in this area became narrowly focussed on the technology of coating quartz tubes with immobilized stationary phases. One of them is the prediction of exact values of the retention times in programmed temperature GC from isothermal data. The equation relating these different parameters cannot be solved in closed form, but the solution is easily calculated [27]. Nevertheless algorithms for the calculation of these solutions are not available in chromatographic data packages. Similarly, by contrast with LC, surprisingly little has been accomplished in the area of GC optimization. The simple extension of the approaches used fruitfully in LC has not even been investigated. It seems that, because GC samples are on the average simpler, and GC open tubular columns have a much larger separa-

tion power than LC packed columns, great returns could be expected from such studies.

#### *Instrumental problems*

As observed by Lochmüller [1], we see a growing demand for inexpensive, high performance equipment. The science of designing and manufacturing scientific equipments has made great progress in the last ten years. Minor adjustment of performances may permit considerable savings. This is particularly important for the instruments sold to the bioscientists who seem to be less demanding on certain types of high performance instruments, such as chromatographs with quadruple gradient programmers, and fast scanning UV diode-array photometers.

There has not been a real innovation in instrument design for years. Still some needs are unmet. I sometimes wonder whether there has been a better gas chromatograph than the short-lived Perkin-Elmer 226 of the mid 1960s. The weakest parts of the current chromatographs remain the sampling system in both GC and LC, and the LC detectors. The sensitivity and dynamic linear range of the UV detector have nearly reached their theoretical limits [28]. No principle has been suggested yet on which could be based the design of an LC detector having performance (i.e., detection limits and dynamic linear range) comparable to those of the flame ionization detector in GC. In a related area, the development of detectors based on polarimetry and circular dichroism will bring a useful complement to the present detector collection. A most attractive addition to the pride would be an instrument specially designed to perform multidimensional chromatography as easily as LC column chromatography. This is currently carried out.

Ten years ago, there was a raging controversy regarding the miniaturization of the chromatographic columns. Optimistic analysts kept predicting the coming of age of open tubular columns for LC, or at least the wide-spread use of micro-columns. Except for some attractive but yet academic works, little progress is to be seen on the instrument market. A few dedicated pumps, gradient generators and detectors are available in what is still considered as a small market niche.

The pessimists who kept insisting on the nature and magnitude of the problems to be solved were, unfortunately, right. Slowly, however, knowledge is acquired and accumulated on the design and behavior of microcolumns and the situation will probably change within the next ten years. After all, miniaturization permits faster analysis and/or higher separation powers. It would allow considerable reductions in the amount of waste generated, thus satisfying administrative requirements. The market keeps pushing in these directions, slowly but decisively.

### Conclusions

Although chromatography has now become a mature technique, it enjoys a unique cross-road position which will ensure it a bright future before it is entirely assimilated in the cultural background of chemists.

On the one hand, chromatography is an extremely powerful tool for physico-chemical studies of nearly all molecular interactions. All phase equilibria, their thermodynamics and kinetics can be studied more easily, accurately, rapidly than with any other technique. The method can be used as easily to carry out measurements at extremely low concentrations (below 1 ppb) as to make them at very high concentrations (close to 100%). It will be a long time before this gold mine is exhausted.

On the other hand, chromatography is the premier separation method for molecular sciences. As biochemistry and all the life sciences are becoming more and more molecular, they will generate a nearly endless source of challenging analytical problems. The same chromatographic principle permits the production of purified amounts of biochemicals with negligible concentrations of any specified impurities. The development of suitable procedures is also a major task of the immediate future.

More importantly, however, chromatography is one of the critical tools required for the application of the tide of rules which aim at giving us total safety and a long life. Legal requirements regarding the handling of toxic chemicals (all chemicals are presumed to be so, until proven innocuous), and the monitoring of exposure to

them by workers and by the public at large is the powerful drive towards the development of more sensitive trace analysis, highly selective detection, cheap microchromatographs able to monitor individual exposure to certain compounds, and complex instruments able to separate and quantize hundreds of pollutants in samples containing thousands of poorly known natural compounds. The inability of the toxicologists to make sense of the tide of numbers we can so easily generate, and the frenzy of the press to misinterpret them are the only limiting factor to a tremendous growth.

Legal requirements regarding drug certification lead to a similar drive, one of the main differences being the terms in which cost and benefits are balanced, another being the need to prepare extremely pure compounds (“pharmaceuticals”) and document their purity. The separation of complex mixtures and the identification of their components requires new progress in instrumentation, but mainly in the mere fundamentals of the methods.

These great promises could entirely vanish, however, if the regulations on the use of chemicals in research laboratories become too drastic, a distinct possibility at this time. In this case this would be the entire future of chemistry which would be in question. We have to be ready for a fight, even though we hope we will be spared.

### REFERENCES

- 1 C.H. Lochmüller, *J. Chromatogr. Sci.*, 25 (1987) 583.
- 2 M. Roman and P. Brown, *J. Chromatogr.*, 592 (1992) 3.
- 3 K.P. Hupe, H. McNair, L.S. Ettre, K.Th. Kok, G.J. Bruin, H. Poppe, C. Poole, T.L. Chester, R.L. Wimalasena, G.S. Wilson, B. Bidlingmeyer, D.W. Armstrong, R.P.W. Scott, H.M. Widmer, R.E. Majors and G.I. Ouchi, *LC-GC*, 10 (1992) 238.
- 4 A.M. Siouffi, *Chromatographia*, in press.
- 5 M.S. Tswett, *Tr. Protok. Varshav. Obshch. Estestvoispyt., Otd. Biol.*, 14 (1903, publ. 1905) 20. On the new Category of Adsorption Phenomena and their Applications in Biochemical Analysis. Reprinted and Translated in G. Hesse and H. Well, *Michael Tswett's erste chromatographische Schrift*, Woelm, Eschwegen, 1954. As cited in Ref. 6.
- 6 K. Sakodinskii, *J. Chromatogr.*, 73 (1972) 303.
- 7 A.T. James and A.J.P. Martin, *Biochem. J.*, 50 (1952) 679.

- 8 M. Verzele and C. Dewaele, *Preparative High Performance Liquid Chromatography*, TEC, Gent, 1986, Chap. I.
- 9 M.S. Tswett, *Ber. Dtsch. Bot. Ges.*, 24 (1906) 316.
- 10 M.S. Tswett, *Ber. Dtsch. Bot. Ges.*, 24 (1906) 384.
- 11 I. Hais, *J. Chromatogr.*, 86 (1973) 283.
- 12 R. Kuhn and E. Lederer, *Naturwissenschaften*, 19 (1931) 306.
- 13 A.J.P. Martin and R.L.M. Synge, *Biochem. J.*, 35 (1941) 1358.
- 14 J.C. Giddings, in H.J. Cortes (Ed.), *Multidimensional Chromatography: Techniques and Applications*, Marcel Dekker, New York, 1990, p. 1.
- 15 J.C. Giddings, *Unified Separation Science*, Wiley-Interscience, New York, 1991.
- 16 F.J. Oros and J.M. Davis, *J. Chromatogr.*, 591 (1992) 1.
- 17 W.O. McReynolds, *Gas Chromatography Retention Data*, Preston Technical Abstract, Evanston, IL, 1966.
- 18 J.H. Park, A. Hussam, P. Couasnon, D. Fritz and P.W. Carr, *Anal. Chem.*, 59 (1987) 1970.
- 19 L. Rohrschneider, *J. Chromatogr. Sci.*, 11 (1973) 160.
- 20 B.R. Kersten and C.F. Poole, *J. Chromatogr.*, 452 (1988) 191.
- 21 D.E. Martire and R.E. Boehm, *J. Phys. Chem.*, 91 (1987) 2433.
- 22 W.J. Cheong and P.W. Carr, *Anal. Chem.*, 60 (1988) 820.
- 23 B.P. Johnson, M.G. Khaledi and J.G. Dorsey, *Anal. Chem.*, 58 (1986) 2354.
- 24 C.R. Yonker and R.D. Smith, *J. Chromatogr.*, 459 (1986) 183.
- 25 P.J. Schoenmakers, *J. Chromatogr.*, 315 (1985) 1.
- 26 A.M. Katti and G. Guiochon, *Adv. Chromatogr.*, 31 (1991) 1.
- 27 G. Guiochon and C. Guillemin, *Quantitative Gas Chromatography*, Elsevier, Amsterdam, 1988.
- 28 J.G. Atwood, *ACS Natl. Meeting*, Philadelphia, PA, Fall 1985.



# Standard pH values in non-aqueous mobile phases used in reversed-phase liquid chromatography

J. Barbosa and V. Sanz-Nebot

*Department of Analytical Chemistry, University of Barcelona, Avda. Diagonal 647, 08028 Barcelona (Spain)*

(Received 8th September 1992; revised manuscript received 28th January 1993)

## Abstract

Standard  $\text{pH}_s$  values for three reference buffer solutions (0.05 mol  $\text{kg}^{-1}$  potassium dihydrogenphosphate; 0.1 mol  $\text{l}^{-1}$  acetic acid + 0.1 mol  $\text{l}^{-1}$  sodium acetate; 0.03043 mol  $\text{kg}^{-1}$  disodium hydrogenphosphate + 0.008695 mol  $\text{kg}^{-1}$  potassium dihydrogenphosphate) in 10, 30, 40, 50 and 70% (w/w) acetonitrile–water mixtures at 298.15 K were determined from e.m.f. measurements of the reversible cell Pt/Ag/AgCl/standard buffer + KCl, in acetonitrile–water/glass electrode. In order to obtain  $\text{pH}_s$  values in each of the unlimited number of possible acetonitrile–water mixtures,  $\text{pH}_s$  values were correlated with mole fraction, % (w/w) and % (v/v) of acetonitrile in solvent mixtures and the methodology of linear solvation energy relationship, based on the Kamlet–Taft multiparametric scales, was applied and  $\text{pH}_s$  data were correlated with  $\pi^*$ ,  $\alpha$  and  $\beta$  solvatochromic parameters of the acetonitrile–water mixtures.

**Keywords:** Liquid chromatography; Acetonitrile; pH; Standard pH values

Mixed aqueous–organic solvents are widely used in chemistry to enhance the reactivities, solubilities, biological absorption properties and chromatographic properties of a wide variety of chemical substances. As in aqueous solutions, the pH of the solvent will be affected by solutes and its control will often be necessary in order to obtain optimum chemical results. The solvent system chosen in this study was acetonitrile–water because of its wide use in reversed-phase liquid chromatography (RPLC).

Many different methods have been devised for optimizing the selectivity of chromatographic separations [1–3]. Usually, the methods focus on the optimization of the mobile phase composition, i.e., on the concentrations of water and organic

solvents. However, for separating ionic or ionogenic solutes, variations in the mobile phase pH may easily lead to dramatic variations in selectivity [4]. The degree of ionization of solutes, stationary phases (e.g., ion exchangers) and mobile phase additives (e.g., ion-pairing reagents) may be affected by the pH. Hence pH is potentially a very powerful parameter for optimizing selectivity in RPLC. However, the optimization of the mobile phase pH is complicated as the problem of pH measurements in aqueous–organic mixtures has not been solved [5].

Usually, the operational pH in mixed aqueous–organic solvents is measured assuming that the mobile phase pH is the same on that of the aqueous fraction, in which case errors due to the medium effects contribute to the uncertainty in the true pH. In acetonitrile–water mixtures the influence of the co-solvent on the pH is substantial [6,7].

*Correspondence to:* J. Barbosa, Department of Analytical Chemistry, University of Barcelona, Avda. Diagonal 647, 08028 Barcelona (Spain).

From the point of view of practical chromatography, it is possible to measure the activity of the hydronium ion in mixed aqueous–organic solvents if reference pH values of standard buffer solutions in these solvents are known. The conventional electrometric technique for pH measurements is dependent on an operational definition of pH:

$$\text{pH}_x = \text{pH}_s + \frac{E_s - E_x}{g}$$

where X denotes the solution of unknown pH and S the standard reference solution of known or assigned pH,  $E$  is the electromotive force of a suitable galvanic cell consisting of an electrode reversible to hydrogen ions (usually a glass electrode) coupled with a suitable reference electrode (commonly a silver/silver chloride electrode) and  $g = (\ln 10) RT/F$ .

The aim of this present work was the assessment of  $\text{pH}_s$  values for three standard buffer solutions (citrate, acetate and phosphate buffers) in acetonitrile–water mixtures containing 10, 30, 40, 50 and 70% (w/w) acetonitrile, according to the criteria recently endorsed by IUPAC [5,8]. Also, considering the unlimited number of possible binary acetonitrile–water mixtures, relationships between  $\text{pH}_s$  values and different characteristics of the solvent mixtures were examined and the methodology of linear solvation energy relationship (LSER) [9–11] were used to correlate  $\text{pH}_s$  values with solvent dipolarity/polarizability ( $\pi^*$ ), solvent hydrogen bond-donating acidity ( $\alpha$ ) and solvent hydrogen bond-accepting basicity ( $\beta$ ) [12,13].

## EXPERIMENTAL

E.m.f. values were measured with a Crison 2002 potentiometer ( $\pm 0.1$  mV) using a radiometer G202C glass electrode and a reference Ag/AgCl electrode prepared according to the electrolytic method [14]. The cell was thermostated externally at  $25 \pm 0.1^\circ\text{C}$ . All of the potentiometric assembly was automatically controlled with a Stronger AT microcomputer.

## Reagents

Analytical-reagent grade chemicals were used unless indicated otherwise. All the solutions were prepared by mixing doubly distilled, freshly boiled water and acetonitrile (Merck, chromatography grade).

The concentrations of the standard reference solutions used in this work were chosen as those recommended by IUPAC [8]. The compositions of the buffer solutions prepared for standardization were as follows:  $0.05 \text{ mol kg}^{-1}$  potassium dihydrogen citrate (citrate buffer),  $0.1 \text{ mol l}^{-1}$  acetic acid +  $0.1 \text{ mol l}^{-1}$  sodium acetate (acetate buffer) and  $0.03043 \text{ mol kg}^{-1}$  disodium hydrogenphosphate +  $0.008695 \text{ mol kg}^{-1}$  potassium dihydrogenphosphate (phosphate buffer).

## Procedures

Reference pH values of the standard buffer solutions in acetonitrile–water mixtures containing 10, 30, 40, 50 and 70% (w/w) acetonitrile,  $\text{pH}_s$ , were assigned by using the procedure adopted by the IUPAC [5]. This procedure involves three steps. The first step is the measurement of the e.m.f. of the cell

Pt/Ag/AgCl/standard buffer

+ KCl in acetonitrile–water/glass electrode

(cell A) where the reference standard buffer solutions contains potassium chloride at different and accurately known concentration. The e.m.f.,  $E$ , of this cell is directly related to the activities of the hydrogen ions and chloride ions in solution:

$$E = E^0 + g \log(a_{\text{H}^+} a_{\text{Cl}^-}) \quad (1)$$

where  $E^0$  is the standard e.m.f. of the cell, values of which are essential and have been determined in previous work [14].

The second step is the determination of the different pH values for each concentration of potassium chloride,  $c_{\text{Cl}^-}$ , examined using the Nernst expression of e.m.f.,  $E$ , for cell A:

$$\begin{aligned} p(a_{\text{H}^+} a_{\text{Cl}^-}) &= \text{pH} + py_{\text{Cl}^-} \\ &= [(E^0 - E)/g] - pc_{\text{Cl}^-} \end{aligned} \quad (2)$$

where  $p(a_{\text{H}^+} a_{\text{Cl}^-})$  is a thermodynamic quantity that can be determined in thermodynamically ex-



TABLE 2

Values of standard e.m.f.,  $E^0$ , of cell A, dielectric constants,  $\epsilon$ , densities,  $\rho$ , and solvatochromic Kamlet–Taft parameters at various concentrations of acetonitrile in acetonitrile–water mixtures

Acetonitrile concentration (% w/w)	$E^0$ (mV)	$\epsilon$	$\rho$ ( $\text{g mol}^{-1}$ )	$\pi^*$	$\alpha$	$\beta$
0	401.03	78.36	0.9971	1.17	1.285	0.47
10	406.44	75.01	0.9809	1.14	1.137	0.30
30	426.87	65.52	0.9389	1.03	0.971	0.37
40	442.64	60.38	0.9150	0.97	0.919	0.40
50	458.57	55.44	0.8912	0.91	0.891	0.41
70	515.43	46.82	0.8465	0.84	0.859	0.40

knowledge of the ionic strength  $I$  of the standard buffer + KCl mixed electrolyte solutions:

$$I = I_S + C_{\text{Cl}^-} \quad (5)$$

but  $I$  is, in turn, a function of the  $\text{H}^+$  concentration,  $c_{\text{H}^+}$ , which is expressed by

$$pc_{\text{H}^+} = \frac{(E^0 - E)}{g} - pc_{\text{Cl}^-} - p(y_{\text{H}^+} + y_{\text{Cl}^-}) \quad (6)$$

and of the ionization constants,  $pK$ , corresponding to the equilibria involved in the standard buffer solutions in acetonitrile–water mixtures. These  $pK$  values required were determined previously [16].

Calculation of  $py_{\text{Cl}^-}$  values must proceed by successive iterations. Initially one takes  $I = c_S + C_{\text{Cl}^-}$  and obtain  $py_{\text{Cl}^-}$  by Eqn. 3 for their subsequent insertion in Eqn. 6 to obtain  $pc_{\text{H}^+}$  and a better value of  $I$  by Eqn. 5. Thus, one calculates again the  $py_{\text{Cl}^-}$  value by Eqn. 3, and so on until constancy of  $I$  is obtained.

Inserting  $py_{\text{Cl}^-}$  in Eqn. 2, one distinct pH value is obtained for each concentration  $c_{\text{Cl}^-}$  examined. The standard value,  $\text{pH}_s$ , for standard buffer alone at the fixed molality recommended for International pH Standards [8] can finally be obtained, step (iii), as the intercept at  $c_{\text{Cl}^-} = 0$  of the pH vs.  $c_{\text{Cl}^-}$  linear regression at each mole fraction  $x$  of acetonitrile studied.

## RESULTS AND DISCUSSION

E.m.f. measurements for cell A were made at different concentrations of KCl,  $c_{\text{Cl}^-}$ , added to

each standard buffer as recommended [8] constant concentration solutions in 10, 30, 40, 50 and 70% (w/w) acetonitrile–water mixtures at 298.15 K. At each solvent composition and for each pH reference material studied, various series of measurements were made, giving total of 560 independent measurements over the solvent interval explored. To simplify the tabulation,  $E$  values for only one series of different  $c_{\text{Cl}^-}$  concentrations in each standard reference solutions are quoted in Table 1. Table 1 also reports the corresponding values of molar activity coefficients of monoprotonated species and pH.

Values of the dielectric constants,  $\epsilon$ , and densities,  $\rho$ , involved in the calculation of the Debye–Hückel parameters  $A$  and  $a_0B$  in Eqn. 3, were taken from the literature [17–20] and are given in Table 2. The determination of standard

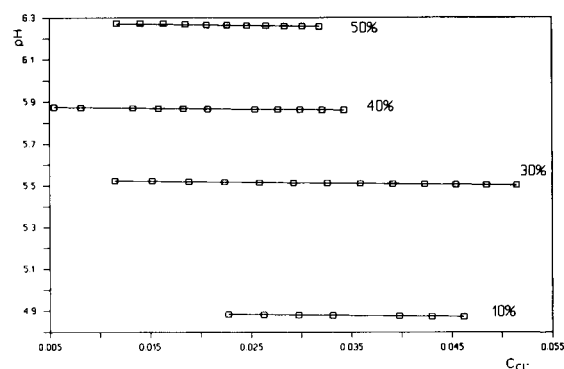


Fig. 1. Variation of pH with concentration of chloride added to acetate buffer in acetonitrile–water mixtures. Acetonitrile concentrations in % (w/w) are given adjacent to the lines.

TABLE 3

pH<sub>s</sub> values for standard reference solutions and pK values of the involved equilibria in various acetonitrile–water mixtures at 298.15 K

Primary standard	Parameter	Acetonitrile concentration (% w/w)					
		0	10	30	40	50	70
Citrate buffer	pH <sub>s</sub>	3.776	3.994	4.470	4.702	4.995	5.610
	pK <sub>1</sub>	3.13	3.40	3.81	4.06	4.31	5.00
	pK <sub>2</sub>	4.76	5.01	5.50	5.81	6.08	7.03
	pK <sub>3</sub>	6.40	6.68	7.29	7.63	7.91	8.86
Acetate buffer	pH <sub>s</sub>	4.644	4.898	5.532	5.875	6.275	–
	pK <sub>1</sub>	4.75	4.97	5.63	5.99	6.41	5.57
Phosphate buffer	pH <sub>s</sub>	7.413	7.697	8.151	8.436	8.646	–
	pK <sub>2</sub>	7.20	7.46	8.02	8.24	8.53	9.42

e.m.f. values,  $E^0$ , for the glass electrode, silver/silver chloride electrochemical cell A containing mixtures of acetonitrile and water has been described previously [14]. The  $E^0$  values obtained are stable, the average deviation being as low as 0.2 mV. Also, the ionization constant values required for the iterative calculations (pK<sub>1</sub>, pK<sub>2</sub> and pK<sub>3</sub> of citric acid, pK of acetic acid and pK<sub>2</sub> of phosphoric acid) were determined previously [16]. All these values, given in Tables 2 and 3, now permit the assignment of standard pH values to reference solutions in acetonitrile–water mix-

tures by using procedures and conventions described.

When the pH for each buffer solution in each acetonitrile–water mixture was plotted as a function of  $c_{\text{Cl}^-}$ , straight lines of small slope were obtained. Typical regression lines are shown in Fig. 1 for the acetate buffer in acetonitrile–water mixtures studied.

Table 3 gives the pH<sub>s</sub> values determined for the citrate, acetate and phosphate buffers, standard reference solutions in 10, 30, 40, 50 and 70% (w/w) acetonitrile–water mixture together

TABLE 4

Relationships between pH<sub>s</sub> values and weight ( $w$ ) and volume ( $v$ ) percentages and mole fraction of acetonitrile in acetonitrile–water mixture and linear solvation energy relationships for pH<sub>s</sub> values

Buffer solution	Relationship	$r$	$n$
Citrate	$\text{pH} = 3.775 + 2.18 \times 10^{-2} w - 1.24 \times 10^{-5} w^2 + 7.13 \times 10^{-6} w^3$	0.999	6
	$\text{pH} = 3.775 + 1.74 \times 10^{-2} v - 2.72 \times 10^{-7} v^2 + 1.15 \times 10^{-6} v^3$	0.999	6
	$\text{pH} = 3.777 + 4.803 x - 3.348 x^2 + 2.011 x^3$	0.999	6
	$\text{pH} = 10.917 - 7.416 \pi^* + 1.824 \alpha - 1.733 \beta$	0.991	6
Acetate	$\text{pH} = 4.642 + 2.42 \times 10^{-2} w + 1.81 \times 10^{-4} w^2 - 2.45 \times 10^{-7} w^3$	0.999	5
	$\text{pH} = 4.643 + 1.88 \times 10^{-2} v + 1.26 \times 10^{-4} v^2 - 7.23 \times 10^{-7} v^3$	0.999	5
	$\text{pH} = 4.641 + 5.692 x - 0.355 x^2 - 2.505 x^3$	0.999	5
	$\text{pH} = 12.310 - 6.741 \pi^* + 0.422 \alpha - 0.685 \beta$	0.996	5
Phosphate	$\text{pH} = 7.418 + 2.78 \times 10^{-2} w - 1.21 \times 10^{-4} w^2 + 1.19 \times 10^{-6} w^3$	0.999	5
	$\text{pH} = 7.417 + 2.23 \times 10^{-2} v + 8.29 \times 10^{-5} v^2 + 1.23 \times 10^{-6} v^3$	0.999	5
	$\text{pH} = 7.422 + 5.880 x - 8.080 x^2 + 6.588 x^3$	0.999	5
	$\text{pH} = 12.837 - 3.852 \pi^* + 0.531 \alpha - 0.500 \beta$	0.993	5

with the literature standard  $\text{pH}_s$  values in water [21].

Determination of  $\text{pH}_s$  values must be carried out at each distinct composition of the solvent but, considering the unlimited number of possible binary acetonitrile–water mixtures, some procedure for predicting  $\text{pH}_s$  values, including pure water as the extreme case, is highly desirable. To this end, the different sets of results for the various solvent mixtures investigated were analysed in terms of a multilinear regression procedure. The usually used concentration by volume, % (v/v),  $v$ , the mole fraction of acetonitrile,  $x$ , and concentration by weight, % (w/w),  $w$ , are the independent variables and the third-order polynomials shown in Table 3 were obtained.

To provide an independent interpretation of the  $\text{pH}_s$  results, the linear solvation energy relationship (LSER) method based on the Kamlet–Taft multiparameter scales [9] was utilized. The solvatochromic LSER approach of Kamlet and Taft seeks to relate a  $\text{pH}_s$  value or a dissociation constant value,  $XYZ$ , with three types of terms as shown below, based on the differential evaluation of solvent dipolarity/polarizability,  $\pi^*$ , solvent hydrogen bond-donating acidity,  $\alpha$ , and solvent hydrogen bond accepting basicity,  $\beta$ :

$$XYZ = XYZ_0 + a\alpha + b\beta + s\pi^* \quad (4)$$

where  $a$ ,  $b$  and  $s$  represent the susceptibilities of  $XYZ$  to changes in the solvent solvatochromic properties [22]. Values of the Kamlet–Taft solvatochromic parameters  $\pi^*$  [10],  $\alpha$  [12] and  $\beta$  [13] for acetonitrile–water mixtures are known. As a result of the application of the LSER method to  $\text{pH}_s$  values determined in this work, the relationships shown in Table 4 were obtained. These equations allow the  $\text{pH}_s$  value of a primary standard buffer in any acetonitrile–water mixture to be calculated.

The financial support of the DGICYT (Project PB91-0262) is gratefully acknowledged.

## REFERENCES

- 1 P.J. Shoenmakers, *Optimization of Chromatographic Selectivity: a Guide to Method Development*, Elsevier, Amsterdam, 1986.
- 2 W.J. Cheong and P.W. Carr, *Anal. Chem.*, 61 (1989) 1524.
- 3 D.W. Armstrong, G.L. Bertrand, K.D. Ward, T.J. Ward, H.S. Secor and J.I. Seeman, *Anal. Chem.*, 61 (1990) 332.
- 4 P.J. Shoenmakers, S. van Molle, C.M.G. Hayes and L.C.M. Uunk, *Anal. Chim. Acta*, 250 (1991) 1.
- 5 S. Rondinini, P.R. Mussini and T. Mussini, *Pure Appl. Chem.*, 59 (1987) 1549.
- 6 S. Rondinini and A. Nese, *Electrochim. Acta*, 32 (1987) 1499.
- 7 T. Mussini, A.K. Covington, P. Longhi, S. Rondinini and S. Tettamanti, *Anal. Chim. Acta*, 174 (1985) 331.
- 8 A.K. Covington, R.G. Bates and R.A. Durst, *Pure Appl. Chem.*, 57 (1985) 531.
- 9 M.J. Kamlet, J.M.L. Abboud, M.H. Abraham and R.W. Taft, *J. Org. Chem.*, 48 (1983) 2877.
- 10 W.J. Cheong and P.W. Carr, *Anal. Chem.*, 60 (1988) 820.
- 11 J. Barbosa and V. Sanz-Nebot, *Talanta*, submitted for publication.
- 12 J.H. Park, M.D. Jang, D.S. Kim and P.W. Carr, *J. Chromatogr.*, 513 (1990) 107.
- 13 T.M. Krygowski, P.K. Wrona, U. Zielkowska and C. Reichardt, *Tetrahedron*, 41 (1985) 4519.
- 14 J. Barbosa and V. Sanz-Nebot, *Anal. Chim. Acta*, 244 (1991) 183.
- 15 T. Mussini, A.K. Covington, P. Longhi and S. Rondinini, *Pure Appl. Chem.*, 57 (1985) 865.
- 16 J. Barbosa and V. Sanz-Nebot, *Anal. Chim. Acta.*, submitted for publication.
- 17 S. Rondinini, C. Confalonieri, P. Longhi and T. Mussini, *Electrochim. Acta*, 30 (1985) 981.
- 18 T. Mussini, P. Longhi and P. Giammarino, *Chim. Ind. (Milan)*, 53 (1971) 1124.
- 19 P. Longhi, T. Mussini, F. Penotti and S. Rondinini, *J. Chem. Thermodyn.*, 17 (1985) 355.
- 20 C. Moreau and G. Douhéret, *J. Chem. Thermodyn.*, 8 (1976) 403.
- 21 R.G. Bates, *CRC Crit. Rev. Anal. Chem.*, 10 (1981) 247.

# Liquid chromatographic study of the photochemical decomposition of sodium ethylmercurithiosalicylate

M. Pilar da Silva, Jesús R. Procopio and Lucas Hernández

*Departamento de Química Analítica y Análisis Instrumental, Facultad de Ciencias, Universidad Autónoma de Madrid, E-28049 Madrid (Spain)*

(Received 8th September 1992; revised manuscript received 20th January 1993)

## Abstract

A liquid chromatographic (LC) method with electrochemical detection was developed for the determination of sodium ethylmercurithiosalicylate (thimerosal) by ligand exchange with tetramethylenedithiocarbamate. This method was used to study the photodecomposition of thimerosal under several solution conditions. The results obtained were compared with those obtained by a previously reported LC assay and a standard cold vapour atomic absorption spectrometric method.

**Keywords:** Ion chromatography; Liquid chromatography; Contact lens solution; Sodium ethylmercurithiosalicylate; Photodecomposition; Thimerosal

Thimerosal (sodium ethylmercurithiosalicylate; TMS) is a relatively stable organomercurial compound used as an antiseptic and preservative. It is the preservative used in most soft contact lens care solutions. TMS is fairly stable in aqueous solutions [1,2] in glass bottles, although it can be lost from ophthalmic solutions stored in plastic containers [3,4]. It has also been reported that the presence of chloride in the solution can have an adverse influence on its stability [5]. It is known that the major decomposition products of TMS are thiosalicylic acid (TSA), 2,2'-dithiosalicylic acid (DTSA) (formed by oxidation of TSA), the ethylmercury ion and, in the presence of light, elemental mercury [4].

Analytical methods previously developed for TMS determination in ophthalmic solutions include spectrophotometry [3,5,6], atomic absorption spectrometry [7–9] and polarography [10,11].

*Correspondence to:* J.R. Procopio, Departamento de Química Analítica y Análisis Instrumental, Facultad de Ciencias, Universidad Autónoma de Madrid, E-28049 Madrid (Spain).

These methods, based on total mercury assay, do not indicate accurately the amount of intact TMS present in solution. Liquid chromatography (LC) has been suggested as a specific method for the determination of intact TMS and its degradation compounds [3,4,7,12–18].

The antimicrobial activity of TMS probably resides in the ethylmercury (EtHg) part of compound. Accordingly, the total EtHg, from intact TMS and free EtHg, may afford a better chemical assessment of the active antimicrobial activity. If this is the case, then the methods for determining TMS levels in ophthalmic solutions based on LC techniques do not indicate accurately the degree of its antimicrobial activity (total EtHg concentration).

In studies of degradation and for routine analytical purposes in the quality control of manufactured products, it is important to develop assays that provide information about TMS levels and its degradation products. In a previous study [18] an ion-suppression reversed-phase chromatographic assay, using electrochemical detection,

was developed for the determination of TMS and its degradation products TSA and DTSA, which was used to study the levels of these compounds in recent and old soft contact lens care solutions. Although useful, the main disadvantage of this method was the absence of information about the fraction of degraded TMS that contains mercury and antimicrobial activity. In order to obtain this information, Parkin [17] used two dithiocarbamate complexing agents for the development of an EtHg ligand-specific assay for thermally and photochemically degraded aqueous solutions of TMS, obtaining information of total EtHg present in samples.

The aim of this work was to obtain more information about the degradation of TMS by light under several solution conditions and in various containers, using both ion-suppression and dithiocarbamate complex-formation chromatographic methods. In the latter methods ammonium tetramethylenedithiocarbamate (ammonium pyrrolidinedithiocarbamate) was tested. Amperometric detection with a glassy carbon electrode was chosen in order to obtain more sensitive and selective detection.

## EXPERIMENTAL

### *Reagents*

Thimerosal (Alcon Iberhis, Spain), thiosalicylic acid, 2,2'-dithiosalicylic acid, ammonium tetramethylenedithiocarbamate (Py) (Sigma, St. Louis, MO), phenylmercury (PhHg) chloride and ethylmercury (EtHg) chloride (Chem Service, West Chester, PA) were used as received. Methanol and other reagents were of ACS grade (Carlo Erba, Milan). Stock solutions of thimerosal and ethylmercury and phenylmercury chloride were prepared in water and stock solutions of thiosalicylic and dithiosalicylic acids in methanol, all at concentrations of  $100 \mu\text{g ml}^{-1}$ . These solutions were stored at  $4^\circ\text{C}$  and protected against light.

### *Apparatus*

The LC system consisted of a Gilson Model 302 pumping system equipped with a membrane damper and a Rheodyne Model 7125 injector

equipped with a  $20\text{-}\mu\text{l}$  loop. The detector was a Metrohm Model 461 amperometric detector equipped with a Metrohm Model 656 flow cell. A glassy carbon electrode (Metrohm 6.0850.010) with an area of  $7 \text{ mm}^2$  was used as the working electrode. The column temperature was thermostated at  $25.0 \pm 0.2^\circ\text{C}$  with a glass jacket using a Selecta Digiterm S-613 thermostat. A Spectra-Physics SP-4290 integrator was used to record the chromatograms. For photochemical degradation of compounds, an Osram 300-W high-pressure mercury arc lamp was used.

### *Chromatographic conditions*

The column was a  $150 \times 4 \text{ mm}$  i.d. stainless-steel prepacked reversed-phase column containing  $5\text{-}\mu\text{m}$  Spherisorb  $\text{C}_{18}$  particles (Tracer, Spain). In the dithiocarbamate complex-formation chromatographic method the mobile phase was methanol–water (75 + 25, v/v) containing 0.02 M potassium nitrate. In the ion-suppression chromatographic method the mobile phase was methanol–water (60 + 40, v/v) containing 0.02 M phosphoric acid. These solutions were filtered through a Millipore Durapore filter ( $0.45\text{-}\mu\text{m}$  pore size) and deaerated by stirring under vacuum for 10 min. The detector was operated at 1.15 V vs. Ag/AgCl with a sensitivity of 100 nA full-scale in the dithiocarbamate complex-formation method and at 1.2 V with a sensitivity of 10 nA full scale in the ion-suppression method.

### *Degradation studies*

Samples of TMS, TSA, DTSA and EtHg were submitted to degradation in glass tubes or in plastic bottles, used as commercial product containers, in the presence or absence of 0.5% (w/v) sodium chloride. To investigate the degradation of TMS in ophthalmic solutions, the same procedure was applied to two types of commercial solutions. The solutions were irradiated by the lamp at a distance of 15 cm in a cold water-bath. Test samples were taken at regular time intervals.

For the determination of TMS, TSA and DTSA the samples were filtered and  $20 \mu\text{l}$  were injected into the chromatographic system; quantification was carried out by comparison of the peak areas obtained from test solutions with those obtained



from standard solutions under the same conditions. For total EtHg determination, a 250- $\mu\text{l}$  aliquot of sample solution was mixed with 750  $\mu\text{l}$  of a methanolic solution containing 5.3 M Py and 5.0  $\mu\text{g ml}^{-1}$  PhHg in methanol. PhHg was added to the sample as an internal standard. The mixture was stirred and, after a short time for completion of the reaction, filtered and 20  $\mu\text{l}$  were injected into the chromatograph. Quantification was carried out by comparing the EtHg to PhHg peak-area ratios obtained for standard solutions of EtHg.

## RESULTS AND DISCUSSION

### Chromatographic studies

The electrochemical behaviour of dithiocarbamate complexes of EtHg and PhHg was characterized by voltammetry on a glassy carbon rotating-disc electrode. In these studies, it was observed that the addition of an excess of Py complexing agent to solutions of EtHgCl or PhHgCl led to the rapid formation of EtHg–Py and PhHg–Py complexes when the pH of the solution was  $> 4$ . The optimum reaction rate and analytical signal were obtained at pH values  $> 6$ . The same conclusions were later obtained in chromatographic studies.

As shown in hydrodynamic voltammograms (Fig. 1), both complexes give the highest signal at a potential of 1.15 V, and this potential was chosen for their simultaneous detection.

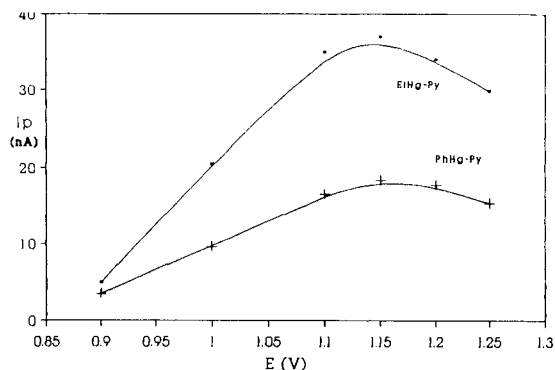


Fig. 1. Hydrodynamics curves of EtHg–Py and PhHg–Py at 10  $\mu\text{g ml}^{-1}$  concentration under chromatographic conditions.

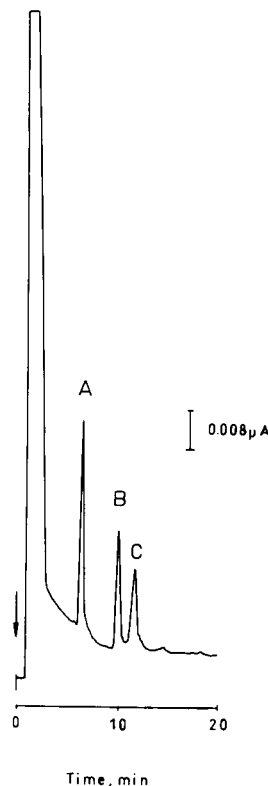


Fig. 2. Chromatograms of EtHg (A), PhHg (B) and  $\text{Hg}^{2+}$  (C) as pyrrolidine complex at a concentration of 5  $\mu\text{g ml}^{-1}$ .

The EtHg–Py and PhHg–Py complexes formed elute as separate peaks when the proportion of methanol in the eluent is lower than 80% (v/v) in water and the pH value is  $> 4$ . Under the chromatographic conditions employed,  $\text{HgPy}_2$  complexes elute separately at a longer elution time than PhHg–Py and can be easily characterized. TSA and DTSA elute at the void volume at pH  $> 4$  and do not interfere in the analysis. Figure 2 shows a typical chromatogram of EtHg, PhHg and  $\text{Hg}^{2+}$  as Py complexes.

The addition of an excess of Py reagent to a solution of TMS also leads to rapid ligand exchange to form EtHg–Py, which leads to the same chromatographic peak area as would be expected for a solution of EtHg of the same concentration. The complexation reactions of Py with EtHg, PhHg and TMS proceed quickly, the complexes are stable for at least 30 min once formed and the formation is independent of the

complexing agent concentration for ligand: compound ratios of 1:1 to 10:1. For all subsequent studies a complexing agent concentration of  $4 \times 10^{-4}$  M was used, which corresponds to a fivefold excess when EtHg is present in the sample at a concentration of  $10 \mu\text{g ml}^{-1}$ . Because the ligand is oxidized on a glassy carbon electrode at the working potential, it was not added to the eluent, but to the samples only. Disodium ethylenediaminetetracetate (EDTA- $\text{Na}_2$ ), usually added in low concentration to the eluent in complex chromatography to minimize the possibility of interference from other metals ion in the system, was not added for the same reason. No interference from other metals was observed during this work because the excess of ligand ensures complete complex formation of metals at trace levels.

In order to obtain a high signal-to-noise ratio, several electrolytes, such as  $\text{KClO}_4$ ,  $\text{NH}_4\text{OAc}$  and  $\text{KNO}_3$ , at different concentrations levels were tried. Linearity, sensitivity and limits of detection were evaluated for concentrations ranging from 0.10 to  $10.0 \mu\text{g ml}^{-1}$ , with an eluent of methanol–water (75 + 25, v/v) containing 0.02 M  $\text{KNO}_3$ . The results are given in Table 1. The sensitivity obtained was of the same order of magnitude as that in the ion-suppression method [18] and one order of magnitude higher than with UV detection. The method described exhibits good reproducibility with relative standard deviations (R.S.D.s) of 2.5 and 1.9% for EtHg and PhHg, respectively, at the  $1 \mu\text{g ml}^{-1}$  level. Using PhHg as an internal standard, an R.S.D. of 0.5% for EtHg at the same concentration level was obtained.

#### Determination of TMS in ophthalmic solutions

Several soft lens products containing TMS at concentrations of 0.001 and 0.004% (Alcon Iber-

TABLE 1

Statistical treatment of calibration graphs and limits of detection (signal-to-noise = 1:3)

Compound	Sensitivity (nA ml $\mu\text{g}^{-1}$ )	Limit of detection ( $\mu\text{g ml}^{-1}$ )	Correlation coefficient
EtHg	13.2	0.05	0.9995
PhHg	5.5	0.10	0.9995

TABLE 2

Comparison of the determination of TMS in ophthalmic solutions at the time of their manufacture by complex-formation (CF) and cold vapour atomic absorption spectrometric (CV-AAS) methods

Sample <sup>a</sup>	TMS ( $\mu\text{g ml}^{-1}$ ) <sup>b</sup>	
	CF	CV-AAS
A <sub>1</sub>	10.77 ± 0.05	10.73 ± 0.04
A <sub>2</sub>	11.00 ± 0.05	10.85 ± 0.05
B <sub>1</sub>	41.30 ± 0.1	42.28 ± 0.08
B <sub>2</sub>	42.41 ± 0.09	42.56 ± 0.08
C <sub>1</sub>	10.80 ± 0.08	10.91 ± 0.03
C <sub>2</sub>	10.70 ± 0.04	10.87 ± 0.04

<sup>a</sup> Initial concentration of TMS: A and C, 0.001%; B, 0.004%.

<sup>b</sup> Mean ± standard deviation ( $n = 3$ ).

his) were analysed at the time of their manufacture using the complex-formation method. The results obtained are summarized in Table 2 together with those obtained by the standard cold vapour atomic absorption spectrometric (CV-AAS) method. From these data, it can be inferred that concomitants present in samples do not interfere for the three solution types assayed. Figure 3 shows the chromatogram obtained for a real sample containing 0.004% TMS. The results obtained indicate the suitability of the complex-formation method with electrochemical detection for the quality control of commercial products containing TMS.

#### Decomposition studies

Both the ion-suppression [18] and complex-formation methods were used to assay TMS, TSA, DTSA and EtHg in samples of aqueous solutions of TMS at concentrations of 0.004% after irradiation by the lamp. The irradiation was applied to samples in various containers including glass tubes and two types of plastic bottles.

After irradiation in glass tubes, the plain solutions of TMS give ion-suppression assay values lower than those obtained by the complex-formation method, but both tended to show total degradation at irradiation times higher than 60 min (Table 3). These differences were more important in solutions containing 0.5% NaCl. Under these conditions, the TMS concentration determined by the ion-suppression method dropped

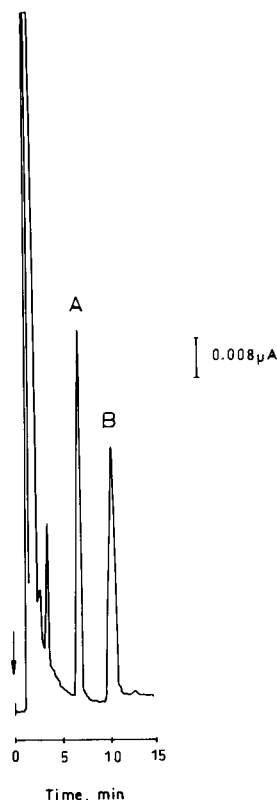


Fig. 3. Chromatogram of a real sample containing 0.004% in TMS. Compounds: EtHg (A) and PhHg (B).

TABLE 3

Results of the determination of TMS after direct irradiation in glass tubes by the ion-suppression (IS) and complex-formation (CF) methods

Time (min)	TMS remaining (%) <sup>a</sup>			
	Plain solution		0.5% NaCl solution	
	IS	CF	IS	CF
5	92.5	90.1	86.0	95.3
10	70.0	86.0	78.0	90.2
15	32.5	81.9	52.0	80.4
20	32.5	62.6	40.0	73.3
30	17.5	52.7	14.0	58.4
45	12.5	23.4	n.d. <sup>b</sup>	48.6
60	5.0	7.7	n.d.	48.3

<sup>a</sup> Initial concentration of TMS = 0.004% (w/v). <sup>b</sup> Not detected.

to zero after exposure times longer than 30 min, whereas the EtHg concentration tended to a constant value after the same time (Table 3).

TABLE 4

Determination of DTSA by the ion-suppression method after irradiation of TMS solution containing NaCl, expressed as the percentage of TMS remaining

Time (min)	TMS remaining (%)	Time (min)	TMS remaining (%)
5	17.5	30	n.d. <sup>a</sup>
10	23.4	45	n.d.
15	26.3	60	n.d.
20	35.0		

<sup>a</sup> Not detected.

On irradiation of both plain and NaCl solutions, no signal corresponding to  $\text{Hg}^{2+}$  was observed. In the absence of NaCl, no formation of TSA or DTSA during the TMS decomposition was observed, because their decomposition is faster than that of TMS (Tables 3 and 4). However, in the presence of NaCl, DTSA was observed in some of the assays (Table 4). The DTSA concentration in these samples increased with time up to 20 min. After longer irradiation times the DTSA signal disappeared. Under this solution condition, EtHg is more stable than in plain solution (Table 5), and a redox reaction could take place between TSA and EtHg, leading to DTSA and, probably,  $\text{Hg}^0$  (no  $\text{Hg}^{2+}$  was detected). The reaction stoichiometry could be 2 mol of TSA per 1 mol of EtHg. This hypothesis is in agreement with the 50% of TMS remaining in the complex formation assay (Table 3).

TABLE 5

Results of determination analysis of TSA and DTSA by the ion-suppression method and of EtHg by the complex-formation method after direct irradiation in glass tubes

Time (min)	Proportion remaining (%) <sup>a</sup>					
	Plain solution			0.5% NaCl solution		
	TSA	DTSA	EtHg	TSA	DTSA	EtHg
5	67.9	47.1	94.0	61.4	100.2	100.0
10	47.1	18.5	96.4	16.5	80.5	100.5
15	16.1	7.3	95.2	n.d. <sup>b</sup>	65.2	99.8
20	n.d.	1.7	91.7	n.d.	54.4	101.2
30	n.d.	n.d.	90.5	n.d.	45.6	99.9
45	n.d.	n.d.	94.0	n.d.	10.9	100.2
60	n.d.	n.d.	95.2	n.d.	n.d.	100.4

<sup>a</sup> Initial concentrations: TSA 6.19, DTSA 6.40 and EtHg 6.19  $\mu\text{g ml}^{-1}$ . <sup>b</sup> Not detected.

Table 5 shows the decomposition of TSA, DTSA and EtHg in glass tubes by light. The results for the irradiation of TSA solutions in glass tubes confirm the rapid decomposition shown by this compound in plain and NaCl solutions. Photodegradation of TSA was faster than TMS decomposition. This result explains the absence of TSA in undegraded samples of TMS. However, DTSA degradation was fast in plain solution and slower than that of TSA and TMS in NaCl solutions. The slower decomposition of DTSA in NaCl solutions allows its detection, at moderate levels, in TMS solutions degraded in this medium.

EtHg solutions irradiated in glass tubes showed decomposition by light in plain solution but no degradation in the presence of NaCl (Table 5). These results are in agreement with the data obtained for TMS decomposition in NaCl but not in plain solutions. It is considered that in this latter instance, the decomposition products of TMS cause a reduction of EtHg to metallic mercury or the formation of organomercurials not detected by the proposed method.

The effect of the kind of plastic container on the decomposition rate of TMS was also studied. Two types of polyethylene bottles were studied, one made of a white plastic, which absorbs strongly at wavelengths shorter than 250 nm, and the other colourless, which absorbs only slightly

TABLE 6

Comparison of results of the determination of TMS after irradiation in plastic containers by the ion-suppression (IS) and complex-formation (CF) methods

Time (min)	TMS remaining (%)			
	White plastic container		Colourless plastic container	
	IS	CF	IS	CF
5	99.6	100.1	91.6	80.9
10	97.2	97.8	65.3	74.2
15	96.7	99.9	43.7	48.6
20	97.2	98.4	22.9	41.0
30	98.7	97.8	6.6	10.5
45	92.1	95.7	n.d. <sup>b</sup>	3.8
60	93.0	92.1	n.d.	0.5

<sup>a</sup> Initial concentration of TMS = 0.004% (w/v). <sup>b</sup> Not detected.

TABLE 7

Results obtained for TMS photodegradation in contact lens care solutions in glass tubes by the ion-suppression (IS) and complex-formation (CF) methods

Time (min)	TMS remaining (%) <sup>a</sup>			
	Solution A		Solution B	
	IS	CF	IS	CF
5	95.4	98.1	88.9	93.8
10	92.6	85.9	81.3	91.1
15	69.1	76.7	74.7	87.3
20	40.8	68.9	68.3	85.4
30	6.9	56.7	50.3	77.8
45	n.d. <sup>b</sup>	46.3	35.2	64.9
60	n.d.	38.8	10.2	61.8

<sup>a</sup> Initial TMS concentration: A, 0.001%; B, 0.004% (w/v).

<sup>b</sup> Not detected.

at these wavelengths. The obtained data (Table 6) show that irradiation of TMS in the white polyethylene container results in a low decomposition, similar results being obtained by both methods. However, irradiation in a colourless container gives a faster decomposition rate than in glass tubes. These results could be due to adsorption of mercury compounds on plastic materials, favouring decomposition of both TMS and EtHg [4]. Adsorption could also be the reason for a loss of about 8% of TMS in the white container.

In order to obtain information about the effect that concomitants in commercial products have on the photodecomposition of TMS, similar irradiation studies were performed with samples of two contact lens care solutions, A and B, containing 0.001% and 0.004% TMS, respectively, and 0.5% NaCl, 0.01% EDTA-Na<sub>2</sub> and other compounds, in glass tubes. The main difference between the two solutions was, apart from TMS concentration, the presence of several polymers in compounds B that absorb strongly at wavelengths shorter than 250 nm. The results are given in Table 7. A higher degradation rate in solution A than solution B can be observed, mainly shown in the complex-formation assays. These results indicate that the presence of light-absorbing polymers delays TMS decomposition. Similar results to those in Table 6 were obtained

TABLE 8

Comparison of ion-suppression (IS), complex-formation (CF) and cold-vapour atomic absorption spectrometric (CV-AAS) assays of several aged contact lens solutions

Sample	Date of manufacture <sup>a</sup>	Concentration ( $\mu\text{g ml}^{-1}$ )					
		TMS			TSA (CF)	DTSA (CF)	$\text{Hg}^{2+}$ (CF)
		IS	CF	CV-AAS			
A <sub>3</sub>	4/91	n.d.	n.d.	6.8	n.d.	n.d.	2.90
A <sub>4</sub>	5/91	n.d.	n.d.	6.4	0.03	n.d.	1.54
A <sub>5</sub>	5/91	n.d.	n.d.	6.4	0.08	n.d.	1.27
B <sub>3</sub>	5/91	43.4	42.0	43.2	n.d.	n.d.	n.d.
B <sub>4</sub>	5/91	41.1	40.7	40.8	n.d.	n.d.	n.d.
C <sub>3</sub>	4/91	6.72	9.00	10.80	0.72	0.08	n.d.
C <sub>4</sub>	6/91	6.97	8.70	11.20	0.48	0.68	n.d.

<sup>a</sup> Date of assay: 6/92.

for solutions A and B irradiated in plastic containers.

#### Assay of aged ophthalmic solutions

Because of the different information obtained by the three methods used in these studies (ion-suppression and complex-formation chromatography and CV-AAS), several ophthalmic samples that were at least 1 year old were analysed by the different methods. The results are summarized in Table 8 and important differences are observed.

Type B solutions have a complex light-absorbing formulation and they remain unchanged after 1 year, with similar results being obtained by the three techniques. On the other hand, chromatographic methods give lower TMS concentrations than CV-AAS for type C solutions. According to these results, the assayed solutions maintain their original level of total mercury, but the chromatographic methods indicate lower levels of TMS and EtHg in solution than expected. The absence of  $\text{Hg}^{2+}$  in the samples shows that the portion of mercury detected by the CV-AAS method and not detected by the complex-formation method is not present in samples in this chemical form, but as elemental mercury or as another organomercurial compound. The presence of TSA and DTSA, easily degradable by light, indicates TMS degradation through a reaction mechanism other than photodecomposition.

The formulations that were most strongly degraded after 1 year were of type A. Neither TMS

nor EtHg was detected in these solutions, but the presence of mercury was detected by CV-AAS. The TMS levels obtained by this method cannot be fully explained by the presence of  $\text{Hg}^{2+}$  in the samples, and again indicate the formation of other compounds of mercury in solutions.

The results obtained by the three methods show that the degradation of TMS in aged ophthalmic solutions cannot be explained solely by photodecomposition and apparently other reactions can take place.

#### Conclusions

The complex-formation method described here can be readily used in the quality control of commercial products and, also may reflect more correctly the remaining antimicrobial activity of TMS in aged ophthalmic formulations. In conjunction with the ion-suppression method, it is possible to make a more complete study of the decomposition of such samples.

The authors thank the Autónoma University of Madrid for financial support of this work (Aids to Precompetitive Groups) and Alcon Iberhis for the supply of samples.

#### REFERENCES

- 1 K. Tsuji, Y. Yamawaki and Y. Miyazaki, Arch. Pract. Pharm., 24 (1951) 110.

- 2 E.O. Davisson, H.M. Powell, J.O. MacFarlane, R. Hodson, R.L. Stone and C.G. Culbertson, *J. Lab. Clin. Med.*, 47 (1956) 8.
- 3 N.E. Richardson, D.J.G. Davies, V.J. Meakin and D.A. Norton, *J. Pharm. Pharmacol.*, 29 (1977) 717.
- 4 M.J. Reader and C.D. Lines, *J. Pharm. Sci.*, 72 (1983) 1406.
- 5 E. Lüdtke, H. Darsow and R. Pohloudek-Fabini, *Pharmazie*, 32 (1977) 99.
- 6 J. Viska and A. Okac, *Cesk. Farm.*, 16 (1967) 29.
- 7 S.N. Ibrahim, N. Stroud and V.J. Meakin, *J. Pharm. Pharmacol.*, 30 (1978) 52.
- 8 B.J. Meakin and Z.M. Khammas, *J. Pharm. Pharmacol.*, 31 (1979) 653.
- 9 P.G. Takla and V. Valajanian, *Analyst*, 107 (1982) 378.
- 10 S. Pinzauti, G. Bramanti, G. Mazzi, P. Mura and P. Papini, *Boll. Chim. Farm.*, 119 (1980) 719.
- 11 S. Pinzanti and M. Casini, *Farmaco*, 35 (1980) 92.
- 12 C. Fu and M.J. Sibley, *J. Pharm. Sci.*, 66 (1977) 738.
- 13 R.C. Meyer and L.D. Cohn, *J. Pharm. Sci.*, 67 (1978) 1636.
- 14 S.W. Lam, R.C. Meyer and L.T. Takahashi, *J. Parent. Sci. Technol.*, 35 (1981) 262.
- 15 D.S. Bushee, *Analyst*, 133 (1988) 1167.
- 16 G.C. Visor, R.A. Kenley, J.S. Fleitman, D.A. Neu and I.W. Partridge, *Pharm. Res.*, 2 (1985) 73.
- 17 J.E. Parkin, *J. Chromatogr.*, 542 (1991) 137.
- 18 J.R. Procopio, M.P. da Silva, M.C. Asensio, M.T. Sevilla and L. Hernández, *Talanta*, 39 (1992) 1619.

# Determination of the stability of morphine tablets by ion-pair reversed-phase liquid chromatography

I. Ismail Salem and A. Cerezo Galan

*Department of Pharmacy and Pharmaceutical Technology, University of Granada, E-18071 Granada (Spain)*

(Received 8th September 1992; revised manuscript received 4th January 1993)

## Abstract

The main objective of this study was to develop and test the applicability of a sensitive and rapid ion-pair reversed-phase liquid chromatographic method for evaluating a new dosage form for the oral administration of morphine, based on ion pairing with heptane-1-sulphonic acid. Pseudomorphine was identified by gas chromatography–mass spectrometry as the major degradation product of liquid samples of morphine hydrochloride (used as control) that had been subjected to accelerated decomposition. No degradation product was found in the analyses of tablets. Validation of the method yielded a linear regression  $r = 0.9988$ ; the relative standard deviation was 1.10% at  $0.24 \text{ mg ml}^{-1}$  (more than 200 samples). The limits of detection were  $0.006 \text{ mg ml}^{-1}$  for morphine and  $0.012 \text{ mg ml}^{-1}$  for pseudomorphine. The results of stability studies performed during 12 months confirmed the marked stability of tablets prepared in the laboratory.

*Keywords:* Ion chromatography; Liquid chromatography; Morphine; Pharmaceuticals

Morphine continues to be the most effective analgesic available for the treatment of chronic cancer pain [1–4]. It was therefore decided to develop a new long-acting oral dosage form of tablets of morphine hydrochloride in a hydrophilic matrix. The main objective of this research was to develop and test the applicability of a specific, precise, sensitive analytical technique to the study of the stability of morphine-containing tablets prepared in the laboratory. The aims of the stability studies were twofold: to ensure maximum shelf-life of the new preparation, and to compile statistically valid data regarding the expiry date of the drug.

The use of ion-pair reversed-phase liquid chromatography (IP-RPC) has become popular in recent years as it is considered to be an effective

alternative to ion-exchange chromatography, but eliminates the problems associated with the latter, e.g., temperature control, precise pH, reproducibility and short column lifetime. The ion-pair reagent enhances retention times and improves the resolution and symmetry of the chromatographic peaks [5]. All these considerations are of great importance in the search for degradation products in dosage forms during the stability study period.

The retention can be regulated by modifying the hydrophobicity of the mobile and stationary phase, introducing complexing reagents or altering the pH of the eluent if the solute is ionic. In ion-pair chromatography, the ionic reagents are able to act as counter ions ( $Y^+$ ) and can react with the sample ions ( $X^-$ ) to form non-dissociated ion pairs ( $X^-Y^+$ ). These ion pairs substantially alter the retention behaviour of ionic compounds, forming complexes that are more or less polar than the parent compounds. An additional

*Correspondence to:* I. Ismail Salem, Department of Pharmacy and Pharmaceutical Technology, University of Granada, E-18071 Granada (Spain).

parameter therefore becomes available for optimization of the separation or for the identification of ionic species in a complex mixture by the peak-shifting technique [6].

## EXPERIMENTAL

Stability determinations and the detection of possible degradation products were carried out by IP-RPLC analyses of tablets that had been previously subjected to accelerated ageing.

### Apparatus

A Waters (Milford, MA) liquid chromatograph was used, consisting of an M-45 high-pressure pump and Model 440 UV-visible detector operating at 280 nm. Detector outputs were monitored by a Model 740 Data Module plotter/integrator. Injections were made with a Rheodyne (Berkeley, CA) Model 7125 injector with a 20- $\mu$ l loop.

A prepacked 30 cm  $\times$  3.9 mm i.d.  $\mu$ Bondapak C<sub>18</sub> (10  $\mu$ m particle size) (Waters) was used. Flow-rates of 1–1.5 ml min<sup>-1</sup> were found to give adequate resolution. The column back-pressure ranged between 1200 and 1500 p.s.i. Separations were performed at ambient temperature.

Samples and solvents were clarified by filtration through Millex-GV (0.22  $\mu$ m) and Durapore (0.45  $\mu$ m) porous membranes (Waters).

For gas chromatography–mass spectrometry (GC–MS), GC separation was effected on a Hewlett-Packard HP-5890 gas chromatograph with a 25 m  $\times$  0.2 mm i.d. HP-1 fused-silica capillary column and mass spectra were recorded on an HP 5988-A mass spectrometer with 70 eV electron impact ionization.

### Reagents

Methanol (LiChrosolv) and glacial acetic acid were purchased from Merck (Darmstadt), sodium heptane-1-sulphonate from Sigma (St. Louis, MO) and pentanesulphonic acid (PIC 5) and hexanesulphonic acid (PIC 6), used as the pairing species, from Waters. Morphine hydrochloride and pseudomorphine hydrochloride were kindly supplied by Palex Laboratory (Barcelona). LC-grade water

was produced using a Milli-Q purification system (Millipore, Milford, MA).

### Procedures

All mobile phases were prepared mixing 0.0036 M pairing ion with water–methanol (72 + 28), the final pH being adjusted to 3.50 with anhydrous acetic acid.

The morphine standard was dissolved in the mobile phase to a final concentration of 0.240 mg ml<sup>-1</sup>; standards and mobile phases were prepared freshly each day and degassed before use. In each analysis, a representative sample of the batch was weighed and pulverized and a final weight of morphine of 24 mg was dissolved in 100 ml of the mobile phase. Five determinations and their corresponding chromatograms were recorded for each sample.

An extensive series of preliminary assays including changes in mobile phase composition, type of ion-pair reagent used, temperature and flow-rate were performed to determine the optimum analytical conditions.

Given that the retention time of morphine is conditioned by the carbon chain length of the pairing ions [7], the effects of three ion-pair reagents (pentanesulphonic acid, hexanesulphonic acid and heptane-1-sulphonic acid) on morphine retention times were studied. Experiments showed that increases in retention time and an improved resolution of the chromatographic peaks corresponded to an increase in the number of carbon atoms (Table 1).

The increase in retention time did not indicate

TABLE 1

Reproducibility of retention time values for morphine and resolution factors for morphine/pseudomorphine using a C<sub>18</sub> column and a flow-rate of 1.2 ml min<sup>-1</sup>

Ion-pair reagent	Retention time (min) <sup>a</sup>	R.S.D. (%)	Resolution factor <sup>a</sup>	R.S.D. (%)
Pentanesulphonic acid	6.34	1.36	–	–
Hexanesulphonic acid	7.63	0.97	1.73	2.73
Heptanesulphonic acid	8.51	0.08	2.66	1.57

<sup>a</sup> Mean of ten results.



which of the three reagents should be used, as at this stage it was still unknown which would yield the best separation of the possible degradation products. In order to evaluate the separation capacity of the method, the appearance of degradation products was induced by submitting several aliquots of morphine standard dissolved in methanol to accelerated ageing at 45°C in the presence of oxygen and light [8]. This would be expected to result in the production of pseudomorphine and morphine *N*-oxide, with the former being by far the major product. These samples were then analysed by IP-RPLC with the three different reagents. The resulting chromatographic peaks corresponded to morphine and its degradation products. The best separation and resolution were achieved with heptane-1-sulphonic acid (Fig. 1); the resolution factor ( $R_s$ ) between morphine and pseudomorphine was never less than 2.64. The use of the other pairing reagent, was discounted as very poor peak separations were obtained (pentanesulphonic acid did not adequately resolve morphine and pseudomorphine under the same conditions).

One of the degradation products isolated by IP-RPLC was identified by GC-MS as pseudomorphine (oxydimorphine). Confirmatory evidence for this conclusion comes from the mass assignments; the principal peaks are at  $m/z$  44, 568, 42 and 81.

Once the major degradation product has been identified (there were peaks of another two unidentified substances, one of which was thought to correspond to morphine *N*-oxide), the following procedure was carried out: serial dilutions of standard solutions of both morphine and pseudomorphine were freshly prepared in the concentration range 0.20–0.28 mg ml<sup>-1</sup>, and calibration graphs were constructed. In both instances each standard solution was injected into the C<sub>18</sub> column five times so that final values could be obtained from the means of the five measurements.

Varying the temperature and flow-rate of the mobile phase did not substantially affect the chromatographic resolution.

Once the analytical technique had been optimized, it was used to carry out the content uni-

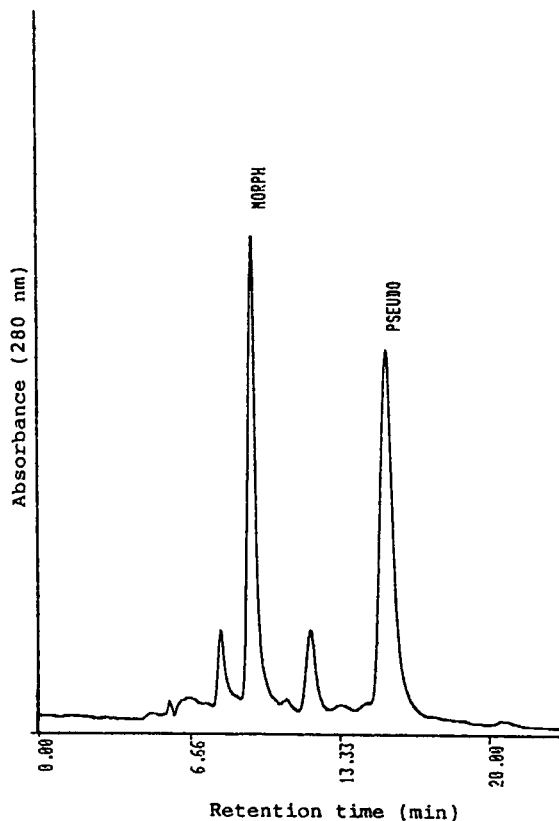


Fig. 1. Chromatographic separation of morphine degradation products using a  $\mu$ Bondapak C<sub>18</sub> column and methanol-water (72+28) containing 0.0036 M heptanesulphonic acid as mobile phase. Analysis was carried out at 280 nm (0.32 absorbance full-scale).

formity test (CUT), which is considered as the most important quality control for individual doses in solid dosage forms. This requirement indicates the increasing attention paid to the homogeneity problem of solid dosage forms where a small amount of highly potent active ingredients is to be distributed throughout a relatively large amount of excipients. Four different dosage forms were analysed (100, 60, 30 and 10 mg of morphine hydrochloride), and significant samples of the different doses were tested under different temperature and storage conditions, according to a widely used and well known protocol for stability studies, involving continuous sampling at different temperatures and times.

## RESULTS AND DISCUSSION

*Validation of the analytical technique*

The current good manufacturing practice regulations [21 CFR 211.194(a) (2)] [9] require that test methods that are used for assessing compliance of pharmaceutical products with established specifications must meet proper standards of accuracy and reliability.

Five concentrations of the standard solution were tested. The analysis was run on each of two days ( $n_{\text{total}} = 50$ ), and linear calibration plots were obtained with correlation coefficients  $r = 0.9988$  and  $0.9987$ . The same procedure was used for pseudomorphine solutions, and  $r = 0.9976$  and  $0.9976$  were obtained.

The precision of the IP-RPLC assay was studied over a 2-day period, calculating the standard deviation (S.D.) and relative standard deviation (R.S.D.) for five determinations per day of two different solutions of morphine standard ( $0.24 \text{ mg ml}^{-1}$ ). The resulting S.D. and R.S.D. were  $0.002 \text{ mg}$  and  $0.85\%$ , respectively. Morphine analysis over the whole study period yielded an R.S.D. of  $1.10\%$ .

The limit of detection was defined as the concentration which gave a signal-to-noise ratio of 3:1. Values of  $0.006$  and  $0.012 \text{ mg ml}^{-1}$  for morphine and pseudomorphine hydrochloride, respectively, were obtained.

The results of the content uniformity test are given in Table 2, which gives the theoretical dose of the morphine hydrochloride tablets prepared in the laboratory and the IP-RPLC results. A fluctuation was observed in the doses, although it remained within the permissible limits given by the pharmacopoeias consulted ([9,10]). This variability may be due to the small amount of drug available at the time of preparing the tablets, which made exact dosage difficult to achieve. The information obtained in this study was applied to improve the dosage of a batch of tablets. No

TABLE 2

Results of content uniformity test for morphine hydrochloride tablets (mg)

	100-mg tablets	60-mg tablets	30-mg tablets	10-mg tablets
	99.17	54.21	28.51	9.06
	94.31	55.62	26.25	8.83
	95.92	57.40	25.92	9.08
	94.55	57.51	28.62	–
	93.83	52.29	24.93	–
Mean	95.56	55.41	26.25	8.99
S.D.	2.16	2.21	1.64	0.13
R.S.D. (%)	2.26	3.99	6.26	1.54

degradation products were found in a stability study performed by IP-RPLC over a 12-month period.

The authors thank Palex I + D Department for providing morphine and pseudomorphine hydrochloride.

## REFERENCES

- 1 J.E.F. Reynolds (Ed.), Martindale. The Extra Pharmacopoeia, Pharmaceutical Press, London 29th edn., 1989, p. 1310.
- 2 A.M. Banning, J.F. Schmidt and B. Chroemmer, *Anesth. Analg.*, 65 (1986) 385.
- 3 J. Säwe, B. Dahlström and A. Rane, *Eur. J. Clin. Pharmacol.*, 24 (1983) 537.
- 4 P.J. Slattery and R.A. Boas, *Drugs*, 30 (1985) 539.
- 5 S. Lindsay, in D. Kealey (Ed.), *High Performance Liquid Chromatography*, Wiley, Chichester, 1987, p. 116.
- 6 G. Szepesi, *How to Use Reverse-Phase HPLC*, VHC, Weinheim, 1992.
- 7 J.W. Munson, in J.W. Munson (Ed.), *Pharmaceutical Analysis (Modern Methods)*, Part B, Dekker, New York, 1984, p. 69.
- 8 P. Proksa, Z. Voticky, L. Molnar, J. Putekan and M. Stefek, *Chem. Zvesti*, 32 (1978) 710.
- 9 United States Pharmacopoeia XXII Revision, USP Convention, Rockville, MD, 1990, pp. 906 and 1710.
- 10 British Pharmacopoeia 1988, H.M. Stationary Office, London, 1988, p. 971.

# Separation and determination of betaine in an oriental medicine by liquid chromatography

Nobu Kikuchi, Kyoko Matsuno and Taihei Miki

Laboratory of Instrumental Analysis, Tokyo University of Agriculture, 1-1, Sakuragaoka-1, Setagaya, Tokyo 156 (Japan)

(Received 8th September 1992; revised manuscript received 4th December 1992)

## Abstract

Recent interest in assaying betaine in plant tissue stimulated work on the complete separation of this substance from numerous impurities. A suitable separation of betaine was achieved by liquid chromatography on an amino-bonded silica gel. Pretreatment of samples of an aqueous extract of Jikoppi, an oriental medicine, was primarily based on a method developed by Vialle et al. in which an extract of Jikoppi was passed through a Dowex 50W-X8 (H<sup>+</sup>) column. The betaine retained in the column was eluted with 4% ammonia solution. The solution was then purified by passing it through a purification column containing a mixed bed of Amberlite IRC-50 [H<sup>+</sup>] and Dowex 1-X4 (OH<sup>-</sup>). The combined effluent and washings from the purification column were evaporated into a syrup. A 15-mg portion of glycine was added to this condensed product as an internal standard. A laboratory-packed Kaseisorb LC NH<sub>2</sub> super (5 μm) column satisfactorily separated betaine and glycine from impurities using acetonitrile–water (75 + 25) containing 0.1% of Brij-35 with a detection wavelength of 210 nm. Linearity of the calibration based on the peak-area ratio was demonstrated over the entire working range of 0.25–18 μg μl<sup>-1</sup>. The relative 95% fiducial limits of betaine were determined to be 1.3–1.6% for the 0.5–12-μg range and 0.5–1.2% for the 14–18-μg range (*n* = 5). The recovery of betaine through the whole analytical procedure was 93% (*n* = 5). Betaine contents in six Jikoppi powders were also determined.

**Keywords:** Liquid chromatography; Betaine; Pharmaceuticals

Jikoppi (Kuko in Japanese), the powdered root-skin of *Lycium chinense* Miller, is widely used in oriental medicine for its lenitive and antifebrile properties. Glycinebetaine, (carboxymethyl)trimethylammonium hydroxide, has been known as a major component of Jikoppi since the early stages of investigation. Previous analytical methods have relied on non-specific precipitation with periodate [1–3] or reineckate [4], purification followed by isotope dilution and micro-Kjeldahl determination [5], enzymatic determination [6], NMR spectroscopy [7] and UV spec-

trophotometry of the ester with  $\alpha$ -*p*-dibromoacetophenone [8]. Methods for the separation of this substance have included thin-layer chromatography or thin-layer electrophoresis, with or without scanning densitometry [9,10]. Gas chromatography was also carried out with thermal degradation of the hydroxide form of the compound [11] or other derivatives [12,13], and unidentified products of trimethylsilylation [14]. Usually these methods show poor accuracy and/or precision and involve complex pretreatment or loss of analyte by adsorption or decomposition of the compound. Despite the above difficulties, there have been a number of reports of the liquid chromatographic (LC) separation of betaine from sugars on amino-bonded silica or

*Correspondence to:* T. Miki, Laboratory of Instrumental Analysis, Tokyo University of Agriculture, 1-1, Sakuragaoka-1, Setagaya, Tokyo 156 (Japan).

“carbohydrate” columns [15–17]. Considering the chemical constitution of this quaternary ammonium salt, ion-pair partition chromatography on non-polar stationary phases [18–21] and high-performance ion-exchange chromatography with the application of an amino acid analyser [22–28] have also been considered.

Control of the elution of betaine with good repeatability of retention times in ion-pair chromatography is very difficult. Exact controls of ion strengths and pH values in ion-exchange chromatography are also painstaking problems. Vialle et al. [15] condensed betaine from wine with a 96% recovery, using the strong cation-exchange resin Dowex 50W-X8 ( $H^+$ ). After successive purification, the sample solution was subjected to reversed-phase LC with an amino-modified silica gel column and acetonitrile–water as eluent. In this work the separation and purification of this polar analyte from aqueous extracts of Jikoppi powders were investigated with a modification of Vialle et al.’s procedure. Successful determinations of the analyte by LC are also described.

## EXPERIMENTAL

### *Instruments*

An LC-5A liquid chromatograph, furnished with an SPD-2A variable-wavelength detector (Shimadzu, Kyoto, Japan), a Rheodyne (Cotati, CA) Model 7125 injector with a 10- $\mu$ l sample loop and an R-301 strip-chart recorder with auto-zero suppression circuit (Rikadenki Kogyo, Tokyo) were used. A Chromatopak C-R4ATD data processor (Shimadzu) was also connected to the detector for quantitative data handling and further calculations.

### *Test materials*

All Jikoppi powders were supplied by Dr. Seon Kwan Seoig of the Chung-Nam Office of Rural Developments, Korea.

### *Reagents and ion exchangers*

Analytical-reagent grade betaine monohydrate was supplied by Aldrich (Milwaukee, WI) and the

internal standard guaranteed-reagent grade glycine, from Tokyo Kasei Kogyo (Tokyo). LC-grade acetonitrile, methanol and 2-propanol (Cica–Merck, supplied by Kanto Chemical, Tokyo), and Milli-Q ultra-pure water with a specific resistance of approximately  $10^{18} M\Omega cm^{-1}$  (Japan Millipore, Tokyo) were used throughout. Dowex (Midland, MI) ion exchangers were supplied by Muromachi Chemical (Tokyo) and Amberlite resin by Japan Organo (Tokyo).

### *Preparation of liquid chromatographic*

Vialle et al. [15] employed LiChrosorb  $NH_2$  (10  $\mu$ m particle diameter) (Merck) as the separation column. The present authors selected Nucleosil 5  $NH_2$  (5  $\mu$ m) (Macherey–Nagel, Düren, Germany) and Kaseisorb LC  $NH_2$  super (5  $\mu$ m) (Tokyo Kasei Kogyo), expecting higher column efficiencies owing to their low surface activities, spherical shapes and smaller particle diameters than those of LiChrosorb. Each column packing was first treated with a suitable volume of packing solution in a 200 W ultrasonic bath for 3 min. This packing solution consisted of detergent and methanol. The resulting slurry was transferred into a packer (internal volume ca. 50 ml) and packed into a stainless-steel column (25 cm  $\times$  4.6 mm i.d., filter pore size 2  $\mu$ m). A 500 kg  $cm^{-2}$  pressure was maintained throughout the packing process. In the initial stage, the column was immersed in an ultrasonic bath and treated for 15 min while passing through methanol–2-propanol (85 + 15, v/v). After 40 min of continuous pumping, the solution was changed to pure methanol, then to acetonitrile–water (75 + 25), pumping for 45 min each at the same pressure. Three to four hours of conditioning were also required to obtain freshly packed column under the analytical conditions.

### *Ion-exchange columns for absorption and purification of betaine*

The absorption column was 30 cm  $\times$  1.6 cm i.d. glass column packed with Dowex 50W-X8 ( $H^+$ ) ion exchanger (50–100 mesh) up to 25 cm.

The purification column was a 30 cm  $\times$  1.6 cm i.d. glass column packed with a 1 + 2 (v/v) mixture of Amberlite IRC-50 ( $H^+$ ) (50–100 mesh)

and Dowex 1-X4 (OH<sup>-</sup>) (50–100 mesh) up to 25 cm.

Each ion exchanger was properly generated by following the manufacturer's, instructions.

#### *Preparation of sample solution from Jikoppi powders*

A 200-ml volume of water was added to each 15 g of Jikoppi powder and the pH was adjusted to 3.2–3.4 using 1 M hydrochloric acid. After leaving for 1 h, the mixture was filtered. The same volume of water was added to the residual cake and extracted at 70–80°C for 1 h at the same pH, then filtered to remove the residue. All filtrates and washings were combined and passed through the absorption column at a flow-rate of 1 ml min<sup>-1</sup>. The column was washed with water until the effluent became clear and was free from chloride ion. The betaine retained in the column was eluted with 200 ml of 4% ammonia solution and successive washing with 150 ml of water. The alkaline effluent and washings were combined and condensed to ca. 50 ml under diminished pressure at 37°C. The remaining solution was poured into the purification column at a flow-rate of 1 ml min<sup>-1</sup>, and the column was washed with two 50-ml portions of water. The effluent and washings were again combined and condensed to a syrupy concentrate. A portion of solution containing 15 mg of glycine was added to the above colourless syrup as an internal standard, then diluted to 5 ml with water. The sample solution thus prepared was filtered through Millipore SJHVOO4NS membrane filter cartridge (pore size 0.45 μm) and 1 μl of the filtrate was analysed by LC. The content of betaine in this 1 μl of filtered sample solution were calculated as the mean value of five repeated analyses.

## RESULTS AND DISCUSSION

#### *Effects of ion exchangers for concentration and purification of betaine*

A strong cation exchanger, Dowex 50W-X8 (H<sup>+</sup>), quantitatively concentrated betaine in plant extracts. And a mixed bed of Dowex 1-X4 (OH<sup>-</sup>) and Amberlite IRC-50 (H<sup>+</sup>) effectively removed

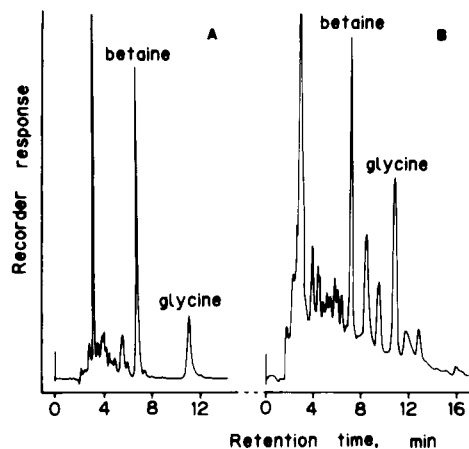


Fig. 1. Effects of ion exchangers on the purification of betaine. Ion-exchange columns: (A) 25 cm × 1.6 cm i.d., showing impurities are almost removed; (B) 15 cm × 1.8 cm I.D., as reported by Vialle et al. [15], indicating incomplete removal of impurities from the Jikoppi extracts. Dimensions are the same for both absorption and purification columns. LC conditions: column, Kaseisorb LC NH<sub>2</sub> super (25 cm × 4.6 mm i.d.); mobile phase, acetonitrile–water (75 + 25) containing 0.1% of Brij 35; flow rate, 1 ml min<sup>-1</sup>; UV detection at 210 nm.

impurities from the sample solutions. It was necessary to change the bed volume of the ion exchangers according to their matrix concentrations and sample volumes (Fig. 1). Regeneration of the exchangers by the usual methods was almost impossible because a thick brown pigment appeared, covering all surfaces of the exchangers. The use of such “regenerated” resins produced a low recovery of betaine and/or a large distribution of analytical values.

#### *Selection of internal standards for betaine determination*

Different types of nitrogenous compounds, such as phenacetin, alloxan, triphenyltetrazolium chloride, quinolin-8-ol, *p*-aminobenzoic acid and several amino acids, were tested with betaine with respect to both their chromatographic retention behaviours and spectrophotometric responses in the range 210–215 nm. Of this series of compounds, glycine was selected as the internal standard for betaine determination as shown in Fig. 2.

### Effects of mobile phase composition and addition of “modifier”

Vialle et al. [15] utilized acetonitrile–water (75 + 25) for the separation of betaine. The present authors tested 70, 75 and 80% aqueous solutions of acetonitrile in preliminary work on the separation of a betaine–glycine mixture (each 3  $\mu$ g). Acetonitrile–water (75 + 25) was found to give the best results on both Nucleosil and Kaseisorb columns. These results were obtained from values of the sample capacity factors ( $k'$ ), column efficiencies, analysis times and separation factor (data not shown).

To decrease peak tailing, the addition of a “modifier” to the mobile phase was considered. In Fig. 3, the effects of a surfactant, Brij-35 (polyoxyethylene lauryl ether), on the separation of the two compounds are shown. The polarities of non-ionic surfactants and the ionic strengths of ionic surfactants were also considered for the selection of the “modifier”. It was found that addition of 0.1% Brij-35 to the mobile phase gave the best results for increasing the column efficiency, decreasing the analysis time and reducing peak tailing.

### Selection of analytical columns

Generally, the lifetime of an amino-bonded silica gel column is much shorter than that of an ODS-modified column. Also, it is very difficult to prepare a high-efficiency column. The column efficiency was evaluated by comparing the num-

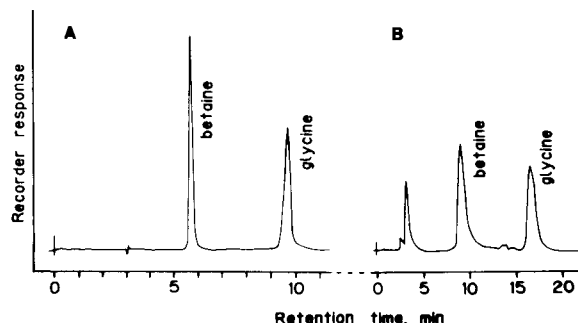


Fig. 2. Retention behaviours of betaine and internal standard. Separation columns: (A) Kaseisorb LC NH<sub>2</sub> super (25 cm × 4.6 mm i.d.); (B) Nucleosil 5 NH<sub>2</sub> (25 cm × 4.6 mm i.d.). Mobile phase, acetonitrile–water (75 + 25) containing 0.1% of Brij 35; flow-rate, 1 ml min<sup>-1</sup>; UV detection at 210 nm.

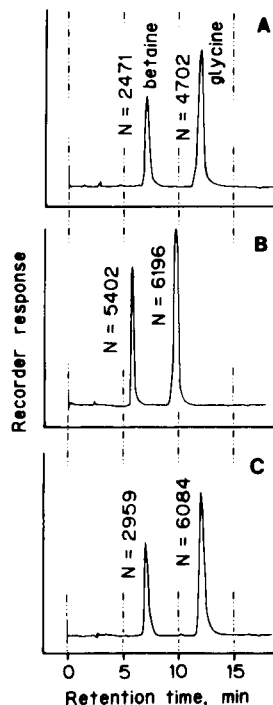


Fig. 3. Effects of addition of modifier (Brij 35) to the mobile phase indicating changes in retention times and numbers of theoretical plates ( $N$ ). (A) Control; (B) 0.1% addition; (C) 0.2% addition. Analytical condition as in Fig. 1.

bers of theoretical plates of the Nucleosil 5 NH<sub>2</sub> and Kaseisorb LC NH<sub>2</sub> super (5  $\mu$ m) columns. With the same packing method and analytical conditions, the Kaseisorb column gave a larger number of theoretical plates ( $N = 5400$  for betaine and 6200 for glycine; Fig. 3B) than the Nucleosil column ( $N = 590$  and 1730, respectively; Fig. 2B). It can be suggested that the packing method used was inadequate for the preparation of the Nucleosil 5 NH<sub>2</sub> column, considering that the theoretical plate number of betaine at  $k' \approx 2.3$  was much lower than that of glycine at  $k' \approx 5.8$ .

### Analytical parameter settings of data processor

All analytical parameter settings of the processor were set by the automatic correction mode with the exception of the slope sensitivity. A manually “fixed” slope sensitivity value set ca. 10% higher (lower sensitivity) than that given by an “automatic correction”, 200  $\mu$ V min<sup>-1</sup>, gave a

TABLE 1

Analysis of variance for the calibration graph of betaine <sup>a</sup>

Amount of betaine ( $\mu\text{g}$ )	Betaine to glycine peak-area ratio	$\sigma^2$	$\sigma^2$ , relative (%)
0.25	0.0788	0.014	5.6
0.5	0.144	0.008	1.6
1.0	0.328	0.017	1.7
2.0	0.620	0.035	1.7
4.0	1.202	0.054	1.4
6.0	1.776	0.074	1.2
8.0	2.412	0.105	1.3
10.0	3.127	0.139	1.4
12.0	3.704	0.165	1.3
14.0	4.178	0.069	0.5
16.0	4.886	0.104	0.7
18.0	5.504	0.230	1.3

<sup>a</sup> Five determinations in each instance.

reliable and stable count against an artificial mixture of betaine and the internal standards.

#### Regression line for betaine

A series of artificial test mixtures, containing 0.25, 0.5, 1.0, 2.0, 4.0, 6.0, 8.0, 10.0, 12.0, 14.0 and 18.0  $\mu\text{g}$  of betaine and 3  $\mu\text{g}$  of glycine in 1  $\mu\text{l}$  of water, were injected into the separation column. Each calibration point was tested five times. The calibration graph of betaine to glycine peak-area ratio versus betaine concentration was linear over the entire working betaine concentration range of 0.25–18  $\mu\text{g } \mu\text{l}^{-1}$ . The linear regression equation for the above betaine concentration range was peak-area ratio = 0.305(betaine amount,  $\mu\text{g}$ ) – 0.0013. The 95% fiducial limits were obtained for this regression line as given in Table 1. The

average relative  $\sigma^2$  value in the betaine concentration range 0.5–18  $\mu\text{g } \mu\text{l}^{-1}$  was ca. 1.3%. From these statistical results, it can be suggested that this method of separation and determination is reasonably acceptable for the determination of betaine in plant tissues.

#### Total recovery of betaine through the analytical procedure

A solution consisting of 18  $\mu\text{g}$  of betaine in 100 ml of water was charged into the absorption column and successively treated as described under Experimental. This procedure was repeated five times. Each sample thus obtained was analysed under the same conditions as described in Fig. 1. The amounts of glycine were determined from the calibration graph and the recovery was calculated as follows: betaine added, 18.0  $\mu\text{g}$ ; average betaine to glycine peak-area ratio, 5.35; betaine found, 16.7  $\mu\text{g}$ ; recovery, 92.7% ( $n = 5$ ). This calculated recovery of 93% is lower than the 96% recovery stated by Vialle et al. [15], but the stability was constant throughout the processes.

#### Betaine contents in Jikoppi powders

Six Jikoppi powders from different origins but cultivated in South Korea were analysed and the results are summarized as in Table 2.

The authors are indebted to Professor Dr. Yoshizo Kaneki of this University for giving them the opportunity to carry out this work, and to Dr. Seon Kwan Seoig of the Chung-Nam Office of Rural Developments, Dae Jeon, Korea, for the gifts of Jikoppi powders.

TABLE 2

Betaine contents in different Jikoppi powders <sup>a</sup>

Parameter	Korean			Japanese <sup>b</sup>	Chinese <sup>b</sup>	
	Untreated	Treated with 3KR <sup>60</sup> Co	Treated with 0.1% colchicine		Hae Nan <sup>c</sup>	Cheong Yang <sup>c</sup>
Betaine to glycine peak-area ratio	2.4823	2.8803	1.6866	2.9209	2.3313	1.7501
Betaine observed ( $\mu\text{g } \mu\text{l}^{-1}$ )	8.10	9.40	5.50	9.55	7.60	5.70
Betaine calculated ( $\text{mg g}^{-1}$ of material)	2.70	3.10	1.83	3.18	2.53	1.90
Betaine recovery, corrected ( $\text{mg g}^{-1}$ of material)	2.90	3.33	1.97	3.42	2.69	2.04

<sup>a</sup> Five determinations in each instance. <sup>b</sup> Untreated. <sup>c</sup> Originally grown in these areas.

## REFERENCES

- 1 J.S. Wall, D.D. Christianson, R.J. Dimler and F.R. Senti, *Anal. Chem.*, 32 (1960) 870.
- 2 R. Strey and R.G. Wyn Jones, *Phytochemistry*, 16 (1977) 447.
- 3 A.J. Barak and D.J. Tuma, *Lipids*, 14 (1979) 860.
- 4 V.Y. Pavinov and V. Egerts, *Nauchn. Konf. Khim. Anal. Pribolt Resp., USSR*, (1974) 109.
- 5 A.D. Hanson and G.E. Nelson, *Plant Physiol.*, 62 (1978) 305.
- 6 J.J. Martin and J.D. Finkelstein, *Anal. Biochem.*, 111 (1981) 72.
- 7 F. Chastellain and P. Hirsbrunner, *Fresenius' Z. Anal. Chem.*, 278 (1976) 207.
- 8 J. Gorham, E. McDonnel and R.G. Wyn Jones, *Anal. Chim. Acta*, 138 (1982) 277.
- 9 A. Corrao and A.M. Gattuso, *Riv. Viticol. Enol.*, 31 (1978) 358.
- 10 J. Gorham, S.J. Coughlan, R. Storey and R.G. Wyn Jones, *J. Chromatogr.*, 210 (1981) 550.
- 11 W.D. Hits and A.D. Hanson, *Phytochemistry*, 10 (1980) 2371.
- 12 P. Dubois and C.R. Dupuy, *Seances Acad. Agric.*, 60 (1974) 62.
- 13 P. Dubois and P. Simand, *Ann. Technol. Agric.*, 25 (1976) 337.
- 14 K. Ranfft and R. Gerstl, *Fresenius' Z. Anal. Chem.*, 276 (1975) 51.
- 15 J. Vialle, M. Kolosky and J.L. Rocca, *J. Chromatogr.*, 204 (1981) 429.
- 16 G. Steinle and E. Fischer, *Zuckerindustrie*, 103 (1978) 129.
- 17 J.C. Linden and C.L. Lawhead, *J. Chromatogr.*, 105 (1975) 125.
- 18 I. Molnár and Cs. Horváth, *J. Chromatogr.*, 142 (1977) 623.
- 19 M.T.W. Hearn, B. Grego and W.S. Hancock, *J. Chromatogr.*, 185 (1979) 429.
- 20 J. Gorham, *J. Chromatogr.*, 362 (1986) 243.
- 21 P.E. Minkler, T.S. Ingalls, L.S. Kormos, D.E. Wier and C.L. Hoppel, *J. Chromatogr.*, 336 (1984) 271.
- 22 S. Konosu, A. Shinagawa and K. Yamaguchi, *Nihon Suisangakukai-shi*, 52 (1986) 869.
- 23 C.W. Ford, *J. Sci. Food Agric.*, 35 (1984) 881.
- 24 G. Mozzola and C. Kent, *Anal. Biochem.*, 141 (1984) 137.
- 25 J. Gorham, *J. Chromatogr.*, 361 (1986) 301.
- 26 N.W. Kerby, R.H. Reed and P. Rowell, *J. Chromatogr.*, 479 (1989) 353.
- 27 J. Gorham, *J. Chromatogr.*, 287 (1984) 345.
- 28 R.H. Reed, *Mar. Biol. Lett.*, 4 (1983) 173.



# On-line trace metal ion preconcentration in ion chromatography using carboxymethyl and hydroxamate dextran-coated silicas

N. Ryan and J.D. Glennon

*Department of Chemistry, University College, Cork, (Ireland)*

D. Muller

*LRM, CNRS URA 502, Institut Galilee, 93430 Villeteuse (France)*

(Received 30th October 1992; revised manuscript received 24th December 1992)

## Abstract

While dextrans have cation binding properties, their chemical modification to carboxymethyl and hydroxamate dextrans increase the degree of metal ion chelation. This paper describes recent findings on the use of dextran coated silica materials for the on-line preconcentration of metal ions in ion chromatography. Results presented include the effects of flow-rate and pH on metal ion uptake and elution, metal ion complexation capacities and applications to trace metal analysis in aqueous environmental samples.

*Keywords:* Atomic absorption spectrometry; Ion chromatography; Dextrans; Preconcentration

While trace metal ion preconcentration based on liquid–liquid extraction, ion-exchange and co-precipitation are widely used in trace metal analysis [1], the high preconcentration factors and increased selectivity of chelating solid phases are increasingly being recognised as important advantages. Different solid supports (e.g. ion-exchange resin, controlled pore-glass, octadecylsilica and polymers) have extensively been used for the immobilization of chelating ligands [2]. Such sorbents have been used for the uptake and enrichment of trace metal ions from aqueous samples utilising mechanisms of ion-exchange, adsorption [3], partition and chelation [4]. Among the grafted ligands, dithiocarbamates, primary and secondary amines [5] and 8-quinolinol [6] immobilized on

silica have been used for trace metal preconcentration. Enrichment of a series of metal traces has been investigated in detail using stearylpyrazolane [7] and pyridinium ion [8] loaded silica gels prior to atomic absorption spectrometric determination. The selectivity advantage of such chelating solid phases should be particularly advantageous in the quantification of trace and ultra trace metals in sea water and brines. The extremely high levels of alkali and alkaline-earth metals and other matrix interferences in such samples, compared to the low levels of transition metals can present a formidable obstacle to direct determination of these trace metal components.

A technique termed chelation ion chromatography has been described, which utilizes an iminodiacetic acid resin prior to the analytical column and has been successfully applied to trace metal determination in sea water and other high ionic strength media [9]. However, Ca and Mg must be

*Correspondence to:* J.D. Glennon, Department of Chemistry, University College, Cork (Ireland).

removed from the resin prior to the elution of trace metals.

Hydroxamic acids, well known for their biochelation activity in microbial systems, have attracted attention as analytical reagents owing to their good complexing behaviour with a broad range of metal ions [10–12]. A number of papers concerning the synthesis, properties and applications of solid phases containing hydroxamic acid groups have been published [13–16]. The solid phase extraction properties of a silica-based chelating phase containing immobilised hydroxamic acid groups have recently been described [17]. Hydroxamic acids have a distinct advantage over carboxylate reagents in that they form stronger transition metal complexes and are selective for transition metal ion uptake. The present work illustrates the use of carboxymethyl dextran coated silica (CMD-Si) (designed for the ion exchange of proteins, polysaccharides and nucleic acids [18]) and CMD-Si derivatised to contain hydroxamic acid groups (HAD-Si) for the preconcentration of a series of transition metal ions. On-line trace metal enrichment coupled with ion chromatographic separation is demonstrated, using the loading and back flushing of a precolumn incorporated in the loop of a single high pressure switching valve. This paper also describes the solid phase extraction properties of a trace metal cartridge utilising the chelating dextran coated silica phase (HAD-Si).

## EXPERIMENTAL

### Materials

The chelating dextran-coated silica was prepared from carboxymethyl dextran coated silica by reaction with hydroxylamine as described previously [17]. Silica beads (40–100  $\mu\text{m}$ , pore size 1250 Å) provided by Sepracor-IBF (Villeneuve La Garenne) were coated with DEAE-dextran (MW 70 000) as previously reported [19,20]. Hydroxylammonium chloride, potassium hydroxide, sodium hydroxide, lead nitrate [ $\text{Pb}(\text{NO}_3)_2$ ], cadmium nitrate tetrahydrate [ $\text{Cd}(\text{NO}_3)_2 \cdot 4\text{H}_2\text{O}$ ], cobalt chloride hexahydrate ( $\text{CoCl}_2 \cdot 6\text{H}_2\text{O}$ ), standard zinc chloride ( $\text{ZnCl}_2$ ), copper chloride

( $\text{CuCl}_2$ ) and nickel chloride ( $\text{NiCl}_2$ ) solutions were purchased from Merck (Darmstadt). Oxalic acid and lithium hydroxide were purchased from Sigma (Poole). Analytical grade reagents were used throughout.

### Solutions

Stock solutions of metals (1000  $\mu\text{g ml}^{-1}$ ) were used in all instances, from which standards with concentrations ranging from 10  $\text{ng ml}^{-1}$  to 5  $\mu\text{g ml}^{-1}$  were prepared by dilution with water. Appropriate calibration graphs were constructed for ion chromatographic and atomic absorption spectroscopic analysis. Solution pH values were adjusted to 7.0 with 0.5 M LiOH prior to injection. De-ionized water from an Elgastat spectrum water purification unit, with a resistivity of 16  $\text{M}\Omega \text{ cm}$  or better, was used throughout. Tap water, domestic water and river water were collected from the laboratory, from Wilton Court (Cork) and on campus from the river Lee (Cork). Metal ion separations were carried out by using a mobile phase of 0.05  $\text{mol dm}^{-3}$  oxalic acid and 0.095  $\text{mol dm}^{-3}$  LiOH (pH 4.8) with a flow-rate of 1  $\text{ml min}^{-1}$ .

### Instrumentation

A schematic diagram of the ion chelation chromatographic instrumentation used is shown in Fig. 1. On-line metal preconcentration was carried out on chelating material (ca. 0.28 g) packed

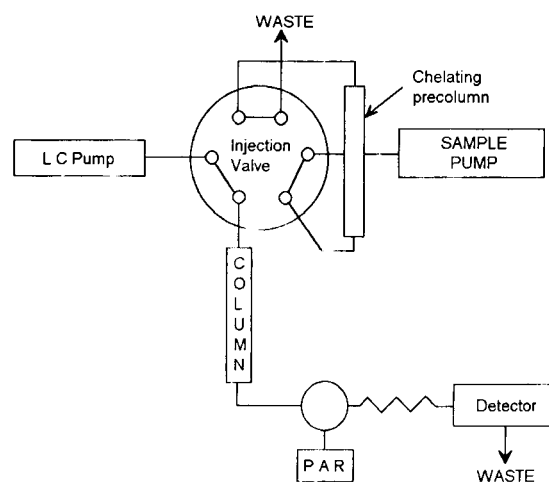


Fig. 1. Instrumental configuration for on-line preconcentration in ion chromatography.

in a  $5 \times 0.4$  cm i.d. Tefzel precolumn. Off-line analysis was carried out using a cartridge (plastic cartridge,  $1.3 \times 0.9$  cm i.d.) packed with ca. 0.25 g of sorbent. Metal ion solutions were loaded on the material using a Pharmacia peristaltic p-1 pump. All pH values were recorded using an EA 920, Orion pH meter. A Dionex 4500i ion-chromatographic system was used, with a  $3 \times 10^{-4}$  M solution of 4-(2'-pyridylazo)resorcinol (PAR) for post-column derivatization. The PAR flow-rate was  $0.6 \text{ ml min}^{-1}$ . The wavelength chosen for metal ion detection was 520 nm. A Dionex Analytical CS5 column was used for metal separation. Pye Unicam SP9 and 2380 Perkin-Elmer flame atomic absorption spectrometers were also used for metal ion determinations (air-acetylene). Resonance lines used for metal ion analysis include Cu (324.8 nm), Zn (213.9 nm), Mn (279.5 nm), Cd (228.8 nm), Pb (217 nm), Co (240.7 nm) and Ni (232 nm). Ultraviolet and visible absorption spectra were measured on a Shimadzu UV 260 spectrophotometer.

#### Procedures

*Characterisation of metal loaded dextran-coated silica.* The characterisation of the metal loaded hydroxamic acid dextran coated silica (HAD-Si)

was carried out by spectrophotometric analysis. Spectra for metal loaded carboxymethyl dextran coated silica were recorded throughout for comparison. Cu(II) and Fe(III) were loaded to capacity on both sorbents at pH values of 6.0 and 2.5 respectively. The sorbents were ground to fine powders and the absorption spectra were obtained as slurries in ethylene glycol using a 1-mm cell.

*Metal ion complexation capacities.* The metal ion complexation capacities of the chelating silicas were studied as a function of pH using a continuous flow cartridge method. In the cartridge experiment, a 25 ml sample solution of a  $5 \mu\text{g ml}^{-1}$  metal ion mixture [i.e.  $5 \mu\text{g l}^{-1}$  each of Pb(II), Cu(II), Mn(II), Cd(II), Co(II), Zn(II) and Ni(II)] was adjusted to the desired pH using 0.5 M LiOH and was passed through the cartridge using a peristaltic pump at  $1 \text{ ml min}^{-1}$ . The effluent and washings were then collected for analysis by ion chromatography (IC) and atomic absorption spectrometry (AAS), respectively. Breakthrough capacities were measured singly for each metal at the pH of maximum uptake using  $10 \mu\text{g ml}^{-1}$  metal solutions at a flow-rate through the cartridge of  $1 \text{ ml min}^{-1}$ . The effluent was collected every minute and analysed by IC for the

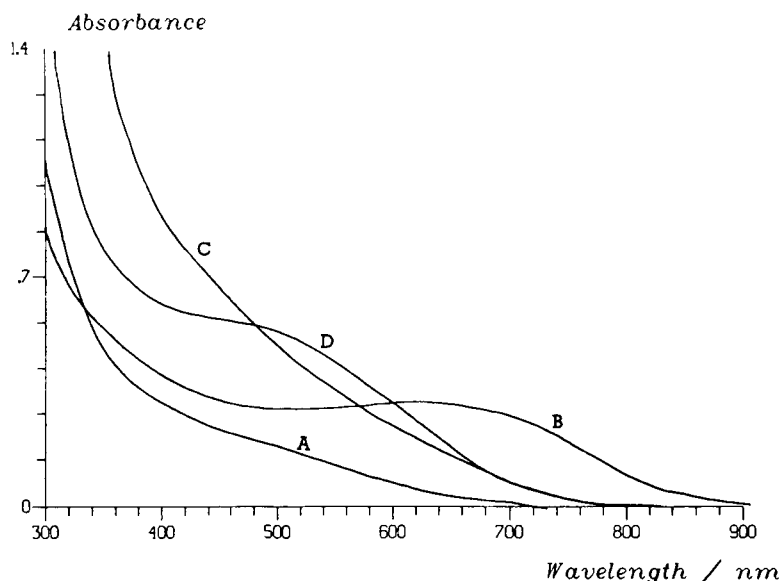


Fig. 2. Absorption spectra of Cu(II) on (A) CMD-Si, (B) HAD-Si, and Fe(III) on (C) CMD-Si, (D) HAD-Si.

presence of metal. The volume at which metal appeared was used to determine the breakthrough capacity.

**Preconcentration of metal ions from standard solutions and environmental samples.** The preconcentration of metal ions from aqueous solutions was studied on-line using a Tefzel precolumn packed with chelating HAD-Si. Standards and samples were adjusted to a pH of 7.0 with 0.5 M LiOH, from which 1 ml quantities were loaded onto the precolumn. Metal ions were subsequently eluted for detection using the mobile phase. Based on a comparison of the peak area obtained for a direct 25- $\mu$ l sample injection with the peak area for a 1 ml on-line preconcentrated sample, a twenty-five fold enrichment factor operates for the given precolumn dimensions. The two approaches of on-line and off-line preconcentration were used in analysing aqueous environmental samples. Samples were first prefiltered using Millipore 0.45- $\mu$ m filters and the sample pH lowered to 2.5 with 2 M hydrochloric acid. Following a second filtration, 1 ml of the sample was loaded on the precolumn following adjustment to the desired loading pH. For off-line preconcentration using the chelating cartridge containing HAD-Si, 250 ml of the environmental sample was similarly pretreated and loaded at 1 ml min<sup>-1</sup> using a peristaltic pump. The metal ions were subsequently eluted using 25 ml of water acidified to pH 2.0 with 2 M HCl and determined by AAS.

## RESULTS AND DISCUSSION

The presence of hydroxamic acid groups on the HAD-Si was confirmed by the visible absorption spectra recorded for Fe(III) and Cu(II) loaded on HAD-Si. The spectra obtained are shown in Fig. 2 and provide strong evidence of the presence of hydroxamate chelating groups on the silica phase, displaying the characteristic bands for Fe(III) and Cu(II) complexation by hydroxamate [17].

The effect of pH on the percentage metal uptake by the chelating dextran coated silica (HAD-Si) for the transition metals studied, is

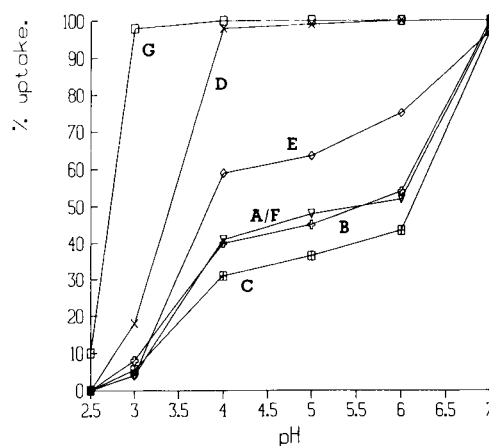


Fig. 3. Percentage uptake of metal ions on HAD-Si as a function of pH: (A) Mn(II), (B) Ni(II), (C) Co(II), (D) Cu(II), (E) Zn(II), (F) Cd(II), (G) Pb(II).

shown in Fig. 3. In general, among these metals two groups can be distinguished with respect to the nature of their complexation by hydroxamic acids, i.e. Pb(II) and Cu(II) where complete complexation occurs in the pH range 2–4.5 and Mn(II), Ni(II), Co(II), Cd(II) and Zn(II) which only begin to be complexed above pH 5.0 and require high pH for complete complexation. From Fig. 3 it is clear that the latter group of metal ions, however, is taken up on the chelating dextran coated silica (HAD-Si) in the low pH region and that a further region of complexation occurs after pH 6.0. The results are diagnostic of the condition of the sorbent material in that, for this group of metals, ion exchange on the residual carboxylic acid groups is occurring at low pH and further coordination to the hydroxamic acid groups on the surface, takes place at higher pH.

A comparison of the metal uptake behaviour of the chelating dextran coated silica and the carboxymethyl dextran coated silica is given in Fig. 4 for two representative metal ions, Cu(II) and Co(II). The decrease in the Co(II) uptake on HAD-Si from that on CMD-Si in the pH range 3–6 is in proportion to the extent of derivatisation of the carboxylate groups to hydroxamate. Higher uptake on CMD-Si is understandable for Co(II) as the complete carboxylic acid coverage is available for ion exchange in this pH range, whereas on HAD-Si fewer ion exchange sites are

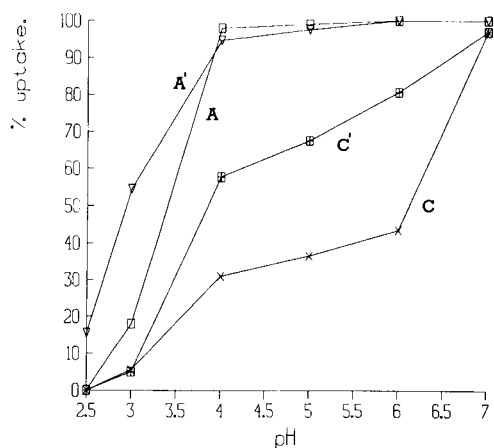


Fig. 4. Percentage uptake of metal ions as a function of pH for (1) Cu(II) on (A) HAD-Si and (A') CMD-Si and (2) Co(II) on (C) HAD-Si and (C') CMD-Si.

available for metal ion uptake. However at higher pH on HAD-Si, the hydroxamate groups become available for Co(II) coordination resulting in increased metal uptake. The profiles for Cu(II) uptake on the two sorbent materials are similar, as expected.

The elution of metal ions from the chelating HAD-Si was examined using the cartridge. Competing ligands such as EDTA and oxalic acid were investigated. It was found that 100% elution of metal ions loaded on the cartridge was readily achieved using 0.02 M EDTA. Significantly, it was also found that 100% elution of metal ions from HAD-Si was possible using 0.05 M oxalic acid (pH 4.8). As this is a major constituent of the mobile phase used for the ion chromatographic separation of metal ions, on-line elution of metal ions by the mobile phase itself from a precolumn conveniently takes place. It is also clear from studies of the pH variation that elution can be achieved readily by pH control for certain metal ions including Cu(II), Zn(II), Co(II) and Ni(II), which are eluted quantitatively with acidified water (pH 2.0). The elution of metal ions from the cartridge with 0.02 M EDTA, 0.05 M oxalic acid or acidified water (pH 2.0) was found to be independent of the flow-rate of these eluting solutions.

Using the precolumn for on-line preconcentration in ion chromatography, the chromatographic

responses obtained as a function of loading volume over the range 0.1–4.0 ml were examined [21]. A loading volume of 1.0 ml was chosen for further use, as higher volumes led to some loss of resolution and poorer peak shape. Under these conditions limits of detection were assigned to metal ion concentrations producing chromatographic responses three times greater than the background noise and were found to be between 5 and 10 ng ml<sup>-1</sup> for Cu(II), Mn(II), Co(II), Zn(II) and Ni(II) but were > 100 ng ml<sup>-1</sup> for Pb(II) and Cd(II).

#### APPLICATION

Breakthrough capacities for the metal ions on HAD-Si were determined to be between 28 and 34  $\mu\text{mol g}^{-1}$ . This complexation capacity of the chelating dextran coated silica (HAD-Si) was utilised for the on-line and off-line preconcentration of metal ions in river, domestic and laboratory tap water samples. In the former case ion chromatography was employed for metal ion separation and analysis and in the latter, atomic absorption spectroscopic analysis was carried out following the elution of the metals from the chelating cartridge.

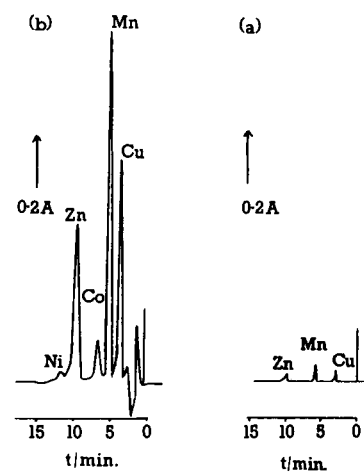


Fig. 5. Comparison of (a) direct injection of 25  $\mu\text{l}$  of river water with (b) on-line preconcentration of 1 ml of river water using HAD-Si. A = Absorbance output range.

TABLE 1

Metal ion analysis in water samples <sup>a</sup>[IC, ion chromatography (direct injection, 25  $\mu$ l). PIC, on-line preconcentration in ion chromatography (1 ml loading volume). PAAS, off-line preconcentration using AAS (using cartridge)]

	Copper			Manganese			Zinc		
	IC	PIC	PAAS	IC	PIC	PAAS	IC	PIC	PAAS
Laboratory tap water	310 $\pm$ 0.1	310 $\pm$ 0.4	318 $\pm$ 0.1	61 $\pm$ 0.1	55 $\pm$ 0.2	62 $\pm$ 0.1	51 $\pm$ 0.1	46 $\pm$ 0.2	56 $\pm$ 0.1
Domestic tap water	– <sup>b</sup>	19 $\pm$ 0.2	14 $\pm$ 0.2	35 $\pm$ 0.1	29 $\pm$ 0.3	24 $\pm$ 0.1	– <sup>b</sup>	13 $\pm$ 0.2	19 $\pm$ 0.2
River water	40 $\pm$ 0.1	35 $\pm$ 0.3	28 $\pm$ 0.1	42 $\pm$ 0.1	42 $\pm$ 0.2	40 $\pm$ 0.1	44 $\pm$ 0.1	40 $\pm$ 0.2	48 $\pm$ 0.1

<sup>a</sup>  $\mu$ g dm<sup>-3</sup>  $\pm$  S.D. for 5 replicate injections or aspirations. <sup>b</sup> Values below limit of detection.

The improvement in sensitivity obtained using HAD-Si is shown in Fig. 5, where the chromatogram obtained for a direct injection of 25  $\mu$ l of river water is compared with that obtained using on-line preconcentration. However the ion chromatographic (CSS) column used in the present study has a similar selectivity for Cu(II) and Pb(II) resulting in similar retention times without base-line separation. While peak overlap is possible, atomic absorption results on the studied preconcentrated environmental samples indicated that Pb(II) levels were insignificant relative to the Cu(II) levels present. Typical results obtained using the three approaches of direct ion chromatography (where sensitivity allowed its use), on-line preconcentration in ion chromatography and flame AAS following off-line preconcentration, are given in Table 1 for Cu(II), Mn(II) and Zn(II).

## REFERENCES

- M.S. Cresser, L.C. Ebdon, C.W. McLeod and J.C. Burridge, *J. Anal. At. Spectrom.*, 1 (1986), 1R.
- R. Van Grieken, *Anal. Chim. Acta*, 43 (1982) 3.
- R.E. Sturgeon, S.S. Berman and S.N. Willie, *Talanta*, 29 (1982)167.
- R. Mendez, N. Vadasseril and P. Sivasankara, *Analyst*, 115 (1990) 213.
- D.E. Leyden and G.H. Luttrell, *Anal. Chem.*, 47 (1975) 1612.
- O. Abollino, E. Mentasti, V. Porta and C. Sarzanini, *Anal. Chem.*, 62 (1990) 21.
- A. Tong, Y. Akama and S. Tanaka, *Analyst*, 115 (1990) 947.
- M.S. Yamamoto and Y. Gushikem, *Analyst*, 114 (1989) 983.
- A. Siriraks, H.M. Kingston and J.M. Riviello, *Anal. Chem.*, 62 (1990) 1185.
- Y.K. Agrawal and R.D. Roshania, *Bull. Soc. Chim. Belg.*, 89 (1980) 159.
- Y.K. Agrawal and S.A. Patel, *Anal. Chem.*, 4 (1980) 237.
- A.T. Senior and J.D. Glennon, *Anal. Chim. Acta.*, 196 (1987) 333.
- F. Vernon and H. Eccles, *Anal. Chim. Acta.*, 83 (1976) 187.
- A. Shah and S. Devi, *Analyst*, 110 (1985) 1501.
- A. Shah and S. Devi, *Analyst*, 112 (1987) 325.
- R.J. Phillips and J.S. Fritz, *Anal. Chim. Acta.*, 139 (1982) 237.
- S. Srijaranai and J.D. Glennon, *Analyst*, 115 (1990) 627.
- J. Novotný, *FEBS Lett.*, 14 (1977) 7.
- X. Santarelli, D. Muller and J. Jozefonvicz, *J. Chromatogr.*, 443 (1988) 55.
- F.L. Zhou, D. Muller, X. Santarelli and J. Jozefonvicz, *J. Chromatogr.*, 476 (1989) 195.
- N. Ryan and J.D. Glennon, *Anal. Proc.*, 29 (1992) 21.

# Simultaneous determination of lanthanum, strontium and copper in superconductor materials by ion chromatography

Eduardo A. Gautier, Raquel T. Gettar and Roberto E. Servant

*Departamento Química Analítica, Div. Espectrometría de Masas, Comisión Nacional de Energía Atómica, Av. Libertador 8250, 1429 Buenos Aires (Argentina).*

(Received 8th September 1992; revised manuscript received 24th December 1992)

## Abstract

A precise and rapid procedure for the determination of metallic macro-components in ceramic superconductor samples of the La–Sr–Cu–O type is described. Lanthanum, strontium and copper are determined by ion chromatography using a complexing mobile phase (EDTA solution) and UV detection. Calibration graphs were linear in the concentration ranges 0.4–100, 0.1–100 and 0.05–100  $\mu\text{g ml}^{-1}$ , respectively, and practical determination limits of 0.1, 0.04 and 0.025  $\mu\text{g ml}^{-1}$  of La(III), Sr(II), Cu(II) ions, respectively, were achieved.

*Keywords:* Ion chromatography; Copper; Lanthanum; Strontium; Superconductors

Since the discovery of the oxide superconductors, one of the problems was to correlate stoichiometry and superconducting properties. Chemical characterization of the materials was usually based on the nominal weighted composition, without taking into account the presence of hydroxides in the starting oxide materials, especially for La- and Nd-based ceramic compounds [1]. The importance of the determination of oxygen content and speciation is also known [2].

Schwarz [3] pointed out the importance of future research focusing on details of well characterized compounds for optimization of properties and reproducibility in the production of ceramic materials.

Improvements in ion chromatography (IC) methodology have significantly enhanced its po-

tential usefulness for metal ion separation and determination using chelating agents as eluents [4–6]. This technique is mainly recommended for low concentrations of analytes. However, when only small amounts of sample such as monocrystals or surface coatings are available, IC becomes an important tool. EDTA is a powerful chelating agent and its metallic complex anions show a strong absorption band in the UV region. The objective of this work was the stoichiometric characterization of metallic macro-components in La–Sr–Cu–O-type superconductor materials.

## EXPERIMENTAL

### *Apparatus*

Measurements were performed using a Konik (Barcelona) KNK-500A liquid chromatograph, a Rheodyne Model 7125 injector with a 100- $\mu\text{l}$  sample loop and a Vydac 302IC4.6 silica-based anion-exchange column in series with a Linear

*Correspondence to:* E.A. Gautier, Departamento Química Analítica, Div. Espectrometría de Masas, Comisión Nacional de Energía Atómica, Av. Libertador 8250, 1429 Buenos Aires (Argentina).

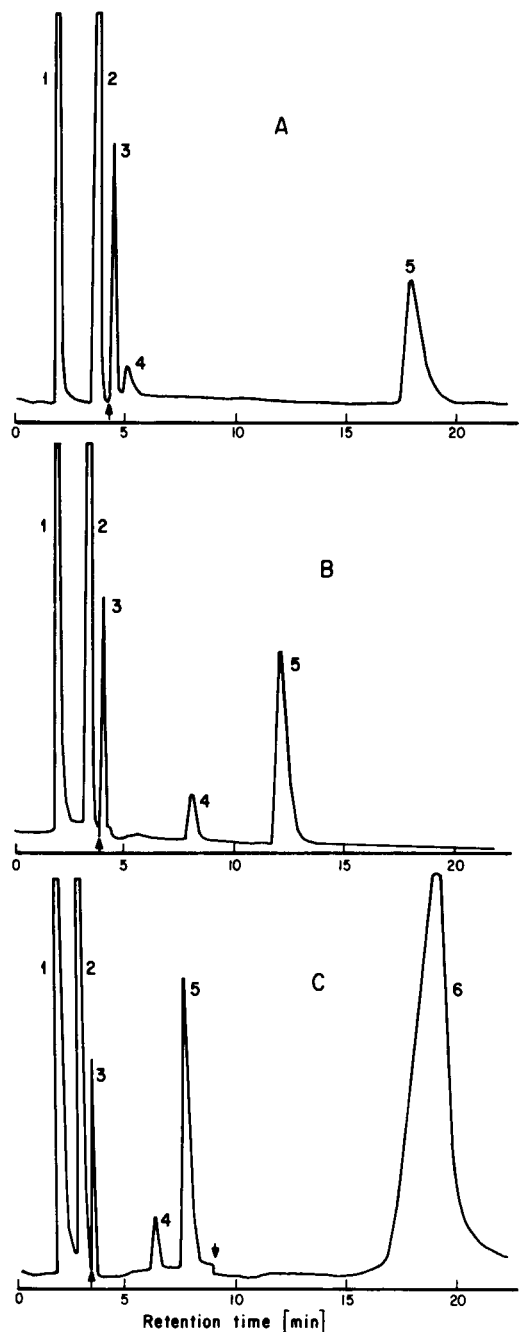


Fig. 1. Effect of pH of the eluent on chromatograms of synthetic samples obtained under the conditions indicated in the analytical procedure. (A) pH = 4.5; (B) pH = 5.05; (C) pH = 5.65. Peaks: 1 = injection; 2 =  $\text{Cl}^-$ ; 3 =  $\text{LaEDTA}^-$ ; 4 =  $\text{SrEDTA}^{2-}$ ; 5 =  $\text{CuEDTA}^{2-}$ ; 6 = system peak. Inversion signal direction:  $\uparrow$ , to positive;  $\downarrow$ , to negative.

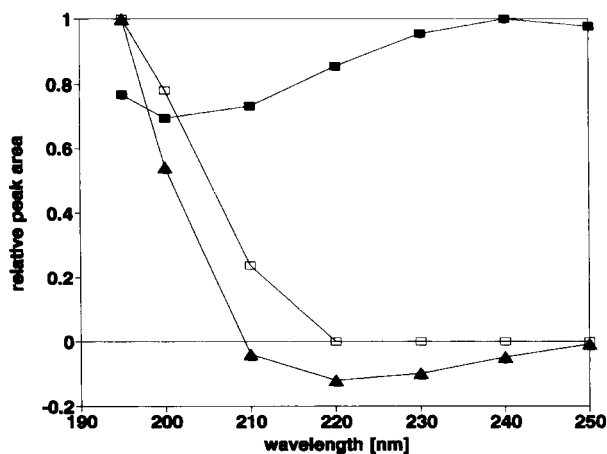


Fig. 2. Relative absorbance signal as a function of wavelength for (▲)  $\text{LaEDTA}^-$ , (□)  $\text{SrEDTA}^{2-}$  and (■)  $\text{CuEDTA}^{2-}$ . The data were measured from chromatograms obtained under the conditions indicated in the analytical procedure.

(Reno, NV) UVis 204 detector and a Spectra-Physics (San José, CA) SP4290 integrator. A switch was added before the integration device to allow negative and positive peak integration in the same chromatogram.

#### Reagents

LC-grade water was obtained by passing distilled water through a Nanopure water purification unit (Sybron/Barnstead, Boston, MA). Eluents were prepared by dissolution of EDTA disodium salt in water. pH was adjusted with 1 M sodium hydroxide solution. Each solution was filtered through a 0.22- $\mu\text{m}$  pore filter prior to use and degassed with helium.

#### Preparation of standards

Stock solutions of 1000  $\mu\text{g ml}^{-1}$  of each metal ion were prepared as follows.

**Sr(II):** the solution was prepared by dissolving  $\text{SrCO}_3$  (previously dried for 2 h at 110°C in an electric oven) in 3 M HCl. The mixture was warmed until total dissolution, then evaporated to dryness and the residue was dissolved in and made up to volume with water.

**Cu(II):** a stock solution was prepared by dissolution of the appropriate amount of clean and grease-free drillings of spectrographic copper metal in concentrated HCl with a few drops of



TABLE 1

Regression data of integrated absorbance vs. concentration: equation  $y = a + bx$  where  $y$  = peak area (arbitrary units),  $x$  = concentration ( $\mu\text{g ml}^{-1}$ ),  $a$  = intercept and  $b$  = slope

Element	$a \times 10^4$	$b \times 10^4$	$r^a$	$n^b$
La	-2.4 (0.9) <sup>c</sup>	2.32 (0.02)	0.99944	11
Sr	1.7 (0.8)	8.07 (0.02)	0.99998	10
Cu	6.4 (3.7)	14.27 (0.08)	0.99987	11

<sup>a</sup> Correlation coefficient. <sup>b</sup> No. of data points. <sup>c</sup> Standard deviations in parentheses.

concentrated  $\text{HNO}_3$ . After evaporation to dryness, residue was dissolved in and was made up to volume with water.

La(III): the solution was prepared from  $\text{La}_2\text{O}_3$  (heated for 2 h at  $950^\circ\text{C}$  in a muffle furnace [1] to remove  $\text{H}_2\text{O}$  and  $\text{CO}_2$ ). The solid was dissolved by slow addition of concentrated HCl. After evaporation to dryness, 0.1 M HCl was added to dissolve the residue, avoiding lanthanum hydrolysis, and the solution was diluted to volume with 0.1 M HCl.

Dissolutions were performed in Teflon beakers to avoid contamination.

#### Sample preparation

About 60.0 mg of solid superconductor sample were dissolved in 0.1 M HCl. The solution was then transferred into a 50-ml volumetric flask and diluted to volume with water. Quantification of the elements was performed after tenfold dilution with water. The final concentration of HCl was ca.  $5 \times 10^{-4}$  M.

TABLE 2

Analytical results ( $\mu\text{g g}^{-1}$ ) with standard deviations in parentheses

Method	Sample 1			Sample 2			Sample 3		
	La	Sr	Cu	La	Sr	Cu	La	Sr	Cu
AAS	63.2 (1)	4.6 (0.3)	17.1 (0.5)	58.7 (0.9)	3.8 (0.3)	18.5 (0.5)	54.1 (0.8)	4.5 (0.4)	–
ICP-AES	61.3 (0.5)	4.5 (0.1)	17.8 (0.1)	58.92 (0.7)	3.7 (0.1)	19.7 (0.2)	–	–	–
This work $n = 5$	60.2 (0.9)	4.7 (0.04)	17.7 (0.3)	59.9 (0.9)	4.0 (0.04)	20.4 (0.04)	54.9 (0.9)	3.8 (0.04)	14.7 (0.3)

#### Analytical procedure

Volumes of 100  $\mu\text{l}$  of sample solution were injected into the chromatographic system, operated in the isocratic mode at  $30^\circ\text{C}$ . The eluent was 2 mM EDTA (pH 5.65) at a flow-rate of 1.8  $\text{ml min}^{-1}$ . Data evaluation was based on integration of the response signals, by comparison with calibration graphs in the appropriate concentration range for each metal ion.

## RESULTS AND DISCUSSION

#### Selection of operating conditions

The experimental parameters were optimized to achieve suitable separation, the highest sensitivity and the shortest time of analysis. Hydrochloric acid was selected to dissolve the sample because chloride has a lower retention time than any other anion of the metal chelates under study, hence it is eluted first.

Different concentrations of eluent EDTA solutions, from 0.5 to 2.0 mM, were tested. Lower concentrations caused long retention times, resulting in peak broadening. Concentrations higher than 2.0 mM were not tested to avoid the risk of damage to the stainless-steel components of the chromatographic system (when the eluent is used for long periods of time).

At the selected optimum concentration of the eluent (2.0 mM EDTA), the flow-rate of the mobile phase was varied from 0.5 to 2.0  $\text{ml min}^{-1}$ . A flow-rate of 2  $\text{ml min}^{-1}$  gave the shortest analysis time. However, lanthanum peak-area evaluation is difficult owing to the proximity of the negative chloride peak. The best flow-rate

was found to be  $1.8 \text{ ml min}^{-1}$ . Lower flow-rate result in long analysis times and broader peaks.

Good resolution between metals chelate anions was observed at several different flow-rates.

The effect of pH variation in the range 4.50–5.65 was tested. The results were in agreement with reported values [4–6]. The influence of pH has two main pathways: first, the strength of the eluent changes owing to variation in the concentration of eluting species, affecting the retention time of each anion retained in the column. Second, the apparent stability constant of metal complexes diminishes when the pH decreases. This effect is greater for complexes with a low stability constant. Evidence of considerable dissociation of the  $\text{SrEDTA}^{2-}$  complex was detected at  $\text{pH} < 5$ . Results for the complexes  $\text{LaEDTA}^-$ ,  $\text{SrEDTA}^{2-}$  and  $\text{CuEDTA}^{2-}$  with stability constants of 15.50, 8.63 and 18.80, respectively [7], are shown in Fig. 1. Mathematical considerations regarding the effect of pH variation were presented by Matsushita [3].

The effect of the presence of EDTA in the injected volume was also considered. EDTA concentrations from 0.5 to 20 mM were tested; 2 mM EDTA at pH 5.65 was used as the eluent. Negligible effects were found up to 5 mM. Above this concentration, distortion of the  $\text{CuEDTA}^{2-}$  peak shape was observed. In addition, the signal decreased for all the metal complexes. As a consequence, the results indicate that adding EDTA to the original sample dilution does not contribute to a better performance for the selected operating conditions.

Detection wavelengths were tested in the range 195–250 nm. The results are shown in Fig. 2. For Cu(II), the best sensitivities were achieved at 240 and 195 nm. For Sr(II) and La(III), 195 nm gave the best response, but the higher noise level made the analysis of low-concentration samples difficult. A compromise wavelength of 200 nm was selected for the three determined elements.

#### Calibration

Plots of peak area vs. concentration gave linear calibration graphs (Table 1) for lanthanum, strontium and copper complexes from 0.4, 0.1 and  $0.05 \mu\text{g ml}^{-1}$ , respectively, up to  $100 \mu\text{g}$

$\text{ml}^{-1}$  (maximum tested concentration). The slightly lower quality of the regression data for the  $\text{LaEDTA}^-$  anion could result from the proximity of the  $\text{Cl}^-$  ion negative peak.

The sensitivity decreases in the order  $\text{CuEDTA}^{2-} > \text{SrEDTA}^{2-} > \text{LaEDTA}^-$  complexes. Practical determination limits for copper, strontium and lanthanum were 0.025, 0.04 and  $0.1 \mu\text{g ml}^{-1}$ , respectively.

Quantification was based on multi-component calibration runs. At least three standards were employed to fit a calibration graph using the least-squares procedure.

#### Analytical application

The method was applied to the characterization of superconductor samples of nominal stoichiometry  $\text{La}_{1.8}\text{Sr}_{0.2}\text{CuO}_4$ . Results are given in Table 2. Samples 1 and 2 were prepared as indicated in [8]. Reference sample 3 was prepared by directly mixing the appropriate amount of dried oxides of La and Cu with dried  $\text{SrCO}_3$ . The chromatographic results were compared with those obtained by Barnes [9] with a sequential multi-element inductively coupled plasma atomic emission spectrometric (ICP-AES) procedure and by atomic absorption spectrometry (AAS) [8].

The authors are deeply grateful to Daniel A. Batistoni for stimulating discussions. They also acknowledge Pablo F. Garat for technical collaboration.

#### REFERENCES

- 1 C.E. Hamrin, Jr., W.D. Arnett, R.J. De Angelis, X.X. Ding and W.D. Ehmann, *Solid State Commun.*, 69 (1989) 1063.
- 2 A.L. Robinson, *Science*, 236 (1987) 1063.
- 3 K. Schwarz, *Mikrochim. Acta*, II (1990) 149.
- 4 S. Matsushita, *J. Chromatogr.*, 312 (1984) 327.
- 5 G. Schwedt and B. Kondratjonok, *Fresenius' J. Anal. Chem.* 332 (1989) 861.
- 6 W.-F. Lien, B.K. Boerner and J.G. Tarter, *J. Liq. Chromatogr.*, 10 (1987) 3213.
- 7 F.J. Welcher, *The Analytical Uses of Ethylenediaminetetraacetic Acid*, Van Nostrand, Princeton, NJ, 1961, p. 3.
- 8 R.O. Crubellati, P.N. Smichowski, D.A. Batistoni, G. Polla and E. Manghi, *Solid State Commun.*, 75 (1990) 101.
- 9 R.M. Barnes, personal communication, 1990.

# Measurement of the speciation of iron in the nanogram range: investigation of chromatographic peaks induced by iron blanks

G. Weber

*Institut für Spektrochemie und Angewandte Spektroskopie, Bunsen-Kirchhoff-Strasse 11, Postfach 10 13 52, W-4600 Dortmund 1 (Germany)*

(Received 2nd November 1992; revised manuscript received 14th December 1992)

## Abstract

The sources of iron blanks in liquid chromatography and interactions of these blanks with injected samples were investigated. The main sources of the blanks are the chemicals used and the chromatographic equipment. Even so-called "metal-free" systems contain iron blanks in the low-ng range, which can be a source of error in speciation analysis of iron. The effects induced by iron blanks include the formation of additional peaks (positive and negative) and changes in the recovery of injected species. Especially free ligands, which are present in the sample, interact strongly with blanks. The mechanism of interaction of blanks with injected species was investigated in some detail using organic acids as complexing agents for Fe(II), Fe(III) or both. The experimental results were compared with computer-simulated chromatograms. It is shown that the observed effects can be explained by using a model based on chemical equilibria in the stationary and mobile phases.

**Keywords:** Liquid chromatography; Blank values; Iron; Speciation

Speciation analysis of iron in environmental or biotic matrices is important for the assessment of its bioavailability and biological activity, which are strongly dependent on the species (such as oxidation states and complexation of iron). One of the most promising concepts for the analysis of such species is the combination of liquid chromatography (LC) with either element-specific detectors (atomic spectrometry) or species-specific detectors e.g., an electrochemical detector as a specific detector for iron (II) species [1].

One problem in using LC for determination of the speciation of metals in the low-ng range is the metal blank of the chromatographic system. Especially for ubiquitous metals such as iron the

blank may be close to the injected concentration of iron species. Even if so-called "metal-free" or "biocompatible" systems are used (made of titanium or polymer), considerable iron blanks may be present, which not only limit the detection power of the system but can also seriously affect the accuracy of the method by interacting with metal species or free ligands.

An example of the interaction of metals with free ligands is the variation in metal species as a result of spiking of the sample [2,3]. This implies that the commonly used standard addition technique for quantification may be problematic in speciation analysis.

The influence of metals (present in the eluent) on chromatographic retention processes has been investigated in some detail [4–7], especially for organic compounds capable of complexing metals. Additionally, some work has been published

*Correspondence to:* G. Weber, Institut für Spektrochemie und Angewandte Spektroskopie, Bunsen-Kirchhoff-Strasse 11, Postfach 10 13 52, W-4600 Dortmund 1 (Germany).

on the stability of metal chelates in LC [8,9] and on the influence of temperature on stability [10,11].

Although most workers in the field of speciation analysis are well aware of the problems related to stability of the species (e.g., risk of dissociation or redistribution of species [12]), the problems related to interactions of metal blanks with the sample are often ignored, probably because the blanks are thought to be negligible. This may be correct (e.g., with some organometallic species, which are not likely to be present in chromatographic systems), but it is definitely wrong in the case of metal chelates and/or oxidation states if the concentration of the species lies in the ng-range.

In this paper, phenomena are presented and discussed that were observed during the determination of iron species in the low-ng range, especially low-molecular-weight complexes of iron(II/III) with organic acids [1]. The aim of this work is to call attention to the problem of blanks in speciation analysis as part of the general problem of accuracy in speciation analysis.

## EXPERIMENTAL

### *LC equipment*

Two different systems were used, as follows.

The “stainless-steel system” consisted of a Milton Roy Constametric III pump, a Rheodyne Model 7125 injection valve (50- $\mu$ l sample loop) and a 250  $\times$  4 mm i.d. column packed with Spherisorb S5 ODS 2. The column, filters and capillaries were made of stainless steel.

The “polymer–titanium system” consisted of a Spectra-Physics SP 8810 pump (titanium), a Knauer injection valve (made of PEEK, 50- $\mu$ l sample loop) and a PEEK column packed with Spherisorb S5 ODS 2. All capillaries and filters were made of PEEK, titanium or ceramic material.

### *Chromatographic solvents*

Two different eluents were used that differ in pH, buffering and complexing properties: acetate eluent, 0.05 M ammonium acetate (pH 4.0)–

methanol (70 + 30); and sulphate eluent, ammonium sulphate–sulphuric acid (pH 2.5) (ionic strength 0.1 M)

All chemicals used were of at least analytical-reagent grade and doubly distilled water was used throughout.

### *Detection of iron species*

On-line detection by atomic absorption spectrometry (AAS) was done using a Knauer HHPN system as interface to a Varian 1000 flame atomic absorption spectrometer [13]. The detection limit of this system is about 5 ng of iron, corresponding to an injected concentration of 100 ng ml<sup>-1</sup>.

Electrochemical detection of iron(II) species was done using a Metrohm 656 electrochemical detector (glassy carbon working electrode) operated at a potential of +0.5 V versus Ag/AgCl/KCl (3 M). This detector enables sub-ng amounts of iron(II) species to be detected.

## RESULTS AND DISCUSSION

### *Sources of iron blanks*

There are two main sources of iron blanks; the chemicals used to prepare the eluent and the LC system itself. The contribution of each eluent component to the blank depends on its purity (with respect to iron) and on its relative amount. Therefore, blanks of the main solvents (water, methanol), although usually much lower than those of other chemicals, can add up to the most significant contribution to the blank. For example, the iron blank for methanol was determined to be 0.63 ng ml<sup>-1</sup>, corresponding to 189 ng of iron per litre of the acetate eluent, whereas the contribution of ammonium acetate (iron blank 34.6 ng g<sup>-1</sup>) was 133 ng l<sup>-1</sup>. Theoretically the overall blank of the eluent can be calculated in this way from the individual blanks of its components (acetate eluent, 450 ng l<sup>-1</sup>; sulphate eluent, 320 ng l<sup>-1</sup>). In reality, however, the blank (as determined after preparation of the eluent) was at least 1–2  $\mu$ g l<sup>-1</sup> because of contamination from glassware, the laboratory atmosphere, etc., which is inevitable in a “normal” analytical laboratory (for clean rooms this would be different).

The blank contribution of the LC equipment (pump, filters, column, capillaries, etc.) depends on the material used (stainless steel, titanium, PEEK), on the active surface, which is in contact with the eluent, and also on the composition of the eluent (pH, salt content, complexing properties).

If the stainless-steel system is used, more than 90% of the total blank originates from the LC equipment. The total blank is about 40–60 ng Fe ml<sup>-1</sup> for both eluents. By replacing all the system components successively with “inert” components, it was found that especially solvent filters (highly active surface), capillaries and pump (in this order) are responsible for high blanks, whereas the contribution of the column and detector is relatively low. Surprisingly, the iron blank of the “metal-free” PEEK column was not lower than that of the similar stainless-steel column. Obviously it is not primarily the column wall that contributes to the blank, but mainly iron traces adsorbed on the column inlet and outlet filters or on the packing material. The contribution of a detector flow cell to the blank is normally negligible (if no stainless-steel capillaries are included in the detector). This also holds for the HHPN system (all parts including the AAS spray chamber are made of titanium or polymer), but may be different for complicated interfaces or for autosampler systems. The overall blank of the carefully cleaned titanium–PEEK system was 2–5 ng Fe ml<sup>-1</sup>.

#### *Effects of iron blanks*

After equilibration of the LC system with the eluent, a steady-state concentration of iron is reached, which depends on the above-discussed factors. As long as this steady-state equilibrium is maintained, the only effect of the iron blank is to limit the detection power of the system. For electrochemical detection in the oxidative mode the equilibrium concentration of iron(II) is the limiting factor [14]. If a sample is injected into the system, the steady-state equilibrium of iron can be disturbed in different ways, as follows.

*Decreasing/increasing the iron concentration.* The simplest form of disturbance is the injection of a sample with an iron concentration higher or

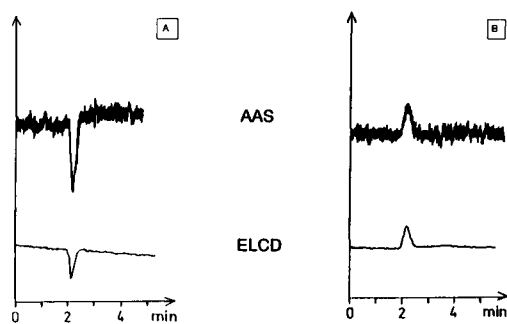


Fig. 1. Liquid chromatogram of a sample with a different iron concentration to the mobile phase. (A) Injection of pure solvent (lower iron concentration); (B) injection of eluent enriched in iron (1 µg ml<sup>-1</sup>). AAS = atomic absorption spectrometric detection; ELCD = electrochemical detection. The stainless-steel system and acetate eluent was used.

lower than that of the eluent. This results in a positive or negative peak at the retention time of free iron, as shown in Fig. 1 for a stainless-steel system. It should be noted that a negative peak is obtained even by injecting pure eluent into this system. This is because the eluent (after passing the filters, pump and capillaries) is enriched in iron by at least a factor of 10 compared with the same eluent which is injected as a sample (without passing the filters, pump, etc.).

Injection of samples containing more iron than the mobile phase is the normal situation for real samples (free iron is present to a greater or lesser extent). The problem in this instance is not the iron peak itself, but the fact that free iron is often not eluted quantitatively. Considerable amounts can be adsorbed on the column or filters and may be remobilized later (memory effects). For example, the recovery of inorganic iron injected into the sulphate eluent is much lower than 100% and the reproducibility is not good. In contrast, inorganic iron is completely recovered using the acetate eluent, because it is complexed by acetate and this organic complex is eluted quantitatively.

*Dissociation of iron species.* A problem that is often addressed in papers on speciation is the risk of dissociation of injected iron species. An example is shown in Fig. 2 using both eluents. If a pure iron complex is injected (without excess of ligand), this dissociation results in a small peak at

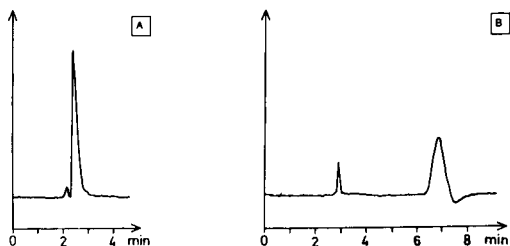


Fig. 2. Liquid chromatogram of an iron complex with electrochemical detection. Fe(II)-citrate (Fe: citrate = 1:1;  $1 \mu\text{g Fe ml}^{-1}$ ) was injected into the titanium-PEEK system. (A) Acetate eluent; (B) sulphate eluent.

the retention time of free iron and a complex peak. Whereas a considerable degree of dissociation to free iron plus free ligand is only a problem for very labile complexes, a change in the stoichiometry of a complex (from a metal to ligand ratio of 1:2 to 1:1) is much more probable. This liberates free ligand, which then can interact with iron blanks, according to the overall reaction  $\text{FeL}_2 + \text{Fe}_{\text{blank}} \rightarrow 2\text{FeL}$ . As a consequence, not only the chemical form of the species is changed, but also the total recovery of complexed iron.

*Interaction of free ligands with iron blank.* The interaction of an excess of ligand with iron blanks is one of the most serious effects, because the recovery of injected species is changed and new species are formed that were not present in the sample. Figure 3 demonstrates this effect by injection of pure citric acid into the LC system. This ligand instantly complexes free iron (blank), leaving a negative peak at the retention time of

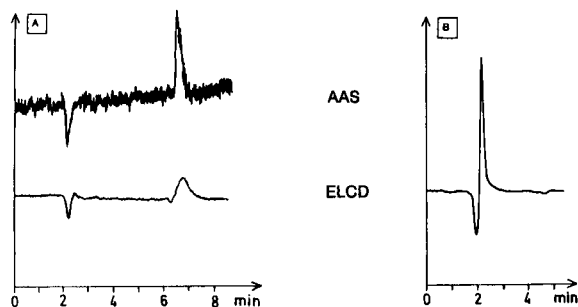


Fig. 3. Liquid chromatogram of pure ligand (citric acid). A  $10\text{-}\mu\text{g}$  amount of citric acid was injected into the titanium-PEEK system. (A) Sulphate eluent; (B) acetate eluent. AAS = atomic absorption spectrometric detection; ELCD = electrochemical detection.

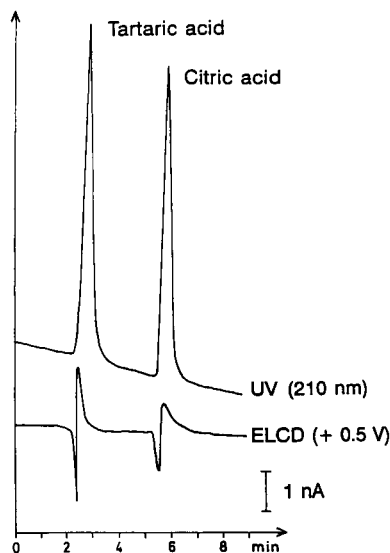


Fig. 4. Liquid chromatogram of tartaric and citric acid with UV and electrochemical detection. A  $20\text{-}\mu\text{g}$  amount of each acid was injected into the titanium-PEEK system; sulphate eluent.

free iron and a positive peak at the retention time of the complex formed (iron-citrate). In Fig. 3A these two peaks are well separated (sulphate eluent), whereas in Fig. 3B (acetate eluent) the two peaks overlap. The uptake of iron from the system by a ligand is a source of error especially for environmental or biotic samples, because usually ligands are present in excess and the species (e.g., iron-citrate) formed during chromatography cannot be distinguished from the respective species originally present in the sample.

Figure 4 demonstrates, that such effects are observed even for the titanium-polymer LC system (blank only  $2\text{-}5 \text{ ng ml}^{-1}$ ). However, the on-line determination of iron by AAS is impossible in this instance owing to the low concentration changes, whereas electrochemical detection of iron(II) is possible at this low concentration. The electrochemical peaks are a result of the interaction of the two ligands (citric and tartaric acid) with the (low) iron blank of the system. Because of the "S-shaped" peaks (combination of negative and positive peaks) the determination of the iron species is difficult, but the concentration lies in the low-ng or even sub-ng range.

### Computer-simulated chromatograms

In order to check the experimental results and to verify the explanations given above (shifting of metal–ligand equilibria), computer simulations were done. The computer simulation model was similar to that used by Deming and co-workers [15,16] for the explanation of induced peaks and component interactions in LC. It is based on a Craig-type repetitive distribution and does not depend on a special retention mechanism.

The simulation process is explained by the following steps: (1) the chromatographic system is initialized with a “blank” of iron; (2) a “sample” is injected consisting of variable amounts of iron and/or ligand; (3) the sample plug is moved step by step across the stationary phase (transport); (4) complex formation equilibria in the mobile phase and distribution equilibria between the two phases are calculated simultaneously by using estimated complex formation and distribution constants; (5) steps (3) and (4) are repeated until the separation is complete; (6) the concentration of iron species is plotted against the mobile phase compartments, which have eluted step by step from the column.

For the estimation of complex formation constants literature data are used, if available. For the estimation of distribution constants [of the general form  $K = c(s)/c(m)$ , where  $c(s)$  is the concentration in the stationary phase and  $c(m)$  that in the mobile phase] assumptions are made, which are in agreement with experimental data (the elution order of species is given by the respective  $K$  values).

If the experimental data suggests strong interactions between components in the stationary phase (e.g., the distribution of iron between the stationary and mobile phases is affected by the presence of excess of ligand in the stationary phase), this is simulated by a first-order dependence of the distribution of one component on the stationary phase concentration of the other component [16].

Some typical results of the simulations are shown in Figs. 5 and 6. The plot in Fig. 5A demonstrates the effect of injecting an iron-free sample into a mobile phase containing a certain blank concentration (normalized to 1). A negative

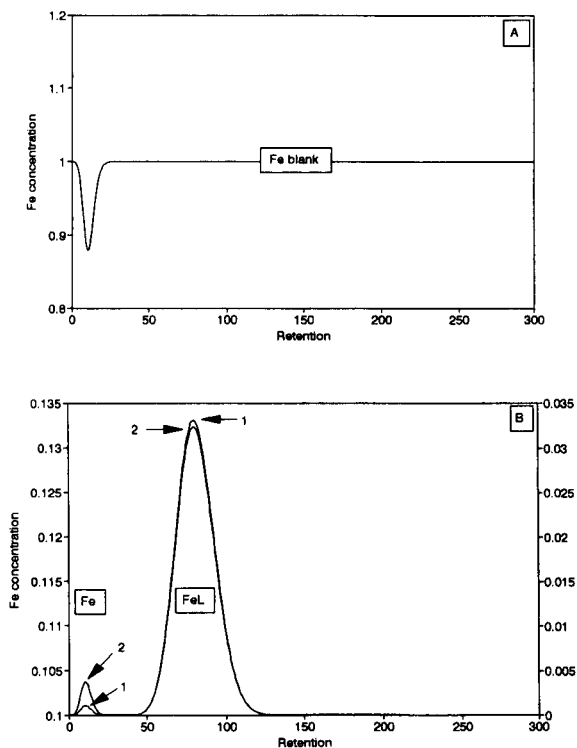


Fig. 5. Computer-simulated chromatograms. (A) Injection of pure eluent (iron-free); (B) injection of an iron complex (1:1, stability constant = 1000) into the LC system, (1) with and (2) without iron blank. Fe = free iron; FeL = iron complex.

peak is produced of about 12% of the blank level. This is in good agreement with the experimental results (see Fig. 1).

The dissociation of an injected iron complex (Fe:ligand = 1:1) is shown in Fig. 5B for two cases: (1) is the chromatogram for a system with a blank close to the injected iron concentration (blank = 10% of injected iron) and (2) is the respective chromatogram for a blank-free system. In both instances the degree of dissociation is below 5% of the injected complex. However, the free iron concentration is lower for the blank system (only 1% dissociation instead of 3%), because the presence of the blank shifts the dissociation equilibrium towards the side of the undissociated complex. In reality, dissociation of complexes can be more pronounced if other factors (kinetic, etc.) play a role.

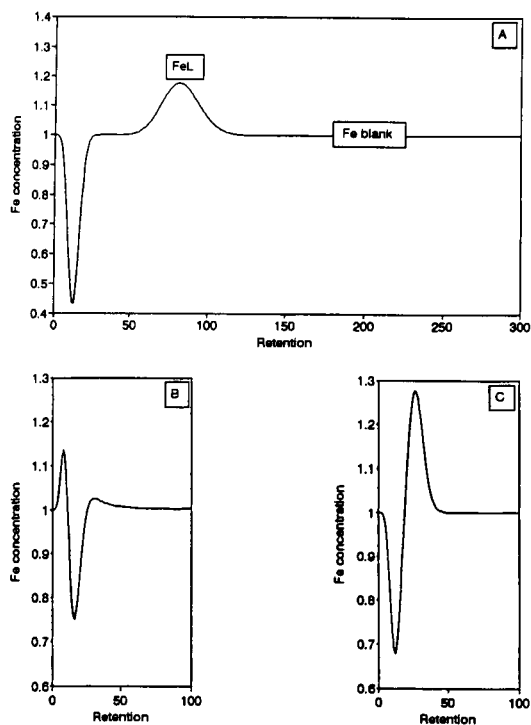


Fig. 6. Computer simulation of ligand-blank interactions. (A) Injection of ligand (concentration ten times higher than blank); (B, C) peak shapes in the case of strong interaction of iron and ligand (for details, see text).

In Fig. 6A the interaction of injected free ligand with the iron blank is simulated. As expected, a negative peak and a corresponding complex peak are formed. Fig. 6B and C illustrate two different peak forms for the case of strong interaction of iron and ligand not only in the mobile phase (complex formation), but also in the stationary phase. The peak in Fig. 6C is similar to the experimental peaks in Fig. 4. It was obtained under the assumption of a strong effect of adsorbed ligand on the chromatographic behaviour of iron (this is equivalent to the model of a column locally “modified” with the ligand). This assumption seems reasonable in the case of a large excess of free ligand and a high complexing power of that ligand. The retention of the resulting peak is close to that of the respective ligand, whereas the peak shape in Fig. 6B was obtained for a peak at the retention time of free

iron under the assumption of strong interaction with the ligand.

### Conclusions

Iron blanks are present not only in stainless-steel systems, but also in so-called “metal-free” or “biocompatible” systems. The blank concentration depends on the purity of the chemicals and on the LC equipment. It generally lies in the range 50–100 ng ml<sup>-1</sup> for stainless-steel systems and 1–10 ng ml<sup>-1</sup> for polymer or titanium systems. Effects of iron blanks (induced peaks) are observed if speciation analysis is done in the ng range and a sensitive detector is used. The most serious effects are observed, if free ligands are present in the sample.

These effects are not restricted to iron, but (in principle) can be observed for every trace metal, provided that speciation analysis is done in a concentration range close to the blank present in the system (“close to” in this sense means about 1–2 orders of magnitude higher than the blank, because LC involves dilution of the sample).

This work was supported by the Bundesministerium für Forschung und Technologie der Bundesrepublik Deutschland and by the Ministerium für Wissenschaft und Forschung des Landes Nordrhein-Westfalen.

### REFERENCES

- 1 G. Weber, *Fresenius' J. Anal. Chem.*, 340 (1991) 161.
- 2 L. Dunemann and H. Reinecke, *Fresenius' J. Anal. Chem.*, 333 (1989) 737.
- 3 H. Reinecke and L. Dunemann, *Fresenius' J. Anal. Chem.*, 338 (1990) 630.
- 4 P.C. Sadek, C.J. Koester and L.D. Bowers, *J. Chromatogr. Sci.*, 25 (1985) 489.
- 5 S.J. Bale, R.M. Smith, S.G. Westcott and M. Martin-Smith, *Anal. Proc.*, 25 (1988) 62.
- 6 R.M. Smith, S.J. Bale, S.G. Westcott and M. Martin-Smith, *Analyst*, 114 (1989) 771.
- 7 R.M. Smith, S.J. Bale, S.G. Westcott and M. Martin-Smith, *Analyst*, 115 (1990) 1517.
- 8 A.R. Timerbaev and O.M. Petrukhin, *Zh. Anal. Khim.*, 44 (1989) 1424.
- 9 Y. Liu and J.D. Ingle, Jr., *Anal. Chim. Acta*, 222 (1989) 279.



- 10 D.E. Henderson, B.J. O'Connor, J.F. Kirby and C.P. Sears, III, *J. Chromatogr. Sci.*, 23 (1985) 477.
- 11 S. Liodakis, A. Pappa and G. Parissakis, *J. Chromatogr. Sci.*, 27 (1989) 149.
- 12 P.M. Bertsch and M.A. Anderson, *Anal. Chem.*, 61 (1989) 535.
- 13 G. Weber and H. Berndt, *Chromatographia*, 29 (1990) 65.
- 14 R. Shoup and M. Bogdan, *LC·GC Int.*, 3 (1990) 16.
- 15 J.J. Stranahan and S.N. Deming, *Anal. Chem.*, 54 (1982) 1540.
- 16 S. Seshadri and S.N. Deming, *Anal. Chem.*, 56 (1984) 1567.

# Rapid separation of fluorescein derivatives using a micromachined capillary electrophoresis system

D. Jed Harrison, Zhonghui Fan and Kurt Seiler

*Department of Chemistry, University of Alberta, Edmonton, Alberta T6G 2G2 (Canada)*

Andreas Manz and H. Michael Widmer

*Forschung Analytik, Ciba-Geigy, CH-4002 Basel (Switzerland)*

(Received 8th September 1992; revised manuscript received 19th January 1993)

## Abstract

Using micromachining techniques electrophoresis systems consisting of sample injectors and separation capillaries have been fabricated in planar glass structures. A device with a total capillary channel length of 13.9 cm was used to inject and separate fluorescein and fluorescein sulfonate dyes within 3 min, with an injector to detector distance of 6.0 cm, and an applied field of 520 V/cm. A similar device with a capillary length of 1.6 cm effected injection and separation within 4 s for an injector to detector length of 0.75 cm at an applied field of 1875 V/cm. Injected sample volumes of 60 pl or less were readily injected and analyte detected at 10  $\mu$ M concentrations.

*Keywords:* Electrophoresis; Sensors; Fluorescein; Capillary electrophoresis; Micromachining

The automation of chemical analysis has been achieved using a systems approach [1–5], through the coupling of sample handling with separation and detection to give an analytical instrumentation package. While robotics provides one route for this, the use of flow systems as in flow injection analysis (FIA) [6], coupled with separation and detection methods [5] to facilitate sample handling, pretreatment and analysis is another promising method. Systems prepared using this strategy have been designated total chemical analysis systems (TAS) [4]. Examples include gas chromatograph-based monitors for trace analysis in air [7], on-line glucose analyzers [3] and a supercritical fluid chromatograph coupled with a sampling system for process control [8].

Miniaturization of the TAS concept ( $\mu$ -TAS)

to incorporate all sample handling operations on a monolithic structure about the size of a silicon chip is an attractive concept [4,5]. Such a device could conceivably function as a dip-type probe, useful for analysis of samples in a complex matrix in a manner comparable to that of a highly selective chemical sensor [5,9]. Miniaturization also offers advantages for many separation methods, as has been well established, and integration of capillaries, detectors and injectors could increase separation efficiency by reduction of dead volumes. Practical benefits of  $\mu$ -TAS devices include considerable reductions in solvent and reagent use, smaller sample volumes, and increased speed of analysis [5,9,10].

We have designed a  $\mu$ -TAS system based on capillary electrophoresis (CE). It consists of an injector and a capillary column integrated together on a glass chip. It utilizes electroosmotic pumping to drive solution flow in the injector

*Correspondence to:* D.J. Harrison, Department of Chemistry, University of Alberta, Edmonton, Alberta T6G 2G2 (Canada).

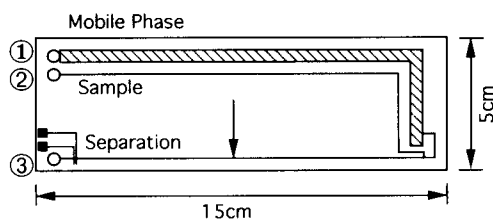
manifold and electrophoresis for separation of sample components [9–12]. The structure is fabricated in glass using integrated circuit technology for micromachining of the capillary channels. We have recently shown that separations can be effected in such a planar structure [9,10], and that the efficiencies obtained are similar to those for electrophoresis in fused silica capillaries [9]. In this report we examine the efficiency of separation using a more sophisticated detector design, and establish that sample injection and separation can be achieved within only a few seconds using these devices. Quantification of the picolitre scale volumes injected has also been demonstrated.

## EXPERIMENTAL

A pH 8.0 buffer was prepared from 0.050 M boric acid (reagent grade) and 0.050 M tris(hydroxymethyl)amino methane (Tris, reagent grade). Stock solutions of 100  $\mu\text{M}$  fluorescein ( $\text{Na}^+$  salt, Aldrich) and fluorescein-5 (and -6) sulfonate ( $\text{Na}^+$  salt, Molecular Probes, Eugene, OR) were used to prepare 10 and 50  $\mu\text{M}$  dye solutions. Elemental analysis of the sulfonated dye was inconclusive as to purity, because of the presence of  $\text{Na}^+$  and the dye's hygroscopic character. Solutions were filtered with 0.2  $\mu\text{m}$  membranes and sparged with He.

The capillary electrophoresis TAS (CETAS) device, Fig. 1, was fabricated by Mettler AG (Switzerland) under contract using a proprietary lithographic process [9]. The sample channel length between reservoir 2 and the intersection was 16.7 cm, while the separation channel from reservoir 3 to the intersection was 13.9 cm. About 91% of a voltage applied between reservoirs 1 and 3 was dropped between the intersection and reservoir 3. The distance from injection point (i.e., intersection) to detection point was 6.0 cm for CETAS in these experiments. Device JH-1 was fabricated at the Alberta Microelectronic Centre in fine-annealed Pyrex glass, using a photolithographic process to be described elsewhere [11]. The bottom glass plates were etched to form channels. Top plates with holes located appropri-

### (a) CETAS



### (b) JH-1

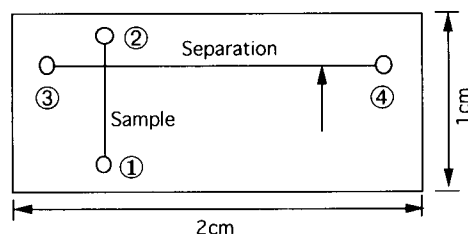


Fig. 1. Layout of two devices fabricated in glass. (a) CETAS device, showing channels and overall dimensions, (b) device JH-1. The contact reservoirs are numbered for reference in the text, and the approximate location of the detector is shown with an error.

ately were then bonded to these to form capillaries, using a high temperature process (620 to 650°C) described previously [9,11]. The channel length from reservoir 1 to 2 was 0.80 cm, and from reservoir 3 to 4 was 1.6 cm. The distance from injection point (i.e. intersection) to detection point was 0.75 cm for JH-1.

The high voltage power supplies and computer control system used has been described elsewhere [9,12]. A 488 nm air-cooled, Ar ion laser (Uniphase/Cyomics) operated at about 4 mW served as a fluorescence excitation source. A 30 cm focal length lens focused the beam into the capillary channel, and a 10:1 microscope objective mounted at 45° to the excitation beam was used to collect emitted light and direct it onto a Hamamatsu R1477 photomultiplier tube (PMT). A 100  $\mu\text{m}$  slit was positioned at the image focal plane of the objective, along with an Omega 505 to 538 nm bandpass filter. The PMT signal was electronically filtered with a 6-pole Butterworth, active filter with a 40 ms (with CETAS) or 5 ms (with

JH-1) time constant and then digitally acquired with a National Instruments NB-MIO-16 board mounted in a Mac II, as described elsewhere [12].

## RESULTS AND DISCUSSION

The size and geometric layout of two devices made in glass are shown in Fig. 1, and the channel contact points (reservoirs) referred to in the text by number are indicated. The channels of the CETAS device were etched to a depth of  $10\ \mu\text{m}$  and the small channels were  $30\ \mu\text{m}$  wide, while the larger channel was  $1\ \text{mm}$  wide [9]. In the other device, JH-1, all the channels were  $10\ \mu\text{m}$  deep and  $30\ \mu\text{m}$  wide. CETAS was used to test sample injection and separation efficiencies, while JH-1 was used for rapid separations.

Current–voltage curves in CETAS, with pH 8, 50 mM Tris, 50 mM boric acid buffer, were linear up to at least 10 kV with a voltage applied between reservoirs 1 and 3, indicating no joule-heating effects were observed. This corresponds to  $650\ \text{V/cm}$  within the separation capillary, two- to three-fold higher than is typically used in CE. For the 6.0 cm separation distance used in these studies this means the maximum potential between the point of injection and detection in CETAS was 3900 V. In device JH-1 linear current voltage curves were obtained for up to 4 kV across the separation channel (potential applied between reservoirs 3 and 4) and 2 kV in the sample channel (reservoirs 1 and 2). This corresponds to up to  $2500\ \text{V/cm}$  across either channel before Joule heating effects cause non-linearity in the current response due to a temperature rise. For the separation channel in JH-1 a maximum of about 1900 V was dropped across the 0.75 cm between the injection and detection points.

Figure 2 shows the separation of two dyes, fluorescein and (5- or 6-)fluorescein sulfonate in the CETAS structure. By introducing sample into reservoir 2 and applying a voltage between reservoirs 2 and 3 it was possible to inject plugs of sample into channel 3. The length of the plug was readily controlled by the injection voltage and time of application [9]. Fluorescein is readily separated from the more negatively charged sul-

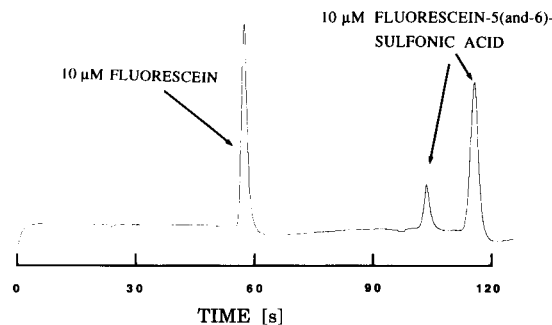


Fig. 2. Electropherogram of fluorescein and isomers of fluorescein sulfonate in pH 8.0 buffer separated in the CETAS device. Sample was injected with 110 V applied for 60 s between reservoirs 2 and 3, followed by a 10 s delay. An 8 kV separation voltage was then applied between reservoirs 1 and 3.

fonate derivative as shown in the figure, with a combined injection and separation time of 180 s. The fluorescein sulfonate was separated into two components. These may be the two different isomers, or one peak may represent an impurity in the material. Despite this uncertainty, the separation of the two dyes is clearly effected in the planar glass device.

Quantitative sample injection was achieved over a large range of sample volumes in the CETAS device, as shown in Fig. 3. The length of the zone was calculated from the measured electrophoretic mobility of each component, the ap-

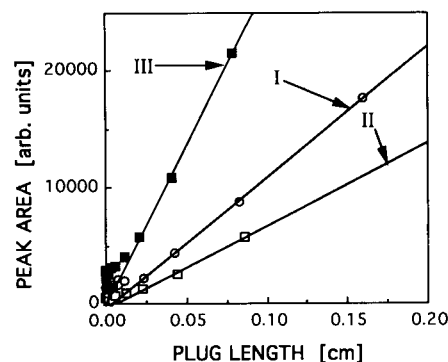


Fig. 3. Peak area (arbitrary units) as a function of plug length for fluorescein (I) and the first (II) and second (III) peaks arising from 5- (and 6-)fluorescein sulfonate in the CETAS device. Injection voltage and time were varied to change the plug length, but the total injection and delay time was 70 s. The separation voltage was constant at 4 kV.

plied voltage and the period of injection. The figure shows there is a linear relationship for sample zone lengths longer than about 200  $\mu\text{m}$  (ca. 60 pl or greater injection volume). Below this value the amount injected decreases in an approximately linear fashion, but with a much lower slope. This effect has not been examined in detail yet, but it must arise at least in part from sample diffusion effects during the period of injection and any delay period between separations. It should be noted that the quantitative relationship *between* the three components is skewed by the fact they move at different velocities, so that the integration times for peaks are different at different migration times. This effect has been discussed [13] and is well understood.

The efficiency of separation in CETAS was evaluated for all three peaks. The height equivalent to a theoretical plate,  $H$ , is given by [9]

$$H = \frac{2Dt_m}{d} + \frac{W_{inj}^2}{12d} + \frac{W_{det}^2}{12d} + \frac{2Dt_{inj}}{d} \quad (1)$$

where  $D$  is the analyte diffusion coefficient,  $t_m$  is the migration time of the peak,  $t_{inj}$  is the period of sample injection and an additional delay of 10 s before separation begins, and  $d$  is the distance from injection point to detection point.  $W_{det}$  and  $W_{inj}$  are the detector cell and injected plug lengths. The equation is derived assuming longitudinal diffusion is the only contribution to band broadening within the capillary, and the injector and detector volumes are rectangular [13,14]. Diffusion of the sample plug during injection or delay periods will also contribute to dispersion and so this is also considered.

A plot of observed  $H$  versus  $t_m$  is shown in Fig. 4 for the components separated in the CETAS device. The value of  $t_m$  is inversely dependent on the applied voltage, which covers a range of 3.5 to 10 kV for the data shown (230 to 650 V/cm). The two components of fluorescein sulfonate show a near linear dependence of  $H$  on  $t_m$ , with a common intercept within experimental error, except at the highest applied voltages (shortest  $t_m$ ). The intercept is not consistent with the indicated contributions to band broadening. For the estimated values of  $W_{det}$  (10  $\mu\text{m}$ ),  $W_{inj}$

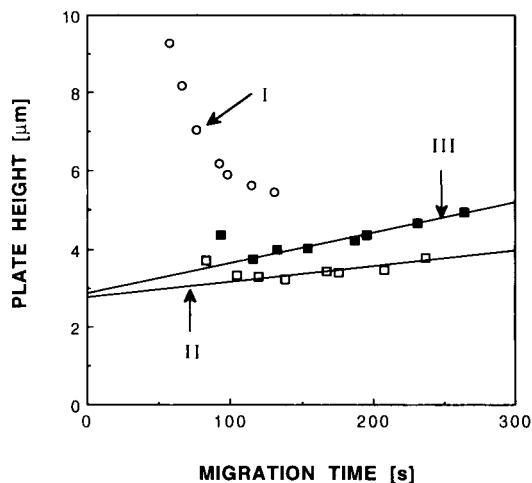


Fig. 4. Measured plate height plotted versus the peak migration time in the CETAS device for fluorescein (I) and the first (II) and second (III) peaks arising from 5- (and 6-) fluorescein sulfonate. The separation voltage varied from 3.5 to 10 kV, with constant injection conditions (110 V, 60 s) and a 10 s delay, in pH 8.0 buffer.

(ca. 200  $\mu\text{m}$ ),  $D$  of ca.  $2 \times 10^{-6}$   $\text{cm}^2/\text{s}$  (obtained from the slope of the plots in Fig. 4), and  $t_{inj}$  of 70 s the calculated intercept is 0.6  $\mu\text{m}$ . This compares poorly with the actual intercept of 2.8  $\mu\text{m}$  shown in Fig. 4. At the shortest times the bands became notably asymmetric and exhibited tailing, which accounted for the obvious increase in  $H$ . The peaks for fluorescein tailed even more at the higher voltages, resulting in very significant  $H$  values and the unexpected trend with migration time shown in Fig. 4. These deviations from theory may arise from adsorption of the components on the capillary walls [13], although further study is required to evaluate the effect.

In a previous study [9] of the separation of fluorescein and calcein in a CETAS device we reported nearly ideal separation efficiency, and a maximum number of plates of about 19000 for fluorescein and about 35000 for calcein. In that study the voltage range utilized was 1 to 5 kV, the pH was 8.5 (Tris, boric acid buffer) and the detector provided the most significant contribution to band broadening. In the present study the voltage range was higher, and the detector made no significant contribution. It is clear from this work that additional band broadening effects

would begin to show up only near the maximum potential range used in the previous study.

The data for fluorescein sulfonate shows that relatively high efficiencies can be obtained. For the latest eluting peak  $H$  was approximately 4  $\mu\text{m}$ , corresponding to about 15 000 theoretical plates across 6 cm. This efficiency was achieved for electric fields ranging from 220 to 400 V/cm. This indicates that a metre long column in a planar glass substrate could give about 250 000 plates with 22 kV or more applied. This is comparable to conventional CE in fused silica capillaries, although values close to  $10^6$  in an open fused silica capillary have been reported.

Figure 5 shows a very rapid separation of the same dye mixture in device JH-1. Sample was introduced into the device in reservoir 1 and driven along the channel to reservoir 2 with 500 V applied. The plug of sample at the intersection of the channels (a geometric volume of 9 pL) was then separated by application of a voltage between reservoirs 3 and 4. The migration time of the peaks decreased linearly with the inverse of the applied voltage, as expected [9,13,14]. Fig. 5 shows that the two dyes were separated within 3 s at an applied potential of 3000 V (1875 V/cm). The two components of the second peak were not resolved, accounting for the peak's broadness. The sample injection time was 1 s, leading to a total analysis cycle time of under 4 s. We found that the magnitude of the injection voltage be-

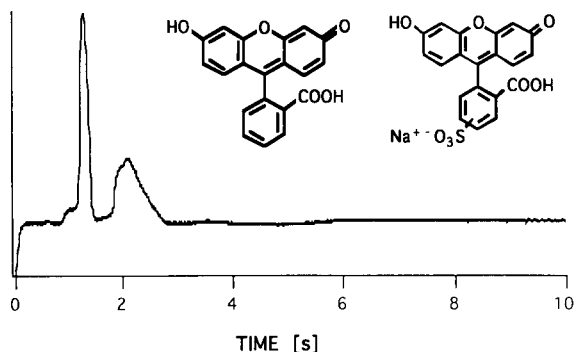


Fig. 5. Rapid separation of 50  $\mu\text{M}$  fluorescein from 50  $\mu\text{M}$  fluorescein sulfonate in device JH-1. Injection was accomplished by applying 500 V for 1 s between reservoirs 1 and 2, and then switching to apply 3000 V between reservoirs 3 and 4 in the pH 8.0 buffer.

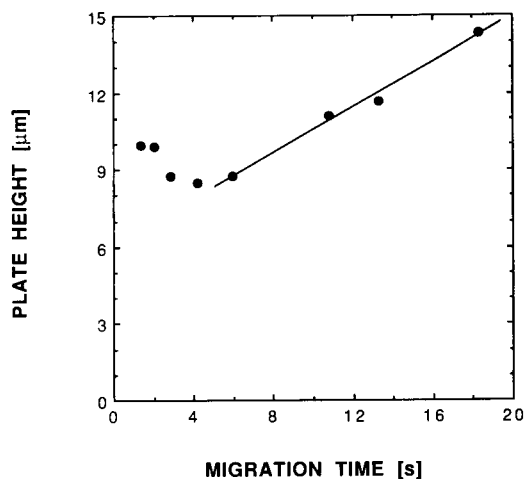


Fig. 6. Measured plate height plotted versus migration time in device JH-1. The separation voltage varied from 200 to 3000 V, with constant injection conditions of 500 V for 1 s between reservoirs 1 and 2.

tween reservoirs 1 and 2 affected the peak area upon separation, as did the period of time the potential was applied. Additional study of this is underway, but the data clearly indicate the injected plug is much larger than the geometric volume. Furthermore, if the geometric size of the intersection is assumed to define  $W_{\text{inj}}$  as 30  $\mu\text{m}$ , while the terms in Eqn. 1 are used to calculate the intercept of  $H$  versus  $t_m$ , the result is substantially smaller than the 7  $\mu\text{m}$  intercept evident in Fig. 6. Using  $D$  for fluorescein of  $3.3 \times 10^{-6}$   $\text{cm}^2/\text{s}$  [9],  $t_{\text{inj}} = 1$  s,  $W_{\text{det}} = 14$   $\mu\text{m}$  and  $d = 0.75$  cm gives a calculated intercept of only 0.1  $\mu\text{m}$ . This is a much greater discrepancy than observed with CETAS. The most probable reason is that diffusion and mixing effects at the intersection mean that the geometric volume is a significant underestimate of the actual volume.

The number of plates obtained for fluorescein in device JH-1 ranged from 520 at 200 V (125 V/cm) across the separation channel, to 900 plates at 1000 V (625 V/cm), and 780 plates at 3000 V (1875 V/cm). A plot of  $H$  versus  $t_m$  for fluorescein in this device is shown in Fig. 6. At longer times  $H$  depends linearly on  $t_m$  as predicted by the equation, but it plateaus and then increases at very short times, just as seen in the CETAS device (Fig. 4). Overall, the efficiency in

device JH-1 is much lower than that observed in CETAS. This is due to the shorter capillary lengths in JH-1, and the consequently greater contribution to band broadening from “off-separation capillary” effects [13–15]. Preliminary work indicates it is possible to reduce these effects by optimizing the injected plug size.

### Conclusions

The difference in separation efficiency of the two devices demonstrates the classic trade-off in separation methods between speed and efficiency. The results in the larger CETAS structure show that efficient separations can be achieved in glass substrates. The smaller device shows that very rapid separations can be achieved in these structures. The rapid separations mean the devices could be coupled with flow injection analysis or another separation method such as liquid chromatography to create two dimensional separation [16] or sample handling systems. Similarly, the cycle time is comparable to the response time required in chemical sensor applications, making these systems competitive with chemical sensors.

The devices studied include sample injectors integrated into the capillary column. The ability to control sample flow by applied voltages in the T and cross intersections utilized demonstrates the feasibility of using electroosmotic flow for more complex sample handling within a manifold of capillaries. Micromachining of such manifolds, and electroosmotic pumping of fluid can clearly be used to provide low dead volume systems for handling very small volumes of samples, reagents and carriers in a liquid system in a precise manner.

We thank the Natural Sciences and Engineering Research Council of Canada and Ciba-Geigy

for support of the work performed at the University of Alberta. We thank G. MacKinnon of the Alberta Microelectronic Centre (AMC) for valuable assistance in device fabrication, and the AMC for use of their facilities.

### REFERENCES

- 1 N. Graber, H. Lüdi and H. M. Widmer, *Sensors Actuators*, B1 (1990) 239.
- 2 M. Gisin and C. Thommen, *Anal. Chim. Acta*, 190 (1986) 165.
- 3 M. Garn, P. Cevy, M. Gisin and C. Thommen, *Biotechnol. Bioeng.*, 34 (1989) 423.
- 4 A. Manz, N. Graber and H. M. Widmer, *Sensors Actuators*, B1 (1990) 244.
- 5 A. Manz, J.C. Fettinger, E. Verpoorte, H. Lüdi, H.M. Widmer and D.J. Harrison, *Trends Anal. Chem.* 10 (1991) 144.
- 6 J. Ruzicka and E.H. Hansen, *Anal. Chim. Acta*, 161 (1984) 1.
- 7 H.M. Widmer, J.F. Erard and G. Grass, *Int. J. Environ. Anal. Chem.*, 18 (1984) 1.
- 8 A. Giorgetti, N. Periclé, H.M. Widmer, K. Anton and P. Dätwyler, *J. Chromatogr. Sci.*, 27 (1989) 318.
- 9 D.J. Harrison, A. Manz, H. Lüdi and H.M. Widmer, *Anal. Chem.*, 64 (1992) 1926.
- 10 A. Manz, D.J. Harrison, E.M.J. Verpoorte, J.C. Fettinger, A. Paulus, H. Lüdi and H.M. Widmer, *J. Chromatogr.* 593 (1992) 253.
- 11 Z. Fan and D.J. Harrison, *Anal. Chem.*, submitted for publication.
- 12 K. Seiler, D.J. Harrison and A. Manz, *Anal. Chem.*, (1993) in press.
- 13 X. Huang, W.F. Coleman and R.N. Zare, *J. Chromatogr.*, 480 (1989) 95.
- 14 J.C. Sternberg, *Adv. Chromatogr.*, 2 (1966) 206.
- 15 J.W. Jorgenson and K.D. Lukacs, *Anal. Chem.*, 53 (1981) 1298.
- 16 C.A. Monnig and J.W. Jorgenson, *Anal. Chem.*, 63 (1991) 802.

# Solid surface photoluminescence and flow analysis: a happy marriage

Alfredo Sanz-Medel

*Department of Physical and Analytical Chemistry, Faculty of Chemistry, University of Oviedo, 33006 Oviedo (Spain)*

(Received 7th October 1992; revised manuscript received 4th January 1993)

## Abstract

A specially active field of scientific research in photoluminescence nowadays is its use to study microheterogeneous systems and, conversely, to investigate how the emission properties of a lumiphor can be improved by manipulating the physico-chemical properties of its microenvironment. Applications of such basic chemical knowledge to improve analytical detection, particularly in flowing systems, is arousing a great deal of interest. A major breakthrough in this vein was the use of "organized media" to improve luminescence quantum yields in solution. An alternative to the use of "ordered media" to further enhance the rigidity of the lumiphor is by adsorbing or binding it to a solid matrix, as in solid surface luminescence (SSL). Unfortunately SSL is a rather discontinuous technique and so less suited than fluid "organized media" for detection in a flow system. An elegant way-out to such a limitation is the coupling (marriage) of SSL with FIA techniques. Solid surface photoluminescence and flow analysis have had a most fortunate encounter, as the merging of the two techniques is providing new avenues for optical sensor transduction and SSL techniques improvement. Fluorimetric advantages of such combinations for new optical sensor development are dealt with and illustrated with the development of a very sensitive and selective optosensor for low aluminium levels in samples of utmost importance in renal failure disease control. However, the potential advantages and increased scope of SSL-FIA combinations are more fully realised when using room temperature phosphorescence (RTP) detection in an aqueous flow system. It is shown how new possibilities for fundamental and applied studies on the SS-RTP phenomenon are opened. SS-RTP-FIA analytical applications to sensing of cations (e.g., by using ferron reagent to bind the cation and retaining this RTP chelate in a flow-through cell), of anions (e.g., an optically "active" phase with the complex Al-8-hydroxyquinoline becomes phosphorescent in the flow-through cell only when iodide is bound to it) or oxygen (which quenches the RTP signal of a phosphorescent "active" phase) which can be analyzed in gas mixtures or dissolved in solutions. Finally, basic measurements carried out in our laboratory will be used to explain the amazingly strong RTP signals obtained in aqueous solutions by using anion-exchange resins to retain the studied phosphors.

*Keywords:* Chemiluminescence; Fluorimetry; Flow system; Phosphorimetry; Photoluminescence

Solid surface photoluminescence (SS-PL) can be considered today to be a well established analytical technique based on the measurement of luminescence emitted from solid compounds or, more frequently, from analytes which are adsorbed on or are chemically bound to a suitable

solid support, which is then interrogated by an external excitation light. Using this measuring principle several techniques have evolved that have proved to be suitable for a wide variety of analytical applications, particularly in the pharmaceutical, clinical and biological fields [1–4]. The two basic techniques derived from photoluminescence phenomena, fluorimetry and phosphorimetry, have been extensively used for the determination of lumiphors [3] because at low

*Correspondence to:* A. Sanz-Medel, Department of Physical and Analytical Chemistry, Faculty of Chemistry, University of Oviedo, 33006 Oviedo (Spain).



concentrations of these analytes (trace analysis), in homogeneous solutions, both fluorescence and phosphorescence emissions follow the basic equations [4]

$$I_F = 2.3\Phi_F I_0 \epsilon l c$$

(singlet-state radiational deactivation)

$$I_P = 2.3\Phi_P I_0 \epsilon l c$$

(triplet-state radiational deactivation)

where  $I_F$  and  $I_P$  are the intensity of the corresponding radiative emissions and  $\Phi_F$  and  $\Phi_P$  the quantum yields,  $I_0$  is the intensity of the exciting radiation,  $\epsilon$  is the lumiphor molar absorptivity,  $l$  is the light path length for excitation and  $c$  is the lumiphor analytical concentration.

Thus, the striking differences for  $I_F$  and  $I_P$  signals observed at room temperature will come from differences in the values of  $\Phi_F$  and  $\Phi_P$ . Acceptable values for  $\Phi_F$  are observed at room temperature and in solution, the most common conditions for carrying out analytical fluorescence. Under these conditions, however, the value of  $\Phi_P$  is very low or close to zero owing to the relatively long lifetime of the triplet state favouring radiationless deactivations.

Therefore, direct phosphorescence in liquid solutions at room temperature is a rare phenomenon and, if strong analytical signals have to be obtained,  $\Phi_P$  should be carefully optimized. Observation of measurable phosphorescence depends on the overall efficiency of two basic processes (see Fig. 1): intersystem crossing populating the triplet,  $\Phi_T$ , and phosphorescence itself,  $\Phi_P$ :

$$\Phi_P = \Phi_T \Phi_P = \Phi_T \cdot \frac{K_P}{K_P + K_{UD} + K_{PQ}}$$

where  $K_P$  is the rate of phosphorescence,  $K_{UD}$  is the rate of radiationless unimolecular processes which deactivate the triplet,  $T_1$  and  $K_{PQ}$  is the rate of phosphorescence bimolecular quenching proportional to the concentration of the quencher:  $K_{PQ} = K_q [Q]$ .

At room temperature in non-viscous solutions where the triplet state is prone to deactivation

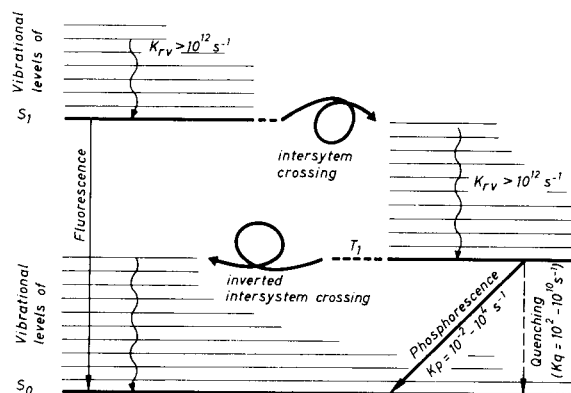


Fig. 1. Simplified energy level diagram of an organic luminescent molecule showing the basic photophysical process to obtain phosphorescence.

processes, the following approximation can be made:

$$K_{UD} + K_{PQ} \gg K_P$$

and thus

$$\Phi_P = \frac{K_P}{K_{UD} + K_{PQ}}$$

A typical  $K_P$  value, for a  $T_1 (\pi, \pi^*)$ , is 0.1 s and  $\Phi_P > 10^{-4}$  if we wish to observe measurable phosphorescence. Hence, to observe phosphorescence,  $K_{UD} + K_{PQ} \leq 10^3 \text{ s}^{-1}$ .

If it is assumed, according to Turro [5], that Q is a diffusional quencher (for a non-viscous organic solvent the rate constant for diffusion of quenchers,  $K_{dif}$ , is ca.  $10^{-10} \text{ l mol}^{-1} \text{ s}^{-1}$ ), then

$$K_q [Q] = K_{dif} [Q] \leq 10^3$$

Hence  $[Q] \leq 10^{-7} \text{ M}$  (collisional quenching predominates over  $K_{UD}$ ). In other words, at room temperature in fluid solutions, even extremely low concentrations of quenchers effectively deactivate the triplet  $T_1$  (see Fig. 1), particularly if it is a  $\pi, \pi^*$ -type excited state [5].

A possible solution to this problem may be the careful purification of solutions, a cumbersome and impractical task for analytical purposes. A preferable alternative is to act on  $K_q$ , decreasing its magnitude by hindering the motion of lumiphors and quenchers. Such a goal has been pursued by increasing the "rigidity" of the envi-

ronment which surrounds the analyte (lumiphor) via its incorporation in a solid matrix: either at cryogenic temperatures by physical trapping of the lumiphor in the rigid glass formed on lowering the temperature of the solution to 77 K (low-temperature luminescence), where very low detection limits can be obtained in rigid glass, or at room temperature by bonding of the lumiphor to a solid surface (SS-PL). As both solid matrix immobilization techniques are intrinsically discontinuous in operation, neither is well suited for detection in continuous-flow systems (e.g., flow injection and liquid chromatographic methodologies).

The fluidity of solutions can be preserved, while securing rigidity of the environment, by resorting to the so-called “organized media”. Organized media, particularly micelles and vesicles, provide a microscopically heterogeneous fluid solution with unique properties [6–8], especially their ability to organize reactants at a molecular level and to enhance luminescence emissions due to increased rigidity of the lumiphor microenvironment. In fact, fluorescence enhancements of around 50-fold in micelles have been reported [7] and micelle (and cyclodextrin)-stabilized-room temperature phosphorescence (MS-RTP) has become a powerful technique for the trace analysis of organic compounds [4] and has been applied to metal ions [9].

It is worth noting that in organized media, the lumiphor is in dynamic equilibrium between the bulk solution and the aggregates. Hence the analyte is not as “rigidly held” as in solid matrices and therefore it must have a residence time in the micelle long enough, when compared with spectroscopic rate constants, if the special “microenvironment” of aggregates is going to influence effectively the lumiphor emissions.

A most interesting development along these lines is the introduction of SS-PL in flowing systems. Here fluidity for continuous-flow operation and rigidity for strong emissions are elegantly combined. The marriage between SS-PL and flow analysis can be very fertile, both for fluorescence and phosphorescence, because it arises from the merging of two apparently independent streams: conventional SS-PL principles and new optosens-

ing technologies. They are emerging as complementary or even synergetic, as will be illustrated later. The following discussion considers how this marriage has been possible, with details of the techniques involved and the possible analytical future, particularly in the revival of analytical phosphorescence, a neglected technique for many analytical chemists.

#### CONVENTIONAL SS-PL SPECTROMETRY

SS-PL analysis, based on fluorescence and phosphorescence measurements of compounds adsorbed on or bound to a solid material, has proved to be useful analytical tool for organic trace analysis [1,3,4]. High sensitivity, comparable to low-temperature work, is perhaps its greatest virtue as nanogram or even picogram amounts of important organics, e.g., pesticides, and carcinogenic compounds, can be detected and determined at acceptable precision levels (2–20%) on the microlitre scale. The selectivity achieved is relatively good and can be improved considerably because this detection technique, very simple and inexpensive, is very well suited to be combined directly with planar (thin-layer and paper) chromatography [10,11]. On the other hand, the most important breakthrough in phosphorescence, the development of room temperature phosphorescence (RTP) techniques, was made possible by adsorbing the phosphor/analyte on a solid surface to obtain the required rigidity in an alternative manner to cryogenic freezing.

These favourable analytical performance characteristics of SS-PL and new advances in investigations on lumiphor–solid surface interactions have provided the basis for hundreds of applications of SS-fluorescence for the analysis of simple mixtures of organics and its extension to identification and control analysis in important and pharmaceutical real-life problems [1]. During the last decade, there has been a most impressive growth of analytical applications of SS-RTP, mostly related to environmental and biological samples [2–4]. This technique has proved especially useful for the analysis and control of low levels of organic pollutants which today are the

subject of concern of many environmental scientists. Several pesticides and closely related compounds, biphenyls, polychlorinated biphenyls and dibenzo-*p*-dioxins, have been investigated by SS-PL techniques. Of special interest are the SS-RTP techniques developed for polycyclic aromatic hydrocarbons (PAHs) and analogous nitrogen heterocyclics, extensively studied by Vo-Dinh and co-workers [12,13], who showed that SS-RTP is a simple and convenient screening tool for monitoring these dangerous compounds in different samples and practical situations (e.g., permeation of PAHs from petroleum, coal and combustion products through protective clothing materials) [13].

Further applications of SS-PL in the pharmaceutical and clinical fields have continued to appear [3], with a clear thrust from the RTP side [4].

Finally, The application of fluorescence and phosphorescence probes to study important analyte–microenvironment interactions in solid sur-

faces should be stressed, e.g., the use of pyrene fluorescence as a probe to study chemical bonding with or physical adsorption on chromatographic stationary phases [14,15] in the search for a displacement model for liquid–solid chromatography [16]. SS-RTP is also a very suitable and sensitive technique for these purposes.

In some instances, SS-PL can be somewhat lengthy, and the procedure discontinuous. Filter-paper is the most convenient and commonly used solid support, for both fluorescence and phosphorescence measurements; in a typical RTP experiment, 1.5  $\mu\text{l}$  of analyte solution are delivered to a manually pretreated disc of filter-paper (Fig. 2). After deposition of the sample, the paper is placed under an infrared lamp for drying and, finally, the dried sample is placed in a suitable sample holder in the spectrometer, probably purged with dry air or nitrogen, in order to measure the RT luminescence signal.

Although there are different RTP techniques and their corresponding experimental procedures differ from one another, the four main steps (see Fig. 2) described are more or less common to all SS-PL methodologies in use.

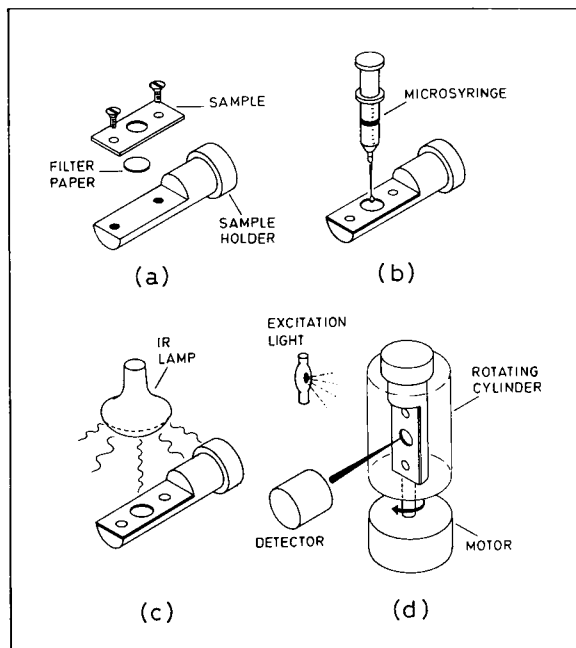


Fig. 2. Schematic illustration of the procedure for RTP analysis using filter-paper as solid support (reprinted with permission from T. Vo-Dinh, Room Temperature Phosphorimetry for Chemical Analysis, Wiley, New York, 1984, p. 99).

#### OPTICAL SENSING AT SOLID SURFACES

A few years ago, Ruzicka and Hansen [17] coined the term “optosensing at active surfaces” and defined it as a new detection principle in flow-injection analysis (FIA) based on the change in optical properties of a surface situated in a flowing stream. Optosensing at active surfaces “will exploit absorbance, reflectance or fluorescence of visible and/or UV radiation as it is changed by chemical reactions taking place at, or in close proximity to, a surface surrounded by a flowing solution” [17]. Using FIA miniconduits, fibre-optics and reflectance measurements, they described [17] a flow-through sensor for pH. This optosensor was also applied to ammonia and urea sensing, providing the first demonstration of the great analytical potential of such detectors when used integrated in FIA manifolds [18].

Valcárcel and Luque de Castro [19], from a different perspective, published an excellent sys-

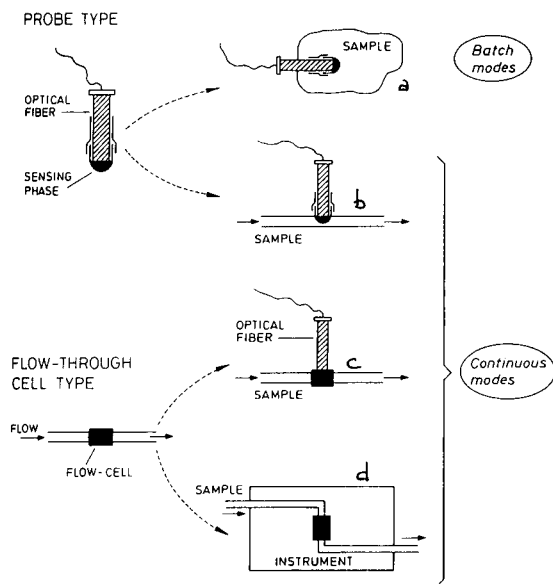


Fig. 3. Schematic diagram illustrating basic differences between probe-type and flow-through cell-type optical sensors. Different uses in (a) batch and (b-d) continuous modes of operation are shown.

tematic classification of possible ways of carrying out the integration of reaction/retention and spectroscopic detection in continuous-flow systems. They also proposed that (bio)chemical sensors could be divided into two broad groups: the more familiar "probe" type and the "flow-through" cell type (bio)chemical sensors. In their paper, the use of optical fibres, and hence the possibility of remote analysis, appear to be exclusive to probe-type sensors. However, it has been shown [17,18,20] that optical fibres and remote analysis can be also achieved in "flow-through" minicell sensors (see Fig. 3). The main difference between the two types of sensors is that fibre-optic probe sensors can be used in batch and in flow systems, allowing for "in-line" analysis, whereas flow-through cells need a continuous-flow system for adequate function. Thus, "on-line" sampling of the material in the process being monitored is usually essential. It should be stressed here that flow-through cells are almost always indispensable devices for more basic studies in optical sensor development.

It is now common knowledge that a sensor consists of at least two basic components [21]: an element able to recognize the analyte selectively (through a chemical reaction, in chemical sensors, and through biochemical reactions, in biochemical sensors) and a physico-chemical transduction element. The recognitive element is usually a selected or tailored organic or bio-organic material immobilized (e.g., as a thin film) on a suitable solid support. The transductive element is a suitable analytical analytical transducer, e.g., electrochemical, optical or thermal, able to translate the selective recognitive reaction into a measurable signal. Therefore, the recognition reaction (selectivity) should provide a sufficient free energy change, on binding, for optical transduction (sensitivity).

There is no doubt that both recognitive and transductive elements are present in the flow-through cell type of sensor. However, as shown by Valcárcel and Luque de Castro [19], the conveniently packed flow cell of a non-destructive detector can be used to immobilize on the solid support any of the participants of the recognitive optical reaction in a permanent mode, as in probe-type sensors, or during a short period just to allow signal measurement due to the analyte or its reaction product. Therefore, the flow-through devices are more versatile than conventional probe-type dedicated sensors, which integrate the reaction/retention/transduction processes on the surface of the "sensing" layer immobilized permanently on the solid support. Flow-through cell devices are analytically more flexible because they allow the recognizing reaction of the retention/transduction processes to be separated and the introduction, on-line with the detector, of the most varied chemistries, taking advantage of the numerous FIA techniques developed so far. Notwithstanding that versatility, the more common approach in flow optodes involves the integration of the basic reaction/retention/detection processes at the solid support in the flow cell. This approach can subsequently be miniaturized and then, if adequate, extended to the construction of probe-type sensors as shown by comparing Fig. 4, a flow optode design, with Fig. 3c and b.

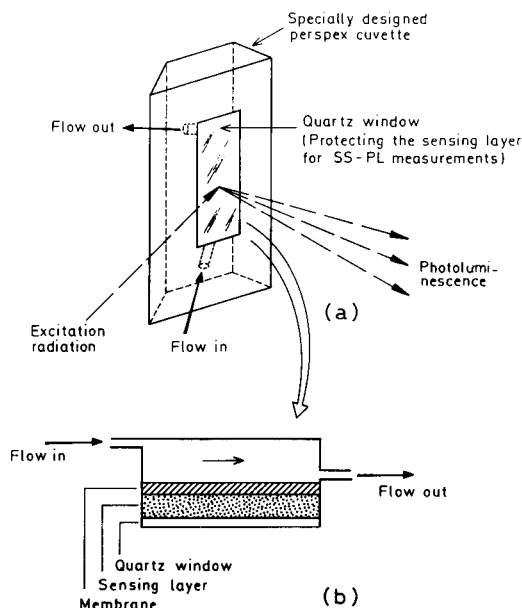


Fig. 4. Schematic view of a flow optical sensor. (a) The flow cell for photoluminescence optosensing; (b) the "sensing layer" position in the flow cell.

#### PHOTOLUMINESCENCE-BASED OPTOSENSING: THE HAPPY MARRIAGE

We have seen before that SS-PL analysis has proved to be a sensitive, selective and inexpensive tool for organic trace analysis. Unfortunately, the manual steps of sample deposition, drying and other necessary manipulations of sample solutions on the solid support (Fig. 2) are more complicated and less precise than those we are used to in conventional fluorescence of solutions. Such steps, on the other hand, had been considered essential to analytical SS-RTP. Besides, SS-PL analysis is like graphite furnace atomic absorption spectrometry, an intrinsically discontinuous technique (some steps, such as deposition and drying, should be performed before final measurement). Therefore, SS-PL is less appropriate for real-time detection in a flow (e.g. FIA and liquid chromatographic detectors) than solution luminescence. An elegant solution to these limitations is the coupling of SS-PL with FIA techniques via optosensing at solid surfaces. Such a marriage constitutes a real synergistic combination providing, at least, the following advantages

to SS-PL: continuous-flow operation; easier automation and routine analysis; improved precision; and improved selectivity, because adequate on-line separation chemistries can be used before final PL detection.

At the same time, optical sensor development is facilitated. It is well known that in order to produce a sensor the selected "recognitive" reagent of the analyte must be incorporated in the solid support. Such immobilization to obtain the active phase is critical because the following sensing properties should be aimed for in the process: binding capability or activity (which should be maintained on immobilization); reversibility of the recognition process of the analyte; response time of the sensor (it should be short enough to allow for useful real-time measurements); long-term stability of the active phase, in order to obtain adequate lifetimes for the corresponding sensor; and specificity or, at least, high selectivity, of the active phase towards the desired analyte.

The coupling of flow systems and luminescent sensors is really fortunate because the use of imaginative "chemistries in-line" will allow several advantageous developments. First, the "recognitive" reaction itself can be separated spatially from the integrated retention/transduction (e.g., determination of aluminium with an RTP optosensor [22]). Second, irreversible "recognitive" reaction can be used. Only a few reactions with sufficient free energy change for sensitive optical transduction and small binding constant ( $K_f \approx 10^3\text{--}10^4 \text{ l mol}^{-1}$ ) to allow for reversibility are known. In a flow system, irreversible reactions (e.g.,  $K_f > 10^{10} \text{ l mol}^{-1}$ ) can be used, with temporary retention of the analyte on the solid phase, just by lowering the thermodynamic value of  $K_f$  to a desired "conditional" constant (e.g., by adding competing agents in the carrier). If the retention is still too strong (permanent), one can also resort to a discontinuous procedure consisting of the injection of a "plug" of a suitable eluting solution, after the plug of the sample [19,20], which will release the analyte. Hence rapid regeneration of the active surfaces is also straightforward. Third, long-term stability, which is a serious problem in current optode technol-

ogy, can be preserved. In natural receptors (e.g., proteins) which degrade with time, nature has overcome this drawback by continually replacing those proteins in the living organisms, sweeping defective receptors into the biological recycling system. The continuous, or discontinuous, regeneration of the active phases referred to above mimics, nature and thus can preserve the long-term performance of sensing phases. Finally, selectivity (another weakness of current sensors) can be improved. On-line separation chemistries are straightforward in the continuous-flow system and most helpful for obtaining an interference-free final detection of the analyte, as will be illustrated later with the ultratrace fluorimetric determination of aluminium in dialysis concentrates [20].

Hence the beneficial features of such coupling are obvious in two respects: procedural SS-PL limitations are overcome, while the scope of optical sensors is clearly expanded. The following discussion is intended to illustrate, mainly with examples of work carried out in the author's laboratory during the last 2–3 years, that optosensing at solid surfaces offers a new insight into luminescence-based sensors. It opens up new analytical possibilities for developed fluorimetric sensors in their application to real-life analysis and, what is more, the field of luminescence sensors is expanded into the elusive area of RTP transduction.

Fluorescence-based chemical sensors [23–25] and biosensors [26,27] have become a research area of great interest. The high sensitivity of fluorescence allows miniaturization of typical sensing layers (see Fig. 4), which can easily be adapted to optical fibres for remote analysis and probe-type sensor construction. Many interesting fluorimetric sensors have been described for different ions such as  $H^+$ ,  $K^+$  and  $Al^{3+}$  [23] and gases (e.g., and  $O_2$ ,  $CO_2$ ) and they are moving very quickly into the biosensors field (for glucose, lactate, ascorbic acid, etc.), offering a good approach for in vivo sensors [26,27] as biocompatibility of the materials to be implanted is continuously improved. At present, however, the use of such sensors in real-life analytical problems is restricted because the required analytical perfor-

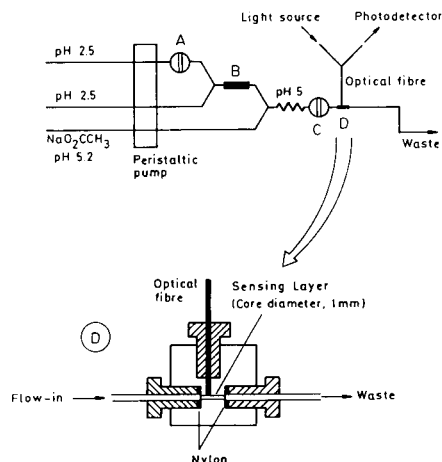


Fig. 5. Flow diagram of a fluorimetric optosensor for aluminium showing the possibility of elimination of interference in a column (B) on-line with the optosensor (D). Expanded view of the flow-through minicell for optical sensing.

mance criteria are not fulfilled. Flow optodes clearly allow more reliable analyses of real-life samples. For example, a sensing layer for Al [20] has been developed by adsorbing Kelex 100 on the resin Amberlite XAD-7. This active solid phase was packed in a small flow cell (see Fig. 5) communicating with the spectrofluorimeter by a laboratory-built optical fibre allowing for remote Al sensing in the flow-through system. Moreover, this FIA configuration allowed the elimination of Cu and Fe interferences by on-line chemical pre-treatment of the sample, and this system proved to be very suitable for the ultratrace determination of Al in samples of dialysis fluids and concentrates, an important analytical problem in hospital dialysis units [20].

#### ROOM TEMPERATURE PHOSPHORESCENCE OPTOSENSING: A FURTHER ANALYTICAL PHOSPHORESCENCE BREAKTHROUGH

Although strong solution RTP has been made possible in the last decade by resorting to the use of organized media to protect the triplet state emission, the best approach to secure strong RTP signals for analytical use is by trapping, adsorbing or binding the phosphor to a solid

matrix, as carried out in SS-RTP. Recent basic work by Ramasamy and Hurtubise [28–31] demonstrated that the stronger the interaction between the phosphor and the solid matrix, and the more rigid the solid matrix, the greater overall rigidity (“rigidly held” mechanism) is achieved. Thus, a more favourable environment results in the prevention of both internal ( $K_{UD}$ ) and collisional ( $K_q$ ) radiationless deactivations of the excited triplet state.

The widespread application of SS-RTP, however, has been hampered so far by the above-mentioned procedural drawbacks (i.e., discontinuous character, more complicated manipulations) and blanks and water/oxygen quenching problems which limit conventional SS-RTP work. In order to make possible continuous and automated operation, Vo-Dinh et al. [32] proposed an automatic instrument for SS-RTP based on a continuous filter-paper where the basic operations for RTP took place. Automatic spraying and drying of samples on the filter-paper strip before SS-RTP measurement and the use an FIA configuration for sample introduction have been reported recently [33]. For all lumiphor–solid support combinations where drying of the solvent is essential, in order to obtain analytically useful signals, this continuous paper strip approach [32,33] is most useful.

A radically different solution is SS-RTP optosensing, on which a considerable part of the latest research time and effort of the author’s group has been devoted.

#### *SS-RTP optosensing of cations and anions*

It is now well known that oxygen and water are the most serious enemies of analytical SS-RTP. Particular attention should be given to water, the most potent quencher of such emissions [34]. In the usual filter-paper supports, water seems to cause swelling of the microporous structure of cellulose and weakening of the phosphor–cellulose hydrogen bonds [35]. This loss of rigidity probably accounts for the strong quenching of RTP by moisture.

Recently it was reported, however, that analytically useful RTP signals in a continuous aqueous flow can be achieved in “flow-through” sensor

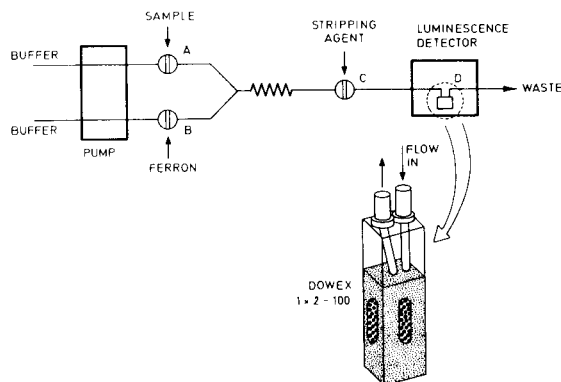


Fig. 6. Phosphorimetric optosensor manifold. A, B, C = injection valves; D = flow-through packed cell [reprinted with permission from R. Pereira et al., *Anal. Chem.*, 63 (1991) 1760].

devices provided that the solid support is adequately selected for a given analyte [22]. In fact, low- $\text{ng ml}^{-1}$  levels of cations and other elements can be determined by this approach. The optosensing device (Fig. 6) is a “flow-through” cell (the primitive technique using paper lint packed in a flow cell [36] for RTP batch measurements could be considered as a forerunner of these devices). The cell interior is packed with the solid support (resin Dowex  $1 \times 2-100$ ), a strong anion exchanger able to retain tightly the negatively charged Al–ferron complex formed in the flow after merging of both sample and reagent solutions (valves A and B). On immobilization of the complex, an RTP signal builds up in the detector at 600 nm, a relatively long wavelength widely separated from the excitation wavelength ( $\lambda_{\text{ex}} = 400 \text{ nm}$ ). Once the RTP has been measured, 2 ml of HCl are injected through valve C to release the Al complex and so to condition the resin before the next sample/reagent injection. The carrier solution contains  $\text{Na}_2\text{SO}_3$  ( $10^{-3} \text{ M}$ ) as oxygen scavenger.

The analytical performance characteristics for Al determinations are good (detection limits of  $2 \text{ ng ml}^{-1}$ ), and the optosensing device has been applied to ultratrace determinations of Al in real samples of clinical interest and good agreement with graphite furnace atomic absorption spectrometric results was obtained [22].

There are very exciting alternatives for extending such a transduction RTP technique to other analytical applications. One is the immobilization of the RTP active reagent in the transduction/detection cell, as in most fluorimetric sensors [24]. When incorporated in the sample flow, the desired analyte should interact selectively with the active phase producing a strong change in the RTP intrinsic emission of the solid support. This is the case with the anion iodide and an active phase of aluminium 5-sulphoquinoline-8-ol adsorbed permanently on Dowex 1- $\times$ 2-100 resin. In a simple FIA manifold, when a sample containing iodide is injected, this anion is retained on the surface of the resin. The strong “heavy atom effect” of iodide on the luminescence of the immobilized complex will change the luminescent emission of the active packing in the cell, by quenching the fluorescence and bringing about RTP signals. Using this principle, an iodide optosensing device, which can be used in fluorescence and phosphorescence modes, has been developed [37]. Its selectivity versus  $\text{Cl}^-$  and  $\text{Br}^-$  in the RTP mode is most striking, as shown in Fig. 7.

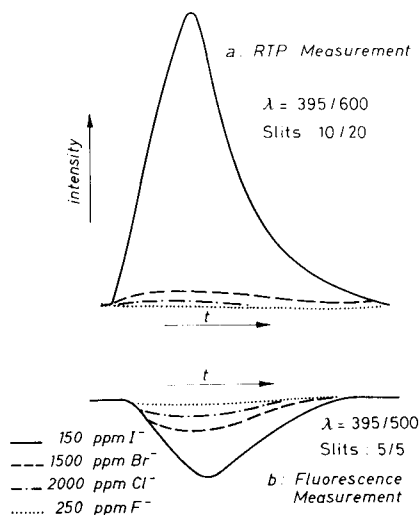


Fig. 7. (a) Typical readout observed in the RTP optosensor coupled to the FIA manifold, for  $150 \mu\text{g ml}^{-1}$  of KI and for other halides (at the concentrations given). (b) The same, using the fluorescence “quenching” mode.

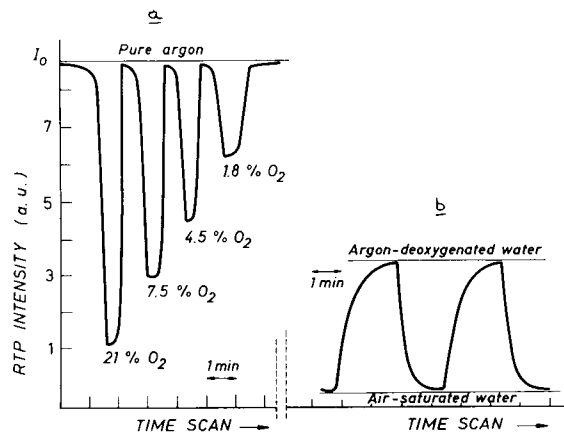


Fig. 8. Typical readouts observed in the RTP oxygen optosensor. (a) Argon–oxygen gas mixtures; (b) oxygen dissolved in water.

#### SS-RTP optosensing of gases

The Al–ferron complex immobilized on Dowex resins is highly phosphorescent. When exposed to water, it proved to be an excellent indicator of oxygen (which quenched such emissions very efficiently). Different metal–ferron chelates such as those of Nb, Zr, Al and Ga have been tested as oxygen RTP indicators. The Al complex provided the strongest phosphorescence and the best indicator properties.

Using such an indicator, a flow-cell type of sensing device was designed using silicone-rubber membranes placed on the rigid support of a quartz slide (as in Fig. 4). This flow cell was used both to determine oxygen in gas mixtures and to determine dissolved oxygen in water in simple flow manifolds [38].

The results showed that this sensor is very attractive for oxygen monitoring (Fig. 8); the response times in gas mixtures are less than 10 s for a full signal change without any hysteresis being observed and the signal being fully reversible. The response times in aqueous solutions are obviously longer, as the results in Fig. 8 demonstrate.

This sensor shows high photochemical stability in the presence of both oxygen and argon; no significant decrease in RTP intensity was observed after 5 h of continuous illumination. The application of this device to real sample analyses was also tested by determining the dissolved oxy-

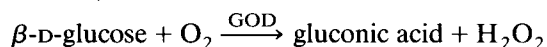


gen concentration in five different water samples. The results were compared with those given by the Winkler's method, as a reference method, and good agreement was found (see Table 1).

This flow-through sensor principle for oxygen sensing is now patent pending [39] and the construction of a probe-type optical fibre device of the design previously reported [40] is straightforward using such RTP active phase.

#### RTP opto-biosensor

The favourable analytical performance characteristics of the described RTP optosensor for oxygen prompted its use for enzymatic biosensing in oxygen-mediated reactions, using the determination of glucose as a model analyte. Glucose oxidase (GOD) covalently immobilized on a nylon net [41] was packed in a minicolumn of a single-channel FIA configuration; the column was located immediately before the flow-through RTP optosensor for oxygen described previously. When a glucose sample is injected into the system, this sensor monitors the oxygen consumption in the column, due to the classical reaction



The observed dynamic linear range of this RTP flow biosensor is adequate for the control of biological levels of glucose in serum (linearity up to 3 mM linearity) with a detection limit below 0.1 mM in glucose and an overall response time of about 2 min. The analytical application of this optosensor to glucose analysis in real samples of serum and fruit juices proves to be satisfactory [42], as shown in Table 2.

TABLE 1

Comparison of the RTP oxygen sensor with the Winkler method determination of dissolved oxygen in water

Water sample	Dissolved oxygen ( $\mu\text{g ml}^{-1}$ )	
	RTP sensor	Winkler's method
1	2.08	2.23
2	4.68	4.75
3	6.67	6.42
4	7.19	7.40
5	8.25	8.34

TABLE 2

Analytical application of RTP glucose biosensor to real samples

Sample <sup>a</sup>	Glucose (mM)	
	Sensor	Alternative method
Serum pool I (DC)	4.85 ± 0.12	4.90 ± 0.12 <sup>b</sup>
Serum pool II (DC)	5.57 ± 0.02	5.64 ± 0.04 <sup>b</sup>
Serum pool III (DC)	6.53 ± 0.13	6.36 ± 0.12 <sup>b</sup>
Apple soft drink (DC)	204.0 ± 0.2	210.0 ± 4.6 <sup>c</sup>
Lemon soft drink <sup>d</sup> :		
DC	390.0 ± 13.3	283.4 ± 9.2 <sup>c</sup>
SA	282.5 ± 3.5	

<sup>a</sup> DC = direct calibration; SA = standard additions. <sup>b</sup> Beckman oxygen electrode. <sup>c</sup> Spectrophotometric determination (hexokinase at 340 nm). <sup>d</sup> The sample was stirred to remove CO<sub>2</sub>.

Antibiotics of the tetracycline type can also be analysed by RTP optosensing in a simple FIA system similar to that depicted schematically in fig. 6. The antibiotic(s), injected with the sample solution, form(s) a strong complex with a suitable cation, such as Eu<sup>3+</sup>, and this complex is immobilized on passing through the packed flow cell (RTP detector). Strong RTP signals are thus originated, providing the basis for detection limits of ca. 0.3 ng ml<sup>-1</sup> (5 × 10<sup>-10</sup> M) of tetracycline in solution. A detailed study of the conditions and potential applications of such RTP optosensor to real samples is in progress [43].

Parallel fundamental studies are being pursued. The fluorescence polarization of the Al-ferron chelate in different environments has been measured at various temperatures in an attempt to explain the high RTP signals observed in spite of the surrounding aqueous flow. This approach is useful in assessing how rigidly the phosphor is held to the surface [31,44,45]. Although limited so far to short temperature ranges (around room temperature, used in the analysis), the preliminary results (see Fig. 9) clearly show that the solid surface of the Dowex resin provides a "rigidly held" effect for the lumiphor that is more intense than that provided by micellar solutions (fluid media). Comparative basic measurements of the effect of moisture and oxygen on the Al-ferron probe adsorbed on filter-paper and on Dowex 1 × 2–200 resin showed that the RTP signals

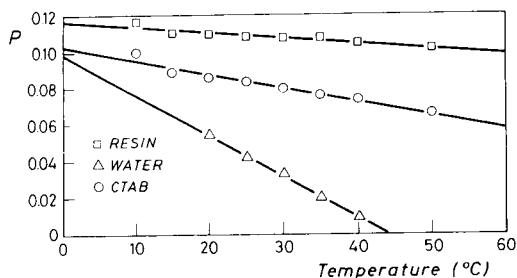


Fig. 9. Fluorescence polarization results of the Al-ferron luminescent probe in different environments. □ = Dowex resin; △ = water; ○ = CTAB micelles.

observed are more than ten times higher in the resin than in filter-paper. In an argon atmosphere, moisture hardly modifies the RTP intensity observed using the resin as support, whereas the signal decreases around three times for the probe adsorbed on filter-paper (see Table 3). Indirectly, therefore, it can be said that Dowex is a solid support for Al-ferron transient immobilization, which provides a much higher “rigidly held” overall mechanism than filter-paper, probably because electrostatic and hydrophobic interactions are acting together in the binding of the complex to the resin (further discussion of this aspect can be found elsewhere [9,22]).

### Conclusions

It appears that SS-PL and flow analysis have had a most fortunate encounter, as the merging of the two fields is providing numerous new analytical possibilities. Particularly attractive developments are expected in the area of flow optodes for (bio)chemical sensing.

Fundamental studies in lumiphor–environment interactions are most interesting because they allow new insights into the “rigidly held” mechanism operating for each lumiphor–solid support system considered. Further increases in the rigidity of the probe in the solid matrix and of the packing around the probe of the matrix itself (e.g., by addition of micelles [46,47] or cyclodextrins [48], perhaps in the flow) can be very useful for obtaining higher quantum efficiencies ( $\Phi_p$  and  $\Phi_F$ ) for the lumiphor and thus for designing new applications of analytical fluorimetry and phosphorimetry.

The analytical potential of RTP optosensing as a detection technique for continuous techniques has been demonstrated. As phosphorescent emissions occur at longer wavelengths than fluorescence emissions, less background (due to scatter and fluorescence) and less photochemical decomposition of reagents can be expected. On the other hand, the intrinsic spectral selectivity of phosphorescence is higher than that of fluorescence (few species phosphoresce at room temperature and temporal discrimination is easier) and it offers much simpler instrumentation for the measurement of lifetimes. Smaller and cheaper instruments might be built for multivariate ( $I_p$ ,  $\lambda_{exc}$ ,  $\lambda_{em}$ , lifetimes) measurements. Suitable chemometric treatment of such information can substantially increase the selectivity of even completely overlapping RTP spectra [49]. Real-life complex spectra could be deconvoluted and reliable analyses achieved without resorting to lengthy and cumbersome separations. In brief, it

TABLE 3

SS-RTP characteristics of the aluminum–ferron complex

Atmosphere	Condition	Support <sup>a</sup>	SS-RTP observed <sup>b</sup>	$\tau$ (ms) <sup>c</sup>
Argon	Dry	Dowex 1- $\times$ 2-100	1640 (87)	0.324
	Wet		1300 (70)	0.206
O <sub>2</sub> (air)	Dry	Filter paper	1560 (85)	0.327
	Wet		256 (20)	–
Argon	Dry	Filter paper	108 (28)	0.309
	Wet		34 (14)	0.172
O <sub>2</sub> (air)	Dry	Filter paper	107 (27)	0.322
	Wet		27 (10)	0.151

<sup>a</sup> The solid support was immersed in a solution containing [Al] =  $1 \times 10^{-5}$  M and [ferron] =  $5 \times 10^{-5}$  M. <sup>b</sup> Values in parentheses correspond to reagent blanks. <sup>c</sup>  $\tau$  is the observed triplet lifetime.

is well known that there are certain potential advantages of phosphorescence over fluorescence hardly realised in practical work. Perhaps the marriage of SS-PL and flow analysis might change this situation. Investigations on the possible realization of such analytical potential still appear very attractive and constitute a fruitful field of research.

Financial support for this work, provided by FICYT in Asturias and by the Comisión Interministerial de Ciencia y Tecnología (CICYT), Project PM88-0183, is gratefully acknowledged.

#### REFERENCES

- 1 R.J. Hurtubise, in S.J. Schulman (Ed.), *Molecular Luminescence Spectroscopy: Methods and Applications, Part 2*, J. Wiley, New York, 1988, Chap. 1.
- 2 T. Vo-Dinh, *Room Temperature Phosphorimetry for Chemical Analysis*, Wiley, New York, 1984.
- 3 R.J. Hurtubise, *Anal. Chem.*, 61 (1989) 889A.
- 4 R.J. Hurtubise, *Phosphorimetry: Theory, Instrumentation and Applications*, VCH, New York, 1990.
- 5 N.J. Turro, *Modern Molecular Photochemistry*, Benjamin/Cummings, Menlo Park, CA, 1978, pp. 129–130.
- 6 L.J. Cline Love, J.G. Habarta and J.G. Dorsey, *Anal. Chem.*, 56 (1984) 1132A.
- 7 W.L. Hinze, H.N. Singh, Y. Baba and N.G. Harvey, *Trends Anal. Chem.*, 3 (1984) 193.
- 8 J. Georges, *Analisis*, 17 (1989) 231.
- 9 A. Sanz Medel, P.L. Martínez and M.E. Díaz García, *Anal. Chem.*, 59 (1987) 774.
- 10 A. Alak, E. Heilweil, W.L. Hinze, H. Oh and D.W. Armstrong, *J. Liq. Chromatogr.*, 7 (1984) 1273.
- 11 J.N. Miller, *Pure Appl. Chem.*, 57 (1985) 515.
- 12 T. Vo-Dinh, *Environ. Sci. Technol.*, 19 (1985) 997.
- 13 D.A. White and T. Vo-Dinh, *Appl. Spectrosc.*, 42 (1988) 285.
- 14 C.H. Lochmüller, A.S. Colborn, M.L. Hunnicutt and J.M. Harvis, *Anal. Chem.*, 55 (1983) 1344.
- 15 J.W. Carr and J.M. Harris, *Anal. Chem.*, 59 (1987) 2546.
- 16 G.J. Burrell and R.J. Hurtubise, *Anal. Chem.*, 60 (1988) 2178.
- 17 J. Ruzicka and E.M. Hansen, *Anal. Chim. Acta*, 173 (1985) 3.
- 18 R.E. Dessy, *Anal. Chem.*, 61 (1989) 1079A.
- 19 M. Valcárcel, and M.D. Luque de Castro, *Analyst*, 115 (1990) 699.
- 20 R. Pereiro, M.E. Díaz and A. Sanz-Medel, *Analyst*, 115 (1990) 575.
- 21 J. Janata, *Principles of Chemical Sensors*, Plenum, New York, 1989.
- 22 R. Pereiro, Y.M. Liu, M.E. Díaz and A. Sanz-Medel, *Anal. Chem.*, 63 (1991) 1759.
- 23 O.S. Wolfbeis, in S.G. Schulman (Ed.), *Molecular Luminescence Spectroscopy: Methods and Applications, Part 2*, Wiley, New York, 1988, chap. 3.
- 24 W.R. Seitz, *CRC Crit. Rev. Anal. Chem.*, 19 (1988) 135.
- 25 O.S. Wolfbeis, *Fresenius' J. Anal. Chem. (Rev.)*, 337 (1990) 522.
- 26 O.S. Wolfbeis, *Fiber Optic Chemical Sensors and Biosensors*, CRC, Boca Raton, FL, 1991.
- 27 D.W. Lübbers, in A.P.F. Turner (Ed.), *Advances in Biosensors, Vol. 2*, JAI Press, London, 1992, pp. 215–260.
- 28 S.M. Ramasamy and R.J. Hurtubise, *Anal. Chem.*, 59 (1987) 432.
- 29 S.M. Ramasamy and R.J. Hurtubise, *Anal. Chem.*, 59 (1987) 2144.
- 30 S.M. Ramasamy and R.J. Hurtubise, *Anal. Chem.*, 60 (1990) 1060.
- 31 S.M. Ramasamy and R.J. Hurtubise, *Appl. Spectrosc.*, 46 (1992) 472.
- 32 T. Vo-Dinh, G.L. Walden and J.D. Winefordner, *Anal. Chem.*, 49 (1977) 1126.
- 33 A.D. Campiglia, A. Berthod and J.D. Winefordner, *Anal. Chim. Acta*, 231 (1990) 289.
- 34 L.A. Citta and R.J. Hurtubise, *Appl. Spectrosc.*, 45 (1991) 1547.
- 35 D.L. McAleese and R.B. Dunlap, *Anal. Chem.*, 56 (1984) 2244.
- 36 J.B.F. Lloyd, *Analyst*, 103 (1978) 775.
- 37 Y.M. Liu, R. Pereiro, M.E. Díaz and A. Sanz-Medel, *Anal. Chim. Acta*, 255 (1991) 245.
- 38 A. Sanz-Medel, M.E. Díaz, Y.M. Liu and M.R. Pereiro, presented at the 1st European Conference on Optical Sensors, Graz, Austria, 1992.
- 39 A. Sanz-Medel, Y.M. Liu, R. Pereiro and M.E. Díaz, *Spanish Pat. Appl.*, 1992.
- 40 R. Pereiro, M.E. Díaz, F. Alava and A. Sanz-Medel, *Clin. Chim. Acta*, 207 (1992) 31.
- 41 W.E. Hornby and D.L. Morris, in H.H. Wheetal (Ed.), *Immobilized Enzymes, Antigens, Antibodies and Peptides*, Marcel Dekker, New York, 1975.
- 42 M.J. Valencia, M.E. Díaz and A. Sanz-Medel, presented at the 12th International Symposium on Microchemical Techniques, Cordoba, 1992.
- 43 F. Alava, MSc Thesis, University of Oviedo, Oviedo, 1992.
- 44 M.D. Richmond and R.J. Hurtubise, *Anal. Chem.*, 63 (1991) 169.
- 45 M.D. Richmond and R.J. Hurtubise, *Anal. Chem.*, 63 (1991) 1073.
- 46 J.J. Aaron, A.D. Campiglia and J.D. Winefordner, *Anal. Chim. Acta*, 236 (1990) 257.
- 47 A. Pal, W. Watts, J. Caraway and T. Vo-Dinh, *Analisis*, 20 (1992) 149.
- 48 A.M. Alak, N. Contolini and T. Vo-Dinh, *Anal. Chim. Acta*, 217 (1989) 171.
- 49 Y.M. Liu, J.I. García Alonso, M.R. Fernández de la Campa, M.E. Díaz García and A. Sanz-Medel, *Mikrochim. Acta*, 1 (1991) 199.

# Flow-injection chemiluminescence determination of cobalt(II) and manganese(II)

Qingxiong Lin, Alfonso Guiraúm and Rosario Escobar

*Departamento de Química Analítica, Facultad de Química, Universidad de Sevilla, 41012 Seville (Spain)*

Francisco F. de la Rosa

*Instituto de Bioquímica Vegetal y Fotosíntesis, Facultad de Biología, Universidad de Sevilla y CSIC, 41012 Seville (Spain)*

(Received 10th September 1992; revised manuscript received 1st December 1992)

## Abstract

Flow-injection analysis (FIA) was applied to the determination of Co(II) and Mn(II). The method is based on the measurement of metal-catalysed light emission from luminol oxidation by potassium periodate. The apparatus consists of a flow-injection analysis system with a flow cell formed by a spiral of transparent tubing suitable for chemiluminescence measurement. Potassium periodate, unlike hydrogen peroxide, which is the oxidant normally used in luminol chemiluminescence systems, is very stable, gives a low baseline and does not generate bubbles in the tubes of the FIA system. The typical signal is a narrow peak, in which the height is proportional to the light emitted and hence to the concentration of metal ions. The detection limit of Co(II) is  $0.01 \text{ ng ml}^{-1}$  and the linear range extends up to  $12 \text{ ng ml}^{-1}$ ; for Mn(II) these limits are 0.02 and  $9 \text{ ng ml}^{-1}$ , respectively. The optimum concentrations for the reagents are  $10^{-3} \text{ M}$  luminol in  $\text{Na}_2\text{CO}_3$ -KOH buffer (pH 12.9) and  $10^{-4} \text{ M}$   $\text{KIO}_4$  in water. The optimum flow-rates are water  $11.1 \text{ ml min}^{-1}$ , luminol  $2.5 \text{ ml min}^{-1}$  and  $\text{KIO}_4$  solution  $2.1 \text{ ml min}^{-1}$ . Interferences by several metal ions were examined.

**Keywords:** Chemiluminescence; Flow injection; Cobalt; Manganese; Waters

The sensitivity of the chemiluminescence (CL) reaction of luminol with hydrogen peroxide in the presence of trace concentrations of certain metal ions is well known [1]. Thus, the reaction is of analytical interest for the determination of species such as Cr(III) [2], Mn(II) [3], Fe(II) [4], Fe(III) [5], Co(II) [6] and Cu(II) [7].

Certain metal ions, or metal-containing species, have been reported to cause CL by luminol oxidation in aqueous solution in the absence of hydrogen peroxide. These chemical species include Fe(II) [8],  $\text{Fe}(\text{CN})_6^{3-}$  [9],  $\text{MnO}_4^-$  [1],  $\text{AuCl}_4^-$

[10],  $\text{SbCl}_6^-$  [11] and V(IV) [12]. Several luminol-CL systems containing  $\text{K}_2\text{S}_2\text{O}_8$  as an oxidant have been described for testing Ag(I) [13], Al(III) [14], Zn(II) [14], V(V) [14] and containing  $\text{KIO}_4$  for Ir(IV) [15], Rh(IV) [15], Ru(IV) [16], V(V) [17] and Mn(II) [18].

It is well known that periodate solution is much more stable than hydrogen peroxide solution. Thus, in flow-injection analysis (FIA) systems, potassium periodate, unlike hydrogen peroxide, does not generate bubbles in tubing and gives a low baseline. All of this makes the use of periodate as an oxidant very convenient for operation in FIA systems.

This paper describes a simple and automatic technique for the sensitive determination of

*Correspondence to:* R. Escobar, Departamento de Química Analítica, Facultad de Química, Universidad de Sevilla, 41012 Seville (Spain).

Co(II) and Mn(II) with the luminol–KIO<sub>4</sub> CL reaction by FIA. In the presence of quinolin-8-ol, only Mn(II) catalyses the luminescence reaction, most ions encountered being masked. Using sodium citrate as a masking reagent, Co(II) and Mn(II) are simultaneously measured, the Co(II) concentration being obtained by the subtraction of the amount of Mn(II) determined in the presence of quinolin-8-ol. The proposed method was applied to the determination of Mn(II) and Co(II) in water samples and vitamin B<sub>12</sub>.

## EXPERIMENTAL

### Instrumentation and procedures

Co(II) and Mn(II) catalysis of luminol oxidation by periodate generating CL was carried out in the FIA system shown in Fig. 1. A four-channel peristaltic pump (Gilson Minipuls 2) is used to pump reagents and sample. Luminol and KIO<sub>4</sub> working solutions are first mixed in a flow stream and then with the flowing water. A 0.32-ml sample is injected into the mixed solution and driven through the flow cell. The flow cell is a transparent coil of 1 mm i.d. PTFE tubing positioned near the photodetector. The light intensity is continuously measured using a Hamamatsu photomultiplier in an Aminco housing and connected to a Knauer recorder. The injection valve and tubing system were obtained from Scharlau Science (FRG).

### Reagents and solutions

All reagents were of analytical-reagent grade. Water was obtained from a Milli-Q purification system (Millipore).

*Co(II) stock standard solution (1 mg ml<sup>-1</sup>).* A 0.4939-g amount of Co(NO<sub>3</sub>)<sub>2</sub> · 6H<sub>2</sub>O (Merck) was dissolved in water in a 100-ml volumetric flask and diluted to volume. Working standard solutions were prepared by diluting this stock solution with water.

*Mn(II) stock standard solution (1 mg ml<sup>-1</sup>).* A 0.3077-g amount of MnSO<sub>4</sub> · H<sub>2</sub>O (Merck) was dissolved in water in a 100-ml volumetric flask and diluted volume with water. Working standard solutions were prepared by diluting this stock solution with water.

*Luminol stock standard solution (0.01 M).* A 0.1772-g amount of luminol (Sigma) was dissolved in 3.5 ml of 1 M KOH solution in a 100-ml volumetric flask and diluted to volume with water. It was stored for more than 1 week before use.

*Luminol working standard solution (0.001 M).* A 15-ml volume of 1 M KOH, 75 ml of 0.2 M Na<sub>2</sub>CO<sub>3</sub> and 10 ml of the 0.01 M luminol solution were mixed.

*KIO<sub>4</sub> stock standard solution (0.01 M).* A 0.23-g amount of KIO<sub>4</sub> was dissolved in 100 ml of water. A 3 × 10<sup>-4</sup> M working standard solution was obtained by dilution of the stock standard solution. These solutions remain stable more than 1 month.

*Quinolin-8-ol (0.002 M).* A 0.073-g amount was dissolved in 250 ml of water.

*Treatment of vitamin B<sub>12</sub> solution.* The vitamin was weighed and dissolved in water. A 5-ml volume of the vitamin solution and the same amount of concentrated nitric acid were heated until dry. The residue was dissolved in a small volume of water, transferred into a 50-ml volumetric flask and diluted to volume with water.

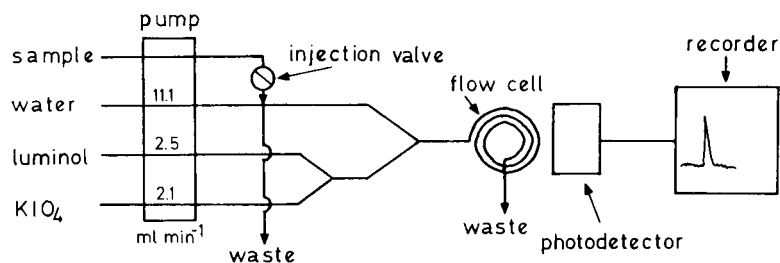


Fig. 1. Schematic diagram of the flow-injection assembly for chemiluminescence monitoring used for the determination of Co(II) and Mn(II).

## RESULTS AND DISCUSSION

*Optimization of assay conditions*

The effect of luminol concentration on the CL intensity for Co(II) and Mn(II) is shown in Fig. 2. The increase in the signal at a concentration above 0.001 M luminol is small and this value was chosen for the remainder of the studies.

The variation of the intensity with  $\text{KIO}_4$  concentration is shown in Fig. 3. For Co(II) the maximum response was obtained at  $\text{KIO}_4$  concentrations between  $1 \times 10^{-4}$  and  $3 \times 10^{-4}$  M. For Mn(II), the light emission increases proportionally with the  $\text{KIO}_4$  concentration below  $3 \times 10^{-4}$  M and decreases above  $3 \times 10^{-4}$  M. Therefore,  $3 \times 10^{-4}$  M  $\text{KIO}_4$  was adapted for the determination of both Co(II) and Mn(II).

The optimum pH was investigated by varying the proportion of  $\text{Na}_2\text{CO}_3$  to KOH in the luminol solution. In Fig. 4, the influence of pH on the CL intensity is shown. Both the Co(II) and Mn(II) profiles showed a maximum at pH 12.9 and this pH was selected for subsequent analyses.

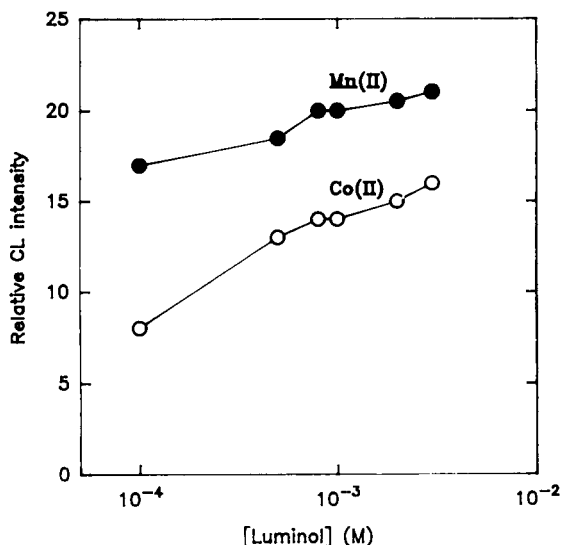


Fig. 2. Variation of chemiluminescence intensity with luminol concentration. Conditions: luminol in 0.15 M  $\text{Na}_2\text{CO}_3$  and 0.15 M KOH, pH 12.9;  $3 \times 10^{-4}$  M  $\text{KIO}_4$  in aqueous solution;  $1 \text{ ng ml}^{-1}$  Co(II) or Mn(II) in  $3 \times 10^{-4}$  M  $\text{H}_3\text{PO}_4$ . Flow-rates: water,  $11.1 \text{ ml min}^{-1}$ ; luminol,  $2.5 \text{ ml min}^{-1}$ ;  $\text{KIO}_4$ ,  $2.1 \text{ ml min}^{-1}$ . Injection volume: 0.32 ml.

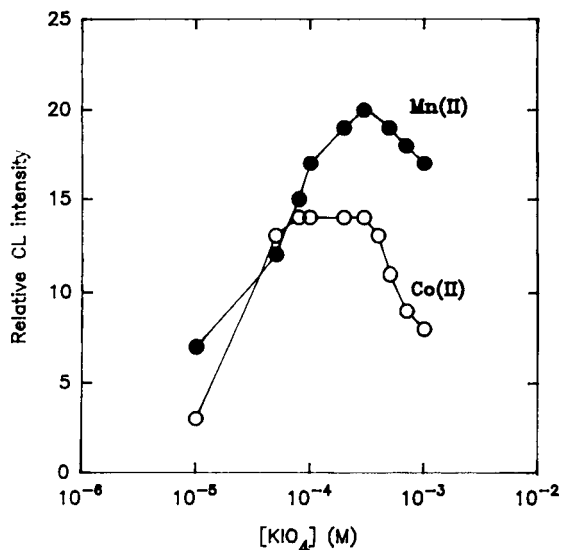


Fig. 3. Variation of chemiluminescence intensity with  $\text{KIO}_4$  concentration. Conditions: 0.001 M luminol in 0.15 M  $\text{Na}_2\text{CO}_3$  and 0.15 M KOH, pH 12.9;  $\text{KIO}_4$  in aqueous solution;  $1 \text{ ng ml}^{-1}$  Co(II) or Mn(II) in  $3 \times 10^{-4}$  M  $\text{H}_3\text{PO}_4$ . Flow-rates: water,  $11.1 \text{ ml min}^{-1}$ ; luminol,  $2.5 \text{ ml min}^{-1}$ ;  $\text{KIO}_4$ ,  $2.1 \text{ ml min}^{-1}$ . Injection volume, 0.32 ml.

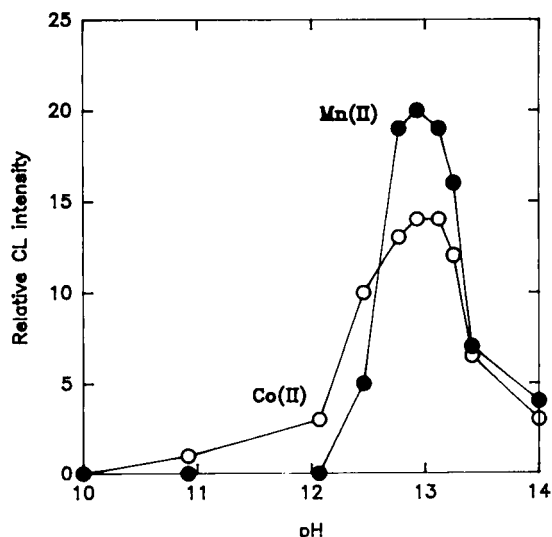


Fig. 4. Influence of pH on chemiluminescence intensity. Conditions: 0.001 M luminol in  $\text{Na}_2\text{CO}_3$ -KOH solution;  $3 \times 10^{-4}$  M  $\text{KIO}_4$  in aqueous solution;  $1 \text{ ng ml}^{-1}$  Co(II) or Mn(II) in  $3 \times 10^{-4}$  M  $\text{H}_3\text{PO}_4$ . Flow-rates: water,  $11.1 \text{ ml min}^{-1}$ ; luminol,  $2.5 \text{ ml min}^{-1}$ ;  $\text{KIO}_4$ ,  $2.1 \text{ ml min}^{-1}$ . Injection volume: 0.32 ml.

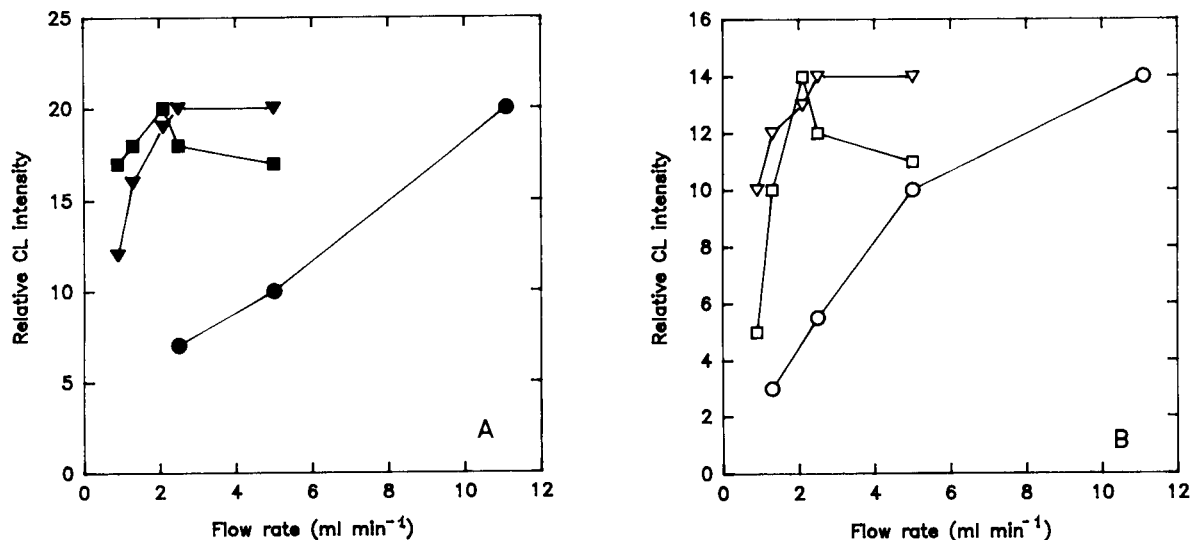


Fig. 5. Influence of flow-rates of (▼) luminol, (■) KIO<sub>4</sub> and (●) water on chemiluminescence intensity for (A) manganese and (B) cobalt determination. Conditions: 0.001 M luminol in 0.15 M Na<sub>2</sub>CO<sub>3</sub> and 0.15 M KOH, pH 12.9; 3 × 10<sup>-4</sup> M KIO<sub>4</sub> in aqueous solution; 1 ng ml<sup>-1</sup> Mn(II) or Co(II) in 3 × 10<sup>-4</sup> M H<sub>3</sub>PO<sub>4</sub>. Flow-rates as indicated. Injection volume: 0.32 ml.

As described previously [19], for the determination of chromium with a similar CL system, the intensity of the emission was dependent on the rate of mixing of the sample and reagents. The flow-rates that gave the most intense signals for both Co(II) and Mn(II), as deduced from Fig. 5, were 2.1 ml min<sup>-1</sup> for KIO<sub>4</sub>, 2.5 ml min<sup>-1</sup> for luminol and 11.1 ml min<sup>-1</sup> for water. These values were used in subsequent analyses.

The influence of H<sub>3</sub>PO<sub>4</sub> concentration on the CL intensity was investigated (data not shown). The maximum emission of light for both Co(II) and Mn(II) determinations was obtained with a concentration of 3 × 10<sup>-4</sup> M H<sub>3</sub>PO<sub>4</sub>. Hence this concentration was used in the assay of water samples.

Quinolin-8-ol was investigated as a masking reagent in the determination of Mn(II). As shown in Fig. 6, its effect on Co(II) and Mn(II) determinations is different; 1 ng ml<sup>-1</sup> of Co(II) can be completely masked by > 5 × 10<sup>-6</sup> M quinolin-8-ol, whereas > 1 × 10<sup>-5</sup> M quinolin-8-ol is necessary to decrease the light intensity when 1 ng ml<sup>-1</sup> of Mn(II) is added. Therefore, 1 × 10<sup>-5</sup> M

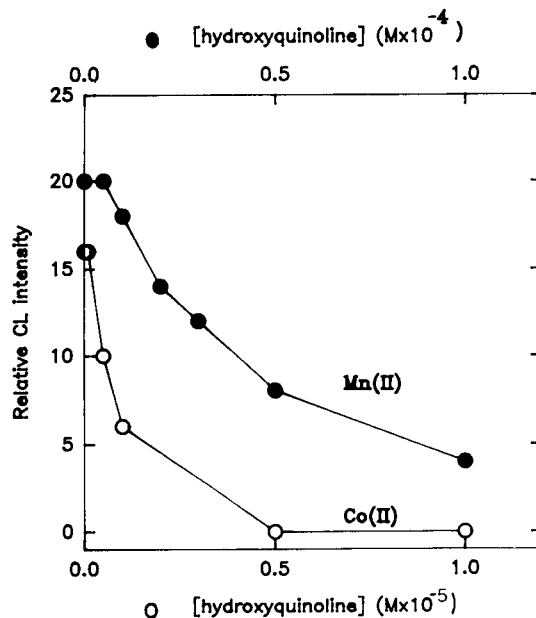


Fig. 6. Influence of quinolin-8-ol concentration on chemiluminescence intensity. Conditions: 0.001 M luminol in 0.15 M Na<sub>2</sub>CO<sub>3</sub> and 0.15 M KOH, pH 12.9; 3 × 10<sup>-4</sup> M KIO<sub>4</sub> in aqueous solution; 1 ng ml<sup>-1</sup> Co(II) or Mn(II) in 3 × 10<sup>-4</sup> M H<sub>3</sub>PO<sub>4</sub> and quinolin-8-ol at the indicated concentrations. Flow-rates: water, 11.1 ml min<sup>-1</sup>; luminol, 2.5 ml min<sup>-1</sup>; KIO<sub>4</sub>, 2.1 ml min<sup>-1</sup>. Injection volume: 0.32 ml.

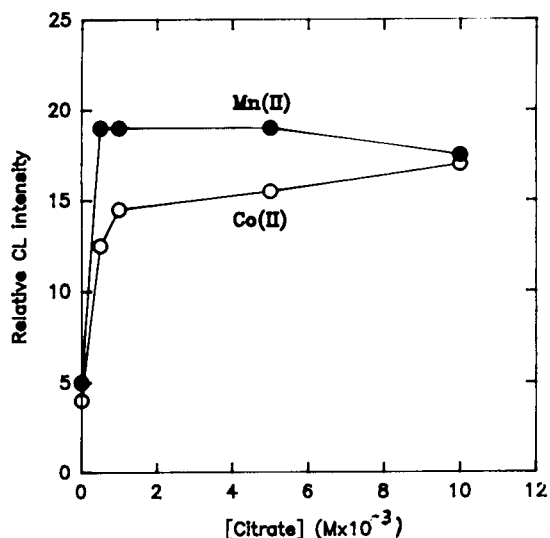


Fig. 7. Influence of sodium citrate concentration on chemiluminescence intensity. Conditions: 0.001 M luminol in 0.15 M  $\text{Na}_2\text{CO}_3$  and 0.15 M KOH, pH 12.9;  $3 \times 10^{-4}$  M  $\text{KIO}_4$  in aqueous solution;  $1 \text{ ng ml}^{-1}$  Co(II) or Mn(II) in sodium citrate solution at the indicated concentrations. Flow-rates: water,  $11.1 \text{ ml min}^{-1}$ ; luminol,  $2.5 \text{ ml min}^{-1}$ ;  $\text{KIO}_4$ ,  $2.1 \text{ ml min}^{-1}$ . Injection volume: 0.32 ml.

quinolin-8-ol was selected as the masking reagent for the determination of Mn(II).

Sodium citrate was used as a masking reagent for the simultaneous determination of Co(II) and Mn(II). Without sodium citrate, the pH of Co(II) and Mn(II) solutions must be adjusted to  $> 3.5$  to minimize hydrolysis. With citrate, the pH of the samples does not influence the CL. Figure 7 shows that the CL intensity increases in the presence of citrate. However, citrate also enhances the CL of the blank solution, probably by complexing trace contaminant. Moreover, higher concentrations of citrate increase the CL of the blank. Hence a high concentration of citrate is detrimental to the system. A concentration of 0.005 M citrate was chosen as the most efficient for further studies.

The injection volume also influences the CL intensity; 0.35 ml gave the most intense signal, and so was selected for subsequent analyses.

### Interferences

In addition to Co(II) and Mn(II), several metal ions, such as Fe(III), Ti(IV), V(V) and Mo(VI), catalyse the luminol–periodate CL reaction. Others, such as Cu(II), Pb(II), Ni(II), Cd(II), In(III) and Ce(IV), inhibit the CL. Table 1 lists the ions that were tested for interferences and their tolerance levels. In the presence of  $1 \times 10^{-5}$  M quinolin-8-ol in a sample, commonly encountered ions, except Mn(II), can be masked (Table 1). Although only  $\leq 10 \text{ ng ml}^{-1}$  Co(II) can be masked, it is good enough to test many samples, such as water. Hence this can be considered to be a highly sensitive and selective method for the determination of Mn(II). Using sodium citrate as a masking agent, without quinolin-8-ol, many ions other than Co(II) and Mn(II) can be masked. Hence traces of Co(II) and Mn(II) can be simultaneously determined in the presence of citrate. The Co(II) concentration alone can be obtained by subtraction of Mn(II) concentration (obtained by quinolin-8-ol masking) from the total. Quinolin-8-ol and citrate mixed solution can mask greater amounts of metals but the CL intensity of the blank is much higher and increases with time, making this mixture unsuitable.

TABLE 1

Tolerance levels of interferences in the determination of Co(II) and Mn(II)

Ions added	Tolerance level <sup>a</sup> ( $\mu\text{g ml}^{-1}$ )	Tolerance level <sup>b</sup> ( $\mu\text{g ml}^{-1}$ )
$\text{F}^-$ , $\text{Cl}^-$ , $\text{Br}^-$ , $\text{I}^-$	$> 10$	$> 10$
Ba(II), Ca(II), Mg(II)	5	5
Cr(VI), Zn(II)	$> 1$	$> 1$
Th(IV), V(V)	1	$> 1$
In(III), Hg(II)	0.1	$> 1$
Fe(III), Cu(II), Cr(III), Ce(IV)	0.1	1
Mo(VI)	0.1	0.1
Pb(II)	0.1	0.2
Cd(II), Ni(II)	0.05	0.2
Ti(IV)	0.02	0.1
Co(II)	–	0.01

<sup>a</sup>  $1 \text{ ng ml}^{-1}$  Co(II) or  $1 \text{ ng ml}^{-1}$  Mn(II) was determined using  $5 \times 10^{-3}$  M sodium citrate as a masking agent. <sup>b</sup>  $1 \text{ ng ml}^{-1}$  Mn(II) was determined using  $1 \times 10^{-5}$  M quinolin-8-ol as a masking agent.



### Calibration graphs

In the presence of quinolin-8-ol as a masking agent, the Mn(II) log–log calibration graph, under the optimum conditions, was linear from 0.02 up to 9 ng ml<sup>-1</sup> Mn(II) with a slope of 1.340. With citrate as a masking agent, the equivalent linear range extends from 0.01 to 12 ng ml<sup>-1</sup> for Co(II) and from 0.06 to 7 ng ml<sup>-1</sup> for Mn(II). In this instance, the slopes are 1.333 for Mn(II) and 1.061 for Co(II) (Fig. 8).

Under the optimum conditions, the relative standard deviation (15 replicates) for 1 ng ml<sup>-1</sup> Co(II) is 4.3% and for 1 ng ml<sup>-1</sup> Mn(II) it is 2.1%. The limits of detection are 0.02 ng ml<sup>-1</sup> for Mn(II) and 0.01 ng ml<sup>-1</sup> for Co(II). These limits of detection were obtained, as indicated by IUPAC, following the method of Long and Winefordner [20].

### Applications

**Water samples.** To measure Mn(II) in water samples, phosphoric acid was added to give a concentration of  $3 \times 10^{-4}$  M, and the solution was made  $1 \times 10^{-5}$  M in quinolin-8-ol. For the determination of Co(II), the sample was made  $5 \times 10^{-3}$  M in sodium citrate, Co(II) plus Mn(II) were determined. The concentration of Co(II) was calculated by subtracting the concentration of Mn(II) (as described above). Table 2 gives the results obtained for different samples of fresh and polluted water.

**Vitamin B<sub>12</sub>.** Vitamin B<sub>12</sub> is a tetrapyrrole complex containing an atom of cobalt. The com-

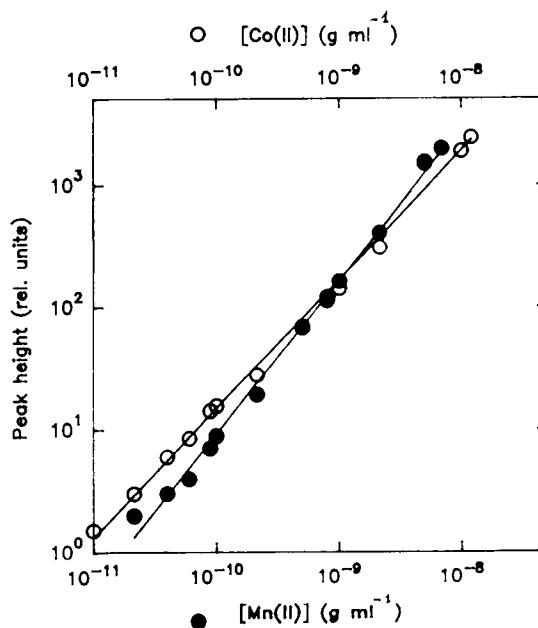


Fig. 8. Calibration graphs for the determination of Mn(II) and Co(II) with  $5 \times 10^{-5}$  M citrate as masking agent. Conditions: 0.001 M luminol in 0.15 M Na<sub>2</sub>CO<sub>3</sub> and 0.15 M KOH, pH 12.9;  $3 \times 10^{-4}$  M KIO<sub>4</sub> in aqueous solution; Mn(II) and Co(II) in  $3 \times 10^{-4}$  M H<sub>3</sub>PO<sub>4</sub>. Flow-rates: water, 11.1 ml min<sup>-1</sup>; luminol, 2.5 ml min<sup>-1</sup>; KIO<sub>4</sub>, 2.1 ml min<sup>-1</sup>. Injection volume: 0.32 ml.

plex does not catalyse light emission by the system. However, when the vitamin B<sub>12</sub> is acidified, Co(II) will be set free and catalyse the CL reaction. Co(II) was determined by using 0.005 M sodium citrate as a masking reagent. The determination of Co(II) in a sample of pure vitamin

TABLE 2

Results of the determination of Co(II) and Mn(II) in different samples <sup>a</sup>

Sample	Mn(II) in sample (ng ml <sup>-1</sup> )	Co(II) in sample (ng ml <sup>-1</sup> )	Mn(II) added (ng ml <sup>-1</sup> )	Recovery (%)	Co(II) added (ng ml <sup>-1</sup> )	Recovery (%)
Fresh water <sup>b</sup> :						
Sample 1	4.7	0.4	0.2	108	0.2	93
Sample 2	7.0	1.5	0.2	102	0.2	98
Sample 3	4.8	0.3	0.2	105	0.2	99
Polluted water <sup>c</sup> :						
Sample 1	4.7	0.3	0.2	93	0.2	108
Sample 2	4.4	0.3 <sub>5</sub>	0.2	110	0.2	103

<sup>a</sup> Results are averages from more than three replicates. <sup>b</sup> The samples of fresh water are from the mains of the city of Seville taken from different sites. <sup>c</sup> Polluted water, samples are from the Guadalquivir river.

B<sub>12</sub> was found to be 3.64% (w/w), a 93% recovery.

### Conclusions

The proposed method is very sensitive and shows good reproducibility. The use of KIO<sub>4</sub>, unlike hydrogen peroxide, prevents the formation of bubbles in the tubing system. The method is rapid and up to 70 samples per hour can be analysed. This method can be used to determine Mn(II) and Co(II) at the ng ml<sup>-1</sup> level in water and Co(II) in vitamin B<sub>12</sub>.

This work was supported by Plan Andaluz de Investigacion. Q.-X. Lin is grateful for financial help from Consejería de Educación of Junta de Andalucía.

### REFERENCES

- 1 W.R. Seitz and D.M. Hercules, in M.J. Cormier, D.M. Hercules and J. Lee (Eds.), *Chemiluminescence and Bioluminescence*, Plenum, New York, 1973, pp. 427–449.
- 2 W.R. Seitz, W.W. Suydam and D.M. Hercules, *Anal. Chem.*, 44 (1972) 957.
- 3 J.L. Burguera and A. Townshend, *Talanta*, 28 (1981) 731.
- 4 C.A. Chang and H.H. Patterson, *Anal. Chem.*, 52 (1980) 653.
- 5 A.T. Philipenko, A.V. Terletskaia and T.A. Bogoslovskaya, *Zh. Anal. Khim.*, 41 (1986) 498.
- 6 J.L. Burguera, A. Townshend and S. Greenfield, *Anal. Chim. Acta*, 114 (1980) 209.
- 7 A.K. Babko and K.I. Dubovenko, *Fresenius' Z. Anal. Chem.*, 200 (1964) 428.
- 8 W.R. Seitz and D.M. Hercules, *Anal. Chem.*, 44 (1972) 2143.
- 9 A.J. Moss, W.A. Nagle and M.L. Baker, *Photobiochem. Photobiophys.*, 2 (1981) 271.
- 10 N.M. Lukovskaya and T.A. Bogoslovskaya, *Ukr. Khim. Zh. (Russ. Ed.)*, 41 (1975) 268.
- 11 V.K. Zinchuk and A.I. Komlev, *Zh. Anal. Khim.*, 28 (1973) 616.
- 12 A.T. Philipenko, E.V. Mitropolitskaya and N.M. Lukovskaya, *Ukr. Khim. Zh. (Russ. Ed.)*, 41 (1975) 1196.
- 13 A.T. Philipenko, A.V. Terletskaia, T.A. Bogoslovskaya and N.M. Lukovskaya, *Zh. Anal. Khim.*, 38 (1983) 807.
- 14 X.-N. Zhang Xinong and Z.-J. Zhang, *Huaxue Xuebao*, 45 (1987) 195.
- 15 N.M. Lukovskaya and N.F. Kushchevsaya, *Ukr. Khim. Zh. (Russ. Ed.)*, 42 (1976) 87.
- 16 N.M. Lukovskaya and A.V. Terletskaia, *Zh. Anal. Khim.*, 31 (1976) 751.
- 17 A.T. Philipenko, E.V. Mitropoliske and N.M. Lukovskaya, *Ukr. Khim. Zh. (Russ. Ed.)*, 39 (1973) 73.
- 18 Z. Geng, Z.-G. Zhang and L.-J. Bian, *Gaodeng Xuexiao Huaxue Xuebao*, 9 (1988) 1114.
- 19 R. Escobar, Q.-X. Lin, A. Giraúm and F.F. de la Rosa, *Analyst*, in press.
- 20 G.L. Long and J.D. Winefordner, *Anal. Chem.*, 55 (1983) 712A.

# Flow-injection and continuous-flow systems for the determination of Se(IV) and Se(VI) by hydride generation atomic absorption spectrometry with on-line prereduction of Se(VI) to Se(IV)

M. Gloria Cobo Fernandez, Maria A. Palacios and Carmen Camara

*Department of Analytical Chemistry, Faculty of Chemistry, Complutense University of Madrid, 28040 Madrid (Spain)*

(Received 10th September 1992; revised manuscript received 7th December 1992)

## Abstract

The on-line reduction of Se(VI) to Se(IV) and subsequent determination of Se(IV) by flow injection-hydride generation atomic absorption spectrometry are proposed. To reduce Se(VI) quantitatively to Se(IV), the sample is acidified with concentrated HCl and the sample coil is heated to 140°C. Hydride generation is performed in an ice-bath to prevent decomposition of the NaBH<sub>4</sub>. The sensitivity of the proposed method is about twice that of the traditional method without heating, the relative standard deviation is below 5%, the recovery is 95–105% and the selectivity is significantly increased. No Se losses occur because the reduction system is closed until the selenium hydride reaches the phase separator. The method has been successfully applied to the determination of Se(IV) and Se(VI) in sea water.

**Keywords:** Atomic absorption spectrometry; Flow system; Continuous flow; Hydride generation; Sea water; Selenium; Speciation

Although selenium levels in ground and surface waters are generally low (less than 10 ng ml<sup>-1</sup>), high concentrations of this element may occur in association with geological features or due to the corrosion of household plumbing by soft, acidic water [1]. Also, at high water pH, selenite may be oxidized to soluble selenate, hence increasing the aqueous selenium concentration to 10–400 ng ml<sup>-1</sup> [2]. The selenium concentration of sea water is generally low (4 pg ml<sup>-1</sup> at the surface and 60 pg ml<sup>-1</sup> in deep water as selenite, and 30 pg ml<sup>-1</sup> at the surface and 120 pg ml<sup>-1</sup> in deep water as selenate [3]), but these

concentrations may increase in the future as a result of the estimated 8000 tons of selenium which are introduced annually into the sea [4]. As the biological effects of selenium are known to depend on its chemical form [Se(IV) is more toxic than Se(VI)], it is important to measure the amount of each selenium species in the environment. Although the pH–pE relationship in water predicts which form of selenium is the more stable under any given conditions, there are contradictory reports on the [Se(IV)]:[Se(VI)] ratio in different natural waters [5].

When tetrahydroborate is used as the reductant in the determination of selenium by hydride generation atomic absorption spectrometry (HG-AAS), only SeH<sub>2</sub> is formed from Se(IV); therefore, to determine the amount of Se(VI), a pre-

*Correspondence to:* C. Camara, Department of Analytical Chemistry, Faculty of Chemistry, Complutense University of Madrid, 28040 Madrid (Spain).

duction step is necessary to reduce Se(VI) to Se(IV). Although several reducing agents have been proposed, such as KI and HBr [6], by far the best results are obtained with hydrochloric acid [7]. A batch system gives a reduction efficiency of about 98% in 4–7 M HCl at 120°C reduction for times of 20–45 min [8]. However selenium may be lost from batch open systems owing to the formation of volatile selenium chloride or other volatile compounds. On-line reduction in a closed system at 140°C (40°C hotter than the usual water-bath) prevents losses of selenium during the prerelution step and provides reducing conditions.

This paper proposes inorganic selenium speciation analysis using an on-line prerelution system coupled to HG-AAS.

## EXPERIMENTAL

### Apparatus

The continuous-flow and FI systems are shown in Fig. 1. In the FI system, the sample is injected into the continuous HCl flow through a six-way valve (Omnifit).

The heating system for on-line reduction of

Se(VI) to Se(IV) is a laboratory-made powdered graphite bath at 140°C. The cooling system is an ice-bath. Hydrogen selenide is generated in the cooled system in order to prevent uncontrolled decomposition of NaBH<sub>4</sub> during hydride generation.

In the continuous-flow system, the sample (previously acidified) and HCl, pumped with a Gilson HP-4 peristaltic pump, are mixed in the first coil and then pass through a heated tube to reduce Se(VI) to Se(IV). The mixture and NaBH<sub>4</sub> are cooled in the cooling system before they enter the reaction coil (0.5 mm i.d.), where the selenium is reduced with NaBH<sub>4</sub>. The hydride formed is carried by argon through the U-tube gas-liquid separator (Philips) to the quartz cell.

A Perkin-Elmer Model 2380 atomic absorption spectrometer equipped with a selenium electrodeless discharge lamp operated with a 6-W power supply was used for all determinations. A spectral bandwidth of 0.7 nm was selected. Signals were recorded on a Perkin-Elmer Model 56 recorder.

### Reagents

All reagents were of analytical-reagent grade or higher purity from Aldrich or Carlo Erba and deionized water from a Milli-Q system (Millipore) was used throughout.

Selenium(IV) stock standard solution (1000 µg ml<sup>-1</sup>) was prepared by dissolving 0.5531 g of sodium selenite in water and diluting to 250 ml. Working standard solutions were prepared daily.

Selenium(VI) stock standard solution (1000 µg ml<sup>-1</sup>) was prepared by dissolving 0.6104 g of sodium selenate in water and diluting to 250 ml. Working standard solutions were prepared daily.

Sodium tetrahydroborate (NaBH<sub>4</sub>) solution (0.5%, w/v) was prepared by dissolving NaBH<sub>4</sub> powder in water and stabilizing with 0.16% (w/v) sodium hydroxide solution. Solutions were filtered before use to eliminate turbidity.

### Procedure

Selenium(IV) and -(VI) speciation analysis was carried out in two steps.

*Determination of selenium(IV).* The sample was pumped in the continuous-flow manifold or in-

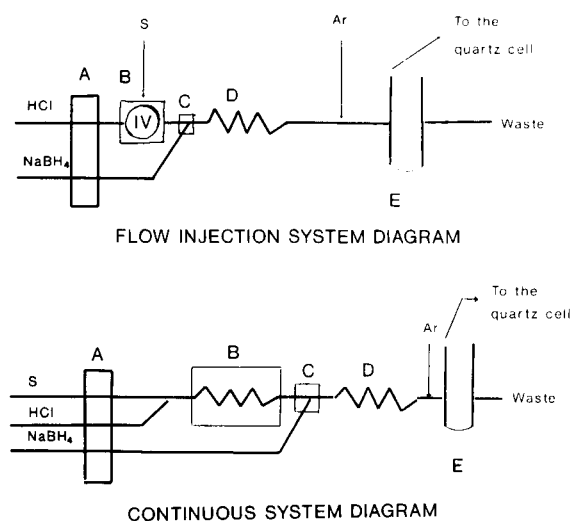


Fig. 1. FI and continuous-flow systems. A = Peristaltic pump; B = heating system; C = cooling system; D = reaction coil; E = gas-liquid separator (U-tube).

TABLE 1

Analytical parameters for hydride generation with and without prereduction

Parameter	FI system	Continuous-flow system
Argon flow-rate	17.5 l h <sup>-1</sup>	17.5 l h <sup>-1</sup>
Pumping speed	1.5 ml min <sup>-1</sup>	1.5 ml min <sup>-1</sup>
[NaBH <sub>4</sub> ]	0.5% (w/v)	0.5% (w/v)
[HCl]		
(without prereduction)	4 M	4 M
[HCl]		
(sample for prereduction)	6 M	6 M
[HCl]		
(with prereduction)	12 M	12 M

jected into the FI system. Hydrogen selenide was generated using 0.5% (w/v) NaBH<sub>4</sub> solution in 4 M HCl in both systems.

*Determination of total selenium.* The sample was previously acidified by adding HCl to a concentration of ca. 6 M. Total selenium was determined after on-line reduction of selenium(VI) to selenium(IV). Hydrogen selenide was generated in the cooled system using 0.5% (w/v) NaBH<sub>4</sub> solution in 12 M HCl in both systems. The Se(VI) concentration was calculated as the difference between total Se and Se(IV). The standard additions method was used in all instances and peaks were recorded as peak height.

## RESULTS AND DISCUSSION

To optimize the conditions for on-line reduction and H<sub>2</sub>Se generation from Se(IV) and Se(VI), the following chemical and physical parameters were adjusted (Table 1).

### Argon flow-rate

The flow-rate of the argon stream used to transport hydrogen selenide was varied from 2.5 to 20 l h<sup>-1</sup>. As shown in Fig. 2, the analytical signal in the continuous-flow system decreases with increasing argon flow-rate in the range 5–9 l h<sup>-1</sup> and then increases with increasing argon flow-rate in the range 9–20 l h<sup>-1</sup>. As the standard deviation is lower in the latter than in the

former range, an argon flow-rate of 17.5 l h<sup>-1</sup> was chosen for subsequent work. In the FI system the signal increased continuously with increasing argon flow-rate. A flow-rate of 17.5 l h<sup>-1</sup> was chosen. The different NaBH<sub>4</sub> concentrations used (3% and 0.5% for H<sub>3</sub>Sb and H<sub>2</sub>Se, respectively) for the two analytes could explain the different behaviour caused by the argon flow-rate. This observation contradicts the results of previous experiments on Sb [9], where the signal decreased with increasing argon flow-rate, becoming negligible at 15 l h<sup>-1</sup>.

### Influence of pumping speed

To evaluate this parameter, the sample, HCl and NaBH<sub>4</sub> were pumped over the range 500–900 rev h<sup>-1</sup> with a tube diameter of 0.5 mm (1.0–1.9 ml min<sup>-1</sup>). In both FI and continuous-flow systems the analytical signal increased and became more nearly perfectly shaped with increasing pumping speed.

A pumping speed of 800 rev h<sup>-1</sup> (1.5 ml min<sup>-1</sup>) was chosen for further experiments in both systems.

### Influence of length and configuration of the reaction coil

Five different lengths, 10, 20, 30, 40 and 50 cm of the reaction coil (0.5 mm i.d.) were studied. No influence on the absorbance or signal shape was observed in either the FI or continuous-flow sys-

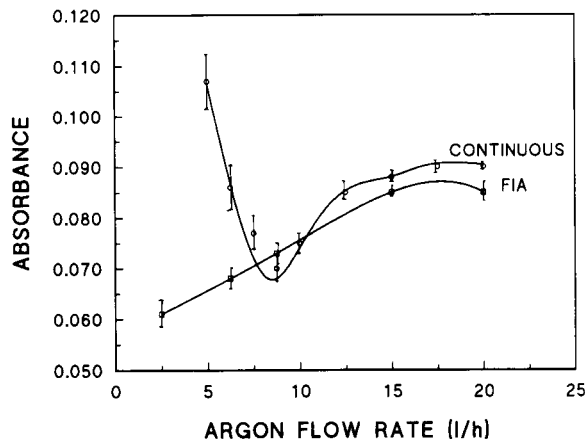


Fig. 2. Optimization of argon flow-rate.

tem, so a reaction coil length of 30 cm was chosen. Using this length, three different coil configurations were studied: linear, looped and knotted. No influence on the signal intensity was observed but the reproducibility was slightly better with a knotted coil. A reaction coil with three knots was therefore chosen for use.

#### *Influence of sample volume injected into the FI system*

As the volume of sample injected can affect the dispersion of the sample, the effect of different volumes of the same Se concentration was investigated. As the slope of the resulting plot of absorbance versus amount of Se was linear for all volumes tested (0.1–1 ml), it was concluded that the volume injected did not significantly affect the sensitivity. Therefore, dilution of excessively concentrated sample material is best achieved by reducing the injection volume.

A sample volume of 0.5 ml was chosen for further experiments.

#### *Optimization of NaBH<sub>4</sub> concentration*

To determine the optimum sodium tetrahydroborate concentration, different concentrations in the range 0.1–5% (w/v) were tested. Figure 3 shows that maximum sensitivity in the FI and continuous-flow systems is obtained at 0.5% (w/v) NaBH<sub>4</sub>. Higher concentrations lead to a decrease

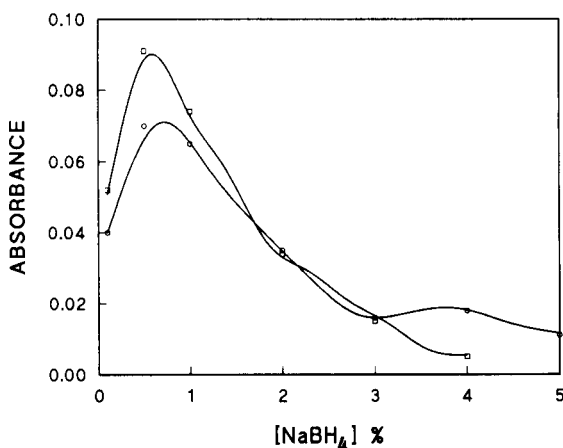


Fig. 3. Optimization of NaBH<sub>4</sub> concentration. ○ = FI system; □ = continuous-flow system.

in sensitivity and the connection tubes become detached because of the pressure. A concentration of 0.5% (w/v) was chosen for further work.

#### *Optimization of hydrochloric acid concentration*

The results were as follows. Two different reduction processes are necessary for the proposed system: on-line reduction of Se(VI) to Se(IV) in the acidified sample; and hydrogen selenide generation from Se(IV) and total Se after prereduction.

In the first instance, two reducing acids (HBr and HCl) were tested. HBr was not significantly better than HCl, therefore the latter was used for further experiments. The results obtained for the on-line reduction of Se(VI) to Se(IV) show that 6 M HBr was required, which means a high sample dilution (8 M HBr is the most concentrated available). The HCl concentration and temperature must be carefully controlled to achieve quantitative on-line reduction of Se(VI) to Se(IV) in both the FI and continuous-flow systems. The HCl concentration added for sample acidification was therefore varied in the range 0–10 M. Figure 4b and d show that the reduction of Se(VI) is quantitative at 6 M HCl for the 100 and 25 ng ml<sup>-1</sup> concentrations tested. Therefore, an HCl concentration of 6 M was chosen for all samples. Further, the effect of sample HCl concentration on the Se(IV) and Se(VI) response with and without heating was studied. No signal was obtained from unheated Se(VI) samples at the 100 ng ml<sup>-1</sup> level (Fig. 4e). The signal from Se(IV) previously heated to 140°C was more than twice that obtained from unheated Se(IV) (Fig. 4a and f), probably because the high temperature favours hydride formation from Se(IV). The maximum signal from Se(VI) after it had been reduced was significantly higher than the optimum obtained for unheated Se(IV) at the same concentration.

In the second instance, the optimum HCl concentration for H<sub>2</sub>Se generation from Se(IV) (at two NaBH<sub>4</sub> concentrations, Fig. 5a and b) was studied over the range 0.1–8 M. The analytical signal for Se(IV) greatly increased with increasing HCl concentration up to 1–2 M. Higher HCl concentrations slightly increased the sensitivity at both the NaBH<sub>4</sub> concentrations tested. There-

TABLE 2  
Interference study <sup>a,b</sup>

Interferent (w/w)			Batch <sup>c</sup>	Interference (%) <sup>f</sup>			
				Without reduction <sup>d</sup>		With pre-reduction <sup>e</sup>	
				FI	Continuous flow	FI	Continuous flow
Fe(powder)	Fe	(1:1000)		74	100	–	–
FeSO <sub>4</sub>	Fe(II)	(1:30)	80	–	–	–	–
Ni(NO <sub>3</sub> ) <sub>2</sub>	Ni(II)	(1:1)		100	100	100	100
		(1:10)	45	87	100	100	100
		(1:100)		64	100	100	100
		(1:1000)		27	100	75	100
(NH <sub>4</sub> ) <sub>2</sub> MoO <sub>4</sub>	Mo(VI)	(1:100)		100	100		
		(1:1000)		100	89		
PdCl <sub>2</sub>	Pd	(1:1)		96	97	100	97
		(1:10)		83	65	100	75
		(1:100)		0	0	65	0
Zr(NO <sub>3</sub> ) <sub>4</sub>	Zr(IV)	(1:10)		100	100		
		(1:100)		75	100		
		(1:1000)		69	100		
Cu <sup>o</sup>	Cu(II)	(1:1)	50	86	92	100	100
		(1:10)	0	56	60	100	100
		(1:100)		0	0	86	85
		(1:1000)				52	57
CrCl <sub>3</sub>	Cr(III)	(1:10)		100	100		
		(1:100)		100	93		
		(1:100)		72	66		
AgNO <sub>3</sub>	Ag(I)	(1:1)		100	100	100	100
		(1:10)		46	100	81	84
		(1:100)		0	0	66	45
As <sub>2</sub> O <sub>3</sub>	As(III)	(1:1)	100	100	100	85	100
		(1:10)	100	100	100	81	100
		(1:100)	90	100	76	84	100
		(1:1000)	20	34	24	84	0
As <sub>2</sub> O <sub>5</sub>	As(V)	(1:10)		100	100		
		(1:100)		89	76		
		(1:1000)		43	24		
Potassium antimonyl tartrate	Sb(III)	(1:10)	100	100	100	100	100
		(1:100)	70	73	21	33	0
		(1:1000)	10	29	21		
Potassium pyroantimonate	Sb(V)	(1:100)		100	100		
		(1:1000)		35	19		
Hg <sup>o</sup>	Hg(II)	(1:1)	100	100	100		
		(1:10)	70	100	100		
		(1:100)	20	100	100		
		(1:1000)		100	100		

<sup>a</sup> [Se(IV)] or [Se(VI)] = 50 ng ml<sup>-1</sup>. <sup>b</sup> Other interferents such as Co [Co(NO<sub>3</sub>)<sub>2</sub>], Mn [Mn(NO<sub>3</sub>)<sub>2</sub>], Mg (MgO), Ba (BaCl<sub>2</sub>), Na (NaCl), K (KCl), Cd[Cd(NO<sub>3</sub>)<sub>2</sub>] and Zn [Zn<sub>2</sub>(NO<sub>3</sub>)<sub>2</sub>] do not interfere at the  $\pm 3\sigma$  level at an Se(VI) or Se(IV) interferent ratio of 1:1000 (w/w). SO<sub>4</sub><sup>2-</sup>, NO<sub>3</sub><sup>-</sup>, Cl<sup>-</sup> and PO<sub>4</sub><sup>3-</sup> do not interfere at the  $\pm 3\sigma$  level at an Se(IV) or Se(VI) interferent ratio of 1:10000 (w/w). <sup>c</sup> Batch study results taken from [10,11]. <sup>d</sup> Interference study carried out with Se(IV). <sup>e</sup> Interference study carried out with Se(VI). <sup>f</sup> % =  $A_i \times 100 / A_{se}$ , where  $A_i$  = absorbance given by a solution containing 50 ng ml<sup>-1</sup> of Se(IV) or Se(VI) and the interferent.  $A_{se}$  = Absorbance given by a solution just containing 50 ng ml<sup>-1</sup> of Se(IV) or Se(VI).

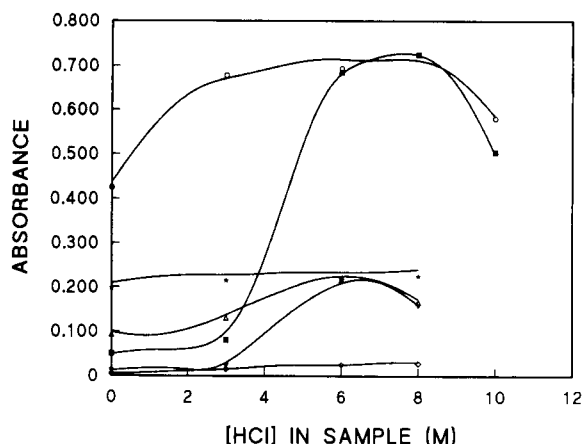


Fig. 4. Optimization of HCl concentration in the sample for the on-line reduction using the FI system. (○) 100 ng ml<sup>-1</sup> Se(IV) with heating; (■) 100 ng ml<sup>-1</sup> Se(VI) with heating; (△) 25 ng ml<sup>-1</sup> Se(IV) with heating; (▼) 25 ng ml<sup>-1</sup> Se(VI) with heating; (◇) 100 ng ml<sup>-1</sup> Se(VI) without heating; (+) 100 ng ml<sup>-1</sup> Se(IV) without heating.

fore, 4 M HCl was chosen for further experiments. The total Se (Fig. 5c) sensitivity increased with increasing acid concentration to a maximum at above 10 M. Experiments carried out at different bath temperature at 12 M HCl showed that quantitative reaction only occurred at temperatures  $\geq 140^\circ\text{C}$ . As temperatures higher than  $140^\circ\text{C}$  lead to rapid tube degeneration, a temperature of  $140^\circ\text{C}$  was chosen for further work. The FI and continuous-flow systems gave similar results.

#### Interferences

Table 2 shows a comparative study of interferences in H<sub>2</sub>Se determination by batch, FI and

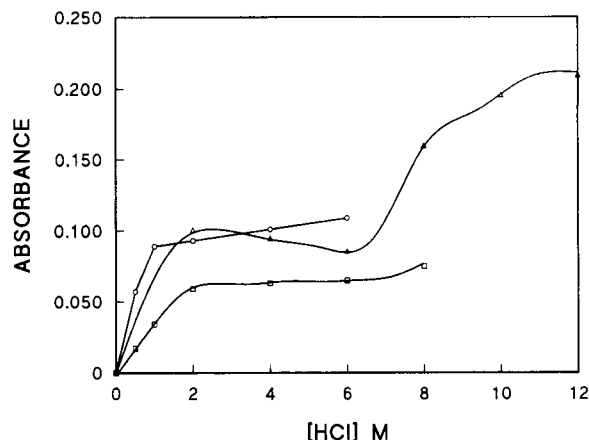


Fig. 5. Optimization of HCl concentration in hydride generation with and without on-line prerelution. (○) 0.5% NaBH<sub>4</sub>, 50 ng ml<sup>-1</sup> Se(IV); (□) 1% NaBH<sub>4</sub>, 50 ng ml<sup>-1</sup> Se(IV); (△) 0.5% NaBH<sub>4</sub>, 50 ng ml<sup>-1</sup> Se(IV) and Se(VI).

continuous-flow methods, with and without prerelution.

As can be seen, on-line determination is always more selective than the batch method. The interference level of foreign ions is similar in the FI and continuous-flow systems and the selectivity increases considerably if the H<sub>2</sub>Se is generated after the on-line prerelution step. This is exemplified by the interference of copper at a weight ratio of 1:10 (Se:Cu), which completely inhibits the analytical signal in batch systems, produces a 50% decrease in FI and continuous-flow systems without reduction and does not interfere in FI and continuous-flow systems with prerelution.

Further, the traditionally observed formation of a metal precipitate does not occur if H<sub>2</sub>Se is

TABLE 3

Analytical characteristics for hydride generation

Parameter	Without prerelution		With on-line prerelution	
	FI	Continuous flow	FI	Continuous flow
Se(IV) detection limit (ng ml <sup>-1</sup> )	2	1.51	0.70	1.50
Se(VI) detection limit (ng ml <sup>-1</sup> )	–	–	0.70	1.50
Precision (%) <sup>a</sup>	2.5	2.1	3	5
Linear range (ng ml <sup>-1</sup> )	6–130	5–125	2–150	5–150

<sup>a</sup>  $n = 10$ . [Se] = 10 and 50 ng ml<sup>-1</sup>.



generated after the on-line reduction step, which is a considerable advantage because the risk of blocked tubing in the system is avoided.

#### Analytical characteristics of FI and continuous-flow systems

Table 3 gives the linear range, precision and detection limits of the FI and continuous-flow methods for Se(IV) and Se(VI) with and without on-line prereduction.

The FI method is recommended over the continuous-flow method because it gives better precision and detection limits than the continuous-flow system with an on-line prereduction step.

#### Sample analysis

The proposed FI method was applied to Se(IV)- and Se(VI)-spiked distilled and sea-water samples (Table 4). The standard addition slopes in distilled water (0.00344 absorbance ml ng<sup>-1</sup>) and sea water (0.00421 absorbance ml ng<sup>-1</sup>) only differ by 23%, indicating the improved sensitivity provided by on-line prereduction.

The recoveries of Se(IV), Se(VI) and a mixture of both in sea water were all 99%.

No Se(IV) was found in the Santander and Canary Islands sea waters analysed. The mea-

sured levels of Se(VI) were  $5 \pm 1$  and  $10 \pm 1$  ng ml<sup>-1</sup> (mean  $\pm$  standard deviation,  $n = 5$ ), respectively.

#### Conclusions

The proposed method allows the on-line determination of both Se(IV) and Se(VI) species and provides higher sensitivity and selectivity than other methods. FI is preferred to continuous flow because it provides better precision and a lower detection limit. Se is not lost during the reduction step in the closed system, as it may be in an open batch system.

The authors are grateful for financial support from the CICYT under project PB 880094 and from BCR under project 5371/1/9/385/90/06/-BCR-E(10).

#### REFERENCES

- 1 W.H. Strain and A.W. Varnes, Trace Subst. Environ. Health, 15 (1981) 104.
- 2 L.W. Newland, The Handbook of Environmental Chemistry, Vol. 3, Part B, Anthropogenic Compounds, Springer Verlag, Heidelberg, 1982, pp. 45–57.
- 3 K.W. Bruland, Chem. Oceanogr., 8 (1983) 188.
- 4 E. Merian, in E.E. Merian, R.W. Frey, W. Härdi and C. Schlatter (Eds.), Carcinogenic and Mutagenic Compounds, Gordon and Breach, London, 1985, pp. 27–32.
- 5 H. Robberecht and R. Van Gratiel, Talanta, 29 (1982) 823.
- 6 Y. Shibita, Analyst, 110 (1985) 1269.
- 7 R. Bye and W.Z. Lund, Anal. Chem., 332 (1988) 242.
- 8 G.A. Cutter, Anal. Chim. Acta, 98 (1978) 59.
- 9 M.B. Calle-Guntiñas, Y. Madrid and C. Camara, Anal. Chim. Acta, 252 (1991) 161.
- 10 B. Welz and M. Melcher, Analyst, 109 (1984) 569.
- 11 M. Verlinden, Fresenius' Z. Anal. Chem., 296 (1979) 253.

TABLE 4

Analytical results for sea-water samples

Sample	[Se(IV)] (ng ml <sup>-1</sup> )	[Se(VI)] (ng ml <sup>-1</sup> )
Sea water (Santander)	< DL <sup>a</sup>	5 ± 1
Sea water (Canary Islands)	< DL	10 ± 1
+ 50 ng ml <sup>-1</sup> Se(IV)	51 ± 0.5	11 ± 1
+ 50 ng ml <sup>-1</sup> Se(VI)	< DL	60 ± 2
+ 25 ng ml <sup>-1</sup> Se(IV)		
+ 25 ng ml <sup>-1</sup> Se(VI)	23 ± 2	36 ± 2

<sup>a</sup> DL = detection limit.

# Flow-injection flame atomic absorption spectrometry for slurry atomization. Determination of calcium, magnesium, iron, zinc and manganese in vegetables

P. Viñas, N. Campillo, I. López García and M. Hernández Córdoba

*Department of Analytical Chemistry, Faculty of Chemistry, University of Murcia, E-30071 Murcia (Spain)*

(Received 23rd October 1992; revised manuscript received 4th January 1993)

## Abstract

A flame atomic absorption spectrometric procedure for determining the iron, zinc, manganese, calcium and magnesium contents of slurries prepared from vegetables is described. Samples were first submitted to a mild calcination step and then suspensions were prepared and introduced into an air-acetylene flame using a simple flow-injection manifold. The calibration for iron, zinc and manganese was carried out using either aqueous standards or a flow-injection sample-to-standard additions method applicable to suspensions. The calcium and magnesium contents were too high for the direct introduction of the slurries into the flame and so an on-line dilution system was used. Excellent agreement was found between the results of the slurry-based procedures and those obtained by an alternative method involving calcination and dissolution in acid. The reliability of the approach was confirmed by analysing two certified reference materials.

*Keywords:* Atomic absorption spectrometry; Flow injection; Calcium; Iron; Magnesium; Manganese; Zinc; Vegetables

Flame atomic absorption spectrometry (FAAS) normally requires complete dissolution of the solid samples to obtain solutions suitable for measurement. However, this dissolution step usually involves considerable time and effort and an interesting alternative is based on the use of suspensions prepared from samples of small particle size, which allows a considerable shortening of the time required for the analysis. Although the essential condition of a fine particle size can be met, the approach is not free from problems, including a serious risk of clogging the nebulizer when the suspension is aspirated.

Previous studies have involved the determina-

tion of metals in foods and biological materials by FAAS and different methods have been applied to overcome problems associated with the direct introduction of the slurries into the flame [1–6]. The discrete nature of sample introduction involved in flow-injection (FI) techniques and the continuous rinsing action of the carrier suggest that this is an adequate way to minimize greatly the problems associated with the use of suspensions in FAAS [7–10]. However, as the linear response range of FAAS is narrow, very dilute suspensions must be prepared when the samples contain high concentrations of analytes so that the signals are within the linear range of the instrument. The use of such dilute slurries generates severe reproducibility problems owing to the small amount of sample to be weighed and the errors associated with suspension sampling [11].

*Correspondence to:* M. Hernández Córdoba, Department of Analytical Chemistry, Faculty of Chemistry, University of Murcia, E-30071 Murcia (Spain).

FI methodology permits an extension of the dynamic determination range and several manifolds for obtaining on-line dilution in FI-FAAS have been reported [12–17].

In this study, a procedure for the determination of metals in vegetables using the slurry-FI-FAAS approach is discussed. Provided that the samples have been previously submitted to a mild calcination step and the suspensions are prepared from the carbonaceous residues, direct calibration using aqueous standards is valid for the determination of iron, zinc and manganese. A sample-to-standard additions method [18] applicable to slurries was also examined as an alternative calibration method. As the calcium and magnesium contents of the samples are very high, a recently reported on-line dilution system [19] was used for the determination of these metals.

## EXPERIMENTAL

### *Apparatus and reagents*

A Pye Unicam Model SP1900 atomic absorption spectrometer was used in most of the experiments. The output of the instrument was interfaced to a personal computer by means of a PCLab-818PG data acquisition card. Data treatment and plotting were done using laboratory-made software written in C language. For the determination of zinc using the sample-to-standard additions method and for comparison purposes, some experiments were made using a Perkin-Elmer Model 1100B atomic absorption spectrometer with deuterium-arc background correction. Measurements were made at 422.7, 285.2, 248.3, 279.5 and 213.9 nm for calcium, magnesium, iron, manganese and zinc, respectively, using conventional hollow-cathode lamps. Air-acetylene flames were used.

The FI manifolds are shown in Fig. 1. A Gilson Minipuls HP4 peristaltic pump with two Omnifit injection valves was used. Sample loops and all connecting lines were made of 0.8 mm i.d. PTFE tubing. As indicated elsewhere [10,20], a three-way connector was included in the manifolds to provide an air inlet and to aid the fragmentation of the sample plug. This T-piece allowed air

compensation for the difference between the nebulizer uptake rate and the pumping flow-rate, thus acting as a prenebulizer. The manifold shown in Fig. 1B was used for the on-line dilution [19] of the slurries.  $S_1$  was a polyethylene syringe used to inject a plug of air via valve  $V_1$ .  $S_2$  was another polyethylene syringe adapted as a variable-volume dilution chamber [17]. Valve  $V_2$  was used to inject the plug of slurry.  $V_3$  was a two-way valve used to switch between the upper and lower outlets of  $S_2$ . Once the sample plug was located in the dilution chamber, the entry of the plug of air permitted rapid and effective mixing. The air replaced the diluted solution, which was propelled towards the spectrometer. In this way, plateaux were obtained for the absorbance-time relationship. A detailed description of the manifold has recently been reported elsewhere [19].

A Fritsch ball-mill of 80-ml capacity and with 20 balls of 1 cm diameter was used. Particle size distributions were obtained with an Imco 10 image computer (Kontron).

Stock solutions ( $1000 \mu\text{g ml}^{-1}$ ) of calcium, magnesium, iron, manganese and zinc were obtained from Fisher Scientific and diluted as necessary to obtain working standards. Glycerol (Fluka), Triton X-100 (Merck) and lanthanum nitrate (Fluka) were used as received.

### *Slurry procedures*

The vegetable samples were washed to eliminate any remains of extraneous materials, rinsed several times with distilled water, cut up and dried in an oven at  $90^\circ\text{C}$  to constant weight. The samples were then ground in a domestic grinder and precalcined in porcelain crucibles at  $500^\circ\text{C}$  for 1.5 h in a muffle furnace. The carbonaceous residues (ca. 5 g) were weighed and ground in the ball mill for 15 min.

For the determination of iron, zinc and manganese using direct calibration, samples of the ashes in the 0.01–0.25 g range (depending on the metal and its level in the sample) were weighed and suspended in 25 ml of a 10% glycerol solution containing 1% hydrochloric acid. The suspensions were submitted to ultrasound for 5 min and then stirred magnetically for another 10 min. While the slurries were being continuously stirred,

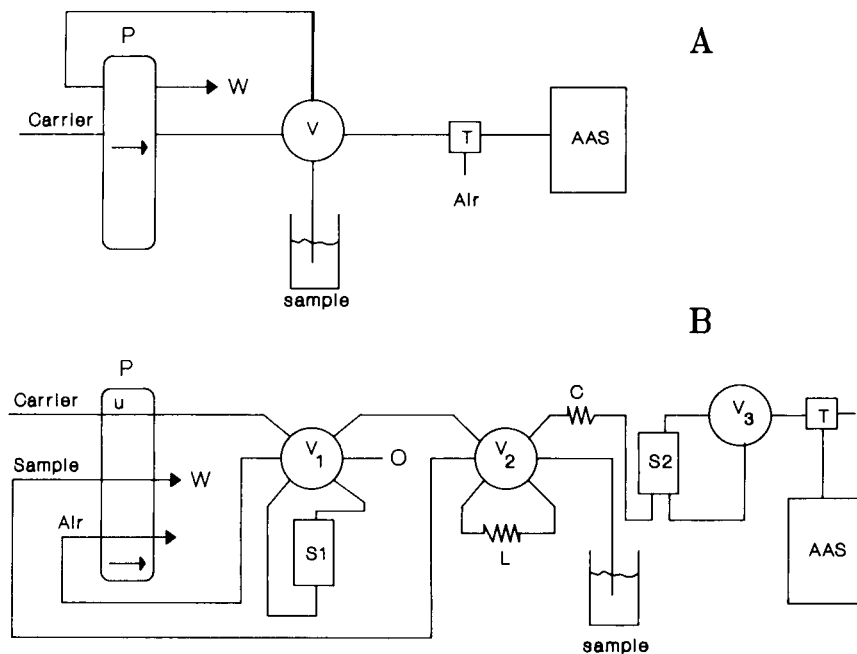


Fig. 1. (A) Flow-injection manifold for the determination of iron, manganese and zinc. P, peristaltic pump; V, injection valve; S, sample reservoir; T, T-piece for air compensation. Sample loop, 150  $\mu\text{l}$ . (B) FI on-line dilution manifold for calcium and magnesium determination (see [19] for a full description).

the sample loop was filled and the plug was injected into the FI manifold using water as the carrier. The peak height of the transitory signal obtained was measured and used as the analytical signal. Calibration was performed by injecting aqueous solutions of iron, zinc or manganese under the same experimental conditions.

When the sample-to-standard additions calibration method [18] was used, the experimental procedure was identical but the carrier was a solution containing 10% glycerol, 1% HCl and a fixed concentration of the analyte to be determined [2.0  $\mu\text{g ml}^{-1}$  of Mn(II) or Fe(III) or 0.3  $\mu\text{g ml}^{-1}$  of Zn(II)].

The determination of calcium and magnesium was carried out using the on-line dilution device shown in Fig. 1B and described in depth elsewhere [19]. The samples were treated as described above. Amounts of 5–25 mg of the ground precalcined samples were suspended in 25 ml of a solution containing 1% hydrochloric acid, 1% lanthanum (as nitrate) and 0.02% Triton X-100. A 35- $\mu\text{l}$  volume of the slurry was injected and the

internal volume of the variable volume dilution chamber was adjusted to 4 ml to obtain an appropriate degree of dilution. The suspending solution was also used as the carrier. The height of the plateau obtained for the absorbance–time relationship was used as the analytical signal. Calibration was performed using aqueous standards.

#### *Procedure for dissolution of samples*

The vegetable samples were previously analysed for comparison purposes. Fractions of the samples were calcined at 500°C for 8 h in porcelain crucibles. The ash was treated with 2 ml of hydrochloric acid and heated to dryness and then again with 5 ml of hydrochloric and 1 ml of nitric acid and the solution was finally diluted to 50 ml. The contents of calcium, magnesium, zinc, manganese and iron were then determined by AAS in the conventional aspiration manner, using the conditions recommended by the manufacturer.

For the particle size distribution study, aliquots of 0.1% slurries were taken while the suspensions

were being continuously stirred and smeared over poly-L-lysine-coated histological slides. The particles were observed through an Zeiss axioscop microscope connected to the image analyser. A commercial software package permitted the particle size distribution to be obtained from the images.

## RESULTS AND DISCUSSION

The introduction of slurries of large particle size into the flame may clog the nebulizer or the FI connections. Dried grapefruit leaves were ground in an agate ball mill for different periods of time to obtain a small particle size. When 1% slurries prepared from these samples were injected into the FI manifold, although clogging of the nebulizer did not occur, the particles agglomerated in the FI connections. This problem was observed even after grinding for 30 min. A different approach consisting of a mild calcination step of the samples in a muffle furnace and preparation of the slurries from the ground ash was therefore chosen. This approach, which is similar to the carbonaceous slurry technique based on wet digestion and described by Faggioli and co-workers [4,5], has already been reported as overcoming problems caused by the physical characteristics of the sample in the case of electrothermal slurry atomization. It allows both a diminution of the particle size and partial destruction of the organic matter, thus minimizing background problems [21–23]. An estimation of particle size distribution was carried out by means of an image analyser on three different calcined vegetable samples that had been ground for 15 min. The

results indicated that at least 90% of the particles had a particle size smaller than 20  $\mu\text{m}$ .

### Determination of iron, manganese and zinc

The stability of the suspensions was studied by preparing 0.6% slurries from calcined grapefruit leaves in the presence of different stabilizing agents. Hexametaphosphate, Triton X-100 (polyethylene glycol *tert*-octylphenyl ether), glycerol, polyoxyethylene sorbitan monolaurate, polyoxyethylene sorbitan monostearate, polyoxyethylene sorbitan trioleate, sorbitane monolaurate, sorbitane monopalmitate and sorbitan monostearate were tried. The suspensions were submitted to ultrasound for 5 min and then stirred magnetically for another 10 min. Stirring was then stopped, aliquots were injected into the FI manifold at 1-min intervals and the absorbance due to iron was obtained. The best results were obtained when a 10% glycerol concentration was used. Although glycerol and the use of ultrasound avoided clogging of the FI tubes, stabilization of the suspension was not total and, for this reason, the sample loop was filled while the suspensions were being continuously stirred.

The instrumental settings, such as air and acetylene flow rates and the height of the burner, were optimized to maximize the absorbances. The optimum values were found to be the same for slurries and for aqueous standards. The effect of both sample loop size and pumping rate were studied in the 35–300  $\mu\text{l}$  and 1–2  $\text{ml min}^{-1}$  ranges, respectively. There was no significant increase in peak height above 150  $\mu\text{l}$  and 1.8  $\text{ml min}^{-1}$ , and these values were chosen as optima. The effect of hydrochloric acid concentration was studied in the range 0.4–1.5% and constant sig-

TABLE 1

Slopes of the standard additions calibration graphs

Sample	Slope <sup>a</sup> (absorbance $\text{ml } \mu\text{g}^{-1}$ )		
	Manganese	Iron	Zinc
Cauliflower slurries	0.0210 $\pm$ 0.0003	0.0100 $\pm$ 0.0005	0.0599 $\pm$ 0.036
Cauliflower leaf slurries	0.0196 $\pm$ 0.0021	0.0093 $\pm$ 0.0002	0.0589 $\pm$ 0.0008
Aqueous standards	0.0192 $\pm$ 0.0012	0.0097 $\pm$ 0.0004	0.0608 $\pm$ 0.0032

<sup>a</sup> Mean values  $\pm$  standard deviations for six graphs. Each graph was constructed from four points and each point was measured three times.

nals were obtained above 0.8%. Therefore, a 1% HCl concentration was selected. The maximum suspension concentration to be used is limited by clogging of the FI system. Using suspensions below 2% there was linearity between the absorbance and the slurry percentage.

To confirm that the simplest calibration approach using aqueous standards was valid, standard additions calibration graphs for the metals were obtained from suspensions prepared from calcined vegetable samples and compared with those obtained for aqueous solutions. Table 1 shows the results for two representative materials. As can be seen, the slopes were similar, indicating the absence of a matrix effect and thus validating direct calibration. Next, slurries were prepared from several precalcined vegetable samples and the iron, manganese and zinc contents obtained by using calibration with aqueous standards. The results, which are shown in Table 2, agreed with those obtained by the acid dissolution procedure.

An alternative approach for calibration is a flow-injection sample-to-standard additions method, which has been reported to be suitable for slurries [18]. In this procedure, which is basically an extension of that discussed by Israel and Barnes [24] and related to another approach reported by Tyson and co-workers [25,26], aliquots of the slurry are injected while a solution of the analyte flows continuously through the FI system.

Positive or negative peaks are obtained, depending on the sample concentration.

The sample loop size and the pumping rate were maintained at the same optimized values. Fig. 2A shows a calibration graph for manganese and Fig. 2B shows the peaks obtained for iron when different slurries were injected into a carrier solution containing  $2 \mu\text{g ml}^{-1}$  of Fe(III).

As discussed elsewhere [18], when a slurry prepared from a sample containing the analyte is injected into the manifold, a  $\beta$  coefficient ( $\beta = K_1/K_2$ ) must be introduced into the equation relating the analytical signal with the unknown concentration.  $K_1$  is the proportionality constant of the detector response for the standard analyte solution in the presence of the solid matrix and  $K_2$  that for the analyte supplied as a slurry. As direct calibration with aqueous standards is valid, the  $\beta$  coefficients must be very close to unity. This was confirmed experimentally, obtaining the  $\beta$  values through separate measurements of  $K_1$  and  $K_2$ . This calibration procedure was applied to the determination of iron, zinc and manganese in the same vegetable samples. Table 2 also shows that the results agreed with those obtained by the reference procedure based on dissolution in acids.

The precision, expressed as the relative standard deviation (R.S.D.), is shown in Table 3. Results for both the detection and the determination limits were calculated according to the criteria  $x \pm 3 \text{ S.D.}$  and  $x \pm 10 \text{ S.D.}$ , respectively, where

TABLE 2

Results for iron, zinc and manganese in vegetables using the slurry and acid dissolution procedures

Sample	Content ( $\mu\text{g g}^{-1}$ )								
	Iron			Zinc			Manganese		
	A <sup>a</sup>	B <sup>a</sup>	C <sup>a</sup>	A <sup>a</sup>	B <sup>a</sup>	C <sup>a</sup>	A <sup>a</sup>	B <sup>a</sup>	C <sup>a</sup>
Cauliflower leaves	115 ± 1	116 ± 6	125 ± 3	50 ± 0.4	52 ± 4	51 ± 3	111 ± 1	106 ± 2	112 ± 6
Cauliflower	58 ± 3	57 ± 5	65 ± 2	51 ± 0.6	51 ± 3	54 ± 2	27 ± 0.7	26 ± 3	24 ± 4
Bean leaves	104 ± 1	106 ± 3	101 ± 5	33 ± 0.8	30 ± 2	32 ± 2	18 ± 0.1	20 ± 1	20 ± 1
Grapefruit leaves	84 ± 1	84 ± 9	85 ± 9	15 ± 0.3	16 ± 1	14 ± 1	13 ± 0.1	14 ± 2	13 ± 1
Cauliflower stem	31 ± 1	35 ± 2	27 ± 5	24 ± 0.4	24 ± 1	23 ± 3	24 ± 0.1	24 ± 1	23 ± 1
Citrus leaves (SRM 1572)	90 ± 10 <sup>b</sup>	88 ± 3	92 ± 4	29 ± 2 <sup>b</sup>	28 ± 2	29 ± 2	23 ± 2 <sup>b</sup>	23 ± 1	22 ± 2
Apple leaves (SRM 1515)	80 <sup>c</sup>	85 ± 4	86 ± 5	12.5 ± 0.3 <sup>b</sup>	12 ± 1	12 ± 1	54 ± 3 <sup>b</sup>	53 ± 2	56 ± 2

<sup>a</sup> (A) Dry-ashing and acid dissolution procedure ( $n = 9$ ); (B) slurry procedure using direct calibration with aqueous standards ( $n = 8$ ); (C) slurry procedure using the sample-to-standard additions procedure for calibration. <sup>b</sup> Certified values. <sup>c</sup> Not certified. Value is given by the supplier for informative purposes.

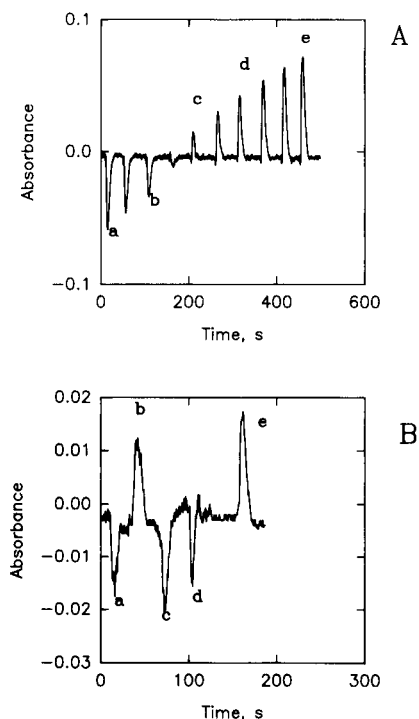


Fig. 2. Sample-to-standard additions method for the determination of manganese and iron. (A)  $2 \mu\text{g ml}^{-1}$  Mn(II) solution as carrier: (a) water; (b) 0.8; (c) 2.8; (d) 4.8; (e)  $7.8 \mu\text{g ml}^{-1}$  Mn(II). (B)  $2 \mu\text{g ml}^{-1}$  Fe(III) solution as carrier: (a) 0.2% slurry prepared from cauliflower leaves; (b) 0.8% slurry from cauliflower leaves; (c) 1.0% slurry from cauliflower stem; (d) 0.1% slurry from bean leaves; (e) 0.7% slurry from bean leaves.

$\bar{x}$  is the mean of ten replicate determinations at the blank level and S.D. is the corresponding standard deviation. A comparison of both the

TABLE 3

Statistical parameters of the method

Parameter	Iron	Zinc	Manganese
R.S.D. (%) <sup>a</sup>	0.8 (57) <sup>d</sup>	0.4 (16) <sup>d</sup>	0.7 (20) <sup>d</sup>
R.S.D. (%) <sup>b</sup>	1.7 (57) <sup>d</sup>	0.9 (16) <sup>d</sup>	0.8 (20) <sup>d</sup>
Detection limit ( $\mu\text{g g}^{-1}$ ) <sup>c</sup>	7.9	1.8	3.5
Determination limit ( $\mu\text{g g}^{-1}$ ) <sup>c</sup>	12.4	3.3	5.7

<sup>a</sup> Relative standard deviation for ten injections of the same slurry. <sup>b</sup> Relative standard deviation for ten injections of different slurries from the same sample. <sup>c</sup> Values calculated for a 2% suspension. <sup>d</sup> Values in parentheses are the contents of the analyte in the sample used in  $\mu\text{g g}^{-1}$ .

aqueous standard calibration and sample-to-standard additions calibration approaches showed no significant differences.

The accuracy was also determined by comparing the results obtained using the suspension procedure with those of the conventional dry-ashing procedure indicated under Experimental. There was agreement between the two analytical approaches as deduced from the Wilcoxon  $T$ -test and the least-squares fitting. The statistical results indicated no significant differences between the procedures at the 95% confidence level. When applying the Wilcoxon  $T$ -test, the value of  $\min(T^+, T^-)$  was always higher than the  $T$  value tabulated ( $T = 11$ ). Application of the least-squares fitting led to experimental values of  $a$  (intercept on the ordinate) and  $b$  (slope) close to 0 and 1, respectively. The Student  $t$ -distribution for these parameters led to total correlation at the 95% confidence level.

The reliability of the procedure was also confirmed by analysing two certified reference materials. The results, which are given in Table 2, were in agreement with the certified values.

#### Determination of calcium and magnesium

As stated above, the analysis of samples containing high concentrations of analyte requires the use of very dilute suspensions, owing to the narrow linear response range of the spectrometer. This applies to calcium and magnesium, which are present in the vegetable samples studied at higher concentrations than the other metals studied. The determination of these elements was carried out using the on-line dilution device illustrated in Fig. 1B. Precalcined samples were used to prepare the slurries. No clogging of the tubes occurred but there was poor homogenization in the dilution device and partial sedimentation of particles at the bottom of the dilution chamber even when using a 10% glycerol solution as the carrier. For this reason, other stabilizing agents were reconsidered. The best results were obtained using 0.02% Triton X-100 in both the sample and the carrier. This agent formed a bubble mesh which avoided the deposition of ash in the dilution chamber. Higher concentrations produced too many bubbles and the appearance

TABLE 4

Results for magnesium and calcium in vegetables using the on-line dilution slurry and the acid dissolution procedures

Sample	Content (%)			
	Magnesium		Calcium	
	A <sup>a</sup>	B <sup>a</sup>	A <sup>a</sup>	B <sup>a</sup>
Cauliflower leaves	0.487 ± 0.004	0.486 ± 0.009	3.559 ± 0.052	3.644 ± 0.093
Cauliflower	0.206 ± 0.003	0.205 ± 0.001	0.417 ± 0.012	0.412 ± 0.006
Bean leaves	0.278 ± 0.007	0.284 ± 0.003	0.919 ± 0.01	0.944 ± 0.019
Grapefruit leaves	0.400 ± 0.007	0.402 ± 0.002	5.269 ± 0.075	5.177 ± 0.083
Cauliflower stem	0.406 ± 0.009	0.417 ± 0.008	2.110 ± 0.099	2.221 ± 0.009
Citrus leaves (SRM 1572)	0.58 ± 0.03 <sup>b</sup>	0.585 ± 0.01	3.15 ± 0.1 <sup>b</sup>	3.115 ± 0.1
Apple leaves (SRM 1515)	0.271 ± 0.008 <sup>b</sup>	0.275 ± 0.004	1.526 ± 0.015 <sup>b</sup>	1.537 ± 0.005

<sup>a</sup> (A) Dry-ashing and acid dissolution procedure ( $n = 9$ ); (B) slurry procedure ( $n = 8$ ). <sup>b</sup> Certified values.

of tailing effects on the plateau. On the other hand, the concentration of acid in the slurry is also an important parameter. Concentrations of hydrochloric acid in the range 0–3% were tried and constant signals were obtained above 0.8%. A 1% HCl concentration was selected.

The variables of the FI system were studied for magnesium using a slurry of cauliflower leaves calcined at 500°C for 1.5 h and prepared in a suspending medium containing 1% lanthanum, 1% hydrochloric acid and 0.02% Triton X-100. Figure 3 shows the results obtained.

Higher pumping rates ( $u$ ) in the range 0.8–4.4 ml min<sup>-1</sup> resulted in increased plateau heights (Fig. 3A). A value of 3.4 ml min<sup>-1</sup> was selected. On the other hand, an increase in the flow-rate produced a decrease in plateau duration ( $\Delta t$ ), as predicted by theoretical considerations [19]. Variations in plateau height ( $h$ ) and  $\Delta t$  according to sample loop size ( $V_0$ ) are shown in Fig. 3B when a 4-ml dilution chamber ( $V_M$ ) was used. Again, as expected, the height of the plateau increased but the duration of the signal remained constant when the sample volume increased. When volumes above 300  $\mu$ l were tried, poorly defined plateaux, showing an initial peak in the absorbance–time profile, were obtained. This is related to a practical limitation of the procedure [19] since homogenization of the sample plug with the carrier in the mixing device does not take place sufficiently rapidly and the concentration of the solution leaving the chamber is not constant. The effect of the dilution chamber volume ( $V_M$ ) on the signals

in the range 1–10 ml, when a 35- $\mu$ l sample loop was chosen, is shown in Figure 3C. The height of the constant signal increased when  $V_M$  decreased as these parameters are inversely proportional,  $\Delta t$  decreasing owing to its direct relationship with the volume of the dilution device. Again, poor plateaux were obtained when the ratio  $V_0/V_M$

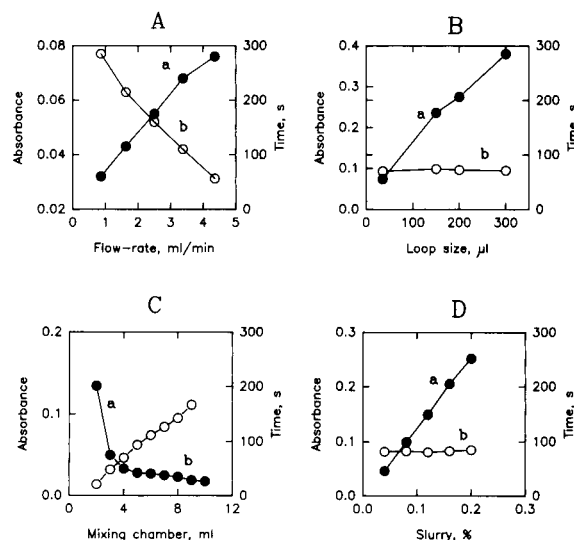


Fig. 3. (a) Variation of the plateau heights and (b) the duration of constant signals with the experimental variables. Slurries prepared from ashed cauliflower leaves. (A) Effect of flow-rate,  $C_0 = 0.02\%$ ,  $V_0 = 35 \mu$ l,  $V_M = 4$  ml; (B) effect of the sample loop size,  $u = 3.4$  ml min<sup>-1</sup>,  $C_0 = 0.02\%$ ,  $V_M = 4$  ml; (C) effect of the dilution chamber volume,  $u = 3.4$  ml min<sup>-1</sup>,  $C_0 = 0.02\%$ ,  $V_0 = 35 \mu$ l; (D) effect of the slurry concentration,  $V_0 = 35 \mu$ l,  $V_M = 4$  ml.



became too high. Finally, Fig. 3D shows the effect of a slurry concentration ( $C_0$ ) of 0.04–0.2% when using a 35- $\mu$ l sample loop and a 4-ml dilution device. The height of the signal increased with  $C_0$ , as they are proportional variables, but the duration of the signal was independent of the slurry concentration. Similar results were obtained when the absorbance from calcium was studied.

To summarize, the manifold shown in Fig. 1B produces a reliable on-line dilution of the slurries. The length of the plateau is dependent on both the volume of the dilution chamber and the flow-rate and is independent of the volume and concentration of the sample. On the other hand, the height of the plateau increases with increasing flow-rate and the volume and concentration of the sample but decreases with increasing volume of the dilution chamber.

Reproducibility was studied using 0.4% slurries prepared from grapefruit leaves. Ten 35- $\mu$ l injections were made of each suspension and R.S.D. values of 1.1% and 1.2% were found for calcium and magnesium, respectively. The results for the two analytes in several vegetables are given in Table 4. A comparison of the results using common statistical tests (Wilcoxon  $T$ -test and least-squares fitting) shows the agreement between the two procedures. Table 4 also shows the results obtained for two certified reference materials using the proposed procedure.

The authors are grateful to the Spanish DGI-CYT (Project 90-0302) for financial support and to Dr. F. Martínez Ortíz (Physical Chemistry Department of the University of Murcia) for developing the software. N. Campillo acknowledges a fellowship from the Consejería de Cultura, Comunidad Autónoma de la Región de Murcia (Spain).

## REFERENCES

- 1 R.C. Fry and M.B. Denton, *Anal. Chem.*, 49 (1977) 1413.
- 2 R.C. Fry and M.B. Denton, *Appl. Spectrosc.*, 33 (1979) 393.
- 3 N. Mohamed and R.C. Fry, *Anal. Chem.*, 53 (1981) 450.
- 4 F. Fagioli, S. Landi, C. Locatelli and C. Bigli, *Anal. Lett.*, 16 (1983) 275.
- 5 F. Fagioli and S. Landi, *Anal. Lett.*, 16 (1983) 1435.
- 6 N. Carrión, Z.A. de Benzo, E.J. Eljuri, F. Ippoliti and D. Flores, *J. Anal. At. Spectrom.*, 2 (1987) 813.
- 7 Z. Fang, B. Welz and G. Schlemmer, *J. Anal. At. Spectrom.*, 4 (1989) 91.
- 8 J.F. Tyson, *Anal. Chim. Acta*, 234 (1990) 3.
- 9 J.C. Andrade, F.C. Strong III and N.J. Martin, *Talanta*, 37 (1990) 711.
- 10 I. López García, F. Ortiz Sobejano and M. Hernández Córdoba, *Analyst*, 116 (1991) 517.
- 11 J.A. Holcombe and V. Majidi, *J. Anal. At. Spectrom.*, 4 (1989) 423.
- 12 J.F. Tyson and J.M.H. Appleton, *Talanta*, 31 (1984) 9.
- 13 J.F. Tyson, J.R. Mariara and J.M.H. Appleton, *J. Anal. At. Spectrom.*, 1 (1986) 273.
- 14 J.F. Tyson and S.R. Bysouth, *J. Anal. At. Spectrom.*, 3 (1988) 211.
- 15 M. de la Guardia, V. Carbonell, A. Morales and A. Salvador, *Fresenius' Z. Anal. Chem.*, 335 (1989) 975.
- 16 V. Carbonell, A. Sanz, A. Salvador and M. de la Guardia, *J. Anal. At. Spectrom.*, 6 (1991) 233.
- 17 E. Beinrohr, P. Csémi and J.F. Tyson, *J. Anal. At. Spectrom.*, 6 (1991) 307.
- 18 I. López García, F. Ortiz Sobejano and M. Hernández Córdoba, *Analyst*, 116 (1991) 831.
- 19 I. López García, J. Arroyo Cortéz and M. Hernández Córdoba, *J. Anal. At. Spectrom.*, 7 (1992) 1291.
- 20 I. López García, M. Hernández Córdoba and C. Sánchez-Pedreño, *Analyst*, 112 (1987) 271.
- 21 L. Ebdon, A.S. Fisher, H.G.M. Parry and A.A. Brown, *J. Anal. At. Spectrom.*, 5 (1990) 321.
- 22 M. Hernández Córdoba and I. López García, *Talanta*, 38 (1991) 1247.
- 23 I. López García, P. Viñas and M. Hernández Córdoba, *J. Anal. At. Spectrom.*, 7 (1992) 529.
- 24 Y. Israel and R.M. Barnes, *Analyst*, 114 (1989) 843.
- 25 J.F. Tyson, J.M.H. Appleton and A.B. Idris, *Anal. Chim. Acta*, 145 (1983) 159.
- 26 J.F. Tyson and A.B. Idris, *Analyst*, 109 (1984) 23.

# Determination of total and free sulphur dioxide in wine with a continuous-flow microdistillation system

A. Maquieira, F. Casamayor and R. Puchades

*Departamento de Química, Universidad Politécnica de Valencia, 46022 Valencia (Spain)*

S. Sagrado

*Departamento de Química Analítica, Universidad de Valencia, 46100 Burjasot, Valencia (Spain)*

(Received 8th September 1992; revised manuscript received 11th February 1993)

## Abstract

A continuous-flow microdistillation system for the determination of SO<sub>2</sub> (free and total) in wine samples is described. The assembly permits the successive addition of discrete volumes of sample to the microdistillation module with the aid of a nitrogen carrier stream. The nitrogen carrier also transports the volatilized SO<sub>2</sub>, after the distillation step, to the absorption module, where the analyte reacts with a solution of 2,2'-dinitro-5,5'-dithiodibenzic acid in phosphate buffer (pH 6) to give a yellow derivative, which is monitored spectrophotometrically at 410 nm. Free and total SO<sub>2</sub> signals are obtained by operating the microdistillation module at room temperature (ca. 20°C) and 100°C, respectively. Total SO<sub>2</sub> requires a previous hydrolysis step, which is carried out on-line with the aid of 4 M NaOH. Chemical and physical parameters were optimized. The influence of some common compounds usually present in wine samples on the analytical signal was also studied. The proposed procedure was compared with two recommended methods: the EEC reference distillation method and the EEC iodimetric method. The proposed method was found to be equally suitable to the reference distillation method, for the rapid and accurate control of wine samples, and additionally competes advantageously with the iodimetric method.

*Keywords:* Flow injection; UV-Visible spectrophotometry; Distillation; Sulphur dioxide; Wines

Analytical techniques for monitoring bioprocesses are increasingly required. The on-line determination of minor components is important with regard to process control. Usually, a separation step is essential in the analysis of complex matrices. Distillation techniques are not often used in automated analytical methods as their incorporation is complicated. However, a continuous distillation configuration should be of interest in relation to the determination of volatile analytes in complex matrices, and it is believed

that a major effort in this matter direction is important.

Continuous-flow distillation assemblies make use of large numbers of channels, peristaltic pumps and connectors. In addition, they feature long start-up times [1]. Other common features are the lack of injection valves and a relatively low sample throughput as a result of the large sample volumes handled.

Continuous analysers with built-in microdistillation systems usually consist of the propulsion module, the microdistillation module (where the gas-liquid separation takes place), the condensation and/or absorption module (which transfers

*Correspondence to:* A. Maquieira, Departamento de Química, Universidad Politécnica de Valencia, 46022 Valencia (Spain).

the gaseous analyte to an outgoing liquid stream) and the continuous detection module.

The relevance of the determination of  $\text{SO}_2$  in food analyses is widely recognized and well documented [2,3]. The presence of both beneficial and toxic effects of  $\text{SO}_2$  in relation to public health and the fact that these properties are related to the relative amounts of “free” or “bound”  $\text{SO}_2$  present, makes the determination and speciation analysis of this analyte of great interest. Numerous methods have been reported, mainly based on gravimetric, volumetric (i.e., iodimetry and alkalimetry), spectrophotometric, chemiluminescence and electroanalytical strategies. However, significant differences in the results obtained when different methods are applied to a given sample are common, especially if complex matrices such as wines are analysed. This implies that the analytical problem still deserves more attention.

Among the currently available methods for the determination of  $\text{SO}_2$  in wines, the European Economic Community (EEC) has adopted a reference method, based on dragging the sample with air or nitrogen, followed by fixation and oxidation of  $\text{SO}_2$  in  $\text{H}_2\text{O}_2$  solution, and final titration of the sulphuric acid formed with a standard  $\text{NaOH}$  solution [4]. Dragging and distillation procedures are widely recognized [5], but

are tedious and time consuming and also lack sensitivity, selectivity, precision and adequate sample throughput. For rapid control, the EEC recommends the iodimetric procedure [4], although this method has been strongly criticized [6].

Adverse reactions in persons hypersensitive to sulphites and the trend towards a decrease in the dosage in food have created a need for rapid, sensitive and reliable analytical techniques. This has promoted studies on flow-injection methods for the determination of  $\text{SO}_2$  in food samples such as wines [7–9]. However, differences in analytical performance parameters and some limitations in applicability were observed with these methods. Further, in some instances the results were not compared with those given by a well established reference method [7,8].

This paper reports studies with a laboratory-made continuous-flow microdistillation unit [10] useful for determining volatile species. The assembly was adapted to determine  $\text{SO}_2$  (free and total) in wine samples. The assembly incorporates the above-mentioned elements and an injection valve, which permits the successive addition of discrete volumes of sample to the microdistillation module with the aid of a nitrogen carrier stream. The nitrogen carrier transports  $\text{SO}_2$ , after distillation, to the absorption module, where

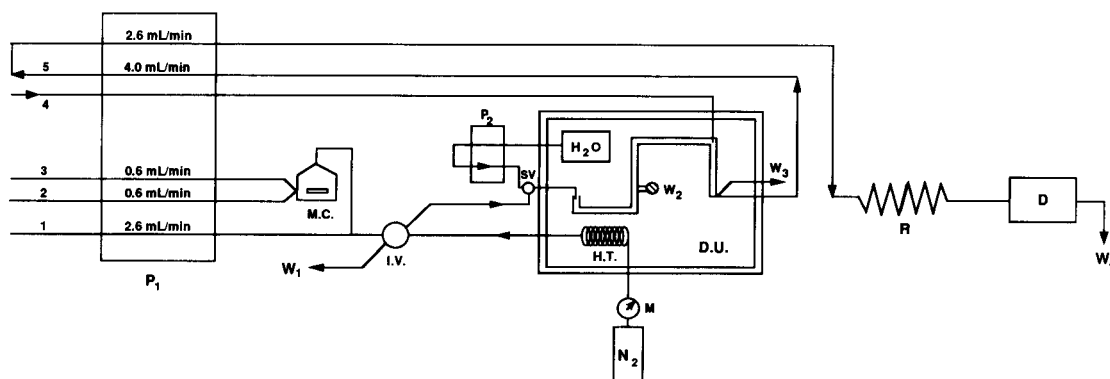


Fig. 1. Schematic diagram of the FIA assembly used for the determination of  $\text{SO}_2$ . Reagent channels: (a) for free  $\text{SO}_2$ , 1 = sample, 2 = distilled water, 3 = 1.2 M phosphoric acid; (b) for total  $\text{SO}_2$ , 1 = 1.2 M phosphoric acid, 2 = 4 M  $\text{NaOH}$ , 3 = sample. In both determinations, channel 4 is for DTNB and channel 5 transports the reaction product to the detector. D = detector; D.U. = distilling unit, thermostatic bath;  $\text{H}_2\text{O}$  = water reservoir; H.T. = heating tube for  $\text{N}_2$ ; I.V. = injection valve; M = manometer; M.C. = mixing chamber;  $\text{N}_2$  = nitrogen cylinder;  $P_1$  and  $P_2$  = peristaltic pumps; R = reaction coil; S.V. = three-way selection valve;  $W_1$  = sample waste;  $W_2$  = washing solution waste;  $W_3$  = debubbler and waste of excess of distillate in DTNB;  $W_4$  = reaction product waste.

it is dissolved/reacted by merging with a solution of 2,2'-dinitro-5,5'-dithiodibenzoic acid (DTNB) in phosphate buffer (pH 6). The yellow derivative formed [11] is monitored spectrophotometrically at 410 nm.

## EXPERIMENTAL

### Reagents

The DTNB indicator reagent was prepared by dissolving 0.32 g of DTNB and 5.23 g of potassium dihydrogenphosphate in 1 l of water and adjusting the pH to 6.0. A 1000  $\mu\text{g ml}^{-1}$   $\text{SO}_2$  stock standard solution was prepared daily by dissolving 1 g of sodium sulphite in a 500-ml volumetric flask, and stabilized by adding 1 ml of 30  $\text{g l}^{-1}$  EDTA and 1 ml of 4 M NaOH. The  $\text{SO}_2$  content was determined by iodimetric titration according to the EEC method [4]. All dilute sulphite solutions were freshly prepared before use. All reagents were of analytical-reagent grade.

### Apparatus

The flow-injection manifold was constructed with two Gilson Minipuls-3 multi-channel peristaltic pumps, a Rheodyne Model 5041 injection valve, PTFE tubes of 0.5 mm i.d., two T-union elements, a 1-ml PTFE mixing chamber and a Hellma quartz flow cell with a 10-mm light path and an 18- $\mu\text{l}$  inner volume. A Philips PU8625 spectrophotometer, a Spectra-Physics Model 4290 integrator for detection and data collection and an LKB Model 2209 Multitemp thermostatic bath were also used.

### Flow-injection system for the determination of $\text{SO}_2$

The whole assembly is depicted in Fig. 1. The assembly permits the successive determination of free and total  $\text{SO}_2$  by changing the reagent channels (total  $\text{SO}_2$  determination requires an on-line hydrolysis step with 4 M NaOH). Discrete volumes of sample are transported to the microdistillation module, which also leads the volatilized  $\text{SO}_2$  through the distillation unit into the absorption module, where the analyte reacts with DTNB to give a derivative that is monitored spectropho-

tometrically at 410 nm. Free and total  $\text{SO}_2$  signals are obtained by operating the microdistillation module at 20 and 100°C, respectively.

### Procedures

*Determination of free  $\text{SO}_2$  in wine samples.* Using the channel-reagent combinations 1 = sample; 2 = distilled water and 3 = 1.2 M phosphoric acid (see Fig. 1), series of sulphite standard solutions (in the 0–30  $\mu\text{g ml}^{-1}$  range) and wine samples are injected.

*Determination of total  $\text{SO}_2$  in wine samples.* Using the channel-reagent combinations 1 = 1.2 M phosphoric acid, 2 = 4 M NaOH and 3 = sample (see Fig. 1), series of sulphite standard solutions (in the 0–200  $\mu\text{g ml}^{-1}$  range) and wine samples are injected.

## RESULTS AND DISCUSSION

### Assembly design considerations

In contrast with other devices described previously [1], this assembly incorporates an injection valve, which permits the discrete addition of sample volumes into the system, and hence the whole assembly falls into the category of flow-injection analysis (FIA) devices. Other components are the propelling unit, the pretreatment module, the injection valve, the distillation unit and the reaction and detection modules. Relevant elements of the assembly are as follows.

The pretreatment unit is formed by channels 1, 2 and 3 and the elements placed before the injection valve. The unit was designed for sample treatment but also for easy sequential determination of free or total  $\text{SO}_2$ . In the determination of free  $\text{SO}_2$  it permits sample acidification with dilute phosphoric acid (pH  $\approx$  1.6) before the mixture fills the sample loop in the injection valve. This was incorporated to displace the sulphite-hydrogensulphite equilibrium to yield  $\text{SO}_2$  (g), thus helping the further volatilization of the analyte. However, the treatment is mild enough to preserve the delicate balance between the free and bound forms of sulphite. In the total  $\text{SO}_2$  determination, it permits alkaline hydrolysis of the sample in a well stirred mixing chamber for

45 s and further acidification with phosphoric acid (pH  $\approx$  3). Alkali treatment to displace bound SO<sub>2</sub> is usual in non-distillation procedures (i.e., iodimetric method or on-line gas diffusion assemblies). In distillation/dragging methods, the pre-hydrolysis treatment is avoided, the thermal treatment at ca. 100°C for 15–30 min apparently sufficient to recover the combined SO<sub>2</sub>. However, the short distillation time imposed by the FIA–volatilisation system suggests the use of the hydrolytic step.

The nitrogen carrier channel is used to transport the sample volume to the distillation unit. The use of a gaseous carrier avoids negative effects such as sample dilution, cooling or steam formation, produced if an aqueous carrier is used. Additionally, the nitrogen is responsible for carrying the gaseous analyte through the distillation unit.

In the glycerine bath, the volatilization column (a component of the distillation unit) is immersed to force SO<sub>2</sub> volatilization. Further, a copper coil carrying the nitrogen is heated in this bath prior to the sample transport into the injection valve. A vessel was also kept in this bath in order to supply hot water to clean the volatilization column.

A cleaning unit, formed by the above-mentioned vessel, a peristaltic pump and a by-pass valve, permits the nitrogen (normal mode) or the water (cleaning mode) to reach the volatilization column. As wine samples produce some residues, with cleaning water is necessary between samples.

The flow-rate of this water channel is 20 ml min<sup>-1</sup>, hence water should be occasionally provided.

The main components of the distillation unit are the following: the volatilization column, which is kept in the glycerine bath, and in which the acidified sample arrives, driven by the nitrogen carrier; a rectification column, communicating with the volatilization column and the absorption unit, which permits the SO<sub>2</sub> transportation (by the nitrogen carrier) with minimum dilution of the analyte with other volatile components (ethanol, water, etc.) of the matrix; an absorption unit, which is cooled by room-temperature circulating water and where SO<sub>2</sub> is dissolved and reacts with the incoming DTNB carrier reagent; and a degasification unit, which allows for the separation of the solution and nitrogen. The solution volume in this last part of the system is kept constant by means of a suitable outgoing flow-rate.

#### *Optimization of the procedure*

Chemical and physical parameters were optimized with the aid of aqueous standards. Table 1 shows the physical parameters adopted, with some comments on their influence on the system behaviour. Chemical parameters were adopted taking into account some previous literature recommendations. The NaOH concentration was 4 M, as used in the iodimetric procedure [4] and in an FIA method [9]. The phosphoric acid concentration chosen was 1.2 M, which is a compromise

TABLE 1  
Optimization of physical parameters

Parameter optimized	Range	Selected value <sup>a</sup>	Comments
N <sub>2</sub> pressure	0.8–3 atm	2 atm	Pressure under 1.2 atm does not eliminate cleaning water; no influence over 2 atm
Bath temperature	37–99°C	Room temp. (f), 100°C (t)	Apparent linear dependence
Pump speed	5–40 rpm	25 rpm	Better compromise between sensitivity and sample passage (see individual flow-rates in Fig. 1)
Sample volume	30–470 $\mu$ l	410 $\mu$ l	Apparent linear dependence. Better compromise between sensitivity and linearity of calibration graph
Coil length	Minimum–200 cm	Minimum	No effect

<sup>a</sup> (f) Free SO<sub>2</sub> determination; (t) total SO<sub>2</sub> determination.

between a low acidity for free  $\text{SO}_2$  determination and a sufficient acidity to maintain an acidic stream after NaOH neutralization in the total  $\text{SO}_2$  determination. DTNB was preferred to other derivatization agents previously used in FIA manifolds to react with  $\text{SO}_2$  [7,8,12], because of its convenience, simple preparation and stability, it being also free from interferences and forming a sensitive derivative. On the other hand the DTNB concentration was at the limit of its solubility at pH 6, as recommended by Brown and Jenke [13] in a paper dealing with the FI determination of sulphite in pharmaceuticals.

#### Study of interferences

Aqueous standards showed an appropriate behaviour and the system was expected to be suitable for the determination of  $\text{SO}_2$  in simple matrices. However, our interest was to establish the potential of the proposed system in relation to complex matrices, such as wines, with a large number of components, some of them with strong internal and external chemical activity and notable heterogeneity in their composition.

An individual study of the influence of some common compounds usually present in wine samples was also carried out using synthetic wine samples. The synthetic wine solution was prepared by mixing 115 ml of 96% ethanol, 7.0 g of citric acid, 2.0 g of glycerine, 3.8 g of L-(+)-tartaric acid, 3.0 g of glucose, 1.23 ml of 18 M sulphuric acid, 70 mg of acetaldehyde and 1 g of Enocianine, using various amounts of the compound to be investigated. Anhydrous acetic acid, L-ascorbic acid and L-cystine were also used. In all instances the mixture was diluted to 1 with distilled water.

The study was conceived in order to compare the EEC iodimetric and the FIA results. For each parameter a series of samples containing various amounts of  $\text{SO}_2$  were prepared for use as standards to construct the free and total  $\text{SO}_2$  calibration graphs. Additionally, a series of samples originally containing  $100 \mu\text{g ml}^{-1}$   $\text{SO}_2$  and various amounts of one of the individual components were also prepared. All solutions were aged for 24 h to permit  $\text{SO}_2$  to react with the components of the matrix. After this maturation step, all samples in each series were analysed by both the

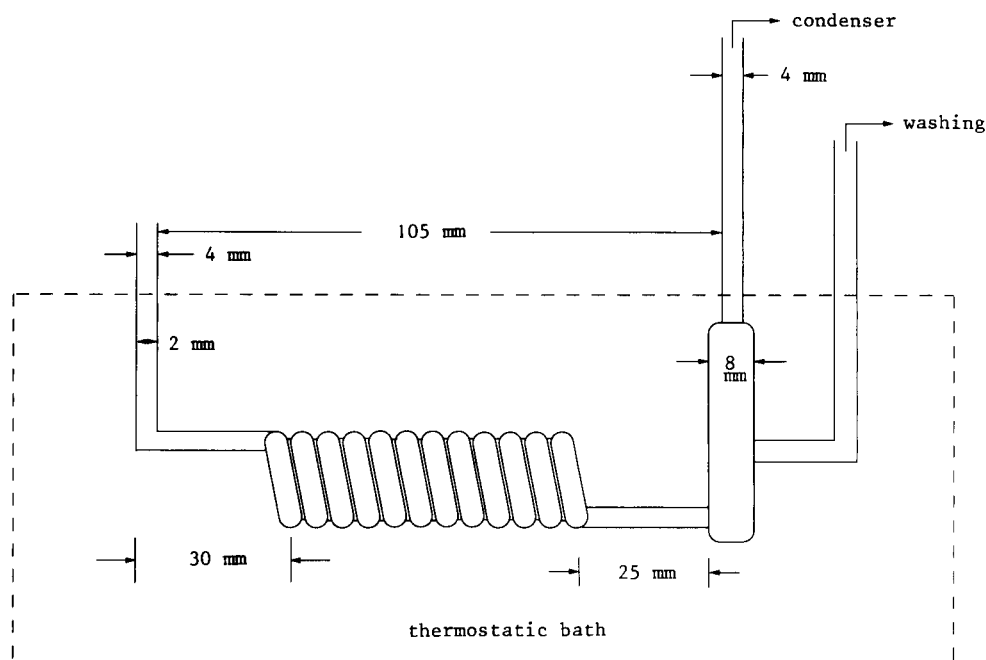


Fig. 2. Detail of the distillation unit

FIA and iodimetric methods. As the real SO<sub>2</sub> content was unknown, the SO<sub>2</sub> values for the standards obtained by the iodimetric method were used as reference values of FIA.

The main conclusions of this study were that acetaldehyde (0–400 µg ml<sup>-1</sup> range) affects both the FIA and iodimetric methods alike and glucose (up to 15 g l<sup>-1</sup>), ethanol (range 8–16%), Enocianina (range 0.3–1.5 g l<sup>-1</sup>), acetic acid (range 0.2–0.8 g l<sup>-1</sup>), L-cysteine (range 6–50 µg ml<sup>-1</sup>) and sample pH (range 3–3.8) had a negligible influence on the SO<sub>2</sub> determination by both methods. Figure 2 shows the influence of ascorbic acid. Unlike in the iodimetric method, the influence of ascorbic acid (range 10–100 µg ml<sup>-1</sup>) was negligible. Ascorbic acid is a common co-adjuvant for SO<sub>2</sub> which can be present if it is added to the wine. The influence of ascorbic acid on the iodimetric determination can be ascribed to the redox character of this determination.

#### Analytical features of the FIA method

Table 2 shows the analytical features of the FIA system. The linear range and detection limits are suitable for the determination of the SO<sub>2</sub> content in wine samples. The precision was not as good as for a typical FIA system owing to the presence of the on-line distillation step. However, it is comparable to that obtainable with the reference methods, with the advantage of a much higher sampling rate than with the off-line methods, thus permitting sufficient repetitions to ensure adequate accuracy. Finally, the sensitivity is acceptable for a normal use of the method; however, it can be increased by increasing the sample

TABLE 2  
Features of the FIA system

SO <sub>2</sub>	Linear range (µg ml <sup>-1</sup> )	Detection limit (µg ml <sup>-1</sup> )	R.S.D. <sup>a</sup> (%)	Sensitivity (absorb and × 10 <sup>3</sup> /µg ml <sup>-1</sup> )	Sampling rate (h <sup>-1</sup> )
Total	200	5	2.9	1.6 ± 0.1	30
Free	30	1	10.4	9.8 ± 0.1	30

<sup>a</sup> Calculated from wine samples in the middle of the linear range with ten consecutive injections.

TABLE 3

Analysis of wine samples <sup>a</sup>: comparison of distillation, iodimetric and FIA method <sup>b</sup>

Wine sample	Parameter	SO <sub>2</sub> concentration (µg ml <sup>-1</sup> ) <sup>b</sup>		
		Distillation method	Iodimetric method	FIA method
White 1	Total SO <sub>2</sub>	91	105	102
	Free SO <sub>2</sub>	14	11	19
White 2	Total SO <sub>2</sub>	77	63	71
	Free SO <sub>2</sub>	2	0	3
White 3	Total SO <sub>2</sub>	75	93	78
	Free SO <sub>2</sub>	10	9	12
Rosé 1	Total SO <sub>2</sub>	57	74	60
	Free SO <sub>2</sub>	5	2	5
Rosé 2	Total SO <sub>2</sub>	37	44	38
	Free SO <sub>2</sub>	2	1	2
Rosé 3	Total SO <sub>2</sub>	73	91	70
	Free SO <sub>2</sub>	4	1	3
Red 1	Total SO <sub>2</sub>	92	107	97
	Free SO <sub>2</sub>	2	3	1
Red 2	Total SO <sub>2</sub>	64	85	65
	Free SO <sub>2</sub>	3	4	3
Red 3	Total SO <sub>2</sub>	84	107	66
	Free SO <sub>2</sub>	2	2	2

<sup>a</sup> From Cheste, Valencia (Spain). <sup>b</sup> Average values for three replicates.

volume, if necessary. From these results it can be concluded that the proposed procedure can be used as a rapid assay method for monitor of the SO<sub>2</sub> content in wine samples.

#### Analysis of wine samples

Table 3 shows a comparison of the EEC distillation method [4], the EEC iodimetric method [4] and the proposed FIA method with representative commercial wine samples. In general, for the total SO<sub>2</sub> content, a better correlation was observed between the FIA and the distillation method than the iodimetric procedure. Some difficulties were experienced with end-point detection in the iodimetric procedure; especially with red wine samples the iodimetric method is not recommended [4]. This can explain the higher values obtained when this method was applied. The results for free SO<sub>2</sub> correlated well with all three methods. Figure 3 shows the good correla-

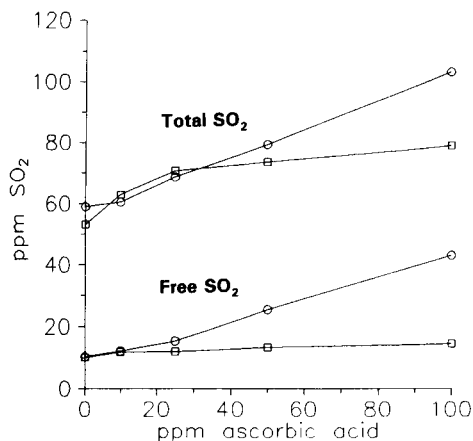


Fig. 3. Influence of ascorbic acid concentration on the determination of SO<sub>2</sub> by the (○) iodimetric and (□) FIA methods.

tion between the FIA and distillation methods for both free and total SO<sub>2</sub>.

### Conclusions

The results demonstrate that the proposed FIA method is adequate and sufficiently accurate for the determination of free and total SO<sub>2</sub> in wine samples. It is also suitable for the determination of SO<sub>2</sub> in other matrices owing to the highly selective on-line volatilization of the analyte. The assembly should also be satisfactory for the determination of other volatile analytes with minor modifications to the manifold.

The advantages of the FIA method over the classical methods are substantial. The FIA method is free from major interferences which occur in other procedures and, consequently, acidic, turbid or highly coloured wine samples can be analysed directly. The FIA method is also much faster for routine control than the distillation (ca. ten times faster) or the iodimetric (ca. five times) procedure, and requires smaller amounts of sample (ca. 50–100 times).

Finally, the results of the FIA method (*y*) are in good agreement with those of the reference EEC distillation method (*x*) (slope =  $0.99 \pm 0.17$ ; *y*-intercept =  $0 \pm 13 \mu\text{g ml}^{-1}$  SO<sub>2</sub>; correlation coefficient = 0.905 for total SO<sub>2</sub>; slope =  $1.39 \pm 0.08$ , *y*-intercept =  $-1.2 \pm 0.5\%$ ; correlation coefficient = 0.989 for free SO<sub>2</sub>; both *n* = 8, confidence limit 95%), the correlation parameters being better than those obtained between the distillation of iodimetric methods.

The authors acknowledge the financial support of the CICYT, Project ALI 90/0633.

### REFERENCES

- 1 M. Valcárcel and M.D. Luque de Castro, *Non-Chromatographic Continuous Separation Techniques*, Royal Society of Chemistry, Cambridge, 1991.
- 2 G. Monier-Williams, *Rep. Publ. Health Med. Subj.*, 43 (1927) 1.
- 3 H. Garza-Ulloa, *Brew. Dig.*, 55 (1980) 20.
- 4 *Off. J. Eur. Commun.*, 3rd October (1990) 125.
- 5 J.J. Sullivan, T.A. Hollingworth, M.M. Wekell, V.A. Meo, H.H. Saba, A. Etemad-Moghadam, C. Eklund, J.G. Phillips and B.H. Gump, *J. Assoc. Off. Anal. Chem.*, 73 (1990) 35.
- 6 J.M. Vahl and J.E. Converse, *J. Assoc. Off. Anal. Chem.*, 63 (1980) 194.
- 7 F. Lazaro, M.D. Luque de Castro and M. Valcárcel, *Anal. Chem.*, 59 (1987) 950.
- 8 J. Bartoli, M. Escalada, C. Jimenez and J. Alonso, *Anal. Chem.*, 63 (1991) 2535.
- 9 T.J. Cardwell, R.W. Cattrall, C.G. Nan, P.J. Iles, I.C. Hamilton and G.R. Scollary, *Electroanalysis*, 3 (1991) 859.
- 10 E. Esteve Juan, R. Puchades Pla and A. Maquieira Catalá, *Span. Pat.*, P9102435, 1991.
- 11 B.L. Wedzicha, L. Bronislaw and K. Michael, *Analyst*, 104 (1979) 694.
- 12 J.J. Sullivan, T.A. Hollingworth, M.M. Wekell, V.A. Meo, A. Etemad-Moghadam, J.G. Phillips and B.H. Gump, *J. Assoc. Off. Anal. Chem.*, 73 (1990) 223.
- 13 D.S. Brown and D.R. Jenke, *Analyst*, 112 (1987) 889.



# Spectrophotometric flow-through sensor for the determination of sulphur dioxide

P. Richter <sup>1</sup>, M.D. Luque de Castro and M. Valcárcel

*Department of Analytical Chemistry, Faculty of Sciences, University of Córdoba, E-14004 Córdoba (Spain)*

(Received 6th July 1992; revised manuscript received 13th October 1992)

## Abstract

A continuous-flow sensor based on integrated separation and spectrophotometric detection was developed for the determination of sulphur dioxide at the  $\text{ng ml}^{-1}$  level by transient immobilization of the reaction product formed between *p*-rosaniline, formaldehyde and sulphur dioxide on an ion exchange support packed in a flow cell. Sulphur dioxide was thus determined in the range  $0.16\text{--}6.0 \mu\text{g ml}^{-1}$  with a relative standard deviation of 2–3% ( $n = 11$ ). The detection limit ( $3\sigma$ ) achieved was  $49 \text{ ng ml}^{-1}$ . The proposed sensor was applied to the determination of free sulphur dioxide in white and rosé wines and the results obtained were consistent with those provided by the EEC recommended method.

**Keywords:** Flow injection; Sensors; UV-Visible; Sulphur dioxide; Wines

The use of sensors in continuous-flow systems reportedly enhances valuable analytical features of both manual and flow methods using the same analytical reaction [1–3]. The sensitivity and selectivity can be dramatically improved through the in situ concentration and separation processes taking place simultaneously on a support packed in the flow cell of a flow-through (bio)chemical sensor. These sensors are based on immobilization of one of the components of a (bio)chemical reaction in a flow cell packed with a suitable support that is placed in the light path of a molecular spectroscopic detector. The different systems developed so far in this context can be classified according to where the analytical reaction takes place along the manifold (the reaction can be homogeneous or heterogeneous de-

pending on whether it is carried out previously or in the flow cell, respectively). The analytical reaction can take place at: the support–solution interface [4–6] when the analyte or the reagent is the species to be immobilized in the flow cell, the catalyst–solution interface [7,8] when the catalyst, usually an enzyme, is to be immobilized or in the reactor, between the injection and detection units, when the support is to retain the reaction product [9–12]. The last approach was used in this work for the determination of sulphur dioxide by measuring the absorbance increase resulting from retention of the reaction product yielded by *p*-rosaniline–formaldehyde and sulphur dioxide in a flow cell packed with an ion-exchange resin.

Various conventional methods have been used to determine  $\text{SO}_2$  in different types of samples [13–17], most of which have some pitfalls as regards sensitivity, selectivity or simplicity. Flow-injection (FI) methods were recently applied to the determination of sulphur dioxide by using different manifolds and detection systems [18–23], all of which showed the high potential of FI for the

*Correspondence to:* M.D. Luque de Castro, Department of Analytical Chemistry, Faculty of Sciences, University of Córdoba, E-14004 Córdoba (Spain).

<sup>1</sup> Permanent address: Department of Chemistry, Faculty of Sciences, University of Chile, P.O. Box 653, Santiago (Chile).

determination of this analyte. However, no integrated retention–detection sensor for the determination of  $\text{SO}_2$  has so far been reported. This paper reports on the analytical advantages and the features of this approach for the determination of this analyte and on its application to wine analyses.

## EXPERIMENTAL

### Reagents

An amount of ca. 0.100 g of anhydrous sodium sulphite was dissolved in 100 ml of doubly distilled water. This solution was standardized iodometrically and more dilute solutions were prepared from it as required. Fresh solutions were prepared daily and stabilized with morpholine (0.01%) [16,17]. A 0.2% *p*-rosaniline (PRA) aqueous solution in 1 M HCl was prepared and purified according to Scaringelli et al. [13]. A 0.4% formaldehyde solution was prepared daily.

The eluent was 2 M HCl saturated with butan-1-ol. The anion-exchange material was rinsed with doubly distilled water and conditioned by triplicate treatment with 4 M HCl, 2 M sodium hydroxide and doubly distilled water, which converted the resin into its chloride form [24].

A Hellma 138-OS flow cell (inner volume 40  $\mu\text{l}$ ) was packed with resin up to 5–8 mm from the bottom. For proper packing of the resin the carrier solution was passed through the cell for 5–10 min.

### Apparatus and instruments

A Unicam Model 8625 UV–visible spectrophotometer equipped with the above-described flow cell and connected to a Knauer *x-t* recorder was used. A laboratory-made assembly including a planar BK7 PCX quartz lens driven by two micrometric screws was placed in the cell compartment in order to focus the light beam precisely at the exact position on the resin. The manifold used consisted of a Gilson Minipuls-2 four-channel peristaltic pump furnished with a rate selector, a Rheodyne Model 5041 injection valve, a Rheodyne Model 5060 rotary switching valve and a Tecator TM III chemifold.

## RESULTS AND DISCUSSION

The manifold used is depicted in Fig. 1. A 2-ml sample volume was inserted into a doubly distilled water or buffered stream at a flow-rate of  $1 \text{ ml min}^{-1}$ . The stream was merged at point M with the reagent solution (0.08% PRA + 0.2% HCHO, pH 0.4) at a flow-rate of  $1 \text{ ml min}^{-1}$ . The reaction product formed (*p*-rosanilinemethylsulphonic acid) in mixing coil r (300 cm  $\times$  0.5 mm i.d.) was retained by the flow cell, packed with Dowex 1-X8 of 200 mesh anion exchanger, when the switching valve (SV) was in position 1. As the plug tail reached the detector (55 s after injection), the concentrated retained reaction product was readily eluted with 2 M HCl saturated with butan-1-ol, which was inserted via SV (position 2), thereby restoring the baseline.

Injection of samples directly into the eluting carrier (2 M HCl) streams resulted in irreproducible signals because the pH difference between sample and carrier could not be offset by merging with the reagent stream.

### Types of signal

Two different types of signal were obtained depending on the order in which valves IV and SV (Fig. 2) were switched. The baseline was established while the eluting agent was circulated through the cell. When SV was switched to position 2, the absorbance signal increased to a con-

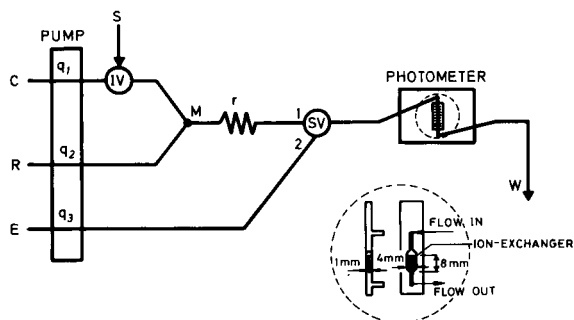


Fig. 1. Manifold used. S = sample; C = carrier; R = reagent (0.08% PRA + 0.2% formaldehyde, pH 0.4); E = eluent (2 M HCl saturated with butan-1-ol); q = flow-rate; IV = injection valve; M = mixing point; r = reaction coil; SV = switching valve; W = waste.

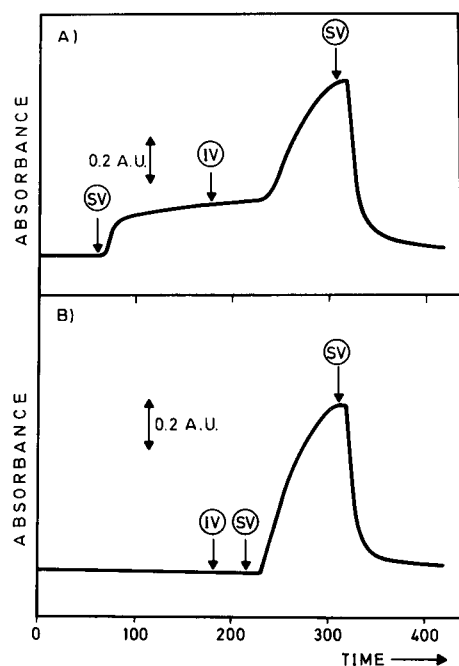


Fig. 2. Types of signal obtained according to the order in which SV and IV (switching and injection valve, respectively) were switched. For details, see text.

stant value of 0.18 on passage of the reagent through the cell (Fig. 2A). Then the sample was inserted via IV and a signal proportional to the concentration of  $\text{SO}_2$  in the sample was obtained 60 s after injection. The other possibility (Fig. 2B), which was ultimately chosen, was to inject the sample by first switching IV and, after 55 s, also switching SV when the retention product arrived at it, thus allowing simultaneous recording of the signals corresponding to the reagent and retained reaction product. Therefore, the reagent contribution to the overall signal corresponded to the blank. In both instances, the eluent was inserted via SV after the tail portion of the plug had reached the flow cell, so the signal was rapidly returned to its baseline.

#### Optimization of the proposed method

The variables affecting the performance of the proposed method were divided into three groups: chemical, FIA and those typical of the retention–elution/detection unit (i.e., characteristic of the sensor). All variables were optimized

by the univariate method; the optimum values and ranges over which they were investigated are given in Table 1.

**Chemical variables.** Both the analytical signal and the absorbance yielded by PRA (blank) were affected by the chemical composition of the reagent stream. Hence these variables were optimized in order to obtain the maximum possible analyte-to-blank ratio. Both contributions to the total peak were found to increase with increasing PRA concentration. Prior to optimization, it was essential to purify PRA [13] because impurities significantly increased the blank compared with the analyte signal. A PRA concentration of 0.08% was selected as optimum.

A similar effect of the reagent stream pH was observed. The colour intensity of the reaction product was enhanced by an increase in pH (that of the reagent stream was also pH dependent). The optimum pH was 0.4. On the other hand, no significant absorbance was obtained at low formaldehyde concentrations. The absorbance increased with increasing concentration of formaldehyde up to a maximum value of 0.14%, above which no effect on the blank signal was observed. A concentration of 0.2% of formaldehyde was selected as optimum.

**FIA variables.** Increased sample volumes resulted in proportionately increased analytical sig-

TABLE 1  
Study of variables

Variable	Range studied	Optimum value
<i>Chemical</i>		
PRA (%)	0.01–0.16	0.08
Formaldehyde (%)	0.02–1	0.2
pH	0–7	0.4
<i>FIA</i>		
Injected volume (ml)	0.1–3.5	2.0
Reactor length (cm)	0–400	300
Flow-rate ( $q_1 + q_2$ ) (ml min <sup>-1</sup> )	0.5–4	2
<i>Retention – detection unit</i>		
Path length (mm)	1–2	1
Particle size (mesh)	50–400	100–200
Eluting agent (HCl) (M)	10 <sup>-3</sup> –3	2
Flow-rate of eluting agent ( $q_3$ ) (ml min <sup>-1</sup> )	0.5–2	1

nals and residence times. A volume of 2 ml was chosen as a compromise between high sensitivity and low sample consumption.

Reaction coil lengths between 0 and 190 cm (i.d. 0.5 mm) influenced the peak height as the reaction was relatively slow. Longer lengths resulted in unchanged signals. A reactor of 300 cm  $\times$  0.5 mm i.d. was adopted in order to increase the dispersion of the reaction product, thus facilitating retention by fitting the concentration of the reaction product in the solution reaching the flow cell to the retention kinetics. The flow-rate had a marked influence on the signal. Increased flow-rates decreased the absorbance even if long reactors were used, which indicated that retention was not instantaneous. Very low total flow rates ( $0.5 \text{ ml min}^{-1}$ ) yielded very high yet irreproducible signals; hence an optimum value of  $2.0 \text{ ml min}^{-1}$  was chosen as a compromise between high sensitivity, reproducibility and sample throughput.

*Variables of the retention–elution / detection unit.* The influence of the cell path length was studied with cells of 1.0, 1.5 and 2.0 mm path length. The absorbance increased in proportion to the path length, but the resin itself saturated the detector capacity when cells of 2.0 mm were used. A cell of 1.0 mm path length yielding a baseline absorbance of 1.300 was chosen for all subsequent experiments.

The reaction product (*p*-rosanilinemethylsulphonic acid) yielded an absorption spectrum with maximum absorbance at 558 nm in solution, and was readily immobilized on anionic Dowex 1-X8 resin under the above-described working conditions (see Experimental), its maximum absorption wavelength being slightly shifted to 560 nm).

Decreasing the particle size of the support packed in the flow cell (50–400 mesh) resulted in an increase in the absorbance of the resin itself through increased compaction of the solid (the analytical signal remained constant). A resin of 100–200 mesh was chosen as optimum for further experiments.

Measurements were made by focusing the light beam 2.5 mm below the top of the resin level. Above this height, the signal decreased dramati-

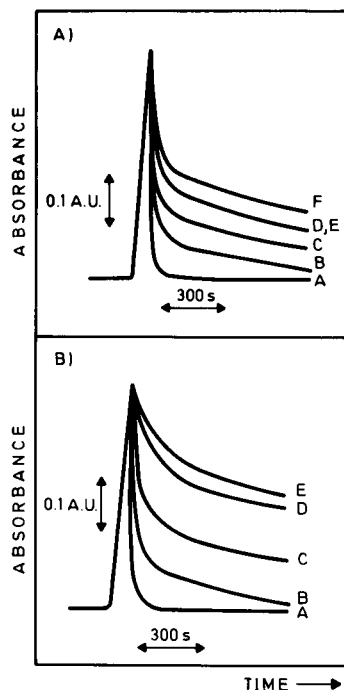


Fig. 3. Effect of various species used as eluting agents. (A) A, 2 M HCl; B, 30% ethanol; C, 30% dimethylformamide; D, E, 10% dimethylformamide and 20% ethanol; F, 10% ethanol. (B) Different concentrations of HCl: A,  $> 2 \text{ M}$ ; B,  $1 \text{ M}$ ; C,  $0.5 \text{ M}$ ; D,  $0.01 \text{ M}$ ; E,  $0.001 \text{ M}$ .

cally because the light beam passed through the solution above the resin. Heights lower than 2.5 mm decreased the absorbance at a rate of  $0.05 \text{ mm}^{-1}$  because the reaction product was largely retained on the resin zone where the flow impinged.

The potential of different species as eluting agents for the reaction product retained on the resin was investigated in order to make the sensor regenerable. As can be seen in Fig. 3A, organic solvents were not efficient for rapid elution. However, increasing HCl concentrations improved the efficiency of the regeneration process and resulted in faster restoration of the baseline at concentrations above 2 M (Fig. 3B). The concentration finally chosen was 2 M. After long working periods, the time required for regeneration increased owing to the sorption of traces of impurities present in PRA after purification. This required using 2 M HCl saturated with butan-1-ol

as the eluent. In this medium, dye impurity traces were eluted in each regeneration step, thus making the system fully re-usable.

#### Features of the proposed method

A series of standards of concentration between 0.10 and 10.0  $\mu\text{g ml}^{-1}$  were injected into the manifold under the optimum working conditions. The calibration graph obtained by plotting peak height against  $\text{SO}_2$  concentration (Fig. 2B) was linear over the range 0.16–6.0  $\mu\text{g ml}^{-1}$ . The corresponding equation obtained by the least-squares method was:

$$\text{absorbance} = 0.18 + 0.25[\text{SO}_2 (\mu\text{g ml}^{-1})]$$

$$(r = 0.9998, \text{R.S.D.} = 2.4\%, n = 11)$$

The standard deviation of the blank absorbance and the limit of detection ( $3\sigma$ ) were 0.004 and 49  $\text{ng ml}^{-1}$ , respectively. Figure 4 shows the recordings obtained. At least 400 sequential determinations can be carried out with the same sensor.

#### Applications

Sulphur dioxide is added to wine in order to avoid undesirable oxidation reactions and also as an antiseptic agent. Its concentration in the wine must therefore be measured. The proposed method was applied to the determination of free sulphur dioxide in wine samples.

Common constituents of wine such as ethanol, tartaric acid and sodium sulphate were tested as potential interferents. Sodium sulphate was found

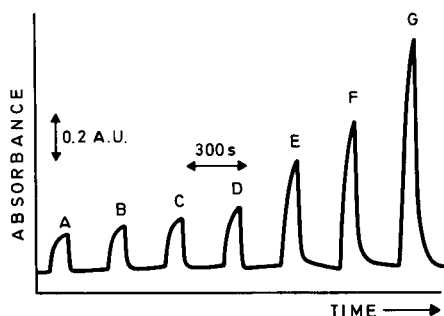


Fig. 4. Response signals from blank and increasing concentrations of  $\text{SO}_2$ . A, Blank signal; B, detection limit; C, determination limit; D, 0.43  $\mu\text{g ml}^{-1}$ ; E, 1.30  $\mu\text{g ml}^{-1}$ ; F, 2.15  $\mu\text{g ml}^{-1}$ ; G, 3.50  $\mu\text{g ml}^{-1}$ .

TABLE 2

Determination of free sulphur dioxide in wines

Sample No.	Found <sup>a</sup>		Error (%)
	Proposed method	Standard method [26]	
1	8.0 ± 0.1	8.3 ± 0.9	-3.0
2	31.4 ± 0.2	30.3 ± 0.4	+3.6
3	28.5 ± 0.2	28.4 ± 0.5	+0.3
4	11.4 ± 0.3	11.2 ± 0.4	+1.3
5	12.0 ± 0.4	12.2 ± 0.3	-2.3

<sup>a</sup> Average ± s.d. of five determinations.

not to interfere at a 2000 (w/w) interferent-to-analyte ratio. The recovery of free  $\text{SO}_2$  was then determined by preparing synthetic samples containing 0.5–3.0  $\mu\text{g ml}^{-1}$   $\text{SO}_2$ , 12% ethanol, 2.0  $\text{g l}^{-1}$  tartaric acid and 0.02 M  $\text{Na}_2\text{SO}_4$ . The R.S.D. of the recoveries was 1.3% ( $n = 5$ ).

Recoveries were also determined on various real wine samples (white and rosé) and the results obtained were compared with those provided by the standard method recommended by the European Economic Community (EEC) [25], which is based on the direct titration of free  $\text{SO}_2$  with iodine. As shown in Table 2, the results obtained by the two methods were consistent. The sensor cannot be applied to red wines because tannins are strongly retained by the support, giving spurious peaks.

#### Conclusions

A critical comparison of the proposed method, which is based on a sensor-integrated approach, with corresponding manual conventional [13], flow-injection [22] and batch ion-exchange absorptiometric counterparts [17], all of which use the same derivatization reaction, is warranted.

The most salient advantages of the proposed method are as follows: reduced human participation (automation capability); higher throughput than the batch alternatives (whether or not ion-exchange resins are used); high selectivity resulting from the in situ concentration kinetics; reusability of the resin, i.e., the sensor can be regenerated by elution of the retained reaction product (in the batch method, the resin is disposable); and simplicity, as reflected in the fact that

all the steps involved are performed in the flow system (the batch method requires manual mixing of the reactants, addition of the resin to the medium, washing, filtration and collection of the resin with the retained product in a conventional cell, followed by measurement).

On the other hand, the most serious disadvantage of the proposed sensor is its detection limit ( $49 \text{ nm ml}^{-1}$ ), which is higher than that of the batch ion-exchange method ( $5 \text{ ng ml}^{-1}$ ). This arises from absorption of the reactants prior to arrival of the product at the detector, i.e., from a high blank signal (see Fig. 4). Nevertheless, the proposed method is fifteen times faster than its batch counterpart, and is also simpler and involves much less human participation.

The Dirección General de Investigación Científica y Técnica (DGICYT) is thanked for financial support (Grant No. PB 90-0925). One of the authors (P.R.) expresses his gratitude to the Fundación Andes de Chile for the award of a post-doctoral grant covering the expenses incurred during his stay in Spain.

#### REFERENCES

- 1 M. Valcárcel and M.D. Luque de Castro, *Analyst*, 115 (1990) 699.
- 2 M.D. Luque de Castro and M. Valcárcel, *Trends Anal. Chem.*, 10 (1991) 114.
- 3 M.D. Luque de Castro and M. Valcárcel, *Lab. Robot. Autom.*, 3 (1992) 199.
- 4 F. Lázaro, M.D. Luque de Castro and M. Valcárcel, *Anal. Chim. Acta*, 214 (1988) 217.
- 5 T.L. Werner, J.G. Cummings and W.R. Seitz, *Anal. Chem.*, 61 (1989) 211.
- 6 S.M. Inman, E.S. Stromvall and S.H. Lieberman, *Anal. Chim. Acta*, 217 (1989) 249.
- 7 K. Hool and T.A. Nieman, *Anal. Chem.*, 60 (1988) 834.
- 8 P. Linares, M.D. Luque de Castro and M. Valcárcel, *Anal. Chim. Acta*, 230 (1990) 199.
- 9 F. Lázaro, M.D. Luque de Castro and M. Valcárcel, *Anal. Chim. Acta*, 219 (1989) 231.
- 10 D. Chen, M.D. Luque de Castro and M. Valcárcel, *Anal. Chim. Acta*, 234 (1990) 345.
- 11 K. Yoshimura, *Analyst*, 113 (1988) 471.
- 12 K. Yoshimura, *Bunseki Kagaku*, 36 (1987) 656.
- 13 F.P. Scaringelli, B.E. Saltzman and S.A. Frey, *Anal. Chem.*, 39 (1967) 1709.
- 14 D. West and G.C. Gaeke, *Anal. Chem.*, 28 (1956) 1816.
- 15 B.G. Stephens and F. Lindstrom, *Anal. Chem.*, 36 (1964) 1308.
- 16 V. Raman, J. Rai, M. Sing and D.C. Parashar, *Analyst*, 111 (1986) 189.
- 17 J.M. Bosque-Sendra, F. Molina and E. López, *Analyst*, 116 (1991) 871.
- 18 P. Linares, M.D. Luque de Castro and M. Valcárcel, *Anal. Chim. Acta*, 225 (1989) 443.
- 19 F. Lázaro, M.D. Luque de Castro and M. Valcárcel, *Anal. Chem.*, 59 (1987) 950.
- 20 J.J. Sullivan and J.E. Larose, *J. Assoc. Off. Anal. Chem.*, 69 (1986) 542.
- 21 P. MacLaurin, K.S. Parker, A. Townshend, P.J. Worsfold, N.W. Barnett and M. Crane, *Anal. Chim. Acta*, 238 (1990) 171.
- 22 G.B. Marshall and D. Midgley, *Analyst*, 108 (1983) 701.
- 23 A. Ríos, M.D. Luque de Castro, M. Valcárcel and H.A. Mottola, *Anal. Chem.*, 59 (1987) 666.
- 24 M. Marhol, *Ion Exchangers in Analytical Chemistry, Their Properties and Use in Inorganic Chemistry*, Elsevier, Amsterdam, 1982, p. 85.
- 25 *Off. J. Eur. Commun.*, May, 55 (1982) 78.

# Continuous-flow spectrophotometric determination of amino acids with 1,2-naphthoquinone-4-sulphonate reagent

J. Saurina and S. Hernández-Cassou

*Departament de Química Analítica, Universitat de Barcelona, Diagonal 647, 08028 Barcelona (Spain)*

(Received 10th September 1992)

## Abstract

A completely continuous-flow method for amino acid determination is proposed. The spectrophotometric detection is based on the reaction between amino acids and 1,2-naphthoquinone-4-sulphonic acid (NQS) in basic sodium carbonate–sodium hydroxide medium (pH 10). The reaction was developed on-line because NQS solutions are unstable in this medium. Phenylalanine (Phe) was chosen as a model amino acid to develop the method. The influence on the absorbance of different variables (pH, buffer and reagent concentrations, temperature, reaction coil length and flow-rate) were studied. For Phe at 470 nm, the calibration graph was linear up to  $1.5 \times 10^{-4}$  M, the reproducibility was 2.5% and the limit of detection was  $2 \times 10^{-6}$  M. The sample throughput was 40 h<sup>-1</sup>. Measurements of reaction product spectra were carried out in the range 290–590 nm. Spectral differences for nineteen amino acids derivatives were studied by using principal component analysis and cluster analysis. On this bases a spectral classification can be made.

*Keywords:* UV–Visible spectrophotometry; Amino acids; Continuous-flow analysis

The determination of amino acids is becoming increasingly important in different areas such as biochemistry, clinical chemistry, nutrition, agrochemistry and pharmaceutical formulations. Many types of samples are generated in which the amino acid contents (from femtomole to micromole amounts), their chemical form and the matrix sample (foods, biological fluids or protein hydrolysates) can be very different. Because of the diversity of and great demand for amino acid analyses, continuous-flow methodologies can play an important role in developing rapid, sensitive and inexpensive methods.

*Correspondence to:* S. Hernández-Cassou, Departament de Química Analítica, Universitat de Barcelona, Diagonal 647, 08028 Barcelona (Spain).

The determination of amino acids is usually carried out by liquid chromatographic techniques [1]. As most common amino acids are not readily detected by spectroscopic techniques (UV–visible spectrophotometry and fluorimetry), a chemical procedure for the derivatization of amino acids is required. Both the amino and the carboxylic groups offer possibilities for this derivatization, but most methods have been devoted to the amino function. The chromatographic step provides selectivity while the derivatization step enhances the sensitivity. Several reagents such as ninhydrin [2], trinitrobenzenesulphonic acid [3], phenyl isothiocyanate [4], dansyl chloride [5] and *o*-phthalaldehyde (OPA) [6] have been used for pre- or post-column derivatization [7].

In this work, a general spectrophotometric method for the determination of amines and

amino acids based on their reaction with 1,2-naphthoquinone-4-sulphonic acid (NQS) in basic medium [8] was developed with a completely continuous-flow analysis (CCFA) system. NQS has several advantages over the reagents mentioned above. In particular, it is water soluble, reacts with primary and secondary amino groups under milder conditions and is inexpensive. The main problem with this reagent is its instability in alkaline solutions. CCFA can overcome the reagent decomposition by obtaining on-line the proper pH conditions for the reaction.

NQS has recently been used in the determination of aliphatic amines in alcoholic drinks by liquid–liquid extraction coupled on-line with a flow-injection system [9]. Stopped-flow kinetic photometric methods have been also developed for the determination of procaine in pharmaceutical preparations [10] and biogenic amines [11]. The electrochemical properties of NQS derivatives have been employed in a post-column detection system for amines [12].

In recent years, diverse chemometric methods [13] have been developed for the resolution of complex mixtures in order to determine simultaneously their individual components without a previous separation step. These methods require the treatment of a large number of data which can be more easily generated by means of continuous-flow methodologies. The CCFA method developed in this work was used to acquire spectral data for nineteen NQS–amino acid products. The spectral differences of these amino acid derivatives allow the amino acids studied to be classified in different groups by applying two mathematical methods, principal component analysis [13] and cluster analysis [14].

## EXPERIMENTAL

### Reagents

All chemicals were of analytical-reagent grade. A set of nineteen aminoacids were supplied by Merck. Stock solutions of 0.01 M of each amino acid were prepared in distilled water. 1,2-Naphthoquinone-4-sulphonate (NQS) (Aldrich) was used as received. Stock solutions of NQS ( $1 \times$

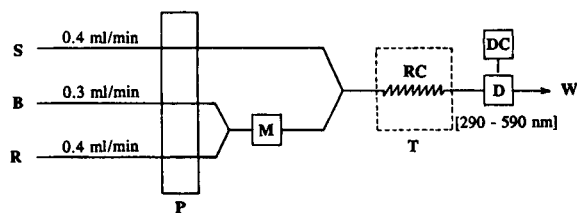


Fig. 1. Completely continuous-flow manifold. P = pump; M = mixing chamber; T = thermostatic bath; RC = reaction coil; D = detector; DC = data acquisition unit; S = sample; R = reagent ( $1 \times 10^{-3}$  M NQS in 0.1 M HCl); B = buffer (0.1 M  $\text{Na}_2\text{CO}_3$  + 0.075 M NaOH); W = waste.

$10^{-3}$  M) in 0.1 M hydrochloric acid are stable for at least 2 weeks. A buffer stock solution consisting of 0.1 M sodium carbonate (Scharlau) and 0.075 M sodium hydroxide (Merck) was employed to neutralize the NQS solution.

### Apparatus

A Beckman DU7 single-beam spectrophotometer with a Hellma flow cell (10-mm path length and 18- $\mu\text{l}$  volume) was used. Spectral data (290–590 nm) were collected with a micro-PC using Dumod software [15]. An SBS TFB-3 thermostatic bath and an SBS A-163 magnetic stirrer were used. pH was recorded with an Orion 8103 ROSS combined electrode connected to a Radiometer PHM84 pH meter.

### Flow manifold and measurement procedure

The three-channel completely continuous-flow manifold is shown in Fig. 1. Standard Tygon pump tubing was used to deliver aqueous solutions by means of a peristaltic pump P (Scharlau HP4). For all connections PTFE tubing and PTFE standard T-pieces were used. The amino acid sample merges with an alkaline stream of reagent as the NQS stock solution has been previously neutralized by the buffer solution in the mixing chamber M with magnetic stirring. This neutralization was done on-line because the reagent quickly decomposes in alkaline media. The colorimetric reaction takes place in the reaction coil RC made of PTFE tubing (10 m  $\times$  0.35 mm i.d.) which was immersed in a water-bath, T, at a controlled temperature of 70°C. The absorbance value corresponds to the difference between the



baseline signal and the steady-state signal, which is attained in about 90 s. The baseline is recorded when water is pumped instead of the amino acid solution.

## RESULTS AND DISCUSSION

The effect of different chemical, physical and flow variables was investigated in order to determine the optimum conditions for the method. The final values selected do not always correspond to the maximum absorbance signal but that they aim to achieve a suitable compromise between signal and other important conditions, such as sample rate (when the residence time is evaluated), spectral noise (when the reagent concentration is studied) or capability to differentiate spectra (when the pH is modified). In all experiments, phenylalanine was selected as a model amino acid to develop the method.

### *Influence of chemical variables*

**pH and buffer concentration.** A set of sodium carbonate–sodium hydroxide buffer solutions were prepared, in which the amount of sodium hydroxide added was varied while the carbonate concentration was kept constant at 0.1 M. In this way, the final pH values for the reaction were in the range 8–12. A  $1 \times 10^{-3}$  M solution of phenylalanine was chosen as an example. The results

TABLE 1

Effect of pH on the absorption maximum wavelength and on the absorbance of NQS–Phe product

pH	Wave-length 1 (nm)	Absorbance	Wave-length 2 (nm)	Absorbance
8.2	475.5	0.024	309.5	0.098
8.9	475.0	0.084	308.0	0.251
9.5	473.5	0.148	307.5	0.413
9.7	473.5	0.161	308.0	0.445
9.9	473.5	0.163	308.0	0.432
10.0	472.5	0.165	307.0	0.436
10.1	471.0	0.171	305.5	0.447
10.2	469.0	0.159	307.5	0.381
10.4	467.5	0.150	307.5	0.344
10.6	465.0	0.140	305.5	0.305

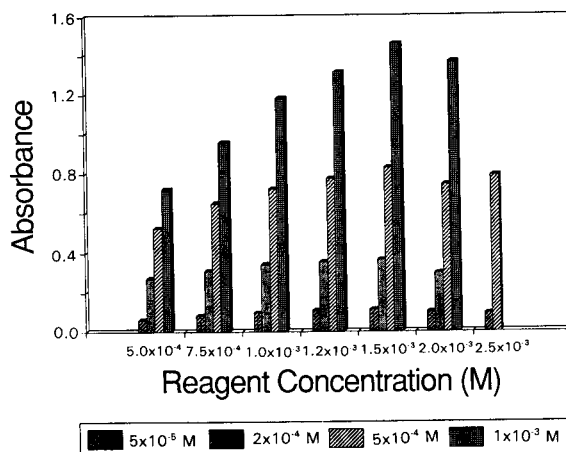


Fig. 2. Effect of reagent concentration on the absorbance at 470 nm of the proline derivative at four concentrations of Phe:  $5 \times 10^{-5}$ ,  $2 \times 10^{-4}$ ,  $5 \times 10^{-4}$  and  $1 \times 10^{-3}$  M.

summarized in Table 1 show that the maximum absorbance value is achieved at about pH 10 at the two absorption maximal wavelengths. When the pH increases there is a small shift of the absorption maxima, denoted by a colour change of the solution from light yellow (pH 8) to orange (pH 11).

The effect of buffer concentration was studied at pH 10 for solutions containing between 0.01 and 1 M of sodium carbonate. The absorbance increases slightly when the buffer concentration diminishes. A buffer concentration of 0.1 M  $\text{CO}_3^{2-}$  was selected.

**Reagent concentration.** This study was carried out at four different concentrations for each of Phe, Lys, Pro and Asp. The concentration of NQS reagent was varied in the range  $5 \times 10^{-4}$ – $2.5 \times 10^{-3}$  M for all sixteen cases. At higher concentrations of amino acid ( $1 \times 10^{-3}$  and  $5 \times 10^{-4}$  M), the absorbance increases when the reagent concentration increases, whereas at lower concentration ( $5 \times 10^{-5}$  and  $2 \times 10^{-4}$  M), the absorbance of Asp increases, that of Lys decreases, and for Pro (as shown in Fig. 2) and Phe the signals were virtually constant. Because the background noise increases greatly with increasing reagent concentration, a value of  $1 \times 10^{-3}$  M was chosen in spite of the fact that the maximum absorbance could not be achieved.

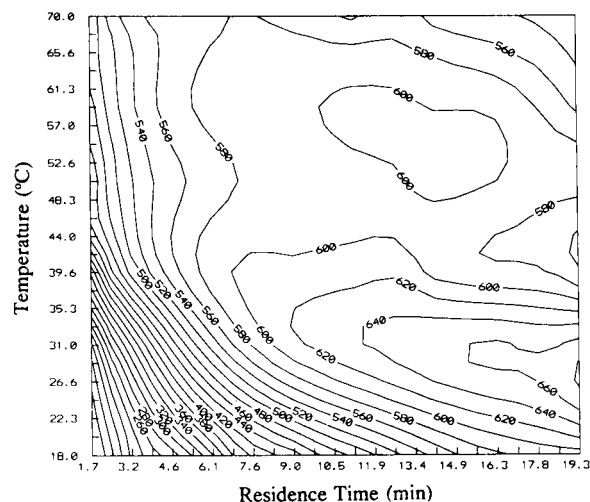


Fig. 3. Effect of residence time and temperature on the absorbance at 470 nm of NQS-Phe product. Contour plots indicate the values of absorbance  $\times 1000$ . Concentration of Phe =  $1 \times 10^{-3}$  M.

**Flow variables and temperature.** The combination of the length and inside diameter of the reactor and the total flow-rate determines the residence time of the sample in the reaction coil. The absorbance for a given residence time hardly changes for any combination of reactor dimensions and total flow-rate (length 2–13 m, i.d. 0.35–1.5 mm, flow-rate 0.4–4 ml min<sup>-1</sup>).

The residence time and the temperature are the factors with the largest effect on the absorbance because of the kinetic reaction between NQS and amino acids. The influence of these parameters on the absorbance was simultaneously studied. Figure 3 shows the response surface obtained by using the SURFER program for a  $1 \times 10^{-3}$  M Phe solution. In this topographic plot the absorbance at 470 nm is represented as level curves versus temperature and residence time. Temperature was varied from 18 to 70°C and residence time from 1.75 to 20 min. A reactor coil of 8 m  $\times$  1.1 mm i.d. was used, and each particular residence time was obtained by changing the total flow-rate while the individual flow channel ratios were kept constant. The graph was constructed from 78 experimental points.

The maximum signal is achieved with a long residence time (17–20 min) and low temperature

(25–30°C), but under these conditions the sample throughput is too slow. Figure 3 also shows that for low residence times the absorbance increases considerably with increasing temperature. The final values selected were total flow-rate 1.1 ml min<sup>-1</sup>, reaction coil 10 m  $\times$  0.35 mm i.d. and temperature 70°C. Under these conditions the sample throughput is about 40 h<sup>-1</sup> although the absorbance is 30% lower than the maximum.

If a method shows an interaction between two or more variables, a univariate optimization may not lead to the optimum response and, in consequence, it may be necessary to apply a multivariate optimization as was done in this work. The presence of an interaction between residence time and temperature can be seen in Fig. 3: at high temperatures when the residence time increases the absorbance becomes lower; it remains constant at medium temperatures (around 55°C) and increases continuously at low temperatures. This behaviour could be explained on the basis of the NQS and NQS-amino acid decompositions in alkaline media, mainly at high temperature.

#### Characteristics of the method

Under the conditions outlined above, the calibration graph for Phe is linear up to  $1.5 \times 10^{-4}$  M. The equation for the straight line at 470 nm was  $A = 1096C_{\text{Phe}} + 0.001$ . The relative standard deviation for a series of fifteen solutions with a concentration of  $5 \times 10^{-5}$  M Phe was 2.5%. The detection limit for Phe was  $2 \times 10^{-6}$  M. The sampling frequency was 40 h<sup>-1</sup>.

#### Spectra classification

Spectra were obtained by means of continuous-flow measurements on the nineteen  $1 \times 10^{-3}$  M amino acid solutions at four different pH values in the range 8–12. The amino acids were classified into groups based on the spectral differences of their NQS derivatives by applying mathematical methods (principal component analysis [13] and cluster analysis [14]).

**Principal component analysis (PCA).** PCA is based on the concentration of data information into a small number of variables (principal factors or principal components) by means of a suitable transformation of the original variables. The first

factor describes the maximum information of the samples while each successive factor explains less of the total information. PCA has been applied to the experimental matrix *M* (NSOLN, NWAWE), where NSOLN is the number of elements (19 amino acids) and NWAWE is the number of sensors (48 working wavelengths between 290 and 590 nm in steps of 6 nm). Thus, the elements of the matrix are the experimental absorbance of each NQS–amino acid product at each wavelength.

Several buffer solutions (0.1 M sodium carbonate/0.05–0.125 M sodium hydroxide) were prepared to study whether pH could influence the spectral distributions. Figure 4 shows how the NQS–amino acid spectra at four given pH values, are distributed on the first and the second princi-

pal components. The graphs indicate that most of the elements belong to a main group with similar NQS–amino acid spectra. At pH 9, there are only a few elements that are spectrophotometrically different [the derivatives of Cys and secondary amino acids (Pro and Hyp)], which are situated on the graph far away from the main group. With increasing pH the spectral differences become more noticeable, as can be seen in Figs. 5 and 6, and the number of elements separated from the main group is greater, i.e., at pH 11 the derivatives of Cys, Pro, Hyp, Lys, Tyr and Trp are clearly differentiated. This behaviour can be also identified by observing how the number of principal components changes with pH (from 8 at pH 9 to 12 at pH 11). The number of principal components was determined from the plot of the indica-

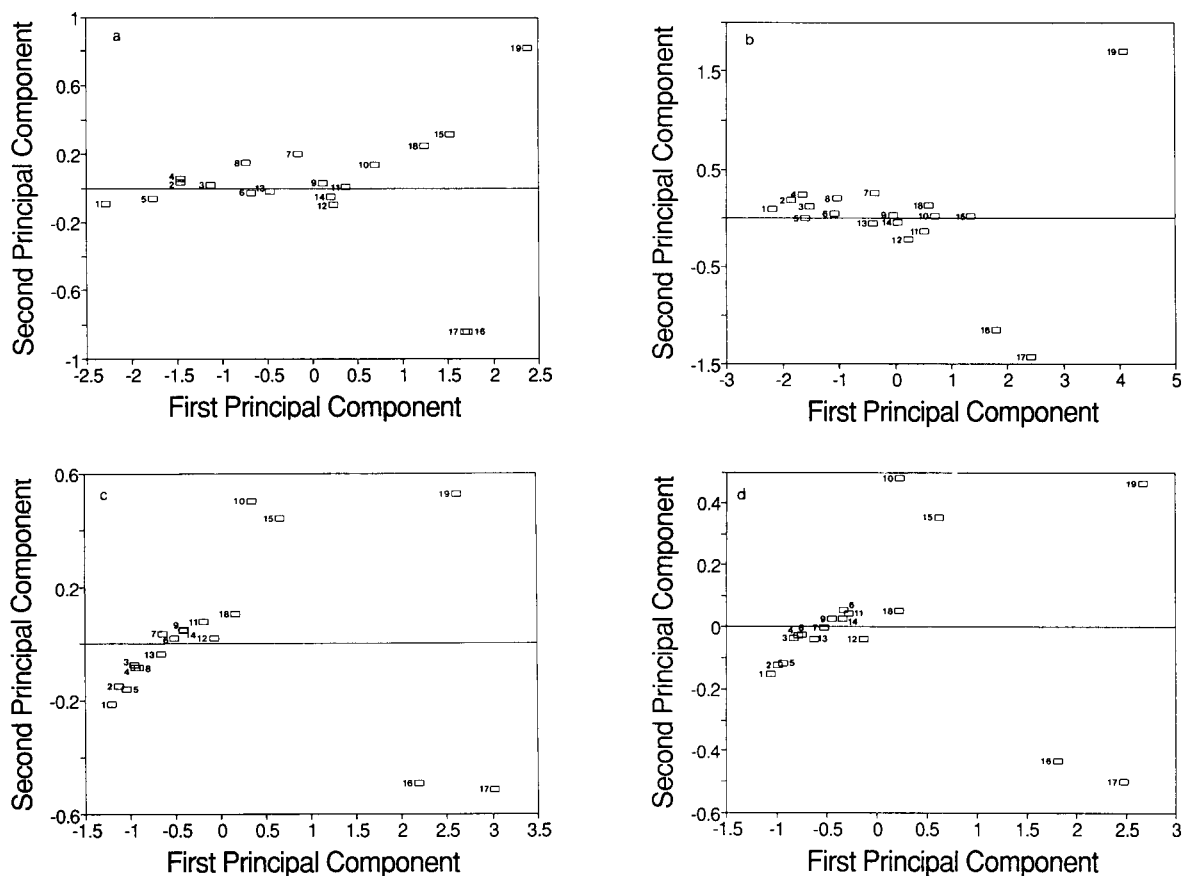


Fig. 4. Distribution of NQS–amino acid spectra on the first and second principal components. 1 = Asp; 2 = Ser; 3 = Thr; 4 = Ala; 5 = Glu; 6 = Gly; 7 = Arg; 8 = Val; 9 = Leu; 10 = His; 11 = Met; 12 = Tyr; 13 = Ile; 14 = Phe; 15 = Lys; 16 = Trp; 17 = Hyp; 18 = Pro; 19 = Cys. pH of reaction: (a) 9; (b) 10; (c) 11; (d) 12.

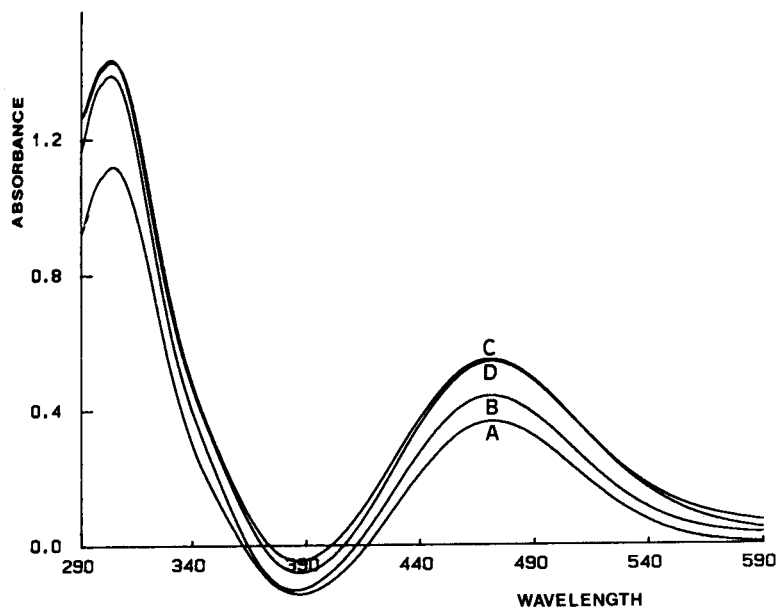


Fig. 5. NQS-amino acid spectra of (A) Arg, (B) Gly, (C) His and (D) Phe at pH 9. Concentrations of amino acids =  $1 \times 10^{-3}$  M.

tor function, described by Malinowski [16,17], and from the plot of the cross-validation results, as proposed by Wold [18]. This number is related to the number of species or groups of species that

are spectrophotometrically different in the system.

*Cluster analysis.* A similar study was carried out by cluster analysis techniques. The divisive

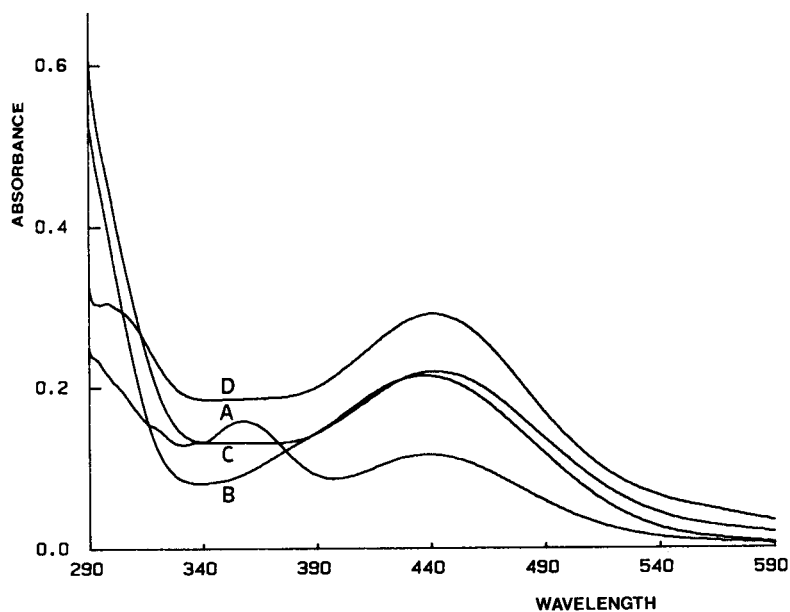


Fig. 6. NQS-amino acid spectra of (A) Arg, (B) Gly, (C) His and (D) Phe at pH 11. Concentrations of amino acids =  $1 \times 10^{-3}$  M.

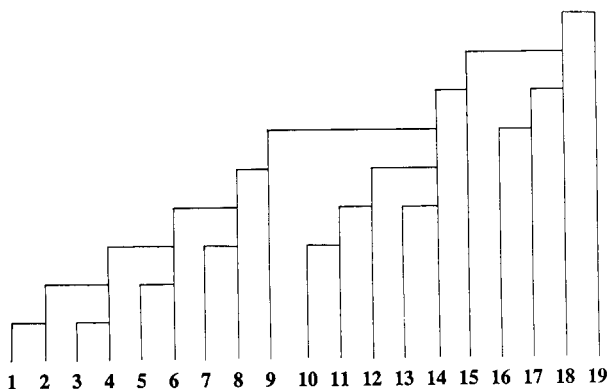


Fig. 7. Dendrogram of NQS–amino acid spectra at pH 10 obtained by cluster analysis. Numbers refer to amino acids as in Fig. 4.

McNaughton–Smith method [19] was applied to spectral data of amino acid derivatives obtained at the four pH values studied, using the euclidean distance as the similarity criterion. Figure 7 shows the dendrogram obtained at pH 10. The results are in agreement with those found from PCA.

### Conclusions

The proposed flow method provides a fast and easy way to acquire and treat spectrophotometric data from amino acid derivatives. Some important limitations can be overcome, such as instability of NQS reagent in basic media. The method shows good reproducibility, a low detection limit and 40 samples can be analysed per hour. These characteristics would make this method suitable for use as a post-column reaction system for the determination of amino acids in several types of samples after their chromatographic separation.

Principal component analysis and cluster analysis have been shown to offer the possibility of establishing a systematic classification of the spectra of NQS–amino acid products. In this way, it would be possible to determine some of the amino acids, i.e., lysine, proline and cysteine, in

real samples without a chromatographic separation step. Further work based on this classification is in progress for the resolution of amino acid mixtures by multivariate calibration methods.

The authors are indebted to Drs. R. Tauler and A. Izquierdo-Ridorsa for their help in this work. One of them (J.S.) also thanks to Ministerio de Educación y Ciencia for a doctoral grant.

### REFERENCES

- 1 W.T. Smith, Jr., and J.M. Patterson, *Anal. Chem.*, 62 (1990) 70R.
- 2 M. Rubinstein, S. Chen-Kiang, S. Stein and S. Udenfriend, *Anal. Biochem.*, 95 (1979) 117.
- 3 J. Molnár-Perl and G. Vitány, *Anal. Chem.*, 16 (1988) 173.
- 4 S.A. Cohen and D.J. Strydom, *Anal. Biochem.*, 174 (1988) 1.
- 5 C. DeJong, G.J. Hughes, E. Van Wieringen and K.J. Wilson, *J. Chromatogr.*, 241 (1982) 345.
- 6 P. Lindroth and K. Mopper, *Anal. Chem.*, 51 (1979) 1667.
- 7 H. Lingeman and W.J.M. Underberg (Eds.), *Detection-Oriented Derivatization Techniques in Liquid Chromatography*, Dekker, New York, 1990.
- 8 K. Hartke and U. Lohmann, *Chem. Lett.*, (1983) 693.
- 9 H. Koizumi and Y. Suzuki, *Anal. Sci.*, 4 (1988) 537.
- 10 M.C. Gutiérrez, A. Gómez-Hens and D. Pérez-Bendito, *J. Pharm. Biomed. Anal.*, 7 (1989) 413.
- 11 M.C. Gutiérrez, A. Gómez-Hens and D. Pérez-Bendito, *Fresenius' Z. Anal. Chem.*, 331 (1988) 642.
- 12 Y. Nakahara, A. Ishigami and Y. Takeda, *J. Chromatogr.*, 489 (1989) 371.
- 13 E.R. Malinowski and D.E. Howery, *Factor Analysis in Chemistry*, Wiley, New York, 1980.
- 14 D.L. Massart and L. Kaufman, *The Interpretation of Analytical Chemical Data by the Use of Cluster Analysis*, Wiley, New York, 1983.
- 15 J.L. Beltrán, G. Centeno, A. Izquierdo and M.D. Prat, *Talanta*, 39 (1992) 981.
- 16 E.R. Malinowski, *J. Chemometr.*, 3 (1988) 39.
- 17 E.R. Malinowski, *J. Chemometr.*, 1 (1987) 33.
- 18 S. Wold, *Technometrics*, 20 (1978) 397.
- 19 P. MacNaughton-Smith, W.T. Williams, M.B. Dale and L.G. Mockett, *Nature*, 202 (1964) 1034.

## Review

# Flow-injection immunoassays

G. Gübitz

*Institute of Pharmaceutical Chemistry, Karl-Franzens University of Graz, Schubertstrasse 1, A-8010 Graz (Austria)*

C. Shellum

*Sanofi Diagnostics Pasteur Inc., 1000 Lake Hazeltine Drive, Chaska, MN 55318-1084 (USA)*

(Received 14th October 1992; revised manuscript received 7th December 1992)

### Abstract

Flow-injection immunoassay is a method of conducting immunoassays using a small, reusable immunoreactor and a continuously flowing buffer stream into which samples and necessary reagents are introduced by valves or by injection. This review focuses on heterogeneous immunoassays. There are numerous potential merits to the use of flow injection and these are discussed. To date there has been much good exploratory work in this area but in general there has been little commercialization using this mode of immunoassay. This aspect is discussed.

*Keywords:* Flow injection; Immunoassay; Review

With the movement toward automation in immunoassays, more and more research is being done with continuous-flow systems. This format is inherently easier to automate than formats using tubes, microtiter plates or other similar reaction vessels and it can lead to very rapid results and very sensitive detection. There is great flexibility as to the type of detection system and, in general, much flexibility in terms of reagent addition.

Both homogeneous and heterogeneous flow-injection immunoassays (FIAs) have been developed. No separation is required in a homogeneous assay, whereas a heterogeneous assay requires the separation of bound from unbound label and typically utilizes a solid phase. The simplest flow-injection immunoassay would be of the homogeneous format. Here samples and reagents are mixed simply by the merging of two

streams or by injection of the sample into a flowing reagent stream. The binding of antigen to antibody typically modulates a standing signal produced by the labeled antibody, and this signal change is measured as the bound complex passes through a detection cell. There are a number of homogeneous flow-injection assays [1–4] including two successful commercial systems, the CE-DIA [5] and EMIT [6] homogeneous enzyme immunoassays.

Although homogeneous assays are very interesting, heterogeneous formats are more straightforward to develop and also offer many advantages. These assays are inherently more sensitive, especially for large proteins, they are less prone to interferences and are extremely flexible as to the choice of detection principle and solid phase. There are a number of examples of heterogeneous flow-injection immunoassays in the literature.

In these examples, the solid phase is typically contained in a small flow cell, termed an im-

*Correspondence to:* G. Gübitz, Institute of Pharmaceutical Chemistry, Karl-Franzens University of Graz, Schubertstrasse 1, A-8010 Graz (Austria)

munoreactor. The solid phase is usually made by coupling antigens or antibodies to preactivated particles, although activated membranes, capillaries or other high-surface-area matrices can also be used. Samples and all reagents are injected into a flowing buffer stream and carried to the immunoreactor where binding to the immobilized antibody or antigen takes place. Washing of unbound reagents is continuous. Detection takes place either directly at the immunoreactor or downstream, depending on the format chosen.

Heterogeneous flow-injection immunoassays offer extremely accelerated binding kinetics. This is true for two reasons. First, there is a very high surface area to volume ratio in the immunoreactor, and hence the effective concentration of capture antibody can be extremely high. Second, the binding reactions do not have to rely on passive diffusion to bring reactants together. The flowing stream actively brings the sample in contact with the solid-phase antibody. These factors result in a greatly enhanced antigen–antibody encounter rate and in nearly quantitative binding during the sample's short residence time in the immunoreactor. This is well documented in the field of affinity chromatography.

The examples given in this review will illustrate exactly what is meant by flow-injection immunoassay and will show the broad variety of approaches that have been examined. The examples will serve to demonstrate the tremendous potential to flow-injection immunoassay and will also point out some current limitations.

#### FLOW-INJECTION ENZYME IMMUNOASSAYS WITH ELECTROCHEMICAL DETECTION

Electrochemical detection (ED) is fairly sensitive, amenable to very small samples and is generally very well suited to flow-injection immunoassays. The flowing stream facilitates transport of the electroactive substance to the electrode surface. In contrast, ED is cumbersome and impractical to apply to immunoassays done in a conventional format. Below are discussed several flow-injection assays which have in common the use of ED.

One of the first heterogeneous flow-injection immunoassays was reported by Uditha de Alwis and Wilson [7]. They developed a flow-injection sandwich enzyme immunoassay for the determination of mouse monoclonal anti-bovine immunoglobulin G (IgG) using amperometric detection. A  $0.2 \times 4$  cm immunoreactor column containing bovine IgG immobilized on Reactigel-6X was used. The assay was performed by injection of sample (anti-bovine IgG), followed by two successive injections of glucose oxidase-labeled anti-bovine IgG and three injections of glucose as a substrate. Detection of the hydrogen peroxide formed by the enzymatic reaction was carried out amperometrically. Regeneration of the immunoreactor was done by a washing step using phosphate buffer (pH 2) followed by equilibration with assay buffer for 10 min. One cycle involving regeneration and equilibration took 30 min. Detection limits were in the low femtomole range. The immunoreactor can be used for about 500 assays during 3 months.

The same workers later described a competitive enzyme immunoassay for human IgG [8].  $F(ab')_2$  fragments of anti-human IgG were immobilized on tresyl-activated Trisacryl and packed into a  $0.2 \times 4$  cm column. The sample (HIgG) together with glucose oxidase-labeled IgG was injected, followed by a 3-min washing period and then by three successive injections of glucose at 3-min intervals. Detection was again carried out amperometrically. The time taken for one assay was 12 min and the between-assay interval was 8 min. A detection limit in the subpicomole range was reported.

Experiments were done to test the activity of the immunoreactor and the stability. The antibody, immobilized through the –SH moiety in its hinge region, retained 75% of its original binding activity and the immunosorbent could be stored for 2 years at 4°C with a negligible decrease in immunological activity. Experiments showed that 600 immunoreactor regenerations could be done over a 2-week period with less than a 5% decrease in activity.

Lee and Meyerhoff [9] described a flow-injection sandwich enzyme immunoassay for the determination of HIgG and  $\alpha_1$ -acid glycoprotein

using potentiometric detection. The instrumental set-up is based on a three-channel peristaltic pump and a three-valve switching system. The immunoreactor was constructed from a four-way rotary Teflon valve by replacing the normal sample loop with a 2.5 cm × 1.5 cm silicone-rubber tube filled with IgG or  $\alpha_1$ -acid glycoprotein antibodies bound to controlled-pore glass. The assay was carried out by injection of the sample followed by a 3-min washing period and then by injection of adenosine deaminase-labeled antibodies. Unbound species were washed away by the carrier buffer and the stream of substrate solution (adenosine) was passed through the immunoreactor. The product formed by the enzymatic reaction, ammonia, was detected with an ammonium-ion selective electrode. The immunoreactor was regenerated by pumping glycine-HCl buffer (pH 2.2) through the reactor for 2 min. The total time for a single assay cycle was 12 min, including regeneration of the reactor. The detection limits for IgG were 5 ng/ml and for AGP 3  $\mu$ g/ml.

Luong and Prusak-Sochaczewski [10] developed an FIIA for the determination of *Salmonella typhimurium*. Antibodies to *Salmonella* were immobilized on Tygon tubing by adsorption or on polyethylene tubing by covalent binding. The assay was carried out by successive injection of the sample, glucose oxidase-conjugated antibodies and the substrate (glucose). During the sample incubation the flow was stopped for 2 min to promote greater binding. The hydrogen peroxide formed by the enzymatic reaction was detected amperometrically. Regeneration of the immunoreactor was carried out with 0.2 M glycine-HCl (pH 2.2). This method allowed the detection of  $10^5$ – $10^6$  *Salmonella* cells ml<sup>-1</sup> in less than 10 min.

#### FLOW-INJECTION IMMUNOASSAYS WITH SPECTROPHOTOMETRIC AND FLUORIMETRIC DETECTION

Mattiasson et al. [11] developed a flow-injection binding assay for carbohydrate analysis. The reactor was a 50- $\mu$ l concanavalin A (Con A)

column, the analytes were glucosides and the competitive label reagent was the glycoprotein horseradish peroxidase (HRP). HRP and the carbohydrate analyte (1-*O*-methyl- $\alpha$ -D-glucopyranoside or methyl- $\alpha$ -D-mannopyranoside) were mixed and injected on to the Con A column where competition for binding sites occurred. HRP substrate was then passed through and the product formed after adding hydrogen peroxide and 4-aminoantipyrine was detected spectrophotometrically in a downstream flow cell. Glycine-HCl (pH 2.2) was used to regenerate the column. Through optimization the cycle time was reduced to one sample every 70 s with a detection limit comparable to that of other methods for these analytes.

An essential improvement in sensitivity in FIIA can be obtained by using fluorescence detection.

Stöcklein and Schmid [12] described the development of an FIIA with fluorescence detection which allows the monitoring of monoclonal antibodies in the course of a hybridoma cell fermentation. The immunoreactor contained either membranes or magnetic particles as supports for the immobilized antibodies. A competitive and a sandwich assay for mouse IgG were carried out, using peroxidase-labeled antibodies against mouse IgG. In the competitive format, the immunoreactor contained immobilized antigens. Sample antigen and conjugated antibodies were injected via a double-valve injector and incubated for 1 min in a mixing coil before passing to the immunoreactor. Hydrogen peroxide and hydroxyphenylpropionic acid were injected via a second valve and allowed to react for 2 min. In the sandwich assay, the reactor contained immobilized antibodies. The sample antigen and conjugate were injected sequentially and allowed to react for 5 min each in the reactor before the substrate injection. The cycle time for the competitive assay was 10 min and for the sandwich assay 25 min.

It is planned both to automate the membrane exchange and to develop a magnetic particle dosage mechanism in order to avoid the necessity of regeneration of the immunoreactors. The goal is efficient on-line monitoring of monoclonal antibody production.

A simple and rapid fluorescence FIIA for DNP derivatives has recently been published by



Kusterbeck et al. [13]. Antibodies directed against the DNP moiety were immobilized to tressyl-activated Sepharose 4B and packed into 200–500- $\mu$ l columns. The binding sites of the immobilized antibodies in the column were saturated with fluorescein-labeled antigens. The sample (DNP derivatives) displaces labeled antigens, resulting in a fluorescence signal downstream at the detector. The readout occurs within 3 min after sample injection. Enough labeled antigen could be loaded on to the solid phase so that several analyses could be done before column regeneration at low pH. A linear calibration graph was obtained for DNP-lysine over a concentration range 60–460 pmol per 200  $\mu$ l and the detection limits were about 50 pmol per 200- $\mu$ l injection.

New fluorescent labels for immunoassays have been introduced by Savitsky et al. [14] and recently been applied to an FIIA for the determination of foot and mouth disease viral antigens [15]. An affinity column specific to the viral antigen and antibodies labeled with highly fluorescent porphyrins were used. The assay time is 10–20 min with a detection limit of about 10 ng ml<sup>-1</sup>. The affinity column was used for over 50 assays and for 3–4 days of continuous work at room temperature.

A new approach, liposome-enhanced flow-injection immunoanalysis, has recently been introduced by Durst and co-workers [16,17]. They showed that the use of liposome-entrapped fluorophore results in a fluorescence signal amplification of more than two orders of magnitude. A competitive assay for theophylline makes use of phospholipid liposomes in which carboxyfluorescein has been entrapped and an immunoreactor column containing anti-theophylline antibodies immobilized on fused-silica particles. The liposomes were surface conjugated with theophyllinephosphatidylethanolamine. The assay was carried out by mixing and injecting the sample and theophylline-conjugated liposomes. The liposomes were then disrupted to release entrapped fluorophore by passing a surfactant or chaotropic agent through the column for 4 min. The fluorescence was detected downstream. KSCN and 1-*O*-octyl- $\beta$ -*D*-glucopyranoside (OG) were compared for the purpose of liposome disruption. Whereas

KSCN resulted in denaturation and significant inactivation of the immunoreactor, OG did not harm the immobilized antibodies. The same immunoreactor was used for about 270 assays over a period of 3 months. The detection limits obtained were about  $3 \times 10^{-8}$  M.

#### FLOW-INJECTION IMMUNOASSAYS WITH CHEMILUMINESCENCE DETECTION

Chemiluminescence (CL) detection has been very successfully implemented in the field of immunoassay within the past decade. It has led to extremely sensitive non-isotopic assays with long shelf-life, simplified assay formats and general applicability to molecules of all sizes. Flow injection is perfectly suited to take advantage of chemiluminescent labels, and several groups have reported its successful application.

The first attempt to use CL detection in a flow-injection system in connection with an immunoassay was reported by Maeda and Tsuji [18]. They developed enzyme immunoassays for  $\alpha$ -fetoprotein, insulin and 17- $\alpha$ -hydroxyprogesterone. However, because the immunoreactions were carried out in a classical way by an overnight incubation of the sample antigen and glucose oxidase-labeled antibodies in antibody-coated tubes, this assay cannot be regarded as a true flow-injection immunoassay. Only the CL reaction was carried out in the flow-injection system. Glucose substrate was added to the reaction mixture and it was injected into the flow system. The hydrogen peroxide was detected with luminol-Fe(CN)<sub>6</sub>.

Osipov et al. [19] reported the development of an FIIA for human IgG using antibodies immobilized on a polystyrene bead and peroxidase-labeled antibodies. The instrumental set-up was based on a two-pump system with a double-valve injector. For detection, an enhanced luminol CL reaction was used.

The assay was carried out in a stop-flow mode. The sample and rabbit anti-human IgG peroxidase conjugate were injected by the double-valve injector and transported successively into a reaction cell containing a 6-mm polystyrene bead with

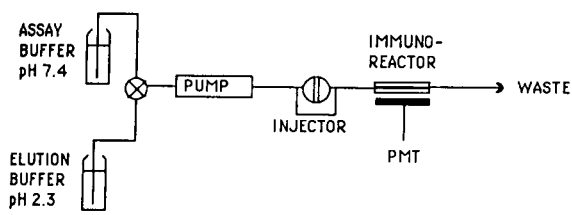


Fig. 1. Instrumental set-up for flow-injection immunoassay based on acridinium ester CL detection.

immobilized antibodies. When the antigen and the antibody conjugate reached the bead, the pump was stopped for 2 min each. After washing, the bead was transferred automatically to the detection cell and mixed with luminol, iodophenol and hydrogen peroxide to initiate the CL reaction. The detection limit for HIgG was  $1 \times 10^{-9}$  M and the overall time of the assay was 5–10 min.

An FIIA using acridinium ester CL detection has been developed [20]. The instrumental set-up is shown in Fig. 1. The system is based on an immunoreactor consisting of a transparent 20- $\mu$ l flow cell packed with immobilized antibodies. The entire immunoassay including CL detection takes place in the packed flow cell. Light is collected directly from the transparent cell. No stopped flow is necessary in this system. The system was optimized by use of mouse IgG as a model analyte and also applied to the determination of HIgG. As a CL label 4-(2-succinimidyl)oxycarbonyl)ethyl)phenyl-10-methylacridinium-9-carboxylate fluorosulphonate was used [21].

A sandwich assay, applicable to proteins, was the first variation explored. The basic scheme is shown in Fig. 2. Anti-IgG antibodies were immobilized on carbonyldiimidazole (CDI)-activated Trisacryl. In the first step the sample (mouse IgG) was injected and became bound to the immobilized antibodies. In the second step, acridinium-labeled antibodies were injected, forming an immunosandwich. In the last step, hydrogen peroxide was injected to initiate the CL reaction. Regeneration the immunoreactor was carried out by washing with acidic buffer or by injection of 60  $\mu$ l of 0.1 M HCl. One assay cycle including regeneration required 12 min with a detection limit of

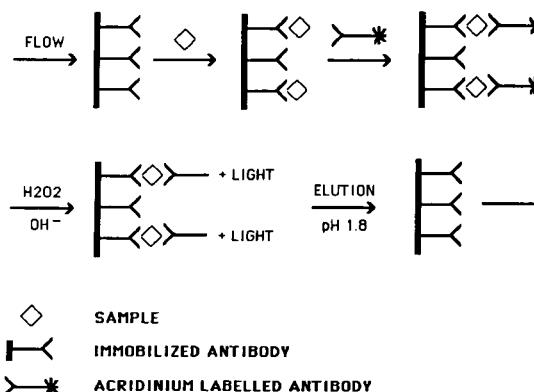


Fig. 2. Chemiluminescence flow-injection immunoassay in the sandwich mode.

200 amol. The linear range of the calibration graph was about two decades. The relative standard deviation for manual injections of 20 fmol of mouse IgG was about 4% ( $n = 10$ ). Similar results were obtained with HIgG.

Another variation explored was a competitive assay (Fig. 3). Sample antigen and labeled antigen were injected together and competed for the binding sites at the immobilized antibodies. The sensitivity obtained for IgG with this more rapid approach was about one order of magnitude less than that with the sandwich assay. This type of assay, however, has potential application to small haptens. In the sandwich format the goal is to couple as much capture antibody on the solid phase as is feasible. The competitive format, on the other hand, demands limiting the capture

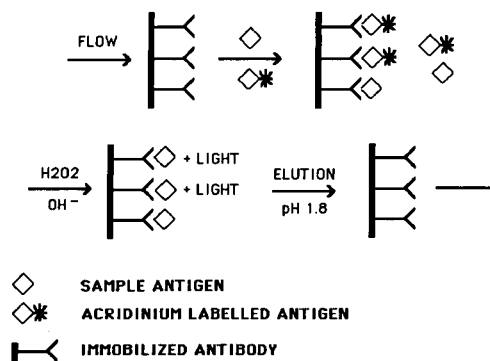


Fig. 3. Chemiluminescence flow-injection immunoassay in the competitive mode.

antibody either by coupling less to the solid phase or by mixing antibody-coupled particles with uncoupled particles before packing the immunoreactor.

A further variation tested was the use of the biotin–streptavidin binding system where the antibody is biotinylated and streptavidin is labeled with acridinium ester [22]. One advantage of this system is the avoidance of direct labeling of the antibodies with dyes, which sometimes causes denaturation. Biotinylated antibodies are often commercially available, or can easily be prepared by commercially available activated biotin. A further advantage is an amplification in sensitivity because streptavidin can be labeled at a higher specific activity than most proteins. Hart and Taffe [23] reported a molar incorporation of eight acridinium ester molecules per streptavidin molecule with no reduction in biotin binding. This is approximately double the incorporation ratio that is feasible for acridinium-labeled antibodies. The detection limit obtained for HIgG was about 50 amol. To improve the reproducibility, reduce the assay time and enhance the sample throughput, full automation of the system is currently in progress.

Recently, Liu et al. [24] developed a similar type of flow-injection CL immunoassay using a membrane-based reactor. The goal was to avoid light scattering from a particle solid phase and to improve the reproducibility of immunoreactor preparation previously obtained with a cylindrical, packed immunoreactor.

They developed a sandwich assay for mouse antiovine IgG with the antigen (bovine IgG) immobilized on a membrane and inserted in a thin-layer flow cell. Horseradish peroxidase-labeled goat anti-mouse IgG was used to catalyze the luminol–hydrogen peroxide reaction for CL detection. The assay was carried out by four successive injections: the sample of mouse antiovine IgG was injected followed by goat anti-mouse peroxidase conjugate, buffer and finally hydrogen peroxide–luminol–iodophenol CL reagent. Light was collected from the membrane through a transparent Plexiglas flow cell window. After detection, the immunoreactor was regenerated by switching to a washing buffer (pH 2.2).

The membrane had to be replaced after three sample injections. The assay time was 8 min with a detection limit of 1 fmol.

Hage and Kao [25] recently reported an automated sandwich immunoassay for the determination of parathyroid hormone (PTH) based on “high-performance immunoaffinity chromatography” with acridinium ester-based CL detection. The set-up is similar to a flow-injection system and consisted of three pumps with a valve-switching system. Sample and acridinium-labeled antibodies were first incubated for 1 h in the autosampler tray. The mixture was then injected on to a 2 cm × 4 mm i.d. HPIAC column containing immobilized anti-PTH antibodies. After washing the column, the PTH-labeled antibody complex was eluted with buffer (pH 3) and combined with hydrogen peroxide–NaOH reagent in the post-column reactor to initiate the CL reaction. The assay required 6 min following 1 h of incubation. The limit of detection was 16 amol. A fully on-line format was also demonstrated but a 1-h preincubation was found to be necessary in this instance to obtain the high level of sensitivity necessary for PTH. This is still 24 times faster than the norm for PTH analysis.

## DISCUSSION

A drawback to the current flow-injection approaches is that the solid phase needs to be regenerated after each sample. It will eventually lose activity on repeated regeneration, although some of the solid phases noted here showed remarkable stability (up to 600 regenerations) [8].

There are many positive aspects to immunoreactor regeneration. It greatly conserves capture antibody and would be ideal for situations using unique or precious antibodies. Also, the antibody or antigen can be covalently coupled so as to give maximum possible activity [8]. This can be done in almost any assay format but it is probably most cost effective when the solid phase is being reused. Finally, flow-injection formats would make it easy and efficient to use universal capture phases such as anti-mouse IgG or anti-rabbit IgG. The immunoreactor regeneration conditions, once opti-

mized, would be identical for all analyses done on that particular phase.

Even with these potential merits to solid-phase regeneration, there is understandably much resistance to the idea, especially for assays where carryover of high samples can be a problem. The solution may lie in the development of exchangeable solid phases where a new charge of particles or a new membrane is used for each sample. This is already under investigation by Stöcklein and Schmid [12] and there are no doubt many potential approaches to this problem.

A second drawback to the FIIA approaches reported here is sample throughput. The flow systems described in this paper were locked into one sample at a time. Thus, even though one can obtain a result in 5–10 min, the sample throughput would be only 6–12 h<sup>-1</sup>. For high-volume testing of hundreds of samples per day, the systems here would require modifications. The most likely solution would be the design of a system with multiple channels. The quickest assay reported here had a sample throughput of 50 h<sup>-1</sup> with a single channel [11]. The use of five channels with this system, for example, would increase the sample throughput to 250 h<sup>-1</sup>, significantly faster than current automated immunoassay systems. There is much precedent for multi-channel systems in the field of flow-injection analysis, and it should be just a matter of time before it is demonstrated in the area of flow-injection immunoassay.

There are various advantages to heterogeneous flow-injection immunoassays. One of the primary advantages is the speed of analyses. In the most rapid assay reported [11], glucosides were analyzed at the rate of one sample every 70 s, and for other methods reported here analysis times of ca. 10 min or less are common. It would be difficult to match a 70-s analysis time with anything other than a flow-injection format and 10 min is more rapid than most non-flow-injection assay formats. The speed is a direct result of the rapid binding that occurs when the sample is pushed through the immunoreactor containing a high surface area and high effective concentration of capture antibody.

Ease of automation is another major advan-

tage. Very little additional engineering was necessary in the assay systems reported here. Most were put together with commercially available chromatographic or flow-injection apparatus with the addition of an immunoreactor of relatively simple construction. The automation of conventional non-flow injection formats, in contrast, is complex and demands more apparatus and more sophisticated computer control. Injecting samples and reagents is simpler and more precise than pipetting, and the washing of the solid phase in a flow-injection system is much simpler than a conventional format. In flow injection, the washing of the solid phase is continuous and inherent in the system. Most conventional automated systems using beads, particles or microtiter wells require multiple additions and aspirations of wash fluid.

Although few direct comparisons of detection limit have been made between flow- and non-flow-injection systems, it is clear from the reports here that FIIA has the potential for very sensitive detection, especially with chemiluminescence. Using acridinium ester-labeled antibodies, Hage and Kao [25] reported a detection limit of 16 amol of PTH, and Shellum and Gübitz [20] a detection limit of 50 amol of IgG. The unique feature of heterogeneous flow-injection assay is that the immunoreactor acts to concentrate the sample. When a sufficient excess of capture antibody is available on the solid phase, increasing the sample volume leads to a direct, proportional decrease in detection limit. In a conventional system, an increase in sample volume dilutes the reaction mixture and the increase in sensitivity is not as dramatic.

Rapid results, ease of automation, good precision and inherently good sensitivity are a powerful combination delivered by flow-injection immunoassays. For the ideas to spread and penetrate further into the commercial area of diagnostics there is a need for more demonstration of efficacy in authentic clinical laboratory situations. This should come soon given the numerous groups working in this area.

There are many fully automated immunoassay systems commercially available [26]. They are typically capable of processing 50–150 samples per hour and some of them are capable of continuous

random access where new samples can be loaded at any time. It is important to point out that the goals of flow-injection immunoassay are not unrelated of those of these current systems. Flow injection is simply a different, potentially more logical, method of carrying out full automation.

## REFERENCES

- 1 C.S. Lim, J.N. Miller and J.W. Bridges, *Anal. Chim. Acta*, 114 (1980) 183.
- 2 T.A. Kelly and G.D. Christian, *Talanta*, 29 (1982) 1109.
- 3 P.J. Worsfold and A. Hughes, *Analyst*, 109 (1984) 339.
- 4 G.F. Blackburn, H.P. Sha, J.H. Kenton, J. Leland, R.A. Kamin, J. Link, J. Peterman, M.J. Powell, A. Shaw, D.B. Talley, S.K. Tyagi, E. Wilkins, T.-G. Wu and R.J. Massey, *Clin. Chem.*, 37 (1991) 1534.
- 5 P.L. Khanna, R.T. Dworschak, W.B. Manning and J.D. Harris, *Clin. Chim. Acta*, 185 (1989) 231.
- 6 R.S. Schneider, P. Lindquist, E.T. Wong, K.E. Rubenstein and E.F. Ullman, *Clin. Chem.*, 19 (1973) 821.
- 7 W. Uditha de Alwis and G.S. Wilson, *Anal. Chem.*, 57 (1985) 2754.
- 8 W. Uditha de Alwis and G.S. Wilson, *Anal. Chem.*, 59 (1987) 2786.
- 9 I.H. Lee and M.E. Meyerhoff, *Anal. Chim. Acta*, 229 (1990) 47.
- 10 J.H.T. Luong and E. Prusak-Sochaczewski, *Anal. Lett.*, 23 (1990) 1809.
- 11 B. Mattiasson, P. Berden and T.G.I. Ling, *Anal. Biochem.*, 181 (1989) 379.
- 12 W. Stöcklein and R.D. Schmid, *Anal. Chim. Acta*, 234 (1990) 83.
- 13 A.W. Kusterbeck, G.A. Wemhoff, P.T. Charles, D.A. Yeager, R. Bredehorst, C.-W. Vogel and F.S. Ligler, *J. Immunochem. Methods*, 135 (1990) 191.
- 14 A.P. Savitsky, D.B. Papkovsky and I.V. Berezin, *Dokl. Akad. Nauk SSSR*, 293 (1987) 744.
- 15 D.B. Papkovsky, A.P. Savitsky, M.M. Poberezhny and V.A. Mischenko, presented at All-Union Conference on New Trends in Biotechnology Puschino, USSR, 1990.
- 16 A.L. Plant, L.L. Brown, M.V. Brizgys and R.A. Durst, *Bio/Technology*, 6 (1988) 266.
- 17 L.L. Brown, A. Plant, V. Horvath and R.A. Durst, *Anal. Chem.*, 62 (1990) 2587.
- 18 M. Maeda and A. Tsuji, *Anal. Chim. Acta*, 167 (1985) 241.
- 19 A.P. Osipov, A.A. Arefyev, S.B. Vlasenko, E.M. Bavrilo and A.M. Yegorov, *Anal. Lett.*, 22 (1989) 1841.
- 20 C. Shellum and G. Gübitz, *Anal. Chim. Acta*, 227 (1989) 97.
- 21 I. Weeks, I. Behesti, F. McCapra, A.K. Campell and J.S. Woodhead, *Clin. Chem.*, 29 (1983) 1474.
- 22 G. Gübitz, C. Shellum and M. Hinterleitner, in preparation.
- 23 R.C. Hart and L.R. Taffe, *J. Immunol. Methods*, 101 (1987) 81.
- 24 H. Liu, J.C. Yu, D.S. Bindra, R.S. Bivens and G.S. Wilson, *Anal. Chem.*, 63 (1991) 667.
- 25 D.S. Hage and P.C. Kao, *Anal. Chem.*, 63 (1991) 586.
- 26 G. Nordblow, *J. Clin. Immunoassay*, 14 (1991) 76.

# Automatic determination of Michaelis–Menten constants by the variable flow-rate technique

Juliana Marcos, Angel Ríos and Miguel Valcárcel

*Department of Analytical Chemistry, Faculty of Sciences, University of Córdoba, 14004 Córdoba (Spain)*

(Received 21st September 1992; revised manuscript received 20th November 1992)

## Abstract

An automatic method for the determination of Michaelis–Menten constants of enzymatic reactions in unsegmented flow systems was developed using the variable flow-rate technique, allowing the substrate concentration to be changed during the experiments in order to obtain different reaction rates. The proposed method can be applied both to enzymes in solution and immobilized, in this case on controlled-pore glass, and packed in a micro-reactor. Various flow-rate–time patterns were used for this purpose and the results were compared. Values of  $1 \times 10^{-2}$  and  $3 \times 10^{-4}$  M were found for Michaelis–Menten constants corresponding to the reaction between  $\beta$ -D-glucose and glucose oxidase by using dissolved and immobilized enzyme, respectively, with standard deviations of  $\pm 0.1 \times 10^{-2}$  (dissolved enzyme) and  $\pm 0.1 \times 10^{-3}$  (immobilized enzyme).

*Keywords:* Enzymatic methods; Flow system; Glucose; Michaelis–Menten constants

The variable flow-rate technique is the foundation of some new unsegmented flow methods [1] as opposed to traditional constant flow-rate procedures implemented in flow manifolds, which have so far prevailed in theoretical and practical studies in this context. Completely continuous and flow-injection manifolds have been used to deliver accurate flow-rate gradients according to different flow-rate–time patterns [2] which have been used for the automatic determination of acidity constants [2,3], stoichiometries of metal complexes [2] and solubility constants and critical micelle concentrations [4]. This approach is also very useful for implementing automatic titrations of one or two species in the same sample [5,6], and simultaneous determinations of metal ions [7,8].

The main advantage of the flow-gradient techniques (and the variable flow-rate technique in general) is that it allows gradients of reagents concentration, pH, etc., along the flow system to be created. This is the basis for various applications that require the concentration of one reagent (or pH) to be changed. This can be very useful in enzyme studies as the kinetics of enzymatic reactions are affected by the concentrations of the enzyme and substrate [9]. The experimental determination of the Michaelis–Menten constant ( $K_m$ ) of an enzyme system is based on the reaction rate versus substrate concentration plot obtained under pseudo-first-order kinetic conditions.  $K_m$  is defined as the concentration of substrate at which half of the maximum reaction rate ( $v_{max}$ ) is reached. This kinetic constant is characteristic of each enzyme system. In this work, variable substrate flow-rate patterns were used in order to develop an automatic methodology for the rapid determination of Michaelis–Menten

*Correspondence to:* M. Valcárcel, Department of Analytical Chemistry, University of Córdoba, 14004 Córdoba (Spain).

constants. The wellknown reaction between  $\beta$ -D-glucose and glucose oxidase was chosen for this purpose. The procedure was applied to the determination of  $K_m$  for both dissolved and immobilized enzymes.

## EXPERIMENTAL

### Reagents

Stock standard aqueous solutions of glucose oxidase (from *Aspergillus niger*, 500 mg l<sup>-1</sup>) (Sigma), and peroxidase (83 mg l<sup>-1</sup>) (Sigma) in 0.01 M tris(hydroxymethyl)aminomethane (Tris) (Merck) buffer (pH 7.0) were used. Aqueous solutions of phenol (0.16 M) (Merck) and 4-aminoantipyrine ( $4 \times 10^{-3}$  M) (Aldrich) were also used.

Controlled-pore glass (CPG) from Electro-Nucleonics ( $77.5 \text{ m}^2 \text{ g}^{-1}$ ) was employed to immobilize the glucose oxidase. The glass was activated with 10% (w/v) 3-aminopropyltriethoxysilane (Sigma) in 0.05 M sodium acetate buffer (pH 5.0) and 12% (v/v) glutardialdehyde (Merck) in 0.1 M sodium phosphate buffer (pH 8.5).

### Immobilization of glucose oxidase

CPG was cleaned by boiling in 5% HNO<sub>3</sub>, dried at 90°C and treated with a 10% solution of 3-aminopropyltriethoxysilane in acetate buffer at 90°C for 2 h. The CPG thus silanized was washed with distilled water, dried and treated with the glutardialdehyde solution at room temperature for 30 min. After washing and drying, 0.3 g of the activated glass was mixed with 3 ml of the enzyme solution for 6 h. The enzyme thus immobilized was washed with distilled water and stored in the buffer at pH 7 and 4°C [10,11].

### Apparatus

A Hewlett-Packard Model 8451A diode-array spectrophotometer furnished with an HP-9121 floppy disk drive, an HP-98155A keyboard and an HP-7470A plotter was used. A Gilson Minipuls-3

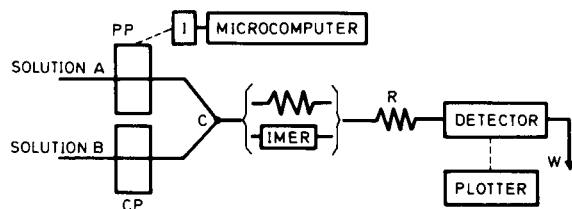


Fig. 1. Manifold used to obtain variable flow-rate patterns. PP = programmable pump; CP = conventional pump; I = electronic interface; C = confluence point; R = reaction coil; IMER = immobilized enzyme reactor (not required if glucose oxidase is used in dissolved form).

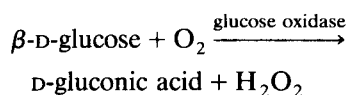
peristaltic pump controlled via a Commodore-64 microcomputer through a laboratory-made interface that allowed flow-rate to be changed as commanded by a BASIC program [2] was also used. A Gilson Minipuls-2 peristaltic pump was employed to ensure a constant flow-rate. A Hellma 178.12 QS flow cell (inner volume 18  $\mu$ l) was also used. All experiments were carried out at ca. 20°C.

### Manifold

The generic configuration used to obtain variable flow-rate patterns is depicted in Fig. 1. It includes two channels that merge at confluence point C. One of them is fitted to the conventional pump (CP), which is operated at a constant flow-rate throughout, while the other channel is fitted to the programable pump (PP), which provides the flow-gradients. This latter channel continuously propels the glucose solution (solution A) and solution B contains the enzyme or not, depending on whether the procedure concerned involves using the enzyme in solution or immobilized in the reactor (IMER = immobilized enzyme reactor), and also the other ingredients of the indicator reaction (phenol, 4-aminoantipyrine and peroxidase in Tris buffer). After the two channels have merged (and after the IMER, if one is required), a reactor coil (R) leads the outgoing stream to the flow cell of a spectrophotometric detector.

## RESULTS AND DISCUSSION

The enzyme system under study was based on the reaction



which was monitored spectrophotometrically by coupling a fast indicator reaction in which the  $\text{H}_2\text{O}_2$  yielded reacted with phenol and 4-aminoantipyrine to produce a quinoneimine absorbing at 500 nm [12].

The manual method for the determination of  $K_m$  involves measuring the initial reaction rate at different substrate concentrations and constant enzyme concentration. The corresponding reaction rate versus substrate concentration plot is a typical exponential curve with a maximum, constant reaction rate ( $v_{\max}$ ) at high substrate concentration.  $K_m$  is defined as the substrate concentration corresponding to a reaction rate equal to half of  $v_{\max}$ . This experimental procedure involves obtaining  $v_{\max}$  from the complete exponential curve. The Lineweaver–Burk procedure avoids the need to record the whole reaction rate–concentration profile as it is based on a graph obtained by plotting the following equation:

$$1/v = (1/v_{\max}) + \{(K_m/v_{\max})(1/[S])\}$$

where  $v$  is the initial reaction rate at a given substrate concentration  $[S]$ . A plot of  $1/v$  versus  $1/[S]$  plot allows  $v_{\max}$  to be calculated from the intercept of the straight line and  $K_m$  from its slope [12].

The optimum pH for the enzymatic reaction studied was ca. 7, which was adjusted by using Tris buffer. The influence of the glucose oxidase concentration was studied by manually calculating  $K_m$  at different enzyme concentrations in the range 2.7–60 mg  $\text{l}^{-1}$ .  $K_m$  was found not to be affected by the enzyme concentration, but the initial reaction rate increased with increasing glucose oxidase (GOD) concentration according to equation

$$v(\text{s}^{-1}) = 0.026 + 0.030[\text{GOD}]$$

( $r = 0.9997$ ,  $n = 7$ )

where  $[\text{GOD}]$  is the enzyme concentration in mg  $\text{l}^{-1}$ . A concentration of 44 mg  $\text{l}^{-1}$  enzyme was chosen for further study. As phenol and 4-aminoantipyrine could be used in excess,  $1.6 \times 10^{-2}$  and  $4 \times 10^{-4}$  M, respectively, were chosen as desirable concentrations. The peroxidase concentration used was 8.3 mg  $\text{l}^{-1}$ . Under these experimental conditions, the following equation for the Lineweaver–Burk plot was obtained:

$$1/v = 0.84 + (0.0102/[\text{glucose}])$$

( $r = 0.9995$ ,  $n = 12$ )

for a glucose concentration range of  $5.5 \times 10^{-4}$ – $5.5 \times 10^{-3}$  M. From this equation, a  $K_m$  value of  $(1.21 \pm 0.14) \times 10^{-2}$  M ( $P = 0.05$ ,  $n = 10$ ), was obtained which is comparable to literature values [ $0.96 \times 10^{-2}$  M for GOD from *Penicillium nutatum* (pH 5.6, 20°C) and  $3.3 \times 10^{-2}$  M for GOD from *Aspergillus niger* (pH 5.6, 25°C)] [13].

#### Determination of $K_m$ by continuous-flow methods

The principles of the proposed flow methods are the same as those of the manual method. However, the substrate concentration in the flow system is automatically changed by altering the flow-rate. Absorbance–time recordings are obtained where the time axis is also a substrate concentration axis, and the absorbance axis can be readily related to the initial reaction rate as the time elapsed from passage by confluence point C in Fig. 1 and the detection point is almost constant in all instances and can be determined.

The manifold in Fig. 1 allows  $K_m$  to be determined in various ways. Solution A contains glucose and solution B a mixture of GOD, peroxidase, phenol and 4-aminoantipyrine in a buffered medium (pH 7.0). This solution contains no GOD when the enzyme is used in immobilized form.

#### Flow methods using dissolved enzyme

Only a reactor coil of 530 cm was used in this instance to connect point C with the detector (Fig. 1). Solution B contained 44 mg  $\text{l}^{-1}$  GOD, 8.3 mg  $\text{l}^{-1}$  peroxidase,  $1.6 \times 10^{-4}$  M phenol and  $4 \times 10^{-4}$  M 4-aminoantipyrine in 0.01 M Tris buffer. As the concentrations of the ingredients



of this solution must remain constant on merging with the substrate stream, a flow-rate of  $2.5 \text{ ml min}^{-1}$  was selected for solution B, whereas the flow-rate of solution A was changed from 0 to  $0.3 \text{ ml min}^{-1}$ . Accordingly, a high glucose concentration in solution A was needed ( $0.17 \text{ M}$ ), which allowed its concentration in the flow system to be changed from 0 to  $5.5 \times 10^{-3} \text{ M}$ .

Several alternatives involving different flow-rate–time patterns that can be used for the automatic determination of  $K_m$  with dissolved GOD enzyme are discussed below.

*With stopped flow and stepwise-variable constant flow-rate.* In this instance the total flow or the substrate flow is stopped after a step in which the flow-rate is kept constant. The flow-rate ( $q$ )–time ( $t$ ) patterns are shown in Fig. 2A. Two variations can be used, as follows.

(a) With completely stopped flow, where  $q_0$  in the flow-rate pattern in Fig. 2A is zero, which means that both CP and PP are simultaneously stopped after cycles in which solutions B and A are circulated at  $2.5 \text{ ml min}^{-1}$  and stepwise-variable constant flow-rates, respectively. Thus, different and known concentrations of the substrate are introduced in each flow cycle. When the signal recorded reaches a constant level in each flow cycle, the flow is stopped and an absorbance–time kinetic curve is acquired in each instance [recording in Figure 2A(1)]. The slope of each straight line obtained corresponds to the reaction rate at a glucose concentration according to

$$C = C_0 q_A / (q_A + q_B)$$

where  $C_0$  is the concentration of glucose in solution A,  $C$  is its concentration after the confluence point (C in Fig. 1) and  $q_A$  and  $q_B$  are the flow-rates of solutions A and B, respectively. The  $C$  and  $v$  values are used to calculate  $K_m$ .

(b) With stopped substrate stream, where  $q_0 = q_B$  for the  $q$ –time pattern in Fig. 2A [a typical recording is shown in Fig. 2A(2)]. In this instance, the peak height can be related to the reaction rate at each glucose concentration calculated from the previous equation. Absorbance peak height–glucose concentration sets are used to calculate the Michaelis–Menten constant.

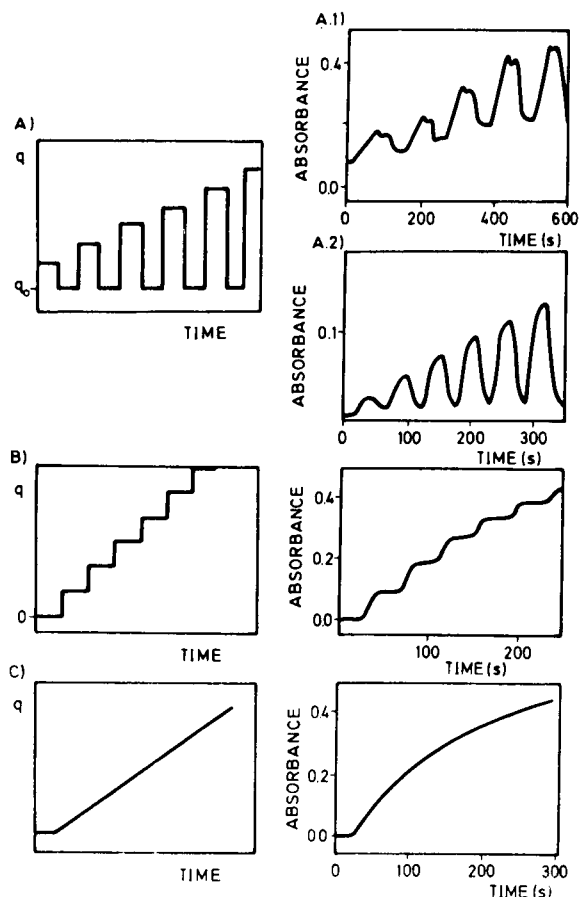


Fig. 2. Flow-rate–time patterns and corresponding absorbance–time recordings provided by the different proposed methods: (A) with stopped-flow and stepwise-variable constant flow-rates, in which all streams are halted (1) or only the substrate stream is stopped (2); (B) with gradual, constant increments in the flow-rate; and (C) by use of the flow gradient technique.

*With gradual, constant increments in the flow-rate.* The flow-rate is changed according the  $q$ –time pattern shown in Fig. 2B, where the flow-rate of the substrate stream is increased to constant levels over short periods of time, thereby providing constant absorbance–time recording steps related to the initial reaction rate as the residence time from point C (Fig. 1) to the detection point (denoted by  $t_r$ ) is almost constant in all instances (25 s). Therefore

$$v = (A_t - A_0) / (t_r - t_0)$$

where  $A_t$  and  $A_o$  are the absorbances at  $t_r$  and  $t_o$  (reaction start), respectively. As the absorbance is zero at  $t_o$ , the initial reaction rate can be calculated from

$$v = A_t/t$$

at each concentration of glucose in the flow system (C).  $K_m$  is calculated from the set of  $v$ - $C$  values.

By the flow-gradient technique. The glucose concentration is changed according to a linear  $q$ -time pattern such as that shown in Fig. 2C.  $C$  is calculated as before, but in this instance

$$q_A = Qt$$

where  $Q$  is the flow gradient ( $\text{ml min}^{-2}$ ) and  $t$  the time (min). Hence,

$$C = C_o Qt / (Qt + q_b)$$

so the concentration of glucose ( $C$ ) is defined each time.

The absorbance-time recordings obtained in this instance are similar to typical Michaelis-Menten plots (Fig. 2C). The absorbance is proportional to the initial rate as well, and can be automatically corrected from  $A_t/t_r$ . The flow gradient ( $Q$ ) is a crucial variable here that must be set according to the time required to perform the measurements. In any event, the  $K_m$  values obtained are obviously not affected by  $Q$  or  $C_o$  shown in Fig. 3.

#### Determination of $K_m$ by use of the immobilized enzyme

The major assets of the immobilized enzymes are well known [12]. Enzymes can be immobilized on a wide variety of supports by numerous procedures. Immobilized enzyme reactors (IMERs) made of enzymes immobilized on controlled-pore glass and packed in reactor coils have been widely used in flow systems [14]. One containing GOD and placed between the confluence point and the detector was used in this work (Fig. 1). Thus, the enzyme reaction only took place in the IMER. The concentration of ingredients contained in solution B had to be reoptimized because the GOD "concentration" (amount of enzyme immobilized in the reactor) had changed. Thus, the

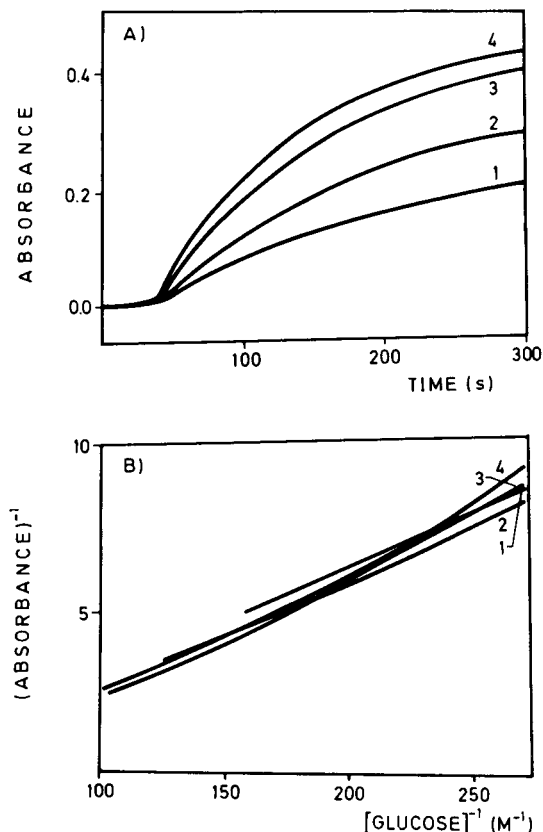


Fig. 3. (A) Absorbance-time recordings provided by the flow gradient technique and (B) corresponding plots of  $(\text{absorbance})^{-1}$  vs.  $[\text{glucose}]^{-1}$  obtained at various concentrations of glucose: (1) 10; (2) 15; (3) 25 and (4) 30  $\text{g l}^{-1}$ .

final composition of solution B was 3.3  $\text{mg l}^{-1}$  peroxidase,  $4.8 \times 10^{-3}$  M phenol and  $1.2 \times 10^{-4}$  M 4-aminoantipyrine. The flow-rate of solution B was kept at  $2.5 \text{ ml min}^{-1}$ , whereas the glucose solution (solution A) was circulated at flow-rates from 0 to  $0.3 \text{ ml min}^{-1}$  according to different constant flow gradients. The glucose concentration in solution A played a major role. At a high enough concentration the recording obtained is like that shown in Fig. 4. From this recording,  $K_m$  can be calculated from  $v_{\text{max}}$  according to the above-stated definition. This parameter was determined by using various concentrations of glucose in solution A, similar values being obtained in all instances. The influence of the IMER length was also studied by using five different reactors. The results obtained are shown in Fig. 5. The

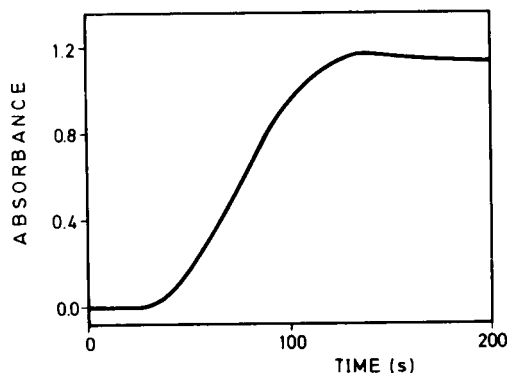


Fig. 4. Automatically obtained Michaelis-Menten plot for the glucose-glucose oxidase enzymatic system, in which the enzyme was used immobilized and packed in a 3.6-cm long reactor. Solution A was  $3.0 \text{ g l}^{-1}$  glucose and the flow gradient was  $0.083 \text{ ml min}^{-2}$ .

plot is a nearly hyperbolic curve, with two asymptotes: one for the shorter reactor and the other for longer reactors.

The  $K_m$  values are obtained from the absorbance-time (reaction rate-glucose concentration) recording shown in Fig. 6. All curves were obtained under the same experimental conditions ( $3.0 \text{ g l}^{-1}$  glucose stock solution concentration,  $2.50 \text{ ml min}^{-1}$  initial flow-rate and a flow gradient of  $8.40 \times 10^{-2} \text{ ml min}^{-2}$ ). It can be seen that the  $K_m$  values increase as the reactor length decreases (from curves 1 to 5). For the shortest reactor (0.45 cm)  $K_m$  is very large and cannot be

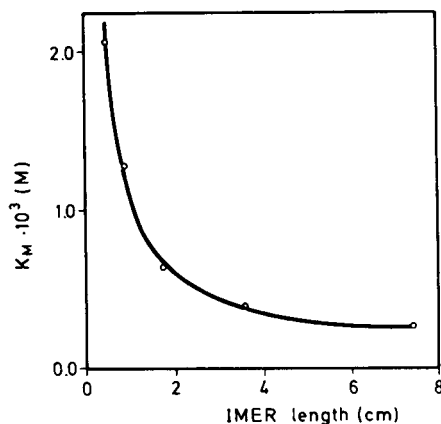


Fig. 5. Influence of the IMER length on  $K_m$ . The inner diameter of the enzyme reactor was 2.0 mm in all instances.

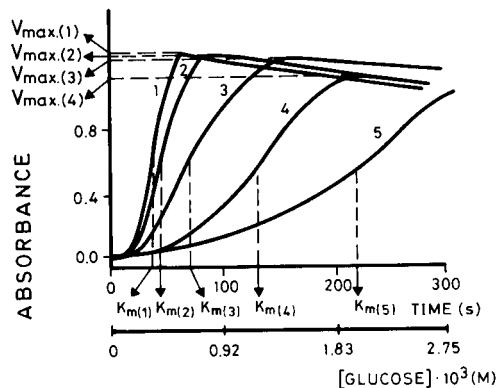


Fig. 6. Absorbance (reaction rate)-time (glucose concentration) recordings obtained by using IMER lengths of (1) 7.5, (2) 3.6, (3) 1.8, (4) 0.9 and (5) 0.45 cm. Maximum reaction rates ( $V_{max}$ ) and  $K_m$  values are indicated for each case.

determined under these experimental conditions because  $V_{max}$  cannot be measured accurately from the graph (in this case  $K_m$  was determined by using a more concentrated glucose solution).

When the enzyme is immobilized, the enzymatic reaction only takes place along the IMER reactor. This is importance because by increasing the IMER length two effects must be considered: the total amount of the enzyme and the reaction time are both increased. On the other hand, if the enzyme is immobilized, the substrate must diffuse from the solution to the solid surface, and this step could limit the rate of the reaction. When the IMER is very short the contact time between the substrate and the IMER is too small. The substrate does not have enough time to arrive at the enzyme on the solid surface and the reaction could be limited by the diffusion process. Also, the enzyme "concentration" could not be in excess of the substrate concentration and pseudo-first-order conditions are not obtained. The resulting curve differs from the typical Michaelis-Menten curve (see curves 3,4 and 5). The reaction time and the amount of enzyme involved increase with increasing IMER length. Hence over its length (6 cm, see Fig. 5) the behaviour of the system is the same as that expected, and  $K_m$  does not change. For practical purposes, a length greater than 6 cm ( $0.2 \text{ cm}^3$  of immobilized material) must be used in order to

TABLE 1

Optimum values of the variables influencing the proposed methods for the determination of  $K_m$ 

Variable	Methods using the dissolved enzyme	Method based on the use of immobilized enzyme
[GOD] ( $\text{mg l}^{-1}$ )	44	
[Peroxidase] ( $\text{mg l}^{-1}$ )	8.3	3.3
[Phenol] (M)	$1.6 \times 10^{-2}$	$4.8 \times 10^{-3}$
[4-aminoantipyrine] (M)	$4 \times 10^{-4}$	$1.2 \times 10^{-4}$
Glucose concentration range (solution A) $\text{g l}^{-1}$	10–30	3–5
Reactor coil length (cm)	530	100
Flow-rates ( $\text{ml min}^{-1}$ ):		
Solution A (glucose)	2.5	2.5
Solution B	0–0.3	0–0.3

ensure first-order kinetics and Michaelis–Menten behaviour.

### Comparison of Results

The optimum values of the variables involved in the proposed methods are given in Table 1. As can be seen, lower concentrations of the reactants were required when the enzyme was used in immobilized form. All the flow methods developed by using dissolved enzyme provided good results; the  $K_m$  values obtained were similar (Table 2) and comparable to that provided by the

manual method. The flow methods offer some major advantages, viz., automatability, use of a single substrate solution and shorter analysis times. The method based on the flow-gradient technique has some interesting features, particularly the highest degree of automatability and the rapidity with which  $K_m$  can be determined. There is great similarity between the completely stopped flow procedure and the manual method, yet the former is implemented in an automatic fashion. The features of the methods based on the use of dissolved enzyme are summarized in Table 3. The flow method using immobilized enzyme is based on the flow gradient technique, so it offers the advantages of this flow methodology and those arising from the use of enzyme immobilized and packed in a reactor. The influence of the IMER length on  $K_m$  is reflected in Table 2, where the correct value must correspond to the greatest length according to the above explanation, but they differed from those provided by the dissolved enzyme in solution, consistent with previous reports.

TABLE 2

$K_m$  values obtained by applying the flow methods ( $n = 10$  and  $P = 0.05$ )

Method	$K_m$ found (M)
Manual	$(1.2 \pm 0.1) \times 10^{-2}$
By use of dissolved enzyme:	
Completely stopped flow	$(0.9 \pm 0.1) \times 10^{-2}$
Stopped substrate stream	$(0.8 \pm 0.1) \times 10^{-2}$
Constant gradual increments in flow-rate	$(1.0 \pm 0.1) \times 10^{-2}$
Flow gradient technique	$(1.05 \pm 0.05) \times 10^{-2}$
By use of immobilized enzyme:	
IMER <sup>a</sup> length (cm)	
0.45	$(2.1 \pm 0.4) \times 10^{-3}$
0.90	$(1.3 \pm 0.2) \times 10^{-3}$
1.80	$(0.7 \pm 0.1) \times 10^{-3}$
3.60	$(0.4 \pm 0.1) \times 10^{-3}$
7.50	$(0.3 \pm 0.1) \times 10^{-3}$

<sup>a</sup> Inner diameter 2.0 mm.

### Conclusion

A straightforward, rapid, automatic method for the spectrophotometric determination of Michaelis–Menten constants has been developed and applied to the glucose–glucose oxidase enzymatic system. The proposed method should equally be applicable to other enzymatic reactions, provided that at least one of the reactants

or reaction products can be monitored or, alternatively, a fast secondary indicator reaction can be coupled (as in the example used in this work).

For enzymatic systems showing induction periods, the following consideration can be made. These systems also follow the typical simplified mechanistic scheme



according to which

$$v = d[P]/dt = k_{+2}[ES]$$

and

$$d[ES]/dt = k_{+1}[E][S] - k_{-1}[ES] + k_{+2}[ES]$$


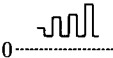
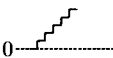
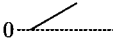
where  $v$  is the rate of the reaction. From these equations, the following can be deduced:

$$v = d[P]/dt = \frac{k_{+2}[E]_0[S]_0}{[S]_0 + (k_{-1} + k_{+2})/k_{+1}} (1 - e^{-t/\tau}) \quad (1)$$

where  $\tau = (k_{+1}[S]_0 + k_{-1} + k_{+2})^{-1}$  and is called the induction period.

TABLE 3

Features of the proposed automatic methods for the determination of  $K_m$  by use of dissolved enzyme

Method	Estimated time for $K_m$ determination (min)	Features	$q-t$ patterns	Advantages and disadvantages
Completely stopped flow	10	Flow-rate ( $q$ ) is kept at various constant but variable values. The reaction is continuously monitored at $q = 0$ The initial-rate is the slope of the absorbance–time curve at $q = 0$		A single substrate solution is needed Time consuming
Stopped substrate stream	6	The enzymatic solution always flows at the sample flow-rate The substrate solution flows according to stepwise variable constant flow-rates between $q = 0$ High peak is related to the initial rate (fixed-time kinetic method)		Single substrate solution Less time consuming
Constant, gradual increments in flow-rate	7	The enzymatic solution always flows at the same flow-rate The substrate solution continuously flows according to stepwise-variable constant flow-rates The absorbance measured in each step is related to the initial rate (fixed time kinetic method)		Single substrate solution A “pseudo” Michaelis–Menten graph is automatically recorded
Flow gradient technique	4	The flow-rate of the enzymatic solution is kept constant, while that of the substrate is changed linearly with time Every absorbance value is proportional to the initial rate corresponding to the substrate concentration in the flow system at this time		Single substrate solution The Michaelis–Menten graph is automatically recorded Rapid $K_m$ determination

It can be seen that at short times ( $t \ll \tau$ ) the exponential has a high enough value, but this term tends to zero at longer times ( $t \gg \tau$ ). Then, the equation simplifies to

$$v = \frac{k_{+2}[E]_0[S]_0}{[S]_0 + (k_{-1} + k_{-2})/k_{+1}} = \frac{v_{\max}[S]_0}{[S]_0 + k_m} \quad (2)$$

which is the Michaelis–Menten equation. After a time  $\tau$  (induction period), a steady state is reached because the enzyme concentration is very low compared with the substrate concentration, so the intermediate complex concentration [ES] can be assumed to be constant with time. The induction period is often very small and its lasts only 2–5 s [16,17], which is why it is not considered in most instances. In addition, to study this induction period methods employed for fast reactions are often required [18].

If an enzymatic reaction has a large induction period, the rate constants can be determined. The product concentration–time relationship is obtained by integrating Eqn. 1:

$$[P] = \frac{k_{+2}[E]_0[S]_0}{[S]_0 + (k_{-1} + k_{+2})/k_{+1}} (t - \tau e^{t/\tau} - 1) \quad (3)$$

The exponential term can be written in the form of a series and, assuming  $t$  to be very small, the product concentration is given by

$$[P] = 0.5k_{+1}k_{+2}[E]_0[S]_0t^2 \quad (4)$$

If an induction period is observed, it can be studied by using the proposed method with totally stopped flow. The reactor might be very short to allow the enzyme–substrate mixture to arrive at the detector very quickly. Then, the flow is stopped and the reaction is followed by measuring the product concentration formed, [P] (an absorbance–time plot is obtained). According to Eqn. 4,  $k_{+1}k_{+2}$  is measured (the enzyme and substrate concentrations are known). On the other hand, other measurements can be made after the induction period (a long reactor must be used) and from these  $K_m$  is calculated by the same methods as proposed here. Finally, a study of induction period with substrate concentration can

be performed manually. The relationship between these two parameters is

$$\tau = (k_{-1} + k_{+2} + k_{+1}[S]_0)^{-1} \quad (5)$$

i.e.,

$$1/\tau = (k_{-1} + k_{+2}) + k_{+1}[S]_0 \quad (6)$$

and for a graph of  $1/\tau$  versus  $[S]_0$ ,  $k_{+1}$  is the slope and  $k_{-1} + k_{+2}$  is the intercept. Consequently,  $k_m$ ,  $k_{+1}$ ,  $k_{-1} + k_{+2}$  and  $k_{+1}k_{+2}$  are thus determined, and the value of each rate constant is calculated through the definition of  $K_m$ :

$$K_m = (k_{-1} + k_{+2})/k_{+1} \quad (7)$$

This recently developed technique has proved to be a powerful tool in a few unusual applications of flow methodologies where the flow-rate is customarily kept constant just because a constant flow is easy to control. However, this cannot be regarded as a premise today if a peristaltic pump accurately controlled via a computer is used to obtain the flow-rate–time patterns required.

The CICYT is acknowledged for financial support (Grant No. PB90/0925). J. Marcos is also grateful to the Bask Government for financial support received through a personal fellowship.

## REFERENCES

- 1 A. Ríos and M. Valcárcel, *Talanta*, 38 (1991) 1359.
- 2 M. Agudo, J. Marcos, A. Ríos and M. Valcárcel, *Anal. Chim. Acta*, 239 (1990) 211.
- 3 J. Marcos, A. Ríos and M. Valcárcel, *Anal. Chem.* 62 (1990) 2237.
- 4 J. Marcos, A. Ríos and M. Valcárcel, *Talanta*, in press.
- 5 J. Marcos, A. Ríos and M. Valcárcel, *Anal. Chim. Acta*, 261 (1992) 489.
- 6 J. Marcos, A. Ríos and M. Valcárcel, *Anal. Chim. Acta*, 261 (1992) 495.
- 7 J. Marcos, G. del Campo, A. Ríos and M. Valcárcel, *Fresenius' J. Anal. Chem.* 342 (1992) 76.
- 8 J. Marcos, A. Ríos and M. Valcárcel, *Analyst*, 117 (1992) 1629.
- 9 H.U. Bergmeyer, *Methods of Enzymatic Analysis*, Verlag Chemie, Weinheim, 1983.
- 10 M. Masoom and A. Townshend, *Anal. Chim. Acta*, 166 (1984) 111.

- 11 L.D. Bowers, and P.R. Johnson, *Biochim. Biophys. Acta*, 661 (1981) 100.
- 12 P.W. Carr, and L.D. Bowers, *Immobilized Enzymes in Analytical and Clinical Chemistry*, Wiley, New York, 1980.
- 13 B.E.P. Swoboda and U. Massey, *J. Biol. Chem.*, 240 (1985) 2209.
- 14 P. Linares, M.D. Luque de Castro and M. Valcárcel, *Rev. Anal. Chem.*, 8 (1985) 229.
- 15 H.A. Mottola, *Analyst*, 112 (1987) 719.
- 16 I.N. Levina, *Fisico-Química*, McGraw-Hill, Mexico D.F., 1987.
- 17 J. Chabas Lopez, *Enzimología, Científico-Médica*, Barcelona, 1969.
- 18 S. Bernhard, *Estructura y Función de las Enzimas*, Blume, Madrid, 1977.

# Optosensing of D-glucose with an immobilized glucose oxidase minireactor and an oxygen room-temperature phosphorescence transducer

M.J. Valencia-González, Y.M. Liu, M.E. Díaz-García and A. Sanz-Medel

*Department of Physical and Analytical Chemistry, Faculty of Chemistry, University of Oviedo, Av. Julián Clavería 8, 33006 Oviedo (Spain)*

(Received 7th October 1992; revised manuscript received 20th January 1993)

## Abstract

Glucose oxidase was immobilized covalently on a nylon membrane and the oxygen consumption was followed via the changes in the room-temperature phosphorescence (RTP) of an oxygen-sensitive metal chelate whose RTP is quenched dynamically by molecular oxygen. The metal chelate was immobilized on an anion-exchange resin and packed into a conventional flow-through cell. As result of the glucose oxidation in the presence of the enzyme, a certain amount of oxygen was consumed, which in turn was indicated by the RTP of the chelate. Measurements were made in flowing air-saturated solutions containing 0.1 M acetate buffer (pH 5.9). The system is linear for 0.5–2.5 mM glucose with a relative standard deviation of 1.6% at 2 mM (ten measurements). The detection limit is  $8 \times 10^{-5}$  M and the application of the system to glucose determination in serum and beverages is demonstrated.

*Keywords:* Biosensors; Enzymatic methods; Flow injection; Phosphorimetry; Glucose; Oxygen

Glucose is among the most frequently determined sugars, especially in clinical samples for the diagnosis of disorders of metabolism [1] and in the food and biotechnology industries for process monitoring.

Conventional chemical methods for determining glucose are based on its reducing properties and so are unselective. Therefore, schemes based on liquid chromatography have been proposed [2] to enhance the selectivity. The use of enzymes and sensors offers a less expensive approach based on enzyme selectivity (and occasional specificity)

and capability of self-regeneration via the catalytic cycle.

There has been much interest in the development of enzyme electrodes for glucose in which oxygen consumption, hydrogen peroxide production or gluconic acid production, resulting from the glucose oxidase reaction, are detected electrochemically by using an oxygen,  $H_2O_2$  or pH electrode, respectively. Of particular practical interest are amperometric enzyme electrodes employing a synthetic mediator (ferrocenes, phenoxazine, quinones, etc.) [3–6], which acts as a shuttle for electrons between the enzyme active site (reaction centre) and the electrode which renders such sensors almost inert towards variations in naturally available (dissolved) oxygen back-

*Correspondence to:* A. Sanz-Medel, Department of Physical and Analytical Chemistry, Faculty of Chemistry, University of Oviedo, Av. Julián Clavería 8, 33006 Oviedo (Spain).



ground. General advantages of optical over electrochemical transduction have been discussed in several papers [7–9], but so far optical glucose sensors are impractical and more work is needed in order to be able to apply them to real analyses. Schultz et al. [10] proposed one of the first optical sensing principles for glucose in their “glucose affinity sensor” based on the competition between sample glucose and fluorescein-labelled dextran for binding sites at surface-immobilized concanavalin A. Uwira et al. [11] described a fibre-optic glucose biosensor based on the measurement of enzymatic oxygen consumption via the changes in the fluorescence of an oxygen-sensitive dye. An important drawback of the device is that the fluorescence indicator (pyrenebutyric acid) has an excitation wavelength in the UV region, not compatible with the transmission characteristics of economic glass or plastic optical fibres. Moreover, slow leaching out of the indicator was observed.

Another type of optical glucose sensor that uses coloured or fluorescent dyes but this time as pH indicators has also been proposed [12,13]. More recently, a glucose biosensor based on the intrinsic green fluorescence of glucose oxidase (GOx), which changes during interaction with glucose, has been developed [14]. Although this sensor is direct (in that it does not need a transducer element), the fairly low intensity of the enzyme fluorescence and the small glucose concentration range in which fluorescence intensity changes occurred severely limit its practical use.

Recently, Papkovskii and co-workers [15–17] described some metal porphyrin chelates for O<sub>2</sub> sensing based on room-temperature phosphorescence (RTP). A sensitive RTP flow-injection method for glucose was developed based on the use of a column of immobilized GOx and the room-temperature phosphorescent indicators Pt<sup>2+</sup>-coproporphyrin III and Pd<sup>2+</sup>-coproporphyrin I as internal molecular oxygen sensors [16]. The method allowed the determination of glucose in biological fluids with low protein contents (0.1%). For samples with high protein contents (e.g., serum) the composition of the elution buffer had to be modified in order to decrease the high background luminescence resulting from interac-

tion of the oxygen sensor with the sample proteins.

Following a similar principle, this paper describes a sensitive flow-injection method for the determination of glucose in food and clinical samples using an immobilized glucose oxidase minireactor. Oxygen consumption during the enzymatic reaction is followed via the changes in the RTP of an oxygen-sensitive metal chelate immobilized on an anion-exchange resin packed into a conventional flow-through cell. The method is simple, consumes only inexpensive reagents (air-equilibrated acetate buffer) and requires no sample preparation for real beverage or serum samples. The use of other enzymes or a combination of two or more enzymes which require oxygen as co-substrate will possibly extend the application of this RTP transducer to other analytes such as ethanol, cholesterol and lactate [18–21], already determined by alternative electrical and/or optical transduction.

## EXPERIMENTAL

### *Chemicals and solutions*

Glucose oxidase (EC 1.1.3.4, Type II, from *Aspergillus niger*) with a specific activity of 25 000 U g<sup>-1</sup> was obtained from Fluka. Lysine (97%, w/w), and glutaraldehyde (50%, w/w) aqueous solutions and dimethyl sulphate were obtained from Fluka.  $\alpha$ -D-Glucose was purchased from Aldrich-Chemie and 2-(*N*-morpholino)ethanesulphonic acid (MES) and bis(2-hydroxyethyl)iminotris(hydroxymethyl)methane (Bis-Tris) from Sigma. All other reagents used were of analytical-reagent grade. A glucose VIS–UV–enzymatic kit was obtained from Sigma.

All aqueous solutions were prepared in 0.1 M sodium acetate–acetic acid buffer (pH 5.9), using water obtained from a Milli-Q system (Millipore). Glucose solutions were allowed to mutarotate overnight before use.

### *Aluminium-7-iodoquinolin-8-ol-5-sulphonic acid chelate solution*

This solution was prepared by mixing 0.3 ml of a 1000  $\mu$ g ml<sup>-1</sup> Al stock solution and 35 ml of

$3 \times 10^{-3}$  M ferron (7-iodoquinolin-8-ol-5-sulphonic acid) in a 100-ml volumetric flask. The solution was diluted to volume with 1 M acetate buffer (pH 5.5). This “chelate solution” did not deteriorate (stable RTP signals) for at least 3 months.

#### Optosensing assembly

In a single-line flow-injection system, a Hellma Model 176.52 flow-through cell of volume  $25 \mu\text{l}$  is packed with the anion-exchange resin and placed in the conventional sample compartment of the detector (see Fig. 1). An Omnifit 1106 rotary valve was used for sample introduction. PTFE tubing (0.5 mm i.d.) and fittings were used for connecting the flow-through cell, the rotary valve, the enzyme minicolumn and the carrier solution reservoir. All the connections were sealed carefully with high-vacuum silicone grease (BDH) to avoid diffusion of oxygen into the system. A Gilson Minipuls-2 peristaltic pump was used to generate the flow stream.

All RTP measurements were made at 600 nm (excitation at 390 nm) with a Perkin-Elmer LS5 spectrofluorimeter which employs a xenon-pulsed (10-s half-width 50 Hz) excitation source and is equipped with a Perkin-Elmer Model 3600 data station. The delay time used was typically 0.04 ms

for optimization of system variables and 0.05 ms for real sample analyses. The gate time used throughout was 2 ms. The instrument excitation and emission slits were set at 10 and 20 nm, respectively, throughout. Steady-state phosphorescent signals were recorded with a Perkin-Elmer Model 560 recorder.

#### Preparation of the oxygen transducer

For immobilization of the oxygen “indicator”, the Al-ferron solution was pumped through the sensing flow cell containing a basic anion-exchange resin. It was found that after passing the carrier solution for 5–6 h the variation in the RTP intensity observed was less than 4–5%. In any case, it was checked that sensor phase “renewal” was accomplished just by injection of 2 ml of 6 M HCl in order to release “old” Al-ferron chelate from the resin. As detailed above, new Al-ferron solution can be then pumped in order to obtain a new active surface for oxygen sensing. Details of this RTP sensing phase production are the subject of a patent application [22].

#### Immobilization of glucose oxidase on nylon

Covalent binding of the enzyme to the inert matrix involved the preparation of the nylon and

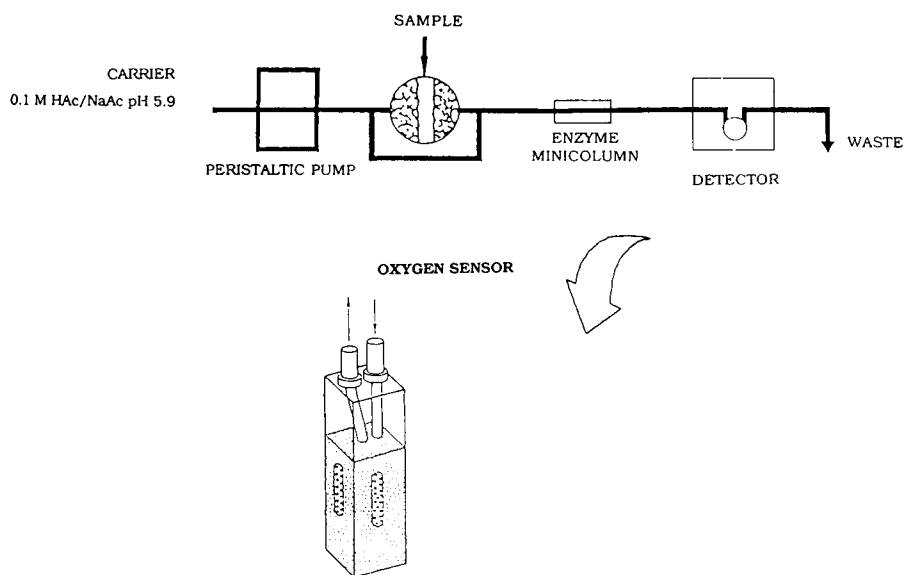


Fig. 1. Schematic diagram of the flow system.

reaction with glutaraldehyde as described elsewhere [23].

Coupling was carried out at room temperature for 2 h, after which the membranes were stored in a refrigerator at 4°C overnight. Finally, the excess of enzyme was washed out with “phosphate buffer” followed by 0.1 M NaCl solution in phosphate buffer and then pure phosphate buffer again.

When not in use, the enzyme membranes were stored at 4°C in 0.1 M phosphate buffer containing 0.1% sodium azide as bactericide.

The enzyme-membrane so obtained was mounted around an open Tygon tube (5 mm i.d.) and inserted in the flow-injection manifold depicted in Fig. 1. The activity after binding of the enzyme was determined by measuring the enzyme activity in the solutions before and after immobilization.

#### *General procedures for glucose determination*

*Calibration.* Glucose solutions (consisting of carrier solution plus a known volume of the glucose standard solution) were injected through the valve (sampling volume 0.2 ml) into the carrier stream. The flow-rate of the carrier was set at 0.40 ml min<sup>-1</sup>. Typical flow-injection RTP signals were measured and peak height was plotted against molar concentration of glucose injected.

*Serum samples.* The serum samples were diluted 1 + 9 with the 0.1 M acetate buffer (pH 5.9). The glucose content was evaluated from calibration graphs obtained using aqueous glucose standards. Comparison was made with results obtained using the Beckman electrode method, routinely used in the Hospital Central de Asturias (from where the samples were obtained).

*Fruit juice and lemonade samples.* Samples of fruit juices with low levels of insoluble ingredients (e.g., fruit pulp) were diluted 200-fold with the acetate buffer solution and injected into the flow system without further treatment. Highly carbonated samples, such as Lemon-Kas, were shaken overnight to decrease the amount of dissolved carbon dioxide because an excess of carbon dioxide disturbs the flow system by generating bubbles. These samples were diluted 500-fold with the buffer solution.

The glucose content in all fruit juices was evaluated from calibration graphs obtained using aqueous glucose standards. The glucose content in lemonades, however, was evaluated using the standard addition technique because the sample matrix interfered in the detection scheme.

## RESULTS AND DISCUSSION

### *Characteristics of the RTP oxygen transducer*

The complex formed by ferron and aluminium immobilized on a strong anion-exchange resin exhibits solid-surface RTP (SS-RTP). The corresponding spectra showed an emission maximum at 600 nm with an excitation maximum at 390 nm. Solid-state membranes of this sensor phase, based on silicone, were also developed to construct oxygen-sensitive membranes. The characterization of such a transducer was performed by monitoring both the RTP intensity and/or lifetime measurements during some oxygenation–deoxygenation cycles in aqueous and in gaseous phases [22].

Immobilization of this phosphor on the solid support seems partially to protect the triplet from non-radiative collisional deactivation by quenchers, even in an aqueous flow. The sensor is completely reversible to oxygen both in gaseous mixtures and aqueous samples and its response to oxygen was linear up to 20% O<sub>2</sub> (v/v) in an argon gas stream. Under the optimum experimental conditions typical response times for full signal change were ca. 20 s for gaseous mixtures and ca. 1 min for solution samples. The sensor exhibited no hysteresis and showed high photochemical stability. More information on the analytical performance of this RTP–O<sub>2</sub> sensing phase is the subject of a patent application [22].

### *Optimization of experimental conditions*

The pH and the ionic strength of the solutions used are important parameters in the continuous-flow system described. Experiments were carried out using sodium acetate buffer to establish the optimum pH for the glucose determination. Figure 2 shows the pH profile for the injection of 2 mM glucose. An RTP signal plateau was found at pH 4–5. Commercially available GOx usually

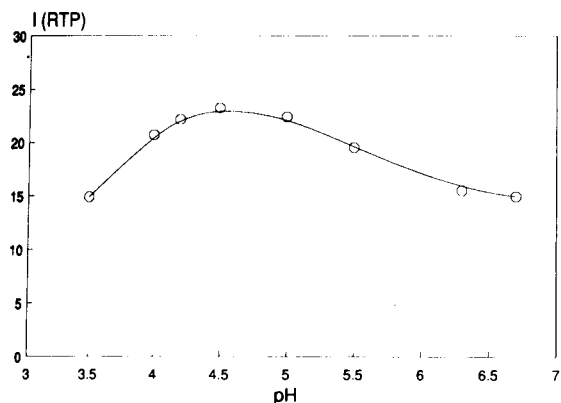


Fig. 2. Influence of pH on the RTP signals.

contains other enzymes as impurities, at pH < 5 GOx activity is reduced but other enzymatic reactions could also take place simultaneously. Data are given in Table 1 for two common sugars. Consequently, all the analyses were done at pH  $6.0 \pm 0.1$ , where GOx activity is high and the oxygen RTP sensor performance is optimum [24].

The effect of the buffer composition is remarkable. MES buffer at pH 5–6 inhibited the enzyme activity gradually with continuous use. Phosphate buffer (1 M) interfered with the oxygen sensor as a continuous flow of phosphate at such a high concentration complexed progressively with aluminium. The behaviours of Bis-Tris and acetate buffer were similar. Therefore, a simple carrier solution of acetate buffer was used throughout.

TABLE 1

Performance of the enzyme minireactor at different pH values

Sugar	pH	Glucose <sup>a</sup> /sugar mole ratio	<i>I</i> <sup>b</sup>
Galactose	4.5	1:10	108
		1:100	135
	6.0	1:10	102
Fructose	4.5	1:100	112
		1:1	110
	6.0	1:5	112
		1:1	100
		1:10	103

<sup>a</sup> 2 mM glucose. <sup>b</sup> *I* = relative RTP intensity.

On increasing the acetate buffer capacity a double effect was observed. Firstly, higher buffer concentrations (e.g., 1 M sodium acetate) inhibited enzyme activity (to even less than 70% of that achieved with low buffer concentrations). On the other hand, the oxygen RTP signals increased with saline content. This could be explained by taking into account that a higher ionic content could result in a more “rigid” solid support [25] of the oxygen sensor and hence to a more rigid environment that could prevent non-radiational RTP deactivations. A 0.1 M sodium acetate concentration in the acetate buffer was used for remainder of the study.

The RTP signals decreased steadily with increasing flow-rate of the carrier solution (from 0.20 to 1.00 ml min<sup>-1</sup>), as would expected owing to the decreased reaction time. A compromise value of 0.40 ml min<sup>-1</sup> was selected as good sensitivity and a relatively short response time were obtained.

To investigate the effect of enzymatically generated H<sub>2</sub>O<sub>2</sub> on the detector signals, the GOx minicolumn was removed from the FIA manifold. Then increasing concentrations of H<sub>2</sub>O<sub>2</sub> (from 0.5 to 50 mM) were injected into the system and the fluorescence [ $\lambda(\text{ex}) = 390 \text{ nm}$ ,  $\lambda(\text{em}) = 498 \text{ nm}$ ] of the immobilized Al-ferron was recorded. No signal changes were observed and only after continuous pumping of a 50 mM H<sub>2</sub>O<sub>2</sub> solution for 15 min did the fluorescence intensity decrease by 6% of its original value. Exactly the same effect was observed for the RTP signals. As these high H<sub>2</sub>O<sub>2</sub> concentrations are not normal in practical assays, it seems that H<sub>2</sub>O<sub>2</sub> will not pose an interference problem for the oxygen detector itself. However, it has been reported [26] that the enzymatically generated H<sub>2</sub>O<sub>2</sub> inhibits the immobilized GOx activity and so catalase (or peroxidase) is sometimes co-immobilized with GOx to circumvent this problem.

The stability of the enzyme column was investigated by comparing the RTP responses observed for 30 repetitive injections of a 2 mM glucose solution. The enzyme was observed to retain only 10–20% of its original reactivity after 25 injections. This inhibition was due to the reversible momentary accumulation of H<sub>2</sub>O<sub>2</sub> and

after a 2–3-min flow of the buffer carrier through the membrane the enzyme activity reached its original value. It is worth mentioning that the use of a co-immobilized enzyme (e.g., catalase or peroxidase) in the present system to avoid the  $H_2O_2$  effect could reduce the sensitivity obtainable because oxygen is produced in the catalase reaction, whereas oxygen is consumed in the measured analytical reaction (GOx reaction).

Regarding the background of RTP signals (dissolved oxygen level), a constant background level was found when air-equilibrated carrier and/or real samples passed over the RTP sensor. This background level was identical with that observed when the sample was split into two fractions, one passing through the enzyme column and the other avoiding the column and feeding the  $O_2$  detector directly. Thus, a constant oxygen supply was always observed with this procedure, and so the analytical signals were obtained by subtracting manually the background close to the value of the RTP total signal measured by the instrument.

#### Analytical features

Figure 3 shows peak and a typical calibration graph for injections of glucose at different con-

centrations. The calibration graph was linear in the glucose concentration range 0.5–2.5 mM, with a detection limit (estimated on the basis of the 3 times the standard deviation of the blank) of  $8 \times 10^{-5}$  M. The reproducibility of the proposed enzymatic glucose assay system was tested by comparing the responses of ten repetitive injections of a 2 mM glucose solution. The relative standard deviation was 1.6%. The stability of the enzyme minicolumn was also investigated over a 4-month period. The reactor retained 100% of its original activity after 2 months and decrease only to 90% after 4 months.

#### Interference study and analytical application

The interferences of fructose, saccharose, lactose and galactose were studied as GOx could be contaminated by other enzyme traces producing interferences in  $O_2$  consumption. Different concentration ratios of glucose to these sugars and their effects on the RTP response to glucose at two different pHs were studied. Only galactose gave positive deviations (ca 12%) for a glucose:galactose ratio of 1:100. This galactose interference was due to galactosidase impurities in the GOx enzyme.

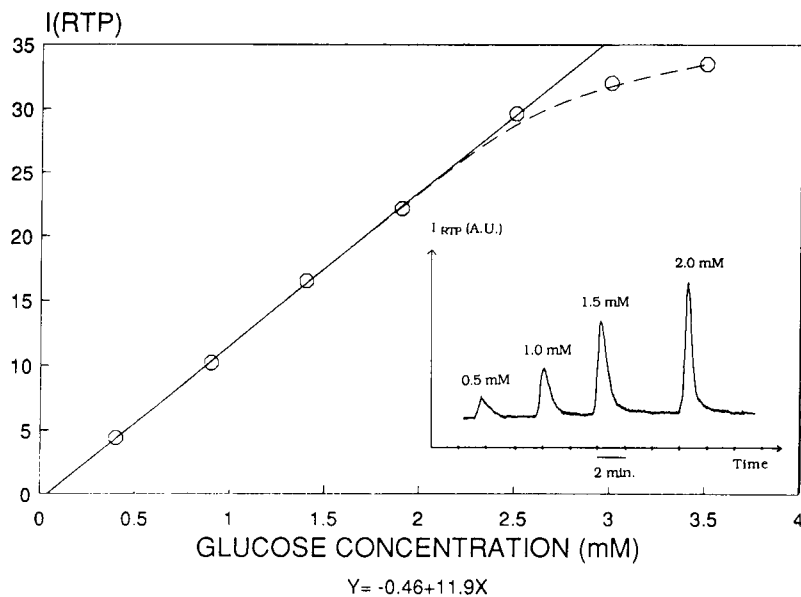


Fig. 3. Calibration graphs for the proposed sensor and response profile [using a 0.2-ml sample loop and 0.1 M acetate buffer (pH 5.9)].

TABLE 2

Analytical applications by direct calibration

Sample	Glucose concentration (mM)	
	This sensor <sup>a</sup>	Alternative method
Serum pool I	4.85 ± 0.12	4.90 ± 0.12 <sup>b</sup>
Serum pool II	5.57 ± 0.02	5.64 ± 0.04 <sup>b</sup>
Serum pool III	6.53 ± 0.13	6.36 ± 0.12 <sup>b</sup>
Apple soft drink	204.0 ± 0.2	210.0 ± 4.6 <sup>c</sup>
Lemon soft drink <sup>d</sup>	390.0 ± 13.3	283.4 ± 9.2 <sup>c</sup>
	282.5 ± 3.5 <sup>e</sup>	

<sup>a</sup> Mean ± S.D. ( $n = 3$ ). <sup>b</sup> Beckman oxygen electrode; mean ± S.D. ( $n = 3$ ). <sup>c</sup> Spectrophotometric determination (hexokinase at 340 nm); mean ± S.D. ( $n = 3$ ). <sup>d</sup> The sample was stirred to remove CO<sub>2</sub>. <sup>e</sup> Standard addition.

Sulphite or other reducing agents can lead to positive deviations of signals because it might react with oxygen (resulting in an enhanced RTP signal) and their possible presence in samples should therefore be taken into account. The effect of possible metals present in biological fluids is not serious using this sensing phase [24] and, in any case, it proved to be negligible in the diluted samples analysed.

In order to assess the validity of the system, several serum samples and beverages were analysed for their glucose content following the general procedure detailed under Experimental. The results obtained compared favourably with those obtained by alternative assays, as shown in Table 2. The alternative techniques used for comparison were the Beckman oxygen electrode and UV method using the HK procedure (Sigma kit). Measurements were made according to the manufacturer's instructions. Hence, it was demonstrated that the proposed RTP optosensing method can be used successfully for the determination of glucose in important clinical and food samples.

### Conclusions

Although not one optosensing approach is clearly superior to all the others in all analytical respects, the RTP detection principle presented here for glucose exhibits the typical advantages of phosphorescence measurements over the more conventional fluorescence mode, namely: in-

creased selectivity because not many substances phosphoresce and there is a time discrimination ability to remove fast emission phenomena (i.e., fluorescence, scattering, Raman, etc.) by using adequate "delay" times, and moreover the RTP sensor is not affected by the protein content in real samples; longer wavelength (less background) and wider separation between excitation and emission maxima are observed (emissions in the long-wavelength visible region allows us the use of cheap optical fibres and photodiode technology currently available); and the measurement of excited triplet state lifetimes ( $\mu\text{s}$ – $\text{s}$ ) is much easier than that for singlet states (ns), hence multi-dimensional analysis with simple instrumentation and increased selectivity by resorting to chemometric treatments [27] can be envisaged.

The RTP sensing principle proposed here can probably be extended to other enzymes involving molecular oxygen consumption (e.g., preliminary experiments with ascorbate oxidase were successful).

Financial support from the Fondo para las Investigaciones Científicas de la Seguridad Social (FISS) and the Fundación para el Fomento en Asturias de la Investigación Científica y Técnica (FICYT) is gratefully acknowledged. Y.M. Liu thanks the Spanish Education and Science Ministry for a Postdoctoral Fellowship.

### REFERENCES

- 1 E. Reach and G.S. Wilson, *Anal. Chem.*, 64 (1992) 381A.
- 2 U.A.Th. Brinkmann, *Chromatographia*, 24 (1987) 190.
- 3 A.E.G. Gass, G. Davis, G.D. Francis, H.A.O. Hill, W.J. Aston, I.J. Higgins, E.V. Plotkin, L.D.L. Scott and A.P.F. Turner, *Anal. Chem.*, 56 (1984) 667.
- 4 M.A. Lange and J.Q. Chambers, *Anal. Chim. Acta*, 175 (1985) 89.
- 5 G. Johnsson and L. Gorton, *Biosensors*, 1 (1985) 355.
- 6 M.F. Cardosi and A.P.F. Turner, in A.P.F. Turner, I. Karube and G.S. Wilson (Eds.), *Biosensors: Fundamentals and Applications*, Oxford University Press, Oxford, 1989, p. 257.
- 7 D.W. Lübbers and N. Opitz, *Sensors Actuators*, 4 (1984) 641.
- 8 M.A. Arnold, *Anal. Chem.*, 64 (1992) 1015A.

- 9 B.P.H. Schaffar and O.S. Wolfbeis, *Biosensors*, 5 (1990) 137.
- 10 J.S. Schultz, S. Mansouri and I.J. Goldstein, *Diabetes Care*, 5 (1982) 245.
- 11 N. Uwira, N. Opitz and D.W. Lübbers, *Adv. Exp. Med. Biol.*, 169 (1984) 913.
- 12 M.J. Goldfinch and C.R. Lowe, *Anal. Biochem.*, 138 (1984) 430.
- 13 W. Trettnak, M.J.P. Leiner and O.S. Wolfbeis, *Biosensors*, 4 (1988) 15.
- 14 W. Trettnak and O.S. Wolfbeis, *Anal. Chim. Acta*, 221 (1989) 195.
- 15 D.B. Papkovskii, A.P. Savitskii and A.I. Yaropolov, *J. Anal. Chem. USSR*, 45 (1990) 1045.
- 16 D.B. Papkovskii, A.P. Savitskii, A.I. Yaropolov, G.V. Ponomarev, V.D. Romyantseva and A.F. Mironov, *Biomed. Sci.*, 2 (1991) 63.
- 17 D.B. Papkovskii, J. Olah, I.V. Troyanovskiy, N.A. Sadovsky, V.D. Romyantseva, A.F. Miranov, A.I. Yaropolov and A.P. Savitsky, *Biosensors Bioelectron.*, 7 (1992) 199.
- 18 D.L. Wise and L.B. Wingard, Jr. (Eds.), *Biosensors with Fiberoptics*, Humana, Clifton, NJ, 1991.
- 19 M. Aizawa, *Anal. Chim. Acta*, 250 (1991) 249.
- 20 R. Lal, *Bioelectrochem. Bioenerg.*, 27 (1992) 121.
- 21 M.A. Arnold, *Anal. Chem.*, 64 (1992) 1015A.
- 22 A. Sanz-Medel, Y.M. Liu, R.M. Pereiro García and M.E. Díaz García, *Spanish Pat. Appl.*, No. P-92/02641 (1992).
- 23 W.E. Hornby and D.L. Morris, in H.H. Weetall (Ed.), *Immobilized Enzymes, Antigens, Antibodies and Peptides*, Dekker, New York, 1975.
- 24 R. Pereiro, Y.M. Liu, M.E. Díaz and A. Sanz-Medel, *Anal. Chem.*, 63 (1991) 1759.
- 25 B.P. Purdy and R.J. Hurtubise, *Appl. Spectrosc.*, 46 (1992) 988.
- 26 N. Opitz and D.W. Lübbers, *Talanta*, 35 (1988) 123.
- 27 Y.M. Liu, J.I. García, R. Fernández, M.E. Díaz and A. Sanz-Medel, *Mikrochim. Acta*, I (1991) 199.

# Spectrophotometric determination of magnesium in serum by using a flow-injection system with an immobilized enzyme reactor

J.M. Fernández-Romero, M.D. Luque de Castro and M. Valcárcel

*Department of Analytical Chemistry, Faculty of Sciences, University of Córdoba, E-14004 Córdoba (Spain)*

R. Quiles-Zafra

*Department of Biochemistry, Hospital Virgen de la Salud, Toledo (Spain)*

(Received 8th July 1992; revised manuscript received 18th December 1992)

## Abstract

A spectrophotometric, continuous flow-injection, merging zones manifold including an enzyme reactor was used for the determination of magnesium ion in serum by exploiting the activating effect of Mg(II) on the hydrolysis of *o*-nitrophenyl- $\beta$ -D-galactopyranoside by  $\beta$ -D-galactosidase immobilized on controlled-pore glass. The advantageous features of the proposed method (determination range 5–20  $\mu\text{mol l}^{-1}$ , within-run and between-run relative standard deviations of 0.78–2.91% and 1.7–3.21%, respectively) allow the determination of the analyte in serum samples with good recoveries (96–113%). The results obtained were consistent with those provided by the conventional atomic absorption spectrometric method.

*Keywords:* Enzymatic methods; Flow injection; UV-Visible spectrophotometry; Enzyme reactor; Magnesium; Serum

Magnesium occurs widely in the human body. It is the second most abundant cation in intracellular fluid. Only 1% of Mg(II) can be found in interstitial liquid. One third of the overall magnesium in serum is bound to proteins and 80% of the other two thirds is carried as free ion, the other 20% forming phosphate and citrate complexes [1,2]. Magnesium plays a mayor role in various biochemical reactions. It is a cofactor of more than 300 enzymatic processes, operates on ATP/ADP activation and is required for the intracellular synthesis of nucleic acids. In addition, it plays a prominent role in the regulation of

membrane cell permeation and the excitability of neuromuscular terminals [3].

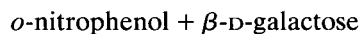
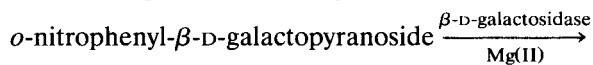
The determination of magnesium in serum is of high clinical significance in the diagnosis and prevention of different organic failures, mainly of the cardiovascular system [4,5]. Thus it is widely documented. Several spectrophotometric methodologies based on metal complex formation [6–11] have been reported, but all are subject to serious interferences [12]. Some atomic absorption spectrometric (AAS) methods have also been reported [13–16]. Recently, some methods based on the ability of magnesium to activate some enzymatic reactions have been developed. Several analytical methods involving hexokinase [17] or glucokinase [18] enzymes and coupling with glucose-6-phosphate dehydrogenase and glycerolki-

*Correspondence to:* M. Valcárcel, Department of Analytical Chemistry, Faculty of Sciences, University of Córdoba, E-14004 Córdoba (Spain).



nase with peroxidase [19] have been proposed with spectrophotometric detection. Also, a chemiluminescence method using L-glutamate dehydrogenase/L-glutamate oxidase was reported [20], and a host of flow-injection (FI) systems have been used to determine magnesium in serum with atomic spectrometry [16,21–24] and with enthalpimetric [25], electroanalytical [26–28], spectrophotometric [29–34] and chemiluminimetric detection [20]. Tabata et al. [20] developed the first FI system for the determination of magnesium using two immobilized enzymes and chemiluminescence detection.

In this paper, a further FI method for the determination of total magnesium based on the method of Berry et al. [35] [dependence of the enzymatic activity of  $\beta$ -D-galactosidase ( $\beta$ -D-galactoside galactohydrolase; EC 3.2.1.23) on the analyte concentration in the medium] is proposed. The enzyme catalyses the hydrolysis *o*-nitrophenyl- $\beta$ -D-galactopyranoside in the presence of Na(I) and Mg(II) ions to yield galactose and *o*-nitrophenol according to the reaction



In the absence of the Mg(II) cation the reaction does not take place. When the substrate, enzyme and other activators are in excess, the analytical signal is proportional to the concentration of magnesium. The species monitored is the *o*-nitrophenol formed in the reaction, which exhibits maximum absorption at 405 nm.

## EXPERIMENTAL

### Apparatus

A Philips PU 8700 spectrophotometer furnished with a Hellma 178.12QS flow cell (18  $\mu$ l inner volume) and a Julabo-5 recirculating thermostat, a Gilson Minipuls-2 four-channel peristaltic pump provided with a rate selector, a laboratory-made double-injection system consisting of two Rheodyne Model 5041 injection valves and Teflon tubing of 0.5 mm i.d. were used. Whenever necessary, the pH was measured by

means of a Beckman Model 072 pH meter. A Perkin-Elmer Model 380 atomic absorption spectrometer was also employed.

### Reagents

$\beta$ -D-Galactoside (grade VIII, from *Escherichia coli*), *o*-nitrophenyl- $\beta$ -D-galactopyranoside (ONPG) and DL-dithiothreitol (DL-DTT) were purchased from Sigma (St. Louis, MO). Sodium chloride, ethylenebis(oxyethylenenitrilo)tetracetic acid (EGTA, Tritriplex VI), magnesium chloride, tris(hydroxymethyl)aminomethane (Tris) and all other reagents were supplied by Merck (Darmstadt).

Reagent A was an aqueous solution containing 100 mmol l<sup>-1</sup> Tris, 4 mmol l<sup>-1</sup> DL-DTT and 0.4 mmol l<sup>-1</sup> EGTA; the pH was adjusted with 6 mol l<sup>-1</sup> HCl. Reagent B was prepared by dissolving 4.7 g of NaCl and 60.3 mg of ONPG in 1 l of reagent A. Reagent C was 1 M NaOH solution.

A 1 g l<sup>-1</sup> standard solution of magnesium was prepared by dissolving MgCl<sub>2</sub> · 6H<sub>2</sub>O in water. Cation Cal serum reference material (Cat. No. B5160-1) from Baxter Healthcare (Miami, FL) was used. Serum samples from a routine clinical laboratory diluted to 1:100 with reagent A were also used.

All solutions were prepared with doubly distilled water purified using a Millipore Milli-Ro system.

### Immobilization of $\beta$ -D-galactosidase

The enzyme was immobilized on controlled-pore glass (CPG, 120–200 mesh; Electronucleonics, Fairfield, CT) by using Masoom and Townshend's procedure [36]. Glass tubes of different lengths and 0.5 mm i.d. were then packed with the supporting enzyme conjugate and stored in buffer solution at 4°C. Under these conditions the enzyme activity was constant for 2 months.

### Configuration and procedure

In order to minimize reagent consumption, the enzyme was immobilized on CPG and a symmetrical merging-zones approach was used [37]. Figure 1 shows the flow-injection manifold used. The configuration consists of a peristaltic pump (P) which propels the reagent stream A through two

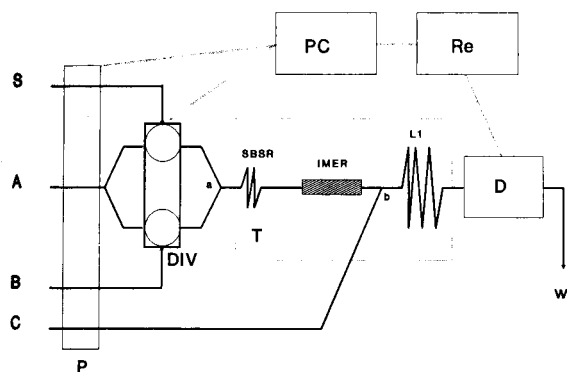


Fig. 1. Flow-injection merging-zones manifold with immobilized enzyme reactor. P = peristaltic pump; DIV = dual injection valve; SBSR = single bead string reactor; IMER = enzymatic reactor;  $L_1$  = open reactor; D = detector; W = waste; Re = recorder; PC = personal computer; T = temperature; S = sample; A, B and C = reagents; a and b = merging points.

channels. A dual-injection valve (DIV) inserts the sample and a solution containing reagent B simultaneously into two reagent streams. A single bead string reactor (SBSR) favours mixing of both injected plugs after merging point a and the hydrolysis reaction occurs on passage through the immobilized enzyme reactor (IMER). At the second merging point (b) the plug is mixed with a basic stream (reagent C) to enhance the colour intensity of the reaction product.

TABLE 1

Studied ranges and optimum values of the variables

Type	Variable	Studied range	Optimum value
Physical	Temperature ( $^{\circ}\text{C}$ )	20–45	73
Chemical	[Tris] ( $\text{mmol l}^{-1}$ )	50–500	100
	Hydrolysis pH	6–9	7.5
	[ $\text{Na}^+$ ] ( $\text{mmol l}^{-1}$ )	200–900	800
	[EGTA] ( $\text{mmol l}^{-1}$ )	0.2–0.8	0.4
	[ONPG] ( $\text{mmol l}^{-1}$ )	2–6	2.0
	[DL-DTT] ( $\text{mmol l}^{-1}$ )	0.5–4.0	4.0
	[NaOH] ( $\text{mol l}^{-1}$ )	–	1.0
FIA	Flow-rate ( $\text{ml min}^{-1}$ )	0.5–2.0	1.2
	Injected sample volume ( $\mu\text{l}$ )	40–200	50
	Injected reagent volume ( $\mu\text{l}$ )	40–200	40
	Length of SBSR (cm)	–	100
	Length of IMER (cm)	0.5–2.0	0.5
	Length of reactor $L_1$ (cm)	50–200	100

## RESULTS AND DISCUSSION

The method proposed by Berry et al. [35] for the determination of sodium was adapted to the FI technique [38]. In both instances, excess magnesium ion was used to enhance the sensitivity. In the presence of excess of sodium ion, the enzyme activity was proportional to the concentration of magnesium in the samples, and thus to the analytical signal.

### Study of variables

A study of the different variables influencing the system was made after grouping them into physical, chemical and hydrodynamic types. Table 1 shows the range over which each variable was studied and the optimum value found.

Increased temperatures accelerated the hydrolysis reaction up to  $37^{\circ}\text{C}$ , above which the signals decreased, possibly owing to denaturation of the biocatalyst.

The influence of the concentration of sodium ion in the sample was studied because this ion is always present at significant concentrations in serum samples (between 135 and  $155 \text{ mmol l}^{-1}$ ), in order to determine the concentration above which its influence on the development of the enzymatic reaction (and on the analytical signal) was negligible. Above  $800 \text{ mmol l}^{-1}$  sodium ion

added to the samples the analytical signal was not affected by such a concentration. The presence of some compounds with thiol groups in the medium can protect the active sites of the enzyme, so 4 mmol l<sup>-1</sup> DL-DTT were added to reagent A.

An ONPG concentration of 2 mmol l<sup>-1</sup> was selected as optimum. Higher concentrations enhanced the uncatalysed reaction and lower concentrations did not result in adequate development of the enzymatic reaction. The influence of pH on the enzymatic reaction was studied between 6.0 and 9.0; the best analytical response was found at pH 7.5. A concentration of 1.0 M NaOH provided a sufficiently basic medium to obtain the highest intensity of the coloured product.

High flow-rates (2 ml min<sup>-1</sup>) decreased the analytical signal and low flow-rates (0.5 ml min<sup>-1</sup>) decreased the sampling frequency. A flow-rate of 1.2 ml min<sup>-1</sup> was selected as a compromise between the two extremes. Injection volumes of 40 and 50 μl for reagent B and the sample solutions, respectively, provided the highest analytical signals.

An SBSR reactor of 100 cm length provided good mixing of the two plugs. A length of 100 cm was also used for the open reactor L<sub>1</sub> to obtain the best possible analytical signal, which also required the use of an enzymatic reactor of 0.5 cm length (ca. 200 U of β-D-galactosidase).

The sampling frequency of the method depended on the flow-rate, the valve loading and injection times and the reaction time. A sampling frequency of 40 h<sup>-1</sup> was achieved.

#### Features of the proposed method

**Calibration and reproducibility.** By using the optimum values of the variables previously found, a series of twelve standards of MgCl<sub>2</sub> · 6H<sub>2</sub>O with concentrations between 5 and 100 μmol l<sup>-1</sup> were injected in triplicate and a typical logarithmic enzymatic curve was obtained that conformed to the following equation:

$$\text{absorbance} = 175.4 \times 10^{-3} \ln[\text{Mg}^{2+} (\mu\text{mol l}^{-1})] - 181.0 \times 10^{-3}$$

(*r* = 0.9967, *n* = 12)

TABLE 2

Study of reproducibility

	Magnesium concentration (μmol l <sup>-1</sup> )					
	Low level <sup>a</sup>			High level <sup>b</sup>		
	<i>x</i>	<i>σ</i> <sub><i>n</i>-1</sub>	R.S.D. (%)	<i>x</i>	<i>σ</i> <sub><i>n</i>-1</sub>	R.S.D. (%)
Within-run ( <i>n</i> = 11)	5.33	0.155	2.91	18.5	0.144	0.78
Between-run ( <i>n</i> = 11)	5.62	0.180	3.21	18.4	0.313	1.70

<sup>a</sup> 5.84 μmol l<sup>-1</sup>, <sup>b</sup> 17.6 μmol l<sup>-1</sup>.

A calibration graph was constructed using different solutions of Cation Cal serum reference material over the concentration range encompassing the maximum slope of the previous graph. For application of the method, a narrower, linear range between 5 and 20 μmol l<sup>-1</sup> was obtained from the equation

$$\text{absorbance} = 14.9 \times 10^{-3} [\text{Mg}^{2+} (\mu\text{mol l}^{-1})] + 0.476 \times 10^{-3}$$

(*r* = 0.9975, *n* = 8)

The reproducibility of the method was studied on eleven solutions prepared from Cation Cal serum at two magnesium concentration levels (5.84 and 17.6 μmol l<sup>-1</sup>). Each solution was injected in triplicate to determine the within-run reproducibility. For the between-run reproducibility, each solution was also injected in triplicate over eleven days. The results obtained are given in Table 2.

**Interferences.** The study of potential interferences was focused on singly and doubly charged cations commonly present in serum. These interferences were added to the samples at higher concentration levels than usually found in real samples. The results showed that sodium and potassium are tolerated up to an 800:1 (interferent: Mg) ratio, whereas ammonium and lithium cause no interference up to a 160:1 ratio and there is no interference from calcium up to a 20:1 ratio. Effects of other species such as Cu(II) and Zn(II) are not significant at a 1:100 dilution of serum samples, which is mandatory for application of the proposed method.

TABLE 3  
Determination of Mg(II) from serum samples

Sample No.	[Mg(II)] ( $\mu\text{mol l}^{-1}$ )	Dilution	1st addition <sup>a</sup>		2nd addition <sup>a</sup>	
			Found ( $\mu\text{mol l}^{-1}$ )	Recov-ery (%)	Found ( $\mu\text{mol l}^{-1}$ )	Recov-ery (%)
1	820	1:100	12.1	97	16.1	96
2	790	1:100	11.7	95	16.0	100
3	630	1:100	10.4	102	14.0	96
4	530	1:100	9.6	108	13.6	104
5	630	1:100	10.8	113	14.2	98
6	590	1:100	10.0	102	14.2	103

<sup>a</sup> 4.01 and 8.04  $\mu\text{mol l}^{-1}$  for the first and second additions, respectively.

*Application of the proposed method.* Six samples of human serum from both healthy and sick individuals were used to validate the proposed method. The analyte concentration in each sample was previously determined by the conventional AAS method. Samples were diluted 100-fold and subjected to two additions of standard (4.01 and 8.04  $\mu\text{mol l}^{-1}$ ) to determine the recovery of magnesium. Table 3 gives the results obtained. The analyte recovery ranged between 96 and 113%.

*Comparison with the AAS method.* The proposed method was compared with the conventional AAS. Thirty serum samples were analysed by both methods. The linear correlation found can be expressed by

$$[\text{FIA}] = 0.93[\text{AAS}] + 0.12$$

with standard deviations of the intercept, slope and *xy* estimate of 0.05, 0.06 and 0.04, respectively, and a correlation coefficient of 0.9502. These results show good consistency between the two methods.

### Conclusion

The simplicity, reproducibility and sensitivity of the proposed method make it a valid alternative to earlier spectrophotometric methods. It is a novel approach to enzyme analysis of metals. This is the first method for the determination of magnesium involving a single enzymatic step. The use of an immobilized enzyme and the merging-zones

mode significantly reduces sample and reagent consumption.

The high dilution of samples allows potential interferences arising from the analysis of complex biological samples to be avoided or minimized.

### REFERENCES

- 1 M. Walser, Rev. Physiol. Biochem. Exp. Pharmacol., 59 (1967) 185.
- 2 J. Ronal, Clin. Chem., 33 (1987) 1965.
- 3 J.K. Alkawa, Magnesium: its Biological Significance (CRC Series on Cations of Biological Significance), CRC, Boca Raton, FL, 1981, pp. 1–27.
- 4 L.J. Iseri, J. Freed and A.R. Bures, Am. J. Med., 58 (1975) 837.
- 5 T. Dycknert, Acta. Med. Scand., 207 (1980) 59.
- 6 C.K. Mann and J.H. Yoe, Anal. Chem., 28 (1985) 202.
- 7 v. Crony, X. Svodoba and I. Stepanora, Biochem. Med., 7 (1973) 208.
- 8 E.M. Gindler and D.A. Heth, Clin. Chem., 17 (1971) 663.
- 9 R.J. Henry, D.C. Cannon and J.W. Winkleman, Clinical Chemistry: Principles and Techniques, Harper and Row, New York, 1974, pp. 670–679.
- 10 D.H. Basinski, Clin. Chem., 5 (1965) 137.
- 11 E.S. Baginski and S.S. Maril, Sel. Methods Clin. Chem., 9 (1982) 227.
- 12 E.C. Farrell, in L.A. Kaplan and A.J. Pesce (Eds.), Clinical Chemistry: Theory, Analysis and Correlations, Mosby, St. Louis, MO 1984, pp. 1065–1070.
- 13 J.A. Nisbet and J.A. Owen, Clin. Chim. Acta, 92 (1979) 367.
- 14 S.A. Lewis, T.C. O'Haver and J.M. Harnly, Anal. Chem., 56 (1984) 1066.
- 15 T. Uchida and B.L. Valle, Anal. Sci., 2 (1986) 243.
- 16 M. Zhuang and R.M. Barnes, Appl. Spectrosc., 39 (1985) 793.
- 17 M. Tabata, T. Kido, M. Totani and T. Murachi, Clin. Chem., 31 (1985) 703.
- 18 P. Fossati, M. Sirtoli, G. Tarengi, M. Gianchetti and G. Berti, Clin. Chem., 35 (1989) 2212.
- 19 M.C. Wimmer, J.D. Artiss and B. Zak, Clin. Chem., 32 (1986) 629.
- 20 M. Tabata, M. Totani and T. Murachi, Biomed. Chromatogr., 4 (1990) 123.
- 21 B.F. Rocks, R.A. Sherwood and C. Riley, Ann. Clin. Biochem., 21 (1984) 51.
- 22 R.A. Sherwood, B.F. Rocks and C. Riley, Analyst, 110 (1985) 493.
- 23 J.L. Burguera, M. Burguera, M. de la Guardia, A. Salvador and V. Carbonell, J. Flow Inject. Anal., 7 (1990) 11.
- 24 M.F. Gine, H. Gergamin, H.F. Reis and R.L. Tuon, Anal. Chim. Acta, 234 (1990) 207.

- 25 W.A. de Oliveira and A.S. Mendes, *Talanta*, 34 (1987) 543.
- 26 V.A. Mirkin and A.V. Fenin, *Zh. Anal. Khim.*, 43 (1988) 1195.
- 27 R. Goldik, C. Yarnitzky and M. Ariel, *Anal. Chim. Acta*, 234 (1990) 161.
- 28 T. Imato, M. Ishii and N. Ishibashi, *Bunseki Kagaku*, 39 (1990) 135.
- 29 A.T. Haj-Hussein and G.D. Christian, *Microchem. J.*, 34 (1986) 67.
- 30 R. Forteza, V. Cerdá, S. MasPOCH and M. Blanco, *Análisis*, 15 (1987) 136.
- 31 F. Cañete, A. Ríos, M.D. Luque de Castro and M. Valcárcel, *Analyst*, 112 (1987) 267.
- 32 Y. Yuan, Y. Wang and K. Qu, *Fenxi Huxue*, 16 (1988) 546.
- 33 Y. Yuan, *Anal. Chim. Acta*, 212 (1988) 291.
- 34 J. Fu, G. Lin, J. Yang, Z. Wang and C. Ma, *Huaxue Tongbao*, 39 (1990) 48.
- 35 M.N. Berry, R.D. Mazzachi, M. Pejakovic and J. Peare, *Clin. Chem.*, 34 (1991) 2295.
- 36 M. Masoom and A. Townshend, *Anal. Chim. Acta*, 166 (1984) 111.
- 37 P.J. Worsfold and A. Nabi, *Anal. Chim. Acta*, 179 (1987) 307.
- 38 R. Quiles, J.M. Fernández-Romero, E. Fernández, M.D. Luque de Castro and M. Valcárcel, *Clin. Chem.*, in press.

# Trends in kinetic methods of analysis

Stanley R. Crouch

*Department of Chemistry, Michigan State University, East Lansing, MI 48824 (USA)*

(Received 8th October 1992)

## Abstract

Seven trends in kinetic methods of analysis are identified and described. These trends include the increasing use of automation and multidimensional instrumentation, the continuing development of sophisticated data processing approaches and error compensation methods, the improvements in multicomponent and single component determinations and the exploitation of the kinetic approach for transient responses that are not the result of chemical reactions. The trends described should continue throughout the 1990s and lead the way into the next century. These trends are helping to make kinetic methods competitive with those methods based on processes at equilibrium or at steady state.

*Keywords:* Kinetic methods; Chemometrics; Data processing; Multidimensional instrumentation

The field of kinetic methods of analysis has been developing since the late 1950s. Although the field is now mature, it has recently been undergoing a major resurgence in activity. The renewed interest can be attributed to advances that have been made in principles, in automated instrumentation, in understanding chemical and instrumental systems, in data treatment methods, and in analytical application. Also, it is becoming clear that the kinetic approach to analytical chemistry is rather general with several advantages over the traditional equilibrium approach [1–3]. Thus we are beginning to see kinetic-based procedures being used in situations other than those involving chemical reactions.

The purpose of this paper is to identify and describe the major trends in kinetic methods for the 1990s. These are the trends that are helping to reshape and revitalize kinetic determinations so that they are becoming competitive with equi-

librium-based procedures in many cases. These are also the trends that are likely to continue for the next several years and lead the way into the next century. At the outset, let us make it clear that this author prefers to have his “trends” spoken and not written down. The spoken word is so much more volatile and less prone to be regurgitated. As a second disclaimer, the trends discussed below are solely this one scientist’s opinion regarding the major directions in which the field is headed. This opinion is to be considered biased and clouded by a certain attachment to his own research ideas. Likewise, any predictive remarks made below should be tempered by the fact that this author’s “success” rate in forecasting the future is negligibly small. That and a firm belief in Edmund Burke’s statement, “You cannot plan the future by the past”, will not, however, deter this author from making the attempt.

In the sections that follow, seven major trends in kinetic methods are examined. Many of the trends identified overlap to some extent. Thus, advances in multicomponent determinations depend heavily on progress made in data processing

*Correspondence to:* S.R. Crouch, Department of Chemistry, Michigan State University, East Lansing, MI 48824-1322 (USA)

TABLE 1

## Major trends in kinetic methods

- 
- (1) Increasing use of “intelligent automation”
  - (2) Growing utilization of multidimensional instrumentation
  - (3) Continuing development of sophisticated data processing techniques
  - (4) Additional progress in error-compensation methods
  - (5) Innovations in multicomponent kinetic procedures
  - (6) Expanding applications of kinetic determinations
  - (7) Enlarging the kinetic approach to include miscellaneous time-dependent responses
- 

and in multidimensional instrumentation. This treatment is not intended to be solely a review of past work, but instead a look to the future. It will draw heavily from recent work, but will not attempt to be comprehensive. Undoubtedly the fu-

ture will see some tremendous breakthroughs that are not predictable from extrapolating current trends. That’s what will make it so exciting.

## MAJOR TRENDS

*“If you can look into the seeds of time and say, which grain will grow, and which will not, speak then to me”. (Shakespeare, ‘Macbeth’)*

Kinetic methods of analysis make use of the response of a dynamic system in order to determine the concentrations of analytes in samples. Typically, kinetic methods are based on the kinetics of chemical reactions. However, the kinetic approach is general and can be based on such processes as diffusion, vaporization, radiative decay, and many others [1,2]. The seven major trends

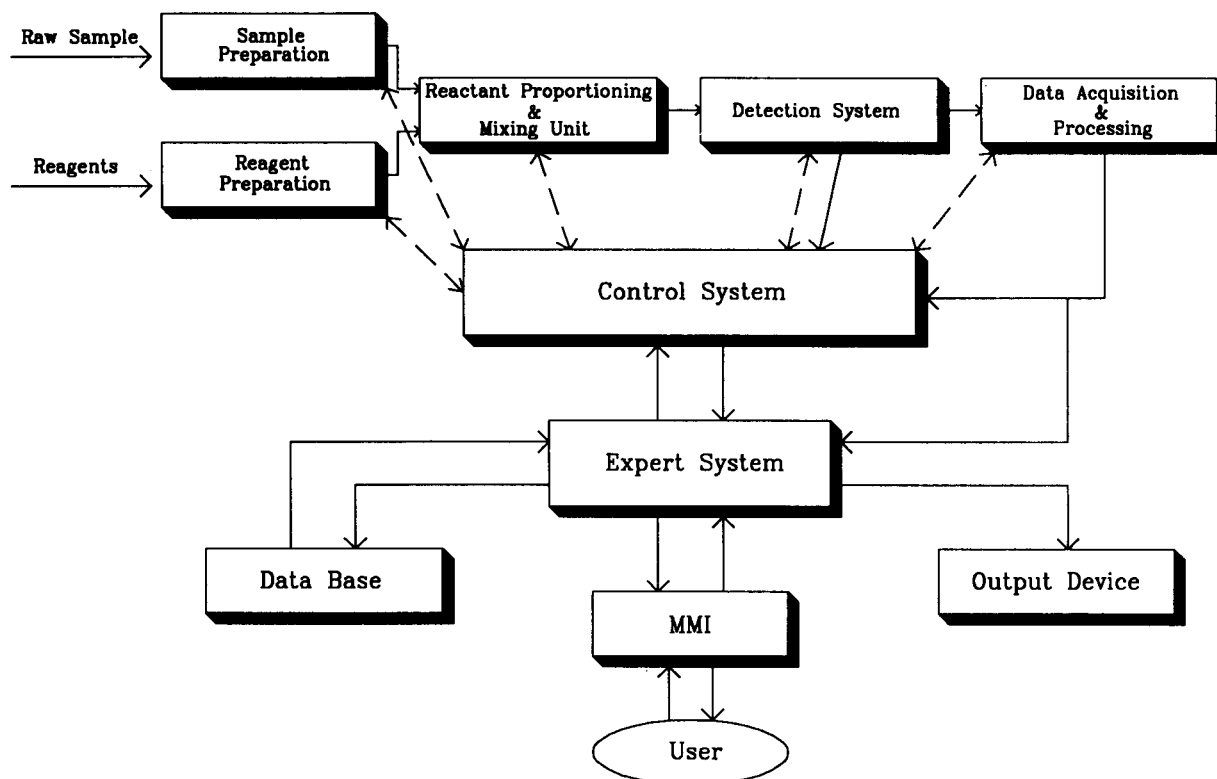


Fig. 1. Block diagram of intelligent kinetic analyzer. Reproduced with permission from Ref. 4. The dotted lines indicate control and status information. Note that the detection system can send raw data back to the controller for diagnostic purposes. The data acquisition and processing system sends processed data to the control system for control purposes and the the expert system for interpretation, display and storage in the data base.

that have been identified in kinetic methods are listed in Table 1. Most of these deal with methods that are based on chemical reactions. However, *Trend 7* discusses the extension of kinetic principles to processes other than chemical reactions.

*Trend 1: Increasing use of “intelligent automation”*

*“The intelligence is proved not by ease of learning, but by understanding what we learn”. (Joseph Whitney)*

Kinetic methods of analysis are extremely well-suited to intelligent automation. They require accurate timing, careful control over experimental conditions, precise sample and reagent preparation, proportioning and mixing, and accurate measurements of dynamic signals. Most of the unfavorable comments that are occasionally heard about kinetic methods are a result of a lack of control over some reaction condition (pH, ionic strength, temperature, reactant concentrations, etc.). In previous articles, we have discussed intelligent automation in general [4] and of kinetic methods in particular [5]. Figure 1 gives a block diagram of an intelligently automated kinetic analyzer [5]. It represents a fifth generation system [4] in which the user interacts with an expert system by means of a man-machine interface (MMI). The expert system has its own knowledge base and can interact with a data base. The expert system communicates with the control system which has control over the instrument. Note that the sample and reagent preparation systems are both under computer control as are the reactant proportioning and mixing systems. Note also the many different feedback paths that are possible in this analyzer.

The intelligent kinetic analyzer has yet to be constructed and may seem to be several years away. However, we are seeing many of the necessary developments so that the tools for its construction are nearly ready. The many advances that have been made in computers and in expert systems will not be covered here for these are well-documented elsewhere (see Ref. 4, for example). Instead this discussion will focus on the kinetic analyzer itself.

One of the most difficult tasks to automate is the preparation of samples and reagents. It is desirable not only to automate solution preparation, but to incorporate the preparation system in the feedback loop of the analyzer. This allows new solutions to be prepared under computer control when they are needed. For example, if a sample concentration is outside the range of the calibration graph, it may be desirable to prepare a new standard of higher concentration. Under computer control, the new solution can be prepared if deemed necessary by the results of experiments. While very few systems incorporate this type of dynamic solution preparation, research is being done in this area. As an early example from our laboratory [6], we presented the design of a computer-controlled syringe-based sample preparation system with a dilution range of up to 5 orders of magnitude. More recently, Stewart and Horlick [7] have presented the concept of incorporating a robotic sample preparation system in the feedback loop of an inductively coupled plasma emission spectrometer. Wentzell [8] has discussed solution sample preparation with continuous flow systems, a process he terms “solution robotics”. Hence, we are beginning to see the introduction of dynamic sample preparation systems in analytical instrumentation. Much work remains to be done, however.

It is flow-injection analysis (FIA) that dominates the sample introduction and mixing area [9]. FIA sample introduction is becoming more widely used for kinetic-based procedures. Ruzicka [10] has described the state of the art in FIA and emphasized the use of stopped-flow and sequential injection methodologies, particularly for kinetic-based determinations. In stopped-flow injection, the sample is injected into a carrier stream, reagent is added, and the mixture transported into the flow cell where the flow is stopped. Stopping the flow causes dispersion to become negligible and allows rate measurements to be made on a selected portion of the sample zone trapped inside the flow cell. Christian and Ruzicka [11] have described numerous examples of assays using stopped-flow injection methods. Sequential injection [10–12] is a second-generation stopped-flow technique based on the sequential



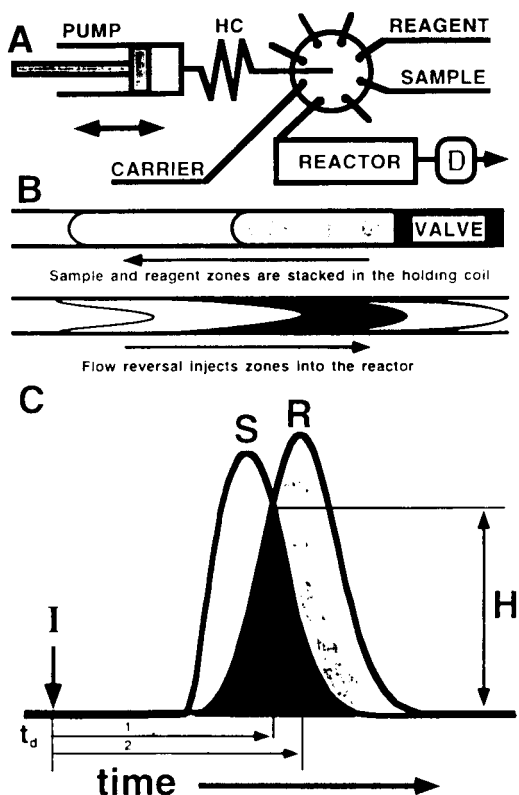


Fig. 2. Sequential injections principle (reproduced with permission from Ref. 10). The flow scheme is shown in (A), while (B) shows the structure of the stacked and injected zones. The concentration profiles seen by the detector are shown in (C). HC, holding coil; D, detector; S, sample; R, reagent; H peak height; I, point of injection.

aspiration of sample and reagent zones through a selector valve into a holding coil as shown in Fig. 2. A stack of well defined zones is obtained in this manner. The direction of flow is then reversed, and the zones are injected into a reactor and detector. The flow reversal creates a composite zone in which sample and reagent zones penetrate each other. For kinetic determinations, the flow is then stopped and a portion of the composite zone is trapped inside the flow cell of the detector. This allows the measurement of the rate of reaction. The sequential injection technique should allow great versatility in configuring analytical systems because injection volumes, reaction times and zone dispersion can all be changed readily by varying stroke volumes, flow-rates,

stopped-flow time, and reversals via computer control of the pump. Since many reagents, reactors and detectors can be positioned around a single selector valve, multi-reagent procedures and multi-detector determinations can be carried out in a single system. Although the technique is in its infancy, it seems to have great potential for kinetic-based determinations and should become widely used.

Stopped-flow, air-segmented continuous flow has also been proposed for kinetic determinations [5,13]. Here, the air segments prevent dispersion and promote good mixing prior to stopping the flow. With an electronic bubble gating system, the flow can be stopped when the cell is filled with liquid. Alternatively, the flow can be stopped after the bubbles are removed. Kinetic information can also be obtained with air-segmented continuous flow systems by using flow reversals or flow recycling methods [14]. Here the advantage is that there is limited dispersion during the process which makes it easy to extract chemical kinetic information.

Chung and Ingle [15] have described a new procedure for obtaining kinetic data from FIA peak profiles by correcting for the effects of dispersion. Their method acquires and stores the peak profiles of a non-reacting reference solution and a reacting sample solution. The dispersion coefficients obtained from the reference profile are used to normalize the profile of the sample solution. Rate information was extracted by the fixed-time approach [1–3].

The rapid-mixing stopped-flow technique is also very useful for kinetic-based procedures. In this method, reagent and samples are mixed under turbulent flow conditions, and the flow is abruptly stopped. Rapid mixing methods allow the monitoring of reactions much faster than those observed with stopped-flow FIA. Reaction times on the millisecond time scale are possible, which expands greatly the range of rate constants observed. The stopped-flow mixing technique has been recently reviewed by Gomez-Hens and Perez-Bendito [16]. Joseph et al. [17] and Takahashi et al. [18] have reported systems in which continuous flow methodology is combined with the rapid mixing stopped-flow technique. This

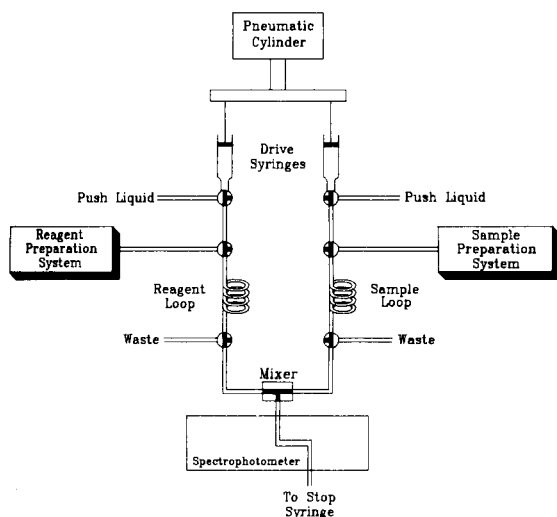


Fig. 3. Schematic diagram of automated stopped-flow system. Prepared samples and reagents are pumped into loops. Inert push liquids push sample and reagent into mixing chamber and mixed solution into observation cell of spectrophotometer. A stop syringe stops the flow and allows absorption measurements to be taken.

can overcome some of the disadvantages of the stopped-flow method. Figure 3 shows an updated version of the system originally conceived by Joseph et al. [17]. Here the reagent and sample preparation systems are continuous flow (either air-segmented or FIA) systems. Prepared reagents and samples are introduced into loops contained in the path of the rapid mixing stopped-flow system. The loops can be inert holding coils or can incorporate immobilized reagents such as enzymes. After a suitable holding time in the loops, valves are turned to isolate the reagent and sample preparation systems and to connect the drive syringes which have been filled with inert pushing liquid. The drive syringes are then activated and the contents of the loops are forced through a mixer into the spectrophotometric observation cell. The flow of liquid through the cell activates a stop syringe and allows measurement of rate information on the stopped mixture in the observation cell. Such combinations of continuous-flow sample preparation and stopped-flow mixing would seem to be particularly advantageous for kinetic-based determinations over a wide range of reaction times and conditions.

Another technique that appears quite promising for the study and analytical use of fast reactions is the continuous addition of reagent technique [19,20]. This method makes use of simple instrumentation, yet allows rate measurements to be made on the millisecond time scale. In the continuous addition technique, a reagent with which the analyte reacts, is added continuously to the solution. The analyte concentration varies because of both reaction and dilution. By using appropriate kinetic expressions, the initial analyte concentration can be obtained by initial rate methods or by integral methods [19]. A major drawback of the method was its high sample consumption, but this has been overcome [20] by use of an immersion probe for measuring absorbance in conjunction with a small reaction vessel. This combination allows microliter volumes of sample to be determined. The method appears to be generally applicable and should enjoy increasing use. Its second-order kinetic nature has allowed it to be exploited in multicomponent determinations (see *Trend 5* below).

Detection, data acquisition and data processing are also areas in which a great deal of progress has been made. In one novel detection approach, integration of reaction and spectroscopic detection has been proposed for continuous flow systems [21]. Such techniques have promise for developing biochemical sensors. Many of the other detection advances are in the area of multidimensional instrumentation which is discussed in *Trend 2* below. Likewise the developments in data acquisition and processing are so important that *Trend 3* is devoted to them.

### *Trend 2: Growing utilization of multidimensional instrumentation*

*“Even if you’re on the right track, you’ll get run over if you just sit there.” (Will Rogers)*

Most kinetic methods, as well as most fundamental studies of kinetics, utilize a reaction monitoring system that produces a single response (proportional to the reactant or product concentration) versus time. All the kinetic information must be extracted from that one response. With modern instrumentation it is possible to obtain

much more information about time-dependent systems. With absorption or fluorescence spectrometry, for example, array detectors allow entire spectra to be obtained in a time short enough to be useful for extracting kinetics information. The ability to acquire time-dependent absorption or fluorescence information simultaneously at many wavelengths can allow the user to monitor multiple species, observe transient intermediates, obtain information on species with overlapping spectra, and correct for background absorbances. Early array detector spectrometers employed vidicon tube-type detectors [22,23]. More recently, diode array spectrometers have been most popular for fluorescence [24] and absorption spectrometry [25]. An example of the use of a diode array spectrometer is shown in Fig. 4, which gives some spectra observed at various times in the Co(II) complexation reaction with 4-(2'-pyridylazo)resorcinol (PAR). Although these detectors are linear arrays, rather than two-dimensional arrays, they do not exhibit the blooming and lag problems of vidicon tubes [26]. When combined with microchannel plate image intensifiers, they can be quite sensitive, which is highly desirable in fluorescence spectrometry.

It is the current generation of array detectors, charge-coupled devices (CCDs) and charge-injection devices (CIDs) [27,28], that appears most promising for optical spectroscopy, particularly when their two-dimensional nature can be used. These devices have many of the advantages of the photomultiplier tube in terms of sensitivity and linear range, yet are two-dimensional like a photographic plate. Such systems should be valuable in instruments like two-dimensional fluorescence spectrometers [29] that simultaneously display a series of emission spectra taken at various excitation wavelengths. For example, we have described a system previously [5] that can collect absorption and fluorescence spectra nearly simultaneously by time-sharing a diode array detector. Instead of time-sharing a linear detector, one should be able to spatially separate and display absorption and fluorescence spectra on a CCD detector. Likewise in continuous flow systems, the imaging capabilities of the CCD detector could be used to collect spectra at different points (reaction times)

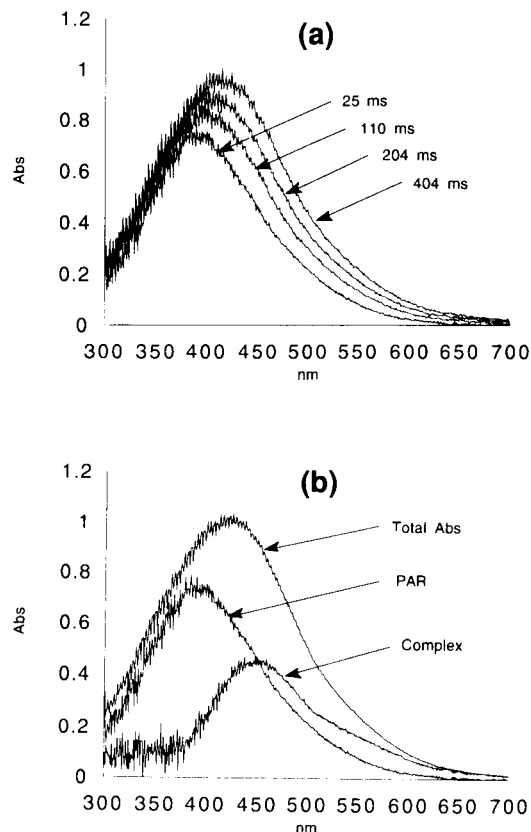


Fig. 4. Spectra of reactants and products in Co(II)-PAR system taken with diode array stopped-flow spectrophotometer. (a) Spectra of the mixture at various times. The apparent shift of the wavelength of maximum absorption is explained by the spectra in (b) of the mixture, PAR and the complex after subtracting the PAR absorption. pH 8.0,  $I = 0.1$  M,  $[Co(II)] = 1.70 \times 10^{-5}$  M,  $[PAR] = 2.11 \times 10^{-4}$ .

along an observation tube. There are now commercially available imaging spectrographs that have 5–35 fiber optic input channels. Each fiber optic can collect a spectrum corresponding to a different time during the reaction. If the number of sampling points is too small to accurately define the reaction progress curve, flow reversal or flow recycle techniques [14] could be used to obtain more sampling points (times). Multi-detection has been shown [30,31] to be advantageous for obtaining kinetics information. Even for fast reactions, rapid mixing continuous flow techniques could be used with imaging spectroscopy to obtain kinetics information without the waste-

ful use of large volumes of solution. The future should see an increase in the use of CCD and CID detectors in kinetic methods, particularly those involving multiple components (see *Trend 5*).

Of course multidimensional detection can also be achieved by combining two or more types of detectors. For example spectrophotometry could be combined with pH monitoring or a bulk property technique such as conductance. In fact several years ago we developed a combined adsorption spectrophotometric/conductometric detection system [32] based on the bipolar pulse conductivity technique [33]. A unique cell was developed that allowed for simultaneous measurements of single wavelength adsorption, solution conductance, and solution temperature. With array detectors one can now readily combine multi-wavelength measurements with conductance and temperature measurements. One can imagine combining a variety of different detection techniques, each giving a different type of information, in a multidimensional instrument. Such an instrument would be extremely powerful for fundamental studies of kinetics and could be used to perform some unique functions in routine kinetic determinations. For example, Campi and Ingle [34] have shown that rates can be corrected for the influence of temperature and pH during fluorimetric kinetic measurements by simultaneously monitoring fluorescence, pH and temperature. They showed that temperature variations of more than 1 degree and pH changes of over 0.28 pH units could be corrected with their method. Hence multidimensional information can be used to provide compensation information in addition to information about multiple species. Again we should see a great deal more of this approach in the future.

### *Trend 3: Continuing development of sophisticated data processing techniques*

*“Statistics are like a bikini. What they reveal is suggestive, but what they conceal is vital.” (Aaron Levenstein)*

The widespread use of computers in analytical chemistry has brought about many new develop-

ments in data processing for kinetic methods. The tremendous advances in instrumentation and automation have all been stimulated by inexpensive computational power. Hand in hand with the development of automated systems and multidimensional instrumentation have come enormous improvements in data processing methods. In this section, the general trends in data processing for kinetics methods are discussed. Specific data processing methods aimed at error compensation or multicomponent determinations are discussed in *Trends 4* and *5* below. The techniques discussed in this section fall under the general category of chemometrics, that discipline that uses statistical and mathematical methods to provide chemical information or select optimum measurement conditions.

Otto [35] has reviewed the applications of chemometrics in kinetic analysis including uses in filtering, smoothing, curve-fitting, experimental design, optimization and multicomponent determinations. Hence, the discussion here will focus on a few recent trends and attempt to project into the future.

Kalman filtering has received a great deal of attention for use in kinetic methods. The Kalman filter [36] is an algorithm for the recursive estimation of the parameters and states of a system from a series of noisy measurements. A system model and a measurement model are used in the filter. The system model describes the system dynamics, or how the measurements vary with one or more of the system variables. The measurement model describes the measurement process and how the measured values relate to the parameters desired. The adjustable parameters of the model are known as the state vector. Estimates of each of the parameters in the state vector are adjusted after each measurement. The first step in Kalman filtering is a prediction step, where the next output is predicted from the model. The observed output is then compared to the predicted value and the resulting difference is used to correct the current estimate of the state of the system. The filter can be used with a linear or nonlinear model. For the case in which absorption spectrophotometry is used with a kinetic system, the model is linear if the rate constants

are known and nonlinear if they are unknown. The nonlinear form of the Kalman filter is not as stable as the linear form and requires better initial estimates of the parameters for fast convergence. Kalman filter estimates are, with some restrictions, optimal in the least squares sense [36].

Kalman filter-based methods have several advantages over batch processing methods for measurement and control applications. Because the calculations are relatively fast, often on the order of seconds, estimates of the system states can, in principle, be obtained as the data are acquired (real-time filtering). Second, the state variables need not be constants, but can vary with time. Finally, since the Kalman filter is recursive, it is unnecessary to store and manipulate large data arrays.

The Kalman filter has been applied to a variety of situations in analytical chemistry [36,37]. Rutan and Brown [38] have shown how kinetic models can be tested with the Kalman filter. The Kalman filter can also be used to detect and correct model errors in the case of unsuspected components, synergistic effects or poorly modeled background. For linear systems, adaptive filtering can be used when models are in error. The adaptive Kalman filter [39] decreases the effect of model error by changing the Kalman gain in a manner that underweights data collected when the model is in error. Unfortunately, with a nonlinear system, ordinary adaptive filtering is not possible. However, this problem can be dealt with by a coupled adaptive filter-nonlinear filter approach [40,41].

Many of the applications of the Kalman filter to kinetic methods have been in error-compensation procedures and in multicomponent determinations. These uses are discussed below. The Kalman filter shows great promise as a data processing technique for kinetic methods. Its greatest utility would seem to be in real-time filtering applications. The real-time applications that are likely in the future await the introduction of faster computers and/or the availability of hardware signal processing chips.

The multidimensional instruments that are becoming popular for use in kinetics can create

serious data storage and processing problems. Fortunately, there are modern chemometric techniques that can help us short through this vast amount of information. One of these methods is factor analysis [42], a technique that is applicable to linear systems in which a data matrix can be represented as the product of two matrices of lower dimensionality. Reacting systems, monitored by multiwavelength optical spectrometric methods are particularly amenable to study by factor analysis techniques.

Abstract factor analysis, also known as principle component analysis, can provide information regarding the number of components in a multicomponent system. The results of abstract factor analysis can be target transformed into physically significant factors (e.g., concentrations or concentration–time profiles) via target factor analysis. The general process for converting the abstract factor analysis solution to a real one has been recently discussed for linear systems [43]. Factor analysis has been applied primarily to multicomponent systems at equilibrium. Only a few applications have been reported dealing with kinetic studies [42].

In some cases factor analysis and Kalman filtering have been combined. For example, Gerow and Rutan [41] used factor analysis to develop weighting factors for the Kalman filter in order to subtract background in fluorescence spectrometry. In another approach Wentzell and Vanslyke [44] used parallel Kalman filter networks to implement principle component analysis recursively on multiwavelength chromatographic data. In this case several different models were employed with differing numbers of components, and the model giving minimum differences between predicted measurement values and actual values was selected. This approach has the advantages of speed and simplicity and can be used for real-time principle component analysis.

Response surface methodology has also been used for modeling various chemical processes including reaction kinetics [35]. Here the model can be empirical or based on a reaction mechanism. Such models can be used to provide multidimensional information about chemical systems and for optimization purposes. Statistical considera-

tions in fitting data to discrete or continuous models have been addressed by Marshall [45]. In the case of empirical models, a second-order polynomial is most often used for fitting the data. In our laboratory [46], we have applied the Kalman filter instead of more traditional least squares methods for fitting the data. The automated exploration and exploitation of response surfaces in flow-injection studies has been reported [47]. Multidimensional visualization of the chemical data obtained in such studies can be highly informative as illustrated in Fig. 5. Here the response surface was mapped by data taken

during optimization studies. Eventually, modeling based on chemical mechanisms and response surface mapping will be combined in even more powerful approaches for the study of chemical reactions.

Optimization of kinetic methods has also been accomplished with various search methods, such as grid searches and simplex optimizations [35]. It has been reported [47] that pattern search methods should be preferable to simplex procedures when the number of experimental variables is small (three or less). In such cases, the grid search methods can accurately map an entire

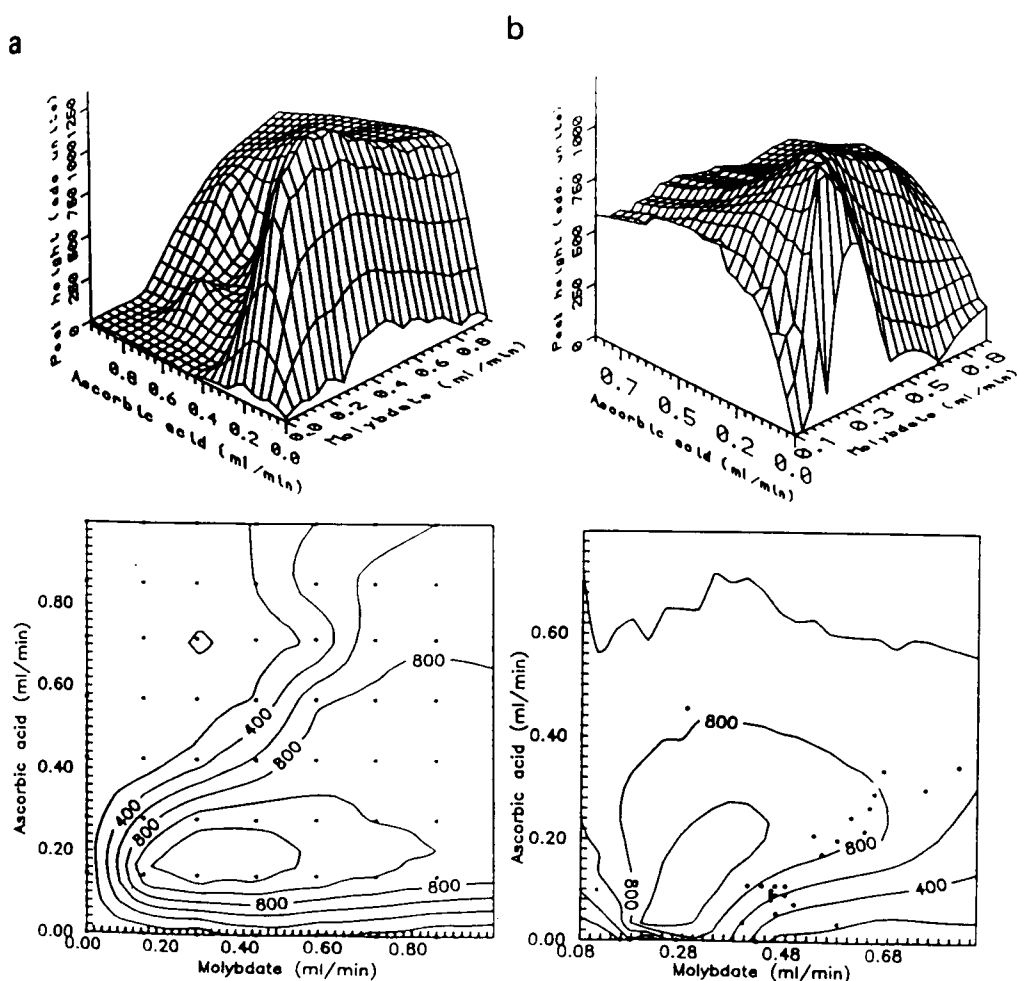


Fig. 5. Response surface plots for the reaction of Mo(VI) with the phosphate in the presence of ascorbic acid as a reducing agent (reproduced with permission from Ref. 47). In (a) the FIA peak absorbance is shown for 64 regularly spaced points taken during a grid search optimization. In (b) the FIA peak absorbance is shown for 40 irregular spaced points taken during a simplex optimization.

surface in less time than manual simplex methods. Note in Fig. 5 that a grid search gives a more global coverage of the surface than the simplex optimization. The latter gives good coverage, however, near the maximum. For systems with four or more variables, it was concluded [47] that simplex methods may provide the only reasonable approach for automated optimization.

The past few years have seen a tremendous increase in computational power and a simultaneous decrease in the cost of such power. This trend seems destined to continue for several years. Because of this, we will see powerful data processing techniques, such as those described here, becoming routinely useful for kinetic studies and methods. Real-time processing methods, such as the Kalman filter, should be major beneficiaries of the next generation of computers.

#### *Trend 4: Additional progress in error-compensation methods*

*“If error is corrected whenever it is recognized as such, the path of error is the path of truth”.  
(Hans Reichenbach)*

Kinetic methods are generally more susceptible than equilibrium methods to changes in such experimental variables as pH, temperature, ionic strength, reagent concentrations, and the presence or absence of catalysts, inhibitors and activators. Hence, it is usually considered necessary to control experimental conditions extremely carefully in order to obtain precise and accurate results. In recent years, however, error-compensation methods have been introduced that reduce the need for such careful control. Since it is not always possible to control all the variables that could cause errors, such compensation methods appear to have wide utility.

Many different approaches have been described for error compensation in kinetic methods [1–3,5]. One of the early methods was a predictive method [48] in which the signal value at equilibrium was predicted from a multiple regression analysis of kinetic data. This has the effect of compensating for changes in variables that effect the kinetics, but not the position of equilibrium. Wentzell [49] applied the Kalman

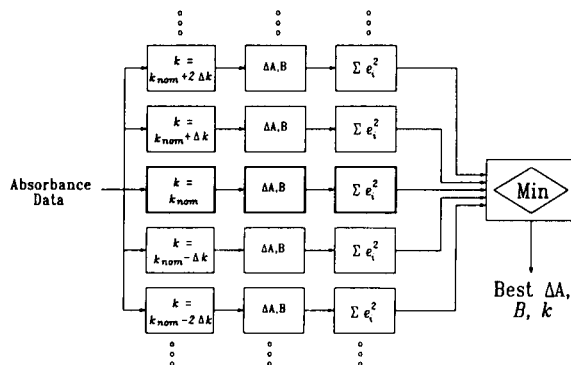


Fig. 6. Parallel Kalman filter network for correction of errors arising from between-sample variations in rate constant  $k$  (reproduced with permission from Ref. 50).

filter in this same mode to estimate the equilibrium absorbance of a mixture from data acquired early during the reaction. He found that compensation for sample-to-sample variations in the rate constant for a first or pseudo-first-order system could be accomplished with the nonlinear form of the Kalman filter. In more recent work, Wentzell and Vanslyke [50] used parallel Kalman filter networks to correct for between sample variations in the rate constant. Here, a set of 40 or more linear models were employed in parallel. The models were based on the following first-order equation:

$$A_t = \Delta A [1 - \exp(-kt)] + B$$

where  $A_t$  is the absorbance at time  $t$ ,  $\Delta A$  is the change in absorbance due to the product formation at  $t = \infty$ ,  $k$  is the pseudo-first-order rate constant and  $B$  is the background absorbance. Each model had a slightly different value of the rate constant as shown in Fig. 6. By examining the differences between the measurement values predicted by the current parameter estimate and the actual measurement values (the innovations sequence) for each model, the best model can be selected and the parameters extracted. This approach has as its major advantages speed, simplicity and flexibility. The parallel Kalman filter method can be applied in real time and is ideally suited for hardware processing and parallel computing architectures.

Most of the procedures for error compensation require knowledge of the kinetic model for the chemical process (reaction order) or the rate constant. In fact, most error-compensation methods are based on the assumption of pseudo-first-order behavior. The recent trend, however, has been to develop error-compensation methods in which these constraints are relaxed. Larsson and Pardue [51] were the first to describe methods that did not require knowledge of the reaction order or rate constant. The algorithm developed is based on a generalized nonlinear rate equation for arbitrary order. The method fails for orders of exactly unity or zero, although orders slightly different from these values are tolerated. Kinetic determinations are based on the predictive approach. A curve-fitting procedure is used to find the best-fit values of rate constant, reaction order, and initial and final values of the detector signal. In related work [52], the same authors developed an algorithm that uses a linearized version of the general rate equation along with time-dependent rates and time-dependent signal values. This linear predictive method produced results that were not as reliable as the nonlinear curve-fitting method for reaction orders greater than two. It is, however, applicable to reaction orders of unity or very nearly unity where the nonlinear method fails. Like the nonlinear method, this method determines the rate constant and reaction order separately for each sample. It should thus be able to compensate for changes in variables that affect these parameters.

Another algorithm has been developed for the determination of analyte concentration and rate constants  $k_1$  and  $k_2$  in a successive reaction  $A \xrightarrow{k_1} B \xrightarrow{k_2} C$  [53]. The method depends on measuring a signal  $S_t$  that is proportional to the concentration of the intermediate  $B$  at time  $t$ . The signal as a function of time is given by:

$$S_t = S_0 + \frac{\alpha A_0}{1-r} (e^{-k_1 r t} - e^{-k_1 t})$$

where  $S_0$  is the initial value of the signal,  $A_0$  is the initial analyte concentration,  $\alpha$  is the detector sensitivity and  $r = k_2/k_1$ . In the proposed algorithm, the above equation is fitted to the data by

a nonlinear least squares method. The values  $A_0$ ,  $k_1$  and  $r$  are calculated. The algorithm was tested using simulated data with varying amounts of superimposed noise. A wide range of rate constants, initial concentrations and data densities were evaluated. Initial estimates of the parameters within an order of magnitude were found to be sufficient. Schechter and Schroder [54] have also discussed error-compensated kinetic determinations in systems of mixed first- and second-order reactions.

It is clear from the discussion above that error-compensation methods have become extremely sophisticated and are able to perform in situations where little prior knowledge is available. This trend should continue in the future. It is also possible to combine several of the approaches to achieve extreme freedom from errors. Thus methods that use measured values of variables such as temperature and pH and fit generalized models in real time are on the horizon. Error-compensation methods are also being applied to multicomponent kinetic methods as discussed in *Trend 5*. The development of such advanced error-compensation and correction techniques will continue to help kinetic methods approach equilibrium methods in terms of accuracy and precision.

#### *Trend 5: Innovations in multicomponent kinetic procedures*

*“In solitude, be a multitude to thyself.” (Tibullus)*

Multicomponent kinetic determinations, often called differential rate methods, are also receiving a good deal of current attention in research laboratories. The various approaches to multicomponent determinations have been reviewed recently by Perez-Bendito [55]. These methods make possible the simultaneous determination of two or more analytes without prior physical separation of the components. Instead discrimination occurs because of the different rates of the analytes. Multicomponent kinetic methods usually rely on chemical reaction rates, but they can be based on the rates of physical processes such as diffusion, vaporization or radioactive decay. Re-



cent work has focused on the development of instrumentation geared for multicomponent determinations and on new computer data processing approaches. These new processing methods are capable of handling multidimensional data and/or of providing error compensation.

Array detector spectrophotometers have become highly useful in multicomponent determinations, particularly when coupled with stopped-flow mixing systems [25]. Here the absorption spectrum is acquired as a function of time. When the spectra of the components are highly overlapped, resolution can be achieved by means of differences in kinetics. Alternatively, when the spectra are resolved, resolution can be achieved on the basis of the spectra. For the majority of cases, spectra are partially overlapped and advantage can be taken of both spectral and kinetic differences.

One new approach that has been proposed for dealing with overlapping spectra is the kinetic wavelength-pair method [56]. For a mixture of two components, the method relies on measuring the difference in the rate of change of absorbance with time at two preset wavelength pairs (four wavelengths). Either one or both components can contribute to the rate of absorbance change at each wavelength pair. The approach was evaluated on four systems with data acquired from a diode array spectrophotometer. As long as the molar absorptivities of the components are significantly different at the two wavelength pairs, mixtures could be resolved even if the reactions occur at the same rate. The method is not, however, applicable to reactions yielding a common product, and the sensitivity is lower than for methods that depend on measurements at wavelengths of maximum absorption.

The Kalman filter has also been successfully applied to the determination of multiple components. For two or more components that react with a common reagent to give similar absorbing products, the linear Kalman filter can be employed if the rate constants are known [57]. Resolution of components with rate constant ratios as small as 2.0 was shown to be feasible. The method was tested on amino acid samples based on their reaction with trinitrobenzenesulfonic acid.

Corcoran and Rutan [58] have employed a similar approach based on the Kalman filter for the determination of species separated on thin-layer chromatography (TLC) plates. Co-eluting amino acids were resolved by means of kinetic differences in their reaction with ninhydrin. The authors had the best success with the linear Kalman filter and concluded that Kinetic resolution two-component mixtures on TLC plates was highly feasible.

The performance of both linear and nonlinear Kalman filters for multicomponent kinetic determinations has been investigated by Xiong et al. [59]. The authors used a kinetic model of the form

$$\Delta A_t = \Delta A_1 [1 - \exp(-k_1 t)] + \Delta A_2 [1 - \exp(-k_2 t)] + B$$

where  $\Delta A_t$  is the total absorbance at time  $t$  and  $\Delta A_1$  and  $\Delta A_2$  and  $k_1$  and  $k_2$  are the net absorbance changes and the rate constants of components 1 and 2 respectively. The authors successfully resolved mixtures of cortisone and hydrocortisone based on their reaction with Blue Tetrazolium despite a low pseudo-first-order rate constant ratio of 1.8. The Kalman filter algorithm was shown to be successful under conditions where classical multicomponent kinetic techniques failed.

Quencer and Crouch [60] have used the Kalman filter in multiwavelength, multicomponent kinetic determinations. They studied the case where the rate constants are unknown and used the nonlinear Kalman filter. Multiwavelength data from an array detector spectrophotometer was used. For pseudo-first-order reactions in two components  $C_1$  and  $C_2$  with common reagent  $R$  to form products  $P_1$  and  $P_2$  the absorbance per unit pathlength at wavelength  $j$  and time  $t$ ,  $A_{jt}$ , can be written

$$A_{jt} = \epsilon_{jC_1} [C_1]_t + \epsilon_{jC_2} [C_2]_t + \epsilon_{jR} [R]_t + \epsilon_{jP_1} [P_1]_t + \epsilon_{jP_2} [P_2]_t$$

If the relationships between product concentrations and reactant concentrations (assuming 1:1 stoichiometry) are substituted into this expression

and the concentrations expressed in terms of their initial values, the result is:

$$A_{jt} = (\epsilon_{jC_1} + \epsilon_{jR} - \epsilon_{jP_1})[C_1]_0 e^{-k_1't} \\ + (\epsilon_{jP_1} - \epsilon_{jR})[C_1]_0 \\ + (\epsilon_{jC_2} + \epsilon_{jR} - \epsilon_{jP_2})[C_2]_0 e^{-k_2't} \\ + (\epsilon_{jP_2} - \epsilon_{jR})[C_2]_0 + \epsilon_{jR}[R]_0$$

where  $k_1' = k_1[R]_0$ ,  $k_2' = k_2[R]_0$ , the  $\epsilon_{C_x}$  values are the molar absorptivities of the reactants and products, and the  $[C_x]_0$  values are the initial concentrations of components  $C_x$ . This measurement model was supplied to the Kalman filter which then determined the initial concentrations and the pseudo-first-order rate constants. Excellent results were obtained even for cases where there were no kinetic differences as long as the spectral differences were sufficient. The method also provides error compensation in that a large variation in rate constants is tolerated with little error.

Another method, called the H-point standard-additions method [61], is capable of dealing with two-component systems in which one component reacts much faster than the other or both components show overlapping time evolutions. The methods both depend on using standard additions and data taken at two wavelengths to obtain the concentration of the components. If the technique can be automated, it would appear to have some advantages in multicomponent determinations.

The continuous addition of reagent technique has also been applied to multicomponent kinetic determinations [62]. Here reactions on the millisecond time scale can be exploited using quite simple instrumentation. The simultaneous determination of copper and iron was demonstrated based on their complex formation with pyridoxal thiosemicarbazone. The latter reagent was continuously added to the mixture and the resulting absorbance of the complexes were obtained at 420 nm. Excellent results were obtained even on serum samples.

Flow-injection methods have been applied to multicomponent determinations. One approach is to use a two-channel system and to stop the flow

twice [63]. In another flow injection method [64], iron(II) and iron(III) were determined by their different catalytic behavior in the redox reaction between leucomalachite green and peroxodisulphate with and without the activator 1,10-phenanthroline. Two different approaches were used because one of the reactions is very rapid compared to the other. In one method a two-line system was used, and two individual zones of sample were injected simultaneously into separate carrier streams of reagent. The samples had different residence times in the manifold and therefore had reacted for different times when they reached the detectors. In the second method, a single-line FIA system was used and a double peak was formed as a result of injecting a large sample zone sandwiched between reagent zones. Two time-resolved signals for the processes were obtained and used in the determination. In another example, a double flow-injection system was presented for simultaneous determinations of nickel and iron [65]. The authors used least squares, principal components regression and partial least squares to analyze the complex time profiles produced.

The simultaneous determination of catalysts based on differences in the rate constants for inhibition by a common reagent has been investigated [66] by computer simulation methods. Both derivative and integral models for the kinetic responses were studied. Effects of rate constants, ratios of rate constants, fitting ranges, data density, and number of replicate determinations on various figures of merit were presented. Figure 7 illustrates the effects of fitting range and rate constant ratio on the accuracy of computed velocities. The fitting range represents the number of half-lives of the slowest reacting components. It can be seen that errors are largest at low ratios of rate constant and small fitting ranges where the first-order response of the inhibitors are highly correlated. Cladera et al. [67] have also presented a new computational approach for the simultaneous determination of catalysts and activators. They developed a mathematical expression based on a multiple standard addition model that accounted for a non-catalytic reaction, a catalytic reaction, and an activating effect on the catalytic

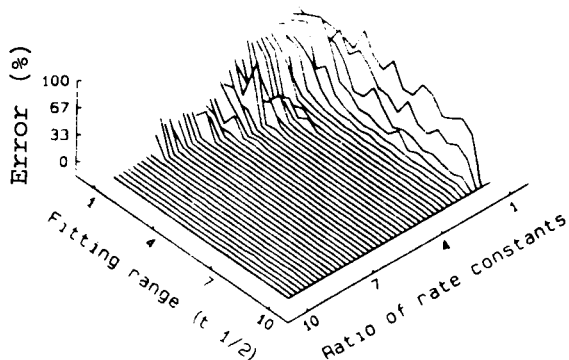


Fig. 7. Effects of fitting range and ratio of rate constants on accuracy of computed catalytic velocities for two-component inhibition of catalytic reaction (reproduced with permission from Ref. 66).

reaction. The method was applied to the determination of Mn(II) and Pb(II).

Schechter [68] has presented a new error-compensating algorithm for kinetic determinations of two-component mixtures based on general-order reactions. The method does not require prior knowledge of the reaction order or rate constants and is an extension of the Larsson and Pardue [51] single component case. Schechter found that the method could be used for a wide range of concentrations, rate constants and reaction orders, but the algorithm fails for a reaction order of exactly unity. An extensive error analysis based on simulations was presented.

Multicomponent kinetic determinations are being steadily improved as is clear from the above discussion. The application of multidimensional instrumentation and multivariate data processing techniques is only just beginning. We will certainly see a great deal more of the Kalman filter approach with array detector spectrometers in the future. Likewise, new FIA and air-segmented continuous flow techniques for multicomponent determinations will certainly be developed. The incorporation of error-compensation methods should greatly increase reliability. Multicomponent kinetic methods have always had great potential, but somehow have never quite produced the anticipated benefits. We should see a realization of this potential in the coming years.

### *Trend 6: Expanding applications of kinetic determinations*

*“Change is certain, progress is not.” (E.H. Carr)*

In the clinical area, kinetic methods have always played an important role because of their use in determining enzyme activities. In other areas, however, the proof of the worthiness of kinetic methods will come when they are considered as standard analytical tools and routinely used in situations where they are advantageous. As a result of some of the progress described above, we are beginning to see truly significant problems being solved by kinetic techniques. Most of the practical determinations that have appeared have been reviewed [69,70]. Hence, we will consider here only some recent and unique applications.

Several factors are important for the successful development of a kinetic based determination. Automation is extremely important to ensure reproducible conditions. In addition, optimization of conditions can be significant in enhancing precision and accuracy. Optimization can be based on an empirical approach or on a detailed study of kinetics of the reaction involved. As discussed in *Trend 1* above, an intelligently automated system can be extremely valuable in developing optimized analytical methods.

Flow injection is proving to be highly useful for methods development as well as for kinetic-based determinations. For kinetic determinations the automated sample handling, controlled sample dispersion and precise timing aspects of FIA are distinct advantages. Hansen [71] has recently given many examples of how FIA can be used for kinetic-based determinations where advantage can be taken of kinetic discrimination or kinetic enhancement. Christian and Ruzicka [11] have also discussed how stopped-flow injection methods can be exploited in quantitative determinations. Tyson [72] has written an extremely interesting article on *Putting the Chemistry Back into Analytical Chemistry*, which focuses on FIA methods and includes a discussion of kinetic-based determinations. In the future we should see many more examples of FIA being exploited for kinetic determinations.

Kinetic methods based on catalytic reactions

are becoming increasingly popular. Because catalysts can be determined with extremely high sensitivity, these methods are very useful in trace analysis. One of the prevailing trends in this area is the increasing use of automation for existing catalytic methods. Kawashima and Nakano [73] have recently reviewed the progress that has been made in using FIA for automating kinetic methods based on catalytic reactions. Such techniques are useful for determining catalysts, activators and inhibitors.

The area of micellar catalysis [74] is one that is beginning to be exploited for kinetic determinations. Micelles have the ability to arrange reactants at the molecular level by bringing analytes and reagents close together. While micelles have been exploited in chromatography, continuous flow analyses and room temperature phosphorescence applications, their use in kinetic methods has only just begun. The strategies devised thus far for using micellar catalysis in kinetic-based single and multiple component determinations have been recently discussed [75]. Because of the many intriguing possibilities in using organized media for enhancement of reaction rates, we should see many more applications in the coming years.

Antibody–antigen reactions have also been used to advantage in analytical methods. Several of the immunological assay methods take advantage of the speed of kinetic methods. For example, a recent article by Fotiou [76] describes the automated kinetic determination of apolipoproteins AI (APA) and B (APB) by consecutive addition of antibodies. A surfactant was used to inhibit the reaction of APB and to enhance the reactivity of APA. The rate was determined by nephelometry. Catalysis by antibodies is an area receiving a good deal of attention. Catalytic antibodies are a new class of biomolecules that are useful for molecular recognition in biosensors. With catalytic antibodies it should be possible to construct reversible immunobiosensors that can be continuously regenerated [77].

Catalysis by immobilized bioreagents such as enzymes remains an area of active interest. In our laboratory, for example, we have been developing immobilized enzyme flow injection systems for

the determination of sugars [78]. Such systems are reliable and the immobilized enzymes are useful for long periods of time (approaching one year with appropriate treatment).

Another trend in practical applications of kinetics is the determination of multiple components simultaneously as discussed above. Such multicomponent or differential rate methods are sure to increase dramatically in the future as some of the developments in instrumentation and data processing become more routinely available.

*Trend 7: Enlarging the kinetic approach to include miscellaneous time-dependent responses*

*“This time, like all times, is a very good one, if we but know what to do with it.” (Ralph Waldo Emerson)*

Increasingly we are seeing the kinetic approach being used for responses other than those obtained from chemical reactions. The kinetic approach can result in faster determinations or in increased resolution of mixtures. With error-compensation approaches, these advantages can be achieved with little or no increase in random or systematic errors. Mottola [79] has written a very interesting article *Some Incidental Kinetic Aspects in Analytical Chemistry* which, although focusing on kinetic considerations in electrode reactions and absorption spectrometry, makes it clear that most analytical techniques have kinetic as well as equilibrium aspects. There are many other examples [2]. Flow-injection methods are by their very nature transient methods with kinetic characteristics [9]. There are also kinetic aspects to the responses obtained from air-segmented continuous flow methods. Advantage can be taken of the slow approach to steady-state with air-segmented continuous flow signals. Here, the steady-state signal can be obtained from measurements taken during the exponential rising portion of the signal [80], a predictive kinetic method, which can increase sample throughput. Most separation techniques are highly dependent on the kinetics of various mass transport processes as well as chemical interactions. Conductivity and electrophoresis are dependent on the mobilities of ions in

solution. Dynamic electrochemical methods involve the kinetics of mass transport as well as the kinetics of the electrode reaction. Most spectroscopic methods have kinetic characteristics. For example, electrothermal atomization atomic absorption spectrometry is a kinetically controlled method. Time of flight mass spectrometry is another technique that is dependent on the velocity of ion drift in a field-free region.

While all of the above techniques have kinetic aspects [2], these are often ignored and seldom used to advantage. One of the techniques where dynamic behavior is being exploited is molecular luminescence spectrometry, where more and more use is being made of lifetime information for resolving mixtures. Lifetimes can be obtained by time-resolved spectroscopic methods or by frequency-domain techniques. Wong and Harris [81] have used a reiterative regression algorithm to obtain quantitative information about individual components in multiexponential data obtained from time-correlated single photon counting measurements of fluorescence. Hart and Daniels [82] have employed a gated detection approach along with nonlinear least-squares fitting to obtain fluorescence lifetime information on a sub-nanosecond time scale. Carroll and Hieftje [83] described a fiber-optic-based instrument for the measurement of phosphorescence intensities and lifetimes, and the same authors [84] used a fiber-optic-based pump-probe instrument to examine the excited state kinetics of 2,7-diphenylphenanthrene.

Frequency-domain fluorescence [85] has also become quite popular. Here the phase shift between the fluorescence emission signal and the modulated excitation signal is related to the fluorescence lifetime. In principle, tuning the instrument to detect a certain phase shift can introduce selectivity by discriminating against components with different lifetimes. One can also use frequency-domain methods for enhanced spectral resolution of mixtures. For example, Millican and McGown have used multiway analysis [86] and evolving factor analysis [87] for lifetime resolution of spectra in the frequency domain. In another application, Bowman and Crouch [88] used lifetime information obtained in the frequency do-

main to correct for quenching. They constructed an instrument that can readout directly the ratio of fluorescence intensity to lifetime. It has been shown by Hieftje and Haugen [89] that such measurements should be independent of quencher concentration if the quenching is collisional.

In another application of a technique originally developed for chemical kinetic methods, Pardue and McNulty [90] adapted the predictive kinetic method to transient responses obtained from an ammonia-selective potentiometric electrode. The steady-state voltage from the electrode was predicted from measurements made while the voltage was changing with time. Originally a first-order model was used, even though more complicated models have been proposed for potentiometric electrodes. In more recent work [91] several different models were applied to the same system. All but one of the models gave reliable results. The predictive kinetic method allows measurement times to be reduced several-fold in comparison to obtaining the steady-state response. Uhegbu and Pardue [92] also applied the predictive kinetic method to an oxygen-selective amperometric electrode. The steady-state current was predicted from measurements made early in time. Both first-order and a variable-order models were used. Only the latter was found to give satisfactory results. Again a substantial decrease in measurements time resulted from using the predictive method.

It is clear from the above discussion that the kinetic approach is beginning to be used in many areas other than chemical kinetic methods. Since these approaches can have major advantages, such as speed and selectivity, we expect to see many additional applications in the future.

### *Conclusions*

Seven major trends in kinetic methods have been identified and described in the discussion above. While the specific nature of the most important trends in the field can be argued, there should be no argument that the trends discussed here are important and should continue to be significant throughout most of the 1990s. The trends described are making kinetic methods more reliable, more selective, more independent

of conditions, more automated and more likely to succeed in actual real-life analytical situations. We have attempted here, in the words of the opening quote from Macbeth, to *look into the seeds of time and say which grain will grow*. We suspect that all seven of the grains described here will not only grow, but flourish.

## REFERENCES

- 1 H.L. Pardue, *Anal. Chim. Acta*, 216 (1989) 67.
- 2 H.A. Mottola, *Kinetic Aspects of Analytical Chemistry*, Wiley, New York, 1988, pp. 19–21.
- 3 D. Perez-Bendito and M. Silva, *Kinetic Methods in Analytical Chemistry*, Ellis Horwood, Chichester, 1988, pp. 190–247.
- 4 A.P. Wade and S.R. Crouch, *Spectroscopy*, 3 (1988) 24.
- 5 S.R. Crouch, *Chemom. Intell. Lab. Syst.* 8 (1990) 259.
- 6 R. Balciunas, F.J. Holler, P.K. Notz, E.R. Johnson, L.D. Rothman and S.R. Crouch, *Anal. Chem.*, 53 (1981) 1484.
- 7 M. Stewart and G. Horlick, *Chemom. Intell. Lab. Syst.*, 8 (1990) 290.
- 8 P.D. Wentzell, *Chemom. Intell. Lab. Syst.*, 8 (1990) 283.
- 9 J. Ruzicka and E.H. Hansen, *Flow Injection Analysis*, Wiley, New York, 2nd edn. 1988.
- 10 J. Ruzicka, *Anal. Chim. Acta*, 261 (1992) 3.
- 11 G. D. Christian and J. Ruzicka, *Anal. Chim. Acta*, 261 (1992) 11.
- 12 J. Ruzicka and G.D. Marshall, *Anal. Chim. Acta*, 237 (1990) 329.
- 13 B.J. Compton, J.R. Weber and W.C. Purdy, *Anal. Lett.*, 13 (1980) 861.
- 14 E.B. Townsend and S.R. Crouch, *Trends Anal. Chem.* 11 (1992) 90.
- 15 H.K. Chung and J.D. Ingle, Jr., *Anal. Chem.*, 62 (1990) 2547.
- 16 A. Gomez-Hens and D. Perez-Bendito, *Anal. Chim. Acta*, 242 (1991) 147.
- 17 M.D. Joseph, D. Kasprzak and S.R. Crouch, *Clin. Chem.*, 23 (1977) 1033.
- 18 K. Takahashi, S. Taniguchi, T. Kuroishi, K. Yasuda and T. Sano, *Anal. Chim. Acta*, 220 (1989) 13.
- 19 M. Marquez, M. Silva and D. Perez-Bendito, *Analyst*, 113 (1988) 1733.
- 20 D. Perez-Bendito, M. Silva and A. Gomez-Hens, *Trends Anal. Chem.*, 8 (1989) 302.
- 21 M. Valcarcel and M.C. Luque de Castro, *Analyst*, 115 (1990) 699.
- 22 R.E. Santini, M.J. Milano and H.L. Pardue, *Anal. Chem.*, 45 (1973) 915A.
- 23 M.J. Milano and H.L. Pardue, *Clin. Chem.*, 21 (1975) 211.
- 24 J.D. Ingle, Jr. and M.A. Ryan, in E.L. Wehry (Ed.), *Modern Fluorescence Spectroscopy*, Vol. 3, Plenum Press, New York, 1981, pp. 95–142.
- 25 M.C. Gutierrez, A. Gomez-Hens and D. Perez-Bendito, *Anal. Chim. Acta*, 225 (1989) 115.
- 26 J.D. Ingle, Jr. and S.R. Crouch, *Spectrochemical Analysis*, Prentice-Hall, Englewood Cliffs, NJ, 1988, pp. 116–117.
- 27 J.V. Sweedler, R.B. Bilhorn, P.M. Esperson, G.R. Sims and M.B. Denton, *Anal. Chem.*, 60 (1988) 282A.
- 28 P.M. Esperson, J.V. Sweedler, R.B. Bilhorn, G.R. Sims and M.G. Denton, *Anal. Chem.*, 60 (1988) 327A.
- 29 I.M. Warner, G. Patonay and M.P. Thomas, *Anal. Chem.*, 57 (1985) 463A.
- 30 D.J. Hooley and R.E. Dessy, *Anal. Chem.*, 55 (1983) 313.
- 31 M.D. Luque de Castro and M. Valcarcel, *Trends Anal. Chem.*, 5 (1986) 71.
- 32 F.J. Holler, Ph.D. Thesis, Michigan State University, East Lansing, MI, 1977.
- 33 K.J. Caserta, F.J. Holler, S.R. Crouch and C.G. Enke, *Anal. Chem.*, 50 (1978) 1534.
- 34 G.L. Campli and J.D. Ingle, Jr., *Anal. Chim. Acta*, 224 (1989) 275.
- 35 M. Otto, *Analyst*, 115 (1990) 685.
- 36 S.D. Brown, *Anal. Chim. Acta*, 181 (1986) 1.
- 37 R.L. Tranter, *Anal. Proc.*, 27 (1990) 134.
- 38 S.C. Rutan and S.D. Brown, *Anal. Chim. Acta*, 167 (1985) 23.
- 39 S.C. Rutan, *Anal. Chem.*, 63 (1991) 1103A.
- 40 S.D. Brown, *Trends Anal. Chem.*, 6 (1987) 260.
- 41 D.D. Gerow and S.C. Rutan, *Anal. Chem.*, 60 (1988) 847.
- 42 E.R. Malinowski, *Factor Analysis in Chemistry*, Wiley, New York, 2nd edn., 1991.
- 43 R. Laatikainen and K. Tuppurainen, *Comput. Chem.*, 14 (1990) 109.
- 44 P.D. Wentzell and S.J. Vanslyke, *Anal. Chim. Acta*, 257 (1992) 173.
- 45 D.B. Marshall, *Anal. Chem.*, 61 (1989) 660.
- 46 P.D. Wentzell, A.P. Wade and S.R. Crouch, *Anal. Chem.*, 60 (1988) 905.
- 47 A.P. Wade, P.M. Shiundu and P.D. Wentzell, *Anal. Chim. Acta*, 237 (1990) 361.
- 48 G.E. Mielsing and H.L. Pardue, *Anal. Chem.*, 50 (1978) 1611.
- 49 P.D. Wentzell, Ph.D. thesis, Michigan State University, East Lansing, MI, 1987.
- 50 P.D. Wentzell and S.J. Vanslyke, *Anal. Chim. Acta*, 257 (1992) 173.
- 51 J.A. Larsson and H.L. Pardue, *Anal. Chim. Acta*, 224 (1989) 289.
- 52 J.A. Larsson and H.L. Pardue, *Anal. Chem.*, 61 (1989) 1949.
- 53 I. Schechter, *Anal. Chem.*, 63 (1991) 1303.
- 54 I. Schechter and H. Schroder, *Anal. Chem.*, 64 (1992) 325.
- 55 D. Perez-Bendito, *Analyst*, 115 (1990) 689.
- 56 J.M. Pena, S. Rubio and D. Perez-Bendito, *Anal. Chim. Acta*, 244 (1991) 81.
- 57 P.D. Wentzell, M.I. Karayannis and S.R. Crouch, *Anal. Chim. Acta*, 224 (1989) 263.
- 58 C.A. Corcoran and S.C. Rutan, *Anal. Chim. Acta*, 224 (1989) 315.

- 59 R. Xiong, A. Velasco, M. Silva and D. Perez-Bendito, *Anal. Chim. Acta*, 251 (1991) 313.
- 60 B.M. Quencer and S.R. Crouch, *Analyst*, submitted for publication.
- 61 F. Bosch-Reig, P. Campins-Falco, A. Sevillano-Cabeza, R. Herraiz-Hernandez and C. Molins-Legua, *Anal. Chem.*, 63 (1991) 2424.
- 62 M. Marquez, M. Silva and D. Perez-Bendito, *Anal. Chim. Acta*, 239 (1990) 221.
- 63 M.D. Luque de Castro and M. Valcarcel, *Trends Anal. Chem.*, 8 (1989) 172.
- 64 H. Muller, V. Muller and E.H. Hansen, *Anal. Chim. Acta*, 230 (1990) 113.
- 65 D.A. Whitman, M.B. Seasholtz, G.D. Christian, J. Ruzicka and B.R. Kowalski, *Anal. Chem.*, 63 (1991) 775.
- 66 C.P. Fitzpatrick and H.L. Pardue, *Anal. Chem.*, 61 (1989) 2551.
- 67 A. Cladera, A. Caro, E. Gomez, J.M. Estela and V. Cerda, *Talanta*, 39 (1992) 887.
- 68 I. Schechter, *Anal. Chem.*, 64 (1992) 729.
- 69 H.A. Mottola, D. Perez-Bendito and H.B. Mark, Jr., *Anal. Chem.*, 62 (1990) 441R.
- 70 H.A. Mottola and D. Perez-Bendito, *Anal. Chem.*, 64 (1992) 407R.
- 71 E.H. Hansen, *Anal. Chim. Acta*, 261 (1992) 125.
- 72 J.F. Tyson, *Microchem. J.*, 45 (1992) 143.
- 73 T. Kawashima and S. Nakano, *Anal. Chim. Acta*, 261 (1992) 167.
- 74 D. Sicillia, S. Rubio and D. Perez-Bendito, *Analyst*, 115 (1990) 1613.
- 75 D. Perez-Bendito and S. Rubio, *Trends Anal. Chem.*, submitted for publication.
- 76 F.K. Fotiou, *Anal. Chem.*, 64 (1992) 1698.
- 77 D.B. Talley, P.M. Booth, C.N. Durfor, M.T. Martin, A.D. Napper and A.R. Rees, *Anal. Chem.*, 62 (1990) 2211.
- 78 K.S. Kurtz and S.R. Crouch, *Anal. Chim. Acta*, 254 (1991) 201.
- 79 H.A. Mottola, *Analyst*, 115 (1990) 679.
- 80 R.E. Thiers, R.R. Cole and W.J. Kirsch, *Clin. Chem.*, 13 (1967) 451.
- 81 A.L. Wong and J.M. Harris, *Anal. Chem.*, 61 (1989) 2310.
- 82 L.P. Hart and M. Daniels, *Appl. Spectrosc.*, 46 (1992) 191.
- 83 M.K. Carroll and G.M. Hieftje, *Appl. Spectrosc.*, 46 (1992) 126.
- 84 M.K. Carroll and G.M. Hieftje, *Appl. Spectrosc.*, 46 (1992) 317.
- 85 L.B. McGown and F.V. Bright, *CRC Crit. Rev. Anal. Chem.*, 18 (1987) 245.
- 86 D.W. Millican and L.B. McGown, *Anal. Chem.*, 62 (1990) 2242.
- 87 D.W. Millican and L.B. McGown, *Appl. Spectrosc.*, 46 (1992) 28.
- 88 L.E. Bowman and S.R. Crouch, *Appl. Spectrosc.*, 46 (1992) 925.
- 89 G.M. Hieftje and G.R. Haugen, *Anal. Chim. Acta*, 123 (1981) 255.
- 90 H.L. Pardue and P.J. McNulty, *Anal. Chem.*, 60 (1988) 1351.
- 91 M.D. Love, H.L. Pardue and G. Pagan, *Anal. Chem.*, 64 (1992) 1269.
- 92 C.E. Uhegbu and H.L. Pardue, *Anal. Chim. Acta*, 237 (1990) 413.

# Simultaneous kinetic-photometric determination of imipramine and desipramine by stopped-flow mixing technique

Lourdes de la Peña, Agustina Gómez-Hens and Dolores Pérez-Bendito

*Department of Analytical Chemistry, Faculty of Sciences, University of Córdoba, 14004 Córdoba (Spain)*

(Received 8th September 1992)

## Abstract

A kinetic-photometric method for the individual determination of imipramine and desipramine and a differential kinetic method for the resolution of mixtures of these tricyclic antidepressants based on the stopped-flow mixing technique were developed for the first time and applied to the determination of these species in serum. Both methods rely on the oxidative coupling of these compounds with 3-methylbenzothiazolin-2-one hydrazone in the presence of ammonium iron(III) sulphate in hydrochloric acid. On the basis of the initial rate and absorbance amplitude of the kinetic curves obtained for each analyte, the resolution of the mixture was accomplished by using the proportional equation method. The linear range of the calibration graphs was  $0.3\text{--}7.0\ \mu\text{g ml}^{-1}$  for imipramine and  $0.3\text{--}5.0\ \mu\text{g ml}^{-1}$  for desipramine. Mixtures of imipramine and desipramine in ratios between 2:1 and 1:8 were satisfactorily resolved. The determination of these analytes in serum called for a prior separation step for matrix removal.

**Keywords:** Flow system; Kinetic methods; Spectrophotometry; Desipramine; Imipramine; Serum samples; Stopped-flow technique

Imipramine and desipramine are two dibenzazepine drugs widely used as antidepressants. On oral administration, imipramine undergoes extensive first-pass metabolism by demethylation to yield desipramine, which is its major active metabolite. Thus, both compounds can occur together in human serum.

A number of methods have so far been developed for the determination of these compounds, of which chromatographic and immunoassay methods are the most sensitive for biological fluids analyses. Thus, several gas [1,2] and liquid [3–5] chromatographic procedures usually involving prior extraction of the analytes from the ma-

trix have been proposed. Also, different immunoassay techniques (radioimmunoassay [6], enzyme immunoassay [7], and fluorescence polarization immunoassay [8]) allow the determination of these tricyclic antidepressants.

An alternative to the use of chromatographic or immunoassay methods, which require expensive instrumentation and reagents, respectively, is the use of the kinetic methodology, a fast approach to individual determinations based on the stopped-flow mixing methodology [9] and also a simple, inexpensive means of resolving mixtures of compounds with similar features by using differential kinetic methods.

The lack of kinetic methods for the determination of imipramine and desipramine led us to carry out a kinetic study of the coloured products obtained by reaction of these compounds with

*Correspondence to:* D. Pérez-Bendito, Dept. de Química Analítica, Facultad de Ciencias, Universidad de Córdoba, 14004 Córdoba (Spain).



3-methylbenzothiazolin-2-one hydrazone (MBTH) in the presence of ammonium iron(III) sulphate. The resolution of this mixture by equilibrium measurements is impossible owing to the similar spectral features of the coloured products, so only the individual determination of each analyte had so far been achieved [10]. However, the resolution can be accomplished on the basis of the difference in reaction rate between the analytes as shown in this work.

## EXPERIMENTAL

### *Instrumentation*

A Perkin-Elmer Lambda 5 spectrophotometer fitted with a stopped-flow module [11] supplied by Quimi-Sur was used for reaction rate measurements. The module, with an observation cell of 1 cm, was controlled by the associated electronics and a Hewlett-Packard 98640A computer. The spectrophotometer cell compartment was thermostated by means of an electronic Peltier system and the solutions in the stopped-flow module were kept at the same constant temperature by a circulating water-bath.

### *Reagents*

All reagents used were of analytical-reagent grade. Imipramine hydrochloride ( $500 \mu\text{g ml}^{-1}$ ) and desipramine hydrochloride ( $500 \mu\text{g ml}^{-1}$ ) stock solutions were prepared by dissolving 12.5 mg of the corresponding compound (Sigma) in 25 ml of distilled water in a calibrated flask. Standard solutions were obtained by appropriate dilution of the stock solutions with distilled water. A 3-methylbenzothiazolin-2-one hydrazone (MBTH) solution ( $1.85 \times 10^{-2}$  M) was prepared by dissolving 4 g of reagent (Aldrich) in 100 ml of distilled water. An ammonium iron(III) sulphate solution ( $4.15 \times 10^{-2}$  M) was made by dissolving 2 g of  $\text{NH}_4\text{Fe}(\text{SO}_4)_2 \cdot 12\text{H}_2\text{O}$  (Merck) in 100 ml of 0.1 M hydrochloric acid.

### *Procedures*

*Individual determination of imipramine and desipramine.* Two solutions, A and B, were pre-

pared to fill the two 2-ml drive syringes of the stopped-flow module. Solution A contained imipramine or desipramine standard or treated sample solution, in a final concentration range between  $0.3$  and  $7.0 \mu\text{g ml}^{-1}$  of imipramine or between  $0.3$  and  $5.0 \mu\text{g ml}^{-1}$  of desipramine and hydrochloric acid ( $5 \times 10^{-2}$  M). Solution B contained MBTH ( $3.7 \times 10^{-3}$  M), ammonium iron(III) sulphate ( $1.7 \times 10^{-2}$  M) and hydrochloric acid ( $5 \times 10^{-2}$  M).

In each run, 0.15 ml of each solution was mixed in the mixing chamber. The absorbance increase during the reaction was monitored at 625 nm and followed via a chart recorder. All measurements were carried out at  $25^\circ\text{C}$ . The initial rate method was applied to the acquired absorbance values, which were processed by linear regression using the microcomputer. The reaction rate was determined in about 2–3 min and each standard was assayed in triplicate. The blank signal was found to be negligible.

*Determination of mixtures.* The procedure used for the resolution of imipramine and desipramine mixtures was the same as described above, but syringe A was filled with appropriate concentrations of imipramine and desipramine to give final concentrations of  $0.5$ – $4.0 \mu\text{g ml}^{-1}$  in each. Two calibration plots (initial rate and absorbance obtained 5 min after the reaction was started) against the analyte concentration were run for imipramine and desipramine, and the data thus obtained were processed by using the proportional equation method as described below.

*Determination of imipramine and desipramine in human serum.* A volume of human serum (1–5 ml) was mixed with 2.5 ml of 0.1 M sodium hydroxide, 8 ml of heptane and 0.75 ml of isoamyl alcohol. The mixture was stirred for 5 min. The resulting aqueous layer was removed by aspiration and 1.25 ml of 0.1 M sodium hydroxide was added. The tube was then shaken for 5 min and centrifuged for 5 min. A volume of 7 ml of the organic phase was transferred to a centrifuge tube containing 2 ml of 0.1 M hydrochloric acid and the tube was shaken for 5 min and subsequently centrifuged. The organic phase was then discarded and 1.5 ml of the acid phase was treated as described above.

## RESULTS AND DISCUSSION

MBTH is a widely used chromogenic reagent for analytical purposes [12]. It forms a strongly electrophilic diazonium salt when acted upon by an oxidizing agent. The coloured products obtained from the reaction of MBTH with imipramine and desipramine in the presence of ammonium iron(III) sulphate in an acidic medium show maximum absorbance at 625 nm and take about 15 min to attain equilibrium [10]. The use of the kinetic methodology can improve the individual equilibrium determination of these compounds because initial rate measurements can be made in only 2–3 min (Fig. 1). Also, the difference in the variation of the absorbance of both reactions with the time allows one to resolve mixtures of the two compounds by using the proportional equation method and performing measurements of initial rate or of absorbance exactly 5 min after the reaction is started (fixed time method).

There are no significant differences in the reaction rates obtained for these systems by using the batch or the stopped-flow technique, which is an exceptional behaviour compared to other chemical systems studied elsewhere [13,14]. This can be ascribed to the slow rate of coupling between the dibenzazepine and the oxidized reagent, which is not modified despite the rapid, thorough mixing of the streams from the drive syringes of the stopped-flow module. However,

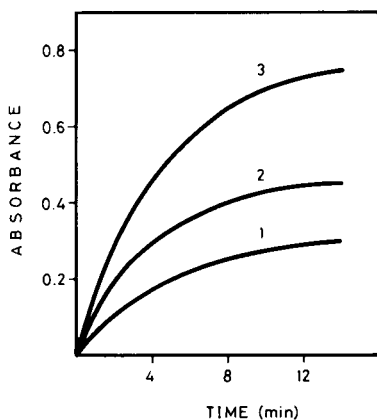


Fig. 1. Kinetic curves obtained for imipramine (1), desipramine (2) and a mixture of both (3). [imipramine]=[desipramine]=  $2 \mu\text{g ml}^{-1}$ .

we opted for using the stopped-flow technique because it allows a rapid handling of reagents for routine determinations.

*Effect of the reaction variables*

The optimization of variables affecting the systems was done by the univariate method. All concentrations given here are initial concentrations in the syringes (twice the actual concentrations in the reaction mixture at time zero after mixing). The optimum values taken were those yielding the minimum possible relative standard deviation for the initial rate measurements under conditions where the reaction order with respect to the species concerned was zero or near zero, and those where the initial rate and absorbance increments obtained after 5 min were additive for imipramine–desipramine mixtures.

Because the reaction was developed in an acidic medium, various acids (HCl, HClO<sub>4</sub>, HNO<sub>3</sub> and H<sub>2</sub>SO<sub>4</sub>) were tested at a final concentration of 0.2 M in each syringe; the highest reaction rates were obtained with HCl and HClO<sub>4</sub>. However, owing to the lack of additivity in the reaction rate in the presence of HClO<sub>4</sub>, HCl was selected. The reaction rate and absorbance values of both the imipramine and the desipramine system remained constant over the HCl concentration range 0.05–0.3 M. Both parameters were also constant and independent of the MBTH concentration over the range  $9.25 \times 10^{-4}$ – $7.4 \times 10^{-3}$  M. From the study of the effect of the ammonium iron(III) sulphate concentration on both systems (Fig. 2), a  $1.7 \times 10^{-2}$  M concentration was selected. Increasing temperatures between 20 and 30°C resulted in only slight increases in the reaction rate and absorbance of both systems, while higher temperatures had no effect.

The initial slopes of the absorbance–time curves obtained under the above optimal experimental conditions were indicative of a first-order reaction with respect to imipramine and desipramine.

*Features of the analytical methods*

The absorbance–time curves obtained for imipramine and desipramine under the optimum

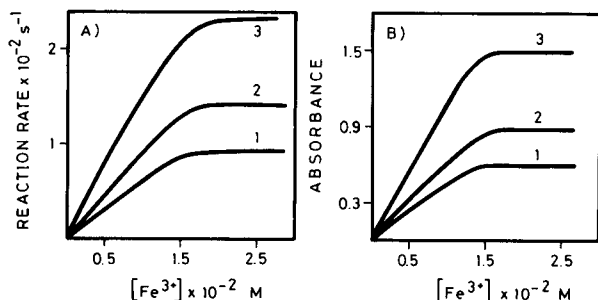


Fig. 2. Effect of the iron(III) concentration on the reaction rate (A) and absorbance (B) obtained for imipramine (1), desipramine (2) and a mixture of both (3).

conditions were processed by two kinetic quantification methods involving initial rate and fixed time measurements. Table 1 shows the features of both methods.

The initial rate method was preferred for the individual determination of each analyte because measurements of this parameter only require running the kinetic curve for 2–3 min. Thus, this method is faster than the proposed equilibrium method [10], which entails waiting for 15 min before any measurements can be made. Also, the linear range is somewhat wider than that of the equilibrium method, which is 0.5–4.0  $\mu\text{g ml}^{-1}$  for both imipramine and desipramine. The quantification limits of the kinetic methods are also better. The detection limits listed in Table 1 were calculated according to IUPAC recommendations [15]. The Pearson's correlation coefficients indicate very good calibration linearity. The relative standard deviations obtained were in the range 2.0–3.5%.

TABLE 1

Quantitative performance of the proposed method

Compound	Method	Linear range ( $\mu\text{g ml}^{-1}$ )	Detection limit <sup>a</sup> ( $\mu\text{g ml}^{-1}$ )	Slope $\pm$ S.D. <sup>b</sup>	Intercept	$r$ <sup>c</sup>	R.S.D. <sup>d</sup> (%)
Imipramine	Initial rate	0.3–7.0	0.11	$(8.1 \pm 0.9) \times 10^{-3}$	$(1.6 \pm 0.7) \times 10^{-3}$	0.998	3.2 <sup>e</sup> , 3.3 <sup>f</sup>
	Fixed time	0.3–7.0	0.10	$(6.1 \pm 0.4) \times 10^{-2}$	$(1.7 \pm 0.6) \times 10^{-2}$	0.9995	2.9, 2.7
Desipramine	Initial rate	0.3–5.0	0.09	$(12.7 \pm 1.5) \times 10^{-3}$	$(3.4 \pm 0.4) \times 10^{-3}$	0.9995	3.5, 2.7
	Fixed time	0.3–5.0	0.09	$(9.2 \pm 0.6) \times 10^{-2}$	$(2.8 \pm 0.1) \times 10^{-2}$	0.9998	3.2, 2.0

<sup>a</sup>  $3\sigma$ . <sup>b</sup> Units: initial rate method:  $\text{min}^{-1} \mu\text{g}^{-1} \text{ml}$ ; fixed time method:  $\text{A} \mu\text{g}^{-1} \text{ml}$  (A = absorbance). <sup>c</sup>  $n = 6$ . <sup>d</sup>  $P = 0.05$ ;  $n = 8$ . <sup>e</sup> 0.5  $\mu\text{g ml}^{-1}$ . <sup>f</sup> 2.5  $\mu\text{g ml}^{-1}$ .

TABLE 2

Resolution of imipramine–desipramine mixtures

Imipramine–desipramine wt. ratio	Imipramine ( $\mu\text{g ml}^{-1}$ )		Desipramine ( $\mu\text{g ml}^{-1}$ )	
	Taken	Found <sup>a</sup>	Taken	Found <sup>a</sup>
2:1	2.0	2.12	1.0	0.95
2:2	2.0	2.10	2.0	1.92
1:1	1.0	1.00	1.0	1.02
1.5:1.5	1.5	1.53	1.5	1.48
1:2	1.0	0.96	2.0	1.91
1:4	1.0	0.95	4.0	4.10
1:5	0.8	0.84	4.0	4.00
1:8	0.5	0.49	4.0	4.05

<sup>a</sup> Average of three determinations.

A brief study of the selectivity of these methods showed that other tricyclic antidepressants such as amitriptyline and nortriptyline are tolerated in 20- and 50-fold excesses, respectively, but trimipramine interferes at the same concentration level as imipramine and desipramine.

Mixtures of imipramine (I) and desipramine (D) can be resolved by the proportional-equation method using two equations derived from two kinetic parameters, viz. the initial rate ( $v$ ) or absorbance ( $\Delta A$ ) obtained exactly 5 min after the reaction is started:

$$v = a_I[I] + a_D[D] + b_I + b_D$$

$$\Delta A = a'_I[I] + a'_D[D] + b'_I + b'_D$$

where  $a$  and  $a'$  are the corresponding slopes of the calibration graphs,  $b$  and  $b'$  their corresponding intercepts and  $[I]$  and  $[D]$  the concentrations

TABLE 3

Recovery of imipramine and desipramine added to human serum samples

Sample	Imipramine ( $\mu\text{g ml}^{-1}$ )			Desipramine ( $\mu\text{g ml}^{-1}$ )		
	Added	Found <sup>a</sup>	Recovery (%)	Added	Found <sup>a</sup>	Recovery (%)
1	0.50	0.43	86	1.00	1.20	120
2	1.00	1.11	111	2.00	1.92	96
3	0.50	0.55	110	0.50	0.48	96
4	1.00	1.05	105	1.00	0.90	90
5	1.00	0.94	94	0.50	0.57	114
6	2.00	1.70	85	1.00	1.07	107

<sup>a</sup> Average of three determinations.

of imipramine and desipramine, respectively. A simple BASIC program was used to solve these equations.

In this case, although the method is not so fast, it is a simple means of resolving this mixture while avoiding the use of expensive chromatographic [1–5] procedures. The absence of synergistic effects ensured the parameters obtained from the kinetic curve for a mixture of the two analytes were the sum of the corresponding parameters obtained for each analyte separately. The method was applied to solutions of known imipramine and desipramine concentrations in different ratios. Table 2 summarizes the results obtained from the calibration graphs.

#### *Analysis of human serum samples*

Imipramine and desipramine were determined in differently spiked human serum samples by using the above described procedures. The matrix was removed in a previous extraction process with heptane and isoamyl alcohol [16,17]. Table 3 summarizes the analytical recoveries obtained.

The authors are grateful to the CICYT for financial support (Grant No. PB91-0840).

#### REFERENCES

- 1 D. Thompson, J. Pharm. Sci., 71 (1982) 536.
- 2 Y. Sasaki and S. Baba, J. Chromatogr., 426 (1988) 93.
- 3 A. Fazio, E. Spina and F. Pisani, J. Liq. Chromatogr., 10 (1987) 223.
- 4 W. Lin and P.D. Frade, Ther. Drug. Monit., 9 (1987) 448.
- 5 P. Ni, F. Guyon, M. Caude and R. Rosset, J. Liq. Chromatogr., 11 (1988) 1087.
- 6 G.F. Read and D.R. Fahmy, Clin. Chem., 24 (1978) 36.
- 7 S. Pankey, C. Collins, A. Jaklitsch, S. Azutsu, M. Hu and M. Pirio, Clin. Chem., 32 (1986) 768.
- 8 P. Jatlow, Clin. Biochem., 18 (1985) 143.
- 9 A. Gómez-Hens and D. Pérez-Bendito, Anal. Chim. Acta, 242 (1991) 147.
- 10 S.A. Hussein, M.E. El-Kommos, H.Y. Hassan and A.M. Mohamed, Talanta, 36 (1989) 941.
- 11 A. Loriguillo, M. Silva and D. Pérez-Bendito, Anal. Chim. Acta, 199 (1987) 29.
- 12 M. Pesez and J. Bartos, Colorimetric and Fluorimetric Analysis of Organic Compounds and Drugs, Marcel Dekker, New York, 1974, p. 536.
- 13 M. Toledano, M.C. Gutiérrez, A. Gómez-Hens and D. Pérez-Bendito, Analyst, 114 (1989) 211.
- 14 S. Antón, M.C. Gutiérrez, A. Gómez-Hens and D. Pérez-Bendito, Anal. Chim. Acta, 230 (1990) 145.
- 15 G.L. Long and J.D. Winefordner, Anal. Chem., 55 (1983) 712A.
- 16 J.R. Gillette, J.V. Dingell, F. Sulser, R. Kuntzman and B.B. Bradie, Experientia, 17 (1961) 377.
- 17 J.V. Dingell, F. Sulser and J.R. Gillette, J. Pharmacol. Exptl. Therap., 143 (1964) 14.

# Kinetic determination of cobalt and nickel by flow-injection spectrophotometry

M.A.Z. Arruda, E.A.G. Zagatto and N. Maniasso

*Centro de Energia Nuclear na Agricultura, Universidade de São Paulo, P.O. Box 96, 13400 Piracicaba SP (Brazil)*

(Received 12th March 1992; revised manuscript received 13th May 1992)

## Abstract

Reactor replacement is proposed as means of realizing different sample residence times in flow-injection analysis. As an application, an improved spectrophotometric determination of cobalt and nickel is proposed. The method exploits differences in reaction rates between cobalt and nickel citrate complexes and 4-(2-pyridylazo)resorcinol (PAR). The influence of pH, reagent concentrations, temperature, ionic strength, flow-rates and masking agent addition were investigated. Selectivity was enhanced by adding EDTA plus pyrophosphate and exploiting kinetic discrimination. The system is very stable and allows the determination of cobalt and nickel up to  $5.00 \text{ mg l}^{-1}$  with a sampling frequency of  $40 \text{ h}^{-1}$ . For tool steel samples characterized by low nickel/cobalt concentration ratios, the system can be simplified, allowing kinetic masking of nickel and single cobalt determination. The reagent consumption is  $65.3 \mu\text{g}$  of PAR per determination, and precise results (R.S.D.  $< 1\%$ ) in agreement with inductively coupled plasma atomic emission spectrometry are obtained at a sampling frequency of  $100 \text{ h}^{-1}$ .

*Keywords:* Flow injection; Kinetic methods; UV-Visible spectrophotometry; Cobalt; Nickel; Steels

In flow-injection analysis, chemical kinetics have been efficiently exploited by recording several peaks after a single injection [1]. To this end, the formation of two reaction zones in a dispersed sample, stream splitting, reversed or oscillating flows, detector relocation [2], stopped-flow systems, etc., have been utilized [3]. As a consequence, flow-injection procedures exploiting differential kinetics [4–6] have been proposed mainly for simultaneous determinations in binary or ternary mixtures [7,8].

This paper describes an alternative procedure for multi-peak recording based on reactor re-

placement, which can be accomplished by commutation. The method deals with differences in kinetics, because to each commutation status corresponds a given mean available time for reaction development.

As an application, an improved spectrophotometric determination of cobalt and nickel in steels is proposed. The method is based on complexation with citrate followed by time-dependent dissociation and reaction with 4-(2-pyridylazo)resorcinol (PAR) [9]. Stream splitting and thermostated water-baths used in the original work to emphasize kinetic discrimination are not needed. Moreover, the contribution of nickel to the analytical signal can be modified or almost suppressed, allowing system simplification for tool steel analysis where only the determination of cobalt is required.

*Correspondence to:* E.A.G. Zagatto, Centro de Energia Nuclear na Agricultura, Universidade de São Paulo, P.O. Box 96, 13400 Piracicaba SP (Brazil).

## EXPERIMENTAL

## Solutions

All solutions were prepared with analytical-reagent grade chemicals and distilled, deionized water.

Working standard solutions (0.00–5.00 mg Co l<sup>-1</sup> and/or 0.00–1.00 mg Ni l<sup>-1</sup>) also contained 0.01 M HCl in order to match the mean sample acidity. To minimize pH gradients, 0.01 M HCl was used as sample carrier stream C (Figs. 1 and 2).

Reagents R<sub>1</sub>, R<sub>2</sub> and R<sub>4</sub> were 0.01 M sodium citrate, 0.1 M sodium tetraborate and 0.1 M Na<sub>2</sub>EDTA plus 0.01 M sodium pyrophosphate, respectively. Reagent R<sub>3</sub> (0.001 M PAR) was freshly prepared by dissolving 25.92 mg of PAR in 100 ml of water.

Samples were solubilized by accurately weighing ca. 0.5 g of finely ground steel filings (50–100 mesh) and placing them in crucibles with 5.0 ml of aqua regia [HNO<sub>3</sub>–HCl (1 + 3, v/v)]. The mixture was heated to complete dissolution (160°C, ca. 15 min) and, after cooling, the volume was made up to 100 ml with water. Before injection, the samples were diluted 1000-fold manually with 0.01 M HCl.

## Flow-injection system

The system for the simultaneous determination of cobalt and nickel (Fig. 1) was constructed using components described elsewhere [10] and provided two different reaction times depending on the presence of P<sub>1</sub> or P<sub>2</sub> in the analytical path. The sample plug selected by the loop L<sub>2</sub> was transported by carrier stream C and merged with reagent R<sub>1</sub> for quantitative metal–citrate complexation inside coil B<sub>1</sub>. After additions of R<sub>2</sub> and R<sub>3</sub>, metal–PAR complexes were formed inside P<sub>2</sub> under buffered alkaline conditions. As the metal–citrate decomplexation rate is slower for nickel than cobalt [9], a long P<sub>2</sub> coil was needed to increase the mean available time for Ni–PAR formation. R<sub>4</sub> was thereafter added, and foreign ions were masked by EDTA inside B<sub>2</sub>. The coloured zone was monitored at 520 nm, with the recorded peak height reflecting the contributions of cobalt and nickel.

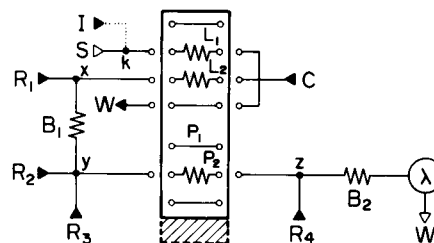


Fig. 1. Flow diagram of the system for the simultaneous determination of cobalt and nickel. S = Sample at 2.0 ml min<sup>-1</sup>; L<sub>1</sub> and L<sub>2</sub> = 20- and 100-cm sampling loops (100 and 500 μl); C = carrier stream (0.01 M HCl, 2.9 ml min<sup>-1</sup>); R<sub>1</sub>, R<sub>2</sub>, R<sub>3</sub> and R<sub>4</sub> = 0.1 M Na<sub>2</sub>B<sub>4</sub>O<sub>7</sub>, 0.01 M sodium citrate, 0.001 M PAR and 0.1 M Na<sub>2</sub>EDTA + 0.01 M Na<sub>4</sub>P<sub>2</sub>O<sub>7</sub> at 0.42 ml min<sup>-1</sup>; B<sub>1</sub> and B<sub>2</sub> = 20 and 50-cm reactors; P<sub>1</sub> and P<sub>2</sub> = 1- and 400-cm paths; λ = detector (520 nm); x, y, z and k = confluence points; W = waste; I = optional stream at 2.0 ml min<sup>-1</sup> for studying interferences; black arrows = sites where pumping is applied. Boxed components are linked to movable portions of the commutator with the next position specified by the dashed area.

By switching the commutator, the content of loop L<sub>1</sub> was intercalated in stream C and the sample plug similarly processed. As Co–citrate decomplexation was quantitative within a few seconds [9] and Ni–citrate decomplexation was relatively slow, P<sub>2</sub> was replaced with the injector path (P<sub>1</sub>), resulting in a very short time for decomplexation and reaction with PAR. Therefore, the recorded signal reflected mainly the cobalt concentration in the sample. Nickel determination was then based on peak heights associated with P<sub>2</sub> and P<sub>1</sub>.

The simplified system for cobalt determination in tool steels (Fig. 2) was similarly operated. To minimize the formation of Ni–PAR, a twofold increase in flow-rates was effected and P<sub>1</sub> was

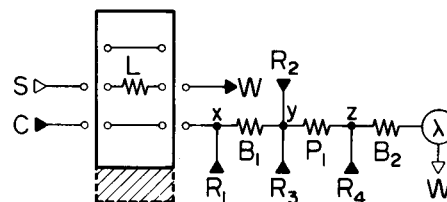


Fig. 2. Flow diagram of the system proposed for cobalt determination in tool steels. L = 50-cm sampling loop; P<sub>1</sub> = 10-cm reactor. Other components and symbols as in Fig. 1.

chosen as short as possible (10 cm), yet sufficient for providing suitable conditions for Co–PAR formation.

#### Procedure

PAR and sodium citrate concentrations were varied within the ranges 0.0001–0.01 and 0.001–1.0 M. PAR solutions with different ages and storage conditions (presence or absence of light) were used. The influence of ionic strength was studied by using an extra stream (2.0 ml min<sup>-1</sup> at confluence x) which added sufficient NaCl to provide ionic strengths of 1–3 for the solution inside B<sub>2</sub>. The effects of temperature in the range 0–50°C were studied by immersing coil B<sub>3</sub> in a thermostated water-bath.

The chemistry involved was studied either by varying the length of P<sub>2</sub> (10–500 cm) or by placing standard solutions in a situation of “infinite volume” and stopping the peristaltic pump after achievement of a steady state [3]. Whenever required, the pump speed was varied in order to provide flow-rates of 25–200% relative to those in Fig. 1.

A merging zones approach [11] was used to investigate selectivity. Concentrations of potentially interfering ions [10.00 mg W(VI) l<sup>-1</sup>, 5.00 mg Cu(II) l<sup>-1</sup>, 50.00 mg Fe(III) l<sup>-1</sup>, 5.00 mg V(V) l<sup>-1</sup>, 5.00 mg Mn(II) l<sup>-1</sup>, 5.00 mg Mo(VI) l<sup>-1</sup> and 5.00 mg Cr(VI) l<sup>-1</sup>; solution I, Fig. 1] were well above those usually found in solubilized tool steels. In these experiments, the pH was varied (5.0–11.0) by adding HCl or NaOH to R<sub>2</sub> and the ionic strength inside B<sub>2</sub> was always adjusted to 1.0 by adding NaCl to the buffer solution.

## RESULTS AND DISCUSSION

For 0.1 mM PAR, decomplexation rates of Co– and Ni–citrate were too low and kinetic discrimination could not be exploited owing to the small analytical signals (ca. 0.017 and 0.009 absorbance for Co and Ni). With R<sub>3</sub> = 0.001 M PAR, a stable baseline of about 0.06 absorbance was attained. For R<sub>3</sub> > 0.01 M PAR, high baselines were observed and kinetic discrimination became less pronounced. PAR reagent prepared

immediately before use yielded results in general 10% higher than those obtained with solutions aged for 5–10 days. In addition to the decrease of the signal, baseline drift (ca. 0.004 absorbance h<sup>-1</sup>) was observed for old R<sub>3</sub> reagents. No differences in peak heights were found for PAR solutions stored in the presence or absence of light. Therefore, the use of R<sub>3</sub> reagents older than 3 days is not recommended.

With 0.001 M citrate, kinetic discrimination was not observable because the citrate/PAR concentration ratio was not sufficient to promote pronounced differences in decomplexation rates. In the range 0.001–0.01 M citrate, an increased R<sub>2</sub> concentration decreased the nickel signal without a significant effect on the cobalt signal. Further, when R<sub>2</sub> was varied from 0.01 to 1.0 M citrate, the nickel signal decreased by about 12%. These results can be attributed to the mass effect with the consequent lowering of decomplexation rates and sensitivity losses.

The proposed procedure is slightly dependent on ionic strength. For 1.00 mg Co l<sup>-1</sup>, peak heights of 0.302, 0.300 and 0.270 absorbance were observed for ionic strengths of 1, 2 and 3 inside B<sub>2</sub>, respectively. The signal related to this cobalt concentration underwent an 8% increase when the water-bath temperature was varied from 0 to 50°C. A 54% increase was observed for nickel, emphasizing the influence of temperature on kinetic discrimination. A water-bath thermostated at 25°C was used thereafter. An ice-bath, although beneficial [9], was not used because the enhancement of the kinetic discrimination was too small to justify addition of an extra apparatus in a system intended for steel-making analysis.

Increasing the pH from 7.0 to 9.0 resulted in sensitivity and selectivity improvement also because of the more effective action of EDTA. Higher pH values were not selected because under more alkaline conditions kinetic discrimination became worse. At pH 11.0 a twofold increase in peak height was observed for nickel but the colour of the PAR solution led to a baseline of 0.9 absorbance. Also, effects of foreign ions became more pronounced, probably owing to precipitation as hydroxides. As a compromise between kinetic discrimination, selectivity and sensi-

tivity, a pH of 8.9 was chosen (coil B<sub>2</sub>), which corresponds to pH 9.2 in the solution R<sub>1</sub>.

Metal interferences in the absence of cobalt or nickel were mostly negligible, manifesting themselves only at increased analyte concentrations. EDTA masked most of the tested ions and iron(III) interference was noted only for higher flow-rates (pump speed > 150% of the nominal speed). Improvements in selectivity were investigated further by adding to R<sub>4</sub> other masking agents such as triethanolamine, EGTA, tartrate, fluoride, KCN and Na<sub>4</sub>P<sub>2</sub>O<sub>7</sub> (0.01 M). For most of the masking agents, inhibition of kinetic discrimination between cobalt and nickel was observed. With triethanolamine or EGTA, reaction development for cobalt and nickel was almost quantitative and interferences of foreign ions were still unacceptable, probably owing to synergistic effects. With Na<sub>4</sub>P<sub>2</sub>O<sub>7</sub>, iron interference was reduced to about one tenth and the analytical signals underwent only a 5% reduction. This can be explained by the fact that the stability constant of Fe(III)–Na<sub>4</sub>P<sub>2</sub>O<sub>7</sub> is twice that of Fe(III)–EDTA [12].

The combination of R<sub>2</sub> and R<sub>4</sub> was tried in order to eliminate one pumping tube, but the analytical signals decreased to about 70%. This

TABLE 1

Comparative results for cobalt and nickel contents (mg l<sup>-1</sup>) in dissolved alloys as determined by the proposed procedure (Fig. 1) and by inductively coupled plasma atomic emission spectrometry (ICP-AES)

Sample	Proposed procedure <sup>a</sup>		ICP-AES <sup>b</sup>	
	Co	Ni	Co	Ni
1	2.73 (3.2)	– <sup>c</sup>	2.67	0.08
2	1.40 (1.1)	– <sup>c</sup>	1.38	0.10
3	3.30 (< 1)	0.39 (4.5)	3.36	0.41
4	3.15 (1.4)	0.47 (3.0)	3.20	0.50
5	3.88 (1.9)	0.55 (2.6)	4.00	0.50
6	2.00 (2.1)	0.29 (5.3)	2.05	0.30
7	4.09 (2.3)	0.12 (7.0)	3.90	0.15
a <sub>1</sub> <sup>d</sup>	4.83 (1.2)	0.91 (1.3)	4.81	0.89
a <sub>2</sub> <sup>d</sup>	5.24 (0.8)	0.87 (0.9)	5.20	0.86
a <sub>3</sub> <sup>d</sup>	3.81 (1.0)	0.95 (1.2)	3.86	0.99

<sup>a</sup> Numbers in parentheses are relative standard deviations (%) for five injections. <sup>b</sup> R.S.D. of ICP-AES result was about 1.7%. <sup>c</sup> R.S.D. > 10%. <sup>d</sup> a<sub>i</sub> = Synthetic samples.

TABLE 2

Comparative results for cobalt contents (mg l<sup>-1</sup>) in solubilized tool steels as determined by the proposed procedure (Fig. 2) and by ICP-AES

Sample	Proposed procedure <sup>a</sup>	ICP-AES <sup>a</sup>
1	1.09 (1.7)	1.13 (1.6)
2	0.60 (1.8)	0.64 (1.8)
3	0.60 (0.6)	0.65 (1.5)
4	0.39 (2.7)	0.38 (2.1)
5	0.32 (1.4)	0.31 (3.3)
6	1.09 (0.3)	1.06 (1.4)
7	0.53 (0.1)	0.58 (0.8)

<sup>a</sup> Numbers in parentheses are relative standard deviations (%) for five injections.

leads to the conclusion that metal–PAR complexes are formed only inside P<sub>1</sub> (or P<sub>2</sub>) and EDTA addition blocks the further formation of Co– and Ni–PAR.

The mean available time for metal–PAR formation, proportional to the lengths of P<sub>1</sub> and P<sub>2</sub>, is an important parameter. P<sub>1</sub> was short enough to impair Ni–PAR formation and to guarantee reproducible results. Regarding P<sub>2</sub>, for lower values (external loop < 5 cm), additivity was not observed owing to the low nickel contribution to the analytical signal, and the measurement reproducibility was unacceptable (R.S.D. 7%). When P<sub>2</sub> was 10 cm, the reproducibility was improved (R.S.D. < 3%) and the additivity was determined to be 98–102%, but the nickel signal was still low. Better reproducibility (R.S.D. 1.1%) and almost quantitative Ni–PAR formation were achieved with P<sub>2</sub> = 400 cm. This length could not be reduced to improve the sampling rate, because at 200 cm nickel complexation was only about 70% and the reproducibility was poorer (R.S.D. 2%).

In spite of P<sub>1</sub> and P<sub>2</sub> replacement, baseline drift or a double baseline was not observed. As the length of B<sub>2</sub> was 50 cm and the commutator was switched after the peak maximum, carryover effects due to sample entrapment inside P<sub>2</sub> were not detected. With a sample frequency of 40 h<sup>-1</sup>, only 32.5 of μg PAR were consumed per determination and accurate results were obtained (Table 1).



TABLE 3

Selectivity for single determination of cobalt using the system in Fig. 2

Ion	Tolerance ratio <sup>a</sup>
W(VI)	200
Cr(VI), Fe(III), Mn(II), Mo(VI)	20
Cu(II)	3
V(V)	2
Ni(II)	1

<sup>a</sup> Maximum tolerance ratios of interfering metal concentrations causing a 10% error in measurement related to 0.50 mg Co l<sup>-1</sup>.

For single cobalt determination, the flow system was simplified (Fig. 2) and the pumping speed was doubled as sensitivity was not critical and the mean available time for Ni-PAR formation should be reduced. In this context, the length of P<sub>1</sub> was decreased to 10 cm and Na<sub>4</sub>P<sub>2</sub>O<sub>7</sub> concentration was increased to 0.1 M. This system does not require thermostating, as only a 3.8% increase in analytical signal per 10°C was calculated. After an 8-h working period, the slope of calibration equation underwent only slight variations (< 5%). Linearity ( $r < 0.999$ ;  $n = 7$ ) was observed in the range 0.0–4.0 mg Co l<sup>-1</sup> and the detection limit associated with a 250- $\mu$ l sampling loop was calculated according to IUPAC recommendations [13] to be 180  $\mu$ g Co l<sup>-1</sup>. Precise results (R.S.D. < 2%) were obtained at a sampling rate of about 100 h<sup>-1</sup>. PAR consumption was calculated to be 65.3  $\mu$ g per determination. The accuracy and selectivity can be assessed from Tables 2 and 3.

Partial support of this work by FAPESP (Fundação de Amparo a Pesquisa do Estado de São Paulo) and CNPq (Conselho Nacional de Desenvolvimento Científico e Tecnológico) is greatly appreciated. B.F. Reis, J.A. Nobrega and O.M. Matsumoto are thanked for critical comments.

## REFERENCES

- 1 M.D. Luque de Castro and M. Valcarcel, Trends Anal. Chem., 5 (1986) 71.
- 2 E.A.G. Zagatto, H. Bergamin F<sup>0</sup>, S.M.B. Brienza, M.A.Z. Arruda, A.R.A. Nogueira and J.L.F.C. Lima, Anal. Chim. Acta, 261 (1992) 59.
- 3 M. Valcarcel and M.D. Luque de Castro, Flow-Injection Analysis. Principles and Applications, Horwood, Chichester, 1st edn., 1987.
- 4 H.A. Mottola and H.B. Mark, Jr., Anal. Chem., 56 (1984) 96R.
- 5 H.A. Mottola, M.D. Perez-Bendito and H.B. Mark, Jr., Anal. Chem., 60 (1988) 181R.
- 6 M.D. Luque de Castro and M. Valcarcel, Analyst, 109 (1984) 413.
- 7 A. Rios, M.D. Luque de Castro and M. Valcarcel, Anal. Chim. Acta, 179 (1986) 463.
- 8 A. Fernandez, M.D. Luque de Castro and M. Valcarcel, Anal. Chem., 56 (1984) 1146.
- 9 D. Betteridge and B. Fields, Fresenius' Z. Anal. Chem., 314 (1983) 386.
- 10 M.A.Z. Arruda and E.A.G. Zagatto, Anal. Chim. Acta, 199 (1987) 137.
- 11 M.A.Z. Arruda, E.A.G. Zagatto, A.O. Jacintho and S.M.B. Brienza, J. Braz. Chem. Soc., 2 (1991) 47.
- 12 A. Ringbom, Complexation in Analytical Chemistry (Chemical Analysis, Vol. XVI), Interscience, New York, London, 1963.
- 13 Analytical Methods Committee, Analyst, 112 (1987) 199.

# Simultaneous determination of arsenate and phosphate by use of the kinetic wavelength-pair method

M. López Carreto, D. Sicilia, S. Rubio and D. Pérez-Bendito

*Department of Analytical Chemistry, Faculty of Sciences, University of Córdoba, 14004 Córdoba (Spain)*

(Received 20th October 1992)

## Abstract

Application of the kinetic wavelength-pair method was extended to the fixed-time kinetic variant with the simultaneous determination of arsenate and phosphate based on the formation of a heteropoly acid with molybdate and subsequent reduction with ascorbic acid to molybdenum blue compounds with strongly overlapping spectra. Resolution of the mixture by using discrete wavelengths was impossible. Selectivity in the resolution was achieved by measuring the absorbance difference at the wavelength pair 820–740 nm and a fixed time of 100 s, where the contribution of phosphate was greatly decreased. Arsenate and phosphate were simultaneously determined in weight ratios between 5:1 and 0.3:1 at concentrations from 0.5 to 6  $\mu\text{g ml}^{-1}$ , with relative standard deviations between 3% and 5% for arsenate and between 1.5% and 2.5% for phosphate. The theoretical basis adapted to first-order kinetic-based determinations was established.

**Keywords:** Kinetic methods; UV-Visible spectrophotometry; Arsenate; Phosphate; Waters

Chromatography is the most suitable and commonly used technique for the determination of individual components in complex mixtures. However, when the individual components are known and limited in number, and adsorb UV-visible radiation, spectrophotometric measurements can be employed without the need for tedious, time-consuming separation techniques [1].

The time required for multi-component analyses based on spectrophotometric measurements at a discrete wavelength on each component has been considerably reduced with the advent of diode-array detectors. Likewise, diode-array detectors have opened up new prospects for differential kinetic analysis by permitting simultaneous

monitoring of the absorbance as a function of time and wavelength [2]. Both equilibrium- and kinetic-based determinations using multi-wavelength detection require a maximum difference between the molar absorptivity ratios of the components being analysed at the different measurement wavelengths in order to obtain the most accurate estimate of their concentration [3,4]. If the absorptivity ratios for two or more components at discrete wavelengths are similar, one approach improving on the accuracy of the simultaneous determination of these species involves using a wavelength pair for each component where the absorptivities for the component being determined are as different as possible at the two wavelengths and as small as possible for the other components in the mixture. This principle has been applied to the kinetic-based determination of formaldehyde and acrolein by reaction with 3-methylbenzothiazolin-2-one hydrazone by mea-

*Correspondence to:* D. Pérez-Bendito, Department of Analytical Chemistry, Faculty of Sciences, University of Córdoba, 14004 Córdoba (Spain).

asuring the rate of change of absorbance of the reaction product at two selected wavelength pairs [5]. This approach, called the “kinetic wavelength-pair method”, is especially useful for the resolution of mixtures of components with similar reactivities and spectra. It can also be used to resolve mixtures of components involved in reactions taking place at the same rate provided that the difference between the molar absorptivity ratios at the two selected wavelength pairs is large enough. Its main shortcoming is a lower sensitivity than methods based on peak wavelengths. It is to be preferred whenever spectral overlap between the components is strong enough to preclude the use of discrete multi-wavelength spectrophotometry.

In this work, the above approach was extended to the fixed-time kinetic method and applied to the simultaneous determination of arsenate and phosphate by the formation of a heteropolyacid with molybdate and subsequent reduction to molybdenum blue compounds by ascorbic acid. As the spectra of the reaction products from arsenate and phosphate are strongly overlapped and the reactivity of the heteropoly complexes against ascorbic acid is similar, their simultaneous resolution is difficult, and procedures based on this reaction use two sample aliquots, arsenate being determined from the absorbance difference between a reduced and an unreduced sample [6,7]. The kinetic wavelength-pair method improves on the accuracy of analyses to an extent allowing the simultaneous resolution of arsenate and phosphate with arsenate-to-phosphate weight ratios between 5 : 1 and 0.3 : 1.

#### THEORETICAL BACKGROUND

The mathematical treatment of the kinetic wavelength-pair method was described in terms of rates in a previous paper [5]. In this work it was extended to the fixed-time kinetic approach.

Consider the analytes M and N, which react with R to yield X and Y, respectively. The kinetic equations for these reactions on the assumption that both are first order and that the chemical

reaction rate is controlled by the formation of X and Y are

$$\frac{dX}{dt} = K_M C_M^0 \quad (1)$$

$$\frac{dY}{dt} = K_N C_N^0 \quad (2)$$

where  $K_M$  and  $K_N$  are the first-order rate constants and  $C_M^0$  and  $C_N^0$  are the initial concentrations of M and N. These equations can be readily integrated, so the concentration, X or Y, of the reaction product at any time can be expressed as follows:

$$X = C_M^0 (1 - e^{-K_M t}) \quad (3)$$

$$Y = C_N^0 (1 - e^{-K_N t}) \quad (4)$$

If X and Y absorb UV-visible radiation, then the absorbance at a given wavelength,  $\lambda_i$ , and time,  $t_i$ , will be

$$A_{M,\lambda_i} = C_M^0 (1 - e^{-K_M t_i}) \epsilon_{M,\lambda_i} \quad (5)$$

$$A_{N,\lambda_i} = C_N^0 (1 - e^{-K_N t_i}) \epsilon_{N,\lambda_i} \quad (6)$$

for a path length of 1 cm.

Simultaneous resolution of M and N by application of the wavelength-pair method involves measuring absorbance at a fixed time and two wavelengths pairs,  $\lambda_1$  and  $\lambda_2$  and  $\lambda_3$  and  $\lambda_4$  (for simplicity, subscripts 1–4 in the expressions below denote measurements made at  $\lambda_1$ – $\lambda_4$ , respectively), which are chosen in such a way that the difference between the absorbances at the selected time for the first wavelength pair is as large as possible for one of the components (e.g., M) and minimal for the other (e.g., N), and the opposite holds for the second wavelength pair. If the measured absorbances are additive, then the following equations can be used for the simultaneous determination of M and N:

$$\Delta A_{2-1} = A_2 - A_1 = C_M^0 (1 - e^{-K_M t_i}) (\epsilon_{M,2} - \epsilon_{M,1}) + C_N^0 (1 - e^{-K_N t_i}) (\epsilon_{N,2} - \epsilon_{N,1}) \quad (7)$$

$$\Delta A_{4-3} = A_4 - A_3 = C_M^0 (1 - e^{-K_M t_i}) (\epsilon_{M,4} - \epsilon_{M,3}) + C_N^0 (1 - e^{-K_N t_i}) (\epsilon_{N,4} - \epsilon_{N,3}) \quad (8)$$

The method is particularly useful for reactions with similar constants (e.g.  $K_M \approx K_N$ ) in which

the components being monitored have similar molar absorptivities (i.e.  $\epsilon_M/\epsilon_N \approx 1$ ) at all wavelengths. Achieving the maximum possible accuracy in estimating M and N entails finding the conditions where the difference between  $(\epsilon_{M,2} - \epsilon_{M,1})/(\epsilon_{N,2} - \epsilon_{N,1})$  and  $(\epsilon_{M,4} - \epsilon_{M,3})/(\epsilon_{N,4} - \epsilon_{N,3})$  is maximal. As the kinetic wavelength-pair method is less sensitive than methods based on peak wavelengths, combining wavelength pairs and discrete wavelengths can be useful for reactions in which one component yields a greater signal than all the others at any wavelength and time (e.g.,  $\epsilon_M/\epsilon_N > 1$ ). In this case, simultaneous resolution of M and N can be accomplished by using the following equations:

$$A_1 = C_M^0(1 - e^{-K_M t_j})\epsilon_{M,1} + C_N^0(1 - e^{-K_N t_j})\epsilon_{N,1} \quad (9)$$

$$\Delta A_{3-2} = C_M^0(1 - e^{-K_M t_j})(\epsilon_{M,3} - \epsilon_{M,2}) + C_N^0(1 - e^{-K_N t_j})(\epsilon_{N,3} - \epsilon_{N,2}) \quad (10)$$

where  $(\epsilon_{N,3} - \epsilon_{N,2})/(\epsilon_{M,3} - \epsilon_{M,2}) > 1$ . Selection of the wavelength pairs to be used at a given time is made by computer.

## EXPERIMENTAL

### Apparatus

Kinetic measurements were made on a Hewlett-Packard Model 8452A diode-array spectrophotometer furnished with 1-cm quartz and glass cells. The temperature of the cell compartment was kept constant by circulating water through it. Kinetic data were acquired and processed by a Hewlett-Packard Vectra E/S 12 computer interfaced to a ThinkJet printer.

### Reagents

All reagents were of analytical-reagent grade and were employed as supplied. Doubly distilled water was used throughout. Solutions were stored in polyethylene bottles. Because dissolved molybdate polymerizes to some extent, all Mo(VI) solutions were prepared at least 24 h prior to their first use in order to ensure that any molybdate aggregates had reached a stable equilibrium [8].

A stock molybdate solution ( $3.6 \times 10^{-2}$  M) was prepared by dissolving  $(\text{NH}_4)_6\text{Mo}_7\text{O}_{24} \cdot 4\text{H}_2\text{O}$  (Merck) in nitric acid and diluting to  $[\text{HNO}_3] = 2.04$  M. An aqueous L-ascorbic acid (Merck) solution (0.358 M) was prepared fresh daily to avoid oxidation. A 40% aqueous solution of glycerine was employed to prevent precipitation of the reaction products. A  $1.33 \times 10^{-2}$  M standard solution of  $\text{Na}_2\text{HAsO}_4 \cdot 7\text{H}_2\text{O}$  (Merck) and a  $3.23 \times 10^{-2}$  M standard solution of  $\text{KH}_2\text{PO}_4$  (Merck) were also prepared. More dilute standard solutions were prepared by appropriate dilution.

### Procedure for the simultaneous determination of phosphate and arsenate

To a 10-ml volumetric flask were added, in sequence, 2 ml of  $3.6 \times 10^{-2}$  M molybdate, 1.2 ml of 40% glycerine, appropriate volumes of phosphate and arsenate standard solutions to obtain a final concentration for each analyte between 0.5 and  $6 \mu\text{g ml}^{-1}$  and 1.5 ml of 0.358 M ascorbic acid. The stop-clock was then started and the solution was diluted to the mark with doubly distilled water. An aliquot of the reaction mixture was transferred to a cell kept at  $65 \pm 0.1^\circ\text{C}$  and measurements were started exactly 60 s after mixing the solutions. Absorbance–time data between 740 and 820 nm were acquired at 2-s intervals for 2 min by using the spectrophotometer's bundled software. Blank solutions were prepared in the same way as the samples but with no analytes.

### Data processing

The DUALCHANGESIGNAL program [5], written in BASIC, was modified for application of the kinetic wavelength-pair method to the fixed-time approach. The set of background data generated from a blank solution was subtracted from each set of sample data. In order to select the most appropriate wavelength pairs, the  $(A_{M,2} - A_{M,1})/(A_{N,2} - A_{N,1})$  ratio was plotted as a function of wavelength at several times and absorbance increments. This ratio is proportional to the  $(\epsilon_{M,2} - \epsilon_{M,1})/(\epsilon_{N,2} - \epsilon_{N,1})$  ratio since the other parameters (e.g., those in Eqn. 5) are independent of wavelength. Wavelength pairs at which the difference between  $(A_{M,2} - A_{M,1})/(A_{N,2} -$

$A_{N,1}$ ) and  $(A_{M,4} - A_{M,3}) / (A_{N,4} - A_{N,3})$  (Eqns. 7 and 8) and between  $A_{M,1} / A_{N,1}$  and  $(A_{M,3} - A_{M,2}) / (A_{N,3} - A_{N,2})$  (Eqns. 9 and 10) were maximal were thus obtained. Selection of the optimum wavelength pair or discrete wavelength for the determination of each component was also dictated by the sensitivity and linear range of the calibrations graphs previously obtained.

For the phosphate–arsenate mixture the most accurate and sensitive measurement conditions were found to be 740 and 820–740 nm at a fixed time of 100 s. The dependence of the absorbance at these wavelengths and time on the concentration of the analytes in binary mixtures was found to conform to the following functions:

$$A(740) = \beta_0 + \beta_1[\text{AsO}_4^{3-}] + \beta_2[\text{PO}_4^{3-}] \quad (11)$$

$$A(820 - 740) = \beta'_0 + \beta'_1[\text{AsO}_4^{3-}] + \beta'_2[\text{PO}_4^{3-}] + \beta'_3[\text{AsO}_4^{3-}][\text{PO}_4^{3-}] \quad (12)$$

where the concentration of the analytes is expressed in  $\mu\text{g ml}^{-1}$ . The coefficients  $\beta_0$ ,  $\beta_1$ ,  $\beta_2$ ,  $\beta'_0$ ,  $\beta'_1$ ,  $\beta'_2$  and  $\beta'_3$  were estimated by multiple linear regression (MLR) from 20 binary mixtures containing arsenate and phosphate at concentrations between 0.5 and 6  $\mu\text{g ml}^{-1}$  using the modified DUALCHANGESIGNAL program. The MLR expression for Eqns. 11 and 12 in matrix notation is

$$y = X \cdot \beta + e$$

where  $y$  is the measurement vector [ $A(740)$  or  $A(820-740)$ ],  $e$  the residual vector,  $\beta$  the parameter vector and  $X$  the independent variable matrix. The least-squares estimates,  $b$ , of  $\beta$  can be obtained from  $b = (X'X)^{-1}X'y$  where  $X'$  is the transpose of  $X$  and  $(X'X)^{-1}$  the inverse of  $X'X$ . Once the coefficient estimates have been obtained, unknown samples can be analysed by substituting the measured parameters  $A(740)$  and  $A(820-740)$  into Eqns. 11 and 12 and calculating the analyte concentrations by using the DUALCHANGESIGNAL program.

## RESULTS AND DISCUSSION

In strongly acidic solutions, molybdenum(VI) forms yellow unreduced 12-molybdophosphoric

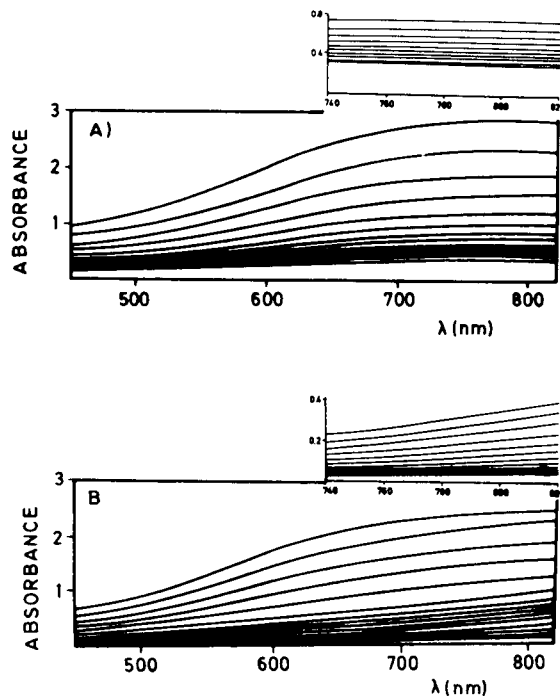


Fig. 1. Absorption spectra of the reduced blue heteropoly complexes [(A) 12-MPA<sub>R</sub> and (B) 12-MAsA<sub>R</sub>] at different reaction times. Measurements made every 10 s.  $[\text{AsO}_4^{3-}] = [\text{PO}_4^{3-}] = 1.5 \times 10^{-5}$  M.

acid (12-MPA) and 12-molybdoarsenic acid (12-MAsA) with phosphate and arsenate, respectively. Addition of ascorbic acid reduces these complexes to blue heteropoly compounds, which will be referred to here as 12-MPA<sub>R</sub> and 12-MAsA<sub>R</sub>.

Figure 1 shows the absorption spectra of these reduced blue heteropoly compounds at different reaction times under the above-described experimental conditions. It also shows a magnified detail of the spectral region between 740 and 820 nm at the initial reaction times which illustrates more clearly some of the considerations on these spectra made below.

The spectra of 12-MPA<sub>R</sub> and 12-MAsA<sub>R</sub> are strongly overlapped, which makes it very difficult to resolve simultaneously the two analytes by using the discrete multi-wavelength approach. The similar spectral features of these compounds are the reason why the usual procedures relying on this reaction use two sample aliquots and

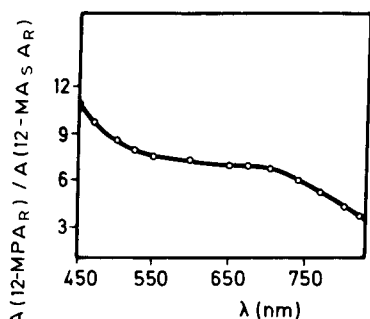


Fig. 2. Variation of the 12-MPA<sub>R</sub>/12-MAsA<sub>R</sub> absorbance ratio as a function of wavelength. Measurements were made at 100 s.  $[\text{AsO}_4^{3-}] = [\text{PO}_4^{3-}] = 1.5 \times 10^{-5}$  M.

determine arsenate from the absorbance difference between a reduced and an unreduced sample.

12-MAsA<sub>R</sub> yields a smaller signal than 12-MPA<sub>R</sub> at any wavelength and equivalent concentrations of arsenate and phosphate. This is apparent from Fig. 2, where the 12-MPA<sub>R</sub>/12-MAsA<sub>R</sub> absorbance ratio, measured at 100 s, is plotted as a function of the wavelength. This poses a major problem to the analysis of water samples from different environments if the phosphate concentration exceeds that of arsenate.

12-MAsA<sub>R</sub> yields a smaller signal than 12-MPA<sub>R</sub> at any time and equivalent concentrations of arsenate and phosphate, as shown in Fig. 3A, where the absorbance–time kinetic curves obtained for these complexes at a discrete wavelength ( $\lambda = 740$  nm) are plotted. Evolution of the blank reaction causes the absorbance to decrease

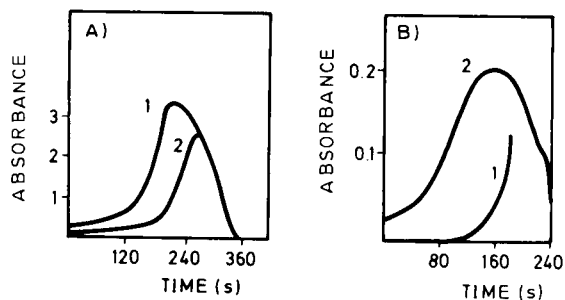


Fig. 3. Absorbance–time kinetic curves run at (A) 740 and (B) 820–740 nm. 1 = 12-MPA<sub>R</sub> complex; 2 = 12-MAsA<sub>R</sub> complex.

at a given time. The response curves possess no linear region from which the reaction rate may be obtained. For this reason, the fixed-time kinetic approach was used for measurements.

As can be seen in the magnified spectrum of 12-MPA<sub>R</sub> (Fig. 1), there is a spectral region in which, over a given time interval, 12-MPA<sub>R</sub> absorbance measurements do not depend on the wavelength. As 12-MAsA<sub>R</sub> behave differently in this spectral region (see the magnified 12-MAsA<sub>R</sub> spectrum in Fig. 1), the contribution of the 12-MPA<sub>R</sub> complex to the measured absorbance can be greatly reduced by subtracting absorbances at the 820–740 wavelength pair and fixed reaction times shorter than 120 s (Fig. 3B).

Taking into account that the sensitivity achieved by using wavelength pairs was lower (compare the ordinates in Fig. 3A and B), the selected wavelengths for simultaneous resolution of phosphate and arsenate in mixtures were 740 nm, where  $A(12\text{-MPA}_R) > A(12\text{-MAsA}_R)$ , and 820–740 nm, where  $A(12\text{-MAsA}_R) > A(12\text{-MPA}_R)$ . The optimum discrete wavelength (740 nm) was chosen in order to achieve the maximum possible 12-MPA<sub>R</sub>/12-MAsA<sub>R</sub> absorbance ratio and the minimum likelihood of interferences from coloured matrices in the analysis of real samples. This latter objective excluded selection of the shortest wavelengths (e.g., between 450 and 550 nm).

#### Optimization of the reaction conditions

In order to achieve the highest possible accuracy and sensitivity in the determination of arsenate and phosphate, reactant concentrations were chosen with two aims, namely that the  $A(12\text{-MPA}_R)/A(12\text{-MAsA}_R)$  ratio should be maximum at 740 nm and minimum at 820–740 nm, respectively, and the opposite should hold for the  $A(12\text{-MAsA}_R)/A(12\text{-MPA}_R)$  ratio and that the absolute values of the measured absorbances for 12-MPA<sub>R</sub> and 12-MAsA<sub>R</sub> should be maximum at 740 and 820–740 nm, respectively. If either condition was not fulfilled at a given value of the studied parameter, then the selected value was that which resulted in the maximum  $A(12\text{-MAsA}_R)/A(12\text{-MPA}_R)$  ratio at 820–740 nm, as the absorbance values at this wavelength pair

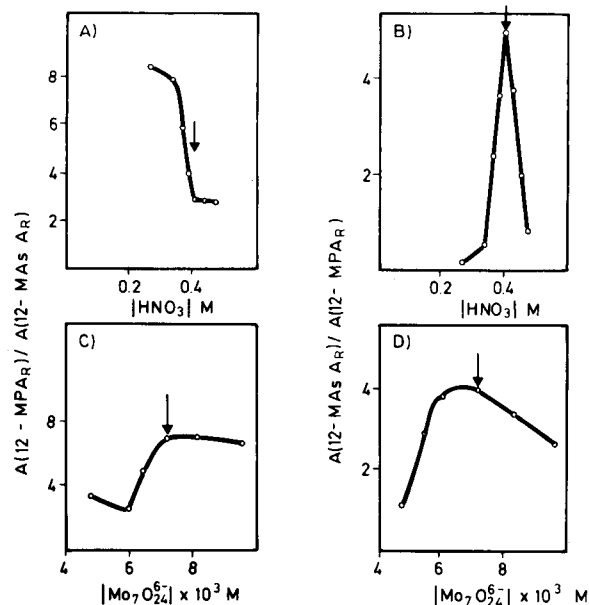


Fig. 4. Variation of the absorbance ratio between the 12-MPA<sub>R</sub> and 12-MAsA<sub>R</sub> complexes at (A and C) 740 and (B and D) 820–740 nm as a function of (A and B) nitric acid and (C and D) heptamolybdate concentration.

were always smaller than those at 740 nm. It should be noted that measurements were made in the kinetic region, so obtaining signals in real time throughout the spectral region entailed the use of a diode-array detector. The effect of different variables affecting the reaction was studied by changing each in turn while keeping all others constant.

Some of the results obtained are shown in Figs. 4 and 5, where the 12-MPA<sub>R</sub>/12-MAsA<sub>R</sub> absorbance ratio at 740 nm and the 12-MAsA<sub>R</sub>/12-MPA<sub>R</sub> absorbance ratio at 820–740 nm are plotted as a function of each parameter affecting the reaction. The selected values are marked with arrows. Absorbance measurements were made at 100 s, the optimum time derived from Fig. 3B. The most salient features of this study are commented upon below.

The hydrogen concentration was found to affect significantly the formation and reduction of 12-MPA. Thus, above 0.1 M HNO<sub>3</sub>, the overall rate of this reaction decreased markedly as the acid concentration was raised. The formation of 12-MAsA and its reduction proceeded at a virtu-

ally constant rate over the concentration range 0.1–0.4 M HNO<sub>3</sub>, above which both rates decreased slightly as increasing amounts of acid were added to the reaction medium. The hydrogen ion concentration also affected the spectral features of the region of interest, so the 12-MPA<sub>R</sub> absorbance was only independent of the wavelength at acid concentrations of ca. 0.41 M, which was selected as optimum (Fig. 4B).

The molybdenum concentration did not affect the spectral features of the 12-MPA<sub>R</sub> complex in the region of interest over the studied interval ( $4.5 \times 10^{-3}$ – $1 \times 10^{-2}$  M heptamolybdate). Concentrations above  $8 \times 10^{-3}$  M caused the reaction products gradually to precipitate. A  $7.2 \times 10^{-3}$  M heptamolybdate concentration yielded the maximum absorbance ratios (Fig. 4C and D), so it was chosen for subsequent experiments.

The presence of a concentration of glycerine greater than 2% in the reaction medium was required in order to avoid precipitation of the reaction products. The rate of reduction of the 12-MPA and 12-MAsA complexes decreased slightly as the glycerine concentration increased.

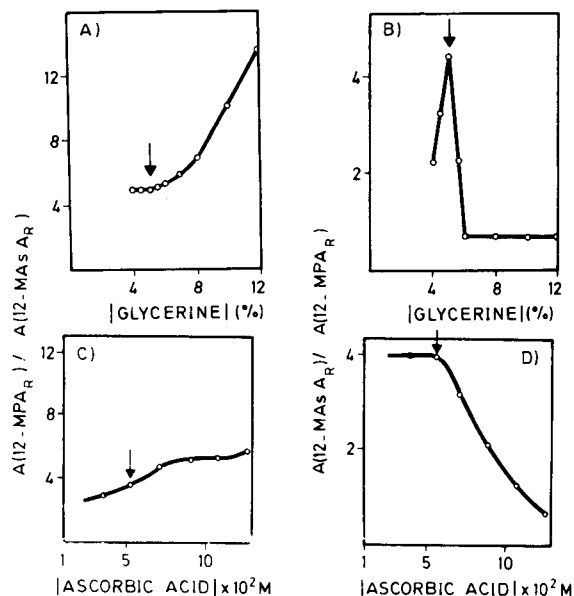


Fig. 5. Variation of the absorbance ratio between the 12-MPA<sub>R</sub> and 12-MAsA<sub>R</sub> complexes at (A and C) 740 and (B and D) 820–740 nm as a function of (A and B) glycerine and (C and D) ascorbic acid concentration.

A glycerine content of 5% was selected as optimum (Fig. 5A and B).

Ascorbic acid influenced the rate of reduction of both the 12-MPA and the 12-MAsA complexes, although the former was more markedly dependent. The selected value was that at which the maximum 12-MAsA<sub>R</sub>/12-MPA<sub>R</sub> absorbance ratio was obtained (Fig. 5D).

Increasing temperatures between 40 and 70°C resulted in slightly increased rates of reduction of both the 12-MPA and 12-MAsA complexes. Above 70°C, phosphate was found to contribute significantly to the signal obtained at 740–820 nm. The optimum absorbance ratio at the selected wavelength pair was obtained at 65°C, which was therefore chosen for subsequent experiments.

#### *Simultaneous determination of arsenate and phosphate*

Small amounts of phosphate have been reported to accelerate markedly the development of the As(V) complex when the reaction rate is monitored at 865 nm as a function of time [9]. Likewise, mixed As–P standards have been shown to yield lower molybdate absorbances than the sum of those of the two elements in isolation when reaction equilibrium is reached [7]. Experimental evidence suggests formation of a discrete As–P mixed complex with Mo that features a low molar absorptivity at 865 nm.

In order to detect any potential synergistic effects under the experimental conditions used, calibration graphs for arsenate in the presence of different phosphate concentrations were con-

structed at 740, 820 and 820–740 nm (Fig. 6). The occurrence of such effects was found to depend on the wavelength. Thus, at the shortest wavelength, 740 nm, the absorbance measured at 100 s was the sum of the values obtained for the two compounds separately (Fig. 6A). However, the rate of reduction of the 12-MAsA complex was increased at 820 nm, as reflected by the gradual increase in the slope of the calibration graph obtained with increase in phosphate concentration (Fig. 6B). As a result of the behaviour of the system at 820 nm, synergistic effects were encountered at the wavelength pair used in this study (820–740 nm) (Fig. 6C). Some calibration graphs for phosphate obtained in the presence of different arsenate concentrations showed similar results.

In order to calculate the concentration of arsenate and phosphate in the mixtures, Eqns. 11 and 12 (see Experimental) were solved by using the DUALCHANGESIGNAL program. Coefficients  $\beta_0$ ,  $\beta_1$ ,  $\beta_2$ ,  $\beta'_0$ ,  $\beta'_1$ ,  $\beta'_2$  and  $\beta'_3$  were estimated by multiple linear regression (MLR) from twenty observations of the variables  $A(740)$  and  $A(820-740)$  on twenty samples containing different combinations of analyte concentrations. The program also used statistical criteria to determine potential interactions between the response values of the analytes, i.e., the occurrence of synergistic effects. The coefficients of Eqns. 11 and 12, expressed as  $\beta \pm \text{S.D.}$ , were found to be  $\beta_0 -0.007 \pm 0.006$ ,  $\beta_1 0.029 \pm 0.001$ ,  $\beta_2 0.235 \pm 0.001$ ,  $\beta'_0 0.03 \pm 0.01$ ,  $\beta'_1 0.018 \pm 0.003$ ,  $\beta'_2 0.019 \pm 0.04$  and  $\beta'_3 0.0074 \pm 0.0009$ . The correlation coefficients for Eqns. 11 and 12 were 0.9998 and 0.997, re-

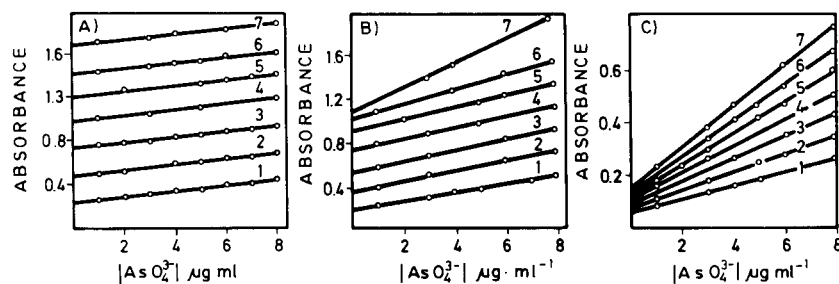


Fig. 6. Calibration graphs for arsenate in the presence of different phosphate concentrations: (1) 1; (2) 2; (3) 3; (4) 4; (5) 5; (6) 6; (7) 7  $\mu\text{g ml}^{-1}$ . (A) 740; (B) 820; (C) 820–740 nm.



TABLE 1

Multiple linear regression prediction for mixtures of arsenate and phosphate

Analyte ratio	Actual concentration ( $\mu\text{g ml}^{-1}$ )		Relative error (%)	
	Arse-nate	Phos-phate	Arse-nate	Phos-phate
1:1	1.0	1.0	3.3	2.6
	5.0	5.0	3.4	-0.3
	6.0	6.0	3.9	0.2
1:2	1.0	2.0	-8.6	1.0
	3.0	6.0	-1.1	-0.7
2:1	6.0	3.0	8.8	-0.9
3:1	3.0	1.0	-2.4	-1.3
	6.0	2.0	5.1	-1.4
4:1	4.0	1.0	2.5	-1.6
5:1	5.0	1.0	-3.8	0.7
1:3	1.0	3.0	7.4	0.5

spectively. The standard error of the estimate was  $9.24 \times 10^{-3}$  absorbance for Eqn. 11 and  $1.23 \times 10^{-2}$  absorbance for Eqn. 12. The precision of the proposed method, expressed as relative standard deviation, was 3.1% for arsenate and 1.6% for phosphate in a 1:1 mixture ( $[\text{AsO}_4^{3-}] = [\text{PO}_4^{3-}] = 3 \mu\text{g ml}^{-1}$ ), and 4.5% for arsenate and 2.1% for phosphate for an arsenate-to-phosphate ratio of ca. 2.3 ( $[\text{AsO}_4^{3-}] = 7 \mu\text{g ml}^{-1}$ ,  $[\text{PO}_4^{3-}] = 3 \mu\text{g ml}^{-1}$ ).

The predictive ability of indirect calibration by MLR for the binary mixture was tested by using eleven mixtures containing the analytes in different ratios as unknown samples and making measurements under the same experimental conditions as those used for calibration. Table 1 summarizes the results obtained from Eqns. 11 and 12. The relative errors were greater for arsenate, which is logical taking into account that synergistic effects on the system resulted in an increased contribution of phosphate to Eqn. 12. However, most of the arsenate determinations featured relative errors less than 5%, which confirms the good accuracy of the proposed method.

### Conclusions

The kinetic wavelength-pair method is an elegant approach to the resolution of mixtures of components with strongly overlapped spectra. Application of this approach to the determination of arsenate and phosphate by formation of molybdenum blue compounds avoids the arsenate reduction step, which is time consuming (3 h for reducing an arsenate concentration of ca.  $1 \mu\text{M}$  [7] and 15 min for less than  $0.15 \mu\text{M}$  [6]). The proposed method is well suited to the determination of arsenate and phosphate in waters, where they occur in not too low ratios of the former to the latter. Thus, it can be very useful for a variety of geothermal waters, polluted groundwaters and lake waters which have been treated with sodium arsenite for weed control in the past. On the other hand, for lower arsenate-to-phosphate ratios (e.g., in deep ocean waters, where the ratio is generally between 0.01 and 0.1) other methods [10] are more precise than the proposed method.

The authors gratefully acknowledge financial support from the CICYT (Project No. PB91-0840).

### REFERENCES

- 1 C.W. Brown, P.F. Lynch, R.J. Obremski and D.S. Lavery, *Anal. Chem.*, 54 (1982) 1472.
- 2 D. Pérez Bendito and M. Silva, *Kinetic Methods in Analytical Chemistry*, Horwood, Chichester, 1988.
- 3 E.I. Stearns, in M.G. Mellon (Ed.), *Analytical Absorption Spectroscopy*, Wiley, New York, 1950, p. 370.
- 4 M.C. Gutiérrez, A. Gómez Hens and D. Pérez Bendito, *Anal. Chim. Acta*, 225 (1989) 115.
- 5 J.M. Peña, S. Rubio and D. Pérez Bendito, *Anal. Chim. Acta*, 224 (1991) 81.
- 6 D.L. Johnson, *Environ. Sci. Technol.*, 5 (1971) 411.
- 7 D.L. Johnson and M.E.Q. Pilson, *Anal. Chim. Acta*, 58 (1972) 289.
- 8 S.R. Crouch and H.V. Malmstadt, *Anal. Chem.*, 39 (1967) 1084.
- 9 R.E. Stauffer, *Anal. Chem.*, 55 (1983) 1205.
- 10 D.G. Ballinger, R.J. Lishka and M.E. Gales, *J. Am. Water Works Assoc.*, 54 (1962) 1424.

# Kinetic flow-injection spectrofluorimetric method for the determination of fluoride

V. Marco, F. Carrillo, C. Pérez-Conde and C. Cámara

*Departamento de Química Analítica, Facultad de Ciencias Químicas, Universidad Complutense, 28040 Madrid (Spain)*

(Received 10th September 1992)

## Abstract

A flow injection–spectrofluorimetric method is reported for the determination of fluoride, based on the ability of trace fluoride to increase the rate of formation of a fluorescent Al(III)–Eriochrome Red B complex in the presence of hexamethylenetetramine. Various chemical and physical variables affecting the reaction and its kinetics in the flow system were evaluated. The proposed method is very sensitive, with a detection limit of  $10 \mu\text{g l}^{-1}$  and a linear calibration graph in the range  $1 \times 10^{-6}$ – $2 \times 10^{-4}$  M. The method was successfully applied to the determination of fluoride in tap and mineral waters.

*Keywords:* Flow injection; Kinetic methods; Fluorimetry; Fluoride; Waters

The monitoring of fluoride has recently received attention because of its dual role as an essential trace element and at high levels as a toxic substance. Both very high and very low fluoride intakes can cause mottling of teeth and bone disorders.

Potentiometry with a fluoride ion-selective electrode (ISE) is an effective and convenient technique commonly used to determine fluoride [1], but inaccurate results may be obtained at low concentrations of this analyte. Other methods reported include molecular absorption spectrometry (MAS) with electrothermal atomization [2] and spectrophotometric [3] and spectrofluorometric [4] methods based on ternary complex formation or catalytic reactions [5], some of them using flow-injection systems [6,7].

In a previous paper the slow rate of formation of an unstable fluorescent complex by aluminium

and Eriochrome Red B (ERB) in the presence of hexamethylenetetramine (HMTA) and the use of this reaction to determine Al(III) were reported [8].

This paper presents a sensitive flow-injection–spectrofluorimetric method for the determination of fluoride based on the ability of trace fluoride to increase the rate of formation of the Al(III)–ERB complex.

## EXPERIMENTAL

### *Instrumentation*

The flow-injection equipment consisted of a Gilson HP4 peristaltic pump, an Omnifit injection valve (six-way), PTFE segments with a 120–120 Y (i.d. 0.8 mm) configuration, 0.5 mm i.d. PTFE connecting tubing and various end fittings and connectors (Omnifit), a Perkin-Elmer MPF-44A spectrofluorimeter equipped with a xenon-lamp source, a 18- $\mu\text{l}$  (10-mm light path) flow cell and a Perkin-Elmer Model 56 recorder. The

*Correspondence to:* C. Cámara, Departamento de Química Analítica, Facultad de Ciencias Químicas, Universidad Complutense, 28040 Madrid (Spain).

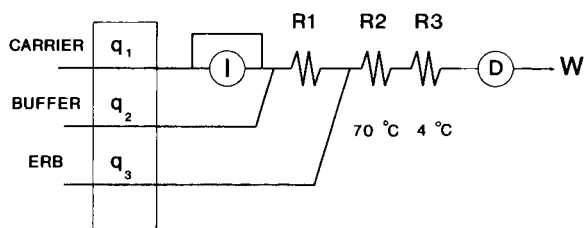


Fig. 1. Schematic diagram of flow-injection system. I = injection valve; R1 = reaction coil (50 cm  $\times$  0.5 mm i.d.); R2 = reaction coil (600 cm  $\times$  0.5 mm i.d.); R3 = reaction coil (200 cm  $\times$  0.5 mm i.d.); D = detector (spectrofluorimeter); W = waste;  $q_1$  and  $q_3 = 0.45 \text{ ml min}^{-1}$ ;  $q_2 = 0.60 \text{ ml min}^{-1}$ .

flow-injection manifold is shown in fig. 1. Mixing loop R1 was 50 cm long. The lengths of the injection and mixing loops R2 and R3 were varied for reasons of optimization.

Readings of pH were made on a Crison Model 2001 pH meter. All glassware was prepared for use by immersion for 24 h in 20% (v/v) nitric acid and subsequent rinsing in deionized water obtained from a Milli-Q system (Millipore).

#### Reagents

Analytical-reagent grade chemicals and Milli-Q-purified water were used in all experiments. A stock standard solution of fluoride ( $1 \times 10^{-2} \text{ M}$ ) was prepared by dissolving sodium fluoride in water. An aluminium solution ( $1.000 \mu\text{g ml}^{-1}$ ) was prepared by dissolving  $\text{Al}(\text{NO}_3)_3 \cdot 9\text{H}_2\text{O}$  in water and standardizing by titration with EDTA. These solutions were diluted when required immediately before use. The ERB solution was prepared by dissolving 10 mg in 100 ml of ethanol. Buffer solutions were prepared by adding perchloric acid to hexamethylenetetramine (HMTA).

#### General procedure

Into a  $0.5 \text{ mg l}^{-1}$  Al(III) solution used as a carrier at a flow-rate of  $0.45 \text{ ml min}^{-1}$ ,  $100 \mu\text{l}$  of sample containing up to  $4000 \mu\text{g l}^{-1}$  and carrier were mixed with the buffer solution (1.5 M  $\text{H}_2\text{MTA}^+ - \text{HMTA}$ ) in reaction coil R1 of length 50 cm (at a flow-rate of  $0.6 \text{ ml min}^{-1}$ ). The flow from R1 was mixed with the 0.01% (w/v) ERB solution (at a flow-rate of  $0.45 \text{ ml min}^{-1}$ ) in reaction coil R2 of length 600 cm, thermostated

at  $70^\circ\text{C}$ , and then cooled to  $4^\circ\text{C}$  in reaction coil R3 of length 200 cm. The fluorescent signal was measured as peak height at 595 nm with excitation at 470 nm and both slits at 18 nm (Fig. 1). The fluoride concentration was evaluated directly from a calibration graph.

## RESULTS AND DISCUSSION

#### Effect of fluoride on reaction kinetics

The slow rate of formation of the unstable fluorescent complex by aluminium and ERB in the presence of HMTA was strongly influenced by the concentration of fluoride in solution. At room temperature, fluoride concentrations above  $10^{-4} \text{ M}$  gave rise to a fluorescence signal intensity which decreased with increase in concentration. At high temperature ( $80^\circ\text{C}$ ), fluoride concentrations below  $10^{-3} \text{ M}$  markedly increased the rate of complex formation and maximum fluorescence intensity was achieved in less than 1 min, which is considerably shorter than the 15 min required in the absence of fluoride at the same temperature (Fig. 2). Although in the presence of fluoride the maximum signal intensity was lower, it was much higher than that obtained in the absence of fluoride at 1 min or less and it was proportional to fluoride concentration. This effect was most pronounced in flow-injection applications, where the measuring time was usually less than 1 min.

#### Effect of temperature

In the absence of fluoride, when the conditions were similar to those described under General procedure, the fluorescence intensity decreased slightly with increasing temperature (Fig. 3). At room temperature the presence of trace fluoride only quenched the fluorescence signal, but as the temperature increased the rate-enhancing effect indicated above became more significant. A temperature of  $70^\circ\text{C}$  was chosen for further experiments as it was difficult to work at higher temperatures.

The fluorescence intensity decreased with time when exposed to higher temperatures, so reaction

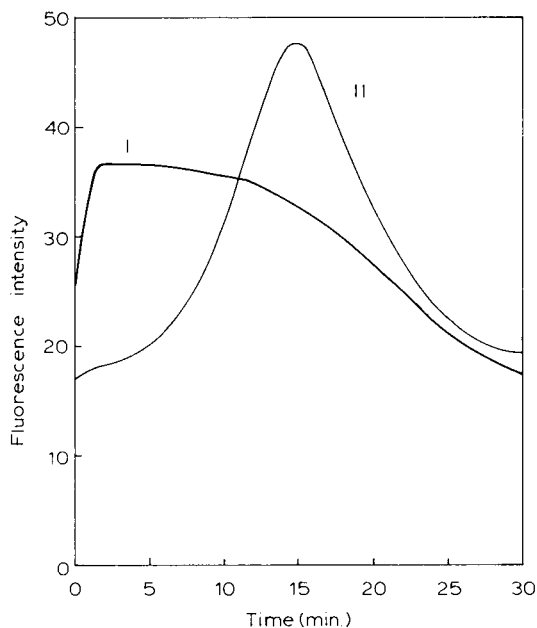


Fig. 2. Fluorescence intensity of  $50 \mu\text{g l}^{-1}$  Al(III) versus time at  $80^\circ\text{C}$ : (I) in the presence of  $1 \times 10^{-4}$  M fluoride; (II) in the absence of fluoride.

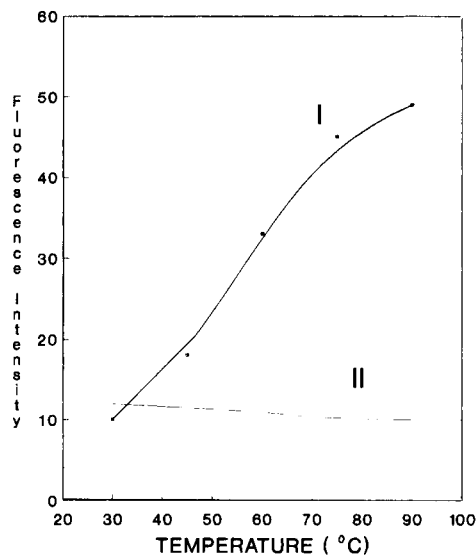


Fig. 3. Influence of temperature on fluorescence intensity: (I) in the presence of  $1 \times 10^{-4}$  M fluoride; (II) in the absence of fluoride.

coil R3 was added to allow rapid cooling to  $4^\circ\text{C}$ , thus improving the sensitivity and precision.

#### *Effects of pH and buffer concentration*

Different buffers were tested for their effect on the fluorescent complex formation in the flow system. The kinetic effect of fluoride was only observed with  $\text{H}_2\text{MTA}^+-\text{HMTA}$  buffer, so this buffer at pH 6.0 was chosen as the most suitable for fluoride determination by the proposed method.

When the  $\text{H}_2\text{MTA}^+-\text{HMTA}$  concentration was increased from 0.5 to 2 M, the analytical signal increased by over 15%. This variation could be explained by the direct participation of HMTA in the fluorescent complex formation. A concentration of 1.5 M  $\text{H}_2\text{MTA}^+-\text{HMTA}$  was chosen as the most appropriate for further experiments because of difficulties in working at higher concentrations owing to high viscosity.

#### *Effect of Al(III) concentration*

The optimum Al(III) concentration for complex formation at pH 6.0 was  $0.5 \text{ mg l}^{-1}$ . Higher Al(III) concentrations caused poor reproducibility owing to precipitation of  $\text{Al}(\text{OH})_3$ .

#### *Effect of ERB concentration*

The effect of ERB concentration on complex formation was evaluated in the range 0.002–0.05% (w/v). The optimum concentration was in the range 0.008–0.05% (w/v). A working concentration of 0.01% (w/v) was chosen for further experiments.

#### *Effect of reactor coil parameters*

The length, inner diameter and shape of the reaction coil were varied. Figure 4 shows that sensitivity increased with increasing tube length up to 600 cm. Greater lengths produced higher dispersion and decreased sensitivity. The reaction coil parameters chosen as optimum were length 600 cm, knotted, and i.d. 0.5 mm.

#### *Effect of flow-rate*

Flow-rates from 0.1 to  $1.5 \text{ ml min}^{-1}$  were tested in the three channels of the flow-injection system and flow-rates of 0.45, 0.6 and  $0.45 \text{ ml min}^{-1}$

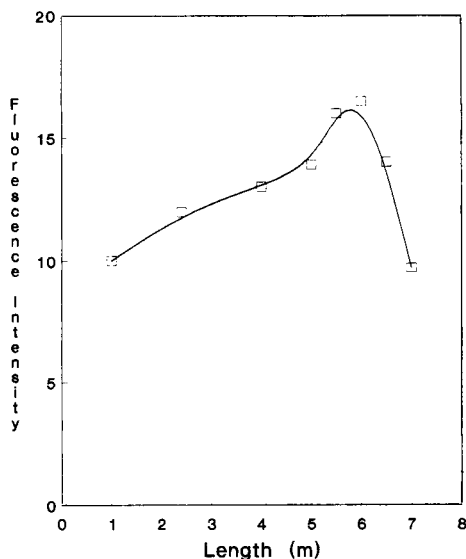


Fig. 4. Effect of reactor coil length on fluorescence intensity

$\text{min}^{-1}$  were chosen for the carrier, buffer and ERB channels, respectively.

#### Effect of injection volume

Different injection volumes were tested. The signal increased with increase in the volume injected but volumes above  $100 \mu\text{l}$  gave rise to very wide, and at times double, analytical peaks. The optimum injection volume chosen was  $100 \mu\text{l}$ .

TABLE 1

Study of interferences in the determination of  $5 \times 10^{-5}$  M fluoride

Cation	Concentration ( $\text{mg l}^{-1}$ )	Relative sensitivity (%) <sup>a</sup>	Anion	Concentration (M)	Relative sensitivity (%) <sup>a</sup>
Na(I)	250	100	$\text{Cl}^-$	$1 \times 10^{-2}$	100
K(I)	300	100	$\text{Br}^-$	$1 \times 10^{-2}$	100
Ca(II)	150	100	$\text{I}^-$	$5 \times 10^{-3}$	100
$\text{NH}_4^+$	0.1 M	100	$\text{NO}_3^-$	$3 \times 10^{-2}$	100
Ba(II)	0.5	100	$\text{ClO}_4^-$	$3 \times 10^{-2}$	100
Mg(II)	100	100	$\text{SO}_4^{2-}$	$1 \times 10^{-3}$	100
Cd(II)	1	100	$\text{PO}_4^{3-}$	$5 \times 10^{-6}$	100
Pb(II)	1	100		$1 \times 10^{-5}$	81
Co(II)	1	100	$\text{CO}_3^{2-}$	$5 \times 10^{-3}$	100
Zn(II), Ni(II), Cu(II)	1	100	Acetate	$1 \times 10^{-2}$	100
	10	85			
Cr(III)	0.01	100			
Fe(III)	0.1	100			
	1	91			

<sup>a</sup> Expressed as the ratio of the fluoride signal in the presence of interference to that of fluoride alone.

#### Analytical characteristics

The calibration graph obtained was linear over the range  $1 \times 10^{-6}$ – $2 \times 10^{-4}$  M. At fluoride concentrations above  $10^{-3}$  M the fluorescence signal decreased because of the predominance of the quenching effect of fluoride on the fluorescent complex.

The method is very sensitive, with a detection limit of  $10 \text{ ng ml}^{-1}$ . The precision, expressed as the relative standard deviation evaluated from ten independent determinations at the  $5 \times 10^{-5}$  and  $1 \times 10^{-4}$  M levels, was 7% and 4%, respectively.

Several species that could potentially interfere in the determination of  $5 \times 10^{-5}$  M fluoride were examined (Table 1). The presence of certain heavy metal cations reduced the analytical signal but only at concentrations higher than those usually found in tap and mineral waters. The most severe interference was caused by Fe(III). The anion that interfered most seriously was phosphate, which acted by complexing Al(III).

The method allowed the determination of 20 samples per hour.

#### Water analysis

The proposed method was applied to the determination of fluoride in different tap and min-

TABLE 2

Determination of fluoride in tap and mineral water samples

Sample	F <sup>-</sup> added (10 <sup>-5</sup> M)	F <sup>-</sup> found <sup>a</sup> (10 <sup>-5</sup> M)	Recovery (%)	Fluoride ISE (10 <sup>-5</sup> M)
Tap water 1	0	2.05 ± 0.08		2.4 ± 0.3
	2.5	4.82 ± 0.06	106	
	5.0	6.56 ± 0.16	93	
Tap water 2	0	0.24 ± 0.08		0.3 ± 0.1
	1	1.26 ± 0.03	102	
	2	2.33 ± 0.03	104	
Mineral water 1	0	1.25 ± 0.07		1.6 ± 0.3
	2.5	3.76 ± 0.15	100	
	5.0	3.76 ± 0.24	101	
Mineral water 2	0	0.23 ± 0.08		0.3 ± 0.1
	1	1.19 ± 0.03	97	
	2	2.19 ± 0.02	98	

<sup>a</sup> Mean ± standard deviation (*n* = 10).

eral waters. The performance of the method was evaluated by recovery studies (adding known amounts of fluoride to the samples) and also by analysing the same samples with a fluoride-selective electrode. The average recovery was 100%. The results of ten independent determinations are given in Table 2; there are no significant differences at the 95% confidence level.

### Conclusions

The proposed method allows the rapid spectrofluorimetric determination of fluoride. The analytical performance of the proposed method, i.e., sensitivity, precision, simplicity and linear calibration range, is better than that previously reported. Other important advantages are the large number of samples that can be processed (up to 20 h<sup>-1</sup>) and the suitability for complete automation in routine analysis.

This method is easy to use and offers a wider calibration range than the MAS method and is

more convenient than the use of a ISE for the determination of low fluoride concentrations.

The authors thank the DCICYT for financial support under Project No. 88/0094 and Max Gormann for revising the manuscript.

### REFERENCES

- 1 W. Frenzel and P. Brätter, *Anal. Chim. Acta*, 185 (1986) 127; 187 (1986) 1; 188 (1986) 151.
- 2 M. Gómez, M.A. Palacios and C. Cámara, *Analyst*, 113 (1988) 1109.
- 3 M. Hanocq and L. Molle, *Anal. Chim. Acta*, 40 (1968) 13.
- 4 T.L. Har and T.S. West, *Anal. Chem.*, 43 (1971) 136.
- 5 K. Toda, I. Sanemas and T. Deguchi, *Bunseki Kagaku*, 34 (1985) 297.
- 6 Danhua Chen, M.D. Luque de Castro and M. Valcarcel, *Anal. Chim. Acta*, 230 (1990) 137.
- 7 M.E. Leon-González, M.J. Santos-Delgado and L.M. Polo-Diez, *Anal. Chim. Acta*, 219 (1989) 329.
- 8 F. Carrillo, C. Pérez-Conde and C. Cámara, *Anal. Chim. Acta*, 243 (1991) 121.

# Detecting errors in micro and trace analysis by using statistics

K. Heydorn

*Isotope Division, Risø National Laboratory, DK-4000 Roskilde (Denmark)*

(Received 10th September 1992)

## Abstract

By assigning a standard deviation to each step in an analytical method it is possible to predict the standard deviation of each analytical result obtained by this method. If the actual variability of replicate analytical results agrees with the expected, the analytical method is said to be in statistical control. Significant deviations between analytical results from different laboratories reveal the presence of systematic errors, and agreement between different laboratories indicate the absence of systematic errors. This statistical approach, referred to as the analysis of precision, was applied to results for chlorine in freshwater from BCR certification analyses by highly competent analytical laboratories in the EC. Titration showed systematic errors of several percent, while radiochemical neutron activation analysis produced results without detectable bias.

*Keywords:* Analysis of precision; Error detection; Standard deviation prediction

Far-reaching conclusions and important decisions are made every day based on analytical results. It is the responsibility of the analytical chemist to ascertain that analytical results are of impeccable quality, which means that (a) their uncertainty is accurately known; (b) their bias is negligible; and that there is no significant risk of extracting misleading information; this also means that the analytical chemist should refrain from analyzing samples without knowing their past history!

As a consequence, most laboratories have introduced internal quality assurance as a tool to maintain the quality of their analyses, and many participate in external intercalibration schemes to ascertain measurement compatibility within a specified organisational, geographical, or methodological area.

*Correspondence to:* K. Heydorn, Isotope Division, Risø National Laboratory, DK-4000 Roskilde (Denmark).

Nevertheless, when intercomparisons are made between different organisations in different countries using different analytical methods, differences are frequently observed that could not be attributed to known or suspected analytical errors. Such differences were traditionally referred to as systematic errors, implying that they could not be dealt with by statistical methods.

This in time led to abandoning the concept of a true value in favour of democracy in analysis: all analyses are equal, they just have different, but unknown, biases. Therefore, the most popular value is the consensus value, one that minimizes the average bias.

Although consensus values may be very useful, they have no scientific basis, and with the growing realization that there is no fundamental difference between random and systematic errors [1], both types of error can be detected and controlled by statistical methods.

This will in time make it possible to identify analyses with the smallest absolute bias, and to

discard the others. Science is basically not democratic.

#### ANALYSIS OF PRECISION

The key to detecting systematic errors by means of statistical methods is to carry out the analysis of precision until statistical control has been achieved [2].

An analytical method consists of a large number of unit operations each carried out according to a prescribed procedure. Many of these procedures are common to many other methods of analysis used in the same laboratory, others are common to many different laboratories using the same equipment or apparatus.

All such unit processes contribute to the uncertainty of the analytical result, and their individual contribution  $\sigma_p$  can be determined experimentally or may be known from experience.

Therefore, using the law of error propagation we can predict the uncertainty  $\hat{\sigma}$  of a result  $y$  of an analytical method from a description of the method, even before we have made any analyses,

$$\hat{\sigma}^2 = \sum_1^p \left( \frac{\delta y}{\delta x_i} \right)^2 \hat{\sigma}_{x_i}^2 \quad (1)$$

By pooling errors of the same type we can express  $\hat{\sigma}^2$  as a combination of absolute, relative, and counting errors

$$\hat{\sigma}^2 = \sigma_a^2 + y^2 \sigma_r^2 + \sigma_c^2 \quad (2)$$

Equation 2 is a property of the analytical method and is often referred to as its a priori precision [3].

The a posteriori precision is experimentally determined after replicate analysis of  $i$  samples of a homogeneous material

$$s^2 = \sum_1^n \frac{(y_i - \bar{y})^2}{n-1} \quad (3)$$

Agreement between a priori and a posteriori precision signals that the method and its results

are in a state of statistical control; this is tested by calculating the statistic  $T$

$$T = \sum_1^n (y_i - \hat{\mu})^2 / \hat{\sigma}_i^2 \quad (4)$$

where

$$\hat{\mu} = \sum_1^n \frac{y_i}{\hat{\sigma}_i^2} / \sum_1^n \frac{1}{\hat{\sigma}_i^2}$$

is the weighted mean. If there is no significant difference between the expected (a priori) and the actual (a posteriori) standard deviations the statistic  $T$  is closely approximated by a chi-square distribution with  $n - 1$  degrees of freedom (d.f.). Significant deviations from this distribution show that there is disagreement between the sources of variability that are expected to influence the result according to Eqn. 1 and the observed variability.

The process of identifying the sources and magnitudes of variability that influence the actual analytical results is called the analysis of precision [4].

Most applications of the analysis of precision are found in neutron activation analysis, where the last term in Eqn. 2 assumes particular importance.

Many types of systematic error have been detected in this way and later identified and eliminated or quantified: sample contamination [3], calibration errors [5], erroneous blank values [6], interference [7,8], sample heterogeneity [9,10], sample interchange [4], inadequate computer programs [11,12] etc. [13].

#### TRACE ANALYSIS OF FRESHWATER REFERENCE MATERIAL

In a recent certification programme under the auspices of the European Community Bureau of Reference [14] we determined chlorine in two different batches of freshwater by radiochemical neutron activation analysis (RNAA).



### Experimental

Approximately 2 cm<sup>3</sup> of sample were weighed into a 2-dram polyethylene vial, which was heat-sealed, and irradiated for 100–200 s at a neutron flux density of  $2.5 \times 10^{13}$  n cm<sup>-2</sup> s<sup>-1</sup> together with an exactly similar comparator standard with a known concentration of approximately 200 μg g<sup>-1</sup>.

After rinsing the exterior with water the sample vial was cut open, and 5 mg Cl carrier in 0.2 cm<sup>3</sup> of solution was added together with 60 mm<sup>3</sup> of HNO<sub>3</sub>. After equilibration for 15 min in a water bath at 60°C, AgCl was precipitated by adding 30 mg of AgNO<sub>3</sub> in 0.25 cm<sup>3</sup> of aqueous solution.

After another 5 min the sample vial was cooled by immersion in cold water and centrifuged; the supernatant was then discarded. The AgCl precipitate was dissolved in 0.4 cm<sup>3</sup> of concentrated ammonia solution and transferred to another polyethylene vial to which was added 1 cm<sup>3</sup> of 1 M HNO<sub>3</sub> and 0.5 cm<sup>3</sup> of H<sub>2</sub>O used for washing the irradiated sample vial.

After heat-sealing, the sample and comparator were counted for 10–15 min at 10 cm from a germanium semiconductor detector, and the 1642 keV photopeak areas were calculated by a method known to be in statistical control [11].

The chemical yield was determined by re-irradiation of the sample together with a comparator of pure water to which was added the exactly same amount of carrier; actual yields averaged 97%.

### A priori precision

The standard deviation  $\hat{\sigma}$  of a single analytical result is now estimated from the standard deviations of all the parameters known or expected to influence the analytical result in accordance with Eqn. 1.

Since RNAA is characterized by the absence of reagent blanks we may disregard absolute sources of error and eliminate  $\sigma_a^2$  from Eqn. 2. The a priori precision is therefore determined only by the coefficients of variation,  $\sigma_r$ , of the relevant parameters listed in Table 1.

The quantities of sample and comparator are determined using an ordinary analytical balance,

TABLE 1

Parameters affecting the analytical results for chlorine determined by radiochemical neutron activation analysis

Parameter	Mean	$\hat{\sigma}_p$	$\hat{\sigma}_r(\%)$
Sample weight	2 g	0.2 mg	
Comparator	2 g	0.2 mg	
Concentration	0.2 mg g <sup>-1</sup>	–	< 0.5
Half-life	$\tau = 37.24$ min	0.05 min	
Fluence rate	$2.5 \times 10^{13}$ n cm <sup>-2</sup> s <sup>-1</sup>	–	2.3
Decay corr.	$t_1 - t_2 = 40$ min	0.1 min	
Carrier	0.2 cm <sup>3</sup>	0.6 mm <sup>3</sup>	
Peak area	> 22000 counts	≈ 150 counts	< 0.7

which yields a relative precision of the order of 0.01%. This is probably insignificant compared with the uncertainty of the concentration of Cl in the comparator standard, which was prepared by dissolving a weighed amount of NH<sub>4</sub>Cl (Merck, 99.8%) in water.

The sample and comparator are irradiated together, so that there is no influence from irradiation time; but then the two of them cannot also be irradiated at the same position, which gives rise to a difference in fluence rate during irradiation. This would traditionally be referred to as a systematic error, but since the orientation of the irradiation container in the reactor during irradiation cannot be controlled, its contribution to the uncertainty of the results is exactly the same as for a random error. The standard deviation of this randomized difference between the fluence rates has been estimated both by experiment and by calculation [6].

Sample and comparator have the same volume and are counted in identical counting geometry by the same detector and counting system; these parameters therefore do not contribute to the uncertainty of the final results. However, then the sample and comparator cannot be counted at the same time, and therefore they have individual decay correction factors,  $e^{\lambda t_1}$  and  $e^{\lambda t_2}$ . The analytical result depends upon the ratio  $f$  of the decay correction factors

$$f = e^{\lambda(t_1 - t_2)}$$

Their contributions to the uncertainty are now calculated according to Eqn. (1)

$$\begin{aligned}\hat{\sigma}_r^2 &= \hat{\sigma}_f^2 / f^2 = \hat{\sigma}_{\ln f}^2 \\ &= \hat{\sigma}_{\ln f}^2 = \left[ \frac{\delta \ln f}{\delta \tau} \right]^2 \hat{\sigma}_\tau^2 + \left[ \frac{\delta \ln f}{\delta t} \right]^2 (\hat{\sigma}_{t_1}^2 + \hat{\sigma}_{t_2}^2) \\ &= \lambda^2 \left[ \left( \frac{t_1 - t_2}{\tau} \right)^2 \hat{\sigma}_\tau^2 + \sigma_{t_1}^2 + \hat{\sigma}_{t_2}^2 \right]\end{aligned}$$

Using values listed in Table 1 and with  $\lambda \cdot \tau = \ln 2$  we find  $\hat{\sigma}_r = 0.3\%$ .

The standard deviation of the analytical result is now obtained by combining the a priori relative standard deviation with the counting statistics according to Eqn. 2

$$\begin{aligned}\hat{\sigma}_r^2 &= \hat{\sigma}_{\text{sample}}^2 + \hat{\sigma}_{\text{comparator}}^2 \\ \sigma_r^2 &= (0.01^2 + 0.01^2 + 0.5^2 + 2.3^2 \\ &\quad + 2.3^2 + 0.3^2) \%^2 \\ \sigma_r &= 3.3\% \quad \hat{\sigma}_c = 0.7\% \\ \hat{\sigma} &= 3.4\%\end{aligned}$$

Results are presented in Table 2 together with the analysis of precision according to Eqn. 4. For the analytical method we obtain a total of  $T = 10.42$  for 8 degrees of freedom, corresponding to a probability  $P(\chi^2 \geq T)$  of 0.24. Thus, both high and low concentrations of Cl give results in statis-

TABLE 2

Analytical results for the determination of chlorine in BCR freshwater reference materials

Sample No. bottle	Result (mg kg <sup>-1</sup> ± S.D.)	Sample No. bottle	Result (mg kg <sup>-1</sup> ± S.D.)
398/007	9.91 ± 0.34	399/024	46.46 ± 1.56
398/007	10.24 ± 0.35	399/024	47.91 ± 1.61
398/186	10.06 ± 0.34	399/202	48.16 ± 1.61
398/186	10.55 ± 0.36	399/202	50.86 ± 1.71
398/186	9.40 ± 0.32	399/202	47.24 ± 1.61
398/mean	10.00 ± 0.15	399/mean	48.04 ± 0.72
<i>T</i>	6.42	<i>T</i>	4.00
d.f.	4	d.f.	4
Yield corrected	10.31 ± 0.19	Yield corrected	49.53 ± 0.92

TABLE 3

Results for chlorine from certification analyses of BCR freshwater reference materials

Lab. No., method	CRM 398		CRM 399	
	mg kg <sup>-1</sup>	$\hat{\sigma}$	mg kg <sup>-1</sup>	$\hat{\sigma}$
12, RNAA	10.31	0.19	49.53	0.92
06, INAA	9.78	0.17	50.25	0.84
01, TITR	10.64	0.10	50.02	0.10
03, TITR	10.59	0.10	51.34	0.10
07, TITR	9.98	0.10	49.62	0.10
11, TITR	9.25	0.10	–	–
14, TITR	10.52	0.11	50.50	0.11

tical control, which means that there is no significant difference in the chemical yields.

For the yield determination the addition of carrier has an expected standard deviation of 0.3%, and the overall standard deviation is expected to be

$$\begin{aligned}\sigma_r^2 &= (0.3^2 + 0.3^2 + 2.3^2 + 2.3^2 + 0.3^2) \%^2 \\ \sigma_r &= 3.3\% \quad \hat{\sigma}_c \approx 0.7\% \\ \hat{\sigma} &= 3.4\%\end{aligned}$$

Results for yield determinations were also in statistical control with  $T = 5.16$  for 9 degrees of freedom; the mean values in Table 2 are therefore corrected for a mean yield of  $97.0 \pm 1.0\%$ .

TABLE 4

Verification of results for chlorine by RNAA in BCR freshwater reference materials

Sample type	Nominal (mg kg <sup>-1</sup> )	Laboratory No.	Ratio ± S.D.
CRM 398 low level	10	06	0.978 ± 0.017
		12	1.031 ± 0.019
CRM 399 high level	50	06	1.005 ± 0.017
		12	0.991 ± 0.018
Weighted mean			1.000 ± 0.009
<i>T</i>			4.61
Degrees of freedom			3
$P(\chi^2 > T)$			> 0.20

## DISCUSSION

These results and those of other laboratories participating in this certification are listed in Table 3; for these others, however, the a priori precision is unavailable and has to be estimated from the measured, individual data.

For laboratory 06 we assume that the precision of an individual result is the same as for our own results; this is consistent with the actual variability of their results, which yield a value of  $T = 9.27$  at 10 degrees of freedom. With 6 instead of 5 replicates the  $\hat{\sigma}$  of the mean is reduced by approximately 10%.

Unknown to participants, the BCR had prepared the fresh-water solutions with nominal concentrations of 10 mg/kg and 50 mg kg<sup>-1</sup>. Results in statistical control can thus be compared with the nominal values as previously proposed [8]. Results by RNAA in Table 4 confirm that this analytical method is without bias when all sources of variability are in statistical control.

For laboratories doing titrations (TITR) we find that the sample variances for the results by laboratories 01, 03, 07 and 11 are not significantly different (the critical value for Hartley's test at  $\alpha = 0.05$  is 33.6) with a maximum  $F$ -value of 9.2 for 7 sets of quintuplicate results. The estimated precision of titration is therefore taken as the

square root of the average variance, which is applied to all laboratories including laboratory 14 which contributed only 4 results.

With  $T > 300$  for 7 degrees of freedom as calculated by Eqn. 4 titration is beyond any reasonable control, and results are affected by highly significant systematic errors. Their magnitude can be estimated by the techniques described by Lyons [15], based on the minimization of  $\chi^2$ . In the present case where the systematic errors dominate statistical ones we calculate a simple mean and variance for each concentration, and after subtracting the small variance contribution from random variations we find no significant difference between variances at the two levels. The pooled variance for 7 degrees of freedom is 0.4241 corresponding to a standard deviation of 0.65 mg kg<sup>-1</sup> for the systematic contribution.

Quality assurance of the titration method is now carried out in the same way as for RNAA and results are shown in Table 5. This confirms the underlying assumption that the systematic errors follow a normal distribution with zero mean and variance independent of concentration.

The identification of the sources of systematic error requires detailed knowledge of the individual steps of each analyses, and their contributions to the a priori precision can be determined by means of the analysis of precision.

TABLE 5

Verification of results for chlorine by titration in BCR fresh-water reference materials

Sample type	Nominal (mg kg <sup>-1</sup> )	Laboratory No.	Ratio $\pm$ S.D.
CRM 398 low level	10	01	1.064 $\pm$ 0.066
		03	1.059 $\pm$ 0.066
		07	0.998 $\pm$ 0.066
		11	0.925 $\pm$ 0.066
		14	1.052 $\pm$ 0.066
CRM 399 high level	50	01	1.000 $\pm$ 0.013
		03	1.027 $\pm$ 0.013
		07	0.992 $\pm$ 0.013
		14	1.008 $\pm$ 0.013
Weighted mean			1.007 $\pm$ 0.006
$T$			7.39
Degrees of freedom			8
$P(\chi^2 > T)$			0.50

## Conclusions

Results in statistical control were found to be unbiased, while results not in statistical control were subject to systematic errors that were large compared with the reproducibility of the analyses.

This means that for laboratories relying on titrations, requirements (a) and (b), as mentioned in the introductory part, are not fulfilled, and there is a significant risk of drawing misleading conclusions from results obtained by this method.

However, if the systematic errors observed are accounted for by achieving statistical control, no such risk remains, and titration can yield unbiased results and qualify as a reference method with better precision than NAA at the 50 mg kg<sup>-1</sup> level.

REFERENCES

- 1 P. Giacomo, *Metrologia*, 17 (1981) 73.
- 2 K. Heydorn and K. Nørgaard, *Talanta*, 20 (1973) 835.
- 3 K. Heydorn, *Natl. Bur. Stand. Special Publ.* 422 (1976) 127.
- 4 K. Heydorn, in *International Symposium on the Development of Nuclear-based Techniques for the Measurement, Detection, and Control of Environmental Pollutants*, Vienna 15–19 March 1976, IAEA STI/PUB/432, 1976, p. 61.
- 5 K. Heydorn, *Mikrochim. Acta (Wien)*, III (1991) 1.
- 6 K. Heydorn, *Aspects of Precision and Accuracy in Neutron Activation Analysis*, Risø Report No. 419, Risø National Laboratory, Roskilde, 1980.
- 7 L.H. Christensen and K. Heydorn, *J. Radioanal. Nucl. Chem.*, 113 (1987) 19.
- 8 L.H. Christensen and K. Heydorn, *Nucl. Instrum. Methods*, A299 (1990) 562.
- 9 K. Heydorn, E. Damsgaard and B. Rietz, *Anal. Chem.*, 52 (1980) 1045.
- 10 K. Heydorn and E. Damsgaard, *J. Radioanal. Nucl. Chem.*, 110 (1987) 539.
- 11 K. Heydorn, in *Computers in Activation Analysis and Gamma-Ray Spectroscopy*, U.S. Dept. Energy, Symposium Series, 49 (1979) 85.
- 12 K. Heydorn, in *Proceedings of the 5th International Conference on Nuclear Methods in Environmental and Energy Research*, U.S. Dept. Energy, CONF-840408, 1985, p. 620.
- 13 K. Heydorn, *Neutron Activation Analysis for Clinical Trace Element Research Vols. 1 and 2*, CRC Press, Boca Raton, FL, 1984.
- 14 P. Quevauviller, K. Vercoutere, D. Bousfield and B. Griepink, *The certification of the contents (mass fractions) of Al, Ca, Cl, Fe, K, Mg, Mn, Na, P and S in freshwater*, Community Bureau of Reference, EUR 14062 (1992) 64 pp.
- 15 L. Lyons, *J. Phys. A: Math. Gen.*, 25 (1992) 1967.

# Fuzzy logic for spectra interpretation

Matthias Otto

*Department of Chemistry, Bergakademie Freiberg, Institute of Analytical Chemistry, Leipziger Strasse 29, D-O-9200 Freiberg (Germany)*

(Received 10th September 1992; revised manuscript received 11th February 1993)

## Abstract

Problems with conventional spectra interpretation systems based on either statistical or knowledge-based approaches are discussed and possibilities for circumventing them by means of fuzzy systems are outlined.

**Keywords:** Atomic emission spectrometry; X-ray fluorescence spectrometry; Fuzzy logic; Spectra interpretation

The interpretation of atomic and molecular spectra has been automated by means of several tools at varying performance levels. In atomic spectrometry, such as x-ray fluorescence or atomic emission spectrometry, spectra interpretation has been often limited to library searching methods where the presence of an element is deduced from comparison of the measured atomic lines with the tabulated lines in a related spectral library. More recent approaches exploit the feasibilities of rule-based expert systems, e.g., for interpretation of energy-dispersive x-ray fluorescence (EDXRF) spectra with a Pascal-based computer system [1].

In molecular spectrometry, more advanced systems based on artificial intelligence (AI) tools have been developed since the mid-1970s, the prototype being the DENDRAL interpretation system for organic mass spectrometry [2], which was the first application of AI for solving a real practical problem.

*Correspondence to:* M. Otto, Department of Chemistry, Bergakademie Freiberg, Leipziger Strasse 29, D-O-9200 Freiberg (Germany).

## METHODS FOR SPECTRA INTERPRETATION

The methods used for spectra interpretation can be summarized as follows.

### *Statistical approach*

Grouping of spectra of one element or of similar structural features by cluster analysis, conventional projection and related methods, such as principal components analysis (PCA) and unsupervised neural network models [3]. Classification of unknown spectra is then performed by determining a classification line around the found clusters or by means of supervised pattern recognition methods, e.g., linear discriminant analysis, SIMCA or the KNN method.

Recent examples of this multivariate statistical approach are the application of PCA for the identification of molecular structures from vapour-phase infrared spectra [4], the use of cluster and factor analysis for grouping inductively coupled plasma (ICP) optical emission spectra [5] and the application of neural networks to interpret organic mass spectra [6].

### *Knowledge-based systems*

The use of rules and knowledge bases for spectra interpretation approaches human action

more closely. The interpretation rules can be derived either by experts' knowledge or by methods of machine learning. For example, in IR spectrometry both approaches have been explored from several perspectives. Interpretation systems based on expert's knowledge were developed by Sasaki et al. [7] with CHEMICS and Tomellini et al. [8] with PAIRS.

Systems that use machine learning techniques are known for the method of inductive inference with the Iterative Dichotomizer 3 (ID3) [9], for the exploitation of Bayesian conditional probabilities [10] or for rule generation based on frequency distributions of functionalities [11].

In elemental analysis, the above mentioned EDXRF interpretation system [1] is an example of an automated human-like interpretation system.

General problems with these approaches were found with respect to the following aspects.

#### *Discretization problem*

In the case of statistical procedures, the spectrum has to be ascribed to a vector of fixed length. If the whole spectrum is used for cluster analysis or pattern recognition methods, the digitization rate can be chosen as narrow as possible with respect to the computer system used.

With rule-based systems, however, the spectral feature in the form of a line position or its intensity has to be attributed to a predefined spectral or intensity interval. Thus, in IR spectrometry a fixed interval of  $3100\text{--}3000\text{ cm}^{-1}$  means that a line at  $3001\text{ cm}^{-1}$  is assumed to lie in this interval but a line at  $2999\text{ cm}^{-1}$  would not be assigned to that interval. Interval boundaries are sharp or crisp in the algorithms whereas a human interpreter would work with flexible boundaries.

#### *Decision problem*

Decisions are usually based on exact criteria, such as in atomic emission spectrometry, e.g., an element is present if two prominent lines can be detected. What about further prominent lines or additional non-prominent lines? A more general rule would state that at least two prominent lines should be found in the spectrum and additional

lines will ensure to some extent the existence of a certain element.

#### *Knowledge representation problem*

Human spectra interpretation even works if vague knowledge is to be processed. For example, in XRF spectrometry the intensity ratio of  $K\alpha$  and  $K\beta$  lines should be "about 5" and nobody expects it to be exactly 5:1. Of course, conventionally one could describe this situation again with an interval, say an intensity ratio between 4 and 6. This, however, is not very human-like, because a human expert values the distance of the found ratio from the expected value of 5 by terms such as "very near to 5" or "rather far from 5".

With symbolic knowledge interpretation, there is another problem. Reasoning is confined to symbols that have been defined once in the expert system. In other words, interpolation between symbols is not feasible. For example, if in a symbolic system the colours "blue" and "green" are stored and a query about "greenish" is presented to the system, it will not match either "blue" nor "green". Interpolative reasoning, however, is one of the very important features of human-like knowledge processing. In spectroscopy the same might happen if the intensity of a given line is expected to be "low" or "high" and then in practice a "medium" intensity is found.

#### *Knowledge acquisition problem*

Machine learning can be carried out by both numerical statistical methods and symbolic knowledge processing. Up to now, however, these two approaches have been used alternatively and not supplementarily. Hence methods are needed that will enable symbolic and numerical knowledge to be acquired simultaneously with the same general approach.

The approach to solving the above general problems may be based on fuzzy systems. The basic idea of fuzzy logic was introduced by Zadeh [12] in 1965 with a paper entitled "fuzzy sets". Since then this theory has been mainly used in industrial control but other areas such as expert systems and fuzzy data analysis has become in-

creasingly important. In chemistry, the first application was related to library searching in the infrared spectral range in 1984 by Blaffert [13]. The basic notions of fuzzy set theory have been presented [14,15]. Several implementations in connection with spectra interpretation systems are known. These applications will be considered in detail in this paper together with recent developments in the author's laboratory.

#### FUZZY KNOWLEDGE REPRESENTATION

Fuzzy set theory was developed in order to represent uncertain knowledge. In general, there are different kinds of uncertainty. If we characterize the selectivity of a spectroscopic system as being rather selective, then this kind of uncertainty is *lack of specificity*. We do not have the exact value for the resolution of the bands and, therefore, we are able to characterize the selectivity only roughly by a broad category that is a member of some set. The uncertainty about the outcome of an analytical experiment, e.g., a parallel spectrophotometric determination of nickel, is a kind of variability that is usually interpreted by *randomness*. A third kind of uncertainty is *fuzziness*, which is to be ascribed to situations where no crisp distinction between a concept and its negation can be made. For example, the intensity of a spectroscopic line being "strong" or "not strong (weak)" is a typical concept of this kind. Between "strong" and "weak" exists an overlapping range where lines belong to both concepts (Fig. 1).

In other words, fuzziness models the uncertainty about what is meant. In spectroscopy,

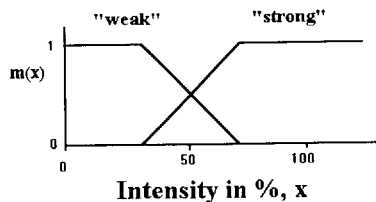


Fig. 1. Overlapping membership functions "weak" and "strong" characterizing the intensity of a spectral line.

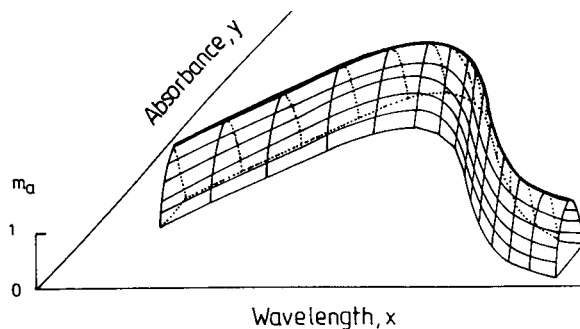


Fig. 2. A fuzzy function representing the uncertainty of a UV absorption spectrum.

fuzziness is not due to measuring or other errors but to physical or chemical reasons. The shape of a UV spectrum depends on the actual solvent composition and the exact position of an IR band results from the vibrational combination of all substructures present in the molecule. With the use of fuzzy set theory it is not intended to level out such kinds of uncertainty, e.g., by averaging over intensities or by defining crisp intervals for a line position, but one tries to describe this uncertainty as closely as possible by a mathematical function, the so-called membership function.

In classical set theory, the membership function is confined to two values only, i.e. 1 and 0. A membership value of 1 is assigned to all elements that are contained in the considered subset,  $A$ , of the universe  $X$ . Membership values of 0 are assigned to all elements that are not member of the set  $A$ :

$$m(x) = \begin{cases} 1 & \text{if } x \in A \subseteq X \\ 0 & \text{if } x \notin A \subseteq X \end{cases} \quad (1)$$

Fuzzy set theory comprises the concept of gradual membership to a set. Thus, the membership function,  $m(x)$ , can represent any monotonous

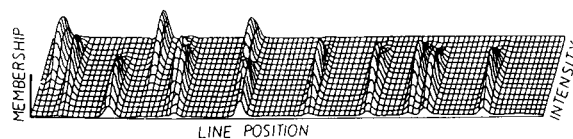


Fig. 3. Example of a two-dimensional membership function for line position and line intensity taken from IR spectrometry [13].

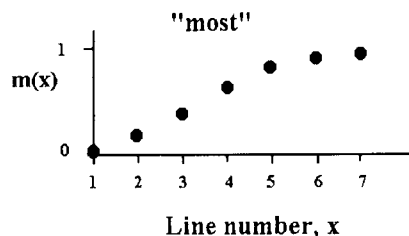


Fig. 4. Membership function for "most" detected lines in atomic emission spectrometry.

increasing or decreasing function. Examples are given in Figs. 1–4.

#### *Uncertainty about the spectra*

The spectral information can be used either as the appropriately preprocessed full spectrum or in the form of a line table. To describe the uncertainty of the full spectrum, the measured intensities are considered as fuzzy numbers at every wavelength or energy value. The degree of uncertainty might vary from wavelength to wavelength, i.e., varying distributions of the membership functions along the wavelength axis are realistic. Also, there are no restrictions with respect to the symmetry of the membership function over the intensity variable. The collection of all these fuzzy numbers can be considered then as a fuzzy function as depicted in Fig. 2.

If the spectrum is represented as a line table, which usually contains the line position, intensity and band width, the uncertainty can be represented as a fuzzy set. The membership function for a situation where line position and intensity are considered simultaneously is given in Fig. 3, i.e., a two-dimensional membership function is obtained.

#### *Fuzzy facts*

Apart from the primary spectral information, uncertain spectroscopic knowledge also has to be treated in connection with an interpretation system. In ICP atomic emission spectroscopy (AES), a typical fact could be: "most of the prominent lines of an element should be found". This statement implies that as many lines as detectable should be found in the spectrum.

A suitable membership function for "most" increases with increasing number of detected lines as given in Fig. 4. We use Yager's OWA (ordered weighted averaging) operator for specifying this kind of membership function. The mathematical details can be found in [16].

Sometimes the importance of a fact is expressed by a membership value in the sense of a Bayes or uncertainty value. Thus, the following rule has been derived in a spectrum interpretation system for ICP-OES [17]:

IF a peak at 228.802 nm indicates the presence of Cd

AND the sample has a peak at 228.802 nm to a membership value of 0.80

THEN the sample shows indications of the presence of Cd to a truth value of 0.75.

#### KNOWLEDGE PROCESSING

As a preliminary to spectrum interpretation, library searching is used to narrow the range of candidate molecules or elements. The search can be based on full spectra represented as fuzzy functions or on line tables that are described by fuzzy sets. Successful applications of fuzzy functions are known for spectral library searches in the UV range [18] and are further used for comparing depth profiles in materials analysis [19]. Comparing the candidate library spectrum with the sample spectrum is based on computing the difference spectrum by fuzzy subtraction. A similarity index is then deduced from integrating over the fuzzy difference function and normalizing the resulting number to the interval [0,1].

The fuzzy model for representing position, intensity or band width as fuzzy sets is the basis of existing library searching systems in the infrared spectral range, such as the SpecInfo System [20] or an expert system for wavelength-dispersive XRF (WDXRF) analysis [21]. Apart from the paper by Blaffert [13], however, the line position is used solely in those systems.

Spectra interpretation based on fuzzy reasoning can be based on several approaches. The basis for the different inference methods is the formulation of the appropriate rules. For exam-



ple, in IR spectrometry the following rules might be valid for the spectral range 1500–1700  $\text{cm}^{-1}$ :

IF Position = low THEN Substituent =  
secondary Amine  
IF Position = high THEN Substituent =  
primary Amine

In general, we consider spectra with variables  $V$  (here position) and  $U$  (here substituent) taking their values in the sets  $X$  and  $Y$ . Then, if  $A'$ ,  $A_1$ ,  $A_2, \dots, A_n$  and  $B'$ ,  $B_1, B_2, \dots, B_n$  are subsets in  $X$  and  $Y$ , respectively, the following general rules can be derived:

IF  $V = A_1$  THEN  $U = B_1$   
IF  $V = A_2$  THEN  $U = B_2$   
:  
IF  $V = A_n$  THEN  $U = B_n$  (2)

If we have the additional proposition

$V = A'$

we can reason about the unknown fuzzy set of  $U$ , i.e.,  $B'$ , by means of one of the different inference schemes. The propositions  $A'$  and  $B'$  represent the available information about the unknown compound.

The most common way is to use the compositional rule of inference introduced by Zadeh [12]. The IF–THEN rule is described by a fuzzy relation between the fuzzy sets  $A$  and  $B$  expressed by their membership functions:

$$M_{A \times B}(x, y) = \min\{m_A(x), m_B(y)\} \quad (3)$$

The compositional rule of inference provides the membership function for the consequence  $B'$  according to

$$m_{B'}(y) = \max \min\{m_{A'}(x), m_{A \times B}(x, y)\} \quad (4)$$

Of course, the inference would have to be performed with any of the rules previously defined. Finally, the results for the  $B_i$ s have to be aggregated, e.g., by calculating the minimum over all  $B_i$ s.

Although this inference rule is mainly used in fuzzy control, its application to spectral reasoning is straightforward.

A different reasoning scheme was introduced by Yager [22], likewise in the sense of approximate reasoning.

Based on the above implication statements (Eqns. 2), it is assumed that every implication induces a relation  $H(y)$  on the fuzzy relation  $X \times Y$  such that

$$\begin{aligned} H_1(y) &= \text{Poss}(\bar{A}_1 | A') \vee B_1(y) \\ H_2(y) &= \text{Poss}(\bar{A}_2 | A') \vee B_2(y) \\ &\vdots \\ H_n(y) &= \text{Poss}(\bar{A}_n | A') \vee B_n(y) \end{aligned} \quad (5)$$

with the complement  $\bar{A}(x) = 1 - A(x)$ , the possibility  $\text{Poss}(A | B) = \text{Max}[A(x) \wedge B(x)]$  and  $\vee = \text{AND}$ ,  $\wedge = \text{OR}$ .

Aggregation of the inferred values  $H_i(y)$  can be carried out by ANDing them according to

$$B' = H_1 \wedge H_2 \wedge \dots \wedge H_n \quad (6)$$

The advantages of Yager's scheme are its feasibility to apply default reasoning and its flexibility to choose freely the connectives AND and OR, conventionally min and max, respectively, as well as the aggregation operator in Eqn. 6.

The first steps in implementing fuzzy reasoning in spectra interpretation have been made in ICP-AES [17], in XRF [21] and in Elyashberg et al.'s IR interpretation system [23]. However, until now only simple inferences have been applied so that fuzzy knowledge processing remains one of the challenges for implementation in spectra interpretation systems.

#### RULE GENERATION BY NEURAL NETWORKS

In the beginning of the development of spectra interpretation systems, the rules were derived from experts' knowledge only. The same is true for specifying membership functions in fuzzy expert systems to account for the uncertainty in the sense of fuzziness. The sources for specifying those fuzzy sets were experience, subjective aspects and orientation on statistical material.

This strategy is successfully applied if one or two variables with one- or two-dimensional mem-

bership functions, respectively, are considered and if well defined systems are under study. With multi-dimensional membership functions the specification of membership functions is difficult. Also, in many situations, such as in IR spectrometry, explicitly known relationships between spectra and substructures are lacking. Therefore, current research is aimed at learning or at least tuning membership functions automatically by neural networks.

Neural networks are designed to imitate the parallel distributed processing in the brain. Although artificial neural networks are still far from brain-like functioning, the high degree of their complexity and the iterative nature of network training provide an additional powerful method in the field of machine learning.

To adjust membership functions in a fuzzy expert system several approaches already exist. An easily understandable method is based on Kosko's fuzzy associative memories or FAM's [24]. Every rule in Eqns. 2 is expressed by an individual FAM rule as given in Fig. 5. The antecedent  $A_i$  is interpreted now as the input to the neural net and the consequence  $B_i$  is the output of the neural network. Training of the different neural networks, which correspond to the different rules, by spectra-structure data adjusts the weights such that presentation of an unknown spectrum will recall the associated chemical structure. In order to arrive at fuzzy rules the input and output space are partitioned into overlapping fuzzy sets as given in Fig. 6. Similar input–output data will

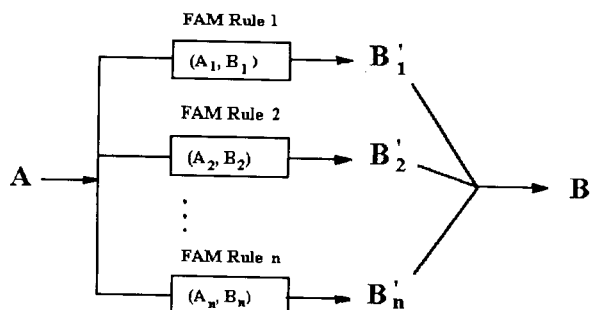


Fig. 5. Kosko's fuzzy associative memory (FAM). Reasoning about  $B$  is performed by input of the fuzzy set  $A$  to all rules and aggregating the result by a suitable operator, e.g., by computing the maximum.

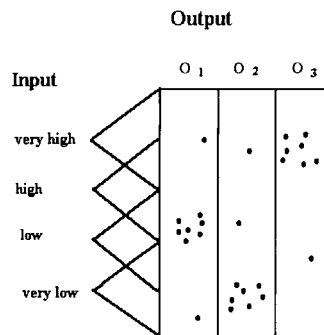


Fig. 6. In the FAM, fuzzy sets are specified for the input to the network. The output is assumed to be crisp. Data cluster correspond to rules.

now cluster in the different FAM cells providing the sought interpretation rules. FAM cells have already been used for rule generation in IR spectrometry. Limitations with this approach arise, however, from the simple linear relationship between input and output. The temptation to apply FAMs for spectroscopic rule generation lies in the availability of user friendly software, e.g., the TILGen program by Togai/Infra Logic.

A more complex approach for spectrometry is based on neural networks prewired with fuzzy rules. A rule as given above for a "high" or "low" position of a spectral line can be modelled by an input neuron that receives the actual line position, two neurons in a subsequent layer that model the fuzzy sets "high" and "low" by a sigmoid function, a third layer specifying the importance of a rule and the output layer representing the substructures in molecular spectrometry or the elements in atomic spectrometry. A network ex-

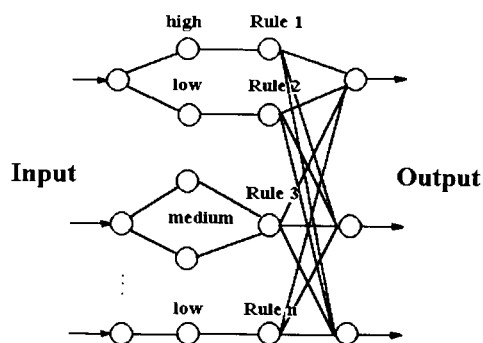


Fig. 7. Neural network prewired with fuzzy rules.

ample for several inputs corresponding to the interpretation of several lines simultaneously is depicted in Fig. 7.

With this kind of rule generation one can also imagine inputting the full spectrum rather than the line tables. The membership functions are then interpreted as the fuzzy numbers given in Fig. 2.

An application of prewired networks was presented recently by Wegscheider [25] for spectra interpretation in WDXRF based on line table information.

Another approach is based on approximating the fuzzy expert system by a neural network. In this application, a neuron does not represent an interval for a line position or an intensity range but several neurons describe the input of a fuzzy set to the neural network. Figure 8 outlines this network architecture graphically. The output might be crisp or fuzzy.

A typical application is known for IR spectrometry. The crisp input consists of 256 input neurons in the range between 3927 and 400  $\text{cm}^{-1}$ . Digitization was carried according to [26]:

$$i = 6.0(\bar{\nu})^{1/2} - 120.0$$

where  $\bar{\nu}$  = wavenumber. The spectral window ranges between 6.7  $\text{cm}^{-1}$  at low frequencies and about 21  $\text{cm}^{-1}$  at high frequencies.

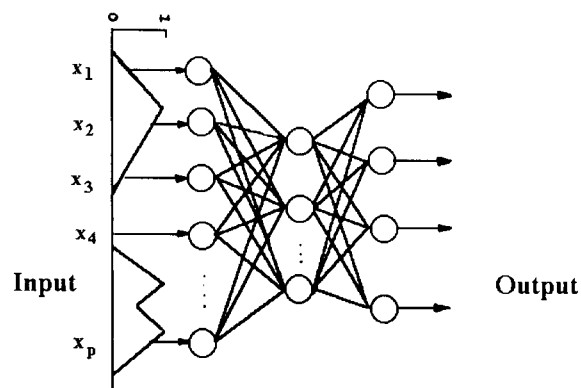


Fig. 8. Approximation of a fuzzy expert system by a neural network.

TABLE 1

Output of a neural network for substructure classification of IR spectra.

Output unit	Functionality	Averaged output value	
		Crisp input	Fuzzy input
1	OH/NH bond	0.66	0.74
2	Alcohol/phenol	0.49	0.52
3	Alcohol	0.58	0.56
4	Primary alcohol	0.37	0.40
5	Secondary alcohol	0.22	0.31
6	Amine	0.50	0.59
7	C=O	0.65	0.73
8	Ester	0.50	0.65
9	Ethyl ester	0.44	0.55
10	Aldehyde	0.25	0.41
11	Ketone	0.62	0.65
12	Amide	0.14	0.40
13	C=C	0.49	0.52
14	Vinyl group	0.51	0.57
15	Aromatic	0.93	0.92
16	C-O single bond	0.65	0.69
17	Ether/ester	0.33	0.42

For fuzzy spectra representation a trapezoidal type of fuzzy set was chosen with the following membership function:

$$m(\bar{\nu}) = \begin{cases} 1/20\bar{\nu} & \text{for } (z - 30) < \bar{\nu} < (z - 10) \\ 1 & \text{for } (z - 10) < \bar{\nu} < (z + 10) \\ 1 - 1/20 & \text{for } (z + 10) < \bar{\nu} < (z + 30) \\ 0 & \text{for } (z + 30) < \bar{\nu} < (z - 30) \end{cases}$$

where  $z$  is the line position as given in the line table.

In the spectral range from 4000 to 400  $\text{cm}^{-1}$  the number of input neurons was chosen to be 500. Up to 36 substructures were assigned to the output neurons representing the most common functionalities as given in the first application of neural networks for IR spectra interpretation by Robb and Munk [26]; 700 IR spectra from the SpecInfo database were trained with the back propagation algorithm and an additional 300 spectra were used as the test spectra. The classification ability was studied for recalling the test spectra and averaging over the individual output values that represent a certain functionality. In Table 1 some results are compared for crisp and fuzzy data input. Even if only the line position is

used as in the demonstrated example there is already an improvement by applying a fuzzy input to the network. If fuzzified intensities and line widths are additionally used the results can be further improved.

The authors thank the Bundesminister für Forschung und Technologie and the Deutsche Forschungsgemeinschaft for supporting this research.

#### REFERENCES

- 1 K. Janssens and P. Van Espen, *Anal. Chim. Acta*, 184 (1986) 117.
- 2 R.K. Lindsay, B.G. Buchanan, E.A. Feigenbaum and E.A. Lederberg, *Applications of Artificial Intelligence for Organic Chemistry – The Dendral Project*, McGraw-Hill, New York, 1980.
- 3 J. Zupan and J. Gasteiger, *Anal. Chim. Acta*, 248 (1991) 1.
- 4 E.J. Hasenoehrl, J.H. Perkins and P.R. Griffiths, *Anal. Chem.*, 64 (1992) 656.
- 5 D.F. Wirsz and M.W. Blades, *Anal. Chem.*, 58 (1986) 51.
- 6 B. Curry and D.E. Rumelhart, *Tetrahedron Comput. Methodol.*, 3 (1990) 213.
- 7 S. Sasaki, Y. Kudo, S. Ochiani and H. Abe, *Mikrochim. Acta*, (1971) 726.
- 8 S.A. Tomellini, R.A. Hartwick and H.B. Woodruff, *Appl. Spectrosc.*, 39 (1985) 331.
- 9 W.A. Schlieper, T.L. Isenhour and J.C. Marshall, *J. Chem. Inf. Comput. Sci.*, 28 (1988) 159.
- 10 H.J. Luinge, *Trends Anal. Chem.*, 9 (1990) 66.
- 11 M. Passlack and W. Bremser, in J. Zupan (Ed.), *Computer-Supported Spectroscopic Databases*, Horwood, Chichester, 1986, p. 93.
- 12 L.A. Zadeh, *Inf. Control*, 8 (1965) 338.
- 13 T. Blaffert, *Anal. Chim. Acta*, 161 (1984) 135.
- 14 H. Bandemer and M. Otto, *Mikrochim. Acta*, II (1986) 93.
- 15 M. Otto, *Chemometr. Intell. Lab. Syst.*, 4 (1988) 101.
- 16 C. Schierle, M. Otto and W. Wegscheider, *Fresenius' J. Anal. Chem.*, 343 (1992) 561.
- 17 R. Neuböck, W. Wegscheider and M. Otto, *Microchem. J.*, 45 (1992) 343.
- 18 M. Otto and H. Bandemer, *Anal. Chim. Acta*, 191 (1986) 193.
- 19 M. Otto, G. Stingeder, K. Piplits, M. Grasserbauer and M. Heinrich, *Mikrochim. Acta*, 106 (1992) 163.
- 20 W. Bremser, *Angew. Chem., Int. Ed. Engl.*, 27 (1988) 247.
- 21 T. George, *Dissertation*, Bergakademie Freiberg, Freiberg, 1992.
- 22 R.R. Yager, *Artif. Intell.*, 31 (1987) 99.
- 23 M.E. Elyashberg, V.V. Serov and L.A. Gribov, *Talanta*, 34 (1987) 21.
- 24 B. Kosko, *Neural Networks and Fuzzy Systems – a Dynamical Systems Approach to Machine Intelligence*, Prentice-Hall, London, 1992.
- 25 W. Wegscheider, paper presented at COMPANA '92, Jena, 24–27 August, 1992.
- 26 E.W. Robb and M.E. Munk, *Mikrochim. Acta*, (1990) 131.

# Non-linear modelling of chemical data by combinations of linear and neural net methods

Beata Walczak<sup>1</sup> and Wolfhard Wegscheider

*Institute of Analytical Chemistry, Micro- and Radiochemistry, Graz University of Technology, Technikerstrasse 4, A-8010 Graz (Austria)*

(Received 10th September 1992)

## Abstract

The combinations of classical bilinear models and neural nets, extended to neural net models on residuals from partial least squares (PLS) are discussed. The performances of principal component regression (PCR), PLS, neural networks (NN), principal component analysis (PCA)-NN and PLS residuals-NN are compared on simulated data, near-infrared data and quantitative structure-activity relationship data.

*Keywords:* Multivariate calibration; Neural networks; Non-linear modelling

A modelling technique that has attracted increasing interest in recent years is the artificial neural networks approach. Since Hopfield's work in 1982 [1], and particularly since Rumelhart and McClelland's popularization of the back-propagation algorithm in 1986 [2], intensive work has been done on the application of such a methodology to pattern recognition, process control, optimization and many other branches of engineering and scientific analysis. In the light of the hitherto successful applications, neural networks seem to be a most promising candidate for treating a large class of chemical problems, but in comparison with other fields the reports in the chemometrics literature are scarce [3–28]. A very broad spectrum of possible applications includes spectroscopy, chromatography, food, environmental and geochemistry, quantitative structure-activity

relationships (QSAR) studies, diagnosis and the control of chemical processes. In other words neural networks (NN) can be applied to many classification and multivariate calibration (quantitative structure-reactivity, structure-property, structure-activity and composition-property) problems. It has been demonstrated [10] that the use of direct connections in NN and principal component scores as input ensures that the NN performance is never worse than that obtained with principal component regression (PCR) [29], the standard linear methods. A major drawback for the application of NN to science problems appears to be the difficulty of interpreting the internal structure of a net in the light of the physical problem to be solved. In particular, the weights between synapses, the actual knowledge storage of a net, defies obvious interpretability.

The aim of this work was to study combinations of classical linear methods, such as PCR and partial least squares (PLS), with NN for chemical data sets with proved or suspected non-linearities. It is proposed that PLS can be supplemented in a second modelling step by a minimal

*Correspondence to:* W. Wegscheider, Institute of Analytical Chemistry, Micro- and Radiochemistry, Graz University of Technology, Technikerstrasse 4, A-8010 Graz (Austria).

<sup>1</sup> On leave from Silesian University, Katowice, Poland.

neural network if the data suggest the presence of non-linearities.

## NEURAL NETWORKS

Artificial neural networks (ANN) are mathematical algorithms, inspired by the current understanding of neurophysiology, that try to model the human brain and its ability to learn. It ought to be mentioned that the first significant attempt to explain the brain's enormous ability was made in 1943 by McCulloch and Pitts [30], and the basic learning theory comes from a book by Hebb [31] in 1949. In other words, ANN are the greatly simplified essence of the dendrites, axons, synapses and interconnects found in living systems. ANN can be considered as a group of interconnected nodes (neurons) forming a net, where every node receives a weighted input signal, through its inputs (synapses), from every node connected to it. The efficiency of signal transmission depends on the weights, which correspond to the strength of the synapses joining dendrites. The summation of all the input signals to the node (neuron body) excites it and up to a threshold makes the node (neuron) produce an output signal through its output (axon). If the input signal is too high, only a maximum output signal is produced.

ANN have ability to “learn” during a training process where they are presented with a sequence of stimuli and a set of expected responses. In ANN, learning means any change in a synapse.

Typical attributes of NN are [22] parallel processing, non-linear transfer, non-algorithmic processing, adaptation (learning), self-organization, generalization, fault tolerance, high connectivity, potential high speed and feedback paths.

One of the most popular NN is the feedforward net trained with the back-propagation learning algorithm [2]. The architecture of an NN, which consists of three layers of processing nodes, namely an input layer (LX), a hidden layer (LH) and an output layer (LY), is presented in Fig. 1.

The information processing in the three-layer network in Fig. 1 can be described in the follow-

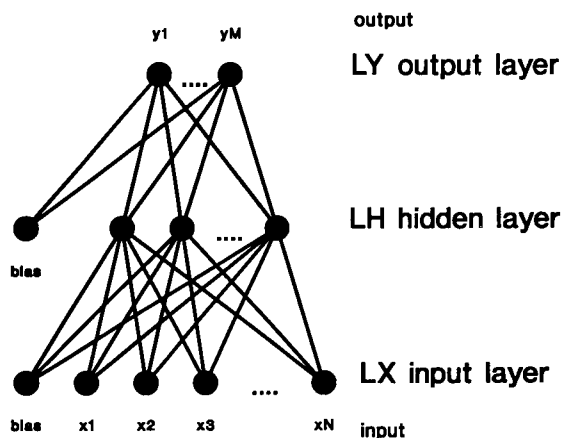


Fig. 1. The NN architecture.

ing manner. The input nodes serve as distributors of the input to the hidden-layer nodes. The network illustrated has only one hidden layer, although others may be used. The nodes in the hidden layer perform a weighted summation of the inputs followed by a non-linear transformation. The output nodes, which receive inputs from the hidden nodes, perform a weighted summation of these inputs. For classification hidden nodes, perform a weighted summation of these inputs. For classification purposes the output nodes can also perform a non-linear transformation, but for calibration purposes linear output nodes are usually applied. A neuron, which is connected to the hidden and output nodes, outputs a constant value of 1.0. This permits incorporation of non-zero intercepts into NN calibration.

The weights are the adjustable parameters altered by training. During the learning procedure, a series of input patterns with their corresponding expected output values are presented to the network in an iterative fashion while the weights are adjusted. Training can be performed by applying certain rules to the adaptation of the weights when a given input expects a certain output. The back-propagation training algorithm [2], which is equivalent to the steepest descent technique of function minimization, compares the actual and desired output of the NN and adjusts the weights of the network to decrease the output error in the direction of local downhill gradient.

Prior to the start of training, all of the weights in the network are set to random values. The weights between neural layers are modified recursively. The algorithm first modifies the weights between the output (LY) and the hidden (LH) layers, then uses this information to modify the weights between the hidden (LH) and the input layers (LX).

The training is usually stopped before the NN reaches the minimum error on the calibration set, because this is one way to avoid overfitting, which results in a loss of generality, leading to greater prediction error for the test data. By stopping the training before NN reaches equilibrium one can prevent it from fitting the details of the training data set (to model random noise specific to the calibration data) and to exploit the full potential of all its weights. Another way to avoid overfitting is through the choice of a lean network topology with only a minimum of elements. This reduces the number of weights to be trained accordingly.

Principal component analysis (PCA) is often applied as a preprocessor to the NN. This usually allows the dimension of the input vector to be reduced which is effected by the reduction in the number of weights emerging from the first layer of the NN, leading to the so-called optimum minimum neural network [10]. According to our experience, the main advantage of the application of PCA is the input vector orthogonalization (decorrelation). As the input vector is decorrelated by the PCA preprocessing, the NN models only the non-redundant part of the information, hidden in the raw data, thus adapting faster and better to the input while at the same time reducing the number of nodes substantially.

## COMPUTATIONS

The performance of the NN and PCA–NN approaches is presented in terms of one simulated and two real examples. The simulated example was chosen to demonstrate the performance of PCA–NN and NN on a very noisy, non-linear data set with large input variance which poorly correlates with the output. The real examples demonstrate the efficiency of NN and PCA–NN when applied to highly collinear data.

For comparison, PCR [29], PLS [29], NN and PCA–NN were applied in the discussed examples. For all these methods the same model (or training) and test sets are considered. The standard error of prediction (SEP) over the test data set is used to measure a method's performance. SEP is defined as

$$\text{SEP} = \left\{ \frac{\sum [y(\text{desired}) - y(\text{predicted})]^2}{n} \right\}^{1/2}$$

where  $n$  is the number of samples in the test data set.

SEP over the test set is also used as a stop criterion for the net training, because with small data sets (examples I and IV) one has to pay much attention to avoiding net overfitting, which results in a discrepancy between the SEP value over the training set diminishing in the course of learning, and the SEP value over the test set passing through its minimum. However, with more abundant data sets the most practical stop criterion is the SEP value over the so-called monitoring set [10].

In all the examples discussed the linear function is used for the output node(s), the inputs are scaled by maximum–minimum scaling and all weights are initially set to random values from  $-0.1$  to  $+0.1$ . As NN adjustable parameters, the type of non-linear transfer function, their gain, the number of hidden nodes and the number of PCA scores were considered. To optimize NN structure the so-called pruning [32] was applied. When not mentioned, mean centring and data standardization before PCA and PLS are assumed.

## RESULTS AND DISCUSSION

### *Example I: protein calibration*

One of the possible applications of NN is in the multivariate calibration of spectroscopic data, where the real and apparent non-linear responses can be attributed to several different sources [11], and where the standard linear PLS and PCR methods are sub-optimum. In this example, the application of NN to the Fearn data set [33] as published in [34], which consists of the near-in-

TABLE 1

Protein calibration data

No.	Reflectance			Protein (%)
	X1	X2	X3	
1	246	374	386	9.23
2	240	359	353	10.95
3	236	352	340	11.67
4	242	370	377	8.67
5	243	367	378	9.95
6	324	448	467	11.87
7	271	407	451	8.09
8	274	406	407	8.38
9	260	385	374	9.64
10	242	366	353	9.70
11	255	376	383	10.75
12	276	396	404	11.47
13	258	393	377	8.05
14	288	415	443	10.57
15	236	386	383	8.01
16	243	366	371	10.41
17	273	404	433	9.51
18	238	370	353	7.75
19	264	384	398	11.39
20	233	365	365	8.25
21	293	421	450	10.23
22	360	484	524	12.55
23	269	389	391	11.35
24	285	410	445	10.75

frared reflectance at three different wavelengths and the protein content measured for 24 samples (see Table 1), is discussed.  $X$  values at all three wavelengths are highly correlated with each other.

The presented data set was divided into a model set (samples 1–14) and a test set (samples

TABLE 2

NN architecture

Example	Method	Output layer		Hidden layer		Number of nodes in the hidden layer
		lr <sup>a</sup>	m <sup>a</sup>	lr <sup>a</sup>	m <sup>a</sup>	
I: protein calibration data	NN	0.01		0.05	0.05	1 + direct
	PCA–NN	0.01		0.05	0.05	1
	RES–NN	0.05	0.03	0.05		1
II: peptide QSAR	NN (145)	0.01		0.01		1
	NN (15)	0.05		0.01	0.02	2
	RES–NN (145)	0.01	0.02	0.01	0.02	1
	RES–NN (15)	0.01	0.02	0.05	0.05	1
III: Simulated cubic data	NN	0.05		0.05		2
	PCA–NN	0.01		0.02		2
	RES–NN	0.06	0.03	0.01		2

<sup>a</sup> lr = Learning rate; m = momentum.

TABLE 3

Results of PLS, PCR, NN and PCA–NN applied to protein calibration

Method	SEP	Description
PLS	1.34	3 factors
PCR	1.34	3 factors
NN	0.51	
PCA–NN	0.39	3 scores

15–24). PLS applied to these data gives three significant components, describing 96.2% of variance in protein content. The SEP over the test data set is 1.34. Exactly the same results are observed for the PCR.

Direct application of NN to these data allows a decrease in the SEP to 0.51. The optimum NN architecture that was deduced consisted of three input nodes, one node with a sigmoidal transfer function in the hidden layer and direct connections between input and output layers (see Table 2).

When PCA is applied to data preprocessing, the three factors emerge from cross-validation [29]. The NN fed with the three PCA scores gives a further decrease in the SEP, to 0.39. In this instance the best NN consists of only one node in the hidden layer. The results of all the methods discussed are summarized in Table 3.

It is well known [33,35] that the dominant variance in the reflectance measurements does not result from variances in protein composition



but rather from variances in the average particle size, so the results of PCR, which exploits variances in the input data, might be worse than results of PLS, which uses the covariance between the input and output data to improve the regression. Nevertheless, in the case studied, three significant factors (according to cross-validation), explaining 100% of the variance in the block of independent variables, emerge from both types of analysis and their results are identical. The best NN derived for processing of the raw data includes direct connections between linear input and output layers. Such a type of connections seems to be necessary when the linear dependence between  $X$  and  $Y$  blocks of variables is dominant [10]. Theoretically the sigmoidal node in the hidden layer should also be able to recover linear performance, but in practice this is often not so or the training is stopped beforehand. Expectation of good linear performance of NN is based on the fact that during the training process, the bias weight to the output layer can be automatically adjusted, thereby selecting approximately the linear part of the sigmoidal curve. Nevertheless, as reported [3,35] a sigmoid transfer function inadequately reproduces a linear input–output relationship. Then, fed with the PCA scores, NN with only one sigmoidal node in the hidden layer performs well and reduces the RMS error by 70% when compared with PLS and PCR. This indicates that when non-linearity is present in the data set, PCA–NN gives a superior performance for spectroscopic calibration. This seems also be supported by one of the examples in [10].

#### *Example II: peptide QSAR*

The problem of experimentally evaluating the potential biological activity of organic compounds has received much attention in the past few years. The primary objective of a QSAR is to give a predictive relationship between the structure and activity data. Then the activity of future compounds similar to those used in the calibration data set can be predicted from their structure data within the model's validity.

In this example, the application of NN and PLS–NN procedures to model the variation in chemical structure of the bradykinin potentiating

TABLE 4

Peptide code

No.	Peptide	No.	Peptide
1	Val-Glu-Ser-Ser-Lys	16	Ala-Ala-Ala-Ala-Ala
2	Val-Glu-Ser-Ala-Lys	17	Ala-Ala-Tyr-Ala-Ala
3	Val-Glu-Ala-Ser-Lys	18	Ala-Ala-Trp-Ala-Ala
4	Val-Glu-Ala-Ala-Lys	19	Val-Ala-Trp-Ala-Ala
5	Val-Lys-Ala-Ala-Lys	20	Val-Ala-Trp-Ala-Lys
6	Val-Glu-Trp-Ala-Lys	21	Val-Lys-Trp-Ala-Ala
7	Val-Glu-Ala-Ala-Pro	22	Val-Trp-Ala-Ala-Lys
8	Val-Glu-His-Ala-Lys	23	Val-Ala-Ala-Trp-Lys
9	Val-Ala-Ala-Ala-Lys	24	Glu-Lys-Trp-Ala-Pro
10	Gly-Glu-Ala-Ala-Lys	25	Val-Lys-Trp-Ala-Pro
11	Leu-Glu-Ala-Ala-Lys	26	Arg-Lys-Trp-Ala-Pro
12	Phe-Glu-Ala-Ala-Lys	27	Val-Glu-Trp-Val-Lys
13	Val-Glu-Gly-Gly-Lys	28	Pro-Gly-Phe-Ser-Pro
14	Val-Glu-Phe-Ala-Lys	29	Phe-Ser-Pro-Phe-Arg
15	Val-Glu-Leu-Ala-Lys	30	Arg-Tyr-Leu-Pro-Thr

pentapeptides with the variation in their biological activity is discussed. Experimental data were taken from [36].

The five positions of amino acids are described with the 29 variables (physical and chemical parameters) for each of amino acids, giving an  $X$ -matrix with 145 descriptors. The biological activity is modelled as the logarithm of the activity index relative to peptide 1 (see Table 4).

Let us consider the first fifteen peptides as the model set (M1) and the remaining peptides as the test set (T1). The PLS analysis, applied to these data, gives six significant components, describing 99.3% of the variance in biological activity. The SEP for the test set is 0.98. The PCR analysis gives twelve factors, also describing 99.3% of variance in biological activity. The SEP in this instance is 0.96.

The amino acids in each position have also been described by three so-called principal properties, derived from a PCA of a matrix of 29 variables for 20 amino acids coded by RNA in the amino acid synthesis [36,37]. A principal component model of this data set with three significant factors was obtained, explaining together about 60% of the data variance. The three score vectors, regarded as “principal properties” of the amino acids, can be used to code each amino acid position in the peptide structure. Then the model

TABLE 5

Results of PLS, PCR, NN and PCA–NN applied to the peptide data

Method	Model set	Test set	SEP	Description
PLS	M1	T1	0.98	6 factors
PCR	M1	T1	0.96	12 factors
NN	M1	T1	0.50	
PLS	M2	T2	0.55	3 factors
PCR	M2	T2	0.50	5 factors
NN	M2	T2	0.32	

and test matrices (M2 and T2, respectively) reduce to ones with 15 orthogonal descriptors (5 positions  $\times$  3 principal properties). In this instance the SEP of the PLS analysis is 0.55 and that of the PCR analysis is 0.50. It ought to be mentioned that when principal properties of

amino acids are used as the peptide variables, then no scaling of data prior to PLS and PCR analysis is applied.

Application of NN to the full data set (M1, T1 with 145 descriptors) allows the SEP to be decreased to 0.58, and when applied to the second data set (M2, T2 with 15 orthogonal descriptors) gives an SEP of 0.32. In both instances the best NN contains only one or two sigmoidal nodes in the hidden layer (see Table 2), and direct linear connection between the input and output does not improve the results.

The results of PLS, PCR, NN and PCA–NN methods applied to the peptide data sets are presented in Table 5.

It ought to be mentioned that the performance of PLS or PCR methods can, of course, be improved by including squared terms and cross-terms as additional  $x$ -variables, but one usually

TABLE 6

Simulated cubic data

Set	No.	X1	X2	X3	X4	Y
Training set	1	-2.188	-1.940	-6.397	-0.032	-8.000
	2	-1.148	-1.213	0.846	-0.183	-2.370
	3	-0.679	-0.578	5.422	0.169	-0.296
	4	-0.154	0.036	-1.794	0.086	0.000
	5	0.693	0.583	-4.459	0.093	0.296
	6	1.225	1.183	6.361	-0.095	2.370
	7	1.919	2.145	1.302	-0.160	8.000
Test set	1	-1.928	-1.857	2.377	-0.159	-8.000
	2	-1.805	-1.859	6.358	-0.198	-5.832
	3	-1.724	-1.727	0.064	0.104	-4.096
	4	-1.364	-1.400	6.165	-0.155	-2.744
	5	-1.268	-1.355	-0.405	0.119	-1.728
	6	-1.103	-0.936	-2.412	0.173	-1.000
	7	-0.868	-0.648	6.611	0.138	-0.512
	8	-0.728	-0.696	3.901	0.085	-0.216
	9	-0.517	-0.354	-5.486	-0.172	-0.064
	10	-0.197	-0.221	-7.825	-0.012	-0.008
	11	0.148	0.193	-1.067	-0.120	0.000
	12	0.229	0.345	-0.160	0.134	0.008
	13	0.516	0.573	7.146	-0.091	0.064
	14	0.451	0.783	2.560	0.154	0.216
15	0.977	0.814	7.853	0.062	0.512	
16	0.834	0.953	-7.662	0.188	1.000	
17	1.282	1.275	-9.544	0.120	1.728	
18	1.562	1.567	-6.424	0.200	2.744	
19	1.411	1.491	8.917	-0.058	4.096	
20	1.614	1.716	-1.681	0.031	5.832	
21	1.879	2.011	-1.373	-0.080	8.000	

does not know which descriptor variables will be important in the final QSAR model and which quadratic and cross-terms are needed. As is demonstrated, the performance of NN applied to the raw data processing is as good as the performance of PCR or PLS after intensive data pre-treatment.

#### Example III: simulated cubic data

In both examples considered above the PCA–NN approach outperforms NN. To demonstrate that this should not be considered as a rule, the Holcomb and Morari tutorial example [35], in which very noisy data with a large input variance that does not correlate with the output is discussed, is presented. For such data set the PCA preprocessing to a neural net is not expected to improve the performance of NN.

Let us consider the following cubic input–output relationship, proposed by Holcomb and Morari [35]:

Four inputs:

$$X1 = a + 0.2v$$

$$X2 = a + 0.2v$$

$$X3 = 10v$$

$$X4 = 0.2v$$

One output:

$$y = aaa$$

where  $v [-1,1]$  is a uniformly distributed random variable; the  $vs$  in the above equations are independent. The training set consists of seven  $as$  evenly spaced over the interval  $[-2,2]$  and the test set consists of 21  $as$  evenly spaced over the interval  $[-2,2]$  (see Table 6).

Two of the inputs are noisy measurements of the true  $a$  variable and the other two just contain random numbers. This noisy data incorporates not only non-linearity but, as was mentioned above, also the large variance in the input data, which does not correlate with the output. The results of PLS, PCR, NN and PCA–NN methods are presented in Table 7.

It is well known that when very low-noise data are available, PLS and PCR techniques can give good approximations even to non-linear data, by incorporating extra factors in the calibration

TABLE 7

Results of PLS, PCR, NN and PCA–NN applied to the cubic simulated data <sup>a</sup>

Method	SEP	Description
PLS	2.10	1 factor
PCR	2.28	1 factor
NN	1.30	
PCA–NN	0.86	2 scores

<sup>a</sup> Training set, 7 samples; test set, 21 samples.

model [27]. When applied to very noisy data, such as those studied, they perform very poorly. As expected, the performance of PLS is slightly better than that of PCR. The application of NN allows the SEP to be decreased efficiently, but again the best result is observed for PCA–NN, which is unexpected [33]. When additional data sets were simulated, bringing the total to 21 elements, then the SEP of NN was 0.59 and that of PCA–NN (two scores) was 0.93. These results allow the conclusion that for very noisy data the sampling error can have a substantial influence.

#### PLS residuals–NN approach (RES–NN)

As a compromise between the undesirable “black-box” approach and the demand for NN performance, a tandem linear calibration method and NN can be proposed. When the PLS error of prediction is not acceptable, then PLS residuals can be treated by the NN approach. This tandem method does not always guarantee a decrease in

TABLE 8

Model data set

No.	Model set M			Y block of dependent variable(s): Protein (%)
	X block of independent variables: Reflectance			
	X1	X2	X3	
1	246	374	386	9.23
2	240	359	353	10.95
3	236	352	340	11.67
4	242	370	377	8.67
5	243	367	378	9.95
6	324	448	467	11.87
7	271	407	451	8.09

TABLE 9

Computed residuals from PLS to be used as input for NN

No.	Reflectance			Protein observed (%)	Protein predicted (%)	Resi- duals
	X1	X2	X3			
8	274	406	407	8.38	8.17	0.21
9	260	385	374	9.64	9.56	0.08
10	242	366	353	9.70	9.43	0.27
11	255	376	383	10.75	11.05	-0.30
12	276	396	404	11.47	11.77	-0.30
13	258	393	377	8.05	6.57	1.48
14	288	415	443	10.57	10.55	0.02
15	236	386	383	8.01	2.23	5.78
16	243	366	371	10.41	10.19	0.22
17	273	404	433	9.51	9.14	0.36
18	238	370	353	7.75	6.99	0.76
19	264	384	398	11.39	11.69	-0.30
20	233	365	365	8.25	7.33	0.92
21	293	421	450	10.23	10.39	-0.16
22	360	484	524	12.55	13.13	-0.58
23	269	389	391	11.35	11.48	-0.13
24	285	410	445	10.75	11.23	-0.48

the error, as the source of PLS residuals can be not only non-linearity of data but also noise. Nevertheless, if some type of non-linear pattern in the PLS residuals is observed, then the application of NN can be fruitful.

The proposed procedure requires partitioning of the data set into the three following sets: model (M), calibration (C) and test (T) sets. The model set (M) is used to construct the PLS model. Based on this model and using *X*-blocks of data

TABLE 10

Results of PLS-NN on Fearn data

Set	No.	<i>X</i> block of independent variables: Reflectance			<i>Y</i> block of dependent variable(s) (PLS residuals):
		X1	X2	X3	
Calibration set C	8	274	406	407	0.21
	9	260	385	374	0.08
	10	242	366	353	0.27
	11	255	376	383	-0.30
	12	276	396	404	-0.30
	13	258	393	377	1.48
	14	288	415	443	0.02
Test set T	15	236	386	383	5.78
	16	243	366	371	0.22
	17	273	404	433	0.36
	18	238	370	353	0.76
	19	264	384	398	-0.30
	20	233	365	365	0.92
	21	293	421	450	-0.16
	22	360	484	524	-0.58
	23	269	389	391	-0.13
	24	285	410	445	-0.48

sets C and T, the respective *Y*-blocks of these sets can be predicted. The differences between true and predicted *Y* values (residuals) are then used together with the *X*-blocks of C and T data sets to calibrate (set C) and to test (set T) the neural net.

Let us consider the application of the RES–NN procedure to the Fearn data presented in Table 1. The first seven samples were chosen as the model data set, M (Table 8).

*X* and *Y* blocks of model set M were used to construct a PLS model. Based on the constructed PLS model, the protein content for the remaining 17 samples (samples 8–24) was predicted and differences between observed (true) and predicted values were calculated (Table 9).

The above set of 17 samples (8–24) was then split into two sets, calibration C set and test T set, but now as dependent variables the PLS residuals were considered (Table 10).

Calibration set C was used to train NN and set T to test NN performance.

The results of the proposed RES–NN procedure applied to the examples discussed above are presented in Table 11. In all instance the SEP for the same test set was calculated.

The RES–NN procedure outperforms PLS in all the examples studied. For the Fearn and peptide data the results of RES–NN are comparable to those of PCA–NN or NN. As expected for very noisy cubic data, the performances of the NN and PCA–NN approaches are better than that of RES–NN.

### Conclusions

Orthogonal transformation of the input variables can not only significantly improve speed of

neural net convergence, but also improve the accuracy of prediction. Application of the PCA–NN procedure to real data allows the SEP to be decreased efficiently in comparison with PLS, PCR or NN. However, in the case of very noisy data with an input variance that does not correlate with the output the PCA data preprocessing prior to NN does not improve the performance of NN. The superior performance of the PCA–NN approach should not be regarded as a rule. Each data set has its own characteristics, which ought to be considered before method selection. Nevertheless, in the all the examples discussed NN (with or without PCA data preprocessing) perform better than the standard linear multivariate methods such as PLS or PCR, even with a limited number of samples in the training set.

As a compromise between the undesirability of NN as a “black-box” approach and the demand for NN performance, a tandem calibration procedure has been proposed. Its performance is comparable to that of NN or PCA–NN. The advantage is that the linear portion (PCR or PLS) retains, of course, the commonly acknowledged ease of interpretation; this is only supplemented by a non-linear NN treatment if the residuals from the first step appear large enough for non-linear behaviour unexplained by PCR or PLS to be expected.

### REFERENCES

- 1 J.J. Hopfield, *Proc. Natl. Acad. Sci. U.S.A.*, 79 (1982) 2554.
- 2 D.E. Rumelhart and J.L. McClelland, *Parallel Distributed Processing*, Vol. 1, MIT Press, Cambridge, MA, 1986.
- 3 J.R. Long, V.G. Gregoriou and P.J. Gemperline, *Anal. Chem.*, 62 (1990) 1791.
- 4 B.J. Wythoff, S.P. Levine and S.A. Tomellini, *Anal. Chem.*, 62 (1990) 2702.
- 5 J. Zupan and J. Gasteiger, *Anal. Chim. Acta*, 248 (1991) 1.
- 6 N. Qian and T.J. Sejnowski, *J. Mol. Biol.*, 202 (1988) 865.
- 7 L.H. Holley and M. Karplus, *Proc. Natl. Acad. Sci. U.S.A.*, 86 (1989) 152.
- 8 N.V. Bhat, P.A. Minderman, T. McAvoy and N.S. Wang, *IEEE Control Syst. Mag.*, (1990) 24.
- 9 J.U. Thomsen and B. Meyer, *J. Magn. Reson.*, 84 (1989) 212.
- 10 C. Borggaard and H.H. Thodberg, *Anal. Chem.*, 64 (1992) 545.

TABLE 11

SEP values for PLS, PCR, NN, PCA–NN and RES–NN applied to real and simulated examples

Method	Fearn data	Peptide data		Cubic data
		145	15	
PLS	1.34	0.98	0.55	2.10
PCR	1.34	0.96	0.50	2.28
NN	0.51	0.50	0.32	1.30
PCA–NN	0.39			0.86
RES–NN	0.34	0.57	0.33	1.65

- 11 P.J. Gemperline, J.R. Long and V.G. Gregoriou, *Anal. Chem.*, 63 (1991) 2313.
- 12 B. Meyer, T. Hansen, D. Nute, P. Albersheim, A. Darbill, W. York and J. Seilers, *Science*, 251 (1991) 542.
- 13 E.W. Robb and M.E. Munk, *Mikrochim. Acta*, I (1990) 131.
- 14 E.W. Elrod, G.M. Maggoria and R.G. Trenary, *J. Chem. Inf. Comput. Sci.*, 20 (1990) 477.
- 15 M. Bos, A. Bos and W.E. Van der Linden, *Anal. Chim. Acta*, 233 (1990) 31.
- 16 T. Amayama and H.T. Tchikawa, *Chem. Pharm. Bull.*, 39 (1991) 358, 372.
- 17 V. Kvasnicka, *Chem. Zvesti*, 44 (1990) 775.
- 18 M. Otto, T. George, C. Schierle and W. Wegscheider, *Pure Appl. Chem.*, 64 (1992) 497.
- 19 C. Schierle, M. Otto and W. Wegscheider, *Fresenius' J. Anal. Chem.*, 343 (1992) 561.
- 20 B.W. Pack and P.B. Harrington, *Book of Abstracts of the Pittsburgh Conference PITTCON '92*, abstract no. 175.
- 21 LL. McDermott, *Book of Abstracts of the Pittsburgh Conference PITTCON '92*, abstract no. 176.
- 22 P.A. Jansson, *Anal. Chem.*, 63 (1991) 357A.
- 23 J.R. Long, H.T. Mayfield, M.V. Henley and P.R. Kromann, *Anal. Chem.*, 63 (1991) 1256.
- 24 A.L. Sumner, S.K. Rogers, G.L. Tarr, M. Kabrisky and D. Norman, *Proc. SPIE Int. Soc. Opt. Eng.*, 1294 (1990) 138.
- 25 M. Sundgren, F. Winqvist, I. Lukkari and I. Lundstrom, *Meas. Sci. Technol.*, 2 (1991) 464.
- 26 S.M. Chang, Y. Iwasaki, M. Suzuki, E. Tamiya, I. Karube and M. Muramatsu, *Anal. Chim. Acta*, 249 (1991) 323.
- 27 T. Nakamoto, K. Fukunishi and T. Moriizumi, *Sensors Actuators*, B1 (1990) 473.
- 28 P. Olmos, J.C. Diaz, J.M. Perez, P. Gomez, V. Rodeilar, P. Aguayo, A. Bru, G. Garcia-Belmonte and J.L. De Pablos, *IEEE Trans. Nucl. Sci.*, 38 (1991) 971.
- 29 H. Martens and T. Naes, *Multivariate Calibration*, Wiley, Chichester, 1989.
- 30 W.S. McCulloch and W.H. Pitts, *Bull. Math. Biophys.*, 5 (1943) 115.
- 31 D.O. Hebb, *The Organization of Behavior*, Wiley, New York, 1949.
- 32 H.H. Thodberg, *Int. J. Neural Syst.*, 1 (1991) 317.
- 33 T. Fearn, *Appl. Stat.*, 32 (1983) 73.
- 34 J. Mandel, *J. Res. Natl. Bur. Stand.*, 90 (1985) 465.
- 35 T.R. Holcomb and M. Morari, *Comput. Chem. Eng.*, (1992) in press.
- 36 S. Hellberg, *Dissertation*, University of Umea, Umea, 1986.
- 37 S. Wold, M. Sjostrom, R. Carlson, T. Lundstedt, S. Hellberg, B. Skagerberg, C. Wikstrom and J. Ohman, *Anal. Chim. Acta*, 191 (1986) 17.

# Expert systems in trace analysis

F.X. Rius

*Department of Chemistry, University of Tarragona, Pl. Imperial Tàrraco 1, E-43005 Tarragona (Spain)*

(Received 10th September 1992; revised manuscript received 6th January 1993)

## Abstract

A brief overview of the fundamental principles of knowledge-based systems and their development and usefulness is given. The main differences from conventional computer programs are indicated together with the main advantages and drawbacks. A variety of recent applications of expert systems in trace analysis are reviewed, novel approaches to the field are reported and the future trends of these systems in the development of intelligent instrumentation are evaluated.

*Keywords:* Expert systems; Knowledge-based systems; Trace analysis

The aim of this paper is to give an overview of expert systems dedicated to trace analysis. Belonging to the realm of artificial intelligence, expert systems are useful tools for solving problems where expertise is needed. If we ourselves do not have this expertise, the problem can be solved by consulting with the most readily available human expert. Of course, a useful alternative is to have a computer system that offers intelligent advice for such a problem requiring such expertise. This is precisely what expert systems try to do. Expert systems have been defined as software products containing encoded knowledge about a limited and substantial domain that are able to apply reasoning to obtain useful information [1–7].

A brief description of the terminology used is appropriate. These systems solve problems by manipulating the knowledge previously embedded. At present, they are able to assimilate and reproduce the ability of human experts to find solutions, but it is difficult for them to acquire

new or to modify previous knowledge on their own. The name “expert” systems, therefore, exaggerates their actual capabilities. More adequate labels such as knowledge-based, deductive, production or rule-based systems can be found in the recent literature [8–10].

The structure and characteristics of expert systems have been thoroughly discussed [1–10], and therefore, only the principal concepts associated with these tools are briefly summarized here. The main focus is on the features of expert systems, both conceptual and structural, that make them different from conventional numerical programs. The literature devoted to expert systems in trace analysis is critically assessed and some future trends are envisaged with an emphasis on the role of these systems in the development of intelligent trace analysers.

## STRUCTURE OF THE EXPERT SYSTEMS

Basically, expert systems are integrated computer programs but, unlike conventional programs, a clear distinction exists between the loca-

*Correspondence to:* F.X. Rius, Department of Chemistry, University of Tarragona, Pl. Imperial Tàrraco 1, E-43005 Tarragona (Spain).

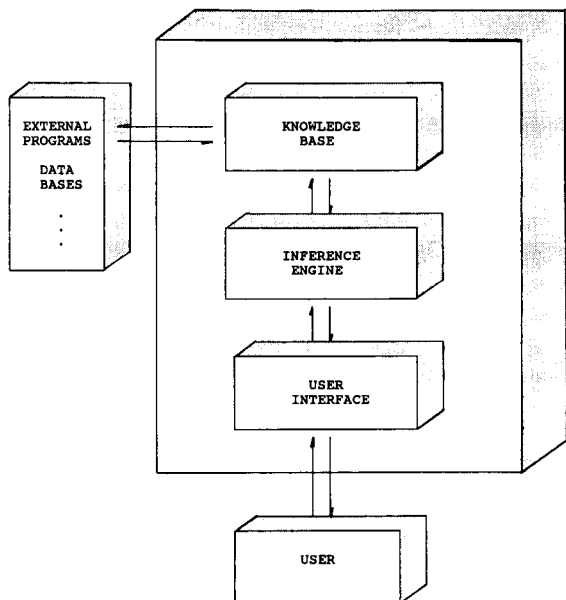


Fig. 1. Structure of expert systems.

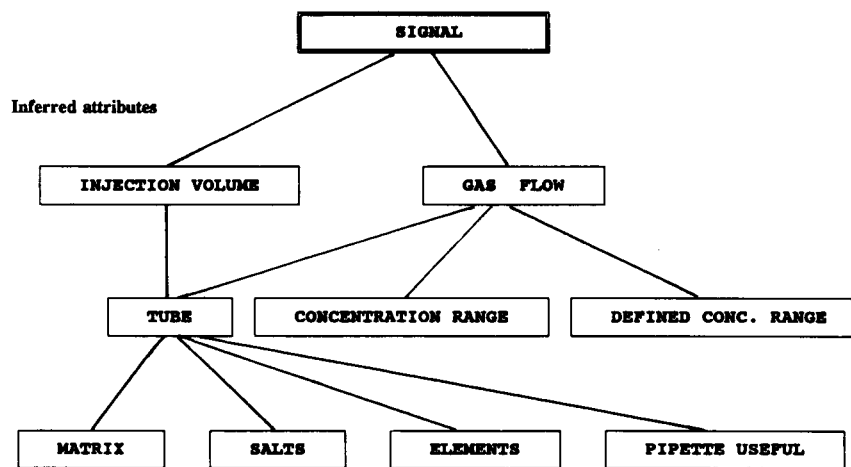
tion of the embedded knowledge, the way in which it is manipulated and the system utilities. The first is contained in the knowledge base, the second is the inference engine and the last is included in the third main part of expert systems, the user interface, which serves to facilitate communication between system and users. A schematic view of the overall structure of expert

systems is given in Fig. 1. To develop the knowledge base the technologists who physically generate the system, or knowledge engineers, must conduct repeated exchanges with human experts. This is one of the key points in the development of the systems and will be dealt with further below. The knowledge base can also contain information from books or other sources (data tables, chemical structures, numerical programs, references, etc.) which can also be linked to the expert system through external programs. The knowledge can be encoded in different ways; rules, frames or planning networks are the most common [2,11,12]. The production of rules is the most usual way of representing the encoded knowledge. They follow the pattern:

```

if....(antecedent 1)
    and..(antecedent 2)
    :
then...(action 1)
    and..(action 2)
    :
else...(action j)
    and..(action i)
    :
    
```

The rules are linked to each other in such a way that the antecedent of one is provided by the actions of others, as shown in the following example taken from an expert system on graphite



Input attributes

Fig. 2. Example of a hierarchical tree corresponding to the graphite furnace atomic absorption spectrometry expert system [14].



### furnace atomic absorption spectrometry (GFAAS) method development [13]:

#### rule 1 tube:

```

if
  elements = Al|Cu|Mn and
  pipette useful = yes and
  matrix = inorganic and
  salts = concentrated
then
  tube = pyrocoated – with – Lvov platform.
endif.

```

#### rule 2 gas flow:

```

if
  tube = pyrocoated – with – Lvov platform and
  elements = Cd and
  pipette useful = yes and
  concentration range = defined and
  def conc range sol ge 2
then
  gas flow = fifty ml per min.
endif.

```

#### rule 3 injection volume:

```

if
  tube = pyrocoated – with – Lvov platform
then
  injection volume = ten microlitres.
endif.

```

In this way, they form the structure of a hierarchical tree like that shown in Fig. 2 corresponding to the GFAAS prototype expert system [13,14].

The inference engine uses the knowledge embedded in the knowledge base and input information from the user to infer the solution to the problems. Once the goal has been established by the user, the inference engine links adequate rules to achieve it. It could be said that the inference engine is the part of the expert system that carries out the reasoning. In rule-based systems, some special rules, called meta-rules, are used sometimes. These are rules designed not to act directly on facts from the knowledge base but to control the selection of other rules [2].

The user interface conveys information between the user and the system. The user should

provide values for input attributes and the system will give the solution, with an indication of its reliability, the reasoning used to obtain it and explanations about the questions asked of the end user.

A very important aspect of expert systems development is their validation. Several features must be verified: first, it must be ensured that the system has been built according to specifications. Second, the program (software) performance must be checked and finally, the expertise embedded (knowledge base) and interfaces must be examined for correctness [8,15,16].

### DIFFERENCES FROM CONVENTIONAL COMPUTER PROGRAMS. ADVANTAGES AND DRAWBACKS

#### *Conceptual*

Once the experience and knowledge of human experts have been incorporated into the program, expert systems do the reasoning on their own. This is the key difference from other programs, or computer-based systems: the knowledge-based system has to choose the best solution among a wealth of paths and possible answers. The captured human expertise is then made permanent, accessible and easily transportable.

Expert systems manipulate symbolic rather than numerical knowledge. Since they have this feature, expert systems must be developed with a clear strategy: only in cases where experience and expertise are needed, can knowledge-based systems be useful. They are not suitable for solving problems of an algorithmic or procedural nature.

The characteristics of the end user must be considered from the very first stages of the development process.

Expert systems can deduce answers, but only in a limited domain. This is, in fact, a fundamental limitation of artificial intelligence in its present stage of development rather than a difference between conventional programs and expert systems. The “intelligence” of expert systems is very limited since they are not able to cope with unforeseen situations. Humans are much more flexible when it comes to complicated problems. Books or data-based systems, however, do not

have the capacity to understand problems, to explain the reasoning behind the answers, to justify the approach to the problem or to explain the way the solutions have been obtained [1,15].

#### *Structural*

In order to encode the heuristics and symbolic knowledge, expert systems are usually not written in conventional languages such as Fortran, Basic or C. Special languages such as LISP or PROLOG have been developed and applied [17–21].

The “knowledge engineer”, the person who physically develops the system, must have considerable skill and experience as a programmer to build the system from scratch. Expert system-building tools, or shells, offer an alternative. To use these commercially available tools the user must follow a series of fixed syntax norms that can be learnt without much difficulty by the non-specialist. Shells already incorporate the user interface and only the knowledge has to be added to them [8,10,22,23].

Shells have development components and run-time components. Development components are utilities used during editing and compiling phases of the development while run time components are necessary just to run the compiled systems. They are user-friendly and do not require specific programming experience; however, run-time modules are not always readily available. Since they are necessary to run the systems, this may in practice, make the dissemination of these systems difficult.

As mentioned above, knowledge base and inference engine are well separated parts in expert systems. The knowledge base does not have a fixed structure, i.e., a sequence of pre-established instructions. This makes it possible to enlarge the knowledge base without rebuilding the whole system. Although it is not necessary to write the rules in order, the hierarchical tree does have to be maintained coherent [24].

The chemical knowledge from human experts must be structured and shaped according to the different ways of encoding knowledge. Consequently, knowledge engineers must have not only programming skills, but also a considerable amount of human features such as understand-

ing, an ability to communicate and patience. Working together with the often singular human experts, knowledge engineers have to be able to extract, formalize and validate coherent reasoning iteratively.

In order to overcome the above-mentioned difficulties, which Feigenbaum [25] called the “bottleneck problem of artificial intelligence”, techniques of automatic knowledge acquisition can be applied in some cases [26,27]. Inductive expert systems are one of the best known procedures. Developed on the basis of the ID3 algorithm devised by Quinlan [28], inductive systems try to extract rules from known examples. In this way, the human expert must provide a series of examples with known solutions. The induction algorithm builds the proper rules so that conclusions can be predicted for new examples. Often, the inductive systems involve procedures that develop decision trees [29] and are especially suitable for classification problems [30,31].

#### APPLICATION OF EXPERT SYSTEMS IN TRACE ANALYSIS

The applications of expert systems in trace analysis can be classified according to diverse criteria. In this paper a distinction has been made between applications related to qualitative and quantitative analysis. The latter has been ordered according to the analytical technique used.

#### *Applications related to qualitative analysis*

A wealth of expert systems have been dedicated to structure elucidation of compounds from spectra. At first glance it may appear that these systems are of interest only to the “synthetic” chemist who is concerned with knowing the structure of the newly synthesized compounds. However, the development of expert systems devoted to the interpretation of spectral information with structural purposes is also very useful to the analytical chemist with qualitative purposes in trace analysis. These systems have a direct incidence on the interpretation of data obtained through spectroscopic techniques which have been coupled with separation techniques. Munk

[32] stated that a suitably programmed computer can answer the question, "Do the spectral data of this compound support its proposed structure?". Expert systems can play an important role within any programmed computer and, therefore, they contribute to the tremendous potential of coupled techniques inasmuch as the interpretative data section is concerned [33].

In addition to the general interest in this type of expert systems, the reader should be aware of the different analytical aims that have guided their development. Thus, within the applications which have a more analytical character, Luinge et al. [34,35] used IR, MS,  $^{13}\text{C}$  NMR,  $^1\text{H}$  NMR and UV data as well as other relevant preinformation such as chromatographic retention data for the structure analysis of unknown compounds. However, this approach has not yet been tested on practical problems related to trace analysis.

Tomellini and co-workers [36–38] devised an expert system that acts as the core of an integrated analytical system devoted to environmentally hazardous mixtures. Their main aim was the preliminary screening for principal organic components handled on waste sites, so the whole system had to be transportable in order to carry out on-site analysis. To cope with this characteristic, Fourier transform (FT) IR spectrometry was chosen and this selection had, in turn, a direct influence on the concentration range of the analyte compounds. Hence, although the direct incidence in trace analysis is limited, the numerous ideas developed regarding such different aspects as automated knowledge acquisition, self-training or self-optimization could be adapted to other expert systems.

Hasenoehrl et al. [39] developed an expert system to identify molecular structures from vapour-phase IR spectra using principal component analysis (PCA). This step was prior to its application to the rapid functional group characterization by means of GC-FT-IR spectra [40]. The system is relevant to trace analysis because it acts as a selective detector of functional groups such as alcohols, carboxylic acids, ketones or aldehydes in complex mixtures. The system does not require the use of standards as the PCA transformed spectra of the eluted compounds are

compared with a training set of transformed library spectra. However, the type of sigmoid discriminant function used to classify the PCA results makes it difficult to increase the limited number of different functional groups studied to date.

Janssens and Van Espen [41] described an expert system for the qualitative interpretation of x-ray fluorescence spectra. Developed in Pascal for a mainframe computer under a VMS operating system, the expert system has proved to be reliable in the inorganic trace analysis of industrial aerosol particles by using an electron microprobe. Although up to 2000 rules may be required to deal with all situations, cases of severe absorption may cause the expert system to produce an erroneous interpretation. Like many other expert systems, they cannot substitute the human expert when complicated situations are encountered, but they can act as useful assistants in routine analysis.

Recently, Holzer et al. [42] developed an expert system to detect petroleum based volatiles in suspect arson samples on the basis of GC-MS analysis. The system can be very useful in this selected domain of trace analysis but, as it was developed from scratch for a specific operating system, it would require some adaptation before being suitable for use in different equipment and computer environments.

Scott and co-workers, who have been interested for a long time in the identification of hazardous compounds from mass spectra [43], recently reported an improved version of a previous inductive expert system [44,45]. Developed using a shell in which the ID3 algorithm was implemented, the system is capable of identifying and classifying toxic and other volatile organic compounds on the basis of low-concentration mass spectra. The system has been thoroughly tested with both field and library spectra with a high degree of identification and classification accuracy. Compared with library search techniques, it has obvious advantages in speed and provision of identification information. Scott [46,47] also developed a rule-based system to estimate the molecular weights of volatile organic compounds from low-resolution mass spectra. The

importance of this specific domain system resides in its useful ability to exclude some candidate structures in mass spectral interpretation in either automated searches or manual interpretation.

Two expert systems related to classical inorganic microanalysis have been developed with clear educational purposes. Settle [48] reported two applications in the general chemistry laboratory and Larrechi and Rius [49] developed an expert system for the separation and identification of 24 metal ions in solution. Both systems are written using commercially available shells, are easy to handle and can be run on PCs. Not designed to solve specific domain problems, these rule-based systems were conceived to help students in their reasoning process to arrive at the correct solutions to problems.

#### *Applications related to quantitative analysis*

Method development is one of the activities that need a lot of expertise. Accordingly, many useful expert systems in quantitative trace analysis are devoted to providing the user with useful advice for developing different steps in the analytical process.

Several systems have been devoted to procedures that involve stages prior to analytical determination. Settle and co-workers [50,51] reported a knowledge-based system for sample preparation by microwave dissolution. They showed how standard methods can be encapsulated in computer programs that can be shared among laboratories. Moors and Massart [52] presented a small system that gives advice on solid-phase extraction of drugs from aqueous samples or plasma. This work is valuable also for all those who want to learn the development of expert systems using the shell KES, as graphs on attribute hierarchy and decision trees together with a complete listing of the implemented expert system are given. Xu et al. [53] reported an expert system for the liquid-liquid extraction of rare earths. The system, which has been developed in LISP and runs on a PC, can be very valuable for those users working in the area as it includes information on frequently used extractants, separation of the seventeen ele-

ments of the rare earth family, recommendations on the procedures for the separation of mixtures or economics of the processing. It is worth noting that very few expert systems have been reported in the field of sampling, one of the areas in which few specialists exist and, therefore, in which much advice is needed. Olivero and Bottrell [54] described several systems used by the US Environmental Protection Agency and discussed their design, operation and impact on environmental applications. Their paper, rather than describing the characteristics of individual expert systems, introduces the reader to the guidelines and requirements set up for expert systems to support environmental sampling, analysis and data validation.

Of all the separation techniques, liquid chromatography (LC) has received most attention and effort. However, a simple expert system for drug separation using thin-layer chromatography has also been reported [21]. Moll and Clerc [21] did not intend to develop a system which could be of immediate practical use for the trace analyst; rather, the value of their work resides in the detailed explanations, practical hints and examples of the system development using PROLOG.

It is not surprising that several groups have developed expert systems to give advice on method development by using LC. Because of the many types of analytes incorporating a variety of functional groups, samples, matrices and experimental conditions involving type and composition of mobile and stationary phases, pH, isocratic or gradient elution, detection modes, etc., this technique is an excellent field in which expert systems can be exploited to the full. A macro project called ESCA has given rise to several publications involving chemical knowledge, such as mobile phase selection or detection mode, and chemometric knowledge, such as precision or ruggedness tests [8,55–57]. The series of rule-based systems in this project have been developed with practical purposes in mind and, as the systems are currently running in several companies and institutions, this aim has been achieved. Other workers have developed rule-based systems for the selection of separation mode, stationary and mobile phases, including peak identi-

fication [58], peak purity [59], mobile phase selection [60,61], planning LC separations with the use of meta-knowledge (or control knowledge) [11], LC method development [62–65] and LC separations of steroids [66] and drugs [67].

A set of modular expert systems designed to provide real-time assistance to the analyst in completing trace metal analyses using automated sample introduction and atomic absorption spectrometry is being developed by Stillman and co-workers [68,69]. The set of systems, which can act either individually or interconnected, give advices not only on method selection or control of the instrumental settings and data acquisition but also on problem diagnosis [70] and assistance in the execution of a laboratory quality assurance programme. Other expert systems within this technique involve practical guidance on method development in GFAAS including some chemometric knowledge focused on the calibration step and methods validation [13,14] and atomic line selection [71].

Voltammetric techniques are not easy to master owing to the variety of the existing modes, their complexity, the number of analytes that can be determined and the presence of systematic errors due to many possible interferences. In spite of these features, which make these techniques attractive to be tackled by expert systems, the first system devoted to trace electrochemical analysis appeared only very recently [72]. Esteban and co-workers [73,74] developed a rule-based system that gives recommendations on sample pretreatment and the selection of a suitable methodology for the voltammetric determination of a number of metal ions. The system, which is being extended at present to incorporate the determination of more metal ions [75], provides advice on the development of both standard and well established methodologies for qualitative and quantitative analysis. Developed using the shell KES and running with PCs, the system can be linked to the polarograph so that experimental data can be stored and retrieved by the expert system when necessary. In order to facilitate the transportability and implementation of the system in different environments, commercially available material has been used when possible.

Other expert systems have been conceived to give advice, within trace analysis, for specific purposes. This is the case with a rule-based system for environmental pollutant analysis [54,76,77] and a system for evaluating published data on selenium in foods [78]. Finally, other expert systems are of a general nature, and therefore not addressed specifically to trace analysis, although they can be used in several steps of the trace analytical process. Thus, Marsili et al. [79] reported a system containing specific chemometric knowledge such as the selection of appropriate methods for data analysis and for experimental design, Wolters et al. [80] developed an expert system-based program for the quantitative validation of the results of analytical methods and Danzer et al. [81] reported a system for the evaluation and interpretation of interlaboratory comparisons.

#### FUTURE TRENDS. EXPERT SYSTEMS IN INTELLIGENT TRACE ANALYSIS

New facilities are incorporated in order to overcome some of the difficulties previously encountered. In this way, hypermedia tools can simplify the building of prototypes and their maintenance. Hypermedia is a new information management technology which includes facilities to produce texts, graphics, sound and animation so that they can be used to build man-machine interfaces which are much more attractive to the end user [82]. The information is distributed in portions and this combination of facilities allows users to manoeuvre through the different pieces of information in an unordered way and according to his or her needs. The distinct parts in which the information has been modelled are linked to each other by at least one connection. As many sections are connected to others by several links, the user can follow many paths, having access to the information with no pre-established order. Very few applications of these tools have been reported in analytical chemistry to date [83,84], but new studies are being developed in this direction [85,86].

Inductive expert systems have been referred to above as tools that can overcome, in those cases in which enough data examples exist, the problem of knowledge acquisition. However, the existence of a series of examples with a known solution is often a severe restriction. Eriksson [87] has recently proposed a smart shortcut whose performance will have to be tested under different situations, heuristics and new future knowledge. He has provided a knowledge acquisition tool, specialized in the field of protein purification, which enables the human expert to develop expert systems without the need for a knowledge engineer. By means of a graphical user interface, the expert has to fill in forms and to enter schemes which are automatically transformed into knowledge bases, that is, knowledge encoded in such a way as to be interpretable by the expert system. The knowledge base generator transforms the closely resembling experts' own conceptual model of the domain into knowledge bases that can be used immediately for testing. Such a strategy is relevant in that it would reduce the role of knowledge engineers to a minimum. The task of the analysts who are experts in trace analysis, or any other domain, and want to develop expert systems would be made considerably easier if the efficiency of tools such as that proposed by Eriksson were to be verified in the future.

A clear trend of expert systems in chemical analysis is the development of intelligent analysers. Once automation of many parts of the analytical process have been achieved [88] and computers are being used extensively in instrument control, data acquisition [89] and data analysis [90], the next logical step consists in introducing some intelligence into those instruments [27]. Crouch [91] recently reviewed the attributes of an intelligent instrument, including features such as selection of appropriate methods, automatic development of such methods or self-calibration and optimization. Expert systems, acting as intelligent cores of instruments, will play the important role of managing and controlling these steps of the chemical process. A variety of tools such as inductive learning or neural networks [92,93] for automatic knowledge acquisition will be activated from the expert system that will address the suit-

able artificial intelligence technique to each circumstance. Isenhour and co-workers pioneered work with intelligent robots [94] and provided a number of applications [95–98]. Other intelligent instruments are being developed for atomic absorption spectrometry [71], kinetic measurements [91] and spectroscopic flow systems [99].

Expert systems are evolving from isolated support systems which complemented human intelligence [100] to the main parts of integrated intelligent analysers. Their functions will range from advisors for taking decisions concerning the development, testing and implementation of sophisticated analysis processes to diligent managers of tireless automated systems in the laboratory. However, it will take some time until instruments possess one of the most appreciated human qualities, common sense, together with other features of human intelligence such as the "ability to do something appropriate under unpredictable conditions" [101].

The author is grateful to D.L. Massart and J. Smeyers-Verbeke for helpful scientific discussions and advice and acknowledges financial support from the DGICYT (project BP90–453).

#### REFERENCES

- 1 R.E. Dessy, *Anal. Chem.*, 56 (1984) 1200A.
- 2 J.W.A. Klaessens, G. Kateman and B.G.M. Vandeginste, *Trends Anal. Chem.*, 4 (1985) 114.
- 3 P. Jackson, *Introduction to Expert Systems*, Addison-Wesley, New York, 1986.
- 4 D.A. Waterman, *A Guide to Expert Systems*, Addison-Wesley, Reading, MA, 1986.
- 5 A.R. De Monchy, A.R. Foster, J.R. Arretteig, L. Lan and S.N. Deming, *Anal. Chem.*, 60 (1988) 1355A.
- 6 A.P. Wade, S.R. Crouch and D. Betteridge, *Trends Anal. Chem.*, 7 (1988) 358.
- 7 B.A. Hohne and T.A. Pierce, in B.A. Hohne and T.A. Pierce (Eds.), *Expert System Applications in Chemistry* (ACS Symposium Series, Vol. 408), American Chemical Society, Washington, DC, 1989, pp. 2–9.
- 8 J.A. van Leeuwen, L.M.C. Buydens, B.G.M. Vandeginste and G. Kateman, *Trends Anal. Chem.*, 9 (1990) 49.
- 9 D. Yurman, in J.M. Hushon (Ed.), *Expert Systems for Environmental Applications* (ACS Symposium Series, Vol. 431), American Chemical Society, Washington, DC, 1990, pp. 25–38.

- 10 F.A. Settle, Jr., and M.A. Pleva, *Chemometr. Intell. Lab. Syst.*, 11 (1991) 13.
- 11 A.L. Ananda, S.M. Foo and H. Gunasingham, *J. Chem. Inf. Comput. Sci.*, 28 (1988) 82.
- 12 L. Buydens, A. Peeters and D.L. Massart, *Chemometr. Intell. Lab. Syst.*, 5 (1989) 73.
- 13 J. Smeyers-Verbeke, F.X. Rius, P. Vankeerberghen and D.L. Massart, unpublished work.
- 14 D.L. Massart and F.X. Rius, in S. Alegret, J.J. Arias, D. Barceló, J. Casal and G. Rauret (Eds.) *Miscellània Enric Casassas, Universitat Autònoma de Bellaterra, Barcelona, 1991*, pp. 237–240.
- 15 M. Stunder, in J.M. Hushon (Ed.), *Expert Systems for Environmental Applications (ACS Symposium Series, Vol. 431)*, American Chemical Society, Washington, DC, 1990, pp. 39–51.
- 16 R. Wehrens, L. Buydens and G. Kateman, *Chemometr. Intell. Lab. Syst.*, 12 (1991) 57–67.
- 17 B.J. MacLennan, *Principles of Programming Languages*, Holt, Rinehart and Winston, New York, 1983.
- 18 G.J. Postma, B.G.M. Vandeginste, C.J.G. van Halen and G. Kateman, *Trends Anal. Chem.*, 6 (1987) 2, and references cited therein.
- 19 G.J. Kleywegt, H. Luinge and B.P. Schuman, *Chemometr. Intell. Lab. Syst.*, 4 (1988) 273.
- 20 G.J. Kleywegt, H. Luinge and B.P. Schuman, *Chemometr. Intell. Lab. Syst.*, 5 (1989) 117.
- 21 H. Moll and J. Clerc, in J. Zupan (Ed.), *PCs for Chemists*, Elsevier, Amsterdam, 1990, pp. 105–133.
- 22 M.H. Richer, *Expert Systems*, 3 (1986) 166.
- 23 G. Wünsch and M. Gansen, *Fresenius' Z. Anal. Chem.*, 333 (1989) 607.
- 24 M. De Smet and D.L. Massart, *Trends Anal. Chem.*, 6 (1987) 266.
- 25 E.A. Feigenbaum, in *The Art of Artificial Intelligence. 1: Themes and Case Studies of Knowledge Engineering*, Publ. No. STAN-CS-77-621, Department of Computer Science, Stanford University, Stanford, CA, 1977.
- 26 D. Michie and I. Bratko, *Expert Systems. Automatic Knowledge Acquisition*, Addison-Wesley, Wokingham, 1986.
- 27 E.D. Salin and P.H. Winston, *Anal. Chem.*, 64 (1992) 49A.
- 28 J.R. Quinlan, *Machine Learning*, 1 (1986) 81.
- 29 P. Vankeerberghen and D.L. Massart, *Trends Anal. Chem.*, 10 (1991) 110.
- 30 L. Buydens, D.L. Massart and P.K. Hopke, *Chemometr. Intell. Lab. Syst.*, 3 (1988) 199.
- 31 R.L. Erskine, in R. Brereton (Ed.), *Course Notes of the European Spring School in Chemometr.*, University of Bristol, 10–15 April 1988.
- 32 M.E. Munk, *J. Chem. Inf. Comput. Sci.*, 32 (1992) 263.
- 33 C.F. Poole and S.K. Poole, *Chromatography Today*, Elsevier, Amsterdam, 1991, pp. 947–1003.
- 34 H.J. Luinge, G.J. Kleywegt, H.A. Van't Klooster and J.H. Van der Maas, *J. Chem. Inf. Comput. Sci.*, 27 (1987) 95.
- 35 H.J. Luinge, *Trends Anal. Chem.*, 9 (1990) 66.
- 36 L. Ying, S.P. Levine, S.A. Tomellini and S.R. Lowry, *Anal. Chim. Acta*, 210 (1988) 51, and references cited therein.
- 37 B.J. Wythoff and S.A. Tomellini, *Anal. Chim. Acta*, 227 (1989) 359.
- 38 L. Ying, S.P. Levine, S.A. Tomellini and S.R. Lowry, *Anal. Chem.*, 59 (1987) 2197.
- 39 E.J. Hasenoehrl, J.H. Perkins and P.R. Griffiths, *Anal. Chem.*, 64 (1992) 656.
- 40 E.J. Hasenoehrl, J.H. Perkins and P.R. Griffiths, *Anal. Chem.*, 64 (1992) 705.
- 41 K. Janssens and P. Van Espen, *Anal. Chim. Acta*, 184 (1986) 117.
- 42 G. Holzer, W. Bertsch and Q.W. Zhang, *Anal. Chim. Acta*, 259 (1992) 225.
- 43 M. Sarker, W. G. Glen, L. Yin, W.J. Dunn, III, D.R. Scott and S. Swanson, *Anal. Chim. Acta*, 257 (1992) 229, and references cited therein.
- 44 D.R. Scott, *Anal. Chim. Acta*, 265 (1992) 43.
- 45 D.R. Scott, *Anal. Chim. Acta*, 223 (1989) 105.
- 46 D.R. Scott, *Anal. Chim. Acta*, 246 (1991) 391.
- 47 D.R. Scott, *Chemometr. Intell. Lab. Systems*, 16 (1992) 193.
- 48 F.A. Settle, Jr., *J. Chem. Educ.*, 64 (1987) 340.
- 49 M.S. Larrechi and F.X. Rius, *J. Chem. Educ.*, 68 (1991) 659.
- 50 F.A. Settle, Jr., B.I. Diamondstone, H.M. Kingston and M.A. Pleva, *J. Chem. Inf. Comput. Sci.*, 29 (1989) 11.
- 51 F.A. Settle, Jr., P.J. Walter, H.M. Kingston, M.A. Pleva, T. Snider and W. Boute, *J. Chem. Inf. Comput. Sci.*, 32 (1992) 349.
- 52 M. Moors and D.L. Massart, *Trends Anal. Chem.*, 9 (1990) 164.
- 53 L. Xu, Y. Xiao and D. Li, *J. Chem. Inf. Comput. Sci.*, 32 (1992) 437.
- 54 R.A. Olivero and D.W. Bottrell, in J.M. Hushon (Ed.), *Expert Systems for Environmental Applications (ACS Symposium Series, Vol. 431)*, American Chemical Society, Washington, DC, 1990, pp. 69–81.
- 55 J.A. van Leeuwen, B.G.M. Vandeginste, G.J. Postma and G. Kateman, *Chemometr. Intell. Lab. Syst.*, 6 (1989) 239.
- 56 P. Conti, T. Hamoir, M. De Smet, H. Piryns, N. Vanden Driessche, F. Marais, H. Hindriks, P.J. Schoenmakers and D.L. Massart, *Chemometr. Intell. Lab. Syst.*, 11 (1991) 27, and references cited therein.
- 57 J.A. van Leeuwen, L.M.C. Buydens, B.G.M. Vandeginste, G. Kateman, A. Cleland, M. Mulholland, C. Jansen, F.A. Marais, P.H. Hoogkamer and J.H.M. van den Berg, *Chemometr. Intell. Lab. Syst.*, 11 (1991) 161, and references cited therein.
- 58 Y. Zhang, H. Zou and P. Lu, *J. Chromatogr.*, 515 (1990) 13.
- 59 T.P. Bridge, M.H. Williams and A.F. Fell, *J. Chromatogr.*, 465 (1989) 59.
- 60 M.A. Tischler and E.A. Fox, *Comput. Chem.*, 11 (1987) 125.
- 61 T.P. Bridge, *Chromatogr. Anal.*, 11 (1990) 13.

- 62 S.S. Williams, *Trends Anal. Chem.*, 9 (1990) 63.
- 63 S.A. Borman, *Anal. Chem.*, 58 (1986) 1192 A.
- 64 T.P. Bridge, M.H. Williams and A.F. Fell, *Anal. Proc.*, 25 (1988) 43.
- 65 J.C. Pearce, A. Churchill and A.C. Terry, *Chemometr. Intell. Lab. Syst.*, 17 (1992) 213.
- 66 H. Gunasingham, B. Srinivasan and A.L. Ananda, *Anal. Chim. Acta*, 182 (1986) 193.
- 67 B.J. Clark, A.F. Fell, K.T. Milne and M.H. Williams, *J. Pharm. Pharmacol.*, 37 (1985) 1298.
- 68 W.R. Browett, T.A. Cox and M.J. Stillman, in B.A. Hohne and T.A. Pierce (Eds.), *Expert System Applications in Chemistry* (ACS Symposium Series, Vol. 408), American Chemical Society, Washington, DC, 1989, pp. 210–235.
- 69 W.R. Browett and M.J. Stillman, *Prog. Anal. Spectrosc.*, 12 (1989) 73.
- 70 S. Lahiri and M.J. Stillman, *Anal. Chem.*, 64 (1992) 283A.
- 71 D.P. Webb and E.D. Salin, *J. Anal. At. Spectrom.*, 4 (1990) 793.
- 72 I. Ruisánchez, M.S. Larrechi, F.X. Rius and M. Esteban, *Trends Anal. Chem.*, 11 (1992) 135.
- 73 M. Esteban, I. Ruisánchez, M.S. Larrechi and F.X. Rius, *Anal. Chim. Acta*, 268 (1992) 95.
- 74 M. Esteban, I. Ruisánchez, M.S. Larrechi and F.X. Rius, *Anal. Chim. Acta*, 268 (1992) 107.
- 75 M. Esteban, C. Ariño, I. Ruisánchez, M.S. Larrechi and F.X. Rius, *Anal. Chim. Acta*, submitted for publication.
- 76 H. Hirayama, R. Wohlsen and C. Brede, in B.A. Hohne and T.A. Pierce (Eds.), *Expert System Applications in Chemistry* (ACS Symposium Series, Vol. 408), American Chemical Society, Washington, DC, 1989, pp. 200–209.
- 77 J.M. Hushon (Ed.), *Expert Systems for Environmental Applications* (ACS Symposium Series, Vol. 431), American Chemical Society, Washington, DC, 1990.
- 78 D.W. Bigwood, S.R. Heller, W.R. Wolf, A. Schubert and J.M. Holden, *Anal. Chim. Acta*, 200 (1987) 411.
- 79 M. Marsili, E. Marengo and H. Saller, *Anal. Chim. Acta*, 210 (1988) 33.
- 80 R. Wolters, A.C.M. Van Den Broek and G. Kateman, *Chemometr. Intell. Lab. Syst.*, 9 (1990) 143.
- 81 K. Danzer, U. Wank and D. Wienke, *Chemometr. Intell. Lab. Syst.*, 12 (1991) 69.
- 82 N. Woodhead, *Hypertext and Hypermedia: Theory and Applications*, Addison Wesley, Reading, MA, 1991.
- 83 M. Farkas, M. Cadish and E. Pretsch, *Scientific Computing and Automation*, Elsevier, Amsterdam, 1990.
- 84 B. Bourguignon, P. Vankeerberghen and D.L. Massart, *J. Chromatogr.*, 592 (1992) 51.
- 85 W. Penninckx, J. Smeyers-Verbeke, D.L. Massart, L.G.C.W. Spanjers and F. Maris, *Chemometr. Intell. Lab. Syst.*, 17 (1992) 193.
- 86 W. Penninckx, J. Smeyers-Verbeke, D.L. Massart, L.G.C.W. Spanjers and F. Maris, in preparation.
- 87 H. Eriksson, *J. Chem. Inf. Comput. Sci.*, 32 (1992) 90.
- 88 M. Valcárcel and M.D. Luque de Castro, *Automatic Methods of Analysis*, Elsevier, Amsterdam, 1988.
- 89 V. Cerdà and G. Ramis, *An Introduction to Laboratory Automation*, Wiley, Chichester, 1990.
- 90 S.D. Brown, R.S. Bear, Jr., and T.B. Blank, *Anal. Chem.*, 64 (1992) 22R.
- 91 S.R. Crouch, *Chemometr. Intell. Lab. Syst.*, 8 (1990) 259.
- 92 J. Zupan, *Anal. Chim. Acta*, 235 (1990) 53.
- 93 J. Zupan and J. Gasteiger, *Anal. Chim. Acta*, 248 (1991) 1.
- 94 T.L. Isenhour and J.C. Marshall, *J. Res. Natl. Bur. Stand.*, 93 (1988) 209.
- 95 T.L. Isenhour, S.E. Eckert and J.C. Marshall, *Anal. Chem.*, 61 (1989) 805A.
- 96 T.L. Isenhour and P.B. Harrington, *J. Chem. Inf. Comput. Sci.*, 28 (1988) 215.
- 97 J.R. Lee, T.L. Isenhour and J.C. Marshall, *J. Chem. Inf. Comput. Sci.*, 31 (1991) 546.
- 98 S.E. Eckert-Tilotta, T.L. Isenhour and J.C. Marshall, *Anal. Chim. Acta*, 254 (1991) 215.
- 99 I. Ruisánchez, A. Rius, M.P. Callao, M.S. Larrechi and F.X. Rius, in M. Valcárcel (Ed.), *Proceedings of the 12th International Symposium on Microchemical Techniques*, Córdoba, 1992.
- 100 G. Kateman, *Trends Anal. Chem.*, 3 (1984) VII.
- 101 N. Winkless and I. Browning, *Robots on Your Doorstep*, Robotics Press, Portland, OR, 1978.



# Chemometric study of organic pollution in the aerosol of Madrid

J. Méndez

*Centro Nacional de Sanidad Ambiental, Instituto de Salud Carlos III, 28220 Majadahonda, Madrid (Spain)*

A.J. Quejido, R. Pérez-Pastor and M. Pérez-García

*División de Química, CIEMAT, Avda. Complutense 22, 28040 Madrid (Spain)*

(Received 8th September 1992; revised manuscript received 1st February 1993)

## Abstract

The incomplete combustion of fossil fuels is one of the more important contributions of organic compounds to the atmosphere. Most of them can be detected in the aerosol and a number of these are known to be carcinogenic and mutagenic. For this reason, it is necessary to control their emission for environmental protection. Multivariate techniques were applied to the results obtained after a previous development of analytical methodologies, including sampling and determination by gas chromatography–mass spectrometry of the aliphatics and polynuclear aromatic hydrocarbons compounds in airborne particulate matter. Both chemical parameters [e.g. biogenic and anthropogenic alkanes, carbon predominance index (CPI), unresolved complex mixture (UCM) and aromatic hydrocarbons] and meteorological (temperatures, rainfall and daily sunlight period) parameters were determined weekly during the period January 1989–December 1990 at two sampling sites located in the centre of Madrid (a highly polluted area). Another site was located in a residential area and another one far from any polluting source. Correlation studies, factor analysis and cluster analysis were applied to the raw and transformed data, showing different patterns related to the anthropogenic activity along the year, that can be distinguished by means of these studies with the organic pollutant values and the meteorological conditions during sampling.

*Keywords:* Gas chromatography–mass spectrometry; Pattern recognition; Air; Cluster analysis; Factor analysis; Organic aerosols

In the last decade, there has been growing concern about the concentration of organic compounds in the atmosphere of urban areas [1]. Some of these compounds, such as the polynuclear aromatic hydrocarbons (PAHs), have well known mutagenic and carcinogenic activity [2,3]. Long-range transport of PAHs, with relatively good chemical stability, becomes feasible, promoting the formation of secondary pollutants with

higher toxicity by photochemical reactions [4,5]. The large number and wide variety of pollution sources of these compounds in urban areas is increased by industrial activity, natural sources and atmospheric reactions.

Other compounds associated with airborne particulate matter include aliphatic hydrocarbons. Two main sources of these compounds are known: compounds generated in biogenic processes, such as vegetation activity, wood-burning fires and the oceanic aerosols, and characterized by a range from  $C_{15}$  to  $C_{35}$  with an odd carbon number predominance above  $C_{25}$ , and with  $C_{27}$ ,

*Correspondence to:* J. Méndez, Centro Nacional de Sanidad, Instituto de Salud Carlos III, 28220 Majadahonda, Madrid (Spain).

$C_{29}$ ,  $C_{31}$  and  $C_{33}$  being the more significant  $n$ -alkanes associated with vegetable waxes [6,7]; and compounds generated by anthropogenic sources, such as fossil fuel combustion and vehicle exhausts, and showing a predominance of low carbon numbers (below  $C_{21}$ ) [8,9].

In order to evaluate the effects of different pollution sources and their variability with time, large numbers of samples must be analysed. In addition, several variables, both chemical and meteorological, must be measured. For this reason, modern multivariate techniques, such as pattern recognition, have been selected to extract and evaluate information from data according to the studied area and the sampling date [10–12].

The aim of this work was to establish pollution patterns in urban areas according to organic compound sources and meteorological conditions during the year. A comparison with an unpolluted area was carried out in order to discriminate anthropogenic and biogenic sources.

## EXPERIMENTAL

### *Sampling*

Particulate matter samples were collected by high-volume samplers. About 800 m<sup>3</sup> (in urban sites) or 1800 m<sup>3</sup> (in rural site) of air were drawn through a glass-fibre filter in 24 h.

Sampling was done in the metropolitan area of Madrid, with a population about 3.1 million and with very dense traffic. Sampling points were selected inside the city and at distances of not more than 10 km. Ciudad Universitaria (sampling point 1) is located in the north-west of the city, 2 km from the centre, and is characterized by open areas, university buildings and large garden extensions. The main pollutant sources are automobile exhausts and domestic heating. These are not important pollution sources and, therefore, it can be considered as a “residential area”. Paseo del Prado (sampling point 2) is located inside the city with dense traffic and a wide variety of buildings, some of them with very old and badly regulated central heating. There is also a large park near this point. Legazpi (sampling point 3) is located in the south of the city with numerous mobile and stationary emission sources in the vicinity.

In addition to these urban sites, a rural station was selected (sampling point 4), located at San Pablo de los Montes (Toledo), 130 km from Madrid. This site is a EMEP (Environmental Monitoring Evaluating Program) station.

Two sampling campaigns were carried out weekly during the period 1989–90. A total of 278 samples were collected.

Several meteorological parameters, such as maximum and minimum temperature, rainfall and daily sunlight period, were measured during sampling.

### *Analytical procedure*

Samples were Soxhlet extracted with methylene chloride and cleaned up by silica gel column chromatography. The experimental procedure has been described previously [13].

The two different fractions thus obtained were subjected to gas chromatographic (GC) and gas chromatographic–mass spectrometric (GC–MS) analysis.

Several chemical parameters were determined: Aliphatic biogenic and anthropogenic and aromatic hydrocarbon concentrations were measured. The carbon predominance index (CPI) is the summation of the odd carbon number alkanes over a range divided by the summation of the even carbon number homologues over the same range. A high CPI (> 4) indicates the major incorporation of biological constituents into the sample. The addition of contaminants reduces the CPI, such that values of about 1 reflect a significant input of anthropogenic compounds. The unresolved complex mixture (UCM) area is the envelope of unresolved complex hydrocarbons derived from petroleum residues. The ratio of unresolved and resolved aliphatic hydrocarbons (U : R) was also measured.

### *Data processing*

A commercial statistics software package, Statgraphics (Statistical Graphics, 1990) and a BASIC program called CLUSTER, developed by one of the authors [14], were used for the chemometric study of data. Statgraphics is implemented on a personal computer, whereas CLUSTER is implemented on a VAX 8350 computer.

## RESULTS AND DISCUSSION

In Table 1 the descriptive statistics of both the chemical and meteorological data obtained from the samples are given. As the different orders of magnitude of some of these data could produce a bias in the conclusions obtained, standardization of the raw data is needed. A z-transform was carried out in order to convert the Gaussian distribution of each variable from  $N(\mu_i, \sigma_i)$  to  $N(0, 1)$ .

*Correlation and factor analysis*

In studies of the environment, many variables are measured in order to characterize the system. However, not all of these variables are independent of one another. Hence it is essential to have mathematical techniques that permit the study of the simultaneous variation of multiple variables. One such analysis is based on examining the relationship between pairs of variables (correlation study). This correlation analysis, however, does not always provide a clear view of the multiple interactions in the data. Thus, various forms of eigenvectors analysis are used to convert the correlation data into multivariate information. Factor analysis (FA) is the name given to one of the variety of forms of eigenvector analysis. It was originally developed and used in psychology to provide mathematical models of psychological theories of human ability and behaviour [15].

However, eigenvector analysis has found wide application throughout the physical and life sciences. Unfortunately, a great deal of confusion exists in the literature with regard to the termi-

nology of eigenvector analysis. Various changes in the way the method is applied have resulted in it being called factor analysis, principal component analysis, principal component factor analysis, empirical orthogonal function analysis, Karhunen–Loewe transform and so on, depending on the way in which the data are scaled before analysis or how the resulting vectors are treated after the eigenvector analysis is completed. Even so, a further treatment of the eigenvectors obtained has been developed by several workers [16] in order to establish better variability between factors, including rotation of these components, such as varimax and quartimax.

All of the eigenvector methods have the same basic objective: the compression of data into fewer dimensions and the identification of the structure of interrelationships that exist between the variables measured or the samples being studied. In many chemical studies, the measured properties of a system can be considered to be the sum of the terms representing the fundamental effects of the system multiplied by appropriate weighting factors. Another use of such methods can be found in the resolution of environmental mixtures according to their source contributions. For example, a sample of airborne particulate matter collected at a specific site at a specific time is made up of particles of several sources (soils, motor vehicle exhausts, industrial point sources, domestic heating sources, etc.). It may be of interest to determine how much of the total collected mass of particles comes from each source [17].

TABLE 1

Descriptive statistics of raw data

Variable	Average	Standard deviation	Minimum value	Maximum value
Total <i>n</i> -alkanes (ng m <sup>-3</sup> )	123.8	142.1	4.3	726.8
Biogenic <i>n</i> -alkanes (ng m <sup>-3</sup> )	12.1	7.6	1.3	70.3
CPI	1.7	0.9	1	6.2
UCM (ng m <sup>-3</sup> )	1444.9	1476.6	6.8	6283.8
U:R	11.9	4.9	0.8	27.1
PAHs (ng m <sup>-3</sup> )	22.5	32.4	0.1	147.2
Max. temperature (°C)	19.8	8.8	4	39
Min. temperature (°C)	9.9	6.5	-4	24.5
Rainfall (l m <sup>-2</sup> )	1.2	3.5	0	21
Daily sunlight period (h)	7.6	3.8	0	13

TABLE 2

Correlation coefficients of total samples

No. <sup>a</sup>	1	2	3	4	5	6	7	8	9	10
1	1									
2	0.28	1								
3	-0.40	0.16	1							
4	0.94	0.25	-0.48	1						
5	-0.06	-0.12	-0.48	0.16	1					
6	0.82	0.13	-0.39	0.80	-0.01	1				
7	-0.38	0.17	0.54	-0.35	-0.01	-0.44	1			
8	-0.40	0.12	0.50	-0.37	0.05	-0.48	0.90	1		
9	-0.07	-0.10	-0.06	-0.08	0.03	-0.09	-0.19	-0.02	1	
10	-0.14	0.22	0.35	-0.13	-0.04	-0.18	0.70	0.52	-0.38	1

<sup>a</sup> 1 = Total *n*-alkanes; 2 = biogenic *n*-alkanes (*n*-C<sub>27</sub>-*n*-C<sub>33</sub>); 3 = CPI; 4 = UCM; 5 = U : R; 6 = PAHs; 7 = maximum temperature; 8 = minimum temperature; 9 = rainfall; 10 = daily sunlight period.

Hence factor analysis can help to compress multivariate data to sufficiently few dimensions to make visualization possible and to assist in identifying the interrelated variables. Depending on the approach used, the results can be interpreted statistically or they can be directly related to the structural variables that describe the system being studied. However, in all instances, the researcher must interpret the interrelationships determined by the analysis within the context of the problem concerned to provide a more detailed understanding of the system.

In this paper, factor analysis, including varimax rotation and correlation analysis between variables, was applied in order to achieve interre-

lationships between the measured variables and the effect of several environmental conditions on these measurements.

In Table 2 the correlation coefficients between variables considering all samples are given. The high value observed between total alkanes and UCM ( $r = 0.94$ ) confirm that an increase in pollution promotes increases in alkane concentration and the UCM value. A high value is also obtained between PAHs and alkanes and between PAHs and UCM, which can be explained by the assumption that both groups of organic compounds come from the same source.

The correlation coefficient values follow the sequence Legazpi > Paseo del Prado ≥ Ciudad

TABLE 3

Correlation coefficients of rural station samples

No. <sup>a</sup>	1	2	3	4	5	6	7	8	9	10
1	1									
2	0.85	1								
3	0.53	0.81	1							
4	0.50	0.07	0.14	1						
5	-0.23	0.46	-0.44	0.59	1					
6	0.10	-0.15	-0.33	0.17	0.06	1				
7	0.40	0.51	0.59	0.08	-0.32	-0.42	1			
8	0.33	0.47	0.53	0.06	-0.26	-0.43	0.95	1		
9	-0.35	-0.27	-0.14	-0.23	-0.07	-0.13	-0.34	-0.20	1	
10	0.43	0.47	0.51	0.18	-0.25	-0.32	0.76	0.68	-0.42	1

<sup>a</sup> 1 = Total *n*-alkanes; 2 = biogenic *n*-alkanes (*n*-C<sub>26</sub>-*n*-C<sub>33</sub>); 3 = CPI; 4 = UCM; 5 = U : R; 6 = PAHs; 7 = maximum temperature; 8 = minimum temperature; 9 = rainfall; 10 = daily sunlight period.

Universitaria  $\gg$  rural station. This shows the importance of the anthropogenic sources with regard to alkanes and UCM values.

A negative correlation coefficient is observed between alkanes and CPI. An increase in the CPI value can be ascribed to an increase in biogenic emissions, which are more important during spring and summer periods. This assumption is confirmed when a correlation study for different seasons is carried out. During spring and summer, the anthropogenic alkane sources (mainly domestic heating) decrease in activity. For this

reason, a negative correlation between these two variables is obtained. However, at the rural sampling point, where there is no anthropogenic activity, a positive correlation coefficient should be obtained as the only source of alkanes is the biogenic activity. This is shown in Table 3, where the correlation coefficients between variables are described, considering samples collected at the rural site.

This is confirmed by the low correlation coefficient between total and biogenic alkanes in Table 2 (0.28), whereas a high coefficient (0.85) is ob-

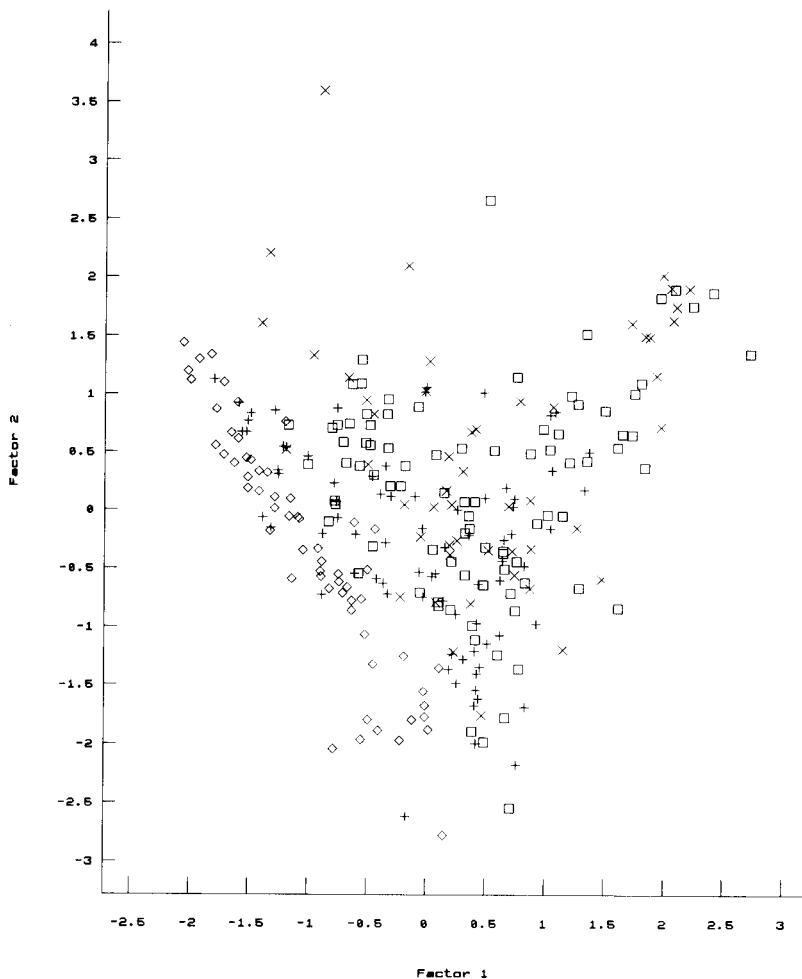


Fig. 1. Plot of the first two factors. + = Site 1;  $\square$  = site 2;  $\times$  = site 3;  $\diamond$  = site 4.

TABLE 4

Eigenvalues and associated variance of factors

Factor	Eigenvalue	Variance (%)	Accumulated variance (%)
Factor 1	3.99	39.93	39.93
Factor 2	2.06	20.66	60.59
Factor 3	1.32	13.23	73.82
Factor 4	0.98	9.78	83.60
Factor 5	0.67	6.75	90.35
Factor 6	0.38	3.82	94.17
Factor 7	0.30	2.99	97.16
Factor 8	0.19	1.89	99.05
Factor 9	0.06	0.64	99.69
Factor 10	0.03	0.31	100.00

tained when rural samples only are considered. At urban sites, the biogenic alkanes can be considered as a minimum percentage of the total amount of these compounds. At these sites, correlation coefficients lower than 0.4 are obtained.

Significant positive correlation coefficients are obtained between CPI and temperature, as biogenic activity is higher during warm periods, as has been mentioned above.

Diagonalization of the correlation matrix provides the eigenvalues shown in Table 4, which also includes the variance associated with each factor. Many criteria to retain the significant factors have been described. Kaiser [18] proposed that only factors whose eigenvalue is greater than unity should be considered. From Table 4, only three factors (including 73.82% of the system variance) should be retained. Table 5 gives the eigenvector components of these first three factors.

The main contribution to factor 1 is due to alkanes, UCM, PAHs and, negatively, CPI and temperature. This factor should therefore be assigned to high pollution conditions. The assignment of the two remaining factors to real behaviour cannot be done. This is shown in Fig. 1, where the projections of the samples in a factor 1 vs. factor 2 plot are represented. Higher values of factor 1 indicate higher pollution conditions. For this reason, samples located on the right-hand side of the plot are those collected at the centre of Madrid, whereas samples located on the left-hand side are those sampled at the rural site.

TABLE 5

Eigenvector components of the first three factors

No.	Eigenvector	Factor 1	Factor 2	Factor 3
1	Total <i>n</i> -alkanes	0.79	0.52	-0.08
2	Biogenic <i>n</i> -alkanes	0.01	0.63	-0.19
3	CPI	-0.70	0.19	-0.52
4	UCM	0.80	0.50	0.13
5	U:R	0.13	-0.14	0.91
6	PAHs	0.80	0.39	-0.07
7	Max. temperature	-0.81	0.45	0.21
8	Min. temperature	-0.79	0.31	0.23
9	Rainfall	0.08	-0.49	-0.13
10	Daily sunlight period	-0.54	0.63	0.20

When factor analysis for different sampling points is carried out, similar results are obtained for urban sites, whereas for the rural site the first factor (including more than 50% of the total variance) is related to alkanes, biogenic hydrocarbons, CPI and temperature, indicating the emission of organic compounds during periods of mild meteorological conditions.

In order to achieve more reliable information about the data obtained, a varimax rotation was carried out. In Table 6, eigenvector components of the first three rotated factors are given.

The first rotated factor is mainly related to alkanes, UCM and aromatics (chemical variables), whereas the second is associated with meteorological parameters (temperature and daily sunlight period) and the third with U:R and CPI

TABLE 6

Eigenvector components of the first three factors after varimax rotation

No.	Eigenvector	Factor 1	Factor 2	Factor 3
1	Total <i>n</i> -alkanes	0.95	-0.07	0.00
2	Biogenic <i>n</i> -alkanes	0.40	0.42	0.31
3	CPI	-0.41	0.39	0.69
4	UCM	0.93	-0.02	-0.20
5	U:R	-0.03	0.09	-0.93
6	PAHs	0.88	-0.17	-0.03
7	Max. temperature	-0.38	0.86	0.08
8	Min. temperature	-0.45	0.75	0.02
9	Rainfall	-0.23	-0.46	0.01
10	Daily sunlight period	-0.06	0.85	0.06

values. Hence a varimax rotation is useful for obtaining “latent variables” from the studied system. The same results are obtained when varimax rotation for different sampling points and different seasons is applied.

In Fig. 2, a plot of the first two rotated factors is given. An increase on the abscissa denotes higher pollution values, whereas samples at the top of the figure correspond to those collected during mild meteorological conditions (spring and summer seasons). It must be taken into account

that this plot shows only 60.56% of the total system variance. For this reason, an alternative mathematical technique is needed to represent the relative “likelihood” between the collected samples, such as cluster analysis.

#### Cluster analysis

The objective of cluster analysis is to sort objects into groups of similar characteristics. If  $m$  variables are measured for each of  $n$  objects, these can be represented by  $n$  points in an  $m$ -di-

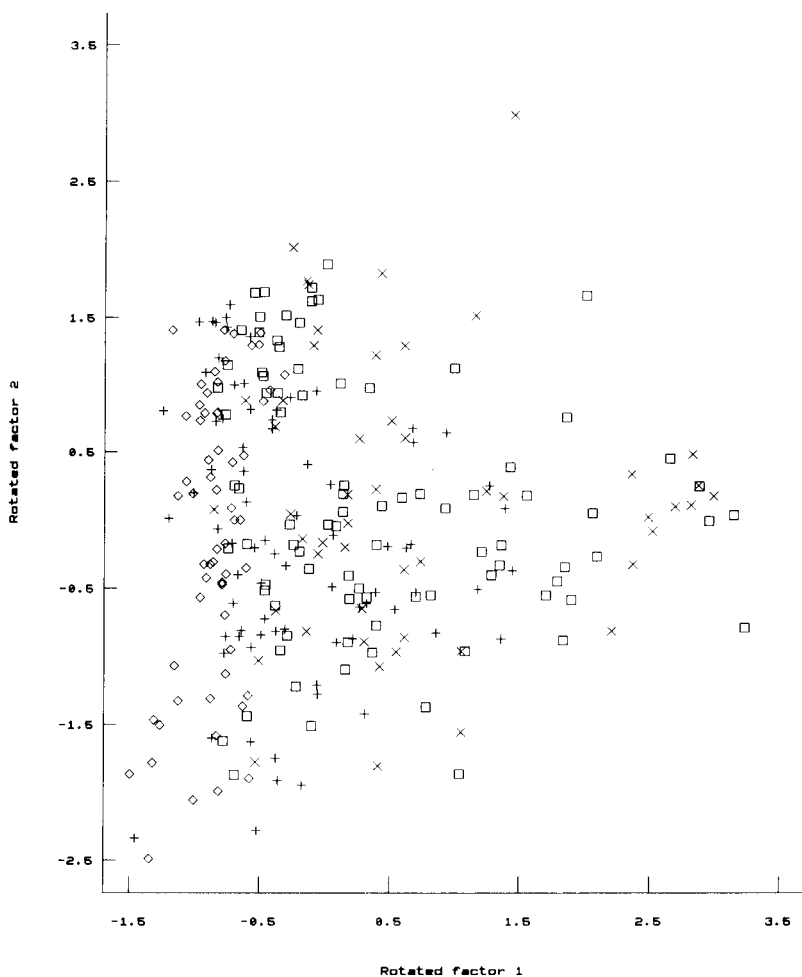


Fig. 2. Plot of the first two rotated factors. Symbols as in Fig. 1.

dimensional space. It is possible to define the similarity (or dissimilarity) between these points in terms of various geometric parameters such as the distance between the objects in the space. Using these inter-object similarity measures, groups of “close” objects can be found that form a cluster. There are a number of ways in which the differences between objects can be expressed and how to group objects based on these various distances measured. This subject was thoroughly reviewed by Massart and Kaufman [19]. In this

work, four similarity “distances” (Manhattan, Euclidean and Minkowski third- and fourth-order distances) were applied and five different strategies to group the objects (nearest, furthest, average, centroid and Ward strategies) were considered).

However, the significance of the groups formed must be evaluated, owing to the “blind” procedure used by the commercial clustering programs. In some instances, the grouping of two objects (or clusters) cannot be considered to be significant

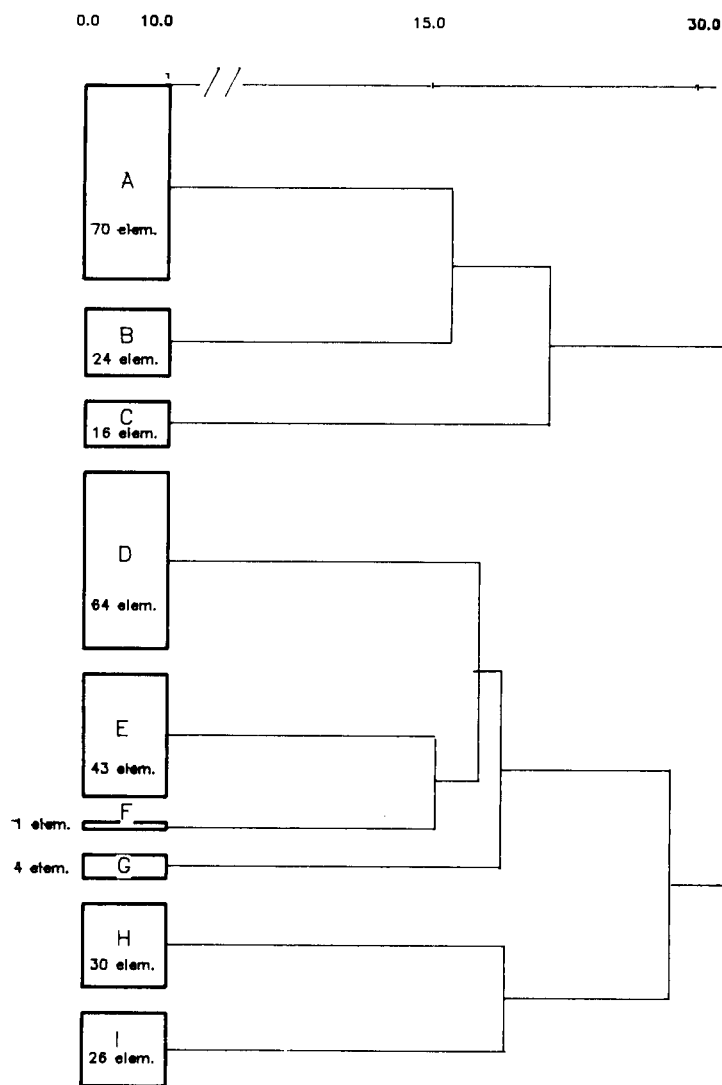


Fig. 3. Simplified dendrogram of the collected samples.



according to the relative values of their measured (or evaluated) variables. For this reason, although the program considers these objects to be grouped, it cannot be inferred statistically that these objects are similar.

Here, the significance of the groups formed was evaluated continuously by calculating both Mahalanobis distance between groups and the  $F$  statistic of the grouped objects (or previous clusters).

The use of different similarity measurements or clustering strategies leads to similar results. Figure 3 shows the simplified dendrogram obtained when Manhattan distance and furthest strategy are considered.

Nine main clusters can be defined and the block size is proportional to the number of samples or elements included in each cluster.

In Table 7 the average values of the variables for the clusters obtained are summarized. These values are useful for pointing out the characteristics of the samples grouped into the nine categories.

Category A (70 samples) corresponds to medium or slightly high values of pollutants and mild meteorological conditions. In this group samples collected during the autumn and winter period at urban sites are clustered. The large number of samples grouped in this category indicates that during 1989 and 1990 moderate pollution levels were reached in Madrid.

Category B (24 samples) includes those samples collected during autumn and winter at urban sites, but during more severe meteorological conditions and at higher pollutant concentrations.

The samples collected during highest pollution conditions are grouped in category C (16 samples).

These three categories are grouped at higher distance values and can be explained as a "polluted samples group".

An important number of samples (64) are included in category D. This group is characterized by an increase in the CPI and  $C_{\max}$  values, a decrease in the total alkane concentration and milder meteorological conditions.

Category E (43 samples) includes those samples collected during typical summer conditions and at low pollution levels, mainly from residential and rural areas.

A single element category (group F) is characterized by similar conditions to category E, but with high rainfall. This case can be isolated from the other samples, but it is clustered at higher distance values with the latter group owing to their similarity.

These three groups (D, E and F) can be defined as "slightly polluted samples collected under mild meteorological conditions".

Four peculiar samples are grouped in category G. These elements show high pollutant values (similar to categories A, B and C) but mild mete-

TABLE 7

Mean values of variables for each category

Variable	Clusters group								
	A	B	C	D	E	F	G	H	I
Total <i>n</i> -alkanes (ng m <sup>-3</sup> )	148	163	539	73	24	43	222	70	13
Biogenic <i>n</i> -alkanes (ng m <sup>-3</sup> )	12	13	15	12	13	24	54	8	6
IPC	1	1	1	1.5	3	2.8	2	1	2
UCM (ng m <sup>-3</sup> )	1814	2726	5245	754	189	477	1883	159	67
U:R	13	10	10	15	7	11	9	16	7
$C_{\max}$	23	22	22	26	29	31	26	23	29
PAHs (ng m <sup>-3</sup> )	27	65	11	7	1.4	6.1	16	15	1
Max. temperature (°C)	15	10	12	26	32	31	29	13	15
Min. temperature (°C)	6	3	4	14	18	16	15	9	6
Rainfall (l m <sup>-2</sup> )	0.3	1.6	0.1	0.3	0.2	18	1	6	2
Daily sunlight period (h)	7	5	7	10	11	12.4	1	1.5	5

orological parameters (close to categories D, E and F). According to the similarity distance and clustering strategy used, this category is grouped with the above mentioned A–B–C or D–E–F classes.

Category H (30 samples) includes those samples collected at the residential site during the year. They are characterized by low pollution values and intermediate temperatures but high rainfall values.

Finally, 26 samples are grouped in category I. These samples have similar pollution levels to category E but show lower rainfall values, moderate temperatures and higher sunlight periods. These samples were collected during the year at the rural site.

These two categories (H and I) can be defined as “low polluted samples collected under moderate meteorological conditions”.

### Conclusions

Multivariate techniques were applied to the study of organic pollution in the aerosol of Madrid during the period 1989–90. High correlation coefficients were obtained between variables directly connected with pollution (alkanes and aromatic hydrocarbons) and between meteorological measured parameters. Factor analysis, followed by varimax rotation, provides two significant latent variables related to pollution index and meteorological conditions, respectively.

The application of pattern recognition methods (cluster analysis) allows the clarification of similarities among samples according to sampling site and stational variations.

### REFERENCES

- 1 K.E. Thrane and A. Mikalsen, *Atmos. Environ.*, 15 (1981) 909.
- 2 G. Grimmer, *Fate of Hydrocarbons in the Environment. An Analytical Approach*, Vol. 10, Gordon and Breach, New York, 1986, p. 181.
- 3 J. Arey, B. Zielinska, W.P. Harges, R. Atkinson and A.M. Winer, *Mutat. Res.*, 207 (1988) 45.
- 4 T. Nielsen and B. Seitz, *Atmos. Environ.*, 10 (1984) 2159.
- 5 B. Zielinska, J. Arey, R. Atkinson and A.M. Winer, *Atmos. Environ.*, 23 (1989) 223.
- 6 B.R. Simoneit and M.A. Mazurek, *Atmos. Environ.*, 16 (1982) 2139.
- 7 R.E. Cox, M.A. Mazurek and B.R. Simoneit, *Nature*, 296 (1982) 848.
- 8 M.A. Mazurek and B.R. Simoneit, *Identification and Analysis of Organic Pollutants in Air*, Ann Arbor Science, Ann Arbor, MI, 1984, p. 353.
- 9 B.R. Simoneit, *Atmos. Environ.*, 18 (1984) 51.
- 10 S.A. Edgerton and M.W. Holdren, *Environ. Sci. Technol.*, 21 (1987) 1102.
- 11 L.M. Hildemann, M.A. Mazurek, G.R. Cass and B.R. Simoneit, *Environ. Sci. Technol.*, 25 (1991) 1331.
- 12 H. Lohninger and K. Varmuza, *Anal. Chem.*, 59 (1987) 236.
- 13 M. Pérez-García, J. Méndez and M.T. Bomboi, *Informe CIEMAT*, No. 619 (1988).
- 14 A.J. Quejido, PhD Thesis, Universidad Complutense de Madrid, Madrid, 1989.
- 15 H.H. Harman, *Modern Factor Analysis*, University of Chicago Press, Chicago, 3rd edn., 1976.
- 16 E.R. Malinowski and D.G. Howery, *Factor Analysis in Chemistry*, Wiley, New York, 1980.
- 17 P.K. Hopke, *Receptor Modeling in Environmental Chemistry*, Wiley, New York, 1985.
- 18 H.F. Kaiser, *Psychometrika*, 23 (1958) 187.
- 19 D.L. Massart and L. Kaufman, *The Interpretation of Analytical Chemical Data by the Use of Cluster Analysis*, Wiley, New York, 1983.

# Application of an evolving factor analysis-based procedure to speciation analysis in the copper(II)–polyuridylic acid system

E. Casassas, R. Gargallo, I. Giménez, A. Izquierdo-Ridorsa and R. Tauler

*Departament de Química Analítica, Universitat de Barcelona, Avda. Diagonal 647, 08028 Barcelona (Spain)*

(Received 10th September 1992; revised manuscript received 14th December 1992)

## Abstract

The acid–base properties and the copper(II)-complexing behaviour of the polynucleotide polyuridylic acid were studied by means of potentiometric, spectrophotometric and electron spin resonance titrations in a working aqueous medium of 0.15 M ionic strength and at 37°C. Spectrophotometric data were treated with an evolving factor analysis-based procedure that allows different sets of spectrometric titrations of the same multi-equilibria system to be analysed simultaneously. A dimeric macromolecular complex species between copper(II) ions and polyuridylic acid was detected in the system and its formation constant was evaluated.

**Keywords:** Electron spin resonance spectrometry; Potentiometry; Titrimetry; UV–Visible spectrophotometry; Copper complexes; Evolving factor analysis; Polynucleotides; Polyuridylic acid; Speciation

This work is part of a wider study concerning the interpretation of metal ions and proton interactions with nucleic acids and their constituents in aqueous solution under physiological conditions [1–3]. In this work, the acid–base properties and the copper(II)-complexing behaviour of the polynucleotide polyuridylic acid [poly(U)], where all the nitrogen bases are uracil molecules (see Scheme 1), are presented. This study was carried out by means of potentiometric, spectrophotometric and electron spin resonance (ESR) titrations in a working aqueous medium of 0.15 M ionic strength and at 37°C, which can be considered physiological conditions.

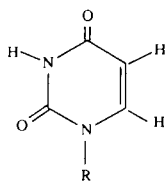
Because the information obtained by the different techniques is in certain respects comple-

mentary, it is worth using them simultaneously in the study of complicated systems, such as that investigated here, which contains a macromolecular ligand.

Complex formation by macromolecular ligands is influenced by some secondary effects [4], viz., polyfunctional effects, conformational changes and polyelectrolyte effects, which affect the stability of the species formed and vary with the degree of site occupation (complexation) and/or site deprotonation. Thus, the interpretation of experimental data using traditional least-squares curve fitting approaches, which are based on the postulation of a chemical model and on compliance with the mass action law, is difficult or even impossible for multi-equilibria systems involving macromolecular ligands.

In this work, an approach which is an improvement of a previously developed SPFAC procedure [5–8] was applied to the spectrophotometric

*Correspondence to:* A. Izquierdo-Ridorsa, Departament de Química Analítica, Universitat de Barcelona, Avda. Diagonal 647, 08028 Barcelona (Spain).



Scheme 1. R = ribose-5'-monophosphate in poly(U).

titrations. SPFAC is an evolving factor analysis-based procedure, which can be advantageously used for the study of multi-equilibria systems, in order to define the number of species present and to evaluate their concentrations, their individual spectra and their stability constants, without the requirement of postulating a chemical model and without making any use of the mass action law. Whereas in the previously described SPFAC procedure evolving factor analysis techniques were applied to the treatment of individual spectrometric titrations, in the modified SPFAC program [8] the simultaneous analysis can be performed on different sets of spectrometric titrations for the same multi equilibria system under different experimental conditions if the spectra in all the analysed titrations are measured at the same set of wavelengths. Some of the ambiguities that may appear when a single titration is analysed are removed when several spectrometric titrations under different starting conditions (different initial concentrations of the constituents) are analysed simultaneously and the individual spectra of the common species in the different spectrometric titrations are forced to be equal.

In the macromolecular system studied here, the results obtained from SPFAC analysis may be a good starting point for chemical modelling and application of the traditional least-squares procedures, which cannot ensure by themselves the validity of the postulated model.

The copper(II) complexation results obtained with poly(U) were compared with those obtained previously with the mononucleotide uridine-3,5'-cyclic monophosphate (cyclic UMP) [3], which can be considered as a model compound as it contains the same coordinating centres as poly(U).

## EXPERIMENTAL

### Reagents and solutions

Nitric acid, copper(II) oxide, sodium nitrate (Merck, analytical-reagent grade) and polyuridylic acid sodium salt (Sigma) were used without further purification. All the solutions were prepared using CO<sub>2</sub>-free deionized water.

Stock solutions of copper(II) ion were standardized by iodimetric titration. Stock solutions of poly(U) were prepared from a known amount of the solid reagent and dissolution in water. The concentration of these solutions was referred to the concentration of the nucleotide uridine-3',5'-cyclic monophosphate, which is the monomeric unit in the polynucleotide chain. CO<sub>2</sub>-free sodium hydroxide (Merck, analytical reagent grade) solutions were prepared by Kolthoff's procedure [9] and standardized with potassium hydrogenphthalate.

The ionic strength of the measured solutions was kept at 0.15 mol dm<sup>-3</sup> by adding, when necessary, the appropriate amount of sodium nitrate.

### Apparatus

Visible absorption spectra at 37°C were recorded on a Beckman DU-7 spectrophotometer interfaced (RS232) to an IBM personal computer. Spectra acquisition was controlled through Beckman data capture software.

ESR spectra were recorded on a Varian E-109 spectrometer in capillary glass tubes of diameter 1 mm (Wilmad, Cat. No. 800)<sup>a</sup>.

pH measurements were performed with a Radiometer PHM-64 pH meter (with a precision of ±0.1 mV) and a combined Ross pH electrode (Orion 81-02). Titrant was added with a Metrohm Dosimat 655 autoburette equipped with an exchange unit of 5 cm<sup>3</sup> (with a precision of ±0.005 cm<sup>3</sup>). Sample solutions were titrated in a double-walled vessel maintained at 37.0 ± 0.1°C by circulating water and stirred magnetically under a continuous flow of nitrogen.

<sup>a</sup> Belonging to the Inst. of Development and Investigation, CSIC, Barcelona, whose cooperation is acknowledged.

### Procedure

Potentiometric titrations were carried out automatically. The potentiometric assembly was controlled by an HP 9816 microcomputer via an HP 3421 A data acquisition control unit (for details, see [10]).

Solutions for ESR and visible spectrometric studies were obtained during the potentiometric titration, with a standardized sodium hydroxide solution, of slightly acidic solutions containing different copper(II) ion concentrations and different ligand-to-metal ion concentration ratios. With the aid of a peristaltic pump the solution being titrated was introduced continuously into the flow cell in the spectrophotometer. After each titrant addition the pH of the solution was measured, the visible spectrum obtained (the absorbance was measured every 10 nm between 520 and 820 nm) and a sample of 100  $\mu$ l withdrawn for ESR spectrum determination.

For every titration, a previous calibration of the potentiometric cell was carried out by Gran's method [11]. In aqueous medium of 0.15 M ionic strength and at 37°C the value of the ionic product of the medium is  $-\log K_w = 13.30 \pm 0.03$ , and in the working pH range the pH dependence of the liquid junction potential is negligible.

The experimental conditions of the titrations performed are given in Table 1.

All the titrations can be performed up to basic pH values without the formation of any precipitate in the solutions.

### Data treatment

Data treatment of the experimental potentiometric data was carried out with the SUPERQUAD program [12], which uses traditional least-squares curve-fitting approaches, and is based on the postulation of a chemical model and on compliance with the mass action law. The accuracy of the results obtained is indicated by the value of the parameter SIGMA, which is the ratio of the root mean square of the weighted residuals to the estimated error under our working conditions (0.005 ml for the autoburette volume readings and 0.1 mV for the e.m.f. readings), and by the value of the statistical parameter  $\chi^2$ , which is based on weighted residuals of e.m.f. readings [12].

The interpretation of the experimental spectrophotometric data was carried out with the new version of the SPFAC program [8] and also, whenever possible, using the computer program SQUAD [13], which is a traditional least-squares curve-fitting approach based on the postulation of a chemical model and on compliance with the mass action law.

The SPFAC program is written in FORTRAN 77 and runs either on an IBM 3090 mainframe (large sets of data) or in an IBM PC environment (for small sets of data). Essentially, the data treatment consists of the following tasks:

(1) Building up of the data matrix *D*(NSOLN, NWAIVE). When an individual titration is analysed, the matrix *D* contains the spectra at

TABLE 1  
Experimental conditions of the titrations performed

Titration	Titration number	[Ligand] <sub>0</sub> (mM)	[Cu] <sub>0</sub> (mM)	Ligand-to-metal ratio
Potentiometric	1	2.173	–	–
	2	2.911	–	–
	3	3.861	–	–
	4	2.135	2.013	1.0:1
	5	3.015	2.329	1.3:1
	6	3.178	2.145	1.5:1
	7	2.575	1.161	2.2:1
Spectrophotometric and ESR	8	10.51	10.91	0.96:1
	9	12.63	4.849	2.6:1
	10	8.24	4.872	1.7:1

NWAVE wavelengths of the NSOLN mixtures obtained at the successive titration points of the spectrometric titration. When more than one titration is analysed simultaneously, the augmented data matrix  $D$  contains the same number of columns (NWAVE), as the spectra in all the titrations are measured at the same set of wavelengths, and a number of rows (NSOLN) equal to the total number of solutions in all the titrations. Matrix  $D$  is treated in the same way whether augmented or not.

(2) Factor analysis of the experimental data matrix  $D$ : calculation of the eigenvalues and eigenvectors of the matrix  $DD^T$  and estimation of the number of absorbing species in the system. This number is estimated using different independent methods: (a) from the changes in magnitude of the eigenvalues and from the plot of the RSD function (residual standard deviation function) obtained using the principles of the theory of error in factor analysis as proposed by Malinowski [14–16]; (b) from the plot of the SEP function (standard error of prediction function) obtained from cross-validation of the complete spectral matrix data as proposed by Wold [17]; and (c) from the abstract distribution plot ob-

tained in evolving factor analysis [18,19] (see below).

(3) Evolving factor analysis (EFA). This is based on the evolution with pH of the magnitudes of the eigenvalues during the spectrometric titration. From the results obtained in the EFA, and considering the previously deduced number of species present in the system, an abstract representation of the concentration profiles is obtained.

(4) From the initial estimation of the concentration profiles obtained using EFA, the generalized Beer's law equation in matrix form is solved iteratively by least-squares (alternating least-squares procedure) to obtain the matrices of individual spectra  $A$  and of concentration profiles  $C$  which best fit the data. The concentration profiles in matrix  $C$  should be unimodal and positive; only a certain amount (given in the input data) of departure from the unimodal condition is allowed at any instant. The total amount of absorbing material at each titration point is experimentally known and used in the iterations as a constraint. Negative values of absorbance obtained in the iterative least-squares estimation of  $A$  are set equal to zero. To these general con-

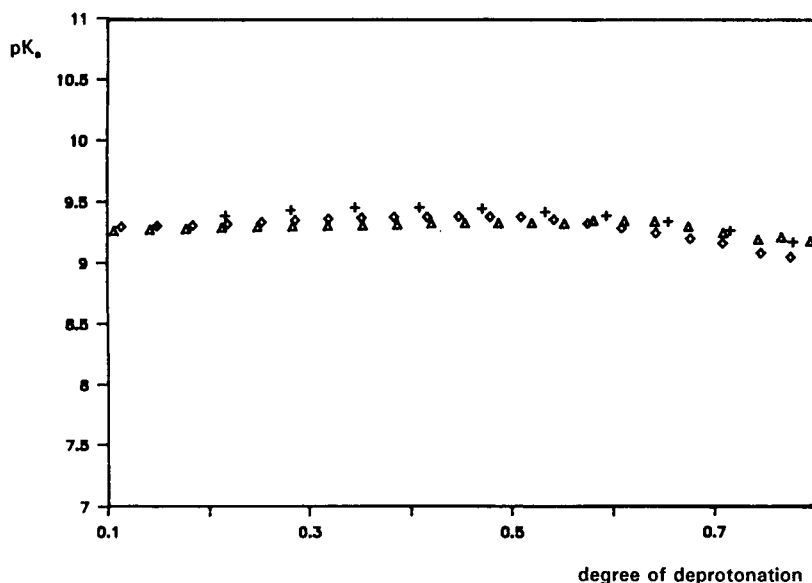


Fig. 1. Plot of  $pK_a$  versus the degree of dissociation for poly(U). + = Titration 1;  $\Delta$  = titration 2;  $\diamond$  = titration 3.

straints present in both SPFAC versions, a new constraint is added in the new one: the unitary spectrum (i.e., the variation of molar absorptivity with wavelength) of any individual species is equal in any one of the different titrations.

In SPFAC and SQUAD programs the goodness of the fit is measured by the standard deviation of the residuals.

## RESULTS AND DISCUSSION

### Potentiometric study of the H-poly(U) system

The polynucleotide poly(U) presents no polyfunctional effect as it contains the same monomeric unit repeated along its structure: the nucleotide cyclic UMP. This nucleotide has only one protonation site to be taken into account under the working conditions, which is the nitrogen atom in position 3 (N-3) in the nitrogen base moiety. The first acidic group in the phosphate residue has a  $pK$  value of acid dissociation lower than 1, and hence it is always deprotonated in the working pH range. In the polynucleotide the protonation site is repeated along the molecule, conferring to poly(U) a polyelectrolytic character, which must be taken into account in the study of its acid–base properties. As deprotonation takes place, there is an increase in the negative charge on the molecule surface, which could affect the acid–base characteristics of the next dissociation site and could lead to a dependence of the disso-

ciation constant on the degree of site deprotonation. Actually, the plot (Fig. 1) of the  $pK$  value of acid dissociation for the N-3 site in poly(U) as a function of the degree of deprotonation indicates the absence of appreciable polyelectrolytic effects as the  $pK$  value is hardly dependent on the number of deprotonated positions. Thus, to determine with the required precision the protonation constant of the N-3 site in poly(U), this macromolecular ligand can be assimilated to a group of individual monomeric units, and the numerical treatment of the experimental e.m.f. data can be performed with a traditional program for the determination of stability constants, such as the program SUPERQUAD. The value of the protonation constant for the N-3 site in the polynucleotide, obtained in aqueous solution of 0.15 M ionic strength and at 37°C is  $\log K = 9.363 \pm 0.004$ .

### ESR study of the copper(II)–poly(U) system

Figure 2 shows some of the ESR spectra obtained for one of the titrations performed. At  $pH < 5$  no copper(II) complexation is observed as the experimental ESR spectra coincide with that of free copper(II) (Fig. 2, spectrum A). Copper(II) complexation takes place between ca.  $pH 5$  and 6, as indicated by the decrease in the intensity of the band due to free copper(II) (Fig. 2, spectra B–E). The disappearance of the band at  $pH 6$  indicates that at this pH copper(II) is already quantitatively complexed.

In the pH range of complexation there is no appearance of new bands at higher magnetic field owing to the hyperfine interaction between the unpaired electron and the complexed copper(II) nucleus, which is consistent with the formation of diamagnetic copper(II) species, that is, with the formation of dimeric species that contain two copper(II) ions close enough to each other to allow interaction between their unpaired electrons. A probable dimeric species would be that formed by two copper(II) ions each bonded to a nitrogen atom in poly(U) and with two hydroxo bridges between them, as the complex is formed in a pH region where the formation of the binary hydroxo complexes  $Cu(OH)^+$  and  $Cu_2(OH)_2^{2+}$  [20] must be taken into account.

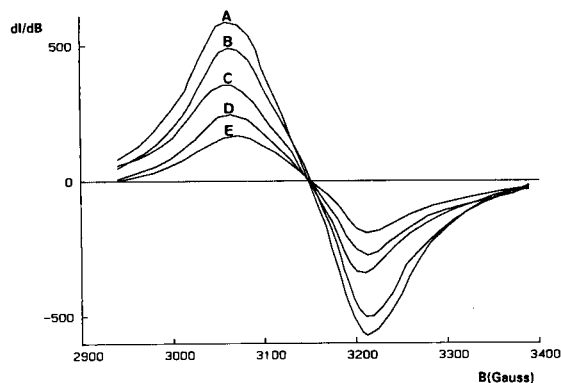


Fig. 2. Experimental ESR spectra for the copper(II)–poly(U) system, obtained in one of the titrations performed (titration 8).  $pH =$  (A) 1.82, (B) 5.10, (C) 5.39 (D) 5.48 and (E) 5.54.

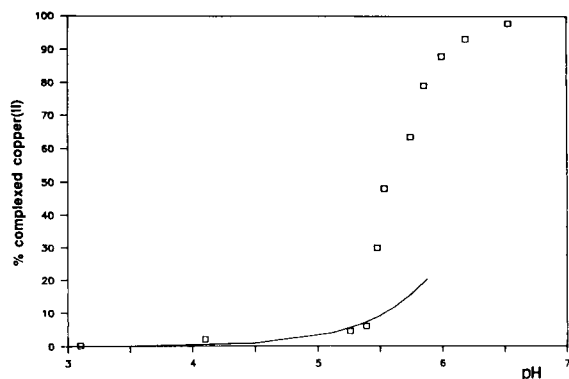


Fig. 3. Plot of the proportion of complexed copper(II) at every pH value for the copper(II)-poly(U) (□) and copper(II)-cyclic UMP (continuous line) systems.

From the ESR signal obtained for the free copper(II) present at every point of the titration, it is possible to determine the proportion of complexed copper(II) ion at every pH value. The results obtained are presented in Fig. 3, together with those obtained when the ligand is the monomeric nucleotide cyclic UMP, the copper(II) complexation of which has been studied previously [3]. While the nucleotide cyclic UMP at pH values around 6 always yields a precipitate from the copper(II) solutions under the working conditions, which is attributed to a basic salt of copper(II), the polynucleotide poly(U) yields much stronger complexes and copper(II) remains in solution over the whole pH range studied and for all the studied copper(II)-to-ligand ratios.

#### Potentiometric study of the copper(II)-poly(U) system

The experimental formation curves obtained for the titrations performed in the potentiometric study of the copper(II)-poly(U) system are shown in Fig. 4. They suggest the presence of hydroxo and polynuclear species in the system. Thus, in order to avoid additional difficulties, the study of this system was only performed up to pH values around 6.5, where complexation is already almost quantitative.

The experimental e.m.f. data were treated with the SUPERQUAD program, and the best fit of the experimental data was found with the model that contains as a major species the dimeric

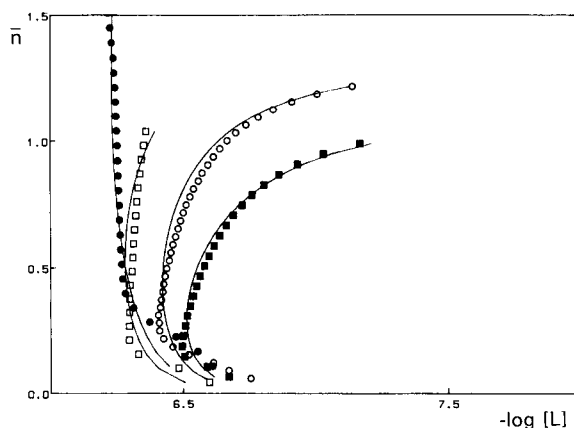


Fig. 4. Experimental formation curves for the copper(II)-poly(U) system. ■ = Titration 4; ○ = titration 5; □ = titration 6; ● = titration 7. Continuous lines are the theoretical curves obtained with the calculated set of constants.

species already proposed from the ESR results. This species is usually denoted by its stoichiometric coefficients, 2:2:-2 for Cu(II):L:proton stoichiometry, where L represents the deprotonated N-3 sites in the ligand that are bound to copper(II) ions and the negative sign indicates hydroxide ions.

When the ligand-to-metal ion ratio is around 1:1, additional hydroxo ligands enter into the

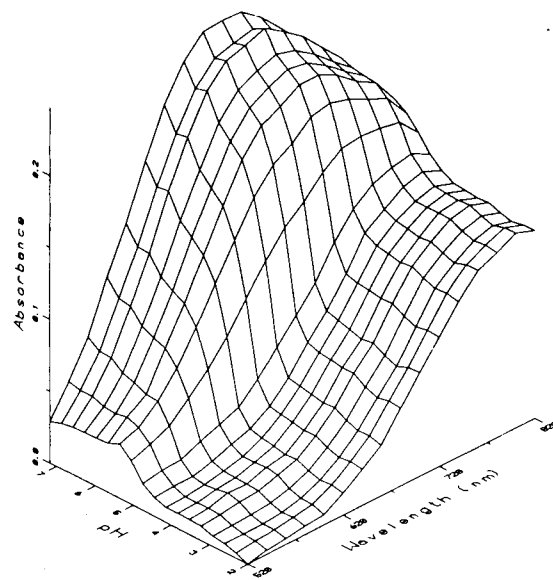


Fig. 5. Three-dimensional plot of the spectrometric data for titration 8.



complex. Thus, a 2:2:–4 species is also detected in the system.

The values obtained for the logarithm of the formation constants show a great lack of precision, probably because complexation causes conformational changes in the polymer, the extent which may depend on the ligand-to-metal ion ratio and on the concentration of the different reagents. For the 2:2:–2 species  $\log \beta = 3.1 \pm 0.2$  and for the 2:2:–4 species  $\log \beta = -9.1 \pm 0.4$ .

In Fig. 4 the calculated formation curves are also shown. It can be concluded that they show good agreement with the experimental data, taking into account that the studied system is very complicated as it contains a macromolecular ligand whose complexing behaviour may be greatly affected by possible conformational changes and

polyelectrolytic effects due to the presence of the metal ion.

#### *Spectrophotometric study of the copper(II)-poly(U) system*

Figure 5 shows a three-dimensional plot of the experimental visible spectra obtained in a titration of a solution containing copper(II) ions and poly(U). There is no variation of the absorption band due to the copper(II) ion until a pH value of ca. 5, which is indicative of the beginning of complexation. In the pH range where complexation takes place, ca. 5–6, the absorption band moves towards lower wavelengths and there is an increase in intensity.

The numerical treatment of the experimental absorption data was carried out with the SPFAC program [8]. First, each of the spectrophotomet-

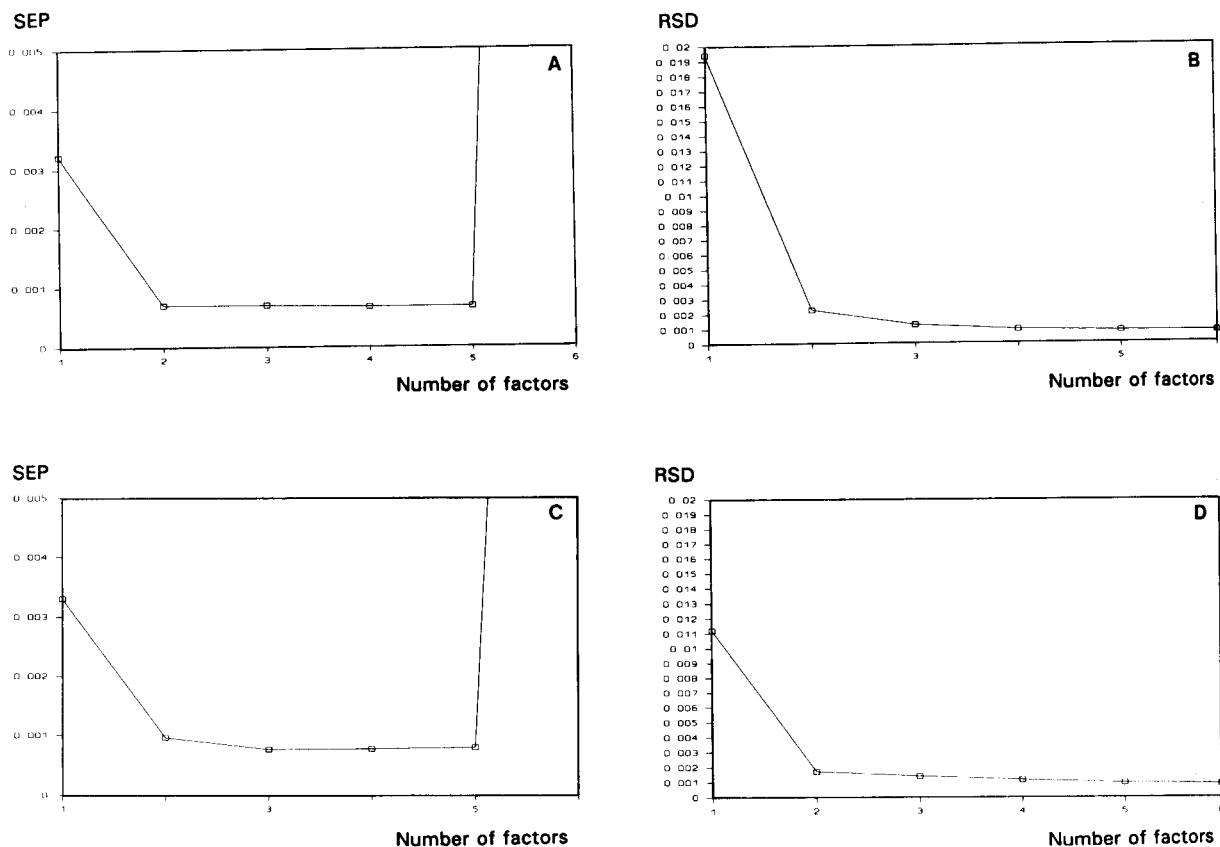


Fig. 6. Determination of the number of components: (A) and (B) are plots of the SEP and RSD functions versus the number of factors for titration 8; (C) and (D) are plots of the SEP and RSD functions versus the number of factors for titration 9.

ric titrations performed was studied individually in order to ascertain if the results obtained by the SPFAC treatment are dependent or not on the ligand-to-metal ion ratio present in the solutions.

Figure 6 includes plots of SEP and RSD functions for titrations 8 and 9. These plots show the presence of only two main factors and, perhaps, of a third whose contribution is very much lower. As the instrumental random error is ca. 0.002

absorbance units, the variation in the experimental data is completely explained when only the two first main factors are considered.

Figure 7 displays the results obtained in the evolving factor analysis of the two titrations mentioned before, and the abstract distribution plot resulting from the evolving factor analysis results and considering the presence of only two absorbing species in the system. The first factor, which

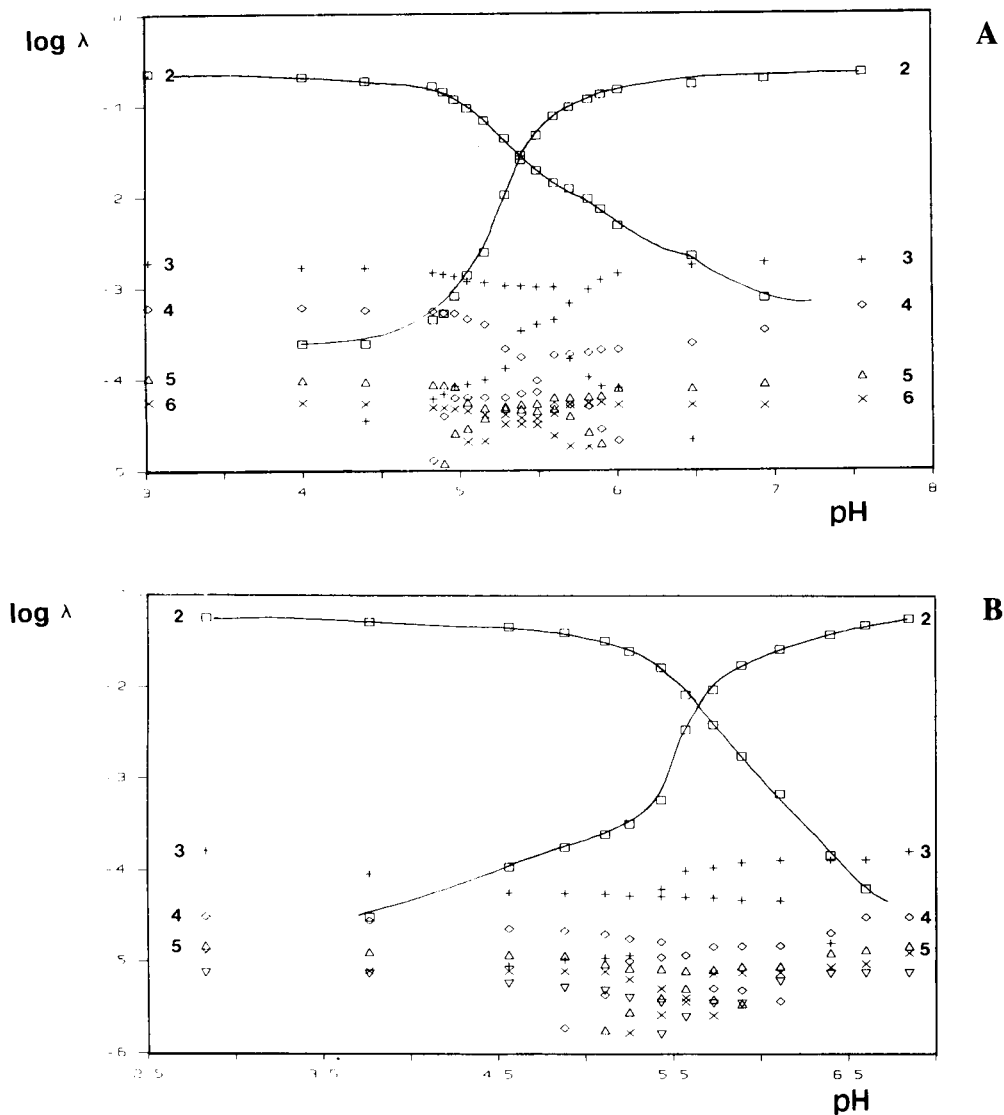


Fig. 7. Evolving factor analysis plots for (A) titration 8 and (B) titration 9. Continuous lines give the abstract estimated concentration profiles of the two detected species. Symbols refer to the upsurging and decreasing factors in the evolving factor analysis. Each factor is numbered to the left for the backward eigenanalysis and to the right for the forward eigenanalysis.

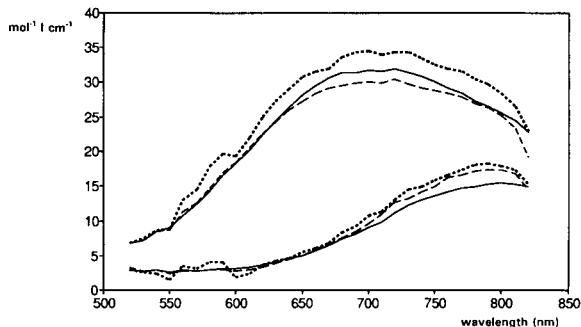


Fig. 8. Spectra of the individual species obtained in the individual treatment of the spectrometric titrations with the SPFAC program. Solid line, titration 8; short dashed line, titration 9; long dashed line, titration 10.

is not represented in the forward evolving factor analysis, as it is present from the beginning of the titration, can be related to free copper(II) ions. From the reverse evolving factor analysis it can be concluded that at  $\text{pH} > 6.5$  the concentration of free copper(II) ions is already negligible, which shows that complexation is quantitative. The second factor appears at a  $\text{pH} \approx 5$  and can be attributed to the complex formed between copper(II) ions and poly(U).

The next step is the estimation of the concentration profiles and the spectra of the individual

species which best explain the data matrix for every titration. Figure 8 shows the individual spectra obtained in the individual analysis of each titration. It is observed that, depending on the ratio of the ligand site to copper(II) ion concentration in the titrated solution, the spectra of the individual species have the same shape and spectral features but a different intensity. This was observed whenever several titrations at different concentrations of the metal ion and of the macromolecule were analysed independently [21], and can be interpreted as if the intensity of the individual spectra and the concentration of the related species are exchangeable to a certain extent for a similar fit of the experimental data. In order to remove this ambiguity, the different experimental data matrices of spectra obtained in the three titrations were analysed together with the improved SPFAC version. The results obtained for the unitary spectra of the two species are presented in Fig. 9. It is found that the standard deviation of the residuals between the factor analysis reduced data matrix and the calculated data matrix using the best set of species spectra and of species concentration is around 0.01 absorbance units, which falls well within the error in the experimental conditions.

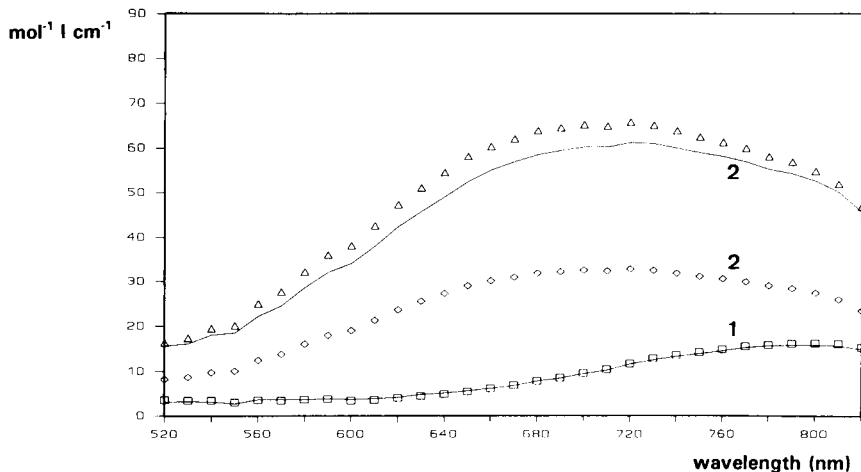


Fig. 9. Comparison of SQUAD and SPFAC procedures in the study of the copper(II)-poly(U) system. Continuous lines refer to SQUAD results and symbols to SPFAC results obtained in the simultaneous analysis of the titrations. Numbers refer to the following species: 1 = free copper(II) ions; 2 = 2:2: -2 species.  $\square$  = SPFAC spectrum for free copper(II) ions;  $\diamond$  = spectrum directly obtained from SPFAC analysis for the copper(II)-poly(U) complex;  $\triangle$  = spectrum of this complex if it is dimeric (its molar absorptivities being twice those given by SPFAC; see text).

From the results obtained in the ESR study of the copper(II)–poly(U) system, the complex found in the SPFAC treatment of the spectrophotometric data could be attributed to the dimeric 2:2:–2 species.

The experimental spectrophotometric data were also treated with the computer program SQUAD [13]. The value obtained for the formation constant of the 2:2:–2 species is  $\log K = 3.0 \pm 0.3$ . Figure 9 shows the visible spectra of free copper(II) ions and of the dimeric species calculated with the SQUAD program. For the studied system the SPFAC program applies, in the alternating least-squares step, the mass balance equation for copper(II) ions, and hence the concentration of every individual species detected is given in relation to the concentration of copper(II) ions that it contains. As the dimeric complex contains two copper(II) ions per molecule, the concentration of dimeric species given by the SPFAC program is the double of that found with the SQUAD program and, therefore, for compliance with Beer's law, the absorbances for this species evaluated with SPFAC program are approximately half those found with SQUAD program. There is a very close agreement between the results obtained with both programs (see Fig. 9) when the visible spectrum found with the SPFAC program is multiplied by two.

### Conclusions

Evolving factor analysis-based techniques, such as SPFAC, are powerful tools for the study of systems involving macromolecular ligands, when difficulties are encountered with traditional least-squares fitting approaches owing to poly-electrolyte, polyfunctional or conformational effects.

In the copper(II)–poly(U) system, only one complexed copper(II) species was clearly detected with the SPFAC program. Whereas in the absence of copper(II) ions poly(U) is known to have a random coil conformation, the dimeric copper(II) complex formed must lead to conformational changes in the polynucleotide, as each of the two complexed copper(II) ions is assumed to be bonded to a nitrogen atom in poly(U) and with two hydroxo bridges between them. These

conformational changes, whose relative importance may vary with the ligand-to-metal ion ratio and with the copper(II) and poly(U) concentrations present in the solutions, contribute to the stability of the species found and, thus, the application of traditional least-squares procedures to this system gives results that show a great lack of precision and which do not by themselves allow the model to be validated. The results obtained with SPFAC give real proof of the validity of the model assumed.

This research was supported by a CICYT grant, No. PB90-0821.

### REFERENCES

- 1 R. Tauler, J.F. Cid and E. Casassas, *J. Inorg. Biochem.*, 39 (1990) 277.
- 2 E. Casassas, A. Izquierdo-Ridorsa and R. Tauler, *J. Inorg. Biochem.*, 39 (1990) 327.
- 3 E. Casassas, I. Giménez, A. Izquierdo-Ridorsa and R. Tauler, *J. Inorg. Biochem.*, submitted for publication.
- 4 J. Buffle, *Complexation in Aquatic Systems: an Analytical Approach*, Horwood, Chichester, 1988.
- 5 R. Tauler and E. Casassas, *J. Chemometr.*, 3 (1988) 151.
- 6 R. Tauler and E. Casassas, *Anal. Chim. Acta*, 223 (1989) 257.
- 7 R. Tauler, E. Casassas and A. Izquierdo-Ridorsa, *Anal. Chim. Acta*, 248 (1991) 447.
- 8 R. Tauler, A. Izquierdo-Ridorsa and E. Casassas, *Chemometr. Intell. Lab. Syst.*, (1992) in press.
- 9 I.M. Kolthoff, E.B. Sandell, E.J. Meehan and S. Bruckenstein, *Quantitative Chemical Analysis*, Collier–Macmillan Canada, Toronto, 1969, p. 781.
- 10 E. Casassas, G. Fonrodona and R. Tauler, *Polyhedron*, 6 (1987) 1517.
- 11 G. Gran, *Analyst*, 77 (1952) 661.
- 12 P. Gans, A. Sabatini and A. Vacca, *J. Chem. Soc., Dalton Trans.*, (1985) 1195.
- 13 D.J. Leggett, S.L. Kelly, L.R. Shiue, Y.T. Wu, D. Chang and K.M. Kadish, *Talanta*, 30 (1983) 579.
- 14 E.R. Malinowski and D.E. Howery, *Factor Analysis in Chemistry*, Wiley, New York, 1980.
- 15 E.R. Malinowski, *J. Chemometr.*, 1 (1987) 33.
- 16 E.R. Malinowski, *J. Chemometr.*, 3 (1988) 39.
- 17 S. Wold, *Technometrics*, 20 (1978) 397.
- 18 H. Gampp, M. Maeder, C.J. Meyer and A.D. Zuberbühler, *Talanta*, 32 (1985) 1133.
- 19 H. Gampp, M. Maeder, C.J. Meyer and A.D. Zuberbühler, *Talanta*, 33 (1986) 943.
- 20 C.W. Childs, *Inorg. Chem.*, 9 (1970) 2465.
- 21 R. Tauler and E. Casassas, *Chemometr. Intell. Lab Syst.*, 14 (1992) 305.

# Factor analysis applied to the study of the effects of solvent composition and nature of the inert electrolyte on the protonation constants in dioxane–water mixtures

E. Casassas, N. Domínguez, G. Fonrodona and A. de Juan

*Departament de Química Analítica, Universitat de Barcelona, Avda. Diagonal 647, 08028 Barcelona (Spain)*

(Received 10th September 1992; revised manuscript received 8th December 1992)

## Abstract

The effect of solvent properties on protonation constants was studied for water–dioxane mixtures covering a wide range of solvent compositions, from data sets on several solutes with a variety of functional groups. The establishment of the model was carried out using different approaches: the use of a classical procedure, where the best multiparametric fit to the Kamlet and Taft equation was evaluated for each substance; and the application of combined factor analysis and target factor analysis to quantify and identify the factors affecting the variation of the whole data sets, without the need to postulate any a priori hypothetical model. Further, a preliminary overview of the influence of different inert electrolytes on the values of the solute protonation constants in this solvent mixture was also obtained through factor analysis.

*Keywords:* Dioxane; Factor analysis; Protonation constants; Solvatochromic parameters; Solvent effects; Waters

Factor analysis (FA) has been demonstrated to be a powerful technique in the study of complex chemical phenomena, whose interpretation requires multivariate approaches [1]. It has often been used to explain solute–solvent interactions, as a helpful tool in the field of linear free energy relationships [2] when medium effects have to be described and to understand better some solvent effects on solute physico-chemical properties [3–5]. This wide application in the study of pure solvent effects contrasts with the scarceness of analogous works devoted to solvent mixtures.

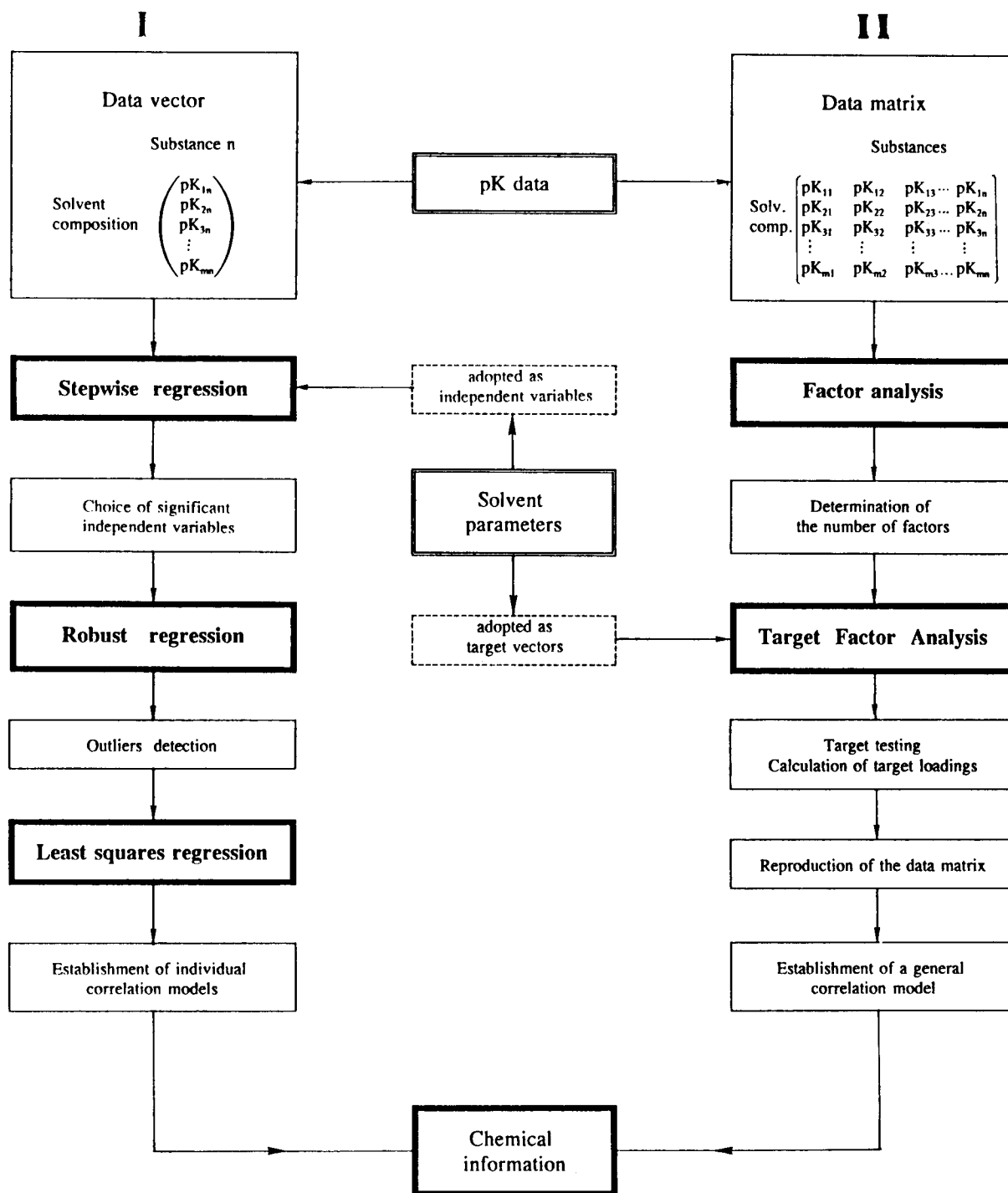
In the latter field, in previous studies [6] FA was used to find the number of factors involved in the variation of the protonation constants of carboxylate groups of several substances when

the composition of water–dioxane mixtures is modified and target factor analysis (TFA) was then applied to identify these factors. The analysed data set revealed that this variation could be expressed through the general equation  $pK_s = pK_0 + s\pi^*$ , where  $\pi^*$  is the microscopic polarity parameter proposed by Kamlet et al. [7], and  $s$  is a constant.

In this work, the same study was extended to several acidic solutes with different functional groups (phenolic and amino groups) and to a wider composition range of mixtures, in order to propose a more general model. To achieve this objective, two different parallel approaches were applied, as described briefly in Scheme 1.

The first attempt was carried out in a classical way, trying to fit the behaviour of each substance to a previously proposed model, using the more extended form of the multiparametric equation proposed by Kamlet et al. [7],  $XYZ = XYZ_0 + aa$

*Correspondence to:* E. Casassas, Departament de Química Analítica, Universitat de Barcelona, Avda. Diagonal 647, 08028 Barcelona (Spain)



Scheme 1. Outline of the approaches used: classical approach (data treatment I) and FA + TFA approach (data treatment II).

$+b\beta + s\pi^*$ , where  $\alpha$ ,  $\beta$  and  $\pi^*$  are solvatochromic parameters related to the hydrogen bond acidity, hydrogen bond basicity and polarity–polarizability, respectively [7–9],  $XYZ$  is the solute property studied ( $pK_s$ ) and  $XYZ_0$  is the hypothetical value for this property in a solvent where  $\alpha = \beta = \pi^* = 0$ . For this purpose, a stepwise procedure was first applied to select the significant solvent properties to be included in the model. Thereafter, a robust analysis was performed to detect outliers, and finally a least-squares fit was carried out with the appropriate data and variables to lead to the definite expressions for each compound. The second approach involved the application of the hypothesis-free model technique, FA, to establish how many sources of variation affect the solute property studied. Thereafter, these factors were identified using TFA and combined to yield the best general model for all the substances studied.

The classical approach gives force-fitted equations, whereas FA provides a much less arbitrary criterion for selecting the quantity and nature of the possible causes of variation in the data sets, avoiding the introduction of a priori hypotheses. From the combination of the two procedures, interesting conclusions can be inferred relating to the variation of protonation constants with the solvent composition in water–dioxane mixtures.

To complete the study of the acid–base behaviour of solutes in water–dioxane mixtures, a preliminary overview of the influence of different inert electrolytes on the values of the solute protonation constants in this solvent system by FA was also obtained.

## EXPERIMENTAL

### Reagents

Analytical-reagent grade chemicals were used, unless indicated otherwise. Water was deionized and distilled twice over potassium permanganate.

Dioxane (Probus) was purified by Eigenberger's method [10]. 4-Nitroanisole (Merck) was purified by treatment with active carbon in an acetone solution and recrystallization in water. 2-Nitroanisole, 4-ethylnitrobenzene and *N,N*-di-

ethyl-4-nitroaniline were obtained from Aldrich, 4-nitroaniline and sodium salicylate from Carlo Erba and 2,6-diphenyl-4-(2,4,6-triphenyl-1-pyridinio)phenolate from Professor E. Bosch. Potassium hydroxide (Merck) was prepared as a  $\text{CO}_2$ -free solution in dioxane–water by the ion-exchange procedure [11]. Sodium hydroxide, nitric acid, propionic acid, potassium nitrate, sodium nitrate and potassium chloride were obtained from Merck. Salicylic acid (Merck) was purified by sublimation and 3-hydroxynaphthalene-2-carboxylic acid (Merck) by treatment with active carbon and recrystallization from ethanol.

### Apparatus

A Beckman DU-7 spectrophotometer was interfaced (RS232) to an IBM personal computer. Acquisition of spectra was controlled through Beckman data capture software. An Orion SA 720 potentiometer (precision  $\pm 0.1$  mV), an Orion 90-05 AgCl/Ag reference electrode with ceramic junction and internal reference solution of saturated KCl in the working aqueous–organic mixture, an Orion 91-01 glass electrode, a double-jacketed cell thermostated at  $25 \pm 0.1^\circ\text{C}$ , a Metrohm 665 Dosimat autoburette (precision 0.01 ml) with an exchange unit of  $5\text{ cm}^3$  with an antidiffusion burette tip and a magnetic stirrer were used. The whole titration set-up was connected to a personal computer (HP Vectra ES/12 or HP 9133) through an HP 3421 A interface, which allows full automation of the titration process.

### Determination of acid dissociation constants ( $pK_a$ ) of several acidic solutes in water–dioxane mixtures

$pK_s$  values for 3-hydroxynaphthalene-2-carboxylic acid (HNCA), propionic acid and salicylic acid using  $\text{KNO}_3$  as inert electrolyte were determined previously [12,13]. Values for propionic acid in other inert electrolytes were obtained by potentiometric titrations performed at a constant temperature ( $25^\circ\text{C}$ ) and constant ionic strength. The potentiometric cell used was GE/working solution ( $b\text{ mol l}^{-1}$ )– $n\%$  dioxane/RE ( $\text{KCl}_{\text{sat}}$ ,  $n\%$  dioxane), where GE is the glass electrode, RE the reference electrode,  $b$  the constant con-

centration of inert electrolyte and  $n$  the percentage of dioxane in the working aqueous–organic mixture. The Gran method [14] was used for in situ calibration of the cell and determination of the standard potential. After calibration, a known amount of acid solute was added to the cell and the titration continued until a suitable pH value. The experimental e.m.f. readings were processed with the SUPERQUAD program [15] to obtain the  $pK_s$  values. Glycine  $pK_s$  values were taken from the literature [16]. All the  $pK_s$  values and the experimental conditions used in their determination are given in Table 1.

*Determination of solvatochromic parameters in water–dioxane mixtures*

Solvatochromic parameters were determined from spectroscopic measurements of certain substances, the so-called solvatochromic indicators, whose shift in the wavelength of maximum absorption is sensitive only to the solvent property that must be measured and is free from contributions produced by other causes. For amphiprotic solvents or amphiprotic mixtures, the solvatochromic indicators proposed by Kamlet and Taft were used as follows: 2-nitroanisole, 4-nitroanisole and 4-ethylnitrobenzene (all of them showing spectral shifts sensitive only to the polarity of the solvent) were used to determine the  $\pi^*$  parame-

ter; both 2,6-diphenyl-4-(2,4,6-triphenyl-1-pyridinio)phenolate (whose spectra shifts are sensitive to the polarity and to the hydrogen bond donor acidity of solvent) and 4-nitroanisole were used to determine the  $\alpha$  parameter and both 4-nitroaniline (with spectral shifts sensitive to the polarity and to the hydrogen bond acceptor basicity of solvent) and *N,N*-diethyl-4-nitroaniline (whose spectral shifts are sensitive only to the polarity) were used to determine the  $\beta$  parameter. All the wavelength values used to evaluate the solvatochromic parameters were determined by the authors [12,13,17], except several betaine wavelengths values which were taken from the literature [18].

To determine the required wavelengths, the spectrum of each test solution (solvatochromic indicator in the binary mixture) is recorded against a blank formed by a solvent mixture of composition identical with that of the solvent used in the test solution. Both the test solution and the blank circulate through continuous-flow systems in which the mixture composition is changed stepwise with additions of dioxane until the whole composition range of the binary mixture is covered. Replicates of each spectrum are made from identical independently prepared test solutions. Thereafter, a digitization procedure yields the wavelength corresponding to the ab-

TABLE 1

Experimental conditions and acid dissociation constants ( $pK_a$ ) of several acidic compounds in water–dioxane mixtures

Experimental conditions							
Substance	Propionic acid	Propionic acid	Salicylic acid <sup>a</sup>	Salicylic acid <sup>b</sup>	HNCA <sup>a,c</sup>	Glycine <sup>a</sup>	Glycine <sup>d</sup>
Ionic strength (M)	0.2	0.2	0.2	0.2	0.1	0.1	0.1
Inert electrolyte	KNO <sub>3</sub>	NaNO <sub>3</sub>	KNO <sub>3</sub>	KNO <sub>3</sub>	KNO <sub>3</sub>	NaClO <sub>4</sub>	NaClO <sub>4</sub>
Dioxane (% v/v)	$pK_a$ values						
10	4.825	4.8334	2.897	12.789			
20	5.091		3.067	13.23	2.964	2.6	9.64
30	5.395	5.382	3.318	13.43	3.171		
40	5.676		3.524	13.51	3.448	2.94	9.7
50	6.063	6.0236	3.789	13.94	3.762	3.17	9.76
60	6.494		4.305	14.12		3.45	9.84
65	6.745		4.478	14.46	4.382		
70	6.879	6.861	4.654	14.84	4.653	3.81	9.98
75		7.052			4.998	4.05	10.07
80					5.289	4.33	10.23

<sup>a</sup> COOH group. <sup>b</sup> OH group. <sup>c</sup> HNCA = 3-hydroxynaphthalene-2-carboxylic acid. <sup>d</sup> NH<sub>2</sub> group.



TABLE 2

Solvent parameters for water–dioxane mixtures

Dioxane (% v/v)	$\alpha$	$\beta$	$\pi^*$	$n_2$
10	0.94	0.217	1.143	0.023
20	0.81	0.296	1.124	0.05
30	0.74	0.379	1.088	0.083
40	0.67	0.433	1.049	0.123
50	0.61	0.474	0.989	0.174
60	0.57	0.486	0.92	0.241
65	0.55	0.465	0.885	0.282
70	0.54	0.469	0.849	0.33
75	0.51	0.501	0.823	0.388
80	0.48	0.532	0.781	0.458
85	0.45	0.552	0.748	0.545
90	0.4	0.551	0.704	0.655
95	0.35	0.518	0.636	0.801
100	-0.07	0.360	0.54	1

sorption maximum. The gross averages of the different wavelengths obtained for each solvent composition conveniently processed give the values of the solvatochromic parameters. The  $\beta$  values have been revised and modified in this work. Numerical values for  $\alpha$ ,  $\beta$  and  $\pi^*$  parameters are given with some other solvent parameters in Table 2.

*Study of the variation of protonation constants in water–dioxane mixtures*

*Classical approach.* For each substance, a correlation model based on the general equation of Kamlet et al. [7],  $XYZ = XYZ_0 + a\alpha + b\beta + s\pi^*$ , where  $XYZ$  is the property of the solvent studied (in this instance  $pK_a$ ) and  $\alpha$ ,  $\beta$  and  $\pi^*$  are the microscopic parameters related to hydrogen bond donor acidity, hydrogen bond acceptor basicity and polarity–polarizability of the solvent, respectively, is proposed. As was pointed out by Kamlet and Taft [19], the number of terms in the equation can be larger or smaller depending on the significance of the different solvent parameters with respect to the solute property being studied.

The effect of the different solvent properties (quantified through solvatochromic parameters) on the variation of  $pK_s$  values of one substance over the entire range of mixture compositions (dependent variable) is first analysed using a stepwise procedure, in which  $\alpha$ ,  $\beta$  and  $\pi^*$  are the possible independent variables, whose significance is tested. The stepwise procedure used is a combination of both forward selection and backward elimination of variables, as implemented in the PARVUS statistical package [20]. For each selection step of a new independent variable the

TABLE 3

A.1 and A.2 data matrices <sup>a</sup>:  $pK_a$  values for several acidic compounds in water–dioxane mixtures of different composition

Dioxane (% v/v)	Compound <sup>b</sup>					
	HNCA	gly1	gly2	PropK	Sal1	Sal2
20	2.964	2.6	9.64	5.091	3.067	13.23
30	3.171	2.71	9.67	5.395	3.318	13.43
40	3.448	2.94	9.7	5.676	3.524	13.51
50	3.762	3.17	9.76	6.063	3.789	13.94
60	4.288	3.45	9.84	6.494	4.305	14.12
70	4.653	3.81	9.98	6.879	4.654	14.84
75	4.998	4.05	10.07			
80	5.289	4.33	10.23			

<sup>a</sup> Dashed box = A.1 data matrix; solid box = A.2 data matrix. <sup>b</sup> HNCA = 3-hydroxynaphthalene-2-carboxylic acid (COOH group); gly1 = glycine (COOH group); gly2 = glycine (NH<sub>2</sub> group); PropK = propionic acid at ionic strength 0.2MKNO<sub>3</sub>; Sal1 = salicylic acid (COOH group); sal2 = salicylic acid (OH group).

program computes alternatively one of the following  $F$ -tests. In the first, an  $F$ -to-enter value is computed for each non-entered variable to evaluate the significance of the decrease in variance in the fit. In the second  $F$ -test, an  $F$ -to-delete value is computed for the variables already entered. The process continues until any one of the unselected variables gives  $F$  values larger than the user-defined control  $F$  value. Once it has been decided which of the variables in the model are significant, the regression analysis is performed by using the PROGRESS program [21]. The first step in this program includes a robust approach [least median of squares regression (LMS)] to detect the presence of outliers. The outliers diagnostic is performed through the application of two different high breakdown point methods, such as the study of the standardized LMS residuals and the robust diagnostic method proposed by Rousseeuw and Leroy [21]. To avoid the removal of good leverage data points, only data to be considered as outliers through both previous methods have been removed by the authors. Thereafter, a least-squares fit is performed to obtain the definite model for each substance.

**FA and TFA approach.** Input data referring to  $pK_a$  for all substances and all mixture compositions are collected to build up two different experimental data matrices. In the first (A.1 data matrix), the main interest is in finding a general model for substances with different functional groups; in the second (A.2 data matrix), the general model is deduced from  $pK_a$  data for a smaller number of solutes, but covering a wider range of mixture compositions. This separate treatment was adopted to avoid the use of extrapolated  $pK_s$  data, which necessarily would come from the application of an external hypothetical chemical model. For both matrices, no pretreatment of the data was necessary. The A.1 and A.2 data matrices are shown in Table 3.

Factor analysis (FA), also known as principal component analysis (PCA), has been primarily used to determine how many causes affect the variation of  $pK_a$  values with solvent composition. The correct number of abstract factors is obtained through (1) the application of the IND function [22], (2) the study of the evolution of

standard error in prediction (SEP) function, through cross-validation techniques, as proposed by Malinowski [22] and Wold [23], (3) the application of an  $F$ -test to check the significance of the eigenvalue [24] and (4) the study of the real error (RE) [22]. Both the empirical indicator function, IND (which is calculated from the magnitude of the eigenvalues), and standard error of prediction, SEP, should have a minimum for the correct number of factors (NF). When the  $F$ -test is performed, the number of factors is obtained from the break in the evolution of the values of the percentage of significance level (%SL, Table 6) associated with the successive  $F$  values evaluated for an increasing number of factors. The correct NF is given by the RE function when the difference between the calculated value of this function and the experimental error passes through a minimum. These tests yield the number of factors which explain the variation of data; they are abstract factors and the assignment of a physical meaning to them requires further information and data treatment.

For the A.1 data matrix all four methods were applied, whereas for the A.2 data matrix only methods 3 and 4 were used.

When the number of factors has been established, TFA is developed to identify the chemical nature of these factors. Up to this point, in contrast with the classical approach, no hypothetical model is necessary. A target is defined as a vector representing known experimental data other than those under analysis, which is tentatively proposed as a possible real factor causing the observed variation of the data within the original data matrix. Geometrically, a target vector accepted as a real factor lies in the space determined by the abstract factors found in FA.

As both the A.1 and A.2 data matrices are formed by equilibrium constants determined at different solvent compositions, the variation within the original data matrices has to be related to modifications in the solute–solvent interactions, well described by the Kamlet and Taft parameters. Hence these solvent parameters and the mole fraction are accepted as targets and checked as possible real factors present in a future general model. No other solvent parameters

TABLE 4

B.1 and B.2 data matrices <sup>a</sup>:  $pK_a$  values for several acidic compounds in water–dioxane mixtures of different composition

Compound <sup>b</sup>	Dioxane (% v/v)				
	20	40	50	70	60
HCNA	2.964	3.448	3.762	4.653	4.288
Sal1	3.067	3.524	3.789	4.654	4.305
Sal2	13.23	13.51	13.94	14.84	14.12
PropK	5.091	5.676	6.063	6.879	6.494
gly1	2.6	2.94	3.17	3.81	3.45
gly2	9.64	9.7	9.76	9.98	9.84

<sup>a</sup> Dashed box = B.1 data matrix; solid box = B.2 data matrix.

<sup>b</sup> See Table 3.

(macroscopic or microscopic) have been proposed as possible targets, because previous studies yielded much worse results for them in comparison with those related to the chosen parameters [6]. The validity of each target is analysed through an *F*-test [24] and evaluating its SPOIL function [25]. Targets which lie in the factor space should have SPOIL values below 3 and a percent signifi-

cance level, %SL, for the *F*-test above 5. The accepted targets are thereafter combined to reproduce the original data matrix. The best combination of target test vectors is that which yields the lowest error in the estimation of the loadings and the lowest root mean square error (RMS) in the reproduction of the data matrix.

All the data treatment was performed using the TARGET90 program [24].

*Study of the effect of the inert electrolyte on the determination of protonation constants in water–dioxane mixtures*

Because it has not been possible to accept any general model that could explain the effect of using different inert electrolytes on the values of protonation constants in water–dioxane mixtures, no classical procedure of model fitting was used for data treatment.

FA was then applied to detect the possible existence of the effect referred to above, by comparison of the number of factors calculated for the two following matrices: (B.1)  $pK_s$  data for several solutes determined at the same solvent composition and using the same inert electrolyte ( $KNO_3$ ); and (B.2) the B.1 data matrix enlarged

TABLE 5

Individual  $pK_a$  correlation models, according to the classical approach

Solute <sup>a</sup>	Significant variable <sup>b</sup>	Correlation model <sup>c,d</sup>
Propionic acid, <i>I</i> = 0.2 M $KNO_3$	$\alpha, \pi^*$	$pK = -1.3(2)\alpha - 5.4(3)\pi^* + 12.1(1)$ $r^2 = 0.999$ ; sc.est. <sup>e</sup> = 0.03
Propionic acid, <i>I</i> = 0.2 M $NaNO_3$	$\pi^*$	$pK = -6.7(3)\pi^* + 12.5(3)$ $r^2 = 0.994$ ; sc.est. = 0.08
Sal1, <i>I</i> = 0.2 M $KNO_3$	$\pi^*$	$pK = -5.9(1)\pi^* + 9.7(1)$ $r^2 = 0.996$ ; sc.est. = 0.04
Sal2, <i>I</i> = 0.2 M $KNO_3$	$\pi^*$	$pK = -5.9(5)\pi^* + 19.7(5)$ $r^2 = 0.960$ ; sc.est. = 0.1
HNCA, <i>I</i> = 0.1 M $KNO_3$	$\pi^*$	$pK = -6.6(2)\pi^* + 10.4(2)$ $r^2 = 0.991$ ; sc.est. = 0.09
Gly1, <i>I</i> = 0.1 M $NaClO_4$	$\pi^*$	$pK = -4.9(3)\pi^* + 8.0(2)$ $r^2 = 0.980$ ; sc.est. = 0.08
Gly2, <i>I</i> = 0.1 M $NaClO_4$	$\pi^*$	$pK = -1.4(1)\pi^* + 11.2(1)$ $r^2 = 0.950$ ; sc.est. = 0.04

<sup>a</sup> For abbreviations, see Table 3. <sup>b</sup> Significant variables were deduced through stepwise regression (SR). <sup>c</sup> Correlation models were obtained from the successive application of robust regression [least median of squares regression (LMS)] and least-squares regression without the presence of outlier data. <sup>d</sup> Values in parentheses are the errors associated with the last figure. <sup>e</sup> Scale estimate.

by the inclusion of  $pK_s$  data for both glycine functional groups, determined employing  $\text{NaClO}_4$  as an inert electrolyte.

An increase in the number of factors from B.1 to B.2 could probably be attributed to the effect of the new different electrolyte. The determination of the correct number of factors was carried out with the four methods listed previously. The small size of the B.1 data matrix limited the range of procedures to the study of RE and the significance of eigenvalues, whereas with the B.2 data matrix all methods were applied. Both B.1 and B.2 data matrices are given in Table 4.

## RESULTS AND DISCUSSION

### *Study of the variation of protonation constants in dioxane–water mixtures*

Table 5 gives the results provided by the classical approach. For each substance, the significant independent variables selected by applying the stepwise procedure to build up the model are listed, together with the definitive fit to the appropriate form of the Kamlet and Taft equation with its associated quality parameters.

The results obtained with the application of FA for both the A.1 and A.2 data matrices are presented as follows. Table 6 shows RE values and the study of the significance of the eigenvalues through an  $F$ -test. For the A.1 data matrix, Fig. 1 plots the evolution of IND function vs. number of factors and Fig. 2 the evolution of SEP (standard error or prediction) functions vs. num-

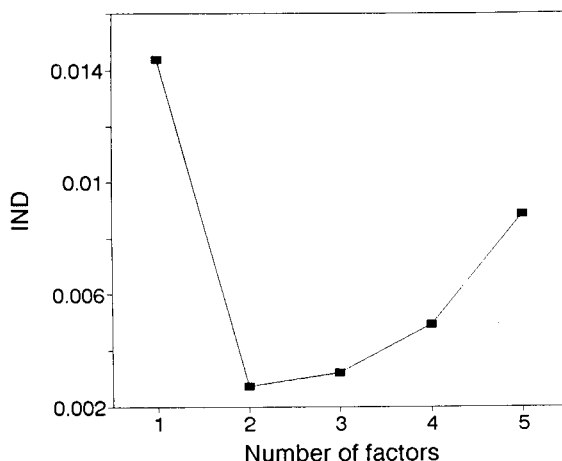


Fig. 1. Evolution of the IND function vs. the number of factors for the A.1 data matrix.

ber of factors, evaluated according to Malinowski and Wold cross-validation techniques.

For both the A.1 and A.2 data matrices, all the methods used lead to the confirmation that two factors are sufficient to explain the variation of the studied data sets. Hence this number of factors was adopted for the target testing.

Table 7 shows the results of testing the Kamlet and Taft parameters, with  $n_2$  and unity as targets. The target vector unity must be included in the target set in order to take into account the chemical nature of each substance, this nature being a constant contribution in all data referring to each substance. For the A.1 data matrix  $n_2$ ,  $\pi^*$  and unity were accepted as targets lying in

TABLE 6

Determination of the number of factors, NF

NF	A.1 data matrix				A.2 data matrix			
	RE <sup>a</sup>	Log(EV)	$F(\text{calc.})$	SL(%) <sup>b</sup>	RE <sup>a</sup>	Log(EV)	$F(\text{calc.})$	SL(%) <sup>b</sup>
1	0.360	3.335	850.89	0.0	0.579	2.885	148.35	0.7
2	0.043	0.584	101.53	<i>0.01</i> <sup>c</sup>	<i>0.016</i> <sup>c</sup>	0.605	1067.06	<i>1.9</i> <sup>c</sup>
3	0.029	-1.519	1.75	27.8		-2.821		
4	0.019	-1.979	1.25	37.9				
5	0.008	-2.378	2.22	37.6				
6		-3.325						

<sup>a</sup> RE = real error, according to [22]. <sup>b</sup> SL = percentage significance level associated with each  $F$ -value, calculated using  $\log(\text{eigenvalues})$  [log(EV)] according to [24]. <sup>c</sup> Values in italics indicate the correct number of factors according to the different criteria.

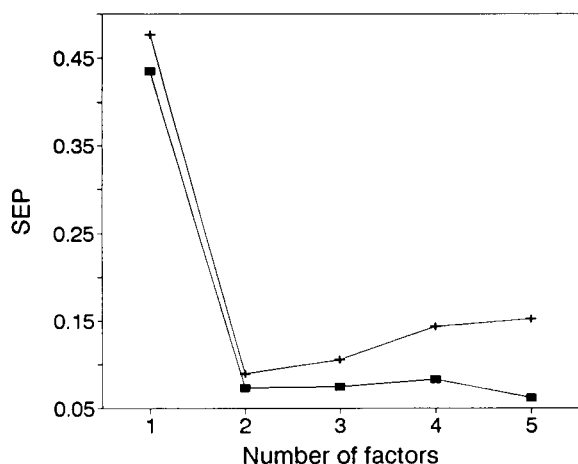


Fig. 2. Evolution of the SEP functions according to (■) Malinowski and (+) Wold vs. the number of factors for the A.1 data matrix.

the factor space. Of the two reasonable combinations of targets,  $\pi^*$ -unity and  $n_2$ -unity, the former reproduces the data matrix with an RMS = 0.052, whereas the latter yields an RMS = 0.060. Even though the difference does not seem very significant, the results of target testing for the A.2

TABLE 7

Summary of target errors using two factors based on covariance for A.1 and A.2 data matrices

Target	A.1 data matrix <sup>a</sup>						
	AET	EDM	SPOIL	F	df1	df2	SL (%)
$\alpha$	$3.59 \times 10^{-2}$	$6.55 \times 10^{-3}$	5.39	9.14	4	4	2.7
$\beta$	$4.55 \times 10^{-2}$	$2.19 \times 10^{-3}$	20.78	131.50	4	4	0.0
$\pi^*$	$1.76 \times 10^{-2}$	$8.15 \times 10^{-3}$	1.92	1.42	4	4	37.1
Unity	$8.91 \times 10^{-3}$	$3.50 \times 10^{-3}$	2.30	1.97	4	4	26.4
$n_2$	$1.33 \times 10^{-2}$	$4.72 \times 10^{-3}$	2.63	2.40	4	4	20.8
	A.2 data matrix <sup>a</sup>						
	AET	EDM	SPOIL	F	df1	df2	SL (%)
$\alpha$	$3.51 \times 10^{-2}$	$2.91 \times 10^{-3}$	11.98	55.30	4	1	10.0
$\beta$	$4.73 \times 10^{-2}$	$9.70 \times 10^{-4}$	48.80	911.59	4	1	2.5
$\pi^*$	$9.08 \times 10^{-3}$	$3.77 \times 10^{-3}$	2.19	2.22	4	1	46.1
Unity	$5.07 \times 10^{-3}$	$1.83 \times 10^{-3}$	2.58	2.93	4	1	40.9
$n_2$	$3.27 \times 10^{-2}$	$1.59 \times 10^{-3}$	20.56	162.16	4	1	5.9

<sup>a</sup> AET = apparent error in the target; EDM = error from data matrix; SPOIL = spoil associated with the target; df1 and df2 = degrees of freedom; SL = percentage significance level.

TABLE 8

Factor loadings for the reproduction of the A.1 and A.2 data matrices

(Number of factors = 2. Factor loadings based on covariance)

Compound <sup>a</sup>	A.1 data matrix <sup>b</sup>		A.2 data matrix <sup>b</sup>	
	$\pi^*$	Unity	$\pi^*$	Unity
PropK	-6.4(2)	12.4(2)		
Sal1	-5.8(2)	9.5(2)		
Sal2	-5.4(4)	19.3(4)		
HNCA	-6.3(1)	9.9(1)	-6.7(2)	10.5(2)
Gly1	-4.38(9)	7.5(1)	-4.9(2)	8.1(2)
Gly2	-1.18(9)	10.95(9)	-1.6(2)	11.4(1)

<sup>a</sup> For abbreviations, see Table 3. <sup>b</sup> Values in parentheses are the errors associated with the last figures.

data matrix confirm clearly the superiority of the  $\pi^*$ -unity over the  $n_2$ -unity combination. When the composition range includes a higher percentage of dioxane,  $n_2$  is not admitted as a correct target, and only  $\pi^*$  and unity are considered to be valid. For the reproduction of the A.2 data matrix, the combination of  $\pi^*$  and unity yields an RMS = 0.060. Definite loadings [which are defined as coefficients related to the weight of each real factor in each different column (each different substance) of the original data matrix] for the reproduction of the A.1 and A.2 data matrices are given in Table 8.

This study confirms the greater usefulness of microscopic parameters, such as  $\pi^*$ , over bulk parameters, such as  $n_2$ , in the explanation of microscopic processes, as the solvent properties in the cybotactic zone, which are often very different from those in the bulk solvent, are the ones which affect directly the solutes when a process such as acid-base equilibrium occurs.

The application of FA and TFA to the study of the effect of solvent properties on the solute protonation constants in water-dioxane mixtures confirms the model suggested in the classical attempt for most substances, leading to the reduced form of the Kamlet and Taft equation  $pK = pK_0 + s\pi^*$ , independent of the functional group and composition range studied.

Only for propionic acid, determined at  $I = 0.2$  M in  $KNO_3$ , should the  $\alpha$  parameter also be introduced into the model, according to the step-

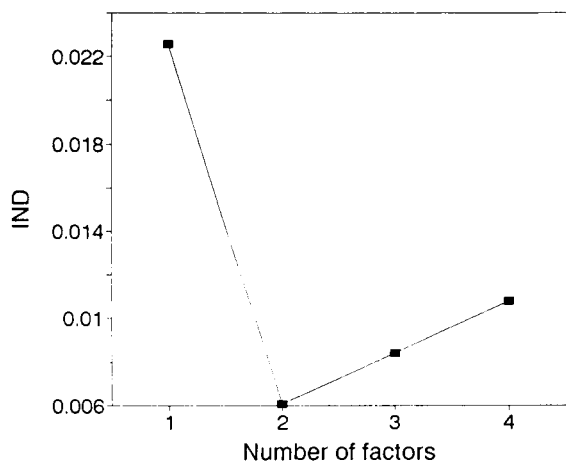


Fig. 3. Evolution of the IND function vs. the number of factors for the B.2 data matrix.

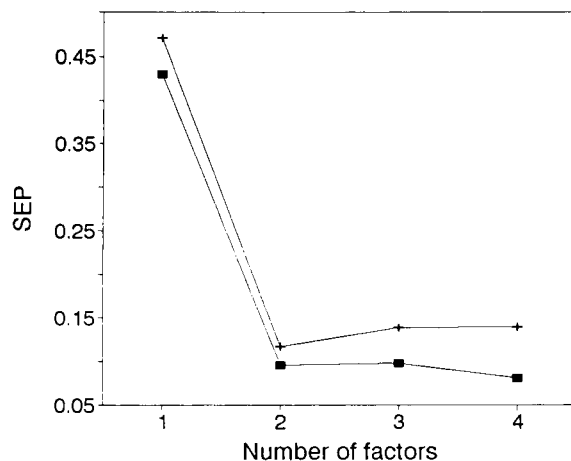


Fig. 4. Evolution of the SEP functions according to (■) Malinowski and (+) Wold vs. the number of factors for the B.2 data matrix.

wise procedure. This difference in the model is actually of minor significance, because  $\pi^*$  explains 98.9% of the total variance in the data, and the introduction of  $\alpha$  increases the level of explanation to 99.8%. In fact, the expression obtained including only  $\pi^*$  yields a high-quality fit:  $pK_s = (-6.5 \pm 0.2)\pi^* + (12.5 \pm 0.2)$ ;  $r^2 = 0.996$ ; scale estimate = 0.05.

The subtle numerical differences between loadings and correlation coefficients for every substance are easily explained, as the amount of data used for establishing the two parallel models is not always the same and in the case of the amino group of glycine one outlier has been removed. Of the expressions obtained by the two methods, individual models are to be preferred,

because they are built using a larger number of quality-checked data.

The results obtained in the study of the effect of the inert electrolyte on the protonation constants does not lead to very clear inferences. There is no evident variation in the number of factors when data determined with a different electrolyte are added to the B.1 data matrix, as can be seen from Table 9 and Figs. 3 and 4. As the size of the B.1 data matrix used is small (other work is in progress), the only tentative conclusion that can be extracted from the present data sets is that no apparent electrolyte effect can be observed or, at least, that if it is present, its magnitude is so small that it is masked by some other main effects.

TABLE 9

Determination of the number of factors, NF

NF	B.1 data matrix				B.2 data matrix			
	RE <sup>a</sup>	Log(EV)	F(calc.)	SL(%) <sup>b</sup>	RE <sup>a</sup>	Log(EV)	F(calc.)	SL(%) <sup>b</sup>
1	0.364	3.011	536.19	0.0	0.362	3.263	777.54	0.0
2	<i>0.050</i> <sup>c</sup>	0.197	42.79	2.3 <sup>c</sup>	<i>0.055</i> <sup>c</sup>	0.489	57.45	0.5 <sup>c</sup>
3	0.007	-1.695	22.57	13.2	0.034	-1.396	1.97	29.5
4		-3.650			0.011	-1.891	6.11	24.5
5						-3.153		

<sup>a</sup> RE = real error, according to [22]. <sup>b</sup> SL = percentage significance level associated with each  $F$ -value, calculated using  $\log(\text{eigenvalues})$  [ $\log(\text{EV})$ ] according to [24]. <sup>c</sup> Values in italics indicate the correct number of factors according to the different criteria.

This research was supported by the Spanish Comision Interministerial de Ciencia y Tecnologia (CICYT), Grant No. PB90-0821, and by a grant from the Generalitat de Catalunya (CIRIT).

## REFERENCES

- 1 E.R. Malinowski and D.G. Howery, *Factor Analysis in Chemistry*, Wiley, New York, 1980.
- 2 P.H. Weiner, *J. Am. Chem. Soc.*, 95 (1973) 5845.
- 3 W.R. Fawcett and T.M. Krygowski, *Can. J. Chem.*, 54 (1976) 3283.
- 4 J.T. Edward and S.C. Wong, *J. Am. Chem. Soc.*, 99 (1977) 4229.
- 5 E.M. Kosower, *An Introduction to Physical Organic Chemistry*, Wiley, New York, 1968.
- 6 E. Casassas, G. Fonrodona, A. de Juan and R. Tauler, *Chemometr. Intell. Lab. Syst.*, 12 (1991) 29.
- 7 M.J. Kamlet, J.J. Abboud and R.W. Taft, *J. Am. Chem. Soc.*, 99 (1977) 6027.
- 8 R.W. Taft and M.J. Kamlet, *J. Am. Chem. Soc.*, 98 (1976) 2886.
- 9 M.J. Kamlet and R.W. Taft, *J. Am. Chem. Soc.*, 98 (1976) 377.
- 10 A.I. Vogel, *A Text Book of Practical Organic Chemistry*, Longmans Green, London, 5th edn., 1989, p. 407.
- 11 J.E. Powell and M.A. Hiller, *J. Chem. Educ.*, 34 (1957) 330.
- 12 E. Casassas and G. Fonrodona, *J. Chim. Phys.*, 86 (1989) 391.
- 13 E. Casassas, G. Fonrodona and A. de Juan, *Inorg. Chim. Acta*, 187 (1991) 187.
- 14 G. Gran, *Acta Chem. Scand.*, 4 (1950) 559; *Analyst*, 77 (1952) 661.
- 15 P. Gans, A. Sabatini and A. Vacca, *J. Chem. Soc., Dalton Trans.*, (1985) 1195.
- 16 K.K. Mui, W.A.E. McBryde and E. Nieboer, *Can. J. Chem.*, 52 (1974) 1821.
- 17 E. Casassas, G. Fonrodona and A. de Juan, *J. Solution Chem.*, 21 (1992) 147.
- 18 C. Reichardt, in H. Ratajczak and W.J. Orville-Thomas (Eds.), *Molecular Interactions*, Vol. 3, Wiley, Chichester, 1982, p. 241.
- 19 M.J. Kamlet and R.W. Taft, *Acta Chem. Scand., Ser. B*, 39 (1985) 611.
- 20 M. Forina, R. Leardi, C. Armanino and S. Lanteri, *PARVUS, an Extendable Package of Programs for Data Exploration, Classification and Correlation*, Elsevier, Amsterdam, 1988.
- 21 P.J. Rousseeuw and A.M. Leroy, *Robust Regression and Outlier Detection*, Wiley, New York, 1981.
- 22 E.R. Malinowski, *J. Chemom.*, 1 (1987) 33.
- 23 S. Wold, *Technometrics*, 20 (1978) 397.
- 24 E.R. Malinowski, *J. Chemom.*, 3 (1988) 49.
- 25 E.R. Malinowski, *Anal. Chim. Acta*, 103 (1978) 339.

# Computer experimentation in and teaching of modern instrumental techniques using circular dichroism measurement as an example

Edward Voigtman

*LGRT-102 (Chemistry), University of Massachusetts at Amherst, Amherst, MA 01003-0035 (USA)*

(Received 2nd September 1992)

## Abstract

Several different circular dichroism measurement techniques and instrument schemes have been examined by means of detailed Jones calculus computer simulations. The simulations are easy to set-up, extremely realistic and accurately predict what would happen if careful, well-characterized experiments were to be performed. Students can see how experiments are supposed to work and become familiar with the operational parameters. Experts can explore instrument designs and configurations, determine parameter sensitivities, predict signal-to-noise ratios, calibration linearities, dynamic ranges, and so on.

*Keywords:* Circular dichroism; Computer simulations

Modern chemical instrumentation is extremely powerful and sophisticated, capable of routine analyses that would have been essentially impossible as little as a generation ago. The many factors contributing to the remarkable advances in instrumentation and associated technologies are not considered further, because what is of interest here is the matter of training students, and other analysts, to use sophisticated instruments and techniques. How can we teach students to use instruments which, all too often, are simply too expensive or too delicate to be placed in teaching laboratories? How are we to teach students to use instruments, if the instruments are designed never to be “opened up” by users (and instructors)? How can we teach students how best to select among alternative techniques

when so little quantitative performance information, of true intrinsic significance, i.e., *not* detection limits, is available? The standard textbooks tend not to be of much help in this regard, and the primary literature is fragmented and of highly variable quality, so what can be done to remedy the situation?

There are no general answers to these questions, and related ones, but one partial solution is to use carefully crafted computer simulations of instruments and instrumental techniques. It has recently become possible to craft such simulations in simple, powerful, and elegant fashion. The models are constructed using a commercially available simulation program named Extend<sup>TM</sup> (Imagine That, Inc., San Jose, CA), augmented with a collection of 133 component blocks custom-programmed by the author. The libraries of custom blocks, named Voigt fx<sup>TM</sup>, comprise a complete implementation of the Jones and Mueller optical calculi and also include an assort-

*Correspondence to:* E. Voigtman, LGRT-102 (Chemistry), University of Massachusetts at Amherst, Amherst, MA 01003-0035 (USA).



ment of conventional electronic signal processing components and a versatile noise generator. The optical calculi have been described, in detail, elsewhere [1,2]. Several applications of the Voigt fx blocks have also been described [3–7].

This paper details the use of Extend plus the Voigt fx software for the analysis of several published circular dichroism instruments and techniques. Circular dichroism (CD) was selected as a typical example of the type of instrumental technique which can be accurately simulated with the combination of Extend plus Voigt fx. Circular dichroism measurement is an increasingly important matter because of its utility in the structural study of both chemical and biological systems, especially polymeric systems. Yet most modern teaching curricula have ignored CD because of its instrumental costs, the cumbersomeness of describing polarized light, especially circularly and elliptically polarized light, and the difficulties in dealing with CD in quantitative fashion.

## EXPERIMENTAL

All simulations were performed on a Macintosh IIfx computer (Apple, Cupertino, CA) with 20 M RAM, system 7.0.1 (enhanced), and an Extend 1.1n memory allocation of 4000 Kbytes. A Macintosh Plus with 4 M RAM is a satisfactory, though much slower, alternative. The Voigt fx

optical calculus and signal processing libraries were widely released as copyrighted shareware on January 2, 1992. Interested readers may contact the author.

The coordinate system in all of the Voigt fx optical simulations is right-handed, with  $x$  being horizontal,  $y$  being vertical, and  $z$  as the light beam propagation direction. In all the simulations described below, Jones calculus was used, though Mueller calculus was equally serviceable. All Mueller matrices in the Voigt fx blocks are in standard Shurcliff form [1], including those in references using other matrix element arrangements, e.g., Jensen et al. [8].

The Appendix shows the dialog boxes, of the more complicated blocks, present in the figures in the simulations. Necessary operational parameters are entered into the appropriate dialog box entries, as may be understood by examining the dialog boxes in the Appendix, and then the simulation is performed by specifying a starting time, an ending time, and the desired number of simulation steps.

## RESULTS

A simplified conventional, but noiseless, circular dichroism simulation model is shown in Fig. 1. Each of the blocks in Fig. 1 is a portion of the simulation computer code, requiring appropriate

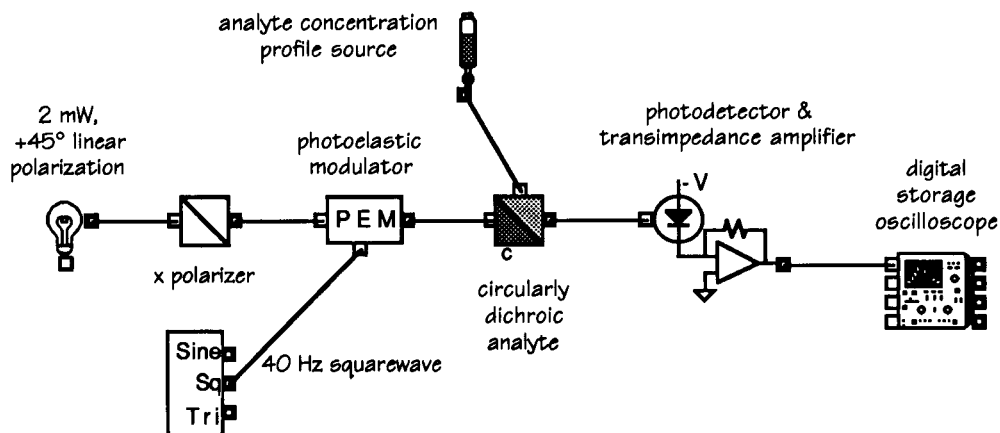


Fig. 1. A conventional circular dichroism measurement scheme using photoelastic modulation.

input parameter specification via individual dialog box parameters. The figure is the over-all simulation computer program itself.

The physical principles of operation of the model are quite simple. The light source produces linearly polarized light having its polarization axis at  $+45^\circ$  to the horizontal. The  $x$  polarizer converts the light to a pure horizontal polarization and passes it on to the photoelastic modulator (PEM). The modulation axis of the PEM is oriented at  $+45^\circ$  relative to the  $x$  axis. With appropriate squarewave drive voltage, the PEM behaves as a quarter wave retardation plate, alternating between  $+90^\circ$  and  $-90^\circ$  retardation. The output is therefore circularly polarized, alternating, with 50% duty factor, between right circular polarization (RCP) and left circular polarization (LCP).

The polarization-modulated beam then passes through a sample cell containing a circularly dichroic material, wherein the RCP and LCP states are absorbed unequally. The CD material may be present in a static cell, at fixed concentration, or it may flow through a dynamic cell, in

which case the concentration is determined by another block. This is the situation shown in Fig. 1. The differentially absorbed circular polarizations then pass to the photodetector and preamplifier, which produce voltages proportional to the incident light intensities. The digital storage oscilloscope provides for signal acquisition and processing. Phase sensitive detection, via lock-in amplifier, is the customary signal processing option of choice. It is demonstrated in a later figure, when source and photodetector/preamplifier noise sources have been added to the model.

Figure 1 is much more than simply a schematic of a simplified CD instrument: it is a computer program modeling, via the use of Jones calculus, the performance and behavior of a CD instrument. For Fig. 1, the starting time was 0 s, the ending time was 0.8 s, and 640 steps were specified. Before observing the time-domain output of the instrument, it is useful to see how the blocks accomplish their modeling tasks.

A circularly dichroic medium, by definition, unequally absorbs incident RCP and LCP light. Therefore, CD may be measured by performing

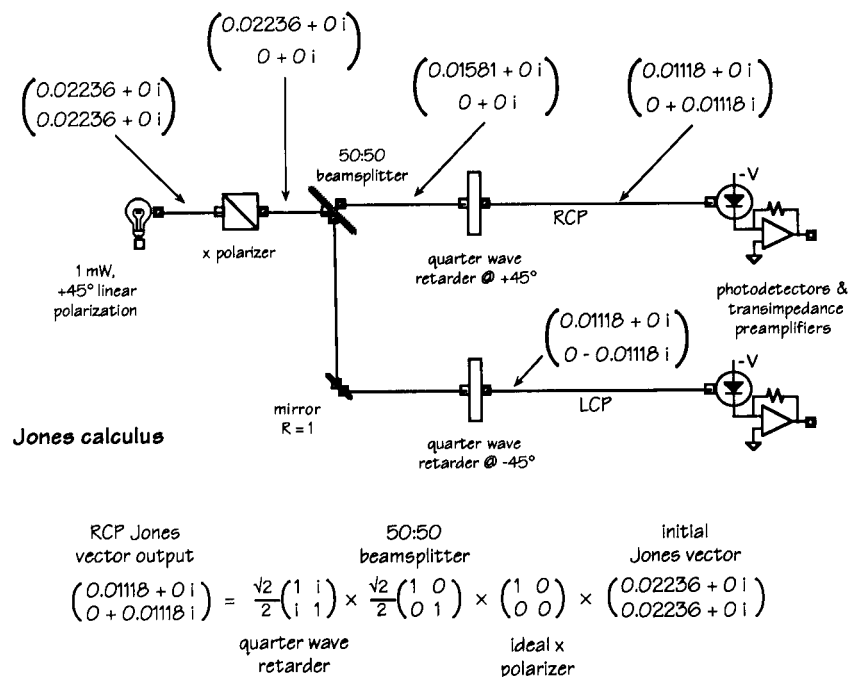


Fig. 2. Converting linearly polarized light to circularly polarized light.

appropriate absorbance measurements, using RCP and LCP light. The conventional method of preparing RCP and LCP light is shown in Fig. 2. The incident light beam is converted to a pure linearly polarized state, in this case the  $x$  polarization, and the resulting state is converted to circularly polarized light by passage through a suitably oriented retarder. The retardance must be  $90^\circ$ , i.e., quarter wave at the wavelength of the incident beam, and the handedness of the circularly polarized light depends on whether the retarder's "fast axis", i.e., axis of minimum index of refraction, is oriented at  $+45^\circ$  to  $x$  or is at  $-45^\circ$  to  $x$ . If it is at  $+45^\circ$  and the retardance is  $+90^\circ$ , the light is RCP; if at  $-45^\circ$  and  $+90^\circ$  retardance, the light is LCP.

Figure 2 also shows the Jones vectors describing the process of converting light, in arbitrary initial polarization state, into both RCP and LCP states. In the figure, the initial polarization state is linear, oriented at  $+45^\circ$  to  $x$ . The Jones vector, a complex two-vector, has equal  $x$  (top) and  $y$  (bottom) polarization components. Passage through the  $x$  polarizer removes the  $y$  component, leaving a pure  $x$  state. The beamsplitter transmits 50% of the incident  $x$  state and reflects the other 50%, which is then totally reflected by an ideal mirror. Passage of the two  $x$  states through the quarter wave retarders gives the RCP and LCP states. The same results are obtained when the retarders have the same orientation, e.g.,  $+45^\circ$ , but differ only in the sign of their  $90^\circ$  retardances.

The component blocks in Fig. 2 can model ideal behavior and various types of non-ideal behaviors. In Fig. 2, the blocks were specified, for reasons of clarity and simplicity, as modeling ideal components. Below the simulation itself is the Jones calculus matrix calculation showing how the RCP state would be obtained. This calculation is automatically performed by the connected blocks, once for each simulation step.

Having obtained Jones vectors for RCP and LCP light, it is only necessary to pass them to a block exhibiting circular dichroism, measure the resultant transmitted intensities, and use Beer's law as appropriate. Figure 3 shows the general circular dichroism and circular birefringence (CB)

Jones matrix for circular dichroism (CD) and circular birefringence (CB)

$$e^{-\eta \cdot A_c/2} \begin{pmatrix} \cosh Q & (CB - i CD) \sinh Q/2Q \\ -(CB - i CD) \sinh Q/2Q & \cosh Q \end{pmatrix}$$

Mueller matrix for circular dichroism (CD) and circular birefringence (CB)

$$e^{-A_c} \begin{pmatrix} \cosh CD & 0 & 0 & \sinh CD \\ 0 & \cos CB & \sin CB & 0 \\ 0 & -\sin CB & \cos CB & 0 \\ \sinh CD & 0 & 0 & \cosh CD \end{pmatrix}$$

Fig. 3. The Jones and Mueller matrices for circular dichroism and optical activity (CB).

Jones and Mueller calculus matrices. Table 1 defines the terms in the matrices and relates them to the usual experimental parameters, e.g., molar ellipticity, molar optical activity, concentration and path length. Note that circular birefringence is also called optical activity or optical rotation. These matrices are subsets of the general anisotropic medium matrices, which are programmed, in full, in another block in the Voigt fx software. The matrices, rearranged into standard Shurcliff form [1], are from Jensen et al. [8].

TABLE 1

Definitions of symbols and expressions

RCP:	right circularly polarized light (+ subscript)
LCP:	left circularly polarized light (– subscript)
$\epsilon_{\pm}$ :	molar absorptivities for RCP and LCP ( $l \text{ mol}^{-1} \text{ cm}^{-1}$ )
$A_{\pm}$ :	absorbances for RCP and LCP
$n_{\pm}$ :	indices of refraction for RCP and LCP
$c$ :	concentration (M)
$l$ :	path length (cm)
$\lambda$ :	wavelength (cm) = $10^{-7} \times$ wavelength (nm)
$n$ :	$(n_{-} + n_{+})/2$ , mean index of refraction
$A_e$ :	$(A_{+} + A_{-})/2$ , mean absorbance
$\eta$ :	$2\pi n l / \lambda$ , phase (radians)
$\theta$ :	molar ellipticity ( $\text{degree cm}^{-1} \text{ M}^{-1}$ )
$\phi$ :	molar optical activity ( $\text{degree cm}^{-1} \text{ M}^{-1}$ )
CD:	$\ln 10 (\epsilon_{-} - \epsilon_{+}) c l / 2 = \theta c l \pi / 180$
CB:	$2\phi c l \pi / 180 = 2\pi (n_{-} - n_{+}) l / \lambda$
$a$ :	$CD^2 - CB^2$
$b$ :	$2CDCB$
$B$ :	$[(a^2 + b^2)^{0.5} + a]^{0.5} / 2\sqrt{2}$
$C$ :	$[(a^2 + b^2)^{0.5} - a]^{0.5} / 2\sqrt{2}$
$Q$ :	$B + iC$

In Fig. 1, it was assumed that the optical activity was zero, the molar ellipticity was  $100^\circ \text{ cm}^{-1} \text{ M}^{-1}$ , the path length was 1 cm, and the reference frequency for the PEM was 40 Hz. The CD analyte concentration had a Gaussian temporal profile, with 0.4 s retention time, 0.1 s standard deviation, and peak concentration as specified below. The mean molar absorptivity was  $1 \text{ l mol}^{-1} \text{ cm}^{-1}$ , unless otherwise stated. The photodetector responsivity was  $0.1 \text{ A W}^{-1}$  and the preamplifier's transimpedance was  $10^4 \text{ V A}^{-1}$ .

Figure 4 shows the effect of increasing the CD analyte concentration, holding everything else constant. The circular dichroism is clearly shown as an AC squarewave signal, modulated by an "envelope" due to the mean molar absorptivity of the analyte. With phase sensitive detection, the AC signal may be separated from the envelope, as will be seen later.

Figure 5 shows the effects of varying the mean

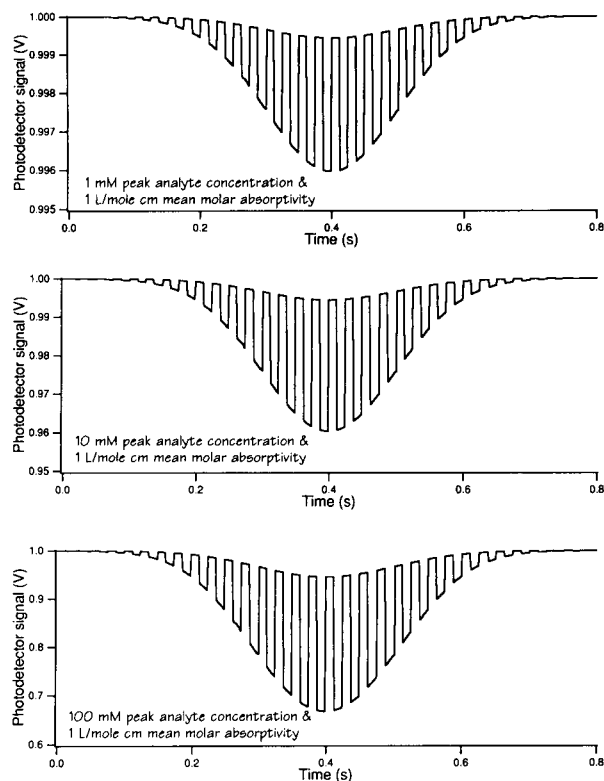


Fig. 4. Typical circular dichroism responses as a function of concentration.

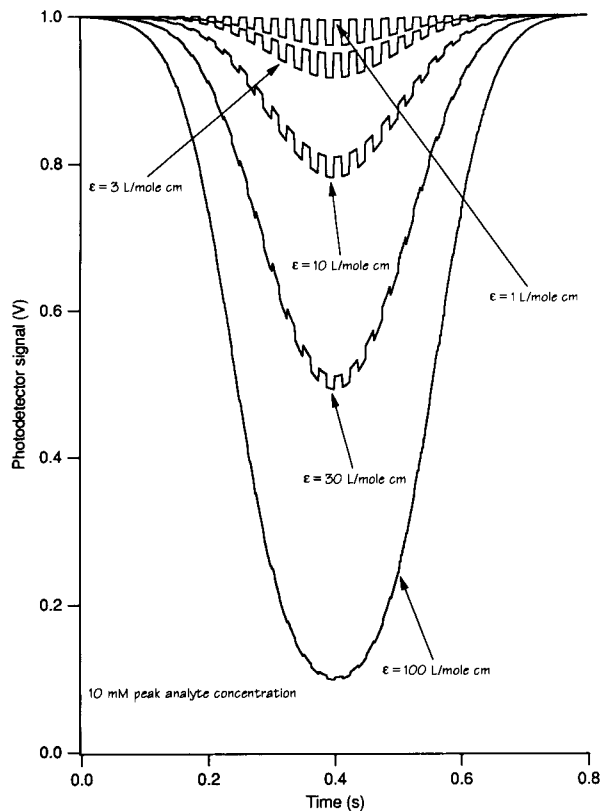


Fig. 5. The detrimental effects of mean molar absorptivity on circular dichroism signals.

molar absorptivity while holding the mean molar ellipticity constant. It is quite evident that the CD signal is dramatically degraded by high mean molar absorptivities, a circumstance that also makes phase sensitive detection less sensitive, since the large "envelope" must be rejected while acquiring the concomitantly small CD signal. An interesting feature of the simulations is that various processes may be "turned off", as desired, to verify the causes of observed effects. In Figs. 4 and 5, it is a simple matter to specify zero molar ellipticity and see the mean absorbance envelope devoid of CD signal squarewave modulation.

An unrealistic feature of Fig. 1 is the complete absence of noise in the simulation. Figure 6 shows a modified version of Fig. 1, allowing for both light source noise and photodetector/preamplifier (PD/preamp) noise. The light source had 0.1% R.S.D. of Gaussian, white noise. The

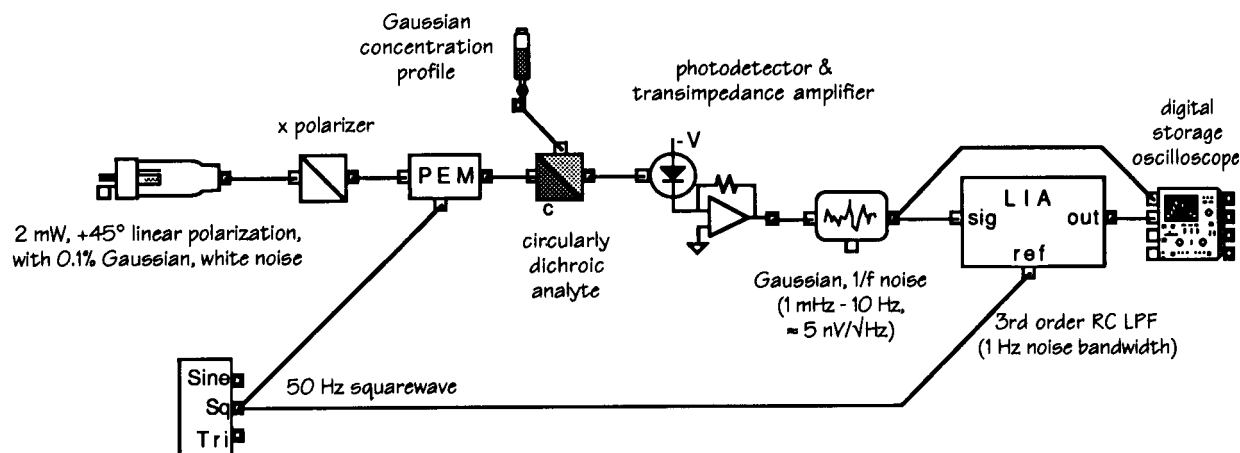


Fig. 6. A conventional CD instrument with noise sources and lock-in amplifier detection.

PD/preamp noise was modeled by a following noise generator block. The noise was Gaussian, bandlimited (1 mHz–10 Hz)  $1/f$  noise, with approximately  $5 \text{ nV Hz}^{-1/2}$  noise amplitude spectral density. The average light intensity reaching the PD/preamp, in the absence of an absorbing analyte, was approximately 1 mW. The PD/pre-

amp responsivity was  $0.1 \text{ A W}^{-1}$  and the transimpedance was  $10000 \text{ V A}^{-1}$ . Therefore, the average PD/preamp output voltage, in the absence of an absorbing analyte, was approximately 1 V. The simulation had a starting time of 0 s, an ending time of 2 s, and the number of simulation steps was 10000.

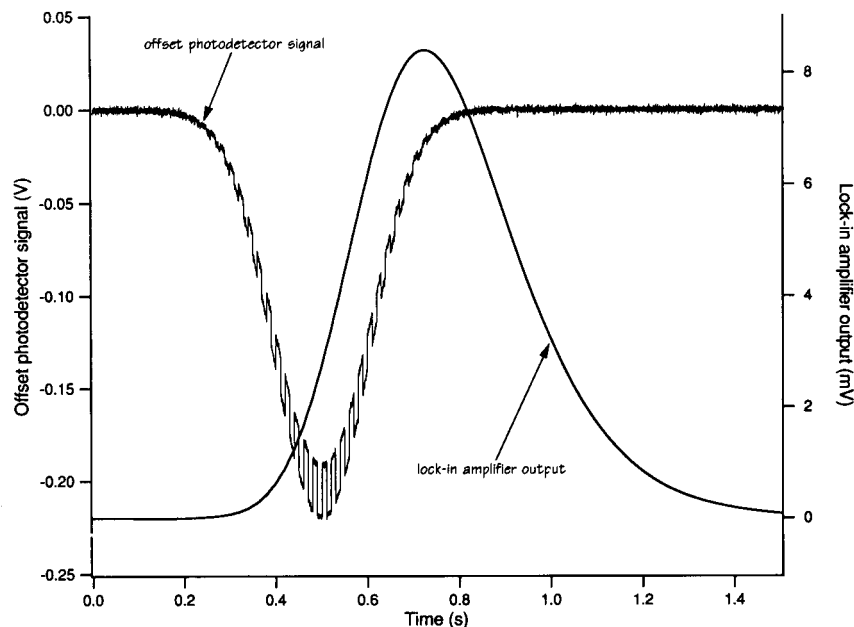


Fig. 7. The output response of the simulation in Fig. 6.

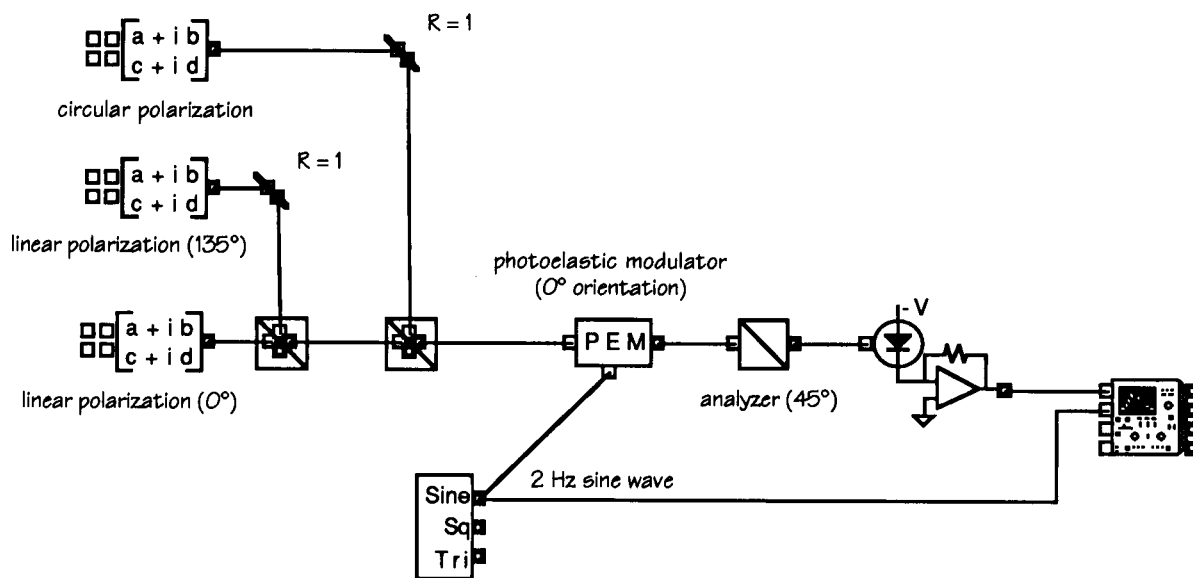


Fig. 8. A simulation showing the use of a photoelastic modulator for polarization analysis.

Figure 7 shows the first 1.5 s, i.e., 7500 data points, of the simulation results. The PD/preamp output was offset to approximately 0 V by using  $-1$  V offset parameter in its dialog box. If this were not done, the lock-in amplifier would have

responded with its step response, partially obscuring the signal peak. The step response can be avoided by simply “out waiting” it, but only at the expense of simulation time. Note that the lock-in amplifier response is quite smooth and both de-

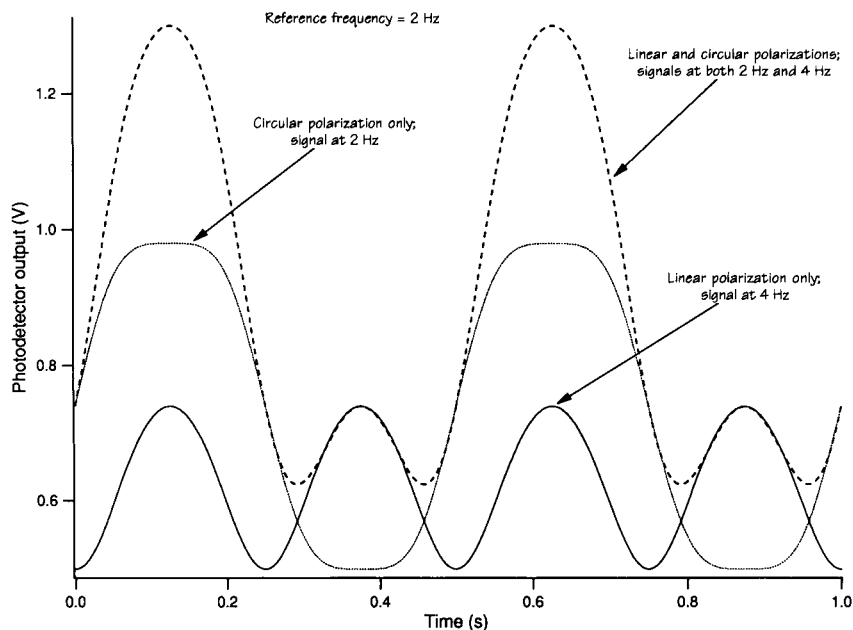


Fig. 9. The waveforms produced by Fig. 8.

laid and stretched. These are necessary consequences of the use of an output filter time constant long relative to the signal duration. For the lock-in amplifier in Fig. 6, the output low pass filter was specified as being a third order RC low pass filter with 1 Hz noise bandwidth.

Clearly, the photoelastic modulator does an excellent job of producing light which is circular polarization-modulated. It has other benefits as well. It may serve, for example, as a polarization analyzer [9]. Figure 8 shows a simulation in which the PEM is used to extract the linear and circular polarization components from a beam comprised of several types of polarized light. A linear component oriented at  $0^\circ$  is aligned with the PEM. It passes through the PEM and is attenuated, by

50%, in passing through the analyzer, oriented at  $+45^\circ$ . There is no intensity modulation impressed on this linearly polarized light component, so it simply contributes a DC offset, of 0.5 V, to the PD/preamp output.

The linearly polarized light component at  $+135^\circ$  was combined with the  $0^\circ$  linearly polarized component via the beamsplitter cube and was then sent to a second beamsplitter cube, where right circularly polarized light was also added. In passing through the PEM, the linearly polarized light at  $135^\circ$  was converted to elliptically polarized light, circularly polarized only at the peaks of the sine wave reference frequency. Accordingly, the output of the analyzer contained a modulated intensity at twice the reference fre-

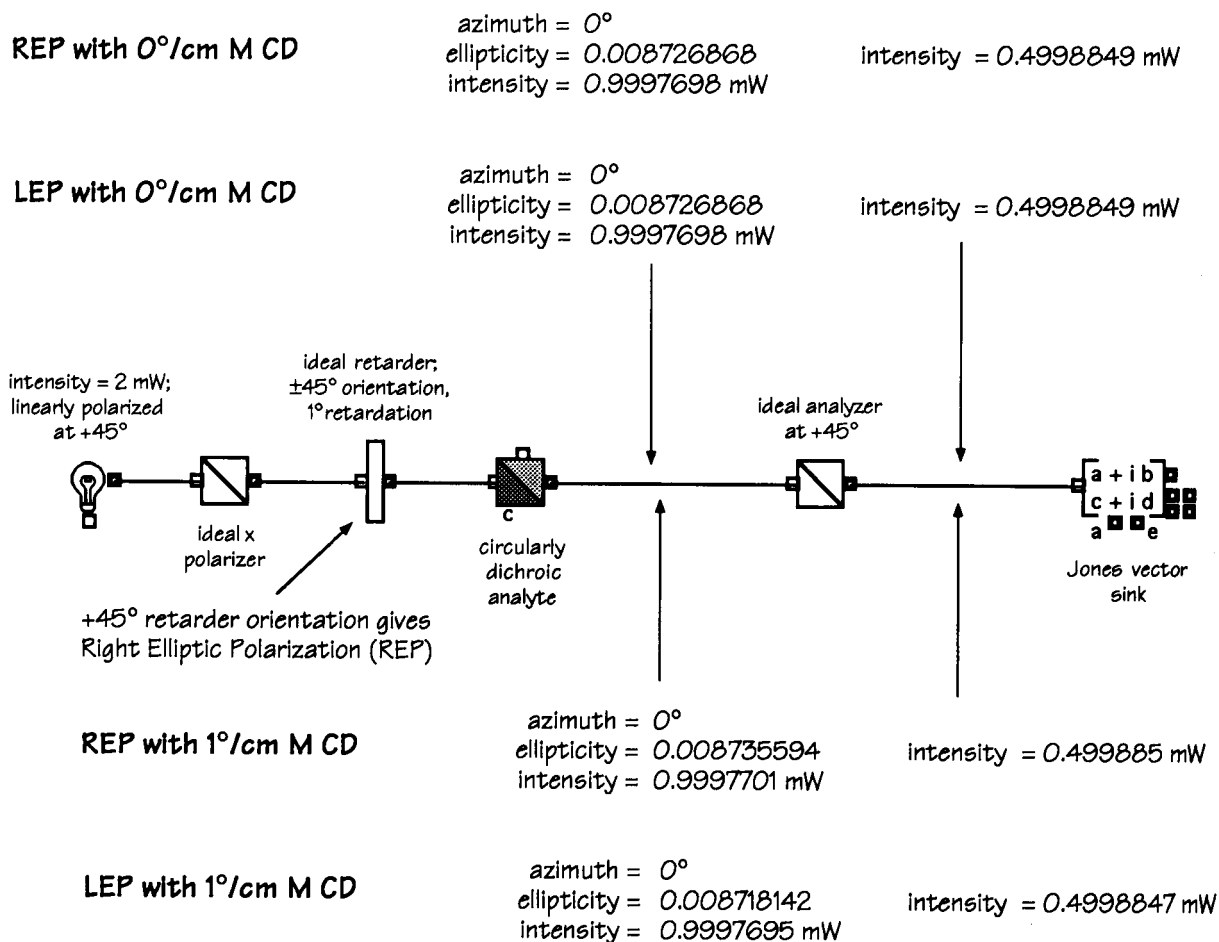


Fig. 10. The simulation used to demonstrate the principles of circular dichroism measurement by ellipticity measurement.

$$\frac{I_{\text{REP}} - I_{\text{LEP}}}{I_{\text{REP}} + I_{\text{LEP}}} \approx \frac{\ln 10 (\epsilon_- - \epsilon_+) c l}{\delta} = \frac{2 \theta c l \pi / 180}{\delta}$$

concentration (M)  
 path length (cm)  
 molar absorptivities (L/mole cm)  
 LCP RCP  
 molar ellipticity (deg/cm M)  
 retardation (radians)  
 normalized light intensity difference  
 for  $\ln 10 (\epsilon_- - \epsilon_+) c l \ll \delta$

Fig. 11. The circular dichroism ellipticity signal expression derived by Goldbeck and Kliger [10].

quency, since both RCP and LCP were produced in each period of the reference frequency and these polarizations yield the maximum transmitted intensity through the analyzer.

The circularly polarized component in the beam incident at the PEM was converted to elliptically polarized light, but at the peaks of the sine wave reference frequency, it is actually linearly polarized. The original retardation of  $90^\circ$  is either increased or decreased by  $90^\circ$  in transiting the PEM. One resultant linear polarization is

aligned with the analyzer, the other is orthogonal to it. Hence, there is an analyzer intensity component at the reference frequency. With phase sensitive detection, the two modulated components are readily found, even in the presence of a substantially larger unmodulated component. Figure 9 shows these results for Fig. 8.

There are other advantages of PEM-based systems, but there are also some disadvantages. Actual PEM devices are resonantly driven, providing modulation frequencies of approximately 50 KHz. Increasing the modulation frequency requires reduction in the size of the device, with concomitant reduction in the optical throughput. There may also be problems with residual birefringence in the PEM device.

Given the relative slowness of PEM devices, it is not possible, at present, to perform CD measurements, using PEM-based instruments, on nanosecond lifetime species. However, there are other ways to measure CD and it is indeed feasible to perform such measurements. One possibility involves the use of ellipticity measurement [2,10].

## Circular Dichroism Ellipticity Signal Detection

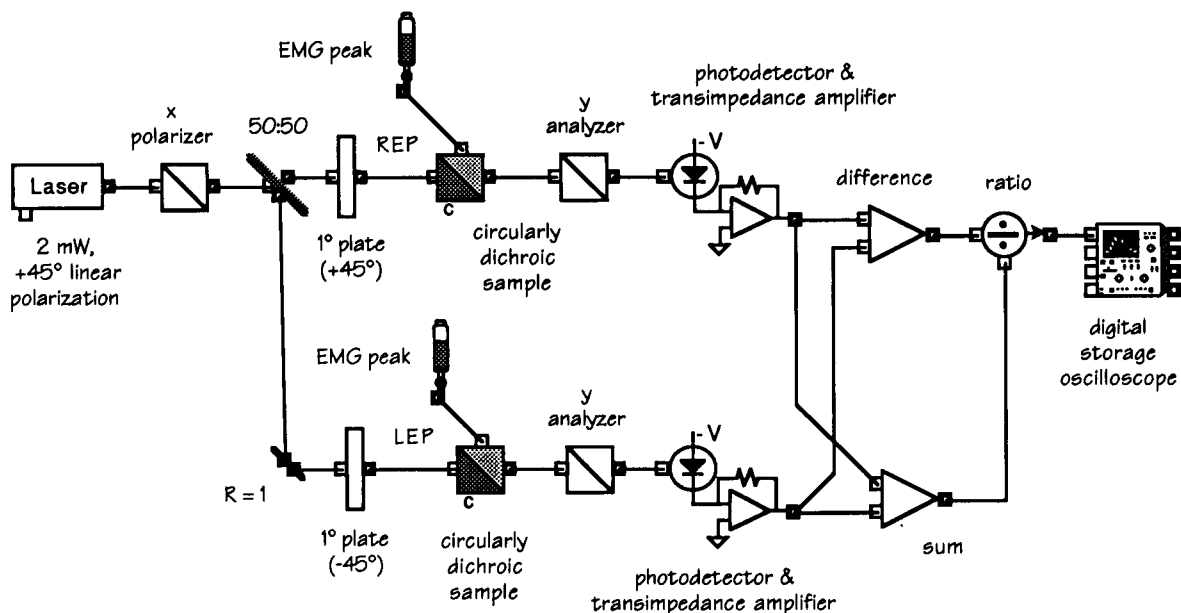


Fig. 12. A "double beam in space" instantiation of the Goldbeck and Kliger circular dichroism ellipticity measurement scheme.



The basic idea is shown in Fig. 10. Linearly polarized light is converted to elliptically polarized light having very small ellipticity, i.e., the light is described by a polarization ellipse which is very thin. The retardation is a small value, typically about  $1^\circ$ , and the retarder is oriented at either  $+45^\circ$  relative to the incident polarized beam or at  $-45^\circ$  relative to the incident beam. In each case, the elliptically polarized resultant beam has an azimuth of  $0^\circ$ , but the  $+45^\circ$  retarder orientation yields right elliptic polarization (REP), while the  $-45^\circ$  retarder orientation yields left elliptic polarization (LEP). As shown in the data in the upper portion of Fig. 10, both REP and LEP light have the same ellipticity and intensity, if they pass through a medium having zero CD. The intensities, after transmission through an analyzer oriented at  $+45^\circ$ , are also equal.

The data in the lower portion of Fig. 10 shows that even a small molar ellipticity causes the REP to become more circularly polarized, i.e., its ellipticity increases, while the LEP becomes more linearly polarized. In Fig. 10, the path length was 1 cm and the analyte concentration was 1 mM, so the CD was only 1 millidegree. After transmission through the analyzer, the intensity difference is easily detected, particularly for larger CD signals.

Goldbeck and Kliger [10] gave an approximate expression, shown in Fig. 11, used to describe the ellipticity signal. Measurement of, e.g., the molar ellipticity, is possible by determining the other parameters and by making measurements of the light intensities ( $I_{\text{REP}}$  and  $I_{\text{LEP}}$ ) for the two orientations of the  $1^\circ$  retarder. An advantage of the technique is that it can be used with nanosecond-pulsed light sources. Another advantage is that polychromatic operation is easily achieved. A disadvantage is that the light intensities would ordinarily be measured in succession. Thus, the retarder would be oriented at  $+45^\circ$  and the transient  $I_{\text{REP}}$  light intensity would be acquired, perhaps with a high speed digital storage oscilloscope. Then the retarder would be switched to  $-45^\circ$  orientation, by  $180^\circ$  rotation about the  $x$  axis, and the transient  $I_{\text{LEP}}$  light intensity would be acquired. High quality digital storage oscilloscopes readily perform file arithmetic on digitized channel data, so calculation of

the normalized light intensity difference is easy, but has the drawback of requiring two light pulses, which then degrades the signal-to-noise ratio ( $S/N$ ) because of pulse-to-pulse light source fluctuations.

Note that the normalized light intensity difference is bounded by  $\pm 1$ , while the other ratios in Fig. 11 are inversely proportional to  $\delta$ , and, therefore, potentially much greater than unity. Decreasing  $\delta$  is a feasible way of improving the measurement only so long as these ratios are much less than unity. If the ratios become too large, temporal distortion occurs, followed by non-linear response.

Figure 12 shows a simple “double beam in space” configuration of the Goldbeck and Kliger ellipticity measurement scheme. Such an arrangement might be useful in cases where source noise was dominant. Two matched sample cells are used and the analyte is supplied by separate, but matched, reservoirs. The PD/preamp outputs would probably be acquired on two channels of a high speed digital storage oscilloscope and the normalized light intensity difference would be calculated in the oscilloscope or in a subsequent computer program. In Fig. 12, the calculation is carried out with unrealistically fast, and accurate, sum, difference, and quotient blocks, for simulation convenience.

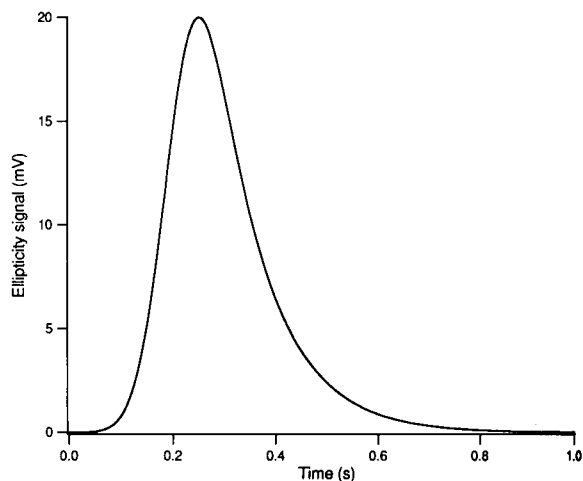


Fig. 13. A typical ellipticity signal waveform produced by the simulation in Fig. 12.

The resulting ellipticity waveform is shown in Fig. 13. The concentration profile was that of an exponentially modified Gaussian (EMG), with asymmetry of 2, and the laser light source was of 2 mW constant intensity, with 1 ppm Gaussian, white noise. The waveform scales with analyte concentration and is almost completely immune to source noise: even 10% R.S.D. Gaussian, white noise on the light source causes no significant change in the waveform. Likewise, changing the light intensity by a factor of 2 has no effect on the signal. This is, of course, a benefit of the “double beam in space” configuration. In practice, it is impossible to match the arms of the instrument perfectly, but the performance should still be impressive.

There are many ways in which to improve upon or change Fig. 12. Suppose the light source is a pulsed laser, with substantial laser noise and also pulse-to-pulse intensity fluctuations. Also suppose the analyte’s circular dichroism is photo-induced, with a 1 ns lag time, and suppose the PD/preamps are noisy. Figure 14 shows a modified version of Fig. 12 having these complications. The laser is modulated with the product of an EMG temporal profile and a noise generator’s output (for pulse-to-pulse fluctuations). The EMG has an amplitude of unity, retention time of 1.5 ns, standard deviation of 0.5 ns, and time

constant of 1 ns [11]. The noise generator produces 1 point per simulation, held throughout a given simulation, having Gaussian distribution,  $\mu \equiv 1$  and  $\sigma \equiv 0.1$ . The resultant product modulated the laser’s 20 mW output, which has 10% R.S.D. of Gaussian, white noise.

The fluctuating laser modulation input serves as the input to an infinite impulse response filter, i.e., digital recursive filter, with 1 ns time constant. The filter is simply a single pole low pass filter. The attenuated output then serves as the “concentration” input to the two sample cells. Therefore, the concentration of CD analyte may be considered as being “photo-generated”, though the laser noise is not used. If it is desired to include the laser noise in the “photo-generation” process, this is readily accomplished by addition of a beamsplitter and PD/preamp after the 50:50 beamsplitter. It should also be noted that far more complicated “kinetics” may be modeled by custom-programming an appropriate block, if the necessary photophysical equations and data are available.

The PD/preamp block has no noise, so it may be made noisy by following it with a noise generator block. As shown, the noise amplitude spectral density is  $10 \text{ nV/}\sqrt{\text{Hz}}$ . The PD/preamp block also has no gain-bandwidth product limitations, so IIR filters, with 1 ns time constants, are used

#### Nanosecond CD Ellipticity Detection

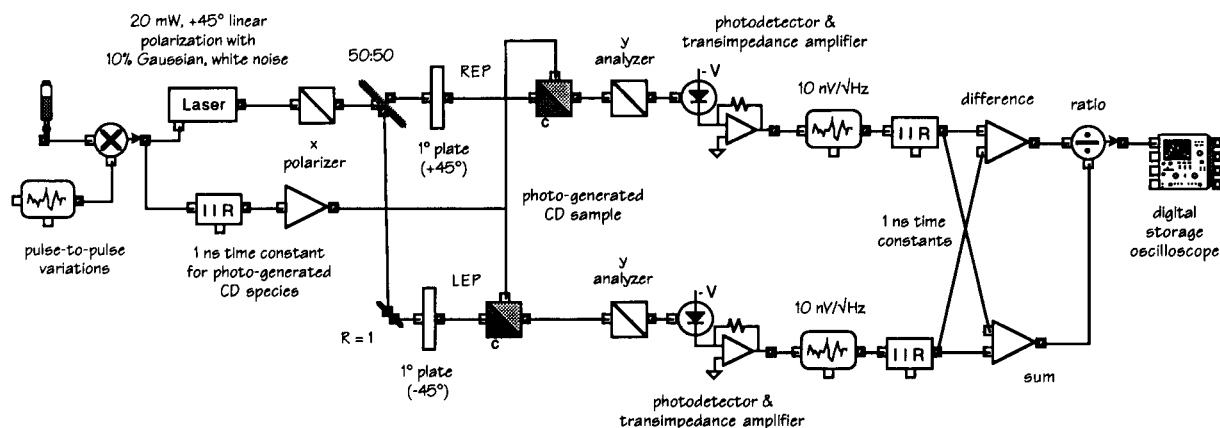


Fig. 14. A more realistic version of the simulation in Fig. 12.

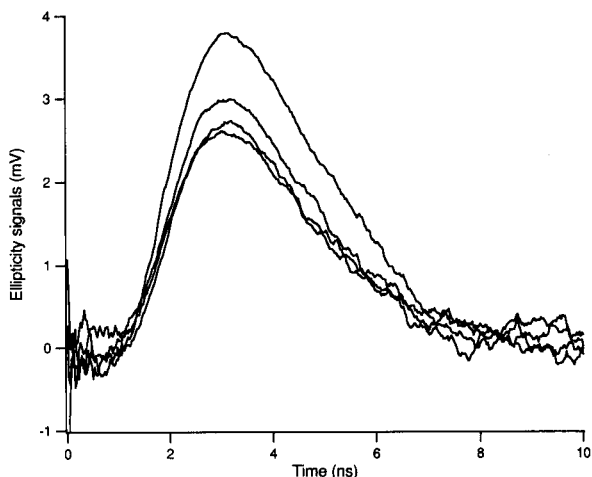


Fig. 15. Four consecutive ellipticity signal waveforms produced by the simulation in Fig. 14.

to roll-off the frequency response. The responsivities of the PD/preamps were  $10^4 \text{ A W}^{-1}$  and the transimpedances were  $1000 \text{ V A}^{-1}$ .

How well does the simulation work? Figure 15 shows 4 consecutive ellipticity signal waveforms. The PD/preamp noise is dominant. The peak analyte concentration was approximately 1 mM, the path length was 10 cm, the mean molar absorptivity was  $5 \text{ l mol}^{-1} \text{ cm}^{-1}$ , and the molar ellipticity was  $0.4^\circ \text{ cm}^{-1} \text{ M}^{-1}$ . Clearly, the laser's pulse-to-pulse intensity fluctuations are not compensated by the light intensity normalization calculation because the fluctuations appear twice: once in the use of the fluctuating laser pulses as the CD probes and a second time in the "photo-generation" of the CD analyte. Another normalization factor is required.

### Conclusions

Several different circular dichroism measurement techniques and instrument schemes have been examined by means of Jones calculus computer simulations. The simulations are easy to set-up, extremely realistic and accurately predict what would happen if careful, well-characterized experiments were to be performed. The simulations are useful for both novices and experts. Novices can see how experiments are supposed to work and become familiar with the operational parameters. Experts can explore instrument de-

signs and configurations, determine parameters sensitivities, predict signal-to-noise ratios, calibration linearities, dynamic ranges, and so on.

It is abundantly clear, from the material presented, that many additional simulations and demonstrations are waiting to be performed. The teaching value of the simulations is enormous and obvious.

This material is based upon work supported by the National Science Foundation under Grant No. CHE-9108707. Thanks are also due to W. Wegscheider and M. Valcárcel for providing the opportunity to participate in the *12th International Symposium on Microchemical Techniques*, in Córdoba.

### APPENDIX

Fig. A1. The dialog box for the polarizers block.

Fig. A2. The dialog box for the photo-elastic modulator block.

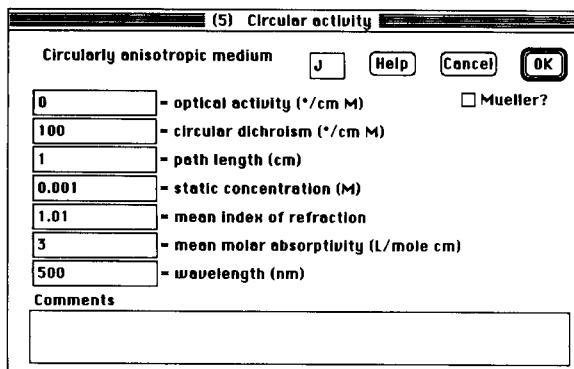


Fig. A3. The dialog box for the circular activity block.

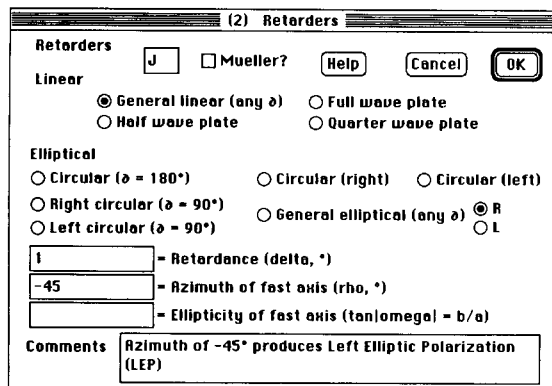


Fig. A6. The dialog box for the retarders block.

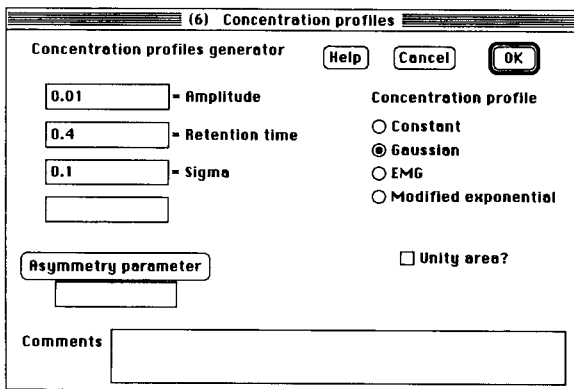


Fig. A4. The dialog box for the concentration profiles block.

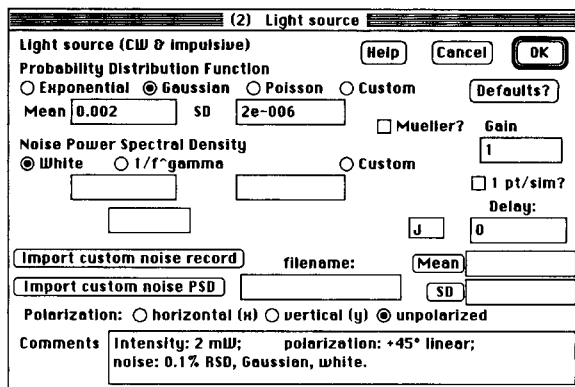


Fig. A7. The dialog box for the light source block.

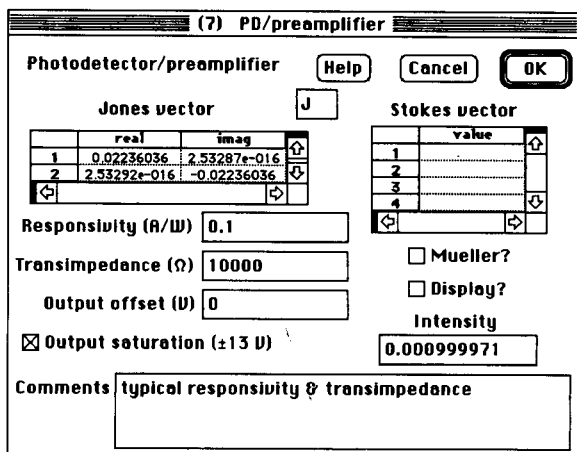


Fig. A5. The dialog box for the PD/preamplifier block.

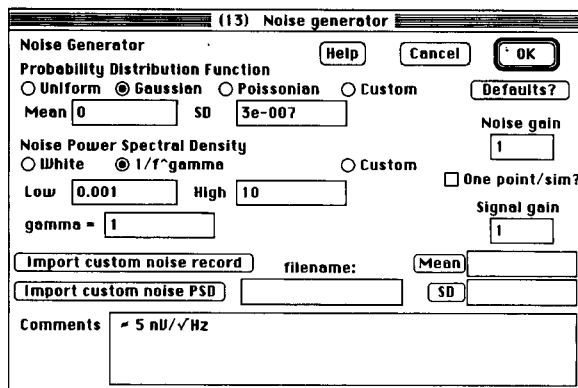


Fig. A8. The dialog box for the noise generator block.

(6) Lock-in amplifier

Lock-in Amplifier and Integrator

1st order RC LPF     3rd order Bessel LPF  
 2nd order RC LPF     1% 'Pickup' LPF  
 3rd order RC LPF     True integration

Time constant

Noise bandwidth     Phase

	Frequency	PoleReal	PoleImag	ZeroReal	ZeroImag
1	0.1591549	-10.66667	0		
2	0.1591549	-10.66667	0		
3	0.1591549	-10.66667	0		

Reference threshold     Hysteresis

Comments

Fig. A9. The dialog box for the lock-in amplifier block.

(1) IIR filter

Digital recursive (IIR) filter

Filter options:

Horowitz & Hill's 'R'     Bibbero's 'K'     external input  
 uniformly distributed     gaussian distributed  
 reciprocal derivative     predator-prey chaos

Time constant options:  constant     proportional

The time constant is  seconds

= Initial filter output

Comments

A simple digital, recursive filter, i.e., infinite impulse response filter, with 1 ns time constant.

Fig. A12. The dialog box for the IIR filter block.

(13) Jones vector source

Jones vector source

Jones vector (rectangular)     Jones vector (polar)

	real	imaginary
1	0.2	0
2	0	0.2

	amplitudes	phases (°)
1	0.2	0
2	0.2	90

Convert rect to polar    Convert polar to rect

   Intensity calculation

Comments

right circular polarization

Fig. A10. The dialog box for the Jones vector source block.

(4) Jones vector sink

Jones vector sink

Display?     Enable separate outputs?

	Real	Imag
1	0.01580896	-0.0001378248
2	0.01580896	-0.0001378248

Intensity =

= azimuth (degrees)

= ellipticity (0 <= b/a <= 1)

Comments

Fig. A11. The dialog box for the Jones vector sink block.

## REFERENCES

- 1 W.A. Shurcliff, Polarized Light, Harvard University Press, Cambridge, MA, 1st edn., 1962.
- 2 D.S. Kliger, J.W. Lewis and C.E. Randall, Polarized Light in Optics and Spectroscopy, Academic Press, Boston, MA 1st edn., 1990.
- 3 E. Voigtman, Anal. Chim. Acta, 246 (1991) 9.
- 4 E. Voigtman, Appl. Spectrosc., 45 (1991) 890.
- 5 U. Kale and E. Voigtman, Appl. Spectrosc., 46 (1992) 1636.
- 6 E. Voigtman, Spectrochim. Acta Electronica, 47B (1992) E1549.
- 7 E. Voigtman, Anal. Chem., 64 (1992) 2590.
- 8 H.P. Jensen, J.A. Schelman and T. Troxell, Appl. Spectrosc., 32 (1978) 192.
- 9 Hinds Instruments, Inc., Hillsboro, OR, PEM-90™ Photoelastic Modulators, brochure and data sheets, 1991.
- 10 R.A. Goldbeck and D.S. Kliger, Spectroscopy, 7 (1992) 17.
- 11 J.P. Foley and J.G. Dorsey, J. Chromatogr. Sci., 22 (1984) 40.

# Certified reference materials: use, manufacture and certification

S. Caroli

*Istituto Superiore di Sanità, Viale Regina Elena 299, 00161 Rome (Italy)*

(Received 8th September 1992; revised manuscript received 18th March 1993)

## Abstract

The present scientific and technological challenges rely heavily on the fundamental support lent by the science of measurement in general and analytical chemistry in particular. For a thorough exploitation of this discipline a massive number of reference materials are required in fields as diverse as environmental protection, biomedicine, industrial activities and many others. It is therefore of the greatest importance that new reference materials are devised and produced. Given the limited financial resources that can be allocated for this purpose at national and international levels, the decision-making process should be judicious enough so as to evaluate carefully actual needs, benefits expected and costs involved. Once the target has been identified as regards the host matrix and properties to be certified, an overall scheme must be designed which should include a plan for the collection of a sufficient amount of material, its preliminary treatment, homogenization and stabilization, selection of participants in the certification campaign, execution of the actual plan, evaluation of experimental results, possible approval of the candidate reference material and eventual release to customers. As all these phases are extremely time consuming and expensive, no effort should be spared toward preventing misuse or incorrect use by unaware operators. Detailed information on this specific aspect should be conveyed to the user in all possible ways in order to minimize the deleterious consequences of erroneous procedures on the quality of analytical data.

*Keywords:* Certified reference materials

“Given the unavailability of reference materials closely matching the matrix composition of the unknowns, the accuracy of measurement could be checked only by resorting to a substance with relatively similar properties.” Sentences such as this are increasingly encountered in analytical chemistry-related papers, clearly testifying the mounting general awareness that the quality of experimental data is now considered an essential attribute, although it may be difficult to pursue.

“Quality” is in effect a term that today has become a commonplace, permeating all possible sectors of science and technology [1]. The more processes and products that can be judged to incorporate quality, the more they satisfy the needs that inspired them. The establishment in the late 1970s and the widespread acceptance soon afterwards of the principles of good laboratory practice (GLP) in the testing of chemicals paved the way to a much deeper understanding of the experimentalist in toxicology and environmental sciences of the need for standardization to guarantee reliability and comparability of data [2].

*Correspondence to:* S. Caroli, Istituto Superiore di Sanità, Viale Regina Elena 299, 00161 Rome (Italy).

Measurement techniques play a major role in production technology as a consequence of increasingly complex processes, their automation and the need to respect norms set at both national and international levels [3,4].

The impact of analytical chemistry on the economy of developed countries is of increasing importance, and quality of measurements must be more and more rigorously guaranteed if the ensuing beneficial effects are to be fully exploited. Accurate chemical measurements will then result in considerable value being added to marketed goods, and in addition reliable data are essential to ensure an effective spread of information among scientists, irrespective of their affiliation or language. In this framework, reference materials (RMs) and certified reference materials (CRMs) have a key function and the major aspects involved in their preparation will be briefly reviewed in subsequent sections. Most of these considerations are in the context of chemical measurements; in spite of this, they are sufficiently broad in coverage to apply to the majority of metrological activities. In order to avoid any misinterpretation, a list of internationally accepted definitions of the terms more frequently used in this paper is given in the Appendix. Further, the focus is mainly on CRMs, as these warrant the highest degree of credibility of the values attached to the property certified, although under less demanding conditions or if CRMs are unavailable, RMs can also be profitably exploited. One of the examples of this inherently different approach is the use of RMs in control charts to monitor the long-term reproducibility of measurements of a quantity expected to be constant, or to test the proficiency of laboratories involved in intercomparison exercises, i.e., when the actual value of a given property of the RM is less important than the agreement among determinations. On the other hand, with CRMs, assessment of accuracy is the goal, so that the validity of the quantification process can be checked. Consequently, the “true” value of the property must be known with the highest possible certainty. It should be stressed that the concepts dealt with hereafter are, from a general standpoint, valid in both instances.

## FEATURING REFERENCE MATERIALS

### *Reliability of experimental information*

Experimental data achieved through an analytical process are characterized by, among other factors, their precision and accuracy, the former referring to the general agreement of measurements (i.e., their dispersion around the central value) and the latter the closeness of such measurements to the true (or deemed such) value of the quantity concerned. It is this last factor that deserves the greatest attention, as the better that accuracy of a quantitative determination, the higher is the ability to generate correct information, with all the attendant consequences on competitiveness of technological products in international markets, the potential for adequately monitoring environmental pollution, safeguards of human health, art conservation, forensic purposes, etc., and ultimately better chances for decision-makers to set up safer, more realistic legal provisions [5–9].

Hence, if accuracy is the target, how can this be attained? Conventionally, it is acknowledged that there are three main options to evaluate the accuracy of measurements in analytical chemistry, namely the use of basically different techniques, each with its own operators and procedural aspects; the organization of interlaboratory exercises; and the incorporation in the analytical scheme of suitable RMs and CRMs, when available. In the first instance, the limitation is obvious; only a few laboratories are in fact so well equipped that they can respect the crucial condition of an array of independent instrumental techniques and personnel, or can afford the burden of frequent analytical replicates. On the other hand, agreement of data obtained under such circumstances is strong evidence of accurate results. As regards the second possibility, this goal is achieved by involving a number of analytical centres, each with specific expertise in a given methodology, with the clear advantage of distributing the load of the undertaking among several participants. Such intercomparisons are always welcome, even though their success depends on the capacity of the coordinator and on the existence of standards suited to the needs in

terms of matrices and analyte levels matching those to be determined. These two approaches virtually combine in the third one, in that the mere existence of a CRM implies the assessment of one or more of its properties through a number of selected techniques.

#### Role of CRMs in the analytical process

CRMs can be considered as only part of the overall situation, although essential to confer consistency to the whole, as summarized by Uriano and Gravatt [10]. Figure 1 highlights the links among and the sequence of the main phases identifiable in an accurate and ideal measurement pattern. This is based on the use of basic measurement units (SI system) and goes through the assessment of definitive methods, i.e., those which quantify chemical or physical entities directly in basic units (or even in derived units, provided that these can be related to the former by univocal mathematical expressions). Today, this definition is thought to be not entirely satis-

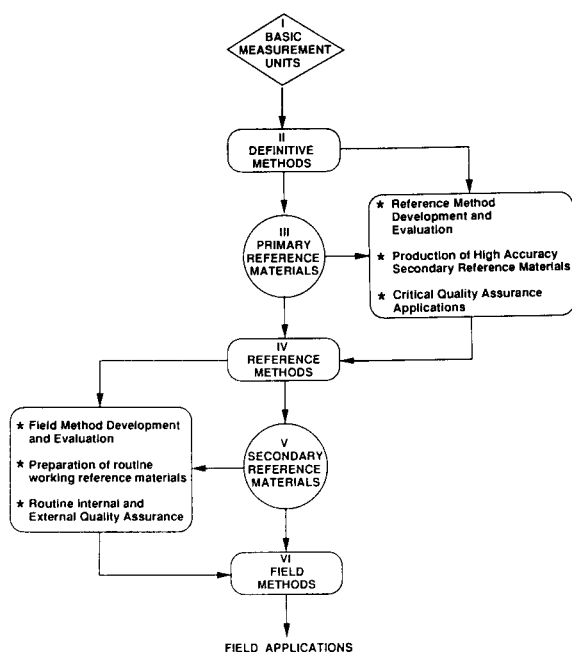


Fig. 1. Hierarchical model of a measurement network [reproduced with permission from G.A. Uriano and C.C. Gravatt, *CRC Crit. Rev. Anal. Chem.*, 6 (1977) 361, by courtesy of CRC Press, Boca Raton, FL].

factory and it is still open to debate which are the minimum prerequisites for a reference method to be labelled as such.

Dependability, freedom from systematic errors and full control of the processes governing the generation of experimental data characterize such methods, which allow primary RMs to be produced. Their use should by no means be extended to current work for which instead the second category of RMs is planned. They lead to reference methods whose role is in checking and calibrating field methods and in setting up routine quality control programmes. Field methods are then encountered which transfer this global strategy to a more accessible level, especially in consideration of the high costs and complexity affecting reference methods. Although less rigorous, their accuracy should be compatible with the needs of the specific analytical problem and therefore find validity only when carefully calibrated. It is apparent that the coverage of primary and secondary RMs coincides, more or less, with that of CRMs and RMs, respectively, according to the definitions given in the Appendix.

Criteria for an appropriate choice of these should include soundness of the methodologies with which such materials were produced, completeness of the information accompanying them, especially insofar as the conditions of use are concerned, and permanent availability. Harmonization of terminology plays a large role in this context, as misleading inconsistencies still persist among producers. Also, the definitions given in the Appendix for RMs and CRMs still leave some margin of misinterpretation, e.g., as concerns the meaning of a “certifying body” [11].

The confusion is not likely to decrease in spite of the efforts being made internationally. In this connection it is worth mentioning that IUPAC recognizes three main types of materials, in the following order: (i) primary substances, intended for the setting up of measurement scales based on SI units or derived units (to be qualified as such, these substances should be obtainable in a pure state by a reliable procedure or should be certified in terms of purity and stability by a highly experienced laboratory); (ii) calibration and test materials, aimed at checking the instrumental



performance and analytical methods and to establish measurement scales other than those envisaged under (i); and (iii) certified reference materials, whose properties are formally guaranteed by an authoritative organization with accuracy better than that needed for practical purposes by substances under (ii) [12]. In turn, to detail further the concept of CRMs, ISO recommends the use, as appropriate, of the terms certified values, uncertified values, consensus values and best estimates, as given in the Appendix [13]. Again, interpretative problems arise in the practical application of such definitions, as boundaries between two subsequent classes are difficult to grasp and no clear criteria are set to grant an RM the qualifying attribute of “certified”. From this cursory survey, what comes out as a general trend is that a number of precisely defined requirements must be satisfied for an RM to be labelled as “certified”. In an attempt to rationalize this aspect, an exhaustive list of essential features has been worked out by ISO, as illustrated in Table 1 [14].

#### FROM CONCEPTION TO EMPLOYMENT

##### *Background information*

The increasing awareness early in this century that the obtainment of comparable results for

similar materials over extended periods of time and among different laboratories could be more and more difficult as the analytical needs were progressively approaching the domain of trace analysis prompted the American Foundrymen’s Association in 1905 to contact the US National Bureau of Standards, formed only 4 years earlier, as better agreement in the analyses of cast iron was needed. This gave birth to the first four standards, consisting of cast iron, certified for chemical content. This opened up a new era in modern analytical chemistry.

Nowadays, the sequence of steps leading to the certification of new RMs should include, in order: decision on the type and amount of material; its collection, preparation and manipulation; assessment of homogeneity and stability; definition of the quantities to be certified; organization of the measurement network; critical evaluation of experimental data; elimination of inaccurate results; statistical treatment; compilation of the certification report; commercialization of the CRM, its use by the customer and follow-up of its adequacy for the analyst’s needs with possible revision of data already certified and/or certification of other parameters; and finally, possible decision on replication of the process if the first lot of CRMs goes out of stock.

With reference to the first step, the conspicuous imbalance existing between present needs in

TABLE 1

Information to be attached to a CRM according to ISO [14]

Name and address of the certifying organization	Special instructions for correct use
Title of the document	Preparation method
Status of the certificate	Evaluation of homogeneity
Name of the material	Values of the certified properties and their confidence limits
Number of the sample and/or the batch	Non-certified values
Certification date	Values obtained by individual methods or laboratories
Availability of the material in other forms or formats	Significance and nature of certified values and their uncertainties
Source of the material	Measurement techniques used for certification
Supplier of the material	Names of participating analysts and laboratories
Preparer of the material	Legal advice
Description of the material	References
Foreseen use	Signatures or names of certifiers
Instructions on stability, transport and storage	

several experimental disciplines and the paucity of CRMs available make it all the more problematic for the producer even only to select likely candidates because of the many different and pressing gaps that require filling. With no claim at exhaustiveness, but in any event well representative of current manufacturers, Table 2 gives an overview of producers of RMs and CRMs to date. The advances in most experimental disciplines and the increasing understanding of the mandatory character of quality control criteria are putting great stress on CRMs. Sectors such as environmental sciences, bioclinical chemistry, food analysis and innovative technologies demand that new certification projects be launched. Nonetheless, priorities must be identified and the driving forces behind this may substantially change with the perception of producers, one of

the main parameters in the decision-making process being the economical return expected by such undertakings to the benefit of both the manufacturer and the community at large. The mass to be collected and the feasibility of the certification for the properties targeted must understandably soon be faced. Collection should then take place so as to ensure the highest uniformity possible of the raw mass with physical and/or chemical characteristics as close as possible to those of the samples for which they are designed. This phase may vary from the simple identification of a suitable substance or chemical at the desired degree of purity for further treatment to the painstaking cultivation of a vegetable species with given features under controlled conditions for subsequent harvesting and attendant manipulation to prepare a multi-elemental CRMs.

TABLE 2

A selection of organizations producing reference materials

Manufacturer	Coverage	Country
Behring Institute (BI)	Biology	Germany
Bundesanstalt für Materialprüfung und -forschung (BAM)	Industry	Germany
Bureau of Analysed Samples (BAS)	Industry	UK
Bureau Communautaire de Référence (BCR)	Biomedicine, food and agriculture, environment, industry, physical chemistry	EC
Central Bureau for Nuclear Measurements (CBNM)	Biology, environment, nuclear, and isotopic applications	Belgium
Ferroetalon Vaskut (FV)	Industry	Hungary
Geological Survey of Japan (GSJ)	Geology	Japan
Institute of Geological Sciences (IGS)	Geology	UK
Institute of Radioecology and Applied Nuclear Techniques (IRANT)	Environment	Czechoslovakia
Instytut Metali Niezależnych (IMN)	Industry	Poland
International Atomic Energy Agency (IAEA)	Biology, environment, nuclear and isotopic applications	International
Kaulson Laboratory (KL)	Biology, environment	USA
Laboratory of the Government Chemist (LGC)	Biology, environment, food and agriculture	UK
National Institute for Environmental Studies (NIES)	Biology, environment	Japan
National Institute of Standards and Technology (NIST)	Biology, environment, food and agriculture, industry, physical chemistry	USA
National Research Council of Canada (NRCC)	Biology, Environment	Canada
National Research Centre for Certified Reference Materials (NRCCRM)	Biology, environment, food and agriculture, physical chemistry	China
New Brunswick Laboratory (NBL)	Nuclear and isotopic applications	USA
Nyegaard (NYE)	Biology	Norway
South African Bureau of Standards (SABS)	Environment	South Africa

### *Preparatory phase*

The start mass may well require some preliminary preparation steps, such as grinding, freeze-drying, purification, cutting or shaping, that would render it more suitable for subsequent manipulation. Two major goals of this pretreatment, although not the only ones, are centred around the achievement of the pre-established degree of homogeneity and of chemical and microbial inertness of the material during its shelf-life. These two fundamental parameters may be optimized before, during or after the other operations mentioned as examples of preliminary elaboration of the material. The need for homogeneity is self-evident as the assessment of a value for a tested quantity carried out on small and separate aliquots of the total mass must be valid and congruous not only for these, but also for the much more abundant unassayed bulk of the substance.

This depends to a large extent on the minimum amount of the material that is likely to be taken for an analysis. Many instrumental techniques actually require tiny portions of sample (often in the sub-milligram range), as is typical in electrothermal atomization atomic absorption spectrometry or laser ablation inductively coupled mass spectrometry. Homogeneity brings with it an accentuated statistical component, i.e., the acceptable uncertainty for a given analyte should be decided first and then the aliquot of the CRM necessary not to exceed that level of imprecision should be calculated. Homogeneity can thus be expressed by the so-called sampling constant,  $K_s$ , resulting from the product  $s^2m$  (where  $s$  is the relative standard deviation of subsampling for the component of interest and  $m$  is the corresponding mass), as recommended by Parr et al. [15]. Further, different levels of homogeneity are to be expected for the various analytes. All this information should be explicitly reported by the producer in the CRM certificate. For most practical purposes, amounts in the range 100–500 mg are adequate in terms of homogeneity-related imprecision of measurements, although the certification process should in this respect be much more demanding to make inhomogeneity negligible with respect to uncertainty of the analytical method.

Alternatively, a statistical tolerance interval can be defined, the centre of which can be accepted as the mean value of the batch, although this would inescapably imply an unacceptable consumption of the CRM, with the associated costs, and more tedious and prolonged analyses. The physical means for homogenizing the candidate mass, moreover, should neither contaminate nor spoil the original content of the analytes concerned to an appreciable extent to avoid any significant alterations of the material that would bring it far away from that planned to satisfy the users' needs. Finally, the homogeneity study must clearly be conducted before the certification campaign by a small group of specialists using the most up-to-date and adequate analytical techniques to test this parameter from bottle to bottle and within bottle.

Stability is an indispensable condition to ensure that the figures attached to the certified properties are not prone to alteration in the course of time. Both organic and inorganic materials are, in different ways, liable to such a fate: chemical phenomena consequent on contact with air, moisture, adsorption, reactions among different components, growth of fungi and bacteria and decomposition by exposure to light may all seriously affect the original status of the CRM. Such deleterious effects must be counteracted at a dual level, namely at the production stage, when sterilization, lyophilization and similar physical measures should be taken, and at the storage phase, when the recommendations given by the producer regarding conditions of temperature, humidity and darkness should be strictly followed. Even in the best case, however, the full validity of the CRM expires after a certain period of time (often several years). The supplier should give notice of this to the best of the available knowledge, although one has to acknowledge that often no reliable information is available when novel materials are put on the market.

Parallel to all the steps already mentioned is the selection of the quantities for which certification is needed. In reality, this decision is foreshadowed at the moment of the conception of a new CRM, which would otherwise not even be planned. However, as the project takes shape, the

actual feasibility of that particular certification may require some adjustments or may require an expansion of the study to other quantities in a feed-back manner that will come to a halt only on completion of the overall exercise. It is also worth emphasizing that, for the best benefit-to-investment ratio to be obtained, the highest number of properties possible should be certified in the same CRM, at least until the price of this latter do not become prohibitive for the customer.

#### *Certification process*

The two basic approaches to the certification exercise have been already briefly mentioned and can be labelled as the single-laboratory and the interlaboratory campaign modes. The first case, most frequently the approach chosen by the National Institute of Standards and Technology (NIST), is much less time consuming, but also requires a well established scientific centre of extremely high competence, capable of mastering even the most difficult experimental challenges and performing all phases of the CRM production cycle. Several independent methods should be applied to arrive at reasonably accurate mean values, even though this may be expensive and thus have an effect on the purchase costs.

In the latter instance this last drawback is appreciably less serious as the expenses associated with certification are shared in part by the laboratories that have accepted to join the inter-comparison exercise under the guidance of a leading organization. The success of the initiative is linked to the scrupulous choice of the participating centres. This pattern is preferred by the International Atomic Energy Agency (IAEA) and the Community Bureau of Reference (BCR) of the European Communities, with different strategies, however.

In terms of accuracy, the latter approach would provide better estimates of the “true” value of a given quantity, whereas it is definitely more problematic for the leading centre to have effective control over the quality of work done by each participant. To circumvent this disadvantage, it is desirable to select carefully the participating laboratories to ensure the presence of at least two or three units using the same analytical methodology

independently of each other and to scrutinize impartially the defensibility of data provided by each partner through general meetings, the attendance at which is a prerequisite for the discussion of the corresponding set of measurements and their possible acceptance. These and other criteria are rigorously applied by BCR in the performance of a certification campaign and ease the task of detecting any bias or inconsistency of experimental results, seeking their causes and eventually discarding unreliable figures and outliers. Not always can such discrepancies be totally resolved and a residual probability still remains that a minority of laboratories (maybe only one) are closer to the true value than the majority.

Another option arises when every participant uses the same experimental technique and a consensus is reached from the statistical distribution of each measurement point in the overall population of data. The risk in this instance is that a systematic and still unsuspected error may plague the method and the mean average is thus biased with respect to the true value. Nor should any statistical treatment be applied considering each single measurement as an independent variable. In fact, each set of data is bound to one of the laboratories and it would be incorrect to merge them all as if they were a single population, whereas this can be safely done taking into account the means from each participant.

In reality, some of the operations listed previously as separate steps for the sake of clarity are, at this stage, closely interconnected: evaluation of data cannot be thought of without an adequate statistical treatment and the attendant rejection of unacceptable results; ultimately, each certified value is accompanied by a confidence interval that reflects the summation of all possible uncertainties encountered along the way. A multiplicity of tests can be used to identify outliers (e.g., those by Dixon or Grubbs), to ascertain the symmetry of the frequency distribution curve of data (coefficient of skewness) or its sharpness (coefficient of kurtosis), to verify the homogeneity of variance among different sets of measurements (Snedecor, Cochran and Bartlett tests). Non-parametric tests are to be applied when the distribution of values does not follow a Gaussian

BAR - GRAPHS FOR LABORATORY MEANS AND 95% CI

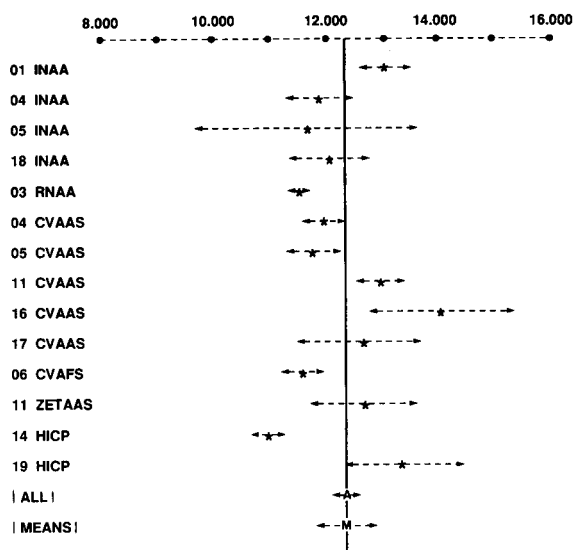


Fig. 2. Bar graph representation of experimental results obtained by eleven laboratories (identified by the code on the left) with the associated uncertainties in the certification of Hg in human hair [reproduced with permission from B. Griepink, Ph. Quevauviller, E.A. Maier, K. Vercoutere and H. Muntau, The Certification of the Contents (Mass Fractions) of Cd, Hg, Pb, Se and Zn in Human Hair, CRM 397, BCR Information Report EUR 13433 EN, 1991, courtesy of the European Communities].

pattern, which is often the case with averages pertaining to different methods. Just as an example of the approach adopted by BCR, Fig. 2 reports a typical bar graph depicting the scattering of results in a certification campaign [16].

A certificate can then be issued containing in a clear, yet exhaustive, way the information set forth in Table 1 and unequivocally distinguishing between certified and simply qualified values. Preferably, a summary of these notices is given in the few sheets comprising the certificate, while a more extended report is available to detail all aspect of the certification campaign. Once the CRM is ready, concerted action is needed to convey to all possible users the message of its availability. For this purpose channels such as scientific journals, supplier catalogues, technical meetings and any other form of announcement are to be exploited.

A similar constant action should be taken to promote the correct use of the product. In the

case of multi-elemental CRMs for trace analysis, in particular, this would mean discouraging its use as a calibrant or for the analysis of specimens with appreciably different matrices, while suggesting the advisable number of intakes that should not be exceeded still to have a substance with characteristics within the prescribed range and strongly recommending appropriate storage conditions. More specifically, four main uses for a CRM can be envisaged: production or evaluation of secondary RMs; direct primary standardization in the field; method/instrument development and evaluation; and quality assurance [4]. All four issues help a chemical laboratory to ensure accuracy and to adopt a valid measurement system by identifying causes of discrepancies and avoiding them. To this end, CRMs must be used consistently to guarantee reliable measurements [17].

An inappropriate use of a CRM is likely not to provide the intended information. Moreover, a clear distinction is made between misuse of a CRM and incorrect use. The first case arises when the CRM is used, e.g., as a "blind" unknown check sample in quality control programmes, owing to the ease with which that CRM can be recognized, especially if only a few CRMs of that type are available. The user should also be fully cognisant the parameters of certification in order to exploit them adequately. In particular, the uncertainty associated with the certified value should never be overlooked, as would happen if an amount of the CRM were taken that is less than that guaranteeing homogeneity. Nor should the user select an analytical method capable of better repeatability than those used for the certification. On the other hand, the chosen CRM should not possess an uncertainty greater than that permitted by the end use of the method (as a rule, the CRM should be characterized by an uncertainty better by a factor of 3–10 than that for the end use).

The term incorrect use applies when the rule of the strictest identity between the CRM and samples is violated because of the lack of a suitable CRM. A similar material must be then resorted to, but the user must be aware of the possible adverse consequences of this choice. In turn, the cost of the CRM cannot be neglected,

especially when an alternative exists at a lower price and does not imply drawbacks, e.g., a poorer uncertainty, yet still adequate for the end use.

It may happen, finally, that at a later period of the CRM shelf-life the certification of another property becomes desirable, thus decreasing considerably the costs of the preparation of a new product. When this occurs, it is usually in response to a desire expressed by some qualified scientific groups that earlier than others have realized the practicality of this solution. A further certification may also become necessary when, for more or less fortuitous reasons, it becomes apparent that a given value is less close to the true value than expected. Fortunately, this very rarely occurs; just to mention one example, a total of 24 elemental concentrations were re-evaluated in some reference materials distributed by the Institute of Geological Sciences (UK), namely those from IGS 21 to IGS 39 [18].

#### FUTURE PROSPECTS

In view of current worldwide economic difficulties, high-quality technical and factual information is needed more than ever and CRMs certainly play a key role in the overall process. Planning of new CRMs, in this framework, should therefore respond promptly and efficaciously to arising needs and even anticipate them, while international bodies and also regional and national authorities should more and more encourage and prescribe in detail the use of such products.

The dramatic expansion of research into global change phenomena and transboundary migration of pollutants, for example, require a much better range of CRMs than currently available. These exigencies will be even more keenly felt when more ambitious projects come of age, such as the scientific programmes in Antarctica, for which there is a serious lack of suitable CRMs [19,20].

As a contribution to the consolidation of a culture in this area, it is suggested that journal editors, collators and publishers should further strengthen the policy followed so far and reject or

request amendment of papers and scientific publications in general when a minimum set of necessary information on quality control schemes, accuracy evaluation and use of CRMs is not unequivocally included, preferably in a tabulated manner, the format of which could be harmonized to a great degree by collaboration among the major publishing houses. Referees should also be requested to make a more systematic judgement of these aspects. If all this can be progressively consolidated, then the validity of experimental information will no longer remain a topic to be dealt with only by specialists.

#### APPENDIX

For a better understanding of the major key terms used in this paper, internationally accepted definitions are given here, with the corresponding literature sources.

*Accuracy:* accuracy relates to the difference between a result (or mean) and the true value [21].

*Best estimate:* an estimate of the value that is optimized by taking into account both metrological and technical judgement and statistical factors [13].

*Certified reference material:* a reference material one or more of whose property values are certified by a technically valid procedure, accompanied or traceable to a certificate or other documentation which is issued by a certifying body [17].

*Certified value:* for a certified reference material, the value that appears in the certificate or other documentation accompanying the material, this value having been certified by a technical valid procedure [13].

*Consensus value:* for a reference material, the value of a quantity obtained by interlaboratory testing or by agreement between appropriate bodies or experts. A consensus value could, through appropriate action by a certifying body, become a certified value [13].

*Precision:* precision relates to the variations between variates, i.e., the “scatter” between variates [21].

*Reference material:* a material or substance one or more properties of which are sufficiently well established to be used for the calibration of an apparatus, the assessment of a measurement method, or for assigning values to materials [17].

*Reproducibility:* precision under reproducibility conditions [21].

*Uncertified values:* for a reference material, the value of a quantity obtained by interlaboratory comparison, but which is not certified by the producer or by any other agency. An uncertified value may be given for information only [13].

## REFERENCES

- 1 S. Caroli and R. Fuoco (Eds.), Quality Control and Assurance in Life Sciences, *Microchem. J.*, 45, No. 3 (Part I) and 46, Nos. 1, 2 and 3 (Parts II, III and IV) (1992).
- 2 OECD Environment Monograph No. 5, Final Report of the Working Group on Mutual Recognition of Compliance with Good Laboratory Practice, London, March 1988.
- 3 G. Tassey, *IEEE Trans. Eng. Manage.*, EM-33 (1986) 162.
- 4 NBS Special Publication 679, National Bureau of Standards, Washington, DC, 1986.
- 5 H. Muntau, *Fresenius' Z. Anal. Chem.*, 324 (1986) 678.
- 6 R. Alvarez, *Fresenius' Z. Anal. Chem.*, 324 (1986) 376.
- 7 M.M. Schantz, B.A. Benner, Jr., S.N. Chesler, B.J. Koster, K.E. Helm, S.F. Stone, W.R. Kelly, R. Zeisler and S.A. Wise, *Fresenius' Z. Anal. Chem.*, 338 (1990) 501.
- 8 S.D. Rasberry, *Fresenius' Z. Anal. Chem.*, 326 (1987) 609.
- 9 K. Okamoto and K. Fuwa, *Analyst*, 110 (1985) 785.
- 10 G.A. Uriano and C.C. Gravatt, *CRC Crit. Rev. Anal. Chem.*, 6 (1977) 361.
- 11 International Organization for Standardization, International Vocabulary of Basic and General Terms in Metrology, ISO, 1984.
- 12 International Union of Pure and Applied Chemistry, Physical Chemistry Division, Commission on Physicochemical Measurements and Standards, *Pure Appl. Chem.*, 40 (1974) 393.
- 13 Terms and Definitions used in Connection with Reference Materials, International Organization for Standardization, ISO Guide 30, 1981.
- 14 Contents of Certificates of Reference Materials, International Organization for Standardization, ISO Guide 31, 1981.
- 15 R.M. Parr, Y. Muramatsu and S.A. Clements, *Fresenius' Z. Anal. Chem.*, 326 (1987) 601.
- 16 B. Griepink, Ph. Quevauviller, E.A. Maier, K. Vercoutere and H. Muntau, The Certification of the Contents (Mass Fractions) of Cd, Hg, Pb, Se and Zn in Human Hair, CRM 397, BCR Information Report EUR 13433 EN, Office for Official Publications of the EC, 1991.
- 17 Uses of Certified Reference Materials, International Organization for Standardization, ISO Guide 33, 1989.
- 18 B. Lister, *Geostand. Newsl.*, 10 (1986) 177.
- 19 XXII Meeting of the Scientific Committee on Antarctica Research (SCAR), Final Reports, 8–19 June 1992, San Carlos de Bariloche, Argentina.
- 20 P. Cescon (Ed.), Antarctica Project, Environmental Impact and Chemical Methodologies, *Ann. Chim. (Rome)*, 81 (1991).
- 21 H. Freiser and G.H. Nancollas (Eds.), *IUPAC Compendium of Analytical Nomenclature. Definitive Rules 1987*. Blackwell, Oxford, 2nd edn., 1987.

# Projects for the improvement and quality control of inorganic and organic analysis in environmental matrices

Ph. Quevauviller, E.A. Maier and B. Griepink

*Commission of the European Communities, Community Bureau of Reference (BCR), 200 Rue de la Loi, B-1040 Brussels (Belgium)*

(Received 8th September 1992)

## Abstract

Owing to the strong need to improve the quality of measurements for the monitoring of inorganic and organic compounds in the environment, the Community Bureau of Reference (BCR) of the Commission of the European Communities has undertaken a series of projects dealing with interlaboratory exercises and the production of reference materials certified for a wide variety of inorganic (major and trace elements) and organic (chlorinated biphenyls and polycyclic aromatic hydrocarbons) compounds in various environmental matrices. This paper provides an overview of the most recent projects in the field of environmental monitoring, i.e., for water (fresh, estuarine and sea water), plants (aquatic and terrestrial), biota and waste.

**Keywords:** Biota; Certified Reference Materials; Foods; Plant materials; Quality control; Waste materials; Waters

Environmental protection is nowadays a priority for many countries. The public concern and hence the economic and political impact of environmental protection have led governments to implement national or international regulations such as EC Directives and international conventions such as the Paris and Oslo convention for the protection of the North Sea. The implementation of these regulations may require monitoring programmes in which measurements of various parameters are carried out to evaluate the situation (e.g., mapping, modelling) and its evolution ("trend" monitoring). The results of the determinations performed are the basis for possible actions and decisions to be taken by the authorities. Their effect is again evaluated on the basis of measurements which are conducted over long periods of time. Trends and even kinetics of

decontamination processes may be established and accordingly actions can be modified. The economic and legal impact of the decisions (e.g., closing of factories, waste management, etc.) and the human effect (unemployment, displacement of populations such as in Seveso, Italy) can be enormous.

Hence the analyses have to be reliable. Many scientists have stated that good reproducibility is sufficient in order to follow trends and demonstrate effects of actions carried out by the authorities to improve the quality of the environment; such a statement overlooks applications of results for modelling and theory development and ignores improvements in equipment and methodology. Accuracy is therefore the prime requirement for environmental analysis.

Many examples have been given to illustrate the economic effects of bad measurements [1], e.g., the amount of money lost every year due to a lack of accuracy in the monitoring of the North Sea has been estimated to be ca.  $2 \times 10^7$  ECU

*Correspondence to:* E.A. Maier, Commission of the European Communities, Community Bureau of Reference (BCR), 200 Rue de la Loi, B-1040 Brussels (Belgium).



[2]. To achieve not only good reproducibility but also good accuracy, various measures are necessary, which have been described in detail in the literature [3,4]; they include the follow-up of good quality control principles {e.g., Good Laboratory Practice (GLP) and ISO and CEN Standards [5,6]}, the need for proper calibration of instrumentation, the use of reference materials and participation in interlaboratory studies.

Owing to the strong need to improve the quality of measurements for the monitoring of inorganic and organic compounds in a wide variety of environmental matrices, the Community Bureau of Reference (BCR) of the Commission of the European Communities has conducted [7] and is currently undertaking a series of projects the aims of which are to improve the state of the art of analysis through interlaboratory exercises and to produce certified reference materials (CRMs). This paper summarizes the most recent projects for quality control in monitoring different environmental compartments (water, wastes, plants, biological tissues); these projects were presented and summarized in the form of posters at the ISM'92 in Córdoba [8–14].

#### ORGANIZATION OF THE PROJECTS

One of the most powerful tools in detecting and removing sources of error due to a particular technique or a lack of quality control (QC) within a laboratory is to participate in intercomparisons [1]. In general, apart from the sampling error, the following main sources of error can be detected in all inorganic and organic analyses: sample pretreatment (e.g., digestion, extraction, preconcentration, clean-up, dilution); separation (e.g., adsorption on column, peak overlap) for organic analysis; final measurement (e.g., calibration errors, spectral interferences, background corrections); and the laboratory itself (e.g., training and education level of workers, care applied to the work, awareness of pitfalls, management, clean bench facilities).

When different laboratories participate in an intercomparison, different sample pretreatment methods and different techniques of final deter-

mination are compared and discussed as well as the laboratories themselves. If the results of such an intercomparison agree, the obtained value is likely to be the best approximation of the truth.

An intercomparison can be held (i) to detect the pitfalls of a commonly applied method and to ascertain its performance in practice, (ii) to measure the quality of a laboratory or a part of a laboratory (e.g., audits for accreditation of laboratories), (iii) to improve the quality of a laboratory in collaborative work in a mutual learning process and (iv) to certify the contents of a reference material [1]. The programmes described in this paper are of types (iii) and (iv).

#### WATER ANALYSES

The topics described here were dealt with in [13]. In recent years, a number of Directives, concerned with the quality of several types of water, have been issued dealing with the quality of drinking (75/440/CEE, 79/869/CEE and 80/778/CEE) and underground waters (80/68/CEE). They prescribe the determination of a series of major compounds (e.g., Al, Ca, Cl, Fe, Mg, Mn, P, K). Other types of water (e.g., rain water) are frequently analysed in the member states for the same elements without the support of a Directive. The need for improvement of the quality of these determinations has led the BCR to produce as part of a larger project two sets of CRMs which are described below:

freshwater samples certified for their content of major elements (Al, Ca, Cl, Fe, K, Mg, Mn, Na, P and S), CRMs 398 (low element content) and 399 (high element content) [15]; and

rain water samples certified for their major element content (Ca, Cl, H<sub>3</sub>O, K, Mg, Na, NH<sub>4</sub>, NO<sub>3</sub> and SO<sub>4</sub>), CRMs 408 (low element content) and 409 (high element content) [16].

In addition, an intercomparison on nitrate in freshwater has been successfully concluded [17]. Typically results obtained at levels of 8 and 50 mg l<sup>-1</sup> NO<sub>3</sub> did not differ by more than a factor of 1.3 [relative standard deviation (R.S.D.) between laboratories less than 6%]; a certification campaign may be organized in 1993.

Other projects on water analysis concern the estuarine and marine environments. National and international programmes have been initiated worldwide, e.g., the Joint Monitoring Programme of the Oslo and Paris Commission. Similar programmes exist to monitor the quality of estuarine environments, e.g., the Rhine monitoring programme. The BCR has initiated a series of projects for the quality of determinations of trace elements in seawater and estuarine waters which are listed below:

sea water certified for its content of trace elements (Cd, Cu, Mo, Ni, Pb and Zn), CRM 403 [18];

intercomparisons on Hg in sea water which were successfully concluded [19]; the state of the art was improved for Hg levels in sea water at a level of 10 and 4 ng l<sup>-1</sup> (R.S.D. between laboratories of 10 and 38%, respectively); further improvements are desired for contemplating certification; and

intercomparison of trace elements in estuarine water: a first intercomparison enabled the feasibility of preparation of estuarine reference materials [20] to be tested and the main sources of

error to be detected and removed [21]; a second intercomparison is planned which could be continued by a certification.

The range of contents of some major elements in the freshwater and rain water CRMs is illustrated in Fig. 1.

#### PLANT ANALYSES

The subjects described here were dealt with in [11,12]. Plant analyses are routinely performed for the assessment of their quality, e.g., for feed and food and/or for their use as indicator organisms for environmental threat (monitoring, mapping, etc.). For instance, clover and grass for animal feed are analysed to determine elements of nutritive importance (e.g., Se, Mo) and of potential toxicity (e.g., As, Co); other plant materials are used to assess the global distribution pattern of a wide range of elements in the ecosystem and to study the element fluxes from rain, airborne dust or soil and water to plants, animals and humans.

In order to improve the quality of results in

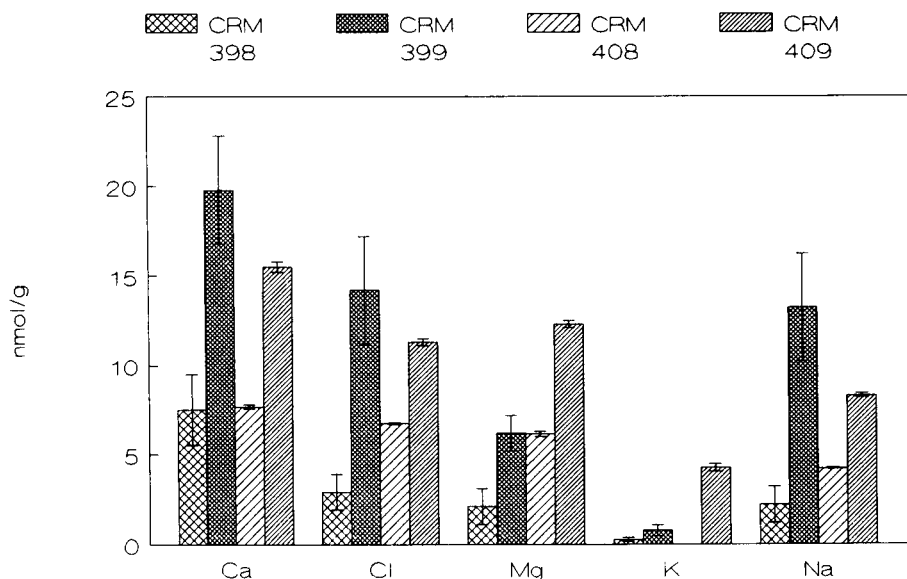


Fig. 1. Range of contents of some major elements in freshwater (CRMs 398 and 399) and rain water (CRMs 408 and 409) certified reference materials. The contents are expressed in nmol g<sup>-1</sup>. In this presentation, the certified values of CRMs 398 and 399 have been divided by 100 and those of Cl and Na in CRMs 408 and 409 by 10 in order to allow an easy visual comparison.

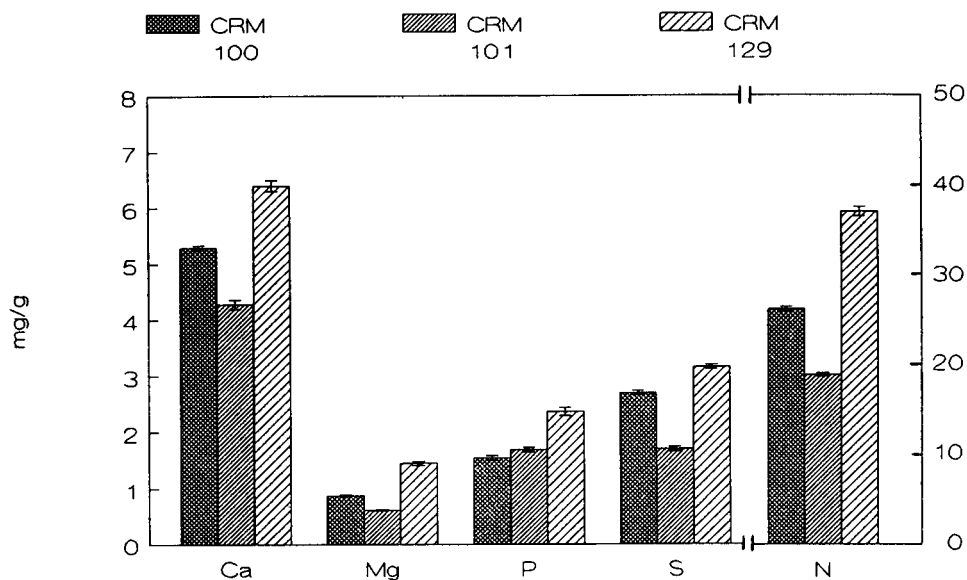


Fig. 2. Range of contents of some major elements in terrestrial plant certified reference materials (CRMs 100, 101 and 129). The contents are expressed in  $\text{mg g}^{-1}$ .

plant analysis, BCR has developed a series of certified reference materials (CRMs) for the monitoring of trace elements in aquatic plants, which are listed below:

*Lagorosiphon major* and *Platihypnidium riparioides* certified for their content of trace elements (Cd, Cu, Hg, Mn, Pb and Zn), CRMs 060 and 061 [22]; and

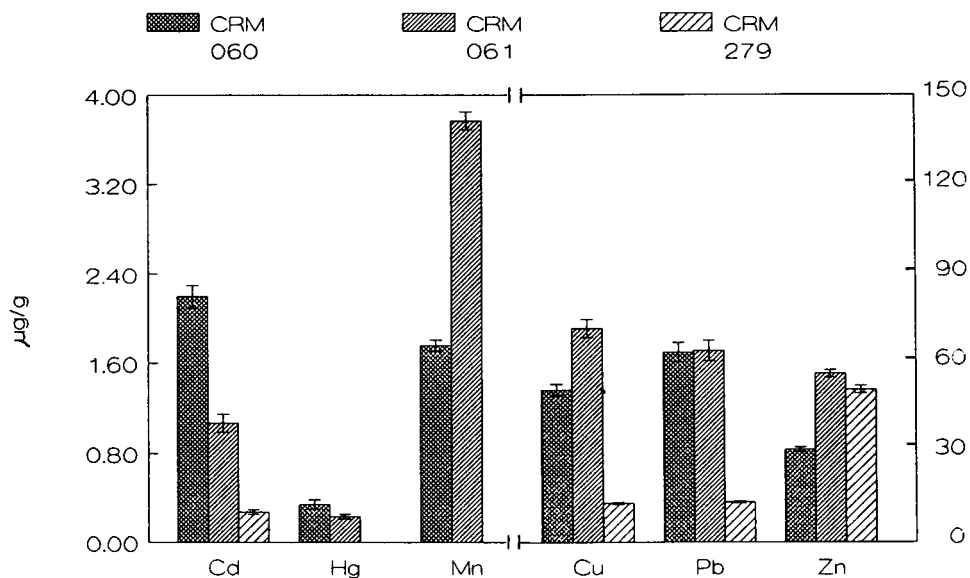


Fig. 3. Range of contents of some trace elements in aquatic plant certified reference materials (CRMs 060, 061 and 279). The contents are expressed in  $\mu\text{g g}^{-1}$ , except for Mn ( $\text{mg g}^{-1}$ ). In this presentation, the certified values of Zn in CRMs 060 and 061 and Cu in CRM 061 have been divided by 10 in order to allow an easy visual comparison.

*Ulva lactuca* (sea lettuce) certified for its content of trace elements (As, Cd, Cu, Pb, Se and Zn, CRM 279 [23].

Other materials have been produced for the quality control of trace elements in terrestrial plants, e.g., olive leaves certified for their contents of trace elements (Cd, Cu, Hg, Mn, Pb and Zn), CRM 062 [22].

Acid deposition damages forests. The chemical determination of various elements in leaves or needles allows more objective criteria for forest damage to be obtained than visual inspection. The monitoring with time of these effects requires quality control. The following two CRMs have been produced for this purpose:

beech leaves certified for their contents of major elements (N, Cl, S and P), CRM 100 [24]; an additional certification of Al, Ca, K and Mg was recently carried out; and

spruce needles certified for their contents of trace and major elements (Al, Mn, Zn, N, Cl, S, P, Ca and Mg), CRM 101 [24].

Analyses of lichen are routinely performed by a number of organizations to monitor the level of atmospheric contamination by toxic elements, e.g., heavy metals. A project for improving the quality

of trace element determinations in lichen has therefore been started by the organization of an interlaboratory exercise [25] which possibly could be followed by the production of a CRM.

Finally, analyses of nutritive elements are routinely performed in grass or hay for animal feed in order to improve the state of health and growth of domestic animals. To control the quality of such determinations, the two following CRMs were produced:

hay powder certified for its content of elements of nutritive interest (Zn, N, S, P, K, I, Ca, Mg and Kjeldahl-N), CRM 129 [26]; and

rye grass certified for its content of some trace elements (As, Cd, Cu, Hg, Mn, Pb, Se, Zn, B, Mo and Ni), CRM 281 [26].

Figures 2 and 3 give the range of contents of some trace elements certified in the CRMs mentioned above.

#### ANALYSES OF BIOTA

The subjects described here were dealt with in [14]. Certified reference materials are strongly needed to ensure the quality of analysis of biolog-

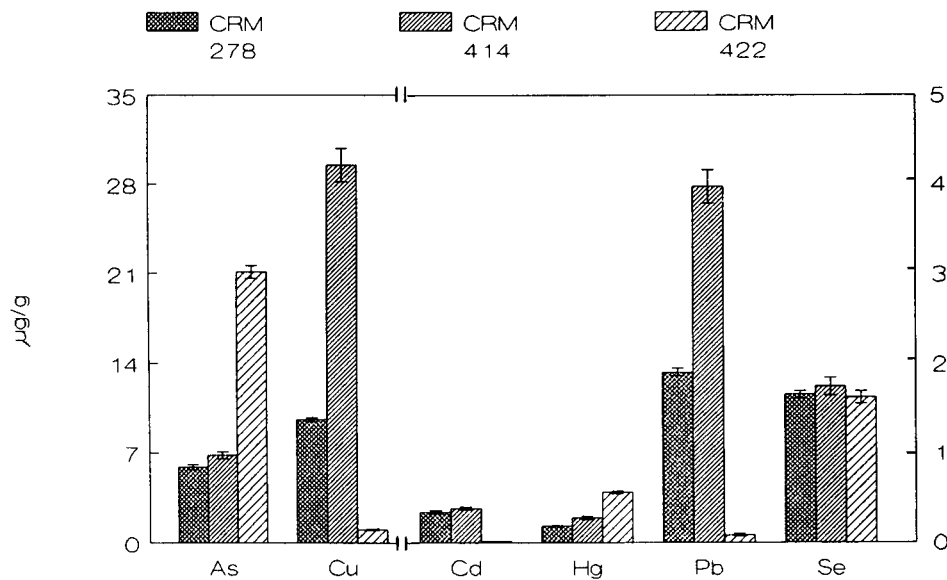


Fig. 4. Range of contents of some trace elements in biota certified reference materials (CRMs 278, 414 and 422). The contents are expressed in  $\mu\text{g g}^{-1}$ .

ical matrices in the aquatic environment both for the control of contamination and for the assessment of the quality of food following the requirements of national or EC legislation. Fish and plankton materials are used as indicators of pollution and to compare the levels of contamination of different areas. Fish is also analysed for nutritional reasons and for assessing human exposure to toxic elements.

Owing to the need for CRMs for the analytical quality control of trace element determination in these matrices, the BCR has already produced a mussel tissue (CRM 278) certified for its content of As, Cd, Cr, Cu, Fe, Hg, Mn, Pb, Se and Zn [27]. Two additional materials were recently certified for the following element contents:

plankton certified for As, Cd, Cr, Cu, Hg, Mn, Ni, Pb, Se, V and Zn, CRM 414 [28]; and

cod muscle certified for As, Cd, Cu, Fe, Hg, I, Mn, Pb, Se and Zn, CRM 422 [29].

The range of some trace elements in the three CRMs mentioned is illustrated in Fig. 4.

#### WASTE ANALYSIS

The subjects described here were dealt with in [8–10]. The illicit contamination of used mineral oils with chlorobiphenyls (CBs) continues to be a serious problem. These waste materials need to be checked for the level of the CBs which may have been added prior to their treatment. Simple tests to verify whether the PCB content in a certain (waste) oil exceeds the maximum level of  $50 \mu\text{g g}^{-1}$  set in most countries have been developed or are being developed (e.g., JRC, Ispra). However such tests need occasional verification for which CRMs of waste mineral oil with certified contents of major PCB congeners have been produced, namely CRM 420 (low level) and CRM 449 (high level); CRM 420 has been certified for CBs (IUPAC numbers) 28, 101, 118, 153 and 180 [30] and CRM 449 has been certified for CBs 28, 52, 101, 105, 118, 153, 156, 170 and 180 [31].

Polycyclic aromatic hydrocarbons (PAHs) generally enter the environment through combustion processes, e.g., as a result of smoke production in the combustion of organic materials. They may

contaminate the food chain through various pathways e.g., deposition on soils followed by plant uptake, contamination of water or by concentration in sewage sludge which may be used for soil amendment. Therefore, the PAHs have to be determined in a variety of matrices from all parts of the ecosystem. For impact studies, the required precision and accuracy pose severe analytical difficulties. The BCR has organized a series of intercomparisons to help laboratories to improve the quality of their analyses, the last one being a round-robin of a PAH-spiked sediment. Finally, a material (CRM 088) has been certified for its content of eight PAHs (pyrene, benz[*a*]anthracene, benzo[*a*]pyrene, benzo[*e*]pyrene, benzo[*k*]fluoranthene, benzo[*b*]fluoranthene, benzo[*b*]naphtho[2,1-*d*]thiophene and indeno[1,2,3-*cd*]pyrene) [32].

#### FOOD ANALYSIS

CBs are lipophilic compounds that bioconcentrate in the food chain. Hence they may be present in milk or dairy products, which must be monitored for the presence of these contaminants. CRM 450 has been produced for the purpose of quality control in CB determinations in milk; this material is certified for its incurred content of CBs (IUPAC numbers) 52, 118, 153, 156, 170 and 180 [33].

#### AVAILABILITY

The CRMs are available from the BCR at the authors' address. Each CRM is accompanied by a certificate and a report that contains a full description of the certification work, of all individual results and of the methods applied.

Collaboration with J. Hirschberger, J. Jacob, K.J.M. Kramer, H. Muntau, H. Schimmel, H.F.R. Reijnders, M. Valcarcel, D. Van Renterghem, K. Vercoetere, D.E. Wells and Th. Westermair is gratefully acknowledged. The authors thank the participants in the different projects for all their efforts which allowed a considerable improve-

ment in the state of the art of chemical analysis to be achieved.

## REFERENCES

- 1 E.A. Maier, *Trends Anal. Chem.*, 10 (1991) 340.
- 2 W. Cofino, personal communication.
- 3 B. Griepink and M. Stoeppler, in M. Stoeppler (Ed.), *Hazardous Metals in the Environment*, Elsevier, Amsterdam, 1992, p. 517.
- 4 B.E. Broderick, W.P. Cofino, R. Cornelis, K. Heydorn, W. Horwitz, D.T.E. Hunt, R.C. Hutton, H.M. Kingston, H. Muntau, R. Baudo, D. Rossi, J.G. Van Raaphorst, T.T. Lub, P. Schramel, F.T. Smyth, D.E. Wells and A.G. Kelly, *Mikrochim. Acta*, II (1991) 523.
- 5 Quality Management and Quality Assurance Standards. Guidelines for Selection and Use. ISO/IEC Standard 9000, International Organization for Standardization, Geneva.
- 6 General Criteria for the Operation of Testing Laboratories. European Standard EN 45001-12, CEN/CENELEC, Brussels, 1989.
- 7 B. Griepink, E.A. Maier, Ph. Quevauviller and H. Muntau, *Fresenius' J. Anal. Chem.*, 339 (1991) 599.
- 8 E.A. Maier, H. Schimmel, J. Hirschberger, D.E. Wells and B. Griepink, poster presented at the ISM'92 Conference, Córdoba, 7–11 September 1992.
- 9 E.A. Maier, H. Schimmel, J. Hirschberger, D.E. Wells, Th. Westermair and B. Griepink, poster presented at the ISM'92 Conference, Córdoba, 7–11 September 1992.
- 10 E.A. Maier, H. Schimmel, J. Jacob, J. Hirschberger, H. Muntau and B. Griepink, poster presented at the ISM'92 Conference, Córdoba, 7–11 September 1992.
- 11 E.A. Maier, K. Vercoutere, D. Van Renterghem, M. Valcarcel, H. Muntau and B. Griepink, poster presented at the ISM'92 Conference, Córdoba, 7–11 September 1992.
- 12 Ph. Quevauviller, D. Van Renterghem, G.N. Kramer, H. Muntau and B. Griepink, poster presented at the ISM'92 Conference, Córdoba, 7–11 September 1992.
- 13 Ph. Quevauviller, D. Van Renterghem and B. Griepink, poster presented at the ISM'92 Conference, Córdoba, 7–11 September 1992.
- 14 Ph. Quevauviller, G.N. Kramer, H. Muntau and B. Griepink, poster presented at the ISM'92 conference, Córdoba, 7–11 September 1992.
- 15 Ph. Quevauviller, K. Vercoutere and B. Griepink, *Mikrochim. Acta*, in press.
- 16 Ph. Quevauviller, D. Van Renterghem, B. Griepink, H.F.R. Reijnders and H. Van der Jagt, EUR Report, CEC, Brussels, in press.
- 17 Ph. Quevauviller, D. Van Renterghem, M. Valcarcel, M.D. Luque de Castro, J. Cabnillas and B. Griepink, *Anal. Chim. Acta*, submitted for publication.
- 18 Ph. Quevauviller, K.J.M. Kramer, E.M. Van der Vlies, K. Vercoutere and B. Griepink, *Mar. Pollut. Bull.*, 24 (1992) 33.
- 19 Ph. Quevauviller, K.J.M. Kramer and B. Griepink, *Mar. Pollut. Bull.*, submitted for publication.
- 20 K.J.M. Kramer, Vinhas T., Van der Vlies L.M. and B. Griepink, *An. Inst. Hidrogr.*, 10 (1989) 77.
- 21 Ph. Quevauviller, K.J.M. Kramer, D. Van Renterghem and B. Griepink, *An. Inst. Hidrogr.*, in press.
- 22 B. Griepink, H. Muntau and E. Colinet, *Fresenius' J. Anal. Chem.*, 315 (1983) 193.
- 23 B. Griepink and H. Muntau, EUR Report, No. 11185, CEC, Brussels, 1987.
- 24 E.A. Maier, H. Muntau and B. Griepink, *Fresenius' J. Anal. Chem.*, 335 (1989) 833.
- 25 E.A. Maier, B. Griepink, Ph. Quevauviller, H. Muntau and L. De Angelis, *Mikrochim. Acta*, III (1990) 87.
- 26 Ph. Quevauviller, D. Van Renterghem, H. Muntau and B. Griepink, *Int. J. Environ. Anal. Chem.*, submitted for publication.
- 27 B. Griepink and H. Muntau, EUR Report, no. 11838, CEC, Brussels, 1988.
- 28 Ph. Quevauviller, K. Vercoutere, H. Muntau and B. Griepink, *Fresenius' J. Anal. Chem.*, in press.
- 29 Ph. Quevauviller, G.N. Kramer and B. Griepink, *Mar. Pollut. Bull.*, in press.
- 30 B. Griepink, E.A. Maier and D.E. Wells, EUR Report, CEC, Brussels, in press.
- 31 E.A. Maier, J. Hirschberger, H. Schimmel, D.E. Wells and B. Griepink, EUR Report, CEC Brussels, in preparation.
- 32 E.A. Maier, H. Schimmel, J. Jacob and B. Griepink, EUR Report, CEC, Brussels, in preparation.
- 33 E.A. Maier, H. Schimmel, J. Hirschberger, D.E. Wells, Th. Westermair and B. Griepink, EUR Report, CEC, Brussels, in preparation.

# Interlaboratory studies as a tool for many purposes: proficiency testing, learning exercises, quality control and certification of matrix materials

E.A. Maier, Ph. Quevauviller and B. Griepink

*Community Bureau of Reference (BCR), Commission of the European Communities, rue de la Loi 200, 1049 Brussels (Belgium)*

(Received 8th September 1992)

## Abstract

Interlaboratory studies are collaborative exercises by laboratories to assess or improve the quality for their measurements. They are an important aspect of quality control and quality assurance systems which should be set up by all testing laboratories. They are efficient tools for investigating the method and the laboratory performance and also to certify reference materials. They can be applied with a research or teaching objective but they can also be used to assess the performance of a normalized method or the ability of a laboratory to perform a given task. As such they are a complementary aspect of accreditation audits.

*Keywords:* Certification; Interlaboratory studies; Learning exercises; Matrix materials; Proficiency testing; Quality control

There is an ever increasing demand for measurements and testing and in parallel a growing need to assure the quality of such activities. As a consequence, laboratories have to set up systems that will help to assure the quality of their determinations and limit the risk of producing unreliable data. The accreditation systems which are nowadays being installed are a help to laboratories in achieving this goal.

Quality in chemical analysis means that the laboratory is able to answer properly the question(s) posed by the customer. This means that the entire chain from the definition of the problem through the sampling, the determination and the reporting of the data is under control [1]. To achieve such a high degree of reliability the laboratory must be very well structured at both the technical (including infrastructure) and personnel

levels. The analysts have to use methods that have been validated in detail and that are under statistical control [1]. This means that all possible measures should be applied to achieve the best reproducibility and to assure the accuracy of the determinations. The improvement of precision can be dealt with in the laboratory itself but accuracy can only be achieved by comparing its own performance with those of other laboratories. This can be done by using certified reference materials (CRMs) and by participating in interlaboratory studies. CRMs are materials guaranteed for their stability and homogeneity and in which a certain number of parameters have been accurately and precisely determined by selected and highly experienced bodies. Unfortunately, CRMs are not available for all analytical problems.

Interlaboratory studies are another way of evaluating a laboratory's own performance. In analytical chemistry, interlaboratory studies (often called intercomparisons or round robins) are ex-

*Correspondence to:* E.A. Maier, Community Bureau of Reference (BCR), Commission of the European Communities, rue de la Loi 200, 1049 Brussels (Belgium).

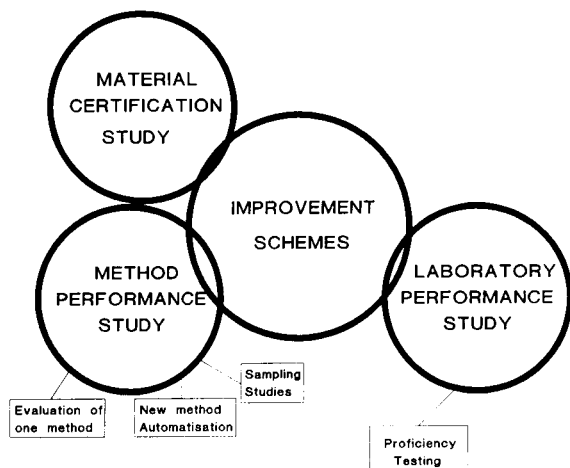


Fig. 1. Various types of interlaboratory studies. Improvement schemes are in fact exercises which cover laboratory and method performance studies and their positive outcome may lead to the certification of reference materials. All types of interlaboratory studies participate in the general quality control and quality assurance scheme that each laboratory should set up.

ercises involving the participation of several laboratories which analyse the same material following a given protocol.

Horwitz has defined in an IUPAC report [2] three types of interlaboratory studies which have different purposes: method performance studies, laboratory performance studies and material certification studies. These three types of studies cover the three main parameters that characterize the work of the analytical chemist: the analytical method or procedure, the analyst in the laboratory and the material to be analysed.

Figure 1 shows the various types of interlaboratory studies and some of their specialized forms. All interlaboratory studies have in common several aspects: several participants; a common material is used; and an organizer is in charge of the study.

#### COMMON ASPECTS

##### *Participants*

Progress or keeping up a good quality requires motivation, which involves the participants believ-

ing that a high standard of working is achievable in their laboratory. Motivation may also be stimulated by making participation in interlaboratory studies mandatory.

The number of participants may change from one type of study to another but at least it should be sufficient to assure that sound conclusions can be drawn from the exercise [2]. With more than 25 participants it is difficult to evaluate the data together with the participants in a meeting.

All participants should have set up beforehand all within-laboratory quality assurance and quality control systems possible [1]. This implies also that the method applied is under statistical control in the laboratory. Otherwise, no clear benefit could result from participation in the study.

##### *Organizer*

The organizer of the interlaboratory study takes the objective of the study into account and adapts the organization to this objective. There is a great difference in responsibility and work involved between a simple exercise on a method performance study and the certification of a reference material. However, in all cases the organizer will be in charge of the supply of clear information to the participants, the production and distribution of the samples (or the preparation of the sampling site), the verification of the quality of the sample and that they are adapted to the objective of the study and the collection, treatment and presentation of the results and possibly the organization of a meeting to discuss them with the participants.

For laboratory studies leading to decisions that affect the professional status of the participants (e.g. proficiency testing within accreditation systems) or leading to certification of materials [3], the organizer must be evaluated. The selection should even be subject to well established rules or procedures. The organizer must guarantee the confidentiality of the data.

##### *Objective of the study*

Another success-determining factor is the clarity of the objectives. Adequate protocols where the objective is clearly stated should be prepared. The materials distributed should be well de-



scribed and well-adapted reporting forms should be distributed so that the data can be compared and properly processed.

#### *Test materials*

All participants must receive identical test samples. The material prepared should meet the requirements of the objective of the study.

*Choice of the material.* The material should be similar to samples that are analysed in the laboratory so that analytical errors can be detected in the methods applied. In most instances this means similarity of the matrix composition, the contents of the analytes, the way of binding of these analytes, the fingerprint pattern of possible interferences and the physical status of the material.

However, for practical reasons this similarity cannot always be entirely respected. As the material has to be homogeneous and stable in order to assure that identical samples are delivered to the laboratories, often compromises have to be made. Therefore, the preparation of the material has to be adapted.

*Preparation of the material.* The material has to be collected in an amount sufficient to supply all participants with test samples or to assure an adequate stock for a CRM. Therefore, the amount to be collected may vary from a few grams to 100 kg or from a few ml to several m<sup>3</sup>. The organizer is in charge of providing the adapted tools to proceed with the preparation.

The collected material has to be stabilized. This is one of the most sensitive and difficult steps of the work. The stabilization has to be adapted to each particular case and should be studied in detail before processing in order to respect as much as possible the integrity of the material. Usually, the materials are dried to avoid chemical and microbiological changes. This can be done by heating or by freeze-drying, depending on the volatility of the analytes and the matrix components. Some materials can be sterilized by irradiation but it should be noted that  $\gamma$ -irradiation destroys some organic substances [e.g., pesticides and polycyclic aromatic hydrocarbons (PAHs)]. Table 1 gives an example for organochlorine pesticides in animal feed. Some materials may be pasteurized or stabilized by fixing the

TABLE 1

Damage caused to organochlorine pesticides in pork fat by  $\gamma$ -irradiation (<sup>60</sup>Co source; irradiation dose = 0, 2.5 and 5.0 kGy)<sup>a</sup>

Pesticide	Irradiation dose (kGy) (n = 5)		
	0	2.5	5.0
HCB	100 ± 4.4	101 ± 5.3	104 ± 1.7
$\alpha$ -HCH	100 ± 2.6	99.1 ± 6.5	95.1 ± 2.0
$\beta$ -HCH	100 ± 7.8	90.1 ± 8.4	101.4 ± 6.2
$\gamma$ -HCH (lindane)	100 ± 3.1	54.3 ± 3.6	51.7 ± 3.0
Heptachlor	100 ± 4.6	110.3 ± 2.6	110.8 ± 2.0
Aldrin	100 ± 2.6	107.9 ± 2.8	106.0 ± 2.2
$\beta$ -Heptachlor epoxide	100 ± 6.5	103.1 ± 2.5	98.6 ± 3.4
$\gamma$ -Chlordane	100 ± 2.3	97.2 ± 4.3	101.5 ± 3.4
$\alpha$ -Endosulfan	100 ± 3.6	78.5 ± 2.6	75.8 ± 3.2
p,p'-DDE	100 ± 4.2	93.9 ± 4.0	102.6 ± 3.0
p,p'-TDE	100 ± 3.4	103.5 ± 4.6	99.0 ± 3.9
o,p'-DDT	100 ± 3.6	97.7 ± 3.5	101.6 ± 2.1
p,p'-DDT	100 ± 2.4	83.7 ± 4.6	85.0 ± 2.2
Dieldrin	100 ± 1.4	92.8 ± 2.7	95.4 ± 5.0
Endrin	100 ± 2.7	102.2 ± 6.9	90.1 ± 2.2

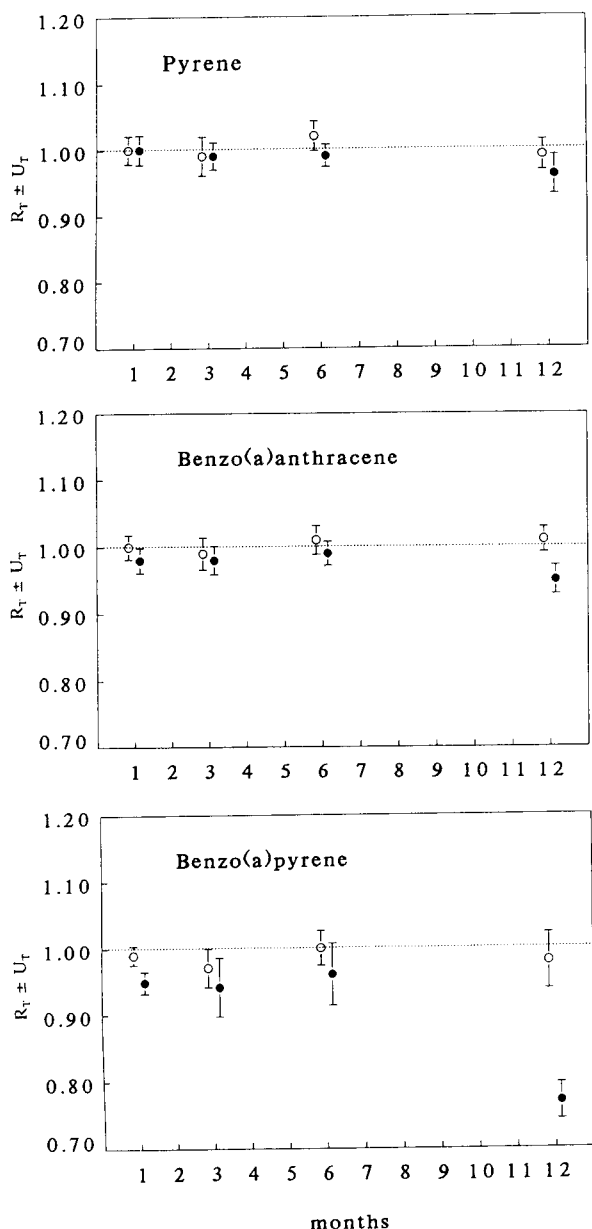
<sup>a</sup> The data have been normalized to the content determined on five test portions which were not irradiated (base = 100). The data given are the normalized means of five determinations and the corresponding standard deviations.

water with chemical additives (e.g., Florisil or sodium sulphate) or sterilized by the addition of preservatives.

The stabilization of the material by simple freezing is also possible but is not very practical because of the difficulties with transport. It is feasible for studies limited in the number of participants. It should be noted that after thawing the samples may no longer be homogeneous and that re-freezing may alter them.

When stabilized, the material must be homogenized to assure sufficient within- and between-vial homogeneity. This means that the inhomogeneity of the material should not significantly affect the total uncertainty of the measurement. This homogeneity should be verified by the organizer with the most repeatable analytical method available and possibly with a multi-elemental or multi-residue method, e.g., neutron activation analysis, inductively coupled plasma atomic emission spectrometry (ICP-OES) or X-ray fluorescence spectrometry, gas or liquid chromatography. The level of intake of these tests should be

at least as low as or lower than the usual sample intake that will be used afterwards by the participants [4]. After having verified the homogeneity, the organizer should study the stability of the material. This means that he should perform studies to verify that the material's integrity is maintained under severe conditions which may be



encountered, e.g., during transport. The stability study has to be conducted at least over the entire duration of the interlaboratory study. For CRMs the monitoring of the stability has to be followed over the lifetime of the material. Accelerated ageing conditions (e.g., storage at high temperatures over longer periods of time) can give a good indication of the behaviour of a material. Figure 2 shows the result of such a study on PAHs in sewage sludge where some compounds showed instability at +40°C. In order to minimize long-term reproducibility problems the measurements are done on samples stored at different temperatures (e.g., -20, +20 and +40°C) and the data are normalized to the results obtained on the samples stored at low temperatures where chemical and microbiological activity is not likely. Strictly this approach either detects a decay in the analyte or matrix but it also may detect a decreased extractability.

The stability and the homogeneity of the material can only be maintained and guaranteed if they are stored in proper vials. The producer should study the type of storage vial and storage and transport conditions beforehand. Usually amber-glass bottles are sufficient for solid materials, trace organics in solvents may be stored in sealed glass or quartz ampoules, water in high-density

Fig. 2. Stability of PAHs in sewage sludge (CRM 088). The stability of eight PAHs in sewage sludge was monitored over 12 months at three different temperatures: +20°C, -40°C and -20°C. The data presented are the ratio of the values found for samples stored at (○) +20°C or (●) +40°C versus the value found for samples stored at -20°C (see text).  $R_T = X_T / X_{-20^\circ\text{C}}$ ;  $X_T$  = mean of five replicates at temperature  $T$  (+20 or +40°C);  $U_T = (CV_T^2 + CV_{-20^\circ\text{C}}^2)^{1/2} (R_T / 100)$ ;  $CV_T$  = coefficient of variation of five replicates at temperature  $T$ . The study did not detect any significant instability for pyrene. Benz[*a*]anthracene seems to decrease at +40°C after 12 months of storage but only marginally. Benz[*a*]pyrene shows a significant decrease at +40°C (ca. 25% of the initial content). This means that at a higher temperature the latter compound is degraded or has changed its extractability. No clear explanation could be given. This example shows clearly that for organic analysis the stability of a material has to be assessed for all compounds to be studied. The conclusion for CRM 088 was that it should be stored in a cool place (+4°C) and that higher temperatures during transport will not affect the certified value.

polymers or glass bottles and gases in aluminium or stainless-steel bottles. Prolonged exposure to high temperatures and to light should be avoided.

The material produced for the study should present the same analytical difficulties as real samples. However, because of the requirement for homogeneity and stability the representativeness of the material may suffer compromises. A material such as “fresh strawberries” cannot be produced in a sufficient amount for a large inter-laboratory study.

If possible the organizer should try to assign a target value to the parameter(s) to be determined in the study. For artificial mixtures (e.g., aqueous or organic solutions, spiked solid samples) prepared under proper metrologically valid conditions with compounds of verified purity and stoichiometry the true value may be established by calculation. This is no longer possible for real matrix samples. For such materials the target value can only be determined by analytical means and will only be known with a certain uncertainty. Where possible this target value should be obtained by a so-called definitive method, e.g., isotope dilution mass spectrometry (IDMS) for some polynuclidic elements [5] and by highly experienced laboratories. Unfortunately, such techniques do not exist for all elements and not for organic trace analysis.

For these parameters the organizer can ask one or several highly experienced laboratories to establish the target value by using different analytical procedures which are all validated in detail. This will decrease the risk of a biased result.

*Analytical protocol.* The protocol should at least recall the goal of the study. This includes the number of test samples to be analysed and the number of replicates. It should also inform the participant on possible storage and handling difficulties which are specific to the material. An example of a protocol can be obtained from the authors on request.

It is always good advice to prepare and complete the analytical protocol with well adapted and carefully prepared report forms. This facilitates the exploitation of the results by the organizer.

#### *Collection and evaluation of the data*

The evaluation of the data generated by the participants in an interlaboratory study and the actions and the conclusions to be drawn by the participants and the organizer depend strongly on the objective of the study. The way results are reported has to be adapted to this objective.

*Collection of results.* In order to allow easy collection of the analytical data, the organizer should prepare report sheets. These sheets may include forms to describe the analytical methods and forms to report the results.

The standard forms to describe the analytical methods are usually not included in proficiency tests nor for normalization purposes. It is an essential element for the evaluation of the performance of a laboratory or of a method in exercises with a training objective (improvement schemes with a step-by-step approach). It is a mandatory part if certification of a material is to be considered. An example of report forms can be obtained from the authors on request.

Adapted report forms and proper protocols will assure that the data are comparable and can be treated adequately by the organizer. This treatment includes a clear presentation of these data so that the participants can extract rapidly and accurately all necessary information. This implies that methods are described in synthetic tables and that the data are shown in tables with means and standard deviations and in understandable bar-graph presentations.

*Technical evaluation.* The technical evaluation of the data consists in a scientific evaluation of the reports submitted by the participants. For maximum benefit by the participants the organizer has to prepare summaries of the method description for the most critical steps in the analytical procedure. The outcome of the exercise should be discussed amongst the participants in a technical meeting where they can exchange their experience.

*Statistical evaluation.* It should be remembered that the statistical evaluation of data cannot explain deviating results, nor can it give any information on the accuracy. Statistics only analyse a population of data and inform on the homogene-

ity of this population. Therefore, the statistical evaluation may raise questions and discussions rather than giving explanations.

Figure 3 shows a good example of the limits of the statistical treatment of data. In this exercise polychlorodibenzo-p-dioxins and polychlorodibenzofurans were determined in a fly ash extract. It appeared in the technical discussion that for one hexachlorodibenzofuran all but one laboratory found an interference for this compound. Careful examination of the chromatograms revealed that only one phase was able to separate compound F118 from F121. A statistical treatment identified the data of the laboratory as outliers. Too often it is considered that outliers are inaccurate. From the example in Fig. 3 it is clear that statistics cannot judge the accuracy of data. The organizer and the participants in interlaboratory studies should be aware of this.

#### Conclusions and actions

The conclusions to be drawn and the actions to be taken depend strongly on the initial objective of the study. They will be briefly discussed in the following presentation of the various types of studies.

#### PARTICULAR ASPECTS

##### Method performance study

A method performance study is an exercise in which each laboratory uses the same method on a set of identical test samples following the same protocol [2]. Such studies are often organized by standardization organizations (e.g., ISO, CEN, national or professional bodies). They have the goal to work out and test the performance of a method.

A method performance study may also be used to evaluate the performance of a new analytical technique or an automated form of an existing technique [2]. Investigations on sampling techniques may also be conducted in interlaboratory exercises. Under certain circumstances a method performance study may be called an intercalibration study. This should only concern exercises where the calibration of methods is investigated,

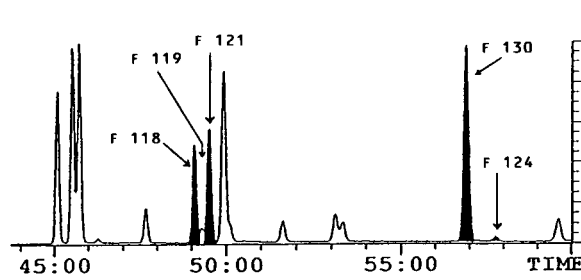
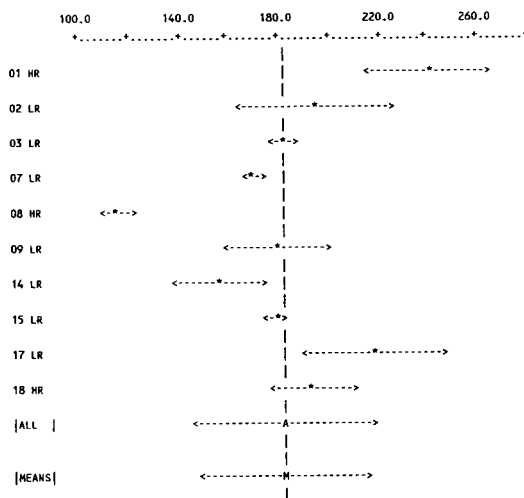


Fig. 3. Interlaboratory study on the certification of polychlorodibenzo-dioxins (PCDDs) and polychlorodibenzofurans (PCDFs) in a fly ash extract [11]. Bar graph presentation of the results obtained and chromatogram detail of laboratory 08. The values in the bar-graph presentation are given as  $\text{ng g}^{-1}$  extract. Mean of means:  $183 \text{ ng g}^{-1}$  S.D. =  $34 \text{ ng g}^{-1}$ . Mean of all individual values:  $183 \text{ ng g}^{-1}$  S.D. =  $37 \text{ ng g}^{-1}$ . HR = high-resolution MS; LR = low resolution MS. The participants had to determine twelve PCDDs and PCDFs including 1,2,3,4,7,8-PCDF (F118). Only laboratory 08 managed to separate F118 and F121 properly from F119 using a new DB dioxin column (J&W Scientific), as can be seen on the chromatogram. A direct statistical analysis of the population of data leads to the exclusion of laboratory 08 as an outlier of means (Nalimov test). This is an example where the majority of the laboratories were wrong and where a rejection of results as being technically wrong on statistical grounds would have led to an erroneous conclusion.

e.g., studies on calibrants, calibrant solutions, etc. Such studies are more frequently encountered for physical measurements for metrological purposes.

The term intercalibration should be avoided for all other type of studies [2]. As such, method performance studies are an essential component of the laboratory quality control and quality assurance system and should be used as often as possible.

#### *Laboratory performance study*

The laboratory performance study is usually intended to evaluate the performance of laboratories. They are also an essential component of the quality control and quality assurance system of the laboratory. Such studies may be requested by regulatory bodies and they are then called proficiency testing studies. Alternatively they may be part of a more ambitious project in which the various steps of the method applied by the participants are studied: improvement schemes by step-by-step approaches.

#### *Proficiency testing*

This particular form of interlaboratory study is mainly characterized by the goal allocated to the exercise. The organizing body has the purpose to evaluate if a laboratory is able to fulfil a given task. The outcome of a proficiency test may affect the professional status of the laboratory and therefore the organizer of the trial has an important responsibility. It has been suggested that the organizing bodies should also be evaluated [6] and that guidelines for the organization and the evaluation of proficiency testing are harmonized at international level [7].

In addition to this regulatory aspect, proficiency testing may be considered as the most stimulating and therefore effective tool for external quality control of the laboratory. Therefore, it has already been introduced by some accreditation bodies, such as the National Association of Testing Authorities, Australia, into their accreditation criteria and procedures.

#### *Certification of materials*

Material certification studies represent the most sophisticated type of interlaboratory studies as they require the participation of selected laboratories and they work on materials presenting all

possible guarantees of homogeneity, stability and representativeness. The organizer must be highly reliable and possibly should have or develop international recognition. The participants should be strictly selected on the basis of their analytical performance as verified before accepting their participation. The methods applied should be validated in detail and be likely to produce accurate results. The organizer should verify that within the group sufficiently different and independent methods exist so that risk of possible bias is minimized unless definitive methods exist [3,8]. The number of laboratories authorized to participate in the study should not exceed 15–25 depending on the diversity of methods available.

The size of the batch of the material should be sufficient to assure an availability over long periods of time. The preparation should be delegated to a highly experienced and well equipped laboratory. The homogeneity and stability tests should be performed by independent laboratories having demonstrated a good performance for the determination of the parameter to be measured.

The results of the interlaboratory study have to be discussed in a meeting with all participants. This technical/chemical discussion should lead to the conclusion that all data used for certification present all guarantees of reliability: accuracy can only be achieved on solid technical grounds. The statistical evaluation is intended to verify that no outliers of mean of variance remain within the population of data. The entire study should be described in an extensive report and the certified values should be given in a certificate. Where no definitive methods (e.g., IDMS for multi-nuclidic elements) exist [5], interlaboratory studies are the only possibility for certifying parameters in matrix materials; in fact, this means many elements and all parameters in the field of organic and organometallic trace analysis.

#### *Improvement schemes*

In addition to the more classical intercomparisons described above, some organizations have developed studies to allow laboratories to validate all steps of their new or existing procedure in adequately organized interlaboratory studies [9–12].

The learning programmes require from the organizer a high ability at both organizational and scientific levels as he has to play an important role in the design of the study, the evaluation and the consequences.

*Various steps.* In general, it can be considered that each critical step of the analytical procedure should benefit from a particular exercise with adapted material. Figure 4 shows the sequence of steps usually encountered in a procedure together with the type of material that can be used to validate the parameter concerned. This sequence is in fact very close to the procedure which each individual should apply when he sets up a new technique in his laboratory. It allows the contribution of each step to the total uncertainty of the determination to be evaluated.

Recent experience obtained from such exercises has shown that the calibration is one of the most critical steps in the analytical procedure. This includes the use of impure compounds with unknown stoichiometry or identity, errors in dilution or transfer of volatile solvents, bad storage of stock solutions, bad introduction or inadequate internal standards and matrix effects. Other difficult aspects are the extraction and clean-up or the matrix destruction of samples and the chromatographic separation.

*Materials.* As can be deduced from Fig. 4, the validation of each step needs a particular material. The composition of this material is discussed in a meeting between the participants and the organizer. In view of the result of a step, it may be decided to repeat the exercise on a different but similar material. Analytical protocols have to be adapted to each step and should include all quality control measures that have been developed beforehand. The final protocol which deals with the entire procedure should include all quality control measures so that errors in the total analytical procedure can be traced back. Such protocols are well adapted for the certification of materials.

*Evaluation of data.* Improvement schemes as described above lead to a large amount of information to be handled by the organizer. They should be condensed into practical and easy to read tables and graphical representations. If pos-

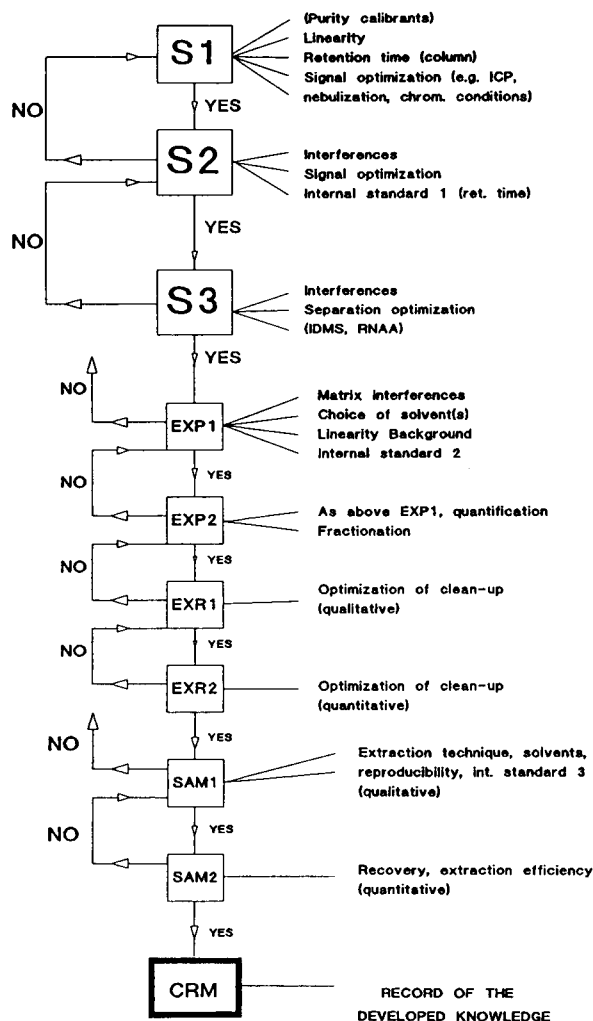


Fig. 4. Step-by-step approach for the validation of analytical procedures in interlaboratory studies. To each step corresponds a material chosen together with the participants (S1 to S3 = pure to complex mixtures of solutions; EXP = cleaned-up extracts or digests; EXR = raw extracts or digests; SAM = natural or spiked samples) in view of critical aspects of the methods to be validated. The successful exercise could lead to certification of a reference material to disseminate the obtained expertise to other laboratories.

sible Youden plots as presented in Fig. 5 may be produced to detect systematic errors [13]. This will compose the basic information for the participants in the meeting where the exercise is discussed. The conclusion of the discussion will lead to the organization of the next step and the

description of the material needed to solve the next difficulties.

**Examples of improvement schemes.** The step-by-step approach is particularly suited for investigations of complex methods, e.g., trace organic or organometallic determinations. Figures 6 and 7 give examples of two improvement schemes conducted within the BCR, leading to high analytical quality and finally allowing certification of certain parameters in environmental matrices. As can be deduced from Fig. 7, some steps can be conducted in successive exercises but for which the samples are distributed together. This block approach allows the number of meetings necessary to be limited. However, each step within a block has to be discussed individually so that the likely consequences may be decided by the participants.

The step-by-step approach if properly conducted helps to achieve the best accuracy possible within the current state of the art. As a consequence, the organizer of such studies should transfer the developed experience to a wider group. This may be performed by certifying the studied parameter(s) in a reference material and by publishing the outcome of the step-by-step exercise.

Figure 1 highlights the link between improvement schemes and all the other types of studies. The improvements benefit the method, the ana-

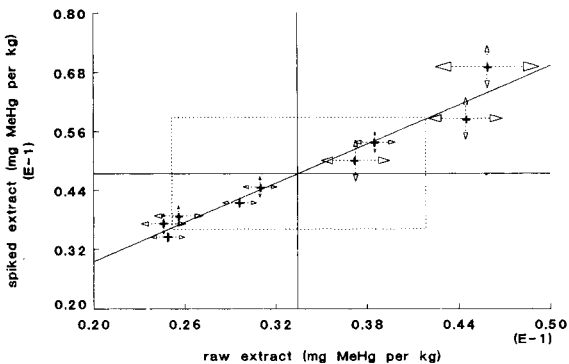


Fig. 5. Youden plot for the determination of methylmercury in a spiked raw extract versus a non-enriched raw extract of fish tissue [13]. The horizontal and vertical continuous lines represent the means of the laboratory means. Dotted lines of the central square show the standard deviation of these means. The length of the dotted lines for each individual laboratory represent the mean  $\pm$  one standard deviation (five replicates).

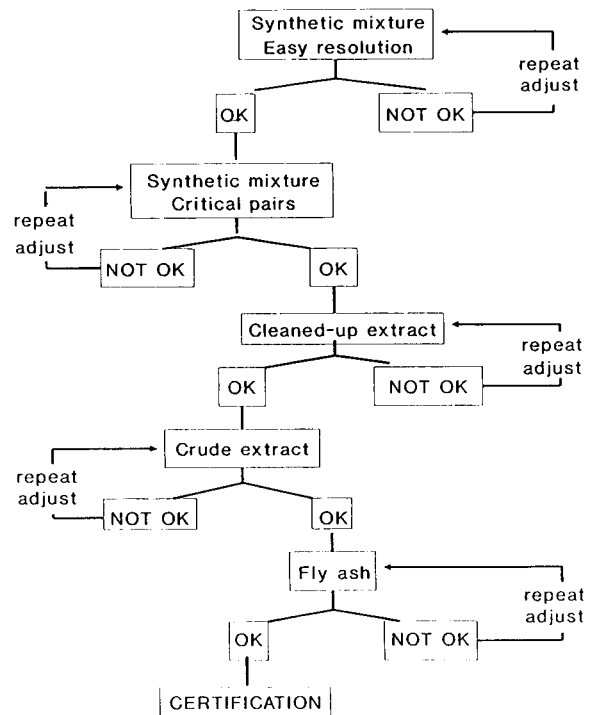


Fig. 6. Improvement scheme for the determination of PCDDs and PCDFs in fly ash [11].

lyst, the laboratory and possibly its structure, materials through the certification of reference materials and finally the customers and all users of analytical data.

### Conclusions

Various types of interlaboratory studies are possible. All participate in the objective to improve the quality of measurements and therefore have their particular place in the quality control and the quality assurance system that each laboratory has to set up. If properly conducted such studies may help the laboratories to achieve accuracy. Together with the use of certified reference materials they help laboratories to link their performance with the scientific community. However, it must be repeated that participation in interlaboratory studies can only be beneficial to the laboratory when a good infrastructure is available, as such "intercomparisons" are only part of the total quality control and quality assurance system.

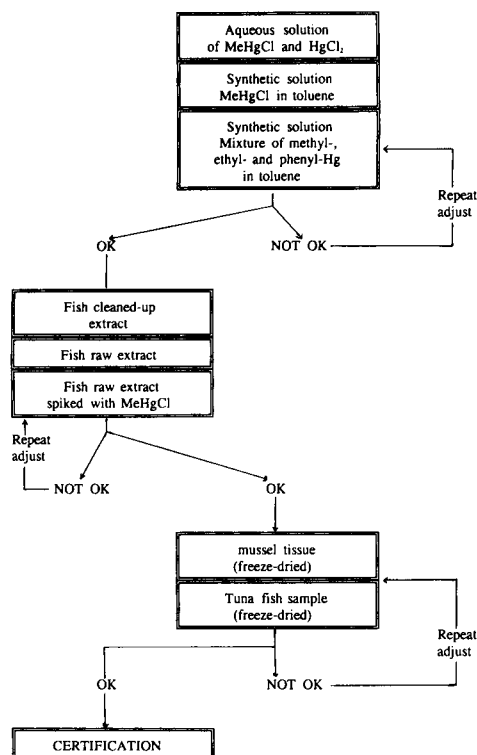


Fig. 7. Improvement scheme for the determination of methylmercury in fish tissue. Each interlaboratory study included several appropriate materials to be analysed. This permitted the scheme to be concentrated into fewer steps.

The major limitation of interlaboratory studies is inherent in their organization. It would be a major help to testing laboratories if private, public or professional organizations would develop efficient and cost-effective systems that would be in charge of organizing such studies. This could be done inside and beside the accreditation systems that exist or are being developed in many countries.

## REFERENCES

- 1 B.E. Broderick, W.P. Cofino, K. Heydorn, R. Cornelis, W. Horwitz, D.T.E. Hunt, R.C. Hutton, H.M. Kingston, H. Muntau, R. Baudo, D. Rossi, J.G. van Raaphorst, T.T. Luh, P. Schramel, F.T. Smyth, D.E. Wells and A.G. Kelly, *Microchim. Acta*, II (1991) 523.
- 2 International Union of Pure and Applied Chemistry (IUPAC), Analytical Chemistry Division, Commission on General Aspects of Analytical Chemistry (V.1), Project 27/87: Nomenclature for Interlaboratory Studies, Fourth Draft, April 1991.
- 3 Certification of Reference Materials – General and Statistical Principles, ISO Guide 35, International Organization for Standardization, Geneva, 1985.
- 4 J. Pauwels and C. Vandecasteele, *Fresenius, J. Anal. Chem.*, in press.
- 5 P. De Bievre, *Fresenius' J. Anal. Chem.*, 337 (1990) 766.
- 6 Accreditation and Interlaboratory Studies. Criteria for the Design and Execution of Interlaboratory Studies and Guidelines for the Use of Results. STERLAB Board of Experts: Interlaboratory Studies, No. 91 (CVDENG) 352 (1991).
- 7 International Harmonized Protocol for the Proficiency Testing of (Chemical) Analytical Laboratories, AOAC/ISO/REMCO. No. 247, Draft, June 1992.
- 8 E.A. Maier, *Trends Anal. Chem.*, 10 (1991) 340.
- 9 D.E. Wells, E.A. Maier and B. Griepink, *Int. J. Environ. Anal. Chem.*, 46 (1992) 255.
- 10 D.E. Wells, J. De Boer, L.G.M.Th. Tuinstra, L. Reutegardh and B. Griepink, *Fresenius' Z. Anal. Chem.*, 322 (1985) 591.
- 11 T. Ryman, J. Hirschberger, E.A. Maier and B. Griepink, The Quantitative Determination of PCDD (Polychlorodibenzo-*p*-dioxin) and PCDF (Polychlorobenzofuran): Improvement of the Analytical Quality up to a Level Acceptable for the Certification of Certified Reference Materials, Report EUR 14357 EN, CEC, Luxembourg, 1992.
- 12 D.T.E. Hunt and A.L. Wilson, *The Chemical Analysis of Water. General Principles and Techniques*, Royal Society of Chemistry, London, 1986.
- 13 Ph. Quevauviller, B. Griepink, I. Drabeak and H. Muntau, in A. Rizzi and G. Sontag (Eds.), *Euroanalysis VII*, Austrian Society for Analytical Chemistry (ASAC), Austrian Chem. Soc., Vienna, August 1990, Book of Abstracts, Vol. 2, p. 132.



# Interlaboratory programme for the quality control of nitrate determination in freshwater

Ph. Quevauviller, D. Van Renterghem and B. Griepink

*Commission of the European Communities, Community Bureau of Reference (BCR), 200 rue de la Loi, B-1049 Brussels (Belgium)*

M. Valcarcel, M.D. Luque de Castro and J. Cosano

*Universidad de Córdoba, Departamento de Química Analítica, E-14004 Córdoba (Spain)*

(Received 5th October 1992; revised manuscript received 5th April 1993)

## Abstract

Analyses of freshwaters and groundwaters are routinely performed to monitor the level of contamination by, e.g., nitrates. To verify the quality of such determinations, the Community Bureau of Reference (BCR) has organised an interlaboratory exercise which allowed to identify most of the pitfalls observed in the determination of nitrate at three levels of concentrations (0.5, 8 and 53 mg kg<sup>-1</sup>). In addition, this first step enabled the BCR to study the feasibility of the preparation of candidate certified reference materials (CRMs) for the determination of nitrate in freshwater. The materials used in this exercise were carefully prepared and their homogeneity and stability were verified by using a flow-injection analysis technique developed for this purpose. This paper presents the main results of the intercomparison.

*Keywords:* Flow injection; Interlaboratory study; Nitrate; Quality control; Waters

A number of European Community Directives have been issued dealing with the quality of drinking (75/440/CEE, 76/869/CEE, 80/778/CEE) or underground water (80/68/CEE). They prescribe the determination of a wide range of major and minor elements and compounds, including nitrates. It has however been demonstrated that systematic errors may occur in the analysis of water e.g. for seawater analysis [1,2] and estuarine water analysis [3]. Sources of errors in the determination of major elements in freshwater were also identified by collaborative trials and removed prior to the certification of ten major elements [4]; the certification of these

freshwater materials (CRMs 398 and 399) excluded nitrate because the water was stabilised by the addition of nitric acid. More recently, two artificial rainwater samples were certified for their contents in major constituents, including nitrate [5]. Other intercomparisons have been organised on nitrate in seawater by the International Council for the Exploration of the Sea (ICES) and showed that systematic errors, likely due to calibration, could still be observed for this type of determination [6]. Studies to investigate the feasibility of preparing artificial freshwater samples containing nitrate were found to be desirable, as well as interlaboratory comparisons which could lead to the production of certified reference materials. Consequently, the Community Bureau of Reference (BCR) of the Commission of the European Communities organised an interlabora-

*Correspondence to:* M. Valcarcel, Universidad de Córdoba, Departamento de Química Analítica, E-14004 Córdoba, (Spain).

tory exercise of which the first step focussed on the analysis of nitrate in three artificial freshwater solutions. This paper describes the preparation of these samples, the development of a flow-injection analysis (FIA) procedure for the verification of the homogeneity and stability of the samples, the main results of the intercomparison and gives an outline of the further development contemplated.

#### AIM OF THE EXERCISE

An intercomparison can be held (i) to detect the pitfalls of a commonly applied method and to ascertain its performance in practice, (ii) to measure the quality of a laboratory or a part of a laboratory (e.g., audits for accreditation of laboratories), (iii) to improve the quality of a laboratory in collaborative work in mutual learning process and (iv) to certify the contents of a reference material (CRM) [7]. The work described here is of type (iii); such an exercise is one of the most powerful tools to detect and remove sources of error due to a particular technique as applied within a laboratory [8,9]. In general, analytical errors in all inorganic analyses may stem from:

- (a) inadequate sample storage;
- (b) the method of sample pretreatment (e.g., digestion, preconcentration, dilution);
- (c) the method of final measurement (e.g., calibration, removal of spectral interferences, background corrections); the influence of blanks is particularly critical for nitrate determinations;

- (d) the laboratory infrastructure (e.g., training and educational level of workers, awareness of pitfalls, management, clean bench facilities); and
- (e) the data treatment.

When different laboratories participate in an intercomparison, different sample pretreatment methods and different techniques of final determination are compared and discussed as well as the actual analytical results from the laboratories.

#### ANALYTICAL DEVELOPMENT

To establish the homogeneity and stability of candidate CRMs, a method has to be chosen which is highly repeatable. In this case FIA was the method of choice. The most frequently used methods of final determination are, in this order, those using photometry, potentiometry and fluorimetry. Photometric methods for nitrate are usually based on the reduction of nitrate to nitrite and the formation of diazo compound which is coupled to sulphanilamide (SPA) [10] and *N*-naphthylethylenediamine (NED) to yield an azo derivative with a maximum absorption at 540 nm. The FIA configuration used is given in Fig. 1; after mixing with the carrier ( $\text{NH}_4\text{Cl}-\text{Na}_2\text{B}_4\text{O}_7-\text{EDTA}$ ) along  $L_1$ , the sample reaches the redox Cd column (copperized with  $\text{EDTA}-\text{CuSO}_4$ ) where nitrate is reduced to nitrite. Then, the reduced analyte solution is sequentially mixed with the SPA and NED solutions to yield the azo compound, which is monitored at 540 nm as it passes through the flow cell of the photometric

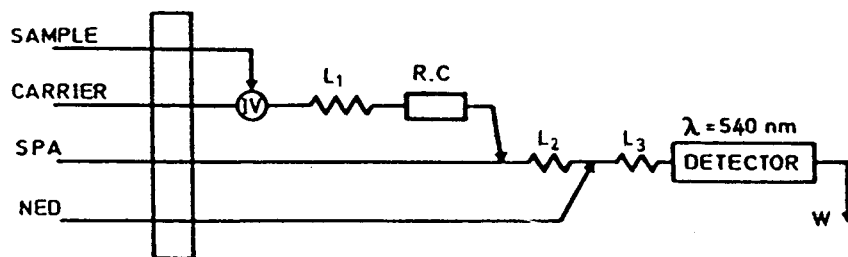


Fig. 1. Configuration selected for the photometric determination of nitrate by the Griess reaction.  $L_1 = 60$  cm,  $L_2 = 15$  cm,  $L_3 = 100$  cm,  $V_i = 200$   $\mu\text{l}$ , C = redox column (8 cm  $\times$  2 mm),  $\lambda = 540$  nm, flow-rate = 3.5 ml  $\text{min}^{-1}$ .

detector. The measured signal is the maximum height of the FIA peak. The determination range is 0.4 to 16 mg l<sup>-1</sup> NO<sub>3</sub><sup>-</sup> with a C.V. (*n* = 11) of the method of ca. 1.5%; and 2% at the 20 and 110 mg l<sup>-1</sup> levels (with a previous dilution), respectively.

## PREPARATION

### Solutions

Freezing was not considered to be a suitable procedure for the long term storage of CRMs as it may also lead to irreversible physico-chemical changes (e.g., formation of insoluble calcium salts) and would necessitate the use of special containers and ways of dispatching. Freeze-drying would be susceptible to the same difficulties. Consequently, in view of the risks of instability of natural waters and of the high variability in composition, it was decided to prepare artificial solutions containing known concentrations of nitrate and other major constituents, if necessary with addition of stabilizing agents.

The pH of the solution was considered to be critical for stability and subject to change when the sample is in contact with CO<sub>2</sub> (e.g., during bottling). The evaporation of CO<sub>2</sub> and the precipitation of CaCO<sub>3</sub> were considered to be possible sources of inhomogeneity and instability. Problems were considered to be less likely to arise if samples could be equilibrated with air and a carbonate buffer added. Therefore 530 mg l<sup>-1</sup> of Na<sub>2</sub>CO<sub>3</sub> was added to each sample and the pH adjusted to 6.8 with HCl to simulate a typical pH observed in natural water.

Implicitly, calcium could only be present to such an extent that precipitation would not occur and all other ions could be added with the exception of e.g. phosphate and ammonium (to avoid the production of a microbiological growth).

The addition of UV absorbing organic matter was also considered; as it was found difficult to prepare water samples containing humic acids, 2 mg l<sup>-1</sup> of lauryl sulphate was added to the samples. Finally, the addition of phenyl-mercury acetate (C<sub>8</sub>H<sub>8</sub>HgO<sub>2</sub>) was recommended against moulds. Different concentrations were studied

and undesirable white precipitate and deleterious effects on the redox copperized Cd column were observed in the samples with concentrations of 100 mg l<sup>-1</sup> of phenyl-mercury acetate. These effects were not noticeable at a 10 mg l<sup>-1</sup> level which was therefore used for the sample preparation.

The nitrate concentrations were chosen to cover the range of levels found in the environment, considering the tolerance level specified in the EC Directive (50 mg l<sup>-1</sup>), i.e., samples with concentrations of 0.80, 8.0 and 53.8 mg l<sup>-1</sup> were prepared (respectively solutions A, B and C). The concentrations of the other compounds were adjusted to obtain water samples simulating a natural water with ca. 10 (French) degrees of hardness, i.e., CaCl<sub>2</sub> 91.7; MgSO<sub>4</sub>, 123; Na<sub>2</sub>CO<sub>3</sub>, 530 mg l<sup>-1</sup>. In addition, 5 mg l<sup>-1</sup> of potassium hydrogen phthalate (C<sub>8</sub>H<sub>5</sub>O<sub>4</sub>K; to introduce K<sup>+</sup> ions and additional organic matter to simulate the presence of humic acids) were added.

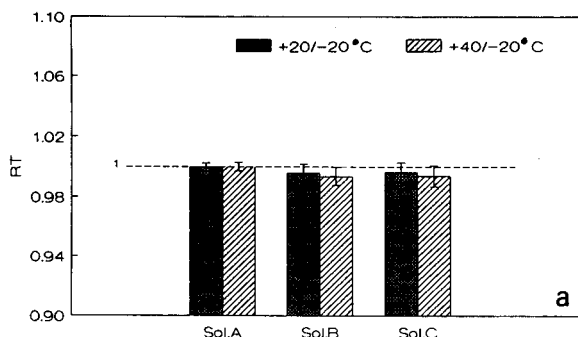
Boiled water was sterilised, homogenised and filtered with sterile filters to 0.2 μm and then the different compounds listed above were added.

### Stability study and selection of container

In order to verify the long term stability of the samples upon storage, white and brown glass ampoules of 200 ml were selected. The short-term stability (3 months) of the three sets of samples was verified at -20, +20 and +40°C. The homogeneity was verified prior to the stability experiments by performing five measurements for each of the three concentrations considered on fifteen ampoules randomly selected during the filling procedure. Any change in the content of an element with time indicates an instability provided that a good long-term reproducibility of analysis is achieved. Instability would be detected by comparing the nitrate contents in the solutions stored at -20°C, for which changes are assumed to be unlikely, with those stored at +20 and +40°C. This procedure was chosen in this case to assess possible changes during storage, even if the storage at -20°C is not recommended (as discussed above) for long-term storage of CRMs due to risks of precipitation. However, the samples did not show any precipitate upon defreezing which

made this procedure acceptable for the purpose of a short term stability study. The ratio  $R_T$  of the mean values  $\bar{X}_{+20^\circ\text{C}}$  or  $\bar{X}_{+40^\circ\text{C}}$  of the measurements performed over a period of three months at  $+20$  and  $+40^\circ\text{C}$ , respectively, versus the mean value  $\bar{X}_{-20^\circ\text{C}}$  from the determinations performed over the same period on samples stored at  $-20^\circ\text{C}$  can be used to evaluate the changes. In the case of ideal stability,  $R_T$  should be 1. In practice however there are some random variations due to the error on the measurement. Figure 2a and b shows the ratio  $R_T$  and its uncertainty  $U_T$  for the three solutions stored in white and brown glass ampoules, respectively. In all the cases the value 1 is between  $R_T - U_T$  and  $R_T + U_T$ . On the basis of these results, it was concluded that no instability could be demonstrated over a period of three months for the three sets of solutions, both in white and brown glass ampoules. Consequently, the white glass ampoules were selected for the storage of the solutions and a temperature of  $+20^\circ\text{C}$  was adopted for the storage conditions.

The homogeneity of the final batch of solutions was verified by selecting 15 ampoules during the filling procedures and performing five replicate determinations on each of the ampoules. In all cases no inhomogeneities could be detected (within a 99% confidence interval) and the samples were therefore considered to be suitable for use in the intercomparison.



#### ANALYTICAL TECHNIQUES USED IN THE INTER-COMPARISON STUDY

The techniques used were of three main categories.

(i) Ten laboratories performed the analyses by reduction of nitrate to nitrite using a Cd column [addition of sulphanilamide and/or *N*-(1-naphthyl)-ethylenediamine dihydrochloride, except one laboratory which used hydrazine], addition of buffer ( $\text{NH}_4\text{Cl}$  in most of the cases) and spectrometric detection. Seven laboratories used a segmented flow method and three laboratories performed flow-injection analysis.

(ii) Twelve laboratories performed the analyses by ion chromatography with a suppressed column system and addition of buffer ( $\text{Na}_2\text{CO}_3$ - $\text{NaHCO}_3$ ). Ten laboratories used conductivity as final detection whereas two performed UV detection. The injection was either manual (10 labs.) or by FIA (2 labs.). No pretreatment (except dilution for laboratories using UV detection) was applied to the solutions.

(iii) One laboratory determined nitrate by differential pulse polarography (DPP) after addition of 0.1 M KCl.

#### DISCUSSION

Each laboratory which participated in the intercomparison study was requested to make a

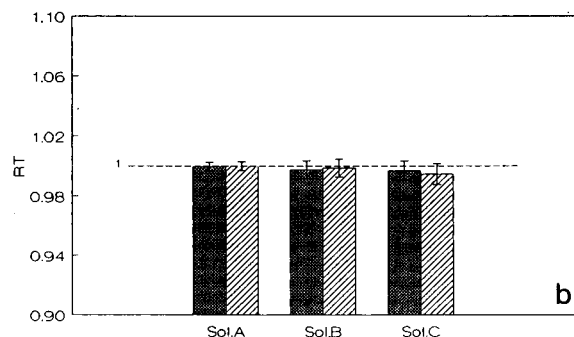


Fig. 2. Three-month stability of nitrate in the solutions A, B and C. This stability was assessed using the concentrations obtained with the  $-20^\circ\text{C}$  as a comparison. The figures present the ratios of concentrations  $R_T$  obtained after two different treatments ( $+20$  and  $+40^\circ\text{C}$ ) divided by the reference concentrations. a and b concern the storage of solutions in (a) white glass and (b) brown glass ampoules, respectively.

minimum of five independent replicate determinations. The results submitted were presented in the form of bar-graphs showing the laboratory codes and the methods used, the individual means and standard deviations and the mean of laboratory means with its standard deviation. The bar-graphs of accepted results for the three sets of solutions are shown in Fig. 3a–c.

The large variation of the standard deviations for ion chromatography was attributed to the application of different columns, different eluents and the use of both chemical and electronic suppression (conductivity detection). In general, small standard deviations were observed at a given concentration level if the laboratory carried out routine analysis at this concentration. The absence of

overlap between different sets of results was at least partly due to the inexplicably (following a priori error estimations) small standard deviations, obtained in some laboratories (not using FIA).

No significant differences were observed between manual and continuous flow methods. This was also verified by ICES in an intercomparison on nitrate in seawater [6]. Some specific remarks were reported for the different solutions.

#### Solution A

The coefficient of variation (C.V.) obtained between laboratories for the raw data was considered to be unacceptably high (13.3%). After removal of some sets of results (e.g., very high

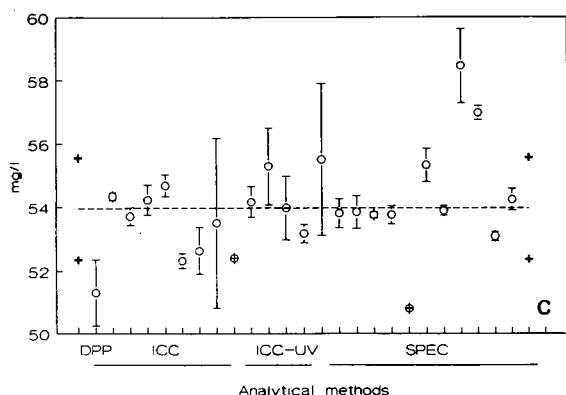
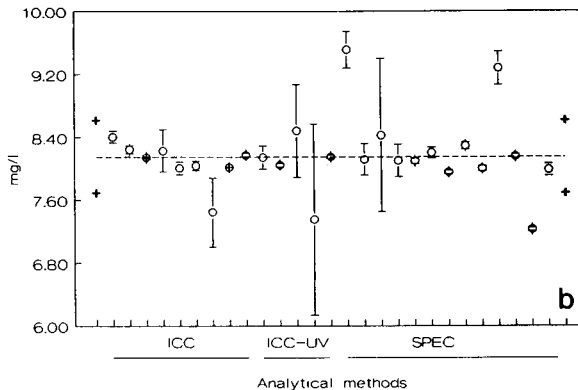
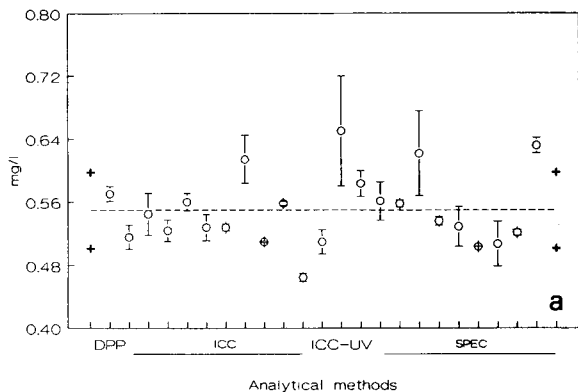


Fig. 3. Bar-graphs of accepted results. The dotted line indicates the mean of the laboratory means; the two crosses on each part of the graph show the standard deviation of the mean of laboratory means. (a) Solution A (expected value,  $0.500 \text{ mg l}^{-1}$  of nitrate); (b) solution B (expected value,  $8.00 \text{ mg l}^{-1}$  of nitrate); (c) solution C (expected value,  $53.8 \text{ mg l}^{-1}$  of nitrate). ICC = Ion chromatography with conductivity detection; ICC-UV = ion chromatography with conductivity and UV detection; SPEC = spectrometry; DPP = differential pulse polarography.

standard deviations for two sets of ion chromatography results observed for one laboratory working close to its limit of detection), the C.V. between laboratories was 8.7% which was still considered to be high. The discrepancies of the results observed were partly explained by the fact that some laboratories probably did not take into account the non-linearity of the calibration curve. The application of bracketing calibrant solutions was considered to be a prerequisite to obtain correct values.

#### *Solution B*

Better results were achieved at this level of concentration. The original bar-graph showed a C.V. between laboratories of 9.6%. This high value was due to a set of differential pulse polarography (DPP) results which were not corrected for residual current; after correction the new value was much closer to the mean of the laboratory means. The C.V. between laboratories of the accepted data was 5.7% which was found acceptable. High results using spectrophotometry were attributed to either contamination or the yield of the reduction. Lower results could be due to not correcting for the blank of the water used for the preparation of the calibrant solutions.

#### *Solution C*

The C.V. between laboratories obtained was 3.0% which was considered to be acceptable for contemplating certification. Low spectrometry results were suspected to be due to an incomplete reduction whereas a negative bias observed in a DPP set of results was probably due to working near the upper limit of determination.

#### *Conclusions*

For solutions B and C, the values expected upon spiking were within the range of uncertainty of the mean of laboratory means (respectively  $8.00 \text{ mg l}^{-1}$  and  $8.15 \pm 0.46 \text{ mg l}^{-1}$  for solution B;  $53.80 \text{ mg l}^{-1}$  and  $53.96 \pm 1.60 \text{ mg l}^{-1}$  for solution C). For solution A, a slightly higher value was obtained ( $0.550 \pm 0.048 \text{ mg l}^{-1}$ , expected value  $0.500 \text{ mg l}^{-1}$ ) which was attributed to a contribution of the reagent blank ( $< 0.12 \text{ mg}$

$\text{l}^{-1}$  of  $\text{NO}_3^-$  corresponding to the detection limits) obtained in the manufacturing laboratory. This agreement confirms that neither losses nor contamination (except from the reagents) occurred during the preparation of the samples which procedure was recognized to be suitable for the preparation of candidate certified reference materials.

#### *Future development*

This interlaboratory exercise enabled the BCR to identify some sources of error occurring in the determination of nitrate in freshwater and to have a clear picture of the present state of the art. Beside the analytical improvements achieved, this exercise enabled to test the feasibility of preparation of artificial freshwater samples for the production of possible certified reference materials (CRMs). Owing to the need for CRMs for the quality control of nitrate determination in freshwater, the participants agreed that a certification should be contemplated. Consequently a programme was designed which focussed on the certification of nitrate at two concentration levels (ca.  $10$  and  $50 \text{ mg l}^{-1}$ ); the preparation will be similar to the procedure used in this exercise. As only three methods were used (DPP, IC, SPEC), the participants recommended the addition of alternative techniques such as, e.g., isotope dilution mass spectrometry (ID-MS).

Two candidate CRMs are presently being prepared by the University of Córdoba. The between-ampoule homogeneity has been tested and the long term stability study will be verified over 12 months. The experience with rainwater CRMs has shown that the nitrate contents are stable at ambient temperature in the dark over one year and therefore no difficulties are expected in the stability of the candidate freshwater CRMs. The certification campaign will start before the end of 1993 and hence the CRMs could be available by the middle of 1994.

The authors thank all the laboratories participating in the intercomparison.

*Preparation homogeneity and stability studies.* University of Córdoba, Department of Analytical Chemistry (Córdoba, Spain).

*Analyses.* Anglian Water Authority (Cambridge, UK); Aristotelian University, Laboratory of Analytical Chemistry (Thessaloniki, Greece); Bureau of Geological and mine Research, BRGM (Orléans, France); Danish Technological Institute (Aarhus, Denmark); Hydrographical Institute (Lisbon, Portugal); Institute for Environmental Protection, Sopra (Milan, Italy); Institute for Freshwater Ecology (Dorset, UK); Italian Institute for Hydrobiology (Pallanza, Italy); Ministry of Economic Affairs (Brussels, Belgium); Multizonal Institute for Prevention, Analytical Section (Venice, Italy); National Service of Parks and Nature Conservation (Lisbon, Portugal); National Scientific Research Centre (CNRS), Central Service of Analysis (Vernaison, France); National Research Centre (CNR), Water Research Institute (Brugherio, Italy); Netherlands Energy Research Foundation, ECN (Petten, Netherlands); Portsmouth Polytechnic, Department of Chemistry (Portsmouth, UK); Public Enterprise of Free Waters, EPAL (Lisbon, Portugal); Research Centre for Environment and Health (Neuherberg, Germany); Swedish Environmental Protection Agency (Uppsala, Sweden); Swedish Environmental Research Institute (Göteborg, Sweden); University of Córdoba, Department of Analytical Chemistry (Córdoba, Spain); University of Plymouth, Department of Environmental Sciences (Plymouth, UK); Water Quality Institute (Hørsholm, Denmark); Waterworks Testing and Research Institute, KIWA (Nieuwegein, Netherlands).

## REFERENCES

- 1 R. Boniforti, R. Ferraroli, P. Frigieri, D. Heltai and G. Queirazza, *Anal. Chim. Acta*, 162 (1984) 33.
- 2 Ph. Quevauviller, K.J.M. Kramer, E.M. van der Vlies, K. Vercoutere and B. Griepink, *Mar. Pollut. Bull.*, 24 (1992) 33.
- 3 Ph. Quevauviller, K.J.M. Kramer and B. Griepink, *Anais do Inst. Hidrogr.*, in press.
- 4 Ph. Quevauviller, K. Vercoutere and B. Griepink, *Mikrochim. Acta*, 108 (1992) 195.
- 5 Ph. Quevauviller, D. Van Renterghem, B. Griepink, H.F.R. Reijnders and H. Van der Jagt, EUR Report, Certification of Major Elements in Simulated Rainwater (CRMs 408 and 409), CEC, Brussels, in press.
- 6 D. Kirkwood, A. Aminot and M. Pertillä, ICES Report, Copenhagen, No. 174 (1991).
- 7 E.A. Maier, *Trends Anal. Chem.*, 10 (1991) 340.
- 8 Royal Society of Chemistry, Analytical Methods Committee, *Analyst*, 112 (1987) 679.
- 9 B. Griepink and M. Stoeppler, in M. Stoeppler (Ed.), *Hazardous Metals in the Environment (Techniques and Instrumentation in Analytical Chemistry, Vol. 12)*, Elsevier, Amsterdam, 1992, p. 517.
- 10 M.B. Shinn, *Ind. Eng. Chem. Anal. Ed.*, 13 (1941) 33.

# Combining fingerprinting capability with trace analytical detection: surface-enhanced Raman spectrometry

J.J. Laserna

*Department of Analytical Chemistry, Faculty of Sciences, University of Málaga, E-29071 Málaga (Spain)*

(Received 8th September 1992)

## Abstract

The demand to measure unique spectral information on trace analytes in complex samples continues to increase. This paper discusses surface-enhanced Raman spectrometric (SERS) methods which are currently being explored for molecular recognition at trace concentration levels. SERS is amenable to the analysis of solids, liquids and gases in a variety of experimental configurations for both qualitative and quantitative tasks. Batch and flow systems are also easily implemented in colloid SERS experiments. Typical instrumental systems for each of these analytical approaches are described and compared. The shape of the calibration graphs and the factors limiting the linear range of response are discussed. Other figures of merit, including limits of detection, precision and selectivity of measurement, are given. Applications to compounds of technical, environmental, biomedical and pharmaceutical interest are presented.

*Keywords:* Raman spectrometry; Trace detection

In its simplest forms, Raman spectroscopy is not a sensitive analytical technique, as the scattering cross-sections for most molecules are several orders of magnitude below those in optical absorption or emission spectroscopy. Fluorescence in the molecule of interest or other sample components further compromises detectability as the luminescence emission often obscures the weak scattering signal. Although some improvements using updated instrumental components (lasers, spectrometers, array and imaging detectors, counting electronics, digital spectral processing) have been achieved, a major breakthrough in Raman detection capability took place with the discovery some years ago of surface-enhanced

Raman spectroscopy (SERS). This is a technique in which lasers are used to excite vibrational transitions in molecules adsorbed on a rough metallic substrate. As a result of large optical fields and resonance-related effects, the Raman cross-section for the molecule on the surface is enhanced by factors of up to  $10^6$ . Even larger factors are observed when the SERS effect is combined with an optical resonance in the molecule. Extensive overviews [1,2] and a full book [3] on the subject have been published.

Both electromagnetic (EM) and charge-transfer (CT) theories have been proposed to explain the great enhancement in Raman-cross sections. It is generally accepted that some form of roughness is necessary for SERS. However, the operational model of roughness vary from one theory to the other. For space reasons only a brief description of the theoretical models will be given

*Correspondence to:* J.J. Laserna, Department of Analytical Chemistry, Faculty of Sciences, University of Málaga, E-29071 Málaga (Spain).



here. A compilation of SERS mechanisms has been published elsewhere [3] and a unifying view of the several models has been presented [4]. The electromagnetic theory relies on the plasma resonance model, which is related to the optical properties of free electron systems such as metals.

The electric field at the tips of protrusions (or particles) in such a surface becomes greatly enhanced if the incident photon energy is in resonance with a normal mode of conduction electrons in the metal. In the Rayleigh limit, where the particle size is much smaller than the incident wavelength, the electric field depends on the dielectric constant of the metal. In this sense, Ag, Au and Cu are unique as their wavelength-dependent dielectric functions produce maximum values of the electric field in the visible region. A molecule located near the particle will experience, in addition to the regular electric field associated to the radiation, an amplified field and will scatter enhanced intensity over that of an isolated molecule. In the CT model, molecules located on atomic-scale sized metal clusters may be physisorbed or chemisorbed on the surface. Electron transfer from the metal to the excited electronic level of the adsorbate via tunnelling or hybridization leaves the molecule in a higher vibrational level when the electron transfers back to the metal. Photon emission is now produced by electron–hole recombination in the metal. The CT process is resonant when the energy difference between the excited level in the adsorbate and the Fermi level in the metal is of the order of the incident photon energy. It is evident that in the CT model the distance dependence of the enhancement must be much more critical than in the case of the EM model, and thus the enhancement would decrease dramatically for a molecule–surface separation of only a few ångströms.

Each model has partial success in explaining the experimental observations of SERS. For instance, the EM model is able to explain long-distance effects in SERS, the importance of metal particle morphology and the critical role of the metal dielectric constant. The CT model explains by non-resonant electron–hole recombination the background continuum ubiquitous to all SERS spectra regardless the type of metal, its active

form and the nature of the scattering molecule. Also, it justifies why the enhancement factor for the first adsorbate layer is much greater than that for subsequent layers. It is at present accepted that the largest enhancement factors are achieved only when both mechanisms are allowed to operate, as the Raman intensity is the product of both electromagnetic and molecular effects. The former enter into the theory through the local field and dipole emission and the latter through the molecular polarizability. The relative importance of EM and CT processes depends very much on the experimental configuration and conditions, which at present cannot be fully controlled [4].

The metal substrates most often used for SERS fall qualitatively into several groups: noble metals (e.g., Ag, Cu and Au), free-electron-like metals (e.g., Al, Na and K) and transition metals (e.g., Ni, Pd and Pt). The necessary roughness can be created in a number of ways: electrochemical (oxidation and reduction of electrodes), photochemical (photoreduction of adsorbates on electrodes, single crystals or powder surfaces), evaporation (vacuum deposition of metallic films on smooth insulating or metallic substrates), lithography (grating structures on Ag surfaces or uniformly shaped Ag microstructures on an array of silica posts), vapour deposition (clusters of a few metal atoms surrounded by a matrix), mechanical polishing (use of different-sized abrasives), and chemical reduction (metal colloids produced in aqueous solution or deposited on rough or flat surfaces). Metal island films provide perhaps the most reproducible substrate. In contrast, electrodes have been mostly used for theoretical studies because favourable conditions are given for supporting the EM and CT models. However, one disadvantage of these static substrates is that the intense laser fields associated with SERS can destroy the surface morphology which gives rise to surface enhancement. In addition, careful attention must be paid to geometrical factors in order to maximize classical field enhancements and light collection. Colloidal hydrosols provide a number of advantages for observation by SERS, including ease of formation and manipulation, simple characterization by absorptiometric techniques and a definite dependence of the en-

hancement on particle size and shape. Disadvantages are that the analyte-induced coagulation of the colloidal dispersion eventually causes instability of the entire system, and that the SERS activity of a given analyte depends to a certain extent on the means of sol preparation and on the exact protocol used for a given preparation.

#### INSTRUMENTAL ADVANCES

One of the advantages of working under the high signal regime typical in SERS experiments is that the instrumentation needed can be greatly simplified over that in conventional Raman spectroscopy (CRS). High-power lasers are not necessary in SERS. In contrast, active substrates can be destroyed under intense optical fields. Although SERS excited by the fundamental frequency of an Nd:YAG laser has been reported [5,6], and it has been pointed out that near-infrared radiation is less likely to cause photochemical changes in the sample [5], near-infrared lasers are of little apparent use in SERS for two main reasons. First, fluorescence is not usually a problem in SERS as a result of charge transfer and radiationless energy transfer to the metal surface, which efficiently quench the luminescence from the adsorbed molecules [7,8]. Thus, the loss of scattering intensity at 1064 nm is not compensated for by a rejection of fluorescence as in CRS. Second, surface enhancement requires the

laser frequency to excite the surface plasma resonance of the metal substrate [9]. This usually appears as a broad band in the visible region (usually between 500 and 700 nm, depending on the metal substrate). Although the spectral distribution of the metal plasma resonance depends on the morphology of the metal particles and the polydispersity of the substrate, it has been shown that maximum enhancement occurs in the visible region [10]. Because the limiting noise source in SERS is elastically or inelastically scattered light rather than detector noise, the multiplex advantage of Fourier transform (FT) spectrometry seem to be non-effective in SERS. However, FT-SERS could still provide a throughput advantage over dispersive SERS.

The trend in modern instrumentation for SERS is towards miniaturization using diode lasers and single spectrometers and toward fast data acquisition using charge-coupled device detectors and diode arrays. However, as SERS always involves a solid substrate, means of rejecting the high level of Rayleigh scattering have to be applied. Usually a combination of filters provides a satisfactory solution to this problem. An interference band-pass filter at the laser frequency is placed after the laser focusing optics and before the sample to reject non-lasing plasma lines of the laser device. Then, laser band rejection filters are placed between the sample and the spectrometer [11,12].

Recently, the construction and evaluation of an inexpensive spectrometer for analytical SERS

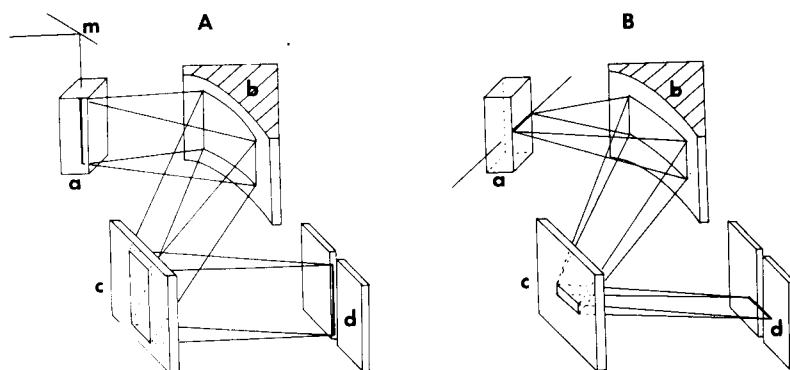


Fig. 1. Configurations for (A) vertical and (B) horizontal sample illumination in a Raman spectrometer. a = Sample cell; b = parabolic collection mirror; c = flat focusing mirror; d = monochromator entrance slit; m = flat mirror.

has been detailed [13]. The system uses a helium–neon laser, which is a rugged, long-lasting device, with none of the cooling requirements necessary in ion and Nd:YAG lasers or the wavelength-drifting effects exhibited by semiconductor lasers. A relatively short focal length (0.22 m) double monochromator provided an adequate compromise between Rayleigh light rejection, throughput and resolution. The refrigerated photomultiplier tube provided good sensitivity with a relatively short acquisition time. For colloidal dispersions, the signal-to-noise ratio (S/N) can be increased significantly by correct imaging the sample optical pathway on to the entrance slit of the spectrometer. This has been achieved by vertical illumination of the cell cuvette as shown in Fig. 1. The S/N obtained with vertical illumina-

tion is about ten times greater than that obtained with the horizontal configuration.

Perhaps the most significant characteristics of SERS with colloidal systems is that the surrounding medium in front of the interface (e.g., several mm of liquid) introduce a large optical loss in the scattered radiation. In addition, attenuation of the exciting laser is also extensive in any colloid SERS experiment. The issue has been treated in detail recently [14]. Using the vertical illumination configuration described above, the Raman intensity profile generated by a collimated laser beam passing through a sample cuvette is shown in Fig. 2. As shown, the intensity is maximum close to the cuvette wall facing the transfer optics. Also, maximum intensity is obtained at a given excitation path length, i.e., at a definite

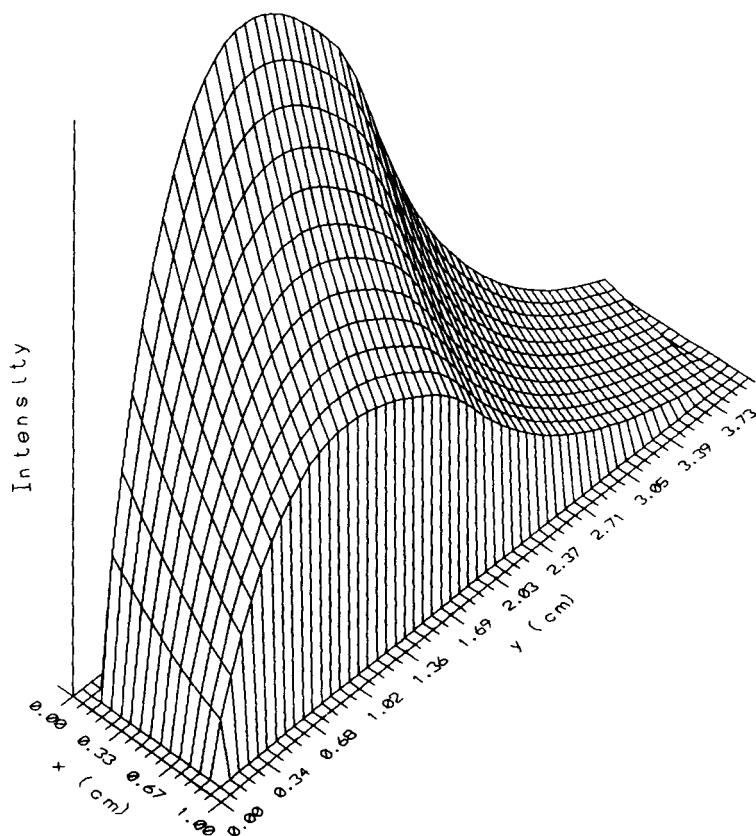


Fig. 2. Raman intensity profile generated by a collimated laser beam passing through a sample cuvette (1 cm  $\times$  4 cm). The laser beam illuminates the sample cuvette along the *y*-axis. The spectrometer is situated along the *x*-axis. (Reprinted with permission from [14]. Copyright ACS, 1992.)

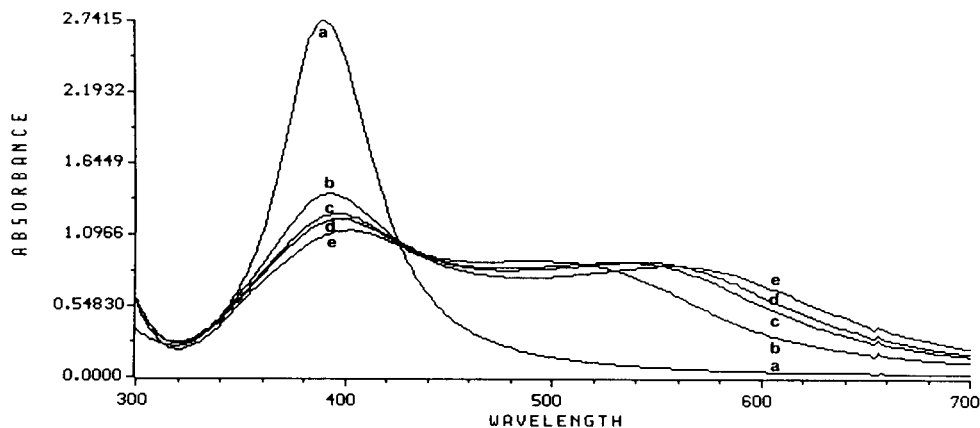


Fig. 3. Absorption spectra of a silver hydrosol following the addition of  $12.5 \mu\text{g ml}^{-1}$  sulphanilamide: (a) immediate; (b) 0.5 min; (c) 1 min; (d) 1.5 min; (e) 6 min. (Reprinted with permission from [15]. Copyright ACS, 1992.)

filling of the cuvette with the sample. Selection of an adequate sample illumination geometry and sample volume contributes significantly to optimizing the quality of measurements by SERS, in particular the S/N, limit of detection and the shape of the variation in SERS response with concentration [14].

Silver hydrosols are easy to characterize in terms of particle size by electronic absorption spectrometry. This point is of relevance in SERS studies as the enhancement factor for a given adsorbate is closely related to the particle size [10]. High SERS intensities occur when the exciting laser line overlaps the longitudinal surface

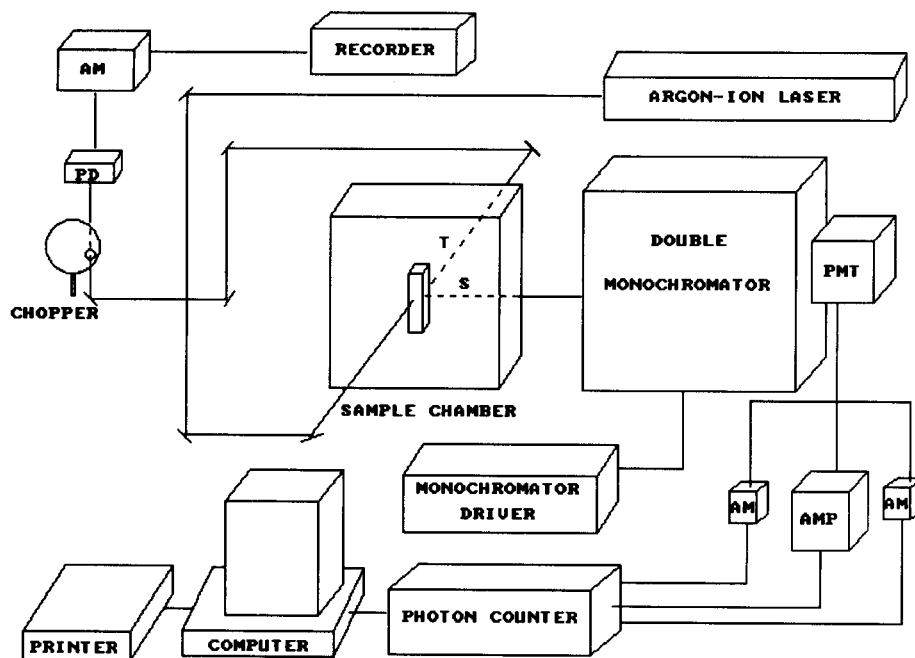


Fig. 4. Block diagram of the instrumental set-up for the simultaneous monitoring of the SERS signal (S) and transmitted light (T). PD = photodiode; AM, AMP = amplifiers.

plasma resonance of the metal, which usually appears as a broad band in the visible region, as discussed above. The spectral distribution of the plasma resonance depends on the particle size, which in turn is a function of the aggregation of the colloid induced by the adsorbate. Figure 3 shows time-dependent absorption spectra of a silver sol aggregated by sulphanilamide. The use of absorption spectrometry as a diagnostic tool in characterizing colloidal systems is of limited scope, however, as the colloid examined spectrophotometrically is usually at a different aggregation stage than that during the SERS measurement. To solve this situation, a method for the simultaneous measurement of SER spectra and absorbance changes occurring in colloid substrates has been reported [15].

Figure 4 shows a block diagram of the instrumental set-up. An argon ion laser is used to excite SERS on the sample. The scattered signal (S) is sampled at right-angles to the exciting beam and focused on the entrance slit of a double spectrometer. The light transmitted through the colloid (T) is detected with a silicon photodiode,

amplified and acquired in a standard recorder. To avoid thermal drifts in the photodiode response, the transmitted beam is chopped at 24 Hz. As the same laser wavelength is used, the transmitted light reflects in real time the colloid absorbance (extinction) at the SERS exciting wavelength, thus providing information on the aggregation state of the colloid while the SERS spectrum is being recorded. Figure 5 shows the data obtained for a colloid aggregated with 9-aminoacridine ( $1.25 \mu\text{g ml}^{-1}$ ). As shown, the transmittance decreases as the SERS signal increases. At about 4 min both signals stabilize, indicating that a steady state has been reached. Distortions in SERS intensities caused by inhomogeneous aggregation and slow adsorption kinetics can thus be readily detected and SERS data are acquired under the most favourable circumstances.

SERS on microprobe equipment has also been developed [16–19]. Several new active silver substrates have been investigated, including filterpapers of different composition and porosity, silver membranes and glass slides [19]. The Raman

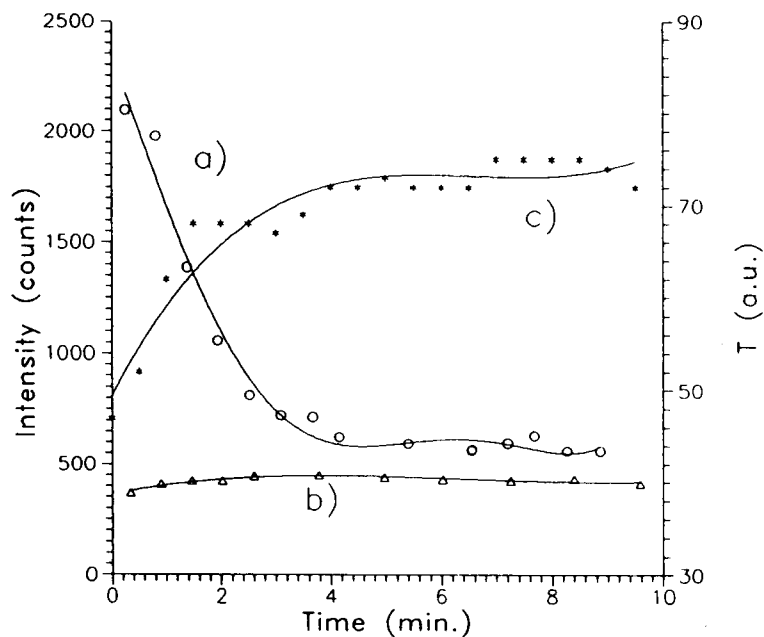


Fig. 5. (a) Transmitted light, (b) background of SERS intensity and (c) SERS intensity of the aggregation kinetics of a silver hydrosol with  $1.25 \mu\text{g ml}^{-1}$  9-aminoacridine. (Reprinted with permission from [15]. Copyright ACS, 1992.)

microprobe facilitated the acquisition of SERS data of 9-aminoacridine, used as a model compound, over several metal microstructures with a lateral resolution of 2  $\mu\text{m}$ . This capability allowed the establishment of practical relationships between the surface morphology and SERS activity.

#### MOLECULAR RECOGNITION AND QUALITATIVE ANALYSIS APPLICATIONS

Unlike conventional Raman spectrometry, apparently not all the molecules are able to produce a high-quality SERS spectrum, the surface-enhanced Raman effect seeming to be associated with the presence in the molecule of certain functional groups. In 1986 Seki [20] published a list with 544 references of molecules considered to be surface-enhanced. An analysis of these data reveals the prevailing presence of ionic, strongly dipolar and highly polarizable species, containing heterocyclic nitrogen atoms, and nitro, amino and carboxylic groups, in addition to groups containing phosphorus and sulphur atoms. This is not surprising as these species promote strong adsorption on the metal surface. SERS has been applied to the identification of compounds of technical, environmental, biomedical and pharmaceutical interest, including polyethylene [21], carbon materials [22], ground water contaminants [23], phthalic acid isomers [24], azole compounds [25], dyes [26,27], polycyclic aromatic hydrocarbons [28,29], organophosphorus pesticides [30], metal complexes [31,32], nitrophenol compounds [33], pH indicators [34], catecholamines [35,36], eye lens pigments [37], amino acids [38], tripeptides [39], nucleic acid bases [40,41], benzopyrene–DNA adducts [42], nitrogen-containing drugs [43], stimulant drugs [44] and sulphonamides [45,46].

Group theory provides a suitable method for the analysis of vibrational spectra. The relevant selection rules predict the number of Raman lines, the number of polarized Raman lines and the activity of overtones and combination bands which are expected from a given molecule. With the rational use of known frequencies and selec-

tion rules, identification and identity confirmation are often possible by Raman spectrometry. Unfortunately, the classical selection rules of Raman scattering apply only to isolated molecules. Environmental factors and intermolecular forces cause intensity changes and newly active vibrational modes which are not predicted by the classical rules. Thus a new set of selection rules has been developed for normal (unenhanced) surface Raman spectrometry [47,48]. These rules apply to smooth surfaces with a highly ordered molecular distribution and, simply stated, predict that vibrations occurring normal to the surface should be the most intense spectral features, whereas those parallel to the surface should be extremely weak and, therefore, commonly absent in the spectrum. Although the image field enhancement (a form of the EM model) at rough surfaces predicts similar rules in SERS, other forms of electromagnetic and chemical enhancements could lead to selection rules different to those for smooth surfaces, thus making vibrational analysis in SERS difficult. In addition, the low symmetry of most molecules when adsorbed on the metal surface makes differences between various adsorption site spectra very subtle; because of this is very difficult to assign definitely to many systems a specific geometry even if the molecular identity is known.

No systematic studies on the use of depolarization ratios for qualitative analysis in SERS have been reported. Although the SERS bands are often totally depolarized, the degree of polarization of the SERS signal varies with the orientation of the molecule at the metal surface, but also with the symmetry as in regular Raman scattering. The interrelation of both aspects tends to complicate the already difficult task of interpreting information on polarization ratios. Work needs to be done with both selection rules and depolarization ratios since these predictors could be extremely useful for molecular recognition and orientation.

The detection of nitrogen-containing aromatic compounds at the nanogram level has been reported [29]. The SERS-active substrate used was a filter-paper coated with chemically reduced silver. The SER spectra of 9-aminoacridine, 2-

aminoanthracene, 5-aminoquinoline and 6-nitroquinoline are shown in Fig. 6. The spectra show highly resolved, narrow bands and are obtained without interference from fluorescence. Each spectrum required only a 5-min single scan. These results show how compounds with similar chemical structures can be identified at trace concentrations, each spectrum serving as a fingerprint of the compound. For instance, 5-aminoquinoline shows a strong peak at  $1368\text{ cm}^{-1}$  which is not exhibited by 6-nitroquinoline.

The spectral fingerprint capability of SERS at trace concentration levels has also been illustrated for sulpha drugs [45]. In this instance colloidal silver was used as a substrate. The SER spectra of sulphadiazine, sulphamerazine and sulphamethazine are shown in Fig. 7A. The close structural similarity of these drugs, which differ only in the presence of a methyl group in the pyrimidine ring of the molecule, should be noted. Peaks at  $738\text{ cm}^{-1}$  in sulphamethazine and a  $762\text{ cm}^{-1}$  in sulphamerazine allow these drugs to be distinguished from sulphadiazine, which shows no

vibration in this frequency range. The conventional Raman spectra of these drugs are shown in Fig. 7B. To obtain a similar S/N to that in the SER spectra, the CR spectra required the crystalline, pure form of the drugs. The CR spectra are superimposed on a strong background, presumably owing to fluorescence of the drug or of some impurity. A comparison of SERS with CRS of these drugs illustrates two interesting differences often encountered among the two spectral approaches. (i) Although in general there is good agreement between SERS and CRS peaks, the vibrational modes in the SER spectra tend to be shifted with respect to the CR spectra. The most prominent peaks in the CR spectra were at  $1150\text{ cm}^{-1}$  for sulphadiazine,  $1153\text{ cm}^{-1}$  for sulphamerazine and  $1144\text{ cm}^{-1}$  for sulphamethazine, whereas the corresponding peaks in the SER spectra appear at  $1114$ ,  $1114$  and  $1112\text{ cm}^{-1}$ , respectively. Sulphamethazine shows a moderately intense SERS band at  $238\text{ cm}^{-1}$  with no counterpart in CRS. This band could be assigned to an Ag–N vibration indicative of adsorbate–

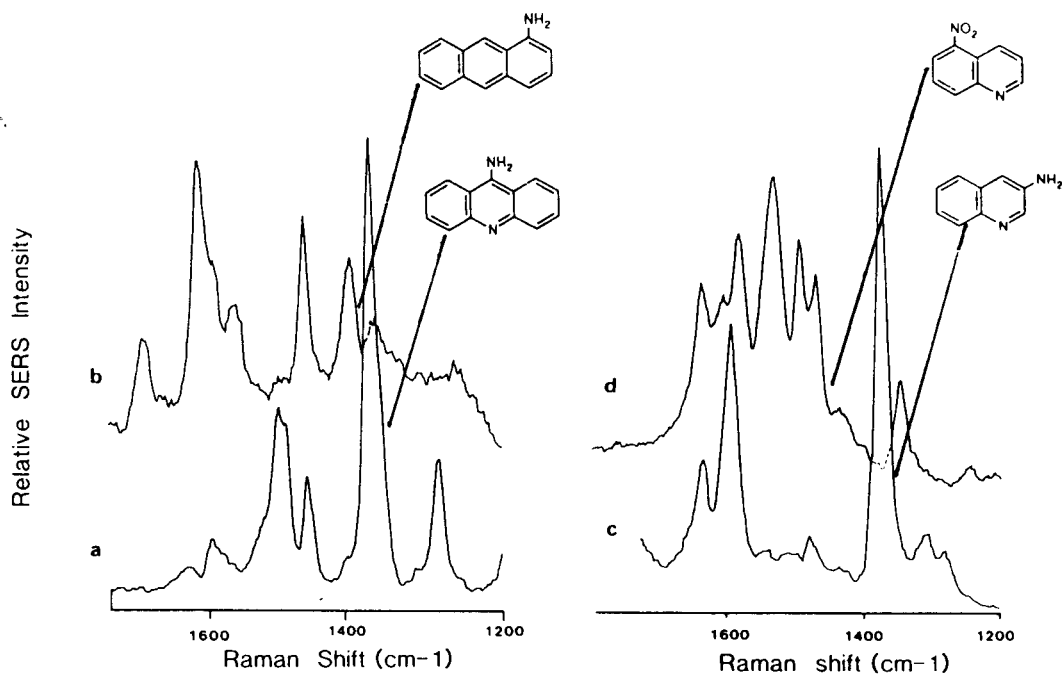


Fig. 6. SER spectra on a silver-coated filter-paper substrate: (a) 9-aminoacridine, 200 ng; (b) 2-aminoanthracene, 200 ng; (c) 5-aminoquinoline, 220 ng; (d) 6-nitroquinoline, 190 ng.

substrate bonding. (ii) The band widths [full width at half maximum intensity (FWHM)] of the solid-state spectra are smaller than those in SERS. For instance, the FWHM for the CRS band of sulphadiazine at  $1598\text{ cm}^{-1}$  was  $12\text{ cm}^{-1}$ ,

whereas for the same vibrational mode in the SER spectrum, held at  $1594\text{ cm}^{-1}$ , it is  $22\text{ cm}^{-1}$ .

Gas-phase species can be also measured by SERS. Nitroaromatic hydrocarbons in the environment are of concern because of their possible

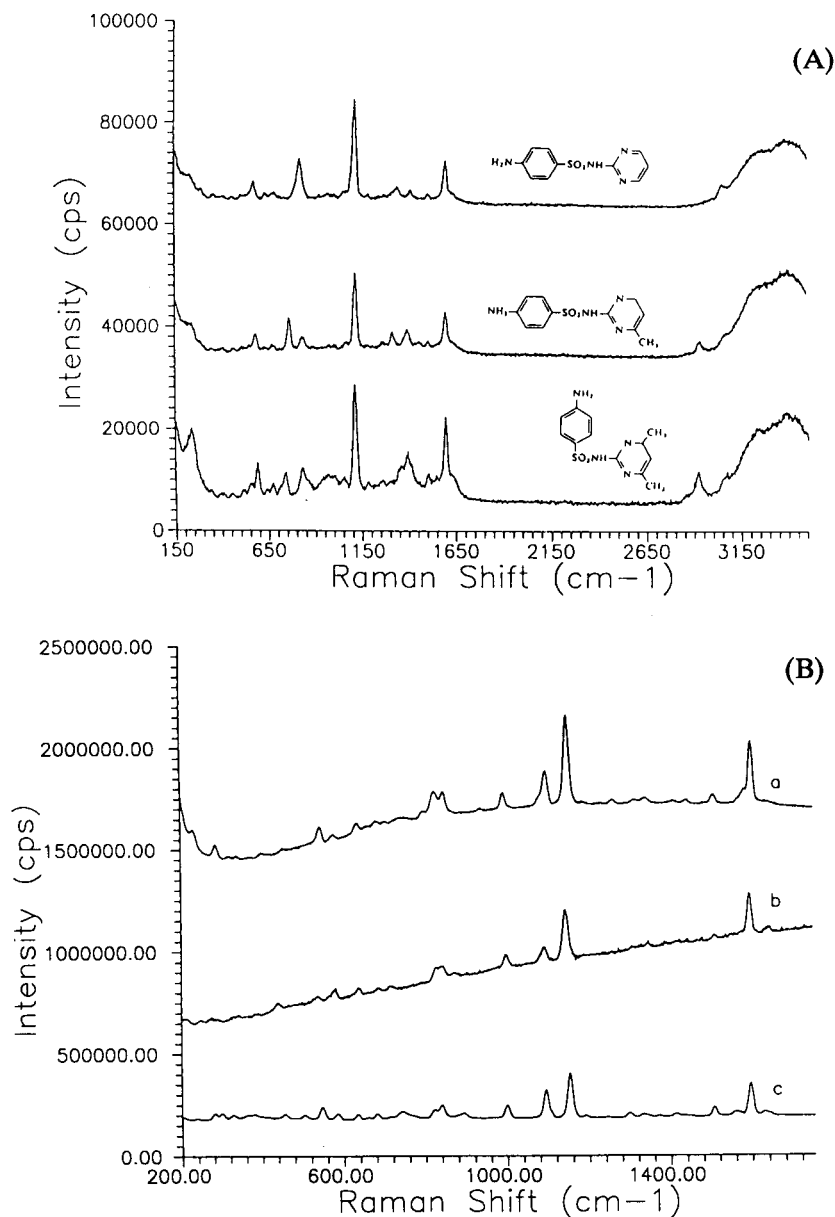


Fig. 7. (A) SER spectra of sulphadiazine (top), sulphamerazine (middle), and sulphamethazine (bottom) on colloidal silver. (B) Unenhanced, conventional Raman spectra of the sulpha drugs (crystalline, pure compounds): (a) sulphadiazine; (b) sulphamerazine; (c) sulphamethazine. (Reprinted with permission from [45]. Copyright ACS, 1990.)



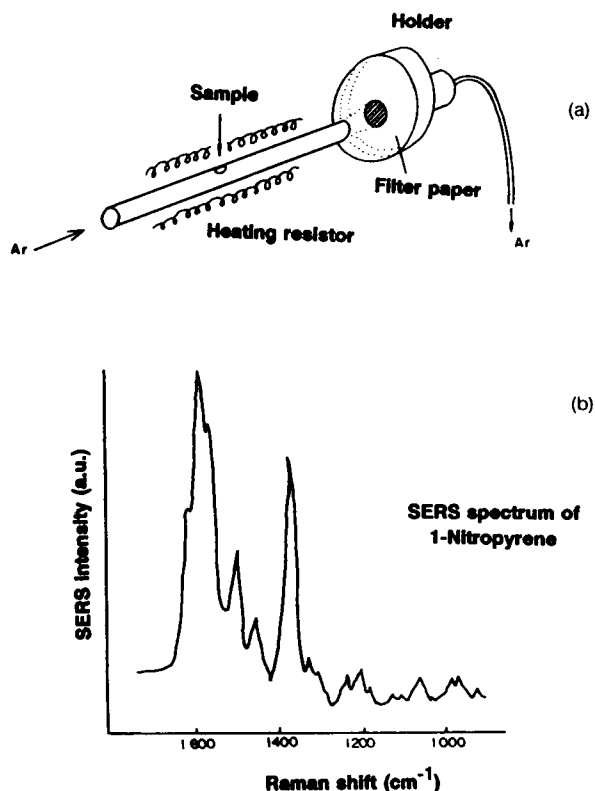


Fig. 8. (a) Set-up used for sampling gas-phase 1-nitropyrene on a silver-coated filter-paper. (b) SER spectrum of 1-nitropyrene sampled with this set-up.

carcinogenicity. Major sources of hydrocarbons in air are the evaporation of solvents and fuels and the partial combustion of fuels. In particular, diesel-engined road vehicles have been found to produce emissions of nitrohydrocarbons. To check for the possible use of SERS in the sampling and determination of these compounds, the device shown in Fig. 8 was used [49]. The source of gas-phase 1-nitropyrene was a ceramic cylinder placed inside a heating oven. The sample, in the form of methanol solution, was placed in the tube through an inlet orifice with the aid of a microsyringe and then evaporated at 300°C for 30 s. The tube was flushed with argon on one side and connected to a high-volume sampler on the other. To trap the evaporated 1-nitropyrene, the sampler contained a silver-coated filter paper. After 30-s exposure to the argon stream, the SERS substrate was removed from the sampler and

examined on a Raman spectrometer. The SER spectrum is shown in Fig. 8. The spectrum is characterized by well defined and resolved bands, the most intense occurring at 1370 and 1570  $\text{cm}^{-1}$ . The SER spectrum agrees fairly well with that published for the same compound under ordinary sampling conditions using the same substrate [50] and silver-coated prolate posts [28].

The analysis of mixtures by SERS has been approached by the use of silver-coated alumina supports [24], silver particles on stochastic-post substrates [51], silver-coated filter-papers [50] and colloidal silver [44,52]. Unlike other spectroscopic techniques in which the spectra of mixtures can be constructed of weighted averages of spectral features of the individual compounds, multi-component SER spectra show a definite dependence on selective molecular adsorption on the metal surface. Figure 9 shows the SER spectra on colloidal silver of two banned drugs in sport, acebutolol (a  $\beta$ -blocking agent) and amiloride (a diuretic drug) at 25  $\mu\text{g ml}^{-1}$  each [53]. The spectrum of a mixture of the two drugs at a concentration ratio of 1:1 is also shown. Amiloride completely dominates the spectrum of the mixture, with no traces of the spectrum of acebutolol, that is, amiloride is readily adsorbed on the silver colloidal particles, causing a displacement of acebutolol from the surface. The results indicate that the drugs are adsorbed selectively on the surface depending on their chemical structure. For the simultaneous determination of components in mixtures selective adsorption can be a limitation and an appropriate separation step would be required prior to SERS analysis. Combined liquid chromatography–SERS provides a suitable approach, although it has not been fully developed (see below).

#### QUANTITATIVE ANALYSIS BY SERS

The signal expression for the SERS intensity in photoelectron counts  $\text{s}^{-1}$  integrated over a specified SERS-active vibration,  $\omega_s$ , is given by [54]

$$I_t = NA\Omega \frac{d\sigma}{d\Omega} E^2 (h\omega)^{-1} P_0 Q T_m T_0 \quad (1)$$

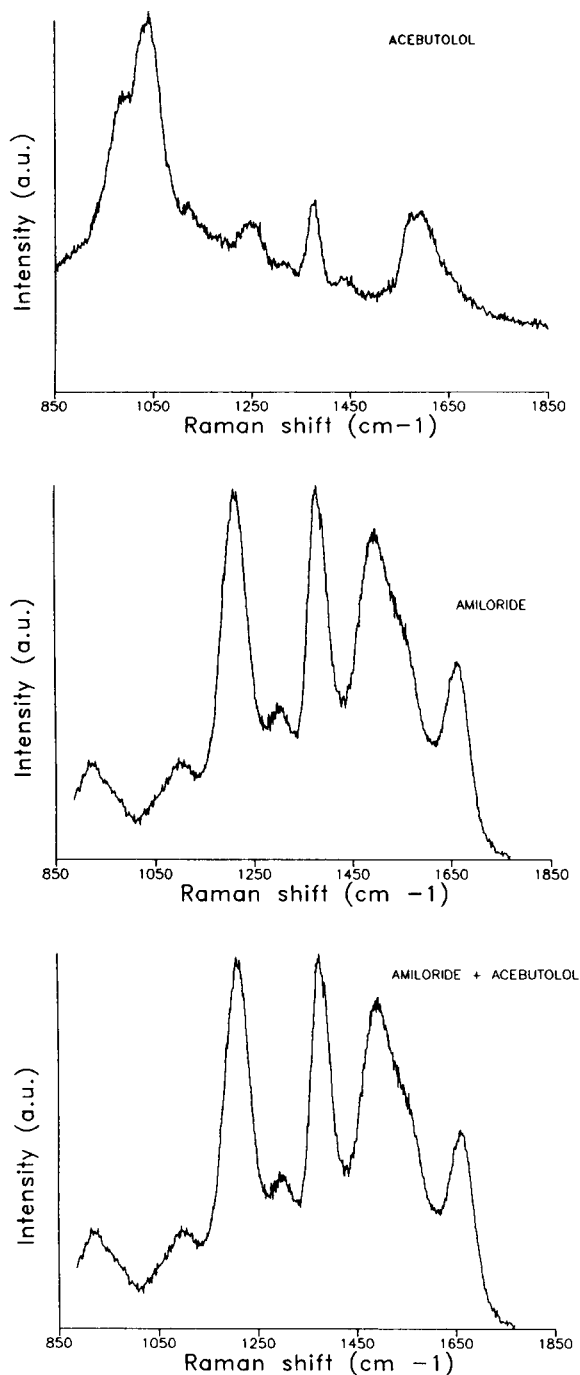


Fig. 9. SER spectra on colloidal silver of acebutolol, amiloride and a mixture of the two at a concentration ratio of 1:1.

where  $N$  is the adsorbate number density (molecules  $\text{cm}^{-2}$ ),  $A$  is the surface area illuminated by the laser beam ( $\text{cm}^2$ ),  $\Omega$  is the solid angle of the collection optics (sr),  $d\sigma/d\Omega$  is the differential Raman scattering cross-section ( $\text{cm}^{-2}$  molecule $^{-1}$  sr $^{-1}$ ),  $E^2 = L(\omega)^2 L(\omega_s)^2$  is the electromagnetic surface-averaged enhancement factor for the excitation and scattering frequencies,  $h\omega$  is the energy of the incident laser photon (J),  $P_0$  is the incident laser beam irradiance ( $\text{W cm}^{-2}$ ) and  $QT_m T_0$  is the product of the detector quantum efficiency, throughput of the dispersion system and transmittance of the collection optics. Equation 1 predicts a linear relationship between intensity and concentration, and indicates that the signal can be increased by improving instrumental factors ( $\Omega$ ,  $QT_m T_0$ ). The linearity of SERS with concentration has been verified experimentally for electrodes, solid substrates and metal colloids. The range of linear response covers 2–3 concentration decades. Higher concentrations tend to produce a flat response, which has been ascribed to saturation of the limited number of active sites on the substrate [55,56].

Equation 1 also predicts that the intensity should scale with the incident laser power. However, the ultimate sensitivity in SERS is limited by the surface damage threshold of the substrate with respect to  $P_0$ . The situation is particularly troublesome for solid substrates where long exposure times to the laser source may lead to substrate destruction. Figure 10 shows the effect of irradiation time on the SER spectrum of acridine on a silver-coated filter-paper [29]. On irradiation the spectrum changes, the structure being completely lost after 45 min. It has not been determined whether this damage process is thermal or photochemical, but it may be due to destruction of the micromorphology of the substrate on irradiation or to induced molecular desorption and decomposition, or both. Metal hydrosols are much more resistant to damage than solid substrates. The continuous renewal of colloid particles in the laser beam by Brownian motion allows much longer exposure times and laser powers to be used. Unfortunately, the dynamic character of aggregation in colloidal systems, and consequently of the SERS intensity, makes careful

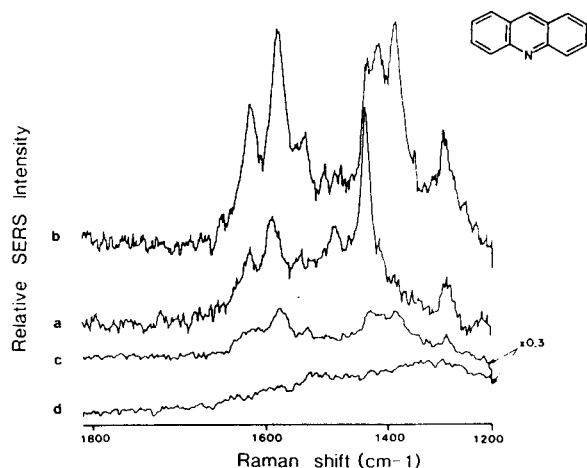


Fig. 10. Effect of laser irradiation on the SER spectrum of acridine (190 ng) on a silver-coated filter-paper. Irradiation time: (a) 0; (b) 10; (c) 22; (d) 45 min.

timing of the measurement process in these substrates essential.

Quantitative analytical applications of SERS are often compromised by the experimental difficulties in measuring intensities with a precision comparable to that in state-of-the-art spectrochemical techniques. Several factors, both substrate and adsorbate dependent, contribute to the poor reproducibility of SERS signals. First, the polydispersity in solid substrates [57] and the different degrees of aggregation and particle sizes in metal colloids [58] have been identified as potential sources of differences in enhancement factors. Second, inhomogeneities in the distribution of molecules at the metal surface, their several possible orientations and various adsorption energies also contribute to the observed reproducibilities [50]. Temperature, pH, ageing of solutions and laboratory practices should be carefully controlled [59,60]. Under ordinary sampling conditions, the precision expected from a SERS experiment is typically 15–20% [relative standard deviation (R.S.D.)]. This number may be compatible with many practical analytical situations, and it can be improved for colloidal substrates by about an order of magnitude by processing both colloids and samples in continuous-flow sampling configurations (see below).

Most Raman studies are conducted on single-beam instruments, so the use of internal standards for quantitative purposes is widely implemented in Raman spectrometry. However, the use of internal standard methods in SERS is at a first glance difficult to implement, for a number of reasons. In addition to the common requirements for a regular internal standard, the candidate molecule should experience the SERS effect when adsorbed on the metal surface. The presence of a limited number of SERS-active sites on the substrate may result in decreased dynamic ranges when both the analyte and the standard compete for the substrate [50]. In addition, selective molecular adsorption may cause great difficulties in the selection of an adequate internal standard.

It should be stressed that depending on the substrate used and on the adsorbate species, changes in the amplitude of SER spectral features with concentration may take place. Figure 11 shows the SER spectra of sulphamerazine on colloidal silver at different drug concentrations [45]. As shown, at lower concentrations the SER spectral features are poorly defined. Also, some vibrational modes grow at a different rate to other modes with increasing concentration. For instance, at low concentrations ( $< 10 \text{ ng ml}^{-1}$ ) the mode at  $1630 \text{ cm}^{-1}$  is more intense than that at

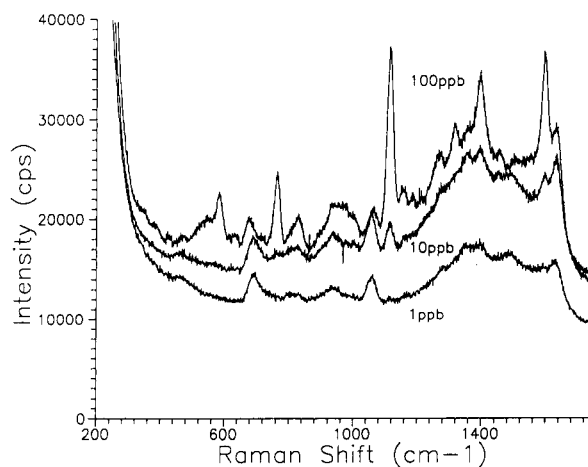


Fig. 11. SER spectra of sulphamerazine obtained at different drug concentrations. (Reprinted with permission from [45]. Copyright ACS, 1990.)

1594  $\text{cm}^{-1}$ . These differences in spectral features may be ascribed to changes in the orientation of the adsorbate at the metal surface as the analyte concentration changes. Although reorientation effects may complicate spectral interpretation, they can provide useful information on structure and activity at solid interfaces. The phenomenon is not general, however. For propranolol on colloidal silver, the intensity distribution of the several vibrational modes is essentially constant from the limit of detection ( $0.1 \mu\text{g ml}^{-1}$ ) to  $25 \mu\text{g ml}^{-1}$  [53]. The choice of the Raman frequency for quantitative monitoring may be of relevance when reorientation effects take place. Several figures of merit of the analytical method may be involved, including the dynamic range, the sensitivity (calibration slope) and the limit of detection [45]. Hence care must be exercised when selecting the vibrational mode, which must be evaluated for each particular analyte.

The limits of detection (LOD) in SERS are several orders of magnitude lower than those in conventional Raman spectrometry and far better than those in infrared spectrometry. Some typical values are given in Table 1. Most reported data refer to silver substrates on a variety of active forms. Absolute limits of detection in the low

nanogram range seem to be typical in solid substrates. When using silver colloids, most LODs are about  $10^{-9}$  M or at the  $\text{ng ml}^{-1}$  level. When the surface-enhanced optical effect is combined with an optical resonance in the adsorbate (surface-enhanced resonance Raman scattering, SERRS), the LODs are even improved. The LOD for rhodamine 6G is reported to be  $5 \times 10^{-12}$  M by SERRS [61]. As an example of the extreme detection power provided by SERS, 9-aminoacridine was deposited on a filter membrane coated with chemically reduced silver. The sample was then examined in a Raman microprobe set-up [19]. The lowest point in the calibration graph represented an absolute amount of 9-aminoacridine added to the substrate of only 60 pg. Although this value itself is an outstanding figure of merit, it is interesting to calculate the number of analyte molecules providing the SERS signal actually being measured. Assuming that the adsorbate spreads equally over the 2-mm diameter sample spot on the substrate, with a  $2\text{-}\mu\text{m}$  diameter laser beam, only one millionth of the applied sample is being observed, i.e., about 0.3 amol or  $1.9 \times 10^5$  9-aminoacridine molecules. It should be noted that this value corresponds to a measured sample, and it is not based on extrap-

TABLE 1  
Limits of detection for various analytes by SERS

Analyte	Substrate	Limit of detection	Ref.
4,4'-Bipyridine	Ag-coated frosted glass slide	$1 \times 10^{-7}$ M	61
Rhodamine 6G	Ag-coated frosted glass slide	$5 \times 10^{-12}$ M	61
<i>p</i> -Aminobenzoic acid	Silver colloid	$0.5 \mu\text{g ml}^{-1}$ (35 ng)	43
	Silver colloid	30 ng	62
Dopamine	Silver electrode	$3 \times 10^{-7}$ M	35
Carbazole	Silver-coated latex spheres on filter-paper	0.2 ng	55
1-Aminopyrene	Silver-coated latex spheres on filter-paper	1.4 ng	55
Pyridine	Silver electrode	8.5 pg	23
Crystal Violet	Silver colloid on filter-paper	500 pg	63
	Silver colloid	$3 \times 10^{-11}$ M	56
Anthracene	Silver-coated fumed silica	18 ng	64
Phthalic acid	Silver-coated fumed silica	17 ng	64
Terephthalic acid	Silver-coated alumina	$24 \text{ ng ml}^{-1}$	24
Pyrene	Silver-coated alumina	2 pg	65
1-Nitropyrene	Silver-coated filter-paper	1 pg	50
9-Aminoacridine	Silver-coated filter membrane	0.3 amol	19
Sulphadiazine	Colloidal silver	$1 \text{ ng ml}^{-1}$	45

olation as in the case of LOD values. It is extraordinary that a Raman experiment could ever provide a quantitatively tractable signal for such a low number density of scatterers.

#### SERS IN FLOWING STREAMS: FLOW-INJECTION AND LIQUID CHROMATOGRAPHIC APPLICATIONS

As described above, one of the weakest points of SERS is the poor precision exhibited by the scattered intensity. This problem has been partially solved for hydrosol substrates by processing both the adsorbate solution and the colloid in a semiautomatic system such as that used in flow-injection analysis [66,67]. An R.S.D. of 3% was reported for replicate injections of *p*-aminobenzoic acid into a stream containing colloidal silver prepared on-line at room temperature. After these reports, other applications of colloid SERS with flowing systems have been described using colloidal silver [41,62,68–70] and silver electrodes [71,72]. The separation and determination of four purine bases (adenine, guanine, hypoxanthine and xanthine) by reversed-phase liquid chromatography in combination with real-time SERS has been demonstrated [73]. Limits of detection in the nanomole range were reported.

For colloidal dispersions in flowing streams, problems associated with clogging of the tubing by silver aggregates and memory effects caused by adsorption on the flow cell walls were observed. These problems can be solved by using an open-flow cell as shown in Fig. 12 [74]. A flow-injection system with two peristaltic pumps permitted the analyte and colloid to flow to a chromatographic mixing T. The windowless flow cell consists of a droplet of mixed solution (aggregated colloid) supported by surface tension between the metal tubing tip and a metal pedestal. SERS is observed at 90° to the excitation beam. The SER spectrum of triamterene (a diuretic drug) obtained by flowing the analyte solution continuously through the system is shown in Fig. 13. The peaks for five consecutive injections of 25  $\mu\text{g ml}^{-1}$  triamterene monitored at 1357  $\text{cm}^{-1}$  are also shown. The R.S.D. for the peak heights (corrected for the baseline) is 1%. Restoration of

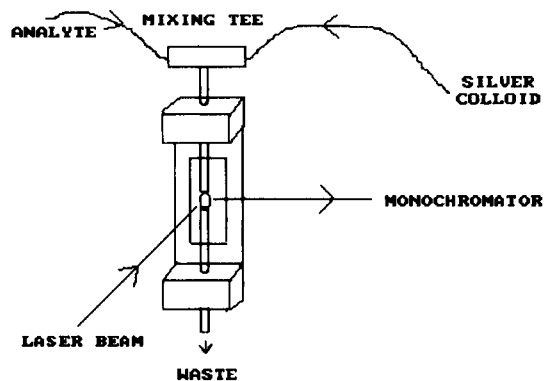


Fig. 12. Windowless flow cell for SERS with flowing streams containing colloidal silver.

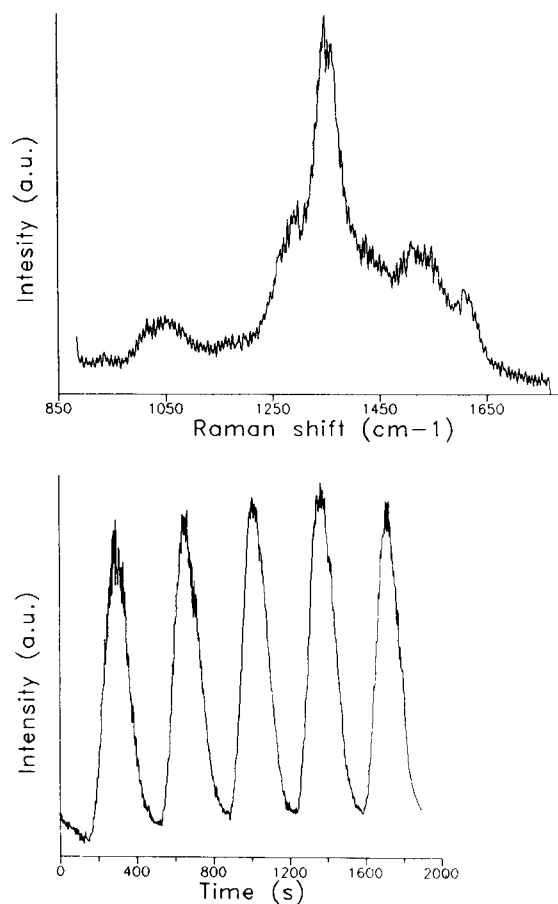


Fig. 13. (Top) SER spectrum of triamterene using the windowless flow cell in Fig. 12. (Bottom) SERS peaks at 1357  $\text{cm}^{-1}$  obtained by replicate injection of 25  $\mu\text{g ml}^{-1}$  triamterene into a flow containing colloidal silver.

the baseline is satisfactory with no drifts characteristic of memory effects.

### Conclusions

SERS provides information on molecular identity at trace concentration levels. The spectral resolution is only slightly inferior to that in CRS and the spatial resolution is comparable to that in techniques of surface analysis. Although some methods of substrate preparation can be demanding, the sampling flexibility is satisfactory. SERS is not as general an analytical tool as other spectroscopic techniques such as mass spectrometry. From a problem-solving standpoint, SERS is not well developed at present. Much work needs to be done on the applicability of this approach to real samples. The development of standardized SERS-active surfaces on a routine basis to become more reproducible and more easily prepared will expand analytical applications, so as to spread the use of this spectroscopic tool among practising analytical scientists.

The research described here is the product of much devoted work by a number of excellent students and postdoctoral associates, including Dr. A. Rupérez, Dr. R. Montes, L.M. Cabalín, N. Calvo and C. Contreras. The author expresses his sincere appreciation to Professor J.D. Winefordner and his students, whose names are cited in the appropriate references. This research on SERS techniques was supported in part by the Dirección General de Investigación Científica y Técnica (Ministerio de Educación y Ciencia, Madrid, Projects PB87-0715 and PB90-0814) and by the Dirección General de Universidades e Investigación (Consejería de Educación y Ciencia, Junta de Andalucía, Seville), Spain.

### REFERENCES

- 1 H. Metiu, *Prog. Surf. Sci.*, 17 (1984) 153.
- 2 J.I. Gersten and A. Nitzan, *Surf. Sci.*, 158 (1985) 165.
- 3 R.K. Chang and T.E. Furtak (Eds.), *Surface Enhanced Raman Scattering*, Plenum, New York, 1982.
- 4 R.K. Chang, *Ber. Bunsenges. Phys. Chem.*, 91 (1987) 296.
- 5 D.B. Chase and B.A. Parkinson, *Appl. Spectrosc.*, 42 (1988) 1186.
- 6 S.M. Angel, L.F. Latz, D.D. Archibald, L.T. Lin and D.E. Honigs, *Appl. Spectrosc.*, 42 (1988) 1327.
- 7 M. Kerker, *Acc. Chem. Res.*, 17 (1984) 271.
- 8 G. Ritchie and C.Y. Chen, *Pure Appl. Chem.*, 52 (1980) 361.
- 9 C.Y. Chen, I. Davoli, G. Ritchie and E. Burstein, *Surf. Sci.*, 101 (1980) 363.
- 10 J.A. Creighton, in R.K. Chang and T.E. Furtak (Eds.), *Surface Enhanced Raman Scattering*, Plenum, New York, 1982, p. 315.
- 11 Y. Wang and R.L. McCreery, *Anal. Chem.*, 61 (1989) 2647.
- 12 Y.W. Alsmeyer and R.L. McCreery, *Anal. Chem.*, 63 (1991) 1289.
- 13 J.J. Laserna and R. Montes, *Spectrosc. Int.*, 3 (1991) 32; *Spectroscopy*, 6 (1991) 34.
- 14 J.J. Laserna, L.M. Cabalín and R. Montes, *Anal. Chem.*, 64 (1992) 2006.
- 15 R. Montes, C. Contreras, A. Rupérez and J.J. Laserna, *Anal. Chem.*, 64 (1992) 2715.
- 16 H. Ishida and A. Ishitani, *Appl. Spectrosc.*, 37 (1983) 450.
- 17 D.M. Hembree, J.C. Oswald and N.R. Smyrl, *Appl. Spectrosc.*, 41 (1987) 267.
- 18 M.L. McGlashen, U. Guhathakurta, K.L. Davis and M.D. Morris, *Appl. Spectrosc.*, 45 (1991) 543.
- 19 J.J. Laserna, W.S. Sutherland and J.D. Winefordner, *Anal. Chim. Acta*, 237 (1990) 439.
- 20 H. Seki, *J. Electron. Spectrosc. Relat. Phenom.*, 39 (1986) 289.
- 21 L.M. Siperko, *Appl. Spectrosc.*, 43 (1989) 226.
- 22 H. Ishida, H. Fukuda, G. Katagiri and A. Ishitani, *Appl. Spectrosc.*, 40 (1986) 322.
- 23 M.M. Carrabba, R.B. Edmonds and R.D. Rauh, *Anal. Chem.*, 59 (1987) 2559.
- 24 J.M. Bello, D.L. Stokes and T. Vo-Dinh, *Anal. Chem.*, 62 (1990) 1349.
- 25 G. Xue and J. Zhang, *Appl. Spectrosc.*, 45 (1991) 760.
- 26 C. Jennings, R. Aroca, A.M. Hor and R.O. Loutfy, *Anal. Chem.*, 56 (1984) 2033.
- 27 E.S. Brandt, *Anal. Chem.*, 61 (1989) 391.
- 28 P.D. Enlow, M. Buncick, R.J. Warmack and T. Vo-Dinh, *Anal. Chem.*, 58 (1986) 1119.
- 29 J.J. Laserna, A.D. Campiglia and J.D. Winefordner, *Anal. Chim. Acta*, (1988) 21.
- 30 A.M. Alak and T. Vo-Dinh, *Anal. Chem.*, 59 (1987) 2149.
- 31 S.M. Angel and M.L. Myrick, *Anal. Chem.*, 61 (1989) 1648.
- 32 K. Carron, K. Mullen, M. Lanouette and H. Angersbach, *Appl. Spectrosc.*, 45 (1991) 420.
- 33 F. Ni and T.M. Cotton, *Anal. Chem.*, 61 (1989) 888.
- 34 K.I. Mullen, D. Wang, L.G. Crane and K.T. Carron, *Anal. Chem.*, 64 (1992) 930.
- 35 N.S. Lee, Y.Z. Hsieh, R.F. Paisley and M.D. Morris, *Anal. Chem.*, 60 (1988) 442.
- 36 M.L. McGlashen, K.L. Davis and M.D. Morris, *Anal. Chem.*, 62 (1990) 846.
- 37 S. Nie, C.G. Castillo, K.L. Bergbauer, J.F.R. Kuck, I.R. Nabiev and N.T. Yu, *Appl. Spectrosc.*, 44 (1990) 571.

- 38 I.R. Navieb, V.A. Savchenko and E.S. Efremov, *J. Raman Spectrosc.*, 14 (1983) 375.
- 39 T.M. Herne, A.M. Ahern and R.L. Garrell, *Anal. Chim. Acta*, 246 (1991) 75.
- 40 E. Koglin and J.M. Sèquaris, *Top. Curr. Chem.*, 134 (1986) 1.
- 41 F. Ni, R. Sheng and T.M. Cotton, *Anal. Chem.*, 62 (1990) 1958.
- 42 T. Vo-Dinh, M. Uziel and A.L. Morrison, *Appl. Spectrosc.*, 41 (1987) 605.
- 43 E.L. Torres and J.D. Winefordner, *Anal. Chem.*, 59 (1987) 1626.
- 44 A. Rupérez, R. Montes and J.J. Laserna, *Vib. Spectrosc.*, 2 (1991) 145.
- 45 W.S. Sutherland, J.J. Laserna, M.J. Angebrannt and J.D. Winefordner, *Anal. Chem.*, 62 (1990) 689.
- 46 R. Montes and J.J. Laserna, *Analyst*, 115 (1990) 1601.
- 47 V.M. Hallmak and A. Campion, *J. Chem. Phys.*, 84 (1986) 2942.
- 48 V.M. Hallmak and A. Campion, *J. Chem. Phys.*, 84 (1986) 2933.
- 49 J.J. Laserna, *Quim. Anal.*, 8 (1989) 321.
- 50 J.J. Laserna, A.D. Campiglia and J.D. Winefordner, *Anal. Chem.*, 61 (1989) 1697.
- 51 T. Vo-Dinh, M. Meier and A. Wokaum, *Anal. Chim. Acta*, 181 (1986) 139.
- 52 J. Thornton and R.K. Forcé, *Appl. Spectrosc.*, 45 (1991) 1522.
- 53 A. Rupérez, L.M. Cabalín and J.J. Laserna, in J. Menon (Ed.), *Trends in Applied Spectroscopy*, Council of Scientific Research, Trivandrum, in press.
- 54 R.P. Van Duyne, K.L. Haller and R.L. Altkorn, *Chem. Phys. Lett.*, 126 (1986) 190.
- 55 T. Vo-Dinh, M.Y.K. Hiromoto, G.M. Begun and R.L. Moody, *Anal. Chem.*, 56 (1984) 1667.
- 56 R.S. Sheng, L. Zhu and M.D. Morris, *Anal. Chem.*, 58 (1986) 1116.
- 57 J.I. Gersten and A. Nitzan, in R.K. Chang and T.E. Furtak (Eds.), *Surface Enhanced Raman Scattering*, Plenum, New York, 1982, p. 89.
- 58 M. Kerker, D.S. Wang, H. Chew, O. Siiman and L.A. Bumm, in R.K. Chang and T.E. Furtak (Eds.), *Surface Enhanced Raman Scattering*, Plenum, New York, 1982, p. 109.
- 59 T.M. Herne and R.L. Garrell, *Anal. Chem.*, 63 (1991) 2290.
- 60 J.J. Laserna, E.L. Torres and J.D. Winefordner, *Anal. Chim. Acta*, 200 (1987) 469.
- 61 F. Ni and T.M. Cotton, *Anal. Chem.*, 58 (1986) 3159.
- 62 J.J. Laserna, A. Berthod and J.D. Winefordner, *Microchem. J.*, 38 (1988) 125.
- 63 C.D. Tran, *Anal. Chem.*, 56 (1984) 824.
- 64 A.M. Alak and T. Vo-Dinh, *Anal. Chem.*, 61 (1989) 656.
- 65 J.M. Bello, D.L. Stokes and T. Vo-Dinh, *Appl. Spectrosc.*, 43 (1989) 1325.
- 66 J.J. Laserna, A. Berthod and J.D. Winefordner, *Talanta*, 34 (1987) 745.
- 67 A. Berthod, J.J. Laserna and J.D. Winefordner, *Appl. Spectrosc.*, 41 (1987) 1137.
- 68 R.D. Freeman, R.M. Hammaker, C.E. Meloan and W.G. Fateley, *Appl. Spectrosc.*, 42 (1988) 456.
- 69 G.T. Taylor, S.K. Sharma and K. Mohanan, *Appl. Spectrosc.*, 44 (1990) 635.
- 70 V.L. Schlegel and T.M. Cotton, *Anal. Chem.*, 63 (1991) 241.
- 71 R.K. Forcé, *Anal. Chem.*, 60 (1988) 1987.
- 72 N.J. Pothier and R.K. Forcé, *Anal. Chem.*, 62 (1990) 678.
- 73 R. Sheng, F. Ni and T.M. Cotton, *Anal. Chem.*, 63 (1991) 437.
- 74 L.M. Cabalín, A. Rupérez and J.J. Laserna, *Talanta*, 40 (1993) in press.

# Analytical characteristics, applications and perspectives in thermal lens spectrometry

Guillermo Ramis-Ramos

*Department of Analytical Chemistry, Faculty of Chemistry, University of Valencia, 46100 Burjassot (Valencia) (Spain)*

(Received 8th September 1992; revised manuscript received 3rd November 1992)

## Abstract

The following selected aspects of thermal lens spectrometry are briefly outlined: fundamentals, sensitivity and background noise, detection approaches, flowing samples, multi-wavelength experiments, thermal lens circular dichroism, associated colateral phenomena and physico-chemical applications and requirements of analytical procedures. The state-of-the-art and problems encountered are discussed.

*Keywords:* UV-Visible spectrophotometry; Thermal lens

Thermal lens spectrometry (TLS) is an extremely sensitive absorptiometric technique. From the analytical viewpoint, other interesting properties are the possibility of reaching very low limits of detection (LODs), the capability of making measurements on microsamples and the expanded dynamic range in comparison with spectrophotometry.

The thermal lens effect was described in the mid-1960s [1,2]; however, significant analytical developments of the technique were not produced until the late 1970s and early 1980s, with a series of papers from the groups of Harris and Dovichi [3,17–20,22–24] and Ishibashi [4,21,25]. Several revisions have been published [3–11], including an exhaustive review by Dovichi [7].

Several mathematical models describing the thermal lens effect have been developed [12–16], and a wide variety of instruments, including single- and dual-cell configurations to perform differential measurements [17–36], single- and mul-

ti-wavelength designs and scanning instruments [37–42] have been described. To improve the signal-to-noise (S/N) ratio, several detection modes and devices have been tried [43–47]. The use of TLS as a detection technique for flowing samples, including flow injection (FI) and liquid chromatography (LC) [48–65], has also been investigated.

New and exciting advances have continued to be produced in recent years, including the development of photothermal circular dichroism [66–68] and research on colateral phenomena and physico-chemical applications [69–78]. Finally, a number of non-chromatographic [79–90] and chromatographic [91–93] analytical applications have been described. Only a few selected topics will be discussed here.

## THE PRINCIPLE OF THERMAL LENS SPECTROMETRY

Thermal lens spectrometry is based on the optical measurement of the thermal gradient generated by absorption of a laser beam. The fre-

*Correspondence to:* G. Ramis-Ramos, Department of Analytical Chemistry, Faculty of Chemistry, University of Valencia, 46100 Burjassot (Valencia) (Spain).



quently used pump–probe coaxial configuration is shown schematically in Fig. 1. Two laser beams are used. The pump beam should be absorbed by the analyte. The thermal gradient is generated by thermal relaxation of the absorbed energy. The gradient is maximized by focusing the pump beam at the sample location.

The intensity of the thermal effect can be measured using a probe beam that is focused at some distance from the sample, thus reaching the sample location with some divergence. In the design in Fig. 1, the thermal gradient causes the divergence of the probe beam to increase. The decrease in intensity at the centre of the probe beam in the far field is proportional to the concentration of the absorbing species.

A complete set-up is shown in Fig. 2. In this instrument, an argon ion laser and a helium–neon laser are used as pump and probe, respectively. Modulation of the pump beam with a chopper gives rise to the alternate formation and dissipation of the gradient. This causes the probe beam divergence to decrease and to increase within a pump cycle. An a.c. signal is generated at the detector. The amplitude of this a.c. signal is also proportional to the concentration of the absorbing species. The TLS signal can be demodulated with a lock-in amplifier, or with a computer, but in the latter instance data acquisition and data treatment periods should be alternated, which makes data throughput slower.

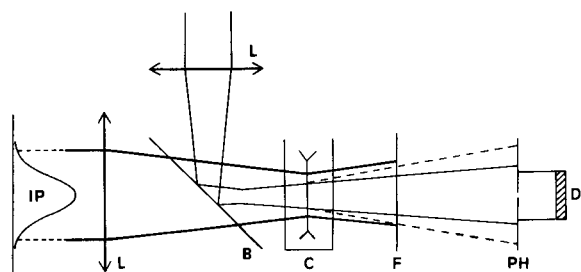


Fig. 1. Working principle of a dual-laser pump–probe coaxial thermal lens spectrometer. IP = intensity profile of the pump beam; L = lens; B = beamsplitter; C = cell; F = filter; PH = pinhole, slit or mask; D = photodiode detector. The diameters of the beams have been greatly exaggerated.

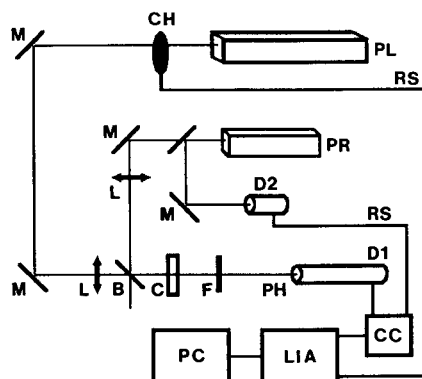


Fig. 2. Scheme of a dual-laser pump–probe coaxial thermal lens spectrometer. CH = chopper; PL = pump laser head; RS = reference signal; PR = probe laser head; D2 = reference detector; D1 = thermal lens signal detector; CC = signal conditioning circuit; LIA = lock-in amplifier; PC = computer; other components as in Fig. 1.

#### SENSITIVITY

The relative change in the beam centre intensity in the far field,  $\Delta I/I$ , is given by

$$\frac{\Delta I}{I} = \frac{1.206PA(-dn/dT)}{\lambda k} \quad (1)$$

where  $P$  and  $\lambda$  are the power and the wavelength of the pump beam, and  $A$ ,  $dn/dT$  and  $k$  are the absorbance, the temperature coefficient of the refractive index and the thermal conductivity of the sample, respectively. Therefore, the sensitivity of thermal lens measurements can be increased by modifying both the pump beam and the sample medium characteristics.

In TLS, the sensitivity is easily increased by using a higher pump power, or by pumping in the UV or the blue visible regions rather than in the infrared. Very high sensitivities are obtained using solvents with good thermo-optical properties, i.e., with a large temperature coefficient of the refractive index and a low thermal conductivity. In particular, the temperature coefficient of the refractive index can be greatly varied by changing the solvent composition.

Water deserves more attention. At 4°C the temperature coefficient of water is zero, which reduces the TLS sensitivity to zero. At 20°C the sensitivity is still low, and it increases by a factor

of about four from 20 to 80°C. The sensitivity can be improved in a factor of about two by adding electrolytes [74], and by larger factors by using mixtures of water with other solvents [7]. In addition, the background noise in water is relatively low, which makes water an acceptable solvent for TLS.

#### BACKGROUND NOISE

It should be kept in mind that, in comparison with spectrophotometry, the main advantage of TLS is the possibility of reaching much lower LODs, and that a low LOD is a consequence of both high sensitivity and low background noise. Frequently, the background noise is also increased when the sensitivity is increased, e.g., by using a higher pump power, or by adding methanol to an aqueous sample. The relationships among the background noise in TLS and the physical properties of the solvent have not been sufficiently studied.

There are two main sources of background noise in TLS, i.e., stability of the lasers and thermal convection. The stability of a powerful continuous-wave (cw) laser is usually very good. Instead, poorly stabilized helium–neon lasers are frequently used as the source of the probe beam. However, the noise produced by the probe beam instability is efficiently filtered out by measuring the TLS signal in a relative form, as indicated in Eqn. 1. This makes the background noise level very low, unless thermal convection is present.

The convective movements of the liquid in the thermal gradient region can be observed by adding a small amount of silica particles and by projecting the beams on a screen. When a long optical path length cell is used (e.g., 1 cm), a strong stream crosses through the thermal gradient from bottom to top, generating alternate layers of clockwise and counter-clockwise whirls around the central vertical axis (Fig. 3) [47]. In a short optical path length cell (e.g., 1 mm), friction on the optical walls hinders whirl formation, and the whole mass of liquid is dragged upwards in the beam region and descends again near the lateral walls of the cell.

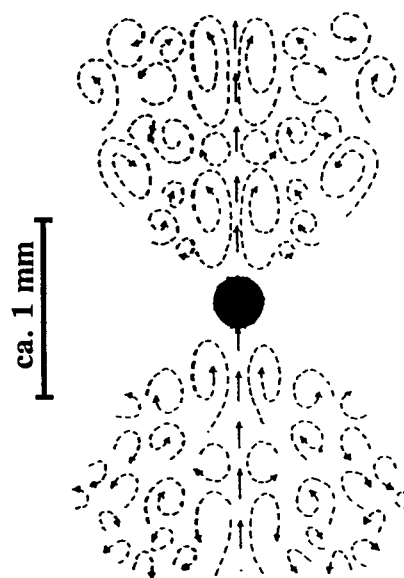


Fig. 3. Scheme of the convective movements in the thermal gradient region. The pump beam was focused at the centre of a standard 1-cm cell. The black circle represents the pump beam profile, the arrows indicate the location of the strongest liquid stream and the dotted lines are whirls.

Convective noise can be attributed to changes in temperature, intensity and direction of this stream. The associated local variations of the refractive index cause the probe beam to undergo deformations and irregular direction changes. In addition, thermal convection should play an important role in dissipating the gradient. This gives rise to the question of how TLS would apply in microgravity conditions. Convective noise would probably be negligible; however, dissipation of the gradient (which is necessary to perform new measurements) would probably be much slower than in normal gravity.

Thermal convection can be reduced and, in favourable situations, it should not be the predominant source of noise. First, thermal convection is reduced when the TLS signal decreases. This is of extreme importance when a blank is repeatedly measured to calculate an LOD. If the absorbance of the blank is very low, thermal convection can be negligible, and a very low LOD can be reached. Further, both a high blank and a large LOD lead to an important decrease in the dynamic range, particularly with solvents with

good thermo-optical properties. Therefore, the use of a separation technique such as liquid–solid or liquid–liquid extraction, volatilization or chromatography to reduce the blank signal when a TLS procedure is to be applied to a real sample will frequently be advisable.

In addition, other means of reducing convective noise should be investigated. As indicated above, and as has been suggested [44], the shape of the cell can strongly influence the form and intensity of the convective streams, and therefore it can be effective in making them more regular, thus reducing convective noise. However, a systematic study to optimize the cell shape, including the possible use of vertical optical paths, has not been performed.

Finally, the selection of the solvent and the use of additives to modify some solvent properties should also be investigated as a means of improving the S/N ratio by reducing the background noise rather than by increasing the sensitivity. The absorbance of water and most common organic solvents in the visible region is not negligible, and convective noise is produced, even in the absence of absorbing species other than the solvent itself.

Molar absorptivity of the solvent is extremely low in the case of some aprotic solvents owing the lack of overtones of the hydrogen bonding stretching frequency [7]. Thus, for instance, a solvent with excellent thermo-optical properties with regard to both high sensitivity and low molar absorptivity is carbon tetrachloride. However, a different solvent with poorer thermo-optical properties can be better than carbon tetrachloride if the blank absorbs, producing thermal convection. The following two aspects can be considered. First, for convective noise to be negligible, the absorbance of the blank should be much smaller the better are the thermo-optical properties of the medium. Thus, for instance, an absorbance of  $10^{-7}$  is negligible in water and ethanol, but it causes a large TLS signal in chloroform or in carbon tetrachloride, giving rise to large background noise of convective origin. Second, background noise also depends on other physical properties of the solvent. Thus, the temperature coefficient of density and the viscosity are very

important in producing and in controlling convection, respectively, and, therefore, they probably have a decisive influence on convective noise. Work on this topic is in progress.

#### ADVANCES IN DETECTION TECHNIQUES

In TLS, spatial noise is produced both by laser pointing instability and convective noise. Spatial noise includes changes in the probe beam direction as a whole and deformations of the probe beam profile. Spatial noise can be reduced by appropriate selection of the shape of the sample of the probe beam profile which is allowed to reach the detector, or by processing the acquired information.

In the simplest approach to TLS detection, a pinhole mask is used to take a circular sample at the centre of the beam profile. However, monitoring at a single point is very sensitive to the sources of spatial noise. A simple way of reducing spatial noise is to use a horizontal slit instead of a pinhole mask [47]. Using this approach, the spatial noise is averaged over one dimension. It has been observed that, when convection is the predominant noise source, the direction changes and deformations of the beam profile are produced laterally rather than in a vertical sense. Consequently, this approach leads to a very effective reduction of the spatial noise and, in addition, it has little effect on sensitivity.

Averaging over one dimension can be also performed using photodiode-array detection [43,45,46]. An optical processor sampling regions of the beam profile other than the beam centre, and over two dimensions, is also effective [5]. Acquisition of the entire beam profile using an image detector, e.g., a CCD camera, is also possible. The information acquired over one or two dimensions can be processed and modelled, e.g., using the Fourier transform. More than a tenfold enhancement of the S/N ratio can be achieved [46]. However, image approaches are more complicated and expensive than the use of a single photodiode, and the time required to acquire and treat the signal is much longer. Image detection can be very useful for performing theoretical

studies, including modelling of the TLS signal and the associated noise.

#### FLOWING SAMPLES

When flowing samples are measured, the sensitivity decreases as a consequence of incomplete formation of the gradient, and noise increases owing to flow fluctuations. Therefore, in the presence of flow, the very low LODs obtained with static samples cannot be reached. Several procedures have been proposed to improve the S/N ratio with flowing samples [48–65]. Good results can be obtained by reducing the flow-rate to a low value, just before a peak is to be measured [94].

In the absence of on-line mixing of reagents, flow programming can be very effective in improving the LODs obtained with both LC and flow-injection (FI) techniques. However, it has been observed that the previous mixing of two streams of reagents of different composition, even at low flow-rates, also produces very high noise on the TLS signal, thus making difficult the practical development and use of LC and FI procedures with on-line chromogenic derivatization [65].

Mixing noise gives rise to changes in the direction and profile deformations of the probe beam. A possible cause of mixing noise is the deformation of the thermal gradient. However, independently of the presence of a thermal gradient, the probe beam undergoes deflection if a concentration gradient is present [65,69]. Therefore, another possible cause of the mixing noise is probe beam refraction through the irregularly shaped liquid–liquid interfaces which are present in the heterogeneous mixture.

In a series of experiments, an aqueous stream containing increasing NaCl concentrations was mixed with a stream of water at a T union and the TLS signal of the resulting mixture was measured using 100 mW laser power. High mixing noise was produced when the NaCl concentration was  $10^{-3}$  M or higher. The same level of noise was obtained when the series was repeated either in the presence of a red dye added only to the

NaCl solution or in the absence of pump power. Therefore, it is concluded that, at least when liquids with similar thermo-optical properties are mixed (e.g., aqueous solutions of different composition), the predominant contribution to the mixing noise arises from the presence of irregularly shaped liquid–liquid interfaces in the heterogeneous mixture, rather than from deformations of the thermal gradient [65].

In addition, monitoring of the intensity of a helium–neon laser in the far field constitutes a simple and sensitive procedure to measure the degree of homogeneity of a mixture of solutions in flowing conditions. No changes of background noise were observed when the same series of experiments were performed using spectrophotometric detection with much higher NaCl and dye concentrations. Therefore, in comparison with a laser beam–photodiode set-up, a spectrophotometer is almost blind to the refractive index changes produced in a heterogeneous mixture.

The procedure was applied to evaluate the mixing efficiencies of packed bead mixing reactors. It has been shown that the mixing noise can be reduced to a negligible level by using these devices [65]. However, the use of a sufficiently efficient mixing device can increase the dead volume of the system excessively.

Finally, when solutions containing relatively high reagent concentrations are mixed, it is very difficult if not impossible to match the concentrations reducing their differences below the  $10^{-3}$  M level. Therefore, high mixing noise would be produced when solutions containing concentrated buffers, masking reagents or organic modifiers are mixed prior to an on-line TLS measurement. In this event, the need to insert an efficient mixing device would complicate the manifold. This applies to the mixing of both injected sample and carrier, and merging of different reagent streams. A way of reducing the need for mixing devices is to use the same reagent stock solution (or the same mixed solvent stock solution) to prepare carriers and injected solutions, instead of using different (independently prepared) stock solutions. The necessary modifications to be made with the stock solution common to a sample and to a carrier, or to different carriers, should be

carefully designed to avoid a mismatch with the concentrations of the concentrated reagents.

#### MULTI-WAVELENGTH TLS EXPERIMENTS

The development of multi-wavelength thermal lens spectrometers has increased the selectivity of the technique. Multi-wavelength instruments are based on the sequential pumping of the sample by the different laser lines emitted by an ion gas laser when used in the multi-line mode. Thus, in an instrument designed by Xu and Tran [41], four lines of an argon ion laser were separated by a prism. The four lines were made coaxial again using a mirror and a series of beamsplitters. The spatial separation of the lines between the prism and the beamsplitters made possible individual mechanical shutting of the lines. Up to four absorbing species could be simultaneously determined using this instrument.

An argon ion laser produces up to nine lines of high or moderate intensity within the visible region, and many lines spread all over the visible region can be obtained using a mixed argon–krypton ion laser. However, the instruments based on the spatial separation and individual shutting of the lines have the drawback of being optically and mechanically too complex to be of practical utility. A recent significant advance is the use of an acousto-optic tunable filter (AOFT) to select the laser lines [42]. AOFTs are active dispersive devices. The lines can be sequentially focused on the sample by applying different radiofrequencies to the AOFT. The need to spatially separate the lines and to make them coaxial again is avoided, and moving parts (shutters) are eliminated, thus greatly simplifying the alignment and operation of the instrument.

#### THERMAL LENS CIRCULAR DICHROISM

Thermal lens circular dichroism (TL-CD) is a recent technique in which the differential thermal lens effect produced by left and right circularly polarized (LCP and RCP) laser radiation is mea-

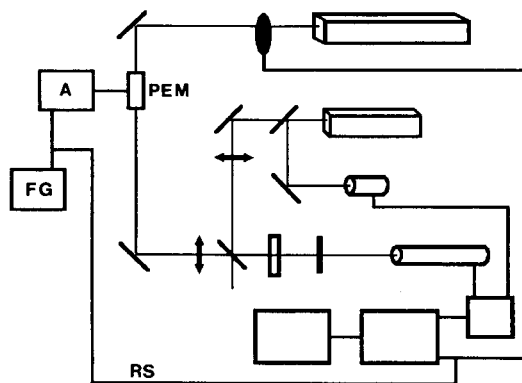


Fig. 4. Conversion of the TLS instrument in Fig. 2 into a TL-CD instrument. A = high-voltage source; PEM = photoelastic modulator; FG = function generator; RS = reference signal; other components as in Fig. 2.

sured. Consequently, in TL-CD the Cotton effect is measured using a photothermal technique rather than the spectrophotometric approach used with conventional dichrographs. This technique has been described and explored by Xu and Tran [66–68] for both static and flowing samples, and it has also been applied to LC detection.

The scheme of a possible instrument is shown in Fig. 4. This instrument was designed on the basis of that shown in Fig. 2 by adding a few elements. Consequently, an advantage is that the same instrument can be used to perform TLS and TL-CD measurements, although operation would be different.

First, a photoelastic modulator or Pockels cell is inserted in the pump beam path. Application of a voltage to the cell causes a delay to be produced on one of the components of the plane polarized beam. By using the appropriate voltages, LCP or RCP laser light can be obtained. In the scheme shown, the Pockels cell operation is controlled by a function generator coupled to a voltage source. Alternate half-periods of LCP and RCP laser light are obtained. As the pump radiation is modulated by the Pockels cell, mechanical chopping of the beam is not needed, and the chopper is set at a permanent open position.

The square wave fed to the Pockels cell is used by the detector system as the timing reference signal.

Both the LCP and RCP laser radiations have the same intensity and, therefore, in the presence of an absorbing substance a permanent thermal gradient is established. However, if a chirophore is present, the different absorption of the LCP and RCP laser radiations causes the thermal lens gradient to increase and decrease within each cycle. An a.c. current is generated at the detector and the amplitude of this current is proportional to the Cotton effect. Further, the dephase of the thermal lens signal with respect to the reference signal indicates the sign of the Cotton effect. If a lock-in amplifier is used to demodulate the signal, a positive or a negative voltage can be obtained for a positive or a negative Cotton effect, respectively.

The TL-CD technique is expected to show the advantages of both CD and TLS when compared with spectrophotometry, i.e., a higher selectivity and capability of giving chiral information, together with the possibility of reaching very low LODs and of analysing microsamples.

However, a difference between the TLS and the TL-CD signals should be noted. In TLS, at sufficiently low values of the signal convective noise is negligible, and very low LODs can be reached. In contrast, the TL-CD signal is inherently differential, and a relatively large thermal gradient should be generated to make the measurements possible. Therefore, the TL-CD signal cannot be obtained in the absence of convective noise. However, reported LODs, of about  $\Delta A = 1 \times 10^{-6}$  and  $4 \times 10^{-6}$  for static and flowing (LC) aqueous samples, respectively [67,68], are of the same order as those reported for TLS absorbance measurements in water.

#### STUDY OF COLATERAL PHENOMENA AND PHYSICO-CHEMICAL APPLICATIONS

Several physico-chemical parameters of solvents and solutes can be determined using TLS. Thus, the  $k$  and  $dn/dT$  values have been determined using Eqn. 1 [74,76]. In addition, if the

solute is a fluorophore, the following energy balance can be established:

$$E = [N(1 - 10^{-A})][h(\nu_{\text{pump}} - \phi_{\text{fluor}}\langle\nu\rangle)] \quad (2)$$

where  $N$ ,  $A$ ,  $h$  and  $\nu_{\text{pump}}$  are the number of photons per laser pulse, the absorbance, Planck's constant and the frequency of the pump radiation, respectively, and  $\phi_{\text{fluor}}$  and  $\langle\nu\rangle$  are the quantum yield of fluorescence and the average energy of an emitted photon, respectively. Equation 2 has been used to evaluate quantum yields of fluorescence, against a standard, with high precision [7]. A similar energy balance can be used to evaluate the quantum yield of a photochemical reaction [7,77].

In addition, the dependence of the TLS sensitivity on the nature of the absorbing species is currently being investigated. In a series of experiments [78], several solutions of non-fluorescent photo-stable dyes were taken, and both the TLS and the spectrophotometric sensitivity factors,  $S$  and  $\epsilon$ , respectively, were measured and compared using the same solvent at the same wavelength. According to Eqn. 1, the sensitivity ratio,  $S/\epsilon$ , should be the same for all solutes. Instead, differences higher than 100% were found. Therefore, some solutes absorb more energy, or less energy than expected or, alternatively, part of the energy absorbed by some solutes is lost to observation, giving rise to smaller thermal gradients than expected.

It has been suggested that the energy could escape the observation region as vibrational energy [73]. Only translational energy contributes to the formation of the thermal gradient and, therefore, vibrational energy cannot be observed in TLS. However, relaxation of vibrational levels is produced within the picosecond range, whereas TLS measurements are made within the millisecond range. In addition, the diameter of the observation region is usually larger than 0.1 mm. A simple calculation shows that a molecule should travel at an excessively high speed to escape from the TLS observation region before undergoing vibrational relaxation. Therefore, another explanation should be found to explain the dependence of the TLS–spectrophotometry sensitivity

ratio on the nature of the absorbing species. Work on this topic is in progress.

#### ANALYTICAL APPLICATIONS

The successful application of an analytical technique always requires a series of physico-chemical conditions to be met, and TLS is not an exception to this rule. When TLS is compared with spectrophotometry, requirements of a similar nature are found, but for TLS procedures they are much more demanding.

Consider the procedures that rely on chromogenic formation of metal complexes. First, the value of the stability constant of the complex should be very high, otherwise the complex would undergo partial dissociation at the very low concentrations used in the vicinity of the LOD and the main advantage of TLS with regard to spectrophotometry would be partially lost. The constant should be correspondingly higher as lower concentrations are involved, that is, the higher is the molar absorptivity of the complex and the better are the thermo-optical properties of the medium. In addition, to maintain a very high value of the conditional stability constant, the concentrations of all possible competing ligands should be greatly reduced. This affects mineral acid anions, pH buffers, and masking agents.

As indicated above, another requirement is to provide a means of reducing the absorbance of the blanks as much as possible to avoid thermal convection in the vicinity of the LOD. The need to obtain low blanks limits in a great extent the number of metal–ligand systems used in spectrophotometric procedures that can be advantageously adapted to TLS.

Thus, for instance, most chromogenic reactions based on a change of the ligand spectrum on complexation cannot be advantageously exploited in TLS. A spectral shift of 50 nm is very good in spectrophotometry, but the TLS signal 50 nm away from the ligand maximum is still very high, which gives a high blank. Under these conditions, the LOD of the TLS procedure cannot be expected to be much lower than the LOD reached using the corresponding spectrophotometric pro-

cedure. For this reason, it is not surprising that most reported TLS procedures involve the formation of strong complexes with colourless ligands, rather than highly absorbing complexes of coloured ligands. Examples are the TLS procedures developed using Cu(II)–EDTA and Fe(II)–1,10-phenanthroline complexes [51,62].

Finally, interferences giving high blanks should also be eliminated. This can be difficult in the case of interfering metals which are widespread in nature, such as iron, aluminium and zinc. In these instances the problem could be alleviated by using a separation technique and/or high-purity reagents. Thus, the very low LOD ( $8 \text{ ng l}^{-1}$ ) obtained for the determination of cadmium using the Cd(II)–dithizone system [81] can be attributed to the excellent selectivity of the extraction of the Cd(II) dithizonate in alkaline medium, and also to the high molar absorptivity of the complex, the excellent thermo-optical properties of carbon tetrachloride and the fulfillment of all the requirements indicated above in a large extent. In contrast other metal dithizonates that were extracted at lower pH values than the Cd(II) complex gave rise to high blanks and, consequently, to worse LODs, owing to the presence of metal impurities which formed coloured dithizonates.

This was also the main drawback of the determination of cerium by using the Ce(IV)–quinolin-8-ol system [88]. All the indicated conditions were fulfilled to a satisfactory extent, but the reagents used contained impurities which were also extracted as coloured quinolin-8-olates. Using analytical-reagent grade reagents, the LOD obtained was  $30 \text{ ng ml}^{-1}$ , which was similar to that obtained with a spectrophotometer. In contrast, when ultrapure ammonia was used, the LOD was  $1 \text{ ng ml}^{-1}$ .

In contrast to most reactions involving the formation of complexes, redox chromogenic reactions are usually largely displaced to the right, if not irreversible. In addition, most redox reagents are colourless and, if necessary, a number of redox indicator reactions can be used. These characteristics make redox reactions particularly attractive to develop analytical TLS procedures. An example is the determination of silicon, phos-

phorus [79,80] and reduced sulphur species [85] using the molybdenum blue reaction.

Further, if organic species are determined, the chances of finding interferences leading to high blanks, due to the lack of purity of the reagents, are much lower than in the determination of metals. A TLS procedure for the determination of the sum of catecholamines in urine has been developed [90]. In this procedure, the catecholamines are selectively isolated from the urine matrix by solid-phase extraction with alumina, which is important to avoid interferences and to reduce the absorbance of the blank. The catecholamines are then oxidized to aminochromes with hexacyanoferrate(III). The absorbance of this reagent is negligible at the low concentration used, and the aminochromes moderately absorb the argon ion pump radiation, giving LODs of about  $1 \text{ ng ml}^{-1}$ .

Differently from the fluorimetric procedures for catecholamine determination, the TLS procedure gave rise to similar sensitivities for all catecholamines. In addition, dopamine showed an intermediate sensitivity when compared with the sensitivities of adrenaline, noradrenaline and L-dopa. This, and the fact that the concentration of dopamine in urine is higher than those of the other catecholamines, made dopamine an excellent standard and reference substance for the determination of the sum of catecholamines by TLS. A calculation showed that systematic errors should be within the 5% range. Therefore, the TLS procedure was of diagnostic value.

A number of FI and LC procedures with TLS detection have been also described [48–65,91–94]. An HPLC procedure has been developed for the determination of catecholamines in urine samples [93,94]. A partially end-capped octadecylsilica (ODS) column and a sodium dodecyl sulphate (SDS) micellar mobile phase are used. The retention is produced by attraction between the protonated amino groups of the aminochromes and both the residual silanol groups and the anionic heads of adsorbed SDS. The synthetic catecholamine isoproterenol was used as an internal standard.

Finally, the determination of coloured species without derivatization can be considered. Several

procedures for the determination of lanthanides have been developed [37,38,86]. Another example is the determination of coloured organic matter (humic substances) in natural water [82]. However, most species of interest, including most organic substances, absorb in the UV region. Today, the development and popularization of analytical procedures based on TLS measurements in the UV region are still difficult owing to the lack of inexpensive and powerful cw UV lasers.

Thanks are due to the DGICYT of Spain for financial support of Project PB-90/425/C2.

## REFERENCES

### *Early descriptions*

- 1 J.P. Gordon, R.C.C. Leite, R.S. Moore, S.P.S. Porto and J.R. Whinnery, *Long-transient effects in lasers with inserted liquid samples*, J. Appl. Phys., 36 (1965) 3.
- 2 F.W. Dabby, R.W. Boyko, C.W. Shank and J.R. Whinnery, *Short time-constant thermal self-defocusing of laser beams*, IEEE J. Quantum Electron., QE-5 (1969) 516.

### *Reviews*

- 3 J.M. Harris and N.J. Dovichi, *Thermal lens calorimetry*, Anal. Chem., 52 (1980) 695A.
- 4 T. Imasaka and N. Ishibashi, *Thermal lens spectrophotometry*, Trends Anal. Chem., 1 (1982) 273.
- 5 J.M. Harris, *Photothermal methods for detection of molecules in liquids*, Opt. News, October (1986) 8.
- 6 M.D. Morris and K. Peck, *Photothermal effects in chemical analysis*, Anal. Chem., 58 (1986) 811A.
- 7 N.J. Dovichi, *Thermo-optical spectrophotometries in analytical chemistry*, CRC Crit. Rev. Anal. Chem., 17 (1987) 357.
- 8 J. Georges and J.M. Mermet, *Thermal lensing spectroscopy: principle and applications*, Anal. Chem., 16 (1988) 203.
- 9 G. Ramis-Ramos and M.C. García-Alvarez-Coque, *Thermo-optical spectrophotometries: ultrasensitive techniques for absorbance measurements*, Opt. Pura Apl., 21 (1988) 133.
- 10 V.I. Grishko and I.G. Yudelevich, *Laser photothermal methods in analytical chemistry*, Zh. Anal. Khim., 44 (1989) 1753.
- 11 G. Ramis-Ramos, *Espectroscopía termo-óptica*, Quím. Anal., 8 (1989) 299.

### *Theory and modelling*

- 12 C. Hu and J.R. Whinnery, *New thermo-optical measurement method and a comparison with other methods*, Appl. Opt., 12 (1973) 72.



- 13 S.J. Sheldon, L.V. Knight and J.M. Thorne, *Laser induced thermal lens effect: a new theoretical model*, Appl. Opt., 21 (1982) 1663.
- 14 C.A. Carter and J.M. Harris, *Comparison of models describing the thermal lens effect*, Appl. Opt., 23 (1984) 476.
- 15 T. Berthoud, N. Delorme and P. Mauchien, *Beam geometry optimization in dual-beam thermal lensing spectrometry*, Anal. Chem., 57 (1985) 216.
- 16 J. Sen, R.D. Lowe and R.D. Snook, *A model for cw laser induced mode-mismatched dual-beam thermal lens spectrometry*, Chem. Phys., 165 (1992) 385.
- Miscellaneous instrumental developments*
- 17 N.J. Dovichi and J.M. Harris, *Laser induced thermal lens effect for calorimetric trace analysis*, Anal. Chem., 51 (1979) 728.
- 18 N.J. Dovichi and J.M. Harris, *Differential thermal lens calorimetry*, Anal. Chem., 52 (1980) 2338.
- 19 N.J. Dovichi and J.M. Harris, *Time-resolved thermal lens calorimetry*, Anal. Chem., 53 (1981) 106.
- 20 C.A. Carter, J.M. Brady and J.M. Harris, *Infrared laser-induced thermal lens calorimetry*, Appl. Spectrosc., 36 (1982) 309.
- 21 K. Mori, T. Imasaka and N. Ishibashi, *Thermal lens spectrophotometry based on pulsed laser excitation*, Anal. Chem., 54 (1982) 2034.
- 22 C.A. Carter and J.M. Harris, *Long path length samples in thermal lens calorimetry*, Appl. Spectrosc., 37 (1983) 166.
- 23 C.A. Carter and J.M. Harris, *Comparison of single- and dual-beam configurations for thermal lens spectrometry*, Anal. Chem., 55 (1983) 1256.
- 24 C.A. Carter and J.M. Harris, *Thermal lens absorption measurements on small volume samples*, Anal. Chem., 56 (1984) 922.
- 25 K. Nakanishi, T. Imasaka and N. Ishibashi, *Thermal lens spectrophotometry of phosphorus using a near-infrared semiconductor laser*, Anal. Chem., 57 (1985) 1219.
- 26 Y. Yang, *Rotoreflected laser beam thermal lens spectrometry*, Anal. Chem., 58 (1986) 1420.
- 27 N. Teramae, E. Voigtman, J. Lanauze and J.D. Winefordner, *Pulsed photothermal refraction spectrometry using an elliptic Gaussian excitation beam*, Anal. Chem., 58 (1986) 761.
- 28 S.R. Erskine, C.M. Foley and D.R. Bobbitt, *Single-laser single-beam pump-probe thermal-lens spectroscopy*, Appl. Spectrosc., 41 (1987) 1189.
- 29 N. Teramae and J.D. Winefordner, *Double-beam lens spectroscopy with dual-beam configuration based on photo-differential detection*, Appl. Spectrosc., 41 (1987) 164.
- 30 T. Berthoud and N. Delorme, *Differential dual-beam thermal-lensing spectrometry: determination of lanthanoids*, Appl. Spectrosc., 41 (1987) 15.
- 31 K. Nakanishi, T. Imasaka and N. Ishibashi, *Single-mode and multi-mode optical fibers for light introduction in thermal-lens spectrophotometry*, Anal. Chem., 59 (1987) 1550.
- 32 T. Imasaka, K. Nakanishi and N. Ishibashi, *A couple of optical fibres for thermal-lens spectrophotometry*, Anal. Chem., 59 (1987) 1554.
- 33 Y. Yang and S.C. Hall, *Differential thermal-lens spectrometry based on high-frequency modulation and rotoreflective double-beam configuration*, Appl. Spectrosc., 42 (1988) 72.
- 34 J. Georges and J.M. Mermet, *Optimization of a compact single-laser dual-beam thermal lens apparatus*, Analyst, 113 (1988) 1113.
- 35 S.R. Erskine and D.R. Bobbitt, *Obliquely crossed, differential thermal-lens measurements under conditions of high background absorbance*, Appl. Spectrosc., 43 (1989) 668.
- 36 J. Slaby, *Background illumination filtering in thermal-lens spectroscopy*, Anal. Chem., 61 (1989) 2496.
- Multiwavelength and scanning TLS experiments*
- 37 N. Omenetto, P. Cavalli, G. Rossi, G. Bidoglio and G.C. Turk, *Thermal-lensing spectrophotometry of uranium(VI) with pulsed laser excitation*, J. Anal. At. Spectrom., 2 (1987) 579.
- 38 C. Moulin, N. Delorme, T. Berthoud and P. Mauchien, *Double beam thermal lens spectroscopy for actinides detection and speciation*, Radiochim. Acta, 44/45 (1988) 103.
- 39 M. Franko and C.D. Tran, *Development of a double-beam, dual-wavelength thermal-lens spectrometer for simultaneous measurement of absorption at two different wavelengths*, Anal. Chem., 60 (1988) 1925.
- 40 M. Franko and C.D. Tran, *Simultaneous determination of two-component mixtures and pH by dual-wavelength thermal-lens spectrometry*, Appl. Spectrosc., 43 (1989) 661.
- 41 M. Xu and C.D. Tran, *Multiwavelength thermal lens spectrophotometer*, Anal. Chim. Acta, 235 (1990) 445.
- 42 C.D. Tran and V. Simianu, *Multiwavelength thermal lens spectrophotometer based on an acousto-optic tunable filter*, Anal. Chem. 64 (1992) 1419.
- Advances in improving the S/N ratio and in detection techniques*
- 43 K. Miyaishi, T. Imasaka and N. Ishibashi, *Thermal lens spectrophotometry based on image detection of a probe laser beam*, Anal. Chem., 54 (1982) 2039.
- 44 L.E. Buffett and M.D. Morris, *Convective effects in thermal lens spectroscopy*, Appl. Spectrosc., 37 (1983) 455.
- 45 K.L. Jansen and J.M. Harris, *Thermal lens measurements by optical computation of the laser beam spot size*, Anal. Chem., 57 (1985) 1698.
- 46 J.F. Power and E.D. Salin, *Mode-mismatched laser-induced thermal lens effect detection via spatial Fourier analysis of beam profiles*, Anal. Chem., 60 (1988) 838.
- 47 E.F. Simó-Alfonso, M.A. Rius-Revert, M.C. García-Alvarez-Coque and G. Ramis-Ramos, *Reduction of convective low-frequency noise in thermal lens spectrometry*, Appl. Spectrosc., 44 (1990) 1501.
- Detection in flowing samples (FI and LC)*
- 48 R.A. Leach and J.M. Harris, *Thermal lens calorimetry. Application to chromatographic detection*, J. Chromatogr., 218 (1981) 15.
- 49 N.J. Dovichi and J.M. Harris, *Thermal lens calorimetry for flowing samples*, Anal. Chem., 53 (1981) 689.

- 50 C.E. Buffet and M.D. Morris, *Thermal lens detection for liquid chromatography*, *Anal. Chem.*, 54 (1982) 1824.
- 51 R.A. Leach and J.M. Harris, *Real-time thermal lens absorption measurements with application to flow-injection systems*, *Anal. Chim. Acta*, 164 (1984) 91.
- 52 M.J. Sepaniak, J.D. Vargo, C.N. Kettler and M.P. Maskarinec, *Open tubular liquid chromatography with thermal lens detection*, *Anal. Chem.*, 56 (1984) 1252.
- 53 W.A. Weimer and N.J. Dovichi, *Time-resolved thermal lens measurements in flowing samples*, *Anal. Chem.*, 57 (1985) 2436.
- 54 T.J. Pang and M.D. Morris, *Differential thermal lens liquid chromatography detector*, *Anal. Chem.*, 57 (1985) 2153.
- 55 T.G. Nolan, B.K. Hart and N.J. Dovichi, *Photothermal refraction as a microbore liquid chromatography detector in femtomole amino acid determination*, *Anal. Chem.*, 57 (1985) 2703.
- 56 S.L. Nickolaisen and S.E. Bialkowski, *Pulsed infrared laser thermal lens spectrophotometry of flowing gas samples*, *Anal. Chem.*, 57 (1985) 758.
- 57 S.L. Nickolaisen and S.E. Bialkowski, *Pulsed-laser thermal-lens spectrophotometry for flowing-liquid detection*, *Anal. Chem.*, 58 (1986) 215.
- 58 Y. Yang, S.C. Hall and M.S. De La Cruz, *Pump-probe thermal lens spectrometry with oppositely propagated beams for liquid chromatography*, *Anal. Chem.*, 58 (1986) 758.
- 59 K.J. Skogerboe and E.S. Yeung, *Single laser thermal lens detector for micro-bore liquid chromatography based on high-frequency modulation*, *Anal. Chem.*, 58 (1986) 1014.
- 60 T.G. Nolan, D.J. Bornhop and N.J. Dovichi, *Crossed-beam thermal-lens detection for 0.25-mm diameter micro-bore liquid chromatography. Separation of 2,4-dinitrophenylhydrazones*, *J. Chromatogr.*, 384 (1987) 189.
- 61 N.J. Dovichi, F. Zarrin, T.G. Nolan and D.J. Bornhop, *Laser detectors for capillary liquid chromatography*, *Spectrochim. Acta, Part B*, 43 (1988) 639.
- 62 J. Georges and J.M. Mermet, *Dual-beam thermal lens spectrophotometry in flowing samples with chopped continuous wave laser excitation*, *Analyst*, 114 (1989) 541.
- 63 S.R. Erskine and D.R. Bobbitt, *Indirect differential thermal lens detection for the reversed-phase separation of underivatized fatty acids*, *Anal. Chem.*, 61 (1989) 910.
- 64 E.F. Simó-Alfonso, M.C. García-Alvarez-Coque, G. Ramis-Ramos, A. Cladera-Forteza, M. Estela-Ripoll and V. Cerdá-Martín, *An automatic system for thermal lens spectrometry and flowing samples*, *Anal. Lett.*, 25 (1992) 573.
- 65 E. Simó-Alfonso, Y. Martín-Biosca, M.C. García-Alvarez-Coque and G. Ramis-Ramos, *On the use of mixing reactors in flow injection analysis with thermal lens calorimetric detection*, *Thermochim. Acta*, in press.
- Photothermal circular dichroism*
- 66 C.D. Tran and M. Xu, *Rev. Sci. Instrum.*, 60 (1989) 3207.
- 67 M. Xu and C.D. Tran, *Thermal lens-circular dichroism spectropolarimeter*, *Appl. Spectrosc.*, 44 (1990).
- 68 M. Xu and C.D. Tran, *Thermal lens-circular dichroism detector for high-performance liquid chromatography*, *Appl. Spectrosc.*, 44 (1990).
- Collateral phenomena and physico-chemical applications*
- 69 J. Pawliszyn, *Laser beam deflection sensor as a detector for high-efficiency chromatography*, *Anal. Chem.*, 58 (1986) 243; see also J. Wu and J. Pawliszyn, *Anal. Chem.*, 64 (1992) 2934.
- 70 C.M. Phillips, S.R. Crouch and G.E. Leroi, *Matrix effects in thermal-lensing spectrometry: determination of phosphate in saline solutions*, *Anal. Chem.*, 58 (1986) 1710.
- 71 C.D. Tran and T.A. Van-Fleet, *Micellar-induced simultaneous enhancement of fluorescence and thermal lensing*, *Anal. Chem.*, 60 (1988) 2478.
- 72 C.D. Tran, *Simultaneous enhancement of fluorescence and thermal lensing by reversed micelles*, *Anal. Chem.*, 60 (1988) 182.
- 73 M. Terazima, M. Horiguchi and T. Azumi, *Limitation of absorbance measurements using the thermal-lens method*, *Anal. Chem.*, 61 (1989) 883.
- 74 M. Franko and C.D. Tran, *Thermal lens effect in electrolyte and surfactant media*, *J. Phys. Chem.*, 95 (1991) 6688.
- 75 R.M. Villanueva-Camañas, J.M. Sanchis-Mallols, E.F. Simó-Alfonso and G. Ramis-Ramos, *Photolytic and transport effects produced by argon ion laser radiation on hexacyanoferrate(III) solutions*, *Anal. Chim. Acta*, 257 (1992) 217.
- 76 M.L. Baesso, J. Shen and R.D. Snook, *Time-resolved thermal lens measurement of thermal diffusivity of soda-lime glass*, *Chem. Phys. Lett.*, 197 (1992) 255.
- 77 R.J. Roach and R.D. Snook, *Anomalous cw thermal lens behaviour of uranyl ion in aqueous carboxylic acid media*, *Anal. Chim. Acta*, 262 (1992) 231.
- 78 E.F. Simó-Alfonso, J.S. Esteve-Romero, Y. Martín-Biosca and G. Ramis-Ramos, in preparation.
- Non-chromatographic analytical applications*
- 79 V.I. Grishko, V.P. Grishko, M.M. Goldshtein and I.G. Yudelevich, *Dual-laser thermal-lens determination of phosphorus in silicon*, *Zh. Anal. Khim.*, 40 (1985) 2155.
- 80 V.I. Grishko, I.G. Yudelevich and V.P. Grishko, *Variations of thermal-lens spectrophotometry with helium-cadmium laser excitation for the determination of traces of phosphorus*, *Anal. Chim. Acta*, 176 (1985) 51.
- 81 G. Ramis-Ramos, M.C. Garcia-Alvarez-Coque, B.W. Smith, N. Omenetto and J.D. Winefordner, *Ultra-trace determination of metals with dithizone by thermal-lens spectrophotometry*, *Appl. Spectrosc.*, 42 (1988) 341.
- 82 J.F. Power and C.H. Langford, *Optical absorbance of dissolved organic matter in natural water studies using the thermal lens effect*, *Anal. Chem.*, 60 (1988) 842.
- 83 R. He, Q. Luo, J. Cao and Y. Deng, *Study of pulsed laser thermal-lens spectrometry. I. Neodymium determination*, *Fenxi Huaxue*, 16 (1988) 21.

- 84 C.D. Tran and M. Franko, *Dual-wavelength thermal-lens spectrometry as a sensitive and selective method for trace gas analysis*, J. Phys. E, 22 (1989) 586.
- 85 V.P. Grishko, V.I. Grishko and I.G. Yudelevich, *New rapid spectrophotometric method for determination of sulphide-sulphur using molybdophosphoric heteropoly acid*, Zh. Anal. Khim., 44 (1989) 434.
- 86 C.D. Tran and W. Zhang, *Thermal lensing detection of lanthanide ions by solvent extraction using crown ethers*, Anal. Chem., 62 (1990) 830.
- 87 E.F. Simó-Alfonso, G. Ramis-Ramos, J.M. Estela-Ripoll, L. Hernández-Guerra and V. Cerdá-Martín, *Determination of metals with pyridylazoresorcinol by thermal-lens spectrometry in static and flow conditions*, Quím. Anal., 9 (1990) 245.
- 88 M.J. Medina-Hernández, J.R. Torres-Lapasió, M.C. García-Alvarez-Coque and G. Ramis-Ramos, *Thermal lens spectrometric determination of cerium with oxine*, Microchem. J., 44 (1991) 222.
- 89 R.D. Lowe and R.D. Snook, *Sensitive spectrophotometric determination of aluminium using thermal lens spectrometry*, Anal. Chim. Acta, 250 (1991) 95.
- 90 J.M. Sanchis-Mallols, R.M. Villanueva-Camañas and G. Ramis-Ramos, *Determination of unconjugated catecholamines in urine as dopamine by thermal lens spectrometry*, Analyst, 117 (1992) 1367.

#### *Chromatographic analytical applications*

- 91 T.G. Nolan and N.J. Dovichi, *Sub-femtomole detection limit for amino-acid determination with laser-induced crossed-beam thermal lens detection*, Anal. Chem., 59 (1987) 2803.
- 92 S.R. Erskine and D.R. Bobbitt, *Indirect differential thermal-lens detection for the reversed-phase separation of un-derivatized fatty acids*, Anal. Chem., 61 (1989) 910.
- 93 R.M. Villanueva-Camañas, J.M. Sanchis-Mallols, E.F. Simó-Alfonso and G. Ramis-Ramos, *Thermal lens spectrometric detection of catecholamines after oxidation to aminochromes*, Anal. Lett., 25 (1992) 1425.
- 94 R.M. Villanueva-Camañas, J.M. Sanchis-Mallols and G. Ramis-Ramos, in preparation.

# Extractive–spectrophotometric determination of amphetamine in urine samples with sodium 1,2-naphthoquinone 4-sulphonate

Carmen Molins Legua, Pilar Campíns Falcó and Adela Sevillano Cabeza

*Departamento de Química Analítica, Universidad de Valencia, Burjassot, Valencia (Spain)*

(Received 2nd December 1992; revised manuscript received 13th April 1993)

## Abstract

Sodium 1,2-naphthoquinone 4-sulphonate (NQS) was tested as a reagent for amphetamine in order to develop an extractive–spectrophotometric method for the determination of the drug in urine samples. The standard additions method showed the absence of proportional bias error whereas the Youden method and the two standard addition plots method showed the presence of a constant bias error [total Youden blank (TYB)]. Acceptable results were obtained by evaluating the TYB error or by using a placebo (urine sample from a normal subject). The dynamic range of concentrations was 1.4–50 mg l<sup>-1</sup> in urine samples and the detection limit was 0.6 mg l<sup>-1</sup> when 10 ml of urine sample were taken.

*Keywords:* UV–Visible spectrophotometry; Amphetamine; Extraction; Urine

Amphetamine at concentrations often found in biological specimens weakly absorbs ultraviolet radiation, and direct ultraviolet measurement of the unchanged drug in biological material is not possible. The problem of enhancing the UV–visible characteristics of amphetamine and other amines has been approached in a number of ways.

Most UV–visible spectrophotometric methods for the determination of amphetamine and related compounds in biological samples require extraction of the analyte with an organic solvent and reaction with a chromogenic reagent in order to obtain a derivative with higher molar absorptivity. Organic solvents such as chloroform [1,2] and 1,2-dichloroethane [3–5] have been used to extract the compound formed and the analyte

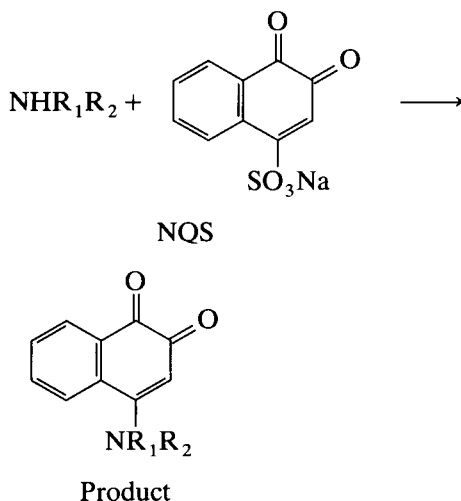
concentration was determined by measuring the intensity of colour in the organic layer when urine, reagent, buffer (pH 1.9–9.4) and organic solvent were mixed. Tropeolin O.O, Bromothymol Blue, Methyl Orange and Eriochrome T have been proposed as chromogenic reagents [1] and Chrome Azurol S [2] has been applied in a screening test of human urine.

Wallace et al. [6] determined amphetamine by spectrophotometry in oxalated blood, serum, urine and homogenized tissue, using hexane as the extraction solvent and cerium oxidation. The reaction product of amphetamine gave a well defined UV absorption curve with a maximum at 287 nm. The detection limit of the method was ca. 0.5 µg ml<sup>-1</sup>, provided that a 10-ml sample was used.

Folin [7] described a method for the determination of amino acids that depends on the combination of the amino groups with sodium 1,2-naphthoquinone 4-sulphonate (NQS) in an alka-

*Correspondence to:* P. Campíns Falcó, Departamento de Química Analítica, Universidad de Valencia, Burjassot, Valencia (Spain).

line solution to form highly coloured compounds. Rosenblatt et al. [8] used NQS for the determination of ethyleneimine and primary amines and reddish dyes were extracted into chloroform. Gürkan [9] applied the reaction to the investigation of sympathomimetic amines, including amphetamines, in pharmaceutical samples, and the highest absorption occurred at pH 10. The dynamic ranges of concentrations were 7.5–30 and 0.05–2  $\mu\text{g ml}^{-1}$  for spectrophotometric and spectrofluorimetric methods, respectively. Hashimoto et al. [10] used NQS for the qualitative analysis of phenethylamine derivatives. The reaction products were isolated by thin-layer chromatography and subjected to elemental analysis and NMR. IR and mass spectrometry. The results suggested that the reaction products have the following general structure:



Endo and Imamichi [11] applied this reagent as a derivatizing agent in the determination of methamphetamine and amphetamine in urine samples by liquid chromatography (LC). Recently Nakahara and co-workers [12–13] described the application of NQS to labelling amines in urine, plasma and saliva samples followed by LC with electrochemical detection.

The aim of this work was to use NQS reagent in a direct extractive–spectrophotometric procedure for the determination of amphetamine in urine samples. The accuracy and precision of the method were tested.

## EXPERIMENTAL

### Reagents

Phosphate buffer (pH 7.5) was prepared by dissolving 3.00 g of sodium hydrogenphosphate dodecahydrate (Probus) and 0.25 g of sodium dihydrogenphosphate dihydrate (Probus) in 100 ml of distilled water. 1,2-Naphthoquinone-4-sulphonate stock solution was prepared by dissolving 0.50 g of the sodium salt (Sigma) in 100 ml of distilled water. This solution was prepared freshly for each experiment and was stored in dark. *D*-Amphetamine sulphate (Sigma) stock solution was prepared by dissolving 100 mg of the solid in distilled water and diluting to 100 ml. Hexane (95%, LC grade) (Sharlau), chloroform (LC grade) with ethanol as preservative (Sharlau), isoamyl alcohol (isomeric mixture for analysis) (Panreac), ethyl acetate (LC grade) (Sharlau), concentrated ammonia solution (Probus) and hydrochloric acid (Probus) were used.

### Apparatus

The organic solvent (hexane) was evaporated to dryness using a Büchi R110 rotary evaporator.

The sample mixtures were heated in a Lauda RM 20 bath, vortex mixed in a Vibromatic-384 mixer and centrifuged in a Heraeus Sepatech Medifuge centrifuge.

All spectrophotometric measurements were made on a Hewlett-Packard HP 8452 A diode-array spectrophotometer furnished with quartz cuvettes of 1 cm path length.

### Standard solutions

Different volumes of the stock solution of amphetamine sulphate were added to 1 ml of phosphate buffer (pH 7.5) and 1 ml of 0.5% (w/v) NQS and diluted with distilled water to 3 ml. The mixture was heated at 70°C for 30 min. After cooling, the mixture was shaken with the same volume of organic solvent for 2 min and then centrifuged for 5 min. The absorbance of the organic phase between 190 and 820 nm was recorded. Absorbances were measured against a reagent blank at 25°C. Three replicates were made in all instances.

#### Urine samples without clean-up treatment

Samples of urine (100 ml) were made alkaline with 1 ml of 1 M NaOH, centrifuged and then adjusted to pH 7.5 with carbonate buffer. Urine samples (50 ml) were taken and spiked with 1 ml of amphetamine sulphate stock solution.

A 1-ml volume of phosphate buffer (pH 7.5), 0.5 ml of 1.0% (w/v) NQS, different volumes of amphetamine sulphate stock solution and distilled water to 2 ml were added to 1-ml samples of urine (with and without amphetamine). The mixture was processed according to the procedure described for standard solutions.

#### Urine samples with clean-up treatment

Samples of urine (5 or 10 ml, previously spiked or not with amphetamine stock solution) were adjusted to pH 10.1 with 0.1 or 0.2 ml of concentrated ammonia solution and the free bases were extracted two or three times with the same volume (5 or 10 ml each time) of hexane. A small volume (50 or 100  $\mu$ l) of concentrated hydrochloric acid–ethanol (1 + 6) was added to the combined hexane extracts to convert the free amines into the hydrochlorides. The solvent was evaporated to dryness using a rotary evaporator. The residue was reconstituted with 1 ml of distilled water, 1 ml of phosphate buffer (pH 7.5) and 1 ml of 0.5% NQS. These samples were processed according to the procedure described for standard solutions.

#### Standard addition and Youden methods

A 1-ml volume of amphetamine sulphate stock solution was added to samples of urine (100 ml). Aliquots of 5 or 10 ml of these samples were taken and spiked with further volumes of amphetamine sulphate stock solution and distilled water to 5.3 or 10.6 ml, respectively. Subsequently 0.1 or 0.2 ml of concentrated ammonia solution was added and the amphetamine extraction was carried out following the procedure described for the treatment of urine samples, and the procedure described for standard samples was followed.

The Youden method [14] was applied to the urine samples (with and without amphetamine). A 1-ml volume of amphetamine sulphate stock

solution or distilled water was added to 100 ml of urine sample and aliquots of 2, 5, 8 and 10 ml (containing amphetamine at concentrations from 5.95 to 29.74 mg l<sup>-1</sup>) were taken and processed according to the procedure described above.

## RESULTS AND DISCUSSION

#### Selection of the organic solvent

According to the literature [7–13], the reaction between NQS and phenylethylamine derivatives is carried out in an alkaline medium adjusted with 8% carbonate buffer with 0.5% (w/v) NQS and heating for 30 min at 70°C. The reaction products are usually extracted with chloroform. Hasmimoto et al. [10] proposed sodium hydrogencarbonate buffer solution, although phosphate buffer (pH 7.0–8.5) also provides good results. When we used the latter at pH 7.5, the blank analytical signal was lower than that obtained with carbonate buffer, whereas the sensitivities of the two methods were similar.

Organic solvents such as isoamyl alcohol, chloroform, ethyl acetate and hexane–ethyl acetate (1 + 1) were tried. Fig. 1 shows the spectra ob-

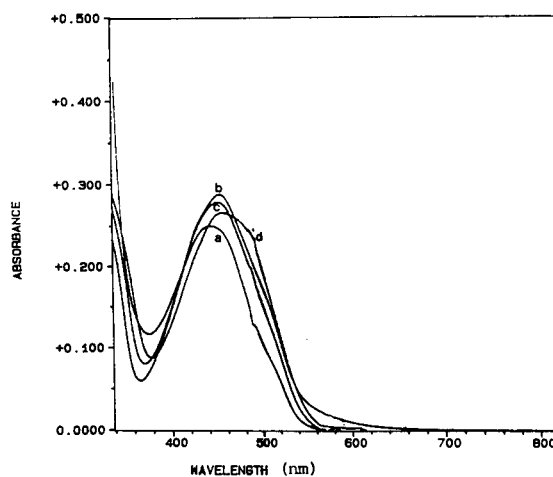


Fig. 1. Absorption spectra of NQS–amphetamine derivatives for different extraction solvents. (a) Hexane–ethyl acetate (1 + 1); (b) chloroform; (c) ethyl acetate; (d) isoamyl alcohol. Conditions: NQS,  $6.4 \times 10^{-3}$  M; phosphate buffer, pH 7.5; amphetamine, 16.6 mg l<sup>-1</sup>, heating for 30 min at 70°C. The spectra were recorded against NQS reagent extracted in the corresponding organic solvent.

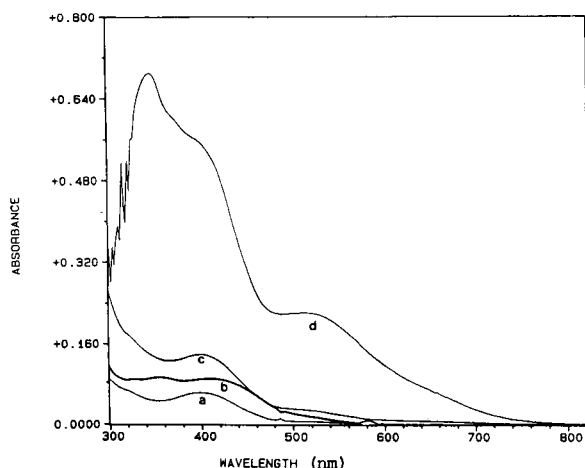


Fig. 2. Absorption spectra of NQS for different extraction solvents. (a) Hexane–ethyl acetate (1 + 1); (b) chloroform; (c) ethyl acetate; (d) isoamyl alcohol. Conditions: NQS,  $6.4 \times 10^{-3}$  M; phosphate buffer, pH 7.5; heating for 30 min at  $70^\circ\text{C}$ . The spectra were recorded against the corresponding organic solvent.

tained for  $16.6 \text{ mg l}^{-1}$  amphetamine solution after reaction with NQS when the different extraction solvents were used. The use of an extraction solvent with greater hydrophilicity allowed better extraction of the reaction product, but also enhanced the analytical signal of the reagent blank (Fig. 2). Isoamyl alcohol showed a different behaviour and was not suitable, as the absorbance of the reagent blank was too high. The products with NQS have absorption maxima in

the visible and UV regions. There is an important band in the visible region that lies between 400 and 500 nm, corresponding to the  $n-\pi^*$  singlet–singlet transition. Although the highest sensitivity was obtained in the bands corresponding to the UV region, we chose the band in the visible region because the interference from the constituents of urine was lower.

The solvents hexane–ethyl acetate (1 + 1) and chloroform were chosen because the analytical signals of blank reagents were lower. The calibration graphs, the dynamic ranges of concentration and the limits of detection obtained with standard solutions for both procedures are given in Table 1. The lower limit of the dynamic range of concentration was the limit of quantification, calculated as  $10S_B/m$ , where  $S_B$  is the standard deviation of the NQS blank and  $m$  is the slope of the calibration graph, and the upper limit was the last point fitted by the linear least-squares method. The limit of detection was calculated as  $3S_B/m$ .

#### Sample clean-up

When the urine samples were processed directly without clean-up treatment, the sensitivity was lower than that obtained with standard solutions. Other compounds in urine different to amphetamine seemed to react with the NQS reagent and inhibited the reaction with the amphetamine. By increasing the reagent concentration to  $12.6 \times 10^{-3}$  M, an increase in sensitivity was obtained,

TABLE 1

Analytical characteristics of the reaction between amphetamine and NQS for different extraction solvents working with standard solutions<sup>a</sup>

Extraction solvent	Calibration graph <sup>b</sup>	$S_B$	Dynamic range of concentration (mg l <sup>-1</sup> in the sample)	Detection limit (mg l <sup>-1</sup> )
Hexane–ethyl acetate (1 + 1)	$a = -8.86 \times 10^{-3}$ $b = 0.01460$ $S_{yx} = 5.9 \times 10^{-4}$ $t_{\text{test}}$ linear	0.006	1.4–50.0	0.4
Chloroform	$a = -9.32 \times 10^{-3}$ $b = 0.01836$ $S_{yx} = 9.9 \times 10^{-3}$ $t_{\text{test}}$ linear	0.030	6.0–50.0	1.8

<sup>a</sup> Conditions: NQS,  $6.4 \times 10^{-3}$  M; phosphate buffer, pH 7.5; heating for 30 min at  $70^\circ\text{C}$ . <sup>b</sup>  $a$  = Intercept;  $b$  = slope;  $S_{yx}$  = variance of the regression line.

and the application of the standard addition method gave a similar slope (0.01718) to that obtained for standard solutions when the extraction solvent was chloroform. These results indicated that there was no matrix bias error, and the concentration of amphetamine present in the urine can be determined with a standard deviation of 2.0% in the 30–100 mg l<sup>-1</sup> range.

Liquid–liquid extraction of the amphetamine from urine samples before reaction with NQS is needed in order to improve the sensitivity, because on cleaning the sample the interferences decreased and larger volumes of urine could be used.

Endo and Imamichi [11] proposed the extraction of amphetamine and related compounds from urine samples with hexane three times, each time using a volume of organic solvent the same as the volume of urine taken. Although the use of two instead of three extractions gave a decrease in the amphetamine recovery of about 20%, this procedure was selected because the blank urine analytical signal was smaller and the evaporation step faster. The use of volumes of organic solvent corresponding to half the volume of urine taken decreased the recovery of the analyte in the organic layer by 30%.

Urine samples with and without amphetamine after the sample clean-up step were treated with NQS and extracted into different organic solvents such as isoamyl alcohol, chloroform, ethyl acetate, hexane and hexane–ethyl acetate (1 + 1). As can be seen in Fig. 3A, the interference from components of the urine samples was lowest with hexane–ethyl acetate (1 + 1), the spectrum showing less irrelevant absorption. With isoamyl alcohol, the urine sample showed strong absorption. In Fig. 3B the spectra for coloured products from urine samples show similar shapes to those obtained for standard solution (Fig. 1).

#### Determination of amphetamine in urine samples

The contents of amphetamine in urine samples previously spiked with amphetamine sulphate stock solution were determined. In order to check for the absence or presence of any constant systematic error due to the sample matrix, the Youden method [14] was applied. This method

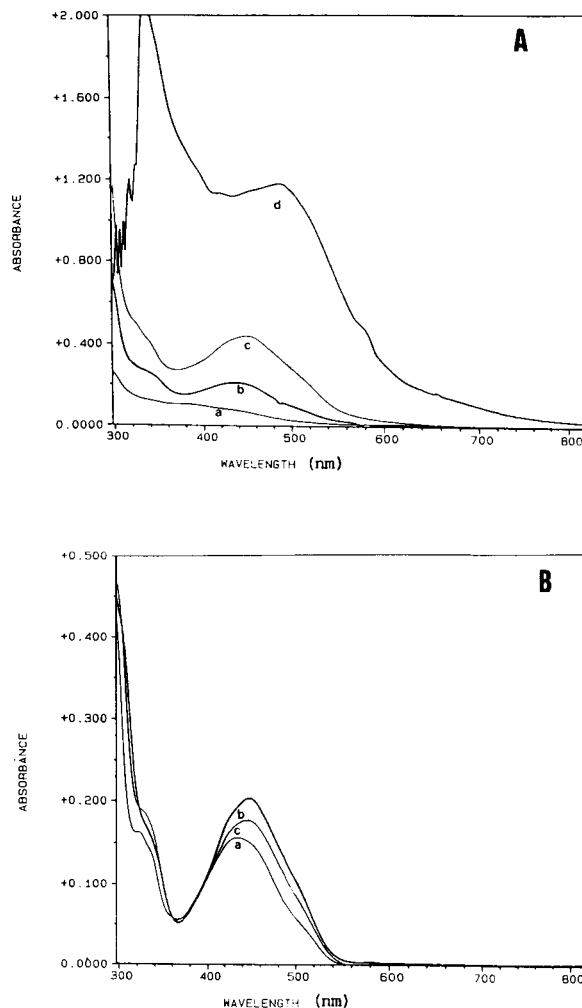


Fig. 3. Absorption spectra for (A) a 5-ml urine sample (the spectra were recorded against NQS reagent extracted in the corresponding organic solvent) and (B) 15.8 mg l<sup>-1</sup> amphetamine in a 5-ml urine sample (the spectra were recorded against a urine sample in the corresponding organic solvent). Extraction solvents: (a) hexane–ethyl acetate (1 + 1); (b) chloroform; (c) ethyl acetate; (d) isoamyl alcohol. Conditions: NQS, 6.4 × 10<sup>-3</sup> M; phosphate buffer, pH 7.5; heating for 30 min at 70°C. The urine samples were previously extracted twice with hexane.

evaluates this error when both analyte and matrix are present. It involves constructing a calibration graph (analytical signal versus sample concentration) and subjecting the data obtained to least-squares analysis in order to obtain an intercept that is known as the total Youden blank (TYB),



which represents the constant error of the method extrapolated to the zero sample level, being independent of the size of sample taken and not attributable to the analyte. If this parameter is not zero-consistent, then measurements must be corrected in order to avoid a constant systematic error.

In order to determine whether the TYB values were zero-consistent, Student's  $t$  was calculated from the equation  $t = a/S_a$ , where  $a$  is intercept of the calibration graph and  $S_a$  its standard deviation.

The application of the Youden method gave an intercept different from zero, i.e., 0.042. This value was similar to that obtained when amphetamine was not present in the sample ( $0.037 \pm 0.002$ ,  $n = 8$ ). These results (Fig. 4) indicated that there was a constant systematic error due to other substances present in the sample, being independent of the urine volume taken.

On the other hand, according to Cardone [15], it was possible to determine the TYB by applying the standard additions method for two different volumes of sample (5 and 10 ml). Figure 5 shows the plots of analytical signal versus (added amount of analyte in the sample/amount of sample) obtained for 5- and 10-ml urine samples previously spiked with amphetamine sulphate stock solution.

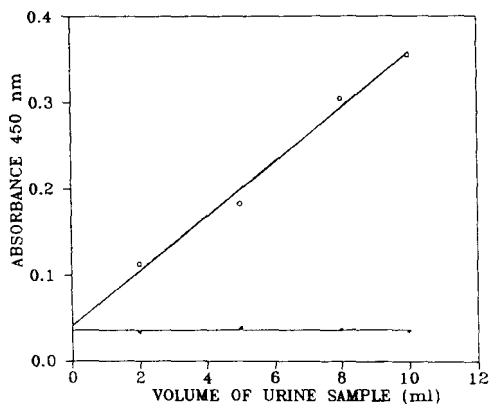


Fig. 4. Youden method for different volumes of urine samples (○) with and (●) without amphetamine. Conditions: NQS,  $6.4 \times 10^{-3}$  M; phosphate buffer, pH 7.5; heating for 30 min at  $70^\circ\text{C}$ ;  $\lambda = 450$  nm; extraction solvent, hexane–ethyl acetate (1+1). The urine samples were previously extracted twice with hexane.

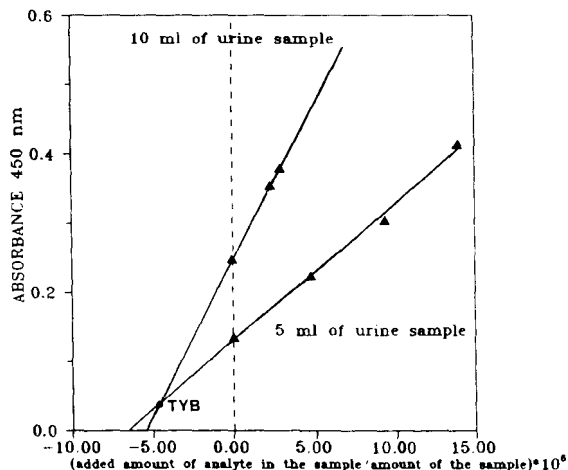


Fig. 5. Absorbance at 450 nm versus (added amount of analyte in urine sample/amount of urine sample) for 5- and 10-ml urine samples. Conditions: NQS,  $6.4 \times 10^{-3}$  M; phosphate buffer, pH 7.5; heating for 30 min at  $70^\circ\text{C}$ ; extraction solvent, hexane–ethyl acetate (1+1). The urine samples were previously extracted twice with hexane.

The two plots cross at a point an an ordinate value corresponding to the TYB value (0.043). This value is similar to that obtained with the Youden method (Fig. 4), although the urine samples were different. This point also allowed the determination of the amphetamine concentration in the sample from the abscissa value as  $4.8 \text{ mg l}^{-1}$ . The concentration actually present in the sample was  $4.6 \text{ mg l}^{-1}$ .

The application of the standard addition method [16] to spiked urine samples revealed that the slope obtained when the urine sample had previously been subjected to three extractions with hexane was the same as that obtained for standard solutions ( $0.01439$ ), so the proportional systematic error that may arise from a matrix difference was not present.

When the sample was subjected to double extraction, the slope obtained was lower ( $0.011 \pm 0.001$ ) as the recovery of amphetamine was  $76 \pm 5\%$ , but no proportional bias error was present because the slope of the calibration graph with standard samples was obtained by considering the mean percentage recovered.

The results obtained by applying the Youden method and standard addition method indicated

that there was a constant bias error (TYB) due to other substances present in the urine, but there was no matrix proportional bias error. For the determination of the unbiased amphetamine concentration, it is necessary to determine the TYB. By subtracting the TYB value from the analytical signal for a urine sample with amphetamine and by taking into account the recovery, the amphetamine concentration could be calculated from a calibration graph with standards. The concentrations of amphetamine in different spiked urine samples were calculated by applying the standard additions method and the calibration graph ob-

tained with standards previously evaluating the TYB constant error. The concentrations of amphetamine found in the samples are given in Tables 2 and 3. The relative error ( $E$ ) is acceptable in all instances.

In addition, different urine samples without amphetamine were processed according to this procedure and all the samples gave similar values at the working wavelength (for  $n = 15$ ,  $A = 0.035 \pm 0.007$ ). This permitted the use, as a placebo, of a urine sample from a normal subject. These values were comparable to those obtained by applying the Youden method, hence providing

TABLE 2

Found concentrations of amphetamine for different volumes and different urine samples by applying the standard additions method <sup>a</sup>

Sample	Volume of urine sample taken (ml) <sup>b</sup>	Amphetamine added to urine sample (mg l <sup>-1</sup> )	Concentration of amphetamine found (mg l <sup>-1</sup> )			
			Youden	$E(\%)$	Placebo	$E(\%)$
1	5	4.6	4.2	-8.7	4.2	-8.7
		10.2	10.4	+2.0	10.6	+3.9
		13.4	12.9	-3.7	13.2	-1.5
		16.1	14.5	-9.9	14.8	-8.1
		18.5	19.3	+4.3	19.7	+6.5
2	5	4.6	4.7	+2.0	4.9	+6.5
		9.2	9.1	-1.1	9.4	+2.1
		13.9	13.2	-5.0	13.4	-3.6
		18.5	18.8	+1.6	19.1	+3.2
		4.6	5.1	+10.8	4.8	+4.3
	10	6.9	7.7	+11.6	7.4	+7.2
		8.1	8.4	+3.7	8.5	+4.9
		9.2	9.7	+5.4	9.8	+6.5
		11.6	12.1	+4.3	12.2	+5.1
3	1 <sup>c</sup>	35.1		33.6	-4.3	
4	5 <sup>d</sup>	10.0		10.7	+7.0	
		14.2		15.4	+7.0	
		25.0		24.3	-2.9	
5	5	4.3		4.3	0.0	
		8.8		9.3	+5.7	
		11.0		10.0	-9.1	
		17.6		17.8	+1.1	
6	5	4.6		4.5	-2.2	
		10.2		9.6	-5.9	
		13.4		12.9	-3.7	
		23.1		21.2	-8.7	
		32.1		34.9	+7.7	

<sup>a</sup> NQS,  $6.4 \times 10^{-3}$  M; phosphate buffer, pH 7.5; heating for 30 min at 70°C;  $\lambda = 450$  nm; extraction solvent, hexane-ethyl acetate (1 + 1). <sup>b</sup> The urine samples were previously extracted twice with hexane. <sup>c</sup> Without liquid-liquid extraction. <sup>d</sup> Three extractions with hexane.

TABLE 3

Found concentrations of amphetamine for different volumes and different urine samples by applying a calibration graph with standards <sup>a</sup>

Sample	Volume of urine sample taken (ml)	Amphetamine added to urine sample (mg l <sup>-1</sup> )	Concentration of amphetamine found (mg l <sup>-1</sup> )			
			Youden	E(%)	Placebo	E(%)
1	5	4.6	4.3	-6.5	4.5	-2.3
		10.2	10.8	+5.9	11.0	+7.8
		13.4	13.3	-0.7	13.6	+1.5
		16.1	15.0	-6.8	15.3	-5.0
		18.5	19.7	+6.5	20.0	+8.1
2	5	4.6	4.7	+2.2	4.7	+2.2
		9.2	9.5	+3.3	9.7	+5.4
		13.9	13.5	-2.9	13.8	-0.7
		18.5	19.2	+3.8	19.8	+7.0
		11.6	12.2	+5.2	12.2	+5.2
	10	4.6	5.1	+10.8	4.8	+4.3
		6.9	7.7	+11.6	7.4	+7.2
		8.1	8.6	+6.2	8.6	+6.2
		9.2	9.9	+7.6	9.8	+6.5
		11.6	12.2	+5.2	12.2	+5.2
3	5	4.3			4.7	+9.3
		13.1			13.1	0.0
		17.6			18.2	+3.4
4	5	4.6			4.3	-6.5
		10.1			10.3	+2.0
		13.4			13.1	-2.2
		16.2			14.6	-9.8
		18.5			19.2	+3.8
5	5 <sup>c</sup>	10.0			10.9	+9.0
		14.0			15.2	+8.6
		20.0			21.6	+8.0
		30.0			30.4	+1.3

<sup>a</sup> Conditions: NQS  $6.4 \times 10^{-3}$  M; phosphate buffer, pH 7.5; heating for 30 min at 70°C;  $\lambda = 450$  nm; extraction solvent, hexane-ethyl acetate (1 + 1). <sup>b</sup> The urine samples were previously extracted twice with hexane. <sup>c</sup> Three extractions with hexane.

yet another possibility for the determination of amphetamine in urine sample, as can be seen in Tables 2 and 3.

The limit of detection calculated from the standard deviation of a blank solution containing NQS and a urine sample ( $S_B = 0.007$ ) and considering the slope of the calibration graph ( $m = 0.011$ ) was  $0.6 \text{ mg l}^{-1}$  amphetamine in urine samples if a 10-ml volume is taken. This value was similar to that obtained with standards.

Another experiment was performed to determine the amphetamine concentration in urine samples by using the absorbance value of a sample ( $A_m$ ) with an unknown amphetamine concen-

tration ( $C_m$ ) and the absorbance value of a reference solution ( $A_r$ ) with a concentration  $C_x = C_m + C_{\text{added}}$  that contains the same volume of urine as the sample and a known addition of amphetamine standard solution ( $C_{\text{added}}$ ). The analytical signal for this solution is  $A_r = A_m + A_{\text{added}}$ ,  $A_r$  being the analytical signal corresponding to  $C_r$ . The unknown concentration can be obtained from the equation

$$C_m = [A_m / (A_r - A_m)] C_{\text{added}} \quad (1)$$

Table 4 gives the results obtained for urine samples using the Eqn. 1 and it can be seen that they are in agreement with those obtained using

TABLE 4

Found concentrations of amphetamine for different volumes and different urine samples by applying Eqn. 1 <sup>a</sup>

Sample	Volume of sample taken (ml) <sup>b</sup>	Amphetamine added to urine sample (mg l <sup>-1</sup> )	Concentration of amphetamine found (mg l <sup>-1</sup> )			
			Youden	E(%)	Placebo	E(%)
1	5	4.6	4.2	-8.7	4.4	-4.3
2	5	4.6	4.9	+6.5	5.2	+13.4
		4.6	5.1	+10.8	5.5	+2.0
		4.6	4.6	0.0	4.9	+6.5
		9.2	8.8	-4.3	9.0	-2.2
		4.6	4.6	0.0	4.7	+2.2
		4.6	5.1	+9.8	5.3	+13.0
3	5	9.2	9.5	+3.3	9.7	+5.4
		4.3			4.0	-6.9
		8.8			9.6	+9.0
4	5	4.6			4.9	+7.1
		4.6			4.9	+7.1
		4.6			4.5	-2.1
		10.1			10.1	0.0
		10.1			9.4	-6.9
		13.4			12.3	-8.2
5	1 <sup>c</sup>	35.1			35.4	+0.9
		35.1			32.7	-6.8
		53.1			48.3	-9.0
6	5 <sup>d</sup>	10.0			10.1	+1.0
		10.0			10.9	+9.0
		13.9			13.8	-0.7

<sup>a</sup> Conditions: NQS,  $6.4 \times 10^{-3}$  M; phosphate buffer, pH 7.5; heating for 30 min at 70°C;  $\lambda = 450$  nm, extraction solvent, hexane-ethyl acetate (1 + 1). <sup>b</sup> The urine samples were previously extracted twice with hexane. <sup>c</sup> Without liquid-liquid extraction.

<sup>d</sup> Three extractions with hexane.

the standard additions method and the calibration graph with standards.

### Conclusions

This paper has shown the possibility of using NQS reagent to determine amphetamine in urine samples by an extractive spectrophotometric procedure. The method was tested and only the TYB bias error was present. Several procedures have been proposed to evaluate the constant bias error, the Youden method, the two standard addition plots proposed by Cardone [15] or even the use, as a placebo, of a urine sample from a normal subject. Sample clean-up prior to the amphetamine determination is proposed, as it allows lower amphetamine concentrations to be

detected. The detection limit was  $0.6 \text{ mg ml}^{-1}$  when 10 ml of urine sample were taken.

The authors are grateful to the CICYT for financial support received for the realization of Project SAF92-0655.

### REFERENCES

- 1 M. Kinness Ajtay, G. Dudutz and G. Coroian, Rev. Med (Tirgu-Mures, Rom.), 33 (1987) 80.
- 2 M. Syoyama and A. Nojima, Kagaku Keisatsu Kenkuyusho Hokoku Hokagaku Hen, 34 (1981) 5.
- 3 T. Sakai and N. Ohmo, Anal. Sci., 2 (1986) 275.
- 4 T. Sakai and N. Ohmo, Analyst, 112 (1987) 149.
- 5 M. Syoyama and S. Toshiyuki, Eisei Kagaku, 31 (1985) 410.

- 6 J.E. Wallace, J.D. Biggs and S.L. Ladd, *Anal. Chem.*, 40 (1968) 2207.
- 7 O. Folin, *J. Biol. Chem.*, 51 (1944) 377.
- 8 D.H. Rosenblatt, P. Hlinka and J. Epstein, *Anal. Chem.*, 27 (1955) 1290.
- 9 T. Gürkan, *Mikrochim. Acta*, I (1976) 165.
- 10 Y. Hashimoto, M. Endo, T. Keido, I. Shigeo and M. Masataka, *Mikrochim. Acta*, II (1978) 493.
- 11 M. Endo and H. Imamichi, *J. Chromatogr.*, 196 (1980) 334.
- 12 Y. Nakahara, A. Ishigami and Y. Takeda, *J. Chromatogr.*, 489 (1989) 371.
- 13 H. Sekine and Y. Nakahara, *Eisei Kagaku*, 37 (1991) 537.
- 14 W.P. Youden, *Anal. Chem.*, 19 (1947) 946.
- 15 M.J. Cardone, *Anal. Chem.*, 59 (1987) 2816.
- 16 M.J. Cardone, *Anal. Chem.*, 58 (1986) 433.

BT

# Microdetermination of sulphate and organic sulphur: potentiometric back-titration using simple coated-wire electrodes

J. Kalous, D. Brázdová and K. Vytřas

*Department of Analytical Chemistry, University of Chemical Technology, 532 10 Pardubice (Czech Republic)*

(Received 10th September 1992; revised manuscript received 8th December 1992)

## Abstract

A method is described for the determination of sulphate, based on precipitation with barium(II) chloride followed by potentiometric back-titration of the excess of barium(II) salt with sodium tetraphenylborate in the presence of polyethylene glycol. To monitor the titrations, simple ion-selective electrodes of the coated-wire type were prepared using an ordinary aluminium conductor, coating the central wire with the membrane formed by plasticized poly(vinyl chloride). The determination of organic sulphur consists in burning the sample in a flask filled with oxygen. The combustion products are absorbed in alkaline hydrogen peroxide and, in an aliquot, the sulphate formed is determined. The procedure was tested on eleven organic substances and applied to the determination of sulphur in samples of asphalt. Compared with visual detection of the end-point of the direct titration of sulphate with barium(II) salt, the results are of the same precision and accuracy. The use of simple potentiometric sensors of the coated-wire type allows objective end-point evaluations and makes the procedure inexpensive.

**Keywords:** Potentiometry; Titrimetry; Coated wire electrodes; Sulphur; Microdetermination

The Schöniger method based on burning organic substances in a flask filled with oxygen is still widely used. Originally used for the determination of halogens [1], the procedure was extended to sulphur [2] and other elements [3]. When an organic substance containing sulphur is burned in oxygen, the sulphur dioxide formed is absorbed in alkaline hydrogen peroxide and determined as sulphate, frequently using barium(II) perchlorate as a titrant in a mixed aqueous–alcoholic medium. As there is no sharp colour change of the indicator (thorin screened by methylene blue is recommended), the analyst should first carry out several standard titrations so that

the eye can become accustomed to locating the end-point [4,5]. Various modifications, including photometric back-titration of the excess of barium(II) perchlorate with sulphuric acid [6], were therefore investigated.

The titration of sulphate as a final step can also be followed potentiometrically using ion-selective electrodes (ISEs) [7–25]. However, there are still some limitations. Potentiometric titration with lead(II) salt and visual titration with barium(II) perchlorate require the use of mixed aqueous–alcoholic media. If a barium(II) liquid membrane ISE is used to monitor the titration, such a mixed medium must not be used because of the limited lifetime of the sensor.

Recently, titrations based on reactions of compounds containing poly(oxyalkylene) chains with bivalent metal ions and lipophilic anions have

*Correspondence to:* K. Vytřas, Department of Analytical Chemistry, University of Chemical Technology, 532 10 Pardubice (Czech Republic).

been studied and the procedures were elaborated for determinations of both metal ions and non-ionic surfactants using sodium tetrphenylborate as titrant (for references, see Table 1 in [26]). The use of simple potentiometric sensors of the coated-wire type in these titrations has been reported previously [26,27]. In the meantime, the formation of ternary complexes has also been used in the indirect determination of sulphate [28–30]. As a continuation of earlier work [31], this paper presents the results of investigations on the determination of sulphate using potentiometric back-titration with simple coated-wire electrodes and its application as a final step in the determination of organic sulphur.

## EXPERIMENTAL

### Solutions

Sodium tetrphenylborate ( $\text{NaBPh}_4$ ) solution (ca.  $0.01 \text{ mol l}^{-1}$ ) was prepared by dissolving a weighed amount (3.427 g) of the substance (VEB Jenapharm Laborchemie, Apolda) in water, adjusting the pH to 9 with sodium hydroxide solution and diluting to 1000 ml with water. The  $\text{NaBPh}_4$  titrant was standardized potentiometrically against standard 0.01 M thallium(I) nitrate solution.

Barium(II) chloride solution ( $0.005 \text{ mol l}^{-1}$ ) was prepared by dissolving ca. 0.611 g of the analytical-reagent grade salt (Lachema, Brno) in water and diluting to 500 ml. The solution was standardized by potentiometric titration of an aliquot against standardized 0.01 M  $\text{NaBPh}_4$  in the presence of an excess of polyethylene glycol (PEG).

PEG solution (ca.  $1 \text{ mol l}^{-1}$ ) was prepared from the substance with a mean molar mass of  $300 \text{ g mol}^{-1}$  (NCHZ, Nováky).

Barium(II) perchlorate solution ( $0.01 \text{ mol l}^{-1}$ ) for visual titrations was prepared by dissolving ca. 3.9 g of the substance in 200 ml of water and diluting to 1000 ml with propan-1-ol. This titrant was standardized visually against a standard substance containing sulphur [*N*-(2-naphthyl)mercaptoacetamide (thionalide)] using a screened indicator (thorin and methylene blue).

The titres of both  $\text{NaBPh}_4$  and propanolic  $\text{Ba}(\text{ClO}_4)_2$  solutions required frequent checking.

### Equipment

Potentiometric titrations were performed using an OP-208/1 pH meter or an OP-271 pH/ion analyser (both from Radelkis, Budapest). The sensing electrodes of the coated-wire type were prepared as described previously [32] using an aluminium conductor as a support for the membrane, which was formed by poly(vinyl chloride) plasticized with 2,4-dinitrophenyl octyl ether. An RCE-102 calomel electrode (Crytur, Turnov) of double-junction construction, filled with saturated potassium chloride and 0.1 M sodium nitrate solution was used to complete the measuring cell. Potentiometric titrations were made in 100-ml beakers. The titrated solution was stirred magnetically, the titrant being added from a 10-ml burette.

For decomposing organic substances, a combustion Erlenmeyer flask (1000 ml) was used, fitted with a ground-in stopper into which a glass rod ending with a platinum spiral was soldered. Visual titrations of the combustion products in an absorption medium were performed as usual [4].

### Samples

For optimizing the potentiometric back-titration, sodium sulphate solution ( $0.005 \text{ mol l}^{-1}$ ) was prepared using the analytical-reagent grade salt (Lachema). Various organic substances containing sulphur (see Table 1) were used to verify the combustion procedure with the potentiometric back-titration as a final operation step. The method was applied to determine the sulphur content in samples of asphalt (AP-80, Paramo, Pardubice) and its volatile fractions.

## RESULTS AND DISCUSSION

### Optimization of sulphate determination by potentiometric back-titration

The procedure consists in precipitation of sulphate with barium(II) salt and titration of the excess of barium(II) with  $\text{NaBPh}_4$  in the presence of PEG. Although the determination is essen-

tially clean, it must be noted that reproducible results can only be achieved when all principles valid for the traditional gravimetric determination of sulphate as  $\text{BaSO}_4$  [33] are fully respected. To find an optimum procedure, portions of 3–7 ml of 0.005 M sodium sulphate solution were measured into a 100-ml titration vessel and subjected to different modes of processing. The best results were obtained when a neutral sulphate solution was acidified with several drops of hydrochloric acid to ca. pH 2. The solution was then heated on a boiling water-bath and precipitated by slowly adding with stirring 10 ml of 0.005 M barium(II) chloride solution. The suspension was left on the boiling water-bath for about 30 min. After cooling to room temperature, PEG solution (5 ml) was added and the mixture was titrated with 0.01 M  $\text{NaBPh}_4$  solution. The resulting titration curves (Fig. 1) were evaluated graphically.

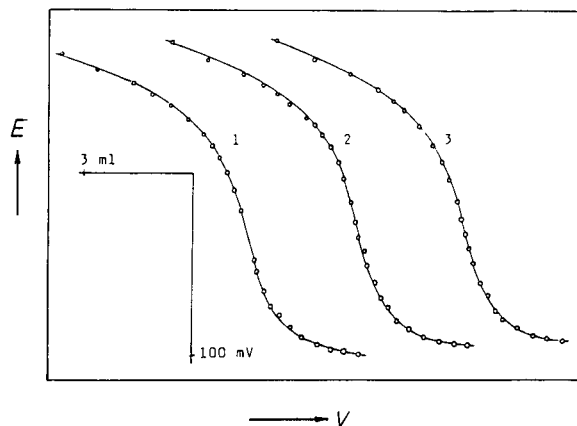


Fig. 1. Potentiometric titration curves of excess of barium(II) salt with 0.01 M  $\text{NaBPh}_4$  in the presence of PEG. Content of sulphur in sample titrated, 0.802 mg. End-point readings, (1) 6.01, (2) 5.97 and (3) 5.98 ml of titrant, serve for appreciating the reproducibility.

TABLE 1

Comparison of results of potentiometric and visual titrations in the determination of organic sulphur after combustion

Substance analysed	Content of sulphur (%)		Lord's test <sup>d</sup> , $u_0$	Moor's test <sup>e</sup> , $U$	
	Theoretical	Found by titration <sup>a</sup>			
		Potentiometric <sup>b</sup>			Visual <sup>c</sup>
<i>N</i> -(2-Naphthyl)-mercaptoacetamide (thionalide) <sup>f</sup>	14.75	14.76 ± 0.05	14.75 ± 0.03	0.077	0.067
<i>S</i> -Benzylthiuronium chloride	15.82	15.80 ± 0.02	15.81 ± 0.04	0.400	0.167
4-Aminobenzene sulphonic acid	18.51	18.45 ± 0.05	18.50 ± 0.01	0.500	0.385
Benzyl sulphone	13.02	13.10 ± 0.16	13.14 ± 0.25	0.195	0.067
Benzyl sulphide	14.96	14.90 ± 0.18	14.76 ± 0.04	0.133	0.292
Thiourea	42.12	42.13 ± 0.06	42.11 ± 0.13	0.063	0.077
Thiosemicarbazide	35.18	35.14 ± 0.22	35.05 ± 0.38	0.073	0.107
Diphenylthiocarbazon	12.51	12.39 ± 0.10	12.43 ± 0.14	0.500	0.141
Benzyl thiocyanate	21.49	21.27 ± 0.04	21.23 ± 0.07	2.444	0.286
5-Sulphosalicylic acid dihydrate	12.60	12.56 ± 0.04	12.51 ± 0.05	0.444	0.385
4-Carboxybenzene sulphonamide	15.94	14.50 ± 0.04	14.47 ± 0.12	14.4	0.158

<sup>a</sup> Given as reliability intervals  $\bar{x} \pm u_0 R$ , where  $\bar{x}$  is the arithmetic mean,  $R$  the range ( $x_{\max} - x_{\min}$ ) and  $u_0$  the Lord's critical value for <sup>b</sup> six or <sup>c</sup> three parallel determinations. <sup>d</sup> Calculated as  $u_0 = |X - \bar{x}|/R$ , where  $X$  is the theoretical value; the critical  $u_0$  value for  $n = 6$  replicates is 0.399. <sup>e</sup> Calculated as  $U = |\bar{x}_A - \bar{x}_B|/(R_A - R_B)$ , where subscripts A and B denote values for two different methods: the critical  $U$  value for  $n_A = 6$  and  $n_B = 3$  replicates is 0.391. In all calculations, a significance level of 0.05 (95% probability) was assumed [34]. <sup>f</sup> Used as a standard substance for standardization of  $\text{Ba}(\text{ClO}_4)_2$  titrant.



*Verification of potentiometric back-titration as a final step in the determination of organic sulphur*

The procedure for the determination of organic sulphur was tested on eleven samples of organic compounds with different structures. A weighed amount of the solid substance (20–25 mg, by difference) was transferred on to a piece of filter-paper, wrapped, placed in platinum basket and subjected to Schöniger combustion in a flask filled with oxygen. An absorption medium, consisting of 0.5 M sodium hydroxide solution (1 ml), 5% hydrogen peroxide (5 ml) and water (25 ml), was placed in the flask before combustion. The burned sample was subsequently allowed to stand in the flask for about 30 min, then the contents of the flask were transferred quantitatively into a 100-ml volumetric flask, acidified by addition of 1 M hydrochloric acid (1 ml) and diluted to the mark with water. An aliquot (10–25 ml) of this solution was pipetted into a titration vessel, heated on a boiling water-bath, precipitated with barium(II) chloride and the above procedure of potentiometric back-titration in the presence of PEG was applied.

In visual titrations, the combustion flask and the platinum spiral were rinsed with propan-1-ol (85%, v/v) after the combustion products were absorbed, acidified, several drops of the screened indicator solution were added and the mixture was titrated with 0.01 M barium(II) perchlorate solution.

A statistical evaluation of the results is given in Table 1. Compared with the visual indication procedure, it can be seen that the potentiometric back-titration gives results of at least the same

precision. Having tested the accuracy of the mean value found by back-titration with the theoretical content of sulphur by use of the Lord's  $u_0$  test, the differences in some instances were statistically significant. However, not all the samples could be assumed to be standard substances. It also followed when coincidence of the results of both methods was examined using Moor's  $U$  test that no value calculated was higher than the critical value of  $U = 0.391$ .

*Determination of sulphur in fractions of asphalt*

Samples of asphalt were analysed by the above potentiometric procedure to find the total organic sulphur content and to differentiate between volatile and non-volatile sulphur compounds. Volatile fractions were obtained by heating a sample in a 250-ml flask at 180–200°C for 30–40 min. Gaseous products were released by a stream of air and condensed in an air-cooled separator as a paste (fraction A). A gas stream was then bubbled through a 5% lead(II) acetate solution in a cylinder where sulphidic compounds were isolated as lead(II) sulphide. These were separated by filtration, washed and dried to a powder (fraction B).

Samples of asphalt and its volatile fractions were combusted (it should be pointed out that the pastes, fraction A, had to be weighed into polyethylene microtubes when combusted) and analysed as above using potentiometric back-titration in final step. The results (Table 2) showed that the content of sulphur bound in volatile compounds (a sum of fractions A and B) is ca. 2.0%, whereas total sulphur represents ca. 2.4% of the sample. The precision of the results corresponded to the character of the samples.

*Conclusion*

As confirmed by statistical evaluation of the results, the method for organic sulphur based on potentiometric back-titration gave the results of the same precision and accuracy when compared with traditional visual titration. However, the potentiometric procedure offers some advantages. First, potentiometric indication is objective and the end-point reading is simpler than with subjective observation of the indicator change. Only an

TABLE 2

Determination of sulphur in asphalt and its volatile fractions

Sample	Number of replicates	Found <sup>a</sup> (%)	R.S.D. <sup>b</sup> (%)
Crude asphalt AP-80	6	2.42 ± 0.09	3.7
Fraction A (paste)	4	1.36 ± 0.18	9.0
Fraction B (powder)	4	0.65 ± 0.13	13.5

<sup>a</sup> Given as reliability intervals for a given number of measurements (see footnote a in Table 1). <sup>b</sup> Relative standard deviation.

aqueous instead of a mixed medium is used. Weighing the same amounts of samples, potentiometric method allows at least twice more replications because the sample, after combustion, is subdivided in more aliquots for titration. Additionally, the method can simply be automated using a titrator. In contrast to the procedure reported by Yu et al. [28], it was found that the precipitated barium(II) sulphate need not be separated by filtration, thus saving one operational step of the determination. Finally, although various plastic membrane ISEs could be employed, the use of simple coated-wire electrodes makes the method inexpensive.

## REFERENCES

- 1 W. Schöniger, *Mikrochim. Acta*, (1955) 123.
- 2 W. Schöniger, *Mikrochim. Acta*, (1956) 869.
- 3 N.E. Gelman and L.M. Kiparenko, *Zh. Anal. Khim.*, 20 (1965) 229.
- 4 V.A. Klimova, *Basic Methods of Organic Microanalysis*, Mir, Moscow, 1977, p. 114.
- 5 L. Mázor, *Methods of Organic Analysis*, Akadémiai Kiadó, Budapest, 1983; Russian translation, Mir, Moscow, 1986, p. 412.
- 6 I. Iida, A. Koizumi and Y. Kabasawa, *Nihon Daigaku Yakugaku Kenkyu Hokoku*, 28 (1988) 25; *Chem. Abstr.*, 114 (1991) 177656s.
- 7 J.W. Ross and M.S. Frant, *Anal. Chem.*, 41 (1969) 967.
- 8 W. Selig, *Mikrochim. Acta*, (1970) 168.
- 9 M. Mascini, *Analyst*, 98 (1973) 325.
- 10 A. Hulanicki, R. Lewandowski and A. Lewenstam, *Analyst*, 101 (1976) 939.
- 11 R. Delmas, *Mikrochim. Acta*, I (1978) 219.
- 12 J. Veselý, *Collect. Czech. Chem. Commun.*, 46 (1981) 369.
- 13 K. Harzdorf, *Fresenius' Z. Anal. Chem.*, 262 (1972) 167.
- 14 W. Selig, *Mikrochim. Acta*, II (1975) 665.
- 15 A.M.Y. Jaber, G.J. Moody and J.D.R. Thomas, *Analyst*, 101 (1976) 179.
- 16 G. Ouzounian and G. Michard, *Anal. Chim. Acta*, 96 (1978) 404.
- 17 M. Gueggi, E. Pretsch and W. Simon, *Anal. Chim. Acta*, 91 (1977) 107.
- 18 J. Kotek, *Chem. Prum.*, 34 (1984) 519.
- 19 A.R. Garifzyanov, A.N. Khramov and V.F. Toropova, *Zh. Anal. Khim.*, 46 (1991) 133.
- 20 N. Akimoto and K. Hozumi, *Anal. Chem.*, 46 (1974) 766.
- 21 J. Veselý, *Anal. Lett.*, 13 (1980) 543.
- 22 A.F. Zhukov, A.V. Kopitin, G.K. Zhavornikova and A.V. Gordievskii, *Zavod. Lab.*, 45 (1979) 492.
- 23 W.S. Selig, *Ind. Eng. Chem., Prod. Res. Dev.*, 23 (1984) 140.
- 24 M. Zancato, A. Pietrogrande and C. Macca, *Ann. Chim.*, 80 (1990) 445.
- 25 G.S. Urazalina and V.A. Mirkin, *Zavod. Lab.*, 58, No. 7 (1992) 7.
- 26 K. Vytřas, V. Dvořáková and I. Zeman, *Analyst*, 114 (1989) 1435.
- 27 M.L. Ruberte Sanchez and K. Vytřas, *Analyst*, 113 (1988) 959.
- 28 R.-Q. Yu, K.-M. Wang and X.-M. Zhou, *Fenxi Huaxue*, 11 (1983) 343.
- 29 V.N. Ivanov, N.I. Bavykina and Yu. S. Pravshin, *Zh. Anal. Khim.*, 40 (1985) 2265.
- 30 X.-F. Yin and X.-D. Zhang, *Huanjing Kexue*, 8 (1987) 63.
- 31 K. Vytřas, J. Kalous and D. Brázdová, in *XXV Celoštatny Seminár o Chémii Alkylénoxidov a ich Derivátov*, NCHZ, Nováky, 1991, p. 114.
- 32 K. Vytřas, *Mikrochim. Acta*, III (1984) 139.
- 33 A. Jílek and J. Kota, *Vážková Analýsa a Elektroanalýsa*, Vol. 3, SNTL, Prague, 1956, p. 262.
- 34 K. Eckschlager and V. Štěpánek, *Information Theory as Applied to Chemical Analysis*, Wiley-Interscience, New York, 1979.

# Copper speciation analysis using a chemically modified electrode

R. Agraz, M.T. Sevilla and L. Hernández

*Department of Analytical Chemistry and Instrumental Analysis, Autónoma University of Madrid, 28049 Madrid (Spain)*

(Received 8th September 1992; revised manuscript received 26th January 1993)

## Abstract

A carbon paste electrode modified with Amberlite IRC-718 resin, containing the chelating agent iminodiacetic acid, was used for speciation analysis. Copper was accumulated on the electrode surface when the electrode was immersed in the sample and then the amount of copper preconcentrated was evaluated by cyclic voltammetry. The chemical reaction studied is based on exchange of the iminodiacetate group attached to the electrode surface with the competing ligand in solution. A kinetic study allowed the determination of the influence of the nature of the interfering ligand on the reaction rate. A comparison of the results obtained by this method with theoretical predictions based on thermodynamic equilibrium constants and natural ligand classification as a function of their effects is presented.

**Keywords:** Voltammetry; Chemically modified electrodes; Copper; Speciation

The speciation analysis of metals in waters is an interesting challenge. To study the toxicity and bioavailability of metals in waters it is necessary not only to determine their total concentration, but also the concentrations of the different physico-chemical forms of the element in aqueous systems.

Electrochemical techniques have proved to be the most suitable methods for trace metal speciation analysis in waters. Analytical approaches based exclusively on these techniques, especially anodic stripping voltammetry (ASV), alone or in combination with other techniques, are widely used [1–5]. However, speciation measurements using ASV have some limitations, such as the disturbance of the natural equilibria as a conse-

quence of the application of a potential to the sample. Therefore, it is impossible to measure the speciation under natural conditions. Other important problems are the adsorption of organic matter and the formation of intermetallic compounds [6] at a mercury electrode, the calibration procedure and the influence of the mobility of species on the electroanalytical signal. The complexing properties of a medium can also affect the redissolution peaks in the ASV approach [7], thus affecting the speciation measurements; this can be avoided to a great extent by using medium exchange, with deposition of metals on the electrode in the original water sample and replacing the sample solution with an electrolyte solution for the stripping step [8].

Other speciation techniques used are selective preconcentration on an ion exchanger, chelating resins being the most widely used [9,10]. Although chelating resins have been used particu-

*Correspondence to:* M.T. Sevilla, Department of Analytical Chemistry and Instrumental Analysis, Autónoma University of Madrid, 28049 Madrid (Spain).

larly for the determination of total metal concentration, one of them, Chelex-100 resin (containing iminodiacetate groups), has been widely used in speciation schemes; fractionation in different types of metal species is based on their thermodynamic and kinetic stability against the complexing active group in the resin [11].

In previous papers results were presented on the suitability of an electrode, modified with a chelating resin containing iminodiacetate as active group, for the preconcentration and determination of metals at the  $\text{ng ml}^{-1}$  level [12,13]. The influence of different complexing substances on the analytical signals with this electrode and its utility for simultaneous trace metal determinations have also been considered recently [14].

In this paper, an analytical approach for the speciation analysis of metals is proposed, using a carbon paste electrode modified with Amberlite IRC-718 chelating resin. This approach is based on the effect of the different types of ligands on the analytical signal of the metal, due to thermodynamic and kinetic parameters that influence the competing equilibria between complexes in the water sample and the resin attached to the electrode surface. A mathematical equation to describe these types is deduced and the experimental results are compared with the theoretical predictions using conditional equilibrium constants. For experimental studies, copper was used as a model together with a series of ligands that could be considered as a model of different types of ligands present in natural waters. The latter included inorganic, organic and polyelectrolytes, such as hydrogencarbonate, sulphate, phosphate, thiourea (TU), urea, glycine (Gly), cysteine (Cys), salicylic acid (Sal), thiosalicylic acid (TSal), nitrilotriacetic acid (NTA), fulvic acid (FA), starch, bovine serum albumin (BSA) and iron colloids, and were tested in the concentration ranges usually present in fresh waters [1].

## THEORETICAL

Chemical competition as a speciation strategy has been widely used, employing spectrophotometric and fluorescence detection of the metal-

discriminator complex, separation and other techniques [15–17]. Several problems associated with these techniques have been reported [1], e.g., the difficulty of finding a ligand that is easy to determine spectrophotometrically or the alteration of equilibria when a separation step is required. Alteration of the equilibria in the sample may occur as a consequence of the addition of a new chelating agent and the consumption of free metal, but also by secondary reactions or sample contamination. These processes lead to results that are difficult to interpret.

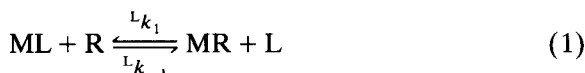
The use of a chemically modified electrode can eliminate most of these problems because the separation procedure is easily implemented by simply removing the electrode from the preconcentration cell. The ligand does not have to conform to special requirements because the complex formed is determined by means of its metal content, preconcentrated on the electrode surface. Another advantage is the very small amount of preconcentrated metal, about  $10^{-13}$  mol, which makes the disturbance of the natural equilibria almost negligible. Contamination of the sample is also avoided because no new ligand is added to the sample. The amount of ligand discriminator in contact with the sample is also very small ( $1.3 \times 10^{-7}$  mol  $\text{cm}^{-2}$ ), which is possible because of the electrochemical detection used. The subsequent determination of the metal complex with the indicator ligand is done in an electrochemical cell with the selectivity and sensitivity that electrochemical methods provide.

Voltammetric methods for speciation analysis include studies in the electrochemical cell of the capability of the metal complex to become dissociated in the diffusion layer, and also the effect of the diffusion coefficients of the species on the analytical signal [18]. In the present scheme, the difference from classical speciation procedures based on electrochemical methods, especially ASV, is that the discrimination between different species is done on the basis of a chemical competition in open circuit, and the voltammetric measurement is done in a clean supporting electrolyte under the optimum electrochemical conditions, avoiding contamination or complexing effects on the redissolution peak. The necessity for the ad-

dition of a buffer to adjust the ionic conductivity of the sample is also avoided.

The choice of the discriminator ligand attached to the electrode surface (Amberlite IRC-718) to develop the chemical competition speciation scheme was made on the basis of the recognized capability of its active group to discriminate between different metal species through thermodynamic and kinetic parameters [11].

The speciation scheme employed is based on the determination of the reaction rate constant  ${}^Lk_1$  for the equilibrium



where R is the discriminator ligand on the electrode surface and L is the interfering natural ligand. The  ${}^Lk_1$  value is affected by the dissociation rate of ML. The kinetic study of the dissociation of ML is done taking into account the different equilibrium reactions for the formation of MR and ML ( $K_1 = k_1/k_{-1}$  and  $K_2 = k_2/k_{-2}$ , respectively) and equilibrium (1):

$${}^LK_1 = {}^Lk_1/{}^Lk_{-1} = K_1/K_2 \quad (2)$$

$${}^Lk_1 = \delta k_1 k_{-2} \quad (3)$$

where  $\delta$  is a factor including the rate constant that is not decisive for speciation results:  $k_{-1}$  and  ${}^Lk_{-1}$  are both determined by the MR dissociation rate and  $k_2$  is limited by the dehydration of M prior to complex formation. The value of  ${}^Lk_1$  will be directly proportional to the MR formation rate ( $k_1$ ) and ML dissociation rate ( $k_{-2}$ ). When ML becomes more inert,  ${}^Lk_1$  value decreases.

The reaction rate for the reaction with the iminodiacetate group attached to the electrode surface is slow and determined by the complexation step, as many studies have shown [19]. Therefore, attainment of the equilibrium implies relatively long preconcentration times, even when working with very low concentration levels. In order to make the analysis time shorter, only initial reaction rates are considered, over a time period of 3–10 min. The initial rate constant for MR formation ( $k_1$  and  ${}^Lk_1$ ) will be denoted by  $k_0$  and  ${}^Lk_0$ . In the initial step of reaction 1, the pseudo-first-order equation describes its reaction

rate [20] and the reaction rate constant is defined by the equation

$${}^Lk_0 = \frac{{}^Lv_0}{[ML]_0} = \frac{1}{[ML]_0} \times \frac{d[MR]}{dt} \quad (4)$$

The slope of the plot of [MR] vs. reaction (preconcentration) time gives the initial reaction rate constant. If the experiment is done in the absence and presence of an interfering ligand,  $k_0$  and  ${}^Lk_0$  are obtained, respectively.

The comparison of  $k_0$  vs.  ${}^Lk_0$  plots can give an idea of the degree of interference for each type of ligand, not only in a thermodynamic but also in a dynamic way. The definition of the kinetic parameter  $\log(k_0/{}^Lk_0)$  allows natural type complexes to be classified as a function of their kinetic characteristics; when no effect is observed,  $\log(k_0/{}^Lk_0) = 0$ . Usually, the observed effect increases with increasing ligand concentration. The amount of interference for any ligand concentration is defined by the slope ( $\beta$ ) of the linear relationship observed between  $\log(k_0/{}^Lk_0)$  and  $\log([M]/[L])$ :

$$\log(k_0/{}^Lk_0) = A + \beta \log([M]/[L]) \quad (5)$$

The operationally defined parameters for discrimination of groups as a function of their kinetic stability will be  $\log(k_0/{}^Lk_0)$  and  $\beta$ .

## EXPERIMENTAL

### Reagents

Ultrapure water obtained with a Milli-Q-Milli-RO system (Millipore) and analytical-reagent grade reagents were used throughout. A copper stock standard solution was prepared by dissolving the ultrapure metal in the minimum amount of nitric acid. Amberlite IRC-718 (Carlo Erba) was purified by successive washing with methanol, 5% HCl and water. Fulvic acid from Quercus soil (donated by the Institute of Pedology, Madrid) was prepared by dissolving a weighed portion in  $1 \times 10^{-3}$  M KOH for 2 h until no pH variation was observed and then filtered over a 0.45- $\mu$ m membrane filter. Iron colloids were prepared as described previously [9]. Stock

standard solutions (0.01 M) of different ligands were prepared in water. All solutions were stored in polyethylene containers at 4°C in the dark.

#### Apparatus

A BAS CV-27 voltammograph and a BAS X-Y recorder, equipped with an Ag/AgCl reference electrode and a platinum counter electrode, were used for cyclic voltammetric determinations. A Perkin-Elmer Model 372 atomic absorption spectrometer equipped with an HGA Model 2200 graphite furnace Controller and a Metrohm Model 654 pH meter were also used.

#### Modified carbon paste electrode preparation

Modified carbon pastes were prepared by placing the following compounds in an agate mortar: 0.3 g of spectrographic graphite powder, 0.2 g of powdered chelating resin and the necessary amount of paraffin oil; these were mixed for ca. 10 min until an uniform paste was obtained. Unmodified carbon paste was prepared in the same way but without the resin powder. The carbon paste obtained was then packed in the end section of a PTFE tube (0.4 cm i.d.) provided with an inner copper contact.

#### Analytical procedure

The electrode was first activated by successive sweeps until a reproducible current was obtained. The electrode was then immersed in a preconcentration cell containing 50 ml of copper solution in 0.01 M KNO<sub>3</sub> at neutral pH and allowed to collect the trace metal for a given period of time in the stirred solution at open circuit. The electrode was removed, rinsed with water and placed in the measurement cell containing the supporting electrolyte (0.1 M HCl). No deaeration of the electrolyte solution was required. A reduction potential of -0.80 V was applied for 30 s and then a cyclic, linear anodic scan was performed at a scan rate of 400 mV s<sup>-1</sup>, obtaining the copper anodic peak at -0.10 V vs. Ag/AgCl. Regeneration of the electrode surface was done by applying a potential of 1.00 V for 2 min in the stirred supporting electrolyte.

Electrode calibration was done by measuring several copper solutions containing increasing

amounts of copper from 0.5 to 2.0 μg l<sup>-1</sup> in 0.01 M KNO<sub>3</sub> at neutral pH, according to the ionic strength and pH of the water samples. The copper peak intensity was obtained as a function of the preconcentration time and employing the slope kinetic method [20], where the proportionality between the initial reaction rate and metal concentration was evaluated.

In order to study the competition between the ligand on the electrode surface and the complex in solution, different copper solutions containing 2 μg l<sup>-1</sup> metal, 0.01 M KNO<sub>3</sub> and increasing concentrations of the test ligand at neutral pH were prepared. These solutions were allowed to equilibrate for 24 h and then tested by the previous procedure, employing the kinetic slope procedure to calculate the recovery.

## RESULTS AND DISCUSSION

The electroanalytical system applied for copper determination shows a reoxidation wave at -0.10 V vs. Ag/AgCl (Fig. 1). The use of the calibration procedure described previously allows different calibration curves graphs to be obtained by plotting peak intensity vs. time for different preconcentration times (Fig. 2) and the kinetic slope method was applied on the basis of the linear relationship obtained from the initial reaction rate  $v_0$  (Eqn. 3) vs. copper concentration (inset, Fig. 2).

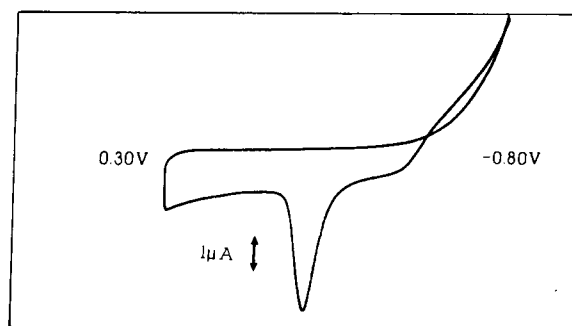


Fig. 1. Copper electrochemical signal with reduction potential -0.80 V, reduction time 30 s and scan rate 400 mV s<sup>-1</sup> for a 3-min preconcentration period over a copper solution containing 2.00 μg l<sup>-1</sup> in 0.01 M KNO<sub>3</sub>.

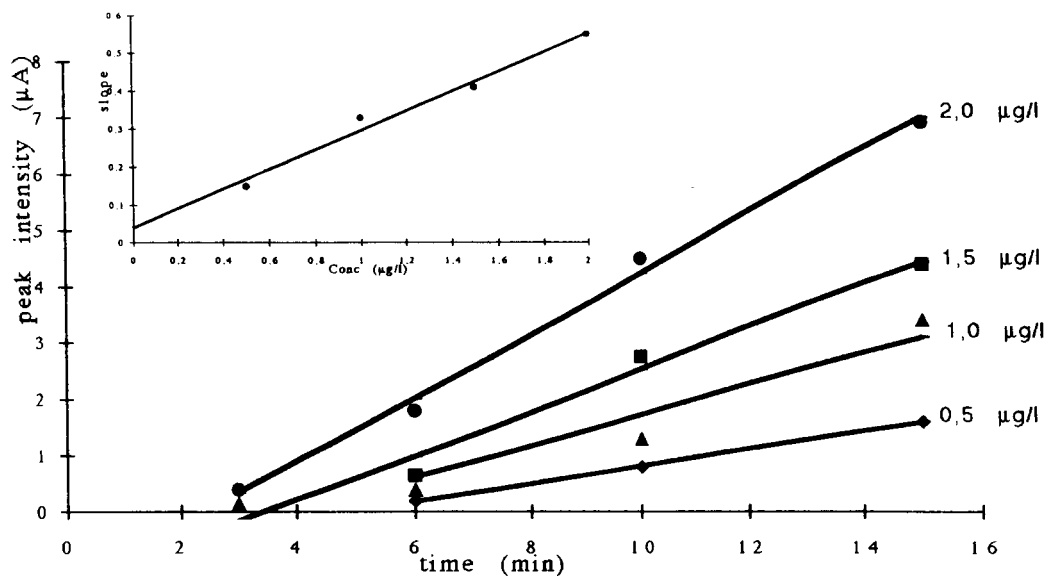


Fig. 2. Electrode calibration for different preconcentration periods. Inset: kinetic slope procedure method. Other parameters as in Fig. 1.

Statistical studies showed a detection limit of  $0.5 \mu\text{g l}^{-1}$  ( $3\sigma$ ) and a determination limit of  $1.0 \mu\text{g l}^{-1}$  ( $10\sigma$ ) for copper with a relative standard

deviation of 7% ( $n=8$ ) and errors below 3% employing the slope kinetic method. A standard solution containing  $2 \mu\text{g l}^{-1}$  copper in 0.01 M

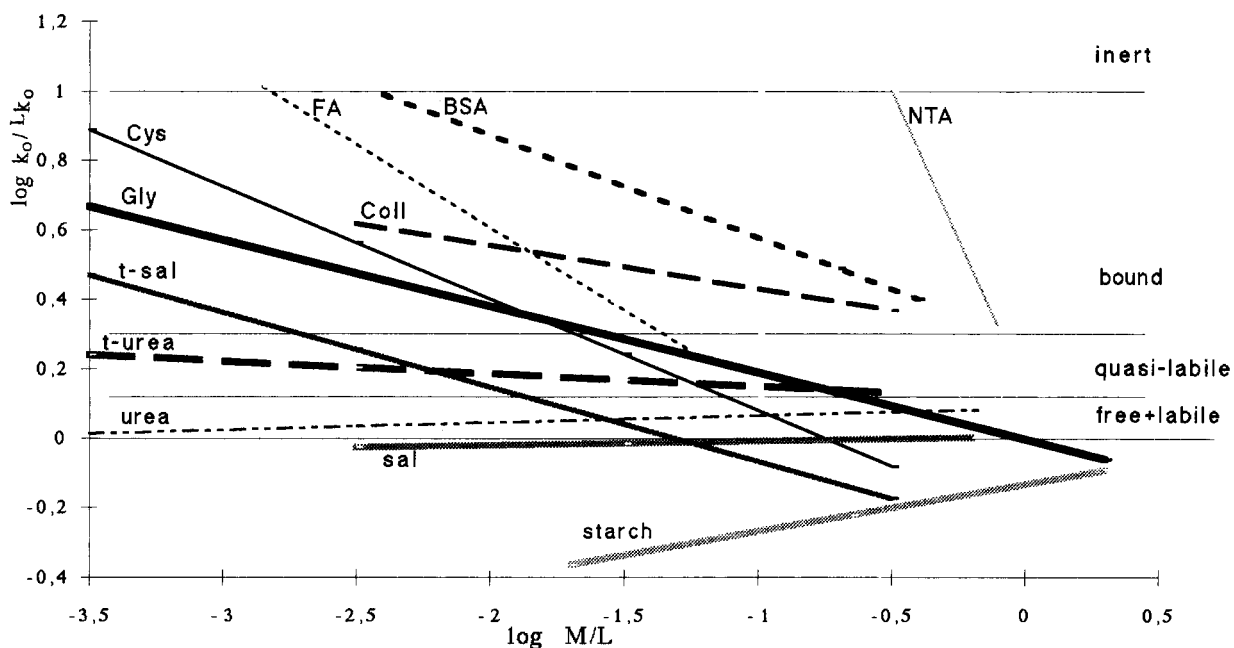


Fig. 3. Kinetic classification for each type of ligand as a function of  $[M]/[L]$  ratio. For further details, see text.

$\text{KNO}_3$  was checked each day before the actual analyses. The results were used as a reference for the activation state of the electrode and the electrochemical system.

The initial reaction rate constant  $k_0$  was also obtained at different copper concentration levels from Eqn. 3, taking into account that the electrochemical signal is due to the metal preconcentrated as MR on the electrode surface, obtaining a  $k_0$  value of  $(1.9 \pm 0.2) \times 10^7 \text{ min}^{-1}$ .

Preconcentration was then done in a copper solution containing different types of ligand and the copper recovery was calculated through the kinetic slope method by measuring the electrochemical copper signal over a predetermined preconcentration time. The  ${}^Lk_0$  value was also obtained from Eqn. 3 and the kinetic factor  $\log(k_0/{}^Lk_0)$  and its linear relationship to  $\log([M]/[L])$  was obtained from Eqn. 5. Results for several model ligands are shown in Fig. 3.

According to these experimental results, an operational criterion for the classification of the types of species in water can be deduced. The difference between the values of the initial reaction rate constant in the absence ( $k_0$ ) and presence ( ${}^Lk_0$ ) of ligand as  $\log(k_0/{}^Lk_0)$  allows four types of species to be established (Table 1) in which the metal complex could be formed in an aquatic system with natural ligands.

The plot  $\log(k_0/{}^Lk_0)$  vs.  $\log([M]/[L])$  illustrates the magnitude of the effect of the addition of each ligand and the type of complex that is formed can be deduced by looking at the zone between defined lines where the ligand is situated for each  $[M]$  to  $[L]$  ratio. In this sense, it can be observed that the complex can change from one type to another depending on the  $[M]$  to  $[L]$  ratio. The slope of their relationship ( $\beta$ ) shows

TABLE 1

Operationally defined lability criteria as a function of the observed effect of each ligand on the initial reaction

$\log(k_0/{}^Lk_0)$	Metal species
< 0.12	Free + labile
0.12–0.30	Quasi-labile
0.30–1.00	Bound
> 1.00	Inert

TABLE 2

$\beta$  and  $\log k'$  values for each ligand as a comparison of the observed kinetic effect and the thermodynamically predicted effect

Ligand	$\beta$	Log $K'$
Starch	0.10	–
Urea	0.02	0.7
Sal	0.01	16.6
TU	–0.04	15.4
Colloids	–0.13	–
TSal	–0.22	–
Gly	–0.23	10.4
BSA	–0.29	9.7
Cys	–0.32	13.9
FA	–0.49	7.8
NTA	–1.70	14.7

the extent of the influence for each ligand (Table 2).

FA presents an example of a change in type as a function of the  $[M]/[L]$  ratio. It can be defined as labile when present at a similar concentration to the metal, but when present in excess it can be considered as an inert complex.

For some compounds, such as inorganic or small organic ligands, the value of  $\log(k_0/{}^Lk_0)$  is very close to zero for any  $[M]/[L]$  ratio and they could be considered as free + labile complexes (Sal and urea). For other ligands, although the value of the kinetic parameter is not very high, it is affected by the  $[M]/[L]$  ratio (TU urea).

Simple amino acids, such as cysteine and glycine, show a behaviour which is highly dependent on the  $[M]/[L]$  ratio, but BSA shows a transition to more complexed metal at lower  $[M]/[L]$  ratios. This has been explained [1] as an effect of its three-dimensional structure, trapping the metal more effectively than simple ligands but not because of a higher complexing capacity, as can be seen from its thermodynamic equilibrium constant (Table 2). These three-dimensional structure effects can also be seen in the comparison of FA with Sal and TSal, where their complexing sites are not very different in strength but their spatial structures are different, leading to a behaviour different from that expected on the basis of their conditional equilibrium constants and that can be deduced from  $\beta$  values obtained.



It can also be observed how low complexing sites situated on the surface of solid colloids such as OH sites in the iron colloid tested can strongly bind copper; this effect can also be deduced from its  $\beta$  value. From these results, according to the description of the absorption of the trace metals on substrates as iron oxides, a two-step kinetic mechanism is supposed, the first step being very fast when the metal/adsorbent ratio is low. Surface sites are in large excess and equilibrium can be achieved in a relatively long time (24 h), leading to a bound behaviour in the colloid–metal complex, as observed [21].

NTA, a ligand with high complexing capability for copper, represents, the inert fraction, with the highest  $\beta$  parameter.

Starch is exceptional, showing a positive  $\beta$  parameter. This can be explained on the basis of its non-polyelectrolyte behaviour and taking into account the nature of the electrode surface, which is predominantly hydrophobic [1]; the starch can favour the metal, staying at the electrode surface, and consequently its preconcentration in the electrode as an MR complex. This could be expected, as it is known that some polysaccharides can form an external layer on the cell wall and favour metal crossing the cell wall.

These results obtained by the kinetic approach can be compared with those deduced from theoretical predictions, according to the values of the conditional thermodynamic constants of the complexes ( $K'$ ). The experimentally calculated kinetic parameters show a better correspondence with the real effect of each ligand as a function of its chemical nature and complexing power than the effect deduced from thermodynamic data only. NTA, Sal and simple amino acids show similar values of their conditional constants but their  $\beta$  values are very different and so are their effects: amino acids behave as labile to the bound fraction whereas NTA can be defined as an inert fraction and Sal behaves as free + labile for the whole  $[M]/[L]$  range. These results are in accord with the structure and complexing capability of each ligand; whereas NTA has strong donor atoms for copper (N, O) in a position that allows multi-

dentate chelate formation, simple amino acids contain the same donor atoms but in a linear arrangement. Sal possesses only simple donor atoms (O) with less complexing power. Other ligand effects, such as for FA, are also well explained through kinetic parameters.

The authors thank the Ministry of Education and Research of Spain and Autonoma Community of Madrid for the financial support of this work and for a research grant to R. Agraz.

## REFERENCES

- 1 J. Buffle, *Complexation Reactions in Aquatic Systems. An Analytical Approach*, Horwood, Chichester, 1988.
- 2 T.S. West, *The determination of Trace Metals in Natural Waters*, Blackwell, Oxford, 1988.
- 3 R.R. de Vitre, M.C. Tercier and J. Buffle, *Anal. Proc.*, 28 (1991) 74.
- 4 T.M. Florence and G.E. Batley, *Talanta*, 24 (1977) 151.
- 5 T.M. Florence, *Analyst*, 111 (1986) 489.
- 6 P. Ostapczuk and Z. Kublick, *J. Electroanal. Chem.*, 83 (1977) 1.
- 7 H. Gunasingham, K.P. Ang and C.C. Ngo, *Analyst*, 113 (1988) 113.
- 8 T.M. Florence and K.J. Mann, *Anal. Chim. Acta*, 200 (1987) 305.
- 9 T.M. Florence, *Anal. Chim. Acta*, 141 (1982) 73.
- 10 T.M. Florence and G.E. Batley, *Talanta*, 23 (1976) 179.
- 11 P. Figura and B. McDuffie, *Anal. Chem.*, 52 (1980) 1433.
- 12 M.T. Sevilla, J.R. Procopio, J.M. Pinilla and L. Hernández, *Int. J. Environ. Anal. Chem.*, 37 (1989) 107.
- 13 R. Agraz, M.T. Sevilla and L. Hernández, *Electroanalysis*, 3 (1991) 393.
- 14 R. Agraz, M.T. Sevilla and L. Hernández, *Anal. Chim. Acta*, 273 (1993) 205.
- 15 D.L. Olson and M.S. Shuman, *Anal. Chem.*, 55 (1983) 1103.
- 16 J.A. Lavigne, C.H. Langford and M.K.S. Mark, *Anal. Chem.*, 59 (1987) 2616.
- 17 M.S. Shuman, *Environ. Sci. Technol.*, 26 (1992) 593.
- 18 H.P. van Leeuwen and J. Buffle, *J. Electroanal. Chem.*, 296 (1990) 359.
- 19 C. Heitner and G. Markovits, *J. Phys. Chem.*, 67 (1963) 2263.
- 20 M.D. Pérez-Bendito and M. Valcárcel, *Métodos Cinéticos de Análisis*, Universidad de Córdoba, 1984.
- 21 G.E. Batley, *Trace Element Speciation: Analytical Methods and Problems*, CRC, Boca Raton, FL, 1990.

# Quinidine ion-selective electrode for potentiometric determinations in pharmaceutical preparations

Manuel N.M.P. Alçada, José L.F.C. Lima and M. Conceição B.S.M. Montenegro

*Departamento de Química Física, Faculdade de Farmácia, 4000 Porto (Portugal)*

(Received 11th September 1992; revised manuscript received 7th December 1992)

## Abstract

The construction and evaluation of a quinidine ion-selective electrode, without an inner reference solution, based on an ion exchanger [quinidine tetrakis(4-chlorophenyl)borate] dissolved in 2-nitrophenyl octyl ether and immobilized in PVC is described. The prepared electrode showed a linear response in the concentration range  $3 \times 10^{-5}$ – $1 \times 10^{-2}$  M in quinidine, with a slope of 57.5 mV per decade when the pH of the solutions was between 5 and 7.5. The reproducibility of the electrode was approximately  $\pm 1$  mV during a day's work, with a response time of less than 10 s for quinidine concentrations between  $10^{-4}$  and  $10^{-2}$  M. The electrode was used for the direct potentiometric determination of quinidine in pharmaceutical preparations, giving results with an average recovery of 100.7% and a mean standard deviation of 2.3%.

**Keywords:** Ion selective electrodes; Potentiometry; Pharmaceuticals; Quinidine

The potentiometric determination of alkaloids in pharmaceutical preparations using ion-selective electrodes has been referred to as an advantageous technique [1] compared with conventional methods described in pharmacopoeias [2,3], because the method has a greater specificity and a more rapid response, simpler measurements as well as more precise and accurate results are obtained.

The results given in the literature of ion-selective electrodes for quinidine and quinine, stereoisomer alkaloids with an antimalarial and antiarrhythmic action [4–7], suggest that these devices should not be employed for routine determinations, especially when applied for direct potentiometry.

*Correspondence to:* M.C.B.S.M. Montenegro, Departamento de Química Física, Faculdade de Farmácia, 4000 Porto (Portugal).

Earlier devices either used a liquid membrane [5] or, when the sensor was immobilized in PVC, an inner reference solution [4,6] and an electrode. These electrodes had certain drawbacks, namely unstable potentials, a lack of reproducibility, long response times and difficult manipulation, all of which affected their application to direct potentiometry. The use, in all instances, of tetraphenylborate as an ion extractor [4–7], alone or in association with mediator solvents such as nitrobenzene [5], contributed to a reduced linear response of the electrodes and a poor selectivity as regards interfering species.

In a previous paper [8], the use of tetrakis(4-chlorophenyl)borate as an ion exchanger for cationic species proved to favour electrodes with a wider linear response, a greater reproducibility of the potentials and better selectivity than similar devices prepared with tetraphenylborate. Further, the elimination of an inner reference solu-

tion in conventionally constructed electrodes and the use of 2-nitrophenyl octyl ether as a mediator solvent in previous work [9] were found to create longer lasting and mechanically more stable devices, which is of importance when they need to be used daily in the laboratory.

On the basis of an analysis of these problems, in this work attempts were made to improve the operating characteristics of quinidine ion-selective electrodes so that they could be applied in direct potentiometry or potentiometric titrations. Hence, electrodes were constructed in which the sensor consisted of a blend of quinidine tetrakis(4-chlorophenyl)borate and 2-nitrophenyl octyl ether immobilized in PVC and were fixed directly on a conductor consisting of a graphite powder-treated epoxy resin. The analytical usefulness of the electrodes was assessed by performing direct potentiometric determinations of quinidine and quinine in pharmaceutical preparations.

## EXPERIMENTAL

### *Apparatus and electrodes*

In order to determine the differences in potential between the electrodes and the reference electrode, a Crison Model 2002 decimillivoltmeter ( $\pm 0.1$  mV) coupled to an electrode switch of the same manufacturer was used.

Potentiometric determinations were made at a controlled temperature of  $25.0 \pm 0.2^\circ\text{C}$ , using an Orion 900200 silver chloride/silver double-junction reference electrode with 0.033 M sodium sulphate solution in the outer compartment. For pH determinations an Ingold 10/402/3092 glass electrode was employed.

### *Reagents and solutions*

In all preparations analytical-reagent grade reagents were used as received. The solutions were prepared with deionized water with a conductivity of  $0.1 \mu\text{S cm}^{-1}$ .

A standard solution of quinidine with a concentration of 0.01 M was prepared by accurately weighing the appropriate amount of quinidine sulphate and subsequently diluting it whenever necessary. The more concentrated solution was

prepared daily and, when not in use, was stored in the dark.

For ionic strength adjustment 0.033 M sodium sulphate solution was used. The buffer used for the direct potentiometric determination of quinidine in pharmaceutical preparations was an  $\text{KH}_2\text{PO}_4\text{-Na}_2\text{HPO}_4$  (pH 6.5), prepared in a 1000-ml flask by adding 98 ml of 0.5 M  $\text{KH}_2\text{PO}_4$  solution to 34 mL of a 0.5 M  $\text{Na}_2\text{HPO}_4$  solution and diluting to volume with deionized water.

### *Membrane preparation and electrode assembly*

Quinidine tetrakis(4-chlorophenyl)borate was prepared by adding 45 ml of 0.014 M aqueous quinidine sulphate to 5 ml of a 0.1 M solution of potassium tetrakis(4-chlorophenyl)borate in acetone. The precipitate obtained was stored in the dark in a dry environment whilst the acetone evaporated. Following this, the precipitate was vacuum filtered and washed with deionized water about three times. The collected crystals were placed in a desiccator at room temperature in the dark.

Approximately 0.06 g of precipitate was dissolved in about of 1.24 g of 2-nitrophenyl octyl ether and 0.18 g of PVC previously dissolved in 6 ml of tetrahydrofuran was added to approximately 0.4 ml of the solution. After evaporation of the tetrahydrofuran, a membrane with an ion-pair complex of 3% (w/w) was obtained.

The prepared membrane was fixed directly on to a support consisting of graphite powder-treated epoxy resin, as described in a previous paper [10].

The constructed electrodes were conditioned by soaking in 0.01 M quinidine sulphate solution for at least 3 days, and when not in use were stored in the same solution.

### *Determination of quinidine in pharmaceutical preparations*

In order to determine quinidine in tablets, ten tablets from the same lot were pulverized and ca. 100 mg of the powder were placed in a 50-ml volumetric flask to which ca. 45 ml of  $\text{KH}_2\text{PO}_4\text{-Na}_2\text{HPO}_4$  solution (pH 6.5) were added. This mixture was then placed in an ultrasonic bath to facilitate its dissolution and diluted to a final volume of 50 ml with the same buffer.

For suppositories, about five suppositories that had been previously homogenized by heating them at 37°C were weighted. Approximately 1.0 g of the homogenized product was mixed in a volumetric flask with 50 ml of  $\text{KH}_2\text{PO}_4$ – $\text{Na}_2\text{HPO}_4$  buffer solution (pH 6.5). This solution was heated at 37°C in an ultrasonic bath to promote its dissolution.

Direct potentiometric determinations were performed on the samples prepared as described above and diluted twofold. First, however, the electrodes were calibrated in quinidine solutions at different concentrations and prepared with the same pH adjustment solution.

In order to evaluate the quality of the potentiometric results obtained, determinations were also performed with the standard addition method and the recovery was determined. For the latter purpose, a small amount (100  $\mu\text{l}$ ) of standard 0.01 M quinidine solution was added to a prepared sample with a concentration approximately as mentioned above. The variation in the potential was recorded and used to calculate the percentage recovery of the amount added.

## RESULTS AND DISCUSSION

### Electrode behaviour

The general operating characteristics of the electrodes constructed were evaluated by repeated calibrations in quinidine solutions without an ionic strength adjustment solution, with the ionic strength adjusted to 0.1 M with sodium

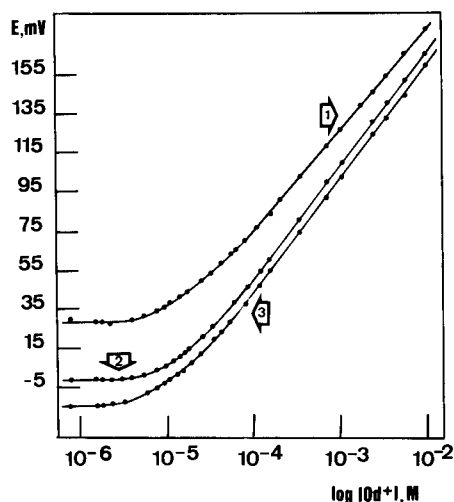


Fig. 1. Calibration graphs for quinidine electrode obtained in solutions (1) without ionic strength adjusted, (2) with ionic strength adjusted (0.1 M  $\text{Na}_2\text{SO}_4$ ) and (3) in  $\text{KH}_2\text{PO}_4$ – $\text{Na}_2\text{HPO}_4$  buffer (pH 6.5,  $I = 0.1$ ).

sulphate and in  $\text{KH}_2\text{PO}_4$ – $\text{Na}_2\text{HPO}_4$  buffer solution (pH 6.5). Figure 1 shows the calibration graphs curves obtained.

The electrode response is very similar regardless of the solution used for calibration. However, there was a slight decrease in the slope values of the devices when the tests were performed in solutions without an ionic strength adjustment solution, probably because such determinations occur when the pH is close to the lower operational limit (pH 5). At this pH value monoprotonated and diprotonated fractions of quinidine co-exist.

TABLE 1

Operating characteristics of the quinidine-selective electrodes

Characteristic	I <sup>a</sup>	II <sup>b</sup>	III <sup>c</sup>
Slope (mV per decade)	$52.3 \pm 1.2$	$57.5 \pm 0.4$	$57.6 \pm 0.4$
LLLR <sup>d</sup> (M)	$3.1 \times 10^{-5}$	$3.2 \times 10^{-5}$	$3.0 \times 10^{-5}$
LLD <sup>e</sup> (M)	$1.3 \times 10^{-5}$	$1.3 \times 10^{-5}$	$9.4 \times 10^{-6}$
pH range <sup>f</sup>	5–7.5	5–7.5	–
Response time (s)	< 6	< 6	< 6
Reproducibility (mV day <sup>-1</sup> )	$\pm 1.5$	$\pm 1.0$	$\pm 0.9$
Lifetime (months)	> 4	> 4	> 4

<sup>a</sup> Results obtained in pure solutions without the ionic strength adjusted. <sup>b</sup> Results obtained in solutions with  $I = 0.1$  M adjusted with  $\text{Na}_2\text{SO}_4$ . <sup>c</sup> Results obtained in  $\text{KH}_2\text{PO}_4$ – $\text{Na}_2\text{HPO}_4$  buffer solutions (pH 6.5 and  $I = 0.1$  M). <sup>d</sup> Lower limit of linear response. <sup>e</sup> Lower limit of detection. <sup>f</sup> Results obtained in 0.01 M quinidine (sulphate) solutions.

Table 1 shows the operating characteristics of the quinidine ion-selective electrodes when tested in solutions with different compositions. The values given are averages of two determinations performed with three different electrodes ( $n = 6$ ). The results show that the electrodes have good operating characteristics, with similar behaviour when tested in different solutions. In comparison with the devices prepared with tetraphenylborate [4–7] and tested under similar conditions, there was an improved linear response, slope and reproducibility of the potential. It is also noteworthy that these electrodes have an increased response rate that may attain values of up to 3 s.

#### Effect of pH

The effect of pH on the potential of the quinidine electrode was evaluated by recording the e.m.f. of the ion-selective electrode in 0.01 M quinidine sulphate solutions, with or without ionic strength adjustment with 0.033 M  $\text{Na}_2\text{SO}_4$ . The pH of the initial solution was modified by adding very small volumes of concentrated sulphuric acid or sodium hydroxide solution. The results in Fig. 2 show that the potential of the electrodes does not change significantly when the pH is between 5 and 7.5. Above pH 7.5 a decrease in potential is observed due both to an increase in the concentration of the non-ionized quinidine fraction ( $\text{p}K_{a_2} = 8.8$ ) [11] and to the dissolution of the precipitate that is formed. Below pH 5, the decrease in potential recorded is due to the in-

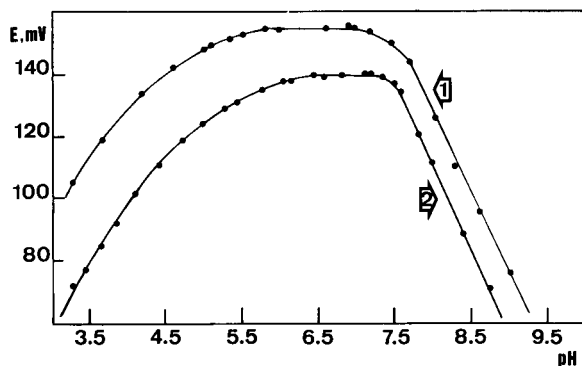


Fig. 2. Effect of pH on the potential of quinidine electrode in 0.01 M quinidine solutions, (1) with ionic strength adjusted to 0.1 M and (2) without ionic strength adjusted.

TABLE 2

Potentiometric selectivity coefficients ( $\log k^{pot}$ ) for quinidine-selective electrodes <sup>a</sup>

Interferent	Concentration	
	$1 \times 10^{-4}$ M	$1 \times 10^{-3}$ M
Calcium	$-3.2 \pm 0.1$	$-3.7 \pm 0.1$
Sodium	$-1.2 \pm 0.2$	$-2.3 \pm 0.2$
Ammonium	$-1.1 \pm 0.1$	$-2.2 \pm 0.1$
Potassium	$-1.3 \pm 0.1$	$-2.4 \pm 0.2$
Atropine	$-0.8 \pm 0.1$	$-1.3 \pm 0.1$
Ephedrine	$-1.0 \pm 0.1$	$-1.8 \pm 0.2$
Pilocarpine	$-0.9 \pm 0.1$	$-1.6 \pm 0.1$
Strychnine	$-0.2 \pm 0.1$	$-0.4 \pm 0.1$
Quinine	$-0.1 \pm 0.1$	$-0.1 \pm 0.1$
Tetrapentylammonium	$+0.5 \pm 0.5$	$+6.0 \pm 0.1$

<sup>a</sup> Means and standard deviations of four values obtained in two determinations with two electrodes.

creased concentration of the diprotonated quinidine fraction ( $\text{p}K_{a_1} = 4.2$ ) according to [11]. These results are similar to those obtained by other workers when testing similar electrodes in solutions of the alkaloid with different pH values [5,6].

#### Selectivity

The interference of several cations was studied by the method of separate solutions [12] at two concentration levels (Table 2). Some of the organic ions were chosen because they represent potentially low-level contaminants in pharmaceutical preparations of quinidine. The bulk of the excipients, usually comprising lactose or glucose as a diluent and maize starch or gelatine as a binder, does not interfere with the electrode response.

The selectivity of the electrode is good when compared with others described previously [4–7]. However, there was high interference from quaternary ammonium compounds, particularly when these are present in high concentrations.

#### Analytical applications

The response characteristics of the quinidine ion-selective electrodes suggest that these devices could be used for the determination of quinidine in pharmaceutical preparations. With a view to proving their analytical usefulness, direct poten-

TABLE 3

Determination of quinidine in some pharmaceutical preparations using the quinidine electrode

Preparation <sup>a</sup>	Quinidine (% w/w) <sup>b</sup>		Recovery (%) <sup>b</sup>
	Direct potentiometry	Standard addition method	
Natisedine (tablets)	25.4 ± 1.3	26.7 ± 0.8	103.2 ± 3.6
Quinocardine (tablets)	59.8 ± 0.4	64.1 ± 0.6	97.8 ± 2.1
Transpulmina (suppositories)	5.1 ± 0.1	4.9 ± 0.2	100.0 ± 1.8
Recto-Pulmo (suppositories)	2.1 ± 0.1	2.2 ± 0.1	101.8 ± 3.7

<sup>a</sup> Commercially available dosage forms. <sup>b</sup> Means and standard deviations of eight determinations with two electrodes.

tiometric determinations were performed. Table 3 gives the results corresponding to these determinations together with the corresponding recoveries. The values presented are the averages of two determinations performed with three electrodes on three different samples of the same product.

The different determinations gave a mean overall recovery of 100.7% (w/w) with a mean standard deviation of 2.3%, hence demonstrating the accuracy of this method.

### Conclusions

The use of tetrakis(4-chlorophenyl)borate as an ion extractor and 2-nitrophenyl octyl ether as a mediator solvent in the preparation of the membranes for quinidine ion-selective electrodes allowed the construction of electrodes with greater linear response ranges, more reproducible potentials, more rapid response times and better overall selectivity. Further, the construction of an electrode in which the internal solution and reference electrode were eliminated resulted

in more stable devices with considerably longer lifetimes. The use of electrodes for the determination of quinidine in pharmaceutical preparations enabled determinations to be performed more rapidly (ca. 15 min), at less cost, with a greater degree of accuracy and without the need for any special treatment of the samples, all of which are considerable advantages over the conventional procedures described in different pharmacopoeias.

The authors gratefully acknowledge financial support from the Instituto Nacional de Investigação Científica (Project 89/SAD/1). M.N.M.P.A. was supported by a grant from JNICT (Lisbon, Portugal). Mrs. Belmira Pereira is thanked for carrying out routine work.

### REFERENCES

- 1 K. Vytras, *J. Pharm. Biomed. Anal.*, 7 (1989) 789.
- 2 British Pharmacopoeia Commission, *British Pharmacopoeia 1988*, Her Majesty's Stationery Office, London, 1988.
- 3 US Pharmacopoeia XXII, *National Formulary XVII*, US Pharmacopoeial Convention, Rockville, MD, 1990.
- 4 J.-I. Anzai, C. Isomura and T. Osa, *Chem. Pharm. Bull.*, 33 (1985) 236.
- 5 S.-Z. Yao and J.-H. Liu, *Huaxue Xuebao*, 43 (1985) 611.
- 6 V.V. Cosofret and R.P. Buck, *J. Pharm. Biomed. Anal.*, 3 (1985) 123.
- 7 E. Hopirtean and E. Stefaniga, *Rev. Roum. Chim.*, 21 (1976) 305.
- 8 G.H. Zhang, T. Imato, Y. Asano, T. Sonoda, H. Kobayashi and N. Ishibashi, *Anal. Chem.*, 62 (1990) 1644.
- 9 G.J. Moody, J.D.R. Thomas, J.L.F.C. Lima and A.A.S.C. Machado, *Analyst*, 113 (1988) 1023.
- 10 R.A.S. Lapa, J.L.F.C. Lima and A.M.R. da Silva, *Far-maco*, 45 (1990) 901.
- 11 *The Merck Index*, Merck, Rahway, NJ, 11th edn., 1989, p. 1283.
- 12 IUPAC Analytical Chemistry Division on Analytical Nomenclature, *Pure Appl. Chem.*, 53 (1981) 1907.

## PUBLICATION SCHEDULE FOR 1994

	S'93	O'93	N'93	D'93	J	F					
Analytica	281/1	282/1	283/1	283/3	284/3	285/3					
Chimica	281/2	282/2	283/2	284/1	285/1	286/1					
Acta	281/3	282/3		284/2	285/2	286/2					
Vibrational Spectroscopy		6/1			6/2						

## INFORMATION FOR AUTHORS

**Detailed "Instructions to Authors"** for *Analytica Chimica Acta* was published in Volume 256, No. 2, pp. 373–376. Free reprints of the "Instructions to Authors" of *Analytica Chimica Acta* and *Vibrational Spectroscopy* are available from the Editors or from: Elsevier Science Publishers B.V., P.O. Box 330, 1000 AH Amsterdam, The Netherlands. Telefax: (+31-20) 5862 845.

**Manuscripts.** The language of the journal is English. English linguistic improvement is provided as part of the normal editorial processing. Authors should submit three copies of the manuscript in clear double-spaced typing on one side of the paper only. *Vibrational Spectroscopy* also accepts papers in English only.

**Abstract.** All papers and reviews begin with an Abstract (50–250 words) which should comprise a factual account of the contents of the paper, with emphasis on new information.

**Figures.** Figures should be prepared in black waterproof drawing ink on drawing or tracing paper of the same size as that on which the manuscript is typed. One original (or sharp glossy print) and two photostat (or other) copies are required. Attention should be given to line thickness, lettering (which should be kept to a minimum) and spacing on axes of graphs, to ensure suitability for reduction in size on printing. Axes of a graph should be clearly labelled, along the axes, outside the graph itself. All figures should be numbered with Arabic numerals, and require descriptive legends which should be typed on a separate sheet of paper. Simple straight-line graphs are not acceptable, because they can readily be described in the text by means of an equation or a sentence. Claims of linearity should be supported by regression data that include slope, intercept, standard deviations of the slope and intercept, standard error and the number of data points; correlation coefficients are optional. Photographs should be glossy prints and be as rich in contrast as possible; colour photographs cannot be accepted. Line diagrams are generally preferred to photographs of equipment.

Computer outputs for reproduction as figures must be good quality on blank paper, and should preferably be submitted as glossy prints.

**Nomenclature, abbreviations and symbols.** In general, the recommendations of the International Union of Pure and Applied Chemistry (IUPAC) should be followed, and attention should be given to the recommendations of the Analytical Chemistry Division in the journal *Pure and Applied Chemistry* (see also *IUPAC Compendium of Analytical Nomenclature, Definitive Rules, 1987*).

**References.** The references should be collected at the end of the paper, numbered in the order of their appearance in the text (not alphabetically) and typed on a separate sheet.

**Reprints.** Fifty reprints will be supplied free of charge. Additional reprints (minimum 100) can be ordered. An order form containing price quotations will be sent to the authors together with the proofs of their article.

**Papers dealing with vibrational spectroscopy** should be sent to: Dr J.G. Grasselli, 150 Greentree Road, Chagrin Falls, OH 44022, U.S.A. Telefax: (+1-216) 2473360 (Americas, Canada, Australia and New Zealand) or Dr J.H. van der Maas, Department of Analytical Molecule Spectrometry, Faculty of Chemistry, University of Utrecht, P.O. Box 80083, 3508 TB Utrecht, The Netherlands. Telefax: (+31-30) 518219 (all other countries).

© 1993, ELSEVIER SCIENCE PUBLISHERS B.V. All rights reserved.

0003-2670/93/\$06.00

No part of this publication may be reproduced, stored in a retrieval system or transmitted in any form or by any means, electronic, mechanical, photocopying, recording or otherwise, without the prior written permission of the publisher, Elsevier Science Publishers B.V., Copyright and Permissions Dept., P.O. Box 521, 1000 AM Amsterdam, The Netherlands.

Upon acceptance of an article by the journal, the author(s) will be asked to transfer copyright of the article to the publisher. The transfer will ensure the widest possible dissemination of information.

Special regulations for readers in the U.S.A.—This journal has been registered with the Copyright Clearance Center, Inc. Consent is given for copying of articles for personal or internal use, or for the personal use of specific clients. This consent is given on the condition that the copier pays through the Center the per-copy fee for copying beyond that permitted by Sections 107 or 108 of the U.S. Copyright Law. The per-copy fee is stated in the code-line at the bottom of the first page of each article. The appropriate fee, together with a copy of the first page of the article, should be forwarded to the Copyright Clearance Center, Inc., 27 Congress Street, Salem, MA 01970, U.S.A. If no code-line appears, broad consent to copy has not been given and permission to copy must be obtained directly from the author(s). All articles published prior to 1980 may be copied for a per-copy fee of US \$2.25, also payable through the Center. This consent does not extend to other kinds of copying, such as for general distribution, resale, advertising and promotion purposes, or for creating new collective works. Special written permission must be obtained from the publisher for such copying.

No responsibility is assumed by the publisher for any injury and/or damage to persons or property as a matter of products liability, negligence or otherwise, or from any use or operation of any methods, products, instructions or ideas contained in the material herein.

Although all advertising material is expected to conform to ethical (medical) standards, inclusion in this publication does not constitute a guarantee or endorsement of the quality or value of such product or of the claims made of it by its manufacturer.

This issue is printed on acid-free paper.

PRINTED IN THE NETHERLANDS

# CHEMOMETRICS TUTORIALS II

edited by **R.G. Brereton**, University of Bristol, Bristol, UK, **D.R. Scott**, U.S. Environmental Protection Agency, Research Triangle Park, NC, USA,

**D.L. Massart**, Vrije Universiteit Brussel, Brussels, Belgium, **R.E. Dessy**, Virginia Polytechnic Institute, Blackburg, VA, USA, **P.K. Hopke**, Clarkson University, Potsdam, NY, USA, **C.H. Spiegelman**, Texas A&M University, College Station, TX, USA and **W. Wegscheider**, Universität Graz, Graz, Austria

The journal *Chemometrics and Intelligent Laboratory Systems* has a specific policy of publishing tutorial papers (i.e. articles aiming to discuss and illustrate the application of chemometric and other techniques) solicited from leading experts in the varied disciplines relating to this subject. This book comprises reprints of tutorials from Volumes 6-11 of this journal, covering the period from mid 1989 to late 1991. The authors of the papers include analytical, organic and environmental chemists, statisticians, pharmacologists, geologists, geochemists, computer scientists and biologists, which reflects the strong interdisciplinary communication. The papers have been reorganized into major themes, covering most of the main areas of chemometrics.

This book is intended both as a personal reference text and as a useful background for courses in chemometrics and laboratory computing.

**Contents:** Foreword.

**Software.** 1. Teaching and Learning Chemometrics with MatLab (*T.C. O'Haver*).

2. Expert System Development Tools for Chemists (*F.A. Settle, Jr., M.A. Pleva*).

3. Spectral Databases (*W.A. Warr*).

**Signal Processing.** 4. Specification and Estimation of Noisy Analytical Signals. Part I. Characterization, Time Invariant Filtering and Signal Approximation (*H.C. Smit*).

5. Specification and Estimation of Noisy Analytical Signals. Part II. Curve Fitting, Optimum Filtering and Uncertainty Determination (*H.C. Smit*).

6. Fast On-Line Digital Filtering (*S.C. Rutan*). **Multivariate Methods.**

7. Cluster Analysis (*N. Bratchell*). 8. Interpretation of Latent-Variable Regression Models (*O.M. Kvalheim, T.V. Karstang*).

9. Quantitative Structure-Activity Relationships (QSAR) (*W.J. Dunn, III*). 10. Analysis of Multi-Way (Multi-Mode) Data (*P. Geladi*).

**Factor Analysis.** 11. Target Transformation Factor Analysis (*P.K. Hopke*). 12. An Introduction to Receptor Modeling (*P.K. Hopke*).

13. The Spectrum Reconstruction Problem. Use of Alternating Regression for Unexpected Spectral Components in Two-Dimensional Spectroscopies (*E.J. Karjalainen*).

**Statistics.** 14. Analysis of Variance (ANOVA) (*L. Stähle, S. Wold*). 15. Multivariate Analysis of Variance (MANOVA) (*L. Stähle, S. Wold*).

16. The Validation of Meas-

urement through Inter-laboratory Studies (*J. Mandel*).

17. Regression and Calibration with Nonconstant Error Variance (*M. Davidian, P.D. Haaland*). 18. Interpolation and Estimation with Spatially Located Data Sets (*D.E. Myers*).

**Optimization.** 19. Optimization Using the Modified Simplex Method (*E. Morgan, K.W. Burton, G. Nickless*).

20. Optimization Using the Super-Modified Simplex Method (*E. Morgan, K.W. Burton, G. Nickless*).

**Fractals.** 21. Fractals in Chemistry (*D.B. Hibbert*). Author Index. Subject Index.

1992 x + 314 pages

Paperback

Price: US \$ 156.50 / Dfl. 250.00

ISBN 0-444-89858-1

## ORDER INFORMATION

For USA and Canada

**ELSEVIER SCIENCE**

**PUBLISHERS**

Judy Weislogel

P.O. Box 945

Madison Square Station,

New York, NY 10160-0757

Tel: (212) 989 5800

Fax: (212) 633 3880

In all other countries

**ELSEVIER SCIENCE**

**PUBLISHERS**

P.O. Box 211

1000 AE Amsterdam

The Netherlands

Tel: (+31-20) 5803 753

Fax: (+31-20) 5803 705

US\$ prices are valid only for the USA & Canada and are subject to exchange rate fluctuations; in all other countries the Dutch guilder price (Dfl.) is definitive. Books are sent postfree if prepaid.



**ELSEVIER**  
SCIENCE PUBLISHERS

414\143\0036



0003-2670(19931115)283:1;1-C

- 4 n.w. 2537